Phys. Lett. B 849 (2024) 138469

Contents lists available at ScienceDirect

Physics Letters B

journal homepage: www.elsevier.com/locate/physletb

Letter

Probing the CP nature of the top–Higgs Yukawa coupling in $t\bar{t}H$ and tH events with $H \to b\bar{b}$ decays using the ATLAS detector at the LHC

The ATLAS Collaboration *

ARTICLE INFO

Editor: M. Doser

ABSTRACT

The CP properties of the coupling between the Higgs boson and the top quark are investigated using 139 fb^{-1} of proton–proton collision data recorded by the ATLAS experiment at the LHC at a centre-of-mass energy of $\sqrt{s} = 13$ TeV. The CP structure of the top quark–Higgs boson Yukawa coupling is probed in events with a Higgs boson decaying into a pair of b-quarks and produced in association with either a pair of top quarks, $t\bar{t}H$, or a single top quark, tH. Events containing one or two electrons or muons are used for the measurement. Multivariate techniques are used to select regions enriched in $t\bar{t}H$ and tH events, where dedicated CP-sensitive observables are exploited. In an extension of the Standard Model (SM) with a CP-odd admixture in the top–Higgs Yukawa coupling, the mixing angle between CP-even and CP-odd couplings is measured to be $\alpha = 11\,^{\circ+52^{\circ}}_{-73^{\circ}}$, compatible with the SM prediction corresponding to $\alpha = 0$.

1. Introduction

Since the observation of the Higgs boson at the LHC [1,2], its properties have been studied in great detail. In particular, the observation of the Higgs boson production in association with a top-quark pair, $t\bar{t}H$ [3,4], provides direct experimental access to the top-quark Yukawa coupling at the tree-level. The increasing datasets at the LHC have recently allowed the ATLAS and CMS Collaborations to probe the charge-conjugation and parity (CP) properties of this coupling using $t\bar{t}H$ events in different decay channels [5–7]. This letter reports on a study of the CP properties of the top-quark Yukawa coupling using $t\bar{t}H$ and tH production, in the $H \to b\bar{b}$ decay channel. The analysis targets final states where at least one top quark decays semi-leptonically to electrons or muons. It uses $\sqrt{s} = 13$ TeV pp collision data recorded by the ATLAS experiment during Run 2, corresponding to an integrated luminosity of 139 fb^{-1}.

The Standard Model (SM) predicts the Higgs boson to be a scalar particle with quantum numbers $J^{CP} = 0^{++}$. Considering the possibility of beyond the Standard Model (BSM) couplings, a CP-odd component of the vector-boson couplings to the Higgs boson is naturally suppressed by the scale at which new physics would become relevant [8,9]. This suppression does not happen for Yukawa couplings, where CP-odd Higgs–fermion couplings may be significant already at tree level [10]. One of the first ATLAS and CMS measurements have excluded the pure $J^P = 0^-$ hypothesis by more than 95% CL using $H \to \gamma\gamma$, $H \to ZZ^*$ and $H \to WW^*$ decays [11,12]. Dedicated searches for CP-mixed couplings between the Higgs boson and vector bosons set stringent limits on the CP-odd components [13–21]. Analyses of $t\bar{t}H$ events with $H \to \gamma\gamma$ decays [5,6] and in the multilepton final state [7] have also excluded pure CP-odd top–Higgs couplings at more than a 3 σ significance. But mixing of CP-odd and CP-even states has not been ruled out and is worth investigating. The observation of a non-zero CP-odd coupling component would in fact signal the existence of BSM physics, and open up the possibility of CP-violation in the Higgs sector [22–25]. Such a new source of CP violation could play a fundamental role in explaining the matter–antimatter asymmetry of the universe. This analysis targets $t\bar{t}H$ and tH events, which are sensitive to the top–Higgs coupling including any potential CP-mixing at the tree-level. This avoids the need for assumptions about the influence of BSM effects which may be present in other, more indirect measurements [26–28]. In particular, current limits on electron and neutron electrical dipole moments place indirect model-dependent constraints on a possible pseudoscalar component of the top-quark Yukawa coupling [29–31].

The top–Higgs interaction can be extended beyond the SM as [26]:

$$\mathcal{L}_{t\bar{t}H} = -\kappa_t' y_t \phi \bar{\psi}_t (\cos\alpha + i\gamma_5 \sin\alpha)\psi_t\,, \tag{1}$$

where y_t is the SM Yukawa coupling strength, modified by a coupling modifier κ_t'; α is the CP-mixing angle; ϕ is the Higgs field; ψ_t and $\bar{\psi}_t$ are top-quark spinor fields and γ_5 is a Dirac matrix. The term containing γ_5 corresponds to a pseudoscalar component. The above expression reduces to the SM case for $\kappa_t' = 1$ and $\alpha = 0$. An anomalous value of α would produce an admixture with a pseudoscalar coupling ($J^{CP} = 0^{+-}$) and change the differential cross-section relative to the SM

* E-mail address: atlas.publications@cern.ch.

https://doi.org/10.1016/j.physletb.2024.138469
Received 13 March 2023; Received in revised form 15 January 2024; Accepted 15 January 2024
Available online 18 January 2024
0370-2693/© 2024 The Author(s). Published by Elsevier B.V. Funded by SCOAP³. This is an open access article under the CC BY license (http://creativecommons.org/licenses/by/4.0/).

expectation, while a variation of κ_t' would induce a change in the total cross-section [22,32–35].

This study measures simultaneously the values of κ_t' and α with a binned profile likelihood fit to data, exploiting dedicated CP-sensitive observables. It closely follows a recent analysis optimised for the measurement of the $t\bar{t}H(\rightarrow b\bar{b})$ production cross-section [36]. This analysis studies an identical phase space using the same physics object definitions and a similar methodology for event selection and evaluation of systematic uncertainties. A notable exception is that this analysis considers both the $t\bar{t}H$ and tH production modes as signals. No attempt was made to optimise the analysis strategy for the tH signal, as its small yield makes this channel relevant only in one analysis region. Other noteworthy differences with respect to the analysis documented in Ref. [36] are detailed in the text. These include the definition of signal regions, the signal-background discrimination strategy and a few details in the definition of systematic uncertainties in signal and background modelling. In the case of tH production, the destructive interference between the diagrams with t–H and W–H couplings leads to the negligible tH production cross-section in the SM. Any change in the relative t–H and W–H coupling strengths would result in a rapid increase in the cross-section. Considering the Lagrangian density in Eqn. 1, the tH production cross-section is expected to grow for values of the mixing angle α different from zero [23]. An opposite and less pronounced dependence exists for the $t\bar{t}H$ cross-section. The ratio of tH to $t\bar{t}H$ cross-sections varies from 0.06 in the SM scenario to more than 1.2 in the pure CP-odd scenario [23]. For the present measurement, the $H \rightarrow b\bar{b}$ branching ratio is assumed to be equal to its SM value of 58.2% ± 0.5% [37].

2. The ATLAS experiment

The ATLAS experiment [38–40] at the LHC is a multipurpose particle detector with a forward–backward symmetric cylindrical geometry and a near 4π coverage in solid angle.[1] It consists of an inner tracking detector surrounded by a thin superconducting solenoid providing a 2 T axial magnetic field, electromagnetic and hadron calorimeters and a muon spectrometer. A two-level trigger system is used to reduce the total event rate to 1 kHz on average, depending on the data-taking conditions [41]. An extensive software suite [42] is used in the reconstruction and analysis of real and simulated data, in detector operations, and in the trigger and data acquisition systems of the experiment. The events used in this analysis are selected using single-lepton triggers [43,44], with either low thresholds for the lepton transverse momentum (p_{T}) and a lepton isolation requirement, or higher thresholds, looser identification criteria and without any isolation requirement. The lowest p_{T} threshold for muons is 20 (26) GeV, while for electrons the threshold is 24 (26) GeV for the data taken in 2015 (2016–2018).

3. Event preselection

Events are required to have at least one primary vertex, formed by two or more associated tracks with transverse momenta greater than 0.5 GeV. The vertex with the highest sum of p_{T}^2 of associated tracks is selected as the hard-scattering primary vertex. Events with exactly one lepton (electrons or muons, denoted as ℓ) or two oppositely charged leptons are considered in this analysis, referred to as the ℓ + jets channel and dilepton channel, respectively. Electrons are identified using the 'Tight' likelihood criterion [45] and are required to have $p_{\mathrm{T}} > 10$ GeV and $|\eta| < 2.47$, excluding those in the calorimeter barrel–endcap transition region ($1.37 < |\eta| < 1.52$). Muons are selected with the 'Medium' identification criterion [46] and are required to have $p_{\mathrm{T}} > 10$ GeV and $|\eta| < 2.5$. Electrons (muons) are required to pass the 'Gradient' ('Fixed-Cut-Tight-Track-Only') isolation requirements [45,46]. All leptons are required to originate from the primary vertex. At least one of the leptons must have $p_{\mathrm{T}} > 27$ GeV and match the corresponding lepton used in the trigger decision. In events with an ee or $\mu\mu$ pair, the dilepton invariant mass is required to be above 15 GeV and outside the Z boson mass window of 83–99 GeV.

This analysis targets events with high jet multiplicities, including b-quark jets expected in the final state of $t\bar{t}H$ and tH events with a subsequent $H \rightarrow b\bar{b}$ decay. Following the same procedure as Ref. [36], jets are reconstructed from topological clusters of energy depositions in the calorimeter [47,48] using the anti-k_t algorithm [49,50] with a radius parameter of $R = 0.4$. The MV2c10 algorithm [51] is used to identify (or 'b-tag') jets containing b-hadrons. By placing different selections on the MV2c10 discriminant, four working points are defined with average b-jet tagging efficiencies of 60%, 70%, 77% and 85% and different c- and light-jet rejection rates. The corresponding efficiencies and rejection rates are calibrated to data [51–53]. A pseudo-continuous b-tagging score is assigned to each jet. A score of two, three, four and five is assigned if a jet passes the 85%, 77%, 70% and 60% working point, but fails the adjacent tighter one. If a jet fails all working points, a score of one is assigned. In the ℓ + jets (dilepton) channel, events are required to have at least five (three) jets with $p_{\mathrm{T}} > 25$ GeV and $|\eta| < 2.5$, and at least four (three) of the jets are required to be b-tagged at the 70% efficiency working point.

The missing transverse momentum is reconstructed as the negative vector sum of the p_{T} of all selected objects in the event, with an extra 'soft term' built from additional tracks associated with the primary vertex [54].

The analysis also exploits the collimated decay topology from high-p_{T} Higgs bosons. Jets with a radius parameter of $R = 0.4$ are reclustered [55] using the anti-k_t algorithm with a radius parameter of $R = 1.0$. The resulting jets are referred to as *large-R* jets. The large-R jets are required to have a mass larger than 50 GeV, $p_{\mathrm{T}} > 200$ GeV and at least two constituent jets with $R = 0.4$.

4. Signal and background modelling

After applying the above selection criteria, background events are dominated by $t\bar{t}$ production with additional jets ($t\bar{t}$ + jets), that contain heavy-flavour hadrons (b- and c-hadrons). Other processes contribute less than 10% of the total expected background. All background processes are estimated using Monte Carlo (MC) simulations, closely following Ref. [36].

The simulated events were produced using the ATLAS detector simulation [56] based on GEANT4 [57]. To simulate the effects of multiple interactions in the same and neighbouring bunch crossings (pile-up), additional interactions were generated using PYTHIA 8.186 [58] with a set of tuned parameters called the A3 tune [59] and overlaid on the simulated hard-scatter event. Simulated events are reweighted to match the pile-up conditions observed in the full Run 2 dataset. All simulated event samples are processed through the same reconstruction algorithms and analysis chain as the data [42].

Events in the simulated $t\bar{t}$ + jets background sample are categorised according to the flavour of the additional jets which do not originate from the top-quark decay. The simulation of each set of backgrounds is treated independently as this allows for a more accurate modelling of $t\bar{t}$ + jets events. The categorisation is based on 'MC-truth jets' that are clustered with stable generated particles (with mean lifetime $\tau > 3 \times 10^{-11}$ s) in the final state using the anti-k_t algorithm with $R = 0.4$. MC-truth jets with $p_{\mathrm{T}} > 15$ GeV and $|\eta| < 2.5$ in the simulated events are used for the categorisation. Their MC-truth flavour is

[1] ATLAS uses a right-handed coordinate system with its origin at the nominal interaction point (IP) in the centre of the detector and the z-axis along the beam pipe. The x-axis points from the IP to the centre of the LHC ring, and the y-axis points upwards. Cylindrical coordinates (r, ϕ) are used in the transverse plane, ϕ being the azimuthal angle around the z-axis. The momentum component in the transverse plane is referred to as the transverse momentum (p_{T}). The pseudorapidity is defined in terms of the polar angle θ as $\eta = -\ln\tan(\theta/2)$. Angular distance is measured in units of $\Delta R \equiv \sqrt{(\Delta\eta)^2 + (\Delta\phi)^2}$.

determined by counting the number of b/c-hadrons contained within $\Delta R = 0.4$ of the jet axis. Events with at least one MC-truth jet containing b-hadrons not originating from a top-quark decay are labelled as $t\bar{t}+\geq 1b$. This can be further separated into subcomponents corresponding to $t\bar{t}+1b$ and $t\bar{t}+\geq 2b$. Events failing to satisfy that criterion but with at least one MC-truth jet containing c-hadrons not originating from top-quark decay are labelled $t\bar{t}+\geq 1c$. The rest of the events are labelled as $t\bar{t}+$light. The dominant $t\bar{t}+\geq 1b$ background is modelled using a sample of $t\bar{t}+b\bar{b}$ events generated at next-to-leading order (NLO) in QCD in the four-flavour scheme, with two additional massive b-quarks produced at the matrix element (ME) level. The ME simulation was performed using the Powheg Box Res generator and OpenLoops [60–63], with the NNPDF3.0nlo nf4 [64] parton distribution function (PDF) set and Pythia 8.230 [58] with the A14 set of tuned parameters [65] for the simulation of the parton shower (PS) and hadronisation. Given that the production rate of $t\bar{t}$ with additional b-jets is observed to be underestimated by the current predictions [66,67], the normalisation of the $t\bar{t}+\geq 1b$ background is determined from the analysed data without prior constraints. The $t\bar{t}+\geq 1c$ and $t\bar{t}+$light backgrounds are modelled from a subset of an inclusive $t\bar{t}+$jets sample generated at NLO in QCD using Powheg Box v2 [68–71] as the ME generator interfaced with Pythia 8.230 for the PS and hadronisation. This inclusive $t\bar{t}+$jets sample is generated with the five-flavour scheme, where c- and b-quarks not originating from a top-quark decay are assumed to be massless. Due to limited knowledge regarding $t\bar{t}+\geq 1c$ production, an additional 100% uncertainty is included in its normalisation. Additionally, a prior uncertainty of 6% is assigned to the inclusive $t\bar{t}+$jets production cross-sections according to the predicted inclusive $t\bar{t}$ production cross-section at NNLO+NNLL [72–78]. Other background processes include the production of $W+$ jets, $Z+$ jets, $t\bar{t}W$, $t\bar{t}Z$, tZq, tWZ, $t\bar{t}t\bar{t}$ and $WW/WZ/ZZ$ events. These are all subdominant and modelled from simulation as detailed in Ref. [36]. A small fraction of events contains misidentified leptons or leptons originating from the decay of heavy-flavour hadrons. The contribution from these events is found to be negligible in the $\ell+$jets channel. In the dilepton channel, this small contribution is modelled using a simulation.

The signal processes, $t\bar{t}H$ and tH, are simulated with different values of α and κ_t'. All other parameters were fixed to their SM values, including the $H\to b\bar{b}$ branching ratio. The alternative scenarios were simulated using the NLO Higgs Characterisation [37,79] model implemented in MadGraph5_aMC@NLO with FeynRules [80,81]. With a few exceptions, all signal samples were generated using the MadGraph5_aMC@NLO 2.6.2 [82] generator at NLO in QCD using the five-flavour scheme with the NNPDF3.0nnlo PDF set, interfaced with Pythia 8.230 with the A14 set of tune parameters for PS and hadronisation. The SM $t\bar{t}H$ events were simulated using MadGraph5_aMC@NLO 2.6.0. The renormalisation and factorisation scales were set to $\sqrt[3]{m_{\mathrm{T}}(t)\cdot m_{\mathrm{T}}(\bar{t})\cdot m_{\mathrm{T}}(H)}$, where $m_{\mathrm{T}}=\sqrt{m^2+p_{\mathrm{T}}^2}$ is the transverse mass of a particle. The cross-section is normalised to 507 fb from the fixed-order calculation including NLO QCD and electroweak corrections, with an uncertainty of 3.6% from variations in PDF and α_{s} and 9.2% due to variations of the renormalisation and factorisation scales [37,83–87]. A K-factor of 1.1 is derived by taking the ratio of the cross-section from the above fixed-order calculation to that from MadGraph5_aMC@NLO, and is applied to all $t\bar{t}H$ samples with different values of α and κ_t'. For the tH signal, two subprocesses, $tHjb$ and tWH, are considered. The $tHjb$ (tWH) events were generated in the four(five)-flavour scheme using the NNPDF3.0nnlo nf4 (NNPDF3.0nnlo) PDF set [64], with the renormalisation and factorisation scales set to the generator's default. The cross-sections for the $tHjb$ and tWH samples are obtained directly from MadGraph5_aMC@NLO. In the SM scenario, the cross-section for $tHjb$ and tWH are 60.1 fb and 16.7 fb, respectively. Variations of the renormalisation and factorisation scales, including the consideration of the flavour scheme choice for the $tHjb$ process, contribute 15% and 6.7% to the uncertainty of the cross-sections of $tHjb$ and tWH respectively. Similarly, variations of the PDFs and α_{s} result in a 3.7% and 6.3% uncertainty in the $tHjb$ and tWH cross-sections, respectively. A diagram removal scheme [88] is applied in the simulation of the tWH events in order to remove diagrams already included in the $t\bar{t}H$ simulation.

The yields of $t\bar{t}H$ and tH signals are parameterised as a function of the model parameters by smoothly interpolating between generated MC samples with varying α and κ_t'. The parameterisation is performed in each analysis bin. Two $t\bar{t}H$ samples with alternative values of α were generated, corresponding to a pure CP-odd interaction ($\alpha=90°$) and maximal CP-odd/CP-even mixing ($\alpha=45°$). The $t\bar{t}H$ yields, $N_{t\bar{t}H}(\kappa_t',\alpha)$, are parameterised using the SM sample and the pure CP-odd sample as $\kappa_t'^2 c_\alpha^2 N_{CP\text{-even}} + \kappa_t'^2 s_\alpha^2 N_{CP\text{-odd}}$, where $c_\alpha=\cos\alpha$, $s_\alpha=\sin\alpha$, and $N_{CP\text{-even}}$ and $N_{CP\text{-odd}}$ are the expected yields predicted by the SM and the CP-odd $t\bar{t}H$ simulations, respectively. This was verified to be a good approximation using the maximal mixing sample ($\alpha=45°$), with the difference in any analysis bin smaller than the uncertainties due to the limited number of simulated events. In the case of tH, the interference between diagrams with CP-even and CP-odd $t-H$ and SM $W-H$ couplings are considered in the parameterisation, assuming contributions from lowest order diagrams of $tHjb$ and tWH processes. The signal yield in each analysis bin is parameterised as $N_{tH}(\kappa_t',\alpha)=A\kappa_t'^2 c_\alpha^2 + B\kappa_t'^2 s_\alpha^2 + C\kappa_t' c_\alpha + D\kappa_t' s_\alpha + E\kappa_t'^2 c_\alpha s_\alpha + F$. Coefficients A-F are derived separately for each analysis bin, by fitting to the yields predicted by multiple simulated samples with varying κ_t' and α. The terms with c_α^2 and s_α^2 correspond to the contribution from CP-even and CP-odd t-H coupling, respectively. The terms at the first order of c_α and s_α account for potential interference effects between CP-even and CP-odd t-H coupling and SM W-H coupling contributions. The term F represents the contribution from only the SM W-H coupling. Ten samples generated with different values of α and κ_t' in addition to the SM tH sample are used for the parameterisation. These samples include: samples where $\kappa_t'=1$ and α is set between 15° to 90° in steps of 15°, samples with $\kappa_t'=$ -1, 0.5, and 2 where $\alpha=0°$ and an additional sample with $\alpha=45°$ and $\kappa_t'=2$. Uncertainties due to limited number of MC events in these simulated samples are considered when performing the parameterisation fit in each bin. Good closure was observed: the largest χ^2 per degree of freedom was 0.19 in any given bin. Uncertainties pertaining to the parameterisation of either signal were found to have a negligible impact on the measured values of α and κ_t'.

5. Analysis strategy

In order to optimise the analysis sensitivity, events satisfying the preselection criteria are categorised into orthogonal regions in two steps. In the first step, control regions (CR) and training regions (TR) are defined using requirements on jet multiplicity, b-tagging and large-R jets. The TRs are defined according to the expected numbers of objects from the decay of the signal events, whilst the CRs with lower object multiplicities are signal depleted. The TRs broadly contain the signals and are used to train various multivariate algorithms (MVA). Dedicated observables are constructed in the TRs to enhance sensitivity to the top-Higgs Yukawa CP coupling. In the second step, MVAs are used to divide the TRs into signal regions (SR) and additional CRs with relatively high and low signal purity, respectively. Given the small contribution expected from tH events, the categorisation, MVAs and CP-sensitive observables are optimised for the $t\bar{t}H$ signal. All regions labelled CR and SR are simultaneously fit to the data using either specific observables or simple yields as specified below. Both steps are described in detail below.

The first step of categorisation adopts a strategy similar to that described in Ref. [36], devised to separate the SM signal from the various backgrounds. A 'boosted' region, labelled as $\mathrm{TR}_{\mathrm{boosted}}$, is firstly defined in the $\ell+$jets channel by requiring the presence of a high-p_{T} Higgs boson candidate which is identified using a deep neural network (DNN). The DNN is trained to identify the boosted Higgs boson candidates from among large-R jets with $p_{\mathrm{T}}>300$ GeV [36]. A mixture of constituent

Table 1
Definition of the CRs and TRs according to the number of jets and b-tagged jets using different b-tagging selection criteria, and the number of boosted Higgs boson candidates. For CRs, the bottom row indicates the observables used in the fit to data in the corresponding regions. For the $\mathrm{TR}_{\mathrm{boosted}}$region, the b-tagged jets flagged with † are not constituents of the boosted Higgs boson candidate. Events must pass $N_{b\text{-tag}}$ requirements for each b-tagging selection criteria.

Region		Dilepton				ℓ + jets			
		$\mathrm{TR}^{\geq 4j,\geq 4b}$	$\mathrm{CR}^{\geq 4j,3b}_{\mathrm{hi}}$	$\mathrm{CR}^{\geq 4j,3b}_{\mathrm{lo}}$	$\mathrm{CR}^{3j,3b}_{\mathrm{hi}}$	$\mathrm{TR}^{\geq 6j,\geq 4b}$	$\mathrm{CR}^{5j,\geq 4b}_{\mathrm{hi}}$	$\mathrm{CR}^{5j,\geq 4b}_{\mathrm{lo}}$	$\mathrm{TR}_{\mathrm{boosted}}$
N_{jets}		≥ 4			$=3$	≥ 6	$=5$		≥ 4
$N_{b\text{-tag}}$	@85%	–				≥ 4			
	@77%	–				–			$\geq 2^{\dagger}$
	@70%	≥ 4	$=3$			≥ 4			–
	@60%	–	$=3$	<3	$=3$	–	≥ 4	<4	–
$N_{\mathrm{boosted\ cand.}}$		–				0			≥ 1
Fit observable		–	Yield			–	$\Delta R^{\mathrm{avg}}_{bb}$		–

Table 2
Summary of the selections used to define SRs and CRs from the TRs, based on the classification BDT score. In the boosted region, the selection requirement is applied and rejected events are removed entirely from further analysis. In the dilepton channel, events with failed reconstruction due to absence of a real solution from the neutrino weighting are categorised into an additional region known as $\mathrm{CR}^{\geq 4j,\geq 4b}_{\text{no-reco}}$. The fitted discriminating variable in each region is indicated in the last column.

Channel (TR)	Final SRs and CRs	Classification BDT selection	Fitted observable
Dilepton ($\mathrm{TR}^{\geq 4j,\geq 4b}$)	$\mathrm{CR}^{\geq 4j,\geq 4b}_{\text{no-reco}}$	–	$\Delta\eta_{\ell\ell}$
	$\mathrm{CR}^{\geq 4j,\geq 4b}$	$\mathrm{BDT}^{\geq 4j,\geq 4b} \in [-1,-0.086)$	b_4
	$\mathrm{SR}^{\geq 4j,\geq 4b}_{1}$	$\mathrm{BDT}^{\geq 4j,\geq 4b} \in [-0.086,0.186)$	b_4
	$\mathrm{SR}^{\geq 4j,\geq 4b}_{2}$	$\mathrm{BDT}^{\geq 4j,\geq 4b} \in [0.186,1]$	b_4
ℓ + jets ($\mathrm{TR}^{\geq 6j,\geq 4b}$)	$\mathrm{CR}^{\geq 6j,\geq 4b}_{1}$	$\mathrm{BDT}^{\geq 6j,\geq 4b} \in [-1,-0.128)$	b_2
	$\mathrm{CR}^{\geq 6j,\geq 4b}_{2}$	$\mathrm{BDT}^{\geq 6j,\geq 4b} \in [-0.128,0.249)$	b_2
	$\mathrm{SR}^{\geq 6j,\geq 4b}$	$\mathrm{BDT}^{\geq 6j,\geq 4b} \in [0.249,1]$	b_2
ℓ + jets ($\mathrm{TR}_{\mathrm{boosted}}$)	$\mathrm{SR}_{\mathrm{boosted}}$	$\mathrm{BDT}^{\mathrm{boosted}} \in [-0.05,1]$	$\mathrm{BDT}^{\mathrm{boosted}}$

jet masses, pseudo-continuous b-tagging scores and jet substructure observables [89] are used as input features for the training. Events failing this DNN selection defining the $\mathrm{TR}_{\mathrm{boosted}}$ region are categorised into CRs and TRs according to the number of jets (j) and various b-tagging (b) requirements. Events in the TRs are required to have at least the number of jets and b-tagged jets expected from the final state of the $t\bar{t}H$ signal. This results in four statistically independent regions in the dilepton channel, named $\mathrm{CR}^{3j,3b}_{\mathrm{hi}}$, $\mathrm{CR}^{\geq 4j,3b}_{\mathrm{lo}}$, $\mathrm{CR}^{\geq 4j,3b}_{\mathrm{hi}}$ and $\mathrm{TR}^{\geq 4j,\geq 4b}$, and three regions in the ℓ + jets channel, named $\mathrm{CR}^{5j,\geq 4b}_{\mathrm{lo}}$, $\mathrm{CR}^{5j,\geq 4b}_{\mathrm{hi}}$ and $\mathrm{TR}^{\geq 6j,\geq 4b}$. The yields of these regions enter the fit. The requirements used to define all CRs and TRs are summarised in Table 1. Regions labelled with 'hi' ('lo') have relatively higher (lower) fractions of events with true b-jets not from top-quark decays, and are selected with tight (loose) b-tagging requirements. The average ΔR separation between b-jets ($\Delta R^{\mathrm{avg}}_{bb}$) is used as the observable which enters the fit for $\mathrm{CR}^{5j,\geq 4b}_{\mathrm{lo}}$ and $\mathrm{CR}^{5j,\geq 4b}_{\mathrm{hi}}$ regions as it better constrains the shape of the backgrounds. All mentioned CRs have different fractions of $t\bar{t}$ + light, $t\bar{t}+\geq 1c$ and $t\bar{t}+\geq 1b$ events and this helps to constrain the systematic uncertainties in each of these components.

In the TRs, two sets of boosted decision trees (BDT) are trained: reconstruction BDTs and classification BDTs. The former is trained to assign jets as coming from the decay of the Higgs boson or top quarks in $t\bar{t}H$ events, while the latter is trained to discriminate the $t\bar{t}H$ signal against the backgrounds. Both the reconstruction and classification BDTs are trained using simulated SM $t\bar{t}H$ events. It was tested that their performance is equally good for a pure CP-odd signal. For both the reconstruction and classification BDTs, the training procedures are performed independently for each TR and are identical to those used in Ref. [36]. The reconstruction BDTs are trained to classify the correct combinations of jet assignments from random ones. The training explores the relative positional information between pairs of objects, and the invariant masses of object pairs and triplets that form W-boson and top-quark candidates. In order to reconstruct the top-quark and Higgs boson candidates, for each event, all possible permutations of jet assignments are evaluated and the permutation with the highest BDT score is selected. The reconstruction BDTs provide important information that improves the performance of the classification BDTs, whilst allowing for the calculation of observables sensitive to the CP nature of the Yukawa coupling. Classification BDT inputs include reconstruction BDT (DNN in the boosted channel) outputs, pseudo-continuous b-tagging discriminant scores of jets, and kinematic features, such as angular separations and invariant masses of pairs of b-tagged jets. The classification BDTs are used to further refine the TRs to define the final CRs and SRs, as detailed later. The classification BDTs used in $\mathrm{TR}^{\geq 4j,\geq 4b}$, $\mathrm{TR}^{\geq 6j,\geq 4b}$ and $\mathrm{TR}_{\mathrm{boosted}}$ are henceforth denoted by $\mathrm{BDT}^{\geq 4j,\geq 4b}$, $\mathrm{BDT}^{\geq 6j,\geq 4b}$ and $\mathrm{BDT}^{\mathrm{boosted}}$, respectively.

Dedicated CP-sensitive observables are computed in $\mathrm{TR}^{\geq 4j,\geq 4b}$ and $\mathrm{TR}^{\geq 6j,\geq 4b}$ and are used in the fit to determine the CP properties of the top-quark Yukawa coupling. Two CP observables, b_2 and b_4 [22,35], were found to provide the best discrimination in $\mathrm{TR}^{\geq 6j,\geq 4b}$ of the ℓ + jets channel and $\mathrm{TR}^{\geq 4j,\geq 4b}$ of the dilepton channel, respectively. They are defined as:

$$b_2 = \frac{(\vec{p}_1 \times \hat{z}) \cdot (\vec{p}_2 \times \hat{z})}{|\vec{p}_1||\vec{p}_2|}, \text{ and } b_4 = \frac{(\vec{p}_1 \cdot \hat{z})(\vec{p}_2 \cdot \hat{z})}{|\vec{p}_1||\vec{p}_2|},$$

where $\vec{p}_i$ with $i = 1,2$ are the momentum three-vectors of the two top quarks in the events and $\hat{z}$ is a unit vector in the direction of the beamline and defines the z-axis. The b_4 observable exploits the enhanced production of top quarks travelling in opposite longitudinal directions and closer to the beamline in CP-odd $t\bar{t}H$ production. The observ-

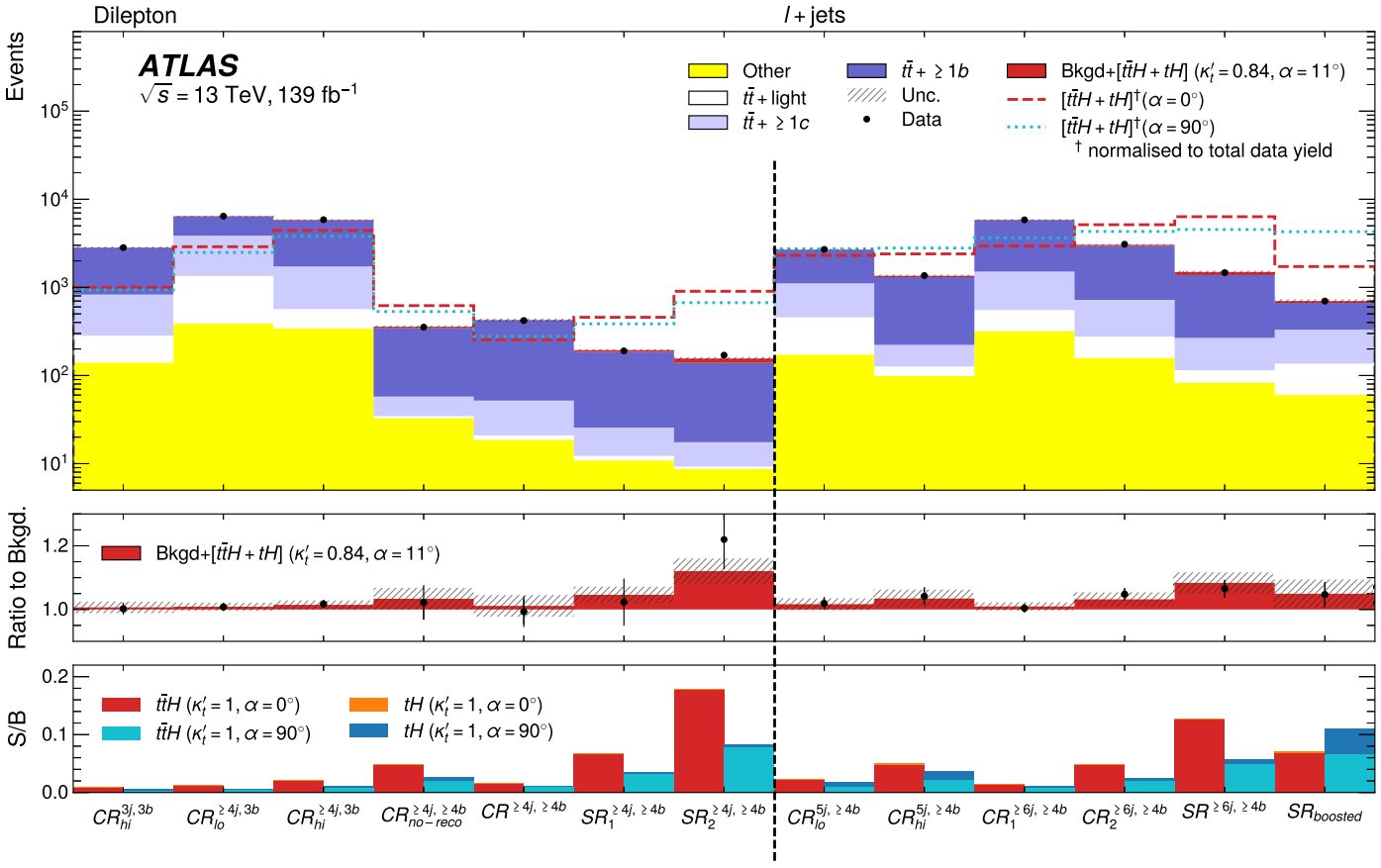

Fig. 1. Yields calculated following a fit with κ_t' and α as free parameters, compared to the observed data in all analysis regions. The different backgrounds and the signal are shown in coloured stack. The background component labelled "other" corresponds to the production of $W+$ jets, $Z+$ jets, $t\bar{t}W$, $t\bar{t}Z$, tZq, tWZ, $t\bar{t}t\bar{t}$ and $WW/WZ/ZZ$ events, as in Ref. [36]. The dashed and dotted lines show the sum of $t\bar{t}H + tH$ signals for pure CP-even and CP-odd hypotheses normalised to the total data yields including all regions. The hashed area around the prediction illustrates the total post-fit uncertainties. In the middle panel, the best-fit model is compared with the data by showing ratios of its value to the post-fit background prediction. The histogram represents the total post-fit model including the best-fit signals. The hashed band represents the total post-fit uncertainty as a ratio to the background. In the bottom panel, the S/B is shown for pure CP-even and CP-odd signals, separately. The histograms are shown as a stack of $t\bar{t}H$ and tH.

able b_2 relies simultaneously on the smaller azimuthal separation of top quarks and on their larger longitudinal fraction of momentum in CP-odd $t\bar{t}H$ production. The calculation of b_2 is performed in the $t\bar{t}H$ rest frame [35], which enhances the discrimination power.

Computation of b_2 and b_4 requires the full reconstruction of both top quarks and the Higgs boson. However, the reconstruction BDTs only resolve the hadronic part of the $t\bar{t}H$ system. In the ℓ + jets channel, the missing transverse momentum is used as a proxy for the p_{T} of the undetected neutrino from the semileptonically decaying top quark. The z component of the neutrino four-momentum is obtained from a quadratic equation constructed from the lepton four-momentum and the missing transverse momentum, using as a constraint the leptonic W boson's mass, assumed to be its on-shell value. Both solutions of the quadratic equation are used to reconstruct the top-quark mass, and the one yielding a mass closer to 172.5 GeV is chosen. In the case of a negative determinant, a solution is obtained by setting the determinant to zero. In the dilepton channel, the neutrino weighting technique is used to determine the four momenta of the two neutrinos [90,91]. Neutrino weighting provides a solution for reconstructing the $t\bar{t}$ pair for 68% of the events in $\mathrm{TR}^{\geq 4j,\geq 4b}$.

In contrast to the $\mathrm{TR}^{\geq 4j,\geq 4b}$ and $\mathrm{TR}^{\geq 6j,\geq 4b}$ regions, the CP-odd signals are strongly enhanced in comparison with the CP-even signals in the $\mathrm{TR}_{\mathrm{boosted}}$ region. The yields of $t\bar{t}H$ with pure CP-even and CP-odd couplings are approximately equal in the $\mathrm{TR}_{\mathrm{boosted}}$ region. Additionally, the yield of the tH signal with a pure CP-odd coupling is comparable to the $t\bar{t}H$ signal yield. The total CP-odd signal is therefore expected to be 50% larger than a CP-even signal in this region. Given the substantial sensitivity provided by the yield in this region, the distribution of the classification BDT ($\mathrm{BDT}^{\mathrm{boosted}}$) is used instead of a dedicated CP-sensitive observable.

In the second step of the categorisation, TRs are further refined to CRs and SRs according to the output of the reconstruction and classification BDTs. A summary of the selections used to define the regions is detailed in Table 2. In $\mathrm{TR}_{\mathrm{boosted}}$, events below a classification BDT score of –0.05 are discarded to reduce contamination of $t\bar{t}+$light events. $\mathrm{TR}^{\geq 4j,\geq 4b}$ and $\mathrm{TR}^{\geq 6j,\geq 4b}$ are further categorised, each into three regions, according to the classification BDT score. The resulting regions have similar background compositions but different expected signal-to-background ratios (S/B). The BDT thresholds are determined by optimising the sensitivity to the SM $t\bar{t}H$ signal. The three regions (one in ℓ + jets and two in dilepton) with an $S/B > 7\%$ are referred to as SRs. The remaining three regions (two in ℓ + jets and one in dilepton) are used as additional CRs to constrain the modelling of the CP observables in the backgrounds events. The highest S/B in the resulting SRs is 22% (10%) for a pure CP-even (CP-odd) signal. For $\mathrm{SR}^{\geq 4j,\geq 4b}$ in the dilepton channel, b_4 cannot be calculated for events where the neutrino weighting fails to provide a solution. These events are categorised as an additional region, $\mathrm{CR}^{\geq 4j,\geq 4b}_{\mathrm{no\text{-}reco}}$, where the difference in η between the two leptons, $\Delta\eta_{\ell\ell}$, is used as a CP-sensitive observable instead [26].

Table 3
The observed data yields and the expected signal and background yields in the ℓ + jets channel. The expected yields of pure CP-even and CP-odd $t\bar{t}H$ and tH signals, with $\kappa_t' = 1$, are shown at the top of the table. The uncertainties in the pure CP-even and CP-odd $t\bar{t}H$ and tH signals are the total uncertainties before fitting to data. Below that are shown the post-fit $t\bar{t}H$ and tH yields, corresponding to $\kappa_t' = 0.84$ and $\alpha = 11°$. The following seven rows show the yields and uncertainties of individual background sources, where "other" corresponds to W+ jets, Z+ jets, $t\bar{t}W$, $t\bar{t}Z$, tZq, tWZ, $t\bar{t}t\bar{t}$ and $WW/WZ/ZZ$ events, as in Ref. [36]. The row labelled 'Total' represents the total signal plus background post-fit yields. The uncertainties in the post-fit yields are evaluated from the post-fit nuisance parameters as well as the post-fit uncertainties in the fitted free parameters (α and κ_t' for the signals and $k_{t\bar{t}+b}$ for the $t\bar{t}+\geq 1b$ background) that affect the corresponding processes. The correlations amongst all fitted parameters are taken into account. Due to these correlations the uncertainties on the total yields do not correspond to the quadrature sum of uncertainties of individual signals and backgrounds.

	$CR_{lo}^{5j,\geq 4b}$	$CR_{hi}^{5j,\geq 4b}$	$CR_{1}^{\geq 6j,\geq 4b}$	$CR_{2}^{\geq 6j,\geq 4b}$	$SR^{\geq 6j,\geq 4b}$	$SR_{boosted}$
$t\bar{t}H$ $(1,0°)$	60±9	63±10	78±11	139±18	173±26	46±6
$tH(1,0°)$	3.5±0.5	3.8±0.6	3.3±0.6	2.3±0.6	1.3±0.4	1.9±0.4
$t\bar{t}H$ $(1,90°)$	28±6	28±6	45±11	61±12	68±16	45±6
$tH(1,90°)$	19.0±2.8	19.4±3.1	17.4±3.1	13.1±3.5	10±4	29±6
$t\bar{t}H$ $(0.84,11°)$	40±30	41±31	50±40	90±70	110±80	30±22
tH $(0.84,11°)$	3±4	3.9±1.9	3.1±1.9	1.9±0.8	1.3±1.7	3±5
$t\bar{t}+\geq 1b$	1530±80	1090±60	4300±120	2220±120	1110±110	335±30
$t\bar{t}+\geq 1c$	650±50	96±11	950±80	450±40	153±15	196±22
$t\bar{t}$+ light	280±40	28±8	230±60	117±26	32±11	76±15
Other	173±30	99±20	320±50	159±21	83±11	60±11
Total	2690±50	1350±40	5870±80	3040±70	1500±50	701±31
Data	2696	1363	5837	3090	1470	699

Table 4
The observed data yields and the expected signal and background yields in the dilepton channel. The expected yields of pure CP-even and CP-odd $t\bar{t}H$ and tH signals, with $\kappa_t' = 1$, are shown at the top of the table. The uncertainties in the pure CP-even and CP-odd $t\bar{t}H$ and tH signals are the total uncertainties before fitting to data. Below that are shown the post-fit $t\bar{t}H$ and tH yields, corresponding to $\kappa_t' = 0.84$ and $\alpha = 11°$. The following seven rows show the yields and uncertainties of individual background sources, where "other" corresponds to W+ jets, Z+ jets, $t\bar{t}W$, $t\bar{t}Z$, tZq, tWZ, $t\bar{t}t\bar{t}$ and $WW/WZ/ZZ$ events, as in Ref. [36]. The row labelled 'Total' represents the total signal plus background post-fit yields. The uncertainties in the post-fit yields are evaluated from the post-fit nuisance parameters as well as the post-fit uncertainties in the fitted free parameters (α and κ_t' for the signals and $k_{t\bar{t}+b}$ for the $t\bar{t}+\geq 1b$ background) that affect the corresponding processes. The correlations amongst all fitted parameters are taken into account. Due to these correlations the uncertainties in the total yields do not correspond to the quadrature sum of uncertainties of individual signals and backgrounds.

	$CR_{hi}^{3j,3b}$	$CR_{lo}^{\geq 4j,3b}$	$CR_{hi}^{\geq 4j,3b}$	$CR_{no\text{-}reco}^{\geq 4j,\geq 4b}$	$CR^{\geq 4j,\geq 4b}$	$SR_{1}^{\geq 4j,\geq 4b}$	$SR_{2}^{\geq 4j,\geq 4b}$
$t\bar{t}H$ $(1,0°)$	26±4	79±8	120±12	16.9±2.1	6.9±1.1	12.5±1.5	24.8±2.9
$tH(1,0°)$	1.12±0.13	0.90±0.13	1.74±0.20	0.19±0.08	0.087±0.035	0.100±0.033	0.09±0.06
$t\bar{t}H$ $(1,90°)$	10.6±1.6	35.6±3.5	54±5	7.2±0.9	4.3±0.6	6.1±0.7	10.9±1.3
$tH(1,90°)$	5.4±0.6	7.0±1.0	10.7±1.2	1.8±0.8	0.48±0.19	0.48±0.16	0.5±0.4
$t\bar{t}H$ $(0.84,11°)$	18±14	50±40	80±60	11±9	4.7±3.4	8±6	17±12
tH $(0.84,11°)$	0.9±0.5	1.0±1.9	1.5±1.3	0.17±0.16	0.068±0.016	0.08±0.14	0.07±0.09
$t\bar{t}+\geq 1b$	1990±80	2520±110	4040±130	288±15	371±16	160±8	122±11
$t\bar{t}+\geq 1c$	550±50	2510±150	1160±90	23±4	31.1±2.5	13.4±1.6	8.2±1.0
$t\bar{t}$+ light	143±27	960±130	230±40	1.7±0.4	2.3±0.8	1.4±0.8	0.57±0.25
Other	140±11	390±19	340±40	33±8	18.6±2.5	10.9±1.3	8.7±1.0
Total	2840±50	6430±80	5850±80	358±12	428±15	194±5	156±6
Data	2827	6429	5865	354	420	190	170

6. Systematic uncertainties

Systematic uncertainties are assessed for three main sources: theoretical modelling of the signal processes, background modelling which is dominated by the uncertainties in the $t\bar{t}+\geq 1b$ background and experimental sources involving the (mis)identification rates and energy calibration of leptons, jets, b-jets and missing transverse momentum. Uncertainties accounting for the limited number of events in all simulated samples are also considered. Systematic variations can affect the overall yields, relative yields between analysis regions and shapes of observables.

Uncertainties associated with the modelling of the $t\bar{t}H$ signals include variations due to initial and final state radiation (ISR and FSR), choice of the NLO matching procedure as well as the PS and hadronisation model. These uncertainties are evaluated using events generated with POWHEG BOX + PYTHIA 8, which are produced with the same PDF set and renormalisation and factorisation scales as the nominal MADGRAPH5_AMC@NLO + PYTHIA 8 sample, unless otherwise specified.

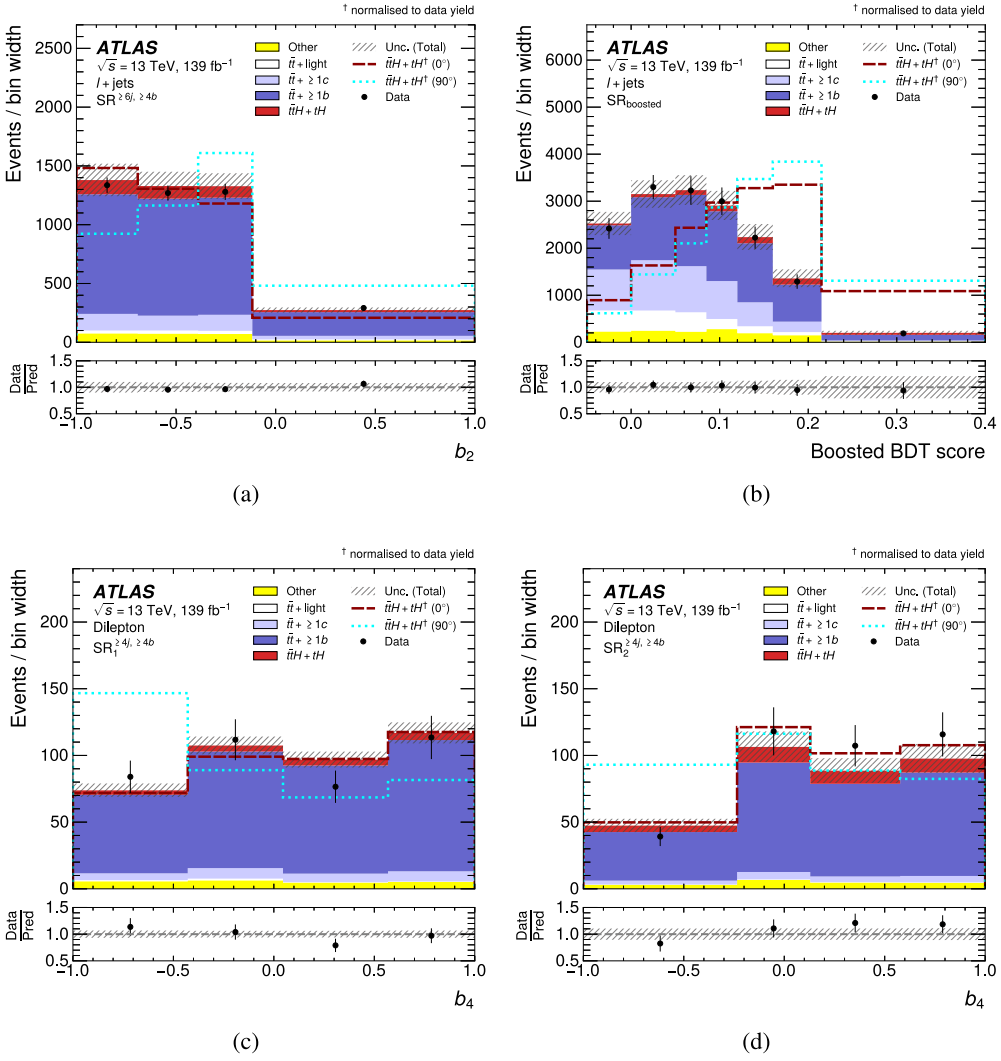

Fig. 2. The distributions of the fitted variables in all signal regions. The stacked histograms represent the predictions from a fit of signal and background to data with both κ_t' and α as free parameters. This is compared with data shown with black dots. The solid red histogram shows the best-fit signal with $\alpha = 11°$ and $\kappa_t' = 0.84$. The dashed and dotted lines show $t\bar{t}H + tH$ signal predictions for pure CP-even and CP-odd hypotheses, respectively, normalised to the total data yield per region in order to illustrate the shapes of the signal distribution. The hashed area around the prediction illustrates the total post-fit uncertainties. The lower panel shows the ratio of data to the predicted yields from a fit of signal and background in which κ_t' and α are free parameters.

Variations relative to the SM hypothesis are propagated to scenarios with alternative values of α and κ_t'. To estimate the uncertainty related to the amount of partonic ISR, the renormalisation and factorisation scales in the ME and α_S^{ISR} in the PS are varied simultaneously [92]. The impact of the FSR is evaluated by varying α_S^{FSR} in the PS. The impact of varying the PS and hadronisation models is estimated by comparing $t\bar{t}H$ samples generated using POWHEG BOX + PYTHIA 8.230 with those generated from POWHEG BOX + HERWIG 7.04 [93]. The uncertainty due to the choice of NLO matching procedure is derived by directly comparing the POWHEG BOX + PYTHIA 8 sample with the nominal MADGRAPH5_AMC@NLO + PYTHIA 8 sample. The uncertainties in the modelling of tH are estimated using the nominal sample generated using MADGRAPH5_AMC@NLO + PYTHIA 8. For each tH subprocess ($tHjb$ and tWH), two sources of modelling uncertainty are considered: that associated with the description of PDFs, and the uncertainty due to missing higher-order QCD contributions. The former is estimated from the standard deviation of the expected yields using 100 NNPDF3.0NLO eigenvector PDF sets, in each analysis bin used to build the likelihood function. The latter is estimated by coherently varying μ_r and μ_f by factors of 0.5 and 2.

The most important uncertainties in the background estimation come from the modelling of the $t\bar{t} + \geq 1b$ background. These uncertainties are designed to account for the choice of NLO matching procedure, PS and hadronisation model as well as the flavour scheme utilised in the $t\bar{t} + \geq 1b$ event generation. An uncertainty in the ME-to-PS matching procedure is assessed by comparing the POWHEG BOX + PYTHIA 8 sample with a sample generated using MADGRAPH5_AMC@NLO + PYTHIA 8, both in the five-flavour scheme. The variation by comparing these two samples is propagated to the nominal $t\bar{t} + \geq 1b$ sample generated with POWHEG BOX RES + PYTHIA 8 in the four-flavour scheme. This uncertainty is separated into three components that are treated independently: one for the dilepton channel, another for the non-boosted regions in the ℓ + jets channel, and a third for the ℓ + jets boosted region. This treatment is found to be important because it provides the fit with enough flexibility to cover the potential background mismodelling. Uncertainties in the choice of the PS model are evaluated by comparing the nominal sample with the one produced with POWHEG BOX + HERWIG 7. These uncertainties are treated in the same way as the uncertainty in the NLO matching procedure. An additional source of systematic uncertainty is introduced to address the choice of flavour scheme used for the generation of the $t\bar{t} + \geq 1b$ events. It is evaluated by

comparing the nominal sample, generated in the four-flavour scheme using POWHEG + PYTHIA 8, with that produced in the five-flavour scheme reweighted to remove differences in scale settings. Uncertainties in ISR and FSR are estimated using the same procedure as used for the $t\bar{t}H$ signals. An uncertainty due to differences in relative fraction of $t\bar{t}+1b$ and $t\bar{t}+\geq 2b$ subcomponents from different MC predictions is also considered. Other uncertainties in $t\bar{t}+\geq 1b$ and uncertainties in other background components are treated identically to the procedure described in Ref. [36].

Aside from the modelling uncertainties described above, experimental uncertainties are also considered. These arise from the modelling of trigger, reconstruction, identification and isolation efficiencies, as well as the calibration of energy and momentum scales for all physics objects, including electrons, muons, jets, b-tagged jets and $E_{\mathrm{T}}^{\mathrm{miss}}$. Uncertainties in the measured integrated luminosity and in the modelling of additional pp collisions are included.

7. Results

A binned profile likelihood fit is performed including all analysis regions simultaneously in order to determine the α and κ_t' parameters. The likelihood function, $\mathcal{L}(\alpha, \kappa_t', \boldsymbol{\theta})$, is constructed as the product of Poisson terms, with each term corresponding to an analysis bin. The value of the likelihood varies according to the expected signal yields, as a function of α and κ_t', and background yields of the analysis bins, as well as $\boldsymbol{\theta}$, representing the nuisance parameters encoding the effects of the systematic uncertainties and a single parameter controlling the normalisation of the $t\bar{t}+\geq 1b$ background. The nuisance parameters are constrained with Gaussian or log-normal functions. The normalisation of the $t\bar{t}+\geq 1b$ background is controlled by an unconstrained parameter $k_{t\bar{t}+b}$. A profile likelihood ratio is used as the test statistic, following Ref. [94]. By scanning the value of the test statistic in grid points in κ_t' and α, two-dimensional exclusion contours in the (κ_t', α) plane are obtained.

Fig. 1 compares the observed yield of data in each analysis region with that expected after the fit to data (post-fit). The expected yields for pure CP-even and CP-odd signals, normalised to the total data yields, are overlaid and shown with dashed lines in the top panels. These illustrate the signal-to-background separation provided by the classification BDTs. In the middle panel, the best-fit model is compared with the data by showing ratios of its value to the post-fit background prediction. The post-fit model agrees well with the observed data. In addition, the expected S/B for pure CP-even and CP-odd signals are shown for both $t\bar{t}H$ and tH. The post-fit yields for all backgrounds and the signals are summarised in Tables 3 and 4 for the $\ell+$jets and dilepton channels, respectively. The expected yields of pure CP-even and CP-odd signals are compared with the post-fit yields. In all fitted regions, the best-fit signal yields are lower than their SM predictions. The fitted value of $k_{t\bar{t}+b}$ is $1.30^{+0.09}_{-0.08}$, consistent with the value measured in Ref. [36]. Fig. 2 shows the distributions of the fitted observables in the four SRs. The post-fit predictions are in agreement with data. Goodness-of-fit was evaluated using a likelihood ratio test, comparing the likelihood value from the nominal fit with the one obtained from a saturated model built with one free-floating normalisation factor for each fitted bin [95]. The probability that the post-fit prediction is compatible with the observed data is 80%. The pure CP-even and CP-odd signals are shown overlaid and normalised to the data yield to indicate the kinematic discrimination of the b_2 and b_4 observables.

The best-fit values and the exclusion contours in α and κ_t' are displayed in Fig. 3 in the $(\kappa_t' \cos\alpha, \kappa_t' \sin\alpha)$ plane. The best-fit value for the CP mixing angle α is $11^{\circ}{}^{+52^{\circ}}_{-73^{\circ}}$ and overall coupling strength κ_t' is $0.84^{+0.30}_{-0.46}$, which are in agreement with the SM expectations of $\alpha = 0^{\circ}$ and $\kappa_t' = 1$. The data disfavour the pure CP-odd hypothesis with a 1.2 σ significance. The significance of the observed $t\bar{t}H$ and tH signals over the background prediction is 1.3 σ. The compatibility of this analysis with the $t\bar{t}H$ cross-section measurement [36] was tested with the same

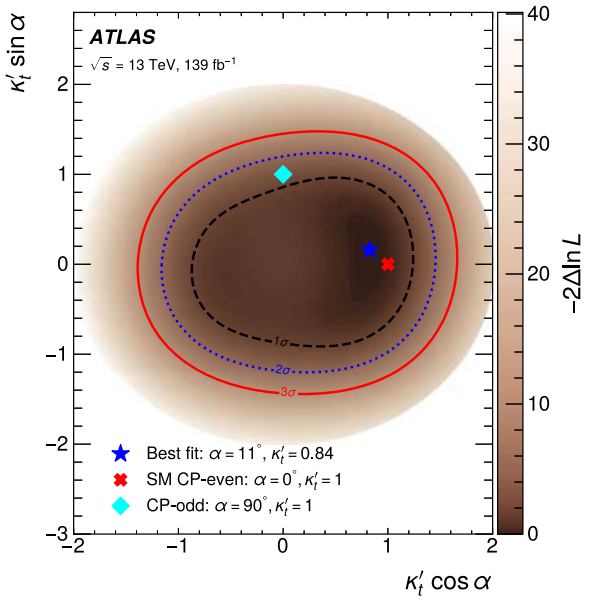

Fig. 3. The observed exclusion contours in the $(\kappa_t' \cos\alpha, \kappa_t' \sin\alpha)$ plane. Regions contained in the dashed, dotted and solid lines are compatible with the best-fit results at 1, 2 and 3 σ standard deviations. The cross (diamond) represents the CP-even (CP-odd) with $\kappa_t' = 1$ and the best-fit result is represented with a pentagram.

parameter of interest: a single free-floating signal strength, $\mu_{t\bar{t}H}$, controlling the normalisation of $t\bar{t}H$ production in the SM scenario. The tH process was fixed to its SM prediction with an identical systematic model. The compatibility is tested using the bootstrap technique [96]. The difference in the measured $\mu_{t\bar{t}H}$ is sampled by fitting to toy datasets generated by varying the event weights entering the Asimov dataset according to the Poisson fluctuations expected in data. The measured values of $\mu_{t\bar{t}H}$ were found to be compatible within one standard deviation, when accounting for the statistical correlations between the two measurements.

The impact of a group of systematic uncertainties on α (κ_t') is assessed by fixing the nuisance parameters to their best fit values and subtracting the subsequent α (κ_t') uncertainty in quadrature from the total α (κ_t') uncertainty. The uncertainty in the measured value of α is dominated by $t\bar{t}+\geq 1b$ modelling uncertainties which contribute $^{+37^{\circ}}_{-51^{\circ}}$ to the overall uncertainty. This is driven by: the NLO matching procedure between the ME and PS; PS and hadronisation; and the choice of flavour scheme. These uncertainties contribute $^{+22^{\circ}}_{-33^{\circ}}$, $^{+16^{\circ}}_{-24^{\circ}}$ and $^{+23^{\circ}}_{-37^{\circ}}$, respectively. Smaller effects from the $t\bar{t}+\geq 1b$ modelling originate from the ISR uncertainty and the relative fractions of $t\bar{t}+\geq 2b$ and $t\bar{t}+1b$, contributing $^{+14^{\circ}}_{-24^{\circ}}$ and $^{+14^{\circ}}_{-21^{\circ}}$. The $t\bar{t}+\geq 1c$ modelling uncertainties contribute only $^{+6.6^{\circ}}_{-11^{\circ}}$ to the uncertainty in α. The 100% $t\bar{t}+\geq 1c$ normalisation uncertainty is constrained to 50% with a pull of 0.6 σ, and has negligible impact on the fitted α and κ_t'. Through a correlation with α, the measured κ_t' contributes $^{+17^{\circ}}_{-33^{\circ}}$ to the α uncertainty. Experimental uncertainties are smaller than the $t\bar{t}+\geq 1b$ modelling uncertainties. The statistical uncertainty is $^{+32^{\circ}}_{-49^{\circ}}$.

8. Summary

In conclusion, the CP properties of the top-quark's Yukawa coupling to the Higgs boson are probed in $t\bar{t}H$ and tH production with $H \to b\bar{b}$ decays, which had not been studied before. Dedicated CP-sensitive variables relying on angular separations between reconstructed top quarks or lepton candidates were used directly. Assuming the SM branching ratio for the Higgs boson decay, the best-fit values of the CP-mixing angle and the overall coupling strength are $\alpha = 11^{\circ}{}^{+52^{\circ}}_{-73^{\circ}}$

and $\kappa_t' = 0.84^{+0.30}_{-0.46}$. These values can be compared with the expected allowed 1 σ ranges of α and κ_t', obtained using Asimov datasets constructed with either a pure CP-even or -odd signal. For a CP-even scenario $\alpha \in [-180°, -173°] \cup [-50°, 52°] \cup [171°, 180°]$ and $\kappa_t' = 1.00^{+0.29}_{-0.27}$, whilst for a pure CP-odd scenario $\alpha \in [-157°, -41°] \cup [43°, 157°]$ and $\kappa_t' = 1.00^{+0.22}_{-0.33}$. The sensitivity of this measurement is driven by the systematic uncertainties.

These results complement previous ATLAS measurements in the $H \to \gamma\gamma$ decay channel and will allow for a future combined measurement of the CP properties of the top-quark Yukawa coupling. Due to the tree-level sensitivity and the high $H \to b\bar{b}$ branching ratio, it can be expected that future measurements in the $t\bar{t}H$ and tH channels will become quite sensitive to the CP properties of the top-quark Yukawa coupling. Additional LHC data and a better theoretical understanding of the $t\bar{t} + \geq 1b$ process will be essential ingredients in order to achieve this sensitivity.

Declaration of competing interest

The authors declare that they have no known competing financial interests or personal relationships that could have appeared to influence the work reported in this paper.

Data availability

Data will be made available on request.

Acknowledgements

We thank CERN for the very successful operation of the LHC, as well as the support staff from our institutions without whom ATLAS could not be operated efficiently.

We acknowledge the support of ANPCyT, Argentina; YerPhI, Armenia; ARC, Australia; BMWFW and FWF, Austria; ANAS, Azerbaijan; CNPq and FAPESP, Brazil; NSERC, NRC and CFI, Canada; CERN; ANID, Chile; CAS, MOST and NSFC, China; Minciencias, Colombia; MEYS CR, Czech Republic; DNRF and DNSRC, Denmark; IN2P3-CNRS and CEA-DRF/IRFU, France; SRNSFG, Georgia; BMBF, HGF and MPG, Germany; GSRI, Greece; RGC and Hong Kong SAR, China; ISF and Benoziyo Center, Israel; INFN, Italy; MEXT and JSPS, Japan; CNRST, Morocco; NWO, Netherlands; RCN, Norway; MEiN, Poland; FCT, Portugal; MNE/IFA, Romania; MESTD, Serbia; MSSR, Slovakia; ARRS and MIZŠ, Slovenia; DSI/NRF, South Africa; MICINN, Spain; SRC and Wallenberg Foundation, Sweden; SERI, SNSF and Cantons of Bern and Geneva, Switzerland; MOST, Taiwan; TENMAK, Türkiye; STFC, United Kingdom; DOE and NSF, United States of America. In addition, individual groups and members have received support from BCKDF, Canarie, Compute Canada and CRC, Canada; PRIMUS 21/SCI/017 and UNCE SCI/013, Czech Republic; COST, ERC, ERDF, Horizon 2020, ICSC-NextGenerationEU and Marie Skłodowska-Curie Actions, European Union; Investissements d'Avenir Labex, Investissements d'Avenir Idex and ANR, France; DFG and AvH Foundation, Germany; Herakleitos, Thales and Aristeia programmes co-financed by EU-ESF and the Greek NSRF, Greece; BSF-NSF and MINERVA, Israel; Norwegian Financial Mechanism 2014-2021, Norway; NCN and NAWA, Poland; La Caixa Banking Foundation, CERCA Programme Generalitat de Catalunya and PROMETEO and GenT Programmes Generalitat Valenciana, Spain; Göran Gustafssons Stiftelse, Sweden; The Royal Society and Leverhulme Trust, United Kingdom.

The crucial computing support from all WLCG partners is acknowledged gratefully, in particular from CRN, the ATLAS Tier-1 facilities at TRIUMF (Canada), NDGF (Denmark, Norway, Sweden), CC-IN2P3 (France), KIT/GridKA (Germany), INFN-CNAF (Italy), NL-T1 (Netherlands), PIC (Spain), ASGC (Taiwan), RAL (UK) and BNL (USA), the Tier-2 facilities worldwide and large non-WLCG resource providers. Major contributors of computing resources are listed in Ref. [97].

References

[1] ATLAS Collaboration, Observation of a new particle in the search for the Standard Model Higgs boson with the ATLAS detector at the LHC, Phys. Lett. B 716 (2012) 1, arXiv:1207.7214 [hep-ex].

[2] CMS Collaboration, Observation of a new boson with mass near 125 GeV in pp collisions at $\sqrt{s} = 7$ and 8 TeV, J. High Energy Phys. 06 (2013) 081, arXiv:1303.4571 [hep-ex].

[3] ATLAS Collaboration, Observation of Higgs boson production in association with a top quark pair at the LHC with the ATLAS detector, Phys. Lett. B 784 (2018) 173, arXiv:1806.00425 [hep-ex].

[4] CMS Collaboration, Observation of $t\bar{t}H$ production, Phys. Rev. Lett. 120 (2018) 231801, arXiv:1804.02610 [hep-ex].

[5] ATLAS Collaboration, CP properties of Higgs boson interactions with top quarks in the $t\bar{t}H$ and tH processes using $H \to \gamma\gamma$ with the ATLAS detector, Phys. Rev. Lett. 125 (2020) 061802, arXiv:2004.04545 [hep-ex].

[6] CMS Collaboration, Measurements of $t\bar{t}H$ production and the CP structure of the Yukawa interaction between the Higgs boson and top quark in the diphoton decay channel, Phys. Rev. Lett. 125 (2020) 061801, arXiv:2003.10866 [hep-ex].

[7] CMS Collaboration, Search for CP violation in ttH and tH production in multilepton channels in proton–proton collisions at $\sqrt{s} = 13\,TeV$, J. High Energy Phys. 07 (2022) 092, arXiv:2208.02686 [hep-ex].

[8] W. Buchmüller, D. Wyler, Effective Lagrangian analysis of new interactions and flavour conservation, Nucl. Phys. B (ISSN 0550-3213) 268 (1986) 621.

[9] V. Hankele, G. Klämke, D. Zeppenfeld, T. Figy, Anomalous Higgs boson couplings in vector boson fusion at the CERN LHC, Phys. Rev. D 74 (2006).

[10] D. Fontes, J.C. Romão, R. Santos, J.P. Silva, Large pseudoscalar Yukawa couplings in the complex 2HDM, J. High Energy Phys. 2015 (2015) 60, arXiv:1502.01720v2 [hep-ph].

[11] ATLAS Collaboration, Evidence for the spin-0 nature of the Higgs boson using ATLAS data, Phys. Lett. B 726 (2013) 120, arXiv:1307.1432 [hep-ex].

[12] CMS Collaboration, Study of the mass and spin-parity of the Higgs boson candidate via its decays to Z boson pairs, Phys. Rev. Lett. 110 (2013) 081803, arXiv:1212.6639 [hep-ex].

[13] ATLAS Collaboration, Search for a CP-odd Higgs boson decaying to Zh in pp collisions at $\sqrt{s} = 8\,TeV$ with the ATLAS detector, Phys. Lett. B 744 (2015) 163, arXiv:1502.04478 [hep-ex].

[14] ATLAS Collaboration, Test of CP invariance in vector-boson fusion production of the Higgs boson in the $H \to \tau\tau$ channel in proton–proton collisions at $\sqrt{s} = 13\,TeV$ with the ATLAS detector, Phys. Lett. B 805 (2020) 135426, arXiv:2002.05315 [hep-ex].

[15] ATLAS Collaboration, Measurements of Higgs boson properties in the diphoton decay channel with 36 fb^{-1} of pp collision data at $\sqrt{s} = 13\,TeV$ with the ATLAS detector, Phys. Rev. D 98 (2018) 052005, arXiv:1802.04146 [hep-ex].

[16] ATLAS Collaboration, Measurement of the Higgs boson coupling properties in the $H \to ZZ^* \to 4\ell$ decay channel at $\sqrt{s} = 13\,TeV$ with the ATLAS detector, J. High Energy Phys. 03 (2018) 095, arXiv:1712.02304 [hep-ex].

[17] CMS Collaboration, Combined search for anomalous pseudoscalar HVV couplings in $VH(H \to b\bar{b})$ production and $H \to VV$ decay, Phys. Lett. B 759 (2016) 672, arXiv:1602.04305 [hep-ex].

[18] CMS Collaboration, Constraints on anomalous Higgs boson couplings using production and decay information in the four-lepton final state, Phys. Lett. B 775 (2017) 1, arXiv:1707.00541 [hep-ex].

[19] CMS Collaboration, Measurements of the Higgs boson width and anomalous HVV couplings from on-shell and off-shell production in the four-lepton final state, Phys. Rev. D 99 (2019) 112003, arXiv:1901.00174 [hep-ex].

[20] CMS Collaboration, Constraints on anomalous Higgs boson couplings to vector bosons and fermions from the production of Higgs bosons using the $\tau\tau$ final state, arXiv:2205.05120 [hep-ex], 2022.

[21] ATLAS Collaboration, Test of CP-invariance of the Higgs boson in vector-boson fusion production and its decay into four leptons, arXiv:2304.09612 [hep-ex], 2023.

[22] J.F. Gunion, X.-G. He, Determining the CP nature of a neutral Higgs boson at the CERN large hadron collider, Phys. Rev. Lett. 76 (1996) 4468, arXiv:hep-ph/9602226.

[23] J. Ellis, D.S. Hwang, K. Sakurai, M. Takeuchi, Disentangling Higgs-top couplings in associated production, J. High Energy Phys. 04 (2014) 004, arXiv:1312.5736 [hep-ph].

[24] X.-G. He, G.-N. Li, Y.-J. Zheng, Probing Higgs boson CP properties with $t\bar{t}H$ at the LHC and the 100 TeV pp collider, Int. J. Mod. Phys. A 30 (2014) 1550156, arXiv:1501.00012 [hep-ph].

[25] F. Boudjema, D. Guadagnoli, R.M. Godbole, K.A. Mohan, Laboratory-frame observables for probing the top-Higgs boson interaction, Phys. Rev. D 92 (2015) 015019, arXiv:1501.03157 [hep-ph].

[26] F. Demartin, F. Maltoni, K. Mawatari, B. Page, M. Zaro, Higgs characterisation at NLO in QCD: CP properties of the top-quark Yukawa interaction, Eur. Phys. J. C 74 (2014) 3065, arXiv:1407.5089 [hep-ph].

[27] H. Bahl, et al., Indirect CP probes of the Higgs-top-quark interaction: current LHC constraints and future opportunities, J. High Energy Phys. 2020 (2020) 127, arXiv:2007.08542 [hep-ph].

[28] D. Gonçalves, J.H. Kim, K. Kong, Y. Wu, Direct Higgs-top CP-phase measurement with $t\bar{t}h$ at the 14 TeV LHC and 100 TeV FCC, J. High Energy Phys. 2022 (2022) 158, arXiv:2108.01083 [hep-ph].

[29] J. Brod, U. Haisch, J. Zupan, Constraints on CP-violating Higgs couplings to the third generation, J. High Energy Phys. 11 (2013) 180, arXiv:1310.1385 [hep-ph].

[30] V. Andreev, et al., Improved limit on the electric dipole moment of the electron, Nature 562 (2018) 355.

[31] C. Abel, et al., Measurement of the permanent electric dipole moment of the neutron, Phys. Rev. Lett. 124 (2020) 081803, arXiv:2001.11966 [hep-ex].

[32] M.R. Buckley, D. Goncalves, Boosting the direct CP measurement of the Higgs-top coupling, Phys. Rev. Lett. 116 (2016) 091801, arXiv:1507.07926 [hep-ph].

[33] D. Gonçalves, J.H. Kim, K. Kong, Probing the top-Higgs Yukawa CP structure in dileptonic $t\bar{t}h$ with M $_2$-assisted reconstruction, J. High Energy Phys. 06 (2018) 079, arXiv:1804.05874 [hep-ph].

[34] D. Azevedo, A. Onofre, F. Filthaut, R. Gonçalo, CP tests of Higgs couplings in $t\bar{t}h$ semileptonic events at the LHC, Phys. Rev. D 98 (2018) 033004, arXiv:1711.05292 [hep-ph].

[35] A. Ferroglia, M.C.N. Fiolhais, E. Gouveia, A. Onofre, Role of the $t\bar{t}h$ rest frame in direct top-quark Yukawa coupling measurements, Phys. Rev. D 100 (2019) 075034, arXiv:1909.00490 [hep-ph].

[36] ATLAS Collaboration, Measurement of Higgs boson decay into b-quarks in associated production with a top-quark pair in pp collisions at $\sqrt{s} = 13\,TeV$ with the ATLAS detector, J. High Energy Phys. 06 (2022) 097, arXiv:2111.06712 [hep-ex].

[37] D. de Florian, et al., Handbook of LHC Higgs cross sections: 4. deciphering the nature of the Higgs sector, arXiv:1610.07922 [hep-ph], 2016.

[38] ATLAS Collaboration, The ATLAS experiment at the CERN large hadron collider, J. Instrum. 3 (2008) S08003.

[39] ATLAS Collaboration, ATLAS insertable B-layer: technical design report, ATLAS-TDR-19; CERN-LHCC-2010-013, https://cds.cern.ch/record/1291633, 2010; Addendum: ATLAS-TDR-19-ADD-1; CERN-LHCC-2012-009, https://cds.cern.ch/record/1451888, 2012.

[40] B. Abbott, et al., Production and integration of the ATLAS insertable B-layer, J. Instrum. 13 (2018) T05008, arXiv:1803.00844 [physics.ins-det].

[41] ATLAS Collaboration, Performance of the ATLAS trigger system in 2015, Eur. Phys. J. C 77 (2017) 317, arXiv:1611.09661 [hep-ex].

[42] ATLAS Collaboration, The ATLAS Collaboration software and firmware, ATL-SOFT-PUB-2021-001, https://cds.cern.ch/record/2767187, 2021.

[43] ATLAS Collaboration, Performance of the ATLAS muon triggers in Run 2, J. Instrum. 15 (2020) P09015, arXiv:2004.13447 [physics.ins-det].

[44] ATLAS Collaboration, Performance of electron and photon triggers in ATLAS during LHC Run 2, Eur. Phys. J. C 80 (2020) 47, arXiv:1909.00761 [hep-ex].

[45] ATLAS Collaboration, Electron and photon performance measurements with the ATLAS detector using the 2015–2017 LHC proton–proton collision data, J. Instrum. 14 (2019) P12006, arXiv:1908.00005 [hep-ex].

[46] ATLAS Collaboration, Muon reconstruction and identification efficiency in ATLAS using the full Run 2 pp collision data set at $\sqrt{s} = 13\,TeV$, Eur. Phys. J. C 81 (2021) 578, arXiv:2012.00578 [hep-ex].

[47] ATLAS Collaboration, Topological cell clustering in the ATLAS calorimeters and its performance in LHC Run 1, Eur. Phys. J. C 77 (2017) 490, arXiv:1603.02934 [hep-ex].

[48] ATLAS Collaboration, Jet energy scale and resolution measured in proton–proton collisions at $\sqrt{s} = 13\,TeV$ with the ATLAS detector, Eur. Phys. J. C 81 (2020) 689, arXiv:2007.02645 [hep-ex].

[49] M. Cacciari, G.P. Salam, G. Soyez, The anti-k_t jet clustering algorithm, J. High Energy Phys. 04 (2008) 063, arXiv:0802.1189 [hep-ph].

[50] M. Cacciari, G.P. Salam, G. Soyez, FastJet user manual, Eur. Phys. J. C 72 (2012) 1896, arXiv:1111.6097 [hep-ph].

[51] ATLAS Collaboration, ATLAS b-jet identification performance and efficiency measurement with $t\bar{t}$ events in pp collisions at $\sqrt{s} = 13\,TeV$, Eur. Phys. J. C 79 (2019) 970, arXiv:1907.05120 [hep-ex].

[52] ATLAS Collaboration, Measurement of b-tagging efficiency of c-jets in $t\bar{t}$ events using a likelihood approach with the ATLAS detector, ATLAS-CONF-2018-001, https://cds.cern.ch/record/2306649, 2018.

[53] ATLAS Collaboration, Calibration of light-flavour b-jet mistagging rates using ATLAS proton–proton collision data at $\sqrt{s} = 13\,TeV$, ATLAS-CONF-2018-006, https://cds.cern.ch/record/2314418, 2018.

[54] ATLAS Collaboration, Performance of missing transverse momentum reconstruction with the ATLAS detector using proton–proton collisions at $\sqrt{s} = 13\,TeV$, Eur. Phys. J. C 78 (2018) 903, arXiv:1802.08168 [hep-ex].

[55] B. Nachman, P. Nef, A. Schwartzman, M. Swiatlowski, C. Wanotayaroj, Jets from jets: re-clustering as a tool for large radius jet reconstruction and grooming at the LHC, J. High Energy Phys. 02 (2015) 075, arXiv:1407.2922 [hep-ph].

[56] ATLAS Collaboration, The ATLAS simulation infrastructure, Eur. Phys. J. C 70 (2010) 823, arXiv:1005.4568 [physics.ins-det].

[57] S. Agostinelli, et al., Geant4 – a simulation toolkit, Nucl. Instrum. Methods A 506 (2003) 250.

[58] T. Sjöstrand, et al., An introduction to PYTHIA 8.2, Comput. Phys. Commun. 191 (2015) 159, arXiv:1410.3012 [hep-ph].

[59] ATLAS Collaboration, The Pythia 8 A3 tune description of ATLAS minimum bias and inelastic measurements incorporating the Donnachie–Landshoff diffractive model, ATL-PHYS-PUB-2016-017, https://cds.cern.ch/record/2206965, 2016.

[60] T. Ježo, J.M. Lindert, N. Moretti, S. Pozzorini, New NLOPS predictions for $t\bar{t}$ + b-jet production at the LHC, Eur. Phys. J. C 78 (2018) 502, arXiv:1802.00426 [hep-ph].

[61] F. Cascioli, P. Maierhöfer, S. Pozzorini, Scattering amplitudes with open loops, Phys. Rev. Lett. 108 (2012) 111601, arXiv:1111.5206 [hep-ph].

[62] A. Denner, S. Dittmaier, L. Hofer, Collier: a fortran-based complex one-loop library in extended regularizations, Comput. Phys. Commun. 212 (2017) 220, arXiv:1604.06792 [hep-ph].

[63] T. Ježo, Powheg-Box-Res ttbb source code, https://gitlab.cern.ch/tjezo/powheg-box-res_ttbb/, 2019.

[64] The NNPDF Collaboration, R.D. Ball, et al., Parton distributions for the LHC run II, J. High Energy Phys. 04 (2015) 040, arXiv:1410.8849 [hep-ph].

[65] ATLAS Collaboration, ATLAS Pythia 8 tunes to 7 TeV data, ATL-PHYS-PUB-2014-021, https://cds.cern.ch/record/1966419, 2014.

[66] ATLAS Collaboration, Measurements of inclusive and differential fiducial cross-sections of $t\bar{t}$ production with additional heavy-flavour jets in proton–proton collisions at $\sqrt{s} = 13\,TeV$ with the ATLAS detector, J. High Energy Phys. 04 (2019) 046, arXiv:1811.12113 [hep-ex].

[67] CMS Collaboration, Measurement of the $t\bar{t}b\bar{b}$ production cross section in the all-jet final state in pp collisions at $\sqrt{s} = 13\,TeV$, Phys. Lett. B 803 (2020) 135285, arXiv:1909.05306 [hep-ex].

[68] P. Nason, A new method for combining NLO QCD with shower Monte Carlo algorithms, J. High Energy Phys. 11 (2004) 040, arXiv:hep-ph/0409146.

[69] S. Frixione, P. Nason, C. Oleari, Matching NLO QCD computations with parton shower simulations: the POWHEG method, J. High Energy Phys. 11 (2007) 070, arXiv:0709.2092 [hep-ph].

[70] S. Alioli, P. Nason, C. Oleari, E. Re, A general framework for implementing NLO calculations in shower Monte Carlo programs: the POWHEG BOX, J. High Energy Phys. 06 (2010) 043, arXiv:1002.2581 [hep-ph].

[71] H.B. Hartanto, B. Jäger, L. Reina, D. Wackeroth, Higgs boson production in association with top quarks in the POWHEG BOX, Phys. Rev. D 91 (2015) 094003, arXiv:1501.04498 [hep-ph].

[72] M. Beneke, P. Falgari, S. Klein, C. Schwinn, Hadronic top-quark pair production with NNLL threshold resummation, Nucl. Phys. B 855 (2012) 695, arXiv:1109.1536 [hep-ph].

[73] M. Cacciari, M. Czakon, M. Mangano, A. Mitov, P. Nason, Top-pair production at hadron colliders with next-to-next-to-leading logarithmic soft-gluon resummation, Phys. Lett. B 710 (2012) 612, arXiv:1111.5869 [hep-ph].

[74] P. Bärnreuther, M. Czakon, A. Mitov, Percent-level-precision physics at the tevatron: next-to-next-to-leading order QCD corrections to $q\bar{q} \to t\bar{t} + X$, Phys. Rev. Lett. 109 (2012) 132001, arXiv:1204.5201 [hep-ph].

[75] M. Czakon, A. Mitov, NNLO corrections to top-pair production at hadron colliders: the all-fermionic scattering channels, J. High Energy Phys. 12 (2012) 054, arXiv:1207.0236 [hep-ph].

[76] M. Czakon, A. Mitov, NNLO corrections to top pair production at hadron colliders: the quark-gluon reaction, J. High Energy Phys. 01 (2013) 080, arXiv:1210.6832 [hep-ph].

[77] M. Czakon, P. Fiedler, A. Mitov, Total top-quark pair-production cross section at hadron colliders through $O(\alpha_S^4)$, Phys. Rev. Lett. 110 (2013) 252004, arXiv:1303.6254 [hep-ph].

[78] M. Czakon, A. Mitov, Top++: a program for the calculation of the top-pair cross-section at hadron colliders, Comput. Phys. Commun. 185 (2014) 2930, arXiv:1112.5675 [hep-ph].

[79] P. Artoisenet, et al., A framework for Higgs characterisation, J. High Energy Phys. 11 (2013) 043, arXiv:1306.6464 [hep-ph].

[80] A. Alloul, N.D. Christensen, C. Degrande, C. Duhr, B. Fuks, FeynRules 2.0 - a complete toolbox for tree-level phenomenology, Comput. Phys. Commun. 185 (2014) 2250, arXiv:1310.1921 [hep-ph].

[81] C. Degrande, et al., UFO - the universal FeynRules output, Comput. Phys. Commun. 183 (2012) 1201, arXiv:1108.2040 [hep-ph].

[82] J. Alwall, et al., The automated computation of tree-level and next-to-leading order differential cross sections, and their matching to parton shower simulations, J. High Energy Phys. 07 (2014) 079, arXiv:1405.0301 [hep-ph].

[83] R. Raitio, W.W. Wada, Higgs-boson production at large transverse momentum in quantum chromodynamics, Phys. Rev. D 19 (1979) 941.

[84] W. Beenakker, et al., NLO QCD corrections to $t\bar{t}H$ production in hadron collisions, Nucl. Phys. B 653 (2003) 151, arXiv:hep-ph/0211352 [hep-ph].

[85] S. Dawson, C. Jackson, L.H. Orr, L. Reina, D. Wackeroth, Associated Higgs boson production with top quarks at the CERN Large Hadron Collider: NLO QCD corrections, Phys. Rev. D 68 (2003) 034022, arXiv:hep-ph/0305087v2 [hep-ph].

[86] Y. Zhang, W.-G. Ma, R.-Y. Zhang, C. Chen, L. Guo, QCD NLO and EW NLO corrections to $t\bar{t}H$ production with top quark decays at hadron collider, Phys. Lett. B 738 (2014) 1, arXiv:1407.1110 [hep-ph].

[87] S. Frixione, V. Hirschi, D. Pagani, H.-S. Shao, M. Zaro, Electroweak and QCD corrections to top-pair hadroproduction in association with heavy bosons, J. High Energy Phys. 06 (2015) 184, arXiv:1504.03446 [hep-ph].

[88] S. Frixione, E. Laenen, P. Motylinski, B.R. Webber, Angular correlations of lepton pairs from vector boson and top quark decays in Monte Carlo simulations, J. High Energy Phys. 04 (2007) 081, arXiv:hep-ph/0702198.

[89] ATLAS Collaboration, Performance of jet substructure techniques for large-R jets in proton–proton collisions at $\sqrt{s} = 7\,TeV$ using the ATLAS detector, J. High Energy Phys. 09 (2013) 076, arXiv:1306.4945 [hep-ex].

[90] DØ Collaboration, Measurement of the top quark mass using dilepton events, Phys. Rev. Lett. 80 (1998) 2063, arXiv:hep-ex/9706014.
[91] ATLAS Collaboration, Measurements of top-quark pair differential cross-sections in the $e\mu$ channel in pp collisions at $\sqrt{s} = 13$ TeV using the ATLAS detector, Eur. Phys. J. C 77 (2017) 292, arXiv:1612.05220 [hep-ex].
[92] ATLAS Collaboration, Study of top-quark pair modelling and uncertainties using ATLAS measurements at $\sqrt{s} = 13$ TeV, ATL-PHYS-PUB-2020-023, https://cds.cern.ch/record/2730443, 2020.
[93] J. Bellm, et al., Herwig 7.0/Herwig++ 3.0 release note, Eur. Phys. J. C 76 (2016) 196, arXiv:1512.01178 [hep-ph].
[94] G. Cowan, K. Cranmer, E. Gross, O. Vitells, Asymptotic formulae for likelihood-based tests of new physics, Eur. Phys. J. C 71 (2011) 1554, arXiv:1007.1727 [physics.data-an]; Erratum: Eur. Phys. J. C 73 (2013) 2501.
[95] R. Cousins, Generalization of chisquare goodness-of-fit test for binned data using saturated models, with application to histograms, http://www.physics.ucla.edu/~cousins/stats/cousins_saturated.pdf, 2013.
[96] ATLAS Collaboration, Evaluating statistical uncertainties and correlations using the bootstrap method, ATL-PHYS-PUB-2021-011, https://cds.cern.ch/record/2759945, 2021.
[97] ATLAS Collaboration, ATLAS computing acknowledgements, ATL-SOFT-PUB-2023-001, https://cds.cern.ch/record/2869272, 2023.

The ATLAS Collaboration

G. Aad [101], B. Abbott [119], D.C. Abbott [102], K. Abeling [55], S.H. Abidi [29], A. Aboulhorma [35e], H. Abramowicz [150], H. Abreu [149], Y. Abulaiti [116], A.C. Abusleme Hoffman [136a], B.S. Acharya [68a,68b,p], B. Achkar [55], L. Adam [99], C. Adam Bourdarios [4], L. Adamczyk [84a], L. Adamek [154], S.V. Addepalli [26], J. Adelman [114], A. Adiguzel [21c], S. Adorni [56], T. Adye [133], A.A. Affolder [135], Y. Afik [36], M.N. Agaras [13], J. Agarwala [72a,72b], A. Aggarwal [99], C. Agheorghiesei [27c], J.A. Aguilar-Saavedra [129f], A. Ahmad [36], F. Ahmadov [38,z], W.S. Ahmed [103], S. Ahuja [94], X. Ai [48], G. Aielli [75a,75b], I. Aizenberg [168], M. Akbiyik [99], T.P.A. Åkesson [97], A.V. Akimov [37], K. Al Khoury [41], G.L. Alberghi [23b], J. Albert [164], P. Albicocco [53], M.J. Alconada Verzini [89], S. Alderweireldt [52], M. Aleksa [36], I.N. Aleksandrov [38], C. Alexa [27b], T. Alexopoulos [10], A. Alfonsi [113], F. Alfonsi [23b], M. Alhroob [119], B. Ali [131], S. Ali [147], M. Aliev [37], G. Alimonti [70a], C. Allaire [36], B.M.M. Allbrooke [145], P.P. Allport [20], A. Aloisio [71a,71b], F. Alonso [89], C. Alpigiani [137], E. Alunno Camelia [75a,75b], M. Alvarez Estevez [98], M.G. Alviggi [71a,71b], Y. Amaral Coutinho [81b], A. Ambler [103], C. Amelung [36], C.G. Ames [108], D. Amidei [105], S.P. Amor Dos Santos [129a], S. Amoroso [48], K.R. Amos [162], C.S. Amrouche [56], V. Ananiev [124], C. Anastopoulos [138], N. Andari [134], T. Andeen [11], J.K. Anders [19], S.Y. Andrean [47a,47b], A. Andreazza [70a,70b], S. Angelidakis [9], A. Angerami [41,ac], A.V. Anisenkov [37], A. Annovi [73a], C. Antel [56], M.T. Anthony [138], E. Antipov [120], M. Antonelli [53], D.J.A. Antrim [17a], F. Anulli [74a], M. Aoki [82], J.A. Aparisi Pozo [162], M.A. Aparo [145], L. Aperio Bella [48], C. Appelt [18], N. Aranzabal [36], V. Araujo Ferraz [81a], C. Arcangeletti [53], A.T.H. Arce [51], E. Arena [91], J-F. Arguin [107], S. Argyropoulos [54], J.-H. Arling [48], A.J. Armbruster [36], O. Arnaez [154], H. Arnold [113], Z.P. Arrubarrena Tame [108], G. Artoni [74a,74b], H. Asada [110], K. Asai [117], S. Asai [152], N.A. Asbah [61], E.M. Asimakopoulou [160], K. Assamagan [29], R. Astalos [28a], R.J. Atkin [33a], M. Atkinson [161], N.B. Atlay [18], H. Atmani [62b], P.A. Atmasiddha [105], K. Augsten [131], S. Auricchio [71a,71b], A.D. Auriol [20], V.A. Austrup [170], G. Avner [149], G. Avolio [36], K. Axiotis [56], M.K. Ayoub [14c], G. Azuelos [107,ag], D. Babal [28a], H. Bachacou [134], K. Bachas [151,s], A. Bachiu [34], F. Backman [47a,47b], A. Badea [61], P. Bagnaia [74a,74b], M. Bahmani [18], A.J. Bailey [162], V.R. Bailey [161], J.T. Baines [133], C. Bakalis [10], O.K. Baker [171], P.J. Bakker [113], E. Bakos [15], D. Bakshi Gupta [8], S. Balaji [146], R. Balasubramanian [113], E.M. Baldin [37], P. Balek [132], E. Ballabene [70a,70b], F. Balli [134], L.M. Baltes [63a], W.K. Balunas [32], J. Balz [99], E. Banas [85], M. Bandieramonte [128], A. Bandyopadhyay [24], S. Bansal [24], L. Barak [150], E.L. Barberio [104], D. Barberis [57b,57a], M. Barbero [101], G. Barbour [95], K.N. Barends [33a], T. Barillari [109], M-S. Barisits [36], J. Barkeloo [122], T. Barklow [142], R.M. Barnett [17a], P. Baron [121], D.A. Baron Moreno [100], A. Baroncelli [62a], G. Barone [29], A.J. Barr [125], L. Barranco Navarro [47a,47b], F. Barreiro [98], J. Barreiro Guimarães da Costa [14a], U. Barron [150], M.G. Barros Teixeira [129a], S. Barsov [37], F. Bartels [63a], R. Bartoldus [142], A.E. Barton [90], P. Bartos [28a], A. Basalaev [48],

A. Basan [99], M. Baselga [49], I. Bashta [76a,76b], A. Bassalat [66,b], M.J. Basso [154], C.R. Basson [100], R.L. Bates [59], S. Batlamous [35e], J.R. Batley [32], B. Batool [140], M. Battaglia [135], M. Bauce [74a,74b], P. Bauer [24], A. Bayirli [21a], J.B. Beacham [51], T. Beau [126], P.H. Beauchemin [157], F. Becherer [54], P. Bechtle [24], H.P. Beck [19,r], K. Becker [166], C. Becot [48], A.J. Beddall [21d], V.A. Bednyakov [38], C.P. Bee [144], L.J. Beemster [15], T.A. Beermann [36], M. Begalli [81b,81d], M. Begel [29], A. Behera [144], J.K. Behr [48], C. Beirao Da Cruz E Silva [36], J.F. Beirer [55,36], F. Beisiegel [24], M. Belfkir [158], G. Bella [150], L. Bellagamba [23b], A. Bellerive [34], P. Bellos [20], K. Beloborodov [37], K. Belotskiy [37], N.L. Belyaev [37], D. Benchekroun [35a], F. Bendebba [35a], Y. Benhammou [150], D.P. Benjamin [29], M. Benoit [29], J.R. Bensinger [26], S. Bentvelsen [113], L. Beresford [36], M. Beretta [53], D. Berge [18], E. Bergeaas Kuutmann [160], N. Berger [4], B. Bergmann [131], J. Beringer [17a], S. Berlendis [7], G. Bernardi [5], C. Bernius [142], F.U. Bernlochner [24], T. Berry [94], P. Berta [132], A. Berthold [50], I.A. Bertram [90], O. Bessidskaia Bylund [170], S. Bethke [109], A. Betti [74a,74b], A.J. Bevan [93], M. Bhamjee [33c], S. Bhatta [144], D.S. Bhattacharya [165], P. Bhattarai [26], V.S. Bhopatkar [6], R. Bi [128], R. Bi [29,aj], R.M. Bianchi [128], O. Biebel [108], R. Bielski [122], N.V. Biesuz [73a,73b], M. Biglietti [76a], T.R.V. Billoud [131], M. Bindi [55], A. Bingul [21b], C. Bini [74a,74b], S. Biondi [23b,23a], A. Biondini [91], C.J. Birch-sykes [100], G.A. Bird [20,133], M. Birman [168], T. Bisanz [36], D. Biswas [169,l], A. Bitadze [100], K. Bjørke [124], I. Bloch [48], C. Blocker [26], A. Blue [59], U. Blumenschein [93], J. Blumenthal [99], G.J. Bobbink [113], V.S. Bobrovnikov [37], M. Boehler [54], D. Bogavac [36], A.G. Bogdanchikov [37], C. Bohm [47a], V. Boisvert [94], P. Bokan [48], T. Bold [84a], M. Bomben [5], M. Bona [93], M. Boonekamp [134], C.D. Booth [94], A.G. Borbély [59], H.M. Borecka-Bielska [107], L.S. Borgna [95], G. Borissov [90], D. Bortoletto [125], D. Boscherini [23b], M. Bosman [13], J.D. Bossio Sola [36], K. Bouaouda [35a], J. Boudreau [128], E.V. Bouhova-Thacker [90], D. Boumediene [40], R. Bouquet [5], A. Boveia [118], J. Boyd [36], D. Boye [29], I.R. Boyko [38], J. Bracinik [20], N. Brahimi [62d,62c], G. Brandt [170], O. Brandt [32], F. Braren [48], B. Brau [102], J.E. Brau [122], W.D. Breaden Madden [59], K. Brendlinger [48], R. Brener [168], L. Brenner [36], R. Brenner [160], S. Bressler [168], B. Brickwedde [99], D. Britton [59], D. Britzger [109], I. Brock [24], G. Brooijmans [41], W.K. Brooks [136f], E. Brost [29], P.A. Bruckman de Renstrom [85], B. Brüers [48], D. Bruncko [28b,*], A. Bruni [23b], G. Bruni [23b], M. Bruschi [23b], N. Bruscino [74a,74b], L. Bryngemark [142], T. Buanes [16], Q. Buat [137], P. Buchholz [140], A.G. Buckley [59], I.A. Budagov [38,*], M.K. Bugge [124], O. Bulekov [37], B.A. Bullard [61], S. Burdin [91], C.D. Burgard [48], A.M. Burger [40], B. Burghgrave [8], J.T.P. Burr [32], C.D. Burton [11], J.C. Burzynski [141], E.L. Busch [41], V. Büscher [99], P.J. Bussey [59], J.M. Butler [25], C.M. Buttar [59], J.M. Butterworth [95], W. Buttinger [133], C.J. Buxo Vazquez [106], A.R. Buzykaev [37], G. Cabras [23b], S. Cabrera Urbán [162], D. Caforio [58], H. Cai [128], Y. Cai [14a,14d], V.M.M. Cairo [36], O. Cakir [3a], N. Calace [36], P. Calafiura [17a], G. Calderini [126], P. Calfayan [67], G. Callea [59], L.P. Caloba [81b], D. Calvet [40], S. Calvet [40], T.P. Calvet [101], M. Calvetti [73a,73b], R. Camacho Toro [126], S. Camarda [36], D. Camarero Munoz [98], P. Camarri [75a,75b], M.T. Camerlingo [76a,76b], D. Cameron [124], C. Camincher [164], M. Campanelli [95], A. Camplani [42], V. Canale [71a,71b], A. Canesse [103], M. Cano Bret [79], J. Cantero [162], Y. Cao [161], F. Capocasa [26], M. Capua [43b,43a], A. Carbone [70a,70b], R. Cardarelli [75a], J.C.J. Cardenas [8], F. Cardillo [162], T. Carli [36], G. Carlino [71a], B.T. Carlson [128,t], E.M. Carlson [164,155a], L. Carminati [70a,70b], M. Carnesale [74a,74b], S. Caron [112], E. Carquin [136f], S. Carrá [70a], G. Carratta [23b,23a], F. Carrio Argos [33g], J.W.S. Carter [154], T.M. Carter [52], M.P. Casado [13,i], A.F. Casha [154], E.G. Castiglia [171], F.L. Castillo [63a], L. Castillo Garcia [13], V. Castillo Gimenez [162], N.F. Castro [129a,129e], A. Catinaccio [36], J.R. Catmore [124],

V. Cavaliere [29], N. Cavalli [23b,23a], V. Cavasinni [73a,73b], E. Celebi [21a], F. Celli [125], M.S. Centonze [69a,69b], K. Cerny [121], A.S. Cerqueira [81a], A. Cerri [145], L. Cerrito [75a,75b], F. Cerutti [17a], A. Cervelli [23b], S.A. Cetin [21d], Z. Chadi [35a], D. Chakraborty [114], M. Chala [129f], J. Chan [169], W.S. Chan [113], W.Y. Chan [152], J.D. Chapman [32], B. Chargeishvili [148b], D.G. Charlton [20], T.P. Charman [93], M. Chatterjee [19], S. Chekanov [6], S.V. Chekulaev [155a], G.A. Chelkov [38,a], A. Chen [105], B. Chen [150], B. Chen [164], C. Chen [62a], H. Chen [14c], H. Chen [29], J. Chen [62c], J. Chen [26], S. Chen [152], S.J. Chen [14c], X. Chen [62c], X. Chen [14b,af], Y. Chen [62a], C.L. Cheng [169], H.C. Cheng [64a], A. Cheplakov [38], E. Cheremushkina [48], E. Cherepanova [113], R. Cherkaoui El Moursli [35e], E. Cheu [7], K. Cheung [65], L. Chevalier [134], V. Chiarella [53], G. Chiarelli [73a], G. Chiodini [69a], A.S. Chisholm [20], A. Chitan [27b], Y.H. Chiu [164], M.V. Chizhov [38], K. Choi [11], A.R. Chomont [74a,74b], Y. Chou [102], E.Y.S. Chow [113], T. Chowdhury [33g], L.D. Christopher [33g], K.L. Chu [64a], M.C. Chu [64a], X. Chu [14a,14d], J. Chudoba [130], J.J. Chwastowski [85], D. Cieri [109], K.M. Ciesla [84a], V. Cindro [92], A. Ciocio [17a], F. Cirotto [71a,71b], Z.H. Citron [168,m], M. Citterio [70a], D.A. Ciubotaru [27b], B.M. Ciungu [154], A. Clark [56], P.J. Clark [52], J.M. Clavijo Columbie [48], S.E. Clawson [100], C. Clement [47a,47b], J. Clercx [48], L. Clissa [23b,23a], Y. Coadou [101], M. Cobal [68a,68c], A. Coccaro [57b], R.F. Coelho Barrue [129a], R. Coelho Lopes De Sa [102], S. Coelli [70a], H. Cohen [150], A.E.C. Coimbra [70a,70b], B. Cole [41], J. Collot [60], P. Conde Muiño [129a,129g], S.H. Connell [33c], I.A. Connelly [59], E.I. Conroy [125], F. Conventi [71a,ah], H.G. Cooke [20], A.M. Cooper-Sarkar [125], F. Cormier [163], L.D. Corpe [36], M. Corradi [74a,74b], E.E. Corrigan [97], F. Corriveau [103,y], A. Cortes-Gonzalez [18], M.J. Costa [162], F. Costanza [4], D. Costanzo [138], B.M. Cote [118], G. Cowan [94], J.W. Cowley [32], K. Cranmer [116], S. Crépé-Renaudin [60], F. Crescioli [126], M. Cristinziani [140], M. Cristoforetti [77a,77b,d], V. Croft [157], G. Crosetti [43b,43a], A. Cueto [36], T. Cuhadar Donszelmann [159], H. Cui [14a,14d], Z. Cui [7], A.R. Cukierman [142], W.R. Cunningham [59], F. Curcio [43b,43a], P. Czodrowski [36], M.M. Czurylo [63b], M.J. Da Cunha Sargedas De Sousa [62a], J.V. Da Fonseca Pinto [81b], C. Da Via [100], W. Dabrowski [84a], T. Dado [49], S. Dahbi [33g], T. Dai [105], C. Dallapiccola [102], M. Dam [42], G. D'amen [29], V. D'Amico [76a,76b], J. Damp [99], J.R. Dandoy [127], M.F. Daneri [30], M. Danninger [141], V. Dao [36], G. Darbo [57b], S. Darmora [6], S.J. Das [29,aj], A. Dattagupta [122], S. D'Auria [70a,70b], C. David [155b], T. Davidek [132], D.R. Davis [51], B. Davis-Purcell [34], I. Dawson [93], K. De [8], R. De Asmundis [71a], M. De Beurs [113], S. De Castro [23b,23a], N. De Groot [112], P. de Jong [113], H. De la Torre [106], A. De Maria [14c], A. De Salvo [74a], U. De Sanctis [75a,75b], M. De Santis [75a,75b], A. De Santo [145], J.B. De Vivie De Regie [60], D.V. Dedovich [38], J. Degens [113], A.M. Deiana [44], F. Del Corso [23b,23a], J. Del Peso [98], F. Del Rio [63a], F. Deliot [134], C.M. Delitzsch [49], M. Della Pietra [71a,71b], D. Della Volpe [56], A. Dell'Acqua [36], L. Dell'Asta [70a,70b], M. Delmastro [4], P.A. Delsart [60], S. Demers [171], M. Demichev [38], S.P. Denisov [37], L. D'Eramo [114], D. Derendarz [85], F. Derue [126], P. Dervan [91], K. Desch [24], K. Dette [154], C. Deutsch [24], P.O. Deviveiros [36], F.A. Di Bello [74a,74b], A. Di Ciaccio [75a,75b], L. Di Ciaccio [4], A. Di Domenico [74a,74b], C. Di Donato [71a,71b], A. Di Girolamo [36], G. Di Gregorio [73a,73b], A. Di Luca [77a,77b], B. Di Micco [76a,76b], R. Di Nardo [76a,76b], C. Diaconu [101], F.A. Dias [113], T. Dias Do Vale [141], M.A. Diaz [136a,136b], F.G. Diaz Capriles [24], M. Didenko [162], E.B. Diehl [105], L. Diehl [54], S. Díez Cornell [48], C. Diez Pardos [140], C. Dimitriadi [24,160], A. Dimitrievska [17a], W. Ding [14b], J. Dingfelder [24], I-M. Dinu [27b], S.J. Dittmeier [63b], F. Dittus [36], F. Djama [101], T. Djobava [148b], J.I. Djuvsland [16], D. Dodsworth [26], C. Doglioni [100,97], J. Dolejsi [132], Z. Dolezal [132], M. Donadelli [81c], B. Dong [62c], J. Donini [40], A. D'Onofrio [14c], M. D'Onofrio [91], J. Dopke [133], A. Doria [71a], M.T. Dova [89], A.T. Doyle [59], M.A. Draguet [125], E. Drechsler [141], E. Dreyer [168], I. Drivas-koulouris [10], A.S. Drobac [157], D. Du [62a], T.A. du Pree [113], F. Dubinin [37],

M. Dubovsky [28a], E. Duchovni [168], G. Duckeck [108], O.A. Ducu [36], D. Duda [109], A. Dudarev [36], M. D'uffizi [100], L. Duflot [66], M. Dührssen [36], C. Dülsen [170], A.E. Dumitriu [27b], M. Dunford [63a], S. Dungs [49], K. Dunne [47a,47b], A. Duperrin [101], H. Duran Yildiz [3a], M. Düren [58], A. Durglishvili [148b], B.L. Dwyer [114], G.I. Dyckes [17a], M. Dyndal [84a], S. Dysch [100], B.S. Dziedzic [85], Z.O. Earnshaw [145], B. Eckerova [28a], M.G. Eggleston [51], E. Egidio Purcino De Souza [81b], L.F. Ehrke [56], G. Eigen [16], K. Einsweiler [17a], T. Ekelof [160], P.A. Ekman [97], Y. El Ghazali [35b], H. El Jarrari [35e,147], A. El Moussaouy [35a], V. Ellajosyula [160], M. Ellert [160], F. Ellinghaus [170], A.A. Elliot [93], N. Ellis [36], J. Elmsheuser [29], M. Elsing [36], D. Emeliyanov [133], A. Emerman [41], Y. Enari [152], I. Ene [17a], S. Epari [13], J. Erdmann [49], A. Ereditato [19], P.A. Erland [85], M. Errenst [170], M. Escalier [66], C. Escobar [162], E. Etzion [150], G. Evans [129a], H. Evans [67], M.O. Evans [145], A. Ezhilov [37], S. Ezzarqtouni [35a], F. Fabbri [59], L. Fabbri [23b,23a], G. Facini [95], V. Fadeyev [135], R.M. Fakhrutdinov [37], S. Falciano [74a], L.F. Falda Ulhoa Coelho [36], P.J. Falke [24], S. Falke [36], J. Faltova [132], Y. Fan [14a], Y. Fang [14a,14d], G. Fanourakis [46], M. Fanti [70a,70b], M. Faraj [68a,68b], A. Farbin [8], A. Farilla [76a], T. Farooque [106], S.M. Farrington [52], F. Fassi [35e], D. Fassouliotis [9], M. Faucci Giannelli [75a,75b], W.J. Fawcett [32], L. Fayard [66], O.L. Fedin [37,a], G. Fedotov [37], M. Feickert [161], L. Feligioni [101], A. Fell [138], D.E. Fellers [122], C. Feng [62b], M. Feng [14b], M.J. Fenton [159], A.B. Fenyuk [37], L. Ferencz [48], S.W. Ferguson [45], J. Ferrando [48], A. Ferrari [160], P. Ferrari [113], R. Ferrari [72a], D. Ferrere [56], C. Ferretti [105], F. Fiedler [99], A. Filipčič [92], E.K. Filmer [1], F. Filthaut [112], M.C.N. Fiolhais [129a,129c,c], L. Fiorini [162], F. Fischer [140], W.C. Fisher [106], T. Fitschen [20,66], I. Fleck [140], P. Fleischmann [105], T. Flick [170], L. Flores [127], M. Flores [33d,ad], L.R. Flores Castillo [64a], F.M. Follega [77a,77b], N. Fomin [16], J.H. Foo [154], B.C. Forland [67], A. Formica [134], A.C. Forti [100], E. Fortin [101], A.W. Fortman [61], M.G. Foti [17a], L. Fountas [9,j], D. Fournier [66], H. Fox [90], P. Francavilla [73a,73b], S. Francescato [61], M. Franchini [23b,23a], S. Franchino [63a], D. Francis [36], L. Franco [112], L. Franconi [19], M. Franklin [61], G. Frattari [26], A.C. Freegard [93], P.M. Freeman [20], W.S. Freund [81b], N. Fritzsche [50], A. Froch [54], D. Froidevaux [36], J.A. Frost [125], Y. Fu [62a], M. Fujimoto [117], E. Fullana Torregrosa [162,*], J. Fuster [162], A. Gabrielli [23b,23a], A. Gabrielli [36], P. Gadow [48], G. Gagliardi [57b,57a], L.G. Gagnon [17a], G.E. Gallardo [125], E.J. Gallas [125], B.J. Gallop [133], R. Gamboa Goni [93], K.K. Gan [118], S. Ganguly [152], J. Gao [62a], Y. Gao [52], F.M. Garay Walls [136a,136b], B. Garcia [29], C. García [162], J.E. García Navarro [162], J.A. García Pascual [14a], M. Garcia-Sciveres [17a], R.W. Gardner [39], D. Garg [79], R.B. Garg [142,q], S. Gargiulo [54], C.A. Garner [154], V. Garonne [29], S.J. Gasiorowski [137], P. Gaspar [81b], G. Gaudio [72a], V. Gautam [13], P. Gauzzi [74a,74b], I.L. Gavrilenko [37], A. Gavrilyuk [37], C. Gay [163], G. Gaycken [48], E.N. Gazis [10], A.A. Geanta [27b], C.M. Gee [135], J. Geisen [97], M. Geisen [99], C. Gemme [57b], M.H. Genest [60], S. Gentile [74a,74b], S. George [94], W.F. George [20], T. Geralis [46], L.O. Gerlach [55], P. Gessinger-Befurt [36], M. Ghasemi Bostanabad [164], M. Ghneimat [140], A. Ghosal [140], A. Ghosh [159], A. Ghosh [7], B. Giacobbe [23b], S. Giagu [74a,74b], N. Giangiacomi [154], P. Giannetti [73a], A. Giannini [62a], S.M. Gibson [94], M. Gignac [135], D.T. Gil [84b], A.K. Gilbert [84a], B.J. Gilbert [41], D. Gillberg [34], G. Gilles [113], N.E.K. Gillwald [48], L. Ginabat [126], D.M. Gingrich [2,ag], M.P. Giordani [68a,68c], P.F. Giraud [134], G. Giugliarelli [68a,68c], D. Giugni [70a], F. Giuli [36], I. Gkialas [9,j], L.K. Gladilin [37], C. Glasman [98], G.R. Gledhill [122], M. Glisic [122], I. Gnesi [43b,f], Y. Go [29,aj], M. Goblirsch-Kolb [26], D. Godin [107], S. Goldfarb [104], T. Golling [56], M.G.D. Gololo [33g], D. Golubkov [37], J.P. Gombas [106], A. Gomes [129a,129b], G. Gomes Da Silva [140], A.J. Gomez Delegido [162], R. Goncalves Gama [55], R. Gonçalo [129a,129c], G. Gonella [122], L. Gonella [20], A. Gongadze [38], F. Gonnella [20], J.L. Gonski [41],

R.Y. González Andana [52], S. González de la Hoz [162], S. Gonzalez Fernandez [13], R. Gonzalez Lopez [91], C. Gonzalez Renteria [17a], R. Gonzalez Suarez [160], S. Gonzalez-Sevilla [56], G.R. Gonzalvo Rodriguez [162], L. Goossens [36], N.A. Gorasia [20], P.A. Gorbounov [37], B. Gorini [36], E. Gorini [69a,69b], A. Gorišek [92], A.T. Goshaw [51], M.I. Gostkin [38], C.A. Gottardo [112], M. Gouighri [35b], V. Goumarre [48], A.G. Goussiou [137], N. Govender [33c], C. Goy [4], I. Grabowska-Bold [84a], K. Graham [34], E. Gramstad [124], S. Grancagnolo [18], M. Grandi [145], V. Gratchev [37,*], P.M. Gravila [27f], F.G. Gravili [69a,69b], H.M. Gray [17a], M. Greco [69a,69b], C. Grefe [24], I.M. Gregor [48], P. Grenier [142], C. Grieco [13], A.A. Grillo [135], K. Grimm [31,n], S. Grinstein [13,v], J.-F. Grivaz [66], E. Gross [168], J. Grosse-Knetter [55], C. Grud [105], A. Grummer [111], J.C. Grundy [125], L. Guan [105], W. Guan [169], C. Gubbels [163], J.G.R. Guerrero Rojas [162], G. Guerrieri [68a,68c], F. Guescini [109], R. Gugel [99], J.A.M. Guhit [105], A. Guida [48], T. Guillemin [4], E. Guilloton [166,133], S. Guindon [36], F. Guo [14a,14d], J. Guo [62c], L. Guo [66], Y. Guo [105], R. Gupta [48], S. Gurbuz [24], S.S. Gurdasani [54], G. Gustavino [36], M. Guth [56], P. Gutierrez [119], L.F. Gutierrez Zagazeta [127], C. Gutschow [95], C. Guyot [134], C. Gwenlan [125], C.B. Gwilliam [91], E.S. Haaland [124], A. Haas [116], M. Habedank [48], C. Haber [17a], H.K. Hadavand [8], A. Hadef [99], S. Hadzic [109], M. Haleem [165], J. Haley [120], J.J. Hall [138], G.D. Hallewell [101], L. Halser [19], K. Hamano [164], H. Hamdaoui [35e], M. Hamer [24], G.N. Hamity [52], J. Han [62b], K. Han [62a], L. Han [14c], L. Han [62a], S. Han [17a], Y.F. Han [154], K. Hanagaki [82], M. Hance [135], D.A. Hangal [41,ac], M.D. Hank [39], R. Hankache [100], J.B. Hansen [42], J.D. Hansen [42], P.H. Hansen [42], K. Hara [156], D. Harada [56], T. Harenberg [170], S. Harkusha [37], Y.T. Harris [125], N.M. Harrison [118], P.F. Harrison [166], N.M. Hartman [142], N.M. Hartmann [108], Y. Hasegawa [139], A. Hasib [52], S. Haug [19], R. Hauser [106], M. Havranek [131], C.M. Hawkes [20], R.J. Hawkings [36], S. Hayashida [110], D. Hayden [106], C. Hayes [105], R.L. Hayes [163], C.P. Hays [125], J.M. Hays [93], H.S. Hayward [91], F. He [62a], Y. He [153], Y. He [126], M.P. Heath [52], V. Hedberg [97], A.L. Heggelund [124], N.D. Hehir [93,*], C. Heidegger [54], K.K. Heidegger [54], W.D. Heidorn [80], J. Heilman [34], S. Heim [48], T. Heim [17a], J.G. Heinlein [127], J.J. Heinrich [122], L. Heinrich [36], J. Hejbal [130], L. Helary [48], A. Held [116], S. Hellesund [124], C.M. Helling [163], S. Hellman [47a,47b], C. Helsens [36], R.C.W. Henderson [90], L. Henkelmann [32], A.M. Henriques Correia [36], H. Herde [142], Y. Hernández Jiménez [144], H. Herr [99], M.G. Herrmann [108], T. Herrmann [50], G. Herten [54], R. Hertenberger [108], L. Hervas [36], N.P. Hessey [155a], H. Hibi [83], E. Higón-Rodriguez [162], S.J. Hillier [20], I. Hinchliffe [17a], F. Hinterkeuser [24], M. Hirose [123], S. Hirose [156], D. Hirschbuehl [170], T.G. Hitchings [100], B. Hiti [92], J. Hobbs [144], R. Hobincu [27e], N. Hod [168], M.C. Hodgkinson [138], B.H. Hodkinson [32], A. Hoecker [36], J. Hofer [48], D. Hohn [54], T. Holm [24], M. Holzbock [109], L.B.A.H. Hommels [32], B.P. Honan [100], J. Hong [62c], T.M. Hong [128], Y. Hong [55], J.C. Honig [54], A. Hönle [109], B.H. Hooberman [161], W.H. Hopkins [6], Y. Horii [110], S. Hou [147], A.S. Howard [92], J. Howarth [59], J. Hoya [89], M. Hrabovsky [121], A. Hrynevich [37], T. Hryn'ova [4], P.J. Hsu [65], S.-C. Hsu [137], Q. Hu [41,ac], Y.F. Hu [14a,14d,ai], D.P. Huang [95], S. Huang [64b], X. Huang [14c], Y. Huang [62a], Y. Huang [14a], Z. Huang [100], Z. Hubacek [131], M. Huebner [24], F. Huegging [24], T.B. Huffman [125], M. Huhtinen [36], S.K. Huiberts [16], R. Hulsken [103], N. Huseynov [12,a], J. Huston [106], J. Huth [61], R. Hyneman [142], S. Hyrych [28a], G. Iacobucci [56], G. Iakovidis [29], I. Ibragimov [140], L. Iconomidou-Fayard [66], P. Iengo [71a,71b], R. Iguchi [152], T. Iizawa [56], Y. Ikegami [82], A. Ilg [19], N. Ilic [154], H. Imam [35a], T. Ingebretsen Carlson [47a,47b], G. Introzzi [72a,72b], M. Iodice [76a], V. Ippolito [74a,74b], M. Ishino [152], W. Islam [169], C. Issever [18,48], S. Istin [21a,ak], H. Ito [167], J.M. Iturbe Ponce [64a], R. Iuppa [77a,77b], A. Ivina [168], J.M. Izen [45],

V. Izzo [71a], P. Jacka [130,131], P. Jackson [1], R.M. Jacobs [48], B.P. Jaeger [141], C.S. Jagfeld [108], G. Jäkel [170], K. Jakobs [54], T. Jakoubek [168], J. Jamieson [59], K.W. Janas [84a], G. Jarlskog [97], A.E. Jaspan [91], T. Javůrek [36], M. Javurkova [102], F. Jeanneau [134], L. Jeanty [122], J. Jejelava [148a,aa], P. Jenni [54,g], C.E. Jessiman [34], S. Jézéquel [4], J. Jia [144], X. Jia [61], X. Jia [14a,14d], Z. Jia [14c], Y. Jiang [62a], S. Jiggins [52], J. Jimenez Pena [109], S. Jin [14c], A. Jinaru [27b], O. Jinnouchi [153], H. Jivan [33g], P. Johansson [138], K.A. Johns [7], C.A. Johnson [67], D.M. Jones [32], E. Jones [166], P. Jones [32], R.W.L. Jones [90], T.J. Jones [91], J. Jovicevic [15], X. Ju [17a], J.J. Junggeburth [36], A. Juste Rozas [13,v], S. Kabana [136e], A. Kaczmarska [85], M. Kado [74a,74b], H. Kagan [118], M. Kagan [142], A. Kahn [41], A. Kahn [127], C. Kahra [99], T. Kaji [167], E. Kajomovitz [149], N. Kakati [168], C.W. Kalderon [29], A. Kamenshchikov [154], N.J. Kang [135], Y. Kano [110], D. Kar [33g], K. Karava [125], M.J. Kareem [155b], E. Karentzos [54], I. Karkanias [151], S.N. Karpov [38], Z.M. Karpova [38], V. Kartvelishvili [90], A.N. Karyukhin [37], E. Kasimi [151], C. Kato [62d], J. Katzy [48], S. Kaur [34], K. Kawade [139], K. Kawagoe [88], T. Kawaguchi [110], T. Kawamoto [134], G. Kawamura [55], E.F. Kay [164], F.I. Kaya [157], S. Kazakos [13], V.F. Kazanin [37], Y. Ke [144], J.M. Keaveney [33a], R. Keeler [164], G.V. Kehris [61], J.S. Keller [34], A.S. Kelly [95], D. Kelsey [145], J.J. Kempster [20], J. Kendrick [20], K.E. Kennedy [41], O. Kepka [130], B.P. Kerridge [166], S. Kersten [170], B.P. Kerševan [92], L. Keszeghova [28a], S. Ketabchi Haghighat [154], M. Khandoga [126], A. Khanov [120], A.G. Kharlamov [37], T. Kharlamova [37], E.E. Khoda [137], T.J. Khoo [18], G. Khoriauli [165], J. Khubua [148b], Y.A.R. Khwaira [66], M. Kiehn [36], A. Kilgallon [122], D.W. Kim [47a,47b], E. Kim [153], Y.K. Kim [39], N. Kimura [95], A. Kirchhoff [55], D. Kirchmeier [50], C. Kirfel [24], J. Kirk [133], A.E. Kiryunin [109], T. Kishimoto [152], D.P. Kisliuk [154], C. Kitsaki [10], O. Kivernyk [24], M. Klassen [63a], C. Klein [34], L. Klein [165], M.H. Klein [105], M. Klein [91], U. Klein [91], P. Klimek [36], A. Klimentov [29], F. Klimpel [109], T. Klingl [24], T. Klioutchnikova [36], F.F. Klitzner [108], P. Kluit [113], S. Kluth [109], E. Kneringer [78], T.M. Knight [154], A. Knue [54], D. Kobayashi [88], R. Kobayashi [86], M. Kocian [142], T. Kodama [152], P. Kodyš [132], D.M. Koeck [145], P.T. Koenig [24], T. Koffas [34], N.M. Köhler [36], M. Kolb [134], I. Koletsou [4], T. Komarek [121], K. Köneke [54], A.X.Y. Kong [1], T. Kono [117], N. Konstantinidis [95], B. Konya [97], R. Kopeliansky [67], S. Koperny [84a], K. Korcyl [85], K. Kordas [151], G. Koren [150], A. Korn [95], S. Korn [55], I. Korolkov [13], N. Korotkova [37], B. Kortman [113], O. Kortner [109], S. Kortner [109], W.H. Kostecka [114], V.V. Kostyukhin [140], A. Kotsokechagia [66], A. Kotwal [51], A. Koulouris [36], A. Kourkoumeli-Charalampidi [72a,72b], C. Kourkoumelis [9], E. Kourlitis [6], O. Kovanda [145], R. Kowalewski [164], W. Kozanecki [134], A.S. Kozhin [37], V.A. Kramarenko [37], G. Kramberger [92], P. Kramer [99], M.W. Krasny [126], A. Krasznahorkay [36], J.A. Kremer [99], T. Kresse [50], J. Kretzschmar [91], K. Kreul [18], P. Krieger [154], F. Krieter [108], S. Krishnamurthy [102], A. Krishnan [63b], M. Krivos [132], K. Krizka [17a], K. Kroeninger [49], H. Kroha [109], J. Kroll [130], J. Kroll [127], K.S. Krowpman [106], U. Kruchonak [38], H. Krüger [24], N. Krumnack [80], M.C. Kruse [51], J.A. Krzysiak [85], A. Kubota [153], O. Kuchinskaia [37], S. Kuday [3a], D. Kuechler [48], J.T. Kuechler [48], S. Kuehn [36], T. Kuhl [48], V. Kukhtin [38], Y. Kulchitsky [37,a], S. Kuleshov [136d,136b], M. Kumar [33g], N. Kumari [101], M. Kuna [60], A. Kupco [130], T. Kupfer [49], A. Kupich [37], O. Kuprash [54], H. Kurashige [83], L.L. Kurchaninov [155a], Y.A. Kurochkin [37], A. Kurova [37], E.S. Kuwertz [36], M. Kuze [153], A.K. Kvam [102], J. Kvita [121], T. Kwan [103], K.W. Kwok [64a], C. Lacasta [162], F. Lacava [74a,74b], H. Lacker [18], D. Lacour [126], N.N. Lad [95], E. Ladygin [38], B. Laforge [126], T. Lagouri [136e], S. Lai [55], I.K. Lakomiec [84a], N. Lalloue [60], J.E. Lambert [119], S. Lammers [67], W. Lampl [7], C. Lampoudis [151], A.N. Lancaster [114],

E. Lançon [29], U. Landgraf [54], M.P.J. Landon [93], V.S. Lang [54], R.J. Langenberg [102], A.J. Lankford [159], F. Lanni [29], K. Lantzsch [24], A. Lanza [72a], A. Lapertosa [57b,57a], J.F. Laporte [134], T. Lari [70a], F. Lasagni Manghi [23b], M. Lassnig [36], V. Latonova [130], T.S. Lau [64a], A. Laudrain [99], A. Laurier [34], S.D. Lawlor [94], Z. Lawrence [100], M. Lazzaroni [70a,70b], B. Le [100], B. Leban [92], A. Lebedev [80], M. LeBlanc [36], T. LeCompte [6], F. Ledroit-Guillon [60], A.C.A. Lee [95], G.R. Lee [16], L. Lee [61], S.C. Lee [147], S. Lee [47a,47b], L.L. Leeuw [33c], H.P. Lefebvre [94], M. Lefebvre [164], C. Leggett [17a], K. Lehmann [141], G. Lehmann Miotto [36], W.A. Leight [102], A. Leisos [151,u], M.A.L. Leite [81c], C.E. Leitgeb [48], R. Leitner [132], K.J.C. Leney [44], T. Lenz [24], S. Leone [73a], C. Leonidopoulos [52], A. Leopold [143], C. Leroy [107], R. Les [106], C.G. Lester [32], M. Levchenko [37], J. Levêque [4], D. Levin [105], L.J. Levinson [168], D.J. Lewis [20], B. Li [14b], B. Li [62b], C. Li [62a], C-Q. Li [62c,62d], H. Li [62a], H. Li [62b], H. Li [14c], H. Li [62b], J. Li [62c], K. Li [137], L. Li [62c], M. Li [14a,14d], Q.Y. Li [62a], S. Li [62d,62c,e], T. Li [62b], X. Li [103], Z. Li [62b], Z. Li [125], Z. Li [103], Z. Li [91], Z. Liang [14a], M. Liberatore [48], B. Liberti [75a], K. Lie [64c], J. Lieber Marin [81b], K. Lin [106], R.A. Linck [67], R.E. Lindley [7], J.H. Lindon [2], A. Linss [48], E. Lipeles [127], A. Lipniacka [16], T.M. Liss [161,ae], A. Lister [163], J.D. Little [4], B. Liu [14a], B.X. Liu [141], D. Liu [62d,62c], J.B. Liu [62a], J.K.K. Liu [32], K. Liu [62d,62c], M. Liu [62a], M.Y. Liu [62a], P. Liu [14a], Q. Liu [62d,137,62c], X. Liu [62a], Y. Liu [48], Y. Liu [14c,14d], Y.L. Liu [105], Y.W. Liu [62a], M. Livan [72a,72b], J. Llorente Merino [141], S.L. Lloyd [93], E.M. Lobodzinska [48], P. Loch [7], S. Loffredo [75a,75b], T. Lohse [18], K. Lohwasser [138], M. Lokajicek [130,*], J.D. Long [161], I. Longarini [74a,74b], L. Longo [69a,69b], R. Longo [161], I. Lopez Paz [36], A. Lopez Solis [48], J. Lorenz [108], N. Lorenzo Martinez [4], A.M. Lory [108], A. Lösle [54], X. Lou [47a,47b], X. Lou [14a,14d], A. Lounis [66], J. Love [6], P.A. Love [90], J.J. Lozano Bahilo [162], G. Lu [14a,14d], M. Lu [79], S. Lu [127], Y.J. Lu [65], H.J. Lubatti [137], C. Luci [74a,74b], F.L. Lucio Alves [14c], A. Lucotte [60], F. Luehring [67], I. Luise [144], O. Lukianchuk [66], O. Lundberg [143], B. Lund-Jensen [143], N.A. Luongo [122], M.S. Lutz [150], D. Lynn [29], H. Lyons [91], R. Lysak [130], E. Lytken [97], F. Lyu [14a], V. Lyubushkin [38], T. Lyubushkina [38], H. Ma [29], L.L. Ma [62b], Y. Ma [95], D.M. Mac Donell [164], G. Maccarrone [53], J.C. MacDonald [138], R. Madar [40], W.F. Mader [50], J. Maeda [83], T. Maeno [29], M. Maerker [50], V. Magerl [54], J. Magro [68a,68c], H. Maguire [138], D.J. Mahon [41], C. Maidantchik [81b], A. Maio [129a,129b,129d], K. Maj [84a], O. Majersky [28a], S. Majewski [122], N. Makovec [66], V. Maksimovic [15], B. Malaescu [126], Pa. Malecki [85], V.P. Maleev [37], F. Malek [60], D. Malito [43b,43a], U. Mallik [79], C. Malone [32], S. Maltezos [10], S. Malyukov [38], J. Mamuzic [13], G. Mancini [53], G. Manco [72a,72b], J.P. Mandalia [93], I. Mandić [92], L. Manhaes de Andrade Filho [81a], I.M. Maniatis [151], M. Manisha [134], J. Manjarres Ramos [50], D.C. Mankad [168], K.H. Mankinen [97], A. Mann [108], A. Manousos [78], B. Mansoulie [134], S. Manzoni [36], A. Marantis [151,u], G. Marchiori [5], M. Marcisovsky [130], L. Marcoccia [75a,75b], C. Marcon [97], M. Marinescu [20], M. Marjanovic [119], Z. Marshall [17a], S. Marti-Garcia [162], T.A. Martin [166], V.J. Martin [52], B. Martin dit Latour [16], L. Martinelli [74a,74b], M. Martinez [13,v], P. Martinez Agullo [162], V.I. Martinez Outschoorn [102], P. Martinez Suarez [13], S. Martin-Haugh [133], V.S. Martoiu [27b], A.C. Martyniuk [95], A. Marzin [36], S.R. Maschek [109], L. Masetti [99], T. Mashimo [152], J. Masik [100], A.L. Maslennikov [37], L. Massa [23b], P. Massarotti [71a,71b], P. Mastrandrea [73a,73b], A. Mastroberardino [43b,43a], T. Masubuchi [152], T. Mathisen [160], A. Matic [108], N. Matsuzawa [152], J. Maurer [27b], B. Maček [92], D.A. Maximov [37], R. Mazini [147], I. Maznas [151], M. Mazza [106], S.M. Mazza [135], C. Mc Ginn [29], J.P. Mc Gowan [103], S.P. Mc Kee [105], T.G. McCarthy [109], W.P. McCormack [17a], E.F. McDonald [104], A.E. McDougall [113], J.A. Mcfayden [145], G. Mchedlidze [148b], R.P. Mckenzie [33g], T.C. Mclachlan [48], D.J. Mclaughlin [95], K.D. McLean [164], S.J. McMahon [133], P.C. McNamara [104], R.A. McPherson [164,y], J.E. Mdhluli [33g], S. Meehan [36],

T. Megy [40], S. Mehlhase [108], A. Mehta [91], B. Meirose [45], D. Melini [149], B.R. Mellado Garcia [33g], A.H. Melo [55], F. Meloni [48], E.D. Mendes Gouveia [129a], A.M. Mendes Jacques Da Costa [20], H.Y. Meng [154], L. Meng [90], S. Menke [109], M. Mentink [36], E. Meoni [43b,43a], C. Merlassino [125], L. Merola [71a,71b], C. Meroni [70a,70b], G. Merz [105], O. Meshkov [37], J.K.R. Meshreki [140], J. Metcalfe [6], A.S. Mete [6], C. Meyer [67], J-P. Meyer [134], M. Michetti [18], R.P. Middleton [133], L. Mijović [52], G. Mikenberg [168], M. Mikestikova [130], M. Mikuž [92], H. Mildner [138], A. Milic [154], C.D. Milke [44], D.W. Miller [39], L.S. Miller [34], A. Milov [168], D.A. Milstead [47a,47b], T. Min [14c], A.A. Minaenko [37], I.A. Minashvili [148b], L. Mince [59], A.I. Mincer [116], B. Mindur [84a], M. Mineev [38], Y. Minegishi [152], Y. Mino [86], L.M. Mir [13], M. Miralles Lopez [162], M. Mironova [125], T. Mitani [167], A. Mitra [166], V.A. Mitsou [162], O. Miu [154], P.S. Miyagawa [93], Y. Miyazaki [88], A. Mizukami [82], J.U. Mjörnmark [97], T. Mkrtchyan [63a], M. Mlynarikova [114], T. Moa [47a,47b], S. Mobius [55], K. Mochizuki [107], P. Moder [48], P. Mogg [108], A.F. Mohammed [14a,14d], S. Mohapatra [41], G. Mokgatitswane [33g], B. Mondal [140], S. Mondal [131], K. Mönig [48], E. Monnier [101], L. Monsonis Romero [162], J. Montejo Berlingen [36], M. Montella [118], F. Monticelli [89], N. Morange [66], A.L. Moreira De Carvalho [129a], M. Moreno Llácer [162], C. Moreno Martinez [13], P. Morettini [57b], S. Morgenstern [166], M. Morii [61], M. Morinaga [152], V. Morisbak [124], A.K. Morley [36], F. Morodei [74a,74b], L. Morvaj [36], P. Moschovakos [36], B. Moser [36], M. Mosidze [148b], T. Moskalets [54], P. Moskvitina [112], J. Moss [31,o], E.J.W. Moyse [102], S. Muanza [101], J. Mueller [128], D. Muenstermann [90], R. Müller [19], G.A. Mullier [97], J.J. Mullin [127], D.P. Mungo [70a,70b], J.L. Munoz Martinez [13], D. Munoz Perez [162], F.J. Munoz Sanchez [100], M. Murin [100], W.J. Murray [166,133], A. Murrone [70a,70b], J.M. Muse [119], M. Muškinja [17a], C. Mwewa [29], A.G. Myagkov [37,a], A.J. Myers [8], A.A. Myers [128], G. Myers [67], M. Myska [131], B.P. Nachman [17a], O. Nackenhorst [49], A. Nag [50], K. Nagai [125], K. Nagano [82], J.L. Nagle [29,aj], E. Nagy [101], A.M. Nairz [36], Y. Nakahama [82], K. Nakamura [82], H. Nanjo [123], R. Narayan [44], E.A. Narayanan [111], I. Naryshkin [37], M. Naseri [34], C. Nass [24], G. Navarro [22a], J. Navarro-Gonzalez [162], R. Nayak [150], P.Y. Nechaeva [37], F. Nechansky [48], T.J. Neep [20], A. Negri [72a,72b], M. Negrini [23b], C. Nellist [112], C. Nelson [103], K. Nelson [105], S. Nemecek [130], M. Nessi [36,h], M.S. Neubauer [161], F. Neuhaus [99], J. Neundorf [48], R. Newhouse [163], P.R. Newman [20], C.W. Ng [128], Y.S. Ng [18], Y.W.Y. Ng [159], B. Ngair [35e], H.D.N. Nguyen [107], R.B. Nickerson [125], R. Nicolaidou [134], J. Nielsen [135], M. Niemeyer [55], N. Nikiforou [36], V. Nikolaenko [37,a], I. Nikolic-Audit [126], K. Nikolopoulos [20], P. Nilsson [29], H.R. Nindhito [56], A. Nisati [74a], N. Nishu [2], R. Nisius [109], J-E. Nitschke [50], E.K. Nkadimeng [33g], S.J. Noacco Rosende [89], T. Nobe [152], D.L. Noel [32], Y. Noguchi [86], T. Nommensen [146], M.A. Nomura [29], M.B. Norfolk [138], R.R.B. Norisam [95], B.J. Norman [34], J. Novak [92], T. Novak [48], O. Novgorodova [50], L. Novotny [131], R. Novotny [111], L. Nozka [121], K. Ntekas [159], E. Nurse [95], F.G. Oakham [34,ag], J. Ocariz [126], A. Ochi [83], I. Ochoa [129a], S. Oda [88], S. Oerdek [160], A. Ogrodnik [84a], A. Oh [100], C.C. Ohm [143], H. Oide [153], R. Oishi [152], M.L. Ojeda [48], Y. Okazaki [86], M.W. O'Keefe [91], Y. Okumura [152], A. Olariu [27b], L.F. Oleiro Seabra [129a], S.A. Olivares Pino [136e], D. Oliveira Damazio [29], D. Oliveira Goncalves [81a], J.L. Oliver [159], M.J.R. Olsson [159], A. Olszewski [85], J. Olszowska [85,*], Ö.O. Öncel [54], D.C. O'Neil [141], A.P. O'Neill [19], A. Onofre [129a,129e], P.U.E. Onyisi [11], M.J. Oreglia [39], G.E. Orellana [89], D. Orestano [76a,76b], N. Orlando [13], R.S. Orr [154], V. O'Shea [59], R. Ospanov [62a], G. Otero y Garzon [30], H. Otono [88], P.S. Ott [63a], G.J. Ottino [17a], M. Ouchrif [35d], J. Ouellette [29,aj], F. Ould-Saada [124], M. Owen [59], R.E. Owen [133], K.Y. Oyulmaz [21a], V.E. Ozcan [21a], N. Ozturk [8], S. Ozturk [21d], J. Pacalt [121], H.A. Pacey [32], A. Pacheco Pages [13], C. Padilla Aranda [13],

G. Padovano [74a,74b], S. Pagan Griso [17a], G. Palacino [67], A. Palazzo [69a,69b], S. Palazzo [52], S. Palestini [36], M. Palka [84b], J. Pan [171], T. Pan [64a], D.K. Panchal [11], C.E. Pandini [113], J.G. Panduro Vazquez [94], H. Pang [14b], P. Pani [48], G. Panizzo [68a,68c], L. Paolozzi [56], C. Papadatos [107], S. Parajuli [44], A. Paramonov [6], C. Paraskevopoulos [10], D. Paredes Hernandez [64b], T.H. Park [154], M.A. Parker [32], F. Parodi [57b,57a], E.W. Parrish [114], V.A. Parrish [52], J.A. Parsons [41], U. Parzefall [54], B. Pascual Dias [107], L. Pascual Dominguez [150], V.R. Pascuzzi [17a], F. Pasquali [113], E. Pasqualucci [74a], S. Passaggio [57b], F. Pastore [94], P. Pasuwan [47a,47b], J.R. Pater [100], J. Patton [91], T. Pauly [36], J. Pearkes [142], M. Pedersen [124], R. Pedro [129a], S.V. Peleganchuk [37], O. Penc [130], C. Peng [64b], H. Peng [62a], M. Penzin [37], B.S. Peralva [81a,81d], A.P. Pereira Peixoto [60], L. Pereira Sanchez [47a,47b], D.V. Perepelitsa [29,aj], E. Perez Codina [155a], M. Perganti [10], L. Perini [70a,70b,*], H. Pernegger [36], A. Perrevoort [112], O. Perrin [40], K. Peters [48], R.F.Y. Peters [100], B.A. Petersen [36], T.C. Petersen [42], E. Petit [101], V. Petousis [131], C. Petridou [151], A. Petrukhin [140], M. Pettee [17a], N.E. Pettersson [36], A. Petukhov [37], K. Petukhova [132], A. Peyaud [134], R. Pezoa [136f], L. Pezzotti [36], G. Pezzullo [171], T. Pham [104], P.W. Phillips [133], M.W. Phipps [161], G. Piacquadio [144], E. Pianori [17a], F. Piazza [70a,70b], R. Piegaia [30], D. Pietreanu [27b], A.D. Pilkington [100], M. Pinamonti [68a,68c], J.L. Pinfold [2], B.C. Pinheiro Pereira [129a], C. Pitman Donaldson [95], D.A. Pizzi [34], L. Pizzimento [75a,75b], A. Pizzini [113], M.-A. Pleier [29], V. Plesanovs [54], V. Pleskot [132], E. Plotnikova [38], G. Poddar [4], R. Poettgen [97], R. Poggi [56], L. Poggioli [126], I. Pogrebnyak [106], D. Pohl [24], I. Pokharel [55], S. Polacek [132], G. Polesello [72a], A. Poley [141,155a], R. Polifka [131], A. Polini [23b], C.S. Pollard [125], Z.B. Pollock [118], V. Polychronakos [29], D. Ponomarenko [37], L. Pontecorvo [36], S. Popa [27a], G.A. Popeneciu [27d], D.M. Portillo Quintero [155a], S. Pospisil [131], P. Postolache [27c], K. Potamianos [125], I.N. Potrap [38], C.J. Potter [32], H. Potti [1], T. Poulsen [48], J. Poveda [162], G. Pownall [48], M.E. Pozo Astigarraga [36], A. Prades Ibanez [162], M.M. Prapa [46], J. Pretel [54], D. Price [100], M. Primavera [69a], M.A. Principe Martin [98], M.L. Proffitt [137], N. Proklova [37], K. Prokofiev [64c], G. Proto [75a,75b], S. Protopopescu [29], J. Proudfoot [6], M. Przybycien [84a], J.E. Puddefoot [138], D. Pudzha [37], P. Puzo [66], D. Pyatiizbyantseva [37], J. Qian [105], Y. Qin [100], T. Qiu [93], A. Quadt [55], M. Queitsch-Maitland [24], G. Rabanal Bolanos [61], D. Rafanoharana [54], F. Ragusa [70a,70b], J.L. Rainbolt [39], J.A. Raine [56], S. Rajagopalan [29], E. Ramakoti [37], K. Ran [14a,14d], V. Raskina [126], D.F. Rassloff [63a], S. Rave [99], B. Ravina [59], I. Ravinovich [168], M. Raymond [36], A.L. Read [124], N.P. Readioff [138], D.M. Rebuzzi [72a,72b], G. Redlinger [29], K. Reeves [45], J.A. Reidelsturz [170], D. Reikher [150], A. Reiss [99], A. Rej [140], C. Rembser [36], A. Renardi [48], M. Renda [27b], M.B. Rendel [109], A.G. Rennie [59], S. Resconi [70a], M. Ressegotti [57b,57a], E.D. Resseguie [17a], S. Rettie [95], B. Reynolds [118], E. Reynolds [17a], M. Rezaei Estabragh [170], O.L. Rezanova [37], P. Reznicek [132], E. Ricci [77a,77b], R. Richter [109], S. Richter [47a,47b], E. Richter-Was [84b], M. Ridel [126], P. Rieck [116], P. Riedler [36], M. Rijssenbeek [144], A. Rimoldi [72a,72b], M. Rimoldi [48], L. Rinaldi [23b,23a], T.T. Rinn [29], M.P. Rinnagel [108], G. Ripellino [143], I. Riu [13], P. Rivadeneira [48], J.C. Rivera Vergara [164], F. Rizatdinova [120], E. Rizvi [93], C. Rizzi [56], B.A. Roberts [166], B.R. Roberts [17a], S.H. Robertson [103,y], M. Robin [48], D. Robinson [32], C.M. Robles Gajardo [136f], M. Robles Manzano [99], A. Robson [59], A. Rocchi [75a,75b], C. Roda [73a,73b], S. Rodriguez Bosca [63a], Y. Rodriguez Garcia [22a], A. Rodriguez Rodriguez [54], A.M. Rodríguez Vera [155b], S. Roe [36], J.T. Roemer [159], A.R. Roepe-Gier [119], J. Roggel [170], O. Røhne [124], R.A. Rojas [164], B. Roland [54], C.P.A. Roland [67], J. Roloff [29], A. Romaniouk [37], E. Romano [72a,72b], M. Romano [23b], A.C. Romero Hernandez [161], N. Rompotis [91], L. Roos [126], S. Rosati [74a], B.J. Rosser [39], E. Rossi [4],

E. Rossi [71a,71b], L.P. Rossi [57b], L. Rossini [48], R. Rosten [118], M. Rotaru [27b], B. Rottler [54], D. Rousseau [66], D. Rousso [32], G. Rovelli [72a,72b], A. Roy [161], A. Rozanov [101], Y. Rozen [149], X. Ruan [33g], A. Rubio Jimenez [162], A.J. Ruby [91], T.A. Ruggeri [1], F. Rühr [54], A. Ruiz-Martinez [162], A. Rummler [36], Z. Rurikova [54], N.A. Rusakovich [38], H.L. Russell [164], J.P. Rutherfoord [7], E.M. Rüttinger [138], K. Rybacki [90], M. Rybar [132], E.B. Rye [124], A. Ryzhov [37], J.A. Sabater Iglesias [56], P. Sabatini [162], L. Sabetta [74a,74b], H.F-W. Sadrozinski [135], F. Safai Tehrani [74a], B. Safarzadeh Samani [145], M. Safdari [142], S. Saha [103], M. Sahinsoy [109], M. Saimpert [134], M. Saito [152], T. Saito [152], D. Salamani [36], G. Salamanna [76a,76b], A. Salnikov [142], J. Salt [162], A. Salvador Salas [13], D. Salvatore [43b,43a], F. Salvatore [145], A. Salzburger [36], D. Sammel [54], D. Sampsonidis [151], D. Sampsonidou [62d,62c], J. Sánchez [162], A. Sanchez Pineda [4], V. Sanchez Sebastian [162], H. Sandaker [124], C.O. Sander [48], J.A. Sandesara [102], M. Sandhoff [170], C. Sandoval [22b], D.P.C. Sankey [133], A. Sansoni [53], L. Santi [74a,74b], C. Santoni [40], H. Santos [129a,129b], S.N. Santpur [17a], A. Santra [168], K.A. Saoucha [138], J.G. Saraiva [129a,129d], J. Sardain [101], O. Sasaki [82], K. Sato [156], C. Sauer [63b], F. Sauerburger [54], E. Sauvan [4], P. Savard [154,ag], R. Sawada [152], C. Sawyer [133], L. Sawyer [96], I. Sayago Galvan [162], C. Sbarra [23b], A. Sbrizzi [23b,23a], T. Scanlon [95], J. Schaarschmidt [137], P. Schacht [109], D. Schaefer [39], U. Schäfer [99], A.C. Schaffer [66], D. Schaile [108], R.D. Schamberger [144], E. Schanet [108], C. Scharf [18], V.A. Schegelsky [37], D. Scheirich [132], F. Schenck [18], M. Schernau [159], C. Scheulen [55], C. Schiavi [57b,57a], Z.M. Schillaci [26], E.J. Schioppa [69a,69b], M. Schioppa [43b,43a], B. Schlag [99], K.E. Schleicher [54], S. Schlenker [36], K. Schmieden [99], C. Schmitt [99], S. Schmitt [48], L. Schoeffel [134], A. Schoening [63b], P.G. Scholer [54], E. Schopf [125], M. Schott [99], J. Schovancova [36], S. Schramm [56], F. Schroeder [170], H-C. Schultz-Coulon [63a], M. Schumacher [54], B.A. Schumm [135], Ph. Schune [134], A. Schwartzman [142], T.A. Schwarz [105], Ph. Schwemling [134], R. Schwienhorst [106], A. Sciandra [135], G. Sciolla [26], F. Scuri [73a], F. Scutti [104], C.D. Sebastiani [91], K. Sedlaczek [49], P. Seema [18], S.C. Seidel [111], A. Seiden [135], B.D. Seidlitz [41], T. Seiss [39], C. Seitz [48], J.M. Seixas [81b], G. Sekhniaidze [71a], S.J. Sekula [44], L. Selem [4], N. Semprini-Cesari [23b,23a], S. Sen [51], D. Sengupta [56], V. Senthilkumar [162], L. Serin [66], L. Serkin [68a,68b], M. Sessa [76a,76b], H. Severini [119], S. Sevova [142], F. Sforza [57b,57a], A. Sfyrla [56], E. Shabalina [55], R. Shaheen [143], J.D. Shahinian [127], N.W. Shaikh [47a,47b], D. Shaked Renous [168], L.Y. Shan [14a], M. Shapiro [17a], A. Sharma [36], A.S. Sharma [163], P. Sharma [79], S. Sharma [48], P.B. Shatalov [37], K. Shaw [145], S.M. Shaw [100], Q. Shen [62c], P. Sherwood [95], L. Shi [95], C.O. Shimmin [171], Y. Shimogama [167], J.D. Shinner [94], I.P.J. Shipsey [125], S. Shirabe [60], M. Shiyakova [38,x], J. Shlomi [168], M.J. Shochet [39], J. Shojaii [104], D.R. Shope [143], S. Shrestha [118], E.M. Shrif [33g], M.J. Shroff [164], P. Sicho [130], A.M. Sickles [161], E. Sideras Haddad [33g], O. Sidiropoulou [36], A. Sidoti [23b], F. Siegert [50], Dj. Sijacki [15], R. Sikora [84a], F. Sili [89], J.M. Silva [20], M.V. Silva Oliveira [36], S.B. Silverstein [47a], S. Simion [66], R. Simoniello [36], E.L. Simpson [59], N.D. Simpson [97], S. Simsek [21d], S. Sindhu [55], P. Sinervo [154], V. Sinetckii [37], S. Singh [141], S. Singh [154], S. Sinha [48], S. Sinha [33g], M. Sioli [23b,23a], I. Siral [122], S.Yu. Sivoklokov [37,*], J. Sjölin [47a,47b], A. Skaf [55], E. Skorda [97], P. Skubic [119], M. Slawinska [85], V. Smakhtin [168], B.H. Smart [133], J. Smiesko [132], S.Yu. Smirnov [37], Y. Smirnov [37], L.N. Smirnova [37,a], O. Smirnova [97], E.A. Smith [39], H.A. Smith [125], J.L. Smith [91], R. Smith [142], M. Smizanska [90], K. Smolek [131], A. Smykiewicz [85], A.A. Snesarev [37], H.L. Snoek [113], S. Snyder [29], R. Sobie [164,y], A. Soffer [150], C.A. Solans Sanchez [36], E.Yu. Soldatov [37], U. Soldevila [162], A.A. Solodkov [37], S. Solomon [54], A. Soloshenko [38], K. Solovieva [54], O.V. Solovyanov [37], V. Solovyev [37], P. Sommer [36], A. Sonay [13], W.Y. Song [155b], A. Sopczak [131], A.L. Sopio [95], F. Sopkova [28b], V. Sothilingam [63a], S. Sottocornola [72a,72b],

R. Soualah [115b], Z. Soumaimi [35e], D. South [48], S. Spagnolo [69a,69b], M. Spalla [109], F. Spanò [94], D. Sperlich [54], G. Spigo [36], M. Spina [145], S. Spinali [90], D.P. Spiteri [59], M. Spousta [132], E.J. Staats [34], A. Stabile [70a,70b], R. Stamen [63a], M. Stamenkovic [113], A. Stampekis [20], M. Standke [24], E. Stanecka [85], B. Stanislaus [17a], M.M. Stanitzki [48], M. Stankaityte [125], B. Stapf [48], E.A. Starchenko [37], G.H. Stark [135], J. Stark [101,ab], D.M. Starko [155b], P. Staroba [130], P. Starovoitov [63a], S. Stärz [103], R. Staszewski [85], G. Stavropoulos [46], J. Steentoft [160], P. Steinberg [29], A.L. Steinhebel [122], B. Stelzer [141,155a], H.J. Stelzer [128], O. Stelzer-Chilton [155a], H. Stenzel [58], T.J. Stevenson [145], G.A. Stewart [36], M.C. Stockton [36], G. Stoicea [27b], M. Stolarski [129a], S. Stonjek [109], A. Straessner [50], J. Strandberg [143], S. Strandberg [47a,47b], M. Strauss [119], T. Strebler [101], P. Strizenec [28b], R. Ströhmer [165], D.M. Strom [122], L.R. Strom [48], R. Stroynowski [44], A. Strubig [47a,47b], S.A. Stucci [29], B. Stugu [16], J. Stupak [119], N.A. Styles [48], D. Su [142], S. Su [62a], W. Su [62d,137,62c], X. Su [62a,66], K. Sugizaki [152], V.V. Sulin [37], M.J. Sullivan [91], D.M.S. Sultan [77a,77b], L. Sultanaliyeva [37], S. Sultansoy [3b], T. Sumida [86], S. Sun [105], S. Sun [169], O. Sunneborn Gudnadottir [160], M.R. Sutton [145], M. Svatos [130], M. Swiatlowski [155a], T. Swirski [165], I. Sykora [28a], M. Sykora [132], T. Sykora [132], D. Ta [99], K. Tackmann [48,w], A. Taffard [159], R. Tafirout [155a], J.S. Tafoya Vargas [66], R.H.M. Taibah [126], R. Takashima [87], K. Takeda [83], E.P. Takeva [52], Y. Takubo [82], M. Talby [101], A.A. Talyshev [37], K.C. Tam [64b], N.M. Tamir [150], A. Tanaka [152], J. Tanaka [152], R. Tanaka [66], M. Tanasini [57b,57a], J. Tang [62c], Z. Tao [163], S. Tapia Araya [80], S. Tapprogge [99], A. Tarek Abouelfadl Mohamed [106], S. Tarem [149], K. Tariq [62b], G. Tarna [27b], G.F. Tartarelli [70a], P. Tas [132], M. Tasevsky [130], E. Tassi [43b,43a], A.C. Tate [161], G. Tateno [152], Y. Tayalati [35e], G.N. Taylor [104], W. Taylor [155b], H. Teagle [91], A.S. Tee [169], R. Teixeira De Lima [142], P. Teixeira-Dias [94], J.J. Teoh [154], K. Terashi [152], J. Terron [98], S. Terzo [13], M. Testa [53], R.J. Teuscher [154,y], A. Thaler [78], N. Themistokleous [52], T. Theveneaux-Pelzer [18], O. Thielmann [170], D.W. Thomas [94], J.P. Thomas [20], E.A. Thompson [48], P.D. Thompson [20], E. Thomson [127], E.J. Thorpe [93], Y. Tian [55], V. Tikhomirov [37,a], Yu.A. Tikhonov [37], S. Timoshenko [37], E.X.L. Ting [1], P. Tipton [171], S. Tisserant [101], S.H. Tlou [33g], A. Tnourji [40], K. Todome [23b,23a], S. Todorova-Nova [132], S. Todt [50], M. Togawa [82], J. Tojo [88], S. Tokár [28a], K. Tokushuku [82], R. Tombs [32], M. Tomoto [82,110], L. Tompkins [142,q], P. Tornambe [102], E. Torrence [122], H. Torres [50], E. Torró Pastor [162], M. Toscani [30], C. Tosciri [39], D.R. Tovey [138], A. Traeet [16], I.S. Trandafir [27b], T. Trefzger [165], A. Tricoli [29], I.M. Trigger [155a], S. Trincaz-Duvoid [126], D.A. Trischuk [163], B. Trocmé [60], A. Trofymov [66], C. Troncon [70a], L. Truong [33c], M. Trzebinski [85], A. Trzupek [85], F. Tsai [144], M. Tsai [105], A. Tsiamis [151], P.V. Tsiareshka [37], S. Tsigaridas [155a], A. Tsirigotis [151,u], V. Tsiskaridze [144], E.G. Tskhadadze [148a], M. Tsopoulou [151], Y. Tsujikawa [86], I.I. Tsukerman [37], V. Tsulaia [17a], S. Tsuno [82], O. Tsur [149], D. Tsybychev [144], Y. Tu [64b], A. Tudorache [27b], V. Tudorache [27b], A.N. Tuna [36], S. Turchikhin [38], I. Turk Cakir [3a], R. Turra [70a], T. Turtuvshin [38], P.M. Tuts [41], S. Tzamarias [151], P. Tzanis [10], E. Tzovara [99], K. Uchida [152], F. Ukegawa [156], P.A. Ulloa Poblete [136c], G. Unal [36], M. Unal [11], A. Undrus [29], G. Unel [159], K. Uno [152], J. Urban [28b], P. Urquijo [104], G. Usai [8], R. Ushioda [153], M. Usman [107], Z. Uysal [21b], V. Vacek [131], B. Vachon [103], K.O.H. Vadla [124], T. Vafeiadis [36], C. Valderanis [108], E. Valdes Santurio [47a,47b], M. Valente [155a], S. Valentinetti [23b,23a], A. Valero [162], A. Vallier [101,ab], J.A. Valls Ferrer [162], T.R. Van Daalen [137], P. Van Gemmeren [6], S. Van Stroud [95], I. Van Vulpen [113], M. Vanadia [75a,75b], W. Vandelli [36], M. Vandenbroucke [134], E.R. Vandewall [120], D. Vannicola [150], L. Vannoli [57b,57a], R. Vari [74a], E.W. Varnes [7], C. Varni [17a], T. Varol [147], D. Varouchas [66],

L. Varriale [162], K.E. Varvell [146], M.E. Vasile [27b], L. Vaslin [40], G.A. Vasquez [164], F. Vazeille [40], T. Vazquez Schroeder [36], J. Veatch [31], V. Vecchio [100], M.J. Veen [113], I. Veliscek [125], L.M. Veloce [154], F. Veloso [129a,129c], S. Veneziano [74a], A. Ventura [69a,69b], A. Verbytskyi [109], M. Verducci [73a,73b], C. Vergis [24], M. Verissimo De Araujo [81b], W. Verkerke [113], J.C. Vermeulen [113], C. Vernieri [142], P.J. Verschuuren [94], M. Vessella [102], M.L. Vesterbacka [116], M.C. Vetterli [141,ag], A. Vgenopoulos [151], N. Viaux Maira [136f], T. Vickey [138], O.E. Vickey Boeriu [138], G.H.A. Viehhauser [125], L. Vigani [63b], M. Villa [23b,23a], M. Villaplana Perez [162], E.M. Villhauer [52], E. Vilucchi [53], M.G. Vincter [34], G.S. Virdee [20], A. Vishwakarma [52], C. Vittori [23b,23a], I. Vivarelli [145], V. Vladimirov [166], E. Voevodina [109], F. Vogel [108], P. Vokac [131], J. Von Ahnen [48], E. Von Toerne [24], B. Vormwald [36], V. Vorobel [132], K. Vorobev [37], M. Vos [162], J.H. Vossebeld [91], M. Vozak [113], L. Vozdecky [93], N. Vranjes [15], M. Vranjes Milosavljevic [15], M. Vreeswijk [113], R. Vuillermet [36], O. Vujinovic [99], I. Vukotic [39], S. Wada [156], C. Wagner [102], W. Wagner [170], S. Wahdan [170], H. Wahlberg [89], R. Wakasa [156], M. Wakida [110], V.M. Walbrecht [109], J. Walder [133], R. Walker [108], W. Walkowiak [140], A.M. Wang [61], A.Z. Wang [169], C. Wang [62a], C. Wang [62c], H. Wang [17a], J. Wang [64a], P. Wang [44], R.-J. Wang [99], R. Wang [61], R. Wang [6], S.M. Wang [147], S. Wang [62b], T. Wang [62a], W.T. Wang [79], W.X. Wang [62a], X. Wang [14c], X. Wang [161], X. Wang [62c], Y. Wang [62d], Y. Wang [14c], Z. Wang [105], Z. Wang [62d,51,62c], Z. Wang [105], A. Warburton [103], R.J. Ward [20], N. Warrack [59], A.T. Watson [20], M.F. Watson [20], G. Watts [137], B.M. Waugh [95], A.F. Webb [11], C. Weber [29], M.S. Weber [19], S.A. Weber [34], S.M. Weber [63a], C. Wei [62a], Y. Wei [125], A.R. Weidberg [125], J. Weingarten [49], M. Weirich [99], C. Weiser [54], C.J. Wells [48], T. Wenaus [29], B. Wendland [49], T. Wengler [36], N.S. Wenke [109], N. Wermes [24], M. Wessels [63a], K. Whalen [122], A.M. Wharton [90], A.S. White [61], A. White [8], M.J. White [1], D. Whiteson [159], L. Wickremasinghe [123], W. Wiedenmann [169], C. Wiel [50], M. Wielers [133], N. Wieseotte [99], C. Wiglesworth [42], L.A.M. Wiik-Fuchs [54], D.J. Wilbern [119], H.G. Wilkens [36], D.M. Williams [41], H.H. Williams [127], S. Williams [32], S. Willocq [102], P.J. Windischhofer [125], F. Winklmeier [122], B.T. Winter [54], M. Wittgen [142], M. Wobisch [96], A. Wolf [99], R. Wölker [125], J. Wollrath [159], M.W. Wolter [85], H. Wolters [129a,129c], V.W.S. Wong [163], A.F. Wongel [48], S.D. Worm [48], B.K. Wosiek [85], K.W. Woźniak [85], K. Wraight [59], J. Wu [14a,14d], M. Wu [64a], S.L. Wu [169], X. Wu [56], Y. Wu [62a], Z. Wu [134,62a], J. Wuerzinger [125], T.R. Wyatt [100], B.M. Wynne [52], S. Xella [42], L. Xia [14c], M. Xia [14b], J. Xiang [64c], X. Xiao [105], M. Xie [62a], X. Xie [62a], J. Xiong [17a], I. Xiotidis [145], D. Xu [14a], H. Xu [62a], H. Xu [62a], L. Xu [62a], R. Xu [127], T. Xu [105], W. Xu [105], Y. Xu [14b], Z. Xu [62b], Z. Xu [142], B. Yabsley [146], S. Yacoob [33a], N. Yamaguchi [88], Y. Yamaguchi [153], H. Yamauchi [156], T. Yamazaki [17a], Y. Yamazaki [83], J. Yan [62c], S. Yan [125], Z. Yan [25], H.J. Yang [62c,62d], H.T. Yang [17a], S. Yang [62a], T. Yang [64c], X. Yang [62a], X. Yang [14a], Y. Yang [44], Z. Yang [62a,105], W-M. Yao [17a], Y.C. Yap [48], H. Ye [14c], J. Ye [44], S. Ye [29], X. Ye [62a], Y. Yeh [95], I. Yeletskikh [38], M.R. Yexley [90], P. Yin [41], K. Yorita [167], C.J.S. Young [54], C. Young [142], M. Yuan [105], R. Yuan [62b,k], L. Yue [95], X. Yue [63a], M. Zaazoua [35e], B. Zabinski [85], E. Zaid [52], T. Zakareishvili [148b], N. Zakharchuk [34], S. Zambito [56], J. Zang [152], D. Zanzi [54], O. Zaplatilek [131], S.V. Zeißner [49], C. Zeitnitz [170], J.C. Zeng [161], D.T. Zenger Jr [26], O. Zenin [37], T. Ženiš [28a], S. Zenz [93], S. Zerradi [35a], D. Zerwas [66], B. Zhang [14c], D.F. Zhang [138], G. Zhang [14b], J. Zhang [6], K. Zhang [14a,14d], L. Zhang [14c], R. Zhang [169], S. Zhang [105], T. Zhang [152], X. Zhang [62c], X. Zhang [62b], Z. Zhang [17a], Z. Zhang [66], H. Zhao [137], P. Zhao [51], T. Zhao [62b], Y. Zhao [135], Z. Zhao [62a], A. Zhemchugov [38], Z. Zheng [142], D. Zhong [161], B. Zhou [105], C. Zhou [169], H. Zhou [7], N. Zhou [62c], Y. Zhou [7], C.G. Zhu [62b],

C. Zhu [14a,14d], H.L. Zhu [62a], H. Zhu [14a], J. Zhu [105], Y. Zhu [62a], X. Zhuang [14a], K. Zhukov [37], V. Zhulanov [37], N.I. Zimine [38], J. Zinsser [63b], M. Ziolkowski [140], L. Živković [15], A. Zoccoli [23b,23a], K. Zoch [56], T.G. Zorbas [138], O. Zormpa [46], W. Zou [41], L. Zwalinski [36]

[1] Department of Physics, University of Adelaide, Adelaide; Australia
[2] Department of Physics, University of Alberta, Edmonton AB; Canada
[3] [(a)] Department of Physics, Ankara University, Ankara; [(b)] Division of Physics, TOBB University of Economics and Technology, Ankara; Türkiye
[4] LAPP, Université Savoie Mont Blanc, CNRS/IN2P3, Annecy; France
[5] APC, Université Paris Cité, CNRS/IN2P3, Paris; France
[6] High Energy Physics Division, Argonne National Laboratory, Argonne IL; United States of America
[7] Department of Physics, University of Arizona, Tucson AZ; United States of America
[8] Department of Physics, University of Texas at Arlington, Arlington TX; United States of America
[9] Physics Department, National and Kapodistrian University of Athens, Athens; Greece
[10] Physics Department, National Technical University of Athens, Zografou; Greece
[11] Department of Physics, University of Texas at Austin, Austin TX; United States of America
[12] Institute of Physics, Azerbaijan Academy of Sciences, Baku; Azerbaijan
[13] Institut de Física d'Altes Energies (IFAE), Barcelona Institute of Science and Technology, Barcelona; Spain
[14] [(a)] Institute of High Energy Physics, Chinese Academy of Sciences, Beijing; [(b)] Physics Department, Tsinghua University, Beijing; [(c)] Department of Physics, Nanjing University, Nanjing; [(d)] University of Chinese Academy of Science (UCAS), Beijing; China
[15] Institute of Physics, University of Belgrade, Belgrade; Serbia
[16] Department for Physics and Technology, University of Bergen, Bergen; Norway
[17] [(a)] Physics Division, Lawrence Berkeley National Laboratory, Berkeley CA; [(b)] University of California, Berkeley CA; United States of America
[18] Institut für Physik, Humboldt Universität zu Berlin, Berlin; Germany
[19] Albert Einstein Center for Fundamental Physics and Laboratory for High Energy Physics, University of Bern, Bern; Switzerland
[20] School of Physics and Astronomy, University of Birmingham, Birmingham; United Kingdom
[21] [(a)] Department of Physics, Bogazici University, Istanbul; [(b)] Department of Physics Engineering, Gaziantep University, Gaziantep; [(c)] Department of Physics, Istanbul University, Istanbul; [(d)] Istinye University, Sariyer, Istanbul; Türkiye
[22] [(a)] Facultad de Ciencias y Centro de Investigaciónes, Universidad Antonio Nariño, Bogotá; [(b)] Departamento de Física, Universidad Nacional de Colombia, Bogotá; Colombia
[23] [(a)] Dipartimento di Fisica e Astronomia A. Righi, Università di Bologna, Bologna; [(b)] INFN Sezione di Bologna; Italy
[24] Physikalisches Institut, Universität Bonn, Bonn; Germany
[25] Department of Physics, Boston University, Boston MA; United States of America
[26] Department of Physics, Brandeis University, Waltham MA; United States of America
[27] [(a)] Transilvania University of Brasov, Brasov; [(b)] Horia Hulubei National Institute of Physics and Nuclear Engineering, Bucharest; [(c)] Department of Physics, Alexandru Ioan Cuza University of Iasi, Iasi; [(d)] National Institute for Research and Development of Isotopic and Molecular Technologies, Physics Department, Cluj-Napoca; [(e)] University Politehnica Bucharest, Bucharest; [(f)] West University in Timisoara, Timisoara; [(g)] Faculty of Physics, University of Bucharest, Bucharest; Romania
[28] [(a)] Faculty of Mathematics, Physics and Informatics, Comenius University, Bratislava; [(b)] Department of Subnuclear Physics, Institute of Experimental Physics of the Slovak Academy of Sciences, Kosice; Slovak Republic
[29] Physics Department, Brookhaven National Laboratory, Upton NY; United States of America
[30] Universidad de Buenos Aires, Facultad de Ciencias Exactas y Naturales, Departamento de Física, y CONICET, Instituto de Física de Buenos Aires (IFIBA), Buenos Aires; Argentina
[31] California State University, CA; United States of America
[32] Cavendish Laboratory, University of Cambridge, Cambridge; United Kingdom
[33] [(a)] Department of Physics, University of Cape Town, Cape Town; [(b)] iThemba Labs, Western Cape; [(c)] Department of Mechanical Engineering Science, University of Johannesburg, Johannesburg; [(d)] National Institute of Physics, University of the Philippines Diliman (Philippines); [(e)] University of South Africa, Department of Physics, Pretoria; [(f)] University of Zululand, KwaDlangezwa; [(g)] School of Physics, University of the Witwatersrand, Johannesburg; South Africa
[34] Department of Physics, Carleton University, Ottawa ON; Canada
[35] [(a)] Faculté des Sciences Ain Chock, Réseau Universitaire de Physique des Hautes Energies – Université Hassan II, Casablanca; [(b)] Faculté des Sciences, Université Ibn-Tofail, Kénitra; [(c)] Faculté des Sciences Semlalia, Université Cadi Ayyad, LPHEA, Marrakech; [(d)] LPMR, Faculté des Sciences, Université Mohamed Premier, Oujda; [(e)] Faculté des sciences, Université Mohammed V, Rabat; [(f)] Institute of Applied Physics, Mohammed VI Polytechnic University, Ben Guerir; Morocco
[36] CERN, Geneva; Switzerland
[37] Affiliated with an institute covered by a cooperation agreement with CERN
[38] Affiliated with an international laboratory covered by a cooperation agreement with CERN
[39] Enrico Fermi Institute, University of Chicago, Chicago IL; United States of America
[40] LPC, Université Clermont Auvergne, CNRS/IN2P3, Clermont-Ferrand; France
[41] Nevis Laboratory, Columbia University, Irvington NY; United States of America
[42] Niels Bohr Institute, University of Copenhagen, Copenhagen; Denmark
[43] [(a)] Dipartimento di Fisica, Università della Calabria, Rende; [(b)] INFN Gruppo Collegato di Cosenza, Laboratori Nazionali di Frascati; Italy
[44] Physics Department, Southern Methodist University, Dallas TX; United States of America
[45] Physics Department, University of Texas at Dallas, Richardson TX; United States of America
[46] National Centre for Scientific Research "Demokritos", Agia Paraskevi; Greece
[47] [(a)] Department of Physics, Stockholm University; [(b)] Oskar Klein Centre, Stockholm; Sweden
[48] Deutsches Elektronen-Synchrotron DESY, Hamburg and Zeuthen; Germany
[49] Fakultät Physik , Technische Universität Dortmund, Dortmund; Germany
[50] Institut für Kern- und Teilchenphysik, Technische Universität Dresden, Dresden; Germany
[51] Department of Physics, Duke University, Durham NC; United States of America
[52] SUPA – School of Physics and Astronomy, University of Edinburgh, Edinburgh; United Kingdom
[53] INFN e Laboratori Nazionali di Frascati, Frascati; Italy
[54] Physikalisches Institut, Albert-Ludwigs-Universität Freiburg, Freiburg; Germany
[55] II. Physikalisches Institut, Georg-August-Universität Göttingen, Göttingen; Germany
[56] Département de Physique Nucléaire et Corpusculaire, Université de Genève, Genève; Switzerland
[57] [(a)] Dipartimento di Fisica, Università di Genova, Genova; [(b)] INFN Sezione di Genova; Italy
[58] II. Physikalisches Institut, Justus-Liebig-Universität Giessen, Giessen; Germany
[59] SUPA – School of Physics and Astronomy, University of Glasgow, Glasgow; United Kingdom
[60] LPSC, Université Grenoble Alpes, CNRS/IN2P3, Grenoble INP, Grenoble; France
[61] Laboratory for Particle Physics and Cosmology, Harvard University, Cambridge MA; United States of America
[62] [(a)] Department of Modern Physics and State Key Laboratory of Particle Detection and Electronics, University of Science and Technology of China, Hefei; [(b)] Institute of Frontier and Interdisciplinary Science and Key Laboratory of Particle Physics and Particle Irradiation (MOE), Shandong University, Qingdao; [(c)] School of Physics and Astronomy, Shanghai Jiao Tong University, Key Laboratory for Particle Astrophysics and Cosmology (MOE), SKLPPC, Shanghai; [(d)] Tsung-Dao Lee Institute, Shanghai; China
[63] [(a)] Kirchhoff-Institut für Physik, Ruprecht-Karls-Universität Heidelberg, Heidelberg; [(b)] Physikalisches Institut, Ruprecht-Karls-Universität Heidelberg, Heidelberg; Germany

[64] [(a)] Department of Physics, Chinese University of Hong Kong, Shatin, N.T., Hong Kong; [(b)] Department of Physics, University of Hong Kong, Hong Kong; [(c)] Department of Physics and Institute for Advanced Study, Hong Kong University of Science and Technology, Clear Water Bay, Kowloon, Hong Kong; China
[65] Department of Physics, National Tsing Hua University, Hsinchu; Taiwan
[66] IJCLab, Université Paris-Saclay, CNRS/IN2P3, 91405, Orsay; France
[67] Department of Physics, Indiana University, Bloomington IN; United States of America
[68] [(a)] INFN Gruppo Collegato di Udine, Sezione di Trieste, Udine; [(b)] ICTP, Trieste; [(c)] Dipartimento Politecnico di Ingegneria e Architettura, Università di Udine, Udine; Italy
[69] [(a)] INFN Sezione di Lecce; [(b)] Dipartimento di Matematica e Fisica, Università del Salento, Lecce; Italy
[70] [(a)] INFN Sezione di Milano; [(b)] Dipartimento di Fisica, Università di Milano, Milano; Italy
[71] [(a)] INFN Sezione di Napoli; [(b)] Dipartimento di Fisica, Università di Napoli, Napoli; Italy
[72] [(a)] INFN Sezione di Pavia; [(b)] Dipartimento di Fisica, Università di Pavia, Pavia; Italy
[73] [(a)] INFN Sezione di Pisa; [(b)] Dipartimento di Fisica E. Fermi, Università di Pisa, Pisa; Italy
[74] [(a)] INFN Sezione di Roma; [(b)] Dipartimento di Fisica, Sapienza Università di Roma, Roma; Italy
[75] [(a)] INFN Sezione di Roma Tor Vergata; [(b)] Dipartimento di Fisica, Università di Roma Tor Vergata, Roma; Italy
[76] [(a)] INFN Sezione di Roma Tre; [(b)] Dipartimento di Matematica e Fisica, Università Roma Tre, Roma; Italy
[77] [(a)] INFN-TIFPA; [(b)] Università degli Studi di Trento, Trento; Italy
[78] Universität Innsbruck, Department of Astro and Particle Physics, Innsbruck; Austria
[79] University of Iowa, Iowa City IA; United States of America
[80] Department of Physics and Astronomy, Iowa State University, Ames IA; United States of America
[81] [(a)] Departamento de Engenharia Elétrica, Universidade Federal de Juiz de Fora (UFJF), Juiz de Fora; [(b)] Universidade Federal do Rio De Janeiro COPPE/EE/IF, Rio de Janeiro; [(c)] Instituto de Física, Universidade de São Paulo, São Paulo; [(d)] Rio de Janeiro State University, Rio de Janeiro; Brazil
[82] KEK, High Energy Accelerator Research Organization, Tsukuba; Japan
[83] Graduate School of Science, Kobe University, Kobe; Japan
[84] [(a)] AGH University of Krakow, Faculty of Physics and Applied Computer Science, Krakow; [(b)] Marian Smoluchowski Institute of Physics, Jagiellonian University, Krakow; Poland
[85] Institute of Nuclear Physics Polish Academy of Sciences, Krakow; Poland
[86] Faculty of Science, Kyoto University, Kyoto; Japan
[87] Kyoto University of Education, Kyoto; Japan
[88] Research Center for Advanced Particle Physics and Department of Physics, Kyushu University, Fukuoka; Japan
[89] Instituto de Física La Plata, Universidad Nacional de La Plata and CONICET, La Plata; Argentina
[90] Physics Department, Lancaster University, Lancaster; United Kingdom
[91] Oliver Lodge Laboratory, University of Liverpool, Liverpool; United Kingdom
[92] Department of Experimental Particle Physics, Jožef Stefan Institute and Department of Physics, University of Ljubljana, Ljubljana; Slovenia
[93] School of Physics and Astronomy, Queen Mary University of London, London; United Kingdom
[94] Department of Physics, Royal Holloway University of London, Egham; United Kingdom
[95] Department of Physics and Astronomy, University College London, London; United Kingdom
[96] Louisiana Tech University, Ruston LA; United States of America
[97] Fysiska institutionen, Lunds universitet, Lund; Sweden
[98] Departamento de Física Teorica C-15 and CIAFF, Universidad Autónoma de Madrid, Madrid; Spain
[99] Institut für Physik, Universität Mainz, Mainz; Germany
[100] School of Physics and Astronomy, University of Manchester, Manchester; United Kingdom
[101] CPPM, Aix-Marseille Université, CNRS/IN2P3, Marseille; France
[102] Department of Physics, University of Massachusetts, Amherst MA; United States of America
[103] Department of Physics, McGill University, Montreal QC; Canada
[104] School of Physics, University of Melbourne, Victoria; Australia
[105] Department of Physics, University of Michigan, Ann Arbor MI; United States of America
[106] Department of Physics and Astronomy, Michigan State University, East Lansing MI; United States of America
[107] Group of Particle Physics, University of Montreal, Montreal QC; Canada
[108] Fakultät für Physik, Ludwig-Maximilians-Universität München, München; Germany
[109] Max-Planck-Institut für Physik (Werner-Heisenberg-Institut), München; Germany
[110] Graduate School of Science and Kobayashi-Maskawa Institute, Nagoya University, Nagoya; Japan
[111] Department of Physics and Astronomy, University of New Mexico, Albuquerque NM; United States of America
[112] Institute for Mathematics, Astrophysics and Particle Physics, Radboud University/Nikhef, Nijmegen; Netherlands
[113] Nikhef National Institute for Subatomic Physics and University of Amsterdam, Amsterdam; Netherlands
[114] Department of Physics, Northern Illinois University, DeKalb IL; United States of America
[115] [(a)] New York University Abu Dhabi, Abu Dhabi; [(b)] University of Sharjah, Sharjah; United Arab Emirates
[116] Department of Physics, New York University, New York NY; United States of America
[117] Ochanomizu University, Otsuka, Bunkyo-ku, Tokyo; Japan
[118] Ohio State University, Columbus OH; United States of America
[119] Homer L. Dodge Department of Physics and Astronomy, University of Oklahoma, Norman OK; United States of America
[120] Department of Physics, Oklahoma State University, Stillwater OK; United States of America
[121] Palacký University, Joint Laboratory of Optics, Olomouc; Czech Republic
[122] Institute for Fundamental Science, University of Oregon, Eugene, OR; United States of America
[123] Graduate School of Science, Osaka University, Osaka; Japan
[124] Department of Physics, University of Oslo, Oslo; Norway
[125] Department of Physics, Oxford University, Oxford; United Kingdom
[126] LPNHE, Sorbonne Université, Université Paris Cité, CNRS/IN2P3, Paris; France
[127] Department of Physics, University of Pennsylvania, Philadelphia PA; United States of America
[128] Department of Physics and Astronomy, University of Pittsburgh, Pittsburgh PA; United States of America
[129] [(a)] Laboratório de Instrumentação e Física Experimental de Partículas – LIP, Lisboa; [(b)] Departamento de Física, Faculdade de Ciências, Universidade de Lisboa, Lisboa; [(c)] Departamento de Física, Universidade de Coimbra, Coimbra; [(d)] Centro de Física Nuclear da Universidade de Lisboa, Lisboa; [(e)] Departamento de Física, Universidade do Minho, Braga; [(f)] Departamento de Física Teórica y del Cosmos, Universidad de Granada, Granada (Spain); [(g)] Departamento de Física, Instituto Superior Técnico, Universidade de Lisboa, Lisboa; Portugal
[130] Institute of Physics of the Czech Academy of Sciences, Prague; Czech Republic
[131] Czech Technical University in Prague, Prague; Czech Republic
[132] Charles University, Faculty of Mathematics and Physics, Prague; Czech Republic
[133] Particle Physics Department, Rutherford Appleton Laboratory, Didcot; United Kingdom
[134] IRFU, CEA, Université Paris-Saclay, Gif-sur-Yvette; France
[135] Santa Cruz Institute for Particle Physics, University of California Santa Cruz, Santa Cruz CA; United States of America
[136] [(a)] Departamento de Física, Pontificia Universidad Católica de Chile, Santiago; [(b)] Millennium Institute for Subatomic physics at high energy frontier (SAPHIR), Santiago; [(c)] Instituto de Investigación Multidisciplinario en Ciencia y Tecnología, y Departamento de Física, Universidad de La Serena; [(d)] Universidad Andres Bello, Department of Physics, Santiago; [(e)] Instituto de Alta Investigación, Universidad de Tarapacá, Arica; [(f)] Departamento de Física, Universidad Técnica Federico Santa María, Valparaíso; Chile
[137] Department of Physics, University of Washington, Seattle WA; United States of America

Eur. Phys. J. C (2025) 85:210
https://doi.org/10.1140/epjc/s10052-025-13740-x

THE EUROPEAN PHYSICAL JOURNAL C

Regular Article - Experimental Physics

Measurement of the associated production of a top-antitop-quark pair and a Higgs boson decaying into a $b\bar{b}$ pair in pp collisions at $\sqrt{s} = 13$ TeV using the ATLAS detector at the LHC

ATLAS Collaboration[*]

CERN,1211 Geneva 23, Switzerland

Received: 16 July 2024 / Accepted: 2 January 2025
© CERN for the benefit of the ATLAS Collaboration 2025

Abstract This paper reports the measurement of Higgs boson production in association with a $t\bar{t}$ pair in the $H \to b\bar{b}$ decay channel. The analysis uses 140 fb^{-1} of 13 TeV proton–proton collision data collected with the ATLAS detector at the Large Hadron Collider. The final states with one or two electrons or muons are employed. An excess of events over the expected background is found with an observed (expected) significance of 4.6 (5.4) standard deviations. The $t\bar{t}H$ cross-section is $\sigma_{t\bar{t}H} = 411\,^{+101}_{-92}$ fb $= 411 \pm 54$(stat.) $^{+85}_{-75}$(syst.) fb for a Higgs boson mass of 125.09 GeV, consistent with the prediction of the Standard Model of 507^{+35}_{-50} fb. The cross-section is also measured differentially in bins of the Higgs boson transverse momentum within the simplified template cross-section framework.

Contents

1 Introduction . . . . . .
2 ATLAS detector . . . . . .
3 Data and Monte Carlo simulation samples . . . . . .
4 Objects and event selection . . . . . .
5 Background modelling . . . . . .
5.1 Modelling of $t\bar{t}$ + jets background . . . . . .
5.2 Non-prompt or mis-identified lepton background
6 Signal extraction . . . . . .
7 Systematic uncertainties . . . . . .
8 Results . . . . . .
9 Conclusion . . . . . .
References . . . . . .

1 Introduction

After the discovery of the Higgs boson [1–3] in 2012 by the ATLAS [4] and CMS [5] collaborations, attention has turned to detailed measurements of its properties and couplings as a means of testing the predictions of the Standard Model (SM) [6–8]. The Higgs boson coupling to the top quark, the heaviest particle in the SM, is of special interest as it could be very sensitive to effects of physics beyond the SM (BSM) [9]. It is indirectly constrained assuming no BSM contributions to loop-induced processes from measurements of gluon–gluon fusion Higgs boson production and decay into $\gamma\gamma$ [10,11]. The Higgs boson production in association with a pair of top quarks ($t\bar{t}H$), where the top quark couples to the Higgs boson at tree level, provides a possibility for a direct measurement of the top-quark's Yukawa coupling without assumptions about the potential presence of BSM physics [12–15]. It was observed by the ATLAS and CMS collaborations using several Higgs boson decay modes [16,17].

The decay into two b-quarks is predicted to have the largest branching fraction of about 58% [18] and has the advantage of allowing for the reconstruction of the Higgs boson four-momentum from the kinematics of its decay products. Furthermore, the $t\bar{t}H(b\bar{b})$ channel involves only fermionic Higgs boson couplings in the production and decay, leading to an enhanced sensitivity for probing them. However, this final state is affected by a large irreducible background arising from the $t\bar{t}$ production in associations with jets ($t\bar{t}$+jets), in particular when the jets originate from b- or c-quarks, which is challenging to predict theoretically.

The ATLAS Collaboration has measured the $t\bar{t}H(b\bar{b})$ production at $\sqrt{s} = 13$ TeV in the final state with at least one lepton using the full Run 2 dataset collected in proton–proton (pp) collisions at the Large Hadron Collider (LHC) [19] between 2015 and 2018, corresponding to an integrated luminosity of 139 fb^{-1} [20]. The measured signal strength, defined as the ratio of the measured cross-section to that predicted by the SM, was found to be $0.35^{+0.36}_{-0.34}$, and corresponds to an observed (expected) significance of 1.0 (2.7) standard deviations. The signal strength was also measured differen-

[*] e-mail: atlas.publications@cern.ch

Published online: 24 February 2025

tially in five intervals of the Higgs boson transverse momentum (p_{T}^{H}) in the simplified template cross-section framework (STXS) [18], probing potential p_{T}^{H}-dependent deviations from the SM expectation.

The CMS Collaboration also recently released a measurement of the $t\bar{t}H(b\bar{b})$ production using 138 fb^{-1} of data collected at $\sqrt{s} = 13$ TeV in 2016–2018 [21]. The analysis achieved an observed (expected) significance of 1.3 (4.1) standard deviation and measured a signal strength of 0.33 ± 0.26. Additionally, the $t\bar{t}H$ production rate was determined in intervals of p_{T}^{H}.

This paper presents a re-analysis of the full Run 2 dataset collected at $\sqrt{s} = 13$ TeV with the ATLAS detector in final states with one or two leptons, referred to in the following as single-lepton and dilepton channels, and supersedes the result of Ref. [20]. Compared with the previous result, this analysis has an increased acceptance by selecting events with less restrictive requirements on the number of jets identified as originating from b-hadrons (b-jets), resulting in an increased efficiency to select $t\bar{t}H$ signal. It utilises a revised treatment of the different flavour components of the $t\bar{t}$ + jets background, and in particular, of the $t\bar{t}$ production in association with b-jets, the main background and the dominant source of the systematic uncertainty in the previous $t\bar{t}H(b\bar{b})$ measurement. For the modelling of this background, a new sample of Monte Carlo (MC) simulated events with improved settings was produced, and a corresponding set of systematic uncertainties was developed [22,23]. This measurement also uses improved analysis techniques: an advanced b-jet identification and an improved event categorisation. In particular, unlike the previous result, where the event categorisation into the background-dominated and signal-rich categories was made based on the number of jets and the number of b-jets, this analysis uses a multiclass neural network to define regions enriched in different components of the main background, the $t\bar{t}$ + jets production processes, and the signal. A more powerful multivariate discriminant is also employed to separate the signal from background and to reconstruct p_{T}^{H}. These improvements lead to better overall sensitivity and allow for a measurement of the $t\bar{t}H(b\bar{b})$ production cross-section in six bins of p_{T}^{H}, 0–60 GeV, 60–120 GeV, 120–200 GeV, 200–300 GeV, 300–450 GeV, and ≥ 450 GeV, as obtained from the MC event record before the Higgs boson decays, in the STXS formalism.

2 ATLAS detector

The ATLAS experiment [24] at the LHC is a multipurpose particle detector with a forward–backward symmetric cylindrical geometry and a near 4π coverage in solid angle.[1] It consists of an inner tracking detector (ID) surrounded by a thin superconducting solenoid providing a 2 T axial magnetic field, electromagnetic and hadronic calorimeters, and a muon spectrometer. The inner tracking detector covers the pseudorapidity range $|\eta| < 2.5$. It consists of silicon pixel, silicon microstrip, and transition radiation tracking detectors. Lead/liquid-argon (LAr) sampling calorimeters provide electromagnetic (EM) energy measurements with high granularity within the region $|\eta| < 3.2$. A steel/scintillator-tile hadronic calorimeter covers the central pseudorapidity range ($|\eta| < 1.7$). The endcap and forward regions are instrumented with LAr calorimeters for EM and hadronic energy measurements up to $|\eta| = 4.9$. The muon spectrometer (MS) surrounds the calorimeters and is based on three large superconducting air-core toroidal magnets with eight coils each. The field integral of the toroids ranges between 2.0 and 6.0 Tm across most of the detector. The muon spectrometer includes a system of precision tracking chambers up to $|\eta| = 2.7$ and fast detectors for triggering up to $|\eta| = 2.4$. The luminosity is measured mainly by the LUCID-2 [25] detector, which is located close to the beampipe. A two-level trigger system is used to select events [26]. The first-level trigger is implemented in hardware and uses a subset of the detector information to accept events at a rate below 100 kHz. This is followed by a software-based trigger that reduces the accepted event rate to 1 kHz on average depending on the data-taking conditions. A software suite [27] is used in data simulation, in the reconstruction and analysis of real and simulated data, in detector operations, and in the trigger and data acquisition systems of the experiment.

3 Data and Monte Carlo simulation samples

This analysis was performed using the pp collision data collected by the ATLAS detector between 2015 and 2018 at $\sqrt{s} = 13$ TeV. After the application of data-quality requirements [28], the dataset corresponds to an integrated luminosity of 140 fb^{-1}. Samples of simulated events were produced to model the different signal and background processes. Additional samples were produced to estimate the modelling uncertainties for each process. The effects of the additional pp collisions in the same or a nearby bunch crossing (pile-up) were modelled by overlaying minimum bias events generated with Pythia8 [29] using the A3 set of tunable parameters [30] onto the simulated hard-scatter

[1] ATLAS uses a right-handed coordinate system with its origin at the nominal interaction point (IP) in the centre of the detector and the z-axis along the beam pipe. The x-axis points from the IP to the centre of the LHC ring, and the y-axis points upwards. Cylindrical coordinates (r, ϕ) are used in the transverse plane, ϕ being the azimuthal angle around the z-axis. The pseudorapidity is defined in terms of the polar angle θ as $\eta = -\ln\tan(\theta/2)$. Angular distance is measured in units of $\Delta R \equiv \sqrt{(\Delta\eta)^2 + (\Delta\phi)^2}$.

event. The MC events were weighted to reproduce the distribution of the average number of interactions per bunch crossing observed in the data. The MC samples were processed using the full ATLAS detector simulation [31] based on GEANT4 [32]. Some alternative samples used to evaluate the modelling uncertainties were produced using fast simulation, where the full GEANT4 simulation of the calorimeter response is replaced by a detailed parameterisation of the shower shapes. For the observables used in this analysis, both simulations were found to give similar modelling. All MC samples were reconstructed using the same software as for collider data. Corrections were applied to the simulated events so that the selection efficiencies, energy scales and energy resolutions of the physics objects closely match those determined from data control samples.

All samples generated with POWHEGBOX [33–36] and MADGRAPH5_AMC@NLO [37] were interfaced to PYTHIA8 [38] to simulate the parton shower (PS), fragmentation, and underlying event with the A14 tune [39] and the NNPDF2.3LO [40] parton distribution function (PDF) set. Some alternative samples use the HERWIG7 [41,42] PS model with the H7UE set of tuned parameters [42] and the MMHT2014LO PDF set [43]. Samples using PYTHIA8 and HERWIG7 have heavy-flavour hadron decays modelled by EvtGen [44]. The masses of the top quark, m_{top}, and of the Higgs boson, m_{H}, are set to 172.5 GeV and 125 GeV, respectively.

The nominal $t\bar{t}H$ signal sample was generated at next-to-leading order (NLO) in the five flavour scheme (5FS) using the POWHEGBOX [45] generator with the NNPDF3.0NLO [40] PDF set. The h_{damp} parameter[2] was set to $3/4 \cdot (m_t + m_{\bar{t}} + m_H) = 352.5$ GeV, and the functional form of the renormalisation and factorisation scales was set to $\sqrt[3]{m_{\text{T}}(t) \cdot m_{\text{T}}(\bar{t}) \cdot m_{\text{T}}(H)}$, where $m_{\text{T}} = \sqrt{m^2 + p_{\text{T}}^2}$ is the transverse mass of a generated particle, m is its mass, and p_{T} is its transverse momentum. It is normalised to the theoretical prediction of Ref. [18] computed at NLO in QCD.[3]

An alternative $t\bar{t}H$ sample generated with the same POWHEGBOX set-up, but interfaced to HERWIG7 is used to evaluate uncertainties due to the choice of parton shower, hadronisation and underlying event model. The uncertainty related to the matching between the matrix element (ME) generator and the PS is accessed by changing the definition of the hardness of the POWHEG emission calculated by PYTHIA8 via the parameter $p_{\text{T}}^{\text{hard}}$ from the value provided by POWHEG to the p_{T} of the POWHEG emission following Refs. [47,48].

Several MC samples with different accuracy in ME generator and with different PS models are used in this analysis to model the main $t\bar{t}$ + jets background. This background is categorised according to the flavour of the additional jets in the event, excluding jets from top-quark or W boson decays, using the same procedure as described in Ref. [49]. Generator-level particle jets are reconstructed from stable particles (mean lifetime $\tau > 3 \times 10^{-11}$ s, excluding muons and neutrinos) using the anti-k_t algorithm [50] with a radius parameter $R = 0.4$, and are required to have transverse momentum $p_{\text{T}} > 15$ GeV and $|\eta| < 2.5$. The flavour of a jet is determined by counting b- or c-hadrons within $\Delta R < 0.4$ of the jet axis. Jets matched to exactly one b-hadron, with p_{T} above 5 GeV, are labelled single-b-jets, while those matched to two or more b-hadrons are labelled B-jets (with no p_{T} requirement on the second b-hadron); single-c- and C-jets are defined analogously, only considering jets not already defined as single-b- or B-jets. Events that have a single-b- or B-jet, are labelled as $t\bar{t}+1b$ and $t\bar{t}+1B$ respectively, events with two or more b-jets are labelled as $t\bar{t}+\geq 2b$. These three categories together are collectively referred to as $t\bar{t}+\geq 1b$. Events with no single-b- or B-jet but at least one single-c- or C-jet are labelled as $t\bar{t}+\geq 1c$. Finally, events not containing any heavy-flavour jets aside from those from top-quark or W boson decays are labelled as $t\bar{t}$ + light.

The $t\bar{t}$ + light and $t\bar{t}+\geq 1c$ contributions are modelled by a MC sample produced with the HVQ programme [34] in the POWHEGBOX generator at NLO in QCD in the five flavour scheme (5FS) with the NNPDF3.0NLO PDF set. The h_{damp} parameter was set to 1.5 m_{top} [39,51]. An additional sample was generated with the h_{damp} parameter increased by a factor of two to evaluate the uncertainty in the modelling of $t\bar{t}$ + light and $t\bar{t}+\geq 1c$ stemming from the choice of the h_{damp} value.

To predict the $t\bar{t}+\geq 1b$ background with the highest available precision, the $t\bar{t}b\bar{b}$ MC sample is generated at NLO, where the additional b-quarks are included in the ME. The four flavour scheme (4FS) was used for this sample. It was produced with the POWHEGBOXRES [52] generator and OPENLOOPS [53–55], using the implementation of this process in POWHEGBOXRES [56], with the NNPDF3.1NNLONF4 [69] PDF set interfaced to PYTHIA8. Based on the studies of Ref. [22], the factorisation scale is set to $\frac{1}{2}\sum_{i=t,\bar{t},b,\bar{b},j} m_{\text{T},i}$, the renormalisation scale is set to $\frac{1}{2} \cdot \sqrt[4]{m_{\text{T}}(t) \cdot m_{\text{T}}(\bar{t}) \cdot m_{\text{T}}(b) \cdot m_{\text{T}}(\bar{b})}$, and the h_{damp} parameter is set to $H_{\text{T}}/2$. The POWHEG internal parameter h_{bzd} that regulates the damping function together with the parameter h_{damp}, was set to 5. The choice of model used for the recoil in the initial state parton shower was found to impact significantly the $t\bar{t}+\geq 1b$ background predictions [23]. The corresponding uncertainty is evaluated by changing the PYTHIA8 parameter from a global recoil to a dipole recoil while keep-

[2] The h_{damp} parameter controls the transverse momentum p_{T} of the first additional emission beyond the leading-order Feynman diagram in the PS and therefore regulates the high-p_{T} emission against which the $t\bar{t}$ system recoils.

[3] A new theoretical computation of the $t\bar{t}H$ production at next-to-next-to-leading order in QCD was published recently in Ref. [46].

ing the rest of the settings identical to the nominal $t\bar{t}b\bar{b}$ sample.

Similar to the $t\bar{t}H$ signal sample, alternative samples were generated to assess the PS and matching uncertainties in the modelling of $t\bar{t}+$light, $t\bar{t}+\geq 1c$ and $t\bar{t}+\geq 1b$ by replacing in the corresponding nominal set-ups the PYTHIA8 shower model by HERWIG and producing samples with a varied $p_{\mathrm{T}}^{\mathrm{hard}}$ parameter.

For an independent pseudo-data test, additional samples of $t\bar{t}$ events were produced to model $t\bar{t}+$light and $t\bar{t}+\geq 1c$ events with the SHERPA [57] generator. The NLO-accurate matrix elements for up to one additional parton, and LO-accurate matrix elements for up to four additional partons were calculated with the COMIX [58] and OPENLOOPS libraries. They were matched with the SHERPA PS [59] with the default set of tuned parameters using the MEPS@NLO prescription [60–63] with a matching scale of 30 GeV. Furthermore, $t\bar{t}+\geq 1b$ events were simulated using SHERPA and OPENLOOPSwith $t\bar{t}b\bar{b}$ ME calculated at NLO accuracy using COMIX in the 4FS using the same functional form of the factorisation and renormalisation scales as in the nominal $t\bar{t}b\bar{b}$ set-up.

Single-top-quark production processes, i.e. tW associated production, t-channel and s-channel production, were modelled using the POWHEGBOX [64–66] generator at NLO in QCD. The t-channel process was generated in the 4FS with the NNPDF3.0NLONF4 PDF set, while for tW and s-channel processes the 5FS NNPDF3.0NLO PDF was used. The tW MC sample was generated using the factorisation and renormalisation scales set to $H_{\mathrm{T}}/2$ with H_{T} defined as a sum of the transverse mass of the W boson, the top quark and the transverse momentum of an additional parton. The overlap between tW and $t\bar{t}$ production [66] was removed using the diagram-removal scheme [67]. An alternative tW MC sample implementing the diagram subtraction scheme [66] was produced to evaluate the systematic uncertainty due to the tW and $t\bar{t}$ interference treatment.

The events in the nominal $t\bar{t}W$ sample were simulated using the SHERPA [68] generator with the NNPDF3.0NNLO PDF set. The ME was calculated for up to one additional parton at NLO and up to two partons at LO using COMIX and OPENLOOPS, and merged with the SHERPA PS using the MEPS@NLO prescription with a merging scale of 30 GeV. The alternative sample was generated with MADGRAPH5_AMC@NLO with up to one additional parton in the final state at NLO accuracy in the strong coupling, using the NNPDF3.1NNLO [69] PDF set. The different jet multiplicities were merged using the FxFx NLO ME and PS merging prescription [70] with a merging scale of 30 GeV. Background events from $t\bar{t}Z/\gamma^*$ and the rare processes $tZq, tWZ, tHjb$, tWH and $t\bar{t}t\bar{t}$ were simulated at NLO in QCD using the MADGRAPH5_AMC@NLO generator. The alternative sample used to evaluate the PS uncertainty in the $t\bar{t}Z$ background was generated with the same set-up as the nominal but interfaced to HERWIG7.

The production of $V+$jets events (where $V = W$ or Z) was simulated with the SHERPA generator using NLO-accurate matrix elements for up to two partons and LO-accurate matrix elements for up to four partons. Samples of diboson final states (VV) were also simulated with the SHERPA generator.

All MC samples corresponding to small backgrounds were normalised to the most precise available theoretical predictions closely following Ref. [20]. The normalisation of the $t\bar{t}W$ background was updated to the most recent prediction of Ref. [71]. The $t\bar{t}+$ light and $t\bar{t}+\geq 1c$ components were normalised to the $t\bar{t}$ cross-section computed at next-to-next-to-leading order (NNLO) in QCD including the resummation of next-to-next-to-leading-logarithmic (NNLL) soft-gluon terms [72] while the $t\bar{t}+\geq 1b$ normalisation is taken from the $t\bar{t}b\bar{b}$ MC simulation.

4 Objects and event selection

Events are selected using single-lepton triggers with variable electron and muon transverse momentum thresholds, and various identification and isolation criteria depending on the lepton flavour and the data-taking period [73,74]. The lowest p_{T} threshold at trigger level used for muons is 20 GeV (26 GeV), while for electrons the threshold is 24 GeV (26 GeV) in 2015 (2016–2018). Events are required to have at least one vertex with at least two associated ID tracks with $p_{\mathrm{T}} > 0.5$ GeV. In each event, the primary vertex is defined as the reconstructed vertex having the highest scalar sum of squared p_{T} of associated tracks [75] among the vertices consistent with the average beam-spot position.

Electron candidates are reconstructed from energy deposits in the electromagnetic calorimeter matched to tracks reconstructed in the ID system and are required to satisfy the *MediumLH* identification criterion [76]. They are required to have $p_{\mathrm{T}} > 10$ GeV and $|\eta| < 2.47$, excluding the calorimeter barrel-endcap transition region ($1.37 < |\eta| < 1.52$). Muon candidates are reconstructed from tracks in the MS that are associated with tracks from the ID and are required to satisfy the *Loose* identification criterion [77] and to have $p_{\mathrm{T}} > 10$ GeV, $|\eta| < 2.5$. Electron (muon) candidates must be associated with the primary vertex of the event: the transverse impact parameter divided by its estimated uncertainty, $|d_0|/\sigma(d_0)$, is required to be less than five (three) for electron (muon) candidates. The longitudinal impact parameter must satisfy $|z_0 \sin(\theta)| < 0.5$ mm for both lepton flavours.

Jets are reconstructed from particle flow objects [78] using the anti-k_t jet clustering algorithm in the FASTJET implementation [79] with a radius parameter $R = 0.4$. Jets are required to satisfy the *Tight* criterion of the *jet vertex tagger* (JVT)

algorithm [80] to mitigate the contribution from pile-up jets, and to have $p_{\mathrm{T}} > 25$ GeV and $|\eta| < 2.5$. The jet energy scale (JES) and resolution are calibrated using simulations with in situ corrections obtained from data [81]. Events containing jets originating from non-collision sources or detector noise are removed.

Jets containing b-hadrons, referred to as b-jets, are identified using the DL1r b-tagging algorithm [82] that uses a neural network based on the distinctive features of b-hadron decays, primarily the impact parameters of tracks and the displaced vertices reconstructed in the ID. Additional input to this network is provided by discriminating variables constructed by a recurrent neural network that exploits the spatial and kinematic correlations between tracks originating from the same b-hadron. A multivariate b-tagging discriminant value is calculated for each jet. The b-tagged jets are required to satisfy the working point (WP) corresponding to an efficiency of 70% or 85% for identifying b-quark initiated jets in $t\bar{t}$ simulated events for the single-lepton and dilepton channels, respectively. For the 70% (85%) WP the rejection factors against light-quark/gluon jets and c-quark jets are 625 and 12 (40 and 3), respectively. To fully exploit the b-tagging information of an event, each jet is assigned a b-tagging score that defines if a jet satisfies a given WP but fails to satisfy the adjacent tighter one. In addition to the standard JES calibration, b-tagged jets satisfying the 85% WP receive additional flavour-specific corrections to their four-vectors to improve their energy measurement (scale and resolution) following the *muon-in-jet* procedure described in Ref. [83].

Hadronically decaying τ-leptons (τ_{had}) are distinguished from jets using their track multiplicity and a multivariate discriminant based on their shower shapes in calorimeter and on tracking information [84]. They are required to have $p_{\mathrm{T}} > 25$ GeV and $|\eta| < 2.5$, and to pass the *Medium* τ-lepton identification working point.

The missing transverse momentum vector, with magnitude $E_{\mathrm{T}}^{\mathrm{miss}}$, is defined as the negative sum of the transverse momenta of the reconstructed and calibrated physical objects, plus a 'soft term' built from all other tracks associated with the primary vertex [85] and not matched to a reconstructed object.

Targeting event topologies with a Higgs boson decaying into collimated hadronic final states, reclustered (RC) jets [86] are reconstructed from the selected jets, using the anti-k_t jet clustering algorithm with a radius parameter $R = 1.0$. RC jets are required to have an invariant mass $M > 50$ GeV, $p_{\mathrm{T}} > 200$ GeV, $|\eta| < 2.0$, have at least two constituent small-R jets (subjets) and have an angular distance $\Delta R > 1.0$ from all electrons.

An overlap removal procedure is applied to avoid the double counting of detector signatures. Electron candidates sharing a track with a muon candidate are first removed. Jets found within a $\Delta R = 0.2$ cone of an electron are removed and electrons within a $\Delta R = 0.4$ cone of a remaining jet are rejected. Jets with less than three associated tracks and within $\Delta R = 0.2$ of a muon and muons within $\Delta R = 0.4$ of a jet with more than two associated tracks are rejected. A τ_{had} candidate is rejected if it is separated by $\Delta R < 0.2$ from any selected electron or muon. No overlap removal is performed between jets and τ_{had} candidates.

Events are selected if they contain exactly one lepton candidate in the single-lepton channel and exactly two lepton candidates with opposite electric charges in the dilepton channel. At least one lepton should have $p_{\mathrm{T}} > 27$ GeV and be matched to the corresponding object at the trigger level. In the events with two electrons, the second lepton is required to have $p_{\mathrm{T}} > 15$ GeV while in the other two dilepton channels, $e\mu$ and $\mu\mu$, it must have $p_{\mathrm{T}} > 10$ GeV. In events with two electrons or two muons, the dilepton invariant mass is required to be above 15 GeV, to suppress contribution from the decays of heavy-flavour resonances and low-mass Drell–Yan processes, and be outside a window of $\pm$ 8 GeV centred at the Z boson mass. To maintain orthogonality with other $t\bar{t}H$ decay channels, events are vetoed if they contain one or more (two or more) τ_{had} candidates in the dilepton (single-lepton) channel.

To reduce the non-prompt and mis-identified lepton background contribution, additional lepton identification and isolation requirements are applied. Electrons (muons) are required to satisfy the *TightLH* (*Medium*) identification criteria and the tight isolation criteria based on the calorimeter and tracking information for electrons [76] and on tracking information only for muons [77]. Events for which the leptons fail to meet these requirements are removed.

In the single-lepton channel two event categories are defined, referred in the following as resolved and boosted categories. The latter is designed to select events in which the Higgs boson is produced with high transverse momentum as a collimated large-R jet. Events that do not satisfy the boosted category selection are assigned to the resolved one. In the single-lepton resolved channel, events are selected if they contain at least five jets, at least three of which satisfy the 70% b-tagging WP. In the single-lepton boosted channel, events are required to have at least one large-R jet and at least four small-R jets, including those contained within the large-R jet, at least three of which must satisfy the 85% b-tagging WP. In the dilepton channel, events are selected if they contain at least three jets satisfying the 85% b-tagging WP, and among these at least two jets that satisfy the 70% b-tagging WP. These requirements are henceforth referred to as "preselection" and have an acceptance of 6.3% for selecting $t\bar{t}H$ events with $H \to b\bar{b}$ decay, an acceptance that is more than a factor of three larger than in the previous analysis [20]. The corresponding acceptance in the signal regions is 2.1%.

5 Background modelling

The largest background from $t\bar{t}$+jets production is modelled by MC simulation with the data-driven corrections described in Sect. 5.1. Small backgrounds include single top production, $t\bar{t}W$, $t\bar{t}Z$, $t\bar{t}t\bar{t}$, rare top-quark processes and non-top-quark processes such as V+jets and diboson production. All of them are estimated from simulations. The contribution from the background arising from non-prompt or mis-identified leptons is determined from data in the single-lepton channel (see Sect. 5.2), and from MC simulation in the dilepton channel, where this background arises primarily from $t\bar{t}$ events with one prompt lepton and is very small.

5.1 Modelling of $t\bar{t}$ + jets background

The $t\bar{t}$ sample used to model the $t\bar{t}$ + light and $t\bar{t} + \geq 1c$ contributions is generated at NLO as described in Sect. 3, with up to one additional parton from the ME calculation. All jets not originating from the decay chain of one of the top quarks, i.e. additional jets, are produced by the parton shower. The dedicated measurement [87] demonstrated deficiencies in modelling the number of additional jets in the $t\bar{t}$ events and the scalar sum of the transverse momenta of the top quarks. Moreover, the rate of $t\bar{t}$ production in association with c- and b-jets was observed to be underestimated in the previous analysis [20]. The new $t\bar{t}b\bar{b}$ MC sample produced for this analysis with lower value of the renormalisation scale than the one used in Ref. [20] predicts larger inclusive $t\bar{t} + \geq 1b$ cross-section, which is expected to match data well. Nevertheless, the rate of the components of the $t\bar{t} + \geq 1b$ background defined in Sect. 3, $t\bar{t} + 1B$, $t\bar{t} + 1b$ and $t\bar{t} + \geq 2b$, could still be mismodelled. Thus, to obtain a reliable estimate of the $t\bar{t}$ + jets background, the $t\bar{t}$ MC events are reweighted using data. The corrections applied include a rescaling of the $t\bar{t}$ + jets flavour components followed by a kinematic reweighting and are described in the next paragraph. Any possible residual mismodelling is accounted for by the systematic uncertainties in the profile-likelihood fit used for the extraction of the signal strength which is described in Sect. 6.

Initial scaling factors for the five $t\bar{t}$ + jets flavour components, $t\bar{t}$ + light, $t\bar{t} + \geq 1c$, $t\bar{t} + 1B$, $t\bar{t} + 1b$ and $t\bar{t} + \geq 2b$, are obtained separately for the single-lepton and dilepton channels from the profile-likelihood fit to data. The fit is performed in background-dominated control regions including all systematic uncertainties (see Sect. 7) prior to the signal extraction fit described in Sect. 6. These scaling factors have similar values to those shown in Table 5. Following the flavour components rescaling, a reweighting is used to mitigate the kinematic mismodelling of the scalar sum of the p_{T}'s of the reconstructed leptons and jets, H_{T}, observed for the $t\bar{t}$ + light and $t\bar{t} + \geq 1c$ components of the inclusive $t\bar{t}$ + jets POWHEG + PYTHIA8 sample. The $t\bar{t} + \geq 1b$ component is excluded from the reweighting since it is simulated by a dedicated $t\bar{t}b\bar{b}$ MC sample. Thus the reweighting derived in the regions dominated by $t\bar{t}$ + light and $t\bar{t} + \geq 1c$ might not be applicable to $t\bar{t} + \geq 1b$. A dedicated reweighting was investigated for the $t\bar{t} + \geq 1b$ component but found to have a negligible effect and is not used in the analysis.

The reweighting corrects the distributions of H_{T} in exclusive jet multiplicity bins from $N_{\mathrm{jets}} = 5$ to $N_{\mathrm{jets}} \geq 8$ in the single-lepton channel and from $N_{\mathrm{jets}} = 3$ to $N_{\mathrm{jets}} \geq 6$ in the dilepton channel. It is derived in $t\bar{t}$ enriched regions selected by using looser b-tagging requirements after subtracting from data all contributions except for $t\bar{t}$ + light and $t\bar{t} + \geq 1c$ and taking the ratio of data to the sum of $t\bar{t}$ + light and $t\bar{t} + \geq 1c$ yields predicted by MC in each H_{T} bin. These regions are orthogonal to the signal and control regions of the analysis and contain less that 0.2% of signal.

The reweighting factors are also derived in the same way for each systematic variation affecting the $t\bar{t}$ + light and $t\bar{t} + \geq 1c$ predictions, such that all systematic variations match the H_{T} distribution in data.

5.2 Non-prompt or mis-identified lepton background

A data-driven method, referred to as "fake factor" method [88], based on the measurement of lepton selection efficiencies using different identification and isolation criteria, is used to estimate the non-prompt or mis-identified (fake) lepton background in the single-lepton channel.

The fake rate is measured in a fake-dominated region selected by requiring exactly one lepton with loose identification and isolation criteria, at least two jets, at least two b-tagged jets satisfying the 70% WP, and a scalar sum of missing transverse energy and the leptonically-decaying W boson mass below 60 GeV. It is parameterised as a function of the leading jet p_{T} and the lepton $|\eta|$. The expected number of events arising from the fake lepton background is determined by applying the measured lepton fake rate to data events satisfying the selection requirements of each analysis region except that the lepton is required to pass loose identification and isolation criteria and to fail the tighter requirements.

6 Signal extraction

After the preselection, events are classified into non-overlapping background-dominated or control regions (CR) and signal-enriched regions (SR) with higher signal-to-background ratios. The CRs provide stringent constraints on the normalisation of the backgrounds and the systematic uncertainties in a combined fit with the signal regions.

To define the regions in the single-lepton and dilepton channels, a multiclass classification neural network based

on the permutation-invariant transformer architecture with attention mechanism [89] is trained to predict the probability of an event to be from the $t\bar{t}H$ signal or from one of the five $t\bar{t}$+jets background categories introduced in Sect. 3: $t\bar{t}+1b$, $t\bar{t}+1B$, $t\bar{t}+\geq 2b$, $t\bar{t}+\geq 1c$, $t\bar{t}+$light jets. The probability p_i of a network class i is converted into a discriminant d_i in order to maximise the separation between the class and all the other classes ($i \neq j$), to yield a similar number of events in the $t\bar{t}+1b$, $t\bar{t}+1B$, and inclusive $t\bar{t}+\geq 2b$ control regions, and to maximise sensitivity. They are defined as

$$d_i = \frac{p_i}{\sum_{j\neq i} p_j \cdot \hat{N}_{ij}}. \quad (1)$$

Here, the denominator of each discriminant is a weighted average of all the remaining class probabilities $p_{j\neq i}$. The weights $\hat{N}_{ij} = N_j/\sum_{k\neq i} N_k$ are the respective fractions of event yields N_j relative to the total yield of all the remaining classes $k \neq i$. These yields are determined from MC simulation after the preselection and incorporate the $t\bar{t}+$ jets scaling factors described in Sect. 5.1.

In the single-lepton (dilepton) channel, events fulfilling $d_{t\bar{t}H} > 4.072$ ($d_{t\bar{t}H} > 9.031$) are assigned to the signal region. The thresholds are defined to maximize the ratio of signal to the square root of the background in the inclusive signal regions. All other events are assigned to the $t\bar{t}+$ jets background category with the highest value of the discriminant. By far the dominant Higgs boson decay mode in the signal region is $H \to b\bar{b}$ with a fraction of more than 97% (94%) of the $t\bar{t}H$ events in the single-lepton (dilepton) channel followed by the $H \to WW$ decay. This motivates the training of a second neural network, based on the same architecture, to identify the two jets most likely originating from the Higgs boson decay, to reconstruct p_{T}^H that is used to further classify the signal region events into the six reconstructed STXS regions. The performance of this reconstruction network to correctly identify both Higgs boson decay products decreases with increasing jet multiplicity and generally increases with increasing true p_{T}^H. Both Higgs boson decay products are correctly identified for 51% (58%) of $t\bar{t}H(b\bar{b})$ events in the single-lepton resolved (dilepton) channel. The boundaries of the regions are optimised to maximise fraction of the events with the corresponding truth p_{T}^H, listed in Fig. 1, separately per $t\bar{t}$ decay channel to capture potential differences due to the final states and separate neural networks. This optimisation leads, in particular, to improved purity in the highest truth p_{T}^H bins, the region of the phase space where this analysis provides a particularly valuable contribution to the global Higgs boson combination. The optimal reconstructed p_{T}^H boundaries are found to be [0, 60, 114, 186, 270, 402, ∞] GeV in the dilepton channel and [0, 60, 114, 192, 282, 408, ∞] GeV in the single-lepton resolved channel. They are referred to in the following as STXS 1–6 regions.

The inclusive control region dominated by the $t\bar{t}+\geq 2b$ background in the single-lepton channel is further split into three categories encompassing STXS regions 1–2, 3–4, and 5–6, to ensure a good control of the $t\bar{t}+\geq 2b$ background modelling over the bins of reconstructed Higgs boson p_{T}. These regions are henceforth referred to as $t\bar{t}+\geq 2b$ CR 1, CR 2, and CR 3. The split is not applied in the dilepton channel due to limited statistics.

Events fulfilling the boosted selection criteria are assigned to dedicated boosted signal and control regions. RC jets are used as input to a multiclass deep neural network (DNN), trained to distinguish high-p_{T} Higgs boson candidates decaying into collimated final states from top quarks and multijet backgrounds following the same strategy as in the previous analysis [20]. An event is flagged as containing a boosted Higgs boson candidate if one of the RC jets has a high probability of originating from a Higgs boson, as estimated by the DNN. Boosted Higgs boson candidates are required to have $p_{\mathrm{T}} \geq 300$ GeV, a mass consistent with the Higgs boson mass window of 100–140 GeV, contain at least two subjets, of which exactly two are required to satisfy the b-tagging 85% WP, and have a DNN score above 0.4. At least two small-R jets that do not form the Higgs boson candidate are required to satisfy the b-tagging 77% WP. The flowchart in Fig. 1 summarises the event classification strategy.

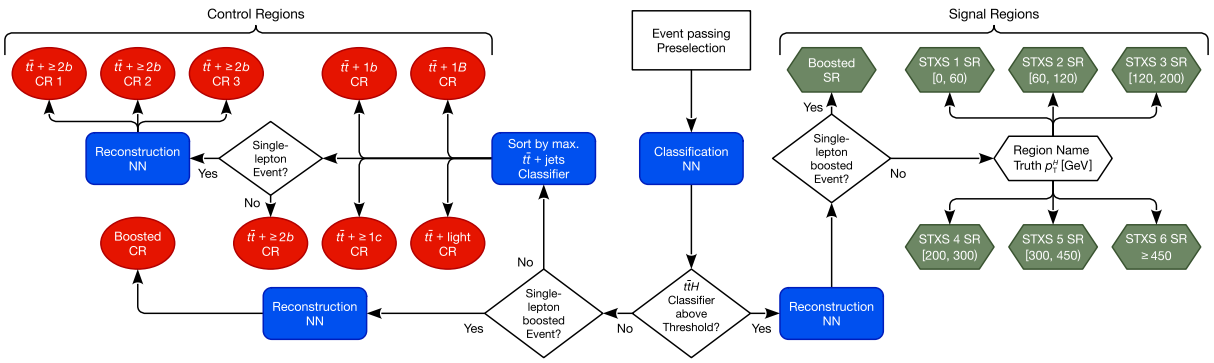

Fig. 1 Flowchart depicting the event classification and Higgs boson p_{T} reconstruction strategy used in the analysis

The transformer networks are trained using low-level features of the reconstructed jets, electrons, muons, and the missing transverse momentum of the event. For each reconstructed object, the kinematic features used are the x-, y- and z-component of the momentum (p_x, p_y, p_z), the energy, the p_{T}, the mass, the pseudorapidity, the azimuthal angle and its sine and cosine. Supplying redundant four-vector information is observed to improve network performance. Additionally, the DL1r pseudo-continuous b-tagging score is included for jets, and the electric charge and a variable indicating if it is an electron or a muon is included for leptons.

The multiclass event-classification network is trained using events sampled from the nominal and alternative $t\bar{t}H$ and $t\bar{t}+$jets background samples to profit from an increased number of events in training. The classification network yields an area under the receiver-operator characteristic curve (AUC) of 0.753 (0.774) for discriminating between $t\bar{t}H$ and the $t\bar{t}+\geq 1b$ background for events satisfying the preselection in the single-lepton resolved (dilepton) channel. The Higgs boson p_{T} reconstruction network is trained using only the $t\bar{t}H$ samples. Figure 2 shows for each bin of truth p_{T}^{H} the fraction of $t\bar{t}H$ events assigned to each of the STXS signal regions.

In the single-lepton channel, a total of 15 analysis regions are defined, including six STXS signal regions, two boosted regions (signal and control) and seven control regions targeting the different components of the $t\bar{t}+$jets background. In the dilepton channel, a total of 11 analysis regions are defined, including the six STXS signal regions and five $t\bar{t}+$jets control regions. The expected yields in the single-lepton (dilepton) signal and control regions are summarised in Tables 1 and 2 (3 and 4) after applying the data-driven corrections to the $t\bar{t}+$jets background discussed in Sect. 5.1.

The $t\bar{t}H$ inclusive signal strength, $\mu_{t\bar{t}H}$, defined as the ratio of the measured $t\bar{t}H$ cross-section including all Higgs boson decay modes to the corresponding SM prediction, or the signal strengths in each of the six STXS bins, μ_i, and the normalisation factors of the components of the $t\bar{t}+$jets background are determined via a binned likelihood fit to the distributions in all signal and control regions defined above. The $t\bar{t}H$ signal sample is split up according to the true p_{T}^{H} in each event, and the μ_i act on the respective component. In the resolved signal and control regions, the corresponding discriminant distribution is used in the likelihood fit, while in the boosted regions, event yields in two bins of the reconstructed p_{T}^{H} distribution, 300–450 GeV and ≥ 450 GeV, are used in the fit.

The $t\bar{t}+1b$, $t\bar{t}+\geq 1c$ and $t\bar{t}+$light normalisation factors are chosen to float independently in the single-lepton and dilepton channels, while the normalisations of the $t\bar{t}+\geq 2b$ and $t\bar{t}+1B$ backgrounds are scaled in a correlated way between the two channels. This choice is made based on studies of the different correlation assumptions between the normalisation factors in the combined fit. The chosen configuration provides enough freedom for the fit model and minimises pulls and constraints of the nuisance parameters in the fit to data.

The inclusive measurement of the signal strength and cross-section is performed in the full phase space. The measurement of these parameters in STXS bins is carried out for $t\bar{t}H$ events with a Higgs boson produced centrally within $|y|\leq 2.5$ at truth level, while the remaining forward events are considered as background.

The statistical model is based on a likelihood function built with HistFactory [90] as the product over every bin of the Poisson probability for the observed data, given the SM prediction. The value of each nuisance parameter, describing the systematic uncertainties for both signal and background processes (see Sect. 7), is constrained by a Gaussian penalty term present in the likelihood function, while all normalisation factors are unconstrained. The statistical uncertainty arising from the limited number of simulated events is included in the likelihood in the form of additional nuisance parameters with Poisson constraint terms. The maximum-likelihood fit is performed with the RooFit package [91]. A test statistic based on the profile-likelihood ratio is used to assess the compatibility of the observed data with the background-only hypothesis ($\mu=0$) [92].

Tests of the statistical model fitted to pseudo-data constructed with the SHERPA $t\bar{t}+$jets samples were performed to help inform the choice of fit variables and uncertainty model, with the goal of minimising bias, maximising robustness and optimising sensitivity.

7 Systematic uncertainties

Multiple sources of systematic uncertainty, arising from detector effects, theoretical assumptions and the limited number of events in the MC simulations, are considered in the analysis. They affect the categorisation of events as well as the normalisation and shape of the distributions used in the signal extraction fit.

All the sources of experimental uncertainty, except the uncertainty in the integrated luminosity, affect both the normalisations and the shapes of the distributions in all simulated samples. The uncertainty in the integrated luminosity is 0.83% [93], obtained using the LUCID-2 detector [25] for the primary luminosity measurements, complemented by measurements using the inner detector and calorimeters. The uncertainty in the pile-up modelling is obtained by varying the pile-up reweighting in the simulation within its uncertainties.

The correction factors applied to the simulated samples to improve the description of the lepton reconstruction, identification and isolation efficiencies, momentum scale and res-

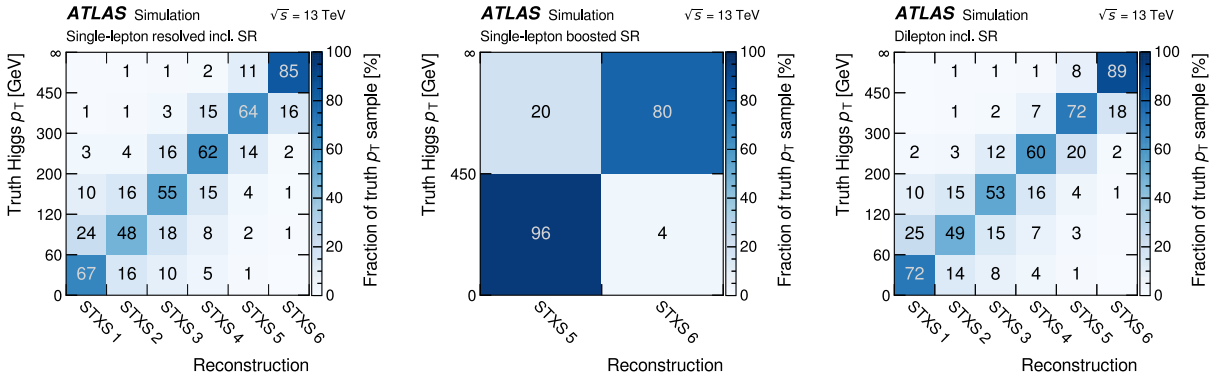

(a) (b) (c)

Fig. 2 STXS migration matrices for the $t\bar{t}H$ signal regions in (**a**) the single-lepton resolved, (**b**) the single-lepton boosted, and (**c**) the dilepton channel. The yield fractions of the predicted STXS bins are normalised per truth STXS sample

Table 1 Expected yields in the single-lepton signal regions before the fit to data. The data-driven corrections to the $t\bar{t}$ + jets background are applied and all uncertainties are included, except the ones associated with the $t\bar{t}$ + jets background normalisation factors, which are not defined pre-fit. The "Other" category includes the s- and t-channel single-top, tZq and tWZ processes. The $t\bar{t}H$ signal is normalised to the SM $t\bar{t}H$ cross-section. For presentation purposes, uncertainties are symmetrised

	STXS 1 SR	STXS 2 SR	STXS 3 SR	STXS 4 SR	STXS 5 SR	STXS 6 SR	Boosted SR
$t\bar{t}H$ truth p_T^H 0–60 GeV	77 ± 12	18.7 ± 3.2	11.1 ± 2.3	5.7 ± 1.0	1.66 ± 0.2	0.42 ± 0.09	0.58 ± 0.13
$t\bar{t}H$ truth p_T^H 60–120 GeV	49 ± 5	99 ± 13	37 ± 6	15.5 ± 2.2	4.4 ± 0.5	1.25 ± 0.19	1.54 ± 0.25
$t\bar{t}H$ truth p_T^H 120–200 GeV	22.7 ± 2.2	37 ± 4	125 ± 16	34 ± 5	8.1 ± 1.3	2.0 ± 0.4	2.31 ± 0.28
$t\bar{t}H$ truth p_T^H 200–300 GeV	4.0 ± 0.5	5.5 ± 0.7	22.5 ± 2.9	88 ± 12	19.4 ± 3.0	2.7 ± 0.4	3.3 ± 0.6
$t\bar{t}H$ truth p_T^H 300–450 GeV	0.39 ± 0.11	0.64 ± 0.16	1.4 ± 0.4	7.6 ± 1.3	32 ± 5	8.0 ± 1.3	20 ± 3
$t\bar{t}H$ truth p_T^H ≥450 GeV	<0.1	<0.1	0.14 ± 0.06	0.21 ± 0.09	1.30 ± 0.31	9.8 ± 1.8	6.9 ± 1.3
$t\bar{t}H$ $\|y\| > 2.5$	0.16 ± 0.06	0.10 ± 0.04	<0.1	<0.1	<0.1	<0.1	<0.1
$t\bar{t}$ + ≥ 2b	870 ± 80	870 ± 90	980 ± 100	640 ± 60	270 ± 40	92 ± 21	103 ± 8
$t\bar{t}$ + 1b	210 ± 60	210 ± 50	250 ± 80	180 ± 60	78 ± 28	25 ± 9	17 ± 5
$t\bar{t}$ + 1B	64 ± 19	73 ± 24	100 ± 40	87 ± 30	46 ± 19	22 ± 11	11 ± 4
$t\bar{t}$ + ≥ 1c	210 ± 50	210 ± 50	250 ± 50	190 ± 50	88 ± 24	27 ± 13	22 ± 8
$t\bar{t}$ + light	42 ± 16	45 ± 12	68 ± 22	64 ± 19	31 ± 11	12 ± 11	3.2 ± 3
$t\bar{t}Z$	36 ± 6	38 ± 6	53 ± 8	43 ± 8	24 ± 5	7.2 ± 1.1	5.8 ± 1.2
tW	20 ± 8	35 ± 12	60 ± 33	55 ± 32	33 ± 25	17 ± 15	5 ± 4
W+jets	10 ± 6	12 ± 8	30 ± 15	29 ± 14	23 ± 12	12 ± 6	3.7 ± 1.9
$t\bar{t}W$	4.2 ± 0.5	5.9 ± 0.8	9.8 ± 1.6	8.9 ± 1.9	5.6 ± 0.7	3.2 ± 0.5	1.06 ± 0.26
Z+jets	2.5 ± 1.1	5.1 ± 2	6.5 ± 2.6	7.4 ± 2.7	3.1 ± 1.1	1.7 ± 0.6	0.5 ± 0.2
Diboson	1.3 ± 0.8	2.5 ± 1.40	4.4 ± 2.3	4.7 ± 2.7	3.1 ± 1.6	1.4 ± 0.7	0.7 ± 0.4
$t\bar{t}t\bar{t}$	5.1 ± 2.2	6.7 ± 3	11 ± 5	9 ± 4	4.8 ± 2.1	2.5 ± 1.1	1.1 ± 0.5
$tHjb$	0.77 ± 0.22	1.06 ± 0.21	1.61 ± 0.32	1.58 ± 0.28	1.11 ± 0.30	0.26 ± 0.12	0.72 ± 0.14
tWH	1.68 ± 0.23	2.16 ± 0.27	3.8 ± 0.4	4.1 ± 0.5	2.22 ± 0.25	1.03 ± 0.12	1.01 ± 0.11
Other	11.3 ± 1.2	11 ± 1.5	14.4 ± 2	11.9 ± 1.5	7.3 ± 1.1	2.43 ± 0.35	2.2 ± 0.6
Fakes	29 ± 12	29 ± 15	27 ± 12	31 ± 19	22 ± 13	3.8 ± 2.5	8 ± 5
Total	1670 ± 160	1710 ± 170	2060 ± 210	1520 ± 150	710 ± 80	250 ± 40	221 ± 19
Data	1672	1657	2016	1441	676	241	216

Table 2 Expected yields in the single-lepton control regions before the fit to data. The data-driven corrections to the $t\bar{t}+$ jets background are applied and all uncertainties are included, except the ones associated with the $t\bar{t}+$ jets background normalisation factors, which are not defined pre-fit. The "Other" category includes the s- and t-channel single-top, tZq and tWZ processes. The $t\bar{t}H$ signal is normalised to the SM $t\bar{t}H$ cross-section. For presentation purposes, uncertainties are symmetrised

	$t\bar{t}+$ light CR	$t\bar{t}+\geq 1c$ CR	$t\bar{t}+1b$ CR	$t\bar{t}+1B$ CR	$t\bar{t}+\geq 2b$ CR 1	$t\bar{t}+\geq 2b$ CR 2	$t\bar{t}+\geq 2b$ CR 3	Boosted CR
$t\bar{t}H$ truth p_{T}^{H} 0–60 GeV	56 ± 6	59 ± 7	89 ± 11	46 ± 6	80 ± 10	12.5 ± 1.7	2.09 ± 0.26	0.54 ± 0.14
$t\bar{t}H$ truth p_{T}^{H} 60–120 GeV	86 ± 5	98 ± 8	133 ± 12	92 ± 13	112 ± 11	33 ± 5	4.5 ± 0.9	1.15 ± 0.23
$t\bar{t}H$ truth p_{T}^{H} 120–200 GeV	59 ± 4	76 ± 7	76 ± 8	88 ± 11	41 ± 4	68 ± 8	5.4 ± 1.1	1.36 ± 0.28
$t\bar{t}H$ truth p_{T}^{H} 200–300 GeV	23 ± 2.5	31.9 ± 3.5	21.2 ± 3.1	41 ± 5	7.3 ± 1.1	34 ± 4	6.7 ± 1.1	1.42 ± 0.32
$t\bar{t}H$ truth p_{T}^{H} 300–450 GeV	7.7 ± 1.0	10 ± 1.5	4.7 ± 0.8	14.3 ± 2	1.12 ± 0.27	4.4 ± 0.8	9.8 ± 1.5	4.8 ± 0.7
$t\bar{t}H$ truth $p_{\mathrm{T}}^{H} \geq 450$ GeV	1.67 ± 0.27	2.4 ± 0.5	0.78 ± 0.19	4.1 ± 0.7	0.18 ± 0.05	0.35 ± 0.12	3 ± 0.7	1.75 ± 0.32
$t\bar{t}H$ $\lvert y\rvert > 2.5$	0.98 ± 0.08	0.72 ± 0.17	1.38 ± 0.22	0.57 ± 0.15	0.37 ± 0.05	0.188 ± 0.029	<0.1	<0.1
$t\bar{t}+\geq 2b$	2320 ± 280	3800 ± 400	5400 ± 600	3500 ± 400	7200 ± 600	4900 ± 500	1140 ± 170	141 ± 10
$t\bar{t}+1b$	3900 ± 400	4600 ± 700	10600 ± 1700	5100 ± 600	2100 ± 500	1120 ± 320	230 ± 100	54 ± 19
$t\bar{t}+1B$	890 ± 80	1390 ± 270	1780 ± 270	5100 ± 400	530 ± 190	380 ± 140	100 ± 50	32 ± 7
$t\bar{t}+\geq 1c$	17000 ± 3300	17900 ± 2600	7800 ± 1000	5400 ± 1300	2500 ± 500	1220 ± 270	240 ± 70	133 ± 35
$t\bar{t}+$ light	31800 ± 3500	5900 ± 1100	4000 ± 600	2000 ± 500	700 ± 180	320 ± 110	49 ± 26	34 ± 8
$t\bar{t}Z$	152 ± 20	171 ± 25	151 ± 21	146 ± 22	122 ± 18	117 ± 15	36 ± 5	5.7 ± 0.9
tW	1040 ± 200	750 ± 220	820 ± 240	560 ± 190	350 ± 140	360 ± 150	130 ± 90	10 ± 6
W+jets	370 ± 180	370 ± 180	230 ± 120	170 ± 80	370 ± 190	250 ± 130	90 ± 40	5.6 ± 2.9
$t\bar{t}W$	100 ± 12	114 ± 17	43 ± 7	44 ± 5	25.6 ± 3.5	26 ± 5	10.5 ± 1.6	1.97 ± 0.33
Z+jets	110 ± 40	110 ± 40	110 ± 40	64 ± 23	100 ± 40	55 ± 20	16 ± 6	0.9 ± 0.4
Diboson	37 ± 19	39 ± 20	23 ± 12	21 ± 11	24 ± 13	23 ± 12	10 ± 5	1.1 ± 0.7
$t\bar{t}t\bar{t}$	2.9 ± 1.2	24 ± 10	7.1 ± 3	19 ± 8	21 ± 9	33 ± 14	17 ± 7	1.4 ± 0.6
$tHjb$	8.2 ± 1.4	5.4 ± 0.9	8.1 ± 1.6	3.5 ± 0.6	5.4 ± 1.1	3.6 ± 0.7	0.53 ± 0.15	0.65 ± 0.20
tWH	7.1 ± 0.7	6.7 ± 0.7	9.6 ± 1	5.7 ± 0.6	5.4 ± 0.6	5.8 ± 0.7	1.78 ± 0.2	0.44 ± 0.07
Other	370 ± 40	370 ± 40	303 ± 35	228 ± 22	179 ± 22	111 ± 12	27.4 ± 2.8	3.9 ± 0.9
Fakes	810 ± 300	800 ± 400	880 ± 350	340 ± 140	660 ± 300	280 ± 130	57 ± 32	6.3 ± 3.3
Total	59000 ± 6000	37000 ± 4000	32500 ± 2900	22900 ± 2200	15200 ± 1700	9400 ± 1000	2190 ± 270	440 ± 50
Data	61954	36528	32887	23245	15595	9397	2097	426

Table 3 Expected yields in the dilepton signal regions before the fit to data. The data-driven corrections to the $t\bar{t}$+jets background are applied and all uncertainties are included, except the ones associated with the $t\bar{t}$+jets background normalisation factors, which are not defined pre-fit. The "Other" category includes the tZq, tWZ and diboson processes. The $t\bar{t}H$ signal is normalised to the SM $t\bar{t}H$ cross-section. For presentation purposes, uncertainties are symmetrised

	STXS 1 SR	STXS 2 SR	STXS 3 SR	STXS 4 SR	STXS 5 SR	STXS 6 SR
$t\bar{t}H$ truth p_{T}^{H} 0–60 GeV	10.6 ± 1.5	2.03 ± 0.31	1.14 ± 0.17	0.63 ± 0.11	0.19 ± 0.07	0.046 ± 0.023
$t\bar{t}H$ truth p_{T}^{H} 60–120 GeV	6.5 ± 0.7	13.0 ± 1.8	4.1 ± 0.7	1.9 ± 0.4	0.7 ± 0.11	0.13 ± 0.07
$t\bar{t}H$ truth p_{T}^{H} 120–200 GeV	3.06 ± 0.34	4.7 ± 0.5	16.3 ± 2.0	5.0 ± 0.7	1.36 ± 0.19	0.24 ± 0.07
$t\bar{t}H$ truth p_{T}^{H} 200–300 GeV	0.5 ± 0.07	0.72 ± 0.08	2.5 ± 0.29	13.0 ± 1.7	4.4 ± 0.6	0.41 ± 0.06
$t\bar{t}H$ truth p_{T}^{H} 300–450 GeV	<0.1	<0.1	0.197 ± 0.033	0.82 ± 0.18	8.0 ± 1.1	1.98 ± 0.32
$t\bar{t}H$ truth $p_{\mathrm{T}}^{H} \geq 450$ GeV	<0.1	<0.1	<0.1	<0.1	0.26 ± 0.08	2.8 ± 0.5
$t\bar{t}H$ $\lvert y \rvert > 2.5$	<0.1	<0.1	<0.1	<0.1	<0.1	<0.1
$t\bar{t} + \geq 2b$	81 ± 8	76 ± 7	81 ± 13	59 ± 4	36.2 ± 3.0	11.7 ± 2.1
$t\bar{t} + 1b$	14 ± 5	15 ± 6	20 ± 9	17 ± 5	11 ± 6	2.9 ± 1.9
$t\bar{t} + 1B$	4.4 ± 2.6	4.8 ± 3.2	5.7 ± 2.3	6.2 ± 1.9	6.6 ± 2.9	3.5 ± 2.3
$t\bar{t} + \geq 1c$	11.3 ± 2.4	11.7 ± 2.6	15.4 ± 3.4	12.5 ± 2.6	7.1 ± 2.6	3.0 ± 1.7
$t\bar{t}$ + light	1.1 ± 0.7	0.9 ± 0.5	1.4 ± 0.8	1.0 ± 0.5	1.0 ± 0.4	0.37 ± 0.30
$t\bar{t}Z$	4.6 ± 0.7	4.6 ± 1.1	7.2 ± 1.1	6.2 ± 1.3	5.3 ± 1.1	2 ± 0.6
tW	1.7 ± 0.8	3 ± 1.8	6 ± 4	8 ± 5	7 ± 5	3.1 ± 2.9
$t\bar{t}W$	0.65 ± 0.11	1.18 ± 0.15	2.1 ± 0.23	2.64 ± 0.3	2.7 ± 0.4	1.2 ± 0.5
Z+jets	1.8 ± 0.9	1.9 ± 0.9	3.4 ± 1.3	3.8 ± 1.4	3.3 ± 1.2	1.8 ± 0.7
$t\bar{t}t\bar{t}$	0.9 ± 0.4	1.1 ± 0.5	1.8 ± 0.7	1.7 ± 0.7	1.3 ± 0.6	0.65 ± 0.28
tWH	0.23 ± 0.04	0.31 ± 0.04	0.57 ± 0.07	0.7 ± 0.08	0.66 ± 0.07	0.24 ± 0.03
Other	<0.1	<0.1	0.28 ± 0.14	0.42 ± 0.19	0.23 ± 0.08	0.29 ± 0.13
Fakes	1.7 ± 0.9	2.2 ± 1.1	3.2 ± 1.6	2.9 ± 1.5	2.6 ± 1.3	1.1 ± 0.6
Total	144 ± 13	144 ± 13	173 ± 20	143 ± 12	100 ± 11	38 ± 6
Data	150	149	161	149	76	35

olution, and lepton trigger efficiencies are varied within their uncertainties [76,77] to estimate the corresponding systematic uncertainty.

The JES uncertainty [81] accounts for contributions from jet-flavour composition, η-intercalibration, punch-through, single-particle response, calorimeter response to different jet flavours, and pile-up, resulting in 31 uncorrelated JES uncertainty components. The jet energy resolution was measured separately for data and MC using two in situ techniques [81]. The systematic uncertainty is defined as the quadratic difference between the jet energy resolutions for data and simulation and split into 13 uncorrelated uncertainty components. The uncertainty associated with the JVT discriminant is obtained by varying the efficiency correction factors [80].

The uncertainties associated with the b-tagging algorithm calibration are derived separately for b-jets, c-jets and light-flavour jets, as a function of the jet p_{T}, and decomposed into several uncorrelated components for each category, corresponding to the number of p_{T} bins multiplied by the number of DL1r pseudo-continuous scores [94–96]. This yields a total of 45 components for b-jets and 20 each for c- and light jets. For jets with a p_{T} above the p_{T} threshold where the b-tagging algorithm is calibrated, high-p_{T} extrapolation uncertainties derived using MC simulation are included.

The uncertainty in $E_{\mathrm{T}}^{\mathrm{miss}}$ results from the propagation of the uncertainties in the energy scales and resolutions of photons, leptons and jets, and from the modelling of its soft term [85].

For the $t\bar{t}H$ signal, two cross-section uncertainties are applied accounting for the effect of varying the PDF and α_S and for missing higher order terms in the fixed order perturbative QCD calculations. They amount to $\pm 3.6\%$ and $\pm 9.2\%$, respectively [18]. The systematic uncertainty in the $t\bar{t}H$ cross-section includes theory uncertainties due to migrations of events between the truth Higgs boson p_{T} bins [97]. An uncertainty of 2.2% is assigned to the $H \to b\bar{b}$ branching fraction [18]. Two uncertainties due to missing higher order terms in the MC simulation are estimated by varying independently the renormalisation and factorisation scales in the ME of the nominal MC sample by a factor of two up and down. The uncertainties in the amount of initial- and final-state QCD radiation (ISR and FSR) predicted by the PS are estimated by varying the scale in α_S^{ISR} according to the values given by *var3c* in the PYTHIA8 A14 tune and by varying

Table 4 Expected yields in the dilepton control regions before the fit to data. The data-driven corrections to the $t\bar{t}$+jets background are applied and all uncertainties are included, except the ones associated with the $t\bar{t}$+jets background normalisation factors, which are not defined pre-fit. The "Other" category includes the tZq, tWZ and diboson processes. The $t\bar{t}H$ signal is normalised to the SM $t\bar{t}H$ cross-section. For presentation purposes, uncertainties are symmetrised

	$t\bar{t}$ + light CR	$t\bar{t} + \geq 1c$ CR	$t\bar{t} + 1b$ CR	$t\bar{t} + 1B$ CR	$t\bar{t} + \geq 2b$ CR
$t\bar{t}H$ truth p_{T}^{H} 0–60 GeV	11.9 ± 1.4	19.7 ± 2.3	19.8 ± 2.3	9.9 ± 1.4	26.0 ± 3.0
$t\bar{t}H$ truth p_{T}^{H} 60–120 GeV	17.0 ± 1.3	34.5 ± 2.9	29.5 ± 3.0	20.4 ± 2.5	42.0 ± 4.0
$t\bar{t}H$ truth p_{T}^{H} 120–200 GeV	10.0 ± 0.9	27.1 ± 2.7	17.0 ± 2.1	19.2 ± 2.4	34.0 ± 3.5
$t\bar{t}H$ truth p_{T}^{H} 200–300 GeV	3.1 ± 0.35	11.1 ± 1.3	4.6 ± 0.7	9.2 ± 1.2	14.9 ± 1.9
$t\bar{t}H$ truth p_{T}^{H} 300–450 GeV	0.94 ± 0.15	3.5 ± 0.5	0.94 ± 0.19	3.3 ± 0.5	5.4 ± 0.8
$t\bar{t}H$ truth $p_{\mathrm{T}}^{H} \geq 450$ GeV	0.33 ± 0.07	0.65 ± 0.12	0.116 ± 0.033	0.97 ± 0.15	1.33 ± 0.26
$t\bar{t}H$ $\lvert y\rvert > 2.5$	0.31 ± 0.05	0.25 ± 0.04	0.4 ± 0.05	0.127 ± 0.028	0.166 ± 0.018
$t\bar{t} + \geq 2b$	495 ± 35	860 ± 60	1080 ± 200	650 ± 100	2700 ± 200
$t\bar{t} + 1b$	1410 ± 130	1790 ± 230	3600 ± 700	1540± 180	1200 ± 400
$t\bar{t} + 1B$	310 ± 40	460 ± 40	540± 210	1560 ± 230	310 ± 110
$t\bar{t} + \geq 1c$	5600 ± 500	7700 ± 600	2210 ± 280	1590 ± 330	1070 ± 170
$t\bar{t}$ + light	9200 ± 1500	2800 ± 400	590 ± 130	410 ± 90	190 ± 70
$t\bar{t}Z$	43 ± 6	81 ± 12	35 ± 6	36 ± 5	92 ± 12
tW	300 ± 60	210 ± 50	220 ± 70	150 ± 50	300 ± 140
$t\bar{t}W$	37 ± 5	72 ± 7	12.1 ± 1.3	14.3 ± 3.3	29.8 ± 3.5
Z+jets	340 ± 130	260 ± 100	250 ± 90	93 ± 34	320 ± 120
$t\bar{t}t\bar{t}$	1.6 ± 0.7	10± 4	1± 0.4	4.8 ± 2	28 ± 12
tWH	0.98 ± 0.11	2.24 ± 0.22	2.69 ± 0.29	1.42 ± 0.14	4.0 ± 0.4
Other	5.6 ± 2.4	8.1 ± 3.1	4.4 ± 2.0	2.1 ± 0.7	12 ± 5
Fakes	110 ± 50	120 ± 60	40 ± 20	40 ± 20	80 ± 40
Total	18000 ± 2000	14400 ± 1100	8700 ± 900	6200 ± 500	6400 ± 700
Data	18557	14361	8624	5830	6448

the scale in α_S^{FSR} by a factor two up and down. To assess the uncertainties associated with the PS, hadronisation and underlying event, the nominal $t\bar{t}H$ sample is compared with the alternative POWHEG+HERWIG7 sample, while the uncertainty due to the NLO matching procedure is estimated with POWHEG+PYTHIA8 with a varied $p_{\mathrm{T}}^{\mathrm{hard}}$ parameter value.

All the modelling uncertainties in the $t\bar{t}$+jets background have independent nuisance parameters for the $t\bar{t}$+$1b$, $t\bar{t}$+$1B$, $t\bar{t}$+$\geq 2b$, $t\bar{t}$+$\geq 1c$ and $t\bar{t}$+light processes. These systematic variations are normalised to conserve the total nominal event count after the preselection for each process. Uncertainties due to missing higher order terms in the perturbative QCD calculations, in the amount of ISR and FSR as well as the uncertainties associated with the PS and hadronisation, and with the NLO matching procedure are estimated in the same way as for the $t\bar{t}H$ signal.

For $t\bar{t} + \geq 1b$, the choice of recoil scheme in the ISR PS has a sizeable effect in the normalisations and shapes of the distributions used in the analysis within the detector acceptance [22]. The uncertainty associated with the choice of the global recoil scheme is assessed by comparing the nominal sample with an alternative sample produced with the dipole recoil scheme. For $t\bar{t}$ + light and $t\bar{t} + \geq 1c$, the uncertainty in the choice of the h_{damp} parameter is estimated by using the alternative POWHEGBOX+PYTHIA8 sample with $h_{\mathrm{damp}} = 3\ m_{\mathrm{top}}$.

Uncertainties related to the H_{T} reweighting procedure described in Sect. 5.1 are assigned independently in the single-lepton and dilepton channels. The $t\bar{t}$ + light and $t\bar{t} + \geq 1c$ normalisation factors are varied within their uncertainties to estimate the corresponding systematic uncertainty. An additional uncertainty is estimated by comparing the distributions with and without the weights derived in the H_{T} reweighting procedure, in bins of jet multiplicity.

A ±5% normalisation uncertainty is considered for the cross-sections of the t- and s- single-top production modes [98,99]. The normalisation uncertainty of the tW background is 3.7% [100]. Modelling uncertainties in the tW production due to the choice of the PS and hadronisation model, the NLO matching and the h_{damp} parameter choice are evaluated in the same way as for the $t\bar{t}$ + light and $t\bar{t} + \geq 1c$ backgrounds. The uncertainty associated with the interference between tW and $t\bar{t}$ production at NLO is assessed by comparing the nominal POWHEGBOX+PYTHIA8 sample pro-

duced using the diagram removal scheme to an alternative sample produced with the same generator but using the diagram subtraction scheme.

The total uncertainty in the theoretical $t\bar{t}W$ cross-section computed at NNLO in the QCD and at NLO in the electroweak interactions is 7.4% [71]. The modelling uncertainty in the $t\bar{t}W$ background is evaluated by comparing the nominal SHERPA simulation with the sample produced using MADGRAPH5_AMC@NLO. For the $t\bar{t}Z$ production, the uncertainty in the predicted cross-section at NLO in QCD is 12% [18]. The modelling uncertainty in the $t\bar{t}Z$ background is evaluated by comparing the nominal MADGRAPH5_AMC@NLO+PYTHIA8 sample with the sample where PYTHIA8 is replaced by HERWIG7 to simulate the PS and hadronisation.

A normalisation uncertainty of $^{+70\%}_{-15\%}$ is assigned for the $t\bar{t}t\bar{t}$ background. The down variation corresponds to the theory uncertainty covering effects from varying the factorisation and renormalisation scales, the PDFs and α_S [101] while the up variation covers the measured $t\bar{t}t\bar{t}$ cross-section [102]. For tZq, the total normalisation uncertainty is 7.9% [37]. A normalisation uncertainty of 15.4% (9.2%) calculated using MADGRAPH5_AMC@NLO at NLO is applied to the $tHjb$ (tWH) background normalisation [103]. For tWZ, an uncertainty of ±50% is used [37].

The treatment of V+jets uncertainties follows the previous analysis [104]. An uncertainty of 40% is assumed for the W+jets cross-section, with an additional 30% normalisation uncertainty used for W boson production in association with heavy-flavour jets, taken as uncorrelated between events with two and events with more than two truth-level heavy-flavour jets. These uncertainties are based on variations of the factorisation and renormalisation scales and of the matching parameters in the SHERPA samples. An uncertainty of 35% is applied to the Z+jets normalisation to account for both the variations of the scales and matching parameters in the SHERPA samples and the uncertainty in the correction factor for the Z boson production accompanied by two b-jets extracted from data. A 50% normalisation uncertainty is used for the diboson background, which includes uncertainties in the inclusive cross-section and additional jet production [105–107].

A 50% normalisation uncertainty is assigned to the fake-lepton background estimate in the single-lepton and dilepton channels separately. An additional uncertainty obtained by using an alternative parameterisation of the fake rate (Sect. 5.2) is considered in the single-lepton channel.

8 Results

An excess of events over the expected background is found with an observed (expected) significance of 4.6 (5.4) standard deviations, in a combined profile-likelihood fit to data in all signal and control regions. The measured $t\bar{t}H$ signal strength for $m_H = 125.09$ GeV [108] is

$$\mu_{t\bar{t}H} = 0.81^{+0.22}_{-0.19} = 0.81 \pm 0.11(\text{stat.})\,^{+0.20}_{-0.16}(\text{syst.}). \quad (2)$$

The total statistical uncertainty is defined as the uncertainty in $\mu_{t\bar{t}H}$ when all nuisance parameters associated with the systematic uncertainties are fixed to their best-fit values. The total systematic uncertainty is then defined as the difference in quadrature between the total and statistical uncertainties. The systematic uncertainty in the signal strength $\mu_{t\bar{t}H}$ includes the theoretical uncertainties in the SM $t\bar{t}H$ cross-section described in Sect. 7. The measured $t\bar{t}H$ signal strength in the single-lepton channel is

$$\mu_{t\bar{t}H} = 0.72 \pm 0.12(\text{stat.})\,^{+0.21}_{-0.17}(\text{syst.}) \quad (3)$$

and in the dilepton channel is

$$\mu_{t\bar{t}H} = 1.03 \pm 0.26(\text{stat.})\,^{+0.28}_{-0.22}(\text{syst.}). \quad (4)$$

The combined $\mu_{t\bar{t}H}$ is converted into an inclusive cross-section using the SM theoretical cross-section of 507^{+35}_{-50} fb for $m_H = 125.09$ GeV and excluding its uncertainty [18]. The resulting cross-section is

$$\sigma_{t\bar{t}H} = 411\,^{+101}_{-92}\ \text{fb} = 411 \pm 54(\text{stat.})\,^{+85}_{-75}(\text{syst.})\ \text{fb}, \quad (5)$$

with a relative uncertainty of $^{+25\%}_{-22\%}$, consistent with the SM prediction. The sensitivity is driven by the single-lepton channel, where the systematic component of the uncertainty dominates. The sensitivity of the dilepton channel is limited by the size of the dataset.

The measured values of the $t\bar{t}+$ jets background normalisation factors, which are free parameters of the fit, are listed in Table 5. They are compatible between the single-lepton and the dilepton channels within two standard deviations. For $t\bar{t}+1b$, the measured value of the normalisation factor is slightly larger in the dilepton channel than in the single-lepton channel.

Compared with the previous analysis using the same dataset, the current analysis selects 64% (29%) new events in the single-lepton (dilepton) SR that did not enter the selection of the previous analysis. This is consistent with the increase of the overall acceptance by a factor of three. The statistical correlation between the two analyses is estimated using a booststrap method to be 19%, assuming that the systematic uncertainties are independent. This assumption is justified by the fact that the systematic model of the most important $t\bar{t}+\geq 1b$ background is different between the two analyses and the experimental uncertainties are updated. Based on

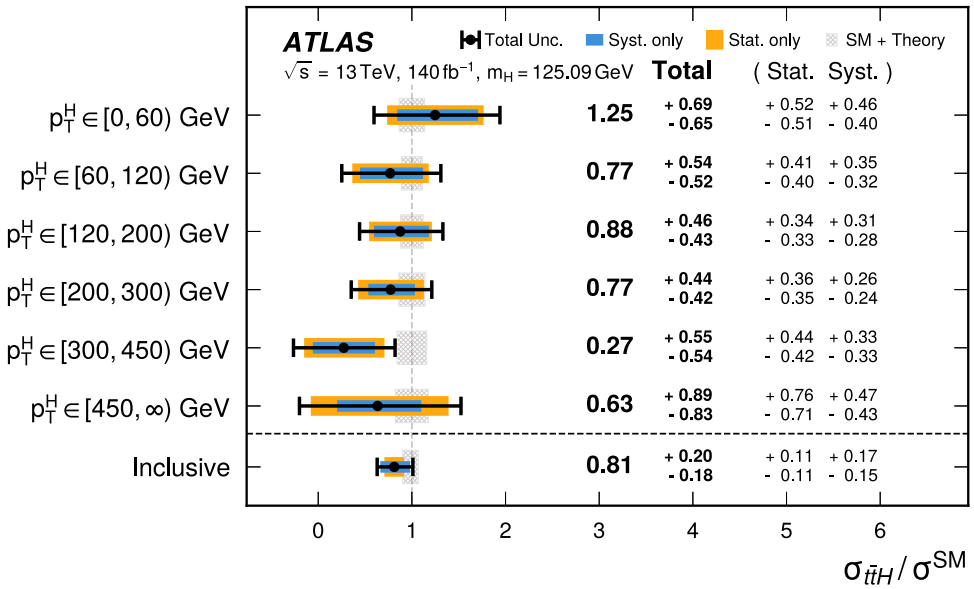

Fig. 3 The $t\bar{t}H$ cross-sections measured in bins of truth Higgs boson p_{T} for a Higgs boson rapidity $|y| \leq 2.5$, and measured inclusively in the full phase space, normalised to their SM predictions, as obtained from a combined profile-likelihood fit to data in all signal and control regions. The uncertainties are shown separately for the measurement and the prediction

Table 5 Best-fit values of the $t\bar{t}+$ jets normalisation factors obtained from the fit to data with a single inclusive $t\bar{t}H$ signal strength parameter. Independent normalisation factors for $t\bar{t}+1b$, $t\bar{t}+\geq 1c$ and $t\bar{t}+$ light components are used in the dilepton and single-lepton channels. Before the fit, the $t\bar{t}+$ light and $t\bar{t}+\geq 1c$ components are normalised to the $t\bar{t}$ cross-section computed at NNLO in QCD including the resummation of NNLL soft-gluon terms [72] while the $t\bar{t}+\geq 1b$ normalisation is taken from the $t\bar{t}b\bar{b}$ MC simulation

Normalisation factor	$t\bar{t}+$ light	$t\bar{t}+\geq 1c$	$t\bar{t}+1b$	$t\bar{t}+1B$	$t\bar{t}+\geq 2b$
Single-lepton	$0.78^{+0.08}_{-0.08}$	$1.51^{+0.19}_{-0.18}$	$1.06^{+0.10}_{-0.10}$	$1.15^{+0.15}_{-0.14}$	$0.94^{+0.08}_{-0.08}$
Dilepton	$0.88^{+0.11}_{-0.10}$	$1.36^{+0.10}_{-0.10}$	$1.24^{+0.09}_{-0.09}$		

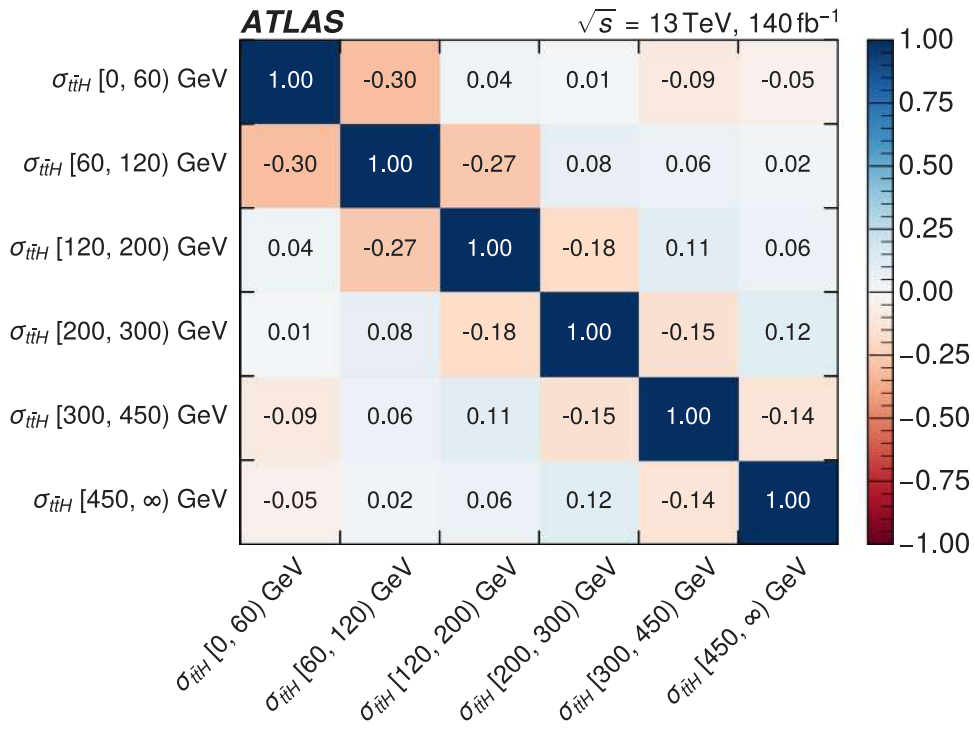

Fig. 4 Post-fit correlations between the measured values of the $t\bar{t}H$ cross-section, $\sigma_{t\bar{t}H}$, in bins of truth p_{T}^{H}

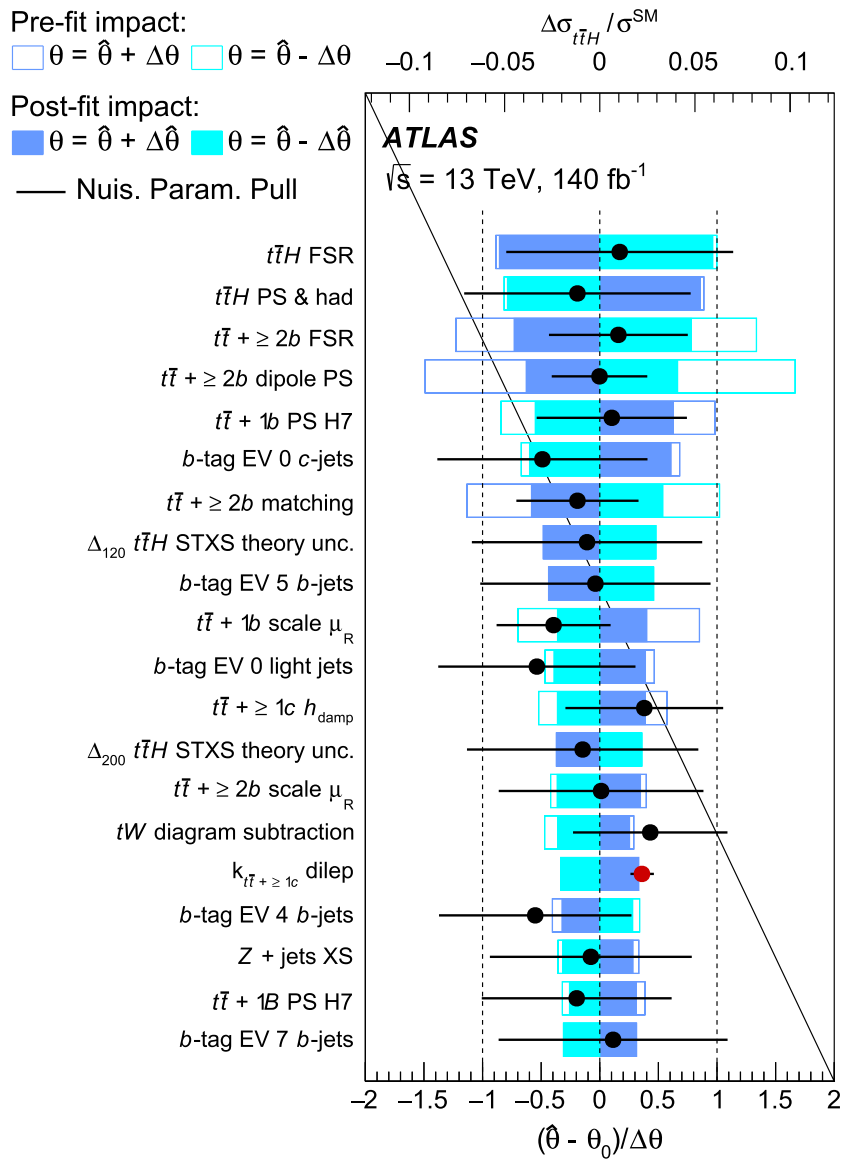

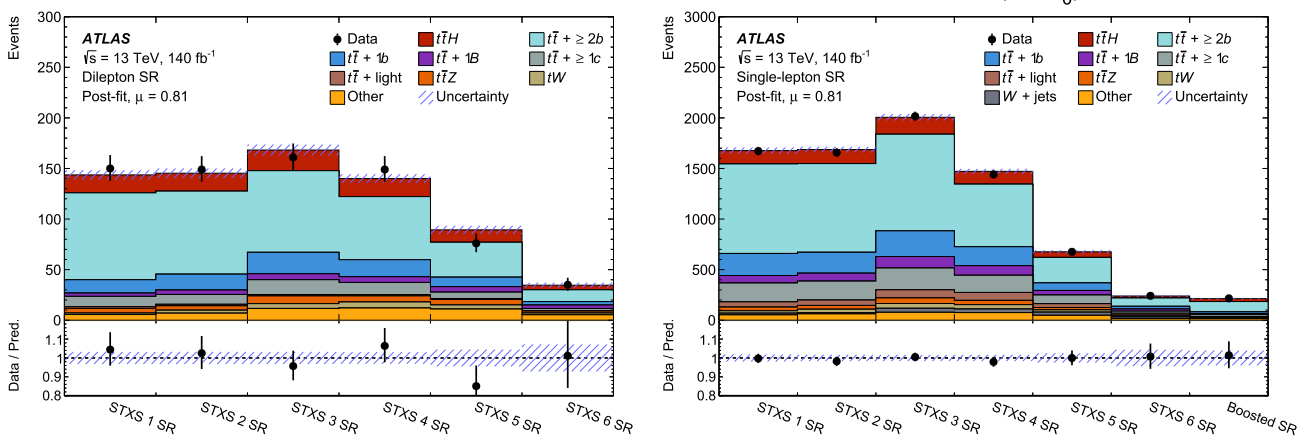

(a) (b)

Fig. 5 Ranking of the 20 modelling and experimental systematic uncertainties with the largest post-fit impact on the inclusive cross-section. The empty (filled) blue rectangles correspond to the pre-(post-)fit impact on $\sigma_{t\bar{t}H}/\sigma^{\mathrm{SM}}$ and refer to the upper scale of the plot. The impact of each nuisance parameter, $\Delta\sigma_{t\bar{t}H}/\sigma^{\mathrm{SM}}$, is computed by comparing the nominal best-fit value of $\sigma_{t\bar{t}H}/\sigma^{\mathrm{SM}}$ with the result of the fit when fixing the considered nuisance parameter to its best-fit value, $\hat{\theta}$, shifted by its pre-fit (post-fit) uncertainties $\pm\Delta\theta$ ($\pm\Delta\hat{\theta}$). The black markers show the pulls of the nuisance parameters relative to their nominal values, $\theta_0 = 0$. The red marker shows the pull of the $t\bar{t} + \geq 1c$ normalisation factor in the dilepton channel relative to its nominal value, $\theta_0 = 1$. No pre-fit uncertainty is defined for the normalisation factor as it is a free parameter of the fit. The pulls and their relative post-fit errors, $\Delta\hat{\theta}/\Delta\theta$, refer to the lower scale of the plot

Fig. 6 Post-fit summary of the yields in the (**a**) dilepton and (**b**) single-lepton signal regions, with all regions aggregated into a single bin each. The uncertainty band includes all uncertainties and their correlations

Table 6 A list of the absolute and relative uncertainties in the measured $\sigma_{t\bar{t}H}$ grouped in categories. The contributions from different sources of uncertainty are evaluated after the fit. The quoted values are obtained by repeating the fit, while fixing the set of nuisance parameters of the sources corresponding to each category to their best-fit values, and subtracting in quadrature the resulting uncertainty from the total uncertainty of the nominal fit presented in the last row. The total uncertainty is different from the sum in quadrature of the different components due to correlations between nuisance parameters in the fit. The $t\bar{t}H$ and $t\bar{t}+\geq 1b$ radiation uncertainty categories include the renormalisation and factorisation scales, ISR and FSR uncertainties. The "$t\bar{t}H$ theory" category includes STXS-related theoretical uncertainties and uncertainty in the $H \to b\bar{b}$ branching fraction. The "Minor background modelling" category includes uncertainties in the fake-lepton background and in minor backgrounds as defined in the text. The total statistical uncertainty includes uncertainties in the normalisation factors

Uncertainty source	$\Delta\sigma_{t\bar{t}H}$ (fb)		$\Delta\sigma_{t\bar{t}H}/\sigma_{t\bar{t}H}$ (%)	
Process modelling				
$t\bar{t}H$ modelling				
$t\bar{t}H$ radiation	+35	−21	+9	−5
$t\bar{t}H$ parton shower	+32	−19	+8	−5
$t\bar{t}H$ matching	<0.1	−0.3	<0.1	−0.1
$t\bar{t}H$ theory	+25	−17	+6	−4
$t\bar{t}+\geq 1b$ modelling				
$t\bar{t}+\geq 1b$ radiation	±31		±8	
$t\bar{t}+\geq 1b$ parton shower	±29		±7	
$t\bar{t}+\geq 1b$ matching	±19		±5	
$t\bar{t}+\geq 1c$ modelling	±18		±4	
$t\bar{t}+$ light modelling	±5		±1	
tW modelling	±16		±4	
Minor background modelling	±19		±5	
Flavour tagging	±36		±9	
Jet modelling	±22		±5	
Monte-Carlo statistics	±17		±4	
Other instrumental	±10		±2	
Total systematic uncertainty	+85	−75	+21	−18
Normalisation factors	±21		±5	
Total statistical uncertainty	±54		±13	
Total uncertainty	+101	− 92	+25	− 22

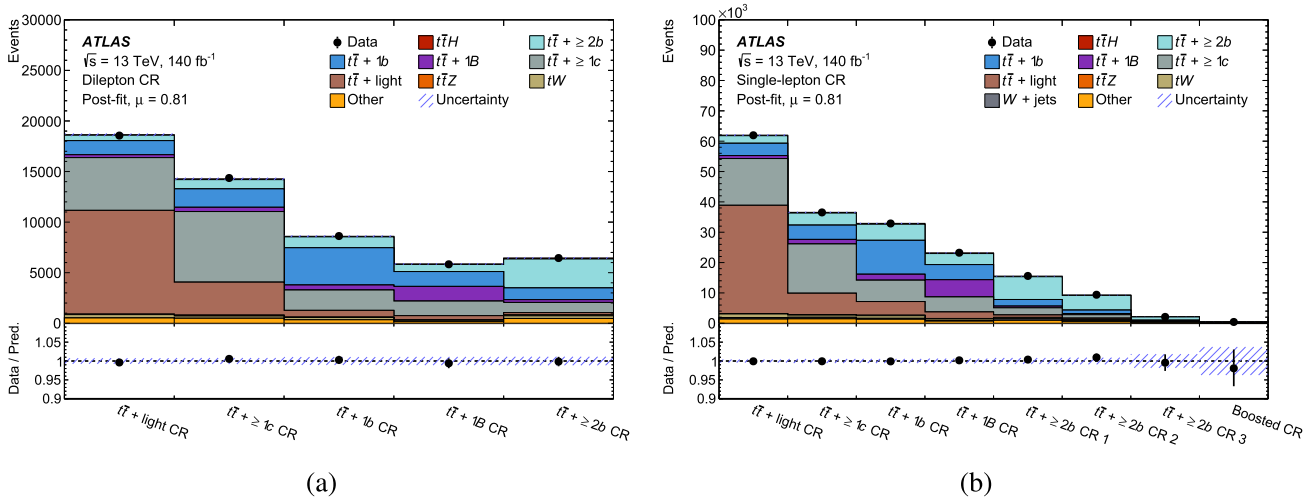

(a) (b)

Fig. 7 Post-fit summary of the yields in the (**a**) dilepton and (**b**) single-lepton control regions, with all regions aggregated into a single bin each. The uncertainty band includes all uncertainties and their correlations

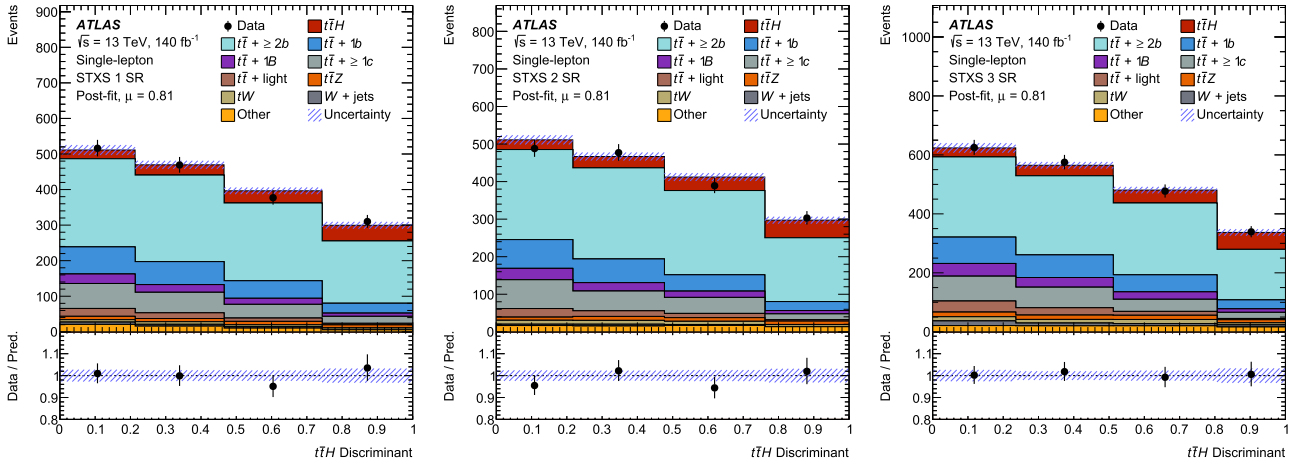

(a)

(b)

(c)

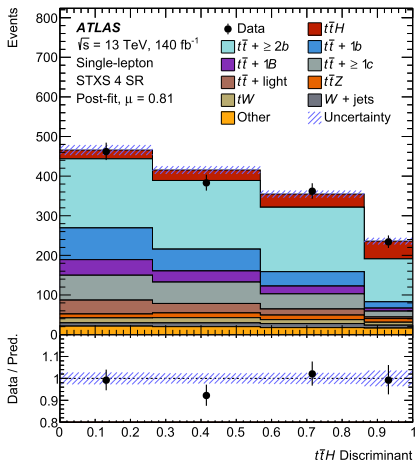

(d)

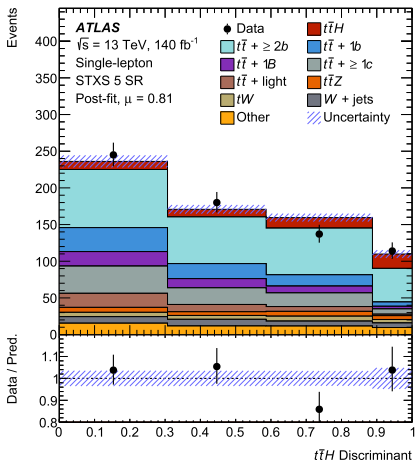

(e)

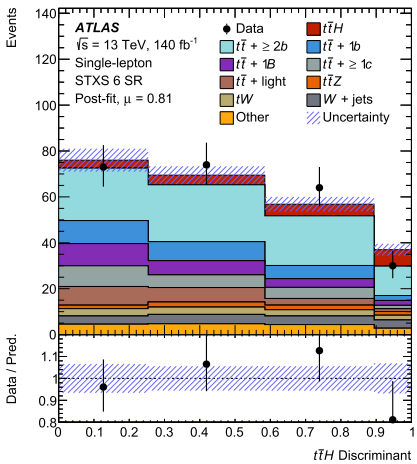

(f)

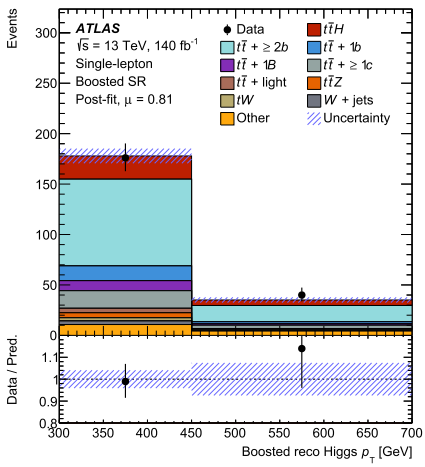

(g)

Fig. 8 Post-fit data/prediction comparisons of the signal region distributions entering the fit in the single-lepton channel. The discriminants are rescaled to lie between zero and one using a logistic function. The signal and background normalisation parameters and the nuisance parameters are set to their best-fit values. The uncertainty band includes all uncertainties and their correlations. For the reconstructed Higgs boson p_{T} in the boosted signal region, the first (last) bin includes the underflow (overflow) contributions

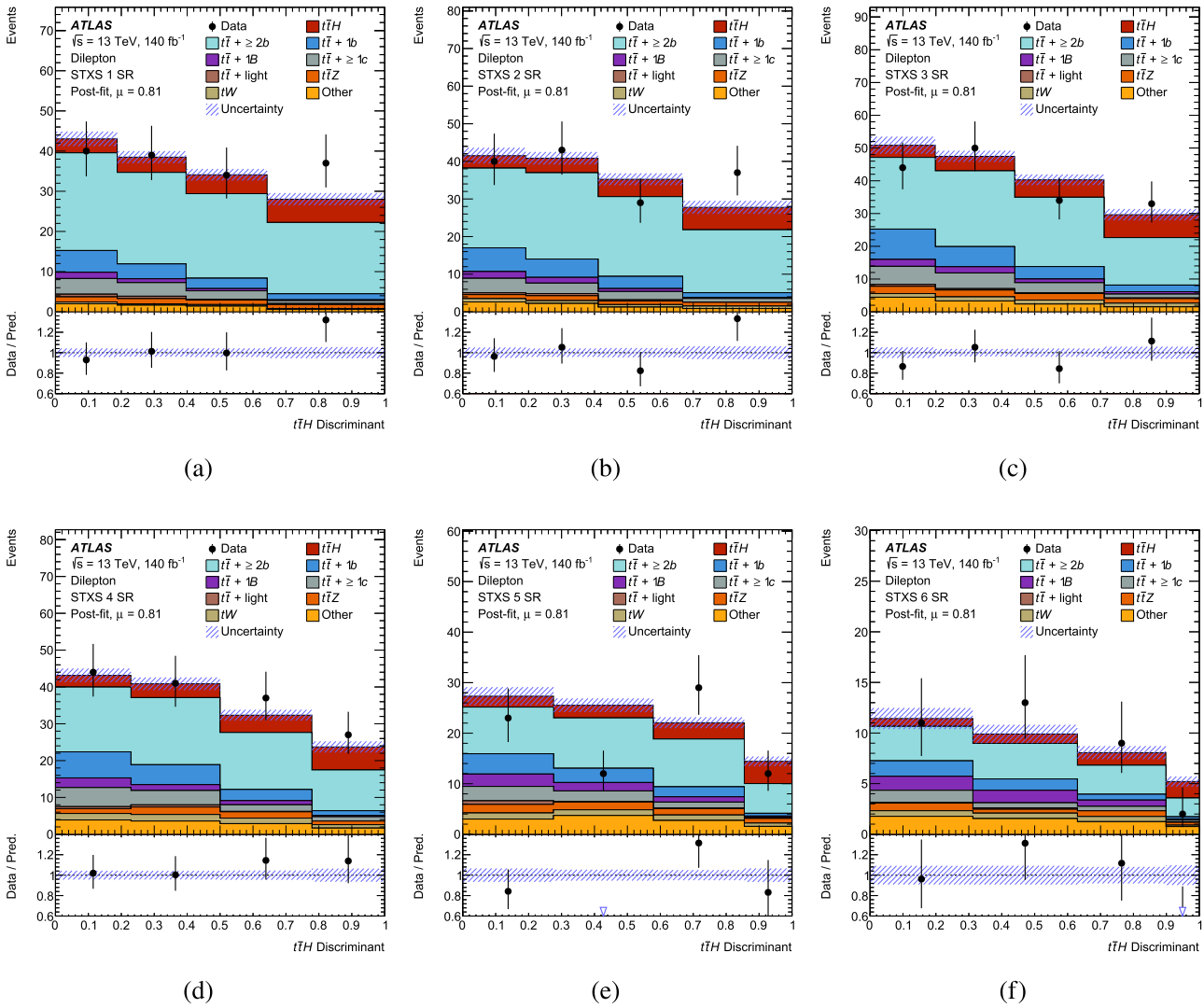

Fig. 9 Post-fit data/prediction comparisons of the signal region distributions entering the fit in the dilepton channel. The discriminants are rescaled to lie between zero and one using a logistic function. The signal and background normalisation parameters and the nuisance parameters are set to their best-fit values. The uncertainty band includes all uncertainties and their correlations

this, the probability that the current result is compatible with the result of Ref. [20] is estimated as 21%.

Figure 3 shows the measured values of $\sigma_{t\bar{t}H}/\sigma^{\mathrm{SM}}$ in bins of the Higgs boson p_{T}, obtained from a combined profile-likelihood fit to data with a free $t\bar{t}H$ signal strength parameter for each bin. The result of this measurement is compatible with the SM prediction with a p-value of 89%, taking into account theoretical uncertainties in the SM $t\bar{t}H$ cross-section. The measured value of the inclusive signal strength is also shown. The measurement of $\sigma_{t\bar{t}H}/\sigma^{\mathrm{SM}}$ in the [300, 450) GeV and [450, ∞) GeV p_{T}^{H} bins is limited by statistical uncertainties. In the remaining bins, there is a similar contribution from statistical and systematic uncertainties. Defining boosted regions improves sensitivity in the [450, ∞) GeV p_{T}^{H} bin by about 15%, compared with the scenario where only the resolved event selection is applied to these events. The correlations between the parameters of interest are shown in Fig. 4. They do not exceed 30% and are larger in the lower Higgs boson transverse momentum region.

The fitted values of $t\bar{t}$ + jets background normalisation factors are consistent with those obtained in the fit with a single $\mu_{t\bar{t}H}$ parameter shown in Table 5.

The absolute and relative systematic uncertainties in the measurement of $\sigma_{t\bar{t}H}$, grouped in categories, are shown in Table 6, and the effect of individual nuisance parameters ranked according to their impact on the inclusive $\sigma_{t\bar{t}H}/\sigma^{\mathrm{SM}}$ is shown in Fig. 5. The largest impact originates from the signal

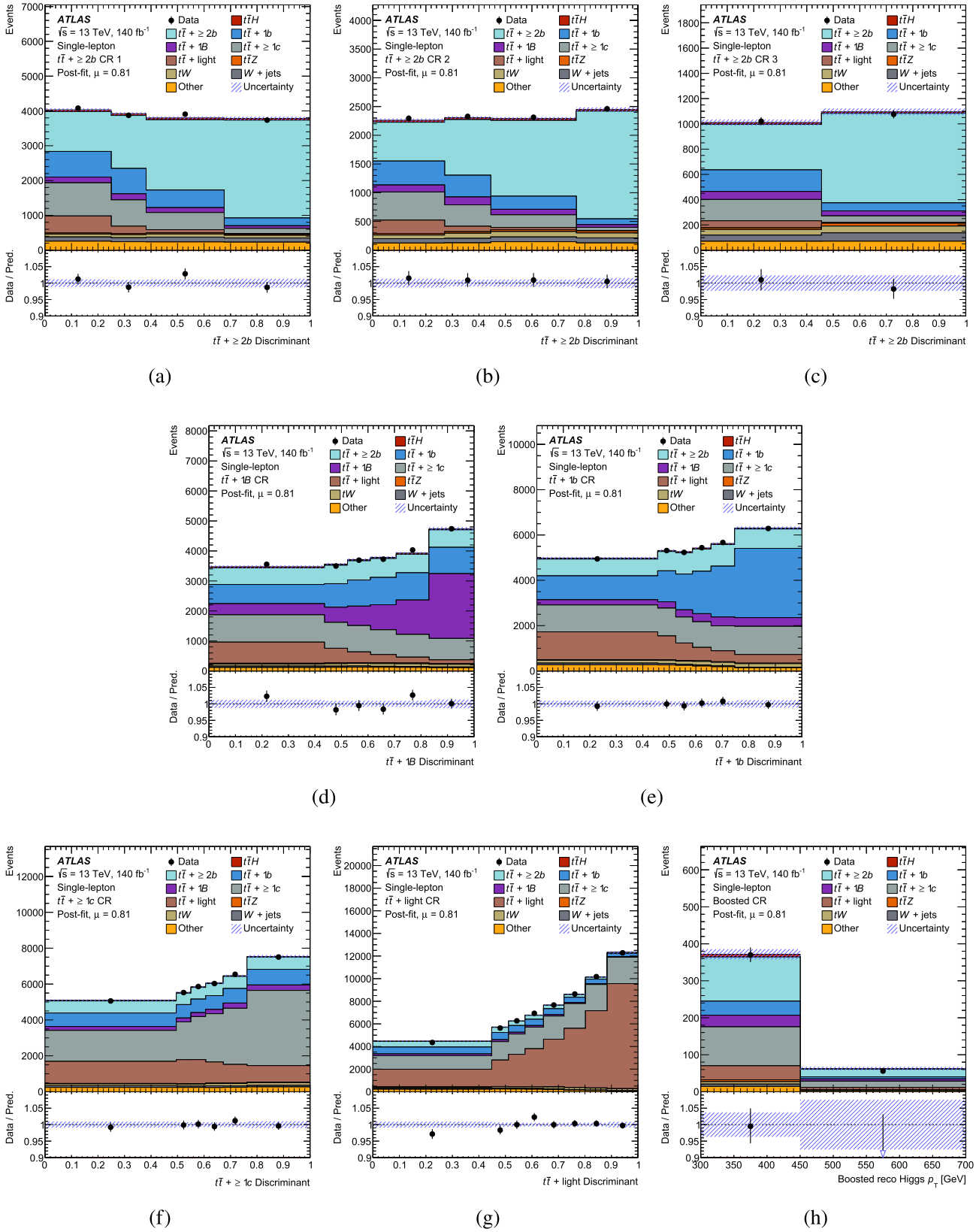

Fig. 10 Post-fit data/prediction comparisons of the control region distributions entering the fit in the single-lepton channel. The discriminants are rescaled to lie between zero and one using a logistic function. The signal and background normalisation parameters and the nuisance parameters are set to their best-fit values. The uncertainty band includes all uncertainties and their correlations. For the reconstructed Higgs boson p_{T} in the boosted control region, the first (last) bin includes the underflow (overflow) contributions

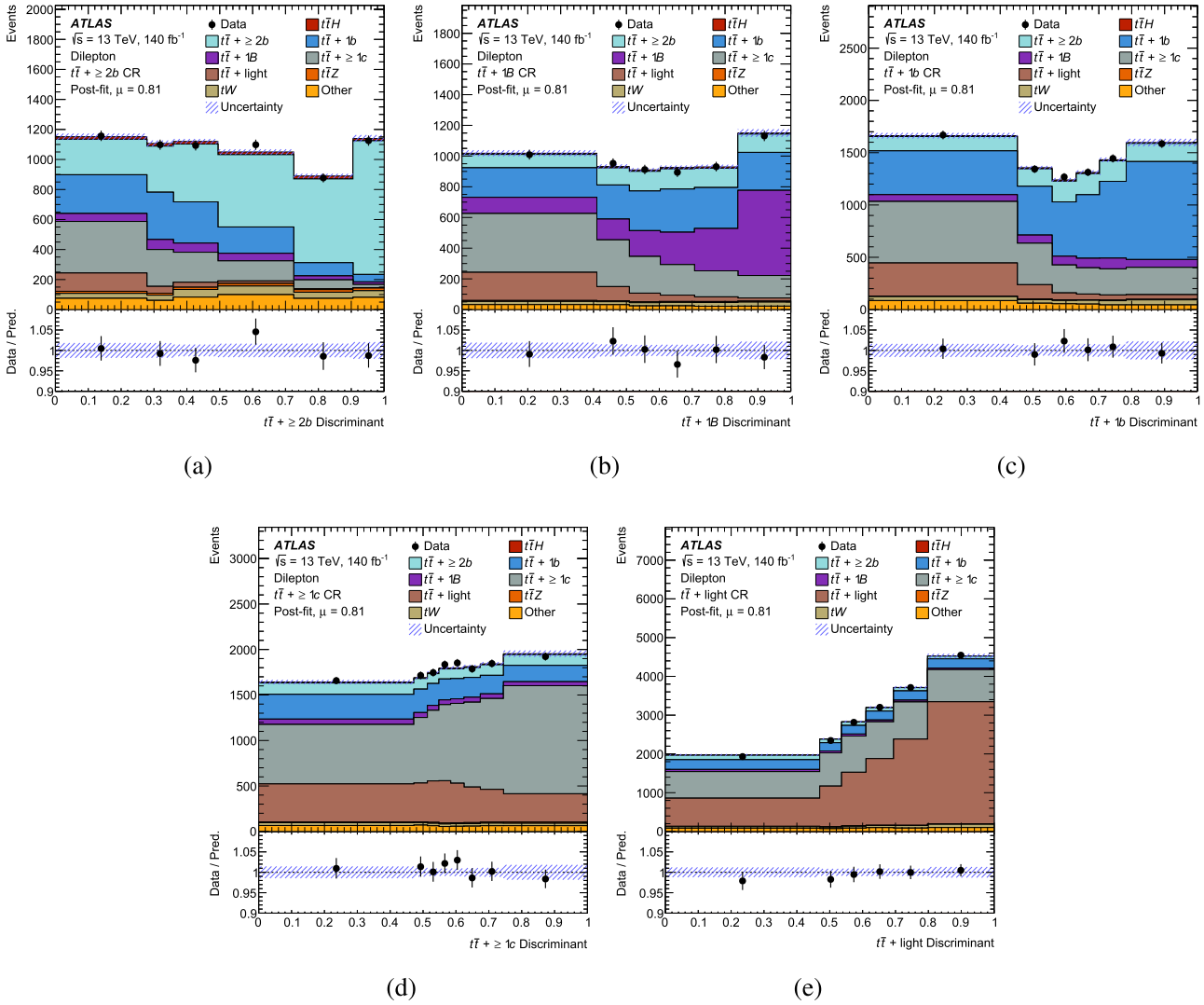

Fig. 11 Post-fit data/prediction comparisons of the control region distributions entering the fit in the dilepton channel. The discriminants are rescaled to lie between zero and one using a logistic function. The signal and background normalisation parameters and the nuisance parameters are set to their best-fit values. The uncertainty band includes all uncertainties and their correlations

modelling, followed by the $t\bar{t}+\geq 2b$ background modelling. In both cases, the dominant effects arise from the modelling of the FSR and the choice of the PS model. Among the experimental uncertainties, the largest effects come from the b-jet tagging and the jet energy scale.

Among the eight highest ranked nuisance parameters in Fig. 5, the largest constraints are observed for the $t\bar{t}+\geq 2b$ uncertainties arising from the dipole shower model and the choice of matching algorithm. These constraints predominantly originate from the single-lepton channel, and more specifically the SRs and the $t\bar{t}+\geq 2b$ CR where the $t\bar{t}+\geq 2b$ background contribution is large. The constraints are more pronounced when the $t\bar{t}+\geq 2b$ CR is split into three in the single-lepton channel to better control the $t\bar{t}+\geq 2b$ background modelling in bins of the reconstructed Higgs boson p_{T}.

The observed yields in all signal and control regions are compared to the post-fit predictions in Figs. 6 and 7. In each region, all bins are aggregated into a single bin. Figures 89 and 10 11 show a more detailed comparison in the single-lepton (dilepton) signal and control regions. The signal and background predictions in all post-fit distributions are obtained by setting the free parameters and the nuisance parameters to their best-fit values. In all post-fit plots, the uncertainty band includes all uncertainties and their correlations. The discriminant output in the plots is rescaled to be between zero and one using a logistic function.

The global goodness of fit [109,110] is 87% for the $\sigma_{t\bar{t}H}/\sigma^{\mathrm{SM}}$ measurement in p_{T}^{H} bins, highlighting that good post-fit modelling is achieved.

Figure 12 shows the event yield in data compared with the post-fit signal (S) and total background (B) predictions. It is ordered by the signal-to-background ratio of the bins from all the fitted regions. The predictions are shown for the best-fit signal strength and for the SM prediction. The observed data shows an excess over the background compatible with the best-fit signal strength $\mu_{t\bar{t}H}=0.81$ in the high $\log_{10}(S/B)$ region.

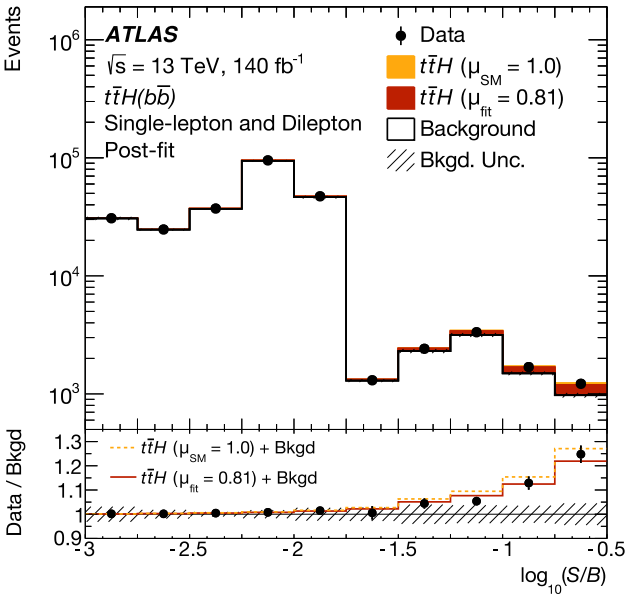

Fig. 12 Observed and expected event yields as a function of $\log_{10}(S/B)$, where S and B are the post-fit signal and total background yields, respectively. The bins in all fitted regions are ordered and grouped in bins of $\log_{10}(S/B)$. The signal is shown for the best-fit signal strength, $\mu=0.81$, or the SM prediction, $\mu=1.0$. The lower panel shows the ratio of the data to the post-fit background prediction, compared with the signal-plus-background prediction with the best-fit signal strength and the SM prediction. The shaded band represents the total uncertainty in the background prediction. The first (last) bin includes the underflow (overflow) contributions

9 Conclusion

The associated production of a Higgs boson with a pair of top quarks was measured in the $H\to b\bar{b}$ decay channel, using the full Run 2 proton–proton collision dataset collected at $\sqrt{s}=13$ TeV by the ATLAS detector at the LHC, corresponding to 140 fb^{-1}. The measurement uses final states containing one or two leptons. The measured inclusive cross-section assuming a Higgs boson mass of 125.09 GeV is $411\pm 54(\mathrm{stat.})\,^{+85}_{-75}(\mathrm{syst.})$ fb with a relative uncertainty of 24%, consistent with the SM prediction. The measurement is dominated by the systematic uncertainties arising from the $t\bar{t}H$ signal modelling followed by the $t\bar{t}+$ jets background modelling. The observed (expected) significance of the $t\bar{t}H$ signal relative to the SM background-only hypothesis is 4.6 (5.4) standard deviations. The cross-section measurement is also performed in six bins of p_{T}^{H} in the STXS framework with the highest bin probing Higgs bosons with p_{T}^{H} above 450 GeV. The uncertainty in the measurement for p_{T}^{H} above 300 GeV is dominated by the limited number of data events.

With respect to the previous iteration of the analysis, this measurement profits from looser selection requirements and improved b-jet identification that increase the $t\bar{t}H$ signal acceptance. Control regions enriched in each of the $t\bar{t}+$ jets components are defined based on a more powerful multi-class neural network. Together with data-driven modelling corrections for the $t\bar{t}+\geq 1c$ and $t\bar{t}+$ light components, and a dedicated MC simulation and systematic model for the $t\bar{t}+\geq 1b$ component, they provide improved signal sensitivity and better control over the background, such that the modelling uncertainty in $t\bar{t}+\geq 1b$ is no longer the dominant contribution to the total systematic uncertainty.

This analysis is the most precise $t\bar{t}H$ cross-section measurement in a single decay channel, inclusively and in each p_{T}^{H} bin.

Acknowledgements We thank CERN for the very successful operation of the LHC and its injectors, as well as the support staff at CERN and at our institutions worldwide without whom ATLAS could not be operated efficiently. The crucial computing support from all WLCG partners is acknowledged gratefully, in particular from CERN, the ATLAS Tier-1 facilities at TRIUMF/SFU (Canada), NDGF (Denmark, Norway, Sweden), CC-IN2P3 (France), KIT/GridKA (Germany), INFN-CNAF (Italy), NL-T1 (Netherlands), PIC (Spain), RAL (UK) and BNL (USA), the Tier-2 facilities worldwide and large non-WLCG resource providers. Major contributors of computing resources are listed in Ref. [111]. We gratefully acknowledge the support of ANPCyT, Argentina; YerPhI, Armenia; ARC, Australia; BMWFW and FWF, Austria; ANAS, Azerbaijan; CNPq and FAPESP, Brazil; NSERC, NRC and CFI, Canada; CERN; ANID, Chile; CAS, MOST and NSFC, China; Minciencias, Colombia; MEYS CR, Czech Republic; DNRF and DNSRC, Denmark; IN2P3-CNRS and CEA-DRF/IRFU, France; SRNSFG, Georgia; BMBF, HGF and MPG, Germany; GSRI, Greece; RGC and Hong Kong SAR, China; ISF and Benoziyo Center, Israel; INFN, Italy; MEXT and JSPS, Japan; CNRST, Morocco; NWO, Netherlands; RCN, Norway; MNiSW, Poland; FCT, Portugal; MNE/IFA, Romania; MSTDI, Serbia; MSSR, Slovakia; ARIS and MVZI, Slovenia; DSI/NRF, South Africa; MICIU/AEI, Spain; SRC and Wallenberg Foundation, Sweden; SERI, SNSF and Cantons of Bern and Geneva, Switzerland; NSTC, Taipei; TENMAK, Türkiye; STFC/UKRI, United Kingdom; DOE and NSF, United States of America. Individual groups and members have received support from BCKDF, CANARIE, CRC and DRAC, Canada; CERN-CZ, FORTE and PRIMUS, Czech Republic; COST, ERC, ERDF, Horizon 2020, ICSC-NextGenerationEU and Marie Skłodowska-Curie Actions, European Union; Investissements d'Avenir Labex, Investissements d'Avenir Idex and ANR, France; DFG and AvH Foundation, Germany; Herakleitos, Thales and Aristeia programmes co-financed by EU-ESF and the Greek NSRF, Greece; BSF-NSF and MINERVA, Israel; NCN and NAWA, Poland; La Caixa Banking Foundation, CERCA Programme Generalitat de Catalunya and PROMETEO and GenT Programmes Generalitat Valenciana, Spain; Göran Gustafssons Stiftelse, Sweden; The Royal Society and Leverhulme Trust, United Kingdom. In addition, individual members wish to acknowledge support from Armenia: Yerevan Physics Institute (FAPERJ); CERN: European Organization for Nuclear Research (CERN PJAS); Chile: Agencia Nacional de Investigación y Desarrollo (FONDECYT 1230812, FONDECYT 1230987, FONDECYT 1240864); China: Chinese Ministry of Science and Technology (MOST-2023YFA1605700), National Natural Science Foundation of China (NSFC - 12175119, NSFC 12275265, NSFC-12075060); Czech Republic: Czech Science Foundation (GACR - 24-11373S), Ministry of Education Youth and Sports (FORTE CZ.02.01.01/00/22_008/0004632), PRIMUS Research Programme (PRIMUS/21/SCI/017); EU: H2020 European Research Council (ERC - 101002463); European Union: European Research Council (ERC - 948254, ERC 101089007), Horizon 2020 Framework Programme (MUCCA - CHIST-ERA-19-XAI-00), European Union, Future Artificial Intelligence Research (FAIR-NextGenerationEU PE00000013), Italian Center for High Performance Computing, Big Data and Quantum Computing (ICSC, NextGenerationEU); France: Agence Nationale de la Recherche (ANR-20-CE31-0013, ANR-21-CE31-0013, ANR-21-CE31-0022, ANR-22-EDIR-0002), Investissements d'Avenir Labex (ANR-11-LABX-0012); Germany: Baden-Württemberg Stiftung (BW Stiftung-Postdoc Eliteprogramme), Deutsche Forschungsgemeinschaft (DFG - 469666862, DFG - CR 312/5-2); Italy: Istituto Nazionale di Fisica Nucleare (ICSC, NextGenerationEU), Ministero dell'Università e della Ricerca (PRIN - 20223N7F8K - PNRR M4.C2.1.1); Japan: Japan Society for the Promotion of Science (JSPS KAKENHI JP22H01227, JSPS KAKENHI JP22H04944, JSPS KAKENHI JP22KK0227, JSPS KAKENHI JP23KK0245); Netherlands: Netherlands Organisation for Scientific Research (NWO Veni 2020 - VI.Veni.202.179); Norway: Research Council of Norway (RCN-314472); Poland: Ministry of Science and Higher Education (IDUB AGH, POB8, D4 no 9722), Polish National Agency for Academic Exchange (PPN/PPO/2020/1/00002/U/00001), Polish National Science Centre (NCN 2021/42/E/ST2/00350, NCN OPUS nr 2022/47/B/ST2/03059, NCN UMO-2019/34/E/ST2/00393, NCN & H2020 MSCA 945339, UMO-2020/37/B/ST2/01043, UMO-2021/40/C/ST2/00187, UMO-2022/47/O/ST2/00148, UMO-2023/49/B/ST2/04085, UMO-2023/51/B/ST2/00920); Slovenia: Slovenian Research Agency (ARIS grant J1-3010); Spain: Generalitat Valenciana (Artemisa, FEDER, IDIFEDER/2018/048), Ministry of Science and Innovation (MCIN & NextGenEU PCI2022-135018-2, MICIN & FEDER PID2021-125273NB, RYC2019-028510-I, RYC2020-030254-I, RYC2021-031273-I, RYC2022-038164-I), PROMETEO and GenT Programmes Generalitat Valenciana (CIDEGENT/2019/027); Sweden: Carl Trygger Foundation (Carl Trygger Foundation CTS 22:2312), Swedish Research Council (Swedish Research Council 2023-04654, VR 2018-00482, VR 2022-03845, VR 2022-04683, VR 2023-03403, VR grant 2021-03651), Knut and Alice Wallenberg Foundation (KAW 2018.0157, KAW 2018.0458, KAW 2019.0447, KAW 2022.0358); Switzerland: Swiss National Science Foundation (SNSF - PCEFP2_194658); United Kingdom: Leverhulme Trust (Leverhulme Trust RPG-2020-004), Royal Society (NIF-R1-231091); United States of America: U.S. Department of Energy (ECA DE-AC02-76SF00515), Neubauer Family Foundation.

Data Availability Statement My manuscript has no associated data. [Authors' comment: All ATLAS scientific output is published in journals, and preliminary results are made available in Conference Notes. All are openly available, without restriction on use by external parties beyond copyright law and the standard conditions agreed by CERN. Data associated with journal publications are also made available: tables and data from plots (e.g. cross section values, likelihood profiles, selection efficiencies, cross section limits, ...) are stored in appropriate repositories such as HEPDATA (http://hepdata.cedar.ac.uk/). ATLAS also strives to make additional material related to the paper available that allows a reinterpretation of the data in the context of new theoretical models. For example, an extended encapsulation of the analysis is often provided for measurements in the framework of RIVET (http://rivet.hepforge.org/). This information is taken from the ATLAS Data Access Policy, which is a public document that can be downloaded from http://opendata.cern.ch/record/413 [opendata.cern.ch].]

Code Availability Statement My manuscript has no associated code/software. [Authors' comment: ATLAS collaboration software is open source, and all code necessary to recreate an analysis is publicly available. The Athena (http://gitlab.cern.ch/atlas/athena) software repository provides all code needed for calibration and uncertainty application, with configuration files that are also publicly available via Docker containers and cvmfs. The specific code and configurations written in support of this analysis are not public; however, these are internally preserved.]

Open Access This article is licensed under a Creative Commons Attribution 4.0 International License, which permits use, sharing, adaptation, distribution and reproduction in any medium or format, as long as you give appropriate credit to the original author(s) and the source, provide a link to the Creative Commons licence, and indicate if changes were made. The images or other third party material in this article are included in the article's Creative Commons licence, unless indicated otherwise in a credit line to the material. If material is not included in the article's Creative Commons licence and your intended use is not permitted by statutory regulation or exceeds the permitted use, you will need to obtain permission directly from the copyright holder. To view a copy of this licence, visit http://creativecommons.org/licenses/by/4.0/.
Funded by SCOAP[3].

References

1. F. Englert, R. Brout, Broken symmetry and the mass of gauge vector mesons. Phys. Rev. Lett. **13**, 321 (1964). https://doi.org/10.1103/PhysRevLett.13.321
2. P.W. Higgs, Broken symmetries and the masses of gauge bosons. Phys. Rev. Lett. **13**, 508 (1964). https://doi.org/10.1103/PhysRevLett.13.508
3. G.S. Guralnik, C.R. Hagen, T.W.B. Kibble, Global conservation laws and massless particles. Phys. Rev. Lett. **13**, 585 (1964). https://doi.org/10.1103/PhysRevLett.13.585
4. ATLAS Collaboration, Observation of a new particle in the search for the Standard Model Higgs boson with the ATLAS detector at the LHC. Phys. Lett. B **716**, 1 (2012). https://doi.org/10.1016/j.physletb.2012.08.020. arXiv:1207.7214 [hep-ex]
5. C.M.S. Collaboration, Observation of a new boson at a mass of 125 GeV with the CMS experiment at the LHC. Phys. Lett. B **716**, 30 (2012). https://doi.org/10.1016/j.physletb.2012.08.021. arXiv:1207.7235 [hep-ex]
6. S.L. Glashow, Partial-symmetries of weak interactions. Nucl. Phys. **22**, 579 (1961). https://doi.org/10.1016/0029-5582(61)90469-2
7. S. Weinberg, A model of leptons. Phys. Rev. Lett. **19**, 1264 (1967). https://doi.org/10.1103/PhysRevLett.19.1264
8. A. Salam, Weak and electromagnetic interactions. Conf. Proc. **C680519**, 367 (1968)
9. C. Englert et al., Precision measurements of Higgs couplings: implications for new physics scales. J. Phys. G **41**, 113001 (2014). https://doi.org/10.1088/0954-3899/41/11/113001. arXiv:1403.7191 [hep-ph]
10. ATLAS Collaboration, A detailed map of Higgs boson interactions by the ATLAS experiment ten years after the discovery. Nature **607**, 52 (2022). https://doi.org/10.1038/s41586-022-04893-w. arXiv:2207.00092 [hep-ex]. [Erratum: Nature **612**, E24 (2022)]. https://doi.org/10.1038/s41586-022-05581-5
11. CMS Collaboration, A portrait of the Higgs boson by the CMS experiment ten years after the discovery. Nature **607**, 60 (2022). https://doi.org/10.1038/s41586-022-04892-x. arXiv:2207.00043 [hep-ex]. [Erratum: Nature **623**, E4 (2023)]. https://doi.org/10.1038/s41586-023-06164-8
12. J.N. Ng, P. Zakarauskas, QCD-parton calculation of conjoined production of Higgs bosons and heavy flavors in $p\bar{p}$ collision. Phys. Rev. D **29**, 876 (1984). https://doi.org/10.1103/PhysRevD.29.876
13. Z. Kunszt, Associated production of heavy Higgs boson with top quarks. Nucl. Phys. B **247**, 339 (1984). https://doi.org/10.1016/0550-3213(84)90553-4
14. S. Dawson, L.H. Orr, L. Reina, D. Wackeroth, Next-to-leading order QCD corrections to $pp \to t\bar{t}h$ at the CERN Large Hadron Collider. Phys. Rev. D **67**, 071503 (2003). https://doi.org/10.1103/PhysRevD.67.071503. arXiv:hep-ph/0211438
15. W. Beenakker et al., Higgs radiation off top quarks at the tevatron and the LHC. Phys. Rev. Lett. **87**, 201805 (2001). https://doi.org/10.1103/PhysRevLett.87.201805. arXiv:hep-ph/0107081
16. ATLAS Collaboration, Observation of Higgs boson production in association with a top quark pair at the LHC with the ATLAS detector. Phys. Lett. B **784**, 173 (2018). https://doi.org/10.1016/j.physletb.2018.07.035. arXiv:1806.00425 [hep-ex]
17. CMS Collaboration, Observation of $t\bar{t}H$ production. Phys. Rev. Lett. **120**, 231801 (2018). https://doi.org/10.1103/PhysRevLett.120.231801. arXiv:1804.02610 [hep-ex]
18. D. de Florian et al., Handbook of LHC Higgs Cross Sections: 4. Deciphering the Nature of the Higgs Sector (2017). https://doi.org/10.23731/CYRM-2017-002. arXiv:1610.07922 [hep-ph]
19. L. Evans, P. Bryant, LHC machine. JINST **3**, S08001 (2008). https://doi.org/10.1088/1748-0221/3/08/S08001
20. ATLAS Collaboration, Measurement of Higgs boson decay into b-quarks in associated production with a top-quark pair in pp collisions at $\sqrt{s} = 13$ TeV with the ATLAS detector. JHEP. **06**, 097 (2022). https://doi.org/10.1007/JHEP06(2022)097. arXiv:2111.06712 [hep-ex]
21. CMS Collaboration, Measurement of the $\mathrm{t\bar{t}}H$ and tH production rates in the $H \to \mathrm{b\bar{b}}$ decay channel using proton-proton collision data at $\sqrt{s} = 13$ TeV (2024). arXiv:2407.10896 [hep-ex]
22. ATLAS Collaboration, Studies of Monte Carlo predictions for the $t\bar{t}b\bar{b}$ process. ATL-PHYS-PUB-2022-006 (2022). https://cds.cern.ch/record/2802806
23. ATLAS Collaboration, Study of $ttbb$ and ttW background modelling for ttH analyses, ATL-PHYS-PUB-2022-026 (2022). https://cds.cern.ch/record/2810864
24. ATLAS Collaboration, The ATLAS experiment at the CERN Large Hadron Collider. JINST. **3**, S08003 (2008). https://doi.org/10.1088/1748-0221/3/08/S08003
25. G. Avoni et al., The new LUCID-2 detector for luminosity measurement and monitoring in ATLAS. JINST **13**, P07017 (2018). https://doi.org/10.1088/1748-0221/13/07/P07017
26. ATLAS Collaboration, Performance of the ATLAS trigger system in 2015. Eur. Phys. J. C **77**, 317 (2017). https://doi.org/10.1140/epjc/s10052-017-4852-3. arXiv:1611.09661 [hep-ex]
27. ATLAS Collaboration, Software and computing for Run 3 of the ATLAS experiment at the LHC (2024). arXiv:2404.06335 [hep-ex]
28. ATLAS Collaboration, ATLAS data quality operations and performance for 2015–2018 data-taking. JINST **15**, P04003 (2020). https://doi.org/10.1088/1748-0221/15/04/P04003. arXiv:1911.04632 [physics.ins-det]
29. T. Sjöstrand, S. Mrenna, P. Skands, A brief introduction to PYTHIA 8.1. Comput. Phys. Commun. **178**, 852 (2008). https://doi.org/10.1016/j.cpc.2008.01.036. arXiv:0710.3820 [hep-ph]
30. ATLAS Collaboration, The Pythia 8 A3 tune description of ATLAS minimum bias and inelastic measurements incorporating the Donnachie–Landshoff diffractive model, ATL-PHYS-PUB-2016-017 (2016). https://cds.cern.ch/record/2206965
31. ATLAS Collaboration, The ATLAS simulation infrastructure. Eur. Phys. J. C **70**, 823 (2010). https://doi.org/10.1140/epjc/s10052-010-1429-9. arXiv:1005.4568 [physics.ins-det]
32. S. Agostinelli et al., GEANT4—a simulation toolkit. Nucl. Instrum. Methods A **506**, 250 (2003). https://doi.org/10.1016/S0168-9002(03)01368-8
33. P. Nason, A new method for combining NLO QCD with shower Monte Carlo algorithms. JHEP **11**, 040 (2004). https://doi.org/10.1088/1126-6708/2004/11/040. arXiv:hep-ph/0409146
34. S. Frixione, G. Ridolfi, P. Nason, A positive-weight next-to-leading-order Monte Carlo for heavy flavour hadroproduction. JHEP **09**, 126 (2007). https://doi.org/10.1088/1126-6708/2007/09/126. arXiv:0707.3088 [hep-ph]
35. S. Frixione, P. Nason, C. Oleari, Matching NLO QCD computations with parton shower simulations: the POWHEG method. JHEP **11**, 070 (2007). https://doi.org/10.1088/1126-6708/2007/11/070. arXiv:0709.2092 [hep-ph]
36. S. Alioli, P. Nason, C. Oleari, E. Re, A general framework for implementing NLO calculations in shower Monte Carlo programs: the POWHEG BOX. JHEP **06**, 043 (2010). https://doi.org/10.1007/JHEP06(2010)043. arXiv:1002.2581 [hep-ph]
37. J. Alwall et al., The automated computation of tree-level and next-to-leading order differential cross sections, and their matching to parton shower simulations. JHEP **07**, 079 (2014). https://doi.org/10.1007/JHEP07(2014)079. arXiv:1405.0301 [hep-ph]

38. T. Sjöstrand et al., An introduction to PYTHIA 8.2. Comput. Phys. Commun. **191**, 159 (2015). https://doi.org/10.1016/j.cpc.2015.01.024. arXiv:1410.3012 [hep-ph]
39. ATLAS Collaboration, ATLAS Pythia 8 tunes to 7 TeV data, ATL-PHYS-PUB-2014-021 (2014). https://cds.cern.ch/record/1966419
40. NNPDF Collaboration, R.D. Ball et al., Parton distributions for the LHC run II. JHEP **04**, 040 (2015). https://doi.org/10.1007/JHEP04(2015)040. arXiv:1410.8849 [hep-ph]
41. M. Bähr et al., Herwig++ physics and manual. Eur. Phys. J. C **58**, 639 (2008). https://doi.org/10.1140/epjc/s10052-008-0798-9. arXiv:0803.0883 [hep-ph]
42. J. Bellm et al., Herwig 7.0/Herwig++ 3.0 release note. Eur. Phys. J. C **76**, 196 (2016). https://doi.org/10.1140/epjc/s10052-016-4018-8. arXiv:1512.01178 [hep-ph]
43. L.A. Harland-Lang, A.D. Martin, P. Motylinski, R.S. Thorne, Parton distributions in the LHC era: MMHT 2014 PDFs. Eur. Phys. J. C **75**, 204 (2015). https://doi.org/10.1140/epjc/s10052-015-3397-6. arXiv:1412.3989 [hep-ph]
44. D.J. Lange, The EvtGen particle decay simulation package. Nucl. Instrum. Methods A **462**, 152 (2001). https://doi.org/10.1016/S0168-9002(01)00089-4
45. H.B. Hartanto, B. Jäger, L. Reina, D. Wackeroth, Higgs boson production in association with top quarks in the POWHEG BOX. Phys. Rev. D **91**, 094003 (2015). https://doi.org/10.1103/PhysRevD.91.094003. arXiv:1501.04498 [hep-ph]
46. S. Catani et al., Higgs boson production in association with a top-antitop quark pair in next-to-next-to-leading order QCD. Phys. Rev. Lett. **130**, 111902 (2023). https://doi.org/10.1103/physrevlett.130.111902. arXiv:2210.07846 [hep-ph]
47. ATLAS Collaboration, Studies on the improvement of the matching uncertainty definition in top-quark processes simulated with POWHEG+PYTHIA8, ATL-PHYS-PUB-2023-029 (2013). https://cds.cern.ch/record/2872787
48. S. Höche, S. Mrenna, S. Payne, C.T. Preuss, P. Skands, A study of QCD radiation in VBF Higgs production with Vincia and Pythia. SciPost Phys. **12**, 010 (2022). https://doi.org/10.21468/SciPostPhys.12.1.010. arXiv:2106.10987 [hep-ph]
49. ATLAS Collaboration, Search for the Standard Model Higgs boson produced in association with top quarks and decaying into $b\bar{b}$ in pp collisions at $\sqrt{s} = 8$ TeV with the ATLAS detector. Eur. Phys. J. C **75**, 349 (2015). https://doi.org/10.1140/epjc/s10052-015-3543-1. arXiv:1503.05066 [hep-ex]
50. M. Cacciari, G.P. Salam, G. Soyez, The anti-k_t jet clustering algorithm. JHEP **04**, 063 (2008). https://doi.org/10.1088/1126-6708/2008/04/063. arXiv:0802.1189 [hep-ph]
51. ATLAS Collaboration, Studies on top-quark Monte Carlo modelling for Top2016, ATL-PHYS-PUB-2016-020 (2016). https://cds.cern.ch/record/2216168
52. T. Ježo, J.M. Lindert, N. Moretti, S. Pozzorini, New NLOPS predictions for $t\bar{t} + b$-jet production at the LHC. Eur. Phys. J. C **78**, 502 (2018). https://doi.org/10.1140/epjc/s10052-018-5956-0. arXiv:1802.00426 [hep-ph]
53. F. Buccioni et al., OpenLoops 2. Eur. Phys. J. C **79**, 866 (2019). https://doi.org/10.1140/epjc/s10052-019-7306-2. arXiv:1907.13071 [hep-ph]
54. F. Cascioli, P. Maierhöfer, S. Pozzorini, Scattering amplitudes with open loops. Phys. Rev. Lett. **108**, 111601 (2012). https://doi.org/10.1103/PhysRevLett.108.111601. arXiv:1111.5206 [hep-ph]
55. A. Denner, S. Dittmaier, L. Hofer, COLLIER: a fortran-based complex one-loop library in extended regularizations. Comput. Phys. Commun. **212**, 220 (2017). https://doi.org/10.1016/j.cpc.2016.10.013. arXiv:1604.06792 [hep-ph]
56. T. Ježo, Powheg-Box-Res $ttbb$ source code (2019). https://gitlab.cern.ch/tjezo/powheg-box-res_ttbb/
57. E. Bothmann et al., Event generation with Sherpa 2.2. SciPost Phys. **7**, 034 (2019). https://doi.org/10.21468/SciPostPhys.7.3.034. arXiv:1905.09127 [hep-ph]
58. T. Gleisberg, S. Höche, Comix, a new matrix element generator. JHEP **12**, 039 (2008). https://doi.org/10.1088/1126-6708/2008/12/039. arXiv:0808.3674 [hep-ph]
59. S. Schumann, F. Krauss, A parton shower algorithm based on Catani–Seymour dipole factorisation. JHEP **03**, 038 (2008). https://doi.org/10.1088/1126-6708/2008/03/038. arXiv:0709.1027 [hep-ph]
60. S. Höche, F. Krauss, M. Schönherr, F. Siegert, A critical appraisal of NLO+PS matching methods. JHEP **09**, 049 (2012). https://doi.org/10.1007/JHEP09(2012)049. arXiv:1111.1220 [hep-ph]
61. S. Höche, F. Krauss, M. Schönherr, F. Siegert, QCD matrix elements + parton showers. The NLO case. JHEP **04**, 027 (2013). https://doi.org/10.1007/JHEP04(2013)027. arXiv:1207.5030 [hep-ph]
62. S. Catani, F. Krauss, B.R. Webber, R. Kuhn, QCD matrix elements + parton showers. JHEP **11**, 063 (2001). https://doi.org/10.1088/1126-6708/2001/11/063. arXiv:hep-ph/0109231
63. S. Höche, F. Krauss, S. Schumann, F. Siegert, QCD matrix elements and truncated showers. JHEP **05**, 053 (2009). https://doi.org/10.1088/1126-6708/2009/05/053. arXiv:0903.1219 [hep-ph]
64. E. Re, Single-top Wt-channel production matched with parton showers using the POWHEG method. Eur. Phys. J. C **71**, 1547 (2011). https://doi.org/10.1140/epjc/s10052-011-1547-z. arXiv:1009.2450 [hep-ph]
65. S. Alioli, P. Nason, C. Oleari, E. Re, NLO single-top production matched with shower in POWHEG: s- and t-channel contributions, JHEP **09**, 111 (2009). https://doi.org/10.1088/1126-6708/2009/09/111. arXiv:0907.4076 [hep-ph], Erratum: **02**, 011 (2010). https://doi.org/10.1007/JHEP02(2010)011JHEP
66. S. Frixione, E. Laenen, P. Motylinski, C. White, B.R. Webber, Single-top hadroproduction in association with a W boson. JHEP **07**, 029 (2008). https://doi.org/10.1088/1126-6708/2008/07/029. arXiv:0805.3067 [hep-ph]
67. ATLAS Collaboration, Studies of $t\bar{t}/tW$ interference effects in $b\bar{b}\ell^+\ell^-\nu\bar{\nu}'$ final states with POWHEG and MADGRAPH5_AMC@NLO setups, ATL-PHYS-PUB-2021-042 (2021). https://cds.cern.ch/record/2792254
68. T. Gleisberg et al., Event generation with SHERPA 1.1. JHEP **02**, 007 (2009). https://doi.org/10.1088/1126-6708/2009/02/007. arXiv:0811.4622 [hep-ph]
69. NNPDF Collaboration, R.D. Ball et al., Parton distributions from high-precision collider data. Eur. Phys. J. C 77, 663 (2017). https://doi.org/10.1140/epjc/s10052-017-5199-5. arXiv:1706.00428 [hep-ph]
70. R. Frederix, S. Frixione, Merging meets matching in MC@NLO. JHEP **12**, 061 (2012). https://doi.org/10.1007/JHEP12(2012)061. arXiv:1209.6215 [hep-ph]
71. L. Buonocore et al., Precise predictions for the associated production of a W boson with a top-antitop quark pair at the LHC. Phys. Rev. Lett. 131 (2023). https://doi.org/10.1103/physrevlett.131.231901. arXiv:2306.16311 [hep-ph]
72. M. Czakon, A. Mitov, Top++: a program for the calculation of the top-pair cross-section at hadron colliders. Comput. Phys. Commun. **185**, 2930 (2014). https://doi.org/10.1016/j.cpc.2014.06.021. arXiv:1112.5675 [hep-ph]
73. ATLAS Collaboration, Performance of the ATLAS muon triggers in Run 2. JINST **15**, P09015 (2020). https://doi.org/10.1088/1748-0221/15/09/p09015. arXiv:2004.13447 [physics.ins-det]
74. ATLAS Collaboration, Performance of electron and photon triggers in ATLAS during LHC Run 2. Eur. Phys. J. C **80**, 47 (2020). https://doi.org/10.1140/epjc/s10052-019-7500-2. arXiv:1909.00761 [hep-ex]

75. ATLAS Collaboration, Vertex Reconstruction Performance of the ATLAS Detector at $\sqrt{s} = 13$ TeV, ATL-PHYS-PUB-2015-026 (2015). https://cds.cern.ch/record/2037717
76. ATLAS Collaboration, Electron and photon performance measurements with the ATLAS detector using the 2015–2017 LHC proton–proton collision data. JINST **14**, P12006 (2019). https://doi.org/10.1088/1748-0221/14/12/P12006. arXiv:1908.00005 [hep-ex]
77. ATLAS Collaboration, Muon reconstruction and identification efficiency in ATLAS using the full Run 2 pp collision data set at $\sqrt{s} = 13$ TeV. Eur. Phys. J. C **81**, 578 (2021). https://doi.org/10.1140/epjc/s10052-021-09233-2. arXiv:2012.00578 [hep-ex]
78. ATLAS Collaboration, Jet reconstruction and performance using particle flow with the ATLAS detector. Eur. Phys. J. C **77**, 466 (2017). https://doi.org/10.1140/epjc/s10052-017-5031-2. arXiv:1703.10485 [hep-ex]
79. M. Cacciari, G.P. Salam, G. Soyez, FastJet user manual. Eur. Phys. J. C **72**, 1896 (2012). https://doi.org/10.1140/epjc/s10052-012-1896-2. arXiv:1111.6097 [hep-ph]
80. ATLAS Collaboration, Performance of pile-up mitigation techniques for jets in pp collisions at $\sqrt{s} = 8$ TeV using the ATLAS detector. Eur. Phys. J. C **76**, 581 (2016). https://doi.org/10.1140/epjc/s10052-016-4395-z. arXiv:1510.03823 [hep-ex]
81. ATLAS Collaboration, Jet energy scale and resolution measured in proton–proton collisions at $\sqrt{s} = 13$ TeV with the ATLAS detector. Eur. Phys. J. C **81**, 689 (2021). https://doi.org/10.1140/epjc/s10052-021-09402-3. arXiv:2007.02645 [hep-ex]
82. ATLAS Collaboration, ATLAS flavour-tagging algorithms for the LHC Run 2 pp collision dataset. Eur. Phys. J. C **83**, 681 (2023). https://doi.org/10.1140/epjc/s10052-023-11699-1. arXiv:2211.16345 [physics.data-an]
83. ATLAS Collaboration, Evidence for the $H \to b\bar{b}$ decay with the ATLAS detector. JHEP **12**, 024 (2017). https://doi.org/10.1007/JHEP12(2017)024. arXiv:1708.03299 [hep-ex]
84. ATLAS Collaboration, Identification of hadronic tau lepton decays using neural networks in the ATLAS experiment, ATL-PHYS-PUB-2019-033 (2019). https://cds.cern.ch/record/2688062
85. ATLAS Collaboration, The performance of missing transverse momentum reconstruction and its significance with the ATLAS detector using 140 fb^{-1} of $\sqrt{s} = 13$ TeV pp collisions (2024). arXiv:2402.05858 [hep-ex]
86. B. Nachman, P. Nef, A. Schwartzman, M. Swiatlowski, C. Wanotayaroj, Jets from jets: re-clustering as a tool for large radius jet reconstruction and grooming at the LHC. JHEP **02**, 075 (2015). https://doi.org/10.1007/JHEP02(2015)075. arXiv:1407.2922 [hep-ph]
87. ATLAS Collaboration, Measurements of top-quark pair differential and double-differential cross-sections in the ℓ+jets channel with pp collisions at $\sqrt{s} = 13$ TeV using the ATLAS detector. Eur. Phys. J. C **79**, 1028 (2019). https://doi.org/10.1140/epjc/s10052-019-7525-6. arXiv:1908.07305 [hep-ex]. [Erratum: Eur. Phys. J. C **80**, 1092 (2020)]. https://doi.org/10.1140/epjc/s10052-020-08541-3
88. ATLAS Collaboration, Tools for estimating fake/non-prompt lepton backgrounds with the ATLAS detector at the LHC. JINST **18**, T11004 (2023). https://doi.org/10.1088/1748-0221/18/11/T11004. arXiv:2211.16178 [hep-ex]
89. A. Vaswani et al., Attention Is All You Need (2023). arXiv:1706.03762 [cs.CL]
90. K. Cranmer, G. Lewis, L. Moneta, A. Shibata, W. Verkerke, HistFactory: a tool for creating statistical models for use with RooFit and RooStats, CERN-OPEN-2012-016 (2012). https://cds.cern.ch/record/1456844
91. W. Verkerke, D. Kirkby, The RooFit toolkit for data modeling (2003). arXiv:physics/0306116 [physics.data-an]
92. G. Cowan, K. Cranmer, E. Gross, O. Vitells, Asymptotic formulae for likelihood-based tests of new physics. Eur. Phys. J. C **71**, 1554 (2011). https://doi.org/10.1140/epjc/s10052-013-2501-z. arXiv:1007.1727 [physics.data-an]. [Erratum: Eur. Phys. J. C **73**, 2501 (2013)]. https://doi.org/10.1140/epjc/s10052-011-1554-0
93. ATLAS Collaboration, Luminosity determination in pp collisions at $\sqrt{s} = 13$ TeV using the ATLAS detector at the LHC. Eur. Phys. J. C **83**, 982 (2023). https://doi.org/10.1140/epjc/s10052-023-11747-w. arXiv:2212.09379 [hep-ex]
94. ATLAS Collaboration, ATLAS b-jet identification performance and efficiency measurement with $t\bar{t}$ events in pp collisions at $\sqrt{s} = 13$ TeV. Eur. Phys. J. C **79**, 970 (2019). https://doi.org/10.1140/epjc/s10052-019-7450-8. arXiv:1907.05120 [hep-ex]
95. ATLAS Collaboration, Measurement of the c-jet mistagging efficiency in $t\bar{t}$ events using pp collision data at $\sqrt{s} = 13$ TeV collected with the ATLAS detector. Eur. Phys. J. C **82**, 95 (2022). https://doi.org/10.1140/epjc/s10052-021-09843-w. arXiv:2109.10627 [hep-ex]
96. ATLAS Collaboration, Calibration of the light-flavour jet mistagging efficiency of the b-tagging algorithms with Z+jets events using 139 fb^{-1} of ATLAS proton–proton collision data at $\sqrt{s} = 13$ TeV. Eur. Phys. J. C **83**, 728 (2023). https://doi.org/10.1140/epjc/s10052-023-11736-z. arXiv:2301.06319 [hep-ex]
97. ATLAS Collaboration, Evaluation of QCD uncertainties for Higgs boson production through gluon fusion and in association with two top quarks for simplified template cross-section measurements, ATL-PHYS-PUB-2023-031 (2023). https://cds.cern.ch/record/2878797
98. N. Kidonakis, Next-to-next-to-leading-order collinear and soft gluon corrections for t-channel single top quark production. Phys. Rev. D **83**, 091503 (2011). https://doi.org/10.1103/PhysRevD.83.091503. arXiv:1103.2792 [hep-ph]
99. N. Kidonakis, Next-to-next-to-leading logarithm resummation for s-channel single top quark production. Phys. Rev. D **81**, 054028 (2010). https://doi.org/10.1103/PhysRevD.81.054028. arXiv:1001.5034 [hep-ph]
100. N. Kidonakis, N. Yamanaka, Higher-order corrections for tW production at high-energy hadron colliders. JHEP **05**, 278 (2021). https://doi.org/10.1007/JHEP05(2021)278. arXiv:2102.11300 [hep-ph]
101. M. van Beekveld, A. Kulesza, L.M. Valero, Threshold resummation for the production of four top quarks at the LHC (2022). arXiv:2212.03259 [hep-ph]
102. ATLAS Collaboration, Observation of four-top-quark production in the multilepton final state with the ATLAS detector. Eur. Phys. J. C **83**, 496 (2023). https://doi.org/10.1140/epjc/s10052-023-11573-0. arXiv:2303.15061 [hep-ex]

103. ATLAS Collaboration, Probing the CP nature of the top-Higgs Yukawa coupling in $t\bar{t}H$ and tH events with $H \to b\bar{b}$ decays using the ATLAS detector at the LHC. Phys. Lett. B **849**, 138469 (2023). https://doi.org/10.1016/j.physletb.2024.138469. arXiv:2303.05974 [hep-ex]
104. ATLAS Collaboration, Probing the CP nature of the top-Higgs Yukawa coupling in $t\bar{t}H$ and tH events with $H \to b\bar{b}$ decays using the ATLAS detector at the LHC. Phys. Lett. B **849**, 138469 (2024). https://doi.org/10.1016/j.physletb.2024.138469. arXiv:2303.05974 [hep-ex]
105. M. Grazzini, S. Kallweit, D. Rathlev, M. Wiesemann, $W^{\pm}Z$ production at hadron colliders in NNLO QCD. Phys. Lett. B **761**, 179 (2016). https://doi.org/10.1016/j.physletb.2016.08.017. arXiv:1604.08576 [hep-ph]
106. ATLAS Collaboration, Multi-boson simulation for 13 TeV ATLAS analyses, ATL-PHYS-PUB-2016-002 (2016). https://cds.cern.ch/record/2119986
107. ATLAS Collaboration, Measurement of $W^{\pm}Z$ production cross sections and gauge boson polarisation in pp collisions at $\sqrt{s} =$ 13 TeV with the ATLAS detector. Eur. Phys. J. C **79**, 535 (2019). https://doi.org/10.1140/epjc/s10052-019-7027-6. arXiv:1902.05759 [hep-ex]
108. ATLAS and CMS Collaborations, Combined measurement of the Higgs boson mass in pp collisions at $\sqrt{s} = 7$ and 8 TeV with the ATLAS and CMS experiments. Phys. Rev. Lett. **114**, 191803 (2015). https://doi.org/10.1103/PhysRevLett.114.191803. arXiv:1503.07589 [hep-ex]
109. S. Baker, R.D. Cousins, Clarification of the use of CHI-square and likelihood functions in fits to histograms. Nucl. Instrum. Methods **221**, 437 (1984). https://doi.org/10.1016/0167-5087(84)90016-4
110. R.D. Cousins, Lectures on Statistics in Theory: Prelude to Statistics in Practice (2024). arXiv:1807.05996 [physics.data-an]
111. ATLAS Collaboration, ATLAS Computing Acknowledgements, ATL-SOFT-PUB-2023-001 (2023). https://cds.cern.ch/record/2869272

ATLAS Collaboration*

G. Aad[104], E. Aakvaag[17], B. Abbott[123], S. Abdelhameed[119a], K. Abeling[56], N. J. Abicht[50], S. H. Abidi[30], M. Aboelela[45], A. Aboulhorma[36e], H. Abramowicz[155], H. Abreu[154], Y. Abulaiti[120], B. S. Acharya[70a,70b,k], A. Ackermann[64a], C. Adam Bourdarios[4], L. Adamczyk[87a], S. V. Addepalli[27], M. J. Addison[103], J. Adelman[118], A. Adiguzel[22c], T. Adye[137], A. A. Affolder[139], Y. Afik[40], M. N. Agaras[13], J. Agarwala[74a,74b], A. Aggarwal[102], C. Agheorghiesei[28c], F. Ahmadov[39,y], W. S. Ahmed[106], S. Ahuja[97], X. Ai[63e], G. Aielli[77a,77b], A. Aikot[166], M. Ait Tamlihat[36e], B. Aitbenchikh[36a], M. Akbiyik[102], T. P. A. Åkesson[100], A. V. Akimov[38], D. Akiyama[171], N. N. Akolkar[25], S. Aktas[22a], K. Al Khoury[42], G. L. Alberghi[24b], J. Albert[168], P. Albicocco[54], G. L. Albouy[61], S. Alderweireldt[53], Z. L. Alegria[124], M. Aleksa[37], I. N. Aleksandrov[39], C. Alexa[28b], T. Alexopoulos[10], F. Alfonsi[24b], M. Algren[57], M. Alhroob[170], B. Ali[135], H. M. J. Ali[93,s], S. Ali[32], S. W. Alibocus[94], M. Aliev[34c], G. Alimonti[72a], W. Alkakhi[56], C. Allaire[67], B. M. M. Allbrooke[150], J. S. Allen[103], J. F. Allen[53], C. A. Allendes Flores[140f], P. P. Allport[21], A. Aloisio[73a,73b], F. Alonso[92], C. Alpigiani[142], Z. M. K. Alsolami[93], M. Alvarez Estevez[101], A. Alvarez Fernandez[102], M. Alves Cardoso[57], M. G. Alviggi[73a,73b], M. Aly[103], Y. Amaral Coutinho[84b], A. Ambler[106], C. Amelung[37], M. Amerl[103], C. G. Ames[111], D. Amidei[108], B. Amini[55], K. J. Amirie[158], S. P. Amor Dos Santos[133a], K. R. Amos[166], D. Amperiadou[156], S. An[85], V. Ananiev[128], C. Anastopoulos[143], T. Andeen[11], J. K. Anders[37], A. C. Anderson[60], S. Y. Andrean[48a,48b], A. Andreazza[72a,72b], S. Angelidakis[9], A. Angerami[42], A. V. Anisenkov[38], A. Annovi[75a], C. Antel[57], E. Antipov[149], M. Antonelli[54], F. Anulli[76a], M. Aoki[85], T. Aoki[157], M. A. Aparo[150], L. Aperio Bella[49], C. Appelt[19], A. Apyan[27], S. J. Arbiol Val[88], C. Arcangeletti[54], A. T. H. Arce[52], J.-F. Arguin[110], S. Argyropoulos[156], J.-H. Arling[49], O. Arnaez[4], H. Arnold[149], G. Artoni[76a,76b], H. Asada[113], K. Asai[121], S. Asai[157], N. A. Asbah[37], R. A. Ashby Pickering[170], K. Assamagan[30], R. Astalos[29a], K. S. V. Astrand[100], S. Atashi[162], R. J. Atkin[34a], M. Atkinson[165], H. Atmani[36f], P. A. Atmasiddha[131], K. Augsten[135], S. Auricchio[73a,73b], A. D. Auriol[21], V. A. Austrup[103], G. Avolio[37], K. Axiotis[57], G. Azuelos[110,ad], D. Babal[29b], H. Bachacou[138], K. Bachas[156,o], A. Bachiu[35], E. Bachmann[51], F. Backman[48a,48b], A. Badea[40], T. M. Baer[108], P. Bagnaia[76a,76b], M. Bahmani[19], D. Bahner[55], K. Bai[126], J. T. Baines[137], L. Baines[96], O. K. Baker[175], E. Bakos[16], D. Bakshi Gupta[8], L. E. Balabram Filho[84b], V. Balakrishnan[123], R. Balasubramanian[4], E. M. Baldin[38], P. Balek[87a], E. Ballabene[24a,24b], F. Balli[138], L. M. Baltes[64a], W. K. Balunas[33], J. Balz[102], I. Bamwidhi[119b], E. Banas[88], M. Bandieramonte[132], A. Bandyopadhyay[25], S. Bansal[25], L. Barak[155], M. Barakat[49], E. L. Barberio[107], D. Barberis[58a,58b], M. Barbero[104], M. Z. Barel[117], T. Barillari[112], M.-S. Barisits[37], T. Barklow[147], P. Baron[125], D. A. Baron Moreno[103], A. Baroncelli[63a], A. J. Barr[129], J. D. Barr[98], F. Barreiro[101], J. Barreiro Guimarães da Costa[14], U. Barron[155], M. G. Barros Teixeira[133a], S. Barsov[38], F. Bartels[64a], R. Bartoldus[147], A. E. Barton[93], P. Bartos[29a], A. Basan[102], M. Baselga[50], A. Bassalat[67,b], M. J. Basso[159a], S. Bataju[45], R. Bate[167], R. L. Bates[60], S. Batlamous[101], B. Batool[145], M. Battaglia[139], D. Battulga[19], M. Bauce[76a,76b], M. Bauer[80], P. Bauer[25], L. T. Bazzano Hurrell[31], J. B. Beacham[52],

T. Beau[130], J. Y. Beaucamp[92], P. H. Beauchemin[161], P. Bechtle[25], H. P. Beck[20,n], K. Becker[170], A. J. Beddall[83], V. A. Bednyakov[39], C. P. Bee[149], L. J. Beemster[16], T. A. Beermann[37], M. Begalli[84d], M. Begel[30], A. Behera[149], J. K. Behr[49], J. F. Beirer[37], F. Beisiegel[25], M. Belfkir[119b], G. Bella[155], L. Bellagamba[24b], A. Bellerive[35], P. Bellos[21], K. Beloborodov[38], D. Benchekroun[36a], F. Bendebba[36a], Y. Benhammou[155], K. C. Benkendorfer[62], L. Beresford[49], M. Beretta[54], E. Bergeaas Kuutmann[164], N. Berger[4], B. Bergmann[135], J. Beringer[18a], G. Bernardi[5], C. Bernius[147], F. U. Bernlochner[25], F. Bernon[37], A. Berrocal Guardia[13], T. Berry[97], P. Berta[136], A. Berthold[51], S. Bethke[112], A. Betti[76a,76b], A. J. Bevan[96], N. K. Bhalla[55], S. Bhatta[149], D. S. Bhattacharya[169], P. Bhattarai[147], K. D. Bhide[55], V. S. Bhopatkar[124], R. M. Bianchi[132], G. Bianco[24a,24b], O. Biebel[111], R. Bielski[126], M. Biglietti[78a], C. S. Billingsley[45], Y. Bimgdi[36f], M. Bindi[56], A. Bingul[22b], C. Bini[76a,76b], G. A. Bird[33], M. Birman[172], M. Biros[136], S. Biryukov[150], T. Bisanz[50], E. Bisceglie[44a,44b], J. P. Biswal[137], D. Biswas[145], I. Bloch[49], A. Blue[60], U. Blumenschein[96], J. Blumenthal[102], V. S. Bobrovnikov[38], M. Boehler[55], B. Boehm[169], D. Bogavac[37], A. G. Bogdanchikov[38], L. S. Boggia[130], C. Bohm[48a], V. Boisvert[97], P. Bokan[37], T. Bold[87a], M. Bomben[5], M. Bona[96], M. Boonekamp[138], C. D. Booth[97], A. G. Borbély[60], I. S. Bordulev[38], G. Borissov[93], D. Bortoletto[129], D. Boscherini[24b], M. Bosman[13], J. D. Bossio Sola[37], K. Bouaouda[36a], N. Bouchhar[166], L. Boudet[4], J. Boudreau[132], E. V. Bouhova-Thacker[93], D. Boumediene[41], R. Bouquet[58a,58b], A. Boveia[122], J. Boyd[37], D. Boye[30], I. R. Boyko[39], L. Bozianu[57], J. Bracinik[21], N. Brahimi[4], G. Brandt[174], O. Brandt[33], F. Braren[49], B. Brau[105], J. E. Brau[126], R. Brener[172], L. Brenner[117], R. Brenner[164], S. Bressler[172], G. Brianti[79a,79b], D. Britton[60], D. Britzger[112], I. Brock[25], R. Brock[109], G. Brooijmans[42], E. M. Brooks[159b], E. Brost[30], L. M. Brown[168], L. E. Bruce[62], T. L. Bruckler[129], P. A. Bruckman de Renstrom[88], B. Brüers[49], A. Bruni[24b], G. Bruni[24b], M. Bruschi[24b], N. Bruscino[76a,76b], T. Buanes[17], Q. Buat[142], D. Buchin[112], A. G. Buckley[60], O. Bulekov[38], B. A. Bullard[147], S. Burdin[94], C. D. Burgard[50], A. M. Burger[37], B. Burghgrave[8], O. Burlayenko[55], J. Burleson[165], J. T. P. Burr[33], J. C. Burzynski[146], E. L. Busch[42], V. Büscher[102], P. J. Bussey[60], J. M. Butler[26], C. M. Buttar[60], J. M. Butterworth[98], W. Buttinger[137], C. J. Buxo Vazquez[109], A. R. Buzykaev[38], S. Cabrera Urbán[166], L. Cadamuro[67], D. Caforio[59], H. Cai[132], Y. Cai[14,114c], Y. Cai[114a], V. M. M. Cairo[37], O. Cakir[3a], N. Calace[37], P. Calafiura[18a], G. Calderini[130], P. Calfayan[69], G. Callea[60], L. P. Caloba[84b], D. Calvet[41], S. Calvet[41], M. Calvetti[75a,75b], R. Camacho Toro[130], S. Camarda[37], D. Camarero Munoz[27], P. Camarri[77a,77b], M. T. Camerlingo[73a,73b], D. Cameron[37], C. Camincher[168], M. Campanelli[98], A. Camplani[43], V. Canale[73a,73b], A. C. Canbay[3a], E. Canonero[97], J. Cantero[166], Y. Cao[165], F. Capocasa[27], M. Capua[44a,44b], A. Carbone[72a,72b], R. Cardarelli[77a], J. C. J. Cardenas[8], G. Carducci[44a,44b], T. Carli[37], G. Carlino[73a], J. I. Carlotto[13], B. T. Carlson[132,p], E. M. Carlson[159a,168], J. Carmignani[94], L. Carminati[72a,72b], A. Carnelli[138], M. Carnesale[37], S. Caron[116], E. Carquin[140f], I. B. Carr[107], S. Carrá[72a], G. Carratta[24a,24b], A. M. Carroll[126], M. P. Casado[13,h], M. Caspar[49], F. L. Castillo[4], L. Castillo Garcia[13], V. Castillo Gimenez[166], N. F. Castro[133a,133e], A. Catinaccio[37], J. R. Catmore[128], T. Cavaliere[4], V. Cavaliere[30], N. Cavalli[24a,24b], L. J. Caviedes Betancourt[23b], Y. C. Cekmecelioglu[49], E. Celebi[83], S. Cella[37], M. S. Centonze[71a,71b], V. Cepaitis[57], K. Cerny[125], A. S. Cerqueira[84a], A. Cerri[150], L. Cerrito[77a,77b], F. Cerutti[18a], B. Cervato[145], A. Cervelli[24b], G. Cesarini[54], S. A. Cetin[83], D. Chakraborty[118], J. Chan[18a], W. Y. Chan[157], J. D. Chapman[33], E. Chapon[138], B. Chargeishvili[153b], D. G. Charlton[21], M. Chatterjee[20], C. Chauhan[136], Y. Che[114a], S. Chekanov[6], S. V. Chekulaev[159a], G. A. Chelkov[39,a], A. Chen[108], B. Chen[155], B. Chen[168], H. Chen[114a], H. Chen[30], J. Chen[63c], J. Chen[146], M. Chen[129], S. Chen[89], S. J. Chen[114a], X. Chen[63c], X. Chen[15,ac], Y. Chen[63a], C. L. Cheng[173], H. C. Cheng[65a], S. Cheong[147], A. Cheplakov[39], E. Cheremushkina[49], E. Cherepanova[117], R. Cherkaoui El Moursli[36e], E. Cheu[7], K. Cheung[66], L. Chevalier[138], V. Chiarella[54], G. Chiarelli[75a], N. Chiedde[104], G. Chiodini[71a], A. S. Chisholm[21], A. Chitan[28b], M. Chitishvili[166], M. V. Chizhov[39,q], K. Choi[11], Y. Chou[142], E. Y. S. Chow[116], K. L. Chu[172], M. C. Chu[65a], X. Chu[14,114c], Z. Chubinidze[54], J. Chudoba[134], J. J. Chwastowski[88], D. Cieri[112], K. M. Ciesla[87a], V. Cindro[95], A. Ciocio[18a], F. Cirotto[73a,73b], Z. H. Citron[172], M. Citterio[72a], D. A. Ciubotaru[28b], A. Clark[57], P. J. Clark[53], N. Clarke Hall[98], C. Clarry[158], J. M. Clavijo Columbie[49], S. E. Clawson[49], C. Clement[48a,48b], Y. Coadou[104], M. Cobal[70a,70c], A. Coccaro[58b], R. F. Coelho Barrue[133a], R. Coelho Lopes De Sa[105], S. Coelli[72a], L. S. Colangeli[158], B. Cole[42], J. Collot[61], P. Conde Muiño[133a,133g], M. P. Connell[34c], S. H. Connell[34c], E. I. Conroy[129], F. Conventi[73a,ae], H. G. Cooke[21], A. M. Cooper-Sarkar[129], F. A. Corchia[24a,24b], A. Cordeiro Oudot Choi[130], L. D. Corpe[41], M. Corradi[76a,76b], F. Corriveau[106,x], A. Cortes-Gonzalez[19], M. J. Costa[166], F. Costanza[4], D. Costanzo[143], B. M. Cote[122], J. Couthures[4], G. Cowan[97], K. Cranmer[173], L. Cremer[50], D. Cremonini[24a,24b], S. Crépé-Renaudin[61],

F. Crescioli[130], M. Cristinziani[145], M. Cristoforetti[79a,79b], V. Croft[117], J. E. Crosby[124], G. Crosetti[44a,44b], A. Cueto[101], H. Cui[98], Z. Cui[7], W. R. Cunningham[60], F. Curcio[166], J. R. Curran[53], P. Czodrowski[37], M. J. Da Cunha Sargedas De Sousa[58a,58b], J. V. Da Fonseca Pinto[84b], C. Da Via[103], W. Dabrowski[87a], T. Dado[37], S. Dahbi[152], T. Dai[108], D. Dal Santo[20], C. Dallapiccola[105], M. Dam[43], G. D'amen[30], V. D'Amico[111], J. Damp[102], J. R. Dandoy[35], D. Dannheim[37], M. Danninger[146], V. Dao[149], G. Darbo[58b], S. J. Das[30], F. Dattola[49], S. D'Auria[72a,72b], A. D'Avanzo[73a,73b], C. David[34a], T. Davidek[136], I. Dawson[96], H. A. Day-hall[135], K. De[8], R. De Asmundis[73a], N. De Biase[49], S. De Castro[24a,24b], N. De Groot[116], P. de Jong[117], H. De la Torre[118], A. De Maria[114a], A. De Salvo[76a], U. De Sanctis[77a,77b], F. De Santis[71a,71b], A. De Santo[150], J. B. De Vivie De Regie[61], J. Debevc[95], D. V. Dedovich[39], J. Degens[94], A. M. Deiana[45], F. Del Corso[24a,24b], J. Del Peso[101], L. Delagrange[130], F. Deliot[138], C. M. Delitzsch[50], M. Della Pietra[73a,73b], D. Della Volpe[57], A. Dell'Acqua[37], L. Dell'Asta[72a,72b], M. Delmastro[4], P. A. Delsart[61], S. Demers[175], M. Demichev[39], S. P. Denisov[38], L. D'Eramo[41], D. Derendarz[88], F. Derue[130], P. Dervan[94], K. Desch[25], C. Deutsch[25], F. A. Di Bello[58a,58b], A. Di Ciaccio[77a,77b], L. Di Ciaccio[4], A. Di Domenico[76a,76b], C. Di Donato[73a,73b], A. Di Girolamo[37], G. Di Gregorio[37], A. Di Luca[79a,79b], B. Di Micco[78a,78b], R. Di Nardo[78a,78b], K. F. Di Petrillo[40], M. Diamantopoulou[35], F. A. Dias[117], T. Dias Do Vale[146], M. A. Diaz[140a,140b], F. G. Diaz Capriles[25], A. R. Didenko[39], M. Didenko[166], E. B. Diehl[108], S. Díez Cornell[49], C. Diez Pardos[145], C. Dimitriadi[164], A. Dimitrievska[21], J. Dingfelder[25], T. Dingley[129], I.-M. Dinu[28b], S. J. Dittmeier[64b], F. Dittus[37], M. Divisek[136], B. Dixit[94], F. Djama[104], T. Djobava[153b], C. Doglioni[100,103], A. Dohnalova[29a], J. Dolejsi[136], Z. Dolezal[136], K. Domijan[87a], K. M. Dona[40], M. Donadelli[84d], B. Dong[109], J. Donini[41], A. D'Onofrio[73a,73b], M. D'Onofrio[94], J. Dopke[137], A. Doria[73a], N. Dos Santos Fernandes[133a], P. Dougan[103], M. T. Dova[92], A. T. Doyle[60], M. A. Draguet[129], M. P. Drescher[56], E. Dreyer[172], I. Drivas-koulouris[10], M. Drnevich[120], M. Drozdova[57], D. Du[63a], T. A. du Pree[117], F. Dubinin[38], M. Dubovsky[29a], E. Duchovni[172], G. Duckeck[111], O. A. Ducu[28b], D. Duda[53], A. Dudarev[37], E. R. Duden[27], M. D'uffizi[103], L. Duflot[67], M. Dührssen[37], I. Duminica[28g], A. E. Dumitriu[28b], M. Dunford[64a], S. Dungs[50], K. Dunne[48a,48b], A. Duperrin[104], H. Duran Yildiz[3a], M. Düren[59], A. Durglishvili[153b], B. L. Dwyer[118], G. I. Dyckes[18a], M. Dyndal[87a], B. S. Dziedzic[37], Z. O. Earnshaw[150], G. H. Eberwein[129], B. Eckerova[29a], S. Eggebrecht[56], E. Egidio Purcino De Souza[84e], L. F. Ehrke[57], G. Eigen[17], K. Einsweiler[18a], T. Ekelof[164], P. A. Ekman[100], S. El Farkh[36b], Y. El Ghazali[63a], H. El Jarrari[37], A. El Moussaouy[36a], V. Ellajosyula[164], M. Ellert[164], F. Ellinghaus[174], N. Ellis[37], J. Elmsheuser[30], M. Elsawy[119a], M. Elsing[37], D. Emeliyanov[137], Y. Enari[85], I. Ene[18a], S. Epari[13], P. A. Erland[88], D. Ernani Martins Neto[88], M. Errenst[174], M. Escalier[67], C. Escobar[166], E. Etzion[155], G. Evans[133a], H. Evans[69], L. S. Evans[97], A. Ezhilov[38], S. Ezzarqtouni[36a], F. Fabbri[24a,24b], L. Fabbri[24a,24b], G. Facini[98], V. Fadeyev[139], R. M. Fakhrutdinov[38], D. Fakoudis[102], S. Falciano[76a], L. F. Falda Ulhoa Coelho[37], F. Fallavollita[112], G. Falsetti[44a,44b], J. Faltova[136], C. Fan[165], K. Y. Fan[65b], Y. Fan[14], Y. Fang[14,114c], M. Fanti[72a,72b], M. Faraj[70a,70b], Z. Farazpay[99], A. Farbin[8], A. Farilla[78a], T. Farooque[109], S. M. Farrington[53], F. Fassi[36e], D. Fassouliotis[9], M. Faucci Giannelli[77a,77b], W. J. Fawcett[33], L. Fayard[67], P. Federic[136], P. Federicova[134], O. L. Fedin[38,a], M. Feickert[173], L. Feligioni[104], D. E. Fellers[126], C. Feng[63b], Z. Feng[117], M. J. Fenton[162], L. Ferencz[49], R. A. M. Ferguson[93], S. I. Fernandez Luengo[140f], P. Fernandez Martinez[68], M. J. V. Fernoux[104], J. Ferrando[93], A. Ferrari[164], P. Ferrari[116,117], R. Ferrari[74a], D. Ferrere[57], C. Ferretti[108], D. Fiacco[76a,76b], F. Fiedler[102], P. Fiedler[135], S. Filimonov[38], A. Filipčič[95], E. K. Filmer[159a], F. Filthaut[116], M. C. N. Fiolhais[133a,133c,c], L. Fiorini[166], W. C. Fisher[109], T. Fitschen[103], P. M. Fitzhugh[138], I. Fleck[145], P. Fleischmann[108], T. Flick[174], M. Flores[34d,aa], L. R. Flores Castillo[65a], L. Flores Sanz De Acedo[37], F. M. Follega[79a,79b], N. Fomin[33], J. H. Foo[158], A. Formica[138], A. C. Forti[103], E. Fortin[37], A. W. Fortman[18a], M. G. Foti[18a], L. Fountas[9,i], D. Fournier[67], H. Fox[93], P. Francavilla[75a,75b], S. Francescato[62], S. Franchellucci[57], M. Franchini[24a,24b], S. Franchino[64a], D. Francis[37], L. Franco[116], V. Franco Lima[37], L. Franconi[49], M. Franklin[62], G. Frattari[27], Y. Y. Frid[155], J. Friend[60], N. Fritzsche[37], A. Froch[55], D. Froidevaux[37], J. A. Frost[129], Y. Fu[63a], S. Fuenzalida Garrido[140f], M. Fujimoto[104], K. Y. Fung[65a], E. Furtado De Simas Filho[84e], M. Furukawa[157], J. Fuster[166], A. Gaa[56], A. Gabrielli[24a,24b], A. Gabrielli[158], P. Gadow[37], G. Gagliardi[58a,58b], L. G. Gagnon[18a], S. Gaid[163], S. Galantzan[155], J. Gallagher[1], E. J. Gallas[129], B. J. Gallop[137], K. K. Gan[122], S. Ganguly[157], Y. Gao[53], F. M. Garay Walls[140a,140b], B. Garcia[30], C. García[166], A. Garcia Alonso[117], A. G. Garcia Caffaro[175], J. E. García Navarro[166], M. Garcia-Sciveres[18a], G. L. Gardner[131], R. W. Gardner[40], N. Garelli[161], D. Garg[81], R. B. Garg[147], J. M. Gargan[53], C. A. Garner[158], C. M. Garvey[34a], V. K. Gassmann[161], G. Gaudio[74a], V. Gautam[13], P. Gauzzi[76a,76b], J. Gavranovic[95], I. L. Gavrilenko[38], A. Gavrilyuk[38], C. Gay[167], G. Gaycken[126],

E. N. Gazis[10], A. A. Geanta[28b], C. M. Gee[139], A. Gekow[122], C. Gemme[58b], M. H. Genest[61], A. D. Gentry[115], S. George[97], W. F. George[21], T. Geralis[47], P. Gessinger-Befurt[37], M. E. Geyik[174], M. Ghani[170], K. Ghorbanian[96], A. Ghosal[145], A. Ghosh[162], A. Ghosh[7], B. Giacobbe[24b], S. Giagu[76a,76b], T. Giani[117], A. Giannini[63a], S. M. Gibson[97], M. Gignac[139], D. T. Gil[87b], A. K. Gilbert[87a], B. J. Gilbert[42], D. Gillberg[35], G. Gilles[117], L. Ginabat[130], D. M. Gingrich[2,ad], M. P. Giordani[70a,70c], P. F. Giraud[138], G. Giugliarelli[70a,70c], D. Giugni[72a], F. Giuli[77a,77b], I. Gkialas[9,i], L. K. Gladilin[38], C. Glasman[101], G. R. Gledhill[126], G. Glemža[49], M. Glisic[126], I. Gnesi[44b], Y. Go[30], M. Goblirsch-Kolb[37], B. Gocke[50], D. Godin[110], B. Gokturk[22a], S. Goldfarb[107], T. Golling[57], M. G. D. Gololo[34g], D. Golubkov[38], J. P. Gombas[109], A. Gomes[133a,133b], G. Gomes Da Silva[145], A. J. Gomez Delegido[166], R. Gonçalo[133a], L. Gonella[21], A. Gongadze[153c], F. Gonnella[21], J. L. Gonski[147], R. Y. González Andana[53], S. González de la Hoz[166], R. Gonzalez Lopez[94], C. Gonzalez Renteria[18a], M. V. Gonzalez Rodrigues[49], R. Gonzalez Suarez[164], S. Gonzalez-Sevilla[57], L. Goossens[37], B. Gorini[37], E. Gorini[71a,71b], A. Gorišek[95], T. C. Gosart[131], A. T. Goshaw[52], M. I. Gostkin[39], S. Goswami[124], C. A. Gottardo[37], S. A. Gotz[111], M. Gouighri[36b], V. Goumarre[49], A. G. Goussiou[142], N. Govender[34c], R. P. Grabarczyk[129], I. Grabowska-Bold[87a], K. Graham[35], E. Gramstad[128], S. Grancagnolo[71a,71b], C. M. Grant[1,138], P. M. Gravila[28f], F. G. Gravili[71a,71b], H. M. Gray[18a], M. Greco[71a,71b], M. J. Green[1], C. Grefe[25], A. S. Grefsrud[17], I. M. Gregor[49], K. T. Greif[162], P. Grenier[147], S. G. Grewe[112], A. A. Grillo[139], K. Grimm[32], S. Grinstein[13,t], J.-F. Grivaz[67], E. Gross[172], J. Grosse-Knetter[56], L. Guan[108], J. G. R. Guerrero Rojas[166], G. Guerrieri[37], R. Gugel[102], J. A. M. Guhit[108], A. Guida[19], E. Guilloton[170], S. Guindon[37], F. Guo[14,114c], J. Guo[63c], L. Guo[49], L. Guo[14], Y. Guo[108], A. Gupta[50], R. Gupta[132], S. Gurbuz[25], S. S. Gurdasani[55], G. Gustavino[76a,76b], P. Gutierrez[123], L. F. Gutierrez Zagazeta[131], M. Gutsche[51], C. Gutschow[98], C. Gwenlan[129], C. B. Gwilliam[94], E. S. Haaland[128], A. Haas[120], M. Habedank[60], C. Haber[18a], H. K. Hadavand[8], A. Hadef[51], S. Hadzic[112], A. I. Hagan[93], J. J. Hahn[145], E. H. Haines[98], M. Haleem[169], J. Haley[124], G. D. Hallewell[104], L. Halser[20], K. Hamano[168], M. Hamer[25], E. J. Hampshire[97], J. Han[63b], L. Han[114a], L. Han[63a], S. Han[18a], Y. F. Han[158], K. Hanagaki[85], M. Hance[139], D. A. Hangal[42], H. Hanif[146], M. D. Hank[131], J. B. Hansen[43], P. H. Hansen[43], D. Harada[57], T. Harenberg[174], S. Harkusha[176], M. L. Harris[105], Y. T. Harris[25], J. Harrison[13], N. M. Harrison[122], P. F. Harrison[170], N. M. Hartman[112], N. M. Hartmann[111], R. Z. Hasan[97,137], Y. Hasegawa[144], F. Haslbeck[129], S. Hassan[17], R. Hauser[109], C. M. Hawkes[21], R. J. Hawkings[37], Y. Hayashi[157], D. Hayden[109], C. Hayes[108], R. L. Hayes[117], C. P. Hays[129], J. M. Hays[96], H. S. Hayward[94], F. He[63a], M. He[14,114c], Y. He[49], Y. He[98], N. B. Heatley[96], V. Hedberg[100], A. L. Heggelund[128], N. D. Hehir[96,*], C. Heidegger[55], K. K. Heidegger[55], J. Heilman[35], S. Heim[49], T. Heim[18a], J. G. Heinlein[131], J. J. Heinrich[126], L. Heinrich[112,ab], J. Hejbal[134], A. Held[173], S. Hellesund[17], C. M. Helling[167], S. Hellman[48a,48b], R. C. W. Henderson[93], L. Henkelmann[33], A. M. Henriques Correia[37], H. Herde[100], Y. Hernández Jiménez[149], L. M. Herrmann[25], T. Herrmann[51], G. Herten[55], R. Hertenberger[111], L. Hervas[37], M. E. Hesping[102], N. P. Hessey[159a], J. Hessler[112], M. Hidaoui[36b], N. Hidic[136], E. Hill[158], S. J. Hillier[21], J. R. Hinds[109], F. Hinterkeuser[25], M. Hirose[127], S. Hirose[160], D. Hirschbuehl[174], T. G. Hitchings[103], B. Hiti[95], J. Hobbs[149], R. Hobincu[28e], N. Hod[172], M. C. Hodgkinson[143], B. H. Hodkinson[129], A. Hoecker[37], D. D. Hofer[108], J. Hofer[166], T. Holm[25], M. Holzbock[37], L. B. A. H. Hommels[33], B. P. Honan[103], J. J. Hong[69], J. Hong[63c], T. M. Hong[132], B. H. Hooberman[165], W. H. Hopkins[6], M. C. Hoppesch[165], Y. Horii[113], M. E. Horstmann[112], S. Hou[152], A. S. Howard[95], J. Howarth[60], J. Hoya[6], M. Hrabovsky[125], A. Hrynevich[49], T. Hryn'ova[4], P. J. Hsu[66], S.-C. Hsu[142], T. Hsu[67], M. Hu[18a], Q. Hu[63a], S. Huang[33], X. Huang[14,114c], Y. Huang[143], Y. Huang[102], Y. Huang[14], Z. Huang[103], Z. Hubacek[135], M. Huebner[25], F. Huegging[25], T. B. Huffman[129], M. Hufnagel Maranha De Faria[84a], C. A. Hugli[49], M. Huhtinen[37], S. K. Huiberts[17], R. Hulsken[106], N. Huseynov[12,f], J. Huston[109], J. Huth[62], R. Hyneman[147], G. Iacobucci[57], G. Iakovidis[30], L. Iconomidou-Fayard[67], J. P. Iddon[37], P. Iengo[73a,73b], R. Iguchi[157], Y. Iiyama[157], T. Iizawa[129], Y. Ikegami[85], N. Ilic[158], H. Imam[84c], G. Inacio Goncalves[84d], T. Ingebretsen Carlson[48a,48b], J. M. Inglis[96], G. Introzzi[74a,74b], M. Iodice[78a], V. Ippolito[76a,76b], R. K. Irwin[94], M. Ishino[157], W. Islam[173], C. Issever[19], S. Istin[22a,ah], H. Ito[171], R. Iuppa[79a,79b], A. Ivina[172], J. M. Izen[46], V. Izzo[73a], P. Jacka[134], P. Jackson[1], C. S. Jagfeld[111], G. Jain[159a], P. Jain[49], K. Jakobs[55], T. Jakoubek[172], J. Jamieson[60], W. Jang[157], M. Javurkova[105], P. Jawahar[103], L. Jeanty[126], J. Jejelava[153a,z], P. Jenni[55,e], C. E. Jessiman[35], C. Jia[63b], H. Jia[167], J. Jia[149], X. Jia[14,114c], Z. Jia[114a], C. Jiang[53], S. Jiggins[49], J. Jimenez Pena[13], S. Jin[114a], A. Jinaru[28b], O. Jinnouchi[141], P. Johansson[143], K. A. Johns[7], J. W. Johnson[139], F. A. Jolly[49], D. M. Jones[150], E. Jones[49], K. S. Jones[8], P. Jones[33], R. W. L. Jones[93], T. J. Jones[94], H. L. Joos[37,56], R. Joshi[122],

J. Jovicevic[16], X. Ju[18a], J. J. Junggeburth[105], T. Junkermann[64a], A. Juste Rozas[13,t], M. K. Juzek[88], S. Kabana[140e], A. Kaczmarska[88], M. Kado[112], H. Kagan[122], M. Kagan[147], A. Kahn[131], C. Kahra[102], T. Kaji[157], E. Kajomovitz[154], N. Kakati[172], I. Kalaitzidou[55], C. W. Kalderon[30], N. J. Kang[139], D. Kar[34g], K. Karava[129], M. J. Kareem[159b], E. Karentzos[55], O. Karkout[117], S. N. Karpov[39], Z. M. Karpova[39], V. Kartvelishvili[93], A. N. Karyukhin[38], E. Kasimi[156], J. Katzy[49], S. Kaur[35], K. Kawade[144], M. P. Kawale[123], C. Kawamoto[89], T. Kawamoto[63a], E. F. Kay[37], F. I. Kaya[161], S. Kazakos[109], V. F. Kazanin[38], Y. Ke[149], J. M. Keaveney[34a], R. Keeler[168], G. V. Kehris[62], J. S. Keller[35], J. J. Kempster[150], O. Kepka[134], B. P. Kerridge[137], S. Kersten[174], B. P. Kerševan[95], L. Keszeghova[29a], S. Ketabchi Haghighat[158], R. A. Khan[132], A. Khanov[124], A. G. Kharlamov[38], T. Kharlamova[38], E. E. Khoda[142], M. Kholodenko[133a], T. J. Khoo[19], G. Khoriauli[169], J. Khubua[153b,*], Y. A. R. Khwaira[130], B. Kibirige[34g], D. Kim[6], D. W. Kim[48a,48b], Y. K. Kim[40], N. Kimura[98], M. K. Kingston[56], A. Kirchhoff[56], C. Kirfel[25], F. Kirfel[25], J. Kirk[137], A. E. Kiryunin[112], S. Kita[160], C. Kitsaki[10], O. Kivernyk[25], M. Klassen[161], C. Klein[35], L. Klein[169], M. H. Klein[45], S. B. Klein[57], U. Klein[94], A. Klimentov[30], T. Klioutchnikova[37], P. Kluit[117], S. Kluth[112], E. Kneringer[80], T. M. Knight[158], A. Knue[50], D. Kobylianskii[172], S. F. Koch[129], M. Kocian[147], P. Kodyš[136], D. M. Koeck[126], P. T. Koenig[25], T. Koffas[35], O. Kolay[51], I. Koletsou[4], T. Komarek[88], K. Köneke[55], A. X. Y. Kong[1], T. Kono[121], N. Konstantinidis[98], P. Kontaxakis[57], B. Konya[100], R. Kopeliansky[42], S. Koperny[87a], K. Korcyl[88], K. Kordas[156,d], A. Korn[98], S. Korn[56], I. Korolkov[13], N. Korotkova[38], B. Kortman[117], O. Kortner[112], S. Kortner[112], W. H. Kostecka[118], V. V. Kostyukhin[145], A. Kotsokechagia[37], A. Kotwal[52], A. Koulouris[37], A. Kourkoumeli-Charalampidi[74a,74b], C. Kourkoumelis[9], E. Kourlitis[112,ab], O. Kovanda[126], R. Kowalewski[168], W. Kozanecki[126], A. S. Kozhin[38], V. A. Kramarenko[38], G. Kramberger[95], P. Kramer[102], M. W. Krasny[130], A. Krasznahorkay[37], A. C. Kraus[118], J. W. Kraus[174], J. A. Kremer[49], T. Kresse[51], L. Kretschmann[174], J. Kretzschmar[94], K. Kreul[19], P. Krieger[158], M. Krivos[136], K. Krizka[21], K. Kroeninger[50], H. Kroha[112], J. Kroll[134], J. Kroll[131], K. S. Krowpman[109], U. Kruchonak[39], H. Krüger[25], N. Krumnack[82], M. C. Kruse[52], O. Kuchinskaia[38], S. Kuday[3a], S. Kuehn[37], R. Kuesters[55], T. Kuhl[49], V. Kukhtin[39], Y. Kulchitsky[38,a], S. Kuleshov[140b,140d], M. Kumar[34g], N. Kumari[49], P. Kumari[159b], A. Kupco[134], T. Kupfer[50], A. Kupich[38], O. Kuprash[55], H. Kurashige[86], L. L. Kurchaninov[159a], O. Kurdysh[67], Y. A. Kurochkin[38], A. Kurova[38], M. Kuze[141], A. K. Kvam[105], J. Kvita[125], T. Kwan[106], N. G. Kyriacou[108], L. A. O. Laatu[104], C. Lacasta[166], F. Lacava[76a,76b], H. Lacker[19], D. Lacour[130], N. N. Lad[98], E. Ladygin[39], A. Lafarge[41], B. Laforge[130], T. Lagouri[175], F. Z. Lahbabi[36a], S. Lai[56], J. E. Lambert[168], S. Lammers[69], W. Lampl[7], C. Lampoudis[156,d], G. Lamprinoudis[102], A. N. Lancaster[118], E. Lançon[30], U. Landgraf[55], M. P. J. Landon[96], V. S. Lang[55], O. K. B. Langrekken[128], A. J. Lankford[162], F. Lanni[37], K. Lantzsch[25], A. Lanza[74a], M. Lanzac Berrocal[166], J. F. Laporte[138], T. Lari[72a], F. Lasagni Manghi[24b], M. Lassnig[37], V. Latonova[134], A. Laurier[154], S. D. Lawlor[143], Z. Lawrence[103], R. Lazaridou[170], M. Lazzaroni[72a,72b], B. Le[103], H. D. M. Le[109], E. M. Le Boulicaut[175], L. T. Le Pottier[18a], B. Leban[24a,24b], A. Lebedev[82], M. LeBlanc[103], F. Ledroit-Guillon[61], S. C. Lee[152], S. Lee[48a,48b], T. F. Lee[94], L. L. Leeuw[34c], H. P. Lefebvre[97], M. Lefebvre[168], C. Leggett[18a], G. Lehmann Miotto[37], M. Leigh[57], W. A. Leight[105], W. Leinonen[116], A. Leisos[156,r], M. A. L. Leite[84c], C. E. Leitgeb[19], R. Leitner[136], K. J. C. Leney[45], T. Lenz[25], S. Leone[75a], C. Leonidopoulos[53], A. Leopold[148], R. Les[109], C. G. Lester[33], M. Levchenko[38], J. Levêque[4], L. J. Levinson[172], G. Levrini[24a,24b], M. P. Lewicki[88], C. Lewis[142], D. J. Lewis[4], L. Lewitt[143], A. Li[30], B. Li[63b], C. Li[63a], C.-Q. Li[112], H. Li[63a], H. Li[63b], H. Li[114a], H. Li[15], H. Li[63b], J. Li[63c], K. Li[14], L. Li[63c], M. Li[14,114c], S. Li[14,114c], S. Li[63c,63d], T. Li[5], X. Li[106], Z. Li[157], Z. Li[14,114c], Z. Li[63a], S. Liang[14,114c], Z. Liang[14], M. Liberatore[138], B. Liberti[77a], K. Lie[65c], J. Lieber Marin[84e], H. Lien[69], H. Lin[108], K. Lin[109], R. E. Lindley[7], J. H. Lindon[2], J. Ling[62], E. Lipeles[131], A. Lipniacka[17], A. Lister[167], J. D. Little[69], B. Liu[14], B. X. Liu[114b], D. Liu[63c,63d], E. H. L. Liu[21], J. B. Liu[63a], J. K. K. Liu[33], K. Liu[63d], K. Liu[63c,63d], M. Liu[63a], M. Y. Liu[63a], P. Liu[14], Q. Liu[63c,63d,142], X. Liu[63a], X. Liu[63b], Y. Liu[114b,114c], Y. L. Liu[63b], Y. W. Liu[63a], S. L. Lloyd[96], E. M. Lobodzinska[49], P. Loch[7], E. Lodhi[158], T. Lohse[19], K. Lohwasser[143], E. Loiacono[49], J. D. Lomas[21], J. D. Long[42], I. Longarini[162], R. Longo[165], I. Lopez Paz[68], A. Lopez Solis[49], N. A. Lopez-canelas[7], N. Lorenzo Martinez[4], A. M. Lory[111], M. Losada[119a], G. Löschcke Centeno[150], O. Loseva[38], X. Lou[48a,48b], X. Lou[14,114c], A. Lounis[67], P. A. Love[93], G. Lu[14,114c], M. Lu[67], S. Lu[131], Y. J. Lu[66], H. J. Lubatti[142], C. Luci[76a,76b], F. L. Lucio Alves[114a], F. Luehring[69], O. Lukianchuk[67], B. S. Lunday[131], O. Lundberg[148], B. Lund-Jensen[148,*], N. A. Luongo[6], M. S. Lutz[37], A. B. Lux[26], D. Lynn[30], R. Lysak[134], E. Lytken[100], V. Lyubushkin[39], T. Lyubushkina[39], M. M. Lyukova[149], M. Firdaus M. Soberi[53], H. Ma[30], K. Ma[63a], L. L. Ma[63b],

W. Ma[63a], Y. Ma[124], J. C. MacDonald[102], P. C. Machado De Abreu Farias[84e], R. Madar[41], T. Madula[98], J. Maeda[86], T. Maeno[30], H. Maguire[143], V. Maiboroda[138], A. Maio[133a,133b,133d], K. Maj[87a], O. Majersky[49], S. Majewski[126], N. Makovec[67], V. Maksimovic[16], B. Malaescu[130], Pa. Malecki[88], V. P. Maleev[38], F. Malek[61,m], M. Mali[95], D. Malito[97], U. Mallik[81,*], S. Maltezos[10], S. Malyukov[39], J. Mamuzic[13], G. Mancini[54], M. N. Mancini[27], G. Manco[74a,74b], J. P. Mandalia[96], S. S. Mandarry[150], I. Mandić[95], L. Manhaes de Andrade Filho[84a], I. M. Maniatis[172], J. Manjarres Ramos[91], D. C. Mankad[172], A. Mann[111], S. Manzoni[37], L. Mao[63c], X. Mapekula[34c], A. Marantis[156,r], G. Marchiori[5], M. Marcisovsky[134], C. Marcon[72a], E. Maricic[16], M. Marinescu[21], S. Marium[49], M. Marjanovic[123], A. Markhoos[55], M. Markovitch[67], E. J. Marshall[93], Z. Marshall[18a], S. Marti-Garcia[166], J. Martin[98], T. A. Martin[137], V. J. Martin[53], B. Martin dit Latour[17], L. Martinelli[76a,76b], M. Martinez[13,t], P. Martinez Agullo[166], V. I. Martinez Outschoorn[105], P. Martinez Suarez[13], S. Martin-Haugh[137], G. Martinovicova[136], V. S. Martoiu[28b], A. C. Martyniuk[98], A. Marzin[37], D. Mascione[79a,79b], L. Masetti[102], J. Masik[103], A. L. Maslennikov[38], S. L. Mason[42], P. Massarotti[73a,73b], P. Mastrandrea[75a,75b], A. Mastroberardino[44a,44b], T. Masubuchi[127], T. T. Mathew[126], T. Mathisen[164], J. Matousek[136], D. M. Mattern[50], J. Maurer[28b], T. Maurin[60], A. J. Maury[67], B. Maček[95], D. A. Maximov[38], A. E. May[103], R. Mazini[152], I. Maznas[118], M. Mazza[109], S. M. Mazza[139], E. Mazzeo[72a,72b], C. Mc Ginn[30], J. P. Mc Gowan[168], S. P. Mc Kee[108], C. A. Mc Lean[6], C. C. McCracken[167], E. F. McDonald[107], A. E. McDougall[117], J. A. Mcfayden[150], R. P. McGovern[131], R. P. Mckenzie[34g], T. C. Mclachlan[49], D. J. Mclaughlin[98], S. J. McMahon[137], C. M. Mcpartland[94], R. A. McPherson[168,x], S. Mehlhase[111], A. Mehta[94], D. Melini[166], B. R. Mellado Garcia[34g], A. H. Melo[56], F. Meloni[49], A. M. Mendes Jacques Da Costa[103], H. Y. Meng[158], L. Meng[93], S. Menke[112], M. Mentink[37], E. Meoni[44a,44b], G. Mercado[118], S. Merianos[156], C. Merlassino[70a,70c], L. Merola[73a,73b], C. Meroni[72a,72b], J. Metcalfe[6], A. S. Mete[6], E. Meuser[102], C. Meyer[69], J.-P. Meyer[138], R. P. Middleton[137], L. Mijović[53], G. Mikenberg[172], M. Mikestikova[134], M. Mikuž[95], H. Mildner[102], A. Milic[37], D. W. Miller[40], E. H. Miller[147], L. S. Miller[35], A. Milov[172], D. A. Milstead[48a,48b], T. Min[114a], A. A. Minaenko[38], I. A. Minashvili[153b], L. Mince[60], A. I. Mincer[120], B. Mindur[87a], M. Mineev[39], Y. Mino[89], L. M. Mir[13], M. Miralles Lopez[60], M. Mironova[18a], M. C. Missio[116], A. Mitra[170], V. A. Mitsou[166], Y. Mitsumori[113], O. Miu[158], P. S. Miyagawa[96], T. Mkrtchyan[64a], M. Mlinarevic[98], T. Mlinarevic[98], M. Mlynarikova[37], S. Mobius[20], P. Mogg[111], M. H. Mohamed Farook[115], A. F. Mohammed[14,114c], S. Mohapatra[42], G. Mokgatitswane[34g], L. Moleri[172], B. Mondal[145], S. Mondal[135], K. Mönig[49], E. Monnier[104], L. Monsonis Romero[166], J. Montejo Berlingen[13], A. Montella[48a,48b], M. Montella[122], F. Montereali[78a,78b], F. Monticelli[92], S. Monzani[70a,70c], A. Morancho Tarda[43], N. Morange[67], A. L. Moreira De Carvalho[49], M. Moreno Llácer[166], C. Moreno Martinez[57], J. M. Moreno Perez[23b], P. Morettini[58b], S. Morgenstern[37], M. Morii[62], M. Morinaga[157], M. Moritsu[90], F. Morodei[76a,76b], P. Moschovakos[37], B. Moser[129], M. Mosidze[153b], T. Moskalets[45], P. Moskvitina[116], J. Moss[32,j], P. Moszkowicz[87a], A. Moussa[36d], E. J. W. Moyse[105], O. Mtintsilana[34g], S. Muanza[104], J. Mueller[132], D. Muenstermann[93], R. Müller[37], G. A. Mullier[164], A. J. Mullin[33], J. J. Mullin[131], A. E. Mulski[62], D. P. Mungo[158], D. Munoz Perez[166], F. J. Munoz Sanchez[103], M. Murin[103], W. J. Murray[137,170], M. Muškinja[95], C. Mwewa[30], A. G. Myagkov[38,a], A. J. Myers[8], G. Myers[108], M. Myska[135], B. P. Nachman[18a], O. Nackenhorst[50], K. Nagai[129], K. Nagano[85], R. Nagasaka[157], J. L. Nagle[30,af], E. Nagy[104], A. M. Nairz[37], Y. Nakahama[85], K. Nakamura[85], K. Nakkalil[5], H. Nanjo[127], E. A. Narayanan[45], I. Naryshkin[38], L. Nasella[72a,72b], M. Naseri[35], S. Nasri[119b], C. Nass[25], G. Navarro[23a], J. Navarro-Gonzalez[166], R. Nayak[155], A. Nayaz[19], P. Y. Nechaeva[38], S. Nechaeva[24a,24b], F. Nechansky[134], L. Nedic[129], T. J. Neep[21], A. Negri[74a,74b], M. Negrini[24b], C. Nellist[117], C. Nelson[106], K. Nelson[108], S. Nemecek[134], M. Nessi[37,g], M. S. Neubauer[165], F. Neuhaus[102], J. Neundorf[49], J. Newell[94], P. R. Newman[21], C. W. Ng[132], Y. W. Y. Ng[49], B. Ngair[119a], H. D. N. Nguyen[110], R. B. Nickerson[129], R. Nicolaidou[138], J. Nielsen[139], M. Niemeyer[56], J. Niermann[56], N. Nikiforou[37], V. Nikolaenko[38,a], I. Nikolic-Audit[130], K. Nikolopoulos[21], P. Nilsson[30], I. Ninca[49], G. Ninio[155], A. Nisati[76a], N. Nishu[2], R. Nisius[112], N. Nitika[70a,70c], J.-E. Nitschke[51], E. K. Nkadimeng[34g], T. Nobe[157], T. Nommensen[151], M. B. Norfolk[143], B. J. Norman[35], M. Noury[36a], J. Novak[95], T. Novak[95], L. Novotny[135], R. Novotny[115], L. Nozka[125], K. Ntekas[162], N. M. J. Nunes De Moura Junior[84b], J. Ocariz[130], A. Ochi[86], I. Ochoa[133a], S. Oerdek[49,u], J. T. Offermann[40], A. Ogrodnik[136], A. Oh[103], C. C. Ohm[148], H. Oide[85], R. Oishi[157], M. L. Ojeda[37], Y. Okumura[157], L. F. Oleiro Seabra[133a], I. Oleksiyuk[57], S. A. Olivares Pino[140d], G. Oliveira Correa[13], D. Oliveira Damazio[30], J. L. Oliver[162], Ö. O. Öncel[55], A. P. O'Neill[20], A. Onofre[133a,133e], P. U. E. Onyisi[11], M. J. Oreglia[40], G. E. Orellana[92], D. Orestano[78a,78b],

N. Orlando[13], R. S. Orr[158], L. M. Osojnak[131], R. Ospanov[63a], Y. Osumi[113], G. Otero y Garzon[31], H. Otono[90], P. S. Ott[64a], G. J. Ottino[18a], M. Ouchrif[36d], F. Ould-Saada[128], T. Ovsiannikova[142], M. Owen[60], R. E. Owen[137], V. E. Ozcan[22a], F. Ozturk[88], N. Ozturk[8], S. Ozturk[83], H. A. Pacey[129], A. Pacheco Pages[13], C. Padilla Aranda[13], G. Padovano[76a,76b], S. Pagan Griso[18a], G. Palacino[69], A. Palazzo[71a,71b], J. Pampel[25], J. Pan[175], T. Pan[65a], D. K. Panchal[11], C. E. Pandini[117], J. G. Panduro Vazquez[137], H. D. Pandya[1], H. Pang[15], P. Pani[49], G. Panizzo[70a,70c], L. Panwar[130], L. Paolozzi[57], S. Parajuli[165], A. Paramonov[6], C. Paraskevopoulos[54], D. Paredes Hernandez[65b], A. Pareti[74a,74b], K. R. Park[42], T. H. Park[158], M. A. Parker[33], F. Parodi[58a,58b], E. W. Parrish[118], V. A. Parrish[53], J. A. Parsons[42], U. Parzefall[55], B. Pascual Dias[110], L. Pascual Dominguez[101], E. Pasqualucci[76a], S. Passaggio[58b], F. Pastore[97], P. Patel[88], U. M. Patel[52], J. R. Pater[103], T. Pauly[37], F. Pauwels[136], C. I. Pazos[161], M. Pedersen[128], R. Pedro[133a], S. V. Peleganchuk[38], O. Penc[37], E. A. Pender[53], S. Peng[15], G. D. Penn[175], K. E. Penski[111], M. Penzin[38], B. S. Peralva[84d], A. P. Pereira Peixoto[142], L. Pereira Sanchez[147], D. V. Perepelitsa[30,af], G. Perera[105], E. Perez Codina[159a], M. Perganti[10], H. Pernegger[37], S. Perrella[76a,76b], O. Perrin[41], K. Peters[49], R. F. Y. Peters[103], B. A. Petersen[37], T. C. Petersen[43], E. Petit[104], V. Petousis[135], C. Petridou[156,d], T. Petru[136], A. Petrukhin[145], M. Pettee[18a], A. Petukhov[38], K. Petukhova[37], R. Pezoa[140f], L. Pezzotti[37], G. Pezzullo[175], A. J. Pfleger[37], T. M. Pham[173], T. Pham[107], P. W. Phillips[137], G. Piacquadio[149], E. Pianori[18a], F. Piazza[126], R. Piegaia[31], D. Pietreanu[28b], A. D. Pilkington[103], M. Pinamonti[70a,70c], J. L. Pinfold[2], B. C. Pinheiro Pereira[133a], J. Pinol Bel[13], A. E. Pinto Pinoargote[138], L. Pintucci[70a,70c], K. M. Piper[150], A. Pirttikoski[57], D. A. Pizzi[35], L. Pizzimento[65b], A. Pizzini[117], M.-A. Pleier[30], V. Pleskot[136], E. Plotnikova[39], G. Poddar[96], R. Poettgen[100], L. Poggioli[130], I. Pokharel[56], S. Polacek[136], G. Polesello[74a], A. Poley[146,159a], A. Polini[24b], C. S. Pollard[170], Z. B. Pollock[122], E. Pompa Pacchi[76a,76b], N. I. Pond[98], D. Ponomarenko[69], L. Pontecorvo[37], S. Popa[28a], G. A. Popeneciu[28d], A. Poreba[37], D. M. Portillo Quintero[159a], S. Pospisil[135], M. A. Postill[143], P. Postolache[28c], K. Potamianos[170], P. A. Potepa[87a], I. N. Potrap[39], C. J. Potter[33], H. Potti[151], J. Poveda[166], M. E. Pozo Astigarraga[37], A. Prades Ibanez[77a,77b], J. Pretel[168], D. Price[103], M. Primavera[71a], L. Primomo[70a,70c], M. A. Principe Martin[101], R. Privara[125], T. Procter[60], M. L. Proffitt[142], N. Proklova[131], K. Prokofiev[65c], G. Proto[112], J. Proudfoot[6], M. Przybycien[87a], W. W. Przygoda[87b], A. Psallidas[47], J. E. Puddefoot[143], D. Pudzha[55], D. Pyatiizbyantseva[38], J. Qian[108], R. Qian[109], D. Qichen[103], Y. Qin[13], T. Qiu[53], A. Quadt[56], M. Queitsch-Maitland[103], G. Quetant[57], R. P. Quinn[167], G. Rabanal Bolanos[62], D. Rafanoharana[55], F. Raffaeli[77a,77b], F. Ragusa[72a,72b], J. L. Rainbolt[40], J. A. Raine[57], S. Rajagopalan[30], E. Ramakoti[38], L. Rambelli[58a,58b], I. A. Ramirez-Berend[35], K. Ran[49,114c], D. S. Rankin[131], N. P. Rapheeha[34g], H. Rasheed[28b], V. Raskina[130], D. F. Rassloff[64a], A. Rastogi[18a], S. Rave[102], S. Ravera[58a,58b], B. Ravina[56], I. Ravinovich[172], M. Raymond[37], A. L. Read[128], N. P. Readioff[143], D. M. Rebuzzi[74a,74b], G. Redlinger[30], A. S. Reed[112], K. Reeves[27], J. A. Reidelsturz[174], D. Reikher[126], A. Rej[50], C. Rembser[37], M. Renda[28b], F. Renner[49], A. G. Rennie[162], A. L. Rescia[49], S. Resconi[72a], M. Ressegotti[58a,58b], S. Rettie[37], J. G. Reyes Rivera[109], E. Reynolds[18a], O. L. Rezanova[38], P. Reznicek[136], H. Riani[36d], N. Ribaric[52], E. Ricci[79a,79b], R. Richter[112], S. Richter[48a,48b], E. Richter-Was[87b], M. Ridel[130], S. Ridouani[36d], P. Rieck[120], P. Riedler[37], E. M. Riefel[48a,48b], J. O. Rieger[117], M. Rijssenbeek[149], M. Rimoldi[37], L. Rinaldi[24a,24b], P. Rincke[56,164], T. T. Rinn[30], M. P. Rinnagel[111], G. Ripellino[164], I. Riu[13], J. C. Rivera Vergara[168], F. Rizatdinova[124], E. Rizvi[96], B. R. Roberts[18a], S. S. Roberts[139], S. H. Robertson[106,x], D. Robinson[33], M. Robles Manzano[102], A. Robson[60], A. Rocchi[77a,77b], C. Roda[75a,75b], S. Rodriguez Bosca[37], Y. Rodriguez Garcia[23a], A. Rodriguez Rodriguez[55], A. M. Rodríguez Vera[118], S. Roe[37], J. T. Roemer[37], A. R. Roepe-Gier[139], O. Røhne[128], R. A. Rojas[105], C. P. A. Roland[130], J. Roloff[30], A. Romaniouk[80], E. Romano[74a,74b], M. Romano[24b], A. C. Romero Hernandez[165], N. Rompotis[94], L. Roos[130], S. Rosati[76a], B. J. Rosser[40], E. Rossi[129], E. Rossi[73a,73b], L. P. Rossi[62], L. Rossini[55], R. Rosten[122], M. Rotaru[28b], B. Rottler[55], C. Rougier[91], D. Rousseau[67], D. Rousso[49], A. Roy[165], S. Roy-Garand[158], A. Rozanov[104], Z. M. A. Rozario[60], Y. Rozen[154], A. Rubio Jimenez[166], A. J. Ruby[94], V. H. Ruelas Rivera[19], T. A. Ruggeri[1], A. Ruggiero[129], A. Ruiz-Martinez[166], A. Rummler[37], Z. Rurikova[55], N. A. Rusakovich[39], H. L. Russell[168], G. Russo[76a,76b], J. P. Rutherfoord[7], S. Rutherford Colmenares[33], M. Rybar[136], E. B. Rye[128], A. Ryzhov[45], J. A. Sabater Iglesias[57], H. F.-W. Sadrozinski[139], F. Safai Tehrani[76a], B. Safarzadeh Samani[137], S. Saha[1], M. Sahinsoy[83], A. Saibel[166], M. Saimpert[138], M. Saito[157], T. Saito[157], A. Sala[72a,72b], D. Salamani[37], A. Salnikov[147], J. Salt[166], A. Salvador Salas[155], D. Salvatore[44a,44b], F. Salvatore[150], A. Salzburger[37], D. Sammel[55], E. Sampson[93], D. Sampsonidis[156,d], D. Sampsonidou[126], J. Sánchez[166], V. Sanchez Sebastian[166], H. Sandaker[128], C. O. Sander[49], J. A. Sandesara[105], M. Sandhoff[174], C. Sandoval[23b],

L. Sanfilippo[64a], D. P. C. Sankey[137], T. Sano[89], A. Sansoni[54], L. Santi[37,76b], C. Santoni[41], H. Santos[133a,133b], A. Santra[172], E. Sanzani[24a,24b], K. A. Saoucha[163], J. G. Saraiva[133a,133d], J. Sardain[7], O. Sasaki[85], K. Sato[160], C. Sauer[64b], E. Sauvan[4], P. Savard[158,ad], R. Sawada[157], C. Sawyer[137], L. Sawyer[99], C. Sbarra[24b], A. Sbrizzi[24a,24b], T. Scanlon[98], J. Schaarschmidt[142], U. Schäfer[102], A. C. Schaffer[45,67], D. Schaile[111], R. D. Schamberger[149], C. Scharf[19], M. M. Schefer[20], V. A. Schegelsky[38], D. Scheirich[136], M. Schernau[162], C. Scheulen[56], C. Schiavi[58a,58b], M. Schioppa[44a,44b], B. Schlag[147], S. Schlenker[37], J. Schmeing[174], M. A. Schmidt[174], K. Schmieden[102], C. Schmitt[102], N. Schmitt[102], S. Schmitt[49], L. Schoeffel[138], A. Schoening[64b], P. G. Scholer[35], E. Schopf[129], M. Schott[25], J. Schovancova[37], S. Schramm[57], T. Schroer[57], H.-C. Schultz-Coulon[64a], M. Schumacher[55], B. A. Schumm[139], Ph. Schune[138], A. J. Schuy[142], H. R. Schwartz[139], A. Schwartzman[147], T. A. Schwarz[108], Ph. Schwemling[138], R. Schwienhorst[109], F. G. Sciacca[20], A. Sciandra[30], G. Sciolla[27], F. Scuri[75a], C. D. Sebastiani[94], K. Sedlaczek[118], S. C. Seidel[115], A. Seiden[139], B. D. Seidlitz[42], C. Seitz[49], J. M. Seixas[84b], G. Sekhniaidze[73a], L. Selem[61], N. Semprini-Cesari[24a,24b], D. Sengupta[57], V. Senthilkumar[166], L. Serin[67], M. Sessa[77a,77b], H. Severini[123], F. Sforza[58a,58b], A. Sfyrla[57], Q. Sha[14], E. Shabalina[56], A. H. Shah[33], R. Shaheen[148], J. D. Shahinian[131], D. Shaked Renous[172], L. Y. Shan[14], M. Shapiro[18a], A. Sharma[37], A. S. Sharma[167], P. Sharma[81], P. B. Shatalov[38], K. Shaw[150], S. M. Shaw[103], Q. Shen[63c], D. J. Sheppard[146], P. Sherwood[98], L. Shi[98], X. Shi[14], S. Shimizu[85], C. O. Shimmin[175], J. D. Shinner[97], I. P. J. Shipsey[129,*], S. Shirabe[90], M. Shiyakova[39,v], M. J. Shochet[40], D. R. Shope[128], B. Shrestha[123], S. Shrestha[122,ag], I. Shreyber[38], M. J. Shroff[168], P. Sicho[134], A. M. Sickles[165], E. Sideras Haddad[34g], A. C. Sidley[117], A. Sidoti[24b], F. Siegert[51], Dj. Sijacki[16], F. Sili[92], J. M. Silva[53], I. Silva Ferreira[84b], M. V. Silva Oliveira[30], S. B. Silverstein[48a], S. Simion[67], R. Simoniello[37], E. L. Simpson[103], H. Simpson[150], L. R. Simpson[108], S. Simsek[83], S. Sindhu[56], P. Sinervo[158], S. Singh[30], S. Sinha[49], S. Sinha[103], M. Sioli[24a,24b], I. Siral[37], E. Sitnikova[49], J. Sjölin[48a,48b], A. Skaf[56], E. Skorda[21], P. Skubic[123], M. Slawinska[88], V. Smakhtin[172], B. H. Smart[137], S.Yu. Smirnov[38], Y. Smirnov[38], L. N. Smirnova[38,a], O. Smirnova[100], A. C. Smith[42], D. R. Smith[162], E. A. Smith[40], J. L. Smith[103], R. Smith[147], M. Smizanska[93], K. Smolek[135], A. A. Snesarev[38], H. L. Snoek[117], S. Snyder[30], R. Sobie[168,x], A. Soffer[155], C. A. Solans Sanchez[37], E.Yu. Soldatov[38], U. Soldevila[166], A. A. Solodkov[38], S. Solomon[27], A. Soloshenko[39], K. Solovieva[55], O. V. Solovyanov[41], P. Sommer[51], A. Sonay[13], W. Y. Song[159b], A. Sopczak[135], A. L. Sopio[53], F. Sopkova[29b], J. D. Sorenson[115], I. R. Sotarriva Alvarez[141], V. Sothilingam[64a], O. J. Soto Sandoval[140b,140c], S. Sottocornola[69], R. Soualah[163], Z. Soumaimi[36e], D. South[49], N. Soybelman[172], S. Spagnolo[71a,71b], M. Spalla[112], D. Sperlich[55], G. Spigo[37], B. Spisso[73a,73b], D. P. Spiteri[60], M. Spousta[136], E. J. Staats[35], R. Stamen[64a], A. Stampekis[21], E. Stanecka[88], W. Stanek-Maslouska[49], M. V. Stange[51], B. Stanislaus[18a], M. M. Stanitzki[49], B. Stapf[49], E. A. Starchenko[38], G. H. Stark[139], J. Stark[91], P. Staroba[134], P. Starovoitov[64a], S. Stärz[106], R. Staszewski[88], G. Stavropoulos[47], A. Stefl[37], P. Steinberg[30], B. Stelzer[146,159a], H. J. Stelzer[132], O. Stelzer-Chilton[159a], H. Stenzel[59], T. J. Stevenson[150], G. A. Stewart[37], J. R. Stewart[124], M. C. Stockton[37], G. Stoicea[28b], M. Stolarski[133a], S. Stonjek[112], A. Straessner[51], J. Strandberg[148], S. Strandberg[48a,48b], M. Stratmann[174], M. Strauss[123], T. Strebler[104], P. Strizenec[29b], R. Ströhmer[169], D. M. Strom[126], R. Stroynowski[45], A. Strubig[48a,48b], S. A. Stucci[30], B. Stugu[17], J. Stupak[123], N. A. Styles[49], D. Su[147], S. Su[63a], W. Su[63d], X. Su[63a], D. Suchy[29a], K. Sugizaki[157], V. V. Sulin[38], M. J. Sullivan[94], D. M. S. Sultan[129], L. Sultanaliyeva[38], S. Sultansoy[3b], T. Sumida[89], S. Sun[173], O. Sunneborn Gudnadottir[164], N. Sur[104], M. R. Sutton[150], H. Suzuki[160], M. Svatos[134], M. Swiatlowski[159a], T. Swirski[169], I. Sykora[29a], M. Sykora[136], T. Sykora[136], D. Ta[102], K. Tackmann[49,u], A. Taffard[162], R. Tafirout[159a], J. S. Tafoya Vargas[67], Y. Takubo[85], M. Talby[104], A. A. Talyshev[38], K. C. Tam[65b], N. M. Tamir[155], A. Tanaka[157], J. Tanaka[157], R. Tanaka[67], M. Tanasini[149], Z. Tao[167], S. Tapia Araya[140f], S. Tapprogge[102], A. Tarek Abouelfadl Mohamed[109], S. Tarem[154], K. Tariq[14], G. Tarna[28b], G. F. Tartarelli[72a], M. J. Tartarin[91], P. Tas[136], M. Tasevsky[134], E. Tassi[44a,44b], A. C. Tate[165], G. Tateno[157], Y. Tayalati[36e,w], G. N. Taylor[107], W. Taylor[159b], R. Teixeira De Lima[147], P. Teixeira-Dias[97], J. J. Teoh[158], K. Terashi[157], J. Terron[101], S. Terzo[13], M. Testa[54], R. J. Teuscher[158,x], A. Thaler[80], O. Theiner[57], T. Theveneaux-Pelzer[104], O. Thielmann[174], D. W. Thomas[97], J. P. Thomas[21], E. A. Thompson[18a], P. D. Thompson[21], E. Thomson[131], R. E. Thornberry[45], C. Tian[63a], Y. Tian[57], V. Tikhomirov[38,a], Yu.A. Tikhonov[38], S. Timoshenko[38], D. Timoshyn[136], E. X. L. Ting[1], P. Tipton[175], A. Tishelman-Charny[30], S. H. Tlou[34g], K. Todome[141], S. Todorova-Nova[136], S. Todt[51], L. Toffolin[70a,70c], M. Togawa[85], J. Tojo[90], S. Tokár[29a], K. Tokushuku[85], O. Toldaiev[69], M. Tomoto[85,113], L. Tompkins[147,l], K. W. Topolnicki[87b], E. Torrence[126], H. Torres[91], E. Torró Pastor[166], M. Toscani[31],

C. Tosciri[40], M. Tost[11], D. R. Tovey[143], I. S. Trandafir[28b], T. Trefzger[169], A. Tricoli[30], I. M. Trigger[159a], S. Trincaz-Duvoid[130], D. A. Trischuk[27], B. Trocmé[61], A. Tropina[39], L. Truong[34c], M. Trzebinski[88], A. Trzupek[88], F. Tsai[149], M. Tsai[108], A. Tsiamis[156], P. V. Tsiareshka[38], S. Tsigaridas[159a], A. Tsirigotis[156,r], V. Tsiskaridze[158], E. G. Tskhadadze[153a], M. Tsopoulou[156], Y. Tsujikawa[89], I. I. Tsukerman[38], V. Tsulaia[18a], S. Tsuno[85], K. Tsuri[121], D. Tsybychev[149], Y. Tu[65b], A. Tudorache[28b], V. Tudorache[28b], A. N. Tuna[62], S. Turchikhin[58a,58b], I. Turk Cakir[3a], R. Turra[72a], T. Turtuvshin[39], P. M. Tuts[42], S. Tzamarias[156,d], E. Tzovara[102], F. Ukegawa[160], P. A. Ulloa Poblete[140b,140c], E. N. Umaka[30], G. Unal[37], A. Undrus[30], G. Unel[162], J. Urban[29b], P. Urrejola[140a], G. Usai[8], R. Ushioda[141], M. Usman[110], F. Ustuner[53], Z. Uysal[83], V. Vacek[135], B. Vachon[106], T. Vafeiadis[37], A. Vaitkus[98], C. Valderanis[111], E. Valdes Santurio[48a,48b], M. Valente[159a], S. Valentinetti[24a,24b], A. Valero[166], E. Valiente Moreno[166], A. Vallier[91], J. A. Valls Ferrer[166], D. R. Van Arneman[117], T. R. Van Daalen[142], A. Van Der Graaf[50], P. Van Gemmeren[6], M. Van Rijnbach[37], S. Van Stroud[98], I. Van Vulpen[117], P. Vana[136], M. Vanadia[77a,77b], U. M. Vande Voorde[148], W. Vandelli[37], E. R. Vandewall[124], D. Vannicola[155], L. Vannoli[54], R. Vari[76a], E. W. Varnes[7], C. Varni[18b], T. Varol[152], D. Varouchas[67], L. Varriale[166], K. E. Varvell[151], M. E. Vasile[28b], L. Vaslin[85], G. A. Vasquez[168], A. Vasyukov[39], L. M. Vaughan[124], R. Vavricka[102], T. Vazquez Schroeder[37], J. Veatch[32], V. Vecchio[103], M. J. Veen[105], I. Veliscek[30], L. M. Veloce[158], F. Veloso[133a,133c], S. Veneziano[76a], A. Ventura[71a,71b], S. Ventura Gonzalez[138], A. Verbytskyi[112], M. Verducci[75a,75b], C. Vergis[96], M. Verissimo De Araujo[84b], W. Verkerke[117], J. C. Vermeulen[117], C. Vernieri[147], M. Vessella[105], M. C. Vetterli[146,ad], A. Vgenopoulos[102], N. Viaux Maira[140f], T. Vickey[143], O. E. Vickey Boeriu[143], G. H. A. Viehhauser[129], L. Vigani[64b], M. Vigl[112], M. Villa[24a,24b], M. Villaplana Perez[166], E. M. Villhauer[53], E. Vilucchi[54], M. G. Vincter[35], A. Visibile[117], C. Vittori[37], I. Vivarelli[24a,24b], E. Voevodina[112], F. Vogel[111], J. C. Voigt[51], P. Vokac[135], Yu. Volkotrub[87b], E. Von Toerne[25], B. Vormwald[37], V. Vorobel[136], K. Vorobev[38], M. Vos[166], K. Voss[145], M. Vozak[117], L. Vozdecky[123], N. Vranjes[16], M. Vranjes Milosavljevic[16], M. Vreeswijk[117], N. K. Vu[63c,63d], R. Vuillermet[37], O. Vujinovic[102], I. Vukotic[40], I. K. Vyas[35], S. Wada[160], C. Wagner[147], J. M. Wagner[18a], W. Wagner[174], S. Wahdan[174], H. Wahlberg[92], C. H. Waits[123], J. Walder[137], R. Walker[111], W. Walkowiak[145], A. Wall[131], E. J. Wallin[100], T. Wamorkar[6], A. Z. Wang[139], C. Wang[102], C. Wang[11], H. Wang[18a], J. Wang[65c], P. Wang[98], R. Wang[62], R. Wang[6], S. M. Wang[152], S. Wang[63b], S. Wang[14], T. Wang[63a], W. T. Wang[81], W. Wang[14], X. Wang[114a], X. Wang[165], X. Wang[63c], Y. Wang[63d], Y. Wang[114a], Y. Wang[63a], Z. Wang[108], Z. Wang[52,63c,63d], Z. Wang[108], A. Warburton[106], R. J. Ward[21], N. Warrack[60], S. Waterhouse[97], A. T. Watson[21], H. Watson[53], M. F. Watson[21], E. Watton[60,137], G. Watts[142], B. M. Waugh[98], J. M. Webb[55], C. Weber[30], H. A. Weber[19], M. S. Weber[20], S. M. Weber[64a], C. Wei[63a], Y. Wei[55], A. R. Weidberg[129], E. J. Weik[120], J. Weingarten[50], C. Weiser[55], C. J. Wells[49], T. Wenaus[30], B. Wendland[50], T. Wengler[37], N. S. Wenke[112], N. Wermes[25], M. Wessels[64a], A. M. Wharton[93], A. S. White[62], A. White[8], M. J. White[1], D. Whiteson[162], L. Wickremasinghe[127], W. Wiedenmann[173], M. Wielers[137], C. Wiglesworth[43], D. J. Wilbern[123], H. G. Wilkens[37], J. J. H. Wilkinson[33], D. M. Williams[42], H. H. Williams[131], S. Williams[33], S. Willocq[105], B. J. Wilson[103], P. J. Windischhofer[40], F. I. Winkel[31], F. Winklmeier[126], B. T. Winter[55], J. K. Winter[103], M. Wittgen[147], M. Wobisch[99], T. Wojtkowski[61], Z. Wolffs[117], J. Wollrath[162], M. W. Wolter[88], H. Wolters[133a,133c], M. C. Wong[139], E. L. Woodward[42], S. D. Worm[49], B. K. Wosiek[88], K. W. Woźniak[88], S. Wozniewski[56], K. Wraight[60], C. Wu[21], M. Wu[114b], M. Wu[116], S. L. Wu[173], X. Wu[57], Y. Wu[63a], Z. Wu[4], J. Wuerzinger[112,ab], T. R. Wyatt[103], B. M. Wynne[53], S. Xella[43], L. Xia[114a], M. Xia[15], M. Xie[63a], S. Xin[14,114c], A. Xiong[126], J. Xiong[18a], D. Xu[14], H. Xu[63a], L. Xu[63a], R. Xu[131], T. Xu[108], Y. Xu[15], Z. Xu[53], Z. Xu[114a], B. Yabsley[151], S. Yacoob[34a], Y. Yamaguchi[85], E. Yamashita[157], H. Yamauchi[160], T. Yamazaki[18a], Y. Yamazaki[86], S. Yan[60], Z. Yan[105], H. J. Yang[63c,63d], H. T. Yang[63a], S. Yang[63a], T. Yang[65c], X. Yang[37], X. Yang[14], Y. Yang[45], Y. Yang[63a], Z. Yang[63a], W.-M. Yao[18a], H. Ye[114a], H. Ye[56], J. Ye[14], S. Ye[30], X. Ye[63a], Y. Yeh[98], I. Yeletskikh[39], B. Yeo[18b], M. R. Yexley[98], T. P. Yildirim[129], P. Yin[42], K. Yorita[171], S. Younas[28b], C. J. S. Young[37], C. Young[147], C. Yu[14,114c], Y. Yu[63a], J. Yuan[14,114c], M. Yuan[108], R. Yuan[63c,63d], L. Yue[98], M. Zaazoua[63a], B. Zabinski[88], E. Zaid[53], Z. K. Zak[88], T. Zakareishvili[166], S. Zambito[57], J. A. Zamora Saa[140b,140d], J. Zang[157], D. Zanzi[55], O. Zaplatilek[135], C. Zeitnitz[174], H. Zeng[14], J. C. Zeng[165], D. T. Zenger Jr[27], O. Zenin[38], T. Ženiš[29a], S. Zenz[96], S. Zerradi[36a], D. Zerwas[67], M. Zhai[14,114c], D. F. Zhang[143], J. Zhang[63b], J. Zhang[6], K. Zhang[14,114c], L. Zhang[63a], L. Zhang[114a], P. Zhang[14,114c], R. Zhang[173], S. Zhang[108], S. Zhang[91], T. Zhang[157], X. Zhang[63c], X. Zhang[63b], Y. Zhang[142], Y. Zhang[98], Y. Zhang[114a], Z. Zhang[18a], Z. Zhang[63b], Z. Zhang[67], H. Zhao[142], T. Zhao[63b], Y. Zhao[139], Z. Zhao[63a], Z. Zhao[63a], A. Zhemchugov[39], J. Zheng[114a],

K. Zheng[165], X. Zheng[63a], Z. Zheng[147], D. Zhong[165], B. Zhou[108], H. Zhou[7], N. Zhou[63c], Y. Zhou[15], Y. Zhou[114a], Y. Zhou[7], C. G. Zhu[63b], J. Zhu[108], X. Zhu[63d], Y. Zhu[63c], Y. Zhu[63a], X. Zhuang[14], K. Zhukov[69], N. I. Zimine[39], J. Zinsser[64b], M. Ziolkowski[145], L. Živković[16], A. Zoccoli[24a,24b], K. Zoch[62], T. G. Zorbas[143], O. Zormpa[47], W. Zou[42], L. Zwalinski[37]

[1] Department of Physics, University of Adelaide, Adelaide, Australia
[2] Department of Physics, University of Alberta, Edmonton, AB, Canada
[3] [(a)]Department of Physics, Ankara University, Ankara, Türkiye; [(b)]Division of Physics, TOBB University of Economics and Technology, Ankara, Türkiye
[4] LAPP, CNRS/IN2P3, Université Savoie Mont Blanc, Annecy, France
[5] APC, CNRS/IN2P3, Université Paris Cité, Paris, France
[6] High Energy Physics Division, Argonne National Laboratory, Argonne, IL, USA
[7] Department of Physics, University of Arizona, Tucson, AZ, USA
[8] Department of Physics, University of Texas at Arlington, Arlington, TX, USA
[9] Physics Department, National and Kapodistrian University of Athens, Athens, Greece
[10] Physics Department, National Technical University of Athens, Zografou, Greece
[11] Department of Physics, University of Texas at Austin, Austin, TX, USA
[12] Institute of Physics, Azerbaijan Academy of Sciences, Baku, Azerbaijan
[13] Institut de Física d'Altes Energies (IFAE), Barcelona Institute of Science and Technology, Barcelona, Spain
[14] Institute of High Energy Physics, Chinese Academy of Sciences, Beijing, China
[15] Physics Department, Tsinghua University, Beijing, China
[16] Institute of Physics, University of Belgrade, Belgrade, Serbia
[17] Department for Physics and Technology, University of Bergen, Bergen, Norway
[18] [(a)]Physics Division, Lawrence Berkeley National Laboratory, Berkeley, CA, USA; [(b)]University of California, Berkeley, CA, USA
[19] Institut für Physik, Humboldt Universität zu Berlin, Berlin, Germany
[20] Albert Einstein Center for Fundamental Physics and Laboratory for High Energy Physics, University of Bern, Bern, Switzerland
[21] School of Physics and Astronomy, University of Birmingham, Birmingham, UK
[22] [(a)]Department of Physics, Bogazici University, Istanbul, Türkiye; [(b)]Department of Physics Engineering, Gaziantep University, Gaziantep, Türkiye; [(c)]Department of Physics, Istanbul University, Istanbul, Türkiye
[23] [(a)]Facultad de Ciencias y Centro de Investigaciónes, Universidad Antonio Nariño, Bogotá, Colombia; [(b)]Departamento de Física, Universidad Nacional de Colombia, Bogotá, Colombia
[24] [(a)]Dipartimento di Fisica e Astronomia A. Righi, Università di Bologna, Bologna, Italy; [(b)]INFN Sezione di Bologna, Bologna, Italy
[25] Physikalisches Institut, Universität Bonn, Bonn, Germany
[26] Department of Physics, Boston University, Boston, MA, USA
[27] Department of Physics, Brandeis University, Waltham, MA, USA
[28] [(a)]Transilvania University of Brasov, Brasov, Romania; [(b)]Horia Hulubei National Institute of Physics and Nuclear Engineering, Bucharest, Romania; [(c)]Department of Physics, Alexandru Ioan Cuza University of Iasi, Iasi, Romania; [(d)]National Institute for Research and Development of Isotopic and Molecular Technologies, Physics Department, Cluj-Napoca, Romania; [(e)]National University of Science and Technology Politechnica, Bucharest, Romania; [(f)]West University in Timisoara, Timisoara, Romania; [(g)]Faculty of Physics, University of Bucharest, Bucharest, Romania
[29] [(a)]Faculty of Mathematics, Physics and Informatics, Comenius University, Bratislava, Slovakia; [(b)]Department of Subnuclear Physics, Institute of Experimental Physics of the Slovak Academy of Sciences, Kosice, Slovak Republic
[30] Physics Department, Brookhaven National Laboratory, Upton, NY, USA
[31] Universidad de Buenos Aires, Facultad de Ciencias Exactas y Naturales, Departamento de Física, y CONICET, Instituto de Física de Buenos Aires (IFIBA), Buenos Aires, Argentina
[32] California State University, Los Angeles, CA, USA
[33] Cavendish Laboratory, University of Cambridge, Cambridge, UK
[34] [(a)]Department of Physics, University of Cape Town, Cape Town, South Africa; [(b)]iThemba Labs, Western Cape, South Africa; [(c)]Department of Mechanical Engineering Science, University of Johannesburg, Johannesburg,

South Africa; [d]National Institute of Physics, University of the Philippines Diliman (Philippines), Quezon City, Philippines; [e]University of South Africa, Department of Physics, Pretoria, South Africa; [f]University of Zululand, KwaDlangezwa, South Africa; [g]School of Physics, University of the Witwatersrand, Johannesburg, South Africa
[35] Department of Physics, Carleton University, Ottawa, ON, Canada
[36] [a]Faculté des Sciences Ain Chock, Université Hassan II de Casablanca, Casablanca, Morocco; [b]Faculté des Sciences, Université Ibn-Tofail, Kenitra, Morocco; [c]Faculté des Sciences Semlalia, LPHEA-Marrakech, Université Cadi Ayyad, Marrakech, Morocco; [d]LPMR, Faculté des Sciences, Université Mohamed Premier, Oujda, Morocco; [e]Faculté des sciences, Université Mohammed V, Rabat, Morocco; [f]Institute of Applied Physics, Mohammed VI Polytechnic University, Ben Guerir, Morocco
[37] CERN, Geneva, Switzerland
[38] Affiliated with an Institute Covered by a Cooperation Agreement with CERN, Geneva, Switzerland
[39] Affiliated with an International Laboratory Covered by a Cooperation Agreement with CERN, Geneva, Switzerland
[40] Enrico Fermi Institute, University of Chicago, Chicago, IL, USA
[41] LPC, CNRS/IN2P3, Université Clermont Auvergne, Clermont-Ferrand, France
[42] Nevis Laboratory, Columbia University, Irvington, NY, USA
[43] Niels Bohr Institute, University of Copenhagen, Copenhagen, Denmark
[44] [a]Dipartimento di Fisica, Università della Calabria, Rende, Italy; [b]INFN Gruppo Collegato di Cosenza, Laboratori Nazionali di Frascati, Cosenza, Italy
[45] Physics Department, Southern Methodist University, Dallas, TX, USA
[46] Physics Department, University of Texas at Dallas, Richardson, TX, USA
[47] National Centre for Scientific Research "Demokritos", Agia Paraskevi, Greece
[48] [a]Department of Physics, Stockholm University, Stockholm, Sweden; [b]Oskar Klein Centre, Stockholm, Sweden
[49] Deutsches Elektronen-Synchrotron DESY, Hamburg and Zeuthen, Germany
[50] Fakultät Physik , Technische Universität Dortmund, Dortmund, Germany
[51] Institut für Kern- und Teilchenphysik, Technische Universität Dresden, Dresden, Germany
[52] Department of Physics, Duke University, Durham, NC, USA
[53] SUPA-School of Physics and Astronomy, University of Edinburgh, Edinburgh, UK
[54] INFN e Laboratori Nazionali di Frascati, Frascati, Italy
[55] Physikalisches Institut, Albert-Ludwigs-Universität Freiburg, Freiburg, Germany
[56] II. Physikalisches Institut, Georg-August-Universität Göttingen, Göttingen, Germany
[57] Département de Physique Nucléaire et Corpusculaire, Université de Genève, Geneva, Switzerland
[58] [a]Dipartimento di Fisica, Università di Genova, Genoa, Italy; [b]INFN Sezione di Genova, Genoa, Italy
[59] II. Physikalisches Institut, Justus-Liebig-Universität Giessen, Giessen, Germany
[60] SUPA-School of Physics and Astronomy, University of Glasgow, Glasgow, UK
[61] LPSC, Université Grenoble Alpes, CNRS/IN2P3, Grenoble INP, Grenoble, France
[62] Laboratory for Particle Physics and Cosmology, Harvard University, Cambridge, MA, USA
[63] [a]Department of Modern Physics and State Key Laboratory of Particle Detection and Electronics, University of Science and Technology of China, Hefei, China; [b]Institute of Frontier and Interdisciplinary Science and Key Laboratory of Particle Physics and Particle Irradiation (MOE), Shandong University, Qingdao, China; [c]School of Physics and Astronomy, Key Laboratory for Particle Astrophysics and Cosmology (MOE), Shanghai Jiao Tong University, SKLPPC, Shanghai, China; [d]Tsung-Dao Lee Institute, Shanghai, China; [e]School of Physics, Zhengzhou University, Zhengzhou, China
[64] [a]Kirchhoff-Institut für Physik, Ruprecht-Karls-Universität Heidelberg, Heidelberg, Germany; [b]Physikalisches Institut, Ruprecht-Karls-Universität Heidelberg, Heidelberg, Germany
[65] [a]Department of Physics, Chinese University of Hong Kong, Shatin, N.T., Hong Kong, China; [b]Department of Physics, University of Hong Kong, Pok Fu Lam, Hong Kong, China; [c]Department of Physics and Institute for Advanced Study, Hong Kong University of Science and Technology, Clear Water Bay, Kowloon, Hong Kong, China
[66] Department of Physics, National Tsing Hua University, Hsinchu, Taiwan
[67] IJCLab, CNRS/IN2P3, Université Paris-Saclay, 91405 Orsay, France
[68] Centro Nacional de Microelectrónica (IMB-CNM-CSIC), Barcelona, Spain
[69] Department of Physics, Indiana University, Bloomington, IN, USA
[70] [a]INFN Gruppo Collegato di Udine, Sezione di Trieste, Udine, Italy; [b]ICTP, Trieste, Italy; [c]Dipartimento Politecnico di Ingegneria e Architettura, Università di Udine, Udine, Italy

[71] [(a)]INFN Sezione di Lecce, Lecce, Italy; [(b)]Dipartimento di Matematica e Fisica, Università del Salento, Lecce, Italy
[72] [(a)]INFN Sezione di Milano, Milan, Italy; [(b)]Dipartimento di Fisica, Università di Milano, Milan, Italy
[73] [(a)]INFN Sezione di Napoli, Naples, Italy; [(b)]Dipartimento di Fisica, Università di Napoli, Naples, Italy
[74] [(a)]INFN Sezione di Pavia, Pavia, Italy; [(b)]Dipartimento di Fisica, Università di Pavia, Pavia, Italy
[75] [(a)]INFN Sezione di Pisa, Pisa, Italy; [(b)]Dipartimento di Fisica E. Fermi, Università di Pisa, Pisa, Italy
[76] [(a)]INFN Sezione di Roma, Rome, Italy; [(b)]Dipartimento di Fisica, Sapienza Università di Roma, Rome, Italy
[77] [(a)]INFN Sezione di Roma Tor Vergata, Rome, Italy; [(b)]Dipartimento di Fisica, Università di Roma Tor Vergata, Rome, Italy
[78] [(a)]INFN Sezione di Roma Tre, Rome, Italy; [(b)]Dipartimento di Matematica e Fisica, Università Roma Tre, Rome, Italy
[79] [(a)]INFN-TIFPA, Povo, Italy; [(b)]Università degli Studi di Trento, Trento, Italy
[80] Universität Innsbruck, Department of Astro and Particle Physics, Innsbruck, Austria
[81] University of Iowa, Iowa City, IA, USA
[82] Department of Physics and Astronomy, Iowa State University, Ames, IA, USA
[83] Istinye University, Sariyer, Istanbul, Türkiye
[84] [(a)]Departamento de Engenharia Elétrica, Universidade Federal de Juiz de Fora (UFJF), Juiz de Fora, Brazil; [(b)]Universidade Federal do Rio De Janeiro COPPE/EE/IF, Rio de Janeiro, Brazil; [(c)]Instituto de Física, Universidade de São Paulo, São Paulo, Brazil; [(d)]Rio de Janeiro State University, Rio de Janeiro, Brazil; [(e)]Federal University of Bahia, Bahia, Brazil
[85] KEK, High Energy Accelerator Research Organization, Tsukuba, Japan
[86] Graduate School of Science, Kobe University, Kobe, Japan
[87] [(a)]AGH University of Krakow, Faculty of Physics and Applied Computer Science, Kraków, Poland; [(b)]Marian Smoluchowski Institute of Physics, Jagiellonian University, Kraków, Poland
[88] Institute of Nuclear Physics Polish Academy of Sciences, Kraków, Poland
[89] Faculty of Science, Kyoto University, Kyoto, Japan
[90] Research Center for Advanced Particle Physics and Department of Physics, Kyushu University, Fukuoka , Japan
[91] L2IT, CNRS/IN2P3, UPS, Université de Toulouse, Toulouse, France
[92] Instituto de Física La Plata, Universidad Nacional de La Plata and CONICET, La Plata, Argentina
[93] Physics Department, Lancaster University, Lancaster, UK
[94] Oliver Lodge Laboratory, University of Liverpool, Liverpool, UK
[95] Department of Experimental Particle Physics, Jožef Stefan Institute and Department of Physics, University of Ljubljana, Ljubljana, Slovenia
[96] School of Physics and Astronomy, Queen Mary University of London, London, UK
[97] Department of Physics, Royal Holloway University of London, Egham, UK
[98] Department of Physics and Astronomy, University College London, London, UK
[99] Louisiana Tech University, Ruston, LA, USA
[100] Fysiska institutionen, Lunds universitet, Lund, Sweden
[101] Departamento de Física Teorica C-15 and CIAFF, Universidad Autónoma de Madrid, Madrid, Spain
[102] Institut für Physik, Universität Mainz, Mainz, Germany
[103] School of Physics and Astronomy, University of Manchester, Manchester, UK
[104] CPPM, CNRS/IN2P3, Aix-Marseille Université, Marseille, France
[105] Department of Physics, University of Massachusetts, Amherst, MA, USA
[106] Department of Physics, McGill University, Montreal, QC, Canada
[107] School of Physics, University of Melbourne, Victoria, Australia
[108] Department of Physics, University of Michigan, Ann Arbor, MI, USA
[109] Department of Physics and Astronomy, Michigan State University, East Lansing, MI, USA
[110] Group of Particle Physics, University of Montreal, Montreal, QC, Canada
[111] Fakultät für Physik, Ludwig-Maximilians-Universität München, Munich, Germany
[112] Max-Planck-Institut für Physik (Werner-Heisenberg-Institut), Munich, Germany
[113] Graduate School of Science and Kobayashi-Maskawa Institute, Nagoya University, Nagoya, Japan
[114] [(a)]Department of Physics, Nanjing University, Nanjing, China; [(b)]School of Science, Shenzhen Campus of Sun Yat-sen University, Guangzhou, China; [(c)]University of Chinese Academy of Science (UCAS), Beijing, China
[115] Department of Physics and Astronomy, University of New Mexico, Albuquerque, NM, USA
[116] Institute for Mathematics, Astrophysics and Particle Physics, Radboud University/Nikhef, Nijmegen, Netherlands

[117] Nikhef National Institute for Subatomic Physics and University of Amsterdam, Amsterdam, Netherlands
[118] Department of Physics, Northern Illinois University, DeKalb, IL, USA
[119] [(a)]New York University Abu Dhabi, Abu Dhabi, United Arab Emirates; [(b)]United Arab Emirates University, Al Ain, United Arab Emirates
[120] Department of Physics, New York University, New York, NY, USA
[121] Ochanomizu University, Otsuka, Bunkyo-ku, Tokyo, Japan
[122] Ohio State University, Columbus, OH, USA
[123] Homer L. Dodge Department of Physics and Astronomy, University of Oklahoma, Norman, OK, USA
[124] Department of Physics, Oklahoma State University, Stillwater, OK, USA
[125] Joint Laboratory of Optics, Palacký University, Olomouc, Czech Republic
[126] Institute for Fundamental Science, University of Oregon, Eugene, OR, USA
[127] Graduate School of Science, Osaka University, Osaka, Japan
[128] Department of Physics, University of Oslo, Oslo, Norway
[129] Department of Physics, Oxford University, Oxford, UK
[130] LPNHE, CNRS/IN2P3, Sorbonne Université, Université Paris Cité, Paris, France
[131] Department of Physics, University of Pennsylvania, Philadelphia, PA, USA
[132] Department of Physics and Astronomy, University of Pittsburgh, Pittsburgh, PA, USA
[133] [(a)]Laboratório de Instrumentação e Física Experimental de Partículas-LIP, Lisbon, Portugal; [(b)]Departamento de Física, Faculdade de Ciências, Universidade de Lisboa, Lisbon, Portugal; [(c)]Departamento de Física, Universidade de Coimbra, Coimbra, Portugal; [(d)]Centro de Física Nuclear da Universidade de Lisboa, Lisbon, Portugal; [(e)]Departamento de Física, Universidade do Minho, Braga, Portugal; [(f)]Departamento de Física Teórica y del Cosmos, Universidad de Granada, Granada, Spain; [(g)]Departamento de Física, Instituto Superior Técnico, Universidade de Lisboa, Lisbon, Portugal
[134] Institute of Physics of the Czech Academy of Sciences, Prague, Czech Republic
[135] Czech Technical University in Prague, Prague, Czech Republic
[136] Charles University, Faculty of Mathematics and Physics, Prague, Czech Republic
[137] Particle Physics Department, Rutherford Appleton Laboratory, Didcot, UK
[138] IRFU, CEA, Université Paris-Saclay, Gif-sur-Yvette, France
[139] Santa Cruz Institute for Particle Physics, University of California Santa Cruz, Santa Cruz, CA, USA
[140] [(a)]Departamento de Física, Pontificia Universidad Católica de Chile, Santiago, Chile; [(b)]Millennium Institute for Subatomic physics at high energy frontier (SAPHIR), Santiago, Chile; [(c)]Instituto de Investigación Multidisciplinario en Ciencia y Tecnología y Departamento de Física, Universidad de La Serena, La Serena, Chile; [(d)]Department of Physics, Universidad Andres Bello, Santiago, Chile; [(e)]Instituto de Alta Investigación, Universidad de Tarapacá, Arica, Chile; [(f)]Departamento de Física, Universidad Técnica Federico Santa María, Valparaiso, Chile
[141] Department of Physics, Institute of Science, Tokyo, Japan
[142] Department of Physics, University of Washington, Seattle, WA, USA
[143] Department of Physics and Astronomy, University of Sheffield, Sheffield, UK
[144] Department of Physics, Shinshu University, Nagano, Japan
[145] Department Physik, Universität Siegen, Siegen, Germany
[146] Department of Physics, Simon Fraser University, Burnaby, BC, Canada
[147] SLAC National Accelerator Laboratory, Stanford, CA, USA
[148] Department of Physics, Royal Institute of Technology, Stockholm, Sweden
[149] Departments of Physics and Astronomy, Stony Brook University, Stony Brook, NY, USA
[150] Department of Physics and Astronomy, University of Sussex, Brighton, UK
[151] School of Physics, University of Sydney, Sydney, Australia
[152] Institute of Physics, Academia Sinica, Taipei, Taiwan
[153] [(a)]E. Andronikashvili Institute of Physics, Iv. Javakhishvili Tbilisi State University, Tbilisi, Georgia; [(b)]High Energy Physics Institute, Tbilisi State University, Tbilisi, Georgia; [(c)]University of Georgia, Tbilisi, Georgia
[154] Department of Physics, Technion, Israel Institute of Technology, Haifa, Israel
[155] Raymond and Beverly Sackler School of Physics and Astronomy, Tel Aviv University, Tel Aviv, Israel
[156] Department of Physics, Aristotle University of Thessaloniki, Thessaloníki, Greece
[157] International Center for Elementary Particle Physics and Department of Physics, University of Tokyo, Tokyo, Japan
[158] Department of Physics, University of Toronto, Toronto, ON, Canada
[159] [(a)]TRIUMF, Vancouver, BC, Canada; [(b)]Department of Physics and Astronomy, York University, Toronto, ON, Canada

[160] Division of Physics and Tomonaga Center for the History of the Universe, Faculty of Pure and Applied Sciences, University of Tsukuba, Tsukuba, Japan
[161] Department of Physics and Astronomy, Tufts University, Medford, MA, USA
[162] Department of Physics and Astronomy, University of California Irvine, Irvine, CA, USA
[163] University of Sharjah, Sharjah, United Arab Emirates
[164] Department of Physics and Astronomy, University of Uppsala, Uppsala, Sweden
[165] Department of Physics, University of Illinois, Urbana, IL, USA
[166] Instituto de Física Corpuscular (IFIC), Centro Mixto Universidad de Valencia-CSIC, Valencia, Spain
[167] Department of Physics, University of British Columbia, Vancouver, BC, Canada
[168] Department of Physics and Astronomy, University of Victoria, Victoria, BC, Canada
[169] Fakultät für Physik und Astronomie, Julius-Maximilians-Universität Würzburg, Würzburg, Germany
[170] Department of Physics, University of Warwick, Coventry, UK
[171] Waseda University, Tokyo, Japan
[172] Department of Particle Physics and Astrophysics, Weizmann Institute of Science, Rehovot, Israel
[173] Department of Physics, University of Wisconsin, Madison, WI, USA
[174] Fakultät für Mathematik und Naturwissenschaften, Fachgruppe Physik, Bergische Universität Wuppertal, Wuppertal, Germany
[175] Department of Physics, Yale University, New Haven, CT, USA
[176] Yerevan Physics Institute, Yerevan, Armenia

[a] Also Affiliated with an Institute Covered by a Cooperation Agreement with CERN, Geneva, Switzerland
[b] Also at An-Najah National University, Nablus, Palestine
[c] Also at Borough of Manhattan Community College, City University of New York, New York, NY, USA
[d] Also at Center for Interdisciplinary Research and Innovation (CIRI-AUTH), Thessaloníki, Greece
[e] Also at CERN, Geneva, Switzerland
[f] Also at CMD-AC UNEC Research Center, Azerbaijan State University of Economics (UNEC), Baku, Azerbaijan
[g] Also at Département de Physique Nucléaire et Corpusculaire, Université de Genève, Geneva, Switzerland
[h] Also at Departament de Fisica de la Universitat Autonoma de Barcelona, Barcelona, Spain
[i] Also at Department of Financial and Management Engineering, University of the Aegean, Chios, Greece
[j] Also at Department of Physics, California State University, Sacramento, USA
[k] Also at Department of Physics, King's College London, London, UK
[l] Also at Department of Physics, Stanford University, Stanford, CA, USA
[m] Also at Department of Physics, Stellenbosch University, Stellenbosch, South Africa
[n] Also at Department of Physics, University of Fribourg, Fribourg, Switzerland
[o] Also at Department of Physics, University of Thessaly, Thessaly, Greece
[p] Also at Department of Physics, Westmont College, Santa Barbara, USA
[q] Also at Faculty of Physics, Sofia University, 'St. Kliment Ohridski', Sofia, Bulgaria
[r] Also at Hellenic Open University, Patras, Greece
[s] Also at Imam Mohammad Ibn Saud Islamic University, Riyadh, Saudi Arabia
[t] Also at Institucio Catalana de Recerca i Estudis Avancats, ICREA, Barcelona, Spain
[u] Also at Institut für Experimentalphysik, Universität Hamburg, Hamburg, Germany
[v] Also at Institute for Nuclear Research and Nuclear Energy (INRNE) of the Bulgarian Academy of Sciences, Sofia, Bulgaria
[w] Also at Institute of Applied Physics, Mohammed VI Polytechnic University, Ben Guerir, Morocco
[x] Also at Institute of Particle Physics (IPP), Ottawa, Canada
[y] Also at Institute of Physics, Azerbaijan Academy of Sciences, Baku, Azerbaijan
[z] Also at Institute of Theoretical Physics, Ilia State University, Tbilisi, Georgia
[aa] Also at National Institute of Physics, University of the Philippines Diliman (Philippines), Quezon City, Philippines
[ab] Also at Technical University of Munich, Munich, Germany
[ac] Also at The Collaborative Innovation Center of Quantum Matter (CICQM), Beijing, China
[ad] Also at TRIUMF, Vancouver, BC, Canada
[ae] Also at Università di Napoli Parthenope, Naples, Italy
[af] Also at Department of Physics, University of Colorado Boulder, Colorado, USA

[ag] Also at Washington College, Chestertown, MD, USA
[ah] Also at Physics Department, Yeditepe University, Istanbul, Türkiye
* Deceased

Published for SISSA by Springer

Received: *August 21, 2025*
Accepted: *September 15, 2025*
Published: *October 10, 2025*

Search for the production of a Higgs boson in association with a single top quark in pp collisions at $\sqrt{s} = 13$ TeV with the ATLAS detector

The ATLAS collaboration

E-mail: atlas.publications@cern.ch

Abstract: A search for the production of a Higgs boson in association with a single top quark, tH, is presented. The analysis uses proton-proton collision data corresponding to an integrated luminosity of 140 fb^{-1} at a centre-of-mass energy of 13 TeV, collected by the ATLAS detector at the LHC. The search targets Higgs-boson decays into $b\bar{b}$, WW^*, ZZ^*, and $\tau\tau$, accompanied by an isolated lepton (electron or muon) from the top-quark decay. Multivariate techniques are employed to enhance the separation between signal and background processes. The observed signal strength, μ_{tH}, defined as the ratio between the measured cross-section and the predicted Standard Model value, is $\mu_{tH} = 8.1 \pm 2.6\,(\text{stat.}) \pm 2.0\,(\text{syst.})$. The significance of the observed (expected) signal above the background-only expectation is 2.8 (0.4) standard deviations. The corresponding observed (expected) upper limit at the 95% confidence level on the tH cross-section is found to be 13.9 (6.1) times the value predicted by the Standard Model. An interpretation with an inverted sign of the top-quark Yukawa coupling is performed, and the signal strength and corresponding limit are reported.

Keywords: Hadron-Hadron Scattering

ArXiv ePrint: 2508.14695

Open Access, Copyright CERN,
for the benefit of the ATLAS Collaboration.
Article funded by SCOAP^3.

https://doi.org/10.1007/JHEP10(2025)093

JHEP10(2025)093

Contents

1 Introduction **1**

2 Analysis strategy **4**

3 ATLAS detector **5**

4 Data and simulated event samples **6**
4.1 Data event samples 6
4.2 Simulated event samples 6

5 Object definitions **11**

6 Event selection and classification **14**
6.1 $H \to b\bar{b}$ channel 15
6.2 2ℓ SS channel 18
6.3 3ℓ channel 19

7 Background estimation **19**
7.1 Background estimation in the $H \to b\bar{b}$ channel 20
7.2 Background estimation in the 2ℓ SS and 3ℓ channels 21

8 Sources of systematic uncertainty **22**
8.1 Common systematic uncertainties 22
8.2 Channel-specific uncertainties: $H \to b\bar{b}$ channel 25
8.3 Channel-specific uncertainties: 2ℓ SS and 3ℓ channels 25

9 Results **25**

10 Conclusion **33**

A List of input variables used to train the different BDTGs **35**

B Pre-fit and post-fit yields tables **40**

The ATLAS collaboration **51**

1 Introduction

The discovery of a particle with properties consistent with the Higgs boson [1, 2] of the Standard Model (SM) in 2012 by the ATLAS and CMS experiments [3, 4] opened a new field of exploration in the realm of particle physics. Studying the Higgs-boson couplings is essential to test whether the observed particle corresponds to the Higgs boson predicted

JHEP10(2025)093

by the SM. In the SM, the strength of these interactions with other elementary particles is proportional to their masses (or masses squared).

Specifically, the Higgs boson interacts with fermions via Yukawa couplings [5]. Among these, the Yukawa coupling to the top quark, y_t, is of special interest as it is the largest with a value close to unity. Given its large value, y_t plays a crucial role in radiative corrections to the Higgs potential [6, 7], influencing the shape of the potential and, consequently, the stability of the electroweak (EW) vacuum [8]. In addition, it significantly affects the running of SM parameters, impacting the scale at which new physics might appear [7]. For all these reasons the Yukawa coupling of the Higgs boson to the top quark is considered a good probe for new physics. In particular, the study of its charge-conjugation and parity (CP) properties could provide insight into the observed baryon asymmetry of the universe [9–11].

The magnitude of y_t can be determined indirectly from Higgs-boson production via a top-quark loop or directly through cross-section measurements of top-quark pair production in association with a Higgs boson ($t\bar{t}H$). The $t\bar{t}H$ production process was observed [12, 13] in 2018. The production cross-section of the Higgs boson in association with a single top quark is sensitive to both the magnitude of y_t and its sign [14–18]. While the sign of y_t is not defined in an absolute sense, it is instead defined relative to the coupling strength of the W boson to the Higgs boson. In the following, this relative-sign convention is adopted throughout, and the sign of y_t is referred to accordingly, without explicitly restating its dependence on the W-boson coupling. Measurements of Higgs-boson processes conducted by the ATLAS and CMS Collaborations, such as the Higgs-boson decay into photon pairs ($H \to \gamma\gamma$) [19, 20], provide insight into the sign of the y_t coupling. Similar information comes from the combination of other Higgs-boson measurements. These include the simplified template cross-section (STXS) combination for gluon-gluon fusion (ggF), vector-boson fusion (VBF), and associated production with vector bosons (VH, where V refers to the W and Z bosons) or $t\bar{t}H$ in different decay channels [21, 22]. These measurements probe indirect effects in loop interactions and currently disfavour a negative value of the coupling [23], under the assumption that only SM particles contribute to the loops.

Higgs-boson production in association with a single top quark occurs via the EW interaction through three distinct production modes: t-channel (tHq), tWH and s-channel [24, 25]. The main production mode in proton-proton (pp) collisions at the Large Hadron Collider (LHC) [26] is the tHq process, followed by the associated tWH process and the s-channel. In this paper, the tHq and tWH processes are collectively referred to as tH production and are the ones used for the measurements presented, while s-channel production is neglected due to its extremely low production cross-section (3% of the total tH cross-section).

In the tHq process, an incoming light-flavour quark (i.e. up-type quark or down-type antiquark) from one of the colliding protons interacts with a b-quark by exchanging a space-like virtual W boson. The origin of the b-quark depends on the flavour scheme (FS) used in the calculation: in the five-flavour scheme (5FS), it is treated as a massless parton originating from the proton sea, while in the four-flavour scheme (4FS), where b-quarks are not included in the proton parton distribution functions (PDFs), it arises from gluon splitting into a $b\bar{b}$ pair [27–29]. In the tWH process, a gluon from one of the protons interacts with a b-quark from the other proton or from gluon splitting, via the exchange of a time-like virtual top

JHEP10(2025)093

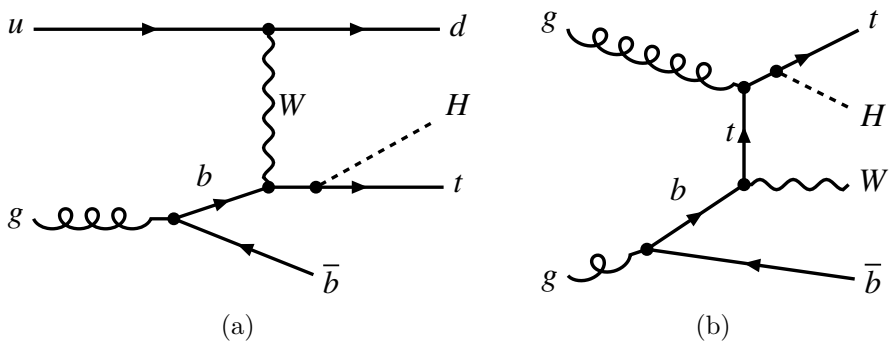

Figure 1. Representative dominant Feynman diagrams for (a) tHq and (b) tWH production at LO, in the 4FS. The tHq event topology (a) is characterised by two heavy objects, the top quark and the Higgs boson plus an energetic light-flavour quark (dominantly a u-quark), referred to as the spectator quark, and an extra soft b-quark from gluon splitting. The tWH event topology (b) is characterised by three heavy objects, the top quark, the Higgs boson and a W boson and an extra soft b-quark from gluon splitting.

quark t. Two examples of dominant leading-order (LO) Feynman diagrams for the tHq and tWH processes, both in the 4FS, are shown in figure 1.

Under the SM hypothesis ($\kappa_t = y_t/y_t^{\mathrm{SM}} = +1$), the interference between diagrams in which the Higgs boson couples to the top quark and those where it couples to the W boson is destructive, leading to a strongly suppressed cross-section. In contrast, in scenarios beyond the SM, such as those involving CP-even and CP-odd admixtures in the top-quark Yukawa coupling structure, the relative sign between the Higgs-boson couplings to the top quark and the W boson can be altered, enhancing the tH cross-section up to an order of magnitude [24, 25]. The maximum enhancement occurs when $\kappa_t = -1$, corresponding to fully constructive interference between the contributing diagrams.

The tHq event topology is characterised by two heavy objects, a top quark and a Higgs boson, which is radiated from the latter, plus an energetic light-flavour quark (dominantly a u- or $\bar{d}$-quark), known as the spectator quark, and an extra soft b-quark from gluon splitting. The top-quark and Higgs-boson systems are produced in the central part of the detector recoiling against each other. The production of tWH is characterised by three heavy objects, the top quark, a W boson, a Higgs boson that is radiated from one of these two particles and an extra soft b-quark from gluon splitting. This event topology closely resembles $t\bar{t}H$ production and has an identical final state.

The CMS Collaboration searched for $tHq + tWH$ production in pp collisions at a centre-of-mass energy of $\sqrt{s} = 13\,\mathrm{TeV}$ with an integrated luminosity of $35.9\,\mathrm{fb}^{-1}$ [30]. The observed cross-section limits are 1.94 pb for the SM and 0.74 pb for the inverted top-quark Yukawa coupling (ITC) (i.e. $\mathrm{sign}(y_t) = \kappa_t = -1$) hypothesis. More recently, using the full Run-2 dataset, the CMS Collaboration reported updated $t\bar{t}H$ and $tHq + tWH$ results in the multi-lepton and $b\bar{b}$ final states in ref. [31] and ref. [32], respectively. In the multi-lepton final state, the measured signal strength is $\mu_{tHq+tWH} = 5.7 \pm 2.7\,(\mathrm{stat.}) \pm 3.0\,(\mathrm{syst.})$. In the $b\bar{b}$ final state, the observed upper limit relative to the SM prediction is 14.6 at 95% confidence level.

JHEP10(2025)093

The analysis presented in this paper uses an integrated luminosity of 140 $\text{fb}^{-1}$of data collected with the ATLAS detector at $\sqrt{s} = 13\,\text{TeV}$ between 2015 and 2018 at the LHC. The search targets signatures that are primarily sensitive to $H \to b\bar{b}$, $H \to WW^*$, $H \to ZZ^*$ and $H \to \tau\tau$ decays. Backgrounds are estimated with a combination of simulation and data-driven techniques, and a global fit in all final states is used to extract the best estimate for the tH production rate under both the SM and ITC hypotheses.

2 Analysis strategy

The search described in this paper considers three mutually orthogonal final states, hereafter referred to as channels, distinguished by the number of light-flavour leptons (ℓ), i.e. electron (e) or muon (μ):

- one lepton ($H \to b\bar{b}$);
- two same-charge leptons ($2\ell\,\text{SS}$);
- three leptons (3ℓ).

Events with τ-leptons decaying into an electron or a muon are part of selection, while events containing hadronically decaying τ-leptons (τ_{had}) are vetoed in all three channels.

Each channel targets different Higgs-boson decay modes. The $H \to b\bar{b}$ channel is most sensitive to the $H \to b\bar{b}$ decay, while the $2\ell\,\text{SS}$ and 3ℓ channels mostly probe $H \to W\,W^*$. In the $2\ell\,\text{SS}$ and 3ℓ channels, subleading contributions arise from $H \to \tau\tau$ and from $H \to ZZ^*$ decays.

These three channels are characterised by different background compositions, therefore they are analysed and fitted separately and combined afterwards.Each channel defines multiple analysis regions: signal regions (SRs), which are enriched in signal events, and control regions (CRs), which are designed to constrain the dominant background contributions. In the $H \to b\bar{b}$ channel, two regions are defined: one SR targeting the signal, and a CR dedicated to top-quark pair ($t\bar{t}$) production in association with b-jets, denoted CR($t\bar{t}+ \geq 1b$). In both the $2\ell\,\text{SS}$ and 3ℓ channels, five regions are defined: one SR, three CRs to constrain backgrounds from non-prompt and fake leptons, and one CR targeting the associated production of a W boson with a top-quark pair ($t\bar{t}\,W$).

To enhance signal-to-background separation, all channels employ multivariate analysis techniques, specifically Boosted Decision Trees (BDTs). These methods are used both to discriminate signal from background and to separate different background components to better constrain them, as well as to define the analysis regions. Details are provided in section 6.

A profile likelihood fit, implemented using the TRExFitter framework [33], is used to simultaneously extract the signal strength, μ_{tH}, and the normalisations of the dominant backgrounds in each channel. The signal strength is first fitted separately in each channel, and then in a combined fit.

The manuscript is structured as follows: section 3 describes the ATLAS detector, while details of the data and MC simulated event samples used in the analysis are provided in

JHEP10(2025)093

section 4. Section 5 outlines the object definitions. The event selection, multivariate analysis techniques, and analysis region definitions for each channel are presented in section 6, while section 7 describes the background estimates and its results. All uncertainties considered in this measurement are discussed in section 8. The resulting constraints on the signal process in both the SM and ITC scenarios are shown in section 9, for each channel and their combination. Finally, the conclusions are presented in section 10.

3 ATLAS detector

The ATLAS detector [34] at the LHC covers nearly the entire solid angle around the collision point.[1] It consists of an inner tracking detector surrounded by a thin superconducting solenoid, electromagnetic and hadronic calorimeters, and a muon spectrometer incorporating three large superconducting air-core toroidal magnets.

The inner-detector system (ID) is immersed in a 2 T axial magnetic field and provides charged-particle tracking in the range of $|\eta| < 2.5$. The high-granularity silicon pixel detector covers the vertex region and typically provides four measurements per track, the first hit generally being in the insertable B-layer (IBL) installed before the LHC Run 2 [35, 36]. It is followed by the SemiConductor Tracker (SCT), which usually provides eight measurements per track. These silicon detectors are complemented by the Transition Radiation Tracker (TRT), which enables radially extended track reconstruction up to $|\eta| = 2.0$. The TRT also provides electron identification information based on the fraction of hits (typically 30 in total) above a higher energy-deposit threshold corresponding to transition radiation.

The calorimeter system covers the pseudorapidity range $|\eta| < 4.9$. Within the region $|\eta| < 3.2$, electromagnetic calorimetry is provided by barrel and endcap high-granularity lead/liquid-argon (LAr) calorimeters, with an additional thin LAr presampler covering $|\eta| < 1.8$ to correct for energy loss in material upstream of the calorimeters. Hadronic calorimetry is provided by the steel/scintillator-tile calorimeter, segmented into three barrel structures within $|\eta| < 1.7$, and two copper/LAr hadronic endcap calorimeters. The solid angle coverage is completed with forward copper/LAr and tungsten/LAr calorimeter modules optimised for electromagnetic and hadronic energy measurements, respectively.

The muon spectrometer (MS) comprises separate trigger and high-precision tracking chambers measuring the deflection of muons in a magnetic field generated by the superconducting air-core toroidal magnets. The field integral of the toroids ranges between 2.0 and 6.0 T m across most of the detector. Three layers of precision chambers, each consisting of layers of monitored drift tubes, cover the region $|\eta| < 2.7$, complemented by cathode-strip chambers in the forward region, where the background is highest. The muon trigger system covers the range $|\eta| < 2.4$ with resistive-plate chambers in the barrel, and thin-gap chambers in the endcap regions.

[1] ATLAS uses a right-handed coordinate system with its origin at the nominal interaction point (IP) in the centre of the detector and the z-axis along the beam pipe. The x-axis points from the IP to the centre of the LHC ring, and the y-axis points upwards. Cylindrical coordinates (r, ϕ) are used in the transverse plane, ϕ being the azimuthal angle around the z-axis. The pseudorapidity is defined in terms of the polar angle θ as $\eta = -\ln\tan(\theta/2)$. Angular distance is measured in units of $\Delta R \equiv \sqrt{(\Delta\eta)^2 + (\Delta\phi)^2}$.

JHEP10(2025)093

The luminosity is measured mainly by the LUCID-2 [37] detector that records Cherenkov light produced in the quartz windows of photomultipliers located close to the beampipe.

Events were selected by the first-level trigger system implemented in custom hardware, followed by selections made by algorithms implemented in software in the high-level trigger [38]. The first-level trigger accepted events from the 40 MHz bunch crossings at a rate close to 100 kHz, which the high-level trigger further reduced in order to record complete events to disk at about 1.25 kHz.

A software suite [39] is used in data simulation, in the reconstruction and analysis of real and simulated data, in detector operations, and in the trigger and data acquisition systems of the experiment.

4 Data and simulated event samples

4.1 Data event samples

This analysis uses data from pp collisions at $\sqrt{s} = 13$ TeV collected with the ATLAS detector at the LHC during 2015–2018. Stringent detector and data-quality requirements were applied [40], resulting in a data sample corresponding to a total integrated luminosity of 140 fb^{-1}. The events were selected by single-lepton triggers with variable electron and muon transverse momentum (p_{T}) thresholds, and various identification and isolation criteria depending on the lepton flavour and the data-taking period [41, 42]. The lowest p_{T} threshold at trigger level used for electrons was 24 GeV (26 GeV), while for muons the threshold was 20 GeV (26 GeV) in 2015 (2016–2018).

4.2 Simulated event samples

Samples of simulated events were produced using different Monte Carlo (MC) event generators including parton shower (PS) and hadronisation models for both signal and background processes. The effect of multiple interactions in the same and neighbouring bunch crossings (pile-up) was modelled by overlaying the hard-scattering event with simulated minimum-bias events generated with Pythia 8.186 [43, 44] using the NNPDF2.3LO set of PDFs [45] and the A3 set of tuned parameters (A3 tune) [46]. Events were reweighted such that the distribution of the average number of interactions per bunch crossing matches that observed in data.

Table 1 presents a summary of all configurations used to generate events for signal (tHq and tWH) and background processes, for both nominal and alternative simulated samples. In all simulated signal and background samples, the top-quark mass was set to $m_{\mathrm{top}} = 172.5$ GeV and the Higgs-boson mass to $m_H = 125.0$ GeV. Moreover, the strong coupling constant was set to $\alpha_{\mathrm{s}} = 0.118$ [47] at the reference scale of the Z-boson mass. These values are also used in the computation of production cross-sections for processes involving these particles. The bottom and charm hadron decays were simulated with EvtGen [48] for all event samples, except those generated with Sherpa.

Systematic uncertainties from different modelling choices are evaluated by comparing alternative simulated samples to the nominal ones. These alternative samples are generated either through reweighting or with dedicated event generators. Each variation is applied

JHEP10(2025)093

Process	Generator	ME order	Parton shower	PDF set	Tune
tHq	MG5_aMC	NLO	Pythia 8	NNPDF3.0nlo	A14
	(MG5_aMC)	(NLO)	(Herwig 7)	(NNPDF3.0nlo)	(Herwig 7.1)
tWH	MG5_aMC	NLO	Pythia 8	NNPDF3.0nlo	A14
	(MG5_aMC)	(NLO)	(Herwig 7)	(NNPDF3.0nlo)	(Herwig 7.1)
$t\bar{t}$	Powheg Box	NLO	Pythia 8	NNPDF3.0nlo	A14
	(Powheg Box)	(NLO)	(Herwig 7)	(NNPDF3.0nlo)	(Herwig 7.1)
	(Powheg Box)	(NLO)	(Pythia 8)	(NNPDF3.0nlo)	(A14 $p_{\mathrm{T}}^{\mathrm{hard}}$)
	(MG5_aMC)	(NLO)	(Pythia 8)	(NNPDF3.0nlo)	(A14)
$t\bar{t}+b\bar{b}$	(Powheg Box Res)	(NLO)	(Pythia 8)	(NNPDF3.0nlo)	(A14)
$t\bar{t}H$	Powheg Box	NLO	Pythia 8	NNPDF3.0nlo	A14
	(Powheg Box)	(NLO)	(Herwig 7)	(NNPDF3.0nlo)	(Herwig 7.1)
	(MG5_aMC)	(NLO)	(Pythia 8)	(NNPDF3.0nlo)	(A14)
$t\bar{t}W$	Sherpa 2.2.10	NLO QCD+EW	Sherpa	NNPDF3.0nnlo	default
	(MG5_aMC)	(NLO QCD+EW)	(Pythia 8)	NNPDF3.0nnlo	(A14)
$t\bar{t}W$ (EW)	Sherpa 2.2.10	LO	Sherpa	NNPDF3.0nnlo	default
	(MG5_aMC)	(LO)	(Pythia 8)	(NNPDF3.0nlo)	(A14)
$t\bar{t}Z$	MG5_aMC	NLO	Pythia 8	NNPDF3.0nlo	A14
	(Sherpa 2.2.10)	(LO)	(Sherpa)	(NNPDF3.0nnlo)	(default)
	(MG5_aMC)	(NLO)	(Herwig 7)	(NNPDF3.0nlo)	(Herwig 7.1)
Single top quark (t-ch., tW, s-ch.)	Powheg Box	NLO	Pythia 8	NNPDF3.0nlo	A14
	(Powheg Box)	(NLO)	(Herwig 7)	(NNPDF3.0nlo)	(Herwig 7.1)
	(MG5_aMC)	(NLO)	(Herwig 7)	(NNPDF3.0nlo)	(Herwig 7.1)
V + jets	Sherpa 2.2.1	MEPS@NLO	Sherpa	NNPDF3.0nlo	default
VV, $qqVV$	Sherpa 2.2.2	MEPS@NLO	Sherpa	NNPDF3.0nnlo	default
	(Powheg Box)	(NLO)	(Pythia 8)	(NNPDF3.0nlo)	(A14)
VVV	Sherpa 2.2.2	MEPS@NLO	Sherpa	NNPDF3.0nnlo	default
tZ	MG5_aMC	NLO	Pythia 8	NNPDF3.1nlo	A14
tWZ	MG5_aMC	NLO DR1	Pythia 8	NNPDF2.3lo	A14
	(MG5_aMC)	(NLO DR2)	(Pythia 8)	NNPDF2.3lo	(A14)
$t\bar{t}t$, $t\bar{t}t\bar{t}$	MG5_aMC	QCD NLO	Pythia 8	NNPDF3.1nlo	A14
ggH, qqH	Powheg Box	QCD NLO	Pythia 8	CTEQ6L1	AZNLO
WH, ZH	Pythia 8	QCD NLO	Pythia 8	NNPDF2.3lo	A14

Table 1. The configurations used to generate events for signal (tHq and tWH) and background processes. The simulation samples used to estimate the systematic uncertainties are shown in parentheses and in grey.

independently, unless explicitly stated otherwise, to ensure a consistent evaluation of its individual impact on the analysis.

4.2.1 Simulated signal event samples

The production of a Higgs boson with a single top quark in the t-channel, tHq, was modelled using MadGraph5_aMC@NLO 2.6.2 [49] with matrix elements (MEs) at next-to-leading-order (NLO) accuracy in QCD in the 4FS using the NNPDF3.0nlo nf4 [50] PDF set. The renormalisation (μ_{r}) and factorisation (μ_{f}) scales were set to $0.5 \times \sum_i \sqrt{m_i^2 + p_{\mathrm{T},i}^2}$, summing over all ME-generated particles with mass m and transverse momentum p_{T}. Events were interfaced with Pythia 8.230 using the A14 set of tuned parameters (A14

JHEP10(2025)093

tune) [51] and the NNPDF2.3LO PDF set. The simulated tHq signal samples were normalised to the NLO QCD theory prediction without NLO EW corrections at $\sqrt{s} = 13\,\text{TeV}$ and in the 5FS of $74.3^{+6.5\%}_{-14.9\%}$ (QCD) $\pm$ 3.7% (PDF+α_s) fb [52, 53]. The PDF and α_s uncertainties are calculated using the PDF4LHC15_nlo_30_pdfas PDF sets [54] and added in quadrature. The QCD uncertainty is computed from a combination of QCD scale variations and the difference of predictions in the 4FS and 5FS schemes, using the PDF4LHC15_nlo_nf4_100 PDF (central) set.

The associated production of a Higgs boson with a single top quark, tWH, was modelled using MadGraph5_aMC@NLO 2.8.1 with MEs at NLO accuracy in QCD in the 5FS using the NNPDF3.0NLO PDF set. The functional forms of the μ_r and μ_f scales were set the same as for the tHq simulation sample. The diagram-removal (DR) scheme (DR1) [55] was employed to remove the overlap between tWH and $t\bar{t}H$ simulation samples [56]. The events were interfaced with Pythia 8.245 using the A14 tune and the NNPDF2.3lo PDF set. The simulated tWH signal samples were normalised to the NLO QCD theory prediction in the 5FS [52, 53] and using the DR2 scheme [25] to handle the overlap between the tWH and $t\bar{t}H$ processes. At $\sqrt{s} = 13\,\text{TeV}$ the predicted cross-section is $\sigma(tWH)_{\text{NLO}} = 15.2^{+4.9\%}_{-6.7\%}$ (QCD scale) $\pm$ 6.3% (PDF+α_s) fb [52, 53].

To assess the modelling uncertainty due to the choice of the PS and hadronisation model, alternative event samples were produced for signal processes. Both tHq and tWH processes were produced using MadGraph5_aMC@NLO with the nominal set-up but interfaced with Herwig 7.1.6 [57, 58] using the MMHT2014nnlo [59] PDF set, with the Herwig 7.1 default set of tuned parameters (Herwig 7.1 tune) [58]. Moreover, simulated signal samples for both tHq and tWH with the ITC hypothesis were produced using similar set-ups as the ones used to produce SM simulated samples. In this case, the samples were normalised to the cross-section, for pp collisions at $\sqrt{s} = 13\,\text{TeV}$, of $\sigma(tHq)^{\kappa_t=-1}_{\text{NLO}} = 873\,\text{fb}$ and $\sigma(tWH)^{\kappa_t=-1}_{\text{NLO}} = 114\,\text{fb}$, respectively. For both nominal and ITC simulated signal samples, alternative variations of μ_r and μ_f scales and initial-/final-state radiation (ISR/FSR) were produced within the nominal set-up (i.e. MadGraph5_aMC@NLO +Pythia 8) as reweighted events.

4.2.2 Simulated background event samples

The production of $t\bar{t}$ events were modelled using Powheg Box v2 [60–63] at NLO QCD in 5FS with the NNPDF3.0NLO PDF set. In this case, the h_{damp} parameter[2] was set to $1.5 \times m_{\text{top}}$ [56]. Events were interfaced with Pythia 8.230 using the A14 tune and the NNPDF2.3LO PDF set. The simulated samples are normalised to the theory prediction at next-to-next-to-leading-order (NNLO) in QCD including the resummation of next-to-next-to-leading logarithmic (NNLL) soft-gluon terms calculated using Top++2.0 [64–70], equals to 834^{+29}_{-37} pb, where the uncertainty is the sum in quadrature of scale, PDF and α_s uncertainties.

A series of alternative $t\bar{t}$ simulated event samples were produced to evaluate the impact of modelling uncertainties. The effect of the choice of the PS and hadronisation model is quantified by comparing the nominal simulation with one produced using the same ME generator but interfaced with Herwig 7.1.6. To evaluate the impact of the choice of the NLO

[2]The h_{damp} parameter controls the p_T of the first additional emission beyond the LO Feynman diagram in the PS and therefore regulates the high-p_T emission against which the $t\bar{t}$ system recoils.

JHEP10(2025)093

matching scheme two samples were produced: one where the parameter $p_{\mathrm{T}}^{\mathrm{hard}}$, which regulates the definition of the vetoed region of the Pythia 8 showering [71], was halved, and other event sample generated by MadGraph5_aMC@NLO and matched to Herwig 7. Moreover, to assess the choice of the value of the h_{damp} parameter, alternative simulated samples generated using the nominal set-up but with $h_{\mathrm{damp}} = 3.0 \times m_{\mathrm{top}}$ were considered. A 4FS $t\bar{t}+b\bar{b}$ simulated sample was produced using Powheg Box Res with the OpenLoops [72–74] library and the NNPDF3.1nnlo nf4 PDF set, interfaced with Pythia 8.244. The simulation used a b-quark mass of 4.95 GeV and dynamic scales μ_{f} set to $0.5 \times \sum_{i=t,\bar{t},b,\bar{b},j} m_{\mathrm{T},i}$ and μ_{r} set to $0.5 \times \sqrt[4]{m_{\mathrm{T},t} \cdot m_{\mathrm{T},\bar{t}} \cdot m_{\mathrm{T},b} \cdot m_{\mathrm{T},\bar{b}}}$, where $m_{\mathrm{T},i} = \sqrt{m_i^2 + p_{\mathrm{T},i}^2}$ denotes the transverse mass of particle i. The h_{damp} parameter was defined as $0.5 \times \sum_{i=t,\bar{t},b,\bar{b}} m_{\mathrm{T},i}$, and the parameter h_{bzd} was set to 5. Here, h_{bzd} controls the suppression of the Born-zero configurations in Powheg. This sample is considered to evaluate the impact of using the 4FS instead of the 5FS and also the effect of generating additional b-quarks explicitly at NLO in the ME in the 4FS, as opposed to their approximate treatment via the PS in the 5FS set-up.

The $t\bar{t}H$ events were simulated using Powheg Box v2 at NLO accuracy in QCD in 5FS with the NNPDF3.0NLO PDF set, and with μ_{r} and μ_{f} scales set to $\sqrt[3]{m_{\mathrm{T},t} \cdot m_{\mathrm{T},\bar{t}} \cdot m_{\mathrm{T},H}}$ [75]. Events were interfaced with Pythia 8.230 using the A14 tune and the NNPDF2.3LO PDF set. The NLO QCD+EW cross-section at $\sqrt{s} = 13$ TeV is 507^{+35}_{-50} fb [52], where the uncertainties were estimated from variations of α_{s} and the μ_{r} and μ_{f} scales. Additional variations use event weights for QCD scales and radiation, with an alternative PS simulated sample using Herwig 7.04.

The $t\bar{t}W$ events were produced using Sherpa 2.2.10 [76] at NLO (LO) accuracy in QCD for up to one (two) additional partons. The NNPDF3.0nnlo PDF set was used along with the dedicated set of tuned PS parameters developed by the Sherpa authors. In addition, EW corrections were also produced with Sherpa 2.2.10 at LO accuracy for up to one additional parton. The $t\bar{t}W$ cross-section is calculated at NLO QCD with up to two additional partons using an improved MadGraph5_aMC@NLO FxFx merging procedure [77, 78] and combines it with leading $\mathcal{O}(\alpha^2\alpha_s^2)$ and subleading $\mathcal{O}(\alpha^3\alpha_s)$ NLO EW corrections. This calculation also includes on-shell LO decays of the $t\bar{t}W$ including the tree-level spin correlations within the narrow-width approximation. At $\sqrt{s} = 13$ TeV, this yields 722^{+70}_{-78} (scale)$^{+7}_{-7}$ (PDF) fb [78]. The choice of the NLO matching scheme was evaluated using an alternative simulated sample produced with MadGraph5_aMC@NLO 2.3.3 with the FxFx [77] merging scheme simulated samples including EW corrections.

The associated production of the Z boson with a top-quark pair ($t\bar{t}Z$) was simulated using MadGraph5_aMC@NLO 2.3.3 at NLO QCD with the NNPDF3.0nlo PDF set, interfaced with Pythia 8.210 using the A14 tune and the NNPDF2.3lo PDF set. The $t\bar{t}Z$ cross-section, including off-shell effects and Z/γ^* interference, was calculated at NLO QCD+EW as $0.88^{+0.09}_{-0.10}$ pb [52, 79], where the uncertainties were estimated from variations of α_{s} and the μ_{r} and μ_{f} scales. The choice of the NLO matching scheme was evaluated using an alternative simulated sample produced with Sherpa 2.2.0 at LO accuracy along with the NNPDF3.0nnlo PDF set, using the MEPS@LO prescription [80], with up to one additional parton for the $t\bar{t}Z(\to \ell\ell)$ sample and two additional partons for the $t\bar{t}Z(\to qq)$ and $t\bar{t}Z(\to \nu\nu)$ samples.

JHEP10(2025)093

All single top-quark events were generated with Powheg Box v2 at NLO in QCD with either the NNPDF3.0nlo nf4 or NNPDF3.0nlo PDF sets, with μ_f and μ_r scales set to $\sqrt{m_b^2 + p_{T,b}^2}$ [81, 82]. The t-channel was produced considering the 4FS, while the s-channel and associated tW processes used the 5FS. The latter process also employed the DR1 scheme to remove the overlap between tW and $t\bar{t}$ [56]. Events were interfaced with Pythia 8.230 using the A14 tune and the NNPDF2.3lo PDF set. Systematic variations include QCD μ_r and μ_f scales and radiation uncertainties, alternative PS using Powheg Box v2 with Herwig 7.16, and matching scheme uncertainties using MadGraph5_aMC@NLO 2.6.2 with Herwig 7.16 and the MMHT2014nnlo PDF set. For associated tW, an additional simulated sample using the diagram subtraction (DS) scheme was produced to evaluate the $t\bar{t}$ interference uncertainties.

The production of single-boson (V + jets), diboson (VV), and triboson (VVV) processes were simulated using either Sherpa 2.2.1 or Sherpa 2.2.2, with varying levels of QCD accuracy depending on the process. The NNPDF3.0nnlo PDF set was used along with a dedicated set of Sherpa-tuned PS parameters. For the V + jets processes, MEs were generated at NLO (LO) accuracy in QCD for up to two (four) partons, using the Comix library [83]. Simulated samples were normalised to NNLO predictions [84]. For the VV processes, MEs accounted for off-shell effects and included Higgs-boson contributions where relevant. Fully leptonic and semileptonic final states, where one boson decays leptonically and the other hadronically, were simulated at NLO (LO) accuracy in QCD for up to one (three) additional partons. Loop-induced processes $gg \to VV$ were generated at LO accuracy in QCD with up to one additional parton, for both fully leptonic and semileptonic final states. The EW production of a VV pair in association with two jets ($VVjj$) was simulated at LO accuracy in QCD. For the VVV processes, MEs were generated with factorised gauge-boson decays at NLO accuracy in QCD for the inclusive process and at LO accuracy in QCD for up to two additional parton emissions. In all cases, NLO MEs were matched to PS using a colour-exact variant of the MC@NLO algorithm [85]. Different jet multiplicities were merged via the CKKW matching procedure [86, 87], extended to NLO QCD accuracy through the MEPS@NLO [80] prescription, with a merging threshold set to 20 GeV. Leading-order MEs were merged using the MEPS@LO prescription. These calculations were performed in the G_μ scheme, which uses the Fermi constant as input, ensuring an optimal description of pure EW interactions at the EW scale.

To assess modelling uncertainties, scale uncertainties were evaluated using seven μ_r and μ_f variations (by factors of 0.5 and 2) as event weights. Furthermore, in the particular case of the VV processes, alternative event simulated samples were produced to evaluate the impact of different ME, PS, and hadronisation models by comparing the nominal diboson Sherpa event samples with Powheg Box v2 simulations of WW, WZ, and ZZ [88] processes at NLO accuracy in QCD. The effects of singly resonant amplitudes and interference due to Z/γ^* exchange, as well as same-flavour lepton combinations in the final state, were included where relevant. However, WW/ZZ interference in same-flavour lepton and neutrino final states was neglected. Events were interfaced with Pythia 8.186 using the AZNLO set of tuned parameters (AZNLO tune) [89]. The CT10 PDF set [90] was used for hard-scattering calculations, while the CTEQ6L1 [91] PDF set was applied for PS. The μ_f and μ_r scales

JHEP10(2025)093

were set to the boson-pair invariant mass, with a requirement of $m_{\ell\ell} > 4\,\text{GeV}$ at the ME level for same-flavour lepton pairs.

The tZq event sample was simulated using MadGraph5_aMC@NLO 2.3.3 at NLO accuracy in QCD in the 4FS with the NNPDF3.0nlo PDF set. The events were interfaced with Pythia 8.230 using the A14 tune and the NNPDF2.3lo PDF set. Off-resonance events away from the Z-mass peak were included. The functional form of the μ_r and μ_f scales was set to $4\sqrt{m_b^2 + p_{\text{T},b}^2}$, where the b-quark was the one produced by a gluon splitting in the event. The uncertainty due to initial-state radiation and to higher/lower parton radiation were estimated following exactly the same prescription as with the t-channel process.

The tWZ event production was modelled using MadGraph5_aMC@NLO 2.3.3 at NLO QCD with the NNPDF3.0nlo PDF set in the 5FS. Events were interfaced with Pythia 8.212, using the A14 tune and the NNPDF2.3lo PDF set. The DR1 scheme was used to remove the overlap between the tWZ and $t\bar{t}Z$ processes. Parton radiation uncertainties follow the same prescription as the t-channel process. An alternative DR scheme [25] was simulated to assess systematic uncertainty.

The production of three top-quark process ($t\bar{t}t$) events was modelled using MadGraph5_aMC@NLO 2.2.2 with NLO accuracy in QCD interfaced with Pythia 8.186, using the NNPDF2.3lo PDF set and the A14 tune. The production of four top-quark process ($t\bar{t}t\bar{t}$) events was modelled using MadGraph5_aMC@NLO 2.3.3 with NLO accuracy in QCD with the NNPDF3.1nlo PDF set. The events were interfaced with Pythia 8.230 for the PS and hadronisation, using the A14 tune and the NNPDF2.3lo PDF set.

Four SM Higgs-boson processes are considered as minor backgrounds: gluon-gluon fusion (ggH), VBF (qqH), and associated production with W and Z bosons (WH and ZH). The ggH and VBF events were modelled with either Powheg Box v2 or v1 (r2856) [92, 93], providing NLO accuracy in QCD with the CT10 PDF set. The μ_r and μ_f scales were set to $\sqrt{m_H^2 + p_{\text{T},H}^2}$. These generated events were interfaced with either Pythia 8.210 or 8.186 for PS and hadronisation, using the AZNLO tune and the CTEQ6L1 PDF set. The WH and ZH production was modelled with Pythia 8.186, using the A14 tune and the NNPDF2.3lo PDF set.

Most of the MC simulated samples used for the nominal estimates were processed through a simulation [94] of the ATLAS detector based on Geant4 [95], while those used for evaluating systematic uncertainties were processed with a fast simulation [94] that relies on a parameterisation of the calorimeter response [96]. Furthermore, fast-simulated event samples were used for certain nominal samples, particularly for the tHq and tWH signal processes and the $t\bar{t}t\bar{t}$ background process with no loss of accuracy.

5 Object definitions

Interaction vertices from the pp collisions are reconstructed from at least two tracks in the ID system with p_T larger than 500 MeV that are consistent with originating from the beam collision region in the x–y plane. If more than one primary vertex candidate is found in the event, the candidate for which the associated tracks form the largest sum of squared p_T is selected as the hard-scatter primary vertex [97].

JHEP10(2025)093

Electron candidates are reconstructed from energy clusters in the electromagnetic calorimeter matched to a track in the ID [98]. They are required to satisfy $p_{\mathrm{T}} > 10\,\mathrm{GeV}$ and $|\eta| < 2.47$, excluding the transition region between the endcap and barrel calorimeters ($1.37 < |\eta| < 1.52$). `Loose` and `Tight` electron identification working points are used, based on a likelihood discriminant employing calorimeter, tracking and combined variables that provide separation between electrons and jets.

Muon candidates are reconstructed from tracks measured in the ID matched to tracks measured in the MS [99, 100]. The resulting muon candidates are re-fitted using the complete track information from both detector systems. They are required to satisfy $p_{\mathrm{T}} > 10\,\mathrm{GeV}$ and $|\eta| < 2.5$. `Loose` and `Medium` muon identification working points are used.

Electron (muon) candidates are matched to the primary vertex by requiring that the significance of their transverse impact parameter, d_0,[3] satisfies $|d_0/\sigma(d_0)| < 5.0\,(3.0)$, where $\sigma(d_0)$ is the measured uncertainty in d_0, and by requiring that their longitudinal impact parameter, $z_0 \sin\theta$,[4] satisfies $|z_0 \sin\theta| < 0.5\,\mathrm{mm}$ [98, 99].

To further suppress leptons from heavy-flavour hadron decays, misidentified jets, or photon conversions (collectively referred to as "non-prompt leptons"), a BDT discriminant, referred to as the non-prompt-lepton BDT [101], based on isolation and lifetime information associated with a track jet that matches the selected electron or muon, is employed. The `Tight` working point based on the non-prompt-lepton BDT is used, which allows prompt muons (barrel/endcap electrons) to be selected with an efficiency that is about 60% (60%/70%) for $p_{\mathrm{T}} \sim 20\,\mathrm{GeV}$ and reaches a plateau of 95% (95%/90%) for $p_{\mathrm{T}} \sim 40$ (40/65)GeV, while the rejection factor against leptons from the decay of b-hadrons is about 20.

For the $2\ell\,\mathrm{SS}$ channel, to further suppress electrons with incorrect charge assignment, a BDT discriminant based on calorimeter and tracking quantities [102] is used, reducing the signal by 1.9% and the total background by approximately 40%, both at preselection level (see section 6.2). The electron candidates are separated into three classes: "material conversion", "internal conversion", and "non-conversion" electron candidates. Most electrons originating from photon conversions, whether from material conversions in the detector or internal conversions, are rejected by the standard electron identification criteria. To further suppress remaining conversion electrons in the $2\ell\,\mathrm{SS}$ and 3ℓ channels, additional vetoes are applied, except in control regions specifically targeting conversion electrons (e^*). Material conversion candidates have a reconstructed displaced vertex with radius $r > 20$ mm that includes the track associated with the electron.[5] The invariant mass of the associated track and the closest (in $\Delta\eta$) opposite-charge track reconstructed in the silicon detector, calculated at the conversion vertex, is required to be $< 100\,\mathrm{MeV}$. Internal conversion candidates must fail to satisfy the requirements for material conversions, and the di-track invariant mass, calculated here at the primary vertex, is required to be $< 100\,\mathrm{MeV}$.

The various lepton working points used are summarised in table 2. Lepton candidates are initially selected using relatively "*Loose*" criteria (labelled as L), and a subset may later

[3]The transverse impact parameter, d_0, is defined in the x–y plane as the distance of closest approach of the track to the beamline.

[4]The longitudinal impact parameter, z_0, is defined as the distance in z between the primary vertex and the point on the track used to evaluate d_0.

[5]The beampipe and IBL inner radii are 23.5 mm and 33 mm, respectively.

JHEP10(2025)093

	Electron		Muon	
Lepton definition	L	T	L	T
Identification	`Loose`	`Tight`	`Loose`	`Medium`
Transverse impact parameter significance $\lvert d_0\rvert/\sigma_{d_0}$	< 5.0		< 3.0	
Longitudinal impact parameter z_0	$\lvert z_0 \sin\theta\rvert < 0.5$ mm			
Isolation (Non-prompt lepton BDT)	No	Yes	No	Yes
Electron charge-misassignment veto	No	Yes	–	
Electron conversion candidate veto	No	Yes (except e^*)	–	

Table 2. Description of the *Loose* (L) and *Tight* (T) lepton definitions. The electron e^* is required to fulfil, in addition to the corresponding lepton definition requirements, those corresponding to an internal or material conversion candidate.

be required to satisfy stricter "*Tight*" criteria (labelled as T) to further optimise the event selection. The choice of working point depends on the main background processes in each category. The specific selections adopted for the signal and control regions are described in section 6. The lepton working points used here (*Loose* and *Tight*) are not to be confused with the identification working points such as `Loose`, `Medium`, and `Tight`.

The constituents for jet reconstruction are identified by combining measurements from both the ID and the calorimeter using a particle flow (PFlow) algorithm [103]. Jet candidates are reconstructed from these PFlow objects using the anti-k_t algorithm [104, 105] with a radius parameter of $\Delta R = 0.4$. They are calibrated using simulation with corrections obtained by using in situ techniques in data [106]. Only jet candidates with $p_{\mathrm{T}} > 20\,\mathrm{GeV}$ and within $|\eta| < 4.5$ are selected. To reduce the effect of pile-up, each jet with $p_{\mathrm{T}} < 60\,\mathrm{GeV}$ and $|\eta| < 2.4$ must satisfy the `Tight` working point of the jet vertex tagger (JVT) [107] criteria used to identify jets that originate from the primary vertex. Moreover, jets within $2.5 < |\eta| < 4.5$ (hereafter called "forward jets") and $p_{\mathrm{T}} < 120\,\mathrm{GeV}$ must satisfy the `Tight` working point of the forward jet vertex tagger (fJVT) [108] criteria. A set of quality criteria is also applied to reject events containing at least one jet arising from non-collision sources or detector noise [109].

Jets containing b-hadrons are identified (b-tagged) via the `DL1r` [110] algorithm that uses a deep feed-forward neural network based on the distinctive features of b-hadron decays, primarily the impact parameters of tracks and the displaced vertices reconstructed in the ID. Additional input to this network is provided by discriminating variables constructed by a recurrent neutral network (RNN) [111], which exploits the spatial and kinematic correlations between tracks originating from the same b-hadron. A multivariate b-tagging discriminant value is calculated for each jet. In this measurement, a jet is considered b-tagged if it passes the working point corresponding to 85%, 77%, 70%, or 60% average expected efficiency to tag a b-quark jet, with a light-jet[6] rejection factor of about 40 to 2500, and a charm-jet (c-jet) rejection factor of about 3 to 40, as determined for jets with $p_{\mathrm{T}} > 20\,\mathrm{GeV}$ and

[6] 'Light jet' or 'Light-flavour jet' refers to a jet originating from the hadronisation of a light-flavour quark (u, d, s) or a gluon.

JHEP10(2025)093

$|\eta| < 2.5$ in simulated $t\bar{t}$ events. This discrete version of the b-tagging discriminant, named pseudo-continuous b-tagging score (PCBT), is also exploited as jet variable.

The reconstruction of the τ_{had} is seeded by jets reconstructed via the anti-k_t algorithm, using calibrated energy clusters as inputs, with a distance parameter of $\Delta R = 0.4$ [112–115]. Jets seeding τ_{had} candidates are additionally required to have $p_{\text{T}} > 10\,\text{GeV}$ and $|\eta| < 2.5$. To separate the τ_{had} candidates initiated by hadronic τ-lepton decays from jets initiated by quarks or gluons, a RNN [114] identification method was trained on information from reconstructed charged-particle tracks and clusters of energy in the calorimeter associated with τ_{had} candidates as well as high-level discriminating variables. A separate multivariate discriminant based on a BDT [113, 115] is also used to reject backgrounds arising from electrons mimicking a τ_{had}. This discriminant (eBDT) is built using information from the calorimeter and the tracking detector. Transition radiation information from the TRT system plays a key role in the performance of this discriminant. Baseline τ_{had} are required to have one or three associated tracks, electric charge of ± 1, $p_{\text{T}} > 20\,\text{GeV}$ and $|\eta| < 2.5$, excluding the barrel-endcap transition region. Each τ_{had} must satisfy the `Medium` RNN identification selection requirement, with efficiencies of 75% for 1-prong and 60% for 3-prong taus, and the `Loose` eBDT requirement, with an efficiency of 95% [113, 115].

Ambiguities between independently reconstructed electrons, muons, jets and τ_{had} can arise. A sequential "overlap removal" procedure is performed to resolve these ambiguities and thus avoid double counting of candidates. This procedure is applied to electrons and muons satisfying the L criteria. If two electrons are separated by $\Delta R < 0.1$, only the one with the higher p_{T} is kept. If an electron and a muon overlap within $\Delta R < 0.1$, the muon is removed if it is reconstructed only from an ID track and calorimeter energy deposits consistent with a minimum-ionising particle (i.e. if it is "calorimeter-tagged"), otherwise the electron is removed. If an electron and a selected jet are found within $\Delta R < 0.2$, the jet is removed. Any electron later found within ΔR of 0.4 of a jet is removed. Muons associated with a jet must satisfy a jet-muon separation of $\Delta R < 0.4$. If the overlapping jet contains less than three tracks with $p_{\text{T}} > 500\,\text{MeV}$, the jet is removed, otherwise the muon is rejected. Any τ_{had} found within a ΔR of 0.2 of an electron is removed. Any τ_{had} found within a ΔR of 0.2 of any type of muon with p_{T} greater than 2 GeV is removed, although if the τ_{had} p_{T} is greater than 50 GeV, it will only be removed if it is found to overlap with a reconstructed muon. Finally, if a jet is found within a ΔR of 0.2 of a τ_{had}, the jet is removed.

The missing transverse momentum $\vec{p}_{\text{T}}^{\,\text{miss}}$ (with magnitude $E_{\text{T}}^{\text{miss}}$) is defined as the negative vector sum of the transverse momenta of all identified and calibrated objects and remaining unclustered energy, the latter of which is estimated from low-p_{T} tracks associated with the primary vertex but not assigned to any lepton or jet candidate [116]. The $E_{\text{T}}^{\text{miss}}$ is taken as a measurement of the undetectable particles, and is affected by energy losses due to detector inefficiencies and acceptance, and by energy resolution.

6 Event selection and classification

Events must satisfy the single-electron or single-muon trigger requirements described in section 4.1. Selected events are required to contain one lepton matched to the corresponding lepton reconstructed by the trigger within $\Delta R < 0.15$ and with $p_{\text{T}} > 27\,\text{GeV}$. These criteria

JHEP10(2025)093

ensure operation on the trigger efficiency plateau, thereby minimising the corrections needed in simulation to reproduce the per-lepton trigger efficiencies measured in data [41, 42].

Events selected by the trigger are required to have at least one primary vertex with at least two associated ID tracks with $p_{\mathrm{T}} > 0.5\,\mathrm{GeV}$. In each event, the primary vertex is defined as the reconstructed vertex having the highest scalar sum of squared p_{T} of associated tracks [97] among the vertices consistent with the average beam-spot position. These events are also required to contain either one lepton and at least three b-tagged jets (70% working point), two leptons with the same electric charge or three leptons, based on the *Loose* lepton definition introduced in section 5. Events containing τ_{had} leptons are explicitly vetoed in all three channels.

The sensitivity of the analysis relies on the discrimination provided by the multivariate response that combines different event-based variables. In each channel, BDTs with gradient boosting (BDTGs) are trained on simulated events in a preselection region using the `XGBoost` Python package [117]. The model performance is evaluated using the hold-out method, in which the considered data sample is randomly divided into an independent training-data sample and a test-data sample that is used as a proxy to evaluate the performance of the model on unseen data. In all channels, only the tHq process is considered as a signal in the BDTG training. This decision is driven by the similarities observed between the tWH and $t\bar{t}H$ topologies, so that including the tWH process in the training weakens the separation between tHq and $t\bar{t}H$ and other background processes. While the tWH sample is not part of the BDTG training, its contribution is fully accounted for in the signal yield and in the limit setting later on. A strong separation of the signal from the $t\bar{t}H$ process leads to a reduced interplay between $t\bar{t}H$ and the tH signal in the results.

Details on the definition of the preselection regions and the background composition are given in the following while the yields are reported in table 3.

6.1 $H \to b\bar{b}$ channel

The $H \to b\bar{b}$ preselection region is defined by requiring the presence of exactly one *Tight* lepton (electron or muon) with $p_{\mathrm{T}} > 27\,\mathrm{GeV}$. The 70% working point of the `DL1r` tagger is used to select at least three b-tagged jets. All events with at least five jets and at least four b-tagged jets are vetoed. This requirement has a negligible impact on the signal acceptance and will help any future combination with other $t\bar{t}H$ analyses. Given the presence of one neutrino coming from the W-boson decay, the event is expected to have a non-zero $E_{\mathrm{T}}^{\mathrm{miss}}$. For this reason an $E_{\mathrm{T}}^{\mathrm{miss}} > 25\,\mathrm{GeV}$ requirement is applied.

As shown in Table 3, the main contribution to the background in the preselection region comes from $t\bar{t}+\mathrm{jets}$ events, constituting 90% of the expected total yield. The $t\bar{t}+\mathrm{jets}$ events are further classified depending on the flavour of the additional jets produced. Simulated events where at least one of the additional jets is matched to a b-hadron are classified as $t\bar{t}+\geq 1b$ (30% of the expected $t\bar{t}+\mathrm{jets}$ yield); if no matched b-jet is found but at least one jet is matched to a c-hadron the event is classified as $t\bar{t}+\geq 1c$ (17% of the expected $t\bar{t}+\mathrm{jets}$ yield) while all the other events are classified as $t\bar{t}+\geq 0$ light (53% of the expected $t\bar{t}+\mathrm{jets}$ yield). The latter contribution also includes $t\bar{t}$ events with no additional jets.

JHEP10(2025)093

Process	$H \to b\bar{b}$	2ℓ SS	3ℓ
tHq	91.1 ± 1.7	12.41 ± 0.17	3.15 ± 0.05
tWH	37.21 ± 0.26	3.97 ± 0.09	2.36 ± 0.07
$t\bar{t}$	–	1430 ± 14	324 ± 6
$t\bar{t}+ \geq 1b$	60170 ± 90	–	–
$t\bar{t}+ \geq 1c$	33585 ± 70	–	–
$t\bar{t}+ \geq 0$ light	106290 ± 120	–	–
e/μ_{Fakes}	8028 ± 80	–	–
$t\bar{t}H$	1676.9 ± 1.5	126.6 ± 1.2	74.62 ± 0.25
$t\bar{t}W$	362.0 ± 1.6	798.0 ± 2.1	205.7 ± 1.1
$t\bar{t}Z$	891.0 ± 6	165.3 ± 1.0	567.8 ± 1.7
tZq	170.5 ± 1.3	88.9 ± 0.5	273 ± 0.9
tWZ	2.22 ± 0.22	18.73 ± 0.08	80.47 ± 0.16
Z/W+jets	4681 ± 34	518 ± 30	131 ± 25
VV, VVV	292 ± 6	298.6 ± 3.3	579 ± 4
Single-top	9331 ± 31	164 ± 4	20.1 ± 1.5
$t\bar{t}t$, $t\bar{t}t\bar{t}$	8.9 ± 0.1	4.81 ± 0.06	4.88 ± 0.06
$VH, \text{VBF}H, ggH$	25.0 ± 0.1	19 ± 4	7.4 ± 2.8
Total	225640 ± 190	3650 ± 33	2274 ± 26

Table 3. Preselection region yields as predicted by the MC simulation. The uncertainty is statistical only and the PDG rounding is applied. The $t\bar{t}$ background is split into $t\bar{t}+ \geq 1b$, $t\bar{t}+ \geq 1c$ and $t\bar{t}+ \geq 0$ light categories for the $H \to b\bar{b}$ channel only; therefore the $t\bar{t}$ contribution for this channel is absent. Moreover, for the $H \to b\bar{b}$ channel only the data-driven estimate of the non-prompt and fake leptons background is given due to lack of a MC-based estimate.

In the $H \to b\bar{b}$ channel, the preselected events are used to train a five-dimensional BDTG including the categories tHq, $t\bar{t}+ \geq 1b$, $t\bar{t}+ \geq 1c$, $t\bar{t}+ \geq 0$ light and others. The "others" category includes all the remaining backgrounds. A Deep Neural Network (DNN) is also tested to validate the results obtained with the BDTG. Since the BDTG shows slightly better performance, it is chosen for the final results.

In total, 25 variables were used in the training, such as the number of jets, the lepton charge and flavour information, invariant mass and angular separation of various reconstructed jets, the minimum χ^2 values from reconstructing the W-bosons and top-quark masses from their decay products under the $t\bar{t}+ \geq 0$ light or $t\bar{t}+ \geq 1b$ hypotheses, as well as the pseudo-continuous b-tagging discriminant of selected jets (see table 6). These variables are motivated by the expected kinematic properties of the signal. The tHq topology features a forward spectator jet from the scattered incoming light-flavour quark, a hadronically decaying top quark, and a different multiplicity of b-jets compared to the dominant $t\bar{t}$ background. The most important variables entering the BDTG reflect these features: the number of jets associated with the reconstructed hadronic top quark from different $t\bar{t}$ reconstruction techniques provides strong separation from the $t\bar{t}$ background; the lepton charge helps distinguish tHq events, as the incoming light-flavour quark is dominantly a u-quark from one of the colliding protons, leading mostly to positively charged top quarks (and hence positive leptons), from charge-

JHEP10(2025)093

Channel	Region	BDT score	Conversion cut	Jets	Leptons flavour (p_{T} ordered)	Other
$H \to b\bar{b}$	SR	—	—	$N^{70}_{\text{not-}b} < 2$ $N^{\text{jet}}_{\text{forward}} \geq 1$	—	—
	CR($t\bar{t}+ \geq 1b$)	—	—	$N^{70}_{\text{not-}b} \geq 2$ $N^{\text{jet}}_{\text{forward}} = 0$	—	
2ℓ SS	SR	BDT(tHq) > 0.65 BDT($t\bar{t}$) < 0.5 BDT($t\bar{t}W$) < 0.6 and BDT(VV) < 0.8	yes	—	—	—
	CR(μ_{HF})	BDT(tHq) < 0.65 BDT($t\bar{t}$) > 0.3 BDT($t\bar{t}W$) < 0.6 and BDT(VV) < 0.9	yes	—	$\mu\ \mu$	—
	CR(e_{HF})	BDT(tHq) < 0.65 BDT($t\bar{t}$) > 0.3 BDT($t\bar{t}W$) < 0.6 and BDT(VV) < 0.9	yes	—	$\mu\ e$, $e\ e$	$H_{\mathrm{T}}(\ell) < 225$ GeV
	CR(e_{conv})	BDT($t\bar{t}$) > 0.3	inverted	—	$\mu\ e$, $e\ e$	m($\ell\ell$) < 150 GeV
	CR($t\bar{t}W$)	BDT($t\bar{t}W$) > 0.6 BDT($t\bar{t}$) < 0.3	yes	—	—	—
3ℓ	SR	BDT(tHq) > 0.7 BDT($t\bar{t}$) < 0.9 BDT($t\bar{t}W$) < 0.8	yes	—	—	—
	CR(μ_{HF})	BDT(tHq) < 0.7 BDT($t\bar{t}$) > 0.5 BDT($t\bar{t}W$) < 0.8	yes	—	$\mu\ \mu\ \mu$, $e\ \mu\ \mu$, $\mu\ e\ \mu$, $e\ e\ \mu$	—
	CR(e_{HF})	BDT(tHq) < 0.7 $BDT(t\bar{t}) > 0.5$ $BDT(t\bar{t}W) < 0.8$	yes	—	$\mu\ \mu\ e$, $e\ \mu\ e$ $\mu\ e\ e$, $e\ e\ e$	—
	CR(e_{conv})	—	inverted	—	$\mu\ \mu\ e$, $e\ \mu\ e$, $\mu\ e\ e$, $e\ e\ e$	—
	CR($t\bar{t}W$)	BDT($t\bar{t}W$) > 0.8	yes	—	—	—

Table 4. Regions selection requirements for $H \to b\bar{b}$, 2ℓ SS and 3ℓ channels. The regions are defined using a mixture of requirements on the BDTGs outputs, the flavour of the leptons, the number of jets and b-tagged jets, the sum of the transverse momentum of the leptons H_{T} (ℓ), the leptons invariant masses ($m(\ell\ell)$) and the conversion criteria.

symmetric backgrounds such as $t\bar{t}$, $t\bar{t}W$, $t\bar{t}Z$ or $t\bar{t}H$; the p_{T} of the highest-p_{T} forward jet is characteristic of the spectator jet in tHq production; and the event sphericity encodes the more isotropic topology of $t\bar{t}$ events compared to the typically more forward-backward structure of tHq events [118]. The complete lists of input variables can be found in section A. Variable importance is evaluated using the "gain" metric provided by the `XGBoost` algorithm, which reflects the relative improvement in model accuracy due to each variable.

The preselection phase-space is then split into two regions, defined by rectangular requirements on the number of forward jets ($N^{\text{jet}}_{\text{forward}}$) and the number of central jets failing to meet the `DL1r` tagger 70% working-point requirement ($N^{70}_{\text{not-}b}$). In the $H \to b\bar{b}$ channel, a jet is classified as forward if its pseudorapodity is $2.5 < |\eta| < 4.5$ or if its pseudorapodity is $2 < |\eta| < 2.5$ and it fails to meet the 70% b-tagging requirement. The two regions are enhanced in the tH contribution and $t\bar{t}+ \geq 1b$ and they are referred to as SR and CR($t\bar{t}+ \geq 1b$), respectively. The SR selection requires at least one forward jet and at most one central jet failing to meet the 70% b-tagging requirement, while for CR($t\bar{t}+ \geq 1b$) no forward jet should be present and at least two central jets must fail to meet the 70% b-tagging requirement. table 4 summarises the selections applied to define the SR and CR.

JHEP10(2025)093

6.2 2ℓ SS channel

The 2ℓ SS preselection region is defined by requiring exactly two *Tight* light leptons (electrons or muons) with the same electric charge. For the selected events, the leading lepton must have $p_{\mathrm{T}} > 27\,\mathrm{GeV}$ and the sub-leading lepton must have $p_{\mathrm{T}} > 20\,\mathrm{GeV}$.

The number of jets with $|\eta| < 4.5$ is required to be between one and six. The 70% working point of the `DL1r` tagger is used to select b-jets. The number of b-jets is required to be between one and three.

As shown in Table 3, the dominant source of background in the preselection region stems from $t\bar{t}$ followed by $t\bar{t}W$ and $Z+$jets production. Both $t\bar{t}$ and $Z+$jets enter the preselection region if a non-prompt or fake lepton is in the event or if the charge of one of the electrons is wrongly measured. The rest of the background processes consists of $t\bar{t}W$, $t\bar{t}Z$ or diboson production.

Four binary-classifier BDTGs are trained in the 2ℓ SS channel, each targeting the tHq signal or one of the main background processes ($t\bar{t}$, $t\bar{t}W$, and diboson) against the sum of the remaining three classes. These classifiers are used to define mutually exclusive enriched regions. In total, 52 variables were used in the training: 28, 19, 29 and 27 for the four BDTGs, respectively. These variables include kinematic and topological quantities that characterise the signal and its main backgrounds. The most important variables include the charge of the two leptons, H_{T},[7] the number of b-tagged jets, the invariant masses and angular separations of pairs of reconstructed jets and leptons (see table 6). The charge of the two leptons is highly discriminating, since the tHq process favours positively charged top quarks as explained before, while dominant backgrounds such as $t\bar{t}$, $t\bar{t}H$, and diboson production are charge-symmetric. Invariant masses of leptons and jets also provide discriminating power, as the decay kinematics and spatial correlations in the tHq topology produce characteristic patterns between leptons from top-quark decays and the forward spectator jet or b-jet. In contrast, in backgrounds such as $t\bar{t}$, $t\bar{t}H$, and dibosons, these correlations are absent or substantially altered due to additional heavy resonances or differing event topologies. The other variables further exploit differences in global event activity, jet and b-jet multiplicities, and the more isotropic topology of $t\bar{t}$, $t\bar{t}W$ and $t\bar{t}Z$ compared to the forward — backward structure of tHq events. The complete lists of input variables can be found in section A.

Five regions are defined in the 2ℓ SS channel: the SR is designed to maximise the tHq contribution, while the CRs target the main background processes. The regions are defined using a mixture of requirements on the BDTGs outputs, selecting a given flavour for the two leptons in the final state or cutting on event kinematic variables such as H_{T} or leptons invariant masses. The material- or internal-conversion cuts defined in section 5 are applied to all the electrons in all regions, except for the conversion control region, CR(e_{conv}), where this requirement is inverted. The regions described here are orthogonal to one another. table 4 summarises the selections applied to define the SR and CRs. Three CRs are defined to derive mis-identified leptons background: CR(μ_{HF}), CR(e_{HF}) and CR(e_{conv}). The CR(e_{conv}) is enriched in events with one electron stemming from γ-conversion (e_{conv}), while CR(μ_{HF})

[7] The H_{T} variable is defined performing the scalar sum of the transverse momentum of all the reconstructed objects in the final state, in this case jets and leptons. The $H_{\mathrm{T}}(\ell)$ variable instead is computed including only leptons.

JHEP10(2025)093

and CR(e_{HF}) are enriched in contributions from non-prompt electrons or muons stemming from heavy-flavoured (containing a b- or c-quark) hadron decay, e_{HF} and μ_{HF}, respectively. One CR is defined to target the irreducible $t\bar{t}W$ background.

6.3 3ℓ channel

The 3ℓ preselection region is defined by requiring the presence of exactly three *Tight* light leptons (electrons or muons). The sum of the leptons' charges is required to be ± 1. The light leptons are ordered based on their p_{T}, with the leading lepton having $p_{\text{T}} > 27\,\text{GeV}$, the sub-leading lepton required to have $p_{\text{T}} > 20\,\text{GeV}$ and the softest lepton to have $p_{\text{T}} > 10\,\text{GeV}$. The number of jets with $|\eta| < 4.5$ is required to be between one and six. The 70% working point of the `DL1r` tagger is used to select b-jets. The number of b-jets is required to be between one and three. As shown in Table 3, the dominant background contributions in the preselection region arise from diboson, $t\bar{t}Z$, and $t\bar{t}$ processes.

Three binary-classifier BDTGs are trained in the 3ℓ channel, each targeting the tHq signal or one of the main background processes ($t\bar{t}$ and $t\bar{t}W$) against the sum of the remaining two classes. These classifiers are used to define regions enriched in tHq and in each of the background processes included in the training. A total of 50 input variables are used in the training: 22, 19, and 30 for each of the three classifiers, respectively. These variables include kinematic and topological quantities that characterise the signal and its main backgrounds. The most important ones include the invariant masses of leptons, the p_{T} of leptons, the sum of leptons' charges, and the multiplicity of central and b-tagged jets. The dilepton invariant masses are powerful discriminants, since in backgrounds such as $t\bar{t}Z$ and diboson production leptons often originate from on-shell Z bosons, producing peaks around the Z-boson mass, while in tHq events they mainly arise from W-boson decays and do not show such resonant structures (see table 6). The sum of leptons' charges is also discriminant similarly to the other two channels. The lepton transverse momenta provide additional separation, as backgrounds with extra vector bosons typically yield harder leptons than those expected in tHq events. Finally, the number of b-tagged jets provides discrimination, as tHq process typically features fewer central and b-jets than backgrounds such as $t\bar{t}$, $t\bar{t}H$, $t\bar{t}W$, and $t\bar{t}Z$. The complete lists of input variables can be found in section A.

Five orthogonal regions are defined in the 3ℓ channel: one SR to maximise the tHq contribution, three CRs to estimate in data the mis-identified leptons background and one CR to estimate the $t\bar{t}W$ background. The regions are defined using a mixture of requirements on the BDTGs outputs, the number of jets and invariant masses. The material- and internal-conversion requirements defined in section 5 are applied to all the electrons in all regions, except for one region where this requirement is inverted to enhance the contribution of the process targeted by that region. Table 4 summarises the selection criteria applied to define the SR and CRs.

7 Background estimation

The background processes satisfying the SR and CR selections are categorised into irreducible and reducible backgrounds. Irreducible backgrounds arise from processes that have an identical number of prompt leptons from weak boson or leptonic τ-lepton decays, and a

JHEP10(2025)093

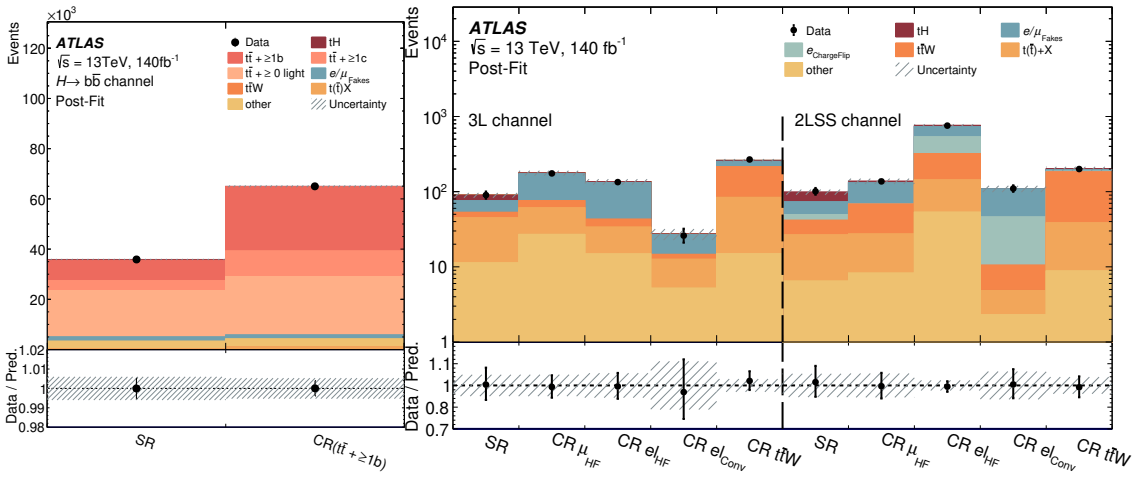

(a) (b)

Figure 2. The data and estimated signal-plus-background yields in the SR and CRs of the (a) $H \to b\bar{b}$ channel and (b) 3ℓ and 2ℓ SS channels. The term e/μ_{Fakes} refers to backgrounds from non-prompt or misidentified leptons, namely contributions from heavy-flavour decays and photon conversions. Both signal and background events are estimated with a likelihood fit to data ("Post-Fit"), as described in sections 7 and 9. The uncertainty band includes statistical and systematic contributions.

similar number of b-jets as the targeted signal. Reducible backgrounds arise instead from particle mis-identification in the detector, mis-assigning of the lepton charge or mis-tagging a charm or light-flavoured jet as a b-jet. Fake and non-prompt leptons can originate from different sources like decays of bottom or charm mesons, photon conversions or light jets creating accidentally a detector signature similar to a light lepton.

The contribution of irreducible backgrounds is generally derived through the respective simulated samples and constrained in CRs where needed. A data-driven estimate is provided for most of the reducible backgrounds and for background processes where the MC prediction is not in good agreement with the data. Figure 2 compares the total data yields in all SRs and CRs as defined in section 6 for the three analysis channels to the signal plus background predictions obtained by the likelihood fit to data described in section 7 and section 9.

7.1 Background estimation in the $H \to b\bar{b}$ channel

As already discussed in section 6.1, the main source of background in the $H \to b\bar{b}$ channel consists of $t\bar{t}$ +jets events. The production of the $t\bar{t}$ in association with heavy flavour jets is known to be not well modelled by the simulation. For this reason, simulated $t\bar{t}$ +jets events are split into $t\bar{t}+ \geq 1b$, $t\bar{t}+ \geq 1c$ and $t\bar{t}+ \geq 0$ light categories and the CR($t\bar{t}+ \geq 1b$) is included in the fit to constrain its contribution from data. The normalisation factor of the $t\bar{t}+ \geq 1b$ background found in the combined fit to data is $k(t\bar{t}+ \geq 1b) = 1.24^{+0.17}_{-0.15}$. The $t\bar{t}+ \geq 1c$ predicted yield has no dedicated correction factor due to the difficulty in building a pure CR. Instead, an overall uncertainty on the $t\bar{t}+ \geq 1c$ prediction is included in the fit as described in section 8.2. The remaining irreducible backgrounds are all estimated by using the MC predictions. The small contribution of reducible background from non-prompt and fake leptons is estimated using the matrix-method technique described in ref. [119].

JHEP10(2025)093

7.2 Background estimation in the 2ℓ SS and 3ℓ channels

In the 2ℓ SS channel, the main irreducible backgrounds originate from $t\bar{t}W$ production, having final states and kinematic properties inherently similar to the tHq signal. Smaller contributions originate from the following rare processes: tZq, $t\bar{t}H$ and tWZ production. Backgrounds with prompt leptons are directly estimated from simulation using the samples described in section 4, except for $t\bar{t}W$, for which the normalisation is fitted. In the 3ℓ channel instead, the main irreducible backgrounds originate from diboson production, $t\bar{t}Z$ and tZq. Other minor irreducible backgrounds are triboson, other Higgs-boson production modes such as ggH, VBF (qqH) and VH, and $t\bar{t}t$ and $t\bar{t}t\bar{t}$. A CR dedicated to the $t\bar{t}W$ background, CR($t\bar{t}W$), is defined in both the 2ℓ and 3ℓ channel to better constrain its contribution from data. The normalisation factor associated with the $t\bar{t}W$ background as estimated from the combined fit is found to be $k(t\bar{t}W) = 1.09 \pm 0.11$.

The most important sources of reducible background in both the 2ℓ SS and 3ℓ channels are the $t\bar{t}$, W/Z+jets and single-top-quark processes. These processes can satisfy the preselection requirement due to the presence of a fake or non-prompt lepton in the final state. These backgrounds are estimated from simulation, with the normalisation determined by the likelihood fit through the use of the dedicated CRs introduced earlier. The non-prompt leptons in the simulated event samples are labelled according to whether they originate from heavy-flavour or light-flavour hadron decays, or from a material/internal conversion. The light-flavour category is negligible. In the 2ℓ SS channel, normalisation factors are extracted to be $k(e_{\text{conv}})_{2\ell\,\text{SS}} = 1.20\pm0.47$, $k(e_{\text{HF}})_{2\ell\,\text{SS}} = 0.55\pm0.65$ and $k(\mu_{\text{HF}})_{2\ell\,\text{SS}} = 0.80\pm0.32$. In the 3ℓ channel, the normalisation factors extracted are $k(e_{\text{conv}})_{3\ell} = 0.82\pm0.59$, $k(e_{\text{HF}})_{3\ell} = 1.47\pm0.42$ and $k(\mu_{\text{HF}})_{3\ell} = 0.91 \pm 0.24$.

Electrons with mis-identified electric charge ("charge-flip"), with one electron either undergoing hard bremsstrahlung followed by an asymmetric conversion ($e^{\pm} \to e^{\pm}\gamma^* \to e^{\pm}e^{+}e^{-}$) or having mismeasured track curvature, represent another source of reducible background. This contribution is negligible in the 3ℓ channel and sizeable in the 2ℓ SS channel. The muon charge misassignment rate is negligible in the p_{T} range relevant to this analysis. The electron charge misassignment rate is measured in data by using samples of $Z \to e^{+}e^{-}$ events reconstructed as either same-charge pairs or opposite-charge pairs, with the non-Z background subtracted via a sideband method utilising events outside the Z-boson mass window. The charge misassignment rate is extracted from the ratio of the numbers of same-charge and opposite-charge events close to the Z-boson mass through a likelihood approach taking into account the possibility that both electron charges are misassigned. The rates are parameterised as a function of electron p_{T} and $|\eta|$, and vary from about 10^{-5} for low-p_{T} electrons ($17 \le p_{\text{T}} \le 50\,\text{GeV}$) with $|\eta| \le 1.37$, to about 4×10^{-3} for high-p_{T} electrons ($p_{\text{T}} \ge 100\,\text{GeV}$) with $2 \le |\eta| \le 2.47$. To estimate the charge-flip background in each 2ℓ SS region, the measured charge misassignment rate is applied to data events satisfying the requirements of the region, except that the two leptons must have opposite charges.

JHEP10(2025)093

8 Sources of systematic uncertainty

Different sources of systematic uncertainty are considered for this measurement. They are grouped into three categories: instrumental uncertainties that affect physics object reconstruction; modelling uncertainties relevant for MC simulation-based estimations; and uncertainties affecting the estimate of fake and non-prompt lepton backgrounds. All uncertainties include both shape and normalisation effect, unless otherwise stated in their description.

The description of the sources of systematic uncertainties is organised as follows: first, those common to all three channels are presented, followed by sections addressing uncertainties specific to the $H \to b\bar{b}$ channel and the 2ℓ SS and 3ℓ channels.

8.1 Common systematic uncertainties

Instrumental systematic uncertainties considered are related to: trigger efficiency; lepton reconstruction, identification and isolation efficiencies; lepton calibration; jet calibration; JVT and fJVT efficiencies; b-tagging efficiency; $E_{\mathrm{T}}^{\mathrm{miss}}$ calibration. The experimental systematic uncertainties are applied either as an event-reweighting correction factor or as a rescaling or smearing of the object energy and momentum for scale and resolution uncertainties.

Uncertainties associated with the lepton selection arise from the trigger, reconstruction, identification and isolation efficiencies, and the lepton momentum scale and resolution as described in refs. [98–100]. Uncertainties on the efficiency of the BDT designed to reject non-prompt leptons are estimated through a $Z \to \ell\ell$ tag-and-probe method and cover contributions related to the $Z(\to \ell\ell)$+jets MC modelling, the template cut/shape, the $m_{\ell\ell}$ window, the tag-and-probe lepton selections, the multijet background, the non-prompt lepton background, the luminosity, the cross-sections of the considered processes, and the limited number of events in simulation and data.

Uncertainties associated with jet reconstruction and calibration arise from the jet energy scale (JES), jet energy resolution (JER) and the JVT/fJVT requirements. The JES uncertainty accounts for contributions from composition of jet flavour, η-intercalibration, punch-through, single-particle response, calorimeter response and pile-up making up for a total of 31 independent variations [106]. The JER is measured separately for data and MC using an in-situ technique and the associated uncertainties are split into 13 components [106]. The JVT efficiency is measured in data and correction factors are applied to simulated events to correct the simulated performance. The uncertainty associated with the JVT performance is obtained by varying the correction factors [107].

The uncertainty in $E_{\mathrm{T}}^{\mathrm{miss}}$ results from the propagation of the uncertainties in the energy scales and resolutions of photons, leptons and jets, and from the modelling of its soft term [120].

The efficiency of the b-tagging algorithm is measured for each jet flavour using control samples in data and in simulation. From these measurements, correction factors are derived to correct the tagging rates in the simulation. For b-jets, the correction factors and their uncertainties are estimated from data using dileptonic $t\bar{t}$ events [110, 121]. For c-jets, they are derived from jets arising from W boson decays in $t\bar{t}$ events [122]. For light-flavour jets, the correction factors are derived from $Z+$jets events [123]. Uncertainties from sources

JHEP10(2025)093

affecting the b-tagging efficiencies of b-jets, c-jets and light-jets are evaluated as a function of jet p_{T}, including bin-to-bin correlations.

The uncertainty in the reweighting of the MC pile-up distribution to match the distribution in data is evaluated by varying the reweighting factors and has a very small impact on either the combined or individual results. The uncertainty in the combined 2015–2018 integrated luminosity is 0.83% [124], obtained using the LUCID-2 detector for the primary luminosity measurements, complemented by measurements using the inner detector and calorimeters.

Systematic uncertainties in the tHq and tWH MC predictions due to missing higher-order QCD corrections in the modelling are estimated by doubling and halving the μ_{r} and μ_{f} scales chosen for the nominal sample. A systematic uncertainty due to the choice of the PS model is estimated as the relative difference between the Powheg +Pythia 8 and Powheg +Herwig 7 predictions and applied to the nominal predictions. An uncertainty is considered on the cross-section summing in quadrature the contributions from QCD scale, flavour scheme, PDF and α_s from a NLO QCD prediction: the values obtained are equal to 15.4% and 9.2% for tHq and tWH, respectively [52, 53].

The uncertainty in the $t\bar{t}$ modelling due to the choice of the h_{damp} parameter, which controls the resummation of higher-order terms, is estimated by comparing the nominal prediction with a Powheg +Pythia 8 sample where the parameter is set to $3 \times m_{\mathrm{top}}$. Reweighted events are used to assess the impact of ISR simulation within the nominal Powheg +Pythia 8 simulation: μ_{f} and μ_{r} scales are varied by 0.5 (high radiation) or 2.0 (low radiation) together with the PS tune `Var3c` [51]. The μ_{r} and μ_{f} scales are varied in both the hard-scatter process and PS and they are modified independently. The hadronisation model uncertainty and other non-perturbative effects in the PS are evaluated by comparing the nominal sample with Powheg+Herwig 7.2.1. The PS scale uncertainty is evaluated using the `Var3c` eigentune variation of the A14 tune [125]. The impact of FSR is evaluated by varying the renormalisation scale for PS emissions by factors of 0.5 and 2.0, using reweighted events.

The uncertainty in $t\bar{t}H$ modelling due to the ISR is estimated by using weights in the ME calculation and the PS. The μ_{r} and μ_{f} scales are varied, and ISR α_{s} variations are evaluated similarly to the $t\bar{t}$ process. The impact of FSR is evaluated using PS weights that vary the renormalisation scale for QCD emission in the FSR by a factor of 0.5 and 2.0. Additionally, uncertainties in the ME (PS, hadronisation and underlying-event modelling) are estimated by comparing the nominal Powheg +Pythia 8 MC simulation with aMC@NLO +Pythia 8 (Powheg +Herwig 7). The predicted $t\bar{t}H$ cross-section uncertainty is $^{+5.8\%}_{-9.2\%}$(scale) + 3.6%(PDF+α_{s}) [52] and the two components are considered uncorrelated.

Systematic uncertainties in the $t\bar{t}W$ MC predictions due to missing higher-order QCD corrections in the modelling are considered. To estimate the uncertainty due to ambiguities in the ME and PS algorithm and parameter choices, the nominal Sherpa prediction is compared with the prediction of the MadGraph5_aMC@NLO +Pythia 8 FxFx sample described in section 4. In addition, a dedicated PS model uncertainty is estimated as the relative difference between the Powheg +Pythia 8 and Powheg +Herwig 7 predictions and applied to the nominal $t\bar{t}W$ prediction. Modelling uncertainties due to μ_{r} and μ_{f} scales [126], and the amounts of ISR/FSR are evaluated similarly to the $t\bar{t}$ and $t\bar{t}H$ processes. Uncertainties in the PDF modelling are included by varying the value of α_{s} and using different PDF sets.

JHEP10(2025)093

The predicted $t\bar{t}W$ cross-section uncertainty is $^{+9.7\%}_{-10.8\%}$(scale) + 7.2%(PDF+α_s) [78] and the two components are considered uncorrelated. The uncertainty on the theoretical prediction of the $t\bar{t}W$ cross-section is dropped in the 3ℓ and 2ℓ SS channels as the normalisation of this background is estimated from data.

Uncertainties due to missing higher orders in QCD are estimated for $t\bar{t}Z$ production by varying the nominal μ_r and μ_f scales are evaluated similarly to the $t\bar{t}$, $t\bar{t}H$ and $t\bar{t}W$ processes. Uncertainties in additional-jet modelling are estimated with ISR α_s variations taken from the A14 tune. To estimate the uncertainty due to ambiguities in the ME and PS algorithm and parameter choices, the nominal prediction is compared with Sherpa. PS, hadronisation and underlying-event modelling uncertainties are estimated by comparing the nominal aMC@NLO +Pythia 8 MC simulation with MadGraph5+Herwig 7. The predicted $t\bar{t}Z$ cross-section uncertainty is $^{+9.6\%}_{-11.3\%}$(scale) + 4%(PDF+α_s) [52].

Systematic uncertainties due to missing higher-order QCD corrections are also considered for the three single-top-quark processes: t-channel, tW and s-channel. The uncertainty due to the choice of the hadronisation model and the other non-perturbative aspects of the PS is evaluated comparing the nominal prediction with that provided by the Powheg+Herwig 7.1.6 simulation. An uncertainty is also attributed to the choice of the Powheg approach to perform the matching between the hard-scatter and the PS. This uncertainty is estimated comparing the nominal Powheg+Pythia 8 prediction with the aMC@NLO+Pythia 8 simulation for the tW process, and the Powheg+Herwig 7.1.6 with the aMC@NLO+Herwig 7.1.6 prediction for the t-channel and s-channel. An additional uncertainty is quoted for the tW process to estimate the difference between the DS and DR schemes. Finally, a conservative 5% uncertainty on the theoretical cross-section of single-top-quark processes (t-channel, tW and s-channel) is considered in the $H \to b\bar{b}$ channel. In the 3ℓ channel, a 5.4% uncertainty on the tW production cross-section [127] is considered. For the 2ℓ SS channel, where single-top-quark contributions are negligible, no uncertainty from these processes is included.

Uncertainties in diboson modelling due to missing higher orders in QCD are estimated by varying the nominal μ_r and μ_f scales by factors of 0.5 and 2.0. In addition, a normalisation uncertainty of 24.5% is considered, as a result of adding in quadrature the theory uncertainty (5%) and 24% per additional jet, accordingly to the Berends-Giele scaling [128].

For minor backgrounds such as Z + jets, W + jets, tZq, tWZ, rare top-quark ($t\bar{t}t$ and $t\bar{t}t\bar{t}$) and other Higgs-boson production modes (ggH, VBF and VH) only the theoretical uncertainty on the predicted cross-section is considered. A normalisation uncertainty of 35% and 40% is considered for the Z + jets and W + jets processes in the $H \to b\bar{b}$ channel only. This is the result of adding in quadrature the theory uncertainty (4% for W + jets and 5% for Z + jets) and 24% per additional jet. In the 2ℓ SS and 3ℓ channels, the normalisation of these processes is derived from data as part of the fake and non-prompt leptons estimate. The predicted tZq cross-section uncertainty is $^{+7.7\%}_{-7.9\%}$(scale) + 0.9%(PDF+α_s) [49] and the two components are considered uncorrelated. The contribution of the tWZ, rare top-quark and other Higgs-boson production processes is small in all the channels, for this reason a conservative 50% uncertainty on their cross-section is applied.

JHEP10(2025)093

8.2 Channel-specific uncertainties: $H \to b\bar{b}$ channel

In the $H \to b\bar{b}$ channel, the effect of every modelling uncertainty associated to the $t\bar{t}$ simulation are considered independently for the three categories, $t\bar{t}+ \geq 1b$, $t\bar{t}+ \geq 1c$ and $t\bar{t}+ \geq 0$ light. In the $t\bar{t}+ \geq 1b$ case, since its yield is estimated from data, the normalisation of alternative samples is rescaled to match the nominal prediction in the preselection region. In addition to the $t\bar{t}$ modelling uncertainties common to all the channels, one from the NLO matching scheme in the $t\bar{t}$ simulated sample is also included comparing the nominal sample to the $p_{\mathrm{T}}^{\mathrm{hard}}$ varied one. A modelling uncertainty due to the differences between the nominal $t\bar{t}+ \geq 1b$ simulation in the 5FS and an alternative $t\bar{t} + b\bar{b}$ simulation in the 4FS is considered [129]. The uncertainty is applied independently to three sub-components of the $t\bar{t}+ \geq 1b$ background, defined according to the number of hadrons matched to the additional jet produced in association with the top-quark pair. The three sub-components are:

- $t\bar{t}$ $+1b$, if one additional jet in the event is matched to a single b-hadron,
- $t\bar{t}$ $+1B$, if one additional jet in the event is matched to a gluon splitting $g \to b\bar{b}$,
- $t\bar{t}$ $+2b$, if two additional jets in the event are matched to a single b-hadron each.

A 50% uncertainty on the normalisation of the $t\bar{t}+ \geq 1c$ is also considered in the fit model [130]. Finally, a theoretical uncertainty of 6% is applied on the $t\bar{t}+ \geq 0$ light normalisation as estimated in a dedicated validation region.

A systematic uncertainty is included to account for the difference between lepton fake rates originating from heavy-flavour decays versus those from misidentified jets. This uncertainty is evaluated separately for muons and electrons and its normalisation component contributes approximately 10% for muons and 30% for electrons.

8.3 Channel-specific uncertainties: 2ℓ SS and 3ℓ channels

For both the 2ℓ SS and 3ℓ channels, all the common $t\bar{t}$ modelling uncertainties are considered, as the $t\bar{t}$ simulation is used to estimate non-prompt lepton backgrounds originating from heavy-flavour decays and conversions. The modelling uncertainties associated to $t\bar{t}$ simulation are considered correlated among the various non-prompt leptons categories and between the 2ℓ SS and 3ℓ channels. Their effect is shape only as the normalisation of these backgrounds is estimated from data. In addition to the $t\bar{t}$ modelling uncertainties common to all the channels, one from the NLO matching scheme in the $t\bar{t}$ simulated sample is also included comparing predictions from Powheg+Herwig 7.1.3 and MadGraph5_aMC@NLO+Herwig 7.1.3 simulations. A conservative uncertainty of 50% is assigned to a small fraction of events, roughly 3% in the preselection region, where the origin of the non-prompt lepton could not be identified.

In the 2ℓ SS channel a systematic uncertainty of 10%–60% is assigned to the estimation of background from electrons with misidentified charge as described in section 7.2.

9 Results

A maximum-likelihood fit to all bins in the three SRs and the nine CRs (see table 4) is performed to simultaneously determine the background and the tH signal yields in the data.

JHEP10(2025)093

The discriminant variable used in the SRs is defined as follows: for the $H \to b\bar{b}$ channel, it is the BDTG response for tHq signal-like events, P(tHq); for the 2ℓ SS and 3ℓ channels, it is given by the output of the BDTG trained to target tHq events, BDT(tHq). In the CR($t\bar{t}+ \geq 1b$), the discriminant is the BDTG response for $t\bar{t}+ \geq 1b$-like events, P($t\bar{t}+ \geq 1b$). The H_{T} variable is used in all the CRs of the 2ℓ SS channel and in the 3ℓ channel control region targeting the $t\bar{t}W$ process. Finally, the $\Delta R(\ell_C, \ell_A + \ell_B)$ variable[8] is used in the CR(μ_{HF}) and CR(e_{HF}) of the 3ℓ channel while the BDTG response of the binary classifier targetting $t\bar{t}$ is used in the CR(e_{conv}).

The likelihood function $\mathcal{L}(\mu, \vec{k}, \vec{\theta})$ is constructed as a product of Poisson probability terms over all bins considered in the measurement, and depends on the following: the signal-strength parameter, μ, defined as a multiplicative factor applied to the predicted yield for the tHq and tWH signal processes; $\vec{k}$, the normalisation factors for several backgrounds; and $\vec{\theta}$, a set of nuisance parameters (NPs) encoding systematic uncertainties in the signal and background expectations [131]. Systematic uncertainties can impact the estimated signal and background rates, the migration of events between categories, and the shape of the fitted distributions; they are summarised in section 8. Both μ and $\vec{k}$ are treated as free parameters in the likelihood fit. The NPs $\vec{\theta}$ allow variations of the expectations for signal and background according to the systematic uncertainties, subject to Gaussian constraints in the likelihood fit. Their fitted values represent the deviations from the nominal expectations that are needed to provide the best fit to the data. Statistical uncertainties in each bin due to the limited size of the simulated event samples are taken into account with dedicated parameters, using the Beeston-Barlow "lite" technique [132]. All systematic uncertainties are fully correlated across channels, except for those that are specific to a given channel.

The best-fit value of the tHq and tWH signal strength, μ_{tH}, is:

$$\mu_{tH} = 8.1 \pm 2.6 \text{ (stat.)} \pm 2.0 \text{ (syst.)}.$$

This value corresponds to a measured value of the cross-section of $\sigma(tH) = 720 \pm 270$ fb. Figure 3(a) shows the signal strength measured in the different channels together with their combined value.

The compatibility of the signal strength evaluated from the different channels and the combined value is assessed by performing a likelihood ratio test and a p-value of 91% is obtained. The significance of the observed (expected) signal above the background-only expectation is 2.8 (0.4) standard deviations. The significance of the observed signal compared with the signal-plus-background hypothesis is instead 2.4. In the absence of a significant deviation from the background-only hypothesis, a 95% CL upper limit on the signal strength is set at 13.9 (6.1) times the observed (expected) SM prediction, as shown in figure 3(b). To quantify how well the fit model describes the data, a goodness-of-fit test is performed. The test consists of comparing the nominal model to a so-called saturated model [133], one constructed with enough degrees of freedom to describe the data perfectly. The probability obtained for the goodness-of-fit test is 98%, confirming excellent fit quality.

[8] Among the three leptons in the event in the 3ℓ channel, the lepton with the highest p_{T} is called ℓ_A, the one with the second highest p_{T} is called ℓ_B while the lepton with the softest p_{T} is called ℓ_C. The variable $\Delta R(\ell_C, \ell_A + \ell_B)$ is defined computing the ΔR value of the ℓ_C lepton with the system composed by summing the four vectors of leptons ℓ_A and ℓ_B.

JHEP10(2025)093

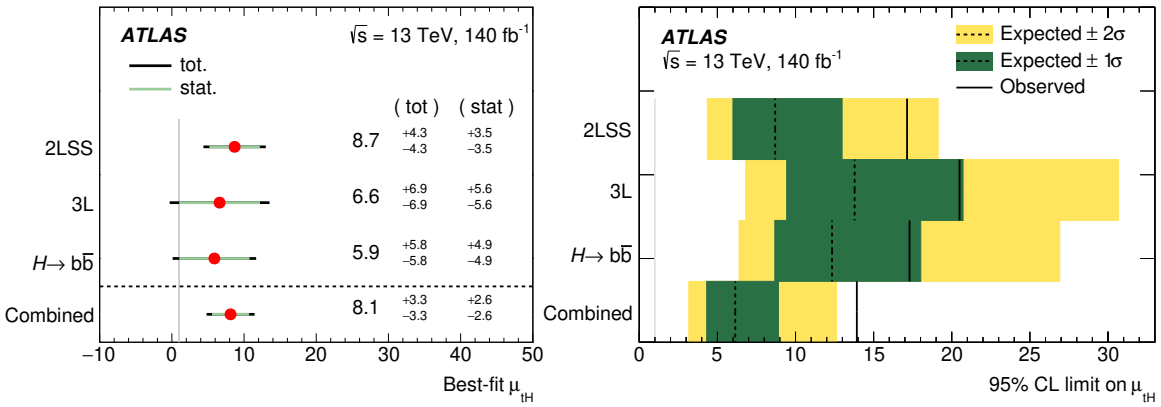

(a) (b)

Figure 3. The (a) fitted values of the μ_{tH} and (b) 95% CL upper limits in the individual channels and in the combined measurement. The values reported for the individual channels are obtained by fitting μ_{tH} separately for each channel, whereas the combined measurement is derived by simultaneously fitting all channels together. The observed limits are shown (solid black lines), together with the expected limits under the SM hypothesis (dotted black lines). A grey line is added in correspondence of the μ_{tH} equal to one. In the case of the expected limits, the one- and two-standard-deviation uncertainty bands are also shown.

The contributions from the different sources of uncertainty affecting the measured μ_{tH} are evaluated using the covariance-matrix decomposition method [134] and are shown, grouped by category, in table 5. The leading source of uncertainty is the statistical uncertainty. The largest source of systematic uncertainty is the theoretical uncertainty with the biggest contribution coming from the uncertainty on the signal prediction and $t\bar{t}$. Among the experimental uncertainties, the leading contribution stems from the JES and JER.

The impact of the top 20 NPs in the fit on μ_{tH} is shown in figure 4 for the SM scenario and it is assessed as follows: if the uncertainty on the parameter is σ_k, the uncertainty on μ_{tH} is σ_μ, and the correlation between the parameter and μ_{tH} is $\rho_{k,\mu}$, the impact is computed as $\sigma_k \rho_{k,\mu} \sigma_\mu$. The plot shows the measured NPs and their agreement with the expected values. The most constrained NP corresponds to the PS uncertainty in the $t\bar{t}+ \geq 0$ light category. All pulls are below one standard deviation with the strongest pull stemming from the PS uncertainty on the $t\bar{t}+ \geq 1b$ category, suggesting a mild mis-modelling of this contribution in the $H \to b\bar{b}$ channel. Overall, the lack of significant pulls or constraints in the NPs indicates a good agreement between data and the fit model, supporting the robustness of the fit and the reliability of the extracted signal strength.

The observed and expected yields in the three SRs and the nine CRs after the combined likelihood fit under the signal-plus-background hypothesis are compared with data in figures 5 and 6. Detailed tables showing pre-fit and post-fit yields for all regions are reported in section B. A good agreement between data and prediction is found in all the regions.

Additional measurements are performed using the ITC hypothesis ($\kappa_t = -1$) as signal model. The best-fit value of the tH signal strength under the ITC hypothesis is:

$$\mu_{tH}(\kappa_t = -1) \;=\; 1.2 \;\pm\; 0.4 \;\;(\text{stat.}) \;\pm\; 0.5 \;\;(\text{syst.})\,.$$

JHEP10(2025)093

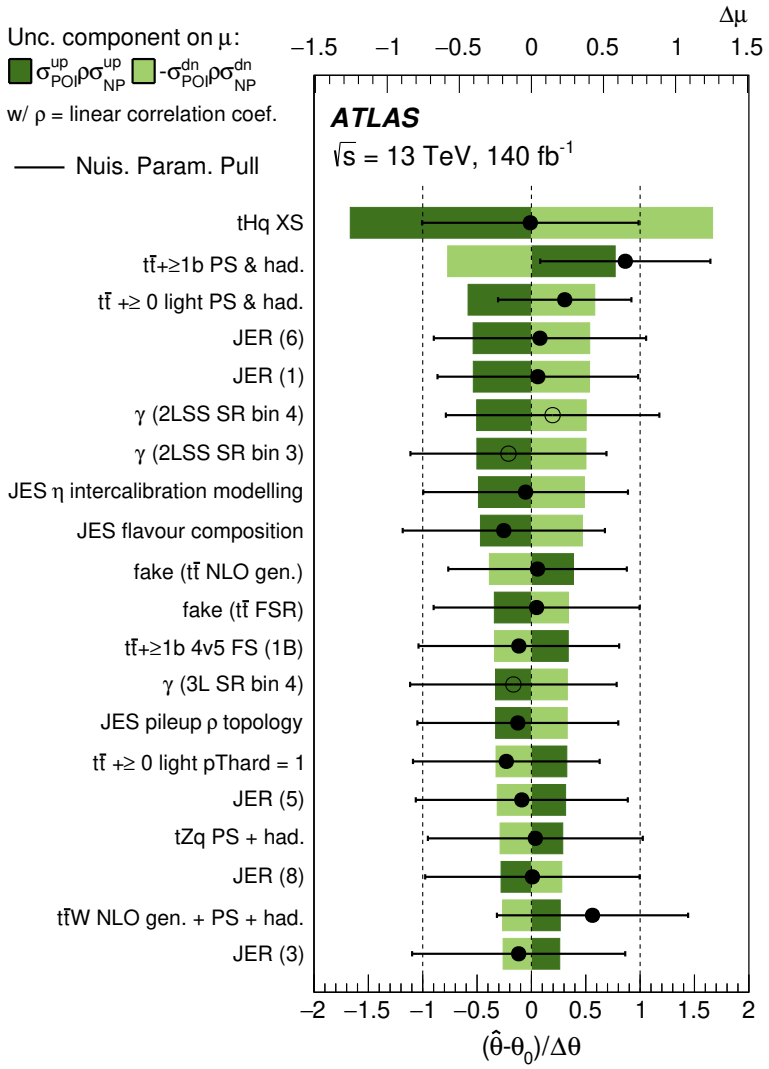

Figure 4. The impact of the top 20 most important systematic uncertainties on the fitted μ_{tH} in the SM scenario. The uncertainties are listed in decreasing order of their impact on μ_{tH}. The filled boxes show the relative impact on μ_{tH}, referring to the top x-axis. The points, referring to the bottom x-axis, show the deviations on the fitted NPs $\boldsymbol{\theta}_0$ from their nominal values, expressed in terms of standard deviations with respect to their nominal uncertainties. The associated black uncertainty bars show the fitted uncertainties of the NPs, relative to their nominal uncertainties. Filled markers refer to systematic uncertainties, while empty black markers refer to statistical uncertainties in the MC simulation in a given bin of an analysis region and they are labelled as γ. The results shown are extracted from the fit including all channels.

JHEP10(2025)093

Source	Impact on μ_{tH}			
	Combination	$H \to b\bar{b}$	2ℓ SS	3ℓ
Theory uncertainties (modelling)	1.69	2.97	1.64	2.63
Signal	1.26	0.88	1.33	1.22
$t\bar{t}+ \geq 1b$	0.70	2.57	—	—
$t\bar{t}+ \geq 0$ light and $t\bar{t}+ \geq 1c$	0.54	1.04	—	—
$t\bar{t}\,W$	0.23	<0.01	0.52	0.18
$t\bar{t}$	0.43	—	0.52	1.95
Rest of backgrounds	0.50	0.60	0.63	1.23
Experimental uncertainties	1.07	0.95	1.61	2.61
JES and JER	1.00	0.51	1.57	2.51
Non-prompt lepton bkg. modelling	0.25	0.59	0.22	0.07
Flavour tagging	0.17	0.52	0.13	0.17
Muons	0.12	< 0.01	0.12	0.40
$E_{\mathrm{T}}^{\mathrm{miss}}$	0.10	0.04	0.20	0.03
Pile-up	0.12	0.04	0.05	0.44
Electrons	0.10	0.07	0.11	0.32
Charge mis-identification	0.07	—	0.06	—
JVT and fJVT	0.04	0.10	0.11	0.06
Luminosity	0.09	0.09	0.10	0.14
Total systematic uncertainty	2.01	3.11	2.30	4.06
Statistical uncertainty	2.56	4.87	3.5	5.60
Normalisation factors	0.50	0.04	0.84	0.73
MC statistics	0.64	< 0.01	1.05	1.67
Total	3.3	5.8	4.3	6.9

Table 5. The absolute contribution of the main sources of uncertainty on the signal strength μ_{tH}. Some NPs with small impacts are grouped into categories, with the impact of the category being the quadrature sum of individual parameter impacts. Indentation is used to denote subcategories.

The observed and expected yields in the three SRs after the combined likelihood fit under the signal-plus-background hypothesis are compared with data in figure 7 for the ITC hypothesis.

The measured inverted-coupling signal strengths in the individual channels and the combined result are summarised in figure 8(a). The corresponding observed (expected) 95% CL exclusion limit is 2.4 (1.2), which is shown in figure 8(b) for both the individual channels and the combined measurement. The goodness-of-fit test probability for the $\kappa_t = -1$ scenario fit is 95%. In contrast to the SM case, under the ITC hypothesis the channel with the highest sensitivity is the $H \to b\bar{b}$ channel, overtaking the multi-lepton channels despite its modest signal-to-background ratio in the SM case (see section B). This inversion arises from the strong enhancement of the tHq cross-section together with the discriminating power of key variables in the $H \to b\bar{b}$ channel, such as the number of jets and number of jets associated with the reconstructed hadronic top quark from different $t\bar{t}$ reconstruction

JHEP10(2025)093

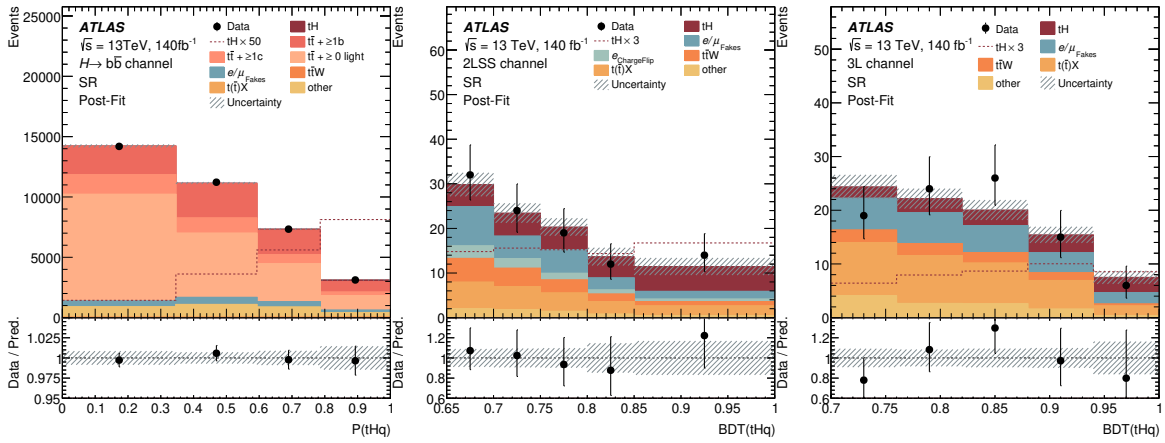

(a) (b) (c)

Figure 5. Comparison between data and the signal-plus-background prediction for the event yields in the (a) $H \to b\bar{b}$, (b) 2ℓ SS and (c) 3ℓ SRs. The term e/μ_{Fakes} refers to backgrounds from non-prompt or misidentified leptons, namely contributions from heavy-flavour decays and photon conversions. The SM signal and the background contributions after the likelihood fit to data ("Post-Fit") under the signal-plus-background hypothesis are shown as filled histograms. A dashed red line is added to the plot to show the signal contribution normalised to the measured value multiplied by 50 for the $H \to b\bar{b}$ channel and by 3 for the 2ℓ SS and 3ℓ channels. The ratio of the data to the total post-fit prediction ("Pred.") is shown in the lower panel. The combined statistical and systematic uncertainty in the prediction is indicated by the grey hatched band.

techniques. By contrast, variables used in training the BDT(tHq) classifiers in the 2ℓ SS and 3ℓ channels, such as invariant masses or angular distances of leptons, show a similar behaviour as the background under the $\kappa_t = -1$ hypothesis, leading to a loss of signal-to-background discrimination power. The uncertainty on the measured signal strength for the ITC hypothesis is dominated by systematic sources. In particular, the absolute uncertainty on $\mu_{tH}(\kappa_t = -1)$ from the theoretical uncertainty in the $t\bar{t}+ \geq 1b$ category is 0.25, the JES and JER together contribute 0.20, the uncertainty from the signal theoretical prediction is 0.18, and that from the modelling of $t\bar{t}$ in the 2ℓ SS and 3ℓ channels is 0.17.

JHEP10(2025)093

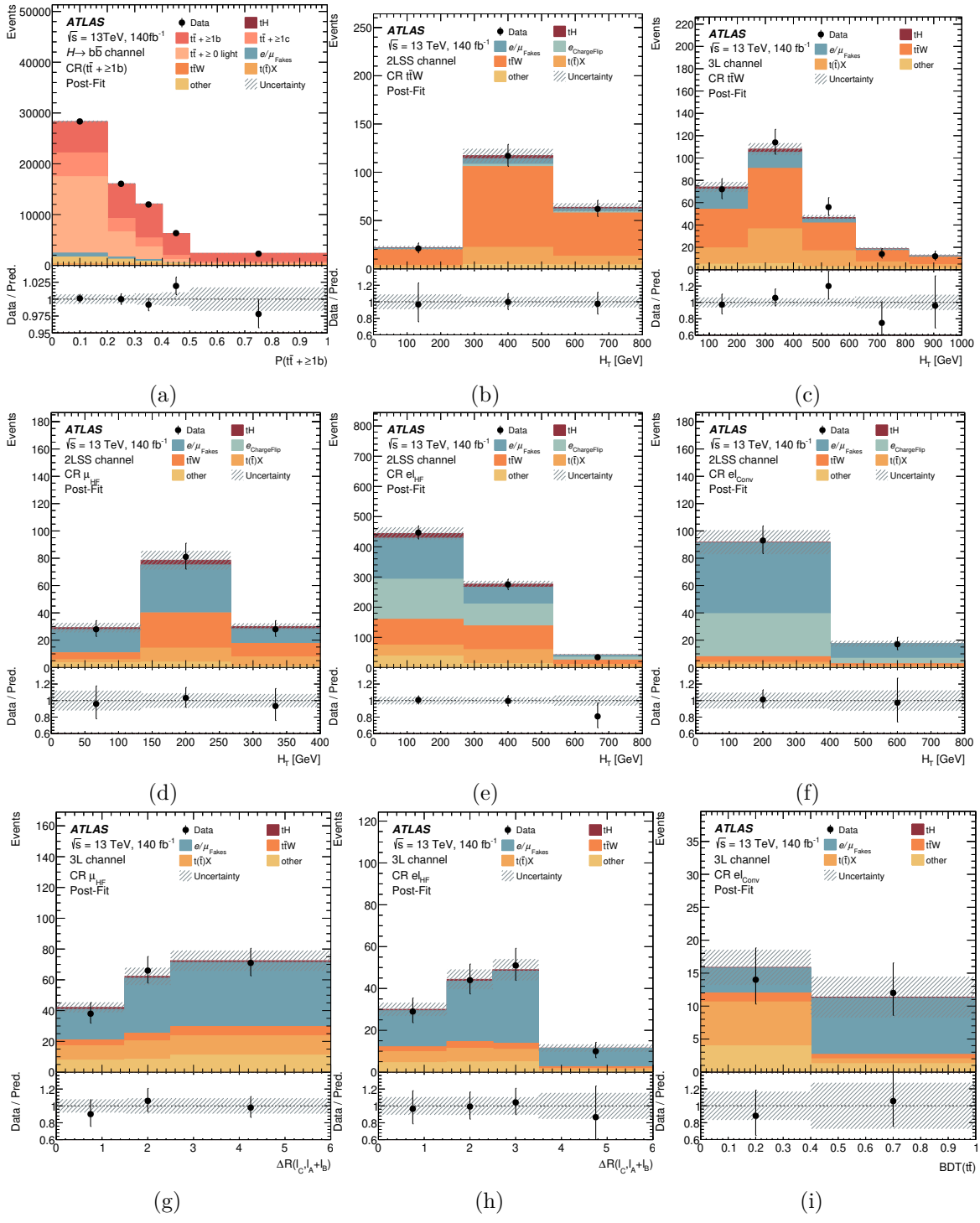

Figure 6. Comparison between data and the signal-plus-background prediction for the event yields in the nine CRs. The term e/μ_{Fakes} refers to backgrounds from non-prompt or misidentified leptons, namely contributions from heavy-flavour decays and photon conversions. The signal and background contributions after the likelihood fit to data ("Post-Fit") under the signal-plus-background hypothesis are shown as filled histograms. The ratio of the data to the total prediction ("Pred.") is shown in the lower panel. The combined statistical and systematic uncertainty in the prediction is indicated by the grey hatched band.

JHEP10(2025)093

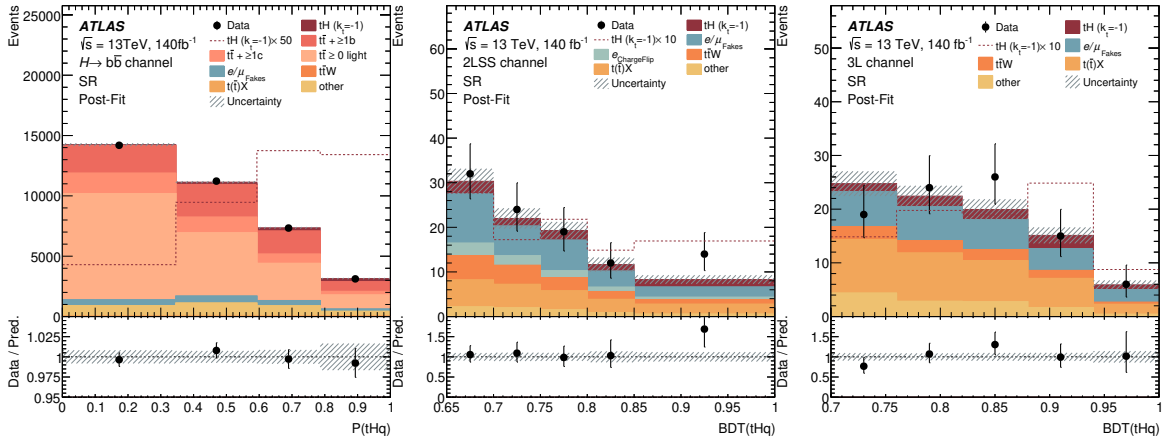

(a) (b) (c)

Figure 7. Comparison between data and the signal-plus-background prediction for the event yields in the (a) $H \to b\bar{b}$, (b) 2ℓSS and (c) 3ℓ SRs in the ITC hypothesis. The term e/μ_{Fakes} refers to backgrounds from non-prompt or misidentified leptons, namely contributions from heavy-flavour decays and photon conversions. The ITC signal and the background contributions after the likelihood fit to data ("Post-Fit") under the signal-plus-background hypothesis are shown as filled histograms. A dashed red line is added to the plot to show the signal contribution normalised to the measured value multiplied by 50 for the $H \to b\bar{b}$ channel and by 10 for the 2ℓSS and 3ℓ channels. The ratio of the data to the total post-fit prediction ("Pred.") is shown in the lower panel. The combined statistical and systematic uncertainty in the prediction is indicated by the grey hatched band.

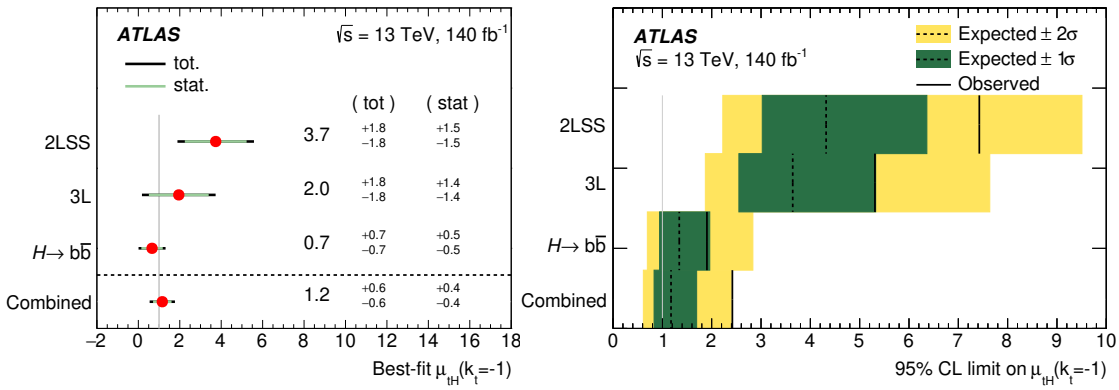

(a) (b)

Figure 8. Fitted values of (a) $\mu_{tH}(\kappa_t = -1)$ and (b) the 95% CL upper limits, shown for the individual channels and the combined measurement. The values reported for the individual channels are obtained by fitting $\mu_{tH}(\kappa_t = -1)$ separately for each channel, whereas the combined measurement is derived by simultaneously fitting all channels together. The observed limits are shown (solid black lines), together with the expected limits under the ITC hypothesis (dotted black lines). A grey line is added in correspondence of the $\mu_{tH}(\kappa_t = -1)$ equal to one. In the case of the expected limits, the one- and two-standard-deviation uncertainty bands are also shown.

JHEP10(2025)093

10 Conclusion

The search for the production of a Higgs boson in association with a single top quark (tH) is presented. The analysis is based on pp collision data at 13 TeV with an integrated luminosity of 140 fb^{-1}, recorded from 2015 to 2018 with the ATLAS detector at the LHC. The signal regions are split into final states with one, two same-sign or three isolated leptons (electrons or muons) probing the $H \to b\bar{b}$, $H \to WW^*$, $H \to ZZ^*$ and $H \to \tau\tau$ decays of the Higgs boson. Additional background-enriched regions are used in the fit to improve the modelling of several leading backgrounds, such as $t\bar{t}+ \geq 1b$, $t\bar{t}W$ and three different categories of the fake and non-prompt leptons background. The tH signal strength is found to be $\mu_{tH} = 8.1 \pm 2.6$ (stat.) $\pm$ 2.0 (syst.) in the SM hypothesis. The measured value of the SM cross-section is $\sigma(tH) = 720 \pm 270$ fb. The main source of uncertainty for this measurement is the one associated with the available experimental data, therefore a better constraint can be obtained analysing a larger event sample. Despite the analysis being optimised to set the best tH limit under the SM hypothesis, it is possible to also test the ITC hypothesis. The signal strength value in this case is found to be $\mu_{tH}(\kappa_t = -1) = 1.2 \pm 0.4$ (stat.) $\pm$ 0.5 (syst.). The excess in data favours the ITC hypothesis, but both hypotheses are compatible with the data.

Acknowledgments

We thank CERN for the very successful operation of the LHC and its injectors, as well as the support staff at CERN and at our institutions worldwide without whom ATLAS could not be operated efficiently.

The crucial computing support from all WLCG partners is acknowledged gratefully, in particular from CERN, the ATLAS Tier-1 facilities at TRIUMF/SFU (Canada), NDGF (Denmark, Norway, Sweden), CC-IN2P3 (France), KIT/GridKA (Germany), INFN-CNAF (Italy), NL-T1 (Netherlands), PIC (Spain), RAL (U.K.) and BNL (U.S.A.), the Tier-2 facilities worldwide and large non-WLCG resource providers. Major contributors of computing resources are listed in ref. [135].

We gratefully acknowledge the support of ANPCyT, Argentina; YerPhI, Armenia; ARC, Australia; BMWFW and FWF, Austria; ANAS, Azerbaijan; CNPq and FAPESP, Brazil; NSERC, NRC and CFI, Canada; CERN; ANID, Chile; CAS, MOST and NSFC, China; Minciencias, Colombia; MEYS CR, Czech Republic; DNRF and DNSRC, Denmark; IN2P3-CNRS and CEA-DRF/IRFU, France; SRNSFG, Georgia; BMFTR, HGF and MPG, Germany; GSRI, Greece; RGC and Hong Kong SAR, China; ICHEP and Academy of Sciences and Humanities, Israel; INFN, Italy; MEXT and JSPS, Japan; CNRST, Morocco; NWO, Netherlands; RCN, Norway; MNiSW, Poland; FCT, Portugal; MNE/IFA, Romania; MSTDI, Serbia; MSSR, Slovakia; ARIS and MVZI, Slovenia; DSI/NRF, South Africa; MICIU/AEI, Spain; SRC and Wallenberg Foundation, Sweden; SERI, SNSF and Cantons of Bern and Geneva, Switzerland; NSTC, Taipei; TENMAK, Türkiye; STFC/UKRI, United Kingdom; DOE and NSF, United States of America.

Individual groups and members have received support from BCKDF, CANARIE, CRC and DRAC, Canada; CERN-CZ, FORTE and PRIMUS, Czech Republic; COST, ERC, ERDF, Horizon 2020, ICSC-NextGenerationEU and Marie Skłodowska-Curie Actions, European

JHEP10(2025)093

Union; Investissements d'Avenir Labex, Investissements d'Avenir Idex and ANR, France; DFG and AvH Foundation, Germany; Herakleitos, Thales and Aristeia programmes co-financed by EU-ESF and the Greek NSRF, Greece; BSF-NSF and MINERVA, Israel; NCN and NAWA, Poland; La Caixa Banking Foundation, CERCA Programme Generalitat de Catalunya and PROMETEO and GenT Programmes Generalitat Valenciana, Spain; Göran Gustafssons Stiftelse, Sweden; The Royal Society and Leverhulme Trust, United Kingdom.

In addition, individual members wish to acknowledge support from CERN: European Organization for Nuclear Research (CERN DOCT); Chile: Agencia Nacional de Investigación y Desarrollo (FONDECYT 1230812, FONDECYT 1240864, Fondecyt 3240661); China: Chinese Ministry of Science and Technology (MOST-2023YFA1605700, MOST-2023YFA1609300), National Natural Science Foundation of China (NSFC — 12175119, NSFC 12275265); Czech Republic: Czech Science Foundation (GACR — 24-11373S), Ministry of Education Youth and Sports (ERC-CZ-LL2327, FORTE CZ.02.01.01/00/22_008/0004632), PRIMUS Research Programme (PRIMUS/21/SCI/017); EU: H2020 European Research Council (ERC — 101002463); European Union: European Research Council (BARD No. 101116429, ERC — 948254, ERC 101089007), European Regional Development Fund (SMASH COFUND 101081355, SLO ERDF), Horizon 2020 Framework Programme (MUCCA — CHIST-ERA-19-XAI-00), European Union, Future Artificial Intelligence Research (FAIR-NextGenerationEU PE00000013), Italian Center for High Performance Computing, Big Data and Quantum Computing (ICSC, NextGenerationEU); France: Agence Nationale de la Recherche (ANR-21-CE31-0022, ANR-22-EDIR-0002); Germany: Baden-Württemberg Stiftung (BW Stiftung-Postdoc Eliteprogramme), Deutsche Forschungsgemeinschaft (DFG — 469666862, DFG — CR 312/5-2); China: Research Grants Council (GRF); Italy: Istituto Nazionale di Fisica Nucleare (ICSC, NextGenerationEU), Ministero dell'Università e della Ricerca (NextGenEU 153D23001490006 M4C2.1.1, NextGenEU I53D23000820006 M4C2.1.1, NextGenEU I53D23001490006 M4C2.1.1, SOE2024_0000023); Japan: Japan Society for the Promotion of Science (JSPS KAKENHI JP22H01227, JSPS KAKENHI JP22H04944, JSPS KAKENHI JP22KK0227, JSPS KAKENHI JP24K23939, JSPS KAKENHI JP24KK0251, JSPS KAKENHI JP25H00650, JSPS KAKENHI JP25H01291, JSPS KAKENHI JP25K01023); Norway: Research Council of Norway (RCN-314472); Poland: Ministry of Science and Higher Education (IDUB AGH, POB8, D4 no 9722), Polish National Science Centre (NCN 2021/42/E/ST2/00350, NCN OPUS 2023/51/B/ST2/02507, NCN OPUS nr 2022/47/B/ST2/03059, NCN UMO-2019/34/E/ST2/00393, UMO-2022/47/O/ST2/00148, UMO-2023/49/B/ST2/04085, UMO-2023/51/B/ST2/00920, UMO-2024/53/N/ST2/00869); Portugal: Foundation for Science and Technology (FCT); Spain: Ministry of Science and Innovation (MCIN & NextGenEU PCI2022-135018-2, MICIN & FEDER PID2021-125273NB, RYC2019-028510-I, RYC2020-030254-I, RYC2021-031273-I, RYC2022-038164-I); Sweden: Carl Trygger Foundation (Carl Trygger Foundation CTS 22:2312), Swedish Research Council (Swedish Research Council 2023-04654, VR 2021-03651, VR 2022-03845, VR 2022-04683, VR 2023-03403, VR 2024-05451), Knut and Alice Wallenberg Foundation (KAW 2018.0458, KAW 2022.0358, KAW 2023.0366); Switzerland: Swiss National Science Foundation (SNSF — PCEFP2_194658); United Kingdom: Royal Society (NIF-R1-231091); United States of America: U.S. Department of Energy (ECA DE-AC02-76SF00515), Neubauer Family Foundation.

JHEP10(2025)093

A List of input variables used to train the different BDTGs

For the 2ℓ SS and 3ℓ channels, leptons are ordered in three different ways:

- *Transverse momentum* ordering: the lepton with the highest p_{T} is called ℓ_A, the one with the second highest p_{T} is called ℓ_B while the lepton with the softest p_{T} is called ℓ_C;
- *Charge and ΔR between leptons* ordering: the lepton with the charge opposite to the sum of the three lepton charges is called ℓ_0, the lepton with the smallest ΔR to ℓ_0 is called ℓ_1, the remaining lepton is called ℓ_2;
- *Charge and ΔR with leading b-jet* ordering: the lepton with the charge opposite to the sum of the three lepton charges is called $\hat{\ell}_0$, the lepton with the smallest ΔR with the leading b-jet is called $\hat{\ell}_1$ while the remaining lepton is called $\hat{\ell}_2$.

The jet satisfying the 70% b-tagging requirement and having the highest p_{T} is called leading b-jet. The jet that fails the b-tagging requirement and maximises the invariant mass with the leading b-jet is called spectator jet, j_{s}. Every jet having $|\eta| > 2.5$ is called forward jet, j_{f}. A forward jet is defined as leading if it has the highest p_{T} among all the forward jets. Every jet with $|\eta| < 2.5$ is called central jet. Using the aforementioned leptons and jet definitions, several variables are constructed.

JHEP10(2025)093

Variable	$H \to b\bar{b}$	2ℓ SS				3ℓ			Description
		BDT($t\bar{t}$)	BDT(VV)	BDT($t\bar{t}W$)	BDT(tHq)	BDT(tHq)	BDT($t\bar{t}$)	BDT($t\bar{t}W$)	
$p^*_{\ell_A}$ (b-jet)	—	—	—	—	—	—	—	×	Momentum of lepton with respect to the leading b-jet rest frame.
$p^*_{\ell_B}$ (b-jet)	—	—	—	—	—	×	—	—	
$p^*_{\ell_C}$ (b-jet)	—	—	—	—	—	—	—	×	
$p_{\mathrm{T,min}}$	—	×	—	×	×	—	—	—	p_{T} of softest lepton.
$\Delta R(\ell_A, \ell_B + \ell_C)$	—	—	—	—	—	—	—	×	ΔR between lepton and the system of the other two leptons.
$\Delta R(\ell_B, \ell_A + \ell_C)$	—	—	—	—	—	—	—	×	
$\Delta R(\ell_A, b\text{-jet})$	—	—	—	—	—	×	—	×	ΔR between lepton and leading b-jet.
$\Delta R(\ell_B, b\text{-jet})$	—	—	—	—	—	—	—	×	
$\Delta R(\text{non-}b\text{-jet}, \ell_1)$	—	—	—	—	×	—	—	—	ΔR or $\Delta\eta$ between lepton and its closest b-jet or non-b-jet.
$\Delta R(\text{non-}b\text{-jet}, \ell_2)$	—	—	—	—	×	—	—	—	
$\Delta R(\ell_1, b\text{-jet})$	—	×	×	—	—	—	—	—	
$\Delta R(\ell_2, b\text{-jet})$	—	×	×	—	—	—	—	—	
$\Delta\eta(\ell_1, b\text{-jet})$	—	×	×	—	—	—	—	—	
$\Delta\eta(\ell_2, b\text{-jet})$	—	×	×	—	—	—	—	—	
$m(\ell, \ell)_{\mathrm{SS}}$	—	—	—	—	—	×	×	×	Invariant mass, ΔR, $\Delta\phi$ or $\Delta\eta$ of same-sign leptons.
$\Delta\eta(\ell, \ell)_{\mathrm{SS}}$	—	—	—	—	×	×	—	—	
$\Delta\phi(\ell, \ell)_{\mathrm{SS}}$	—	—	—	×	—	—	—	—	
$\Delta R(\ell, \ell)_{\mathrm{SS}}$	—	×	—	×	—	—	—	—	
$m(\ell_0, \ell_2)$	—	—	—	—	—	×	×	—	Invariant mass and ΔR of leptons, jets and/or leading b-jet. The lepton ordering is charge and ΔR based.
$m(\ell_0, \ell_1)$	—	—	—	—	—	×	×	×	
$m(\ell_1, b\text{-jet})$	—	—	—	—	—	×	—	×	
$m(\ell_2, b\text{-jet})$	—	—	—	—	—	×	×	—	
$\Delta R(\ell_0, \ell_1)$	—	—	—	—	—	—	—	×	
$m(\ell_2, \mathrm{j}_2)$	—	×	×	×	×	—	—	—	
$m(\ell_2, \mathrm{j}_1)$	—	×	×	—	×	—	—	—	
$m(\ell_1, \mathrm{j}_2)$	—	—	—	—	×	—	—	—	
$m(\ell_1 + \ell_2, \mathrm{j}_2)$	—	—	—	×	—	—	—	—	
$m(\ell_1 + \ell_2, \mathrm{j}_1 + \mathrm{j}_2)$	—	—	—	×	×	—	—	—	
$m(\ell_1 + \ell_2, \mathrm{j}_1)$	—	×	—	—	—	—	—	—	
$m(\mathrm{j}_1 + \mathrm{j}_2)$	—	—	×	×	×	—	—	—	
$m(\ell_1 + \ell_2)$	—	×	×	×	×	—	—	—	
$m_H(WW)$	—	×	—	×	×	—	—	—	Mass of a candidate Higgs Boson when decays into a pair of W bosons.
$m(\text{jet}, \text{jet})_W$	—	—	×	×	×	—	—	—	Mass of the best two jet candidates for the W boson.
$m(\text{jet}, \text{jet})_{\mathrm{top}}$	—	×	×	×	×	—	—	—	Mass of the best top-quark candidate from jets.
$m(\hat{\ell}_0, \hat{\ell}_1)$	—	—	—	—	—	—	×	—	Invariant mass of $\hat{\ell}_0$ and $\hat{\ell}_1$.
$m(\hat{\ell}_0, \hat{\ell}_2)$	—	—	—	—	—	×	—	×	Invariant mass and ΔR of $\hat{\ell}_0$ and $\hat{\ell}_2$.
$\Delta R(\hat{\ell}_0, \hat{\ell}_2)$	—	—	—	—	—	—	—	×	
$m(\hat{\ell}_2, b\text{-jet})$	—	—	—	—	—	×	—	×	Invariant mass and ΔR of leading b-jet and $\hat{\ell}_1$ and $\hat{\ell}_2$.
$\Delta R(\hat{\ell}_2, b\text{-jet})$	—	—	—	—	—	—	×	—	
$m(\ell, b\text{-jet})_{\mathrm{top}}$	—	—	—	—	—	—	×	×	Invariant mass of lepton and b-jet giving best top-quark visible mass.
$m(\ell, \ell)_{\mathrm{top}}$	—	—	—	—	—	×	×	—	Invariant mass of two leptons giving best top-quark visible mass.
p_{FW1}	—	—	—	×	—	—	—	—	First Fox-Wolfram moment [136, 137].

JHEP10(2025)093

Variable	$H \to b\bar{b}$	2ℓ SS				3ℓ			Description
		BDT($t\bar{t}$)	BDT(VV)	BDT($t\bar{t}W$)	BDT(tHq)	BDT(tHq)	BDT($t\bar{t}$)	BDT($t\bar{t}W$)	
p_{FW4}	—	×	×	—	—	—	—	×	Fourth Fox-Wolfram moment.
$p_{\mathrm{T,min}}$	—	—	—	—	—	×	×	×	p_{T} of the softest lepton.
$m(j_{\mathrm{s}})$	—	—	—	—	×	—	—	—	Mass of the spectator jet.
$E(j_{\mathrm{s}})$	—	—	—	—	×	—	—	—	Energy of the spectator jet.
$p_{\mathrm{T}}(j_{\mathrm{s}})$	—	—	—	—	×	—	—	—	p_{T} of the spectator jet.
$E_{\mathrm{T}}^{\mathrm{miss}}/H_{\mathrm{T}}$	—	—	×	—	—	—	—	×	Ratio between $E_{\mathrm{T}}^{\mathrm{miss}}$ and H_{T}.
N(jet)	×	—	—	—	—	—	—	—	Number of non-b-tagged jets.
N(non-b-jet)	—	—	—	—	—	—	—	×	Number of non-b-tagged jets.
N(central-jet)	—	—	—	—	—	×	×	×	Number of central jets.
N(b-jet)	—	—	—	—	—	—	×	×	Number of b-tagged jets.
$\Delta m(Z, \ell\ell_{\mathrm{SF}})_{\mathrm{min}}$	—	×	×	×	—	—	×	×	Minimum difference between the reconstructed invariant mass of two leptons with the same flavour and Z-boson mass.
$\Delta m(Z, \ell\ell)_{\mathrm{min}}$	—	—	—	—	—	×	×	×	Minimum difference between the reconstructed invariant mass of two leptons and Z-boson mass.
$E_{\mathrm{T}}^{\mathrm{miss}}$	—	×	×	×	×	×	×	×	$E_{\mathrm{T}}^{\mathrm{miss}}$.
$\Sigma_i \mathrm{charge}(\ell_i)$	—	×	×	×	×	—	—	—	Sum of lepton charges.
$m(b\text{-jet}, j_{\mathrm{s}})$	—	—	—	×	×	×	—	—	Invariant mass, $\Delta\phi$, $\Delta\eta$ and ΔR of leading b-jet and spectator jet.
$\Delta\phi(b\text{-jet}, j_{\mathrm{s}})$	—	—	—	—	—	×	—	—	
$\Delta\eta(b\text{-jet}, j_{\mathrm{s}})$	—	×	—	—	—	—	—	—	
$\Delta R(b\text{-jet}, j_{\mathrm{s}})$	—	—	—	×	×	—	—	×	
$\Delta R(\ell, j_{\mathrm{f}})$	—	×	—	—	—	—	—	—	ΔR and $\Delta\eta$ between the leading forward jet and its closest lepton.
$\Delta\eta(\ell, j_{\mathrm{f}})$	—	—	—	—	×	—	—	—	
$\Sigma_i q(\ell_i)$	—	—	—	—	—	×	×	×	Sum of lepton charges.
Lepton flavours	—	×	—	—	—	—	—	—	Identification of the flavour of the leptons.
$id(\ell_0)$	×	—	—	—	—	—	—	—	identification number of the lepton combining charge and flavour information.
$e\mu$-events	—	×	×	—	—	—	—	—	Identification of the events $e\mu$.
ee-events	—	—	×	×	×	—	—	—	Identification of the events ee.
H_{T}	—	—	×	—	×	×	×	×	H_{T}.
$H_{\mathrm{T}}(\ell)$	—	×	—	×	×	—	—	—	Sum of the transverse momentum of the leptons.
$H_{\mathrm{T}}(\mathrm{jets})$	—	×	—	×	—	—	—	—	Sum of the transverse momentum of the jets.
$\tilde{m}_{lep}$	—	×	×	×	×	×	—	—	$\sqrt{\Sigma_i (E_{\ell_i}^2 + p_{T,\ell_i}^2)}$.
$\Delta R(\ell, \ell)_{\mathrm{min}}$	—	—	—	—	—	—	—	×	Minimum ΔR between two leptons.
$\Delta\phi(\phi_T^{\mathrm{miss}}, \ell_2)$	—	—	—	×	—	—	—	—	$\Delta\phi$ between ϕ_T^{miss} and ℓ_2.
"custom" χ^2	—	×	×	×	—	—	—	—	$\chi^2(m(\ell_i, \ell_j)_{\mathrm{top}})_{\mathrm{min}}$, minimum χ^2 value between the masses of top-quark candidates given by the combination of leptons.
$m(\ell, \ell)_{\mathrm{top}}$	—	×	×	×	—	—	—	—	Invariant mass of two leptons giving best top-quark visible mass.
$\eta(\mathrm{No}\text{-}b\text{-jet})_{\mathrm{max}}$	—	—	—	×	—	—	—	—	Maximum η value among non-b-tagged jets.
$\Delta\eta(\ell_2, \text{non-}b\text{-jet})$	—	—	—	—	—	—	×	—	$\Delta\eta$ between ℓ_2 and closest non-b-tagged jets.
$\Delta\eta(\ell, j_{\mathrm{f}})$	—	—	—	—	—	×	—	—	$\Delta\eta$ between leading forward jet and closest lepton.
N(non-b-jet)	—	—	×	—	×	—	—	—	Number of non b-tagged jets.
N(central-jet)	—	×	×	×	×	—	—	—	Number of central jets.
N(b-jet)	—	×	×	×	—	—	—	—	Number of b-tagged jets.
$b\text{-score}_1$	—	×	×	×	×	×	×	×	Binned DL1r score (calibrated) of leading b-jet.
$b\text{-score}_2$	—	×	×	×	—	—	—	×	Binned DL1r score (calibrated) of second b-jet.

JHEP10(2025)093

Variable	$H \to b\bar{b}$	2ℓ SS				3ℓ			Description
		BDT($t\bar{t}$)	BDT(VV)	BDT($t\bar{t}W$)	BDT(tHq)	BDT(tHq)	BDT($t\bar{t}$)	BDT($t\bar{t}W$)	
b-score$_3$	—	×	×	×	—	—	—	×	Binned DL1r score (calibrated) of third b-jet.
"custom" n_j	×	—	—	—	—	—	—	—	$n_{j,t_{\text{had}}}(\chi^2_{\text{min, ttl}}, \text{PCBT-bin 4})$, number of jets that belong to the hadronic top-quark found from reconstructing $t\bar{t}$ events but allowing only Hypothesis I within the 4^{th} PCBT bin.
"custom" n_j	×	—	—	—	—	—	—	—	$n_{j,t_{\text{had}}}(\chi^2_{\text{min, ttAll}}, \text{PCBT-bin 4})$, number of jets that belong to the hadronic top-quark found from reconstructing $t\bar{t}$ events within the 4^{th} PCBT bin.
"custom" n_j	×	—	—	—	—	—	—	—	$n_{j,t_{\text{had}}}(\chi^2_{\text{min, ttAll}}, \text{PCBT-bin} \in \{1,2,3\})$, number of jets that belong to the hadronic top-quark found from reconstructing $t\bar{t}$ events within the 1^{st}, 2^{nd} or 3^{rd} PCBT bin.
$p_{\text{T}}^{\text{fwd},0}$	×	—	—	—	—	—	—	—	Transverse momentum of the leading forward-jet.
Sphericity	×	—	—	—	—	—	—	—	as defined in ref. [118].
$\chi^2_{\text{min,ttAll}}$	×	—	—	—	—	—	—	—	The minimum χ^2 value found from reconstructing $t\bar{t}$ events.
"custom" n_j	×	—	—	—	—	—	—	—	$n_{j,\text{not-}t_{\text{had}}}(\chi^2_{\text{min, ttl}}, \text{PCBT-bin} \in \{1,2,3\})$, number of jets that do not belong to the hadronic top-quark found from reconstructing $t\bar{t}$ events but allowing only Hypothesis I within the 1^{st}, 2^{nd} or 3^{rd} PCBT bin.
$p_{\text{T}}^{\text{light},1}$	×	—	—	—	—	—	—	—	Transverse momentum of the 2^{nd} leading jet failing to meet the b-tagging requirement.
"custom" χ^2	×	—	—	—	—	—	—	—	$\chi^2_{\text{top-higgs}}(m_H = 111.5, m_t = 168)$, the minimum χ^2 value found from reconstructing $tHq(H \to b\bar{b})$ events, where the leptonic W from the top-quark decay is reconstructed using the neutrino reconstruction technique.
$\chi^2_{\text{min,ttl}}$	×	—	—	—	—	—	—	—	The minimum χ^2 value found from reconstructing $t\bar{t}$ events allowing only Hypothesis I.
$\text{DL1r}_{\text{light},0}$	×	—	—	—	—	—	—	—	Pseudo-continuous b-tagging distribution for the leading jet failing to meet the b-tagging requirement.
$p_{\text{T}}^{\text{light},2}$	×	—	—	—	—	—	—	—	Transverse momentum of the 3^{rd} leading jet failing to meet the b-tagging requirement.
$\eta_{\text{light},0}$	×	—	—	—	—	—	—	—	Pseudo-rapidity of the leading jet failing to meet the b-tagging requirement.
"custom" χ^2	×	—	—	—	—	—	—	—	$\chi^2_{\text{top-higgs}}(m_H = 113, m_t = 165)$, the minimum χ^2 value found from reconstructing $tHq(H \to b\bar{b})$ events, where the leptonic W from the top-quark decay is reconstructed using the neutrino reconstruction technique.
$p_{\text{T}}^{\text{light},0}$	×	—	—	—	—	—	—	—	Transverse momentum of the leading jet failing to meet the b-tagging requirement.
$\Delta\eta_{\text{top-higgs}}$	×	—	—	—	—	—	—	—	The $\Delta\eta$ between the reconstructed top quark and the reconstructed Higgs boson according to the minimum χ^2 method.
"custom" n_j	×	—	—	—	—	—	—	—	$n_{j,t_{\text{had}}}(\chi^2_{\text{min, ttl}}, \text{PCBT-bin 0})$, number of jets that belong to the hadronic top-quark found from reconstructing $t\bar{t}$ events but allowing only Hypothesis I within the 0^{th} PCBT bin.
$m_{t_{\text{had}}}(\chi^2_{\text{min, ttAll}})$	×	—	—	—	—	—	—	—	The mass of the reconstructed hadronic top-quark found from reconstructing $t\bar{t}$ events.

JHEP10(2025)093

Variable	$H \to b\bar{b}$	2ℓ SS				3ℓ			Description
		BDT($t\bar{t}$)	BDT(VV)	BDT($t\bar{t}W$)	BDT(tHq)	BDT(tHq)	BDT($t\bar{t}$)	BDT($t\bar{t}W$)	
$m_{t_{\text{had}}}(\chi^2_{\text{min, ttl}})$	×	—	—	—	—	—	—	—	The mass of the reconstructed hadronic top-quark found from reconstructing $t\bar{t}$ events but allowing only Hypothesis I.
$\eta_{\text{light,2}}$	×	—	—	—	—	—	—	—	Pseudo-rapidity of the 3^{rd} leading jet failing the b-tagging requirement.
$\Delta R(q_1^W, q_2^W)$	×	—	—	—	—	—	—	—	The minimum ΔR between the two jets assigned to the hadronic W decay from reconstructing $t\bar{t}$ events.
$m(b_{\text{top}}, j_{\text{tag}})$	×	—	—	—	—	—	—	—	The invariant mass of the b-jet from top-quark decay found using a reconstruction of $tHq(H \to b\bar{b})$ events and the light-flavour jet most de-correlated from the top-quark system. The light jet is chosen such that it maximises the invariant mass $m(b_{\text{top}}, j_{\text{tag}})$.
η_{tag}	×	—	—	—	—	—	—	—	The η of the light-flavour jet, η_{tag} most de-correlated from the top-quark system. The light jet is chosen such that it maximises the invariant mass $m(b_{\text{top}}, j_{\text{tag}})$.

Table 6. List of variables considered in the training of the BDTGs in each channel. The × symbol marks in which BDTGs the variable is used. Variables labelled with "custom" are better explained in the description column.

JHEP10(2025)093

$H \to b\bar{b}$ channel				
	Pre-fit		Post-fit	
Process	SR	CR($t\bar{t}+\geq 1b$)	SR	CR($t\bar{t}+\geq 1b$)
tHq	43 ± 7	9.1 ± 2.0	350 ± 130	72 ± 29
tWH	3.4 ± 2.0	14 ± 8	28 ± 20	110 ± 80
$t\bar{t}+\geq 1b$	6800 ± 1100	20100 ± 2600	8100 ± 1000	25600 ± 1900
$t\bar{t}+\geq 1c$	4000 ± 2400	11000 ± 6000	3900 ± 1500	10200 ± 3300
$t\bar{t}+\geq 0$ light	19300 ± 3300	23100 ± 3500	18500 ± 1100	23300 ± 2100
e/μ_{Fakes}	1700 ± 500	1600 ± 500	1700 ± 500	1600 ± 500
$t\bar{t}W$	20.1 ± 3.0	134 ± 19	20.2 ± 2.9	133 ± 19
$t\bar{t}H$	120 ± 15	683 ± 70	120 ± 15	683 ± 70
$t\bar{t}Z$	68 ± 9	340 ± 40	68 ± 9	340 ± 40
tZq	69 ± 7	20.4 ± 1.9	69 ± 6	20.4 ± 1.9
tWZ	0.20 ± 0.10	0.9 ± 0.5	0.20 ± 0.11	0.9 ± 0.5
Wt channel	970 ± 260	1500 ± 500	970 ± 250	1600 ± 500
t-channel	1070 ± 180	350 ± 120	1060 ± 160	350 ± 120
s-channel	43 ± 8	40 ± 11	42 ± 7	39 ± 10
W + jets	740 ± 310	900 ± 400	750 ± 300	890 ± 350
Z + jets	140 ± 50	100 ± 40	140 ± 50	100 ± 40
VV	48 ± 25	70 ± 40	41 ± 22	63 ± 33
other Higgs	6 ± 5	5.3 ± 2.9	7 ± 5	5.2 ± 2.8
Rare top	0.08 ± 0.04	3.3 ± 1.7	0.08 ± 0.04	3.4 ± 1.7
Total	35000 ± 5000	60000 ± 8000	35870 ± 210	65000 ± 340
Data	35869	65002	35869	65002

Table 7. Pre-fit and post-fit event yields in the SR and CR($t\bar{t}+\geq 1b$) of the $H \to b\bar{b}$ channel. Post-fit yields are after the inclusive fit in all channels. All uncertainties are included, taking into account correlations in the post-fit case.

B Pre-fit and post-fit yields tables

Pre-fit and post-fit yields of the analysis regions are reported in table 7 for the $H \to b\bar{b}$ channel. Tables 8 and 9 show the pre- and post-fit yields for the 2ℓSS channel, respectively. Tables 10 and 11 show the pre- and post-fit yields for the 3ℓ channel, respectively.

JHEP10(2025)093

Pre-fit 2ℓ SS channel					
Process	SR	CR(μ_{HF})	CR(e_{HF})	CR(e_{conv})	CR($t\bar{t}W$)
tHq	3.1 ± 0.5	0.65 ± 0.11	2.5 ± 0.4	0.085 ± 0.024	0.30 ± 0.06
tWH	0.09 ± 0.04	0.20 ± 0.04	0.89 ± 0.13	0.016 ± 0.006	0.39 ± 0.05
μ_{HF}	16 ± 5	59 ± 11	19 ± 4	0.24 ± 0.24	3.0 ± 2.0
e_{HF}	4.9 ± 3.1	-	86 ± 17	1.3 ± 0.8	0.9 ± 0.8
e_{conv}	3.4 ± 2.7	-	80 ± 15	47 ± 15	2.8 ± 1.4
other mis-id leptons	4 ± 4	15 ± 12	41 ± 28	3.0 ± 3.0	3.7 ± 2.6
$e_{\text{ChargeFlip}}$	8.3 ± 1.9	-	220 ± 50	37 ± 11	4.4 ± 1.0
$t\bar{t}W$	14.9 ± 2.1	35 ± 4	160 ± 8	5.0 ± 0.4	131 ± 5
$t\bar{t}Z$	3.7 ± 0.6	8.0 ± 1.4	38 ± 6	1.12 ± 0.21	15.3 ± 2.2
$t\bar{t}H$	2.4 ± 0.4	7.2 ± 1.0	30 ± 4	0.77 ± 0.12	13.5 ± 2.0
tZq	14.2 ± 1.9	3.9 ± 0.5	22.0 ± 2.0	0.68 ± 0.09	1.05 ± 0.18
VV	7.3 ± 3.3	9 ± 5	50 ± 15	1.8 ± 1.5	7.2 ± 3.1
others	0.45 ± 0.13	1.1 ± 0.4	7.9 ± 2.1	0.28 ± 0.10	2.0 ± 0.5
4-tops	0.042 ± 0.014	0.050 ± 0.015	0.54 ± 0.15	0.016 ± 0.007	0.83 ± 0.24
Total	83 ± 10	138 ± 16	760 ± 80	98 ± 21	187 ± 8
Data	101	137	756	110	200

Table 8. Pre-fit event yields in the SR and CRs of the 2ℓ SS channel. The 'others' process includes tWZ, Tri-boson, s-channel, 3-tops and VH processes.

Post-fit 2ℓ SS channel					
Process	SR	CR(μ_{HF})	CR(e_{HF})	CR(e_{conv})	CR($t\bar{t}W$)
tHq	25 ± 9	5.3 ± 2.1	21 ± 8	0.67 ± 0.30	2.4 ± 0.9
tWH	0.7 ± 0.4	1.6 ± 0.7	7.3 ± 3.2	0.13 ± 0.07	3.2 ± 1.4
μ_{HF}	13 ± 6	47 ± 18	15 ± 7	0.22 ± 0.17	2.9 ± 1.9
e_{HF}	2.6 ± 3.4	-	50 ± 60	0.7 ± 0.9	0.5 ± 0.7
e_{conv}	3.8 ± 3.1	-	98 ± 35	58 ± 15	3.4 ± 1.6
other mis-id leptons	4 ± 4	15 ± 11	38 ± 25	3.3 ± 2.8	3.2 ± 2.1
$e_{\text{ChargeFlip}}$	8.0 ± 1.8	-	210 ± 50	36 ± 10	4.2 ± 1.0
$t\bar{t}W$	15.0 ± 2.4	41 ± 5	178 ± 17	5.7 ± 0.6	144 ± 13
$t\bar{t}Z$	3.7 ± 0.6	7.9 ± 1.3	37 ± 6	1.07 ± 0.20	15.1 ± 2.1
$t\bar{t}H$	2.4 ± 0.4	7.3 ± 0.9	30 ± 4	0.78 ± 0.11	13.5 ± 1.9
tZq	14.1 ± 1.9	3.9 ± 0.5	22.1 ± 2.0	0.68 ± 0.09	1.03 ± 0.17
VV	6.0 ± 2.4	7.1 ± 3.5	45 ± 13	2.0 ± 1.6	6.0 ± 2.4
others	0.44 ± 0.13	1.1 ± 0.4	7.9 ± 2.1	0.28 ± 0.11	1.9 ± 0.5
4-tops	0.043 ± 0.014	0.050 ± 0.015	0.55 ± 0.15	0.017 ± 0.007	0.85 ± 0.24
Total	99 ± 8	138 ± 11	762 ± 27	109 ± 10	202 ± 12
Data	101	137	756	110	200

Table 9. Post-fit event yields in the SR and CRs of the 2ℓ SS channel. Post-fit yields are after the inclusive fit in all channels. All uncertainties are included, taking into account correlations in the post-fit case. The 'others' process includes tWZ, Tri-boson, s-channel, 3-tops and VH processes.

JHEP10(2025)093

Pre-fit 3ℓ channel					
Process	SR	CR(μ_{HF})	CR(e_{HF})	CR(e_{conv})	CR($t\bar{t}W$)
tHq	1.45 ± 0.24	0.24 ± 0.06	0.159 ± 0.030	0.025 ± 0.007	0.26 ± 0.06
tWH	0.29 ± 0.04	0.24 ± 0.04	0.150 ± 0.023	0.019 ± 0.004	0.64 ± 0.07
μ_{HF}	9 ± 4	84 ± 11	3.2 ± 1.8	0.08 ± 0.11	10 ± 7
e_{HF}	5.3 ± 2.3	2.7 ± 2.2	47 ± 9	0.16 ± 0.04	6.9 ± 3.0
e_{conv}	4.2 ± 1.8	3.5 ± 3.2	14 ± 6	14 ± 9	11 ± 8
other mis-id leptons	4.9 ± 3.0	14 ± 10	8 ± 5	1.0 ± 1.0	10 ± 8
$t\bar{t}W$	7.9 ± 0.9	13.6 ± 0.6	8.1 ± 0.8	1.97 ± 0.33	118 ± 4
tWZ	0.8 ± 0.5	1.4 ± 0.7	0.8 ± 0.5	0.6 ± 0.4	3.5 ± 1.9
$t\bar{t}Z$	14.3 ± 2.1	15.6 ± 2.4	8.2 ± 1.3	4.9 ± 1.1	37 ± 5
$t\bar{t}H$	7.7 ± 1.0	7.6 ± 1.0	4.7 ± 0.7	0.51 ± 0.16	21.0 ± 2.8
tZq	10.8 ± 1.2	9.2 ± 1.1	4.8 ± 0.6	1.8 ± 0.4	6.0 ± 0.7
tW	1.1 ± 0.7	6 ± 4	3.6 ± 2.5	0.9 ± 0.7	1.6 ± 1.2
VV	12 ± 5	22 ± 7	11.0 ± 3.5	4.8 ± 1.7	13 ± 5
others	0.24 ± 0.08	0.44 ± 0.12	0.16 ± 0.05	0.040 ± 0.012	1.0 ± 0.6
4-tops	0.14 ± 0.04	0.15 ± 0.05	0.085 ± 0.026	0.037 ± 0.013	1.7 ± 0.5
Total	80 ± 11	181 ± 17	113 ± 15	31 ± 10	242 ± 14
Data	90	175	134	26	268

Table 10. Pre-fit event yields in the SR and CRs of the 3ℓ channel. The 'others' process includes gluon-gluon fusion and vector-boson fusion Higgs boson production, Tri-boson, s-channel and t-channel single-top, 3-tops and VH processes.

Post-fit 3ℓ channel					
Process	SR	CR(μ_{HF})	CR(e_{HF})	CR(e_{conv})	CR($t\bar{t}W$)
tHq	12 ± 4	2.0 ± 0.9	1.3 ± 0.5	0.20 ± 0.09	2.2 ± 0.9
tWH	2.3 ± 0.9	2.0 ± 0.9	1.2 ± 0.5	0.15 ± 0.07	5.2 ± 2.2
μ_{HF}	8 ± 4	77 ± 18	3.0 ± 1.5	0.07 ± 0.09	9 ± 6
e_{HF}	8 ± 4	3.8 ± 2.9	68 ± 14	0.22 ± 0.08	10 ± 6
e_{conv}	3.1 ± 2.1	3 ± 4	11 ± 6	11 ± 5	9 ± 11
other mis-id leptons	3.8 ± 2.2	13 ± 8	7 ± 4	1.0 ± 0.9	9 ± 7
$t\bar{t}W$	8.3 ± 1.3	15.0 ± 1.6	9.3 ± 1.2	2.0 ± 0.4	131 ± 12
tWZ	0.9 ± 0.5	1.5 ± 0.7	0.9 ± 0.5	0.62 ± 0.33	3.6 ± 1.9
$t\bar{t}Z$	14.2 ± 2.0	15.5 ± 2.3	8.4 ± 1.3	4.6 ± 0.9	38 ± 5
$t\bar{t}H$	7.7 ± 1.0	7.6 ± 1.0	4.7 ± 0.7	0.48 ± 0.14	21.4 ± 2.8
tZq	10.7 ± 1.2	9.3 ± 1.1	4.9 ± 0.6	1.74 ± 0.32	6.0 ± 0.7
tW	1.1 ± 0.7	5 ± 4	4.0 ± 2.7	0.9 ± 0.7	1.4 ± 1.1
VV	10 ± 4	21 ± 6	10.6 ± 3.4	4.2 ± 1.3	11 ± 4
others	0.23 ± 0.08	0.43 ± 0.12	0.15 ± 0.05	0.037 ± 0.011	0.9 ± 0.4
4-tops	0.14 ± 0.04	0.15 ± 0.05	0.087 ± 0.026	0.035 ± 0.012	1.7 ± 0.5
Total	90 ± 7	177 ± 13	135 ± 11	27 ± 5	260 ± 11
Data	90	175	134	26	268

Table 11. Post-fit event yields in the SR and CRs of the 2ℓSS channel. Post-fit yields are after the inclusive fit in all channels. All uncertainties are included, taking into account correlations in the post-fit case. The 'others' process includes gluon-gluon fusion and vector-boson fusion Higgs boson production, Tri-boson, s-channel and t-channel single-top, 3-tops and VH processes.

Data Availability Statement. This article has no associated data or the data will not be deposited.

JHEP10(2025)093

Code Availability Statement. This article has no associated code or the code will not be deposited.

Open Access. This article is distributed under the terms of the Creative Commons Attribution License (CC-BY4.0), which permits any use, distribution and reproduction in any medium, provided the original author(s) and source are credited.

References

[1] F. Englert and R. Brout, *Broken symmetry and the mass of gauge vector mesons*, *Phys. Rev. Lett.* **13** (1964) 321 [INSPIRE].

[2] P.W. Higgs, *Broken symmetries and the masses of gauge bosons*, *Phys. Rev. Lett.* **13** (1964) 508 [INSPIRE].

[3] ATLAS collaboration, *Observation of a new particle in the search for the Standard Model Higgs boson with the ATLAS detector at the LHC*, *Phys. Lett. B* **716** (2012) 1 [arXiv:1207.7214] [INSPIRE].

[4] CMS collaboration, *Observation of a new boson at a mass of 125 GeV with the CMS experiment at the LHC*, *Phys. Lett. B* **716** (2012) 30 [arXiv:1207.7235] [INSPIRE].

[5] M.E. Peskin and D.V. Schroeder, *An introduction to quantum field theory*, Addison-Wesley, Reading, U.S.A. (1995) [DOI:10.1201/9780429503559] [INSPIRE].

[6] G. Degrassi et al., *Higgs mass and vacuum stability in the Standard Model at NNLO*, *JHEP* **08** (2012) 098 [arXiv:1205.6497] [INSPIRE].

[7] D. Buttazzo et al., *Investigating the near-criticality of the Higgs boson*, *JHEP* **12** (2013) 089 [arXiv:1307.3536] [INSPIRE].

[8] C. Englert et al., *Precision measurements of Higgs couplings: implications for new physics scales*, *J. Phys. G* **41** (2014) 113001 [arXiv:1403.7191] [INSPIRE].

[9] J.F. Gunion and X.-G. He, *Determining the CP nature of a neutral Higgs boson at the LHC*, *Phys. Rev. Lett.* **76** (1996) 4468 [hep-ph/9602226] [INSPIRE].

[10] J. Ellis, D.S. Hwang, K. Sakurai and M. Takeuchi, *Disentangling Higgs-top couplings in associated production*, *JHEP* **04** (2014) 004 [arXiv:1312.5736] [INSPIRE].

[11] X.-G. He, G.-N. Li and Y.-J. Zheng, *Probing Higgs boson CP properties with $t\bar{t}H$ at the LHC and the 100 TeV pp collider*, *Int. J. Mod. Phys. A* **30** (2015) 1550156 [arXiv:1501.00012] [INSPIRE].

[12] ATLAS collaboration, *Observation of Higgs boson production in association with a top quark pair at the LHC with the ATLAS detector*, *Phys. Lett. B* **784** (2018) 173 [arXiv:1806.00425] [INSPIRE].

[13] CMS collaboration, *Observation of $t\bar{t}H$ production*, *Phys. Rev. Lett.* **120** (2018) 231801 [arXiv:1804.02610] [INSPIRE].

[14] T.M.P. Tait and C.-P. Yuan, *Single top quark production as a window to physics beyond the standard model*, *Phys. Rev. D* **63** (2000) 014018 [hep-ph/0007298] [INSPIRE].

[15] V. Barger, M. McCaskey and G. Shaughnessy, *Single top and Higgs associated production at the LHC*, *Phys. Rev. D* **81** (2010) 034020 [arXiv:0911.1556] [INSPIRE].

JHEP10(2025)093

[16] S. Biswas, E. Gabrielli and B. Mele, *Single top and Higgs associated production as a probe of the Htt coupling sign at the LHC*, *JHEP* **01** (2013) 088 [arXiv:1211.0499] [INSPIRE].

[17] M. Farina et al., *Lifting degeneracies in Higgs couplings using single top production in association with a Higgs boson*, *JHEP* **05** (2013) 022 [arXiv:1211.3736] [INSPIRE].

[18] J. Chang, K. Cheung, J.S. Lee and C.-T. Lu, *Probing the top-Yukawa coupling in associated Higgs production with a single top quark*, *JHEP* **05** (2014) 062 [arXiv:1403.2053] [INSPIRE].

[19] ATLAS collaboration, *CP properties of Higgs boson interactions with top quarks in the $t\bar{t}H$ and tH processes using $H \to \gamma\gamma$ with the ATLAS detector*, *Phys. Rev. Lett.* **125** (2020) 061802 [arXiv:2004.04545] [INSPIRE].

[20] CMS collaboration, *Measurements of Higgs boson production cross sections and couplings in the diphoton decay channel at $\sqrt{s} = 13$ TeV*, *JHEP* **07** (2021) 027 [arXiv:2103.06956] [INSPIRE].

[21] ATLAS collaboration, *A detailed map of Higgs boson interactions by the ATLAS experiment ten years after the discovery*, *Nature* **607** (2022) 52 [*Erratum ibid.* **612** (2022) E24] [arXiv:2207.00092] [INSPIRE].

[22] CMS collaboration, *A portrait of the Higgs boson by the CMS experiment ten years after the discovery*, *Nature* **607** (2022) 60 [arXiv:2207.00043] [INSPIRE].

[23] ATLAS and CMS collaborations, *Measurements of the Higgs boson production and decay rates and constraints on its couplings from a combined ATLAS and CMS analysis of the LHC pp collision data at $\sqrt{s} = 7$ and 8 TeV*, *JHEP* **08** (2016) 045 [arXiv:1606.02266] [INSPIRE].

[24] F. Demartin, F. Maltoni, K. Mawatari and M. Zaro, *Higgs production in association with a single top quark at the LHC*, *Eur. Phys. J. C* **75** (2015) 267 [arXiv:1504.00611] [INSPIRE].

[25] F. Demartin et al., *tWH associated production at the LHC*, *Eur. Phys. J. C* **77** (2017) 34 [arXiv:1607.05862] [INSPIRE].

[26] L. Evans and P. Bryant, *LHC machine*, 2008 *JINST* **3** S08001 [INSPIRE].

[27] J.M. Campbell, R. Frederix, F. Maltoni and F. Tramontano, *Next-to-leading-order predictions for t-channel single-top production at hadron colliders*, *Phys. Rev. Lett.* **102** (2009) 182003 [arXiv:0903.0005] [INSPIRE].

[28] F. Maltoni, G. Ridolfi and M. Ubiali, *b-initiated processes at the LHC: a reappraisal*, *JHEP* **04** (2012) 095 [*Erratum ibid.* **04** (2013) 095] [arXiv:1203.6393] [INSPIRE].

[29] E. Bothmann, F. Krauss and M. Schönherr, *Single top-quark production with SHERPA*, *Eur. Phys. J. C* **78** (2018) 220 [arXiv:1711.02568] [INSPIRE].

[30] CMS collaboration, *Search for associated production of a Higgs boson and a single top quark in proton-proton collisions at $\sqrt{s} = 13$ TeV*, *Phys. Rev. D* **99** (2019) 092005 [arXiv:1811.09696] [INSPIRE].

[31] CMS collaboration, *Measurement of the Higgs boson production rate in association with top quarks in final states with electrons, muons, and hadronically decaying tau leptons at $\sqrt{s} = 13$ TeV*, *Eur. Phys. J. C* **81** (2021) 378 [arXiv:2011.03652] [INSPIRE].

[32] CMS collaboration, *Measurement of the $t\bar{t}H$ and tH production rates in the $H \to b\bar{b}$ decay channel using proton-proton collision data at $\sqrt{s} = 13$ TeV*, *JHEP* **02** (2025) 097 [arXiv:2407.10896] [INSPIRE].

[33] M. Aly, T. Dado, A. Held, M. Pinamonti and L. Valery, *Trexfitter*, Zenodo, February (2025).

[34] ATLAS collaboration, *The ATLAS experiment at the CERN Large Hadron Collider*, 2008 *JINST* **3** S08003 [INSPIRE].

JHEP10(2025)093

[35] ATLAS collaboration, *ATLAS Insertable B-Layer technical design report*, CERN-LHCC-2010-013, CERN, Geneva, Switzerland (2010).

[36] ATLAS IBL collaboration, *Production and integration of the ATLAS Insertable B-Layer*, 2018 *JINST* **13** T05008 [arXiv:1803.00844] [INSPIRE].

[37] G. Avoni et al., *The new LUCID-2 detector for luminosity measurement and monitoring in ATLAS*, 2018 *JINST* **13** P07017 [INSPIRE].

[38] ATLAS collaboration, *Performance of the ATLAS trigger system in 2015*, *Eur. Phys. J. C* **77** (2017) 317 [arXiv:1611.09661] [INSPIRE].

[39] ATLAS collaboration, *Software and computing for run 3 of the ATLAS experiment at the LHC*, *Eur. Phys. J. C* **85** (2025) 234 [arXiv:2404.06335] [INSPIRE].

[40] ATLAS collaboration, *ATLAS data quality operations and performance for 2015–2018 data-taking*, 2020 *JINST* **15** P04003 [arXiv:1911.04632] [INSPIRE].

[41] ATLAS collaboration, *Performance of electron and photon triggers in ATLAS during LHC run 2*, *Eur. Phys. J. C* **80** (2020) 47 [arXiv:1909.00761] [INSPIRE].

[42] ATLAS collaboration, *Performance of the ATLAS muon triggers in run 2*, 2020 *JINST* **15** P09015 [arXiv:2004.13447] [INSPIRE].

[43] T. Sjostrand, S. Mrenna and P.Z. Skands, *A brief introduction to PYTHIA 8.1*, *Comput. Phys. Commun.* **178** (2008) 852 [arXiv:0710.3820] [INSPIRE].

[44] T. Sjöstrand et al., *An introduction to PYTHIA 8.2*, *Comput. Phys. Commun.* **191** (2015) 159 [arXiv:1410.3012] [INSPIRE].

[45] R.D. Ball et al., *Parton distributions with LHC data*, *Nucl. Phys. B* **867** (2013) 244 [arXiv:1207.1303] [INSPIRE].

[46] ATLAS collaboration, *The Pythia 8 A3 tune description of ATLAS minimum bias and inelastic measurements incorporating the Donnachie-Landshoff diffractive model*, ATL-PHYS-PUB-2016-017, CERN, Geneva, Switzerland (2016).

[47] Particle Data Group collaboration, *Review of particle physics*, *Phys. Rev. D* **110** (2024) 030001 [INSPIRE].

[48] D.J. Lange, *The EvtGen particle decay simulation package*, *Nucl. Instrum. Meth. A* **462** (2001) 152 [INSPIRE].

[49] J. Alwall et al., *The automated computation of tree-level and next-to-leading order differential cross sections, and their matching to parton shower simulations*, *JHEP* **07** (2014) 079 [arXiv:1405.0301] [INSPIRE].

[50] NNPDF collaboration, *Parton distributions for the LHC run II*, *JHEP* **04** (2015) 040 [arXiv:1410.8849] [INSPIRE].

[51] ATLAS collaboration, *ATLAS Pythia 8 tunes to 7 TeV data*, ATL-PHYS-PUB-2014-021, CERN, Geneva, Switzerland (2014).

[52] LHC Higgs Cross Section Working Group collaboration, *Handbook of LHC Higgs cross sections: 4. Deciphering the nature of the Higgs sector*, *CERN Yellow Rep. Monogr.* **2** (2017) 1 [arXiv:1610.07922] [INSPIRE].

[53] ATLAS collaboration, *SM Higgs production cross sections at* $\sqrt{s} = 13$ *TeV*, https://twiki.cern.ch/twiki/bin/view/LHCPhysics/CERNYellowReportPageAt13TeV (2024).

JHEP10(2025)093

[54] J. Butterworth et al., *PDF4LHC recommendations for LHC run II*, *J. Phys. G* **43** (2016) 023001 [arXiv:1510.03865] [INSPIRE].

[55] S. Frixione et al., *Single-top hadroproduction in association with a W boson*, *JHEP* **07** (2008) 029 [arXiv:0805.3067] [INSPIRE].

[56] ATLAS collaboration, *Studies on top-quark Monte Carlo modelling for Top2016*, ATL-PHYS-PUB-2016-020, CERN, Geneva, Switzerland (2016).

[57] M. Bahr et al., *Herwig++ physics and manual*, *Eur. Phys. J. C* **58** (2008) 639 [arXiv:0803.0883] [INSPIRE].

[58] J. Bellm et al., *Herwig 7.0/Herwig++ 3.0 release note*, *Eur. Phys. J. C* **76** (2016) 196 [arXiv:1512.01178] [INSPIRE].

[59] L.A. Harland-Lang, A.D. Martin, P. Motylinski and R.S. Thorne, *Parton distributions in the LHC era: MMHT 2014 PDFs*, *Eur. Phys. J. C* **75** (2015) 204 [arXiv:1412.3989] [INSPIRE].

[60] S. Frixione, P. Nason and G. Ridolfi, *A positive-weight next-to-leading-order Monte Carlo for heavy flavour hadroproduction*, *JHEP* **09** (2007) 126 [arXiv:0707.3088] [INSPIRE].

[61] P. Nason, *A new method for combining NLO QCD with shower Monte Carlo algorithms*, *JHEP* **11** (2004) 040 [hep-ph/0409146] [INSPIRE].

[62] S. Frixione, P. Nason and C. Oleari, *Matching NLO QCD computations with parton shower simulations: the POWHEG method*, *JHEP* **11** (2007) 070 [arXiv:0709.2092] [INSPIRE].

[63] S. Alioli, P. Nason, C. Oleari and E. Re, *A general framework for implementing NLO calculations in shower Monte Carlo programs: the POWHEG BOX*, *JHEP* **06** (2010) 043 [arXiv:1002.2581] [INSPIRE].

[64] M. Beneke, P. Falgari, S. Klein and C. Schwinn, *Hadronic top-quark pair production with NNLL threshold resummation*, *Nucl. Phys. B* **855** (2012) 695 [arXiv:1109.1536] [INSPIRE].

[65] M. Cacciari et al., *Top-pair production at hadron colliders with next-to-next-to-leading logarithmic soft-gluon resummation*, *Phys. Lett. B* **710** (2012) 612 [arXiv:1111.5869] [INSPIRE].

[66] P. Bärnreuther, M. Czakon and A. Mitov, *Percent level precision physics at the Tevatron: first genuine NNLO QCD corrections to $q\bar{q} \to t\bar{t} + X$*, *Phys. Rev. Lett.* **109** (2012) 132001 [arXiv:1204.5201] [INSPIRE].

[67] M. Czakon and A. Mitov, *NNLO corrections to top-pair production at hadron colliders: the all-fermionic scattering channels*, *JHEP* **12** (2012) 054 [arXiv:1207.0236] [INSPIRE].

[68] M. Czakon and A. Mitov, *NNLO corrections to top pair production at hadron colliders: the quark-gluon reaction*, *JHEP* **01** (2013) 080 [arXiv:1210.6832] [INSPIRE].

[69] M. Czakon, P. Fiedler and A. Mitov, *Total top-quark pair-production cross section at hadron colliders through $O(\alpha_S^4)$*, *Phys. Rev. Lett.* **110** (2013) 252004 [arXiv:1303.6254] [INSPIRE].

[70] M. Czakon and A. Mitov, *Top++: a program for the calculation of the top-pair cross-section at hadron colliders*, *Comput. Phys. Commun.* **185** (2014) 2930 [arXiv:1112.5675] [INSPIRE].

[71] S. Höche et al., *A study of QCD radiation in VBF Higgs production with Vincia and Pythia*, *SciPost Phys.* **12** (2022) 010 [arXiv:2106.10987] [INSPIRE].

[72] F. Buccioni et al., *OpenLoops 2*, *Eur. Phys. J. C* **79** (2019) 866 [arXiv:1907.13071] [INSPIRE].

[73] F. Cascioli, P. Maierhofer and S. Pozzorini, *Scattering amplitudes with OpenLoops*, *Phys. Rev. Lett.* **108** (2012) 111601 [arXiv:1111.5206] [INSPIRE].

JHEP10(2025)093

[74] A. Denner, S. Dittmaier and L. Hofer, *Collier: a fortran-based Complex One-Loop LIbrary in Extended Regularizations*, *Comput. Phys. Commun.* **212** (2017) 220 [arXiv:1604.06792] [INSPIRE].

[75] H.B. Hartanto, B. Jager, L. Reina and D. Wackeroth, *Higgs boson production in association with top quarks in the POWHEG BOX*, *Phys. Rev. D* **91** (2015) 094003 [arXiv:1501.04498] [INSPIRE].

[76] SHERPA collaboration, *Event generation with Sherpa 2.2*, *SciPost Phys.* **7** (2019) 034 [arXiv:1905.09127] [INSPIRE].

[77] R. Frederix and S. Frixione, *Merging meets matching in MC@NLO*, *JHEP* **12** (2012) 061 [arXiv:1209.6215] [INSPIRE].

[78] R. Frederix and I. Tsinikos, *On improving NLO merging for $t\bar{t}W$ production*, *JHEP* **11** (2021) 029 [arXiv:2108.07826] [INSPIRE].

[79] ATLAS collaboration, *Modelling of the $t\bar{t}H$ and $t\bar{t}V$ $(V = W, Z)$ processes for $\sqrt{s} = 13$ TeV ATLAS analyses*, ATL-PHYS-PUB-2016-005, CERN, Geneva, Switzerland (2016).

[80] S. Hoeche, F. Krauss, M. Schonherr and F. Siegert, *QCD matrix elements + parton showers: the NLO case*, *JHEP* **04** (2013) 027 [arXiv:1207.5030] [INSPIRE].

[81] S. Alioli, P. Nason, C. Oleari and E. Re, *NLO single-top production matched with shower in POWHEG: s- and t-channel contributions*, *JHEP* **09** (2009) 111 [*Erratum ibid.* **02** (2010) 011] [arXiv:0907.4076] [INSPIRE].

[82] E. Re, *Single-top Wt-channel production matched with parton showers using the POWHEG method*, *Eur. Phys. J. C* **71** (2011) 1547 [arXiv:1009.2450] [INSPIRE].

[83] T. Gleisberg and S. Hoeche, *Comix, a new matrix element generator*, *JHEP* **12** (2008) 039 [arXiv:0808.3674] [INSPIRE].

[84] C. Anastasiou, L.J. Dixon, K. Melnikov and F. Petriello, *High precision QCD at hadron colliders: electroweak gauge boson rapidity distributions at NNLO*, *Phys. Rev. D* **69** (2004) 094008 [hep-ph/0312266] [INSPIRE].

[85] S. Hoeche, F. Krauss, M. Schonherr and F. Siegert, *A critical appraisal of NLO+PS matching methods*, *JHEP* **09** (2012) 049 [arXiv:1111.1220] [INSPIRE].

[86] S. Catani, F. Krauss, R. Kuhn and B.R. Webber, *QCD matrix elements + parton showers*, *JHEP* **11** (2001) 063 [hep-ph/0109231] [INSPIRE].

[87] S. Hoeche, F. Krauss, S. Schumann and F. Siegert, *QCD matrix elements and truncated showers*, *JHEP* **05** (2009) 053 [arXiv:0903.1219] [INSPIRE].

[88] P. Nason and G. Zanderighi, *W^+W^-, WZ and ZZ production in the POWHEG-BOX-V2*, *Eur. Phys. J. C* **74** (2014) 2702 [arXiv:1311.1365] [INSPIRE].

[89] ATLAS collaboration, *Measurement of the Z/γ^* boson transverse momentum distribution in pp collisions at $\sqrt{s} = 7$ TeV with the ATLAS detector*, *JHEP* **09** (2014) 145 [arXiv:1406.3660] [INSPIRE].

[90] H.-L. Lai et al., *New parton distributions for collider physics*, *Phys. Rev. D* **82** (2010) 074024 [arXiv:1007.2241] [INSPIRE].

[91] J. Pumplin et al., *New generation of parton distributions with uncertainties from global QCD analysis*, *JHEP* **07** (2002) 012 [hep-ph/0201195] [INSPIRE].

[92] S. Alioli, P. Nason, C. Oleari and E. Re, *NLO Higgs boson production via gluon fusion matched with shower in POWHEG*, *JHEP* **04** (2009) 002 [arXiv:0812.0578] [INSPIRE].

JHEP10(2025)093

[93] P. Nason and C. Oleari, *NLO Higgs boson production via vector-boson fusion matched with shower in POWHEG*, *JHEP* **02** (2010) 037 [arXiv:0911.5299] [INSPIRE].

[94] ATLAS collaboration, *The ATLAS simulation infrastructure*, *Eur. Phys. J. C* **70** (2010) 823 [arXiv:1005.4568] [INSPIRE].

[95] GEANT4 collaboration, *GEANT4 — a simulation toolkit*, *Nucl. Instrum. Meth. A* **506** (2003) 250 [INSPIRE].

[96] ATLAS collaboration, *The simulation principle and performance of the ATLAS fast calorimeter simulation FastCaloSim*, ATL-PHYS-PUB-2010-013, CERN, Geneva, Switzerland (2010).

[97] ATLAS collaboration, *Vertex reconstruction performance of the ATLAS detector at* $\sqrt{s} = 13$ *TeV*, ATL-PHYS-PUB-2015-026, CERN, Geneva, Switzerland (2015).

[98] ATLAS collaboration, *Electron and photon performance measurements with the ATLAS detector using the 2015–2017 LHC proton-proton collision data*, 2019 *JINST* **14** P12006 [arXiv:1908.00005] [INSPIRE].

[99] ATLAS collaboration, *Muon reconstruction and identification efficiency in ATLAS using the full run 2 pp collision data set at* $\sqrt{s} = 13$ *TeV*, *Eur. Phys. J. C* **81** (2021) 578 [arXiv:2012.00578] [INSPIRE].

[100] ATLAS collaboration, *Studies of the muon momentum calibration and performance of the ATLAS detector with pp collisions at* $\sqrt{s} = 13$ *TeV*, *Eur. Phys. J. C* **83** (2023) 686 [arXiv:2212.07338] [INSPIRE].

[101] ATLAS collaboration, *Evidence for the associated production of the Higgs boson and a top quark pair with the ATLAS detector*, *Phys. Rev. D* **97** (2018) 072003 [arXiv:1712.08891] [INSPIRE].

[102] ATLAS collaboration, *Electron reconstruction and identification in the ATLAS experiment using the 2015 and 2016 LHC proton-proton collision data at* $\sqrt{s} = 13$ *TeV*, *Eur. Phys. J. C* **79** (2019) 639 [arXiv:1902.04655] [INSPIRE].

[103] ATLAS collaboration, *Jet reconstruction and performance using particle flow with the ATLAS detector*, *Eur. Phys. J. C* **77** (2017) 466 [arXiv:1703.10485] [INSPIRE].

[104] M. Cacciari, G.P. Salam and G. Soyez, *The anti-*k_t *jet clustering algorithm*, *JHEP* **04** (2008) 063 [arXiv:0802.1189] [INSPIRE].

[105] M. Cacciari, G.P. Salam and G. Soyez, *FastJet user manual*, *Eur. Phys. J. C* **72** (2012) 1896 [arXiv:1111.6097] [INSPIRE].

[106] ATLAS collaboration, *Jet energy scale and resolution measured in proton–proton collisions at* $\sqrt{s} = 13$ *TeV with the ATLAS detector*, *Eur. Phys. J. C* **81** (2021) 689 [arXiv:2007.02645] [INSPIRE].

[107] ATLAS collaboration, *Performance of pile-up mitigation techniques for jets in pp collisions at* $\sqrt{s} = 8$ *TeV using the ATLAS detector*, *Eur. Phys. J. C* **76** (2016) 581 [arXiv:1510.03823] [INSPIRE].

[108] ATLAS collaboration, *Identification and rejection of pile-up jets at high pseudorapidity with the ATLAS detector*, *Eur. Phys. J. C* **77** (2017) 580 [*Erratum ibid.* **77** (2017) 712] [arXiv:1705.02211] [INSPIRE].

[109] ATLAS collaboration, *Selection of jets produced in 13 TeV proton-proton collisions with the ATLAS detector*, ATLAS-CONF-2015-029, CERN, Geneva, Switzerland (2015).

JHEP10(2025)093

[110] ATLAS collaboration, *ATLAS flavour-tagging algorithms for the LHC run 2 pp collision dataset*, *Eur. Phys. J. C* **83** (2023) 681 [arXiv:2211.16345] [INSPIRE].

[111] ATLAS collaboration, *Identification of jets containing b-hadrons with recurrent neural networks at the ATLAS experiment*, ATL-PHYS-PUB-2017-003, CERN, Geneva, Switzerland (2017).

[112] ATLAS collaboration, *Reconstruction, energy calibration, and identification of hadronically decaying tau leptons in the ATLAS experiment for run-2 of the LHC*, ATL-PHYS-PUB-2015-045, CERN, Geneva, Switzerland (2015).

[113] ATLAS collaboration, *Measurement of the tau lepton reconstruction and identification performance in the ATLAS experiment using pp collisions at* $\sqrt{s} = 13$ *TeV*, ATLAS-CONF-2017-029, CERN, Geneva, Switzerland (2017).

[114] ATLAS collaboration, *Identification of hadronic tau lepton decays using neural networks in the ATLAS experiment*, ATL-PHYS-PUB-2019-033, CERN, Geneva, Switzerland (2019).

[115] ATLAS collaboration, *Reconstruction, identification, and calibration of hadronically decaying tau leptons with the ATLAS detector for the LHC run 3 and reprocessed run 2 data*, ATL-PHYS-PUB-2022-044, CERN, Geneva, Switzerland (2022).

[116] ATLAS collaboration, *Performance of missing transverse momentum reconstruction with the ATLAS detector using proton-proton collisions at* $\sqrt{s} = 13$ *TeV*, *Eur. Phys. J. C* **78** (2018) 903 [arXiv:1802.08168] [INSPIRE].

[117] T. Chen and C. Guestrin, *XGBoost: a scalable tree boosting system*, in *Proceedings of the 22nd ACM SIGKDD International Conference on Knowledge Discovery and Data Mining, KDD '16, (New York, NY, U.S.A.)*, Association for Computing Machinery, U.S.A. (2016), p. 785 [DOI:10.1145/2939672.2939785] [arXiv:1603.02754] [INSPIRE].

[118] ATLAS collaboration, *Measurement of event shapes at large momentum transfer with the ATLAS detector in pp collisions at* $\sqrt{s} = 7$ *TeV*, *Eur. Phys. J. C* **72** (2012) 2211 [arXiv:1206.2135] [INSPIRE].

[119] ATLAS collaboration, *Tools for estimating fake/non-prompt lepton backgrounds with the ATLAS detector at the LHC*, 2023 *JINST* **18** T11004 [arXiv:2211.16178] [INSPIRE].

[120] ATLAS collaboration, *The performance of missing transverse momentum reconstruction and its significance with the ATLAS detector using 140* fb^{-1} *of* $\sqrt{s} = 13$ *TeV pp collisions*, *Eur. Phys. J. C* **85** (2025) 606 [arXiv:2402.05858] [INSPIRE].

[121] ATLAS collaboration, *ATLAS b-jet identification performance and efficiency measurement with* $t\bar{t}$ *events in pp collisions at* $\sqrt{s} = 13$ *TeV*, *Eur. Phys. J. C* **79** (2019) 970 [arXiv:1907.05120] [INSPIRE].

[122] ATLAS collaboration, *Measurement of the c-jet mistagging efficiency in* $t\bar{t}$ *events using pp collision data at* $\sqrt{s} = 13$ *TeV collected with the ATLAS detector*, *Eur. Phys. J. C* **82** (2022) 95 [arXiv:2109.10627] [INSPIRE].

[123] ATLAS collaboration, *Calibration of the light-flavour jet mistagging efficiency of the b-tagging algorithms with Z+jets events using 139* fb^{-1} *of ATLAS proton–proton collision data at* $\sqrt{s} = 13$ *TeV*, *Eur. Phys. J. C* **83** (2023) 728 [arXiv:2301.06319] [INSPIRE].

[124] ATLAS collaboration, *Luminosity determination in pp collisions at* $\sqrt{s} = 13$ *TeV using the ATLAS detector at the LHC*, *Eur. Phys. J. C* **83** (2023) 982 [arXiv:2212.09379] [INSPIRE].

[125] ATLAS collaboration, *Studies on top-quark Monte Carlo modelling with Sherpa and MG5_aMC@NLO*, ATL-PHYS-PUB-2017-007, CERN, Geneva, Switzerland (2017).

JHEP10(2025)093

[126] E. Bothmann, M. Schönherr and S. Schumann, *Reweighting QCD matrix-element and parton-shower calculations*, *Eur. Phys. J. C* **76** (2016) 590 [arXiv:1606.08753] [INSPIRE].

[127] N. Kidonakis, *Two-loop soft anomalous dimensions for single top quark associated production with a W^- or H^-*, *Phys. Rev. D* **82** (2010) 054018 [arXiv:1005.4451] [INSPIRE].

[128] F.A. Berends, H. Kuijf, B. Tausk and W.T. Giele, *On the production of a W and jets at hadron colliders*, *Nucl. Phys. B* **357** (1991) 32 [INSPIRE].

[129] ATLAS collaboration, *Study of ttbb and ttW background modelling for ttH analyses*, ATL-PHYS-PUB-2022-026, CERN, Geneva, Switzerland (2022) [INSPIRE].

[130] ATLAS collaboration, *Measurement of top-quark pair production in association with charm quarks in proton–proton collisions at $\sqrt{s} = 13$ TeV with the ATLAS detector*, *Phys. Lett. B* **860** (2025) 139177 [arXiv:2409.11305] [INSPIRE].

[131] ROOT collaboration, *HistFactory: a tool for creating statistical models for use with RooFit and RooStats*, CERN-OPEN-2012-016, New York U., New York, NY, U.S.A. (2012) [DOI:10.17181/CERN-OPEN-2012-016].

[132] R.J. Barlow and C. Beeston, *Fitting using finite Monte Carlo samples*, *Comput. Phys. Commun.* **77** (1993) 219 [INSPIRE].

[133] R.D. Cousins, *Generalization of chisquare goodness-offit test for binned data using saturated models, with application to histograms*, https://api.semanticscholar.org/CorpusID:5936965 (2013).

[134] A. Pinto et al., *Uncertainty components in profile likelihood fits*, *Eur. Phys. J. C* **84** (2024) 593 [arXiv:2307.04007] [INSPIRE].

[135] ATLAS collaboration, *ATLAS computing acknowledgements*, ATL-SOFT-PUB-2025-001, CERN, Geneva, Switzerland (2025).

[136] G.C. Fox and S. Wolfram, *Observables for the analysis of event shapes in e^+e^- annihilation and other processes*, *Phys. Rev. Lett.* **41** (1978) 1581 [INSPIRE].

[137] C. Bernaciak, M.S.A. Buschmann, A. Butter and T. Plehn, *Fox-Wolfram moments in Higgs physics*, *Phys. Rev. D* **87** (2013) 073014 [arXiv:1212.4436] [INSPIRE].

JHEP10(2025)093

The ATLAS collaboration

G. Aad[104], E. Aakvaag[17], B. Abbott[123], S. Abdelhameed[119a], K. Abeling[55], N.J. Abicht[49], S.H. Abidi[30], M. Aboelela[45], A. Aboulhorma[36e], H. Abramowicz[157], Y. Abulaiti[120], B.S. Acharya[69a,69b,m], A. Ackermann[63a], C. Adam Bourdarios[4], L. Adamczyk[87a], S.V. Addepalli[149], M.J. Addison[103], J. Adelman[118], A. Adiguzel[22c], T. Adye[137], A.A. Affolder[139], Y. Afik[40], M.N. Agaras[13], A. Aggarwal[102], C. Agheorghiesei[28c], F. Ahmadov[39,ad], S. Ahuja[97], X. Ai[143b], G. Aielli[76a,76b], A. Aikot[169], M. Ait Tamlihat[36e], B. Aitbenchikh[36a], M. Akbiyik[102], T.P.A. Åkesson[100], A.V. Akimov[151], D. Akiyama[174], N.N. Akolkar[25], S. Aktas[172], G.L. Alberghi[24b], J. Albert[171], U. Alberti[20], P. Albicocco[53], G.L. Albouy[60], S. Alderweireldt[52], Z.L. Alegria[124], M. Aleksa[37], I.N. Aleksandrov[39], C. Alexa[28b], T. Alexopoulos[10], F. Alfonsi[24b], M. Algren[56], M. Alhroob[173], B. Ali[135], H.M.J. Ali[93,w], S. Ali[32], S.W. Alibocus[94], M. Aliev[34c], G. Alimonti[71a], W. Alkakhi[55], C. Allaire[66], B.M.M. Allbrooke[152], J.S. Allen[103], J.F. Allen[52], P.P. Allport[21], A. Aloisio[72a,72b], F. Alonso[92], C. Alpigiani[142], Z.M.K. Alsolami[93], A. Alvarez Fernandez[102], M. Alves Cardoso[56], M.G. Alviggi[72a,72b], M. Aly[103], Y. Amaral Coutinho[83b], A. Ambler[106], C. Amelung[37], M. Amerl[103], C.G. Ames[111], T. Amezza[130], D. Amidei[108], B. Amini[54], K. Amirie[161], A. Amirkhanov[39], S.P. Amor Dos Santos[133a], K.R. Amos[169], D. Amperiadou[158], S. An[84], C. Anastopoulos[145], T. Andeen[11], J.K. Anders[94], A.C. Anderson[59], A. Andreazza[71a,71b], S. Angelidakis[9], A. Angerami[42], A.V. Anisenkov[39], A. Annovi[74a], C. Antel[37], E. Antipov[151], M. Antonelli[53], F. Anulli[75a], M. Aoki[84], T. Aoki[159], M.A. Aparo[152], L. Aperio Bella[48], M. Apicella[31], C. Appelt[157], A. Apyan[27], M. Arampatzi[10], S.J. Arbiol Val[88], C. Arcangeletti[53], A.T.H. Arce[51], J-F. Arguin[110], S. Argyropoulos[158], J.-H. Arling[48], O. Arnaez[4], H. Arnold[151], G. Artoni[75a,75b], H. Asada[113], K. Asai[121], S. Asatryan[179], N.A. Asbah[37], R.A. Ashby Pickering[173], A.M. Aslam[97], K. Assamagan[30], R. Astalos[29a], K.S.V. Astrand[100], S. Atashi[165], R.J. Atkin[34a], H. Atmani[36f], P.A. Atmasiddha[131], K. Augsten[135], A.D. Auriol[41], V.A. Austrup[103], A.S. Avad[96], G. Avolio[37], K. Axiotis[56], A. Azzam[13], D. Babal[29b], H. Bachacou[138], K. Bachas[158,q], A. Bachiu[35], E. Bachmann[50], M.J. Backes[63a], A. Badea[40], T.M. Baer[108], P. Bagnaia[75a,75b], M. Bahmani[19], D. Bahner[54], K. Bai[126], J.T. Baines[137], L. Baines[96], O.K. Baker[178], E. Bakos[16], D. Bakshi Gupta[8], L.E. Balabram Filho[83b], V. Balakrishnan[123], R. Balasubramanian[4], E.M. Baldin[38], P. Balek[87a], E. Ballabene[24b,24a], F. Balli[138], L.M. Baltes[63a], W.K. Balunas[33], J. Balz[102], I. Bamwidhi[119b], E. Banas[88], M. Bandieramonte[132], A. Bandyopadhyay[25], S. Bansal[25], L. Barak[157], M. Barakat[48], E.L. Barberio[107], D. Barberis[18b], M. Barbero[104], M.Z. Barel[117], T. Barillari[112], M-S. Barisits[37], T. Barklow[149], P. Baron[136], D.A. Baron Moreno[103], A. Baroncelli[62], A.J. Barr[129], J.D. Barr[98], F. Barreiro[101], J. Barreiro Guimarães da Costa[14], M.G. Barros Teixeira[133a], S. Barsov[38], F. Bartels[63a], R. Bartoldus[149], A.E. Barton[93], P. Bartos[29a], M. Baselga[49], S. Bashiri[88], A. Bassalat[66,b], M.J. Basso[162a], S. Bataju[45], R. Bate[170], R.L. Bates[59], S. Batlamous[101], M. Battaglia[139], D. Battulga[19], M. Bauce[75a,75b], M. Bauer[79], P. Bauer[25], L.T. Bayer[48], L.T. Bazzano Hurrell[31], J.B. Beacham[112], T. Beau[130], J.Y. Beaucamp[92], P.H. Beauchemin[164], P. Bechtle[25], H.P. Beck[20,p], K. Becker[173], A.J. Beddall[82],

JHEP10(2025)093

V.A. Bednyakov[39], C.P. Bee[151], L.J. Beemster[16], M. Begalli[83d], M. Begel[30], J.K. Behr[48], J.F. Beirer[37], F. Beisiegel[25], M. Belfkir[119b], G. Bella[157], L. Bellagamba[24b], A. Bellerive[35], C.D. Bellgraph[68], P. Bellos[21], K. Beloborodov[38], I. Benaoumeur[21], D. Benchekroun[36a], F. Bendebba[36a], Y. Benhammou[157], K.C. Benkendorfer[61], L. Beresford[48], M. Beretta[53], E. Bergeaas Kuutmann[167], N. Berger[4], B. Bergmann[135], J. Beringer[18a], G. Bernardi[5], C. Bernius[149], F.U. Bernlochner[25], A. Berrocal Guardia[13], T. Berry[97], P. Berta[136], A. Berthold[50], A. Berti[133a], R. Bertrand[104], S. Bethke[112], A. Betti[75a,75b], A.J. Bevan[96], L. Bezio[56], N.K. Bhalla[54], S. Bharthuar[112], S. Bhatta[151], P. Bhattarai[149], Z.M. Bhatti[120], K.D. Bhide[54], V.S. Bhopatkar[124], R.M. Bianchi[132], G. Bianco[24b,24a], O. Biebel[111], M. Biglietti[77a], C.S. Billingsley[45], Y. Bimgdi[36f], M. Bindi[55], A. Bingham[177], A. Bingul[22b], C. Bini[75a,75b], G.A. Bird[33], M. Birman[175], M. Biros[136], S. Biryukov[152], T. Bisanz[49], E. Bisceglie[24b,24a], J.P. Biswal[137], D. Biswas[147], I. Bloch[48], A. Blue[59], U. Blumenschein[96], V.S. Bobrovnikov[39], L. Boccardo[57b,57a], M. Boehler[54], B. Boehm[172], D. Bogavac[13], A.G. Bogdanchikov[38], L.S. Boggia[130], V. Boisvert[97], P. Bokan[37], T. Bold[87a], M. Bomben[5], M. Bona[96], M. Boonekamp[138], A.G. Borbély[59], I.S. Bordulev[38], G. Borissov[93], D. Bortoletto[129], D. Boscherini[24b], M. Bosman[13], K. Bouaouda[36a], N. Bouchhar[169], L. Boudet[4], J. Boudreau[132], E.V. Bouhova-Thacker[93], D. Boumediene[41], R. Bouquet[57b,57a], A. Boveia[122], J. Boyd[37], D. Boye[30], I.R. Boyko[39], L. Bozianu[56], J. Bracinik[21], N. Brahimi[4], G. Brandt[177], O. Brandt[33], B. Brau[105], J.E. Brau[126], R. Brener[175], L. Brenner[117], R. Brenner[167], S. Bressler[175], G. Brianti[78a,78b], D. Britton[59], D. Britzger[112], I. Brock[25], R. Brock[109], G. Brooijmans[42], A.J. Brooks[68], E.M. Brooks[162b], E. Brost[30], L.M. Brown[171,162a], L.E. Bruce[61], T.L. Bruckler[129], P.A. Bruckman de Renstrom[88], B. Brüers[48], A. Bruni[24b], G. Bruni[24b], D. Brunner[47a,47b], M. Bruschi[24b], N. Bruscino[75a,75b], T. Buanes[17], Q. Buat[142], D. Buchin[112], A.G. Buckley[59], O. Bulekov[82], B.A. Bullard[149], S. Burdin[94], C.D. Burgard[49], A.M. Burger[91], B. Burghgrave[8], O. Burlayenko[54], J. Burleson[168], J.C. Burzynski[148], E.L. Busch[42], V. Büscher[102], P.J. Bussey[59], J.M. Butler[26], C.M. Buttar[59], J.M. Butterworth[98], W. Buttinger[137], C.J. Buxo Vazquez[109], A.R. Buzykaev[39], S. Cabrera Urbán[169], L. Cadamuro[66], H. Cai[37], Y. Cai[24b,114c,24a], Y. Cai[114a], V.M.M. Cairo[37], O. Cakir[3a], N. Calace[37], P. Calafiura[18a], G. Calderini[130], P. Calfayan[35], L. Calic[100], G. Callea[59], L.P. Caloba[83b], D. Calvet[41], S. Calvet[41], R. Camacho Toro[130], S. Camarda[37], D. Camarero Munoz[27], P. Camarri[76a,76b], C. Camincher[171], M. Campanelli[98], A. Camplani[43], V. Canale[72a,72b], A.C. Canbay[3a], E. Canonero[97], J. Cantero[169], Y. Cao[168], F. Capocasa[27], M. Capua[44b,44a], A. Carbone[71a,71b], R. Cardarelli[76a], J.C.J. Cardenas[8], M.P. Cardiff[27], G. Carducci[44b,44a], T. Carli[37], G. Carlino[72a], J.I. Carlotto[13], B.T. Carlson[132,r], E.M. Carlson[171], J. Carmignani[94], L. Carminati[71a,71b], A. Carnelli[4], M. Carnesale[37], S. Caron[116], E. Carquin[140g], I.B. Carr[107], S. Carrá[73a,73b], G. Carratta[24b,24a], C. Carrion Martinez[169], A.M. Carroll[126], M.P. Casado[13,h], P. Casolaro[72a,72b], M. Caspar[48], W.R. Castiglioni[40], F.L. Castillo[4], L. Castillo Garcia[13], V. Castillo Gimenez[169], N.F. Castro[133a,133e], A. Catinaccio[37], J.R. Catmore[128], T. Cavaliere[4], V. Cavaliere[30], L.J. Caviedes Betancourt[23b], E. Celebi[82], S. Cella[37], V. Cepaitis[56], K. Cerny[125], A.S. Cerqueira[83a], A. Cerri[74a,74b,am], L. Cerrito[76a,76b], F. Cerutti[18a], B. Cervato[71a,71b],

JHEP10(2025)093

A. Cervelli[24b], G. Cesarini[53], S.A. Cetin[82], P.M. Chabrillat[130], R. Chakkappai[66], S. Chakraborty[173], A. Chambers[61], J. Chan[18a], W.Y. Chan[159], J.D. Chapman[33], E. Chapon[138], B. Chargeishvili[155b], D.G. Charlton[21], C. Chauhan[136], Y. Che[114a], S. Chekanov[6], S.V. Chekulaev[162a], G.A. Chelkov[39,a], B. Chen[157], B. Chen[171], H. Chen[114a], H. Chen[30], J. Chen[144a], J. Chen[148], M. Chen[129], S. Chen[89], S.J. Chen[114a], X. Chen[144a], X. Chen[15,ah], Z. Chen[62], C.L. Cheng[176], H.C. Cheng[64a], S. Cheong[149], A. Cheplakov[39], E. Cherepanova[117], R. Cherkaoui El Moursli[36e], E. Cheu[7], K. Cheung[65], L. Chevalier[138], V. Chiarella[53], G. Chiarelli[74a], G. Chiodini[70a], A.S. Chisholm[21], A. Chitan[28b], M. Chitishvili[169], M.V. Chizhov[39,s], K. Choi[11], Y. Chou[142], E.Y.S. Chow[116], K.L. Chu[175], M.C. Chu[64a], X. Chu[14,114c], Z. Chubinidze[53], J. Chudoba[134], J.J. Chwastowski[88], D. Cieri[112], K.M. Ciesla[87a], V. Cindro[95], A. Ciocio[18a], F. Cirotto[72a,72b], Z.H. Citron[175], M. Citterio[71a], D.A. Ciubotaru[28b], A. Clark[56], P.J. Clark[52], N. Clarke Hall[98], C. Clarry[161], S.E. Clawson[48], C. Clement[47a,47b], Y. Coadou[104], M. Cobal[69a,69c], A. Coccaro[57b], R.F. Coelho Barrue[133a], R. Coelho Lopes De Sa[105], S. Coelli[71a], L.S. Colangeli[161], B. Cole[42], P. Collado Soto[101], J. Collot[60], R. Coluccia[70a,70b], P. Conde Muiño[133a,133g], M.P. Connell[34c], S.H. Connell[34c], E.I. Conroy[129], M. Contreras Cossio[11], F. Conventi[72a,aj], A.M. Cooper-Sarkar[129], L. Corazzina[75a,75b], F.A. Corchia[24b,24a], A. Cordeiro Oudot Choi[142], L.D. Corpe[41], M. Corradi[75a,75b], F. Corriveau[106,ab], A. Cortes-Gonzalez[159], M.J. Costa[169], F. Costanza[4], D. Costanzo[145], J. Couthures[4], G. Cowan[97], K. Cranmer[176], L. Cremer[49], D. Cremonini[24b,24a], S. Crépé-Renaudin[60], F. Crescioli[130], T. Cresta[73a,73b], M. Cristinziani[147], M. Cristoforetti[78a,78b], V. Croft[117], G. Crosetti[44b,44a], A. Cueto[101], H. Cui[98], Z. Cui[7], B.M. Cunnett[152], W.R. Cunningham[59], F. Curcio[169], J.R. Curran[52], M.J. Da Cunha Sargedas De Sousa[57b,57a], J.V. Da Fonseca Pinto[83b], C. Da Via[103], W. Dabrowski[87a], T. Dado[37], S. Dahbi[154], T. Dai[108], D. Dal Santo[20], C. Dallapiccola[105], M. Dam[43], G. D'amen[30], V. D'Amico[111], J. Damp[102], J.R. Dandoy[35], M. D'Andrea[57b,57a], D. Dannheim[37], G. D'anniballe[74a,74b], M. Danninger[148], V. Dao[151], G. Darbo[57b], S.J. Das[30], F. Dattola[48], S. D'Auria[71a,71b], A. D'Avanzo[72a,72b], T. Davidek[136], J. Davidson[173], I. Dawson[96], K. De[8], C. De Almeida Rossi[161], R. De Asmundis[72a], N. De Biase[48], S. De Castro[24b,24a], N. De Groot[116], P. de Jong[117], H. De la Torre[118], A. De Maria[114a], A. De Salvo[75a], U. De Sanctis[76a,76b], F. De Santis[70a,70b], A. De Santo[152], J.B. De Vivie De Regie[60], J. Debevc[95], D.V. Dedovich[39], J. Degens[94], A.M. Deiana[45], J. Del Peso[101], L. Delagrange[130], F. Deliot[138], C.M. Delitzsch[49], M. Della Pietra[72a,72b], D. Della Volpe[56], A. Dell'Acqua[37], L. Dell'Asta[71a,71b], M. Delmastro[4], C.C. Delogu[102], P.A. Delsart[60], S. Demers[178], M. Demichev[39], S.P. Denisov[38], H. Denizli[22a,l], L. D'Eramo[41], D. Derendarz[88], F. Derue[130], P. Dervan[94,*], A.M. Desai[1], K. Desch[25], F.A. Di Bello[57b,57a], A. Di Ciaccio[76a,76b], L. Di Ciaccio[4], A. Di Domenico[75a,75b], C. Di Donato[72a,72b], A. Di Girolamo[37], G. Di Gregorio[37], A. Di Luca[78a,78b], B. Di Micco[77a,77b], R. Di Nardo[77a,77b], K.F. Di Petrillo[40], M. Diamantopoulou[35], F.A. Dias[117], M.A. Diaz[140a,140b], A.R. Didenko[39], M. Didenko[169], S.D. Diefenbacher[18a], E.B. Diehl[108], S. Díez Cornell[48], C. Diez Pardos[147], C. Dimitriadi[150], A. Dimitrievska[21], A. Dimri[151], Y. Ding[62], J. Dingfelder[25], T. Dingley[129], I-M. Dinu[28b], S.J. Dittmeier[63b], F. Dittus[37],

JHEP10(2025)093

M. Divisek[136], B. Dixit[94], F. Djama[104], T. Djobava[155b], C. Doglioni[103,100], A. Dohnalova[29a], Z. Dolezal[136], K. Domijan[87a], K.M. Dona[40], M. Donadelli[83d], B. Dong[109], J. Donini[41], A. D'Onofrio[72a,72b], M. D'Onofrio[94], J. Dopke[137], A. Doria[72a], N. Dos Santos Fernandes[133a], I.A. Dos Santos Luz[83e], P. Dougan[103], M.T. Dova[92], A.T. Doyle[59], M.P. Drescher[55], E. Dreyer[175], I. Drivas-koulouris[10], M. Drnevich[120], D. Du[62], T.A. du Pree[117], Z. Duan[114a], M. Dubau[4], F. Dubinin[39], M. Dubovsky[29a], E. Duchovni[175], G. Duckeck[111], P.K. Duckett[98], O.A. Ducu[28b], D. Duda[52], A. Dudarev[37], M.M. Dudek[88], E.R. Duden[27], M. D'uffizi[103], L. Duflot[66], M. Dührssen[37], I. Duminica[28g], A.E. Dumitriu[28b], M. Dunford[63a], K. Dunne[47a,47b], A. Duperrin[104], H. Duran Yildiz[3a], A. Durglishvili[155b], G.I. Dyckes[18a], M. Dyndal[87a], B.S. Dziedzic[37], Z.O. Earnshaw[152], G.H. Eberwein[129], B. Eckerova[29a], S. Eggebrecht[55], E. Egidio Purcino De Souza[83e], G. Eigen[17], K. Einsweiler[18a], T. Ekelof[167], P.A. Ekman[100], S. El Farkh[36b], Y. El Ghazali[62], H. El Jarrari[37], A. El Moussaouy[36a], D. Elitez[37], M. Ellert[167], F. Ellinghaus[177], T.A. Elliot[97], N. Ellis[37], J. Elmsheuser[30], M. Elsawy[119a], M. Elsing[37], D. Emeliyanov[137], Y. Enari[84], S. Epari[110], D. Ernani Martins Neto[88], F. Ernst[37], M. Errenst[177], M. Escalier[66], C. Escobar[169], E. Etzion[157], G. Evans[133a,133b], H. Evans[68], L.S. Evans[48], A. Ezhilov[38], S. Ezzarqtouni[36a], F. Fabbri[24b,24a], L. Fabbri[24b,24a], G. Facini[98], V. Fadeyev[139], R.M. Fakhrutdinov[38], D. Fakoudis[102], S. Falciano[75a], L.F. Falda Ulhoa Coelho[133a], F. Fallavollita[112], G. Falsetti[44b,44a], J. Faltova[136], C. Fan[168], K.Y. Fan[64b], Y. Fan[14], Y. Fang[14,114c], M. Fanti[71a,71b], M. Faraj[69a,69b], Z. Farazpay[99], A. Farbin[8], A. Farilla[77a], K. Farman[154], T. Farooque[109], J.N. Farr[178], S.M. Farrington[137,52], F. Fassi[36e], D. Fassouliotis[9], L. Fayard[66], P. Federic[136], P. Federicova[134], O.L. Fedin[38,a], M. Feickert[176], L. Feligioni[104], D.E. Fellers[18a], C. Feng[143a], Y. Feng[14], Z. Feng[117], M.J. Fenton[165], L. Ferencz[48], B. Fernandez Barbadillo[93], P. Fernandez Martinez[67], M.J.V. Fernoux[104], J. Ferrando[93], A. Ferrari[167], P. Ferrari[117,116], R. Ferrari[73a], D. Ferrere[56], C. Ferretti[108], M.P. Fewell[1], D. Fiacco[75a,75b], F. Fiedler[102], P. Fiedler[135], S. Filimonov[39], M.S. Filip[28b,t], A. Filipčič[95], E.K. Filmer[162a], F. Filthaut[116], M.C.N. Fiolhais[133a,133c,c], L. Fiorini[169], W.C. Fisher[109], T. Fitschen[103], P.M. Fitzhugh[138], I. Fleck[147], P. Fleischmann[108], T. Flick[177], M. Flores[34d,ag], L.R. Flores Castillo[64a], L. Flores Sanz De Acedo[37], F.M. Follega[78a,78b], N. Fomin[33], J.H. Foo[161], A. Formica[138], A.C. Forti[103], E. Fortin[37], A.W. Fortman[18a], L. Foster[18a], L. Fountas[9,i], D. Fournier[66], H. Fox[93], P. Francavilla[74a,74b], S. Francescato[61], S. Franchellucci[56], M. Franchini[24b,24a], S. Franchino[63a], D. Francis[37], L. Franco[116], L. Franconi[48], M. Franklin[61], G. Frattari[27], Y.Y. Frid[157], J. Friend[59], N. Fritzsche[37], A. Froch[56], D. Froidevaux[37], J.A. Frost[129], Y. Fu[109], S. Fuenzalida Garrido[140g], M. Fujimoto[151], K.Y. Fung[64a], E. Furtado De Simas Filho[83e], M. Furukawa[159], J. Fuster[169], A. Gaa[55], A. Gabrielli[24b,24a], A. Gabrielli[161], P. Gadow[37], G. Gagliardi[57b,57a], L.G. Gagnon[18a], S. Gaid[85b], S. Galantzan[157], J. Gallagher[1], E.J. Gallas[129], A.L. Gallen[167], B.J. Gallop[137], K.K. Gan[122], S. Ganguly[159], Y. Gao[52], A. Garabaglu[142], F.M. Garay Walls[140a,140b], C. García[169], A. Garcia Alonso[117], A.G. Garcia Caffaro[178], J.E. García Navarro[169], M.A. Garcia Ruiz[23b], M. Garcia-Sciveres[18a], G.L. Gardner[131], R.W. Gardner[40], N. Garelli[164], R.B. Garg[149], J.M. Gargan[33], C.A. Garner[161], C.M. Garvey[34a],

JHEP10(2025)093

V.K. Gassmann[164], G. Gaudio[73a], V. Gautam[13], P. Gauzzi[75a,75b], J. Gavranovic[95], I.L. Gavrilenko[133a], A. Gavrilyuk[38], C. Gay[170], G. Gaycken[126], E.N. Gazis[10], A. Gekow[122], C. Gemme[57b], M.H. Genest[60], A.D. Gentry[115], S. George[97], T. Geralis[46], A.A. Gerwin[123], P. Gessinger-Befurt[37], M.E. Geyik[177], M. Ghani[173], K. Ghorbanian[96], A. Ghosal[147], A. Ghosh[165], A. Ghosh[7], B. Giacobbe[24b], S. Giagu[75a,75b], T. Giani[117], A. Giannini[62], S.M. Gibson[97], M. Gignac[139], D.T. Gil[87b], A.K. Gilbert[87a], B.J. Gilbert[42], D. Gillberg[35], G. Gilles[117], D.M. Gingrich[2,ai], M.P. Giordani[69a,69c], P.F. Giraud[138], G. Giugliarelli[69a,69c], D. Giugni[71a], F. Giuli[76a,76b], I. Gkialas[9,i], L.K. Gladilin[38], C. Glasman[101], M. Glazewska[20], R.M. Gleason[165], G. Glemža[48], M. Glisic[126], I. Gnesi[44b], Y. Go[30], M. Goblirsch-Kolb[37], B. Gocke[49], D. Godin[110], B. Gokturk[22a], S. Goldfarb[107], T. Golling[56], M.G.D. Gololo[34c], D. Golubkov[38], J.P. Gombas[109], A. Gomes[133a,133b], G. Gomes Da Silva[147], A.J. Gomez Delegido[37], R. Gonçalo[133a], L. Gonella[21], A. Gongadze[155c], F. Gonnella[21], J.L. Gonski[149], R.Y. González Andana[52], S. González de la Hoz[169], M.V. Gonzalez Rodrigues[48], R. Gonzalez Suarez[167], S. Gonzalez-Sevilla[56], L. Goossens[37], B. Gorini[37], E. Gorini[70a,70b], A. Gorišek[95], T.C. Gosart[131], A.T. Goshaw[51], M.I. Gostkin[39], S. Goswami[124], C.A. Gottardo[37], S.A. Gotz[111], M. Gouighri[36b], A.G. Goussiou[142], N. Govender[34c], R.P. Grabarczyk[129], I. Grabowska-Bold[87a], K. Graham[35], E. Gramstad[128], S. Grancagnolo[70a,70b], C.M. Grant[1], P.M. Gravila[28f], F.G. Gravili[70a,70b], H.M. Gray[18a], M. Greco[112], M.J. Green[1], C. Grefe[25], A.S. Grefsrud[17], I.M. Gregor[48], K.T. Greif[165], P. Grenier[149], S.G. Grewe[112], A.A. Grillo[139], K. Grimm[32], S. Grinstein[13,x], J.-F. Grivaz[66], E. Gross[175], J. Grosse-Knetter[55], L. Guan[108], G. Guerrieri[37], R. Guevara[128], R. Gugel[102], J.A.M. Guhit[108], A. Guida[19], E. Guilloton[173], S. Guindon[37], F. Guo[14,114c], J. Guo[144a], L. Guo[48], L. Guo[114b,v], Y. Guo[108], Y. Guo[42], A. Gupta[49], R. Gupta[132], S. Gupta[27], S. Gurbuz[25], S.S. Gurdasani[48], G. Gustavino[75a,75b], P. Gutierrez[123], L.F. Gutierrez Zagazeta[131], M. Gutsche[50], C. Gutschow[98], C. Gwenlan[129], C.B. Gwilliam[94], E.S. Haaland[128], A. Haas[120], M. Habedank[59], C. Haber[18a], H.K. Hadavand[8], A. Haddad[41], A. Hadef[50], A.I. Hagan[93], J.J. Hahn[147], E.H. Haines[98], M. Haleem[172], J. Haley[124], G.D. Hallewell[104], K. Hamano[171], H. Hamdaoui[167], M. Hamer[25], S.E.D. Hammoud[66], E.J. Hampshire[97], J. Han[143a], L. Han[114a], L. Han[62], S. Han[14], K. Hanagaki[84], M. Hance[139], D.A. Hangal[42], H. Hanif[148], M.D. Hank[131], J.B. Hansen[43], P.H. Hansen[43], D. Harada[56], T. Harenberg[177], S. Harkusha[179], M.L. Harris[105], Y.T. Harris[25], J. Harrison[13], N.M. Harrison[122], P.F. Harrison[173], M.L.E. Hart[98], N.M. Hartman[112], N.M. Hartmann[111], R.Z. Hasan[97,137], Y. Hasegawa[146], F. Haslbeck[129], S. Hassan[17], R. Hauser[109], M. Haviernik[136], C.M. Hawkes[21], R.J. Hawkings[37], Y. Hayashi[159], D. Hayden[109], C. Hayes[108], R.L. Hayes[117], C.P. Hays[129], J.M. Hays[96], H.S. Hayward[94], M. He[14,114c], Y. He[48], Y. He[98], N.B. Heatley[96], V. Hedberg[100], C. Heidegger[54], K.K. Heidegger[54], J. Heilman[35], S. Heim[48], T. Heim[18a], J.J. Heinrich[126], L. Heinrich[112], J. Hejbal[134], M. Helbig[50], A. Held[176], S. Hellesund[17], C.M. Helling[170], S. Hellman[47a,47b], A.M. Henriques Correia[37], H. Herde[100], Y. Hernández Jiménez[151], L.M. Herrmann[25], T. Herrmann[50], G. Herten[54], R. Hertenberger[111], L. Hervas[37], M.E. Hesping[102], N.P. Hessey[162a], J. Hessler[112], M. Hidaoui[36b], N. Hidic[136], E. Hill[161], T.S. Hillersoy[17], S.J. Hillier[21], J.R. Hinds[109],

JHEP10(2025)093

F. Hinterkeuser[25], M. Hirose[127], S. Hirose[163], D. Hirschbuehl[177], T.G. Hitchings[103], B. Hiti[95], J. Hobbs[151], R. Hobincu[28e], N. Hod[175], A.M. Hodges[168], M.C. Hodgkinson[145], B.H. Hodkinson[129], A. Hoecker[37], D.D. Hofer[108], J. Hofer[169], J. Hofner[102], M. Holzbock[37], L.B.A.H. Hommels[33], V. Homsak[129], B.P. Honan[103], J.J. Hong[68], T.M. Hong[132], B.H. Hooberman[168], W.H. Hopkins[6], M.C. Hoppesch[168], Y. Horii[113], M.E. Horstmann[112], S. Hou[154], M.R. Housenga[168], J. Howarth[59], J. Hoya[6], M. Hrabovsky[125], T. Hryn'ova[4], P.J. Hsu[65], S.-C. Hsu[142], T. Hsu[66], M. Hu[18a], Q. Hu[62], S. Huang[33], X. Huang[14,114c], Y. Huang[136], Y. Huang[114b], Y. Huang[14], Z. Huang[66], Z. Hubacek[135], F. Huegging[25], T.B. Huffman[129], M. Hufnagel Maranha De Faria[83a], C.A. Hugli[48], M. Huhtinen[37], S.K. Huiberts[17], R. Hulsken[106], C.E. Hultquist[18a], D.L. Humphreys[105], N. Huseynov[12], J. Huston[109], J. Huth[61], L. Huth[48], R. Hyneman[7], G. Iacobucci[56], G. Iakovidis[30], L. Iconomidou-Fayard[66], J.P. Iddon[37], P. Iengo[72a,72b], R. Iguchi[159], Y. Iiyama[159], T. Iizawa[159], Y. Ikegami[84], D. Iliadis[158], N. Ilic[161], H. Imam[36a], G. Inacio Goncalves[83d], S.A. Infante Cabanas[140c], T. Ingebretsen Carlson[47a,47b], J.M. Inglis[96], G. Introzzi[73a,73b], M. Iodice[77a], V. Ippolito[75a,75b], R.K. Irwin[94], M. Ishino[159], W. Islam[176], C. Issever[19], S. Istin[22a,ao], K. Itabashi[84], H. Ito[174], R. Iuppa[78a,78b], A. Ivina[175], V. Izzo[72a], P. Jacka[135], P. Jackson[1], P. Jain[48], K. Jakobs[54], T. Jakoubek[175], J. Jamieson[59], W. Jang[159], S. Jankovych[136], M. Javurkova[105], P. Jawahar[103], L. Jeanty[126], J. Jejelava[155a,ae], P. Jenni[54,f], C.E. Jessiman[35], C. Jia[143a], H. Jia[170], J. Jia[151], X. Jia[112,114c], Z. Jia[114a], C. Jiang[52], Q. Jiang[64b], S. Jiggins[48], M. Jimenez Ortega[169], J. Jimenez Pena[13], S. Jin[114a], A. Jinaru[28b], O. Jinnouchi[141], P. Johansson[145], K.A. Johns[7], J.W. Johnson[139], F.A. Jolly[48], D.M. Jones[152], E. Jones[48], K.S. Jones[8], P. Jones[33], R.W.L. Jones[93], T.J. Jones[94], H.L. Joos[55], R. Joshi[122], J. Jovicevic[16], X. Ju[18a], J.J. Junggeburth[37], T. Junkermann[63a], A. Juste Rozas[13,x], M.K. Juzek[88], S. Kabana[140f], A. Kaczmarska[88], S.A. Kadir[149], M. Kado[112], H. Kagan[122], M. Kagan[149], A. Kahn[131], C. Kahra[102], T. Kaji[159], E. Kajomovitz[156], N. Kakati[175], N. Kakoty[13], I. Kalaitzidou[54], S. Kandel[8], N.J. Kang[139], D. Kar[34h], E. Karentzos[25], K. Karki[8], O. Karkout[117], S.N. Karpov[39], Z.M. Karpova[39], V. Kartvelishvili[93], A.N. Karyukhin[38], E. Kasimi[158], J. Katzy[48], S. Kaur[35], K. Kawade[146], M.P. Kawale[123], C. Kawamoto[89], T. Kawamoto[62], E.F. Kay[37], F.I. Kaya[164], S. Kazakos[109], V.F. Kazanin[38], J.M. Keaveney[34a], R. Keeler[171], G.V. Kehris[61], J.S. Keller[35], J.M. Kelly[171], J.J. Kempster[152], O. Kepka[134], J. Kerr[162b], B.P. Kerridge[137], B.P. Kerševan[95], L. Keszeghova[29a], R.A. Khan[132], A. Khanov[124], A.G. Kharlamov[38], T. Kharlamova[38], E.E. Khoda[142], M. Kholodenko[133a], T.J. Khoo[19], G. Khoriauli[172], Y. Khoulaki[36a], J. Khubua[155b,*], Y.A.R. Khwaira[130], B. Kibirige[34h], D. Kim[6], D.W. Kim[47a,47b], Y.K. Kim[40], N. Kimura[98], M.K. Kingston[55], A. Kirchhoff[55], C. Kirfel[25], F. Kirfel[25], J. Kirk[137], A.E. Kiryunin[112], S. Kita[163], O. Kivernyk[25], M. Klassen[164], C. Klein[35], L. Klein[172], M.H. Klein[45], S.B. Klein[56], U. Klein[94], A. Klimentov[30], T. Klioutchnikova[37], P. Kluit[117], S. Kluth[112], E. Kneringer[79], T.M. Knight[161], A. Knue[49], M. Kobel[50], D. Kobylianskii[175], S.F. Koch[129], M. Kocian[149], P. Kodyš[136], D.M. Koeck[126], T. Koffas[35], O. Kolay[50], I. Koletsou[4], T. Komarek[88], K. Köneke[55], A.X.Y. Kong[1], T. Kono[121], N. Konstantinidis[98], P. Kontaxakis[56], B. Konya[100],

JHEP10(2025)093

R. Kopeliansky[42], S. Koperny[87a], K. Korcyl[88], K. Kordas[158,d], A. Korn[98], S. Korn[55], I. Korolkov[13], N. Korotkova[38], B. Kortman[117], O. Kortner[112], S. Kortner[112], W.H. Kostecka[118], M. Kostov[29a], V.V. Kostyukhin[147], A. Kotsokechagia[37], A. Kotwal[51], A. Koulouris[37], A. Kourkoumeli-Charalampidi[73a,73b], C. Kourkoumelis[9], E. Kourlitis[112], O. Kovanda[126], R. Kowalewski[171], W. Kozanecki[126], A.S. Kozhin[38], V.A. Kramarenko[38], G. Kramberger[95], P. Kramer[25], M.W. Krasny[130], A. Krasznahorkay[105], A.C. Kraus[118], J.W. Kraus[177], J.A. Kremer[48], N.B. Krengel[147], T. Kresse[50], L. Kretschmann[177], J. Kretzschmar[94], P. Krieger[161], K. Krizka[21], K. Kroeninger[49], H. Kroha[112], J. Kroll[134], J. Kroll[131], K.S. Krowpman[109], U. Kruchonak[39], H. Krüger[25], N. Krumnack[81], M.C. Kruse[51], O. Kuchinskaia[39], S. Kuday[3a], S. Kuehn[37], R. Kuesters[54], T. Kuhl[48], V. Kukhtin[39], Y. Kulchitsky[39], S. Kuleshov[140d,140b], J. Kull[1], E.V. Kumar[111], M. Kumar[34h], N. Kumari[48], P. Kumari[162b], A. Kupco[134], A. Kupich[38], O. Kuprash[54], H. Kurashige[86], L.L. Kurchaninov[162a], O. Kurdysh[4], Y.A. Kurochkin[38], A. Kurova[38], M. Kuze[141], A.K. Kvam[105], J. Kvita[125], N.G. Kyriacou[142], C. Lacasta[169], F. Lacava[75a,75b], H. Lacker[19], D. Lacour[130], N.N. Lad[98], E. Ladygin[39], A. Lafarge[41], B. Laforge[130], T. Lagouri[178], F.Z. Lahbabi[36a], S. Lai[55,37], W.S. Lai[98], J.E. Lambert[171], S. Lammers[68], W. Lampl[7], C. Lampoudis[158,d], G. Lamprinoudis[102], A.N. Lancaster[118], E. Lançon[30], U. Landgraf[54], M.P.J. Landon[96], V.S. Lang[54], O.K.B. Langrekken[128], A.J. Lankford[165], F. Lanni[37], K. Lantzsch[25], A. Lanza[73a], M. Lanzac Berrocal[169], J.F. Laporte[138], T. Lari[71a], D. Larsen[17], L. Larson[11], F. Lasagni Manghi[24b], M. Lassnig[37], S.D. Lawlor[145], R. Lazaridou[165], M. Lazzaroni[71a,71b], E.T.T. Le[165], H.D.M. Le[109], E.M. Le Boulicaut[178], L.T. Le Pottier[18a], B. Leban[24b,24a], F. Ledroit-Guillon[60], T.F. Lee[162b], L.L. Leeuw[34c], M. Lefebvre[171], C. Leggett[18a], G. Lehmann Miotto[37], M. Leigh[56], W.A. Leight[105], W. Leinonen[116], A. Leisos[158,u], M.A.L. Leite[83c], C.E. Leitgeb[19], R. Leitner[136], K.J.C. Leney[45], T. Lenz[25], S. Leone[74a], C. Leonidopoulos[52], A. Leopold[150], J.H. Lepage Bourbonnais[35], R. Les[109], C.G. Lester[33], M. Levchenko[38], J. Levêque[4], L.J. Levinson[175], G. Levrini[24b,24a], M.P. Lewicki[88], C. Lewis[142], D.J. Lewis[4], L. Lewitt[145], A. Li[30], B. Li[143a], C. Li[108], C-Q. Li[112], H. Li[143a], H. Li[103], H. Li[15], H. Li[62], H. Li[143a], J. Li[144a], K. Li[14], L. Li[144a], R. Li[178], S. Li[14,114c], S. Li[144b,144a], T. Li[5], X. Li[106], Y. Li[14], Z. Li[159], Z. Li[14,114c], Z. Li[62], S. Liang[14,114c], Z. Liang[14], M. Liberatore[138], B. Liberti[76a], G.B. Libotte[83d], K. Lie[64c], J. Lieber Marin[83e], H. Lien[68], H. Lin[108], S.F. Lin[151], L. Linden[111], R.E. Lindley[7], J.H. Lindon[37], J. Ling[61], E. Lipeles[131], A. Lipniacka[17], A. Lister[170], J.D. Little[68], B. Liu[14], B.X. Liu[114b], D. Liu[144b,144a], D. Liu[139], E.H.L. Liu[21], J.K.K. Liu[120], K. Liu[144b], K. Liu[144b,144a], M. Liu[62], M.Y. Liu[62], P. Liu[14], Q. Liu[144b,142,144a], S. Liu[151], X. Liu[62], X. Liu[143a], Y. Liu[114b,114c], Y. Liu[168], Y.L. Liu[143a], Y.W. Liu[62], Z. Liu[66,k], S.L. Lloyd[96], E.M. Lobodzinska[48], P. Loch[7], E. Lodhi[161], K. Lohwasser[145], E. Loiacono[48], J.D. Lomas[21], J.D. Long[42], I. Longarini[165], R. Longo[168], A. Lopez Solis[13], N.A. Lopez-canelas[7], N. Lorenzo Martinez[4], A.M. Lory[111], M. Losada[119a], G. Löschcke Centeno[4], X. Lou[47a,47b], X. Lou[14,114c], A. Lounis[66], P.A. Love[93], M. Lu[66], S. Lu[131], Y.J. Lu[154], H.J. Lubatti[142], C. Luci[75a,75b], F.L. Lucio Alves[114a], F. Luehring[68], B.S. Lunday[131], O. Lundberg[150], J. Lunde[37], N.A. Luongo[6], M.S. Lutz[37], A.B. Lux[26], D. Lynn[30], R. Lysak[134], V. Lysenko[135], E. Lytken[100], V. Lyubushkin[39],

JHEP10(2025)093

T. Lyubushkina[39], M.M. Lyukova[151], M.Firdaus M. Soberi[52], H. Ma[30], K. Ma[62], L.L. Ma[143a], W. Ma[62], Y. Ma[124], J.C. MacDonald[102], P.C. Machado De Abreu Farias[83e], D. Macina[37], R. Madar[41], T. Madula[98], J. Maeda[86], T. Maeno[30], P.T. Mafa[34c,j], H. Maguire[145], M. Maheshwari[33], V. Maiboroda[66], A. Maio[133a,133b,133d], K. Maj[87a], O. Majersky[48], S. Majewski[126], R. Makhmanazarov[38], N. Makovec[66], V. Maksimovic[16], B. Malaescu[130], J. Malamant[128], Pa. Malecki[88], V.P. Maleev[38], F. Malek[60,o], M. Mali[95], D. Malito[97], U. Mallik[80,*], A. Maloizel[5], S. Maltezos[10], A. Malvezzi Lopes[83d], S. Malyukov[39], J. Mamuzic[95], G. Mancini[53], M.N. Mancini[27], G. Manco[73a,73b], J.P. Mandalia[96], S.S. Mandarry[152], I. Mandić[95], L. Manhaes de Andrade Filho[83a], I.M. Maniatis[175], J. Manjarres Ramos[91], D.C. Mankad[175], A. Mann[111], T. Manoussos[37], M.N. Mantinan[40], S. Manzoni[37], L. Mao[144a], X. Mapekula[34c], A. Marantis[158], R.R. Marcelo Gregorio[96], G. Marchiori[5], C. Marcon[71a], E. Maricic[16], M. Marinescu[48], S. Marium[48], M. Marjanovic[123], A. Markhoos[54], M. Markovitch[66], M.K. Maroun[105], M.C. Marr[148], G.T. Marsden[103], E.J. Marshall[93], Z. Marshall[18a], S. Marti-Garcia[169], J. Martin[98], T.A. Martin[137], V.J. Martin[52], B. Martin dit Latour[17], L. Martinelli[75a,75b], M. Martinez[13,x], P. Martinez Agullo[169], V.I. Martinez Outschoorn[105], P. Martinez Suarez[37], S. Martin-Haugh[137], G. Martinovicova[136], V.S. Martoiu[28b], A.C. Martyniuk[98], A. Marzin[37], D. Mascione[78a,78b], L. Masetti[102], J. Masik[103], A.L. Maslennikov[39], S.L. Mason[42], P. Massarotti[72a,72b], P. Mastrandrea[74a,74b], A. Mastroberardino[44b,44a], T. Masubuchi[127], T.T. Mathew[126], J. Matousek[136], D.M. Mattern[49], J. Maurer[28b], T. Maurin[59], A.J. Maury[66], B. Maček[95], C. Mavungu Tsava[104], D.A. Maximov[38], A.E. May[103], E. Mayer[41], R. Mazini[34h], I. Maznas[118], S.M. Mazza[139], E. Mazzeo[37], J.P. Mc Gowan[171], S.P. Mc Kee[108], C.A. Mc Lean[6], C.C. McCracken[170], E.F. McDonald[107], A.E. McDougall[117], L.F. Mcelhinney[93], J.A. Mcfayden[152], R.P. McGovern[131], R.P. Mckenzie[34h], T.C. Mclachlan[48], D.J. Mclaughlin[98], S.J. McMahon[137], C.M. Mcpartland[94], R.A. McPherson[171,ab], S. Mehlhase[111], A. Mehta[94], D. Melini[169], B.R. Mellado Garcia[34h], A.H. Melo[55], F. Meloni[48], A.M. Mendes Jacques Da Costa[103], L. Meng[93], S. Menke[112], M. Mentink[37], E. Meoni[44b,44a], G. Mercado[118], S. Merianos[158], C. Merlassino[69a,69c], C. Meroni[71a,71b], J. Metcalfe[6], A.S. Mete[6], E. Meuser[102], C. Meyer[68], J-P. Meyer[138], Y. Miao[114a], R.P. Middleton[137], M. Mihovilovic[66], L. Mijović[52], G. Mikenberg[175], M. Mikestikova[134], M. Mikuž[95], H. Mildner[102], A. Milic[37], D.W. Miller[40], E.H. Miller[149], A. Milov[175], D.A. Milstead[47a,47b], T. Min[114a], A.A. Minaenko[38], I.A. Minashvili[155b], A.I. Mincer[120], B. Mindur[87a], M. Mineev[39], Y. Mino[89], L.M. Mir[13], M. Miralles Lopez[59], M. Mironova[18a], M. Missio[41], A. Mitra[173], V.A. Mitsou[169], Y. Mitsumori[113], O. Miu[161], P.S. Miyagawa[96], T. Mkrtchyan[37], M. Mlinarevic[98], T. Mlinarevic[98], M. Mlynarikova[136], L. Mlynarska[87a], C. Mo[144a], S. Mobius[20], M.H. Mohamed Farook[115], S. Mohapatra[42], S. Mohiuddin[124], G. Mokgatitswane[34h], L. Moleri[175], U. Molinatti[129], L.G. Mollier[20], B. Mondal[134], S. Mondal[135], K. Mönig[48], E. Monnier[104], L. Monsonis Romero[169], J. Montejo Berlingen[13], A. Montella[47a,47b], M. Montella[122], F. Montereali[77a,77b], F. Monticelli[92], S. Monzani[69a,69c], A. Morancho Tarda[43], N. Morange[66], A.L. Moreira De Carvalho[48], M. Moreno Llácer[169], C. Moreno Martinez[56], J.M. Moreno Perez[23b], P. Morettini[57b], S. Morgenstern[37], M. Morii[61], M. Morinaga[159],

JHEP10(2025)093

M. Moritsu[90], F. Morodei[75a,75b], P. Moschovakos[37], B. Moser[54], M. Mosidze[155b], T. Moskalets[45], P. Moskvitina[116], J. Moss[32], P. Moszkowicz[87a], A. Moussa[36d], Y. Moyal[175], H. Moyano Gomez[13], E.J.W. Moyse[105], T.G. Mroz[88], O. Mtintsilana[34h], S. Muanza[104], M. Mucha[25], J. Mueller[132], R. Müller[37], G.A. Mullier[167], A.J. Mullin[33], J.J. Mullin[51], A.C. Mullins[45], A.E. Mulski[61], D.P. Mungo[161], D. Munoz Perez[169], F.J. Munoz Sanchez[103], W.J. Murray[173,137], M. Muškinja[95], C. Mwewa[48], A.G. Myagkov[38,a], A.J. Myers[8], G. Myers[108], M. Myska[135], B.P. Nachman[149], K. Nagai[129], K. Nagano[84], R. Nagasaka[159], J.L. Nagle[30,al], E. Nagy[104], A.M. Nairz[37], Y. Nakahama[84], K. Nakamura[84], K. Nakkalil[5], A. Nandi[63b], H. Nanjo[127], E.A. Narayanan[45], Y. Narukawa[159], I. Naryshkin[38], L. Nasella[71a,71b], S. Nasri[119b], C. Nass[25], G. Navarro[23a], A. Nayaz[19], P.Y. Nechaeva[38], S. Nechaeva[24b,24a], F. Nechansky[134], L. Nedic[129], T.J. Neep[21], A. Negri[73a,73b], M. Negrini[24b], C. Nellist[117], C. Nelson[106], K. Nelson[108], S. Nemecek[134], M. Nessi[37,g], M.S. Neubauer[168], J. Newell[94], P.R. Newman[21], Y.W.Y. Ng[168], B. Ngair[119a], H.D.N. Nguyen[110], J.D. Nichols[123], R.B. Nickerson[129], R. Nicolaidou[138], J. Nielsen[139], M. Niemeyer[55], J. Niermann[37], N. Nikiforou[37], V. Nikolaenko[38,a], I. Nikolic-Audit[130], P. Nilsson[30], I. Ninca[48], G. Ninio[157], A. Nisati[75a], R. Nisius[112], N. Nitika[175], J-E. Nitschke[50], E.K. Nkadimeng[34b], T. Nobe[159], D. Noll[18a], T. Nommensen[153], M.B. Norfolk[145], B.J. Norman[35], L.C. Nosler[18a], M. Noury[36a], J. Novak[95], T. Novak[95], R. Novotny[135], L. Nozka[125], K. Ntekas[165], D. Ntounis[149], N.M.J. Nunes De Moura Junior[83b], J. Ocariz[130], I. Ochoa[133a], S. Oerdek[48,y], J.T. Offermann[40], A. Ogrodnik[88], A. Oh[103], C.C. Ohm[150], H. Oide[84], M.L. Ojeda[37], Y. Okumura[159], L.F. Oleiro Seabra[133a], I. Oleksiyuk[56], G. Oliveira Correa[13], D. Oliveira Damazio[30], J.L. Oliver[165], R. Omar[68], Ö.O. Öncel[54], A.P. O'Neill[20], A. Onofre[133a,133e,e], P.U.E. Onyisi[11], M.J. Oreglia[40], D. Orestano[77a,77b], R. Orlandini[77a,77b], R.S. Orr[161], L.M. Osojnak[42], Y. Osumi[113], G. Otero y Garzon[31], H. Otono[90], M. Ouchrif[36d], F. Ould-Saada[128], T. Ovsiannikova[142], M. Owen[59], R.E. Owen[137], V.E. Ozcan[22a], F. Ozturk[88], N. Ozturk[8], S. Ozturk[82], H.A. Pacey[129], K. Pachal[162a], A. Pacheco Pages[13], C. Padilla Aranda[13], G. Padovano[75a,75b], S. Pagan Griso[18a], G. Palacino[68], A. Palazzo[70a,70b], J. Pampel[25], J. Pan[178], T. Pan[64a], D.K. Panchal[11], C.E. Pandini[60], J.G. Panduro Vazquez[137], H.D. Pandya[1], H. Pang[138], P. Pani[48], G. Panizzo[69a,69c], L. Panwar[130], L. Paolozzi[56], S. Parajuli[168], A. Paramonov[6], C. Paraskevopoulos[53], D. Paredes Hernandez[64b], A. Pareti[73a,73b], K.R. Park[42], T.H. Park[112], F. Parodi[57b,57a], J.A. Parsons[42], U. Parzefall[54], B. Pascual Dias[41], L. Pascual Dominguez[101], E. Pasqualucci[75a], S. Passaggio[57b], F. Pastore[97], P. Patel[88], U.M. Patel[51], J.R. Pater[103], T. Pauly[37], F. Pauwels[136], C.I. Pazos[164], M. Pedersen[128], R. Pedro[133a], S.V. Peleganchuk[38], O. Penc[134], S. Peng[15], G.D. Penn[178], K.E. Penski[111], M. Penzin[38], B.S. Peralva[83d], A.P. Pereira Peixoto[142], L. Pereira Sanchez[149], D.V. Perepelitsa[30,al], G. Perera[105], E. Perez Codina[37], M. Perganti[10], H. Pernegger[37], S. Perrella[75a,75b], K. Peters[48], R.F.Y. Peters[103], B.A. Petersen[37], T.C. Petersen[43], E. Petit[104], V. Petousis[135], A.R. Petri[71a,71b], C. Petridou[158,d], T. Petru[136], A. Petrukhin[147], M. Pettee[18a], A. Petukhov[82], K. Petukhova[37], R. Pezoa[140g], L. Pezzotti[24b,24a], G. Pezzullo[178], L. Pfaffenbichler[37], A.J. Pfleger[79], T.M. Pham[176], T. Pham[107], P.W. Phillips[137], G. Piacquadio[151], E. Pianori[18a], F. Piazza[126],

JHEP10(2025)093

R. Piegaia[31], D. Pietreanu[28b], A.D. Pilkington[103], M. Pinamonti[69a,69c], J.L. Pinfold[2], B.C. Pinheiro Pereira[133a], J. Pinol Bel[13], A.E. Pinto Pinoargote[130], L. Pintucci[69a,69c], K.M. Piper[152], A. Pirttikoski[56], D.A. Pizzi[35], L. Pizzimento[64b], A. Plebani[33], M.-A. Pleier[30], V. Pleskot[136], E. Plotnikova[39], G. Poddar[96], R. Poettgen[100], L. Poggioli[130], S. Polacek[136], G. Polesello[73a], A. Poley[148], A. Polini[24b], C.S. Pollard[173], Z.B. Pollock[122], E. Pompa Pacchi[123], N.I. Pond[98], D. Ponomarenko[68], L. Pontecorvo[37], S. Popa[28a], G.A. Popeneciu[28d], A. Poreba[37], D.M. Portillo Quintero[162a], S. Pospisil[135], M.A. Postill[145], P. Postolache[28c], K. Potamianos[173], P.A. Potepa[87a], I.N. Potrap[39], C.J. Potter[33], H. Potti[153], J. Poveda[169], M.E. Pozo Astigarraga[37], R. Pozzi[37], A. Prades Ibanez[76a,76b], S.R. Pradhan[145], J. Pretel[171], D. Price[103], M. Primavera[70a], L. Primomo[69a,69c], M.A. Principe Martin[101], R. Privara[125], T. Procter[87b], M.L. Proffitt[142], N. Proklova[131], K. Prokofiev[64c], G. Proto[112], J. Proudfoot[6], M. Przybycien[87a], W.W. Przygoda[87b], A. Psallidas[46], J.E. Puddefoot[145], D. Pudzha[53], H.I. Purnell[1], D. Pyatiizbyantseva[116], J. Qian[108], R. Qian[109], D. Qichen[129], Y. Qin[13], T. Qiu[52], A. Quadt[55], M. Queitsch-Maitland[103], G. Quetant[56], R.P. Quinn[170], G. Rabanal Bolanos[61], D. Rafanoharana[112], F. Raffaeli[76a,76b], F. Ragusa[71a,71b], J.L. Rainbolt[40], S. Rajagopalan[30], E. Ramakoti[39], L. Rambelli[57b,57a], I.A. Ramirez-Berend[35], K. Ran[48,114c], D.S. Rankin[131], N.P. Rapheeha[34h], H. Rasheed[28b], D.F. Rassloff[63a], A. Rastogi[18a], S. Rave[102], S. Ravera[57b,57a], B. Ravina[37], I. Ravinovich[175], M. Raymond[37], A.L. Read[128], N.P. Readioff[145], D.M. Rebuzzi[73a,73b], A.S. Reed[59], K. Reeves[27], J.A. Reidelsturz[177], D. Reikher[37], A. Rej[49], C. Rembser[37], H. Ren[62], M. Renda[28b], F. Renner[48], A.G. Rennie[59], M. Repik[56], A.L. Rescia[57b,57a], S. Resconi[71a], M. Ressegotti[57b,57a], S. Rettie[117], W.F. Rettie[35], M.M. Revering[33], E. Reynolds[18a], O.L. Rezanova[39], P. Reznicek[136], H. Riani[36d], N. Ribaric[51], B. Ricci[69a,69c], E. Ricci[78a,78b], R. Richter[112], S. Richter[47a,47b], E. Richter-Was[87b], M. Ridel[130], S. Ridouani[36d], P. Rieck[120], P. Riedler[37], E.M. Riefel[47a,47b], J.O. Rieger[117], M. Rijssenbeek[151], M. Rimoldi[37], L. Rinaldi[24b,24a], P. Rincke[167,55], G. Ripellino[167], I. Riu[13], J.C. Rivera Vergara[171], F. Rizatdinova[124], E. Rizvi[96], B.R. Roberts[18a], S.S. Roberts[139], D. Robinson[33], M. Robles Manzano[102], A. Robson[59], A. Rocchi[76a,76b], C. Roda[74a,74b], S. Rodriguez Bosca[37], Y. Rodriguez Garcia[23a], A.M. Rodríguez Vera[118], S. Roe[37], J.T. Roemer[37], O. Røhne[128], R.A. Rojas[37], C.P.A. Roland[130], A. Romaniouk[79], E. Romano[73a,73b], M. Romano[24b], A.C. Romero Hernandez[168], N. Rompotis[94], L. Roos[130], S. Rosati[75a], B.J. Rosser[40], E. Rossi[129], E. Rossi[72a,72b], L.P. Rossi[61], L. Rossini[54], R. Rosten[122], M. Rotaru[28b], B. Rottler[54], D. Rousseau[66], D. Rousso[48], S. Roy-Garand[161], A. Rozanov[104], Z.M.A. Rozario[59], Y. Rozen[156], A. Rubio Jimenez[169], V.H. Ruelas Rivera[19], T.A. Ruggeri[1], A. Ruggiero[129], A. Ruiz-Martinez[169], A. Rummler[37], Z. Rurikova[54], N.A. Rusakovich[39], S. Ruscelli[49], H.L. Russell[171], G. Russo[75a,75b], J.P. Rutherfoord[7], S. Rutherford Colmenares[33], M. Rybar[136], P. Rybczynski[87a], A. Ryzhov[45], J.A. Sabater Iglesias[56], H.F-W. Sadrozinski[139], F. Safai Tehrani[75a], S. Saha[1], M. Sahinsoy[82], B. Sahoo[175], A. Saibel[169], B.T. Saifuddin[123], M. Saimpert[138], G.T. Saito[83c], M. Saito[159], T. Saito[159], A. Sala[71a,71b], A. Salnikov[149], J. Salt[169], A. Salvador Salas[157], F. Salvatore[152], A. Salzburger[37], D. Sammel[54], E. Sampson[93], D. Sampsonidis[158,d], D. Sampsonidou[126], M.A.A. Samy[59], J. Sánchez[169],

JHEP10(2025)093

V. Sanchez Sebastian[169], H. Sandaker[128], C.O. Sander[48], J.A. Sandesara[176], M. Sandhoff[177], C. Sandoval[23b], L. Sanfilippo[63a], D.P.C. Sankey[137], T. Sano[89], A. Sansoni[53], M. Santana Queiroz[18b], L. Santi[37], C. Santoni[41], H. Santos[133a,133b], A. Santra[175], E. Sanzani[24b,24a], K.A. Saoucha[85b], J.G. Saraiva[133a,133d], J. Sardain[7], O. Sasaki[84], K. Sato[163], C. Sauer[37], E. Sauvan[4], P. Savard[161,ai], R. Sawada[159], C. Sawyer[137], L. Sawyer[99], C. Sbarra[24b], A. Sbrizzi[24b,24a], T. Scanlon[98], J. Schaarschmidt[142], U. Schäfer[102], A.C. Schaffer[66,45], D. Schaile[111], R.D. Schamberger[151], C. Scharf[19], M.M. Schefer[20], V.A. Schegelsky[38], D. Scheirich[136], M. Schernau[140f], C. Scheulen[56], C. Schiavi[57b,57a], M. Schioppa[44b,44a], B. Schlag[149], S. Schlenker[37], J. Schmeing[177], E. Schmidt[112], M.A. Schmidt[177], K. Schmieden[25], C. Schmitt[102], N. Schmitt[102], S. Schmitt[48], N.A. Schneider[111], L. Schoeffel[138], A. Schoening[63b], P.G. Scholer[35], E. Schopf[147], M. Schott[25], S. Schramm[56], T. Schroer[56], H-C. Schultz-Coulon[63a], M. Schumacher[54], B.A. Schumm[139], Ph. Schune[138], H.R. Schwartz[7], A. Schwartzman[149], T.A. Schwarz[108], Ph. Schwemling[138], R. Schwienhorst[109], F.G. Sciacca[20], A. Sciandra[30], G. Sciolla[27], F. Scuri[74a], C.D. Sebastiani[37], K. Sedlaczek[118], S.C. Seidel[115], A. Seiden[139], B.D. Seidlitz[42], C. Seitz[48], J.M. Seixas[83b], G. Sekhniaidze[72a], L. Selem[60], N. Semprini-Cesari[24b,24a], A. Semushin[179], D. Sengupta[56], V. Senthilkumar[169], L. Serin[66], M. Sessa[72a,72b], H. Severini[123], F. Sforza[57b,57a], A. Sfyrla[56], Q. Sha[14], E. Shabalina[55], H. Shaddix[118], A.H. Shah[33], R. Shaheen[150], J.D. Shahinian[131], M. Shamim[37], L.Y. Shan[14], M. Shapiro[18a], A. Sharma[37], A.S. Sharma[170], P. Sharma[30], P.B. Shatalov[38], K. Shaw[152], S.M. Shaw[103], Q. Shen[14], D.J. Sheppard[148], P. Sherwood[98], L. Shi[98], X. Shi[14], S. Shimizu[84], C.O. Shimmin[178], I.P.J. Shipsey[129,*], S. Shirabe[90], M. Shiyakova[39,z], M.J. Shochet[40], D.R. Shope[128], B. Shrestha[123], S. Shrestha[122,an], I. Shreyber[39], M.J. Shroff[171], P. Sicho[134], A.M. Sickles[168], E. Sideras Haddad[34h,166], A.C. Sidley[117], A. Sidoti[24b], F. Siegert[50], Dj. Sijacki[16], F. Sili[92], J.M. Silva[52], I. Silva Ferreira[83b], M.V. Silva Oliveira[30], S.B. Silverstein[47a], S. Simion[66], R. Simoniello[37], E.L. Simpson[103], H. Simpson[152], L.R. Simpson[6], S. Simsek[82], S. Sindhu[55], P. Sinervo[161], S.N. Singh[27], S. Singh[30], S. Sinha[48], S. Sinha[103], M. Sioli[24b,24a], K. Sioulas[9], I. Siral[37], E. Sitnikova[48], J. Sjölin[47a,47b], A. Skaf[55], E. Skorda[21], P. Skubic[123], M. Slawinska[88], I. Slazyk[17], I. Sliusar[128], V. Smakhtin[175], B.H. Smart[137], S.Yu. Smirnov[140b], Y. Smirnov[82], L.N. Smirnova[38,a], O. Smirnova[100], A.C. Smith[42], D.R. Smith[165], J.L. Smith[103], M.B. Smith[35], R. Smith[149], H. Smitmanns[102], M. Smizanska[93], K. Smolek[135], P. Smolyanskiy[135], A.A. Snesarev[39], H.L. Snoek[117], S. Snyder[30], R. Sobie[171,ab], A. Soffer[157], C.A. Solans Sanchez[37], E.Yu. Soldatov[39], U. Soldevila[169], A.A. Solodkov[34h], S. Solomon[27], A. Soloshenko[39], K. Solovieva[54], O.V. Solovyanov[41], P. Sommer[50], A. Sonay[13], A. Sopczak[135], A.L. Sopio[52], F. Sopkova[29b], J.D. Sorenson[115], I.R. Sotarriva Alvarez[141], V. Sothilingam[63a], O.J. Soto Sandoval[140c,140b], S. Sottocornola[68], R. Soualah[85a], Z. Soumaimi[36e], D. South[48], N. Soybelman[175], S. Spagnolo[70a,70b], M. Spalla[112], D. Sperlich[54], B. Spisso[72a,72b], D.P. Spiteri[59], L. Splendori[104], M. Spousta[136], E.J. Staats[35], R. Stamen[63a], E. Stanecka[88], W. Stanek-Maslouska[48], M.V. Stange[50], B. Stanislaus[18a], M.M. Stanitzki[48], B. Stapf[48], E.A. Starchenko[38], G.H. Stark[139], J. Stark[91], P. Staroba[134], P. Starovoitov[85b], R. Staszewski[88],

JHEP10(2025)093

C. Stauch[111], G. Stavropoulos[46], A. Stefl[37], A. Stein[102], P. Steinberg[30], B. Stelzer[148,162a], H.J. Stelzer[132], O. Stelzer[162a], H. Stenzel[58], T.J. Stevenson[152], G.A. Stewart[37], J.R. Stewart[124], G. Stoicea[28b], M. Stolarski[133a], S. Stonjek[112], A. Straessner[50], J. Strandberg[150], S. Strandberg[47a,47b], M. Stratmann[177], M. Strauss[123], T. Strebler[104], P. Strizenec[29b], R. Ströhmer[172], D.M. Strom[126], R. Stroynowski[45], A. Strubig[47a,47b], S.A. Stucci[30], B. Stugu[17], J. Stupak[123], N.A. Styles[48], D. Su[149], S. Su[62], X. Su[62], D. Suchy[29a], A.D. Sudhakar Ponnu[55], K. Sugizaki[131], V.V. Sulin[38], D.M.S. Sultan[129], L. Sultanaliyeva[25], S. Sultansoy[3b], S. Sun[176], W. Sun[14], N. Sur[100], M.R. Sutton[152], M. Svatos[134], P.N. Swallow[33], M. Swiatlowski[162a], T. Swirski[172], A. Swoboda[37], I. Sykora[29a], M. Sykora[136], T. Sykora[136], D. Ta[102], K. Tackmann[48,y], A. Taffard[165], R. Tafirout[162a], Y. Takubo[84], M. Talby[104], A.A. Talyshev[38], K.C. Tam[64b], N.M. Tamir[157], A. Tanaka[159], J. Tanaka[159], R. Tanaka[66], M. Tanasini[151], Z. Tao[170], S. Tapia Araya[140g], S. Tapprogge[102], A. Tarek Abouelfadl Mohamed[37], S. Tarem[156], K. Tariq[14], G. Tarna[37], G.F. Tartarelli[71a], M.J. Tartarin[91], P. Tas[136], M. Tasevsky[134], E. Tassi[44b,44a], A.C. Tate[168], Y. Tayalati[36e,aa], G.N. Taylor[107], W. Taylor[162b], R.J. Taylor Vara[169], A.S. Tegetmeier[91], P. Teixeira-Dias[97], J.J. Teoh[161], K. Terashi[159], J. Terron[101], S. Terzo[13], M. Testa[53], R.J. Teuscher[161,ab], A. Thaler[79], O. Theiner[56], T. Theveneaux-Pelzer[104], D.W. Thomas[97], J.P. Thomas[21], E.A. Thompson[18a], P.D. Thompson[21], E. Thomson[131], R.E. Thornberry[45], C. Tian[62], Y. Tian[56], V. Tikhomirov[82], Yu.A. Tikhonov[39], S. Timoshenko[38], D. Timoshyn[136], E.X.L. Ting[1], P. Tipton[178], A. Tishelman-Charny[30], K. Todome[141], S. Todorova-Nova[136], L. Toffolin[69a,69c], M. Togawa[84], J. Tojo[90], S. Tokár[29a], O. Toldaiev[68], G. Tolkachev[104], M. Tomoto[84], L. Tompkins[149,n], E. Torrence[126], H. Torres[91], D.I. Torres Arza[140g], E. Torró Pastor[169], M. Toscani[31], C. Tosciri[40], M. Tost[11], D.R. Tovey[145], T. Trefzger[172], P.M. Tricarico[13], A. Tricoli[30], I.M. Trigger[162a], S. Trincaz-Duvoid[130], D.A. Trischuk[27], A. Tropina[39], L. Truong[34c], M. Trzebinski[88], A. Trzupek[88], F. Tsai[151], M. Tsai[108], A. Tsiamis[158], P.V. Tsiareshka[39], S. Tsigaridas[162a], A. Tsirigotis[158,u], V. Tsiskaridze[155a], E.G. Tskhadadze[155a], Y. Tsujikawa[89], I.I. Tsukerman[38], V. Tsulaia[18a], S. Tsuno[84], K. Tsuri[121], D. Tsybychev[151], Y. Tu[64b], A. Tudorache[28b], V. Tudorache[28b], S.B. Tuncay[129], S. Turchikhin[57b,57a], I. Turk Cakir[3a], R. Turra[71a], T. Turtuvshin[39,ac], P.M. Tuts[42], S. Tzamarias[158,d], Y. Uematsu[84], F. Ukegawa[163], P.A. Ulloa Poblete[140c,140b], E.N. Umaka[30], G. Unal[37], A. Undrus[30], G. Unel[165], J. Urban[29b], P. Urrejola[140e], G. Usai[8], R. Ushioda[160], M. Usman[110], F. Ustuner[52], Z. Uysal[82], V. Vacek[135], B. Vachon[106], T. Vafeiadis[37], A. Vaitkus[98], C. Valderanis[111], E. Valdes Santurio[47a,47b], M. Valente[37], S. Valentinetti[24b,24a], A. Valero[169], E. Valiente Moreno[169], A. Vallier[91], J.A. Valls Ferrer[169], D.R. Van Arneman[117], A. Van Der Graaf[49], H.Z. Van Der Schyf[34h], P. Van Gemmeren[6], M. Van Rijnbach[37], S. Van Stroud[98], I. Van Vulpen[117], P. Vana[136], M. Vanadia[76a,76b], U.M. Vande Voorde[150], W. Vandelli[37], E.R. Vandewall[124], D. Vannicola[157], L. Vannoli[53], R. Vari[75a], M. Varma[178], E.W. Varnes[7], C. Varni[118], D. Varouchas[66], L. Varriale[169], K.E. Varvell[153], M.E. Vasile[28b], L. Vaslin[84], M.D. Vassilev[149], A. Vasyukov[39], L.M. Vaughan[124], R. Vavricka[136], T. Vazquez Schroeder[13], J. Veatch[32], V. Vecchio[103], M.J. Veen[105], I. Veliscek[30], I. Velkovska[95], L.M. Veloce[161], F. Veloso[133a,133c], S. Veneziano[75a], A. Ventura[70a,70b], A. Verbytskyi[112], M. Verducci[74a,74b],

JHEP10(2025)093

C. Vergis[96], M. Verissimo De Araujo[83b], W. Verkerke[117], J.C. Vermeulen[117], C. Vernieri[149], M. Vessella[165], M.C. Vetterli[148,ai], A. Vgenopoulos[102], N. Viaux Maira[140g,af], T. Vickey[145], O.E. Vickey Boeriu[145], G.H.A. Viehhauser[129], L. Vigani[63b], M. Vigl[112], M. Villa[24b,24a], M. Villaplana Perez[169], E.M. Villhauer[40], E. Vilucchi[53], M. Vincent[169], M.G. Vincter[35], A. Visibile[117], A. Visive[117], C. Vittori[37], I. Vivarelli[24b,24a], M.I. Vivas Albornoz[48], E. Voevodina[112], F. Vogel[111], J.C. Voigt[50], P. Vokac[135], Yu. Volkotrub[87b], L. Vomberg[25], E. Von Toerne[25], B. Vormwald[37], K. Vorobev[51], M. Vos[169], K. Voss[147], M. Vozak[37], L. Vozdecky[123], N. Vranjes[16], M. Vranjes Milosavljevic[16], M. Vreeswijk[117], N.K. Vu[144b,144a], R. Vuillermet[37], O. Vujinovic[102], I. Vukotic[40], I.K. Vyas[35], J.F. Wack[33], S. Wada[163], C. Wagner[149], J.M. Wagner[18a], W. Wagner[177], S. Wahdan[177], H. Wahlberg[92], C.H. Waits[123], J. Walder[137], R. Walker[111], K. Walkingshaw Pass[59], W. Walkowiak[147], A. Wall[131], E.J. Wallin[100], T. Wamorkar[18a], K. Wandall-Christensen[169], A. Wang[62], A.Z. Wang[139], C. Wang[102], C. Wang[11], H. Wang[18a], J. Wang[64c], P. Wang[103], P. Wang[98], R. Wang[61], R. Wang[6], S.M. Wang[154], S. Wang[14], T. Wang[116], T. Wang[62], W.T. Wang[129], W. Wang[14], X. Wang[168], X. Wang[144a], X. Wang[48], Y. Wang[114a], Y. Wang[62], Z. Wang[108], Z. Wang[144b], Z. Wang[108], C. Wanotayaroj[84], A. Warburton[106], A.L. Warnerbring[147], S. Waterhouse[97], A.T. Watson[21], H. Watson[52], M.F. Watson[21], E. Watton[37], G. Watts[142], B.M. Waugh[98], J.M. Webb[54], C. Weber[30], H.A. Weber[19], M.S. Weber[20], S.M. Weber[63a], C. Wei[62], Y. Wei[54], A.R. Weidberg[129], E.J. Weik[120], J. Weingarten[49], C. Weiser[54], C.J. Wells[48], T. Wenaus[30], T. Wengler[37], N.S. Wenke[112], N. Wermes[25], M. Wessels[63a], A.M. Wharton[93], A.S. White[61], A. White[8], M.J. White[1], D. Whiteson[165], L. Wickremasinghe[127], W. Wiedenmann[176], M. Wielers[137], R. Wierda[150], C. Wiglesworth[43], H.G. Wilkens[37], J.J.H. Wilkinson[33], D.M. Williams[42], H.H. Williams[131], S. Williams[33], S. Willocq[105], B.J. Wilson[103], D.J. Wilson[103], P.J. Windischhofer[40], F.I. Winkel[31], F. Winklmeier[126], B.T. Winter[54], M. Wittgen[149], M. Wobisch[99], T. Wojtkowski[60], Z. Wolffs[117], J. Wollrath[37], M.W. Wolter[88], H. Wolters[133a,133c], M.C. Wong[139], E.L. Woodward[42], S.D. Worm[48], B.K. Wosiek[88], K.W. Woźniak[88], S. Wozniewski[55], K. Wraight[59], C. Wu[161], C. Wu[21], J. Wu[159], M. Wu[114b], M. Wu[116], S.L. Wu[176], S. Wu[14,ak], X. Wu[62], Y.Q. Wu[161], Y. Wu[62], Z. Wu[4], Z. Wu[114a], J. Wuerzinger[112], T.R. Wyatt[103], B.M. Wynne[52], S. Xella[43], L. Xia[114a], M. Xie[62], A. Xiong[126], D. Xu[14], H. Xu[62], L. Xu[62], R. Xu[131], T. Xu[108], Y. Xu[142], Z. Xu[52], R. Xue[132], B. Yabsley[153], S. Yacoob[34a], Y. Yamaguchi[84], E. Yamashita[159], H. Yamauchi[163], T. Yamazaki[18a], Y. Yamazaki[86], S. Yan[59], Z. Yan[105], H.J. Yang[144a,144b], H.T. Yang[62], S. Yang[62], T. Yang[64c], X. Yang[37], X. Yang[14], Y. Yang[159], Y. Yang[62], W-M. Yao[18a], C.L. Yardley[152], J. Ye[14], S. Ye[30], X. Ye[62], Y. Yeh[98], I. Yeletskikh[39], B. Yeo[18b], M.R. Yexley[98], T.P. Yildirim[129], K. Yorita[174], C.J.S. Young[37], C. Young[149], N.D. Young[126], Y. Yu[62], J. Yuan[14,114c], M. Yuan[108], R. Yuan[144b,144a], L. Yue[98], M. Zaazoua[62], B. Zabinski[88], I. Zahir[36a], A. Zaio[57b,57a], Z.K. Zak[88], T. Zakareishvili[169], S. Zambito[56], J.A. Zamora Saa[140d], J. Zang[159], R. Zanzottera[71a,71b], O. Zaplatilek[135], C. Zeitnitz[177], H. Zeng[14], J.C. Zeng[168], D.T. Zenger Jr[27], O. Zenin[38], T. Ženiš[29a], S. Zenz[96], D. Zerwas[66], M. Zhai[14,114c], D.F. Zhang[145], G. Zhang[14,ak], J. Zhang[143a], J. Zhang[6], K. Zhang[14,114c], L. Zhang[62],

JHEP10(2025)093

L. Zhang[114a], P. Zhang[14,114c], R. Zhang[114a], S. Zhang[91], T. Zhang[159], Y. Zhang[142], Y. Zhang[98], Y. Zhang[62], Y. Zhang[114a], Z. Zhang[18a], Z. Zhang[143a], Z. Zhang[66], H. Zhao[142], T. Zhao[143a], Y. Zhao[35], Z. Zhao[62], Z. Zhao[62], A. Zhemchugov[39], J. Zheng[114a], K. Zheng[168], X. Zheng[62], Z. Zheng[149], D. Zhong[168], B. Zhou[108], H. Zhou[7], N. Zhou[144a], Y. Zhou[15], Y. Zhou[114a], Y. Zhou[7], C.G. Zhu[143a], J. Zhu[108], X. Zhu[144b], Y. Zhu[144a], Y. Zhu[62], X. Zhuang[14], K. Zhukov[68], N.I. Zimine[39], J. Zinsser[63b], M. Ziolkowski[147], L. Živković[16], A. Zoccoli[24b,24a], K. Zoch[61], A. Zografos[37], T.G. Zorbas[145], O. Zormpa[46], L. Zwalinski[37]

[1] *Department of Physics, University of Adelaide, Adelaide; Australia*
[2] *Department of Physics, University of Alberta, Edmonton AB; Canada*
[3] [(a)] *Department of Physics, Ankara University, Ankara;* [(b)] *Division of Physics, TOBB University of Economics and Technology, Ankara; Türkiye*
[4] *LAPP, Université Savoie Mont Blanc, CNRS/IN2P3, Annecy; France*
[5] *APC, Université Paris Cité, CNRS/IN2P3, Paris; France*
[6] *High Energy Physics Division, Argonne National Laboratory, Argonne IL; United States of America*
[7] *Department of Physics, University of Arizona, Tucson AZ; United States of America*
[8] *Department of Physics, University of Texas at Arlington, Arlington TX; United States of America*
[9] *Physics Department, National and Kapodistrian University of Athens, Athens; Greece*
[10] *Physics Department, National Technical University of Athens, Zografou; Greece*
[11] *Department of Physics, University of Texas at Austin, Austin TX; United States of America*
[12] *Institute of Physics, Azerbaijan Academy of Sciences, Baku; Azerbaijan*
[13] *Institut de Física d'Altes Energies (IFAE), Barcelona Institute of Science and Technology, Barcelona; Spain*
[14] *Institute of High Energy Physics, Chinese Academy of Sciences, Beijing; China*
[15] *Physics Department, Tsinghua University, Beijing; China*
[16] *Institute of Physics, University of Belgrade, Belgrade; Serbia*
[17] *Department for Physics and Technology, University of Bergen, Bergen; Norway*
[18] [(a)] *Physics Division, Lawrence Berkeley National Laboratory, Berkeley CA;* [(b)] *University of California, Berkeley CA; United States of America*
[19] *Institut für Physik, Humboldt Universität zu Berlin, Berlin; Germany*
[20] *Albert Einstein Center for Fundamental Physics and Laboratory for High Energy Physics, University of Bern, Bern; Switzerland*
[21] *School of Physics and Astronomy, University of Birmingham, Birmingham; United Kingdom*
[22] [(a)] *Department of Physics, Bogazici University, Istanbul;* [(b)] *Department of Physics Engineering, Gaziantep University, Gaziantep;* [(c)] *Department of Physics, Istanbul University, Istanbul; Türkiye*
[23] [(a)] *Facultad de Ciencias y Centro de Investigaciónes, Universidad Antonio Nariño, Bogotá;* [(b)] *Departamento de Física, Universidad Nacional de Colombia, Bogotá; Colombia*
[24] [(a)] *Dipartimento di Fisica e Astronomia A. Righi, Università di Bologna, Bologna;* [(b)] *INFN Sezione di Bologna; Italy*
[25] *Physikalisches Institut, Universität Bonn, Bonn; Germany*
[26] *Department of Physics, Boston University, Boston MA; United States of America*
[27] *Department of Physics, Brandeis University, Waltham MA; United States of America*
[28] [(a)] *Transilvania University of Brasov, Brasov;* [(b)] *Horia Hulubei National Institute of Physics and Nuclear Engineering, Bucharest;* [(c)] *Department of Physics, Alexandru Ioan Cuza University of Iasi, Iasi;* [(d)] *National Institute for Research and Development of Isotopic and Molecular Technologies, Physics Department, Cluj-Napoca;* [(e)] *National University of Science and Technology Politechnica, Bucharest;* [(f)] *West University in Timisoara, Timisoara;* [(g)] *Faculty of Physics, University of Bucharest, Bucharest; Romania*
[29] [(a)] *Faculty of Mathematics, Physics and Informatics, Comenius University, Bratislava;* [(b)] *Department of Subnuclear Physics, Institute of Experimental Physics of the Slovak Academy of Sciences, Kosice; Slovak Republic*
[30] *Physics Department, Brookhaven National Laboratory, Upton NY; United States of America*

JHEP10(2025)093

[31] Universidad de Buenos Aires, Facultad de Ciencias Exactas y Naturales, Departamento de Física, y CONICET, Instituto de Física de Buenos Aires (IFIBA), Buenos Aires; Argentina
[32] California State University, CA; United States of America
[33] Cavendish Laboratory, University of Cambridge, Cambridge; United Kingdom
[34] [(a)] Department of Physics, University of Cape Town, Cape Town;[(b)] iThemba Labs, Western Cape;[(c)] Department of Mechanical Engineering Science, University of Johannesburg, Johannesburg;[(d)] National Institute of Physics, University of the Philippines Diliman (Philippines);[(e)] Department of Physics, Stellenbosch University, Matieland;[(f)] University of South Africa, Department of Physics, Pretoria;[(g)] University of Zululand, KwaDlangezwa;[(h)] School of Physics, University of the Witwatersrand, Johannesburg; South Africa
[35] Department of Physics, Carleton University, Ottawa ON; Canada
[36] [(a)] Faculté des Sciences Ain Chock, Université Hassan II de Casablanca;[(b)] Faculté des Sciences, Université Ibn-Tofail, Kénitra;[(c)] Faculté des Sciences Semlalia, Université Cadi Ayyad, LPHEA-Marrakech;[(d)] LPMR, Faculté des Sciences, Université Mohamed Premier, Oujda;[(e)] Faculté des sciences, Université Mohammed V, Rabat;[(f)] Institute of Applied Physics, Mohammed VI Polytechnic University, Ben Guerir; Morocco
[37] CERN, Geneva; Switzerland
[38] Affiliated with an institute formerly covered by a cooperation agreement with CERN
[39] Affiliated with an international laboratory covered by a cooperation agreement with CERN
[40] Enrico Fermi Institute, University of Chicago, Chicago IL; United States of America
[41] LPC, Université Clermont Auvergne, CNRS/IN2P3, Clermont-Ferrand; France
[42] Nevis Laboratory, Columbia University, Irvington NY; United States of America
[43] Niels Bohr Institute, University of Copenhagen, Copenhagen; Denmark
[44] [(a)] Dipartimento di Fisica, Università della Calabria, Rende;[(b)] INFN Gruppo Collegato di Cosenza, Laboratori Nazionali di Frascati; Italy
[45] Physics Department, Southern Methodist University, Dallas TX; United States of America
[46] National Centre for Scientific Research "Demokritos", Agia Paraskevi; Greece
[47] [(a)] Department of Physics, Stockholm University;[(b)] Oskar Klein Centre, Stockholm; Sweden
[48] Deutsches Elektronen-Synchrotron DESY, Hamburg and Zeuthen; Germany
[49] Fakultät Physik, Technische Universität Dortmund, Dortmund; Germany
[50] Institut für Kern- und Teilchenphysik, Technische Universität Dresden, Dresden; Germany
[51] Department of Physics, Duke University, Durham NC; United States of America
[52] SUPA — School of Physics and Astronomy, University of Edinburgh, Edinburgh; United Kingdom
[53] INFN e Laboratori Nazionali di Frascati, Frascati; Italy
[54] Physikalisches Institut, Albert-Ludwigs-Universität Freiburg, Freiburg; Germany
[55] II. Physikalisches Institut, Georg-August-Universität Göttingen, Göttingen; Germany
[56] Département de Physique Nucléaire et Corpusculaire, Université de Genève, Genève; Switzerland
[57] [(a)] Dipartimento di Fisica, Università di Genova, Genova;[(b)] INFN Sezione di Genova; Italy
[58] II. Physikalisches Institut, Justus-Liebig-Universität Giessen, Giessen; Germany
[59] SUPA — School of Physics and Astronomy, University of Glasgow, Glasgow; United Kingdom
[60] LPSC, Université Grenoble Alpes, CNRS/IN2P3, Grenoble INP, Grenoble; France
[61] Laboratory for Particle Physics and Cosmology, Harvard University, Cambridge MA; United States of America
[62] Department of Modern Physics and State Key Laboratory of Particle Detection and Electronics, University of Science and Technology of China, Hefei; China
[63] [(a)] Kirchhoff-Institut für Physik, Ruprecht-Karls-Universität Heidelberg, Heidelberg;[(b)] Physikalisches Institut, Ruprecht-Karls-Universität Heidelberg, Heidelberg; Germany
[64] [(a)] Department of Physics, Chinese University of Hong Kong, Shatin, N.T., Hong Kong;[(b)] Department of Physics, University of Hong Kong, Hong Kong;[(c)] Department of Physics and Institute for Advanced Study, Hong Kong University of Science and Technology, Clear Water Bay, Kowloon, Hong Kong; China
[65] Department of Physics, National Tsing Hua University, Hsinchu; Taiwan
[66] IJCLab, Université Paris-Saclay, CNRS/IN2P3, 91405, Orsay; France
[67] Centro Nacional de Microelectrónica (IMB-CNM-CSIC), Barcelona; Spain
[68] Department of Physics, Indiana University, Bloomington IN; United States of America

JHEP10(2025)093

[69] [(a)] INFN Gruppo Collegato di Udine, Sezione di Trieste, Udine;[(b)] ICTP, Trieste;[(c)] Dipartimento Politecnico di Ingegneria e Architettura, Università di Udine, Udine; Italy
[70] [(a)] INFN Sezione di Lecce;[(b)] Dipartimento di Matematica e Fisica, Università del Salento, Lecce; Italy
[71] [(a)] INFN Sezione di Milano;[(b)] Dipartimento di Fisica, Università di Milano, Milano; Italy
[72] [(a)] INFN Sezione di Napoli;[(b)] Dipartimento di Fisica, Università di Napoli, Napoli; Italy
[73] [(a)] INFN Sezione di Pavia;[(b)] Dipartimento di Fisica, Università di Pavia, Pavia; Italy
[74] [(a)] INFN Sezione di Pisa;[(b)] Dipartimento di Fisica E. Fermi, Università di Pisa, Pisa; Italy
[75] [(a)] INFN Sezione di Roma;[(b)] Dipartimento di Fisica, Sapienza Università di Roma, Roma; Italy
[76] [(a)] INFN Sezione di Roma Tor Vergata;[(b)] Dipartimento di Fisica, Università di Roma Tor Vergata, Roma; Italy
[77] [(a)] INFN Sezione di Roma Tre;[(b)] Dipartimento di Matematica e Fisica, Università Roma Tre, Roma; Italy
[78] [(a)] INFN-TIFPA;[(b)] Università degli Studi di Trento, Trento; Italy
[79] Universität Innsbruck, Department of Astro and Particle Physics, Innsbruck; Austria
[80] University of Iowa, Iowa City IA; United States of America
[81] Department of Physics and Astronomy, Iowa State University, Ames IA; United States of America
[82] Istinye University, Sariyer, Istanbul; Türkiye
[83] [(a)] Departamento de Engenharia Elétrica, Universidade Federal de Juiz de Fora (UFJF), Juiz de Fora;[(b)] Universidade Federal do Rio De Janeiro COPPE/EE/IF, Rio de Janeiro;[(c)] Instituto de Física, Universidade de São Paulo, São Paulo;[(d)] Rio de Janeiro State University, Rio de Janeiro;[(e)] Federal University of Bahia, Bahia; Brazil
[84] KEK, High Energy Accelerator Research Organization, Tsukuba; Japan
[85] [(a)] Khalifa University of Science and Technology, Abu Dhabi;[(b)] University of Sharjah, Sharjah; United Arab Emirates
[86] Graduate School of Science, Kobe University, Kobe; Japan
[87] [(a)] AGH University of Krakow, Faculty of Physics and Applied Computer Science, Krakow;[(b)] Marian Smoluchowski Institute of Physics, Jagiellonian University, Krakow; Poland
[88] Institute of Nuclear Physics Polish Academy of Sciences, Krakow; Poland
[89] Faculty of Science, Kyoto University, Kyoto; Japan
[90] Research Center for Advanced Particle Physics and Department of Physics, Kyushu University, Fukuoka; Japan
[91] L2IT, Université de Toulouse, CNRS/IN2P3, UPS, Toulouse; France
[92] Instituto de Física La Plata, Universidad Nacional de La Plata and CONICET, La Plata; Argentina
[93] Physics Department, Lancaster University, Lancaster; United Kingdom
[94] Oliver Lodge Laboratory, University of Liverpool, Liverpool; United Kingdom
[95] Department of Experimental Particle Physics, Jožef Stefan Institute and Department of Physics, University of Ljubljana, Ljubljana; Slovenia
[96] Department of Physics and Astronomy, Queen Mary University of London, London; United Kingdom
[97] Department of Physics, Royal Holloway University of London, Egham; United Kingdom
[98] Department of Physics and Astronomy, University College London, London; United Kingdom
[99] Louisiana Tech University, Ruston LA; United States of America
[100] Fysiska institutionen, Lunds universitet, Lund; Sweden
[101] Departamento de Física Teorica C-15 and CIAFF, Universidad Autónoma de Madrid, Madrid; Spain
[102] Institut für Physik, Universität Mainz, Mainz; Germany
[103] School of Physics and Astronomy, University of Manchester, Manchester; United Kingdom
[104] CPPM, Aix-Marseille Université, CNRS/IN2P3, Marseille; France
[105] Department of Physics, University of Massachusetts, Amherst MA; United States of America
[106] Department of Physics, McGill University, Montreal QC; Canada
[107] School of Physics, University of Melbourne, Victoria; Australia
[108] Department of Physics, University of Michigan, Ann Arbor MI; United States of America
[109] Department of Physics and Astronomy, Michigan State University, East Lansing MI; United States of America
[110] Group of Particle Physics, University of Montreal, Montreal QC; Canada
[111] Fakultät für Physik, Ludwig-Maximilians-Universität München, München; Germany

JHEP10(2025)093

[112] Max-Planck-Institut für Physik (Werner-Heisenberg-Institut), München; Germany
[113] Graduate School of Science and Kobayashi-Maskawa Institute, Nagoya University, Nagoya; Japan
[114] [(a)] Department of Physics, Nanjing University, Nanjing;[(b)] School of Science, Shenzhen Campus of Sun Yat-sen University;[(c)] University of Chinese Academy of Science (UCAS), Beijing; China
[115] Department of Physics and Astronomy, University of New Mexico, Albuquerque NM; United States of America
[116] Institute for Mathematics, Astrophysics and Particle Physics, Radboud University/Nikhef, Nijmegen; Netherlands
[117] Nikhef National Institute for Subatomic Physics and University of Amsterdam, Amsterdam; Netherlands
[118] Department of Physics, Northern Illinois University, DeKalb IL; United States of America
[119] [(a)] New York University Abu Dhabi, Abu Dhabi;[(b)] United Arab Emirates University, Al Ain; United Arab Emirates
[120] Department of Physics, New York University, New York NY; United States of America
[121] Ochanomizu University, Otsuka, Bunkyo-ku, Tokyo; Japan
[122] Ohio State University, Columbus OH; United States of America
[123] Homer L. Dodge Department of Physics and Astronomy, University of Oklahoma, Norman OK; United States of America
[124] Department of Physics, Oklahoma State University, Stillwater OK; United States of America
[125] Palacký University, Joint Laboratory of Optics, Olomouc; Czech Republic
[126] Institute for Fundamental Science, University of Oregon, Eugene, OR; United States of America
[127] Graduate School of Science, University of Osaka, Osaka; Japan
[128] Department of Physics, University of Oslo, Oslo; Norway
[129] Department of Physics, Oxford University, Oxford; United Kingdom
[130] LPNHE, Sorbonne Université, Université Paris Cité, CNRS/IN2P3, Paris; France
[131] Department of Physics, University of Pennsylvania, Philadelphia PA; United States of America
[132] Department of Physics and Astronomy, University of Pittsburgh, Pittsburgh PA; United States of America
[133] [(a)] Laboratório de Instrumentação e Física Experimental de Partículas — LIP, Lisboa;[(b)] Departamento de Física, Faculdade de Ciências, Universidade de Lisboa, Lisboa;[(c)] Departamento de Física, Universidade de Coimbra, Coimbra;[(d)] Centro de Física Nuclear da Universidade de Lisboa, Lisboa;[(e)] Departamento de Física, Escola de Ciências, Universidade do Minho, Braga;[(f)] Departamento de Física Teórica y del Cosmos, Universidad de Granada, Granada (Spain);[(g)] Departamento de Física, Instituto Superior Técnico, Universidade de Lisboa, Lisboa; Portugal
[134] Institute of Physics of the Czech Academy of Sciences, Prague; Czech Republic
[135] Czech Technical University in Prague, Prague; Czech Republic
[136] Charles University, Faculty of Mathematics and Physics, Prague; Czech Republic
[137] Particle Physics Department, Rutherford Appleton Laboratory, Didcot; United Kingdom
[138] IRFU, CEA, Université Paris-Saclay, Gif-sur-Yvette; France
[139] Santa Cruz Institute for Particle Physics, University of California Santa Cruz, Santa Cruz CA; United States of America
[140] [(a)] Departamento de Física, Pontificia Universidad Católica de Chile, Santiago;[(b)] Millennium Institute for Subatomic physics at high energy frontier (SAPHIR), Santiago;[(c)] Instituto de Investigación Multidisciplinario en Ciencia y Tecnología, y Departamento de Física, Universidad de La Serena;[(d)] Universidad Andres Bello, Department of Physics, Santiago;[(e)] Universidad San Sebastian, Recoleta;[(f)] Instituto de Alta Investigación, Universidad de Tarapacá, Arica;[(g)] Departamento de Física, Universidad Técnica Federico Santa María, Valparaíso; Chile
[141] Department of Physics, Institute of Science, Tokyo; Japan
[142] Department of Physics, University of Washington, Seattle WA; United States of America
[143] [(a)] Institute of Frontier and Interdisciplinary Science and Key Laboratory of Particle Physics and Particle Irradiation (MOE), Shandong University, Qingdao;[(b)] School of Physics, Zhengzhou University; China
[144] [(a)] State Key Laboratory of Dark Matter Physics, School of Physics and Astronomy, Shanghai Jiao Tong University, Key Laboratory for Particle Astrophysics and Cosmology (MOE), SKLPPC, Shanghai;[(b)] State Key Laboratory of Dark Matter Physics, Tsung-Dao Lee Institute, Shanghai Jiao Tong University, Shanghai; China

JHEP10(2025)093

[145] Department of Physics and Astronomy, University of Sheffield, Sheffield; United Kingdom
[146] Department of Physics, Shinshu University, Nagano; Japan
[147] Department Physik, Universität Siegen, Siegen; Germany
[148] Department of Physics, Simon Fraser University, Burnaby BC; Canada
[149] SLAC National Accelerator Laboratory, Stanford CA; United States of America
[150] Department of Physics, Royal Institute of Technology, Stockholm; Sweden
[151] Departments of Physics and Astronomy, Stony Brook University, Stony Brook NY; United States of America
[152] Department of Physics and Astronomy, University of Sussex, Brighton; United Kingdom
[153] School of Physics, University of Sydney, Sydney; Australia
[154] Institute of Physics, Academia Sinica, Taipei; Taiwan
[155] [(a)] E. Andronikashvili Institute of Physics, Iv. Javakhishvili Tbilisi State University, Tbilisi;[(b)] High Energy Physics Institute, Tbilisi State University, Tbilisi;[(c)] University of Georgia, Tbilisi; Georgia
[156] Department of Physics, Technion, Israel Institute of Technology, Haifa; Israel
[157] Raymond and Beverly Sackler School of Physics and Astronomy, Tel Aviv University, Tel Aviv; Israel
[158] Department of Physics, Aristotle University of Thessaloniki, Thessaloniki; Greece
[159] International Center for Elementary Particle Physics and Department of Physics, University of Tokyo, Tokyo; Japan
[160] Graduate School of Science and Technology, Tokyo Metropolitan University, Tokyo; Japan
[161] Department of Physics, University of Toronto, Toronto ON; Canada
[162] [(a)] TRIUMF, Vancouver BC;[(b)] Department of Physics and Astronomy, York University, Toronto ON; Canada
[163] Division of Physics and Tomonaga Center for the History of the Universe, Faculty of Pure and Applied Sciences, University of Tsukuba, Tsukuba; Japan
[164] Department of Physics and Astronomy, Tufts University, Medford MA; United States of America
[165] Department of Physics and Astronomy, University of California Irvine, Irvine CA; United States of America
[166] University of West Attica, Athens; Greece
[167] Department of Physics and Astronomy, University of Uppsala, Uppsala; Sweden
[168] Department of Physics, University of Illinois, Urbana IL; United States of America
[169] Instituto de Física Corpuscular (IFIC), Centro Mixto Universidad de Valencia — CSIC, Valencia; Spain
[170] Department of Physics, University of British Columbia, Vancouver BC; Canada
[171] Department of Physics and Astronomy, University of Victoria, Victoria BC; Canada
[172] Fakultät für Physik und Astronomie, Julius-Maximilians-Universität Würzburg, Würzburg; Germany
[173] Department of Physics, University of Warwick, Coventry; United Kingdom
[174] Waseda University, Tokyo; Japan
[175] Department of Particle Physics and Astrophysics, Weizmann Institute of Science, Rehovot; Israel
[176] Department of Physics, University of Wisconsin, Madison WI; United States of America
[177] Fakultät für Mathematik und Naturwissenschaften, Fachgruppe Physik, Bergische Universität Wuppertal, Wuppertal; Germany
[178] Department of Physics, Yale University, New Haven CT; United States of America
[179] Yerevan Physics Institute, Yerevan; Armenia

[a] Also at Affiliated with an institute formerly covered by a cooperation agreement with CERN
[b] Also at An-Najah National University, Nablus; Palestine
[c] Also at Borough of Manhattan Community College, City University of New York, New York NY; United States of America
[d] Also at Center for Interdisciplinary Research and Innovation (CIRI-AUTH), Thessaloniki; Greece
[e] Also at Centre of Physics of the Universities of Minho and Porto (CF-UM-UP); Portugal
[f] Also at CERN, Geneva; Switzerland
[g] Also at Département de Physique Nucléaire et Corpusculaire, Université de Genève, Genève; Switzerland
[h] Also at Departament de Fisica de la Universitat Autonoma de Barcelona, Barcelona; Spain
[i] Also at Department of Financial and Management Engineering, University of the Aegean, Chios; Greece
[j] Also at Department of Mathematical Sciences, University of South Africa, Johannesburg; South Africa

JHEP10(2025)093

[k] Also at Department of Modern Physics and State Key Laboratory of Particle Detection and Electronics, University of Science and Technology of China, Hefei; China
[l] Also at Department of Physics, Bolu Abant Izzet Baysal University, Bolu; Türkiye
[m] Also at Department of Physics, King's College London, London; United Kingdom
[n] Also at Department of Physics, Stanford University, Stanford CA; United States of America
[o] Also at Department of Physics, Stellenbosch University; South Africa
[p] Also at Department of Physics, University of Fribourg, Fribourg; Switzerland
[q] Also at Department of Physics, University of Thessaly; Greece
[r] Also at Department of Physics, Westmont College, Santa Barbara; United States of America
[s] Also at Faculty of Physics, Sofia University, 'St. Kliment Ohridski', Sofia; Bulgaria
[t] Also at Faculty of Physics, University of Bucharest; Romania
[u] Also at Hellenic Open University, Patras; Greece
[v] Also at Henan University; China
[w] Also at Imam Mohammad Ibn Saud Islamic University; Saudi Arabia
[x] Also at Institucio Catalana de Recerca i Estudis Avancats, ICREA, Barcelona; Spain
[y] Also at Institut für Experimentalphysik, Universität Hamburg, Hamburg; Germany
[z] Also at Institute for Nuclear Research and Nuclear Energy (INRNE) of the Bulgarian Academy of Sciences, Sofia; Bulgaria
[aa] Also at Institute of Applied Physics, Mohammed VI Polytechnic University, Ben Guerir; Morocco
[ab] Also at Institute of Particle Physics (IPP); Canada
[ac] Also at Institute of Physics and Technology, Mongolian Academy of Sciences, Ulaanbaatar; Mongolia
[ad] Also at Institute of Physics, Azerbaijan Academy of Sciences, Baku; Azerbaijan
[ae] Also at Institute of Theoretical Physics, Ilia State University, Tbilisi; Georgia
[af] Also at Millennium Institute for Subatomic physics at high energy frontier (SAPHIR), Santiago; Chile
[ag] Also at National Institute of Physics, University of the Philippines Diliman (Philippines); Philippines
[ah] Also at The Collaborative Innovation Center of Quantum Matter (CICQM), Beijing; China
[ai] Also at TRIUMF, Vancouver BC; Canada
[aj] Also at Università di Napoli Parthenope, Napoli; Italy
[ak] Also at University of Chinese Academy of Sciences (UCAS), Beijing; China
[al] Also at University of Colorado Boulder, Department of Physics, Colorado; United States of America
[am] Also at University of Sienna; Italy
[an] Also at Washington College, Chestertown, MD; United States of America
[ao] Also at Yeditepe University, Physics Department, Istanbul; Türkiye
[*] Deceased

JHEP10(2025)093

Phys. Lett. B 860 (2025) 139177

Contents lists available at ScienceDirect

Physics Letters B

journal homepage: www.elsevier.com/locate/physletb

Letter

Measurement of top-quark pair production in association with charm quarks in proton–proton collisions at $\sqrt{s} = 13$ TeV with the ATLAS detector

The ATLAS Collaboration *

ARTICLE INFO

Editor: M. Doser

ABSTRACT

Inclusive cross-sections for top-quark pair production in association with charm quarks are measured with proton–proton collision data at a center-of-mass energy of 13 TeV corresponding to an integrated luminosity of 140 fb^{-1}, collected with the ATLAS experiment at the LHC between 2015 and 2018. The measurements are performed by requiring one or two charged leptons (electrons and muons), two b-tagged jets, and at least one additional jet in the final state. A custom flavor-tagging algorithm is employed for the simultaneous identification of b-jets and c-jets. In a fiducial phase space that replicates the acceptance of the ATLAS detector, the cross-sections for $t\bar{t} + \geq 2c$ and $t\bar{t} + 1c$ production are measured to be $1.28^{+0.27}_{-0.24}$ pb and $6.4^{+1.0}_{-0.9}$ pb, respectively. The measurements are primarily limited by uncertainties in the modeling of inclusive $t\bar{t}$ and $t\bar{t} + b\bar{b}$ production, in the calibration of the flavor-tagging algorithm, and by data statistics. Cross-section predictions from various $t\bar{t}$ simulations are largely consistent with the measured cross-section values, though all underpredict the observed values by 0.5 to 2.0 standard deviations. In a phase-space volume without requirements on the $t\bar{t}$ decay products and the jet multiplicity, the cross-section ratios of $t\bar{t} + \geq 2c$ and $t\bar{t} + 1c$ to total $t\bar{t}$ + jets production are determined to be $(1.23 \pm 0.25)\%$ and $(8.8 \pm 1.3)\%$.

1. Introduction

Due to its pivotal role in the Standard Model (SM) of particle physics and its potential interactions with new physics in various beyond-SM frameworks, the study of the top quark (t) remains a cornerstone of contemporary particle physics research. In particular, the ATLAS [1] and CMS [2] experiments at the Large Hadron Collider (LHC) have directed their attention towards exploring rare final states involving top-quark pairs ($t\bar{t}$), such as associated production of $t\bar{t}$ with Higgs bosons ($t\bar{t}H$) or gauge bosons ($t\bar{t}W$, $t\bar{t}Z$, $t\bar{t}\gamma$), and four-top-quark production ($t\bar{t}t\bar{t}$). Measurements of $t\bar{t}H$ with $H \to b\bar{b}$ decay and $t\bar{t}t\bar{t}$ topologies with single-lepton or dilepton final states [3–7] encounter significant challenges due to substantial, irreducible background contributions stemming from $t\bar{t}$ production in association with heavy-flavor quarks, namely bottom (b) and charm (c) quarks. These heavy-flavor quarks can be produced via radiation of a gluon which then splits into a $b\bar{b}$ or $c\bar{c}$ pair. Depending on the kinematics, the $b\bar{b}$ or $c\bar{c}$ pair can form a jet each ($t\bar{t} + b\bar{b}/c\bar{c}$) or merge into a single jet ($t\bar{t} + 1B/1C$). Single b-quark or c-quark production ($t\bar{t} + 1b/c$) can also occur via a b-quark or c-quark originating from the initial state. Illustrative Feynman diagrams for these three production modes are shown in Fig. 1.

Measurements of $t\bar{t} + b\bar{b}$ and $t\bar{t} + c\bar{c}$ production have been limited by the challenging modeling of these processes. While computations of the $t\bar{t} + b\bar{b}$ production cross-section are available at next-to-leading order (NLO) in quantum chromodynamics (QCD) [8–13], the uncertainties in the choice of the renormalization and factorization scales, denoted by μ_R and μ_F, remain sizable, primarily due to the distinct energy scales associated with the $t\bar{t}$ pair and the $b\bar{b}$ pair. Experimental measurements of $t\bar{t} + b\bar{b}$ production were conducted in proton–proton (pp) collision data at the LHC by the ATLAS and CMS experiments at a center-of-mass energy of $\sqrt{s} = 13$ TeV [14–17]. These measurements, along with those of $t\bar{t}H$ ($H \to b\bar{b}$) and $t\bar{t}t\bar{t}$ production, frequently involve determining the $t\bar{t} + \geq 1c$ normalization *in situ* through a free parameter in the fit, compensating for the limited knowledge of this process. Recent ATLAS measurements of $t\bar{t} + b\bar{b}$ and $t\bar{t}H$ ($H \to b\bar{b}$) [5,17] reported the $t\bar{t} + \geq 1c$ normalization factor to be larger than the value predicted by Monte Carlo (MC) simulations. CMS performed a dedicated $t\bar{t} + c\bar{c}$ measurement in $t\bar{t}$ final states with two charged leptons based on Run 2 data corresponding to 41.5 fb^{-1} [18], but did not explicitly measure the $t\bar{t} + 1c/C$ cross-section. The rates of $t\bar{t} + b\bar{b}$, $t\bar{t} + c\bar{c}$, and $t\bar{t}$ + light jets were found to agree with predictions from MC simulations performed at NLO in the matrix element interfaced with a parton shower (PS) algorithm (NLO+PS) within one to two standard deviations of measurement uncertainties.

Using the complete LHC Run 2 data sample of pp collisions corresponding to an integrated luminosity of 140 fb^{-1}, this Letter presents

* *E-mail address:* atlas.publications@cern.ch.

https://doi.org/10.1016/j.physletb.2024.139177
Received 18 September 2024; Received in revised form 13 November 2024; Accepted 2 December 2024

Available online 4 December 2024
0370-2693/© 2024 CERN for the benefit of the ATLAS Collaboration. Published by Elsevier B.V. Funded by SCOAP³. This is an open access article under the CC BY license (http://creativecommons.org/licenses/by/4.0/).

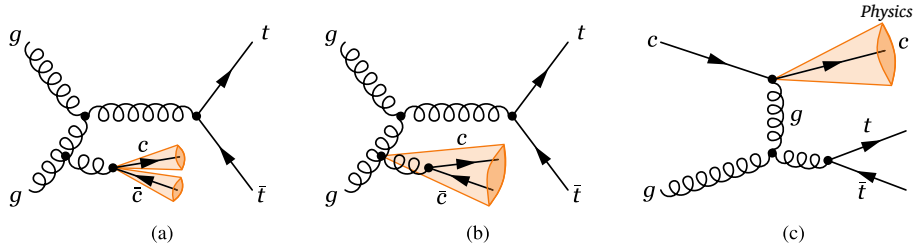

Fig. 1. Illustrative Feynman diagrams for $t\bar{t}+\geq 2c$ and $t\bar{t}+1c$ production: (a) $t\bar{t}+c\bar{c}$ production via initial-state gluon radiation where both c-quarks form a jet each, (b) $t\bar{t}+c\bar{c}$ production via initial-state gluon radiation where the two c-quarks are in the same jet, (c) $t\bar{t}+1c$ production where the c-quark originates from the initial state.

the first ATLAS measurement of $t\bar{t}+\geq 1c$ production. The production rates of $t\bar{t}+\geq 2c$ and $t\bar{t}+1c$ are determined separately to facilitate more detailed comparisons with theoretical predictions, as these processes are expected to be sensitive to different production mechanisms (cf. Fig. 1). The first comprises all final states with two or more c-jets, e.g., $t\bar{t}+c\bar{c}$ production where both c-quarks form separate jets, while the second includes both $t\bar{t}+1c$ production via a c-quark from the initial state and $t\bar{t}+1C$ production. Events with one or two charged leptons in the final state are considered, targeting $t\bar{t}$ topologies where one or both W bosons from the top quarks decay leptonically. While topologies with one charged lepton (single-lepton) offer larger statistics, they introduce additional complexity due to the potential production of extra c-quarks from the hadronically decaying W boson. Conversely, final states with two charged leptons (dilepton) are rarer but expect less background contamination.

The probabilities for $t\bar{t}$ pairs with additional jets initiated by b-quarks, c-quarks, light quarks, and gluons to enter each analysis region are estimated through NLO+PS simulations of inclusive $t\bar{t}$ and of $t\bar{t}+b\bar{b}$ production. This measurement uses a custom flavor tagging algorithm, termed the b/c-tagger, tailored to simultaneous c-jet and b-jet identification, to define analysis regions sensitive to $t\bar{t}+\geq 2c$ and $t\bar{t}+1c$ production. The rates of these processes are then measured in a fiducial phase space designed to replicate the acceptance of the ATLAS detector and in a more inclusive volume. Furthermore, the ratios of $t\bar{t}+\geq 2c$, $t\bar{t}+1c$, and $t\bar{t}+\geq 1b$ to overall $t\bar{t}+$ jets production are extracted and compared with NLO+PS simulations.

2. ATLAS detector

The ATLAS experiment [1] at the LHC is a multipurpose particle detector with a forward–backward symmetric cylindrical geometry and a near 4π coverage in solid angle.[1] It consists of an inner tracking detector (ID) surrounded by a thin superconducting solenoid providing a 2 T axial magnetic field, electromagnetic and hadronic calorimeters, and a muon spectrometer. The ID covers the pseudorapidity range $|\eta| < 2.5$. It consists of silicon pixel, silicon microstrip, and transition radiation tracking detectors. Lead/liquid-argon (LAr) sampling calorimeters provide electromagnetic (EM) energy measurements with high granularity within the region $|\eta| < 3.2$. A steel/scintillator-tile hadronic calorimeter covers the central pseudorapidity range ($|\eta| < 1.7$). The endcap and forward regions are instrumented with LAr calorimeters for EM and hadronic energy measurements up to $|\eta| = 4.9$. The muon spectrometer surrounds the calorimeters and is based on three large superconducting air-core toroidal magnets with eight coils each. The field integral of the toroids ranges between 2.0 and 6.0 T m across most of the detector. The muon spectrometer includes a system of precision tracking chambers up to $|\eta| = 2.7$ and fast detectors for triggering up to $|\eta| = 2.4$. The luminosity is measured mainly by the LUCID–2 [19] detector which is located close to the beampipe. A two-level trigger system is used to select events [20]. The first-level trigger is implemented in hardware and uses a subset of the detector information to accept events at a rate below 100 kHz. This is followed by a software-based trigger that reduces the accepted event rate to 1 kHz on average depending on the data-taking conditions. A software suite [21] is used in data simulation, in the reconstruction and analysis of real and simulated data, in detector operations, and in the trigger and data acquisition systems of the experiment.

3. Simulation of signal and background processes

Samples of simulated events are used to model $t\bar{t}+$ jets production and most background processes. These MC simulated samples were generated employing either the full ATLAS detector simulation [22] based on GEANT4 [23], or a faster simulation where the GEANT4 simulation of the calorimeter response is replaced by a detailed parameterization of the shower shapes [22]. Both simulation methods were found to provide similar modeling for the observables used in this Letter. To account for the effects of multiple interactions in the same and neighboring bunch crossings (pileup), additional interactions were simulated using PYTHIA 8.186 [24] with a set of tuned parameters (*tune*) referred to as A3 [25] and superimposed onto the simulated hard-scatter event. Subsequently, simulated events were reweighted to replicate the pileup conditions observed in the full Run 2 data sample, with a mean number of pp interactions per bunch crossing of 34. All simulated events were processed through the same reconstruction algorithms and analysis chain as the data.

Unless specified otherwise, PYTHIA8 [26] was employed to simulate PS, hadronization, and multi-parton interactions (MPIs). For all samples using PYTHIA8 or HERWIG7 [27–29] for the simulation of the PS, hadronization and MPIs, the decays of b- and c-hadrons were simulated using the EVTGEN program [30]. PYTHIA8 setups use the A14 tune [31] and the NNPDF2.3LO parton distribution function (PDF) set [32]; HERWIG7 setups use the H7UE tune [28] or the default HERWIG tune alongside the MMHT2014LO PDF set [33]. The top-quark mass was set to $m_t = 172.5$ GeV and, unless stated otherwise, the five-flavor scheme (5FS) with massless b-quarks in the matrix element was used for all simulation setups and the corresponding PDF sets.

Inclusive $t\bar{t}$ events were generated with the POWHEG BOX2 [34–37] generator at NLO in QCD employing the NNPDF3.0NLO PDF set [38]. The h_{damp} parameter, which regulates the transverse momentum (p_{T}) of the first additional emission beyond the Born configuration, was set to $1.5\,m_t$ [39]. The hardness scale parameter, which determines the region of phase space vetoed during showering when matched to a PS, was fixed at $p_{\text{T}}^{\text{hard}} = 0$ [40,41]. The scales μ_{R} and μ_{F} were set to the transverse mass of the top quark, $m_{\text{T}}(t) = \sqrt{m_t^2 + p_{\text{T},t}^2}$. In the following, this sample is referred to as $t\bar{t}$ POWHEG+PYTHIA8. To assess uncertainties in the modeling, alternative sets of $t\bar{t}$ events were generated with different configurations: with $p_{\text{T}}^{\text{hard}} = 1$; with $h_{\text{damp}} = 3\,m_t$; and with POWHEG

[1] ATLAS uses a right-handed coordinate system with its origin at the nominal interaction point (IP) in the center of the detector and the z-axis along the beam pipe. The x-axis points from the IP to the center of the LHC ring, and the y-axis points upwards. Polar coordinates (r, ϕ) are used in the transverse plane, ϕ being the azimuthal angle around the z-axis. The pseudorapidity is defined in terms of the polar angle θ as $\eta = -\ln\tan(\theta/2)$ and is equal to the rapidity $y = \frac{1}{2}\ln\left(\frac{E+p_z}{E-p_z}\right)$ in the relativistic limit. Angular distance is measured in units of $\Delta R \equiv \sqrt{(\Delta y)^2 + (\Delta\phi)^2}$.

BOX interfaced to HERWIG7 instead of PYTHIA8. To compare the result with another prediction, an additional set was generated with the MADGRAPH5_AMC@NLO 2.6.0 generator [42] at NLO in QCD, which uses the NNPDF3.0NLO PDF set, MADSPIN [43,44] to simulate top-quark decays, and HERWIG7 for PS and hadronization [45]. All generated sets of events were reweighted to the predicted cross-section of $\sigma(t\bar{t}) = 832 \pm 51$ pb, as calculated with the Top++2.0 program to next-to-next-to-leading order (NNLO) in QCD, including soft-gluon resummation to next-to-next-to-leading-log order (see Ref. [46] and references therein). The uncertainties include independent variations of μ_R and μ_F, and variations in the PDF and α_S, following the PDF4LHC prescription with the MSTW2008 68% CL NNLO, CT10 NNLO and NNPDF2.3 5FS PDF sets (see Ref. [47] and references therein, and Refs. [32,48,49]).

The POWHEG BOX RES [11] generator and OPENLOOPS [50–52] were used to generate $t\bar{t} + b\bar{b}$ events in the four-flavor scheme (4FS) with massive b-quarks, where the generation of the additional $b\bar{b}$ pair is included in the matrix element, employing the NNPDF3.0NLO 4FS PDF set [38]. The μ_R scale was set to $\frac{1}{2}\sqrt[4]{\prod_{i=t,\bar{t},b,\bar{b}} m_{T,i}}$ where $m_{T,i}$ denotes the transverse mass for each parton i. The μ_F scale and the h_{damp} parameter were set to $0.5 \times \sum_i m_{T,i}$ with $i \in \{t, \bar{t}, b, \bar{b}, j\}$ and $i \in \{t, \bar{t}, b, \bar{b}\}$, respectively, where j denotes extra partons. The p_T^{hard} parameter was fixed to 0, and the Born-zero-damp parameter (h_{bzd}), regulating the division between the finite and singular part of the real emission in the NLO calculation, was set to 5. In the following, this sample is referred to as $t\bar{t} + b\bar{b}$ POWHEG+PYTHIA8. To assess uncertainties in the modeling, alternative sets of $t\bar{t} + b\bar{b}$ events were generated with different configurations: with $p_T^{hard} = 1$; using the dipole recoil scheme instead of the nominal global recoil scheme [11,53]; and interfacing POWHEG BOX RES with HERWIG7 instead of PYTHIA8. To compare the result with another prediction, alternative sets of $t\bar{t} + b\bar{b}$ events were generated with $h_{bzd} = 2$. An additional alternative set of events was generated with the SHERPA 2.2.10 generator [54] in the 4FS, for which the virtual corrections for matrix elements at NLO accuracy were provided by COMIX [55] and OPENLOOPS. The SHERPA events were matched with the SHERPA PS algorithm [56] based on Catani–Seymour dipole factorization using the MEPS@NLO prescription [57–60] and a set of tuned parameters developed by the SHERPA authors. All generated sets of events were reweighted to the same prediction cross-section value as computed in POWHEG BOX RES at NLO in QCD.

A dedicated simulation of $t\bar{t} + c\bar{c}$ production in the three-flavor scheme (3FS) is not available. Hence, $t\bar{t} + c\bar{c}$ contributions are estimated solely using $t\bar{t}$ 5FS simulation, where only the gluon radiation process is simulated in the NLO matrix element, but its splitting into a $c\bar{c}$ pair is done in the PS.

Simulated $t\bar{t}$ and $t\bar{t} + b\bar{b}$ events are sorted into four $t\bar{t}$ + jets categories using particle-level information: $t\bar{t} + \geq 2c$, $t\bar{t} + 1c$, $t\bar{t} + \geq 1b$, and $t\bar{t}$ + light. For the categorization, jets are reconstructed from stable particles[2] following PS and hadronization, using the anti-k_t algorithm [61,62] with a radius parameter $R = 0.4$. They are required to have $p_T > 15$ GeV and $|\eta| < 2.5$. The flavor of a particle-level jet is determined by counting b- and c-hadrons with $p_T > 5$ GeV that are *ghost-associated* [63,64] with the jet. Jets with one or more associated b-hadrons are designated as b-jets, while those with one or more associated c-hadrons but no b-hadron are labeled as c-jets. Events are categorized based on the presence of additional particle-level b-jets and c-jets, excluding jets originating from decays of top quarks and W bosons.[3] Events with one or more b-jets are classified as $t\bar{t} + \geq 1b$, those with two or more c-jets but no b-jet are categorized as $t\bar{t} + \geq 2c$, and events with one c-jet but no b-jet are labeled as $t\bar{t} + 1c$. Any remaining events enter the $t\bar{t}$ + light category.

[2] Particle-level objects are considered stable if $\tau > 3 \times 10^{-11}$ s.

[3] The procedure to exclude these jets is as follows: b-quarks and c-quarks originating directly from the decays of top quarks and W bosons are identified in the MC generator record. Then, the b- and c-hadrons closest in ΔR are flagged. Any jet *ghost-associated* with these hadrons is removed from the categorization.

The $t\bar{t}$ + jets categorization at particle level is used to remove the overlap between the inclusive $t\bar{t}$ 5FS simulation and the $t\bar{t} + b\bar{b}$ 4FS simulation. The latter is expected to provide the more accurate modeling of $t\bar{t} + b\bar{b}$ production and is the preferable setup to simulate $t\bar{t} + \geq 1b$ contributions in this analysis. Thus, events are removed from any of the $t\bar{t}$ 5FS setups if they fall into the $t\bar{t} + \geq 1b$ category at particle level. All other events are retained to estimate contributions in the $t\bar{t} + \geq 2c$, $t\bar{t} + 1c$, and $t\bar{t}$ + light categories. Likewise, events from the $t\bar{t} + b\bar{b}$ 4FS simulation are removed if they fall into the $t\bar{t} + \geq 2c$, $t\bar{t} + 1c$, or $t\bar{t}$ + light categories at particle level. The individual cross-sections assigned to the $t\bar{t}$ and $t\bar{t} + b\bar{b}$ samples are retained, and no rescaling is performed after removing the overlapping events.

Various other processes involving top quarks can mimic $t\bar{t}$ + jets topologies. Single-top-quark t-channel, s-channel, and tW production were simulated using POWHEG BOX2 at NLO in QCD. For t-channel production, events were generated in the 4FS with the NNPDF3.0NLO 4FS PDF set. For s-channel and tW production, events were generated in the 5FS using the NNPDF3.0NLO 5FS PDF set. The tW simulation employed the diagram-removal scheme [65] to treat interference with $t\bar{t}$ production [39]. Additional sets of tW events were generated in different setups: using the diagram-subtraction scheme [39,65]; using POWHEG BOX2 interfaced with HERWIG 7.04; and using MADGRAPH5_AMC@NLO 2.6.2 interfaced with PYTHIA8. POWHEG BOX2+HERWIG7 setups were also generated for t-channel and s-channel production. $t\bar{t}H$ production was simulated with POWHEG BOX2 at NLO in QCD in the 5FS, using the NNPDF3.0NLO PDF set. Additionally, $t\bar{t}W$, $t\bar{t}Z$, tZq, and tWZ events were generated using the MADGRAPH5_AMC@NLO 2.3.3 generator at NLO in QCD with the NNPDF3.0NLO PDF set. Secondary sets of $t\bar{t}W$ and $t\bar{t}Z$ events were simulated with SHERPA 2.2.0 at leading order (LO) in QCD. In the following, these processes are collectively referred to as *Other Top*.

W + jets and Z + jets events were simulated using the SHERPA 2.2.1 generator employing NLO matrix elements for up to two partons and LO matrix elements for up to four partons, calculated with the COMIX and OPENLOOPS libraries. Diboson events with semileptonic and fully leptonic decays were simulated using SHERPA 2.2.1 and SHERPA 2.2.2, employing NLO matrix elements for up to one additional parton and LO matrix elements for up to three additional partons. W + jets, Z + jets and diboson events were matched with the SHERPA PS algorithm based on Catani–Seymour dipole factorization using the MEPS@NLO prescription and a set of tuned parameters developed by the SHERPA authors. The NNPDF3.0NNLO PDF set [38] was used, and the cross-sections of the samples were reweighted to NNLO predictions [66]. In the following, W + jets, Z + jets and diboson processes are collectively referred to as *Non-Top*.

The cross-section measurements are conducted within a fiducial volume at particle level, closely resembling the detector-level acceptance, ensuring robustness against variations in acceptance predictions from MC simulations. Events in the single-lepton (dilepton) channel must exhibit five (three) or more jets with $p_T > 25$ GeV and $|\eta| < 2.5$, out of which at least two must be ghost-associated with b-hadrons. No specific requirements are imposed regarding the presence of additional b- or c-jets in the fiducial phase space, but the $t\bar{t}$ + jets categorization is performed as described above. In the single-lepton channel, events must feature exactly one charged lepton ($\ell = e, \mu$), while in the dilepton channel, events must contain exactly two oppositely charged leptons. One lepton must have $p_T > 27$ GeV, any additional lepton must carry $p_T > 10$ GeV, and all are required to be within $|\eta| < 2.5$. Any event featuring a same-flavor lepton pair with an invariant mass below 15 GeV or within the range 83 to 99 GeV is rejected. Leptons are removed if their distance to a jet satisfies $\Delta R < 0.4$. The fiducial phase space accepts approximately 17% of the total number of simulated $t\bar{t} + \geq 1c$ events. The measurements are also performed in a more inclusive phase-space volume without requirements on the $t\bar{t}$ decay products and the jet multiplicity.

Physics Letters B 860 (2025) 139177

4. Event reconstruction and selection

Events are required to have at least one primary vertex with two or more tracks with $p_{\mathrm{T}} > 0.5$ GeV. For events with more than one primary vertex, the hard-scattering primary vertex is selected as the one with the highest sum of squared track p_{T} [67]. A suite of single-electron and single-muon triggers is used to select events with at least one charged lepton [68,69].

Jets are reconstructed using the anti-k_t clustering algorithm with a radius parameter of $R = 0.4$ using particle flow jet constituents that combine measurements from both the ID and the calorimeter [70]. Jet candidates undergo calibration using simulations, with corrections derived from in situ techniques applied to data [71]. They are required to have $p_{\mathrm{T}} > 25$ GeV and $|\eta| < 2.5$, with jets within $|\eta| < 2.4$ and $p_{\mathrm{T}} < 60$ GeV further required to pass the tight working point of the jet vertex tagger [72] to reduce contribution from pileup jets.

Electron candidates are reconstructed from clusters of energy in the EM calorimeter associated with reconstructed tracks from the ID. Their reconstruction, identification, and calibration are detailed in Refs. [73,74]. They must satisfy a set of likelihood-based identification criteria with $p_{\mathrm{T}} > 10$ GeV and $|\eta_{\mathrm{cluster}}| < 2.47$. Electrons in the transition region between the end-caps and barrel region ($1.37 < |\eta_{\mathrm{cluster}}| < 1.52$) are vetoed. Tracks matched to electrons are required to be associated with the primary vertex and satisfy $|z_0 \sin\theta| < 0.5$ mm and $|d_0|/\sigma(d_0) < 5$, where z_0 and d_0 are the longitudinal and transverse impact parameters of the electron track, respectively. For the analysis regions, the identification criteria are tightened, and electrons are required to satisfy a set of variable-radius isolation criteria to reduce contributions from misidentified jets, considering energy depositions in the calorimeter and tracks in the ID [73].

Muons are reconstructed by combining a track from the muon spectrometer with an ID track. Details regarding the reconstruction, identification and calibration of muons are summarized in Refs. [75,76]. The ID tracks must be associated with the primary vertex by passing $|z_0 \sin\theta| < 0.5$ mm and $|d_0|/\sigma(d_0) < 3$. They must fulfill $p_{\mathrm{T}} > 10$ GeV, $|\eta| < 2.5$, and satisfy a set of muon quality criteria. For the analysis regions, the quality criteria are tightened, and muons are required to pass a track-based isolation criterion to reduce contributions from misidentified jets [75].

An overlap removal procedure prevents double counting of energy deposits and improves object resolution and identification efficiencies. Electron candidates sharing tracks with a muon candidate are removed. The nearest jet within $\Delta R < 0.2$ of an electron candidate is removed in favor of the electron. Electrons within $\Delta R < 0.4$ of any jets after this selection are removed in favor of the jet. Muons are removed if they are within $\Delta R < 0.4$ of a jet to reduce contributions from heavy-flavor decays. However, if the jet has fewer than three associated tracks, the muon is kept in favor of the jet.

Jets containing b-hadrons are identified as b-tagged jets using the DL1r algorithm [77], which leverages distinctive b-hadron features like track impact parameters and the presence of displaced vertices in the ID. The algorithm also includes discriminating variables from a recurrent neural network that exploit spatial and kinematic correlations between tracks from the same b-hadron. The DL1r algorithm provides three output scores, p_b, p_c, and p_{light}, and in the standard DL1r calibration, jets are tagged as b-jets using a discriminant $\mathcal{D}_b$ that is built using the Neyman–Pearson lemma [78]:

$$\mathcal{D}_b = \log \frac{p_b}{f_c p_c + (1 - f_c) p_{\mathrm{light}}}.$$

The parameter f_c controls which background contributes more to the decision. To improve the efficiency of selecting jets originating from c-quarks without compromising the b-jet identification performance, the DL1r algorithm was reoptimized as a 2D binned discriminant, the b/c-tagger. This reoptimization was necessary because standard DL1r configurations do not provide calibrated c-tagging working points, requiring a tailored approach to achieve the desired balance between b-jet and c-jet identification. The axes of the discriminant, $\mathcal{D}_c$ and $\mathcal{D}_b$, are calculated from the p_b, p_c, and p_{light} scores following the above formula, with all b- and c-subscripts interchanged for the $\mathcal{D}_c$ discriminant. It was found that $f_b = 0.4$ provides good performance for the b/c-tagger as it leads to a balanced contamination of b-jets and light-flavor jets in the analysis regions; the value of $f_c = 0.018$ was chosen to align the admixture with the standard DL1r calibration.

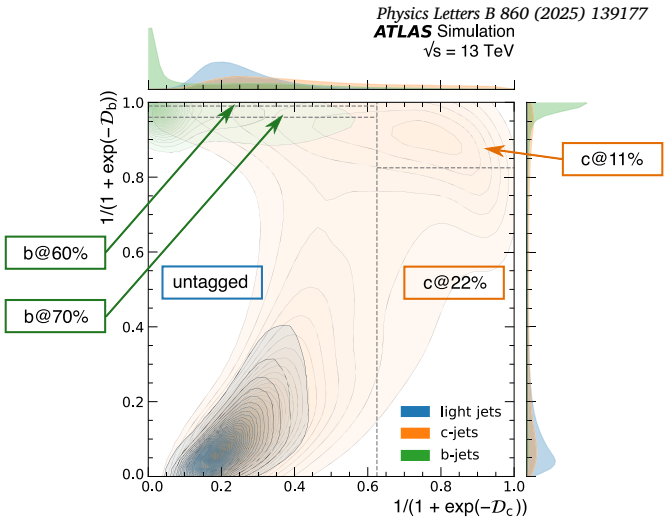

Fig. 2. Distribution of light, c-, and b-jets for the 2D b/c-tagger in simulated $t\bar{t}$ events. Dashed lines correspond to the edges of the working points. For visualization purposes a standard logistic function is applied to both axes of the discriminant. The contours for each jet type are smoothed with a kernel density method to improve readability, with contours corresponding to lines of constant density. The two b-tagging bins comprise the top left corner of the discriminant, with the c-tagging bins to the right of the vertical dashed line. Untagged jets are located in the bottom left corner.

The binning in $\mathcal{D}_c$ and $\mathcal{D}_b$ includes five working points (WPs), two of which are optimized for c-jet identification and two for b-jet identification. The WPs are designed to achieve an approximately constant efficiency for b-jet and c-jet identification across the jet p_{T} and $|\eta|$ range, with $p_{\mathrm{T}} > 20$ GeV. The c-tagging WPs are separated from the others by $\mathcal{D}'_c \geq 0.625$, where the prime indicates that a standard logistic function is applied to the discriminant: $\mathcal{D}'_c = 1/(1 + \exp(-\mathcal{D}_c))$. The tight c-tagging WP includes a tighter cut on $\mathcal{D}'_b$ to increase the light-flavor rejection rate and is designed to achieve an exclusive efficiency of 11% (denoted $c@11\%$).[4] The loose c-tagging WP, which includes $c@11\%$, achieves an inclusive efficiency of 22% ($c@22\%$). The $c@11\%$ and $c@22\%$ WPs yield b-jet rejection rates of 28.7 and 18.9 and light-flavor rejection rates of 1051 and 104 in simulated $t\bar{t}$ events, respectively. The b-tagging WPs, defined for $\mathcal{D}'_c < 0.625$, use the same $\mathcal{D}'_b$ cuts as the two tightest b-tagging WPs in the standard DL1r calibration. The tighter b-tagging WP is designed to achieve an exclusive efficiency of 60% ($b@60\%$), the looser, which includes $b@60\%$, to achieve an inclusive b-tagging efficiency of 70% ($b@70\%$), with c-jet rejection rates of 37.1 and 12.2 and light-flavor rejection rates of 2320 and 573, respectively. Jets not entering any of the four WP bins are classified as untagged. Consequently, the b/c-tagger comprises a total of five orthogonal bins, with the distribution of light, c- and b-jets illustrated in Fig. 2.

The calibration of the five b/c-tagger WPs follows standard procedures applied to the DL1r algorithm [79–81]. Jets originating from b- and c-quarks are calibrated in data using $t\bar{t}$ events, both selections being orthogonal to the events analyzed in this study by limiting the number

[4] Tightening the cut on $\mathcal{D}'_c$ instead of $\mathcal{D}'_b$ would lead to a more balanced increase in the b-jet and light-flavor rejection rate, but it was found that a focus on higher light-flavor rejection rates yields better $t\bar{t} + \geq 1c$ signal sensitivity.

Table 1
Jet multiplicity and tagging criteria for the signal regions (SRs) and control regions (CRs) in the single-lepton and dilepton channels. All single-lepton regions are defined in the 5-jet-exclusive and 6-jet-inclusive jet selections, all dilepton regions in the 3-jet-exclusive and 4-jet-inclusive jet selections. By construction, $SR^{2\ell}_{tight}$ only exists for the 4-jet-inclusive selection. Identical requirements on inclusive and exclusive working points, e.g., one c@22% and one c@11% in the $CR^{1\ell}_{1}$, indicate a veto of additional tags at the inclusive working point.

	$CR^{1\ell}_{1}$	$CR^{1\ell}_{2}$	$CR^{1\ell}_{3}$	$SR^{1\ell}_{loose}$	$SR^{1\ell}_{tight}$	$CR^{2\ell}_{1}$	$CR^{2\ell}_{2}$	$CR^{2\ell}_{3}$	$SR^{2\ell}_{loose}$	$SR^{2\ell}_{tight}$
N_{jets}	$= 5$ or ≥ 6					$= 3$ or ≥ 4				≥ 4
b@70%	2	–	–	2	2	2	–	≥ 3	2	2
b@60%	–	≥ 3	3	–	–	–	≥ 3	≤ 2	–	–
c@22%	1	0	1	≥ 2	–	0	–	–	1	≥ 2
c@11%	1	–	1	1	≥ 2	–	–	–	–	–

of jets to four (two) in single-lepton (dilepton) final states. All b-tagging calibration scale factors (SFs) are close to unity, with statistical uncertainties dominating the high p_T regime. The c-tagging calibration yields more variation in the SF values. For the b@70% WP, the SFs average around 0.9 and some bins in jet p_T are incompatible with unity within their uncertainties. Light-flavor jet calibration employs the *negative-tag* method [82,83] in conjunction with a *flip-tagger* approach following Ref. [81], and all SFs are compatible with unity within uncertainties. For the b@60% working point, the light-flavor SFs cannot be determined due to the large b-jet contamination and so, following the procedure in Ref. [81], are set to unity with additional uncertainties. The c@11% WP also has large uncertainties due to high contamination of heavy-flavor jets and low statistics. Simulation-to-simulation SFs are derived in bins of jet p_T and $|\eta|$ to account for differences between tagging efficiencies for different PS and hadronization algorithms [84].

A preselection is applied and requires at least one electron or muon with $p_T > 27$ GeV that is matched to the trigger object. The single-lepton channel selects events with exactly one lepton, while the dilepton channel selects those with exactly two oppositely charged leptons. Events must have at least five (three) jets in the single-lepton (dilepton) channel, with at least three (two) b-tagged or c-tagged jets using the b@70% or c@22% working points. For dilepton final states with identical lepton flavors, the same invariant-mass criteria as those applied in the fiducial selection at particle level are imposed. In the single-lepton channel, events are split into those with exactly five jets (5-jet-exclusive) and those with six or more jets (6-jet-inclusive). Similarly, in the dilepton channel, events are categorized as either 3-jet-exclusive or 4-jet-inclusive. Based on the number of identified b- and c-tagged jets, events are further classified into signal regions (SRs) enriched in $t\bar{t}+\geq 2c$ and $t\bar{t}+1c$ events, and control regions (CRs), which determine the normalization of the $t\bar{t}+\geq 1b$ and $t\bar{t}+$ light background. An overview of the seven SRs and 12 CRs is shown in Table 1. Approximately 5.3% of the simulated $t\bar{t}+\geq 1c$ events passing the fiducial selection criteria are reconstructed in the analysis regions.

There are four SRs in the single-lepton channel and three SRs in the dilepton channel with different degrees of purity in $t\bar{t}+\geq 2c$ and $t\bar{t}+1c$ events. The $SR^{1\ell}_{tight}$ and $SR^{2\ell}_{tight}$ regions target $t\bar{t}+\geq 2c$ events, while $SR^{1\ell}_{loose}$ and $SR^{2\ell}_{loose}$ are dominated by $t\bar{t}+1c$. All seven regions require exactly two b-tagged jets at b@70%. In the single-lepton channel, events featuring at least two c-tagged jets at c@22% with exactly one satisfying the c@11% working point enter the $SR^{1\ell}_{loose}$ regions. Events with two or more c-tagged jets at c@11% are classified into $SR^{1\ell}_{tight}$. The expected purity in $t\bar{t}+\geq 2c$ events in the single-lepton SRs ranges between 10% and 28%, while the predicted $t\bar{t}+1c$ contributions are between 29% and 38%. In the dilepton channel, events with exactly one c-tagged jet at c@22% are sorted into $SR^{2\ell}_{loose}$, while events with at least two enter $SR^{2\ell}_{tight}$, which is only defined in the 4-jet-inclusive selection. In the dilepton regions, the expected purity in $t\bar{t}+\geq 2c$ and $t\bar{t}+1c$ events is between 4% and 46%, and between 16% and 38%, respectively.

In the single-lepton channel, three CRs with varying compositions in $t\bar{t}+\geq 1b$ and $t\bar{t}+$ light are defined for each of the two jet multiplicity selections. The $CR^{1\ell}_{1}$ regions select exactly two b-tagged jets at b@70% and exactly one c-tagged jet passing c@22% and c@11%. They are dominated by $t\bar{t}+$ light events. The $CR^{1\ell}_{2}$ regions are characterized by events with three or more b-tagged jets at b@60%, with a veto on c-tagged jets, leading to a mix of $t\bar{t}+\geq 1b$ and $t\bar{t}+$ light. The $CR^{1\ell}_{3}$ regions are pure in $t\bar{t}+\geq 1b$ and select events with exactly three b-tagged jets at b@60% and exactly one c-tagged jet satisfying c@22% and c@11%.

Similarly, the dilepton channel features three CRs for each of the two jet multiplicity selections. The $CR^{2\ell}_{1}$ regions require exactly two b-tagged jets at b@70% and veto c-tagged jets. They are dominated by $t\bar{t}+$ light events. The $CR^{2\ell}_{2}$ regions are pure in $t\bar{t}+\geq 1b$ and select events with three or more b-tagged jets at b@60%. The $CR^{2\ell}_{3}$ regions show a mix of $t\bar{t}+\geq 1b$ and $t\bar{t}+$ light by requiring at least three b-tagged jets at b@70%, with no more than two satisfying the b@60% criteria.

Contributions from processes with non-prompt or misidentified leptons to the single-lepton selection, in the following termed *fake leptons*, were estimated by using the data-driven *matrix method* [85] in dedicated CRs. Prompt-lepton efficiencies were derived in data using a tag-and-probe method in Z-boson decays. Fake-lepton efficiencies were estimated in data in bins of lepton p_T and $|\eta|$ using events with at least three jets, at least two b-tagged jets at the 70% working point of the DL1r tagger, and one lepton fulfilling the looser identification and quality criteria. The isolation requirements were completely dropped. To enrich the selection in fake leptons, only events where the scalar sum of the magnitude of the missing-transverse-momentum vector and the leptonically decaying W-boson mass is no larger than 60 GeV were considered.[5] The fake-lepton contributions to the analysis were then estimated by inverting the efficiency matrix and applying it to the observed event yields in the analysis regions using the looser and the nominal lepton identification and isolation criteria. Fake-lepton contributions to the dilepton selection mainly arise from W + jets and single-lepton $t\bar{t}$ + jets events and were estimated from MC simulation.

5. Systematic uncertainties

The extraction of the $t\bar{t}+\geq 2c$ and $t\bar{t}+1c$ cross-sections is subject to various sources of uncertainties, impacting either the overall event yields in a region, the shape of observable distributions considered in the fit, or both.

Experimental sources of uncertainties include uncertainties in the value of the integrated luminosity of the Run 2 data, the simulation

[5] The magnitude of the missing-transverse-momentum vector, denoted E_T^{miss}, is defined as the negative sum of the transverse momenta of the reconstructed and calibrated physical objects, plus a *soft term* built from all other tracks associated with the primary vertex [86] and not matched to a reconstructed object. The mass of the leptonically decaying W boson is calculated from the kinematics of the lepton and the missing transverse momentum.

of pileup events, and effects related to the reconstruction and identification of physics objects used in the analysis. The uncertainty in the combined 2015–2018 integrated luminosity is 0.83% [87], obtained using the LUCID-2 detector [19] for the primary luminosity measurements, complemented by measurements using the inner detector and calorimeters. Uncertainties in the modeling of pileup are evaluated by varying the pileup reweighting in MC simulations within its associated uncertainties. Furthermore, lepton identification and isolation efficiencies, momentum scale and resolution, and lepton trigger efficiencies are varied within their uncertainties to evaluate their impact on the measurement [73–76]. The uncertainty in the jet energy scale (JES) is derived from a combination of simulations, test-beam data, and in situ measurements [71]. This uncertainty incorporates contributions from various sources such as jet-flavor composition, η-intercalibration, punch-through, single-particle response, calorimeter response to different jet flavors, and pileup. It comprises 30 uncorrelated JES uncertainty subcomponents. Additionally, the jet energy resolution in simulation is varied by its corresponding uncertainty, which is divided into thirteen uncorrelated sources. The uncertainty associated with the jet vertex tagger is determined by varying its efficiency correction factors [72]. Moreover, uncertainties in the calibration of the b/c-tagger are separately determined for b-jets, c-jets, and light-flavor jets, following the procedures detailed in Refs. [79–81]. They are derived as a function of jet p_{T} and separately for each WP, yielding a total of 45 components for b-jets and 20 each for c-jets and light-flavor jets. For jets with p_{T} values above the range covered by the calibration, extrapolation uncertainties derived from MC simulation are applied.

Uncertainties in the modeling of $t\bar{t}+\geq 2c$, $t\bar{t}+1c$, and $t\bar{t}+$light are considered through several alternative inclusive $t\bar{t}$ simulation setups. The alternative set of events with $p_{\mathrm{T}}^{\mathrm{hard}}=1$ is used to assess the uncertainty in the NLO matching between the matrix elements and the PS. The $h_{\mathrm{damp}}=3\,m_t$ sample assesses the uncertainty in the choice of that parameter. The POWHEG+HERWIG7 setup evaluates the uncertainty in the choice of the PS and hadronization algorithm. Additionally, the nominal set of events is reweighted to scenarios where μ_{R} and μ_{F} in the matrix element are halved and doubled independently to assess the uncertainty in the choice of these parameters. To estimate uncertainties in the modeling of initial-state radiation (ISR) and final-state radiation (FSR), the factorized parameter α_S^{ISR} is varied using the *var3c* variation of the A14 tune, and the renormalization scale associated with α_S^{FSR} is varied to 0.625 and 2 relative to its nominal setting. The uncertainty in the PDF set is estimated by using 30 PDF variations of the PDF4LHC prescription.

Uncertainties in the modeling of the $t\bar{t}+\geq 1b$ contributions are considered through a similar suite of alternative $t\bar{t}+b\bar{b}$ simulation setups. The alternative set of events with $p_{\mathrm{T}}^{\mathrm{hard}}=1$ is used to assess the uncertainty in the NLO matching between the matrix elements and the PS. The uncertainty in the choice of the recoil scheme is evaluated with the set of events generated with the alternative dipole recoil scheme. The POWHEG+HERWIG7 setup is used to evaluate the uncertainty in the selection of the PS and hadronization algorithm. Event weight variations identical to those applied in $t\bar{t}$ simulations, including μ_{R}, μ_{F}, ISR, FSR, and the PDF set, are considered for $t\bar{t}+b\bar{b}$.

All uncertainties considered in the modeling of $t\bar{t}$ + jets production are treated as uncorrelated between the $t\bar{t}+\geq 1b$, $t\bar{t}+\geq 1c$, and $t\bar{t}+$light processes. Moreover, the NLO matching and PS uncertainties for $t\bar{t}+\geq 1c$ ($t\bar{t}+\geq 1b$) are parameterized independently for the $t\bar{t}+\geq 2c$ and $t\bar{t}+1c$ ($t\bar{t}+\geq 2b$ and $t\bar{t}+1b$) components as the components are sensitive to different effects. Additionally, the $t\bar{t}+$light PS uncertainty is parameterized separately for the 3-jet-exclusive, 4-jet-inclusive, 5-jet-exclusive, and 6-jet-inclusive regions to avoid strong constraints arising from region-to-region migration effects.

For t-channel, s-channel, and tW single-top-quark production, the POWHEG+HERWIG7 setups are used to assess the uncertainty in the choice of the PS and hadronization algorithm. For tW production, the set of events with the diagram-subtraction scheme is used to gauge the uncertainty in the treatment of the interference with $t\bar{t}$, and the NLO matching uncertainty is evaluated using events generated with MADGRAPH5_AMC@NLO+PYTHIA8. An additional 5% normalization uncertainty is assigned to accommodate the uncertainty in the cross-section value [88]. For the t-channel and s-channel predictions, normalization uncertainties of 50% are assigned to cover NLO matching and cross-section uncertainties. The difference between the sets of $t\bar{t}W$ and $t\bar{t}Z$ events generated with MADGRAPH5_AMC@NLO+PYTHIA8 and SHERPA is used as an uncertainty in the prediction for these processes. Additionally, uncertainties of approximately 13% and 11% are assigned to $t\bar{t}W$ and $t\bar{t}Z$, respectively, to accommodate uncertainties in the assigned cross-section values [89]. Conservative normalization uncertainties of 50% are assigned to each of the remaining top-quark processes considered ($t\bar{t}H$, tWZ, tZq) to cover potential mismodeling of the rates of these processes in the probed fiducial phase space. For the W + jets, Z + jets and diboson background, the assigned uncertainties follow those used in previous ATLAS measurements [90]. Normalization uncertainties of 40% and 35% are considered for W + jets and Z + jets processes, based on variations of the μ_{R} and μ_{F} scales and of the matching parameters in the SHERPA generator. Additional 40% uncertainties are assigned to W + jets events with exactly two heavy-flavor jets and at least three heavy-flavor jets based on the same variations. A 50% uncertainty is assigned to the diboson background, which includes uncertainties in the inclusive cross-section and additional jet production [91–93]. None of the modeling uncertainties of the *Other Top* and *Non-Top* categories have any significant impact on the $t\bar{t}+\geq 2c$ and $t\bar{t}+1c$ cross-section measurements.

The fake-lepton estimate in the single-lepton channel is derived from a data sample with finite statistics, leading to bin-by-bin statistical uncertainties for the fake-electron and fake-muon contributions. In addition, conservative 50% normalization uncertainties are assigned to the data-driven single-lepton and MC-based dilepton estimates.

6. Results

The data from all 19 analysis regions are simultaneously fit using a binned profile likelihood approach using the HistFactory [94] and RooFit [95] toolkits. Systematic uncertainties are incorporated as nuisance parameters in the fit and are constrained by a Gaussian penalty term present in the likelihood function. The statistical uncertainty arising from the limited number of simulated events is included in the likelihood in the form of additional nuisance parameters with Poisson constraint terms. To determine the production cross-sections of the $t\bar{t}+\geq 2c$ and $t\bar{t}+1c$ processes, and to control the $t\bar{t}+\geq 1b$ and $t\bar{t}+$light background processes, normalization factors are defined for all four $t\bar{t}$ + jets categories. These factors, μ_i, serve as unconstrained normalization factors in the profile likelihood fit, and they are applied to both fiducial and non-fiducial $t\bar{t}$ + jets events. The inclusive $t\bar{t}$ + jets normalization factor is computed following

$$\mu(t\bar{t}+\text{jets})=\sum_i \mu_i R_i^{\mathrm{MC}} \quad \text{for } i\in\{t\bar{t}+\geq 1b, t\bar{t}+\geq 2c, t\bar{t}+1c, t\bar{t}+\text{light}\}, \tag{1}$$

where R_i^{MC} is the predicted cross-section ratio of process i to overall $t\bar{t}$ + jets production in MC simulation.

Each of the 12 CRs is represented as a single bin in the fit. $\mathrm{SR}_{\mathrm{loose}}^{1\ell 5\mathrm{j}}$ and $\mathrm{SR}_{\mathrm{tight}}^{1\ell 5\mathrm{j}}$ use the invariant mass between the two geometrically closest c-tagged jets to increase sensitivity to differences between the $t\bar{t}+\geq 2c$, $t\bar{t}+1c$, and $t\bar{t}+$light contributions (only considering c-tagged jets passing $c@11\%$ in $\mathrm{SR}_{\mathrm{tight}}^{1\ell 5\mathrm{j}}$). Due to c-jets originating from the decay of the W boson, the contribution from $t\bar{t}+$light is enhanced around the W-boson mass. $\mathrm{SR}_{\mathrm{loose}}^{2\ell 3\mathrm{j}}$ uses the invariant mass between the c-tagged jet and the geometrically closest b-tagged jet. All three regions use four bins with varying width to maximize sensitivity to the $t\bar{t}+\geq 2c$ and $t\bar{t}+1c$ contributions. In the 4-jet-inclusive and 6-jet-inclusive SRs, the jet multiplicity is used to enhance the separation between $t\bar{t}+\geq 1b$, $t\bar{t}+\geq 2c$,

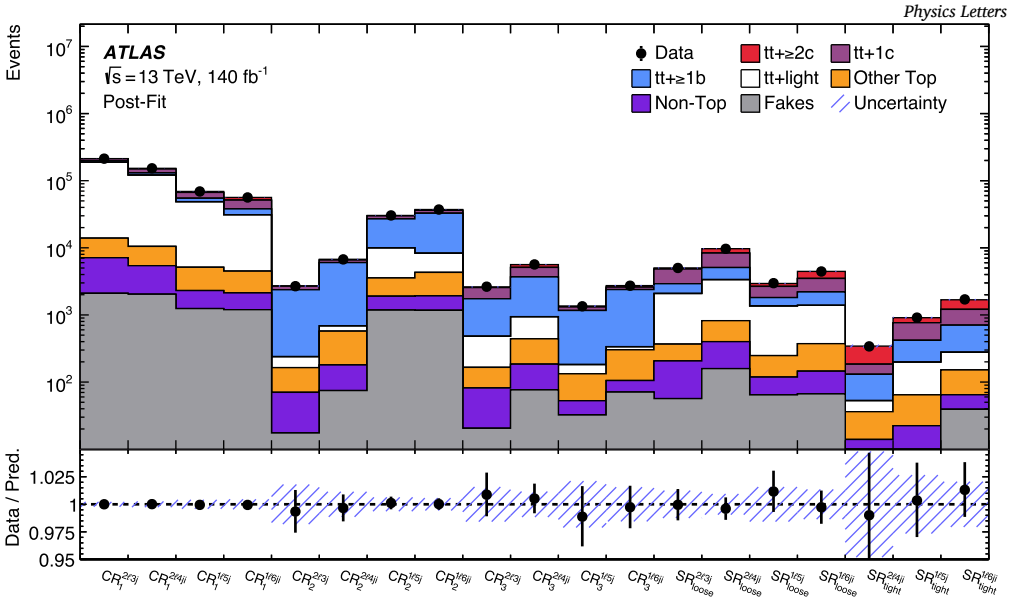

Fig. 3. Post-fit agreement between data and MC simulation in the 12 control regions (CRs) and seven signal regions (SRs). The error bars indicate data statistical uncertainties. The hatched uncertainty bands include all uncertainties and their correlations. *Other Top* includes single-top-quark production and associated production of $t\bar{t}$ and single top quarks with bosons. *Non-Top* includes W + jets, Z + jets, and diboson processes.

$t\bar{t}+1c$, and $t\bar{t}+$ light processes, fitting $6 \leq N_{\text{jets}} \leq 9$ and $4 \leq N_{\text{jets}} \leq 7$ in the single-lepton and dilepton channels, respectively. Overflow events are included in the last bin of each distribution.

Post-fit comparisons between data and simulation for all regions are depicted in Fig. 3. The fitted observable distributions of the SRs are shown in Figs. 4 and 5. Good agreement between data and simulation is observed in all regions and observables with varying relative contributions of the $t\bar{t}$ + jets categories. The goodness of fit was evaluated using a *saturated model* [96] and the compatibility with data was found to be 98%.

The $t\bar{t}+\geq 2c$ and $t\bar{t}+1c$ normalization factors obtained from this fit are used to extract the observed fiducial cross-sections by scaling them with the predicted cross-sections for the fiducial phase space introduced in Section 3. Theoretical uncertainties in the predicted cross-sections owing to the μ_{R} and μ_{F} scale choice and the used PDF set are not propagated to the extracted fiducial cross-section values. The fiducial cross-sections for $t\bar{t}+\geq 2c$ and $t\bar{t}+1c$ processes are determined to be

$$\sigma^{\text{fid}}(t\bar{t}+\geq 2c) = 1.28\,^{+0.16}_{-0.10}\,(\text{stat})\,^{+0.21}_{-0.22}\,(\text{syst})\ \text{pb} = 1.28\,^{+0.27}_{-0.24}\ \text{pb}, \tag{2}$$

$$\sigma^{\text{fid}}(t\bar{t}+1c) = 6.4\,^{+0.5}_{-0.4}\,(\text{stat}) \pm 0.8\,(\text{syst})\ \text{pb} = 6.4\,^{+1.0}_{-0.9}\ \text{pb}. \tag{3}$$

The breakdown into statistical and systematic uncertainties is estimated from the covariance matrix of the profile likelihood fit, following Ref. [97]. The precision of the measured $t\bar{t}+\geq 2c$ and $t\bar{t}+1c$ cross-sections is limited by uncertainties in the modeling of $t\bar{t}+\geq 1c$, $t\bar{t}+\geq 1b$, and $t\bar{t}+$ light, in particular in the NLO matching and the PS, by uncertainties in the b/c-tagger calibration, as well as by data statistics. Table 2 provides a detailed breakdown of the uncertainties that affect the $t\bar{t}+\geq 2c$ and $t\bar{t}+1c$ cross-sections in the fiducial phase space. The uncertainty in the $t\bar{t}+\geq 1b$ and $t\bar{t}+$ light normalization factors on the $t\bar{t}+\geq 2c$ and $t\bar{t}+1c$ cross-sections is included in the data statistics entry. The fit constrains several nuisance parameters that strongly impact the $t\bar{t}+\geq 2c$ and $t\bar{t}+1c$ cross-sections, with none falling below 50% of their prior values. Noteworthy constraints are placed on the $t\bar{t}+\geq 1c$ FSR and $t\bar{t}+1c$ PS nuisance parameters, which arise primarily from discrepancies between the predicted rates of $t\bar{t}+\geq 2c$ and $t\bar{t}+1c$ events in the signal regions. No significant pulls of the nuisance parameters are observed in the fit. The measured $t\bar{t}+\geq 1b$ normalization factor is compatible with those obtained in a dedicated ATLAS $t\bar{t}+b\bar{b}$ measurement performed in a fiducial phase space targeting $e+\mu$ final states [17], reaching a similar level of relative precision.

Table 2
Breakdown of the fiducial $t\bar{t}+\geq 2c$ and $t\bar{t}+1c$ cross-section uncertainties. Systematic uncertainties are grouped into signal and background modeling, instrumental, and MC statistics categories. The table lists the fractional uncertainty in the measured cross-sections in percent and is estimated from the covariance matrix of the profile likelihood fit, following Ref. [97]. Individual groups of uncertainties can be added in quadrature to obtain the total uncertainty. JES and JER denote the jet energy scale and resolution uncertainties, respectively. The fractional uncertainties in the fitted $t\bar{t}+\geq 1b$ and $t\bar{t}+$ light normalization factors are included in the data statistics category. For presentation purposes, all uncertainties are symmetrized.

Uncertainty group	Fractional uncertainty [%] on	
	$\sigma^{\text{fid}}(t\bar{t}+\geq 2c)$	$\sigma^{\text{fid}}(t\bar{t}+1c)$
$t\bar{t}+\geq 1c$ modeling	9	8
Background modeling:		
$t\bar{t}+\geq 1b$	4	4
$t\bar{t}+$ light	6	4
Others	2.5	1.7
Instrumental:		
b-tagging	2.2	1.8
c-tagging	9	4
light mis-tagging	2.2	3.4
JES/JER	6	3.5
Others	1.3	0.9
MC statistics	3.1	2.5
Total systematic uncertainty	17	12
Data statistical uncertainty	11	7
Total	20	14

The measured values for the four processes and the overall $t\bar{t}$ + jets production are depicted in Fig. 6 and listed in Table 3, along with several NLO+PS predictions from different MC simulations. The predictions for $t\bar{t}+\geq 2c$ and $t\bar{t}+1c$ are largely consistent with the measurements, but underpredict the observed cross-sections by 0.5 to 2.0 standard deviations. Considering variations of the μ_{R} and μ_{F} scales and uncertainties in the PDF choice of the predictions, the POWHEG+PYTHIA8 setups agree with the measured $t\bar{t}+\geq 2c$ ($t\bar{t}+1c$) values within 0.5 to 0.8 (0.9 to 1.1) standard deviations of measurement and prediction uncertainties. In contrast, POWHEG+HERWIG7 and MADGRAPH5_AMC@NLO+HERWIG7

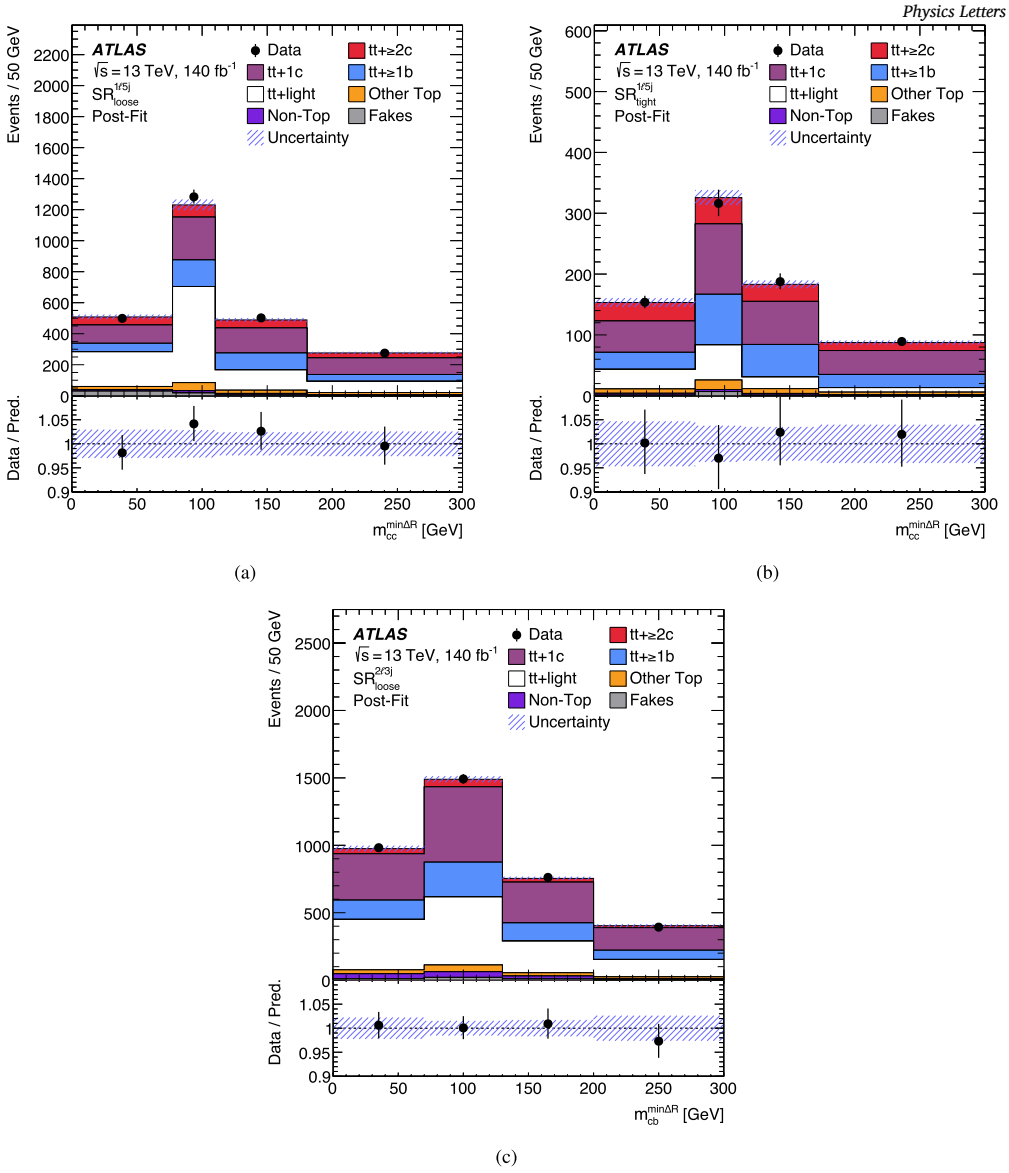

Fig. 4. Post-fit agreement between data and MC prediction for the observables used in the 5-jet-exclusive and 3-jet-exclusive signal regions (SRs): (a) $\mathrm{SR}^{1\ell 5\mathrm{j}}_{\mathrm{loose}}$ and (b) $\mathrm{SR}^{1\ell 5\mathrm{j}}_{\mathrm{tight}}$, both using the invariant mass of the two geometrically closest c-tagged jets, $m_{cc}^{\mathrm{min}\Delta R}$, for the latter only considering c-tagged jets passing $c@11\%$; (c) $\mathrm{SR}^{2\ell 3\mathrm{j}}_{\mathrm{loose}}$ using the invariant mass of the selected c-tagged jet and the geometrically closest b-tagged jet, $m_{cb}^{\mathrm{min}\Delta R}$. The hatched uncertainty bands include all uncertainties and their correlations. The last bins contain overflow events. *Other Top* includes single-top-quark production and associated production of $t\bar{t}$ and single top quarks with bosons. *Non-Top* includes W + jets, Z + jets, and diboson processes.

fall short by 25% to 40%, aligning with the measured values at 1.2 to 2.0 standard deviations. For $t\bar{t}+\geq 1b$, $t\bar{t}+$light, and $t\bar{t}$ + jets, most NLO+PS predictions agree with the measured cross-sections within measurement uncertainties.

To test the compatibility of the two channels, an additional fit was performed where the $t\bar{t}+\geq 2c$ and $t\bar{t}+1c$ normalization factors were parameterized independently in the single-lepton and dilepton regions. The single-lepton channel measures $\sigma^{\mathrm{fid}}(t\bar{t}+\geq 2c) = (1.5 \pm 0.4)$ pb and $\sigma^{\mathrm{fid}}(t\bar{t}+1c) = (6.4 \pm 1.1)$ pb, and the dilepton channel $\sigma^{\mathrm{fid}}(t\bar{t}+\geq 2c) = (1.18 \pm 0.25)$ pb and $\sigma^{\mathrm{fid}}(t\bar{t}+1c) = (6.4 \pm 1.0)$ pb. The results in both channels are consistent with the nominal results within their uncertainties. The compatibility of this fit with the nominal setup was evaluated by performing a χ^2 test on the log-likelihood difference, yielding a compatibility of 58%. In a second test, the $t\bar{t}+\geq 2c$ and $t\bar{t}+1c$ normalization factors were parameterized through one joint parameter of interest, and the NLO matching and PS uncertainties of the two processes were treated as correlated. The resulting cross-section of $\sigma^{\mathrm{fid}}(t\bar{t}+\geq 1c) = (8.2 \pm 0.9)$ pb is consistent with the sum of the $t\bar{t}+\geq 2c$ and $t\bar{t}+1c$ cross-sections in the nominal setup within uncertainties, but shows increased relative precision.

A measurement of the cross-sections in the more inclusive phase space yields $\sigma^{\mathrm{inc}}(t\bar{t}+\geq 2c) = (5.4 \pm 1.1)$ pb and $\sigma^{\mathrm{inc}}(t\bar{t}+1c) = (38 \pm 6)$ pb, showing moderately increased relative uncertainties compared with the fiducial cross-sections.

The normalization factors $\mu(t\bar{t}+\geq 1b)$, $\mu(t\bar{t}+\geq 2c)$, $\mu(t\bar{t}+1c)$, and $\mu(t\bar{t}+\text{light})$ are used to determine the cross-section ratios of these processes to total $t\bar{t}$ + jets production. These measurements benefit from the cancelation of several systematic uncertainties related to detector instrumentation and calibrations, potentially reducing the overall systematic uncertainties. In the more inclusive phase space, the measurement yields ratios of $R^{\mathrm{inc}}_{t\bar{t}+\geq 2c} = (1.23 \pm 0.25)\%$ and $R^{\mathrm{inc}}_{t\bar{t}+1c} = (8.8 \pm 1.3)\%$. In the fiducial phase space, these ratios increase to $R^{\mathrm{fid}}_{t\bar{t}+\geq 2c} = (2.7 \pm 0.5)\%$ and $R^{\mathrm{fid}}_{t\bar{t}+1c} = (13.7 \pm 1.8)\%$. In both phase spaces, the POWHEG+PYTHIA8 simulations underpredict the ratios, but agree with the measured $R^{\mathrm{inc}}_{t\bar{t}+\geq 2c}$ and $R^{\mathrm{inc}}_{t\bar{t}+1c}$ values within 0.9 and 1.1 standard deviations, and in the fidu-

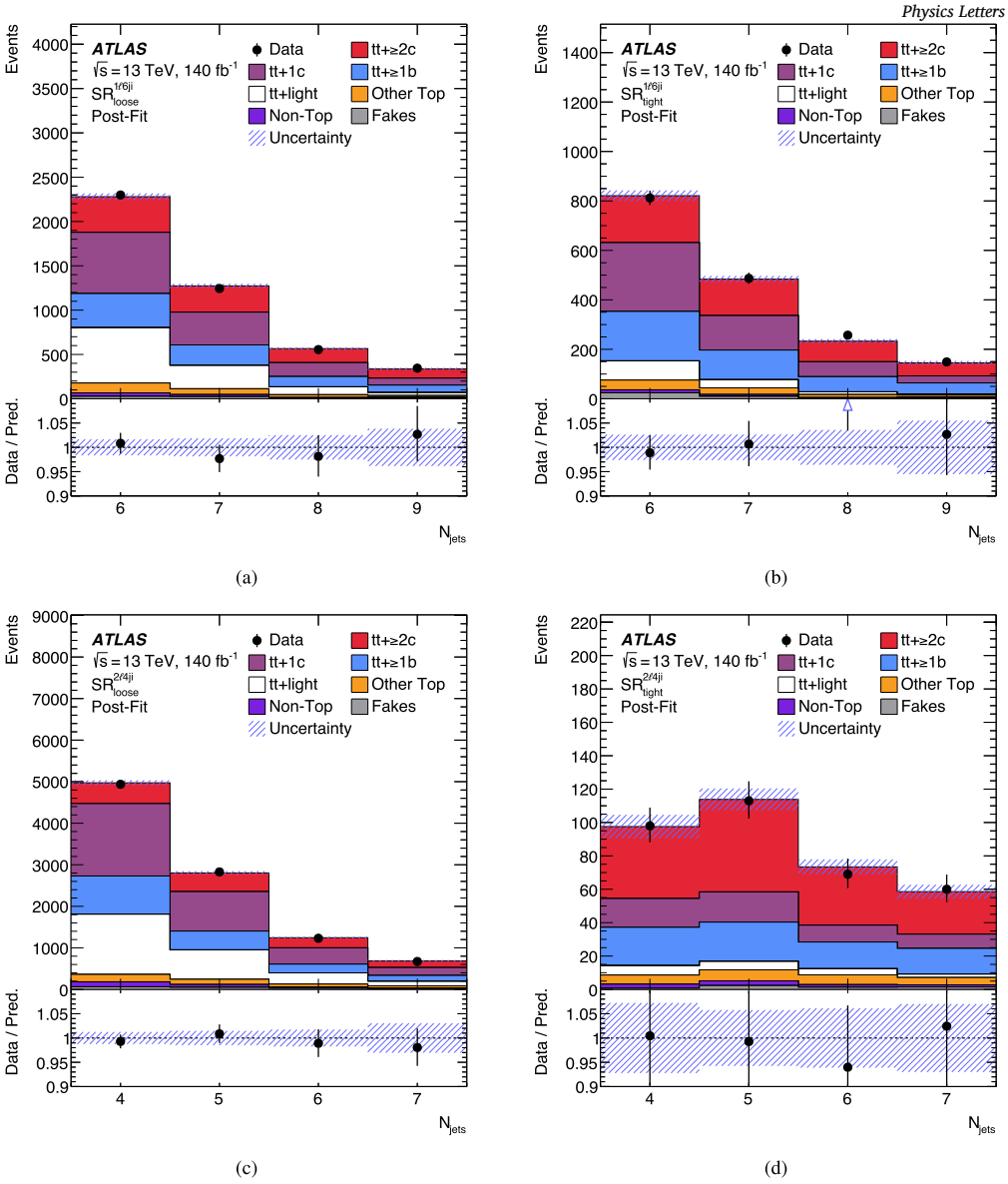

Fig. 5. Post-fit agreement between data and MC prediction for the observables used in the (a) loose 6-jet-inclusive, (b) tight 6-jet-inclusive, (c) loose 4-jet-inclusive, and (d) tight 4-jet-inclusive signal regions (SRs). All regions use the jet multiplicity, N_{jets}, as a fit observable. The hatched uncertainty bands include all uncertainties and their correlations. The last bins contain overflow events. *Other Top* includes single-top-quark production and associated production of $t\bar{t}$ and single top quarks with bosons. *Non-Top* includes W + jets, Z + jets, and diboson processes.

Table 3
Measured fiducial cross-section values in comparison with various NLO+PS predictions. The uncertainties in the predictions include independent and simultaneous variations of the μ_{R} and μ_{F} scales and uncertainties in the choice of the PDF set, but no uncertainties in the parton shower or hadronization. The uncertainties in the measured values include all statistical and systematic uncertainties. For presentation purposes, the quoted measurement and prediction uncertainties are symmetrized.

	$t\bar{t}+\geq 2c$ [pb]	$t\bar{t}+1c$ [pb]	$t\bar{t}+\geq 1b$ [pb]	$t\bar{t}+$ light [pb]	$t\bar{t}+$ jets [pb]
$t\bar{t}$ POWHEG+PYTHIA 8	1.04 ± 0.18	5.1 ± 0.8	3.2 ± 0.5	40 ± 6	50 ± 7
$t\bar{t}$ POWHEG+PYTHIA 8, $h_{\text{damp}} = 3\,m_t$	1.12 ± 0.16	5.4 ± 0.7	3.3 ± 0.5	41 ± 5	51 ± 7
$t\bar{t}$ POWHEG+PYTHIA 8, $p_{\text{T}}^{\text{hard}} = 1$	1.05 ± 0.18	5.2 ± 0.8	3.1 ± 0.5	40 ± 6	50 ± 7
$t\bar{t}$ POWHEG+HERWIG 7	0.94 ± 0.16	4.2 ± 0.7	3.3 ± 0.5	43 ± 6	52 ± 8
$t\bar{t}$ MADGRAPH5_AMC@NLO+HERWIG 7	0.74 ± 0.19	4.0 ± 0.8	2.7 ± 0.6	46 ± 8	53 ± 10
$t\bar{t}+b\bar{b}$ POWHEG+PYTHIA 8	—	—	3.2 ± 1.6	—	—
$t\bar{t}+b\bar{b}$ POWHEG+PYTHIA 8, $p_{\text{T}}^{\text{hard}} = 1$	—	—	2.8 ± 1.3	—	—
$t\bar{t}+b\bar{b}$ POWHEG+PYTHIA 8, $h_{\text{bzd}} = 2$	—	—	3.1 ± 1.5	—	—
$t\bar{t}+b\bar{b}$ POWHEG+PYTHIA 8, dipole recoil	—	—	3.0 ± 1.4	—	—
$t\bar{t}+b\bar{b}$ POWHEG+HERWIG 7	—	—	3.1 ± 1.6	—	—
$t\bar{t}+b\bar{b}$ SHERPA 2.2.10	—	—	3.5 ± 1.0	—	—
Data	1.28 ± 0.25	6.4 ± 0.9	3.46 ± 0.24	36.0 ± 1.8	47.1 ± 2.3

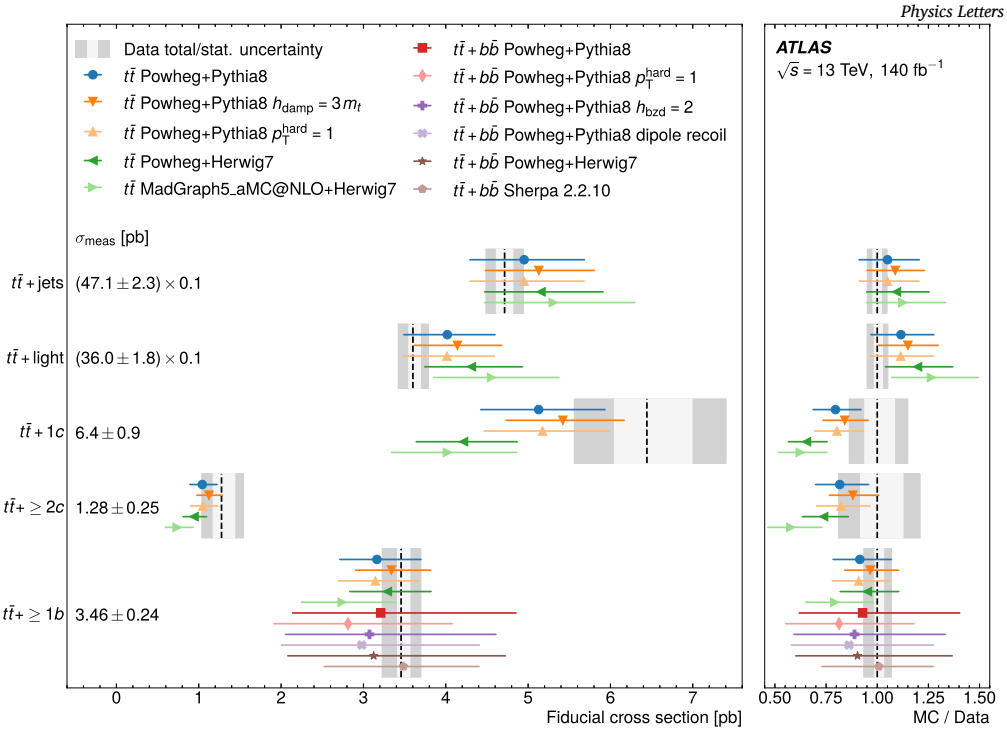

Fig. 6. Measured fiducial cross-section values in comparison with various NLO+PS predictions from inclusive $t\bar{t}$ and $t\bar{t}+b\bar{b}$ simulations. The boxes in the background represent the statistical and total uncertainties of the values extracted from data. The uncertainty bars of the predictions include independent and simultaneous variations of the μ_R and μ_F scales and uncertainties in the choice of the PDF set, but no uncertainties in the parton shower or hadronization. The measured and computed values for $t\bar{t}$ + jets and $t\bar{t}$ + light are scaled by a factor of 0.1 to facilitate visualization. For presentation purposes, the quoted measurement uncertainties are symmetrized.

Table 4
Measured and predicted values for the $t\bar{t}+\geq 1b$, $t\bar{t}+\geq 2c$, and $t\bar{t}+1c$ cross-sections and for the cross-section ratios of these processes to total $t\bar{t}$ + jets production. The quoted uncertainties in the measurements include statistical and systematic uncertainties. The predictions are taken from the nominal setup using inclusive $t\bar{t}$ POWHEG+PYTHIA8 predictions for the $t\bar{t}+\geq 2c$, $t\bar{t}+1c$, and $t\bar{t}$ + light processes, and $t\bar{t}+b\bar{b}$ POWHEG+PYTHIA8 predictions for the $t\bar{t}+\geq 1b$ process. The first use the five-flavor scheme (5FS), the latter the four-flavor scheme (4FS), where the b-quarks are treated as massive particles and are included in the matrix element calculation. The uncertainties in the predictions include independent and simultaneous variations of the μ_R and μ_F scales and uncertainties in the choice of the PDF set.

	Measured	$t\bar{t}$ or $t\bar{t}+b\bar{b}$ POWHEG+PYTHIA8
$\sigma^{fid}(t\bar{t}+\geq 1b)$ [pb]	3.46 ± 0.24	3.2 ± 1.6
$\sigma^{fid}(t\bar{t}+\geq 2c)$ [pb]	1.28 ± 0.25	1.04 ± 0.18
$\sigma^{fid}(t\bar{t}+1c)$ [pb]	6.4 ± 0.9	5.1 ± 0.8
$\sigma^{inc}(t\bar{t}+\geq 1b)$ [pb]	13.0 ± 0.9	12 ± 4
$\sigma^{inc}(t\bar{t}+\geq 2c)$ [pb]	5.4 ± 1.1	4.4 ± 0.7
$\sigma^{inc}(t\bar{t}+1c)$ [pb]	38 ± 6	31 ± 4
$R^{fid}_{t\bar{t}+\geq 1b}$ [%]	7.2 ± 0.4	6.5 ± 3.3
$R^{fid}_{t\bar{t}+\geq 2c}$ [%]	2.7 ± 0.5	2.1 ± 0.4
$R^{fid}_{t\bar{t}+1c}$ [%]	13.7 ± 1.8	10.3 ± 1.6
$R^{inc}_{t\bar{t}+\geq 1b}$ [%]	3.14 ± 0.23	2.6 ± 0.8
$R^{inc}_{t\bar{t}+\geq 2c}$ [%]	1.23 ± 0.25	0.97 ± 0.16
$R^{inc}_{t\bar{t}+1c}$ [%]	8.8 ± 1.3	6.9 ± 1.0

cial phase space within 1.0 and 1.4 standard deviations, respectively. A summary of all results is given in Table 4.

7. Conclusion

The production of $t\bar{t}$ pairs in association with heavy-flavor jets, $t\bar{t}+b\bar{b}$ and $t\bar{t}+c\bar{c}$, is a background in many measurements of rare SM processes and searches for new physics, yet a challenging process to model precisely. This Letter presents a measurement of the production of $t\bar{t}$ with additional jets initiated by charm quarks with the ATLAS experiment at the LHC. The analysis exploits the full ATLAS Run 2 pp collision data sample at a center-of-mass energy of 13 TeV, corresponding to an integrated luminosity of 140 fb^{-1}, and considers events with one or two charged leptons in the final state. A custom flavor tagging algorithm, termed the b/c-tagger, tailored to simultaneously tag c-jets and b-jets, is employed to define analysis regions sensitive to both $t\bar{t}+\geq 2c$ and $t\bar{t}+1c$ production which are determined separately for the first time. Using a profile likelihood fit approach, the cross-sections for $t\bar{t}$ production with two or more additional c-jets and one additional c-jet are found to be $\sigma^{fid}(t\bar{t}+\geq 2c) = 1.28^{+0.27}_{-0.24}$ pb and $\sigma^{fid}(t\bar{t}+1c) = 6.4^{+1.0}_{-0.9}$ pb in a fiducial volume that mimics the acceptance of the ATLAS detector. NLO+PS predictions for $t\bar{t}+\geq 2c$ and $t\bar{t}+1c$ are largely consistent with the measurements, though all underpredict the observed values. POWHEG+PYTHIA8 setups agree with the measured values within 0.5 to 1.1 standard deviations, while POWHEG+HERWIG7 and MADGRAPH5_AMC@NLO+HERWIG7 predict cross-sections up to 40% lower than the measurements, with agreement observed at the level of up to 2.0 standard deviations. The precision of the measured cross-sections is limited by uncertainties in the modeling of $t\bar{t}+\geq 1c$, $t\bar{t}+\geq 1b$, and $t\bar{t}$ + light, and in the b/c-tagger calibration, as well as by data statistics. The cross-section ratios of $t\bar{t}+\geq 2c$ and $t\bar{t}+1c$ to total $t\bar{t}$ + jets production are found to be $R^{inc}_{t\bar{t}+\geq 2c} = (1.23 \pm 0.25)\%$ and $R^{inc}_{t\bar{t}+1c} = (8.8 \pm 1.3)\%$ in a phase-space volume without requirements on the $t\bar{t}$ decay products and the jet multiplicity. These results provide crucial inputs for improving the modeling of $t\bar{t}$ production with additional c-jets, which would benefit from 3FS $t\bar{t}+c\bar{c}$ simulations that incorporate the gluon splitting to a $c\bar{c}$ pair into the matrix element calculation. Understanding $t\bar{t}+\geq 1c$ production is essential for precision measurements of even rarer SM processes and for searches for physics beyond the SM, where $t\bar{t}+\geq 1c$ is an important background.

Declaration of competing interest

The authors declare that they have no known competing financial interests or personal relationships that could have appeared to influence the work reported in this paper.

Acknowledgements

We thank CERN for the very successful operation of the LHC and its injectors, as well as the support staff at CERN and at our institutions worldwide without whom ATLAS could not be operated efficiently.

The crucial computing support from all WLCG partners is acknowledged gratefully, in particular from CERN, the ATLAS Tier-1 facilities at TRIUMF/SFU (Canada), NDGF (Denmark, Norway, Sweden), CC-IN2P3 (France), KIT/GridKA (Germany), INFN-CNAF (Italy), NL-T1 (Netherlands), PIC (Spain), RAL (UK) and BNL (USA), the Tier-2 facilities worldwide and large non-WLCG resource providers. Major contributors of computing resources are listed in Ref. [98].

We gratefully acknowledge the support of ANPCyT, Argentina; YerPhI, Armenia; ARC, Australia; BMWFW and FWF, Austria; ANAS, Azerbaijan; CNPq and FAPESP, Brazil; NSERC, NRC and CFI, Canada; CERN; ANID, Chile; CAS, MOST and NSFC, China; Minciencias, Colombia; MEYS CR, Czech Republic; DNRF and DNSRC, Denmark; IN2P3-CNRS and CEA-DRF/IRFU, France; SRNSFG, Georgia; BMBF, HGF and MPG, Germany; GSRI, Greece; RGC and Hong Kong SAR, China; ISF and Benoziyo Center, Israel; INFN, Italy; MEXT and JSPS, Japan; CNRST, Morocco; NWO, Netherlands; RCN, Norway; MNiSW, Poland; FCT, Portugal; MNE/IFA, Romania; MSTDI, Serbia; MSSR, Slovakia; ARIS and MVZI, Slovenia; DSI/NRF, South Africa; MICIU/AEI, Spain; SRC and Wallenberg Foundation, Sweden; SERI, SNSF and Cantons of Bern and Geneva, Switzerland; NSTC, Taipei; TENMAK, Türkiye; STFC/UKRI, United Kingdom; DOE and NSF, United States of America.

Individual groups and members have received support from BCKDF, Canarie, CRC and DRAC, Canada; CERN-CZ, FORTE and PRIMUS, Czech Republic; COST, ERC, ERDF, Horizon 2020, ICSC-NextGenerationEU and Marie Skłodowska-Curie Actions, European Union; Investissements d'Avenir Labex, Investissements d'Avenir Idex and ANR, France; DFG and AvH Foundation, Germany; Herakleitos, Thales and Aristeia programmes co-financed by EU-ESF and the Greek NSRF, Greece; BSF-NSF and MINERVA, Israel; NCN and NAWA, Poland; La Caixa Banking Foundation, CERCA Programme Generalitat de Catalunya and PROMETEO and GenT Programmes Generalitat Valenciana, Spain; Göran Gustafssons Stiftelse, Sweden; The Royal Society and Leverhulme Trust, United Kingdom.

In addition, individual members wish to acknowledge support from Armenia: Yerevan Physics Institute (FAPERJ); CERN: European Organization for Nuclear Research (CERN PJAS); Chile: Agencia Nacional de Investigación y Desarrollo (FONDECYT 1230812, FONDECYT 1230987, FONDECYT 1240864); China: Chinese Ministry of Science and Technology (MOST-2023YFA1605700), National Natural Science Foundation of China (NSFC - 12175119, NSFC 12275265, NSFC-12075060); Czech Republic: Czech Science Foundation (GACR - 24-11373S), Ministry of Education Youth and Sports (FORTE CZ.02.01.01/00/22_008/0004632), PRIMUS Research Programme (PRIMUS/21/SCI/017); EU: H2020 European Research Council (ERC - 101002463); European Union: European Research Council (ERC - 948254, ERC 101089007), European Union, Future Artificial Intelligence Research (FAIR-NextGenerationEU PE00000013), Italian Center for High Performance Computing, Big Data and Quantum Computing (ICSC, NextGenerationEU); France: Agence Nationale de la Recherche (ANR-20-CE31-0013, ANR-21-CE31-0013, ANR-21-CE31-0022, ANR-22-EDIR-0002); Germany: Baden-Württemberg Stiftung (BW Stiftung-Postdoc Eliteprogramme), Deutsche Forschungsgemeinschaft (DFG - 469666862, DFG - CR 312/5-2); Italy: Istituto Nazionale di Fisica Nucleare (ICSC, NextGenerationEU), Ministero dell'Università e della Ricerca (PRIN - 20223N7F8K - PNRR M4.C2.1.1); Japan: Japan Society for the Promotion of Science (JSPS KAKENHI JP22H01227, JSPS KAKENHI JP22H04944, JSPS KAKENHI JP22KK0227, JSPS KAKENHI JP23KK0245); Netherlands: Netherlands Organisation for Scientific Research (NWO Veni 2020 - VI.Veni.202.179); Norway: Research Council of Norway (RCN-314472); Poland: Ministry of Science and Higher Education (IDUB AGH, POB8, D4 no 9722), Polish National Agency for Academic Exchange (PPN/PPO/2020/1/00002/U/00001), Polish National Science Centre (NCN 2021/42/E/ST2/00350, NCN OPUS 2023/51/B/ST2/02507, NCN OPUS nr 2022/47/B/ST2/03059, NCN UMO-2019/34/E/ST2/00393, NCN & H2020 MSCA 945339, UMO-2020/37/B/ST2/01043, UMO-2021/40/C/ST2/00187, UMO-2022/47/O/ST2/00148, UMO-2023/49/B/ST2/04085, UMO-2023/51/B/ST2/00920); Slovenia: Slovenian Research Agency (ARIS grant J1-3010); Spain: Generalitat Valenciana (Artemisa, FEDER, IDIFEDER/2018/048), Ministry of Science and Innovation (MCIN & NextGenEU PCI2022-135018-2, MICIN & FEDER PID2021-125273NB, RYC2019-028510-I, RYC2020-030254-I, RYC2021-031273-I, RYC2022-038164-I); Sweden: Carl Trygger Foundation (Carl Trygger Foundation CTS 22:2312), Swedish Research Council (Swedish Research Council 2023-04654, VR 2018-00482, VR 2022-03845, VR 2022-04683, VR 2023-03403, VR grant 2021-03651), Knut and Alice Wallenberg Foundation (KAW 2018.0458, KAW 2019.0447, KAW 2022.0358); Switzerland: Swiss National Science Foundation (SNSF - PCEFP2_194658); United Kingdom: Leverhulme Trust (Leverhulme Trust RPG-2020-004), Royal Society (NIF-R1-231091); United States of America: U.S. Department of Energy (ECA DE-AC02-76SF00515), Neubauer Family Foundation.

Data availability

No data was used for the research described in the article.

References

[1] ATLAS Collaboration, The ATLAS experiment at the CERN Large Hadron Collider, J. Instrum. 3 (2008) S08003.

[2] CMS Collaboration, The CMS experiment at the CERN LHC, J. Instrum. 3 (2008) S08004.

[3] CMS Collaboration, Search for $t\bar{t}H$ production in the all-jet final state in proton–proton collisions at $\sqrt{s} = 13$ TeV, J. High Energy Phys. 06 (2018) 101, arXiv:1803.06986 [hep-ex].

[4] CMS Collaboration, Search for $t\bar{t}H$ production in the $H \to b\bar{b}$ decay channel with leptonic $t\bar{t}$ decays in proton–proton collisions at $\sqrt{s} = 13$ TeV, J. High Energy Phys. 03 (2019) 026, arXiv:1804.03682 [hep-ex].

[5] ATLAS Collaboration, Measurement of the associated production of a top-antitop-quark pair and a Higgs boson decaying into a $b\bar{b}$ pair in pp collisions at $\sqrt{s} = 13$ TeV using the ATLAS detector at the LHC, arXiv:2407.10904 [hep-ex], 2024.

[6] ATLAS Collaboration, Measurement of the $t\bar{t}t\bar{t}$ production cross section in pp collisions at $\sqrt{s} = 13$ TeV with the ATLAS detector, J. High Energy Phys. 11 (2021) 118, arXiv:2106.11683 [hep-ex].

[7] CMS Collaboration, Evidence for four-top quark production in proton–proton collisions at $\sqrt{s} = 13$ TeV, Phys. Lett. B 844 (2023) 138076, arXiv:2303.03864 [hep-ex].

[8] A. Bredenstein, A. Denner, S. Dittmaier, S. Pozzorini, NLO QCD corrections to $t\bar{t}b\bar{b}$ production at the LHC: 1. Quark-antiquark annihilation, J. High Energy Phys. 08 (2008) 108, arXiv:0807.1248 [hep-ph].

[9] A. Bredenstein, A. Denner, S. Dittmaier, S. Pozzorini, Next-to-leading order QCD corrections to $pp \to t\bar{t}b\bar{b} + X$ at the LHC, Phys. Rev. Lett. 103 (2009) 012002, arXiv:0905.0110 [hep-ph].

[10] F. Cascioli, P. Maierhöfer, N. Moretti, S. Pozzorini, F. Siegert, NLO matching for $t\bar{t}b\bar{b}$ production with massive b-quarks, Phys. Lett. B 734 (2014) 210, arXiv:1309.5912 [hep-ph].

[11] T. Ježo, J.M. Lindert, N. Moretti, S. Pozzorini, New NLOPS predictions for $t\bar{t} + b$-jet production at the LHC, Eur. Phys. J. C 78 (2018) 502, arXiv:1802.00426 [hep-ph].

[12] F. Buccioni, S. Kallweit, S. Pozzorini, M.F. Zoller, NLO QCD predictions for $t\bar{t}b\bar{b}$ production in association with a light jet at the LHC, J. High Energy Phys. 12 (2019) 015, arXiv:1907.13624 [hep-ph].

[13] G. Bevilacqua, et al., $t\bar{t}b\bar{b}$ at the LHC: on the size of off-shell effects and prompt b-jet identification, Phys. Rev. D 107 (2023) 014028, arXiv:2202.11186 [hep-ph].

[14] ATLAS Collaboration, Measurements of inclusive and differential fiducial cross-sections of $t\bar{t}$ production with additional heavy-flavour jets in proton–proton collisions at $\sqrt{s} = 13$ TeV with the ATLAS detector, J. High Energy Phys. 04 (2019) 046, arXiv:1811.12113 [hep-ex].

[15] CMS Collaboration, Measurement of the $t\bar{t}b\bar{b}$ production cross section in the all-jet final state in pp collisions at $\sqrt{s} = 13$ TeV, Phys. Lett. B 803 (2020) 135285, arXiv:1909.05306 [hep-ex].
[16] CMS Collaboration, Inclusive and differential cross section measurements of $t\bar{t}b\bar{b}$ production in the lepton+jets channel at $\sqrt{s} = 13$ TeV, J. High Energy Phys. 05 (2024) 042, arXiv:2309.14442 [hep-ex].
[17] ATLAS Collaboration, Measurement of $t\bar{t}$ production in association with additional b-jets in the $e\mu$ final state in proton–proton collisions at $\sqrt{s} = 13$ TeV with the ATLAS detector, arXiv:2407.13473 [hep-ex], 2024.
[18] CMS Collaboration, First measurement of the cross section for top quark pair production with additional charm jets using dileptonic final states in pp collisions at $\sqrt{s} = 13$ TeV, Phys. Lett. B 820 (2021) 136565, arXiv:2012.09225 [hep-ex].
[19] G. Avoni, et al., The new LUCID-2 detector for luminosity measurement and monitoring in ATLAS, J. Instrum. 13 (2018) P07017.
[20] ATLAS Collaboration, Performance of the ATLAS trigger system in 2015, Eur. Phys. J. C 77 (2017) 317, arXiv:1611.09661 [hep-ex].
[21] ATLAS Collaboration, Software and computing for Run 3 of the ATLAS experiment at the LHC, arXiv:2404.06335 [hep-ex], 2024.
[22] ATLAS Collaboration, The ATLAS simulation infrastructure, Eur. Phys. J. C 70 (2010) 823, arXiv:1005.4568 [physics.ins-det].
[23] S. Agostinelli, et al., GEANT4 – a simulation toolkit, Nucl. Instrum. Methods A 506 (2003) 250.
[24] T. Sjöstrand, S. Mrenna, P. Skands, A brief introduction to PYTHIA 8.1, Comput. Phys. Commun. 178 (2008) 852, arXiv:0710.3820 [hep-ph].
[25] ATLAS Collaboration, The Pythia 8 A3 tune description of ATLAS minimum bias and inelastic measurements incorporating the Donnachie–Landshoff diffractive model, ATL-PHYS-PUB-2016-017, https://cds.cern.ch/record/2206965, 2016.
[26] T. Sjöstrand, et al., An introduction to PYTHIA 8.2, Comput. Phys. Commun. 191 (2015) 159, arXiv:1410.3012 [hep-ph].
[27] M. Bähr, et al., Herwig++ physics and manual, Eur. Phys. J. C 58 (2008) 639, arXiv:0803.0883 [hep-ph].
[28] J. Bellm, et al., Herwig 7.0/Herwig++ 3.0 release note, Eur. Phys. J. C 76 (2016) 196, arXiv:1512.01178 [hep-ph].
[29] J. Bellm, et al., Herwig 7.1 release note, arXiv:1705.06919 [hep-ph], 2017.
[30] D.J. Lange, The EvtGen particle decay simulation package, Nucl. Instrum. Methods A 462 (2001) 152.
[31] ATLAS Collaboration, ATLAS Pythia 8 tunes to 7 *TeV* data, ATL-PHYS-PUB-2014-021, https://cds.cern.ch/record/1966419, 2014.
[32] NNPDF Collaboration, R.D. Ball, et al., Parton distributions with LHC data, Nucl. Phys. B 867 (2013) 244, arXiv:1207.1303 [hep-ph].
[33] L.A. Harland-Lang, A.D. Martin, P. Motylinski, R.S. Thorne, Parton distributions in the LHC era: MMHT 2014 PDFs, Eur. Phys. J. C 75 (2015) 204, arXiv:1412.3989 [hep-ph].
[34] S. Frixione, G. Ridolfi, P. Nason, A positive-weight next-to-leading-order Monte Carlo for heavy flavour hadroproduction, J. High Energy Phys. 09 (2007) 126, arXiv:0707.3088 [hep-ph].
[35] P. Nason, A new method for combining NLO QCD with shower Monte Carlo algorithms, J. High Energy Phys. 11 (2004) 040, arXiv:hep-ph/0409146.
[36] S. Frixione, P. Nason, C. Oleari, Matching NLO QCD computations with parton shower simulations: the POWHEG method, J. High Energy Phys. 11 (2007) 070, arXiv:0709.2092 [hep-ph].
[37] S. Alioli, P. Nason, C. Oleari, E. Re, A general framework for implementing NLO calculations in shower Monte Carlo programs: the POWHEG BOX, J. High Energy Phys. 06 (2010) 043, arXiv:1002.2581 [hep-ph].
[38] NNPDF Collaboration, R.D. Ball, et al., Parton distributions for the LHC run II, J. High Energy Phys. 04 (2015) 040, arXiv:1410.8849 [hep-ph].
[39] ATLAS Collaboration, Studies on top-quark Monte Carlo modelling for Top2016, ATL-PHYS-PUB-2016-020, https://cds.cern.ch/record/2216168, 2016.
[40] S. Höche, S. Mrenna, S. Payne, C.T. Preuss, P. Skands, A study of QCD radiation in VBF Higgs production with Vincia and Pythia, SciPost Phys. 12 (2022) 010, arXiv:2106.10987 [hep-ph].
[41] ATLAS Collaboration, Studies on the improvement of the matching uncertainty definition in top-quark processes simulated with Powheg+Pythia8, ATL-PHYS-PUB-2023-029, https://cds.cern.ch/record/2872787, 2013.
[42] J. Alwall, et al., The automated computation of tree-level and next-to-leading order differential cross sections, and their matching to parton shower simulations, J. High Energy Phys. 07 (2014) 079, arXiv:1405.0301 [hep-ph].
[43] S. Frixione, E. Laenen, P. Motylinski, B.R. Webber, Angular correlations of lepton pairs from vector boson and top quark decays in Monte Carlo simulations, J. High Energy Phys. 04 (2007) 081, arXiv:hep-ph/0702198.
[44] P. Artoisenet, R. Frederix, O. Mattelaer, R. Rietkerk, Automatic spin-entangled decays of heavy resonances in Monte Carlo simulations, J. High Energy Phys. 03 (2013) 015, arXiv:1212.3460 [hep-ph].
[45] ATLAS Collaboration, Studies on top-quark Monte Carlo modelling with Sherpa and MG5_aMC@NLO, ATL-PHYS-PUB-2017-007, https://cds.cern.ch/record/2261938, 2017.
[46] M. Czakon, A. Mitov, Top++: a program for the calculation of the top-pair cross-section at hadron colliders, Comput. Phys. Commun. 185 (2014) 2930, arXiv:1112.5675 [hep-ph].
[47] J. Butterworth, et al., PDF4LHC recommendations for LHC Run II, J. Phys. G 43 (2016) 023001, arXiv:1510.03865 [hep-ph].
[48] A.D. Martin, W.J. Stirling, R.S. Thorne, G. Watt, Uncertainties on α_S in global PDF analyses and implications for predicted hadronic cross sections, Eur. Phys. J. C 64 (2009) 653, arXiv:0905.3531 [hep-ph].
[49] J. Gao, et al., CT10 next-to-next-to-leading order global analysis of QCD, Phys. Rev. D 89 (2014) 033009, arXiv:1302.6246 [hep-ph].
[50] F. Cascioli, P. Maierhöfer, S. Pozzorini, Scattering amplitudes with open loops, Phys. Rev. Lett. 108 (2012) 111601, arXiv:1111.5206 [hep-ph].
[51] A. Denner, S. Dittmaier, L. Hofer, Collier: a fortran-based complex one-loop library in extended regularizations, Comput. Phys. Commun. 212 (2017) 220, arXiv:1604.06792 [hep-ph].
[52] F. Buccioni, et al., OpenLoops 2, Eur. Phys. J. C 79 (2019) 866, arXiv:1907.13071 [hep-ph].
[53] ATLAS Collaboration, Study of $ttbb$ and ttW background modelling for ttH analyses, ATL-PHYS-PUB-2022-026, https://cds.cern.ch/record/2810864, 2022.
[54] E. Bothmann, et al., Event generation with Sherpa 2.2, SciPost Phys. 7 (2019) 034, arXiv:1905.09127 [hep-ph].
[55] T. Gleisberg, S. Höche, Comix, a new matrix element generator, J. High Energy Phys. 12 (2008) 039, arXiv:0808.3674 [hep-ph].
[56] S. Schumann, F. Krauss, A parton shower algorithm based on Catani–Seymour dipole factorisation, J. High Energy Phys. 03 (2008) 038, arXiv:0709.1027 [hep-ph].
[57] S. Höche, F. Krauss, M. Schönherr, F. Siegert, A critical appraisal of NLO+PS matching methods, J. High Energy Phys. 09 (2012) 049, arXiv:1111.1220 [hep-ph].
[58] S. Höche, F. Krauss, M. Schönherr, F. Siegert, QCD matrix elements + parton showers. The NLO case, J. High Energy Phys. 04 (2013) 027, arXiv:1207.5030 [hep-ph].
[59] S. Catani, F. Krauss, B.R. Webber, R. Kuhn, QCD matrix elements + parton showers, J. High Energy Phys. 11 (2001) 063, arXiv:hep-ph/0109231.
[60] S. Höche, F. Krauss, S. Schumann, F. Siegert, QCD matrix elements and truncated showers, J. High Energy Phys. 05 (2009) 053, arXiv:0903.1219 [hep-ph].
[61] M. Cacciari, G.P. Salam, G. Soyez, The anti-k_t jet clustering algorithm, J. High Energy Phys. 04 (2008) 063, arXiv:0802.1189 [hep-ph].
[62] M. Cacciari, G.P. Salam, G. Soyez, FastJet user manual, Eur. Phys. J. C 72 (2012) 1896, arXiv:1111.6097 [hep-ph].
[63] M. Cacciari, G.P. Salam, Pileup subtraction using jet areas, Phys. Lett. B 659 (2008) 119, arXiv:0707.1378 [hep-ph].
[64] M. Cacciari, G.P. Salam, G. Soyez, The catchment area of jets, J. High Energy Phys. 04 (2008) 005, arXiv:0802.1188 [hep-ph].
[65] S. Frixione, E. Laenen, P. Motylinski, C. White, B.R. Webber, Single-top hadroproduction in association with a W boson, J. High Energy Phys. 07 (2008) 029, arXiv:0805.3067 [hep-ph].
[66] C. Anastasiou, L. Dixon, K. Melnikov, F. Petriello, High-precision QCD at hadron colliders: electroweak gauge boson rapidity distributions at next-to-next-to leading order, Phys. Rev. D 69 (2004) 094008, arXiv:hep-ph/0312266.
[67] ATLAS Collaboration, Vertex reconstruction performance of the ATLAS detector at $\sqrt{s} = 13$ TeV, ATL-PHYS-PUB-2015-026, https://cds.cern.ch/record/2037717, 2015.
[68] ATLAS Collaboration, Performance of electron and photon triggers in ATLAS during LHC Run 2, Eur. Phys. J. C 80 (2020) 47, arXiv:1909.00761 [hep-ex].
[69] ATLAS Collaboration, Performance of the ATLAS muon triggers in Run 2, J. Instrum. 15 (2020) P09015, arXiv:2004.13447 [physics.ins-det].
[70] ATLAS Collaboration, Jet reconstruction and performance using particle flow with the ATLAS Detector, Eur. Phys. J. C 77 (2017) 466, arXiv:1703.10485 [hep-ex].
[71] ATLAS Collaboration, Jet energy scale and resolution measured in proton–proton collisions at $\sqrt{s} = 13$ TeV with the ATLAS detector, Eur. Phys. J. C 81 (2021) 689, arXiv:2007.02645 [hep-ex].
[72] ATLAS Collaboration, Performance of pile-up mitigation techniques for jets in pp collisions at $\sqrt{s} = 8$ TeV using the ATLAS detector, Eur. Phys. J. C 76 (2016) 581, arXiv:1510.03823 [hep-ex].
[73] ATLAS Collaboration, Electron and photon performance measurements with the ATLAS detector using the 2015–2017 LHC proton–proton collision data, J. Instrum. 14 (2019) P12006, arXiv:1908.00005 [hep-ex].
[74] ATLAS Collaboration, Electron and photon efficiencies in LHC Run 2 with the ATLAS experiment, J. High Energy Phys. 05 (2024) 162, arXiv:2308.13362 [hep-ex].
[75] ATLAS Collaboration, Muon reconstruction and identification efficiency in ATLAS using the full Run 2 pp collision data set at $\sqrt{s} = 13$ TeV, Eur. Phys. J. C 81 (2021) 578, arXiv:2012.00578 [hep-ex].
[76] ATLAS Collaboration, Studies of the muon momentum calibration and performance of the ATLAS detector with pp collisions at $\sqrt{s} = 13$ TeV, Eur. Phys. J. C 83 (2023) 686, arXiv:2212.07338 [hep-ex].
[77] ATLAS Collaboration, ATLAS flavour-tagging algorithms for the LHC Run 2 pp collision dataset, Eur. Phys. J. C 83 (2023) 681, arXiv:2211.16345 [physics.data-an].
[78] J. Neyman, E.S. Pearson, On the problem of the most efficient tests of statistical hypotheses, Philos. Trans. R. Soc. A 231 (1933) 289.
[79] ATLAS Collaboration, ATLAS b-jet identification performance and efficiency measurement with $t\bar{t}$ events in pp collisions at $\sqrt{s} = 13$ TeV, Eur. Phys. J. C 79 (2019) 970, arXiv:1907.05120 [hep-ex].
[80] ATLAS Collaboration, Measurement of the c-jet mistagging efficiency in $t\bar{t}$ events using pp collision data at $\sqrt{s} = 13$ TeV collected with the ATLAS detector, Eur. Phys. J. C 82 (2022) 95, arXiv:2109.10627 [hep-ex].
[81] ATLAS Collaboration, Calibration of the light-flavour jet mistagging efficiency of the b-tagging algorithms with Z+jets events using 139 fb^{-1} of ATLAS proton–proton

collision data at $\sqrt{s} = 13$ TeV, Eur. Phys. J. C 83 (2023) 728, arXiv:2301.06319 [hep-ex].

[82] ATLAS Collaboration, Calibration of the performance of b-tagging for c and light-flavour jets in the 2012 ATLAS data, ATLAS-CONF-2014-046, https://cds.cern.ch/record/1741020, 2014.

[83] D0 Collaboration, Measurement of the $t\bar{t}$ production cross section in $p\bar{p}$ collisions at $\sqrt{s} = 1.96$ TeV using secondary vertex b tagging, Phys. Rev. D 74 (2006) 112004, arXiv:hep-ex/0611002.

[84] ATLAS Collaboration, Monte Carlo to Monte Carlo scale factors for flavour tagging efficiency calibration, ATL-PHYS-PUB-2020-009, https://cds.cern.ch/record/2718610, 2020.

[85] ATLAS Collaboration, Tools for estimating fake/non-prompt lepton backgrounds with the ATLAS detector at the LHC, J. Instrum. 18 (2023) T11004, arXiv:2211.16178 [hep-ex].

[86] ATLAS Collaboration, The performance of missing transverse momentum reconstruction and its significance with the ATLAS detector using 140 fb^{-1} of $\sqrt{s} = 13$ TeV pp collisions, arXiv:2402.05858 [hep-ex], 2024.

[87] ATLAS Collaboration, Luminosity determination in pp collisions at $\sqrt{s} = 13$ TeV using the ATLAS detector at the LHC, Eur. Phys. J. C 83 (2023) 982, arXiv:2212.09379 [hep-ex].

[88] N. Kidonakis, N. Yamanaka, Higher-order corrections for tW production at high-energy hadron colliders, J. High Energy Phys. 05 (2021) 278, arXiv:2102.11300 [hep-ph].

[89] D. de Florian, et al., Handbook of LHC Higgs Cross Sections: 4. Deciphering the Nature of the Higgs Sector, arXiv:1610.07922 [hep-ph], 2017.

[90] ATLAS Collaboration, Probing the CP nature of the top-Higgs Yukawa coupling in $t\bar{t}H$ and tH events with $H \to b\bar{b}$ decays using the ATLAS detector at the LHC, Phys. Lett. B 849 (2024) 138469, arXiv:2303.05974 [hep-ex].

[91] M. Grazzini, S. Kallweit, D. Rathlev, M. Wiesemann, $W^{\pm}Z$ production at hadron colliders in NNLO QCD, Phys. Lett. B 761 (2016) 179, arXiv:1604.08576 [hep-ph].

[92] ATLAS Collaboration, Multi-boson simulation for 13 TeV ATLAS analyses, ATL-PHYS-PUB-2016-002, https://cds.cern.ch/record/2119986, 2016.

[93] ATLAS Collaboration, Measurement of $W^{\pm}Z$ production cross sections and gauge boson polarisation in pp collisions at $\sqrt{s} = 13$ TeV with the ATLAS detector, Eur. Phys. J. C 79 (2019) 535, arXiv:1902.05759 [hep-ex].

[94] K. Cranmer, G. Lewis, L. Moneta, A. Shibata, W. Verkerke, HistFactory: a tool for creating statistical models for use with RooFit and RooStats, CERN-OPEN-2012-016, https://cds.cern.ch/record/1456844, 2012.

[95] W. Verkerke, D. Kirkby, The RooFit toolkit for data modeling, arXiv:physics/0306116 [physics.data-an], 2003.

[96] S. Baker, R.D. Cousins, Clarification of the use of CHI-square and likelihood functions in fits to histograms, Nucl. Instrum. Methods Phys. Res. 221 (1984) 437.

[97] A. Pinto, et al., Uncertainty components in profile likelihood fits, Eur. Phys. J. C 84 (2024) 593, arXiv:2307.04007 [physics.data-an].

[98] ATLAS Collaboration, ATLAS computing acknowledgements, ATL-SOFT-PUB-2023-001, https://cds.cern.ch/record/2869272, 2023.

The ATLAS Collaboration

G. Aad [105], E. Aakvaag [17], B. Abbott [124], S. Abdelhameed [120a], K. Abeling [57], N.J. Abicht [51], S.H. Abidi [30], M. Aboelela [46], A. Aboulhorma [36e], H. Abramowicz [156], H. Abreu [155], Y. Abulaiti [121], B.S. Acharya [71a,71b,k], A. Ackermann [65a], C. Adam Bourdarios [4], L. Adamczyk [88a], S.V. Addepalli [148], M.J. Addison [104], J. Adelman [119], A. Adiguzel [22c], T. Adye [138], A.A. Affolder [140], Y. Afik [41], M.N. Agaras [13], A. Aggarwal [103], C. Agheorghiesei [28c], F. Ahmadov [40,y], S. Ahuja [98], X. Ai [64e], G. Aielli [78a,78b], A. Aikot [168], M. Ait Tamlihat [36e], B. Aitbenchikh [36a], M. Akbiyik [103], T.P.A. Åkesson [101], A.V. Akimov [150], D. Akiyama [173], N.N. Akolkar [25], S. Aktas [22a], K. Al Khoury [43], G.L. Alberghi [24b], J. Albert [170], P. Albicocco [55], G.L. Albouy [62], S. Alderweireldt [54], Z.L. Alegria [125], M. Aleksa [37], I.N. Aleksandrov [40], C. Alexa [28b], T. Alexopoulos [10], F. Alfonsi [24b], M. Algren [58], M. Alhroob [172], B. Ali [136], H.M.J. Ali [94,s], S. Ali [32], S.W. Alibocus [95], M. Aliev [34c], G. Alimonti [73a], W. Alkakhi [57], C. Allaire [68], B.M.M. Allbrooke [151], J.S. Allen [104], J.F. Allen [54], C.A. Allendes Flores [141f], P.P. Allport [21], A. Aloisio [74a,74b], F. Alonso [93], C. Alpigiani [143], Z.M.K. Alsolami [94], M. Alvarez Estevez [102], A. Alvarez Fernandez [103], M. Alves Cardoso [58], M.G. Alviggi [74a,74b], M. Aly [104], Y. Amaral Coutinho [85b], A. Ambler [107], C. Amelung [37], M. Amerl [104], C.G. Ames [112], D. Amidei [109], B. Amini [56], K.J. Amirie [159], S.P. Amor Dos Santos [134a], K.R. Amos [168], D. Amperiadou [157], S. An [86], V. Ananiev [129], C. Anastopoulos [144], T. Andeen [11], J.K. Anders [37], A.C. Anderson [61], S.Y. Andrean [49a,49b], A. Andreazza [73a,73b], S. Angelidakis [9], A. Angerami [43], A.V. Anisenkov [39], A. Annovi [76a], C. Antel [58], E. Antipov [150], M. Antonelli [55], F. Anulli [77a], M. Aoki [86], T. Aoki [158], M.A. Aparo [151], L. Aperio Bella [50], C. Appelt [156], A. Apyan [27], S.J. Arbiol Val [89], C. Arcangeletti [55], A.T.H. Arce [53], J-F. Arguin [111], S. Argyropoulos [157], J.-H. Arling [50], O. Arnaez [4], H. Arnold [150], G. Artoni [77a,77b], H. Asada [114], K. Asai [122], S. Asai [158], N.A. Asbah [37], R.A. Ashby Pickering [172], K. Assamagan [30], R. Astalos [29a], K.S.V. Astrand [101], S. Atashi [163], R.J. Atkin [34a], H. Atmani [36f], P.A. Atmasiddha [132], K. Augsten [136], A.D. Auriol [21], V.A. Austrup [104], G. Avolio [37], K. Axiotis [58], G. Azuelos [111,ac], D. Babal [29b], H. Bachacou [139], K. Bachas [157,o], A. Bachiu [35], E. Bachmann [52], A. Badea [41], T.M. Baer [109], P. Bagnaia [77a,77b], M. Bahmani [19], D. Bahner [56], K. Bai [127], J.T. Baines [138], L. Baines [97], O.K. Baker [177], E. Bakos [16], D. Bakshi Gupta [8], L.E. Balabram Filho [85b], V. Balakrishnan [124], R. Balasubramanian [4], E.M. Baldin [39], P. Balek [88a], E. Ballabene [24b,24a], F. Balli [139], L.M. Baltes [65a], W.K. Balunas [33], J. Balz [103], I. Bamwidhi [120b], E. Banas [89], M. Bandieramonte [133], A. Bandyopadhyay [25], S. Bansal [25],

Physics Letters B 860 (2025) 139177

L. Barak [156], M. Barakat [50], E.L. Barberio [108], D. Barberis [59b,59a], M. Barbero [105], M.Z. Barel [118], T. Barillari [113], M-S. Barisits [37], T. Barklow [148], P. Baron [126], D.A. Baron Moreno [104], A. Baroncelli [64a], A.J. Barr [130], J.D. Barr [99], F. Barreiro [102], J. Barreiro Guimarães da Costa [14], M.G. Barros Teixeira [134a], S. Barsov [39], F. Bartels [65a], R. Bartoldus [148], A.E. Barton [94], P. Bartos [29a], A. Basan [103], M. Baselga [51], A. Bassalat [68,b], M.J. Basso [160a], S. Bataju [46], R. Bate [169], R.L. Bates [61], S. Batlamous [102], B. Batool [146], M. Battaglia [140], D. Battulga [19], M. Bauce [77a,77b], M. Bauer [81], P. Bauer [25], L.T. Bazzano Hurrell [31], J.B. Beacham [53], T. Beau [131], J.Y. Beaucamp [93], P.H. Beauchemin [162], P. Bechtle [25], H.P. Beck [20,n], K. Becker [172], A.J. Beddall [84], V.A. Bednyakov [40], C.P. Bee [150], L.J. Beemster [16], T.A. Beermann [37], M. Begalli [85d], M. Begel [30], A. Behera [150], J.K. Behr [50], J.F. Beirer [37], F. Beisiegel [25], M. Belfkir [120b], G. Bella [156], L. Bellagamba [24b], A. Bellerive [35], P. Bellos [21], K. Beloborodov [39], D. Benchekroun [36a], F. Bendebba [36a], Y. Benhammou [156], K.C. Benkendorfer [63], L. Beresford [50], M. Beretta [55], E. Bergeaas Kuutmann [166], N. Berger [4], B. Bergmann [136], J. Beringer [18a], G. Bernardi [5], C. Bernius [148], F.U. Bernlochner [25], F. Bernon [37], A. Berrocal Guardia [13], T. Berry [98], P. Berta [137], A. Berthold [52], S. Bethke [113], A. Betti [77a,77b], A.J. Bevan [97], N.K. Bhalla [56], S. Bhatta [150], D.S. Bhattacharya [171], P. Bhattarai [148], Z.M. Bhatti [121], K.D. Bhide [56], V.S. Bhopatkar [125], R.M. Bianchi [133], G. Bianco [24b,24a], O. Biebel [112], M. Biglietti [79a], C.S. Billingsley [46], Y. Bimgdi [36f], M. Bindi [57], A. Bingham [176], A. Bingul [22b], C. Bini [77a,77b], G.A. Bird [33], M. Birman [174], M. Biros [137], S. Biryukov [151], T. Bisanz [51], E. Bisceglie [45b,45a], J.P. Biswal [138], D. Biswas [146], I. Bloch [50], A. Blue [61], U. Blumenschein [97], J. Blumenthal [103], V.S. Bobrovnikov [39], M. Boehler [56], B. Boehm [171], D. Bogavac [37], A.G. Bogdanchikov [39], L.S. Boggia [131], C. Bohm [49a], V. Boisvert [98], P. Bokan [37], T. Bold [88a], M. Bomben [5], M. Bona [97], M. Boonekamp [139], A.G. Borbély [61], I.S. Bordulev [39], G. Borissov [94], D. Bortoletto [130], D. Boscherini [24b], M. Bosman [13], K. Bouaouda [36a], N. Bouchhar [168], L. Boudet [4], J. Boudreau [133], E.V. Bouhova-Thacker [94], D. Boumediene [42], R. Bouquet [59b,59a], A. Boveia [123], J. Boyd [37], D. Boye [30], I.R. Boyko [40], L. Bozianu [58], J. Bracinik [21], N. Brahimi [4], G. Brandt [176], O. Brandt [33], B. Brau [106], J.E. Brau [127], R. Brener [174], L. Brenner [118], R. Brenner [166], S. Bressler [174], G. Brianti [80a,80b], D. Britton [61], D. Britzger [113], I. Brock [25], R. Brock [110], G. Brooijmans [43], A.J. Brooks [70], E.M. Brooks [160b], E. Brost [30], L.M. Brown [170], L.E. Bruce [63], T.L. Bruckler [130], P.A. Bruckman de Renstrom [89], B. Brüers [50], A. Bruni [24b], G. Bruni [24b], D. Brunner [49a,49b], M. Bruschi [24b], N. Bruscino [77a,77b], T. Buanes [17], Q. Buat [143], D. Buchin [113], A.G. Buckley [61], O. Bulekov [39], B.A. Bullard [148], S. Burdin [95], C.D. Burgard [51], A.M. Burger [37], B. Burghgrave [8], O. Burlayenko [56], J. Burleson [167], J.T.P. Burr [33], J.C. Burzynski [147], E.L. Busch [43], V. Büscher [103], P.J. Bussey [61], J.M. Butler [26], C.M. Buttar [61], J.M. Butterworth [99], W. Buttinger [138], C.J. Buxo Vazquez [110], A.R. Buzykaev [39], S. Cabrera Urbán [168], L. Cadamuro [68], D. Caforio [60], H. Cai [133], Y. Cai [14,115c], Y. Cai [115a], V.M.M. Cairo [37], O. Cakir [3a], N. Calace [37], P. Calafiura [18a], G. Calderini [131], P. Calfayan [35], G. Callea [61], L.P. Caloba [85b], D. Calvet [42], S. Calvet [42], R. Camacho Toro [131], S. Camarda [37], D. Camarero Munoz [27], P. Camarri [78a,78b], M.T. Camerlingo [74a,74b], D. Cameron [37], C. Camincher [170], M. Campanelli [99], A. Camplani [44], V. Canale [74a,74b], A.C. Canbay [3a], E. Canonero [98], J. Cantero [168], Y. Cao [167], F. Capocasa [27], M. Capua [45b,45a], A. Carbone [73a,73b], R. Cardarelli [78a], J.C.J. Cardenas [8], M.P. Cardiff [27], G. Carducci [45b,45a], T. Carli [37], G. Carlino [74a], J.I. Carlotto [13], B.T. Carlson [133,p], E.M. Carlson [170,160a], J. Carmignani [95], L. Carminati [73a,73b], A. Carnelli [139], M. Carnesale [37], S. Caron [117], E. Carquin [141f],

I.B. Carr [108], S. Carrá [73a], G. Carratta [24b,24a], A.M. Carroll [127], M.P. Casado [13,h], M. Caspar [50], F.L. Castillo [4], L. Castillo Garcia [13], V. Castillo Gimenez [168], N.F. Castro [134a,134e], A. Catinaccio [37], J.R. Catmore [129], T. Cavaliere [4], V. Cavaliere [30], L.J. Caviedes Betancourt [23b], Y.C. Cekmecelioglu [50], E. Celebi [84], S. Cella [37], V. Cepaitis [58], K. Cerny [126], A.S. Cerqueira [85a], A. Cerri [151], L. Cerrito [78a,78b], F. Cerutti [18a], B. Cervato [146], A. Cervelli [24b], G. Cesarini [55], S.A. Cetin [84], P.M. Chabrillat [131], D. Chakraborty [119], J. Chan [18a], W.Y. Chan [158], J.D. Chapman [33], E. Chapon [139], B. Chargeishvili [154b], D.G. Charlton [21], M. Chatterjee [20], C. Chauhan [137], Y. Che [115a], S. Chekanov [6], S.V. Chekulaev [160a], G.A. Chelkov [40,a], A. Chen [109], B. Chen [156], B. Chen [170], H. Chen [115a], H. Chen [30], J. Chen [64c], J. Chen [147], M. Chen [130], S. Chen [90], S.J. Chen [115a], X. Chen [64c], X. Chen [15,ab], Y. Chen [64a], C.L. Cheng [175], H.C. Cheng [66a], S. Cheong [148], A. Cheplakov [40], E. Cheremushkina [50], E. Cherepanova [118], R. Cherkaoui El Moursli [36e], E. Cheu [7], K. Cheung [67], L. Chevalier [139], V. Chiarella [55], G. Chiarelli [76a], N. Chiedde [105], G. Chiodini [72a], A.S. Chisholm [21], A. Chitan [28b], M. Chitishvili [168], M.V. Chizhov [40,q], K. Choi [11], Y. Chou [143], E.Y.S. Chow [117], K.L. Chu [174], M.C. Chu [66a], X. Chu [14,115c], Z. Chubinidze [55], J. Chudoba [135], J.J. Chwastowski [89], D. Cieri [113], K.M. Ciesla [88a], V. Cindro [96], A. Ciocio [18a], F. Cirotto [74a,74b], Z.H. Citron [174], M. Citterio [73a], D.A. Ciubotaru [28b], A. Clark [58], P.J. Clark [54], N. Clarke Hall [99], C. Clarry [159], J.M. Clavijo Columbie [50], S.E. Clawson [50], C. Clement [49a,49b], Y. Coadou [105], M. Cobal [71a,71c], A. Coccaro [59b], R.F. Coelho Barrue [134a], R. Coelho Lopes De Sa [106], S. Coelli [73a], L.S. Colangeli [159], B. Cole [43], J. Collot [62], P. Conde Muiño [134a,134g], M.P. Connell [34c], S.H. Connell [34c], E.I. Conroy [130], F. Conventi [74a,ad], H.G. Cooke [21], A.M. Cooper-Sarkar [130], F.A. Corchia [24b,24a], A. Cordeiro Oudot Choi [131], L.D. Corpe [42], M. Corradi [77a,77b], F. Corriveau [107,x], A. Cortes-Gonzalez [19], M.J. Costa [168], F. Costanza [4], D. Costanzo [144], B.M. Cote [123], J. Couthures [4], G. Cowan [98], K. Cranmer [175], L. Cremer [51], D. Cremonini [24b,24a], S. Crépé-Renaudin [62], F. Crescioli [131], M. Cristinziani [146], M. Cristoforetti [80a,80b], V. Croft [118], J.E. Crosby [125], G. Crosetti [45b,45a], A. Cueto [102], H. Cui [99], Z. Cui [7], W.R. Cunningham [61], F. Curcio [168], J.R. Curran [54], P. Czodrowski [37], M.J. Da Cunha Sargedas De Sousa [59b,59a], J.V. Da Fonseca Pinto [85b], C. Da Via [104], W. Dabrowski [88a], T. Dado [37], S. Dahbi [153], T. Dai [109], D. Dal Santo [20], C. Dallapiccola [106], M. Dam [44], G. D'amen [30], V. D'Amico [112], J. Damp [103], J.R. Dandoy [35], D. Dannheim [37], M. Danninger [147], V. Dao [150], G. Darbo [59b], S.J. Das [30], F. Dattola [50], S. D'Auria [73a,73b], A. D'Avanzo [74a,74b], C. David [34a], T. Davidek [137], I. Dawson [97], H.A. Day-hall [136], K. De [8], C. De Almeida Rossi [159], R. De Asmundis [74a], N. De Biase [50], S. De Castro [24b,24a], N. De Groot [117], P. de Jong [118], H. De la Torre [119], A. De Maria [115a], A. De Salvo [77a], U. De Sanctis [78a,78b], F. De Santis [72a,72b], A. De Santo [151], J.B. De Vivie De Regie [62], J. Debevc [96], D.V. Dedovich [40], J. Degens [95], A.M. Deiana [46], F. Del Corso [24b,24a], J. Del Peso [102], L. Delagrange [131], F. Deliot [139], C.M. Delitzsch [51], M. Della Pietra [74a,74b], D. Della Volpe [58], A. Dell'Acqua [37], L. Dell'Asta [73a,73b], M. Delmastro [4], C.C. Delogu [103], P.A. Delsart [62], S. Demers [177], M. Demichev [40], S.P. Denisov [39], L. D'Eramo [42], D. Derendarz [89], F. Derue [131], P. Dervan [95], K. Desch [25], C. Deutsch [25], F.A. Di Bello [59b,59a], A. Di Ciaccio [78a,78b], L. Di Ciaccio [4], A. Di Domenico [77a,77b], C. Di Donato [74a,74b], A. Di Girolamo [37], G. Di Gregorio [37], A. Di Luca [80a,80b], B. Di Micco [79a,79b], R. Di Nardo [79a,79b], K.F. Di Petrillo [41], M. Diamantopoulou [35], F.A. Dias [118], T. Dias Do Vale [147], M.A. Diaz [141a,141b], A.R. Didenko [40], M. Didenko [168], E.B. Diehl [109], S. Díez Cornell [50], C. Diez Pardos [146], C. Dimitriadi [166], A. Dimitrievska [21], J. Dingfelder [25], T. Dingley [130], I-M. Dinu [28b], S.J. Dittmeier [65b], F. Dittus [37], M. Divisek [137], B. Dixit [95], F. Djama [105], T. Djobava [154b],

C. Doglioni [104,101], A. Dohnalova [29a], Z. Dolezal [137], K. Domijan [88a], K.M. Dona [41], M. Donadelli [85d], B. Dong [110], J. Donini [42], A. D'Onofrio [74a,74b], M. D'Onofrio [95], J. Dopke [138], A. Doria [74a], N. Dos Santos Fernandes [134a], P. Dougan [104], M.T. Dova [93], A.T. Doyle [61], M.A. Draguet [130], M.P. Drescher [57], E. Dreyer [174], I. Drivas-koulouris [10], M. Drnevich [121], M. Drozdova [58], D. Du [64a], T.A. du Pree [118], F. Dubinin [39], M. Dubovsky [29a], E. Duchovni [174], G. Duckeck [112], O.A. Ducu [28b], D. Duda [54], A. Dudarev [37], E.R. Duden [27], M. D'uffizi [104], L. Duflot [68], M. Dührssen [37], I. Duminica [28g], A.E. Dumitriu [28b], M. Dunford [65a], S. Dungs [51], K. Dunne [49a,49b], A. Duperrin [105], H. Duran Yildiz [3a], M. Düren [60], A. Durglishvili [154b], B.L. Dwyer [119], G.I. Dyckes [18a], M. Dyndal [88a], B.S. Dziedzic [37], Z.O. Earnshaw [151], G.H. Eberwein [130], B. Eckerova [29a], S. Eggebrecht [57], E. Egidio Purcino De Souza [85e], L.F. Ehrke [58], G. Eigen [17], K. Einsweiler [18a], T. Ekelof [166], P.A. Ekman [101], S. El Farkh [36b], Y. El Ghazali [64a], H. El Jarrari [37], A. El Moussaouy [36a], V. Ellajosyula [166], M. Ellert [166], F. Ellinghaus [176], N. Ellis [37], J. Elmsheuser [30], M. Elsawy [120a], M. Elsing [37], D. Emeliyanov [138], Y. Enari [86], I. Ene [18a], S. Epari [13], P.A. Erland [89], D. Ernani Martins Neto [89], M. Errenst [176], M. Escalier [68], C. Escobar [168], E. Etzion [156], G. Evans [134a], H. Evans [70], L.S. Evans [98], A. Ezhilov [39], S. Ezzarqtouni [36a], F. Fabbri [24b,24a], L. Fabbri [24b,24a], G. Facini [99], V. Fadeyev [140], R.M. Fakhrutdinov [39], D. Fakoudis [103], S. Falciano [77a], L.F. Falda Ulhoa Coelho [134a], F. Fallavollita [113], G. Falsetti [45b,45a], J. Faltova [137], C. Fan [167], K.Y. Fan [66b], Y. Fan [14], Y. Fang [14,115c], M. Fanti [73a,73b], M. Faraj [71a,71b], Z. Farazpay [100], A. Farbin [8], A. Farilla [79a], T. Farooque [110], J.N. Farr [177], S.M. Farrington [138,54], F. Fassi [36e], D. Fassouliotis [9], M. Faucci Giannelli [78a,78b], W.J. Fawcett [33], L. Fayard [68], P. Federic [137], P. Federicova [135], O.L. Fedin [39,a], M. Feickert [175], L. Feligioni [105], D.E. Fellers [127], C. Feng [64b], Z. Feng [118], M.J. Fenton [163], L. Ferencz [50], R.A.M. Ferguson [94], P. Fernandez Martinez [69], M.J.V. Fernoux [105], J. Ferrando [94], A. Ferrari [166], P. Ferrari [118,117], R. Ferrari [75a], D. Ferrere [58], C. Ferretti [109], M.P. Fewell [1], D. Fiacco [77a,77b], F. Fiedler [103], P. Fiedler [136], S. Filimonov [39], A. Filipčič [96], E.K. Filmer [160a], F. Filthaut [117], M.C.N. Fiolhais [134a,134c,c], L. Fiorini [168], W.C. Fisher [110], T. Fitschen [104], P.M. Fitzhugh [139], I. Fleck [146], P. Fleischmann [109], T. Flick [176], M. Flores [34d,z], L.R. Flores Castillo [66a], L. Flores Sanz De Acedo [37], F.M. Follega [80a,80b], N. Fomin [33], J.H. Foo [159], A. Formica [139], A.C. Forti [104], E. Fortin [37], A.W. Fortman [18a], M.G. Foti [18a], L. Fountas [9,i], D. Fournier [68], H. Fox [94], P. Francavilla [76a,76b], S. Francescato [63], S. Franchellucci [58], M. Franchini [24b,24a], S. Franchino [65a], D. Francis [37], L. Franco [117], V. Franco Lima [37], L. Franconi [50], M. Franklin [63], G. Frattari [27], Y.Y. Frid [156], J. Friend [61], N. Fritzsche [37], A. Froch [58], D. Froidevaux [37], J.A. Frost [130], Y. Fu [64a], S. Fuenzalida Garrido [141f], M. Fujimoto [105], K.Y. Fung [66a], E. Furtado De Simas Filho [85e], M. Furukawa [158], J. Fuster [168], A. Gaa [57], A. Gabrielli [24b,24a], A. Gabrielli [159], P. Gadow [37], G. Gagliardi [59b,59a], L.G. Gagnon [18a], S. Gaid [165], S. Galantzan [156], J. Gallagher [1], E.J. Gallas [130], A.L. Gallen [166], B.J. Gallop [138], K.K. Gan [123], S. Ganguly [158], Y. Gao [54], F.M. Garay Walls [141a,141b], B. Garcia [30], C. García [168], A. Garcia Alonso [118], A.G. Garcia Caffaro [177], J.E. García Navarro [168], M. Garcia-Sciveres [18a], G.L. Gardner [132], R.W. Gardner [41], N. Garelli [162], R.B. Garg [148], J.M. Gargan [54], C.A. Garner [159], C.M. Garvey [34a], V.K. Gassmann [162], G. Gaudio [75a], V. Gautam [13], P. Gauzzi [77a,77b], J. Gavranovic [96], I.L. Gavrilenko [39], A. Gavrilyuk [39], C. Gay [169], G. Gaycken [127], E.N. Gazis [10], A.A. Geanta [28b], A. Gekow [123], C. Gemme [59b], M.H. Genest [62], A.D. Gentry [116], S. George [98], W.F. George [21], T. Geralis [48], A.A. Gerwin [124], P. Gessinger-Befurt [37], M.E. Geyik [176], M. Ghani [172], K. Ghorbanian [97],

A. Ghosal [146], A. Ghosh [163], A. Ghosh [7], B. Giacobbe [24b], S. Giagu [77a,77b], T. Giani [118], A. Giannini [64a], S.M. Gibson [98], M. Gignac [140], D.T. Gil [88b], A.K. Gilbert [88a], B.J. Gilbert [43], D. Gillberg [35], G. Gilles [118], L. Ginabat [131], D.M. Gingrich [2,ac], M.P. Giordani [71a,71c], P.F. Giraud [139], G. Giugliarelli [71a,71c], D. Giugni [73a], F. Giuli [78a,78b], I. Gkialas [9,i], L.K. Gladilin [39], C. Glasman [102], G.R. Gledhill [127], G. Glemža [50], M. Glisic [127], I. Gnesi [45b], Y. Go [30], M. Goblirsch-Kolb [37], B. Gocke [51], D. Godin [111], B. Gokturk [22a], S. Goldfarb [108], T. Golling [58], M.G.D. Gololo [34g], D. Golubkov [39], J.P. Gombas [110], A. Gomes [134a,134b], G. Gomes Da Silva [146], A.J. Gomez Delegido [168], R. Gonçalo [134a], L. Gonella [21], A. Gongadze [154c], F. Gonnella [21], J.L. Gonski [148], R.Y. González Andana [54], S. González de la Hoz [168], R. Gonzalez Lopez [95], C. Gonzalez Renteria [18a], M.V. Gonzalez Rodrigues [50], R. Gonzalez Suarez [166], S. Gonzalez-Sevilla [58], L. Goossens [37], B. Gorini [37], E. Gorini [72a,72b], A. Gorišek [96], T.C. Gosart [132], A.T. Goshaw [53], M.I. Gostkin [40], S. Goswami [125], C.A. Gottardo [37], S.A. Gotz [112], M. Gouighri [36b], V. Goumarre [50], A.G. Goussiou [143], N. Govender [34c], R.P. Grabarczyk [130], I. Grabowska-Bold [88a], K. Graham [35], E. Gramstad [129], S. Grancagnolo [72a,72b], C.M. Grant [1,139], P.M. Gravila [28f], F.G. Gravili [72a,72b], H.M. Gray [18a], M. Greco [72a,72b], M.J. Green [1], C. Grefe [25], A.S. Grefsrud [17], I.M. Gregor [50], K.T. Greif [163], P. Grenier [148], S.G. Grewe [113], A.A. Grillo [140], K. Grimm [32], S. Grinstein [13,t], J.-F. Grivaz [68], E. Gross [174], J. Grosse-Knetter [57], L. Guan [109], J.G.R. Guerrero Rojas [168], G. Guerrieri [37], R. Gugel [103], J.A.M. Guhit [109], A. Guida [19], E. Guilloton [172], S. Guindon [37], F. Guo [14,115c], J. Guo [64c], L. Guo [50], L. Guo [14], Y. Guo [109], A. Gupta [51], R. Gupta [133], S. Gurbuz [25], S.S. Gurdasani [56], G. Gustavino [77a,77b], M. Guth [58], P. Gutierrez [124], L.F. Gutierrez Zagazeta [132], M. Gutsche [52], C. Gutschow [99], C. Gwenlan [130], C.B. Gwilliam [95], E.S. Haaland [129], A. Haas [121], M. Habedank [61], C. Haber [18a], H.K. Hadavand [8], A. Hadef [52], A.I. Hagan [94], J.J. Hahn [146], E.H. Haines [99], M. Haleem [171], J. Haley [125], G.D. Hallewell [105], L. Halser [20], K. Hamano [170], M. Hamer [25], E.J. Hampshire [98], J. Han [64b], L. Han [115a], L. Han [64a], S. Han [18a], Y.F. Han [159], K. Hanagaki [86], M. Hance [140], D.A. Hangal [43], H. Hanif [147], M.D. Hank [132], J.B. Hansen [44], P.H. Hansen [44], D. Harada [58], T. Harenberg [176], S. Harkusha [178], M.L. Harris [106], Y.T. Harris [25], J. Harrison [13], N.M. Harrison [123], P.F. Harrison [172], N.M. Hartman [113], N.M. Hartmann [112], R.Z. Hasan [98,138], Y. Hasegawa [145], F. Haslbeck [130], S. Hassan [17], R. Hauser [110], C.M. Hawkes [21], R.J. Hawkings [37], Y. Hayashi [158], D. Hayden [110], C. Hayes [109], R.L. Hayes [118], C.P. Hays [130], J.M. Hays [97], H.S. Hayward [95], F. He [64a], M. He [14,115c], Y. He [50], Y. He [99], N.B. Heatley [97], V. Hedberg [101], A.L. Heggelund [129], N.D. Hehir [97,*], C. Heidegger [56], K.K. Heidegger [56], J. Heilman [35], S. Heim [50], T. Heim [18a], J.G. Heinlein [132], J.J. Heinrich [127], L. Heinrich [113,aa], J. Hejbal [135], A. Held [175], S. Hellesund [17], C.M. Helling [169], S. Hellman [49a,49b], R.C.W. Henderson [94], L. Henkelmann [33], A.M. Henriques Correia [37], H. Herde [101], Y. Hernández Jiménez [150], L.M. Herrmann [25], T. Herrmann [52], G. Herten [56], R. Hertenberger [112], L. Hervas [37], M.E. Hesping [103], N.P. Hessey [160a], J. Hessler [113], M. Hidaoui [36b], N. Hidic [137], E. Hill [159], S.J. Hillier [21], J.R. Hinds [110], F. Hinterkeuser [25], M. Hirose [128], S. Hirose [161], D. Hirschbuehl [176], T.G. Hitchings [104], B. Hiti [96], J. Hobbs [150], R. Hobincu [28e], N. Hod [174], M.C. Hodgkinson [144], B.H. Hodkinson [130], A. Hoecker [37], D.D. Hofer [109], J. Hofer [168], T. Holm [25], M. Holzbock [37], L.B.A.H. Hommels [33], B.P. Honan [104], J.J. Hong [70], J. Hong [64c], T.M. Hong [133], B.H. Hooberman [167], W.H. Hopkins [6], M.C. Hoppesch [167], Y. Horii [114], M.E. Horstmann [113], S. Hou [153], M.R. Housenga [167], A.S. Howard [96], J. Howarth [61], J. Hoya [6], M. Hrabovsky [126],

A. Hrynevich [50], T. Hryn'ova [4], P.J. Hsu [67], S.-C. Hsu [143], T. Hsu [68], M. Hu [18a], Q. Hu [64a], S. Huang [33], X. Huang [14,115c], Y. Huang [144], Y. Huang [103], Y. Huang [14], Z. Huang [104], Z. Hubacek [136], M. Huebner [25], F. Huegging [25], T.B. Huffman [130], M. Hufnagel Maranha De Faria [85a], C.A. Hugli [50], M. Huhtinen [37], S.K. Huiberts [17], R. Hulsken [107], N. Huseynov [12,f], J. Huston [110], J. Huth [63], R. Hyneman [148], G. Iacobucci [58], G. Iakovidis [30], L. Iconomidou-Fayard [68], J.P. Iddon [37], P. Iengo [74a,74b], R. Iguchi [158], Y. Iiyama [158], T. Iizawa [130], Y. Ikegami [86], D. Iliadis [157], N. Ilic [159], H. Imam [85c], G. Inacio Goncalves [85d], T. Ingebretsen Carlson [49a,49b], J.M. Inglis [97], G. Introzzi [75a,75b], M. Iodice [79a], V. Ippolito [77a,77b], R.K. Irwin [95], M. Ishino [158], W. Islam [175], C. Issever [19], S. Istin [22a,ag], H. Ito [173], R. Iuppa [80a,80b], A. Ivina [174], J.M. Izen [47], V. Izzo [74a], P. Jacka [135], P. Jackson [1], C.S. Jagfeld [112], G. Jain [160a], P. Jain [50], K. Jakobs [56], T. Jakoubek [174], J. Jamieson [61], W. Jang [158], M. Javurkova [106], P. Jawahar [104], L. Jeanty [127], J. Jejelava [154a], P. Jenni [56,e], C.E. Jessiman [35], C. Jia [64b], H. Jia [169], J. Jia [150], X. Jia [14,115c], Z. Jia [115a], C. Jiang [54], S. Jiggins [50], J. Jimenez Pena [13], S. Jin [115a], A. Jinaru [28b], O. Jinnouchi [142], P. Johansson [144], K.A. Johns [7], J.W. Johnson [140], F.A. Jolly [50], D.M. Jones [151], E. Jones [50], K.S. Jones [8], P. Jones [33], R.W.L. Jones [94], T.J. Jones [95], H.L. Joos [57,37], R. Joshi [123], J. Jovicevic [16], X. Ju [18a], J.J. Junggeburth [37], T. Junkermann [65a], A. Juste Rozas [13,t], M.K. Juzek [89], S. Kabana [141e], A. Kaczmarska [89], M. Kado [113], H. Kagan [123], M. Kagan [148], A. Kahn [132], C. Kahra [103], T. Kaji [158], E. Kajomovitz [155], N. Kakati [174], I. Kalaitzidou [56], C.W. Kalderon [30], N.J. Kang [140], D. Kar [34g], K. Karava [130], M.J. Kareem [160b], E. Karentzos [25], O. Karkout [118], S.N. Karpov [40], Z.M. Karpova [40], V. Kartvelishvili [94], A.N. Karyukhin [39], E. Kasimi [157], J. Katzy [50], S. Kaur [35], K. Kawade [145], M.P. Kawale [124], C. Kawamoto [90], T. Kawamoto [64a], E.F. Kay [37], F.I. Kaya [162], S. Kazakos [110], V.F. Kazanin [39], Y. Ke [150], J.M. Keaveney [34a], R. Keeler [170], G.V. Kehris [63], J.S. Keller [35], J.J. Kempster [151], O. Kepka [135], J. Kerr [160b], B.P. Kerridge [138], S. Kersten [176], B.P. Kerševan [96], L. Keszeghova [29a], S. Ketabchi Haghighat [159], R.A. Khan [133], A. Khanov [125], A.G. Kharlamov [39], T. Kharlamova [39], E.E. Khoda [143], M. Kholodenko [134a], T.J. Khoo [19], G. Khoriauli [171], J. Khubua [154b,*], Y.A.R. Khwaira [131], B. Kibirige [34g], D. Kim [6], D.W. Kim [49a,49b], Y.K. Kim [41], N. Kimura [99], M.K. Kingston [57], A. Kirchhoff [57], C. Kirfel [25], F. Kirfel [25], J. Kirk [138], A.E. Kiryunin [113], S. Kita [161], C. Kitsaki [10], O. Kivernyk [25], M. Klassen [162], C. Klein [35], L. Klein [171], M.H. Klein [46], S.B. Klein [58], U. Klein [95], A. Klimentov [30], T. Klioutchnikova [37], P. Kluit [118], S. Kluth [113], E. Kneringer [81], T.M. Knight [159], A. Knue [51], D. Kobylianskii [174], S.F. Koch [130], M. Kocian [148], P. Kodyš [137], D.M. Koeck [127], P.T. Koenig [25], T. Koffas [35], O. Kolay [52], I. Koletsou [4], T. Komarek [89], K. Köneke [57], A.X.Y. Kong [1], T. Kono [122], N. Konstantinidis [99], P. Kontaxakis [58], B. Konya [101], R. Kopeliansky [43], S. Koperny [88a], K. Korcyl [89], K. Kordas [157,d], A. Korn [99], S. Korn [57], I. Korolkov [13], N. Korotkova [39], B. Kortman [118], O. Kortner [113], S. Kortner [113], W.H. Kostecka [119], V.V. Kostyukhin [146], A. Kotsokechagia [37], A. Kotwal [53], A. Koulouris [37], A. Kourkoumeli-Charalampidi [75a,75b], C. Kourkoumelis [9], E. Kourlitis [113,aa], O. Kovanda [127], R. Kowalewski [170], W. Kozanecki [127], A.S. Kozhin [39], V.A. Kramarenko [39], G. Kramberger [96], P. Kramer [25], M.W. Krasny [131], A. Krasznahorkay [37], A.C. Kraus [119], J.W. Kraus [176], J.A. Kremer [50], T. Kresse [52], L. Kretschmann [176], J. Kretzschmar [95], K. Kreul [19], P. Krieger [159], K. Krizka [21], K. Kroeninger [51], H. Kroha [113], J. Kroll [135], J. Kroll [132], K.S. Krowpman [110], U. Kruchonak [40], H. Krüger [25], N. Krumnack [83], M.C. Kruse [53], O. Kuchinskaia [39], S. Kuday [3a], S. Kuehn [37], R. Kuesters [56], T. Kuhl [50], V. Kukhtin [40], Y. Kulchitsky [40],

S. Kuleshov [141d,141b], M. Kumar [34g], N. Kumari [50], P. Kumari [160b], A. Kupco [135], T. Kupfer [51], A. Kupich [39], O. Kuprash [56], H. Kurashige [87], L.L. Kurchaninov [160a], O. Kurdysh [68], Y.A. Kurochkin [38], A. Kurova [39], M. Kuze [142], A.K. Kvam [106], J. Kvita [126], T. Kwan [107], N.G. Kyriacou [109], L.A.O. Laatu [105], C. Lacasta [168], F. Lacava [77a,77b], H. Lacker [19], D. Lacour [131], N.N. Lad [99], E. Ladygin [40], A. Lafarge [42], B. Laforge [131], T. Lagouri [177], F.Z. Lahbabi [36a], S. Lai [57], J.E. Lambert [170], S. Lammers [70], W. Lampl [7], C. Lampoudis [157,d], G. Lamprinoudis [103], A.N. Lancaster [119], E. Lançon [30], U. Landgraf [56], M.P.J. Landon [97], V.S. Lang [56], O.K.B. Langrekken [129], A.J. Lankford [163], F. Lanni [37], K. Lantzsch [25], A. Lanza [75a], M. Lanzac Berrocal [168], J.F. Laporte [139], T. Lari [73a], F. Lasagni Manghi [24b], M. Lassnig [37], V. Latonova [135], S.D. Lawlor [144], Z. Lawrence [104], R. Lazaridou [172], M. Lazzaroni [73a,73b], H.D.M. Le [110], E.M. Le Boulicaut [177], L.T. Le Pottier [18a], B. Leban [24b,24a], A. Lebedev [83], M. LeBlanc [104], F. Ledroit-Guillon [62], S.C. Lee [153], S. Lee [49a,49b], T.F. Lee [95], L.L. Leeuw [34c], M. Lefebvre [170], C. Leggett [18a], G. Lehmann Miotto [37], M. Leigh [58], W.A. Leight [106], W. Leinonen [117], A. Leisos [157,r], M.A.L. Leite [85c], C.E. Leitgeb [19], R. Leitner [137], K.J.C. Leney [46], T. Lenz [25], S. Leone [76a], C. Leonidopoulos [54], A. Leopold [149], R. Les [110], C.G. Lester [33], M. Levchenko [39], J. Levêque [4], L.J. Levinson [174], G. Levrini [24b,24a], M.P. Lewicki [89], C. Lewis [143], D.J. Lewis [4], L. Lewitt [144], A. Li [30], B. Li [64b], C. Li [64a], C-Q. Li [113], H. Li [64a], H. Li [64b], H. Li [115a], H. Li [15], H. Li [64b], J. Li [64c], K. Li [14], L. Li [64c], M. Li [14,115c], S. Li [14,115c], S. Li [64d,64c], T. Li [5], X. Li [107], Z. Li [158], Z. Li [14,115c], Z. Li [64a], S. Liang [14,115c], Z. Liang [14], M. Liberatore [139], B. Liberti [78a], K. Lie [66c], J. Lieber Marin [85e], H. Lien [70], H. Lin [109], K. Lin [110], L. Linden [112], R.E. Lindley [7], J.H. Lindon [2], J. Ling [63], E. Lipeles [132], A. Lipniacka [17], A. Lister [169], J.D. Little [70], B. Liu [14], B.X. Liu [115b], D. Liu [64d,64c], E.H.L. Liu [21], J.B. Liu [64a], J.K.K. Liu [33], K. Liu [64d], K. Liu [64d,64c], M. Liu [64a], M.Y. Liu [64a], P. Liu [14], Q. Liu [64d,143,64c], X. Liu [64a], X. Liu [64b], Y. Liu [115b,115c], Y.L. Liu [64b], Y.W. Liu [64a], S.L. Lloyd [97], E.M. Lobodzinska [50], P. Loch [7], E. Lodhi [159], T. Lohse [19], K. Lohwasser [144], E. Loiacono [50], J.D. Lomas [21], J.D. Long [43], I. Longarini [163], R. Longo [167], I. Lopez Paz [69], A. Lopez Solis [50], N.A. Lopez-canelas [7], N. Lorenzo Martinez [4], A.M. Lory [112], M. Losada [120a], G. Löschcke Centeno [151], O. Loseva [39], X. Lou [49a,49b], X. Lou [14,115c], A. Lounis [68], P.A. Love [94], G. Lu [14,115c], M. Lu [68], S. Lu [132], Y.J. Lu [153], H.J. Lubatti [143], C. Luci [77a,77b], F.L. Lucio Alves [115a], F. Luehring [70], O. Lukianchuk [68], B.S. Lunday [132], O. Lundberg [149], B. Lund-Jensen [149,*], N.A. Luongo [6], M.S. Lutz [37], A.B. Lux [26], D. Lynn [30], R. Lysak [135], E. Lytken [101], V. Lyubushkin [40], T. Lyubushkina [40], M.M. Lyukova [150], M. Firdaus M. Soberi [54], H. Ma [30], K. Ma [64a], L.L. Ma [64b], W. Ma [64a], Y. Ma [125], J.C. MacDonald [103], P.C. Machado De Abreu Farias [85e], R. Madar [42], T. Madula [99], J. Maeda [87], T. Maeno [30], P.T. Mafa [34c], H. Maguire [144], V. Maiboroda [139], A. Maio [134a,134b,134d], K. Maj [88a], O. Majersky [50], S. Majewski [127], N. Makovec [68], V. Maksimovic [16], B. Malaescu [131], Pa. Malecki [89], V.P. Maleev [39], F. Malek [62,m], M. Mali [96], D. Malito [98], U. Mallik [82,*], S. Maltezos [10], S. Malyukov [40], J. Mamuzic [13], G. Mancini [55], M.N. Mancini [27], G. Manco [75a,75b], J.P. Mandalia [97], S.S. Mandarry [151], I. Mandić [96], L. Manhaes de Andrade Filho [85a], I.M. Maniatis [174], J. Manjarres Ramos [92], D.C. Mankad [174], A. Mann [112], S. Manzoni [37], L. Mao [64c], X. Mapekula [34c], A. Marantis [157,r], G. Marchiori [5], M. Marcisovsky [135], C. Marcon [73a], M. Marinescu [21], S. Marium [50], M. Marjanovic [124], A. Markhoos [56], M. Markovitch [68], M.K. Maroun [106], E.J. Marshall [94], Z. Marshall [18a], S. Marti-Garcia [168], J. Martin [99], T.A. Martin [138], V.J. Martin [54], B. Martin dit Latour [17], L. Martinelli [77a,77b], M. Martinez [13,t], P. Martinez Agullo [168], V.I. Martinez Outschoorn [106],

P. Martinez Suarez [13], S. Martin-Haugh [138], G. Martinovicova [137], V.S. Martoiu [28b], A.C. Martyniuk [99], A. Marzin [37], D. Mascione [80a,80b], L. Masetti [103], J. Masik [104], A.L. Maslennikov [39], S.L. Mason [43], P. Massarotti [74a,74b], P. Mastrandrea [76a,76b], A. Mastroberardino [45b,45a], T. Masubuchi [128], T.T. Mathew [127], T. Mathisen [166], J. Matousek [137], D.M. Mattern [51], J. Maurer [28b], T. Maurin [61], A.J. Maury [68], B. Maček [96], D.A. Maximov [39], A.E. May [104], R. Mazini [34g], I. Maznas [119], M. Mazza [110], S.M. Mazza [140], E. Mazzeo [73a,73b], J.P. Mc Gowan [170], S.P. Mc Kee [109], C.A. Mc Lean [6], C.C. McCracken [169], E.F. McDonald [108], A.E. McDougall [118], L.F. Mcelhinney [94], J.A. Mcfayden [151], R.P. McGovern [132], R.P. Mckenzie [34g], T.C. Mclachlan [50], D.J. Mclaughlin [99], S.J. McMahon [138], C.M. Mcpartland [95], R.A. McPherson [170,x], S. Mehlhase [112], A. Mehta [95], D. Melini [168], B.R. Mellado Garcia [34g], A.H. Melo [57], F. Meloni [50], A.M. Mendes Jacques Da Costa [104], H.Y. Meng [159], L. Meng [94], S. Menke [113], M. Mentink [37], E. Meoni [45b,45a], G. Mercado [119], S. Merianos [157], C. Merlassino [71a,71c], L. Merola [74a,74b], C. Meroni [73a,73b], J. Metcalfe [6], A.S. Mete [6], E. Meuser [103], C. Meyer [70], J-P. Meyer [139], R.P. Middleton [138], L. Mijović [54], G. Mikenberg [174], M. Mikestikova [135], M. Mikuž [96], H. Mildner [103], A. Milic [37], D.W. Miller [41], E.H. Miller [148], L.S. Miller [35], A. Milov [174], D.A. Milstead [49a,49b], T. Min [115a], A.A. Minaenko [39], I.A. Minashvili [154b], A.I. Mincer [121], B. Mindur [88a], M. Mineev [40], Y. Mino [90], L.M. Mir [13], M. Miralles Lopez [61], M. Mironova [18a], M.C. Missio [117], A. Mitra [172], V.A. Mitsou [168], Y. Mitsumori [114], O. Miu [159], P.S. Miyagawa [97], T. Mkrtchyan [65a], M. Mlinarevic [99], T. Mlinarevic [99], M. Mlynarikova [37], S. Mobius [20], P. Mogg [112], M.H. Mohamed Farook [116], A.F. Mohammed [14,115c], S. Mohapatra [43], G. Mokgatitswane [34g], L. Moleri [174], B. Mondal [146], S. Mondal [136], K. Mönig [50], E. Monnier [105], L. Monsonis Romero [168], J. Montejo Berlingen [13], A. Montella [49a,49b], M. Montella [123], F. Montereali [79a,79b], F. Monticelli [93], S. Monzani [71a,71c], A. Morancho Tarda [44], N. Morange [68], A.L. Moreira De Carvalho [50], M. Moreno Llácer [168], C. Moreno Martinez [58], J.M. Moreno Perez [23b], P. Morettini [59b], S. Morgenstern [37], M. Morii [63], M. Morinaga [158], M. Moritsu [91], F. Morodei [77a,77b], P. Moschovakos [37], B. Moser [130], M. Mosidze [154b], T. Moskalets [46], P. Moskvitina [117], J. Moss [32,j], P. Moszkowicz [88a], A. Moussa [36d], Y. Moyal [174], E.J.W. Moyse [106], O. Mtintsilana [34g], S. Muanza [105], J. Mueller [133], D. Muenstermann [94], R. Müller [37], G.A. Mullier [166], A.J. Mullin [33], J.J. Mullin [132], A.E. Mulski [63], D.P. Mungo [159], D. Munoz Perez [168], F.J. Munoz Sanchez [104], M. Murin [104], W.J. Murray [172,138], M. Muškinja [96], C. Mwewa [30], A.G. Myagkov [39,a], A.J. Myers [8], G. Myers [109], M. Myska [136], B.P. Nachman [18a], K. Nagai [130], K. Nagano [86], R. Nagasaka [158], J.L. Nagle [30,ae], E. Nagy [105], A.M. Nairz [37], Y. Nakahama [86], K. Nakamura [86], K. Nakkalil [5], H. Nanjo [128], E.A. Narayanan [46], Y. Narukawa [158], I. Naryshkin [39], L. Nasella [73a,73b], S. Nasri [120b], C. Nass [25], G. Navarro [23a], J. Navarro-Gonzalez [168], A. Nayaz [19], P.Y. Nechaeva [39], S. Nechaeva [24b,24a], F. Nechansky [135], L. Nedic [130], T.J. Neep [21], A. Negri [75a,75b], M. Negrini [24b], C. Nellist [118], C. Nelson [107], K. Nelson [109], S. Nemecek [135], M. Nessi [37,g], M.S. Neubauer [167], F. Neuhaus [103], J. Neundorf [50], J. Newell [95], P.R. Newman [21], C.W. Ng [133], Y.W.Y. Ng [50], B. Ngair [120a], H.D.N. Nguyen [111], R.B. Nickerson [130], R. Nicolaidou [139], J. Nielsen [140], M. Niemeyer [57], J. Niermann [37], N. Nikiforou [37], V. Nikolaenko [39,a], I. Nikolic-Audit [131], K. Nikolopoulos [21], P. Nilsson [30], I. Ninca [50], G. Ninio [156], A. Nisati [77a], N. Nishu [2], R. Nisius [113], N. Nitika [71a,71c], J-E. Nitschke [52], E.K. Nkadimeng [34g], T. Nobe [158], T. Nommensen [152], M.B. Norfolk [144], B.J. Norman [35], M. Noury [36a], J. Novak [96], T. Novak [96], L. Novotny [136], R. Novotny [116], L. Nozka [126], K. Ntekas [163], N.M.J. Nunes De Moura Junior [85b], J. Ocariz [131], A. Ochi [87], I. Ochoa [134a], S. Oerdek [50,u], J.T. Offermann [41], A. Ogrodnik [137], A. Oh [104], C.C. Ohm [149],

H. Oide [86], R. Oishi [158], M.L. Ojeda [37], Y. Okumura [158], L.F. Oleiro Seabra [134a], I. Oleksiyuk [58], S.A. Olivares Pino [141d], G. Oliveira Correa [13], D. Oliveira Damazio [30], J.L. Oliver [163], Ö.O. Öncel [56], A.P. O'Neill [20], A. Onofre [134a,134e], P.U.E. Onyisi [11], M.J. Oreglia [41], D. Orestano [79a,79b], N. Orlando [13], R.S. Orr [159], L.M. Osojnak [132], Y. Osumi [114], G. Otero y Garzon [31], H. Otono [91], P.S. Ott [65a], G.J. Ottino [18a], M. Ouchrif [36d], F. Ould-Saada [129], T. Ovsiannikova [143], M. Owen [61], R.E. Owen [138], V.E. Ozcan [22a], F. Ozturk [89], N. Ozturk [8], S. Ozturk [84], H.A. Pacey [130], A. Pacheco Pages [13], C. Padilla Aranda [13], G. Padovano [77a,77b], S. Pagan Griso [18a], G. Palacino [70], A. Palazzo [72a,72b], J. Pampel [25], J. Pan [177], T. Pan [66a], D.K. Panchal [11], C.E. Pandini [118], J.G. Panduro Vazquez [138], H.D. Pandya [1], H. Pang [15], P. Pani [50], G. Panizzo [71a,71c], L. Panwar [131], L. Paolozzi [58], S. Parajuli [167], A. Paramonov [6], C. Paraskevopoulos [55], D. Paredes Hernandez [66b], A. Pareti [75a,75b], K.R. Park [43], T.H. Park [159], M.A. Parker [33], F. Parodi [59b,59a], V.A. Parrish [54], J.A. Parsons [43], U. Parzefall [56], B. Pascual Dias [111], L. Pascual Dominguez [102], E. Pasqualucci [77a], S. Passaggio [59b], F. Pastore [98], P. Patel [89], U.M. Patel [53], J.R. Pater [104], T. Pauly [37], F. Pauwels [137], C.I. Pazos [162], M. Pedersen [129], R. Pedro [134a], S.V. Peleganchuk [39], O. Penc [37], E.A. Pender [54], S. Peng [15], G.D. Penn [177], K.E. Penski [112], M. Penzin [39], B.S. Peralva [85d], A.P. Pereira Peixoto [143], L. Pereira Sanchez [148], D.V. Perepelitsa [30,ae], G. Perera [106], E. Perez Codina [160a], M. Perganti [10], H. Pernegger [37], S. Perrella [77a,77b], O. Perrin [42], K. Peters [50], R.F.Y. Peters [104], B.A. Petersen [37], T.C. Petersen [44], E. Petit [105], V. Petousis [136], C. Petridou [157,d], T. Petru [137], A. Petrukhin [146], M. Pettee [18a], A. Petukhov [84], K. Petukhova [37], R. Pezoa [141f], L. Pezzotti [37], G. Pezzullo [177], A.J. Pfleger [37], T.M. Pham [175], T. Pham [108], P.W. Phillips [138], G. Piacquadio [150], E. Pianori [18a], F. Piazza [127], R. Piegaia [31], D. Pietreanu [28b], A.D. Pilkington [104], M. Pinamonti [71a,71c], J.L. Pinfold [2], B.C. Pinheiro Pereira [134a], J. Pinol Bel [13], A.E. Pinto Pinoargote [139], L. Pintucci [71a,71c], K.M. Piper [151], A. Pirttikoski [58], D.A. Pizzi [35], L. Pizzimento [66b], A. Pizzini [118], M.-A. Pleier [30], V. Pleskot [137], E. Plotnikova [40], G. Poddar [97], R. Poettgen [101], L. Poggioli [131], S. Polacek [137], G. Polesello [75a], A. Poley [147,160a], A. Polini [24b], C.S. Pollard [172], Z.B. Pollock [123], E. Pompa Pacchi [124], N.I. Pond [99], D. Ponomarenko [70], L. Pontecorvo [37], S. Popa [28a], G.A. Popeneciu [28d], A. Poreba [37], D.M. Portillo Quintero [160a], S. Pospisil [136], M.A. Postill [144], P. Postolache [28c], K. Potamianos [172], P.A. Potepa [88a], I.N. Potrap [40], C.J. Potter [33], H. Potti [152], J. Poveda [168], M.E. Pozo Astigarraga [37], A. Prades Ibanez [78a,78b], J. Pretel [170], D. Price [104], M. Primavera [72a], L. Primomo [71a,71c], M.A. Principe Martin [102], R. Privara [126], T. Procter [61], M.L. Proffitt [143], N. Proklova [132], K. Prokofiev [66c], G. Proto [113], J. Proudfoot [6], M. Przybycien [88a], W.W. Przygoda [88b], A. Psallidas [48], J.E. Puddefoot [144], D. Pudzha [56], D. Pyatiizbyantseva [39], J. Qian [109], R. Qian [110], D. Qichen [104], Y. Qin [13], T. Qiu [54], A. Quadt [57], M. Queitsch-Maitland [104], G. Quetant [58], R.P. Quinn [169], G. Rabanal Bolanos [63], D. Rafanoharana [56], F. Raffaeli [78a,78b], F. Ragusa [73a,73b], J.L. Rainbolt [41], J.A. Raine [58], S. Rajagopalan [30], E. Ramakoti [39], L. Rambelli [59b,59a], I.A. Ramirez-Berend [35], K. Ran [50,115c], D.S. Rankin [132], N.P. Rapheeha [34g], H. Rasheed [28b], V. Raskina [131], D.F. Rassloff [65a], A. Rastogi [18a], S. Rave [103], S. Ravera [59b,59a], B. Ravina [57], I. Ravinovich [174], M. Raymond [37], A.L. Read [129], N.P. Readioff [144], D.M. Rebuzzi [75a,75b], G. Redlinger [30], A.S. Reed [113], K. Reeves [27], J.A. Reidelsturz [176], D. Reikher [127], A. Rej [51], C. Rembser [37], M. Renda [28b], F. Renner [50], A.G. Rennie [163], A.L. Rescia [50], S. Resconi [73a], M. Ressegotti [59b,59a], S. Rettie [37], J.G. Reyes Rivera [110], E. Reynolds [18a], O.L. Rezanova [39], P. Reznicek [137], H. Riani [36d], N. Ribaric [53], E. Ricci [80a,80b], R. Richter [113], S. Richter [49a,49b], E. Richter-Was [88b], M. Ridel [131], S. Ridouani [36d],

P. Rieck [121], P. Riedler [37], E.M. Riefel [49a,49b], J.O. Rieger [118], M. Rijssenbeek [150], M. Rimoldi [37], L. Rinaldi [24b,24a], P. Rincke [57,166], T.T. Rinn [30], M.P. Rinnagel [112], G. Ripellino [166], I. Riu [13], J.C. Rivera Vergara [170], F. Rizatdinova [125], E. Rizvi [97], B.R. Roberts [18a], S.S. Roberts [140], S.H. Robertson [107,x], D. Robinson [33], M. Robles Manzano [103], A. Robson [61], A. Rocchi [78a,78b], C. Roda [76a,76b], S. Rodriguez Bosca [37], Y. Rodriguez Garcia [23a], A.M. Rodríguez Vera [119], S. Roe [37], J.T. Roemer [37], O. Røhne [129], R.A. Rojas [106], C.P.A. Roland [131], J. Roloff [30], A. Romaniouk [81], E. Romano [75a,75b], M. Romano [24b], A.C. Romero Hernandez [167], N. Rompotis [95], L. Roos [131], S. Rosati [77a], B.J. Rosser [41], E. Rossi [130], E. Rossi [74a,74b], L.P. Rossi [63], L. Rossini [56], R. Rosten [123], M. Rotaru [28b], B. Rottler [56], C. Rougier [92], D. Rousseau [68], D. Rousso [50], A. Roy [167], S. Roy-Garand [159], A. Rozanov [105], Z.M.A. Rozario [61], Y. Rozen [155], A. Rubio Jimenez [168], V.H. Ruelas Rivera [19], T.A. Ruggeri [1], A. Ruggiero [130], A. Ruiz-Martinez [168], A. Rummler [37], Z. Rurikova [56], N.A. Rusakovich [40], H.L. Russell [170], G. Russo [77a,77b], J.P. Rutherfoord [7], S. Rutherford Colmenares [33], M. Rybar [137], E.B. Rye [129], A. Ryzhov [46], J.A. Sabater Iglesias [58], H.F-W. Sadrozinski [140], F. Safai Tehrani [77a], B. Safarzadeh Samani [138], S. Saha [1], M. Sahinsoy [84], A. Saibel [168], M. Saimpert [139], M. Saito [158], T. Saito [158], A. Sala [73a,73b], D. Salamani [37], A. Salnikov [148], J. Salt [168], A. Salvador Salas [156], D. Salvatore [45b,45a], F. Salvatore [151], A. Salzburger [37], D. Sammel [56], E. Sampson [94], D. Sampsonidis [157,d], D. Sampsonidou [127], J. Sánchez [168], V. Sanchez Sebastian [168], H. Sandaker [129], C.O. Sander [50], J.A. Sandesara [106], M. Sandhoff [176], C. Sandoval [23b], L. Sanfilippo [65a], D.P.C. Sankey [138], T. Sano [90], A. Sansoni [55], L. Santi [37,77b], C. Santoni [42], H. Santos [134a,134b], A. Santra [174], E. Sanzani [24b,24a], K.A. Saoucha [165], J.G. Saraiva [134a,134d], J. Sardain [7], O. Sasaki [86], K. Sato [161], C. Sauer [37], E. Sauvan [4], P. Savard [159,ac], R. Sawada [158], C. Sawyer [138], L. Sawyer [100], C. Sbarra [24b], A. Sbrizzi [24b,24a], T. Scanlon [99], J. Schaarschmidt [143], U. Schäfer [103], A.C. Schaffer [68,46], D. Schaile [112], R.D. Schamberger [150], C. Scharf [19], M.M. Schefer [20], V.A. Schegelsky [39], D. Scheirich [137], M. Schernau [141e], C. Scheulen [58], C. Schiavi [59b,59a], M. Schioppa [45b,45a], B. Schlag [148], S. Schlenker [37], J. Schmeing [176], M.A. Schmidt [176], K. Schmieden [103], C. Schmitt [103], N. Schmitt [103], S. Schmitt [50], L. Schoeffel [139], A. Schoening [65b], P.G. Scholer [35], E. Schopf [130], M. Schott [25], J. Schovancova [37], S. Schramm [58], T. Schroer [58], H-C. Schultz-Coulon [65a], M. Schumacher [56], B.A. Schumm [140], Ph. Schune [139], A.J. Schuy [143], H.R. Schwartz [140], A. Schwartzman [148], T.A. Schwarz [109], Ph. Schwemling [139], R. Schwienhorst [110], F.G. Sciacca [20], A. Sciandra [30], G. Sciolla [27], F. Scuri [76a], C.D. Sebastiani [95], K. Sedlaczek [119], S.C. Seidel [116], A. Seiden [140], B.D. Seidlitz [43], C. Seitz [50], J.M. Seixas [85b], G. Sekhniaidze [74a], L. Selem [62], N. Semprini-Cesari [24b,24a], A. Semushin [178,39], D. Sengupta [58], V. Senthilkumar [168], L. Serin [68], M. Sessa [78a,78b], H. Severini [124], F. Sforza [59b,59a], A. Sfyrla [58], Q. Sha [14], E. Shabalina [57], A.H. Shah [33], R. Shaheen [149], J.D. Shahinian [132], D. Shaked Renous [174], L.Y. Shan [14], M. Shapiro [18a], A. Sharma [37], A.S. Sharma [169], P. Sharma [30], P.B. Shatalov [39], K. Shaw [151], S.M. Shaw [104], Q. Shen [64c], D.J. Sheppard [147], P. Sherwood [99], L. Shi [99], X. Shi [14], S. Shimizu [86], C.O. Shimmin [177], I.P.J. Shipsey [130,*], S. Shirabe [91], M. Shiyakova [40,v], M.J. Shochet [41], D.R. Shope [129], B. Shrestha [124], S. Shrestha [123,af], I. Shreyber [39], M.J. Shroff [170], P. Sicho [135], A.M. Sickles [167], E. Sideras Haddad [34g,164], A.C. Sidley [118], A. Sidoti [24b], F. Siegert [52], Dj. Sijacki [16], F. Sili [93], J.M. Silva [54], I. Silva Ferreira [85b], M.V. Silva Oliveira [30], S.B. Silverstein [49a], S. Simion [68], R. Simoniello [37], E.L. Simpson [104], H. Simpson [151], L.R. Simpson [109], S. Simsek [84], S. Sindhu [57], P. Sinervo [159], S. Singh [30], S. Sinha [50], S. Sinha [104], M. Sioli [24b,24a], I. Siral [37],

E. Sitnikova [50], J. Sjölin [49a,49b], A. Skaf [57], E. Skorda [21], P. Skubic [124], M. Slawinska [89], I. Slazyk [17], V. Smakhtin [174], B.H. Smart [138], S.Yu. Smirnov [39], Y. Smirnov [39], L.N. Smirnova [39,a], O. Smirnova [101], A.C. Smith [43], D.R. Smith [163], E.A. Smith [41], J.L. Smith [104], R. Smith [148], H. Smitmanns [103], M. Smizanska [94], K. Smolek [136], A.A. Snesarev [39], H.L. Snoek [118], S. Snyder [30], R. Sobie [170,x], A. Soffer [156], C.A. Solans Sanchez [37], E.Yu. Soldatov [39], U. Soldevila [168], A.A. Solodkov [39], S. Solomon [27], A. Soloshenko [40], K. Solovieva [56], O.V. Solovyanov [42], P. Sommer [52], A. Sonay [13], W.Y. Song [160b], A. Sopczak [136], A.L. Sopio [54], F. Sopkova [29b], J.D. Sorenson [116], I.R. Sotarriva Alvarez [142], V. Sothilingam [65a], O.J. Soto Sandoval [141c,141b], S. Sottocornola [70], R. Soualah [165], Z. Soumaimi [36e], D. South [50], N. Soybelman [174], S. Spagnolo [72a,72b], M. Spalla [113], D. Sperlich [56], G. Spigo [37], B. Spisso [74a,74b], D.P. Spiteri [61], M. Spousta [137], E.J. Staats [35], R. Stamen [65a], A. Stampekis [21], E. Stanecka [89], W. Stanek-Maslouska [50], M.V. Stange [52], B. Stanislaus [18a], M.M. Stanitzki [50], B. Stapf [50], E.A. Starchenko [39], G.H. Stark [140], J. Stark [92], P. Staroba [135], P. Starovoitov [65a], S. Stärz [107], R. Staszewski [89], G. Stavropoulos [48], A. Stefl [37], P. Steinberg [30], B. Stelzer [147,160a], H.J. Stelzer [133], O. Stelzer-Chilton [160a], H. Stenzel [60], T.J. Stevenson [151], G.A. Stewart [37], J.R. Stewart [125], M.C. Stockton [37], G. Stoicea [28b], M. Stolarski [134a], S. Stonjek [113], A. Straessner [52], J. Strandberg [149], S. Strandberg [49a,49b], M. Stratmann [176], M. Strauss [124], T. Strebler [105], P. Strizenec [29b], R. Ströhmer [171], D.M. Strom [127], R. Stroynowski [46], A. Strubig [49a,49b], S.A. Stucci [30], B. Stugu [17], J. Stupak [124], N.A. Styles [50], D. Su [148], S. Su [64a], W. Su [64d], X. Su [64a], D. Suchy [29a], K. Sugizaki [158], V.V. Sulin [39], M.J. Sullivan [95], D.M.S. Sultan [130], L. Sultanaliyeva [39], S. Sultansoy [3b], T. Sumida [90], S. Sun [175], W. Sun [14], O. Sunneborn Gudnadottir [166], N. Sur [105], M.R. Sutton [151], H. Suzuki [161], M. Svatos [135], M. Swiatlowski [160a], T. Swirski [171], I. Sykora [29a], M. Sykora [137], T. Sykora [137], D. Ta [103], K. Tackmann [50,u], A. Taffard [163], R. Tafirout [160a], J.S. Tafoya Vargas [68], Y. Takubo [86], M. Talby [105], A.A. Talyshev [39], K.C. Tam [66b], N.M. Tamir [156], A. Tanaka [158], J. Tanaka [158], R. Tanaka [68], M. Tanasini [150], Z. Tao [169], S. Tapia Araya [141f], S. Tapprogge [103], A. Tarek Abouelfadl Mohamed [110], S. Tarem [155], K. Tariq [14], G. Tarna [28b], G.F. Tartarelli [73a], M.J. Tartarin [92], P. Tas [137], M. Tasevsky [135], E. Tassi [45b,45a], A.C. Tate [167], G. Tateno [158], Y. Tayalati [36e,w], G.N. Taylor [108], W. Taylor [160b], P. Teixeira-Dias [98], J.J. Teoh [159], K. Terashi [158], J. Terron [102], S. Terzo [13], M. Testa [55], R.J. Teuscher [159,x], A. Thaler [81], O. Theiner [58], T. Theveneaux-Pelzer [105], O. Thielmann [176], D.W. Thomas [98], J.P. Thomas [21], E.A. Thompson [18a], P.D. Thompson [21], E. Thomson [132], R.E. Thornberry [46], C. Tian [64a], Y. Tian [58], V. Tikhomirov [39,a], Yu.A. Tikhonov [39], S. Timoshenko [39], D. Timoshyn [137], E.X.L. Ting [1], P. Tipton [177], A. Tishelman-Charny [30], S.H. Tlou [34g], K. Todome [142], S. Todorova-Nova [137], S. Todt [52], L. Toffolin [71a,71c], M. Togawa [86], J. Tojo [91], S. Tokár [29a], K. Tokushuku [86], O. Toldaiev [70], G. Tolkachev [105], M. Tomoto [86,114], L. Tompkins [148,l], E. Torrence [127], H. Torres [92], E. Torró Pastor [168], M. Toscani [31], C. Tosciri [41], M. Tost [11], D.R. Tovey [144], I.S. Trandafir [28b], T. Trefzger [171], A. Tricoli [30], I.M. Trigger [160a], S. Trincaz-Duvoid [131], D.A. Trischuk [27], B. Trocmé [62], A. Tropina [40], L. Truong [34c], M. Trzebinski [89], A. Trzupek [89], F. Tsai [150], M. Tsai [109], A. Tsiamis [157], P.V. Tsiareshka [40], S. Tsigaridas [160a], A. Tsirigotis [157,r], V. Tsiskaridze [159], E.G. Tskhadadze [154a], M. Tsopoulou [157], Y. Tsujikawa [90], I.I. Tsukerman [39], V. Tsulaia [18a], S. Tsuno [86], K. Tsuri [122], D. Tsybychev [150], Y. Tu [66b], A. Tudorache [28b], V. Tudorache [28b], A.N. Tuna [63], S. Turchikhin [59b,59a], I. Turk Cakir [3a], R. Turra [73a], T. Turtuvshin [40], P.M. Tuts [43], S. Tzamarias [157,d], E. Tzovara [103],

F. Ukegawa [161], P.A. Ulloa Poblete [141c,141b], E.N. Umaka [30], G. Unal [37], A. Undrus [30], G. Unel [163], J. Urban [29b], P. Urrejola [141a], G. Usai [8], R. Ushioda [142], M. Usman [111], F. Ustuner [54], Z. Uysal [84], V. Vacek [136], B. Vachon [107], T. Vafeiadis [37], A. Vaitkus [99], C. Valderanis [112], E. Valdes Santurio [49a,49b], M. Valente [160a], S. Valentinetti [24b,24a], A. Valero [168], E. Valiente Moreno [168], A. Vallier [92], J.A. Valls Ferrer [168], D.R. Van Arneman [118], T.R. Van Daalen [143], A. Van Der Graaf [51], P. Van Gemmeren [6], M. Van Rijnbach [37], S. Van Stroud [99], I. Van Vulpen [118], P. Vana [137], M. Vanadia [78a,78b], U.M. Vande Voorde [149], W. Vandelli [37], E.R. Vandewall [125], D. Vannicola [156], L. Vannoli [55], R. Vari [77a], E.W. Varnes [7], C. Varni [18b], D. Varouchas [68], L. Varriale [168], K.E. Varvell [152], M.E. Vasile [28b], L. Vaslin [86], A. Vasyukov [40], L.M. Vaughan [125], R. Vavricka [103], T. Vazquez Schroeder [37], J. Veatch [32], V. Vecchio [104], M.J. Veen [106], I. Veliscek [30], L.M. Veloce [159], F. Veloso [134a,134c], S. Veneziano [77a], A. Ventura [72a,72b], S. Ventura Gonzalez [139], A. Verbytskyi [113], M. Verducci [76a,76b], C. Vergis [97], M. Verissimo De Araujo [85b], W. Verkerke [118], J.C. Vermeulen [118], C. Vernieri [148], M. Vessella [163], M.C. Vetterli [147,ac], A. Vgenopoulos [103], N. Viaux Maira [141f], T. Vickey [144], O.E. Vickey Boeriu [144], G.H.A. Viehhauser [130], L. Vigani [65b], M. Vigl [113], M. Villa [24b,24a], M. Villaplana Perez [168], E.M. Villhauer [54], E. Vilucchi [55], M.G. Vincter [35], A. Visibile [118], C. Vittori [37], I. Vivarelli [24b,24a], E. Voevodina [113], F. Vogel [112], J.C. Voigt [52], P. Vokac [136], Yu. Volkotrub [88b], E. Von Toerne [25], B. Vormwald [37], V. Vorobel [137], K. Vorobev [39], M. Vos [168], K. Voss [146], M. Vozak [118], L. Vozdecky [124], N. Vranjes [16], M. Vranjes Milosavljevic [16], M. Vreeswijk [118], N.K. Vu [64d], R. Vuillermet [37], O. Vujinovic [103], I. Vukotic [41], I.K. Vyas [35], S. Wada [161], C. Wagner [148], J.M. Wagner [18a], W. Wagner [176], S. Wahdan [176], H. Wahlberg [93], C.H. Waits [124], J. Walder [138], R. Walker [112], W. Walkowiak [146], A. Wall [132], E.J. Wallin [101], T. Wamorkar [6], A.Z. Wang [140], C. Wang [103], C. Wang [11], H. Wang [18a], J. Wang [66c], P. Wang [104], P. Wang [99], R. Wang [63], R. Wang [6], S.M. Wang [153], S. Wang [14], T. Wang [64a], W.T. Wang [82], W. Wang [14], X. Wang [167], X. Wang [64c], Y. Wang [64d], Y. Wang [115a], Y. Wang [64a], Z. Wang [109], Z. Wang [64d,53,64c], Z. Wang [109], A. Warburton [107], R.J. Ward [21], N. Warrack [61], S. Waterhouse [98], A.T. Watson [21], H. Watson [54], M.F. Watson [21], E. Watton [61,138], G. Watts [143], B.M. Waugh [99], J.M. Webb [56], C. Weber [30], H.A. Weber [19], M.S. Weber [20], S.M. Weber [65a], C. Wei [64a], Y. Wei [56], A.R. Weidberg [130], E.J. Weik [121], J. Weingarten [51], C. Weiser [56], C.J. Wells [50], T. Wenaus [30], B. Wendland [51], T. Wengler [37], N.S. Wenke [113], N. Wermes [25], M. Wessels [65a], A.M. Wharton [94], A.S. White [63], A. White [8], M.J. White [1], D. Whiteson [163], L. Wickremasinghe [128], W. Wiedenmann [175], M. Wielers [138], C. Wiglesworth [44], D.J. Wilbern [124], H.G. Wilkens [37], J.J.H. Wilkinson [33], D.M. Williams [43], H.H. Williams [132], S. Williams [33], S. Willocq [106], B.J. Wilson [104], D.J. Wilson [104], P.J. Windischhofer [41], F.I. Winkel [31], F. Winklmeier [127], B.T. Winter [56], J.K. Winter [104], M. Wittgen [148], M. Wobisch [100], T. Wojtkowski [62], Z. Wolffs [118], J. Wollrath [37], M.W. Wolter [89], H. Wolters [134a,134c], M.C. Wong [140], E.L. Woodward [43], S.D. Worm [50], B.K. Wosiek [89], K.W. Woźniak [89], S. Wozniewski [57], K. Wraight [61], C. Wu [21], M. Wu [115b], M. Wu [117], S.L. Wu [175], X. Wu [58], X. Wu [64a], Y. Wu [64a], Z. Wu [4], J. Wuerzinger [113,aa], T.R. Wyatt [104], B.M. Wynne [54], S. Xella [44], L. Xia [115a], M. Xia [15], M. Xie [64a], A. Xiong [127], J. Xiong [18a], D. Xu [14], H. Xu [64a], L. Xu [64a], R. Xu [132], T. Xu [109], Y. Xu [143], Z. Xu [54], Z. Xu [115a], B. Yabsley [152], S. Yacoob [34a], Y. Yamaguchi [86], E. Yamashita [158], H. Yamauchi [161], T. Yamazaki [18a], Y. Yamazaki [87], S. Yan [61], Z. Yan [106], H.J. Yang [64c,64d], H.T. Yang [64a], S. Yang [64a], T. Yang [66c], X. Yang [37], X. Yang [14], Y. Yang [46], Y. Yang [64a], W-M. Yao [18a], H. Ye [57], J. Ye [14], S. Ye [30],

X. Ye [64a], Y. Yeh [99], I. Yeletskikh [40], B. Yeo [18b], M.R. Yexley [99], T.P. Yildirim [130], P. Yin [43], K. Yorita [173], S. Younas [28b], C.J.S. Young [37], C. Young [148], C. Yu [14,115c], Y. Yu [64a], J. Yuan [14,115c], M. Yuan [109], R. Yuan [64d,64c], L. Yue [99], M. Zaazoua [64a], B. Zabinski [89], I. Zahir [36a], E. Zaid [54], Z.K. Zak [89], T. Zakareishvili [168], S. Zambito [58], J.A. Zamora Saa [141d,141b], J. Zang [158], D. Zanzi [56], R. Zanzottera [73a,73b], O. Zaplatilek [136], C. Zeitnitz [176], H. Zeng [14], J.C. Zeng [167], D.T. Zenger Jr [27], O. Zenin [39], T. Ženiš [29a], S. Zenz [97], S. Zerradi [36a], D. Zerwas [68], M. Zhai [14,115c], D.F. Zhang [144], J. Zhang [64b], J. Zhang [6], K. Zhang [14,115c], L. Zhang [64a], L. Zhang [115a], P. Zhang [14,115c], R. Zhang [175], S. Zhang [109], S. Zhang [92], T. Zhang [158], X. Zhang [64c], Y. Zhang [143], Y. Zhang [99], Y. Zhang [115a], Z. Zhang [18a], Z. Zhang [64b], Z. Zhang [68], H. Zhao [143], T. Zhao [64b], Y. Zhao [140], Z. Zhao [64a], Z. Zhao [64a], A. Zhemchugov [40], J. Zheng [115a], K. Zheng [167], X. Zheng [64a], Z. Zheng [148], D. Zhong [167], B. Zhou [109], H. Zhou [7], N. Zhou [64c], Y. Zhou [15], Y. Zhou [115a], Y. Zhou [7], C.G. Zhu [64b], J. Zhu [109], X. Zhu [64d], Y. Zhu [64c], Y. Zhu [64a], X. Zhuang [14], K. Zhukov [70], N.I. Zimine [40], J. Zinsser [65b], M. Ziolkowski [146], L. Živković [16], A. Zoccoli [24b,24a], K. Zoch [63], T.G. Zorbas [144], O. Zormpa [48], W. Zou [43], L. Zwalinski [37]

[1] *Department of Physics, University of Adelaide, Adelaide; Australia*
[2] *Department of Physics, University of Alberta, Edmonton AB; Canada*
[3] [(a)] *Department of Physics, Ankara University, Ankara;* [(b)] *Division of Physics, TOBB University of Economics and Technology, Ankara; Türkiye*
[4] *LAPP, Université Savoie Mont Blanc, CNRS/IN2P3, Annecy; France*
[5] *APC, Université Paris Cité, CNRS/IN2P3, Paris; France*
[6] *High Energy Physics Division, Argonne National Laboratory, Argonne IL; United States of America*
[7] *Department of Physics, University of Arizona, Tucson AZ; United States of America*
[8] *Department of Physics, University of Texas at Arlington, Arlington TX; United States of America*
[9] *Physics Department, National and Kapodistrian University of Athens, Athens; Greece*
[10] *Physics Department, National Technical University of Athens, Zografou; Greece*
[11] *Department of Physics, University of Texas at Austin, Austin TX; United States of America*
[12] *Institute of Physics, Azerbaijan Academy of Sciences, Baku; Azerbaijan*
[13] *Institut de Física d'Altes Energies (IFAE), Barcelona Institute of Science and Technology, Barcelona; Spain*
[14] *Institute of High Energy Physics, Chinese Academy of Sciences, Beijing; China*
[15] *Physics Department, Tsinghua University, Beijing; China*
[16] *Institute of Physics, University of Belgrade, Belgrade; Serbia*
[17] *Department for Physics and Technology, University of Bergen, Bergen; Norway*
[18] [(a)] *Physics Division, Lawrence Berkeley National Laboratory, Berkeley CA;* [(b)] *University of California, Berkeley CA; United States of America*
[19] *Institut für Physik, Humboldt Universität zu Berlin, Berlin; Germany*
[20] *Albert Einstein Center for Fundamental Physics and Laboratory for High Energy Physics, University of Bern, Bern; Switzerland*
[21] *School of Physics and Astronomy, University of Birmingham, Birmingham; United Kingdom*
[22] [(a)] *Department of Physics, Bogazici University, Istanbul;* [(b)] *Department of Physics Engineering, Gaziantep University, Gaziantep;* [(c)] *Department of Physics, Istanbul University, Istanbul; Türkiye*
[23] [(a)] *Facultad de Ciencias y Centro de Investigaciónes, Universidad Antonio Nariño, Bogotá;* [(b)] *Departamento de Física, Universidad Nacional de Colombia, Bogotá; Colombia*
[24] [(a)] *Dipartimento di Fisica e Astronomia A. Righi, Università di Bologna, Bologna;* [(b)] *INFN Sezione di Bologna; Italy*
[25] *Physikalisches Institut, Universität Bonn, Bonn; Germany*
[26] *Department of Physics, Boston University, Boston MA; United States of America*
[27] *Department of Physics, Brandeis University, Waltham MA; United States of America*
[28] [(a)] *Transilvania University of Brasov, Brasov;* [(b)] *Horia Hulubei National Institute of Physics and Nuclear Engineering, Bucharest;* [(c)] *Department of Physics, Alexandru Ioan Cuza University of Iasi, Iasi;* [(d)] *National Institute for Research and Development of Isotopic and Molecular Technologies, Physics Department, Cluj-Napoca;* [(e)] *National University of Science and Technology Politechnica, Bucharest;* [(f)] *West University in Timisoara, Timisoara;* [(g)] *Faculty of Physics, University of Bucharest, Bucharest; Romania*
[29] [(a)] *Faculty of Mathematics, Physics and Informatics, Comenius University, Bratislava;* [(b)] *Department of Subnuclear Physics, Institute of Experimental Physics of the Slovak Academy of Sciences, Kosice; Slovak Republic*
[30] *Physics Department, Brookhaven National Laboratory, Upton NY; United States of America*
[31] *Universidad de Buenos Aires, Facultad de Ciencias Exactas y Naturales, Departamento de Física, y CONICET, Instituto de Física de Buenos Aires (IFIBA), Buenos Aires; Argentina*
[32] *California State University, CA; United States of America*
[33] *Cavendish Laboratory, University of Cambridge, Cambridge; United Kingdom*
[34] [(a)] *Department of Physics, University of Cape Town, Cape Town;* [(b)] *iThemba Labs, Western Cape;* [(c)] *Department of Mechanical Engineering Science, University of Johannesburg, Johannesburg;* [(d)] *National Institute of Physics, University of the Philippines Diliman (Philippines);* [(e)] *University of South Africa, Department of Physics, Pretoria;* [(f)] *University of Zululand, KwaDlangezwa;* [(g)] *School of Physics, University of the Witwatersrand, Johannesburg; South Africa*
[35] *Department of Physics, Carleton University, Ottawa ON; Canada*
[36] [(a)] *Faculté des Sciences Ain Chock, Université Hassan II de Casablanca;* [(b)] *Faculté des Sciences, Université Ibn-Tofail, Kénitra;* [(c)] *Faculté des Sciences Semlalia, Université Cadi Ayyad, LPHEA-Marrakech;* [(d)] *LPMR, Faculté des Sciences, Université Mohamed Premier, Oujda;* [(e)] *Faculté des sciences, Université Mohammed V, Rabat;* [(f)] *Institute of Applied Physics, Mohammed VI Polytechnic University, Ben Guerir; Morocco*
[37] *CERN, Geneva; Switzerland*
[38] *Affiliated with an institute formerly covered by a cooperation agreement with CERN*
[39] *Affiliated with an institute covered by a cooperation agreement with CERN*
[40] *Affiliated with an international laboratory covered by a cooperation agreement with CERN*
[41] *Enrico Fermi Institute, University of Chicago, Chicago IL; United States of America*
[42] *LPC, Université Clermont Auvergne, CNRS/IN2P3, Clermont-Ferrand; France*
[43] *Nevis Laboratory, Columbia University, Irvington NY; United States of America*
[44] *Niels Bohr Institute, University of Copenhagen, Copenhagen; Denmark*
[45] [(a)] *Dipartimento di Fisica, Università della Calabria, Rende;* [(b)] *INFN Gruppo Collegato di Cosenza, Laboratori Nazionali di Frascati; Italy*
[46] *Physics Department, Southern Methodist University, Dallas TX; United States of America*

[47] Physics Department, University of Texas at Dallas, Richardson TX; United States of America
[48] National Centre for Scientific Research "Demokritos", Agia Paraskevi; Greece
[49] [(a)] Department of Physics, Stockholm University; [(b)] Oskar Klein Centre, Stockholm; Sweden
[50] Deutsches Elektronen-Synchrotron DESY, Hamburg and Zeuthen; Germany
[51] Fakultät Physik, Technische Universität Dortmund, Dortmund; Germany
[52] Institut für Kern- und Teilchenphysik, Technische Universität Dresden, Dresden; Germany
[53] Department of Physics, Duke University, Durham NC; United States of America
[54] SUPA - School of Physics and Astronomy, University of Edinburgh, Edinburgh; United Kingdom
[55] INFN e Laboratori Nazionali di Frascati, Frascati; Italy
[56] Physikalisches Institut, Albert-Ludwigs-Universität Freiburg, Freiburg; Germany
[57] II. Physikalisches Institut, Georg-August-Universität Göttingen, Göttingen; Germany
[58] Département de Physique Nucléaire et Corpusculaire, Université de Genève, Genève; Switzerland
[59] [(a)] Dipartimento di Fisica, Università di Genova, Genova; [(b)] INFN Sezione di Genova; Italy
[60] II. Physikalisches Institut, Justus-Liebig-Universität Giessen, Giessen; Germany
[61] SUPA - School of Physics and Astronomy, University of Glasgow, Glasgow; United Kingdom
[62] LPSC, Université Grenoble Alpes, CNRS/IN2P3, Grenoble INP, Grenoble; France
[63] Laboratory for Particle Physics and Cosmology, Harvard University, Cambridge MA; United States of America
[64] [(a)] Department of Modern Physics and State Key Laboratory of Particle Detection and Electronics, University of Science and Technology of China, Hefei; [(b)] Institute of Frontier and Interdisciplinary Science and Key Laboratory of Particle Physics and Particle Irradiation (MOE), Shandong University, Qingdao; [(c)] School of Physics and Astronomy, Shanghai Jiao Tong University, Key Laboratory for Particle Astrophysics and Cosmology (MOE), SKLPPC, Shanghai; [(d)] Tsung-Dao Lee Institute, Shanghai; [(e)] School of Physics, Zhengzhou University; China
[65] [(a)] Kirchhoff-Institut für Physik, Ruprecht-Karls-Universität Heidelberg, Heidelberg; [(b)] Physikalisches Institut, Ruprecht-Karls-Universität Heidelberg, Heidelberg; Germany
[66] [(a)] Department of Physics, Chinese University of Hong Kong, Shatin, N.T., Hong Kong; [(b)] Department of Physics, University of Hong Kong, Hong Kong; [(c)] Department of Physics and Institute for Advanced Study, Hong Kong University of Science and Technology, Clear Water Bay, Kowloon, Hong Kong; China
[67] Department of Physics, National Tsing Hua University, Hsinchu; Taiwan
[68] IJCLab, Université Paris-Saclay, CNRS/IN2P3, 91405, Orsay; France
[69] Centro Nacional de Microelectrónica (IMB-CNM-CSIC), Barcelona; Spain
[70] Department of Physics, Indiana University, Bloomington IN; United States of America
[71] [(a)] INFN Gruppo Collegato di Udine, Sezione di Trieste, Udine; [(b)] ICTP, Trieste; [(c)] Dipartimento Politecnico di Ingegneria e Architettura, Università di Udine, Udine; Italy
[72] [(a)] INFN Sezione di Lecce; [(b)] Dipartimento di Matematica e Fisica, Università del Salento, Lecce; Italy
[73] [(a)] INFN Sezione di Milano; [(b)] Dipartimento di Fisica, Università di Milano, Milano; Italy
[74] [(a)] INFN Sezione di Napoli; [(b)] Dipartimento di Fisica, Università di Napoli, Napoli; Italy
[75] [(a)] INFN Sezione di Pavia; [(b)] Dipartimento di Fisica, Università di Pavia, Pavia; Italy
[76] [(a)] INFN Sezione di Pisa; [(b)] Dipartimento di Fisica E. Fermi, Università di Pisa, Pisa; Italy
[77] [(a)] INFN Sezione di Roma; [(b)] Dipartimento di Fisica, Sapienza Università di Roma, Roma; Italy
[78] [(a)] INFN Sezione di Roma Tor Vergata; [(b)] Dipartimento di Fisica, Università di Roma Tor Vergata, Roma; Italy
[79] [(a)] INFN Sezione di Roma Tre; [(b)] Dipartimento di Matematica e Fisica, Università Roma Tre, Roma; Italy
[80] [(a)] INFN-TIFPA; [(b)] Università degli Studi di Trento, Trento; Italy
[81] Universität Innsbruck, Department of Astro and Particle Physics, Innsbruck; Austria
[82] University of Iowa, Iowa City IA; United States of America
[83] Department of Physics and Astronomy, Iowa State University, Ames IA; United States of America
[84] Istinye University, Sariyer, Istanbul; Türkiye
[85] [(a)] Departamento de Engenharia Elétrica, Universidade Federal de Juiz de Fora (UFJF), Juiz de Fora; [(b)] Universidade Federal do Rio De Janeiro COPPE/EE/IF, Rio de Janeiro; [(c)] Instituto de Física, Universidade de São Paulo, São Paulo; [(d)] Rio de Janeiro State University, Rio de Janeiro; [(e)] Federal University of Bahia, Bahia; Brazil
[86] KEK, High Energy Accelerator Research Organization, Tsukuba; Japan
[87] Graduate School of Science, Kobe University, Kobe; Japan
[88] [(a)] AGH University of Krakow, Faculty of Physics and Applied Computer Science, Krakow; [(b)] Marian Smoluchowski Institute of Physics, Jagiellonian University, Krakow; Poland
[89] Institute of Nuclear Physics Polish Academy of Sciences, Krakow; Poland
[90] Faculty of Science, Kyoto University, Kyoto; Japan
[91] Research Center for Advanced Particle Physics and Department of Physics, Kyushu University, Fukuoka; Japan
[92] L2IT, Université de Toulouse, CNRS/IN2P3, UPS, Toulouse; France
[93] Instituto de Física La Plata, Universidad Nacional de La Plata and CONICET, La Plata; Argentina
[94] Physics Department, Lancaster University, Lancaster; United Kingdom
[95] Oliver Lodge Laboratory, University of Liverpool, Liverpool; United Kingdom
[96] Department of Experimental Particle Physics, Jožef Stefan Institute and Department of Physics, University of Ljubljana, Ljubljana; Slovenia
[97] School of Physics and Astronomy, Queen Mary University of London, London; United Kingdom
[98] Department of Physics, Royal Holloway University of London, Egham; United Kingdom
[99] Department of Physics and Astronomy, University College London, London; United Kingdom
[100] Louisiana Tech University, Ruston LA; United States of America
[101] Fysiska institutionen, Lunds universitet, Lund; Sweden
[102] Departamento de Física Teorica C-15 and CIAFF, Universidad Autónoma de Madrid, Madrid; Spain
[103] Institut für Physik, Universität Mainz, Mainz; Germany
[104] School of Physics and Astronomy, University of Manchester, Manchester; United Kingdom
[105] CPPM, Aix-Marseille Université, CNRS/IN2P3, Marseille; France
[106] Department of Physics, University of Massachusetts, Amherst MA; United States of America
[107] Department of Physics, McGill University, Montreal QC; Canada
[108] School of Physics, University of Melbourne, Victoria; Australia
[109] Department of Physics, University of Michigan, Ann Arbor MI; United States of America
[110] Department of Physics and Astronomy, Michigan State University, East Lansing MI; United States of America
[111] Group of Particle Physics, University of Montreal, Montreal QC; Canada
[112] Fakultät für Physik, Ludwig-Maximilians-Universität München, München; Germany
[113] Max-Planck-Institut für Physik (Werner-Heisenberg-Institut), München; Germany
[114] Graduate School of Science and Kobayashi-Maskawa Institute, Nagoya University, Nagoya; Japan
[115] [(a)] Department of Physics, Nanjing University, Nanjing; [(b)] School of Science, Shenzhen Campus of Sun Yat-sen University; [(c)] University of Chinese Academy of Science (UCAS), Beijing; China
[116] Department of Physics and Astronomy, University of New Mexico, Albuquerque NM; United States of America
[117] Institute for Mathematics, Astrophysics and Particle Physics, Radboud University/Nikhef, Nijmegen; Netherlands
[118] Nikhef National Institute for Subatomic Physics and University of Amsterdam, Amsterdam; Netherlands
[119] Department of Physics, Northern Illinois University, DeKalb IL; United States of America
[120] [(a)] New York University Abu Dhabi, Abu Dhabi; [(b)] United Arab Emirates University, Al Ain; United Arab Emirates
[121] Department of Physics, New York University, New York NY; United States of America
[122] Ochanomizu University, Otsuka, Bunkyo-ku, Tokyo; Japan

[123] Ohio State University, Columbus OH; United States of America
[124] Homer L. Dodge Department of Physics and Astronomy, University of Oklahoma, Norman OK; United States of America
[125] Department of Physics, Oklahoma State University, Stillwater OK; United States of America
[126] Palacký University, Joint Laboratory of Optics, Olomouc; Czech Republic
[127] Institute for Fundamental Science, University of Oregon, Eugene, OR; United States of America
[128] Graduate School of Science, Osaka University, Osaka; Japan
[129] Department of Physics, University of Oslo, Oslo; Norway
[130] Department of Physics, Oxford University, Oxford; United Kingdom
[131] LPNHE, Sorbonne Université, Université Paris Cité, CNRS/IN2P3, Paris; France
[132] Department of Physics, University of Pennsylvania, Philadelphia PA; United States of America
[133] Department of Physics and Astronomy, University of Pittsburgh, Pittsburgh PA; United States of America
[134] [(a)] Laboratório de Instrumentação e Física Experimental de Partículas - LIP, Lisboa; [(b)] Departamento de Física, Faculdade de Ciências, Universidade de Lisboa, Lisboa; [(c)] Departamento de Física, Universidade de Coimbra, Coimbra; [(d)] Centro de Física Nuclear da Universidade de Lisboa, Lisboa; [(e)] Departamento de Física, Universidade do Minho, Braga; [(f)] Departamento de Física Teórica y del Cosmos, Universidad de Granada, Granada (Spain); [(g)] Departamento de Física, Instituto Superior Técnico, Universidade de Lisboa, Lisboa; Portugal
[135] Institute of Physics of the Czech Academy of Sciences, Prague; Czech Republic
[136] Czech Technical University in Prague, Prague; Czech Republic
[137] Charles University, Faculty of Mathematics and Physics, Prague; Czech Republic
[138] Particle Physics Department, Rutherford Appleton Laboratory, Didcot; United Kingdom
[139] IRFU, CEA, Université Paris-Saclay, Gif-sur-Yvette; France
[140] Santa Cruz Institute for Particle Physics, University of California Santa Cruz, Santa Cruz CA; United States of America
[141] [(a)] Departamento de Física, Pontificia Universidad Católica de Chile, Santiago; [(b)] Millennium Institute for Subatomic physics at high energy frontier (SAPHIR), Santiago; [(c)] Instituto de Investigación Multidisciplinario en Ciencia y Tecnología, y Departamento de Física, Universidad de La Serena; [(d)] Universidad Andres Bello, Department of Physics, Santiago; [(e)] Instituto de Alta Investigación, Universidad de Tarapacá, Arica; [(f)] Departamento de Física, Universidad Técnica Federico Santa María, Valparaíso; Chile
[142] Department of Physics, Institute of Science, Tokyo; Japan
[143] Department of Physics, University of Washington, Seattle WA; United States of America
[144] Department of Physics and Astronomy, University of Sheffield, Sheffield; United Kingdom
[145] Department of Physics, Shinshu University, Nagano; Japan
[146] Department Physik, Universität Siegen, Siegen; Germany
[147] Department of Physics, Simon Fraser University, Burnaby BC; Canada
[148] SLAC National Accelerator Laboratory, Stanford CA; United States of America
[149] Department of Physics, Royal Institute of Technology, Stockholm; Sweden
[150] Departments of Physics and Astronomy, Stony Brook University, Stony Brook NY; United States of America
[151] Department of Physics and Astronomy, University of Sussex, Brighton; United Kingdom
[152] School of Physics, University of Sydney, Sydney; Australia
[153] Institute of Physics, Academia Sinica, Taipei; Taiwan
[154] [(a)] E. Andronikashvili Institute of Physics, Iv. Javakhishvili Tbilisi State University, Tbilisi; [(b)] High Energy Physics Institute, Tbilisi State University, Tbilisi; [(c)] University of Georgia, Tbilisi; Georgia
[155] Department of Physics, Technion, Israel Institute of Technology, Haifa; Israel
[156] Raymond and Beverly Sackler School of Physics and Astronomy, Tel Aviv University, Tel Aviv; Israel
[157] Department of Physics, Aristotle University of Thessaloniki, Thessaloniki; Greece
[158] International Center for Elementary Particle Physics and Department of Physics, University of Tokyo, Tokyo; Japan
[159] Department of Physics, University of Toronto, Toronto ON; Canada
[160] [(a)] TRIUMF, Vancouver BC; [(b)] Department of Physics and Astronomy, York University, Toronto ON; Canada
[161] Division of Physics and Tomonaga Center for the History of the Universe, Faculty of Pure and Applied Sciences, University of Tsukuba, Tsukuba; Japan
[162] Department of Physics and Astronomy, Tufts University, Medford MA; United States of America
[163] Department of Physics and Astronomy, University of California Irvine, Irvine CA; United States of America
[164] University of West Attica, Athens; Greece
[165] University of Sharjah, Sharjah; United Arab Emirates
[166] Department of Physics and Astronomy, University of Uppsala, Uppsala; Sweden
[167] Department of Physics, University of Illinois, Urbana IL; United States of America
[168] Instituto de Física Corpuscular (IFIC), Centro Mixto Universidad de Valencia - CSIC, Valencia; Spain
[169] Department of Physics, University of British Columbia, Vancouver BC; Canada
[170] Department of Physics and Astronomy, University of Victoria, Victoria BC; Canada
[171] Fakultät für Physik und Astronomie, Julius-Maximilians-Universität Würzburg, Würzburg; Germany
[172] Department of Physics, University of Warwick, Coventry; United Kingdom
[173] Waseda University, Tokyo; Japan
[174] Department of Particle Physics and Astrophysics, Weizmann Institute of Science, Rehovot; Israel
[175] Department of Physics, University of Wisconsin, Madison WI; United States of America
[176] Fakultät für Mathematik und Naturwissenschaften, Fachgruppe Physik, Bergische Universität Wuppertal, Wuppertal; Germany
[177] Department of Physics, Yale University, New Haven CT; United States of America
[178] Yerevan Physics Institute, Yerevan; Armenia

[a] Also Affiliated with an institute covered by a cooperation agreement with CERN.
[b] Also at An-Najah National University, Nablus; Palestine.
[c] Also at Borough of Manhattan Community College, City University of New York, New York NY; United States of America.
[d] Also at Center for Interdisciplinary Research and Innovation (CIRI-AUTH), Thessaloniki; Greece.
[e] Also at CERN, Geneva; Switzerland.
[f] Also at CMD-AC UNEC Research Center, Azerbaijan State University of Economics (UNEC); Azerbaijan.
[g] Also at Département de Physique Nucléaire et Corpusculaire, Université de Genève, Genève; Switzerland.
[h] Also at Departament de Fisica de la Universitat Autonoma de Barcelona, Barcelona; Spain.
[i] Also at Department of Financial and Management Engineering, University of the Aegean, Chios; Greece.
[j] Also at Department of Physics, California State University, Sacramento; United States of America.
[k] Also at Department of Physics, King's College London, London; United Kingdom.
[l] Also at Department of Physics, Stanford University, Stanford CA; United States of America.
[m] Also at Department of Physics, Stellenbosch University; South Africa.
[n] Also at Department of Physics, University of Fribourg, Fribourg; Switzerland.
[o] Also at Department of Physics, University of Thessaly; Greece.
[p] Also at Department of Physics, Westmont College, Santa Barbara; United States of America.
[q] Also at Faculty of Physics, Sofia University, 'St. Kliment Ohridski', Sofia; Bulgaria.
[r] Also at Hellenic Open University, Patras; Greece.

[s] Also at Imam Mohammad Ibn Saud Islamic University; Saudi Arabia.
[t] Also at Institucio Catalana de Recerca i Estudis Avancats, ICREA, Barcelona; Spain.
[u] Also at Institut für Experimentalphysik, Universität Hamburg, Hamburg; Germany.
[v] Also at Institute for Nuclear Research and Nuclear Energy (INRNE) of the Bulgarian Academy of Sciences, Sofia; Bulgaria.
[w] Also at Institute of Applied Physics, Mohammed VI Polytechnic University, Ben Guerir; Morocco.
[x] Also at Institute of Particle Physics (IPP); Canada.
[y] Also at Institute of Physics, Azerbaijan Academy of Sciences, Baku; Azerbaijan.
[z] Also at National Institute of Physics, University of the Philippines Diliman (Philippines); Philippines.
[aa] Also at Technical University of Munich, Munich; Germany.
[ab] Also at The Collaborative Innovation Center of Quantum Matter (CICQM), Beijing; China.
[ac] Also at TRIUMF, Vancouver BC; Canada.
[ad] Also at Università di Napoli Parthenope, Napoli; Italy.
[ae] Also at University of Colorado Boulder, Department of Physics, Colorado; United States of America.
[af] Also at Washington College, Chestertown, MD; United States of America.
[ag] Also at Yeditepe University, Physics Department, Istanbul; Türkiye.
[*] Deceased.

Eur. Phys. J. C (2025) 85:886
https://doi.org/10.1140/epjc/s10052-025-14507-0

THE EUROPEAN PHYSICAL JOURNAL C

Regular Article - Experimental Physics

Search for a new pseudoscalar decaying into a pair of bottom and antibottom quarks in top-associated production in $\sqrt{s} = 13$ TeV proton–proton collisions with the ATLAS detector

ATLAS Collaboration[⋆]

CERN, 1211 Geneva 23, Switzerland

Received: 24 March 2025 / Accepted: 10 July 2025
© The Author(s) 2025

Abstract A search for a pseudoscalar a produced in association with a top-quark pair, or in association with a single top quark plus a W boson, with the pseudoscalar decaying into b-quarks ($a \to b\bar{b}$), is performed using the full Run 2 data sample using a dileptonic decay mode signature. The search covers pseudoscalar boson masses between 12 and 100 GeV and involves both the kinematic regime where the decay products of the pseudoscalar are reconstructed as two standard b-tagged small-radius jets, or merged into a large-radius jet due to its Lorentz boost. No significant excess relative to expectations is observed. Assuming a branching ratio BR($a \to b\bar{b}$) = 100%, the range of pseudoscalar masses between 50 and 80 GeV is excluded at 95% confidence level for a coupling of the pseudoscalar to the top quark of 0.5, while a coupling of 1.0 is excluded at 95% confidence level for the masses considered, with the coupling defined as the strength modifier of the Standard Model Yukawa coupling.

Contents

1 Introduction
2 ATLAS detector
3 Data and simulated event samples
4 Object definition
4.1 Physics objects
4.2 Corrections to physics objects
5 Event selection
5.1 Preselection
5.2 Signal and control regions
6 Background estimate
7 Analysis strategy
7.1 Event reconstruction BDTs
7.2 Signal-versus-background discriminating neural networks
8 Statistical treatment
9 Systematic uncertainties
9.1 Experimental uncertainties
9.2 Modelling uncertainties
10 Results
11 Conclusions
References

⋆ e-mail: atlas.publications@cern.ch

1 Introduction

Since the discovery of the Higgs boson [1,2], there is an ongoing effort at the Large Hadron Collider (LHC) [3] to measure its properties and search for new physics. The Higgs boson was discovered by observing few decay modes [1,2] consistent with the Standard Model (SM) predictions. Part of the interest is about the nature of the discovered particle and whether it is the single boson predicted by the SM or, alternatively, part of an extended Higgs sector as suggested by models such as the two-Higgs-doublet model (2HDM) [4,5], which can be embedded into supersymmetric models [6–11]. It predicts a total of five bosons: a light (h) and a heavy (H) CP-even Higgs boson, with the light one corresponding to the observed Higgs boson; two charged Higgs bosons (H^+ and H^-); and a CP-odd particle (a), also referred to as pseudoscalar. The additional scalar/pseudoscalar states of these models may also provide a portal into dark matter, serving as a mediator between the SM and dark matter sector [12,13]. A pseudoscalar a is also be predicted in axion models [14].

This analysis performs a search for a light pseudoscalar with a mass smaller than the SM Higgs boson, produced in association either with a top-quark pair or a single top quark and a W boson, where the pseudoscalar decays into a bottom-antibottom quark pair, as proposed in [15]. It is based on a simplified model with the following Yukawa lagrangian:

$$\mathcal{L} = -\frac{g_t y_t}{\sqrt{2}} a\bar{t}(i\gamma^5)t - \frac{g_b y_b}{\sqrt{2}} a\bar{b}(i\gamma^5)b,$$

Published online: 19 August 2025

where $y_j/\sqrt{2} = m_j/v$ is the SM Yukawa coupling of particle j to the pseudoscalar a and g_j is the coupling modifier, with $j = t$ or b. Figure 1 shows two example Feynman diagrams for this process. This decay channel is favoured by many models for the range of explored pseudoscalar masses, $m_a < m_h$, although the branching ratios of the pseudoscalar depend on the specific model parameters. This is the first search for this process, exploring the couplings of the pseudoscalar to bottom quarks. Previously, the ATLAS and CMS Collaborations performed similar searches of $t\bar{t}a$ associated production exploiting leptonic decays of the pseudoscalar. The CMS Collaboration studied the decay of a pseudoscalar to the three families of leptons [16], while the ATLAS Collaboration studied the pseudoscalar coupling to muons [17]. None of these searches found significant excesses, but these decay channels are typically disfavoured compared with the $b\bar{b}$ decays when assuming a Yukawa coupling.

The search is performed in the dileptonic decay channel, with both top and antitop quarks (or both W bosons) decaying leptonically. Despite the reduced branching ratio of this decay channel, the reduced jet multiplicity of the final state and the precisely measured kinematics of the two leptons allow for a more efficient identification of the b-jets originating from the top and antitop quark decays than its semileptonic (with only one W boson from either the top or antitop quarks decaying leptonically) or fully hadronic (with the two W bosons decaying hadronically) counterparts.

For masses of the pseudoscalar below ∼30 GeV, the $b\bar{b}$ pair has a large Lorentz-boost and is thus reconstructed as a single large-radius jet. On the other hand, for higher masses, the jets are well separated at detector level. The analysis is designed to exploit both kinematic regimes to have good signal sensitivity, making use of multiple signal regions, reconstructed objects, and machine learning techniques.

2 ATLAS detector

The ATLAS detector [18] at the LHC covers nearly the entire solid angle around the collision point.[1] It consists of an inner tracking detector surrounded by a thin superconducting solenoid, electromagnetic and hadronic calorimeters, and a muon spectrometer incorporating three large superconducting air-core toroidal magnetic systems.

The inner-detector system (ID) is immersed in a 2 T axial magnetic field and provides charged-particle tracking in the range of $|\eta| < 2.5$. The high-granularity silicon pixel detector covers the vertex region and typically provides four measurements per track, the first hit generally being in the insertable B-layer installed before Run 2 [19,20]. It is followed by the SemiConductor Tracker, which usually provides eight measurements per track. These silicon detectors are complemented by the transition radiation tracker (TRT), which enables radially extended track reconstruction up to $|\eta| = 2.0$. The TRT also provides electron identification information based on the fraction of hits (typically 30 in total) above a higher energy-deposit threshold corresponding to transition radiation.

The calorimeter system covers the pseudorapidity range $|\eta| < 4.9$. Within the region $|\eta| < 3.2$, electromagnetic calorimetry is provided by barrel and endcap high-granularity lead/liquid-argon (LAr) calorimeters, with an additional thin LAr presampler covering $|\eta| < 1.8$ to correct for energy loss in material upstream of the calorimeters. Hadronic calorimetry is provided by the steel/scintillator-tile calorimeter, segmented into three barrel structures within $|\eta| < 1.7$, and two copper/LAr hadronic endcap calorimeters. The solid angle coverage is completed with forward copper/LAr and tungsten/LAr calorimeter modules optimised for electromagnetic and hadronic energy measurements respectively.

The muon spectrometer comprises separate trigger and high-precision tracking chambers measuring the deflection of muons in a magnetic field generated by the superconducting air-core toroidal magnets. The field integral of the toroids ranges between 2.0 and 6.0 Tm across most of the detector. Three layers of precision chambers, each consisting of layers of monitored drift tubes, cover the region $|\eta| < 2.7$, complemented by cathode-strip chambers in the forward region, where the background is highest. The muon trigger system covers the range $|\eta| < 2.4$ with resistive-plate chambers in the barrel, and thin-gap chambers in the endcap regions.

The luminosity is measured mainly by the LUCID-2 [21] detector that records Cherenkov light produced in the quartz windows of photomultipliers located close to the beampipe.

Events are selected by the first-level trigger system implemented in custom hardware, followed by selections made by algorithms implemented in software in the high-level trigger [22]. The first-level trigger accepts events from the 40 MHz bunch crossings at a rate below 100 kHz, which the high-level trigger further reduces to record complete events to disk at about 1 kHz.

A software suite [23] is used in data simulation, in the reconstruction and analysis of real and simulated data, in detector operations, and in the trigger and data acquisition systems of the experiment.

[1] ATLAS uses a right-handed coordinate system with its origin at the nominal interaction point (IP) in the centre of the detector and the z-axis along the beam pipe. The x-axis points from the IP to the centre of the LHC ring, and the y-axis points upwards. Polar coordinates (r, ϕ) are used in the transverse plane, ϕ being the azimuthal angle around the z-axis. The pseudorapidity is defined in terms of the polar angle θ as $\eta = -\ln\tan(\theta/2)$ and is equal to the rapidity $y = \frac{1}{2}\ln\left(\frac{E+p_z c}{E-p_z c}\right)$ in the relativistic limit. Angular distance is measured in units of $\Delta R \equiv \sqrt{(\Delta y)^2 + (\Delta\phi)^2}$.

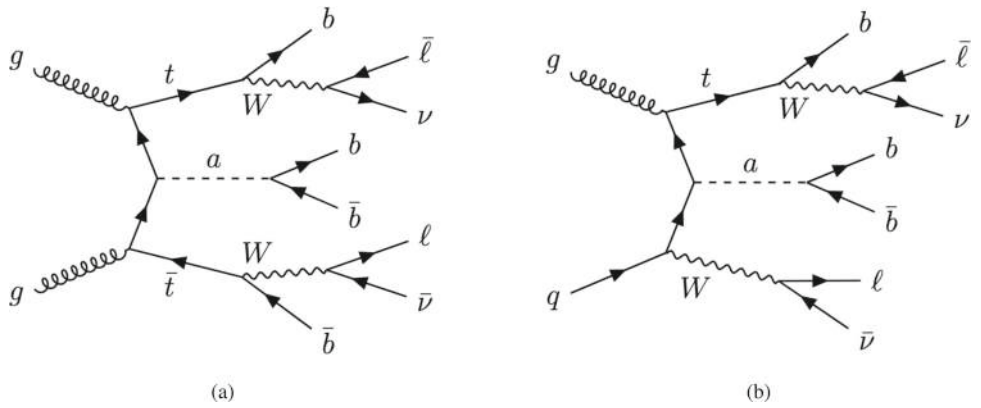

Fig. 1 Feynman diagrams for (**a**) $t\bar{t}$- and (**b**) tW-associated production of a pseudoscalar particle a that decays into a pair of b-quarks

3 Data and simulated event samples

This search is based on proton–proton (pp) collision data at a centre-of-mass energy of 13 TeV collected with the ATLAS detector at the LHC from 2015 to 2018, referred to as the Run 2 data sample in the following. After applying the data quality requirements that ensure that all subdetectors were operational, the integrated luminosity of the data sample is 140.1 ± 1.2 fb^{-1} [24].

The signal consists in the production of a light pseudoscalar a in association with a top-quark pair, $t\bar{t}a$, or in association with a single top quark and a W boson, tWa. The main background in this search is $t\bar{t}$ production in association with jets, followed by smaller contributions from single top quark, $t\bar{t}H$, $t\bar{t}V$, V+jets, diboson and other rare processes involving the production of a top quark. The analysis only considers the decay of the pseudoscalar to a $b\bar{b}$ pair. Decays of the pseudoscalar to other final states like a $\tau\bar{\tau}$ pair or a $c\bar{c}$ pair are not considered, as these are suppressed both by the Yukawa coupling for the masses considered (roughly a factor 5 and 20, respectively) and by the large b-jet multiplicity required in the analysis signal regions.

All signal and background samples are simulated using various Monte Carlo (MC) matrix-element (ME) generators interfaced with different algorithms for the parton shower, hadronisation, and underlying event. The effect from multiple pp interactions originating from the same or neighbouring bunch crossings, usually referred to as pile-up, is simulated by overlaying the simulated hard-scattering event with inelastic pp collisions simulated using PYTHIA 8.1 [25] and the A3 set of tuned parameters (tune) [26]. A reweighting is applied to the simulated samples such that they match the pile-up conditions in data. For the detector simulation two different approaches are used. The full ATLAS detector simulation (FS) is based on GEANT 4 [27], while the "fast" detector simulation (AF2) uses a parameterisation of the calorimeter response [28]. Most background samples are produced with FS while signal samples are produced with AF2. Both MC and data are processed using the same reconstruction and analysis software.

The $t\bar{t}a$ signal samples are simulated with MADGRAPH5_AMC@NLO 2.3.3 [29] generator at next-to-leading order (NLO) in the strong coupling constant α_s. A simplified model based on the decoupling limit of the 2HDM+a type II is used. Additionally, the subdominant tWa signal samples are simulated with the same generator at leading-order (LO). For notational simplicity, in the following $t\bar{t}a$ refers to the production of the pseudoscalar a in association with either a top-quark pair or a single top quark and a W boson. Samples are simulated for the following values of the pseudoscalar mass m_a: 12, 16, 20, 25, 30, 40, 50, 60, 80 and 100 GeV. Additional $t\bar{t}a$ signal samples for 20 and 60 GeV are also simulated with FS to check that no significant differences between the two detector simulations are observed.

The production of top-quark pairs with additional jets represents the main background source, especially the production of $t\bar{t}$ plus heavy flavour ($t\bar{t}$ +HF): $t\bar{t}+b$-jets and $t\bar{t}+c$-jets. For the modelling of $t\bar{t}+b$-jets events, four flavour-scheme samples (4FS), with massive b-quarks, are simulated using the POWHEGBOX-Res framework at NLO [30] and the NNPDF3.1nnlo parton distribution function (PDF) set is used. For the modelling of $t\bar{t}+c$-jets and $t\bar{t}$+light-jets events, five flavour-scheme (5FS) samples with massless b-quarks are simulated using POWHEGBOX-v2 [31–34], also at NLO. To avoid double-counting of events, neither the $t\bar{t}+b$-jets events from the 5FS samples nor the $t\bar{t}+c$-jets nor the $t\bar{t}$+light-jets events from the 4FS samples are used. The simulated $t\bar{t}$ events are categorised based on the number of additional jets matched to b- or c-hadrons with transverse momentum p_T larger than 5 GeV within $\Delta R < 0.3$ of the jet axis.

To model the production of single-top-quark events, which mostly contribute through the tW-channel, and the produc-

tion of $t\bar{t}H$, the same POWHEGBOX-v2 [31–34] settings, as used in the $t\bar{t}$+light/c-jets production, are used. The production of $t\bar{t}Z$ and $t\bar{t}W$ events is modelled using the MADGRAPH5_aMC@NLO 2.3.3 [29] generator at NLO. For all samples listed above, the NNPDF 3.0nlo [35] PDF sets are used and a top-quark mass of $m_{\text{top}} = 172.5$ GeV is set. The events are interfaced with PYTHIA8.230 [36] using the A14 tune [37] and the NNPDF 2.3lo set of PDFs [38] for the parton shower and hadronisation modelling.

The production of tZq and tWZ events is performed using MADGRAPH5_aMC@NLO v2.3.3, at LO and NLO in QCD respectively, in the 4FS with the `CTEQ6L1` PDF set [39] and using PYTHIA 8.212 for the parton shower.

Finally, the production of V+jets and diboson samples (VV) is simulated with different versions of the SHERPA [40] generator and the simulated events are matched with the SHERPA parton shower [41] using the MEPS@NLO prescription [42–45] with the set of tuned parameters developed by the SHERPA authors. All samples and their basic generation parameters are summarised in Table 1.

For all samples, except those generated with SHERPA, the decays of b- and c-hadrons are simulated using the EVTGEN programme [46].

4 Object definition

In this section, the reconstruction and definition of the physics objects are described, together with the additional corrections applied to each.

4.1 Physics objects

Electron candidates are reconstructed from energy deposits (clusters) in the electromagnetic calorimeter associated with reconstructed tracks in the inner detector. Candidates are selected with $p_{\text{T}} > 10$ GeV and $|\eta| < 2.47$, excluding the calorimeter transition region $1.37 < |\eta| < 1.52$. Electrons satisfy the `TightLH` [58] likelihood-based identification criterion and are required to match the PromptLeptonTagger working point `PLVLoose` [59]. They are further required to have $|z_0 \sin\theta| < 0.5$ mm and a d_0 significance $|\frac{d_0}{\sigma(d_0)}| < 5$, where the transverse impact parameter (d_0) is calculated relative to the beamline, and the longitudinal impact parameter (z_0) as the longitudinal distance between the primary vertex and the point where d_0 is measured.

Muon candidates are reconstructed from track segments in the various layers of the muon spectrometer and matched with tracks from the inner detector. The final muon candidates are refitted using the complete track information from both detector systems and must have $p_{\text{T}} > 10$ GeV and $|\eta| < 2.5$. Muons are required to satisfy the `Medium` quality requirements and match the PromptLeptonTagger working point `PLVLoose` [60]. Further requirements are $|\frac{d_0}{\sigma(d_0)}| < 3$, and $|z_0 \sin\theta| < 0.5$ mm.

Small-R jet candidates are reconstructed by clustering particle flow objects [61] using the anti-k_t algorithm [62,63] with a radius parameter of $R = 0.4$ and a four-momentum recombination scheme. The energy of the jet is corrected to the particle level by the application of a jet energy scale calibration derived from $\sqrt{s} = 13$ TeV data and simulation [64]. Baseline jets are required to have $p_{\text{T}} > 20$ GeV and $|\eta| < 2.5$. For pile-up rejection, jets with $p_{\text{T}} \in [20, 60]$ GeV and $|\eta| < 2.4$ are required to have a jet vertex tagger weight [65] larger than 0.5.

The b-tagging is the identification of jets that originate from the decay of b-hadrons using dedicated algorithms. A deep neural-network, called DL1r [66–69] is used. Small-R jets with a DL1r score above a certain threshold are defined as b-tagged jets. The pseudo-continuous (PC) b-tagging working point is used: each jet is classified with an integer from one to five depending on how many calibrated b-tagging working points (WP) the jet fulfils. The four calibrated DL1r WPs are 85%, 77%, 70% and 60%, each corresponding to the approximate average b-tagging efficiency in an inclusive $t\bar{t}$ MC sample. Jets not satisfying any WP are assigned a value of one, and this value is increased by one for every WP that they fulfil. The sum of the PC b-tagging over all jets in an event is defined as `sumPCBTag`. Jets satisfying the 70% WP are referred to as b-jets, while jets satisfying the 85% WP, but not the 70% WP, are classified as loose-b-jets.

Large-R jet candidates are formed by reclustering the small-R jets and tracks with a larger radius parameter of $R = 0.8$ using the anti-k_t algorithm [62,63]. The larger radius for track association allows more tracks from the targeted double b-hadron decays to be associated with the reclustered jet. The tracks in and around the small-R jet associated with the reclustered jet through ghost association [70,71] are selected with a loose track selection [72]. In this procedure, the p_{T} of the tracks is set to infinitesimal values, such that the "ghost" tracks can then be reclustered with the constituents of the reclustered jets with the appropriate radius parameter. Since the p_{T} of the tracks is infinitesimally small, they do not influence the reconstruction of the jet, allowing the use of additional tracks that leak outside the small-R jets.

To resolve the substructure within a large-R jet originating from a boosted $X \to b\bar{b}$ decay, which the small-R jet reconstruction fails to completely capture, additional information is extracted from the large-R jet by reconstructing track-subjets inside the large-R jet. The track-subjets are derived using the tracks that are ghost associated to each large-R jet as inputs to the exclusive-k_T method [73]. The selected tracks for a given jet are clustered using the k_T algorithm with a radius parameter of $R = 0.8$. The clustering stops when there are exactly two track clusters left.

Table 1 Nominal simulated signal and background event samples. The matrix element generator, PDF set, parton-shower (PS) generator and calculation accuracy of the cross section in QCD and EW used for normalisation are shown. MADGRAPH is abbreviated to MG

Process	Matrix element generator	PDF set	PS generator	Normalisation
$t\bar{t}a, a \to b\bar{b}$	MG_aMC@NLO v2.3.3	NNPDF3.0 NLO	PYTHIA 8.230	–
$tWa, a \to b\bar{b}$				
$t\bar{t}$ + jets	POWHEGBOX-v2	NNPDF3.0 NLO	PYTHIA 8.230	$(\text{NLO+NNLL})_{\text{QCD}}$ [47–53]
$t\bar{t} + b\bar{b}$	POWHEGBOX-Res	NNPDF3.1 NNLO	PYTHIA 8.244	–
Single-top	POWHEGBOX-v2	NNPDF3.0 NLO	PYTHIA 8.230	$(\text{NLO+NNLL})_{\text{QCD}}$ [54,55]
$t\bar{t}H$	POWHEGBOX-v2	NNPDF3.0 NLO	PYTHIA 8.230	$\text{NLO}_{\text{QCD+EW}}$ [56]
$t\bar{t}Z$	MG5_aMC@NLO v2.3.3	NNPDF3.0 NLO	PYTHIA 8.210	$\text{NLO}_{\text{QCD+EW}}$ [56]
$t\bar{t}W$	MG5_aMC@NLO v2.3.3	NNPDF3.0 NLO	PYTHIA 8.210	$\text{NLO}_{\text{QCD+EW}}$ [56]
tZq, tWZ	MG5_aMC@NLO v2.3.3	CTEQ6L1	PYTHIA 8.212	–
		NNPDF3.0 NLO		
Z/W + jets	SHERPA 2.2.11	NNPDF3.1 NNLO	SHERPA	NNLO_{QCD} [57]
Diboson	SHERPA 2.2.1	NNPDF3.1 NNLO	SHERPA	–
	SHERPA 2.2.2			

These clusters are used as the track-subjets associated with a given jet. For signal events, each track-subjet should originate from the decay of one b-hadron ideally. The associated large-R jet is required to satisfy $|\eta| < 2.0$ to account for their extended radius and the acceptance of the ID. Furthermore, each track-subjet is required to satisfy $p_{\text{T}} > 5\,\text{GeV}$ where the track-subjet p_{T} is estimated from the sum of its constituent tracks' four-momenta. The four-momentum of the large-R jet is defined as the sum of the four-momenta of its track-subjets.

In addition, secondary vertices (SV) inside the large-R jets are reconstructed to help the identification of b-hadrons. For this purpose, an algorithm that combines the track-cluster-based low-p_{T} vertex tagger (TC-LVT) [74] and the multiple-secondary-vertex finder algorithms (MSVF) [75] is used. The TC-LVT algorithm was developed for soft b-hadron tagging and optimised to reconstruct low-p_{T} b-hadron decays. The clustering algorithm from TC-LVT is used to identify displaced tracks not originating from the primary vertex. The MSVF algorithm is used to identify multiple SVs in the track cluster. The algorithm builds all two-track proto-vertices consistent with displaced tracks that are not compatible with a hadronic material interaction, a photon conversion, or the decay of long-lived light-flavoured hadrons. All displaced tracks reconstructed in the ID are used to build proto-vertices. Proto-vertices define track-to-track relations, since a single track can be associated with more than one proto-vertex. Each set of tracks that are mutually connected to each other forms a secondary vertex. After secondary vertices are formed, tracks not compatible with the vertex are removed, and the ambiguity caused by distant vertices sharing common tracks is resolved. Nearby vertices are also merged by the MSVF algorithm. Finally, reconstructed SVs are required to be ΔR-matched to a large-R jet. Further details and studies about the large-R jets can be found in Ref. [76].

In contrast to b-tagging, the B-tagging is the identification of pairs of b-jets that are too close to be resolved and identified individually. For this purpose the DeXTer tagger is used. It is a double b-tagger based on a deep sets neural network (NN) architecture designed to do flavour tagging of merged reconstructed jets [77] and uses information of the SVs and jet kinematics. This is done in two transverse momentum ranges: a low p_{T} range between 20 and 200 GeV and a high p_{T} one, above 200 GeV. Two working points are defined: the 0–40% tagging interval is referred to as `Tight` WP, and the `Loose` WP is defined by the inclusive 40–60% tagging interval. A sample of Z+jets and $t\bar{t}$ events is used to measure the DeXTer efficiency in data, and to derive B-tagging and b-mistagging rate correction factors for the simulated events. Large-R jets satisfying the `Tight` WP are referred to as B-jets.

The missing transverse momentum $E_{\text{T}}^{\text{miss}}$ measures the event momentum imbalance in the transverse plane of the detector. It is defined as the magnitude of the negative vector sum of p_{T} for all selected and calibrated physics objects in the event, with an extra term added to account for soft energy that is not associated with any of the selected objects. This soft term is calculated from inner detector tracks matched to the primary vertex to make it more resilient to pile-up contamination [78]. The $E_{\text{T}}^{\text{miss}}$ computation is based on the momenta of the objects defined previously, and after applying the overlap removal procedure defined in the next section.

4.2 Corrections to physics objects

The overlap removal is the procedure followed to prevent double-counting of objects. First, electrons that share a track with a muon are removed. To prevent double-counting of electron energy deposits as jets, the closest small-R jet within $\Delta R < 0.2$ of a selected electron is removed. If the nearest jet surviving that selection is within $\Delta R = 0.4$ of the electron, the electron is discarded. To reduce the background from muons from heavy-flavour decays inside jets, muon candidates are required to be separated by $\Delta R > 0.4$ from the nearest small-R jet, removing the muon if the jet has at least three associated tracks, and removing the jet otherwise. This avoids an inefficiency for high-energy muons undergoing significant energy loss in the calorimeter.

To avoid double-counting of jets, the jet overlap removal is done as follows. First, every small-R jet is tested to see if it is eligible to be DeXTer-tagged. This requires the small-R jet to have $p_{\mathrm{T}} > 20$ GeV and be isolated, meaning it is the only constituent of its reclustered jet [79] with the anti-k_t algorithm and radius parameter $R = 0.8$. These jets are then tested by the DeXTer tagger: if a small-R jet passes the `Loose` working point selection, it is defined as a B-tagged large-R jet and removed from the small-R jet list. Otherwise, it is kept as a small-R jet. Thus, this first step gives two jet lists: the DeXTer-tagged large-R jets and the small-R jets, which are either not eligible for DeXTer tagging or fail the tagger. Finally, the jet overlap removal procedure with leptons is repeated for large-R jets using $\Delta R = 0.8$.

The μ-in-jet p_{T} correction is the procedure of adding the muons reconstructed inside of a b-jet to the four-momentum of the respective b-jet. Around 20% of all b-hadron decays produce a low-momentum or soft muon inside of the resulting jet, but those soft muons are removed in the overlap removal as described above. This correction recovers the original energy of those b-jets and reduces biases from the invariant masses calculated with them. The soft muons used are required to have $p_{\mathrm{T}} > 4$ GeV and $|\eta| < 2.5$, and fulfil the `Medium` soft muon quality requirement.

In the case of the DeXTer-tagged jet, the μ-in-jet p_{T} correction is carried out as follows. First, the soft muons are matched to track-subjets within an angular distance of $\Delta R < 0.3$. At most the two highest p_{T} soft muons are taken into account for each track-subjet, and any muon is only matched once to the closest subjet. At last, the matched muons are added to the four-momentum of the track-subjet.

5 Event selection

Only events recorded with a single-electron [80] or single-muon trigger [81] under stable beam conditions and for which all detector subsystems were operational are considered [82]. Single-lepton triggers with p_{T} thresholds varying from 20 to 140 GeV, depending on the year, lepton flavour, isolation requirement and luminosity, are combined in a logical OR to increase the overall efficiency. The triggers with the lower p_{T} thresholds include isolation requirements on the lepton candidate, resulting in inefficiencies at high p_{T} that are recovered by the triggers with higher p_{T} thresholds.

5.1 Preselection

Events are required to have exactly two leptons (electrons, muons, or both) with opposite charge, satisfying the criteria defined in Sect. 4. Since single-lepton triggers are used, at least one of the two reconstructed leptons is required to have a $p_{\mathrm{T}} > 27$ GeV and match a lepton with the same flavour reconstructed by the trigger algorithm within ΔR of 0.15. The chosen p_{T} threshold ensures a fully efficient trigger for the whole Run 2 period. In the ee and $\mu\mu$ channels, the dilepton invariant mass must be above 15 GeV and outside the Z boson mass window 83–99 GeV. Further suppression of the background is achieved by requiring at least three jets (either large-R or small-R) with at least one of which being b-tagged using the DL1r 85% WP. The fraction of signal events in the preselection region is negligible for all masses.

5.2 Signal and control regions

After preselection, the data sample is dominated by background from $t\bar{t}$ events. To take advantage of the high jet and b-object multiplicities of the $t\bar{t}a$ signal process, events are classified into non-overlapping regions based on the total number of B-jets and b-jets. Some of the regions also require the presence of at least one loose (and not tight) b-jet (small-R jets tagged with the DL1r 85% WP but failing to meet the 70% WP). The name of every signal region (SR) or control region (CR) includes the number of B-jets followed by "B" and of b-jets followed by "b". The names of those regions requiring at least an extra loose b-jet indicate it in their name with "+1bL". Due to the high b-jet multiplicity of the signal, only regions with at least three b-objects are considered as signal regions (B-jets count as two b-objects). To maximise the signal sensitivity, signal events are classified into two boosted regions (SR 1B1b+1bL and SR 1B2b) and two resolved regions (SR 0B3b and SR 0B4b). The loose b-tagged jet in one of the signal regions is required to suppress $t\bar{t}$+light events. The complementarity between boosted and resolved regions is illustrated in Fig. 2, which shows the invariant mass of the B-jet in SR 1B2b and the invariant mass of the pair of b-jets with the largest p_T in SR 0B4b for different values of the pseudoscalar mass. Regions containing one B-jet are particularly relevant in the boosted regime ($m_a < 30$ GeV). Regions with no B-jets and a high b-jet multiplicity are more powerful in the resolved regime ($m_a > 30$ GeV).

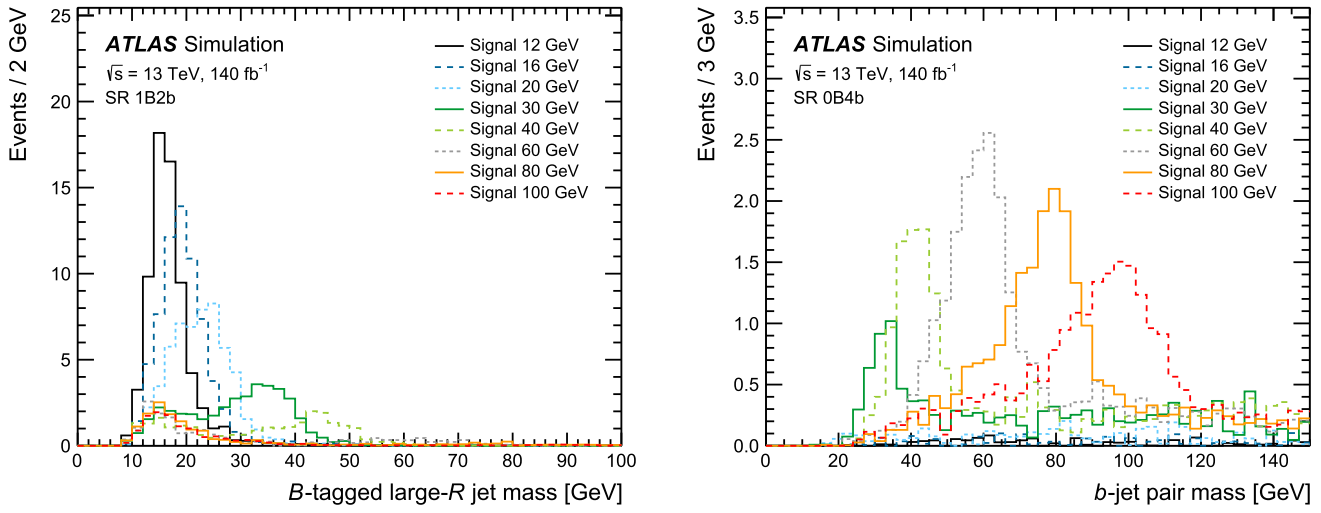

(a) (b)

Fig. 2 Invariant mass of the (**a**) B-jet in SR 1B2b and of the (**b**) pair of b-jets with the largest p_{T} in SR 0B4b for various values of m_a. The distributions are normalised according to the predicted m_a-dependent theoretical cross sections with a Yukawa coupling of the a-boson to the top quark of 0.5

Table 2 Overview of the jet multiplicities considered per region in the fit

Region	Large-R jets	Small-R jets	B-jets	b-jets	Loose b-jets
SR 0B4b	≥ 0	≥ 4	$= 0$	≥ 4	–
SR 0B3b	≥ 0	≥ 3	$= 0$	$= 3$	–
SR 1B2b	≥ 1	≥ 2	$= 1$	≥ 2	–
SR 1B1b+1bL	≥ 1	≥ 2	$= 1$	$= 1$	≥ 1
CR 0B2b+1bL	≥ 0	≥ 3	$= 0$	$= 2$	≥ 1

In addition to the four signal regions described above, a control region is included in the fit to improve the $t\bar{t}$+$\geq$1c normalisation (Sect. 8). The control region (CR 0B2b+1bL), orthogonal to all four signal regions, is composed of events with no B-jets and exactly two b-jets, as well as at least one additional loose (and non-tight) b-jet. Similarly to the SR, the loose b-tagged jet is required to suppress $t\bar{t}$+light events that would otherwise dominate the control region. Finally, events entering the CR are required to have a sum of the pseudo-continuous b-tagging scores between 12 and 15. The number of b-jets in the 0B3b, 1B1b+1bL and 0B2b+1bL regions is exclusive, while it is inclusive in the 0B4b and 1B2b regions. Table 2 summarises the selections for each region, which are applied in addition to the previously mentioned preselection requirements.

6 Background estimate

Data-driven corrections are derived for the $t\bar{t}$ Monte Carlo simulation, the main background process in this search. These corrections are derived to improve the description of the rates of $t\bar{t}$ plus heavy flavour jets and the transverse momenta of lepton and jets observed in data, using a method similar to the one developed for other ATLAS searches [83–85]. The corrections are derived in very inclusive control regions where the contamination of signal is predicted to be below 1% for all considered pseudoscalar mass hypotheses. The region of choice satisfies the preselection requirements described in Sect. 5.1, with an extra requirement of at least two b-jets and no B-jets. Additionally, to suppress the Z+jets contribution, only the different lepton flavour ($e\mu$) region is considered.

The first correction targets the production rate of heavy-flavour jets: c-jets and b-jets. It was observed in previous ATLAS and CMS analyses [86–88] that the rate of $t\bar{t}$+HF events is underestimated in MC simulation. Due to the high b-object multiplicity of the $t\bar{t}a$ signal, these HF events represent a large fraction of the $t\bar{t}$+jets background in the signal regions, and therefore the MC simulation must be corrected. To have a more accurate flavour composition, an event reweighting procedure is applied based on the `sumPCBTag` distribution. Figure 3a shows how the $t\bar{t}$+light production is dominant at low values of `sumPCBTag`, while the $t\bar{t}$+HF

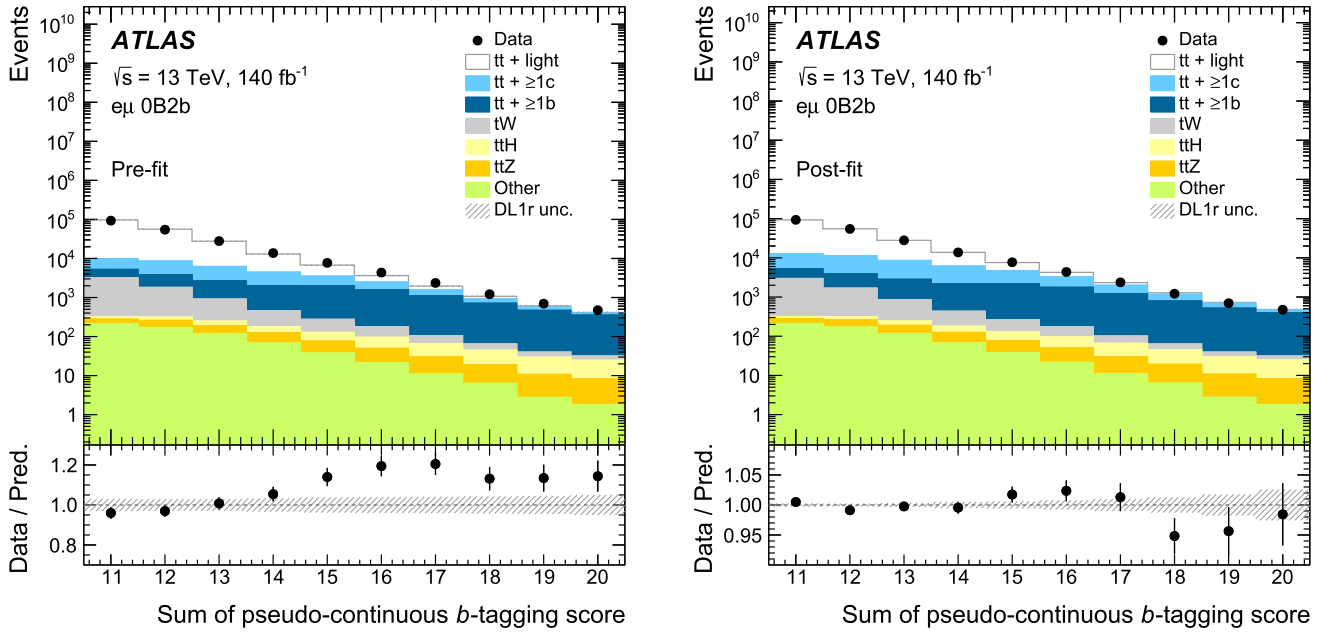

Fig. 3 Comparison of the data versus MC distribution of the sum of the pseudo-continuous b-tagging score of all the jets per event (**a**) before and (**b**) after applying the normalisation factors extracted from the heavy-flavour correction fit

Table 3 Normalisation factors for the three $t\bar{t}$+jets HF categories resulting from the likelihood fit performed using the `sumPCBTag` distribution

HF category	Norm. factor
$t\bar{t}+$ light, tW	0.91 ± 0.03
$t\bar{t}+\geq 1c$	1.58 ± 0.14
$t\bar{t}+\geq 1b$	1.13 ± 0.07

production populates the tail of the distribution. The correction procedure consists in deriving three normalisation factors: one for each component, using a likelihood fit to the `sumPCBTag` MC distributions compared with data. In this fit, DL1r b-tagging systematic uncertainties (detailed in Sect. 9) are included. Figure 3b shows the improved agreement after the fit. The normalisation factors and their corresponding uncertainties are shown in Table 3.

This procedure also corrects the distribution of the number of jets (inclusive of all jet types) per event, N_{jets}, which was also observed to be mismodelled in the simulation. Figure 4 shows the corresponding distribution, before and after applying the normalisation factors from Table 3. In the following, in all Figures and Tables, the category "Other" includes the following minor background processes: Z+jets, $t\bar{t}W$, tq, tZ, tWZ, WW, ZZ, WZ and W+jets.

The second correction targets the transverse momenta of the jets and leptons originating from the decay of top quark/antiquark, a quantity that was also observed to be mismodelled by current $t\bar{t}$ 5FS MC generators. The disagreement between data and MC persists even after applying the $t\bar{t}$+HF correction. To improve the agreement between data and MC for these variables, a kinematic reweighting factor for the $t\bar{t}+\geq 1c$, $t\bar{t}$+light, and tW components is derived from the data/MC ratio, after subtracting other background components from the data. These mismodellings are assumed to be independent of the flavour of the extra radiation, and applied equally to $t\bar{t}$+light, $t\bar{t}+\geq 1c$, and tW.

The event hardness or H_{T}, which is defined as the scalar sum of the p_{T} of all the jets and leptons in the event, is largely correlated with the total number of jets in the event, as every additional jet in the event shifts H_{T} to larger values. Performing the kinematic reweighting directly with H_{T} would therefore spoil the data/MC agreement achieved after the HF correction to the number of jets distribution shown in Fig. 4. To reduce the N_{jets} dependency, a new variable, $H_{\text{T}}^{\text{red}}(n)$, is defined:

$$H_{\text{T}}^{\text{red}}(n) = H_{\text{T}} - (n-3)\Delta H_{\text{T}}(n),$$

where n is the number of jets (small-R and large-R jets, with a minimum of three jets) and $\Delta H_{\text{T}}(n)$ is the average offset in H_{T} caused by the addition of each extra jet to the event. Correction factors are derived over a binned $H_{\text{T}}^{\text{red}}$ distribution, and the results are fitted using a continuous hyperbolic function which is later used for the MC reweighting. Figure 5 shows the H_{T} distribution before and after applying the

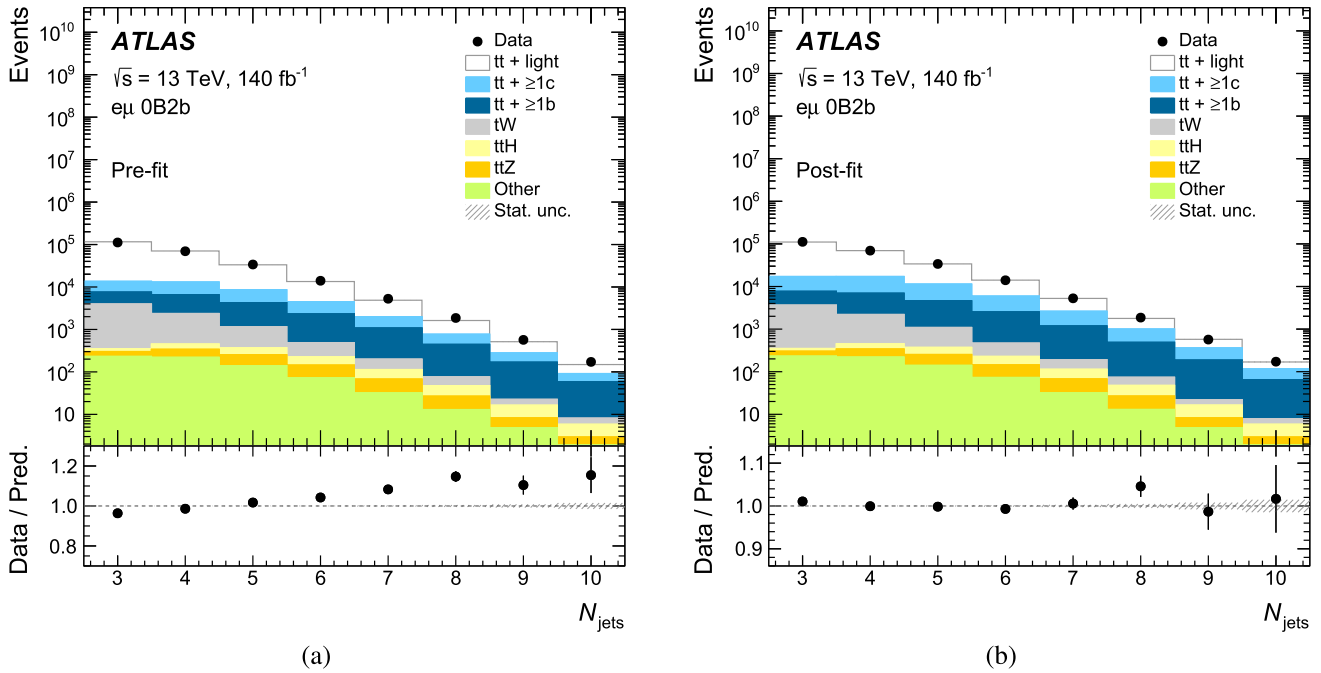

Fig. 4 Comparison of the data versus MC N_{jets} distribution (**a**) before and (**b**) after applying the $t\bar{t}$+jets normalisation factors extracted from the heavy flavour correction fit. Only statistical uncertainties are shown

correction. Similar improvements are observed for individual leptons and jets. No significant changes in the number of jets distribution are observed after the kinematic corrections are applied. Following the same procedure, dedicated kinematic reweighting corrections are derived for the alternative $t\bar{t}$+light, $t\bar{t}$+$\geq$1c, and tW samples employed in the evaluation of systematic uncertainties described in Sect. 9. Residual differences between data and the MC are taken into account in the analysis fit by including free-floating individual normalisations for the various $t\bar{t}$+jets background contributions.

7 Analysis strategy

The analysis uses various machine learning (ML) algorithms to improve the sensitivity to the target signal. First, two different boosted decision trees (BDTs) are trained to identify the jets originating from the decay of the top quark and antiquark and the jets originating from the pseudoscalar decay. Second, a mass-parameterised NN is trained for signal/background discrimination in each of the SRs described in Sect. 5.2. The final fit uses the NN output score distribution in each of the four SRs and the `sumPCBTag` distribution in the CR. In addition to the signal strength μ, three normalisation factors, corresponding to the main background contributions, are left to freely float in the fit. Figure 6 shows a diagram summarising the ML approach followed in the analysis as well as the CR and SRs used in the final fit. Further details on each step are given in the following.

7.1 Event reconstruction BDTs

Two different BDTs are trained to do partial event reconstruction. One targets the identification of the lepton-jet pairs associated with the top quark/antiquark decays, while the other identifies the pair of jets from the pseudoscalar decay. The two BDTs use the five leading small-R jets, together with the two charged leptons in the case of the top quark/antiquark BDT, and in each case select the pair of jets or the lepton/jet pair most likely to correspond to the pseudoscalar or the top quark/antiquark, respectively. Both BDTs were designed to reconstruct resolved topologies, thus they do not use large-R track-jets. Also, no attempt to reconstruct the two neutrinos from the top quark/antiquark decay is made. The two BDTs are trained using all signal samples inclusively, such that they are generic and valid for all considered masses. During the BDT training process, target labels for each jet are assigned based on a one-to-one matching between reconstructed jets at the detector level and parton-level b-quarks/leptons. Consequently, a reconstructed jet/lepton is assigned as originating from a (anti-)top quark, or pseudoscalar decay candidate based on the aforementioned generator information.

The BDT targeting the top quark/antiquark decay attempts to pair each lepton with its corresponding b-jet, considering each lepton in turn. For this, the BDT receives as input several kinematic variables that depend on the tag lepton/jet pair (jl-pair), such as its invariant mass or transverse momentum, or the separation angle between the lepton and the jet. It also uses information about the lepton and jet candidates them-

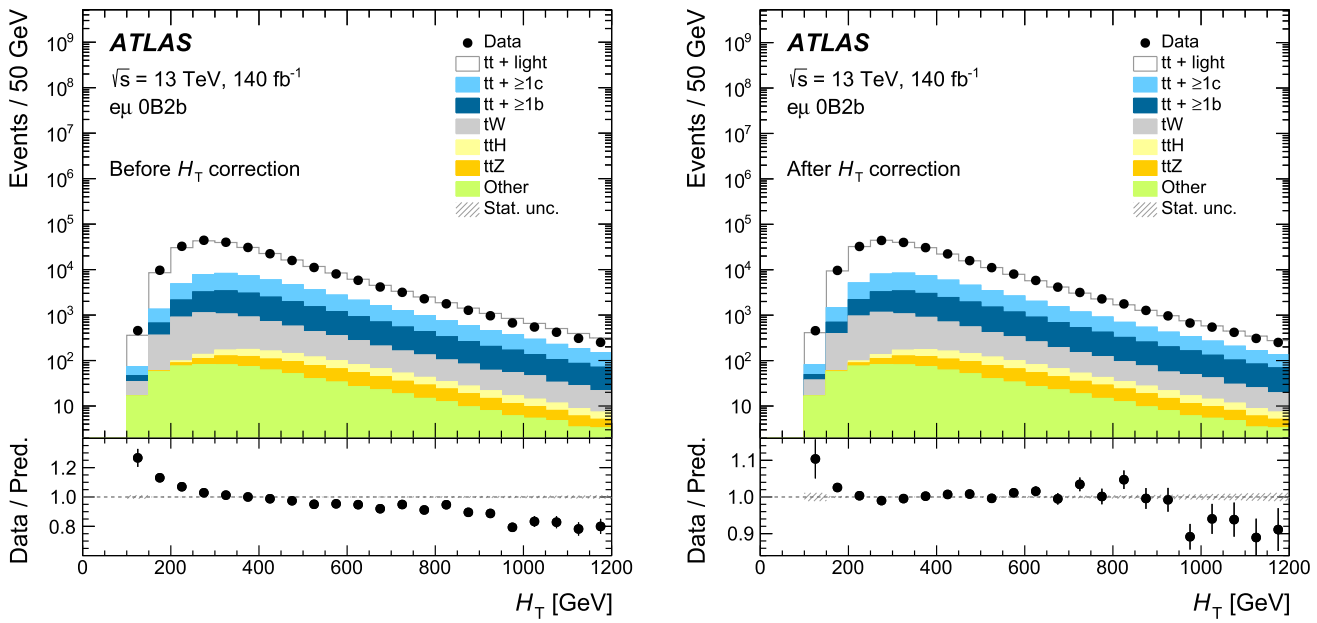

(a) (b)

Fig. 5 Comparison between data and MC of the H_T distribution (**a**) before and (**b**) after correcting it using H_T^{red}. Only statistical uncertainties are shown

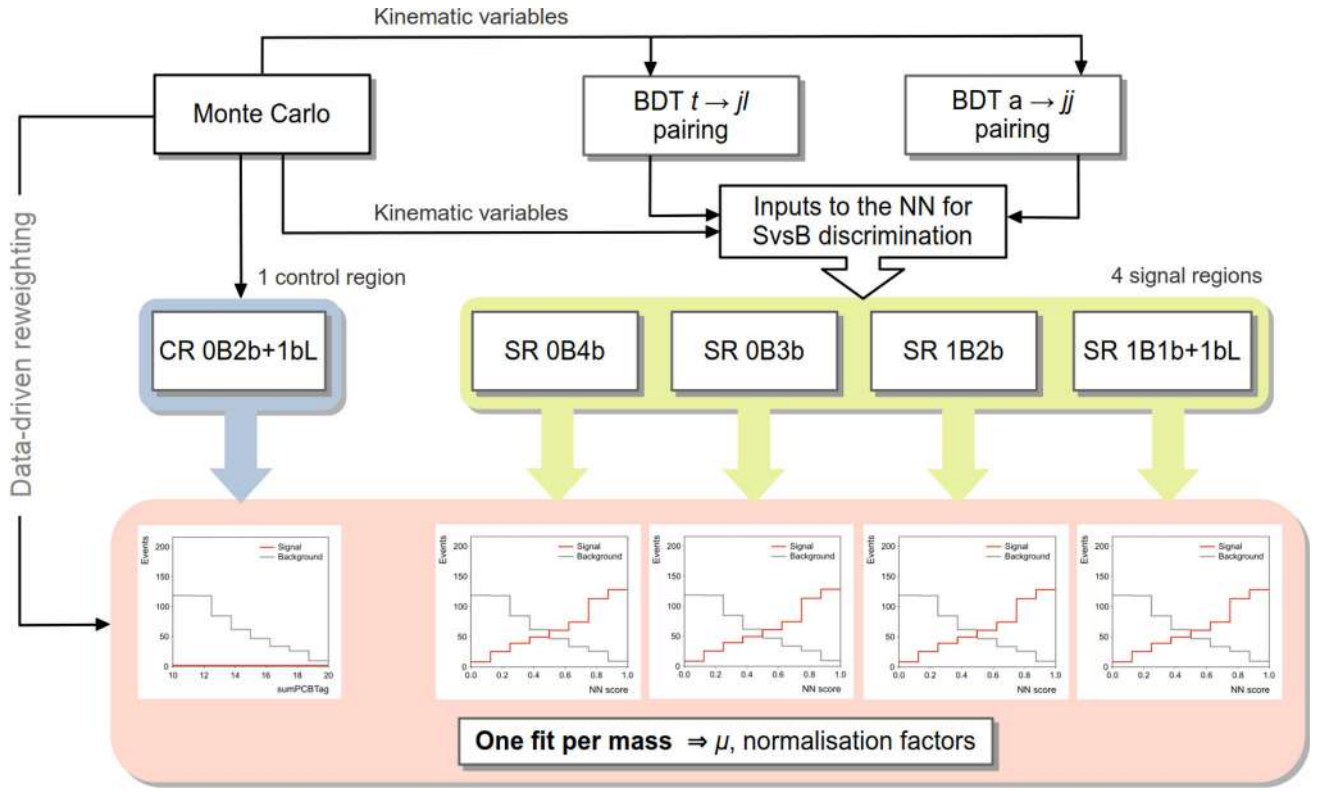

Fig. 6 Diagram of the analysis strategy, illustrating the data-driven corrections, jet/lepton and dijet pairings by two BDTs and the NN for signal versus background discrimination. The CR and SRs are used in the final fits to extract the signal strength (μ) as well as normalisation factors for the main backgrounds

selves, such as their pseudorapidity and transverse momenta, or the jet index indicating in decreasing order the hardness of the jets. In addition, the BDT uses information from the auxiliary jl-pair built with the lepton that is not being evaluated, together with information from the top/antitop system formed by the tag and auxiliary jl-pairs, and variables that refer to the full event. In a similar way, the BDT targeting the pseudoscalar decay receives various kinematic variables connected to the pair of two jets, jj-pair, as its mass or transverse momentum, together with information about the jets themselves or about the overall event. The full list of variables used by each BDT is shown in Table 4.

For the training of both BDTs, generator information is used to define the targets (b-quarks and leptons from the decays of the top quark, top antiquark and pseudoscalar a) and to identify the correct permutations at detector level, which are used as signal (or target) during the training, while all wrong permutations are used as background. A mix of signal and $t\bar{t}$ samples is used during the training of both BDTs. In both cases, two sets of BDTs are trained using k-2 fold training to avoid biases. The BDT trained with odd events is applied to even events and vice versa. The training is performed with the TMVA package of ROOT [89].

Following the training of both BDTs, they are applied to data and MC as follows. For the top quark/antiquark BDT, the lepton/jet permutation with the highest BDT score is identified for each lepton as the most likely jl-pair and the selected jet is assigned to the top quark or antitop quark decay depending on the lepton charge. If both leptons are initially assigned to the same jet, only the one with the highest BDT score keeps the assignment, while the other lepton is reassigned to the second most likely jet in terms of BDT score. In a similar way, for the pseudoscalar BDT, the permutation of two jets with the highest BDT score is selected and the two corresponding jets are assigned to the pseudoscalar decay. The selected jl- and jj-pairs are used to define related variables, such as the top-quark or pseudoscalar reconstructed invariant mass or separation angles, that are later used as input by the signal-versus-background discrimination neural networks. Figure 7 shows the prefit data/MC comparison of the reconstructed mass of the lb-pair selected by the top-quark BDT and of the jj-pair selected by the pseudoscalar BDT in SR 0B3b, the signal region with the largest statistics.

7.2 Signal-versus-background discriminating neural networks

As described in Sect. 5.2, events are divided into four signal regions according to their B- and b-jet multiplicity to better separate signal from background. The four signal regions used in the final fit are SR 0B4b, SR 0B3b, SR 1B2b and SR 1B1b+1bL. Independent NNs are trained individually per region to separate signal from background.

To make better use of the MC samples in the training, five different trainings are performed independently per region, where 80% of the events in the region constitute the training sample and the remaining 20% are used as the validation sample. An appropriate distribution of events in the various samples guarantees that no event is used both in the training and the evaluation of the NNs.

Each NN contains two hidden layers with twice as many nodes as the input layer, connected by Rectified Linear Unit (ReLU) activation functions. The final layer is a single node, normalised by a sigmoid function. The dropout for every layer is set to 0.3. To avoid overtraining, early stopping is implemented when the validation loss function does not improve during the last four epochs. The training is done using PyTorch 1.13.1 [90], and each of the NNs combines basic four-momentum information with high-level variables, such as invariant masses or angular distances, as well as relevant variables from the BDTs described in Sect. 7.1. The full list of input variables depends slightly on the region, given the slightly different signal topologies per region. Table 5 shows the overall list of input variables used by the NNs. Some of the most important variables in the NNs are $H_{\mathrm{T}}^{\mathrm{jets}}$, the invariant mass of two small-R jets or the mass and p_{T} of the large-R jet, among others.

All NNs are mass-parameterised, meaning that they receive the mass hypothesis as input during the evaluation. For the training, background MC samples are randomly assigned a mass from the grid of generated signal samples, while appropriate mass values are assigned to the signal events. Once the NNs are trained, the data scores are evaluated for each value of m_a considered in the analysis. In each SR, the resulting NN score is the distribution used in the profile likelihood fit, as discussed in the next section. Figure 8 shows the prefit distributions of the four NN scores corresponding to the 30 GeV mass hypothesis.

8 Statistical treatment

To test for the presence of a $t\bar{t}a$ signal, for each mass hypothesis, a binned maximum-likelihood fit to the data is performed simultaneously in all SRs and the CR (Sect. 5.2). In each SR, the input to the fit is the corresponding NN distribution described in Sect. 7.2, evaluated at the appropriate mass hypothesis. In the CR, the input to the fit is the `sumPCBTag` distribution. The parameter of interest is the signal strength, μ, a multiplicative factor to the cross section of the signal process. In addition to the signal strength μ, the fit includes three additional free parameters that work as scale factors to the normalisation for the three main background components: $k(t\bar{t}+\text{light}, tW)$, $k(t\bar{t}+{\geq}1c)$, and $k(t\bar{t}+{\geq}1b)$. To estimate the signal strength, a binned likelihood function $\mathcal{L}(\mu, \theta)$ is used,

Table 4 Input variables used in the (a) top quark/antiquark reconstruction BDT and (b) pseudoscalar reconstruction BDT

(a)

Top quark/antiquark reconstruction BDT

Object	Variables
Full event	N_{jets}, $N_{b\text{-jets}}$
Lepton (tag, aux.)	p_{T}, η
Jet (tag, aux.)	p_{T}, η, PC b-tag, jet index
jl pair (tag, aux.)	m, p_{T}, η, ΔR
$t\bar{t}$ pair	m, p_{T}, η, ΔR, $\Delta\phi$
jj pair	ΔR

(b)

Pseudoscalar reconstruction BDT

Object	Variables
Full event	N_{jets}, $N_{b\text{-jets}}$, `sumPCBTag`
Jet (1st, 2nd)	p_{T}, η, PC b-tag, jet index
jj pair	m, p_{T}, η, E, ϕ, ΔR

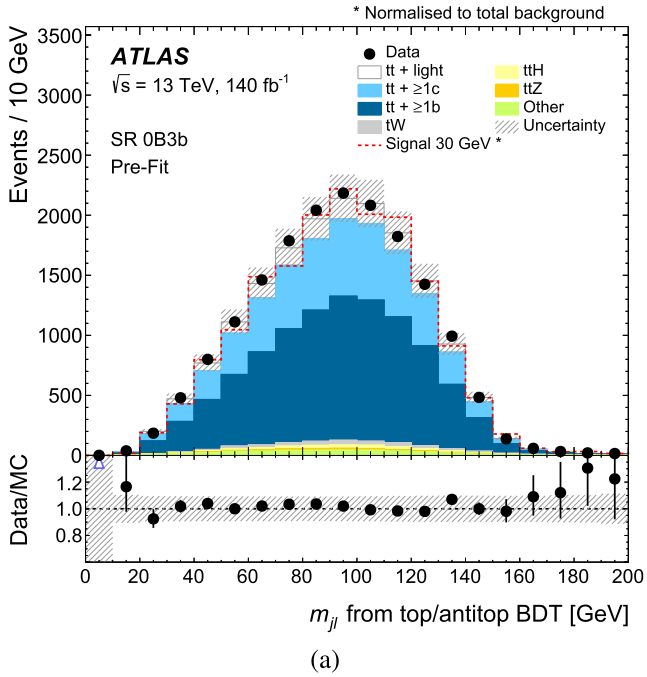

(a)

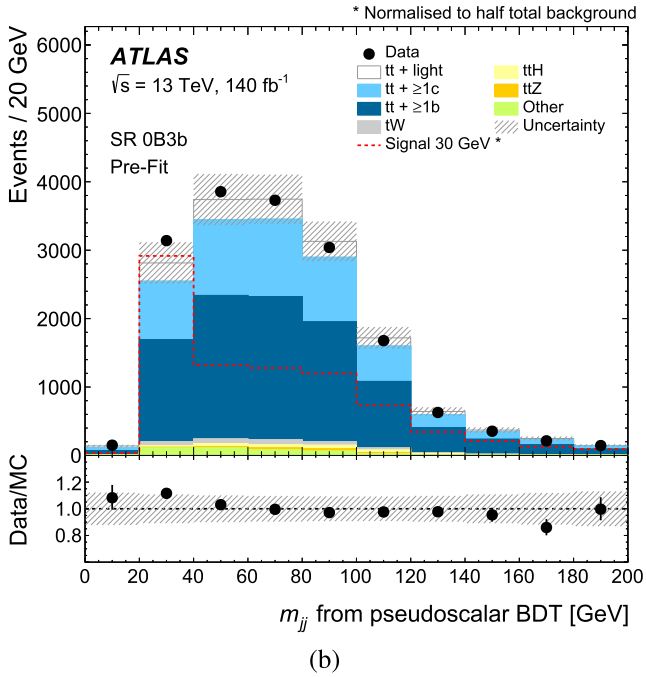

(b)

Fig. 7 Distribution (**a**) of the antitop-quark m_{jl} and (**b**) pseudoscalar m_{jj} selected by the top quark and pseudoscalar BDTs, respectively in SR 0B3b before the fit. The dashed line shows the distribution of the 30 GeV signal normalised to the total or half the total number of events in the region. The band displays the total pre-fit uncertainty

Table 5 List of input variables of the signal-versus-background discrimination NN. The distributions corresponding to both the pair with the maximum p_{T} and minimum ΔR are included for bb variables. Angular variables with one b or one B use the pair with the minimum ΔR. The m_{bbbb} and m_{bbb} variables correspond to the combination with the maximum scalar sum of p_{T}

Object	Variables
Full event	N_{jets}, $H_{\text{T}}^{\text{jets}}$, $E_{\text{T}}^{\text{miss}}$
BDT $t \to jl$	Score, p_{T}^{jl}, ΔR_{jl}, $\Delta\eta_{jl}$, $\Delta\phi_{jl}$, jet index
BDT $a \to jj$	Score, p_{T}^{jj}, η_{jj}, m_{jj}, ΔR_{jj}, $\Delta\eta_{jj}$, $\Delta\phi_{jj}$, jet index
Leptons	ΔR_{ll}, $\Delta\eta_{ll}$, $\Delta\phi_{ll}$, $\Delta\phi_{E_{\text{T}}^{\text{miss}},l}$, $\Delta R_{ll,bb}$, $\Delta R_{ll,B}$, $\Delta R_{ll,b}$
Large-R jets	p_{T}, η, m, ΔR_{Bb}, $\Delta\phi_{E_{\text{T}}^{\text{miss}},B}$
Small-R jets	p_{T}^{bb}, m_{bb}, m_{bbb}, m_{bbbb}, ΔR_{bb}, $\Delta\eta_{bb}$, $\Delta\phi_{bb}$, $\Delta\phi_{E_{\text{T}}^{\text{miss}},b}$
	p_{T}, η, PC b-tag

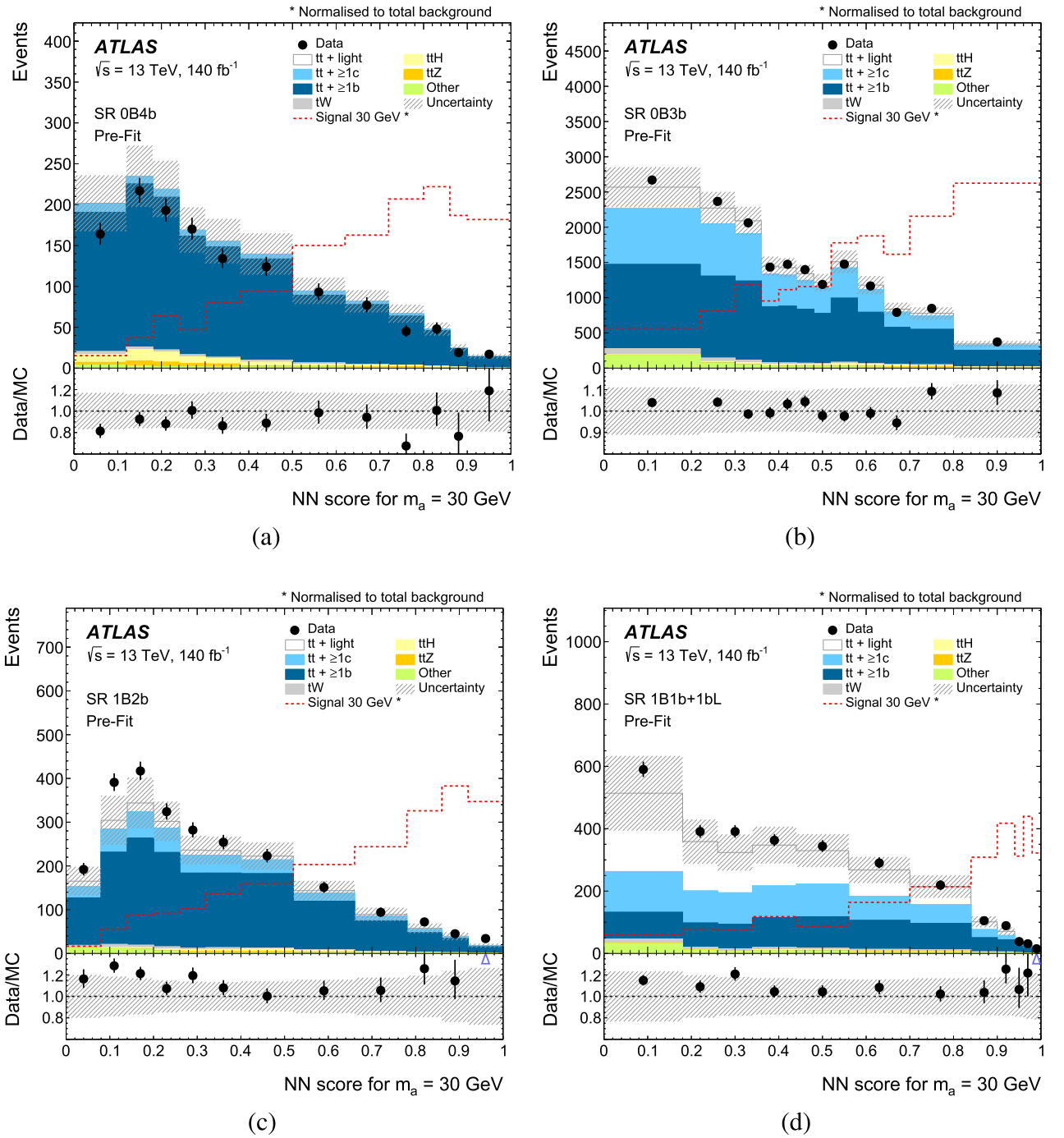

Fig. 8 Pre-fit distributions corresponding to the NN output score of (**a**) SR 0B4b, (**b**) SR 0B3b, (**c**) SR 1B2b and (**d**) SR 1B1b+1bL for the 30 GeV mass hypothesis fit. The dashed line shows the distribution of signal normalised to the total number of events in each region. The band displays the total pre-fit uncertainty. Arrows appearing in the bottom panels indicate the ratio being outside the displayed range

$$\mathcal{L}(\mu,\theta) = \prod_{i}^{N} \frac{(E[n_i(\mu,\theta)])^{n_i}}{n_i!} e^{-E[n_i(\mu,\theta)]} \prod_{\theta_j \in \theta} \rho(\theta_j|\tilde{\theta}_j).$$

The function is constructed as a product of Poisson probability terms with one Poisson term included for every bin i of the NN distribution in the analysis regions. The binning of the NN distributions for each signal is chosen to provide a good separation of signal and background while maintaining a stable performance of the fit. The expected number of events, $E[n_i(\mu,\theta)]$, in each bin, n_i, is a function of μ,

and a set of nuisance parameters, θ. The nuisance parameters encode effects from the normalisation of backgrounds, including the systematic uncertainties and one parameter per bin to model statistical uncertainties in the simulated samples. Unlike the free-floating parameters, all nuisance parameters are constrained by prior distributions, $\rho(\theta|\tilde{\theta})$, which follow Gaussian, log-normal, or Poisson distributions centred around their nominal values, $\tilde{\theta}$. This procedure allows the reduction of the impact of the uncertainties by taking advantage of the separated populations of signal and background. The best-fit value of the signal strength is obtained by performing a fit to the data under the signal-plus-background hypothesis, maximising $\mathcal{L}(\mu, \theta)$ over μ and θ. To set upper limits on μ, the following test statistic is used:

$$\tilde{q}_\mu = \begin{cases} -2\ln \dfrac{\mathcal{L}\left(\mu, \hat{\hat{\theta}}(\mu)\right)}{\mathcal{L}\left(0, \hat{\hat{\theta}}(0)\right)} & \hat{\mu} < 0, \\ -2\ln \dfrac{\mathcal{L}\left(\mu, \hat{\hat{\theta}}(\mu)\right)}{\mathcal{L}\left(\hat{\mu}, \hat{\theta}\right)} & 0 \le \hat{\mu} \le \mu, \\ 0 & \hat{\mu} > \mu. \end{cases}$$

The values of the signal strength and nuisance parameters that maximise the likelihood function are represented by $\hat{\mu}$ and $\hat{\theta}$, respectively. For a given value of μ, the values of the nuisance parameters that maximise the likelihood function are represented by $\hat{\hat{\theta}}(\mu)$. This test statistic measures the compatibility of the observed data with the background-only hypothesis ($\mu = 0$), represented by the p-value, and is estimated by integrating the distribution of $\tilde{q}_0$ based on the asymptotic formula in Ref. [91]. The test statistic is set to zero for $\hat{\mu} > \mu$, as this case indicates that the μ hypothesis is compatible with the observed data and cannot be rejected. Upper limits on μ are derived by using $\tilde{q}_\mu$ in the $\mathrm{CL_s}$ method [92,93].

The systematic uncertainties, including those derived from MC samples, can show fluctuations due to generator weights or statistical variations. To ensure the quality of the templates and the stability of the fit, smoothing algorithms are applied to the histograms before the fit. In addition, systematic uncertainties are pruned to reduce computing time. Only uncertainties with an effect greater than 1% are included in the fit. This is done separately for shape and normalisation effects.

9 Systematic uncertainties

Various sources of systematic uncertainties are considered. Each systematic uncertainty is introduced as a nuisance parameter (NP) in the statistical analysis described in Sect. 8. Section 9.1 describes all experimental uncertainties, related to the luminosity and pile-up or the reconstruction and identification of jets and leptons. They are applied to all MC samples equally and their effects are treated in a correlated way across all four SRs and the CR in the final fit. The signal and background modelling uncertainties are detailed in Sect. 9.2, and can be different depending on the process. They are implemented as decorrelated between regions, given their different coverage of phase spaces, and decorrelated between signal and background samples in the fit.

9.1 Experimental uncertainties

Luminosity and pile-up modelling. The uncertainty in the integrated luminosity for the full Run 2 data sample is 0.83% [24], obtained using the LUCID-2 detector [21] for the primary luminosity measurements. A variation in the pile-up reweighting of simulated events is included to cover the uncertainty in the ratio of the simulated and measured distribution of inelastic cross sections.

Leptons. Uncertainties associated with leptons are related to the trigger, reconstruction, identification and isolation, as well as the lepton energy or momentum scale and resolution. The reconstruction, identification, and isolation efficiency of electrons and muons, as well as the efficiency of the trigger used to record the events, differ slightly between data and simulation, and is corrected by dedicated scale factors. Efficiency scale factors are measured using tag-and-probe techniques on $Z \to ll$ data and simulated samples [58,60], and are applied to the simulation to correct for differences. Additional sources of uncertainty originate from the corrections applied to adjust the lepton momentum scale and resolution in the simulation to match those in data, measured using $Z \to ll$ and $J/\psi \to ll$ events [58,60].

Jets. Uncertainties associated with jets arise from the efficiency of pile-up rejection by the jet vertex tagger (JVT), from the jet energy scale (JES) and resolution (JER), and from the different flavour-tagging algorithms used, DL1r and DeXTer. Scale factors are applied to correct for discrepancies between data and MC for JVT efficiencies, and are estimated by using $Z \to \mu\mu$ with tag-and-probe techniques [65]. The jet energy scale and its uncertainty are derived by combining information from test-beam data, LHC collision data and simulation [64]. The jet energy resolution is measured in Run 2 data and simulation as a function of jet p_{T} and rapidity using dijet events.

To correct flavour-tagging efficiencies in simulated samples to match those measured in data, scale factors are derived. They are calculated as a function of p_{T} for b-jets, c-jets, and light jets separately in dedicated calibration analyses. For b-jet efficiencies, $t\bar{t}$ events in the dilepton topology are used, exploiting the very pure sample of b-jets arising from the decay of the top quarks [67]. For c-jet mistag rates, $t\bar{t}$ events in the single-lepton topology are used, exploiting c-jets from the hadronically decaying W boson [68].

The negative-tag method is used in Z+jets events [69] for light-jets mistag rates. The use of DeXTer introduces additional scale factors to correct for the differences in efficiency between simulated samples and data. The scale factors for DeXTer are derived as a function of p_{T} for B- and b-jets. The calibration measurements with data are performed using both $t\bar{t}$ and Z+jets events simultaneously to measure B-jet tagging and b-jet mistagging efficiency in data. Nevertheless, the DeXTer uncertainties are provided with conservative error bands, leaving the calibration to be performed in situ in the final fit of the analysis. Further details on the methodology can be found in Refs. [77,77].

Missing transverse momentum. All the described uncertainties in energy scales or resolutions of the reconstructed objects (hard components) are propagated to the missing transverse momentum. Additional uncertainties in the scale and resolution of the soft term are considered, to account for the disagreement between data and MC for the p_{T} balance between the hard and soft components [78].

Tracks. Systematic uncertainties related to the track selection efficiency are determined by changing the amount of tracker material and the physical models in the GEANT4 simulation [94,95]. Dedicated uncertainties are considered for the track parameters, including the transverse and longitudinal impact parameters and the track sagitta.

Large- R jet mass scale correction. To correct for the mismodelling in the large-R jet mass, additional mass scale corrections are estimated. The large-R jet mass scale is varied by ±5% and compared with the nominal results.

9.2 Modelling uncertainties

Renormalisation (μ_{r}) *and factorisation* (μ_{f}) *scales.* Variations in the renormalisation and factorisation scales are used to estimate the uncertainty due to missing higher order corrections. The uncertainties are combined by taking an envelope of all the variations.

Initial-state radiation and final-state radiation modelling. For the ISR, the amount of radiation is increased (decreased) using the `Var3cUp` (`Var3cDown`) variation of the A14 tune [37]. For the FSR, the amount of radiation is increased (decreased) varying the coupling of the QCD emission in the final state by a factor of 0.5 (2).

PDF uncertainties. The PDF uncertainties follow the PDF4LHC recommendations [96]. The α_{s} uncertainty is derived using the same PDF set evaluated with two different α_{s} values. The uncertainties from the PDF and α_{s} are added in quadrature.

Parton shower. The uncertainty associated with hadronisation and parton shower is evaluated by comparing samples with different parton shower models. The nominal $t\bar{t}a$ samples simulated using POWHEG+PYTHIA 8 are compared with samples simulated using MADGRAPH5_AMC@NLO+HERWIG 7 [97]. The comparison is done after normalising both $t\bar{t}a$ samples. The nominal $t\bar{t}$ (4FS and 5FS) POWHEG+PYTHIA 8 samples are compared with samples simulated using POWHEG+HERWIG 7. The tW and $t\bar{t}H$ MADGRAPH5_AMC@NLO+PYTHIA 8 samples are compared with MADGRAPH5_AMC@NLO+HERWIG 7 samples.

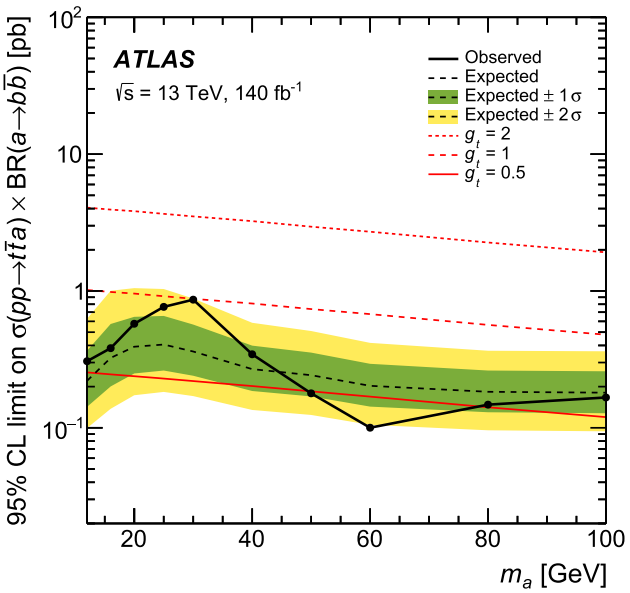

Fig. 9 Expected and observed 95% CL upper limits of $\sigma(t\bar{t}a) \times \mathrm{BR}(a \to b\bar{b})$ as a function of the a-boson mass. The lines correspond to the signal cross sections calculated using different coupling strengths of the a boson to the top quark assuming a $\mathrm{BR}(a \to b\bar{b}) = 100\%$

Matrix element uncertainties. For the 5FS and 4FS $t\bar{t}$ samples, the uncertainty associated with the matching between the Matrix element calculations and the parton shower is calculated by comparing the nominal POWHEG+PYTHIA 8 sample with an alternative set of samples simulated also in POWHEG+PYTHIA 8 but using the `pThard=1` setting. For tW and $t\bar{t}H$, the matrix element uncertainty is evaluated by comparing the nominal POWHEG+PYTHIA 8 samples to those simulated with MADGRAPH5_AMC@NLO+PYTHIA 8. For $t\bar{t}Z$, the nominal samples are compared with an alternative sample simulated using SHERPA 2.2.0, which accounts both for the matrix element and parton shower uncertainties.

POWHEG *damping function.* In the $t\bar{t}b\bar{b}$ (4FS) samples, the effect of the choice of a damping scale h_{bzd} that controls the resummation of infrared divergences is evaluated by comparing the nominal sample ($h_{\mathrm{bzd}} = 5$) with an alternative sample in which the scale is set to 2 [30].

Initial-state shower recoil. The uncertainty due to the recoil choice of ISR emissions is evaluated by comparing the nominal sample, in which the whole final state recoils the ISR emission, with an alternative one, in which only one final-state parton recoils against the ISR emission [30].

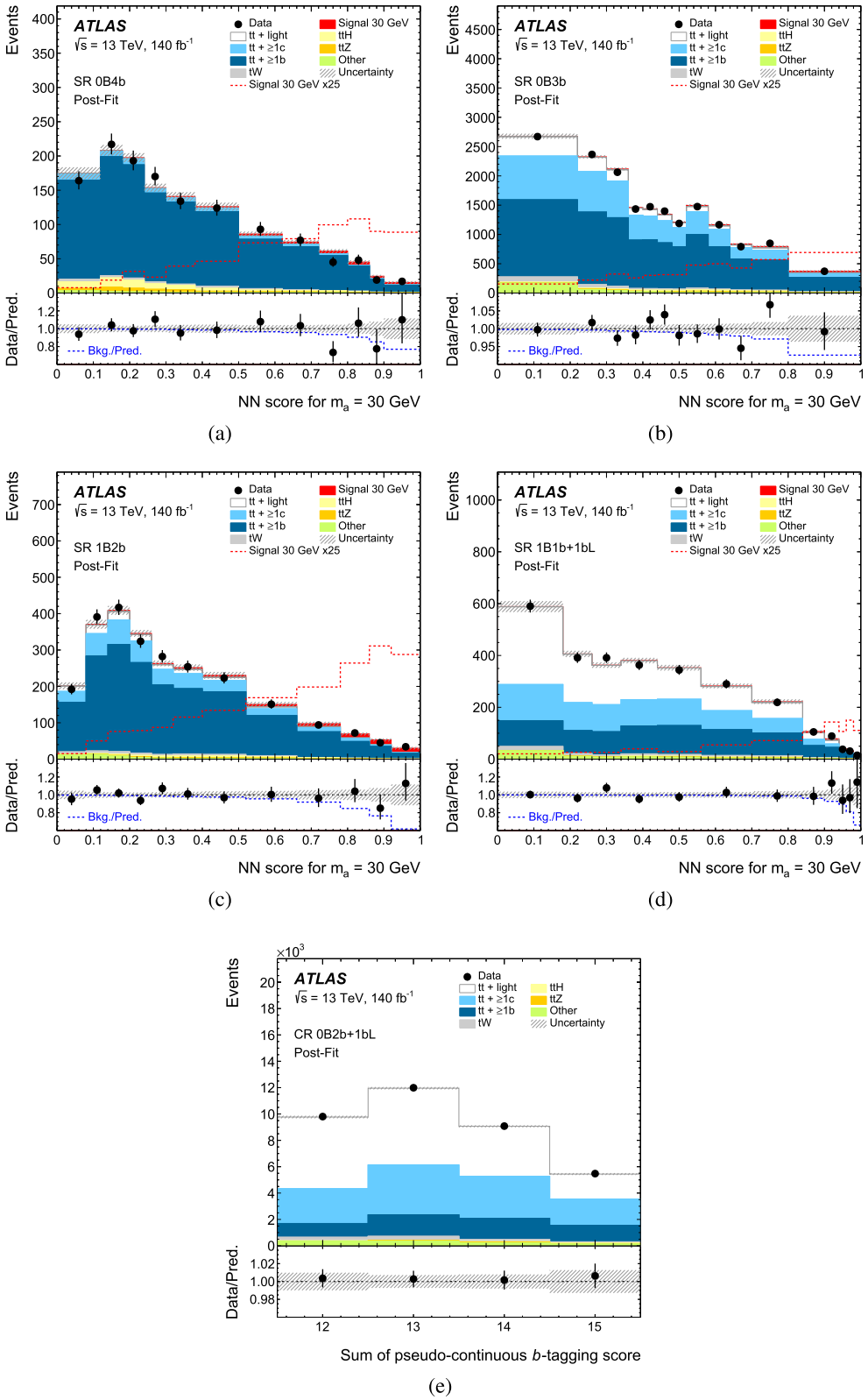

Fig. 10 Post-fit distributions corresponding to the NN output score of (**a**) SR 0B4b, (**b**) SR 0B3b, (**c**) SR 1B2b and (**d**) SR 1B1b+1bL and to the sum of the pseudo-continuous *b*-tagging score of (**e**) CR 0B2b+1bL for the 30 GeV mass hypothesis fit. The dashed lines in the top and ratio panels show the post-fit distribution of the signal scaled by a factor of 25 and the post-fit ratio of the background over the total prediction, respectively. The band displays the total post-fit uncertainty

Table 6 Post-fit background and signal yields in the four signal regions and in the control region for the $m_a = 30$ GeV hypothesis. The uncertainties in each yield are the total uncertainties of each component after the fit

Sample	SR 0B4b	SR 0B3b	SR 1B2b	SR 1B1b+1bL	CR 0B2b+1bL
Signal 30 GeV	28 ± 14	180 ± 98	71 ± 31	35 ± 16	110 ± 63
$t\bar{t}$+light	5 ± 2	1400 ± 320	130 ± 24	1100 ± 180	17,000 ± 3000
$t\bar{t}$+≥1c	58 ± 21	4700 ± 1200	380 ± 140	740 ± 230	12,000 ± 3500
$t\bar{t}$+≥1b	1093 ± 47	9820 ± 700	1758 ± 97	815 ± 70	5510 ± 650
tW	22 ± 12	360 ± 140	46 ± 20	64 ± 17	830 ± 220
$t\bar{t}H$	62 ± 9	222 ± 22	31 ± 4	14 ± 12	136 ± 13
$t\bar{t}Z$	27 ± 6	120 ± 22	15 ± 3	11 ± 2	128 ± 25
Other	14 ± 2	394 ± 35	47 ± 4	78 ± 10	1060 ± 120
Total pred.	1300 ± 35	17,000 ± 130	2500 ± 50	2900 ± 53	36,000 ± 190
Data	1301	17,242	2479	2866	36,350

Table 7 Table of the impact of each group of uncertainties in the fitted cross section for the hypothesis masses of 12, 30 and 80 GeV. The values shown are the average of up and down uncertainties. The fitted cross section values include the BR($t\bar{t} \to WbWb$) × BR($W \to l\nu$) × BR($W \to l\nu$) in addition to the BR($a \to b\bar{b}$)

Fitted cross section [fb]	$m_a = 12$ GeV $\hat{\sigma} = 9$	$m_a = 30$ GeV $\hat{\sigma} = 46$	$m_a = 80$ GeV $\hat{\sigma} = -6.1$
Uncertainty source	$\Delta\hat{\sigma}$	$\Delta\hat{\sigma}$	$\Delta\hat{\sigma}$
Data statistics	6.1	11.0	6.0
MC statistics	2.4	4.2	1.8
Luminosity & pile-up	0.1	0.4	0.1
Jet reconstruction	0.5	4.9	1.2
Lepton reconstruction	<0.1	<0.1	<0.1
$E_{\mathrm{T}}^{\mathrm{miss}}$ reconstruction	<0.1	0.3	<0.1
Track reconstruction	4.1	1.5	0.1
DL1r	0.4	3.5	1.4
DeXTer	4.2	18	1.1
Modelling signal	1.7	7.5	1.3
Modelling $t\bar{t} + b$	2.7	13	5.5
Modelling $t\bar{t} + c$	0.9	1.8	1.4
Modelling $t\bar{t}$+light	0.8	2.0	2.2
Modelling tW	0.3	0.7	0.6
Modelling ttH	0.1	0.3	0.2
Modelling ttZ	0.1	0.2	1.0
Norm factors	0.7	6.7	4.7
Reweighting	<0.1	<0.1	<0.1
Total systematic uncertainty	8.0	22	7.8
Total uncertainty	10	24	9.7

Interference between $t\bar{t}$ and tW. To account for uncertainties in the interference between $t\bar{t}$+jets and tW, the nominal tW sample simulated using diagram removal (DR) is compared with another sample simulated using diagram subtraction (DS).

Reweighting uncertainties. To account for the systematic uncertainties associated with the reweighting functions described in Sect. 6, several uncertainties are determined by the variations of $t\bar{t}$+light + tW, $t\bar{t}$+≥1c and $t\bar{t}$+ ≥1b normalisation factors and the variations of the parameters of the $H_{\mathrm{T}}^{\mathrm{red}}$ hyperbolic fit. The uncertainties are evaluated after diagonalising the fit correlation matrix and propagating the diagonal variations in a correlated way.

10 Results

The expected and observed upper limits on the inclusive $\sigma(t\bar{t}a) \times \mathrm{BR}(a \to b\bar{b})$ are shown in Fig. 9 as a function of the a-boson mass, which ranges from 12 to 100 GeV. This result is compared with the predicted cross sections for the signal corresponding to three different values of the coupling of the a-boson to the top quark, defined as a strength modifier to the SM Yukawa coupling. No significant excess is observed: the largest excess corresponds to the 30 GeV mass hypothesis, with a local significance of 2.0 standard deviations. Assuming $\mathrm{BR}(a \to b\bar{b}) = 100\%$, the mass region between 50 and 80 GeV is excluded for a coupling of the pseudoscalar to the top quark of 0.5, while a coupling of 1.0 is excluded for all masses. Post-fit distributions of the NN output score corresponding to this mass in each of the four signal regions and of the sum of the pseudo-continuous b-tagging score of all jets in the control region are shown in Fig. 10. Table 6 shows the post-fit event yields per signal and background component in each of the signal and control regions for the same mass hypothesis.

Table 7 summarises the impact of the different sources of uncertainties in the fitted signal strength for three different mass hypotheses: 12, 30 and 80 GeV, which are representative of the low, medium and high mass ranges, respectively. Fits to low-mass hypotheses are limited by data statistics, track reconstruction and DeXTer-related uncertainties. Fits to medium-mass hypotheses are dominated by DeXTer-related uncertainties, followed by the modelling of the $t\bar{t}$+$\geq$1b process and data statistics. Finally, fits to high-mass hypotheses are limited mainly by data statistics, the modelling of the $t\bar{t}$+$\geq$1b process and the normalisation of $t\bar{t}$+HF. In all cases, the uncertainties in the modelling of the signal are subdominant compared with that of $t\bar{t}$+$\geq$1b. No large pulls are observed in any of the fits. Including the pre-fit reweighting corrections detailed in Table 3, the final normalisation factors extracted in the fit corresponding to the 30 GeV mass hypothesis are 1.0 ± 0.3 for $t\bar{t}$+light and tW, 1.5 ± 0.5 for $t\bar{t}$+$\geq$1c and 1.2 ± 0.2 for $t\bar{t}$+$\geq$1b. These results are compatible with the latest ATLAS $t\bar{t}H$ Run 2 analysis [98].

11 Conclusions

A search for a pseudoscalar a produced in association with either a pair of top quarks or a single top and a W boson in the dilepton decay channel is performed using the full Run 2 pp data sample collected by the ATLAS detector at the LHC. The search targets the dominant decay channel of the pseudoscalar mass probed in this analysis: $a \to b\bar{b}$. The search covers the pseudoscalar boson mass between 12 and 100 GeV, involving both the kinematic regime where the decay products of the pseudoscalar merge into large B-jets and the regime where the b-tagged jets are resolved. Limits on the signal production cross section times the branching ratio of the decay into a pair of bottom quarks are extracted. Assuming $\mathrm{BR}(a \to b\bar{b}) = 100\%$, the mass region between 50 and 80 GeV is excluded for a coupling of the pseudoscalar to the top quark of 0.5, while a coupling of 1.0 is excluded for all masses. These model independent results are the first limits of their kind and complement previous searches by ATLAS [17] and CMS [16] exploring leptonic decays of the pseudoscalar.

Acknowledgements We thank CERN for the very successful operation of the LHC and its injectors, as well as the support staff at CERN and at our institutions worldwide without whom ATLAS could not be operated efficiently. The crucial computing support from all WLCG partners is acknowledged gratefully, in particular from CERN, the ATLAS Tier-1 facilities at TRIUMF/SFU (Canada), NDGF (Denmark, Norway, Sweden), CC-IN2P3 (France), KIT/GridKA (Germany), INFN-CNAF (Italy), NL-T1 (Netherlands), PIC (Spain), RAL (UK) and BNL (USA), the Tier-2 facilities worldwide and large non-WLCG resource providers. Major contributors of computing resources are listed in Ref. [99]. We gratefully acknowledge the support of ANPCyT, Argentina; YerPhI, Armenia; ARC, Australia; BMWFW and FWF, Austria; ANAS, Azerbaijan; CNPq and FAPESP, Brazil; NSERC, NRC and CFI, Canada; CERN; ANID, Chile; CAS, MOST and NSFC, China; Minciencias, Colombia; MEYS CR, Czech Republic; DNRF and DNSRC, Denmark; IN2P3-CNRS and CEA-DRF/IRFU, France; SRNSFG, Georgia; BMBF, HGF and MPG, Germany; GSRI, Greece; RGC and Hong Kong SAR, China; ICHEP and Academy of Sciences and Humanities, Israel; INFN, Italy; MEXT and JSPS, Japan; CNRST, Morocco; NWO, Netherlands; RCN, Norway; MNiSW, Poland; FCT, Portugal; MNE/IFA, Romania; MSTDI, Serbia; MSSR, Slovakia; ARIS and MVZI, Slovenia; DSI/NRF, South Africa; MICIU/AEI, Spain; SRC and Wallenberg Foundation, Sweden; SERI, SNSF and Cantons of Bern and Geneva, Switzerland; NSTC, Taipei; TENMAK, Türkiye; STFC/UKRI, United Kingdom; DOE and NSF, United States of America. Individual groups and members have received support from BCKDF, CANARIE, CRC and DRAC, Canada; CERN-CZ, FORTE and PRIMUS, Czech Republic; COST, ERC, ERDF, Horizon 2020, ICSC-NextGenerationEU and Marie Skłodowska-Curie Actions, European Union; Investissements d'Avenir Labex, Investissements d'Avenir Idex and ANR, France; DFG and AvH Foundation, Germany; Herakleitos, Thales and Aristeia programmes co-financed by EU-ESF and the Greek NSRF, Greece; BSF-NSF and MINERVA, Israel; NCN and NAWA, Poland; La Caixa Banking Foundation, CERCA Programme Generalitat de Catalunya and PROMETEO and GenT Programmes Generalitat Valenciana, Spain; Göran Gustafssons Stiftelse, Sweden; The Royal Society and Leverhulme Trust, United Kingdom. In addition, individual members wish to acknowledge support from Armenia: Yerevan Physics Institute (FAPERJ); CERN: European Organization for Nuclear Research (CERN DOCT); Chile: Agencia Nacional de Investigación y Desarrollo (FONDECYT 1230812, FONDECYT 1230987, FONDECYT 1240864); China: Chinese Ministry of Science and Technology (MOST-2023YFA1605700, MOST-2023YFA1609300), National Natural Science Foundation of China (NSFC - 12175119, NSFC 12275265); Czech Republic: Czech Science Foundation (GACR - 24-11373S), Ministry of Education Youth and Sports (ERC-CZ-LL2327, FORTE CZ.02.01.01/00/22_008/0004632), PRIMUS Research Programme (PRIMUS/21/SCI/017); EU: H2020 European Research Council (ERC - 101002463); European Union: European Research Council (ERC - 948254, ERC 101089007, ERC, BARD, 101116429), European Regional Development Fund (SMASH COFUND 101081355, SLO ERDF), Horizon 2020 Framework Programme (MUCCA -

CHIST-ERA-19-XAI-00), European Union, Future Artificial Intelligence Research (FAIR-NextGenerationEU PE00000013), Horizon 2020 (EuroHPC - EHPC-DEV-2024D11-051), Italian Center for High Performance Computing, Big Data and Quantum Computing (ICSC, NextGenerationEU); France: Agence Nationale de la Recherche (ANR-21-CE31-0022, ANR-22-EDIR-0002); Germany: Baden-Württemberg Stiftung (BW Stiftung-Postdoc Eliteprogramme), Deutsche Forschungsgemeinschaft (DFG - 469666862, DFG - CR 312/5-2); China: Research Grants Council (GRF); Italy: Istituto Nazionale di Fisica Nucleare (ICSC, NextGenerationEU), Ministero dell'Università e della Ricerca (NextGenEU I53D23000820006 M4C2.1.1); Japan: Japan Society for the Promotion of Science (JSPS KAKENHI JP22H01227, JSPS KAKENHI JP22H04944, JSPS KAKENHI JP22KK0227, JSPS KAKENHI JP23KK0245, JSPS KAKENHI JP24K23939); Norway: Research Council of Norway (RCN-314472); Poland: Ministry of Science and Higher Education (IDUB AGH, POB8, D4 no 9722), Polish National Science Centre (NCN 2021/42/E/ST2/00350, NCN OPUS 2023/51/B/ST2/02507, NCN OPUS nr 2022/47/B/ST2/03059, NCN UMO-2019/34/E/ST2/00393, UMO-2022/47/O/ST2/00148, UMO-2023/49/B/ST2/04085, UMO-2023/51/B/ST2/00920, UMO-2024/53/N/ST2/00869); Portugal: Foundation for Science and Technology (FCT); Spain: Generalitat Valenciana (Artemisa, FEDER, IDIFEDER/2018/048), Ministry of Science and Innovation (MCIN & NextGenEU PCI2022-135018-2, MICIN & FEDER PID2021-125273NB, RYC2019-028510-I, RYC2020-030254-I, RYC2021-031273-I, RYC2022-038164-I); Sweden: Carl Trygger Foundation (Carl Trygger Foundation CTS 22:2312), Swedish Research Council (Swedish Research Council 2023-04654, VR 2021-03651, VR 2022-03845, VR 2022-04683, VR 2023-03403, VR 2024-05451), Knut and Alice Wallenberg Foundation (KAW 2018.0458, KAW 2022.0358, KAW 2023.0366); Switzerland: Swiss National Science Foundation (SNSF- PCEFP2_194658); United Kingdom: Leverhulme Trust (Leverhulme Trust RPG-2020-004), Royal Society (NIF-R1-231091); United States of America: U.S. Department of Energy (ECA DE-AC02-76SF00515), Neubauer Family Foundation.

Open Access This article is licensed under a Creative Commons Attribution 4.0 International License, which permits use, sharing, adaptation, distribution and reproduction in any medium or format, as long as you give appropriate credit to the original author(s) and the source, provide a link to the Creative Commons licence, and indicate if changes were made. The images or other third party material in this article are included in the article's Creative Commons licence, unless indicated otherwise in a credit line to the material. If material is not included in the article's Creative Commons licence and your intended use is not permitted by statutory regulation or exceeds the permitted use, you will need to obtain permission directly from the copyright holder. To view a copy of this licence, visit http://creativecommons.org/licenses/by/4.0/.

Funded by SCOAP[3].

References

1. ATLAS Collaboration, Observation of a new particle in the search for the Standard Model Higgs boson with the ATLAS detector at the LHC. Phys. Lett. B **716**, 1 (2012). https://doi.org/10.1016/j.physletb.2012.08.020. arXiv:1207.7214 [hep-ex]
2. C.M.S. Collaboration, Observation of a new boson at a mass of 125 GeV with the CMS experiment at the LHC. Phys. Lett. B **716**, 30 (2012). https://doi.org/10.1016/j.physletb.2012.08.021. arXiv:1207.7235 [hep-ex]
3. L. Evans, P. Bryant, L.H.C. Machine, JINST **3**, S08001 (2008). https://doi.org/10.1088/1748-0221/3/08/S08001
4. G.C. Branco et al., Theory and phenomenology of two-Higgs-doublet models. Phys. Rep. **516**, 1 (2012). https://doi.org/10.1016/j.physrep.2012.02.002. arXiv:1106.0034 [hep-ph]
5. M. Aoki, S. Kanemura, K. Tsumura, K. Yagyu, Models of Yukawa interaction in the two Higgs doublet model, and their collider phenomenology. Phys. Rev. D **80**, 015017 (2009). https://doi.org/10.1103/PhysRevD.80.015017. arXiv:0902.4665 [hep-ph]
6. Y.A. Golfand, E.P. Likhtman, Extension of the algebra of Poincare group generators and violation of p invariance. JETP Lett. **13**, 323 (1971). https://doi.org/10.1142/9789814542340_0001
7. D.V. Volkov, V.P. Akulov, Is the neutrino a goldstone particle? Phys. Lett. B **46**, 109 (1973). https://doi.org/10.1016/0370-2693(73)90490-5
8. J. Wess, B. Zumino, Supergauge transformations in four dimensions. Nucl. Phys. B **70**, 39 (1974). https://doi.org/10.1016/0550-3213(74)90355-1
9. J. Wess, B. Zumino, Supergauge invariant extension of quantum electrodynamics. Nucl. Phys. B **78**, 1 (1974). https://doi.org/10.1016/0550-3213(74)90112-6
10. S. Ferrara, B. Zumino, Supergauge invariant Yang–Mills theories. Nucl. Phys. B **79**, 413 (1974). https://doi.org/10.1016/0550-3213(74)90559-8
11. A. Salam, J. Strathdee, Super-symmetry and non-Abelian gauges. Phys. Lett. B **51**, 353 (1974). https://doi.org/10.1016/0370-2693(74)90226-3
12. M.R. Buckley, D. Feld, D. Gonçalves, Scalar simplified models for dark matter. Phys. Rev. D **91** (2015). https://doi.org/10.1103/physrevd.91.015017. arXiv:1410.6497 [hep-ph]
13. M. Bauer, U. Haisch, F. Kahlhoefer, Simplified dark matter models with two Higgs doublets: I. Pseudoscalar mediators. JHEP **05**, 138 (2017). https://doi.org/10.1007/jhep05(2017)138. arXiv:1701.07427 [hep-ph]
14. J.E. Kim, Light pseudoscalars, particle physics and cosmology. Phys. Rep. **150**, 1 (1987). https://doi.org/10.1016/0370-1573(87)90017-2
15. M. Casolino, T. Farooque, A. Juste, T. Liu, M. Spannowsky, Probing a light CP-odd scalar in di-top-associated production at the LHC. Eur. Phys. J. C **75**, 498 (2015). https://doi.org/10.1140/epjc/s10052-015-3708-y. arXiv:1507.07004 [hep-ph]
16. CMS Collaboration, Search for a scalar or pseudoscalar dilepton resonance produced in association with a massive vector boson or top quark-antiquark pair in multilepton events at $\sqrt{s} =$ 13 TeV. Phys. Rev. D **110**, 012013 (2024). https://doi.org/10.1103/PhysRevD.110.012013. arXiv:2402.11098 [hep-ex]
17. ATLAS Collaboration, Search for a new pseudoscalar decaying into a pair of muons in events with a top-quark pair at $\sqrt{s} = 13$ TeV TeV with the ATLAS detector. Phys. Rev. D **108**, 092007 (2023). https://doi.org/10.1103/PhysRevD.108.092007. arXiv:2304.14247 [hep-ex]
18. ATLAS Collaboration, The ATLAS Experiment at the CERN Large Hadron Collider. JINST **3**, S08003 (2008). https://doi.org/10.1088/1748-0221/3/08/S08003
19. ATLAS Collaboration, ATLAS Insertable B-Layer: Technical Design Report, ATLAS-TDR-19; CERN-LHCC-2010-013 (2010). https://cds.cern.ch/record/1291633. Addendum: ATLAS-TDR-19-ADD-1; CERN-LHCC-2012-009 (2012). https://cds.cern.ch/record/1451888
20. B. Abbott et al., Production and integration of the ATLAS Insertable B-Layer. JINST **13**, T05008 (2018). https://doi.org/10.1088/1748-0221/13/05/T05008. arXiv:1803.00844 [physics.ins-det]
21. G. Avoni et al., The new LUCID-2 detector for luminosity measurement and monitoring in ATLAS. JINST **13**, P07017 (2018). https://doi.org/10.1088/1748-0221/13/07/P07017

22. ATLAS Collaboration, Performance of the ATLAS trigger system in 2015. Eur. Phys. J. C **77**, 317 (2017). https://doi.org/10.1140/epjc/s10052-017-4852-3. arXiv:1611.09661 [hep-ex]
23. ATLAS Collaboration, Software and computing for Run 3 of the ATLAS experiment at the LHC. Eur. Phys. J. C **85**, 234 (2025). https://doi.org/10.1140/epjc/s10052-024-13701-w. arXiv:2404.06335 [hep-ex]
24. ATLAS Collaboration, Luminosity determination in pp collisions at $\sqrt{s} = 13$ TeV using the ATLAS detector at the LHC. Eur. Phys. J. C **83**, 982 (2023). https://doi.org/10.1140/epjc/s10052-023-11747-w. arXiv:2212.09379 [hep-ex]
25. T. Sjöstrand, S. Mrenna, P. Skands, A brief introduction to PYTHIA 8.1. Comput. Phys. Commun. **178**, 852 (2008). https://doi.org/10.1016/j.cpc.2008.01.036. arXiv:0710.3820 [hep-ph]
26. ATLAS Collaboration, The Pythia 8 A3 tune description of ATLAS minimum bias and inelastic measurements incorporating the Donnachie–Landshoff diffractive model, ATL-PHYS-PUB-2016-017 (2016). https://cds.cern.ch/record/2206965
27. S. Agostinelli et al., Geant4—a simulation toolkit. Nucl. Instrum. Methods A **506**, 250 (2003). https://doi.org/10.1016/S0168-9002(03)01368-8
28. ATLAS Collaboration, The ATLAS simulation infrastructure. Eur. Phys. J. C **70**, 823 (2010). https://doi.org/10.1140/epjc/s10052-010-1429-9. arXiv:1005.4568 [physics.ins-det]
29. J. Alwall et al., The automated computation of tree-level and next-to-leading order differential cross sections, and their matching to parton shower simulations. JHEP **07**, 079 (2014). https://doi.org/10.1007/JHEP07(2014)079. arXiv:1405.0301 [hep-ph]
30. ATLAS Collaboration, Studies of Monte Carlo predictions for the $t\bar{t}b\bar{b}$ process, ATL-PHYS-PUB-2022-006 (2022). https://cds.cern.ch/record/2802806
31. S. Frixione, G. Ridolfi, P. Nason, A positive-weight next-to-leading-order Monte Carlo for heavy flavour hadroproduction. JHEP **09**, 126 (2007). https://doi.org/10.1088/1126-6708/2007/09/126. arXiv:0707.3088 [hep-ph]
32. P. Nason, A new method for combining NLO QCD with shower Monte Carlo algorithms. JHEP **11**, 040 (2004). https://doi.org/10.1088/1126-6708/2004/11/040. arXiv:hep-ph/0409146
33. S. Frixione, P. Nason, C. Oleari, Matching NLO QCD computations with parton shower simulations: the POWHEG method. JHEP **11**, 070 (2007). https://doi.org/10.1088/1126-6708/2007/11/070. arXiv:0709.2092 [hep-ph]
34. S. Alioli, P. Nason, C. Oleari, E. Re, A general framework for implementing NLO calculations in shower Monte Carlo programs: the POWHEG BOX. JHEP **06**, 043 (2010). https://doi.org/10.1007/JHEP06(2010)043. arXiv:1002.2581 [hep-ph]
35. NNPDF Collaboration, R.D. Ball et al., Parton distributions for the LHC run II. JHEP **04**, 040 (2015). https://doi.org/10.1007/JHEP04(2015)040. arXiv:1410.8849 [hep-ph]
36. T. Sjöstrand et al., An introduction to PYTHIA 8.2. Comput. Phys. Commun. **191**, 159 (2015). https://doi.org/10.1016/j.cpc.2015.01.024. arXiv:1410.3012 [hep-ph]
37. ATLAS Collaboration, ATLAS Pythia 8 tunes to 7 TeV data, ATL-PHYS-PUB-2014-021 (2014). https://cds.cern.ch/record/1966419
38. NNPDF Collaboration, R.D. Ball et al., Parton distributions with LHC data. Nucl. Phys. B **867**, 244 (2013). https://doi.org/10.1016/j.nuclphysb.2012.10.003. arXiv:1207.1303 [hep-ph]
39. J. Pumplin et al., New generation of parton distributions with uncertainties from global QCD analysis. JHEP **07**, 012 (2002). https://doi.org/10.1088/1126-6708/2002/07/012. arXiv:hep-ph/0201195
40. E. Bothmann et al., Event generation with Sherpa 2.2. SciPost Phys. **7**, 034 (2019). https://doi.org/10.21468/SciPostPhys.7.3.034. arXiv:1905.09127 [hep-ph]
41. S. Schumann, F. Krauss, A parton shower algorithm based on Catani–Seymour dipole factorisation. JHEP **03**, 038 (2008). https://doi.org/10.1088/1126-6708/2008/03/038. arXiv:0709.1027 [hep-ph]
42. S. Höche, F. Krauss, M. Schönherr, F. Siegert, A critical appraisal of NLO+PS matching methods. JHEP **09**, 049 (2012). https://doi.org/10.1007/JHEP09(2012)049. arXiv:1111.1220 [hep-ph]
43. S. Höche, F. Krauss, M. Schönherr, F. Siegert, QCD matrix elements + parton showers. The NLO case. JHEP **04**, 027 (2013). https://doi.org/10.1007/JHEP04(2013)027. arXiv:1207.5030 [hep-ph]
44. S. Catani, F. Krauss, B.R. Webber, R. Kuhn, QCD matrix elements + parton showers. JHEP **11**, 063 (2001). https://doi.org/10.1088/1126-6708/2001/11/063. arXiv:hep-ph/0109231
45. S. Höche, F. Krauss, S. Schumann, F. Siegert, QCD matrix elements and truncated showers. JHEP **05**, 053 (2009). https://doi.org/10.1088/1126-6708/2009/05/053. arXiv:0903.1219 [hep-ph]
46. D.J. Lange, The EvtGen particle decay simulation package. Nucl. Instrum. Methods A **462**, 152 (2001). https://doi.org/10.1016/S0168-9002(01)00089-4
47. M. Beneke, P. Falgari, S. Klein, C. Schwinn, Hadronic top-quark pair production with NNLL threshold resummation. Nucl. Phys. B **855**, 695 (2012). https://doi.org/10.1016/j.nuclphysb.2011.10.021. arXiv:1109.1536 [hep-ph]
48. M. Cacciari, M. Czakon, M. Mangano, A. Mitov, P. Nason, Top-pair production at hadron colliders with next-to-next-to-leading logarithmic soft-gluon resummation. Phys. Lett. B **710**, 612 (2012). https://doi.org/10.1016/j.physletb.2012.03.013. arXiv:1111.5869 [hep-ph]
49. P. Bärnreuther, M. Czakon, A. Mitov, Percent-level-precision physics at the tevatron: next-to-next-to-leading order QCD corrections to $q\bar{q} \to t\bar{t} + X$. Phys. Rev. Lett. **109**, 132001 (2012). https://doi.org/10.1103/PhysRevLett.109.132001. arXiv:1204.5201 [hep-ph]
50. M. Czakon, A. Mitov, NNLO corrections to top-pair production at hadron colliders: the all-fermionic scattering channels. JHEP **12**, 054 (2012). https://doi.org/10.1007/JHEP12(2012)054. arXiv:1207.0236 [hep-ph]
51. M. Czakon, A. Mitov, NNLO corrections to top pair production at hadron colliders: the quark-gluon reaction. JHEP **01**, 080 (2013). https://doi.org/10.1007/JHEP01(2013)080. arXiv:1210.6832 [hep-ph]
52. M. Czakon, P. Fiedler, A. Mitov, Total top-quark pair-production cross section at hadron colliders through $\mathcal{O}(\alpha_S^4)$. Phys. Rev. Lett. **110**, 252004 (2013). https://doi.org/10.1103/PhysRevLett.110.252004. arXiv:1303.6254 [hep-ph]
53. M. Czakon, A. Mitov, Top++: a program for the calculation of the top-pair cross-section at hadron colliders. Comput. Phys. Commun. **185**, 2930 (2014). https://doi.org/10.1016/j.cpc.2014.06.021. arXiv:1112.5675 [hep-ph]
54. N. Kidonakis, Two-loop soft anomalous dimensions for single top quark associated production with a W^- or H^-. Phys. Rev. D **82**, 054018 (2010). https://doi.org/10.1103/PhysRevD.82.054018. arXiv:1005.4451 [hep-ph]
55. N. Kidonakis, 'Top Quark Production', in *Proceedings, Helmholtz International Summer School on Physics of Heavy Quarks and Hadrons (HQ2013) (JINR, Dubna, Russia, 15th–28th July 2013)*, p. 139. https://doi.org/10.3204/DESY-PROC-2013-03/Kidonakis. arXiv:1311.0283 [hep-ph]
56. D. de Florian et al., Handbook of LHC Higgs Cross Sections: 4. Deciphering the Nature of the Higgs Sector (2017). https://doi.org/10.23731/CYRM-2017-002. arXiv:1610.07922 [hep-ph]
57. C. Anastasiou, L. Dixon, K. Melnikov, F. Petriello, High-precision QCD at hadron colliders: electroweak gauge boson rapidity distributions at next-to-next-to leading order. Phys. Rev. D **69**, 094008 (2004). https://doi.org/10.1103/PhysRevD.69.094008. arXiv:hep-ph/0312266

58. ATLAS Collaboration, Electron and photon performance measurements with the ATLAS detector using the 2015-2017 LHC proton-proton collision data. JINST **14**, P12006 (2019). https://doi.org/10.1088/1748-0221/14/12/P12006. arXiv:1908.00005 [hep-ex]
59. ATLAS Collaboration, Evidence for the associated production of the Higgs boson and a top quark pair with the ATLAS detector. Phys. Rev. D **97**, 072003 (2018). https://doi.org/10.1103/PhysRevD.97.072003. arXiv:1712.08891 [hep-ex]
60. ATLAS Collaboration, Muon reconstruction and identification efficiency in ATLAS using the full Run 2 pp collision data set at $\sqrt{s} = 13$ TeV. Eur. Phys. J. C **81**, 578 (2021). https://doi.org/10.1140/epjc/s10052-021-09233-2. arXiv:2012.00578 [hep-ex]
61. ATLAS Collaboration, Jet reconstruction and performance using particle flow with the ATLAS detector. Eur. Phys. J. C **77**, 466 (2017). https://doi.org/10.1140/epjc/s10052-017-5031-2. arXiv:1703.10485 [hep-ex]
62. M. Cacciari, G.P. Salam, G. Soyez, The anti-k_t jet clustering algorithm. JHEP **04**, 063 (2008). https://doi.org/10.1088/1126-6708/2008/04/063. arXiv:0802.1189 [hep-ph]
63. M. Cacciari, G.P. Salam, G. Soyez, FastJet user manual. Eur. Phys. J. C **72**, 1896 (2012). https://doi.org/10.1140/epjc/s10052-012-1896-2. arXiv:1111.6097 [hep-ph]
64. ATLAS Collaboration, Jet energy scale and resolution measured in proton–proton collisions at $\sqrt{s} = 13$ TeV with the ATLAS detector. Eur. Phys. J. C **81**, 689 (2021). https://doi.org/10.1140/epjc/s10052-021-09402-3. arXiv:2007.02645 [hep-ex]
65. ATLAS Collaboration, Performance of pile-up mitigation techniques for jets in pp collisions at $\sqrt{s} = 8$ TeV using the ATLAS detector. Eur. Phys. J. C **76**, 581 (2016). https://doi.org/10.1140/epjc/s10052-016-4395-z. arXiv:1510.03823 [hep-ex]
66. ATLAS Collaboration, ATLAS flavour-tagging algorithms for the LHC Run 2 pp collision dataset. Eur. Phys. J. C **83**, 681 (2023). https://doi.org/10.1140/epjc/s10052-023-11699-1. arXiv:2211.16345 [physics.data-an]
67. ATLAS Collaboration, ATLAS b-jet identification performance and efficiency measurement with $t\bar{t}$ events in pp collisions at $\sqrt{s} = 13$ TeV. Eur. Phys. J. C **79**, 970 (2019). https://doi.org/10.1140/epjc/s10052-019-7450-8. arXiv:1907.05120 [hep-ex]
68. ATLAS Collaboration, Measurement of the c-jet mistagging efficiency in $t\bar{t}$ events using pp collision data at $\sqrt{s} = 13$ TeV collected with the ATLAS detector. Eur. Phys. J. C **82**, 95 (2022). https://doi.org/10.1140/epjc/s10052-021-09843-w. arXiv:2109.10627 [hep-ex]
69. ATLAS Collaboration, Calibration of the light-flavour jet mistagging efficiency of the b-tagging algorithms with Z+jets events using 139 fb^{-1} of ATLAS proton–proton collision data at $\sqrt{s} = 13$ TeV. Eur. Phys. J. C **83**, 728 (2023). https://doi.org/10.1140/epjc/s10052-023-11736-z. arXiv:2301.06319 [hep-ex]
70. M. Cacciari, G.P. Salam, Pileup subtraction using jet areas. Phys. Lett. B **659**, 119 (2008). https://doi.org/10.1016/j.physletb.2007.09.077. arXiv:0707.1378 [hep-ph]
71. M. Cacciari, G.P. Salam, G. Soyez, The catchment area of jets. JHEP **04**, 005 (2008). https://doi.org/10.1088/1126-6708/2008/04/005. arXiv:0802.1188 [hep-ph]
72. ATLAS Collaboration, Deep Sets based Neural Networks for Impact Parameter Flavour Tagging in ATLAS, ATL-PHYS-PUB-2020-014 (2020). https://cds.cern.ch/record/2718948
73. ATLAS Collaboration, Variable Radius, Exclusive-k_T, and Center-of-Mass Subjet Reconstruction for Higgs($\to b\bar{b}$) Tagging in ATLAS, ATL-PHYS-PUB-2017-010 (2017). https://cds.cern.ch/record/2268678
74. ATLAS Collaboration, Calibration of a soft secondary vertex tagger using proton–proton collisions at $\sqrt{s} = 13$ TeV with the ATLAS detector. Phys. Rev. D **110**, 032015 (2024). https://doi.org/10.1103/PhysRevD.110.032015. arXiv:2405.03253 [hep-ex]
75. V. Kostyukhin, Secondary vertex based b-tagging, tech. rep. ATL-PHYS-2003-033, revised version number 1 submitted on 2003-09-22 11:21:01: CERN (2003). https://cds.cern.ch/record/685550
76. ATLAS Collaboration, Performance of the reconstruction of large impact parameter tracks in the inner detector of ATLAS. Eur. Phys. J. C **83**, 1081 (2023). https://doi.org/10.1140/epjc/s10052-023-12024-6. arXiv:2304.12867 [hep-ex]
77. ATLAS Collaboration, DeXTer: Deep Sets based Neural Networks for Low-p_T $X \to b\bar{b}$ Identification in ATLAS, ATL-PHYS-PUB-2022-042 (2022). https://cds.cern.ch/record/2825434
78. ATLAS Collaboration, The performance of missing transverse momentum reconstruction and its significance with the ATLAS detector using 140 fb^{-1} of $\sqrt{s} = 13$ TeV pp collisions (2024). arXiv:2402.05858 [hep-ex]
79. B. Nachman, P. Nef, A. Schwartzman, M. Swiatlowski, C. Wanotayaroj, Jets from Jets: re-clustering as a tool for large radius jet reconstruction and grooming at the LHC. JHEP **02**, 075 (2015). https://doi.org/10.1007/JHEP02(2015)075. arXiv:1407.2922 [hep-ph]
80. ATLAS Collaboration, Performance of electron and photon triggers in ATLAS during LHC Run 2. Eur. Phys. J. C **80**, 47 (2020). https://doi.org/10.1140/epjc/s10052-019-7500-2. arXiv:1909.00761 [hep-ex]
81. ATLAS Collaboration, Performance of the ATLAS muon triggers in Run 2. JINST **15**, P09015 (2020). https://doi.org/10.1088/1748-0221/15/09/p09015. arXiv:2004.13447 [physics.ins-det]
82. ATLAS Collaboration, ATLAS data quality operations and performance for 2015–2018 data-taking. JINST **15**, P04003 (2020). https://doi.org/10.1088/1748-0221/15/04/P04003. arXiv:1911.04632 [physics.ins-det]
83. ATLAS Collaboration, Search for charged Higgs bosons decaying into a top quark and a bottom quark at $\sqrt{s} = 13$ TeV with the ATLAS detector. JHEP **06**, 145 (2021). https://doi.org/10.1007/JHEP06(2021)145. arXiv:2102.10076 [hep-ex]
84. ATLAS Collaboration, Measurement of the $t\bar{t}t\bar{t}$ production cross section in pp collisions at $\sqrt{s} = 13$ TeV with the ATLAS detector. JHEP **11**, 118 (2021). https://doi.org/10.1007/JHEP11(2021)118. arXiv:2106.11683 [hep-ex]
85. ATLAS Collaboration, Search for a new scalar resonance in flavour-changing neutral-current top-quark decays $t \to qX$ ($q = u, c$), with $X \to b\bar{b}$, in proton–proton collisions at $\sqrt{s} = 13$ TeV with the ATLAS detector. JHEP **07**, 199 (2023). https://doi.org/10.1007/JHEP07(2023)199. arXiv:2301.03902 [hep-ex]
86. CMS Collaboration, Measurement of the $t\bar{t}$ production cross section in the all-jet final state in pp collisions at $\sqrt{s} = 7$ TeV. JHEP **05**, 065 (2013). https://doi.org/10.1007/JHEP05(2013)065. arXiv:1302.0508 [hep-ex]
87. CMS Collaboration, Measurement of the cross section for $t\bar{t}$ production with additional jets and b jets in pp collisions at $\sqrt{s} = 13$ TeV. JHEP **07**, 125 (2020). https://doi.org/10.1007/JHEP07(2020)125. arXiv:2003.06467 [hep-ex]
88. ATLAS Collaboration, Measurements of inclusive and differential fiducial cross-sections of $t\bar{t}$ production with additional heavy-flavour jets in proton–proton collisions at $\sqrt{s} = 13$ TeV with the ATLAS detector. JHEP **04**, 046 (2019). https://doi.org/10.1007/JHEP04(2019)046. arXiv:1811.12113 [hep-ex]
89. A. Hoecker et al., TMVA—Toolkit for Multivariate Data Analysis (2009). arXiv:physics/0703039 [physics.data-an]
90. A. Paszke et al., PyTorch: an imperative style, high-performance deep learning library (2019). https://doi.org/10.48550/arXiv.1912.01703. arXiv:1912.01703 [cs.LG]
91. G. Cowan, K. Cranmer, E. Gross, O. Vitells, Asymptotic formulae for likelihood-based tests of new physics. Eur. Phys. J. C **71**, 1554 (2011). https://doi.org/10.1140/epjc/s10052-011-1554-0. arXiv:1007.1727 [physics.data-an]. Erratum: Eur. Phys. J. C **73**, 2501 (2013)

98. ATLAS Collaboration, Measurement of the associated production of a top-antitop-quark pair and a Higgs boson decaying into a $b\bar{b}$ pair in pp collisions at $\sqrt{s} = 13$ TeV using the ATLAS detector at the LHC. Eur. Phys. J. C **85**, 210 (2025). https://doi.org/10.1140/epjc/s10052-025-13740-x. arXiv:2407.10904 [hep-ex]

99. ATLAS Collaboration, ATLAS Computing Acknowledgements, ATL-SOFT-PUB-2025-001 (2025). https://cds.cern.ch/record/2922210

ATLAS Collaboration*

G. Aad[104], E. Aakvaag[17], B. Abbott[123], S. Abdelhameed[119a], K. Abeling[55], N.J. Abicht[49], S. H. Abidi[30], M. Aboelela[45], A. Aboulhorma[36e], H. Abramowicz[157], Y. Abulaiti[120], B. S. Acharya[69a,69b,n], A. Ackermann[63a], C. Adam Bourdarios[4], L. Adamczyk[86a], S. V. Addepalli[149], M. J. Addison[103], J. Adelman[118], A. Adiguzel[22c], T. Adye[137], A. A. Affolder[139], Y. Afik[40], M. N. Agaras[13], A. Aggarwal[102], C. Agheorghiesei[28c], F. Ahmadov[39,ae], S. Ahuja[97], X. Ai[143b], G. Aielli[76a,76b], A. Aikot[169], M. Ait Tamlihat[36e], B. Aitbenchikh[36a], M. Akbiyik[102], T. P. A. Åkesson[100], A. V. Akimov[151], D. Akiyama[174], N. N. Akolkar[25], S. Aktas[22a], G. L. Alberghi[24b], J. Albert[171], P. Albicocco[53], G. L. Albouy[60], S. Alderweireldt[52], Z. L. Alegria[124], M. Aleksa[37], I. N. Aleksandrov[39], C. Alexa[28b], T. Alexopoulos[10], F. Alfonsi[24b], M. Algren[56], M. Alhroob[173], B. Ali[135], H. M. J. Ali[93,x], S. Ali[32], S. W. Alibocus[94], M. Aliev[34c], G. Alimonti[71a], W. Alkakhi[55], C. Allaire[66], B. M. M. Allbrooke[152], J. S. Allen[103], J. F. Allen[52], P. P. Allport[21], A. Aloisio[72a,72b], F. Alonso[92], C. Alpigiani[142], Z. M. K. Alsolami[93], A. Alvarez Fernandez[102], M. Alves Cardoso[56], M. G. Alviggi[72a,72b], M. Aly[103], Y. Amaral Coutinho[83b], A. Ambler[106], C. Amelung[37], M. Amerl[103], C. G. Ames[111], T. Amezza[130], D. Amidei[108], B. Amini[54], K. Amirie[161], A. Amirkhanov[39], S. P. Amor Dos Santos[133a], K. R. Amos[169], D. Amperiadou[158], S. An[84], C. Anastopoulos[145], T. Andeen[11], J. K. Anders[94], A. C. Anderson[59], A. Andreazza[71a,71b], S. Angelidakis[9], A. Angerami[42], A. V. Anisenkov[39], A. Annovi[74a], C. Antel[56], E. Antipov[151], M. Antonelli[53], F. Anulli[75a], M. Aoki[84], T. Aoki[159], M. A. Aparo[152], L. Aperio Bella[48], M. Apicella[31], C. Appelt[157], A. Apyan[27], S. J. Arbiol Val[87], C. Arcangeletti[53], A. T. H. Arce[51], J-F. Arguin[110], S. Argyropoulos[158], J.-H. Arling[48], O. Arnaez[4], H. Arnold[151], G. Artoni[75a,75b], H. Asada[113], K. Asai[121], S. Asai[159], S. Asatryan[179], N. A. Asbah[37], R. A. Ashby Pickering[173], A. M. Aslam[97], K. Assamagan[30], R. Astalos[29a], K. S. V. Astrand[100], S. Atashi[165], R. J. Atkin[34a], H. Atmani[36f], P. A. Atmasiddha[131], K. Augsten[135], A. D. Auriol[41], V. A. Austrup[103], G. Avolio[37], K. Axiotis[56], G. Azuelos[110,ai], D. Babal[29b], H. Bachacou[138], K. Bachas[158,r], A. Bachiu[35], E. Bachmann[50], M. J. Backes[63a], A. Badea[40], T. M. Baer[108], P. Bagnaia[75a,75b], M. Bahmani[19], D. Bahner[54], K. Bai[126], J. T. Baines[137], L. Baines[96], O. K. Baker[178], E. Bakos[16], D. Bakshi Gupta[8], L. E. Balabram Filho[83b], V. Balakrishnan[123], R. Balasubramanian[4], E. M. Baldin[38], P. Balek[86a], E. Ballabene[24a,24b], F. Balli[138], L. M. Baltes[63a], W. K. Balunas[33], J. Balz[102], I. Bamwidhi[119b], E. Banas[87], M. Bandieramonte[132], A. Bandyopadhyay[25], S. Bansal[25], L. Barak[157], M. Barakat[48], E. L. Barberio[107], D. Barberis[18b], M. Barbero[104], M. Z. Barel[117], T. Barillari[112], M-S. Barisits[37], T. Barklow[149], P. Baron[136], D. A. Baron Moreno[103], A. Baroncelli[62], A. J. Barr[129], J. D. Barr[98], F. Barreiro[101], J. Barreiro Guimarães da Costa[14], M. G. Barros Teixeira[133a], S. Barsov[38], F. Bartels[63a], R. Bartoldus[149], A. E. Barton[93], P. Bartos[29a], A. Basan[102], M. Baselga[49], S. Bashiri[87], A. Bassalat[66,b], M. J. Basso[162a], S. Bataju[45], R. Bate[170], R. L. Bates[59], S. Batlamous[101], M. Battaglia[139], D. Battulga[19], M. Bauce[75a,75b], M. Bauer[79], P. Bauer[25], L. T. Bayer[48], L. T. Bazzano Hurrell[31], J. B. Beacham[112], T. Beau[130], J. Y. Beaucamp[92], P. H. Beauchemin[164], P. Bechtle[25], H. P. Beck[20,q], K. Becker[173], A. J. Beddall[82], V. A. Bednyakov[39], C. P. Bee[151], L. J. Beemster[16], M. Begalli[83d], M. Begel[30], J. K. Behr[48], J. F. Beirer[37], F. Beisiegel[25], M. Belfkir[119b], G. Bella[157], L. Bellagamba[24b], A. Bellerive[35], C. D. Bellgraph[68], P. Bellos[21], K. Beloborodov[38], D. Benchekroun[36a], F. Bendebba[36a], Y. Benhammou[157], K. C. Benkendorfer[61], L. Beresford[48], M. Beretta[53], E. Bergeaas Kuutmann[167], N. Berger[4], B. Bergmann[135], J. Beringer[18a], G. Bernardi[5], C. Bernius[149], F. U. Bernlochner[25], F. Bernon[37], A. Berrocal Guardia[13], T. Berry[97], P. Berta[136], A. Berthold[50], A. Berti[133a], R. Bertrand[104], S. Bethke[112], A. Betti[75a,75b], A. J. Bevan[96], L. Bezio[56], N. K. Bhalla[54], S. Bharthuar[112], S. Bhatta[151], P. Bhattarai[149], Z. M. Bhatti[120], K. D. Bhide[54], V. S. Bhopatkar[124], R. M. Bianchi[132], G. Bianco[24b,24a], O. Biebel[111], M. Biglietti[77a], C. S. Billingsley[45], Y. Bimgdi[36f], M. Bindi[55], A. Bingham[177], A. Bingul[22b], C. Bini[75a,75b], G. A. Bird[33], M. Birman[175], M. Biros[136], S. Biryukov[152], T. Bisanz[49], E. Bisceglie[24b,24a], J. P. Biswal[137], D. Biswas[147],

I. Bloch[48], A. Blue[59], U. Blumenschein[96], J. Blumenthal[102], V. S. Bobrovnikov[39], M. Boehler[54], B. Boehm[172], D. Bogavac[13], A. G. Bogdanchikov[38], L. S. Boggia[130], V. Boisvert[97], P. Bokan[37], T. Bold[86a], M. Bomben[5], M. Bona[96], M. Boonekamp[138], A. G. Borbély[59], I. S. Bordulev[38], G. Borissov[93], D. Bortoletto[129], D. Boscherini[24b], M. Bosman[13], K. Bouaouda[36a], N. Bouchhar[169], L. Boudet[4], J. Boudreau[132], E. V. Bouhova-Thacker[93], D. Boumediene[41], R. Bouquet[57b,57a], A. Boveia[122], J. Boyd[37], D. Boye[30], I. R. Boyko[39], L. Bozianu[56], J. Bracinik[21], N. Brahimi[4], G. Brandt[177], O. Brandt[33], B. Brau[105], J. E. Brau[126], R. Brener[175], L. Brenner[117], R. Brenner[167], S. Bressler[175], G. Brianti[78a,78b], D. Britton[59], D. Britzger[112], I. Brock[25], R. Brock[109], G. Brooijmans[42], A. J. Brooks[68], E. M. Brooks[162b], E. Brost[30], L. M. Brown[171,162a], L. E. Bruce[61], T. L. Bruckler[129], P. A. Bruckman de Renstrom[87], B. Brüers[48], A. Bruni[24b], G. Bruni[24b], D. Brunner[47a,47b], M. Bruschi[24b], N. Bruscino[75a,75b], T. Buanes[17], Q. Buat[142], D. Buchin[112], A. G. Buckley[59], O. Bulekov[82], B. A. Bullard[149], S. Burdin[94], C. D. Burgard[49], A. M. Burger[91], B. Burghgrave[8], O. Burlayenko[54], J. Burleson[168], J. C. Burzynski[148], E. L. Busch[42], V. Büscher[102], P. J. Bussey[59], J. M. Butler[26], C. M. Buttar[59], J. M. Butterworth[98], W. Buttinger[137], C. J. Buxo Vazquez[109], A. R. Buzykaev[39], S. Cabrera Urbán[169], L. Cadamuro[66], D. Caforio[58], H. Cai[132], Y. Cai[24b,114c,24a], Y. Cai[114a], V. M. M. Cairo[37], O. Cakir[3a], N. Calace[37], P. Calafiura[18a], G. Calderini[130], P. Calfayan[35], G. Callea[59], L. P. Caloba[83b], D. Calvet[41], S. Calvet[41], R. Camacho Toro[130], S. Camarda[37], D. Camarero Munoz[27], P. Camarri[76a,76b], C. Camincher[171], M. Campanelli[98], A. Camplani[43], V. Canale[72a,72b], A. C. Canbay[3a], E. Canonero[97], J. Cantero[169], Y. Cao[168], F. Capocasa[27], M. Capua[44b,44a], A. Carbone[71a,71b], R. Cardarelli[76a], J. C. J. Cardenas[8], M. P. Cardiff[27], G. Carducci[44b,44a], T. Carli[37], G. Carlino[72a], J. I. Carlotto[13], B. T. Carlson[132,s], E. M. Carlson[171], J. Carmignani[94], L. Carminati[71a,71b], A. Carnelli[4], M. Carnesale[37], S. Caron[116], E. Carquin[140f], I. B. Carr[107], S. Carrá[73a,73b], G. Carratta[24b,24a], A. M. Carroll[126], M. P. Casado[13,i], M. Caspar[48], F. L. Castillo[4], L. Castillo Garcia[13], V. Castillo Gimenez[169], N. F. Castro[133a,133e], A. Catinaccio[37], J. R. Catmore[128], T. Cavaliere[4], V. Cavaliere[30], L. J. Caviedes Betancourt[23b], E. Celebi[82], S. Cella[37], V. Cepaitis[56], K. Cerny[125], A. S. Cerqueira[83a], A. Cerri[74a,74b,al], L. Cerrito[76a,76b], F. Cerutti[18a], B. Cervato[71a,71b], A. Cervelli[24b], G. Cesarini[53], S. A. Cetin[82], P. M. Chabrillat[130], S. Chakraborty[173], J. Chan[18a], W. Y. Chan[159], J. D. Chapman[33], E. Chapon[138], B. Chargeishvili[155b], D. G. Charlton[21], C. Chauhan[136], Y. Che[114a], S. Chekanov[6], S. V. Chekulaev[162a], G. A. Chelkov[39,a], B. Chen[157], B. Chen[171], H. Chen[114a], H. Chen[30], J. Chen[144a], J. Chen[148], M. Chen[129], S. Chen[89], S. J. Chen[114a], X. Chen[144a], X. Chen[15,ah], Z. Chen[62], C. L. Cheng[176], H. C. Cheng[64a], S. Cheong[149], A. Cheplakov[39], E. Cherepanova[117], R. Cherkaoui El Moursli[36e], E. Cheu[7], K. Cheung[65], L. Chevalier[138], V. Chiarella[53], G. Chiarelli[74a], G. Chiodini[70a], A. S. Chisholm[21], A. Chitan[28b], M. Chitishvili[169], M. V. Chizhov[39,t], K. Choi[11], Y. Chou[142], E. Y. S. Chow[116], K. L. Chu[175], M. C. Chu[64a], X. Chu[14,114c], Z. Chubinidze[53], J. Chudoba[134], J. J. Chwastowski[87], D. Cieri[112], K. M. Ciesla[86a], V. Cindro[95], A. Ciocio[18a], F. Cirotto[72a,72b], Z. H. Citron[175], M. Citterio[71a], D. A. Ciubotaru[28b], A. Clark[56], P. J. Clark[52], N. Clarke Hall[98], C. Clarry[161], S. E. Clawson[48], C. Clement[47a,47b], Y. Coadou[104], M. Cobal[69a,69c], A. Coccaro[57b], R. F. Coelho Barrue[133a], R. Coelho Lopes De Sa[105], S. Coelli[71a], L. S. Colangeli[161], B. Cole[42], P. Collado Soto[101], J. Collot[60], R. Coluccia[70a,70b], P. Conde Muiño[133a,133g], M. P. Connell[34c], S. H. Connell[34c], E. I. Conroy[129], F. Conventi[72a,aj], H. G. Cooke[21], A. M. Cooper-Sarkar[129], L. Corazzina[75a,75b], F. A. Corchia[24b,24a], A. Cordeiro Oudot Choi[142], L. D. Corpe[41], M. Corradi[75a,75b], F. Corriveau[106,ac], A. Cortes-Gonzalez[159], M. J. Costa[169], F. Costanza[4], D. Costanzo[145], B. M. Cote[122], J. Couthures[4], G. Cowan[97], K. Cranmer[176], L. Cremer[49], D. Cremonini[24b,24a], S. Crépé-Renaudin[60], F. Crescioli[130], T. Cresta[73a,73b], M. Cristinziani[147], M. Cristoforetti[78a,78b], V. Croft[117], J. E. Crosby[124], G. Crosetti[44b,44a], A. Cueto[101], H. Cui[98], Z. Cui[7], W. R. Cunningham[59], F. Curcio[169], J. R. Curran[52], M. J. Da Cunha Sargedas De Sousa[57b,57a], J. V. Da Fonseca Pinto[83b], C. Da Via[103], W. Dabrowski[86a], T. Dado[37], S. Dahbi[154], T. Dai[108], D. Dal Santo[20], C. Dallapiccola[105], M. Dam[43], G. D'amen[30], V. D'Amico[111], J. Damp[102], J. R. Dandoy[35], D. Dannheim[37], G. D'anniballe[74a,74b], M. Danninger[148], V. Dao[151], G. Darbo[57b], S. J. Das[30], F. Dattola[48], S. D'Auria[71a,71b], A. D'Avanzo[72a,72b], T. Davidek[136], J. Davidson[173], I. Dawson[96], K. De[8], C. De Almeida Rossi[161], R. De Asmundis[72a], N. De Biase[48], S. De Castro[24b,24a], N. De Groot[116], P. de Jong[117], H. De la Torre[118], A. De Maria[114a], A. De Salvo[75a], U. De Sanctis[76a,76b], F. De Santis[70a,70b], A. De Santo[152], J. B. De Vivie De Regie[60], J. Debevc[95], D. V. Dedovich[39], J. Degens[94], A. M. Deiana[45], J. Del Peso[101], L. Delagrange[130], F. Deliot[138], C. M. Delitzsch[49], M. Della Pietra[72a,72b], D. Della Volpe[56], A. Dell'Acqua[37], L. Dell'Asta[71a,71b], M. Delmastro[4], C. C. Delogu[102], P. A. Delsart[60],

S. Demers[178], M. Demichev[39], S. P. Denisov[38], H. Denizli[22a,m], L. D'Eramo[41], D. Derendarz[87], F. Derue[130], P. Dervan[94], K. Desch[25], F. A. Di Bello[57b,57a], A. Di Ciaccio[76a,76b], L. Di Ciaccio[4], A. Di Domenico[75a,75b], C. Di Donato[72a,72b], A. Di Girolamo[37], G. Di Gregorio[37], A. Di Luca[78a,78b], B. Di Micco[77a,77b], R. Di Nardo[77a,77b], K. F. Di Petrillo[40], M. Diamantopoulou[35], F. A. Dias[117], M. A. Diaz[140a,140b], A. R. Didenko[39], M. Didenko[169], S. D. Diefenbacher[18a], E. B. Diehl[108], S. Díez Cornell[48], C. Diez Pardos[147], C. Dimitriadi[150], A. Dimitrievska[21], A. Dimri[151], J. Dingfelder[25], T. Dingley[129], I-M. Dinu[28b], S. J. Dittmeier[63b], F. Dittus[37], M. Divisek[136], B. Dixit[94], F. Djama[104], T. Djobava[155b], C. Doglioni[103,100], A. Dohnalova[29a], Z. Dolezal[136], K. Domijan[86a], K. M. Dona[40], M. Donadelli[83d], B. Dong[109], J. Donini[41], A. D'Onofrio[72a,72b], M. D'Onofrio[94], J. Dopke[137], A. Doria[72a], N. Dos Santos Fernandes[133a], P. Dougan[103], M. T. Dova[92], A. T. Doyle[59], M. A. Draguet[129], M. P. Drescher[55], E. Dreyer[175], I. Drivas-koulouris[10], M. Drnevich[120], M. Drozdova[56], D. Du[62], T. A. du Pree[117], Z. Duan[114a], F. Dubinin[39], M. Dubovsky[29a], E. Duchovni[175], G. Duckeck[111], P. K. Duckett[98], O. A. Ducu[28b], D. Duda[52], A. Dudarev[37], E. R. Duden[27], M. D'uffizi[103], L. Duflot[66], M. Dührssen[37], I. Duminica[28g], A. E. Dumitriu[28b], M. Dunford[63a], S. Dungs[49], K. Dunne[47a,47b], A. Duperrin[104], H. Duran Yildiz[3a], M. Düren[58], A. Durglishvili[155b], D. Duvnjak[35], B. L. Dwyer[118], G. I. Dyckes[18a], M. Dyndal[86a], B. S. Dziedzic[37], Z. O. Earnshaw[152], G. H. Eberwein[129], B. Eckerova[29a], S. Eggebrecht[55], E. Egidio Purcino De Souza[83e], G. Eigen[17], K. Einsweiler[18a], T. Ekelof[167], P. A. Ekman[100], S. El Farkh[36b], Y. El Ghazali[62], H. El Jarrari[37], A. El Moussaouy[36a], V. Ellajosyula[167], M. Ellert[167], F. Ellinghaus[177], N. Ellis[37], J. Elmsheuser[30], M. Elsawy[119a], M. Elsing[37], D. Emeliyanov[137], Y. Enari[84], I. Ene[18a], S. Epari[110], D. Ernani Martins Neto[87], F. Ernst[37], M. Errenst[177], M. Escalier[66], C. Escobar[169], E. Etzion[157], G. Evans[133a,133b], H. Evans[68], L. S. Evans[97], A. Ezhilov[38], S. Ezzarqtouni[36a], F. Fabbri[24b,24a], L. Fabbri[24b,24a], G. Facini[98], V. Fadeyev[139], R. M. Fakhrutdinov[38], D. Fakoudis[102], S. Falciano[75a], L. F. Falda Ulhoa Coelho[133a], F. Fallavollita[112], G. Falsetti[44b,44a], J. Faltova[136], C. Fan[168], K. Y. Fan[64b], Y. Fan[14], Y. Fang[14,114c], M. Fanti[71a,71b], M. Faraj[69a,69b], Z. Farazpay[99], A. Farbin[8], A. Farilla[77a], T. Farooque[109], J. N. Farr[178], S. M. Farrington[137,52], F. Fassi[36e], D. Fassouliotis[9], L. Fayard[66], P. Federic[136], P. Federicova[134], O. L. Fedin[38,a], M. Feickert[176], L. Feligioni[104], D. E. Fellers[18a], C. Feng[143a], Z. Feng[117], M. J. Fenton[165], L. Ferencz[48], B. Fernandez Barbadillo[93], P. Fernandez Martinez[67], M. J. V. Fernoux[104], J. Ferrando[93], A. Ferrari[167], P. Ferrari[117,116], R. Ferrari[73a], D. Ferrere[56], C. Ferretti[108], M. P. Fewell[1], D. Fiacco[75a,75b], F. Fiedler[102], P. Fiedler[135], S. Filimonov[39], M. S. Filip[28b,u], A. Filipčič[95], E. K. Filmer[162a], F. Filthaut[116], M. C. N. Fiolhais[133a,133c,c], L. Fiorini[169], W. C. Fisher[109], T. Fitschen[103], P. M. Fitzhugh[138], I. Fleck[147], P. Fleischmann[108], T. Flick[177], M. Flores[34d,ag], L. R. Flores Castillo[64a], L. Flores Sanz De Acedo[37], F. M. Follega[78a,78b], N. Fomin[33], J. H. Foo[161], A. Formica[138], A. C. Forti[103], E. Fortin[37], A. W. Fortman[18a], L. Foster[18a], L. Fountas[9,j], D. Fournier[66], H. Fox[93], P. Francavilla[74a,74b], S. Francescato[61], S. Franchellucci[56], M. Franchini[24b,24a], S. Franchino[63a], D. Francis[37], L. Franco[116], V. Franco Lima[37], L. Franconi[48], M. Franklin[61], G. Frattari[27], Y. Y. Frid[157], J. Friend[59], N. Fritzsche[37], A. Froch[56], D. Froidevaux[37], J. A. Frost[129], Y. Fu[109], S. Fuenzalida Garrido[140f], M. Fujimoto[104], K. Y. Fung[64a], E. Furtado De Simas Filho[83e], M. Furukawa[159], J. Fuster[169], A. Gaa[55], A. Gabrielli[24b,24a], A. Gabrielli[161], P. Gadow[37], G. Gagliardi[57b,57a], L. G. Gagnon[18a], S. Gaid[88b], S. Galantzan[157], J. Gallagher[1], E. J. Gallas[129], A. L. Gallen[167], B. J. Gallop[137], K. K. Gan[122], S. Ganguly[159], Y. Gao[52], A. Garabaglu[142], F. M. Garay Walls[140a,140b], C. García[169], A. Garcia Alonso[117], A. G. Garcia Caffaro[178], J. E. García Navarro[169], M. Garcia-Sciveres[18a], G. L. Gardner[131], R. W. Gardner[40], N. Garelli[164], R. B. Garg[149], J. M. Gargan[52], C. A. Garner[161], C. M. Garvey[34a], V. K. Gassmann[164], G. Gaudio[73a], V. Gautam[13], P. Gauzzi[75a,75b], J. Gavranovic[95], I. L. Gavrilenko[133a], A. Gavrilyuk[38], C. Gay[170], G. Gaycken[126], E. N. Gazis[10], A. Gekow[122], C. Gemme[57b], M. H. Genest[60], A. D. Gentry[115], S. George[97], T. Geralis[46], A. A. Gerwin[123], P. Gessinger-Befurt[37], M. E. Geyik[177], M. Ghani[173], K. Ghorbanian[96], A. Ghosal[147], A. Ghosh[165], A. Ghosh[7], B. Giacobbe[24b], S. Giagu[75a,75b], T. Giani[117], A. Giannini[62], S. M. Gibson[97], M. Gignac[139], D. T. Gil[86b], A. K. Gilbert[86a], B. J. Gilbert[42], D. Gillberg[35], G. Gilles[117], D. M. Gingrich[2,ai], M. P. Giordani[69a,69c], P. F. Giraud[138], G. Giugliarelli[69a,69c], D. Giugni[71a], F. Giuli[76a,76b], I. Gkialas[9,j], L. K. Gladilin[38], C. Glasman[101], M. Glazewska[20], R. M. Gleason[165], G. Glemža[48], M. Glisic[126], I. Gnesi[44b], Y. Go[30], M. Goblirsch-Kolb[37], B. Gocke[49], D. Godin[110], B. Gokturk[22a], S. Goldfarb[107], T. Golling[56], M. G. D. Gololo[34c], D. Golubkov[38], J. P. Gombas[109], A. Gomes[133a,133b], G. Gomes Da Silva[147], A. J. Gomez Delegido[169], R. Gonçalo[133a], L. Gonella[21], A. Gongadze[155c], F. Gonnella[21], J. L. Gonski[149], R. Y. González Andana[52], S. González de la Hoz[169], M. V. Gonzalez Rodrigues[48], R. Gonzalez Suarez[167], S. Gonzalez-Sevilla[56], L. Goossens[37], B. Gorini[37],

E. Gorini[70a,70b], A. Gorišek[95], T. C. Gosart[131], A. T. Goshaw[51], M. I. Gostkin[39], S. Goswami[124], C. A. Gottardo[37], S. A. Gotz[111], M. Gouighri[36b], A. G. Goussiou[142], N. Govender[34c], R. P. Grabarczyk[129], I. Grabowska-Bold[86a], K. Graham[35], E. Gramstad[128], S. Grancagnolo[70a,70b], C. M. Grant[1], P. M. Gravila[28f], F. G. Gravili[70a,70b], H. M. Gray[18a], M. Greco[112], M. J. Green[1], C. Grefe[25], A. S. Grefsrud[17], I. M. Gregor[48], K. T. Greif[165], P. Grenier[149], S. G. Grewe[112], A. A. Grillo[139], K. Grimm[32], S. Grinstein[13,y], J.-F. Grivaz[66], E. Gross[175], J. Grosse-Knetter[55], L. Guan[108], G. Guerrieri[37], R. Guevara[128], R. Gugel[102], J. A. M. Guhit[108], A. Guida[19], E. Guilloton[173], S. Guindon[37], F. Guo[14,114c], J. Guo[144a], L. Guo[48], L. Guo[114b,w], Y. Guo[108], A. Gupta[49], R. Gupta[132], S. Gupta[27], S. Gurbuz[25], S. S. Gurdasani[48], G. Gustavino[75a,75b], P. Gutierrez[123], L. F. Gutierrez Zagazeta[131], M. Gutsche[50], C. Gutschow[98], C. Gwenlan[129], C. B. Gwilliam[94], E. S. Haaland[128], A. Haas[120], M. Habedank[59], C. Haber[18a], H. K. Hadavand[8], A. Haddad[41], A. Hadef[50], A. I. Hagan[93], J. J. Hahn[147], E. H. Haines[98], M. Haleem[172], J. Haley[124], G. D. Hallewell[104], L. Halser[20], K. Hamano[171], M. Hamer[25], S. E. D. Hammoud[66], E. J. Hampshire[97], J. Han[143a], L. Han[114a], L. Han[62], S. Han[18a], K. Hanagaki[84], M. Hance[139], D. A. Hangal[42], H. Hanif[148], M. D. Hank[131], J. B. Hansen[43], P. H. Hansen[43], D. Harada[56], T. Harenberg[177], S. Harkusha[179], M. L. Harris[105], Y. T. Harris[25], J. Harrison[13], N. M. Harrison[122], P. F. Harrison[173], M. L. E. Hart[98], N. M. Hartman[112], N. M. Hartmann[111], R. Z. Hasan[97,137], Y. Hasegawa[146], F. Haslbeck[129], S. Hassan[17], R. Hauser[109], M. Haviernik[136], C. M. Hawkes[21], R. J. Hawkings[37], Y. Hayashi[159], D. Hayden[109], C. Hayes[108], R. L. Hayes[117], C. P. Hays[129], J. M. Hays[96], H. S. Hayward[94], M. He[14,114c], Y. He[48], Y. He[98], N. B. Heatley[96], V. Hedberg[100], C. Heidegger[54], K. K. Heidegger[54], J. Heilman[35], S. Heim[48], T. Heim[18a], J. G. Heinlein[131], J. J. Heinrich[126], L. Heinrich[112], J. Hejbal[134], M. Helbig[50], A. Held[176], S. Hellesund[17], C. M. Helling[170], S. Hellman[47a,47b], A. M. Henriques Correia[37], H. Herde[100], Y. Hernández Jiménez[151], L. M. Herrmann[25], T. Herrmann[50], G. Herten[54], R. Hertenberger[111], L. Hervas[37], M. E. Hesping[102], N. P. Hessey[162a], J. Hessler[112], M. Hidaoui[36b], N. Hidic[136], E. Hill[161], T. S. Hillersoy[17], S. J. Hillier[21], J. R. Hinds[109], F. Hinterkeuser[25], M. Hirose[127], S. Hirose[163], D. Hirschbuehl[177], T. G. Hitchings[103], B. Hiti[95], J. Hobbs[151], R. Hobincu[28e], N. Hod[175], A. M. Hodges[168], M. C. Hodgkinson[145], B. H. Hodkinson[129], A. Hoecker[37], D. D. Hofer[108], J. Hofer[169], M. Holzbock[37], L. B. A. H. Hommels[33], V. Homsak[129], B. P. Honan[103], J. J. Hong[68], T. M. Hong[132], B. H. Hooberman[168], W. H. Hopkins[6], M. C. Hoppesch[168], Y. Horii[113], M. E. Horstmann[112], S. Hou[154], M. R. Housenga[168], A. S. Howard[95], J. Howarth[59], J. Hoya[6], M. Hrabovsky[125], T. Hryn'ova[4], P. J. Hsu[65], S.-C. Hsu[142], T. Hsu[66], M. Hu[18a], Q. Hu[62], S. Huang[33], X. Huang[14,114c], Y. Huang[136], Y. Huang[114b], Y. Huang[102], Y. Huang[14], Z. Huang[66], Z. Hubacek[135], M. Huebner[25], F. Huegging[25], T. B. Huffman[129], M. Hufnagel Maranha De Faria[83a], C. A. Hugli[48], M. Huhtinen[37], S. K. Huiberts[17], R. Hulsken[106], C. E. Hultquist[18a], N. Huseynov[12,g], J. Huston[109], J. Huth[61], R. Hyneman[7], G. Iacobucci[56], G. Iakovidis[30], L. Iconomidou-Fayard[66], J. P. Iddon[37], P. Iengo[72a,72b], R. Iguchi[159], Y. Iiyama[159], T. Iizawa[159], Y. Ikegami[84], D. Iliadis[158], N. Ilic[161], H. Imam[36a], G. Inacio Goncalves[83d], S. A. Infante Cabanas[140c], T. Ingebretsen Carlson[47a,47b], J. M. Inglis[96], G. Introzzi[73a,73b], M. Iodice[77a], V. Ippolito[75a,75b], R. K. Irwin[94], M. Ishino[159], W. Islam[176], C. Issever[19], S. Istin[22a,an], K. Itabashi[84], H. Ito[174], R. Iuppa[78a,78b], A. Ivina[175], V. Izzo[72a], P. Jacka[134], P. Jackson[1], P. Jain[48], K. Jakobs[54], T. Jakoubek[175], J. Jamieson[59], W. Jang[159], S. Jankovych[136], M. Javurkova[105], P. Jawahar[103], L. Jeanty[126], J. Jejelava[155a,af], P. Jenni[54,f], C. E. Jessiman[35], C. Jia[143a], H. Jia[170], J. Jia[151], X. Jia[14,114c], Z. Jia[114a], C. Jiang[52], Q. Jiang[64b], S. Jiggins[48], M. Jimenez Ortega[169], J. Jimenez Pena[13], S. Jin[114a], A. Jinaru[28b], O. Jinnouchi[141], P. Johansson[145], K. A. Johns[7], J. W. Johnson[139], F. A. Jolly[48], D. M. Jones[152], E. Jones[48], K. S. Jones[8], P. Jones[33], R. W. L. Jones[93], T. J. Jones[94], H. L. Joos[55,37], R. Joshi[122], J. Jovicevic[16], X. Ju[18a], J. J. Junggeburth[37], T. Junkermann[63a], A. Juste Rozas[13,y], M. K. Juzek[87], S. Kabana[140e], A. Kaczmarska[87], M. Kado[112], H. Kagan[122], M. Kagan[149], A. Kahn[131], C. Kahra[102], T. Kaji[159], E. Kajomovitz[156], N. Kakati[175], N. Kakoty[13], I. Kalaitzidou[54], S. Kandel[8], N. J. Kang[139], D. Kar[34g], K. Karava[129], E. Karentzos[25], O. Karkout[117], S. N. Karpov[39], Z. M. Karpova[39], V. Kartvelishvili[93], A. N. Karyukhin[38], E. Kasimi[158], J. Katzy[48], S. Kaur[35], K. Kawade[146], M. P. Kawale[123], C. Kawamoto[89], T. Kawamoto[62], E. F. Kay[37], F. I. Kaya[164], S. Kazakos[109], V. F. Kazanin[38], J. M. Keaveney[34a], R. Keeler[171], G. V. Kehris[61], J. S. Keller[35], J. J. Kempster[152], O. Kepka[134], J. Kerr[162b], B. P. Kerridge[137], B. P. Kerševan[95], L. Keszeghova[29a], R. A. Khan[132], A. Khanov[124], A. G. Kharlamov[38], T. Kharlamova[38], E. E. Khoda[142], M. Kholodenko[133a], T. J. Khoo[19], G. Khoriauli[172], Y. Khoulaki[36a], J. Khubua[155b,*], Y. A. R. Khwaira[130], B. Kibirige[34g], D. Kim[6], D. W. Kim[47a,47b], Y. K. Kim[40], N. Kimura[98], M. K. Kingston[55], A. Kirchhoff[55], C. Kirfel[25], F. Kirfel[25],

J. Kirk[137], A. E. Kiryunin[112], S. Kita[163], O. Kivernyk[25], M. Klassen[164], C. Klein[35], L. Klein[172], M. H. Klein[45], S. B. Klein[56], U. Klein[94], A. Klimentov[30], T. Klioutchnikova[37], P. Kluit[117], S. Kluth[112], E. Kneringer[79], T. M. Knight[161], A. Knue[49], M. Kobel[50], D. Kobylianskii[175], S. F. Koch[129], M. Kocian[149], P. Kodyš[136], D. M. Koeck[126], T. Koffas[35], O. Kolay[50], I. Koletsou[4], T. Komarek[87], K. Köneke[55], A. X. Y. Kong[1], T. Kono[121], N. Konstantinidis[98], P. Kontaxakis[56], B. Konya[100], R. Kopeliansky[42], S. Koperny[86a], K. Korcyl[87], K. Kordas[158,d], A. Korn[98], S. Korn[55], I. Korolkov[13], N. Korotkova[38], B. Kortman[117], O. Kortner[112], S. Kortner[112], W. H. Kostecka[118], M. Kostov[29a], V. V. Kostyukhin[147], A. Kotsokechagia[37], A. Kotwal[51], A. Koulouris[37], A. Kourkoumeli-Charalampidi[73a,73b], C. Kourkoumelis[9], E. Kourlitis[112], O. Kovanda[126], R. Kowalewski[171], W. Kozanecki[126], A. S. Kozhin[38], V. A. Kramarenko[38], G. Kramberger[95], P. Kramer[25], M. W. Krasny[130], A. Krasznahorkay[105], A. C. Kraus[118], J. W. Kraus[177], J. A. Kremer[48], N. B. Krengel[147], T. Kresse[50], L. Kretschmann[177], J. Kretzschmar[94], K. Kreul[19], P. Krieger[161], K. Krizka[21], K. Kroeninger[49], H. Kroha[112], J. Kroll[134], J. Kroll[131], K. S. Krowpman[109], U. Kruchonak[39], H. Krüger[25], N. Krumnack[81], M. C. Kruse[51], O. Kuchinskaia[39], S. Kuday[3a], S. Kuehn[37], R. Kuesters[54], T. Kuhl[48], V. Kukhtin[39], Y. Kulchitsky[39], S. Kuleshov[140d,140b], J. Kull[1], M. Kumar[34g], N. Kumari[48], P. Kumari[162b], A. Kupco[134], T. Kupfer[49], A. Kupich[38], O. Kuprash[54], H. Kurashige[85], L. L. Kurchaninov[162a], O. Kurdysh[4], Y. A. Kurochkin[38], A. Kurova[38], M. Kuze[141], A. K. Kvam[105], J. Kvita[125], N. G. Kyriacou[108], C. Lacasta[169], F. Lacava[75a,75b], H. Lacker[19], D. Lacour[130], N. N. Lad[98], E. Ladygin[39], A. Lafarge[41], B. Laforge[130], T. Lagouri[178], F. Z. Lahbabi[36a], S. Lai[55], J. E. Lambert[171], S. Lammers[68], W. Lampl[7], C. Lampoudis[158,d], G. Lamprinoudis[102], A. N. Lancaster[118], E. Lançon[30], U. Landgraf[54], M. P. J. Landon[96], V. S. Lang[54], O. K. B. Langrekken[128], A. J. Lankford[165], F. Lanni[37], K. Lantzsch[25], A. Lanza[73a], M. Lanzac Berrocal[169], J. F. Laporte[138], T. Lari[71a], D. Larsen[17], L. Larson[11], F. Lasagni Manghi[24b], M. Lassnig[37], S. D. Lawlor[145], R. Lazaridou[173], M. Lazzaroni[71a,71b], H. D. M. Le[109], E. M. Le Boulicaut[178], L. T. Le Pottier[18a], B. Leban[24b,24a], F. Ledroit-Guillon[60], T. F. Lee[162b], L. L. Leeuw[34c], M. Lefebvre[171], C. Leggett[18a], G. Lehmann Miotto[37], M. Leigh[56], W. A. Leight[105], W. Leinonen[116], A. Leisos[158,v], M. A. L. Leite[83c], C. E. Leitgeb[19], R. Leitner[136], K. J. C. Leney[45], T. Lenz[25], S. Leone[74a], C. Leonidopoulos[52], A. Leopold[150], J. H. Lepage Bourbonnais[35], R. Les[109], C. G. Lester[33], M. Levchenko[38], J. Levêque[4], L. J. Levinson[175], G. Levrini[24b,24a], M. P. Lewicki[87], C. Lewis[142], D. J. Lewis[4], L. Lewitt[145], A. Li[30], B. Li[143a], C. Li[108], C-Q. Li[112], H. Li[143a], H. Li[103], H. Li[15], H. Li[62], H. Li[143a], J. Li[144a], K. Li[14], L. Li[144a], R. Li[178], S. Li[14,114c], S. Li[144b,144a], T. Li[5], X. Li[106], Z. Li[159], Z. Li[14,114c], Z. Li[62], S. Liang[14,114c], Z. Liang[14], M. Liberatore[138], B. Liberti[76a], K. Lie[64c], J. Lieber Marin[83e], H. Lien[68], H. Lin[108], S. F. Lin[151], L. Linden[111], R. E. Lindley[7], J. H. Lindon[37], J. Ling[61], E. Lipeles[131], A. Lipniacka[17], A. Lister[170], J. D. Little[68], B. Liu[14], B. X. Liu[114b], D. Liu[144b,144a], D. Liu[139], E. H. L. Liu[21], J. K. K. Liu[120], K. Liu[144b], K. Liu[144b,144a], M. Liu[62], M. Y. Liu[62], P. Liu[14], Q. Liu[144b,142,144a], X. Liu[62], X. Liu[143a], Y. Liu[114b,114c], Y. L. Liu[143a], Y. W. Liu[62], Z. Liu[66,l], S. L. Lloyd[96], E. M. Lobodzinska[48], P. Loch[7], E. Lodhi[161], T. Lohse[19], K. Lohwasser[145], E. Loiacono[48], J. D. Lomas[21], J. D. Long[42], I. Longarini[165], R. Longo[168], A. Lopez Solis[13], N. A. Lopez-canelas[7], N. Lorenzo Martinez[4], A. M. Lory[111], M. Losada[119a], G. Löschcke Centeno[152], X. Lou[47a,47b], X. Lou[14,114c], A. Lounis[66], P. A. Love[93], M. Lu[66], S. Lu[131], Y. J. Lu[154], H. J. Lubatti[142], C. Luci[75a,75b], F. L. Lucio Alves[114a], F. Luehring[68], B. S. Lunday[131], O. Lundberg[150], J. Lunde[37], N. A. Luongo[6], M. S. Lutz[37], A. B. Lux[26], D. Lynn[30], R. Lysak[134], V. Lysenko[135], E. Lytken[100], V. Lyubushkin[39], T. Lyubushkina[39], M. M. Lyukova[151], M. Firdaus M. Soberi[52], H. Ma[30], K. Ma[62], L. L. Ma[143a], W. Ma[62], Y. Ma[124], J. C. MacDonald[102], P. C. Machado De Abreu Farias[83e], R. Madar[41], T. Madula[98], J. Maeda[85], T. Maeno[30], P. T. Mafa[34c,k], H. Maguire[145], V. Maiboroda[66], A. Maio[133a,133b,133d], K. Maj[86a], O. Majersky[48], S. Majewski[126], R. Makhmanazarov[38], N. Makovec[66], V. Maksimovic[16], B. Malaescu[130], J. Malamant[128], Pa. Malecki[87], V. P. Maleev[38], F. Malek[60,p], M. Mali[95], D. Malito[97], U. Mallik[80,*], A. Maloizel[5], S. Maltezos[10], A. Malvezzi Lopes[83d], S. Malyukov[39], J. Mamuzic[13], G. Mancini[53], M. N. Mancini[27], G. Manco[73a,73b], J. P. Mandalia[96], S. S. Mandarry[152], I. Mandić[95], L. Manhaes de Andrade Filho[83a], I. M. Maniatis[175], J. Manjarres Ramos[91], D. C. Mankad[175], A. Mann[111], T. Manoussos[37], M. N. Mantinan[40], S. Manzoni[37], L. Mao[144a], X. Mapekula[34c], A. Marantis[158], R. R. Marcelo Gregorio[96], G. Marchiori[5], M. Marcisovsky[134], C. Marcon[71a], E. Maricic[16], M. Marinescu[48], S. Marium[48], M. Marjanovic[123], A. Markhoos[54], M. Markovitch[66], M. K. Maroun[105], G. T. Marsden[103], E. J. Marshall[93], Z. Marshall[18a], S. Marti-Garcia[169], J. Martin[98], T. A. Martin[137], V. J. Martin[52], B. Martin dit Latour[17], L. Martinelli[75a,75b], M. Martinez[13,y], P. Martinez Agullo[169],

V. I. Martinez Outschoorn[105], P. Martinez Suarez[13], S. Martin-Haugh[137], G. Martinovicova[136], V. S. Martoiu[28b], A. C. Martyniuk[98], A. Marzin[37], D. Mascione[78a,78b], L. Masetti[102], J. Masik[103], A. L. Maslennikov[39], S. L. Mason[42], P. Massarotti[72a,72b], P. Mastrandrea[74a,74b], A. Mastroberardino[44b,44a], T. Masubuchi[127], T. T. Mathew[126], J. Matousek[136], D. M. Mattern[49], J. Maurer[28b], T. Maurin[59], A. J. Maury[66], B. Maček[95], C. Mavungu Tsava[104], D. A. Maximov[38], A. E. May[103], E. Mayer[41], R. Mazini[34g], I. Maznas[118], S. M. Mazza[139], E. Mazzeo[37], J. P. Mc Gowan[171], S. P. Mc Kee[108], C. A. Mc Lean[6], C. C. McCracken[170], E. F. McDonald[107], A. E. McDougall[117], L. F. Mcelhinney[93], J. A. Mcfayden[152], R. P. McGovern[131], R. P. Mckenzie[34g], T. C. Mclachlan[48], D. J. Mclaughlin[98], S. J. McMahon[137], C. M. Mcpartland[94], R. A. McPherson[171,ac], S. Mehlhase[111], A. Mehta[94], D. Melini[169], B. R. Mellado Garcia[34g], A. H. Melo[55], F. Meloni[48], A. M. Mendes Jacques Da Costa[103], L. Meng[93], S. Menke[112], M. Mentink[37], E. Meoni[44b,44a], G. Mercado[118], S. Merianos[158], C. Merlassino[69a,69c], C. Meroni[71a,71b], J. Metcalfe[6], A. S. Mete[6], E. Meuser[102], C. Meyer[68], J-P. Meyer[138], Y. Miao[114a], R. P. Middleton[137], M. Mihovilovic[66], L. Mijović[52], G. Mikenberg[175], M. Mikestikova[134], M. Mikuž[95], H. Mildner[102], A. Milic[37], D. W. Miller[40], E. H. Miller[149], L. S. Miller[35], A. Milov[175], D. A. Milstead[47a,47b], T. Min[114a], A. A. Minaenko[38], I. A. Minashvili[155b], A. I. Mincer[120], B. Mindur[86a], M. Mineev[39], Y. Mino[89], L. M. Mir[13], M. Miralles Lopez[59], M. Mironova[18a], M. C. Missio[116], A. Mitra[173], V. A. Mitsou[169], Y. Mitsumori[113], O. Miu[161], P. S. Miyagawa[96], T. Mkrtchyan[63a], M. Mlinarevic[98], T. Mlinarevic[98], M. Mlynarikova[37], S. Mobius[20], M. H. Mohamed Farook[115], S. Mohapatra[42], S. Mohiuddin[124], G. Mokgatitswane[34g], L. Moleri[175], U. Molinatti[129], L. G. Mollier[20], B. Mondal[147], S. Mondal[135], K. Mönig[48], E. Monnier[104], L. Monsonis Romero[169], J. Montejo Berlingen[13], A. Montella[47a,47b], M. Montella[122], F. Montereali[77a,77b], F. Monticelli[92], S. Monzani[69a,69c], A. Morancho Tarda[43], N. Morange[66], A. L. Moreira De Carvalho[48], M. Moreno Llácer[169], C. Moreno Martinez[56], J. M. Moreno Perez[23b], P. Morettini[57b], S. Morgenstern[37], M. Morii[61], M. Morinaga[159], M. Moritsu[90], F. Morodei[75a,75b], P. Moschovakos[37], B. Moser[54], M. Mosidze[155b], T. Moskalets[45], P. Moskvitina[116], J. Moss[32], P. Moszkowicz[86a], A. Moussa[36d], Y. Moyal[175], H. Moyano Gomez[13], E. J. W. Moyse[105], O. Mtintsilana[34g], S. Muanza[104], M. Mucha[25], J. Mueller[132], R. Müller[37], G. A. Mullier[167], A. J. Mullin[33], J. J. Mullin[51], A. C. Mullins[45], A. E. Mulski[61], D. P. Mungo[161], D. Munoz Perez[169], F. J. Munoz Sanchez[103], W. J. Murray[173,137], M. Muškinja[95], C. Mwewa[48], A. G. Myagkov[38,a], A. J. Myers[8], G. Myers[108], M. Myska[135], B. P. Nachman[18a], K. Nagai[129], K. Nagano[84], R. Nagasaka[159], J. L. Nagle[30,ak], E. Nagy[104], A. M. Nairz[37], Y. Nakahama[84], K. Nakamura[84], K. Nakkalil[5], A. Nandi[63b], H. Nanjo[127], E. A. Narayanan[45], Y. Narukawa[159], I. Naryshkin[38], L. Nasella[71a,71b], S. Nasri[119b], C. Nass[25], G. Navarro[23a], J. Navarro-Gonzalez[169], A. Nayaz[19], P. Y. Nechaeva[38], S. Nechaeva[24b,24a], F. Nechansky[134], L. Nedic[129], T. J. Neep[21], A. Negri[73a,73b], M. Negrini[24b], C. Nellist[117], C. Nelson[106], K. Nelson[108], S. Nemecek[134], M. Nessi[37,h], M. S. Neubauer[168], J. Newell[94], P. R. Newman[21], Y. W. Y. Ng[168], B. Ngair[119a], H. D. N. Nguyen[110], J. D. Nichols[123], R. B. Nickerson[129], R. Nicolaidou[138], J. Nielsen[139], M. Niemeyer[55], J. Niermann[37], N. Nikiforou[37], V. Nikolaenko[38,a], I. Nikolic-Audit[130], P. Nilsson[30], I. Ninca[48], G. Ninio[157], A. Nisati[75a], N. Nishu[2], R. Nisius[112], N. Nitika[69a,69c], J-E. Nitschke[50], E. K. Nkadimeng[34b], T. Nobe[159], T. Nommensen[153], M. B. Norfolk[145], B. J. Norman[35], M. Noury[36a], J. Novak[95], T. Novak[95], R. Novotny[135], L. Nozka[125], K. Ntekas[165], N. M. J. Nunes De Moura Junior[83b], J. Ocariz[130], A. Ochi[85], I. Ochoa[133a], S. Oerdek[48,z], J. T. Offermann[40], A. Ogrodnik[136], A. Oh[103], C. C. Ohm[150], H. Oide[84], M. L. Ojeda[37], Y. Okumura[159], L. F. Oleiro Seabra[133a], I. Oleksiyuk[56], G. Oliveira Correa[13], D. Oliveira Damazio[30], J. L. Oliver[165], Ö. O. Öncel[54], A. P. O'Neill[20], A. Onofre[133a,133e,e], P. U. E. Onyisi[11], M. J. Oreglia[40], D. Orestano[77a,77b], R. Orlandini[77a,77b], R. S. Orr[161], L. M. Osojnak[131], Y. Osumi[113], G. Otero y Garzon[31], H. Otono[90], G. J. Ottino[18a], M. Ouchrif[36d], F. Ould-Saada[128], T. Ovsiannikova[142], M. Owen[59], R. E. Owen[137], V. E. Ozcan[22a], F. Ozturk[87], N. Ozturk[8], S. Ozturk[82], H. A. Pacey[129], K. Pachal[162a], A. Pacheco Pages[13], C. Padilla Aranda[13], G. Padovano[75a,75b], S. Pagan Griso[18a], G. Palacino[68], A. Palazzo[70a,70b], J. Pampel[25], J. Pan[178], T. Pan[64a], D. K. Panchal[11], C. E. Pandini[60], J. G. Panduro Vazquez[137], H. D. Pandya[1], H. Pang[138], P. Pani[48], G. Panizzo[69a,69c], L. Panwar[130], L. Paolozzi[56], S. Parajuli[168], A. Paramonov[6], C. Paraskevopoulos[53], D. Paredes Hernandez[64b], A. Pareti[73a,73b], K. R. Park[42], T. H. Park[112], F. Parodi[57b,57a], J. A. Parsons[42], U. Parzefall[54], B. Pascual Dias[41], L. Pascual Dominguez[101], E. Pasqualucci[75a], S. Passaggio[57b], F. Pastore[97], P. Patel[87], U. M. Patel[51], J. R. Pater[103], T. Pauly[37], F. Pauwels[136], C. I. Pazos[164], M. Pedersen[128], R. Pedro[133a], S. V. Peleganchuk[38], O. Penc[37], E. A. Pender[52], S. Peng[15], G. D. Penn[178], K. E. Penski[111], M. Penzin[38], B. S. Peralva[83d], A. P. Pereira Peixoto[142], L. Pereira Sanchez[149],

D. V. Perepelitsa[30,ak], G. Perera[105], E. Perez Codina[37], M. Perganti[10], H. Pernegger[37], S. Perrella[75a,75b], O. Perrin[41], K. Peters[48], R. F. Y. Peters[103], B. A. Petersen[37], T. C. Petersen[43], E. Petit[104], V. Petousis[135], A. R. Petri[71a,71b], C. Petridou[158,d], T. Petru[136], A. Petrukhin[147], M. Pettee[18a], A. Petukhov[82], K. Petukhova[37], R. Pezoa[140f], L. Pezzotti[24b,24a], G. Pezzullo[178], L. Pfaffenbichler[37], A. J. Pfleger[37], T. M. Pham[176], T. Pham[107], P. W. Phillips[137], G. Piacquadio[151], E. Pianori[18a], F. Piazza[126], R. Piegaia[31], D. Pietreanu[28b], A. D. Pilkington[103], M. Pinamonti[69a,69c], J. L. Pinfold[2], B. C. Pinheiro Pereira[133a], J. Pinol Bel[13], A. E. Pinto Pinoargote[130], L. Pintucci[69a,69c], K. M. Piper[152], A. Pirttikoski[56], D. A. Pizzi[35], L. Pizzimento[64b], A. Plebani[33], M.-A. Pleier[30], V. Pleskot[136], E. Plotnikova[39], G. Poddar[96], R. Poettgen[100], L. Poggioli[130], S. Polacek[136], G. Polesello[73a], A. Poley[148], A. Polini[24b], C. S. Pollard[173], Z. B. Pollock[122], E. Pompa Pacchi[123], N. I. Pond[98], D. Ponomarenko[68], L. Pontecorvo[37], S. Popa[28a], G. A. Popeneciu[28d], A. Poreba[37], D. M. Portillo Quintero[162a], S. Pospisil[135], M. A. Postill[145], P. Postolache[28c], K. Potamianos[173], P. A. Potepa[86a], I. N. Potrap[39], C. J. Potter[33], H. Potti[153], J. Poveda[169], M. E. Pozo Astigarraga[37], R. Pozzi[37], A. Prades Ibanez[76a,76b], J. Pretel[171], D. Price[103], M. Primavera[70a], L. Primomo[69a,69c], M. A. Principe Martin[101], R. Privara[125], T. Procter[86b], M. L. Proffitt[142], N. Proklova[131], K. Prokofiev[64c], G. Proto[112], J. Proudfoot[6], M. Przybycien[86a], W. W. Przygoda[86b], A. Psallidas[46], J. E. Puddefoot[145], D. Pudzha[53], D. Pyatiizbyantseva[116], J. Qian[108], R. Qian[109], D. Qichen[103], Y. Qin[13], T. Qiu[52], A. Quadt[55], M. Queitsch-Maitland[103], G. Quetant[56], R. P. Quinn[170], G. Rabanal Bolanos[61], D. Rafanoharana[112], F. Raffaeli[76a,76b], F. Ragusa[71a,71b], J. L. Rainbolt[40], J. A. Raine[56], S. Rajagopalan[30], E. Ramakoti[39], L. Rambelli[57b,57a], I. A. Ramirez-Berend[35], K. Ran[48,114c], D. S. Rankin[131], N. P. Rapheeha[34g], H. Rasheed[28b], D. F. Rassloff[63a], A. Rastogi[18a], S. Rave[102], S. Ravera[57b,57a], B. Ravina[37], I. Ravinovich[175], M. Raymond[37], A. L. Read[128], N. P. Readioff[145], D. M. Rebuzzi[73a,73b], A. S. Reed[112], K. Reeves[27], J. A. Reidelsturz[177], D. Reikher[126], A. Rej[49], C. Rembser[37], H. Ren[62], M. Renda[28b], F. Renner[48], A. G. Rennie[59], A. L. Rescia[48], S. Resconi[71a], M. Ressegotti[57b,57a], S. Rettie[37], W. F. Rettie[35], E. Reynolds[18a], O. L. Rezanova[39], P. Reznicek[136], H. Riani[36d], N. Ribaric[51], E. Ricci[78a,78b], R. Richter[112], S. Richter[47a,47b], E. Richter-Was[86b], M. Ridel[130], S. Ridouani[36d], P. Rieck[120], P. Riedler[37], E. M. Riefel[47a,47b], J. O. Rieger[117], M. Rijssenbeek[151], M. Rimoldi[37], L. Rinaldi[24b,24a], P. Rincke[167,55], G. Ripellino[167], I. Riu[13], J. C. Rivera Vergara[171], F. Rizatdinova[124], E. Rizvi[96], B. R. Roberts[18a], S. S. Roberts[139], D. Robinson[33], M. Robles Manzano[102], A. Robson[59], A. Rocchi[76a,76b], C. Roda[74a,74b], S. Rodriguez Bosca[37], Y. Rodriguez Garcia[23a], A. M. Rodríguez Vera[118], S. Roe[37], J. T. Roemer[37], O. Røhne[128], R. A. Rojas[37], C. P. A. Roland[130], A. Romaniouk[79], E. Romano[73a,73b], M. Romano[24b], A. C. Romero Hernandez[168], N. Rompotis[94], L. Roos[130], S. Rosati[75a], B. J. Rosser[40], E. Rossi[129], E. Rossi[72a,72b], L. P. Rossi[61], L. Rossini[54], R. Rosten[122], M. Rotaru[28b], B. Rottler[54], D. Rousseau[66], D. Rousso[48], S. Roy-Garand[161], A. Rozanov[104], Z. M. A. Rozario[59], Y. Rozen[156], A. Rubio Jimenez[169], V. H. Ruelas Rivera[19], T. A. Ruggeri[1], A. Ruggiero[129], A. Ruiz-Martinez[169], A. Rummler[37], Z. Rurikova[54], N. A. Rusakovich[39], H. L. Russell[171], G. Russo[75a,75b], J. P. Rutherfoord[7], S. Rutherford Colmenares[33], M. Rybar[136], P. Rybczynski[86a], A. Ryzhov[45], J. A. Sabater Iglesias[56], H.F-W. Sadrozinski[139], F. Safai Tehrani[75a], S. Saha[1], M. Sahinsoy[82], B. Sahoo[175], A. Saibel[169], B. T. Saifuddin[123], M. Saimpert[138], G. T. Saito[83c], M. Saito[159], T. Saito[159], A. Sala[71a,71b], A. Salnikov[149], J. Salt[169], A. Salvador Salas[157], F. Salvatore[152], A. Salzburger[37], D. Sammel[54], E. Sampson[93], D. Sampsonidis[158,d], D. Sampsonidou[126], J. Sánchez[169], V. Sanchez Sebastian[169], H. Sandaker[128], C. O. Sander[48], J. A. Sandesara[176], M. Sandhoff[177], C. Sandoval[23b], L. Sanfilippo[63a], D. P. C. Sankey[137], T. Sano[89], A. Sansoni[53], L. Santi[37], C. Santoni[41], H. Santos[133a,133b], A. Santra[175], E. Sanzani[24b,24a], K. A. Saoucha[88b], J. G. Saraiva[133a,133d], J. Sardain[7], O. Sasaki[84], K. Sato[163], C. Sauer[37], E. Sauvan[4], P. Savard[161,ai], R. Sawada[159], C. Sawyer[137], L. Sawyer[99], C. Sbarra[24b], A. Sbrizzi[24b,24a], T. Scanlon[98], J. Schaarschmidt[142], U. Schäfer[102], A. C. Schaffer[66,45], D. Schaile[111], R. D. Schamberger[151], C. Scharf[19], M. M. Schefer[20], V. A. Schegelsky[38], D. Scheirich[136], M. Schernau[140e], C. Scheulen[56], C. Schiavi[57b,57a], M. Schioppa[44b,44a], B. Schlag[149], S. Schlenker[37], J. Schmeing[177], E. Schmidt[112], M. A. Schmidt[177], K. Schmieden[102], C. Schmitt[102], N. Schmitt[102], S. Schmitt[48], L. Schoeffel[138], A. Schoening[63b], P. G. Scholer[35], E. Schopf[147], M. Schott[25], S. Schramm[56], T. Schroer[56], H-C. Schultz-Coulon[63a], M. Schumacher[54], B. A. Schumm[139], Ph. Schune[138], H. R. Schwartz[139], A. Schwartzman[149], T. A. Schwarz[108], Ph. Schwemling[138], R. Schwienhorst[109], F. G. Sciacca[20], A. Sciandra[30], G. Sciolla[27], F. Scuri[74a], C. D. Sebastiani[37], K. Sedlaczek[118], S. C. Seidel[115], A. Seiden[139], B. D. Seidlitz[42], C. Seitz[48], J. M. Seixas[83b], G. Sekhniaidze[72a], L. Selem[60], N. Semprini-Cesari[24b,24a], A. Semushin[179], D. Sengupta[56], V. Senthilkumar[169], L. Serin[66], M. Sessa[72a,72b], H. Severini[123],

F. Sforza[57b,57a], A. Sfyrla[56], Q. Sha[14], E. Shabalina[55], H. Shaddix[118], A. H. Shah[33], R. Shaheen[150], J. D. Shahinian[131], M. Shamim[37], L. Y. Shan[14], M. Shapiro[18a], A. Sharma[37], A. S. Sharma[170], P. Sharma[30], P. B. Shatalov[38], K. Shaw[152], S. M. Shaw[103], Q. Shen[144a], D. J. Sheppard[148], P. Sherwood[98], L. Shi[98], X. Shi[14], S. Shimizu[84], C. O. Shimmin[178], I. P. J. Shipsey[129,*], S. Shirabe[90], M. Shiyakova[39,aa], M. J. Shochet[40], D. R. Shope[128], B. Shrestha[123], S. Shrestha[122,am], I. Shreyber[39], M. J. Shroff[171], P. Sicho[134], A. M. Sickles[168], E. Sideras Haddad[34g,166], A. C. Sidley[117], A. Sidoti[24b], F. Siegert[50], Dj. Sijacki[16], F. Sili[92], J. M. Silva[52], I. Silva Ferreira[83b], M. V. Silva Oliveira[30], S. B. Silverstein[47a], S. Simion[66], R. Simoniello[37], E. L. Simpson[103], H. Simpson[152], L. R. Simpson[6], S. Simsek[82], S. Sindhu[55], P. Sinervo[161], S. N. Singh[27], S. Singh[30], S. Sinha[48], S. Sinha[103], M. Sioli[24b,24a], K. Sioulas[9], I. Siral[37], E. Sitnikova[48], J. Sjölin[47a,47b], A. Skaf[55], E. Skorda[21], P. Skubic[123], M. Slawinska[87], I. Slazyk[17], I. Sliusar[128], V. Smakhtin[175], B. H. Smart[137], S. Yu. Smirnov[140b], Y. Smirnov[82], L. N. Smirnova[38,a], O. Smirnova[100], A. C. Smith[42], D. R. Smith[165], J. L. Smith[103], M. B. Smith[35], R. Smith[149], H. Smitmanns[102], M. Smizanska[93], K. Smolek[135], P. Smolyanskiy[135], A. A. Snesarev[39], H. L. Snoek[117], S. Snyder[30], R. Sobie[171,ac], A. Soffer[157], C. A. Solans Sanchez[37], E. Yu. Soldatov[39], U. Soldevila[169], A. A. Solodkov[34g], S. Solomon[27], A. Soloshenko[39], K. Solovieva[54], O. V. Solovyanov[41], P. Sommer[50], A. Sonay[13], A. Sopczak[135], A. L. Sopio[52], F. Sopkova[29b], J. D. Sorenson[115], I. R. Sotarriva Alvarez[141], V. Sothilingam[63a], O. J. Soto Sandoval[140c,140b], S. Sottocornola[68], R. Soualah[88a], Z. Soumaimi[36e], D. South[48], N. Soybelman[175], S. Spagnolo[70a,70b], M. Spalla[112], D. Sperlich[54], B. Spisso[72a,72b], D. P. Spiteri[59], L. Splendori[104], M. Spousta[136], E. J. Staats[35], R. Stamen[63a], E. Stanecka[87], W. Stanek-Maslouska[48], M. V. Stange[50], B. Stanislaus[18a], M. M. Stanitzki[48], B. Stapf[48], E. A. Starchenko[38], G. H. Stark[139], J. Stark[91], P. Staroba[134], P. Starovoitov[88b], R. Staszewski[87], G. Stavropoulos[46], A. Stefl[37], P. Steinberg[30], B. Stelzer[148,162a], H. J. Stelzer[132], O. Stelzer-Chilton[162a], H. Stenzel[58], T. J. Stevenson[152], G. A. Stewart[37], J. R. Stewart[124], M. C. Stockton[37], G. Stoicea[28b], M. Stolarski[133a], S. Stonjek[112], A. Straessner[50], J. Strandberg[150], S. Strandberg[47a,47b], M. Stratmann[177], M. Strauss[123], T. Strebler[104], P. Strizenec[29b], R. Ströhmer[172], D. M. Strom[126], R. Stroynowski[45], A. Strubig[47a,47b], S. A. Stucci[30], B. Stugu[17], J. Stupak[123], N. A. Styles[48], D. Su[149], S. Su[62], X. Su[62], D. Suchy[29a], K. Sugizaki[131], V. V. Sulin[38], M.J. Sullivan[94], D. M. S. Sultan[129], L. Sultanaliyeva[38], S. Sultansoy[3b], S. Sun[176], W. Sun[14], O. Sunneborn Gudnadottir[167], N. Sur[100], M. R. Sutton[152], H. Suzuki[163], M. Svatos[134], P. N. Swallow[33], M. Swiatlowski[162a], T. Swirski[172], I. Sykora[29a], M. Sykora[136], T. Sykora[136], D. Ta[102], K. Tackmann[48,z], A. Taffard[165], R. Tafirout[162a], Y. Takubo[84], M. Talby[104], A. A. Talyshev[38], K. C. Tam[64b], N. M. Tamir[157], A. Tanaka[159], J. Tanaka[159], R. Tanaka[66], M. Tanasini[151], Z. Tao[170], S. Tapia Araya[140f], S. Tapprogge[102], A. Tarek Abouelfadl Mohamed[109], S. Tarem[156], K. Tariq[14], G. Tarna[28b], G. F. Tartarelli[71a], M. J. Tartarin[91], P. Tas[136], M. Tasevsky[134], E. Tassi[44b,44a], A. C. Tate[168], G. Tateno[159], Y. Tayalati[36e,ab], G. N. Taylor[107], W. Taylor[162b], A. S. Tegetmeier[91], P. Teixeira-Dias[97], J. J. Teoh[161], K. Terashi[159], J. Terron[101], S. Terzo[13], M. Testa[53], R. J. Teuscher[161,ac], A. Thaler[79], O. Theiner[56], T. Theveneaux-Pelzer[104], D. W. Thomas[97], J. P. Thomas[21], E. A. Thompson[18a], P. D. Thompson[21], E. Thomson[131], R. E. Thornberry[45], C. Tian[62], Y. Tian[56], V. Tikhomirov[82], Yu. A. Tikhonov[39], S. Timoshenko[38], D. Timoshyn[136], E. X. L. Ting[1], P. Tipton[178], A. Tishelman-Charny[30], K. Todome[141], S. Todorova-Nova[136], S. Todt[50], L. Toffolin[69a,69c], M. Togawa[84], J. Tojo[90], S. Tokár[29a], O. Toldaiev[68], G. Tolkachev[104], M. Tomoto[84,113], L. Tompkins[149,o], E. Torrence[126], H. Torres[91], E. Torró Pastor[169], M. Toscani[31], C. Tosciri[40], M. Tost[11], D. R. Tovey[145], T. Trefzger[172], P. M. Tricarico[13], A. Tricoli[30], I. M. Trigger[162a], S. Trincaz-Duvoid[130], D. A. Trischuk[27], A. Tropina[39], L. Truong[34c], M. Trzebinski[87], A. Trzupek[87], F. Tsai[151], M. Tsai[108], A. Tsiamis[158], P. V. Tsiareshka[39], S. Tsigaridas[162a], A. Tsirigotis[158,v], V. Tsiskaridze[161], E. G. Tskhadadze[155a], M. Tsopoulou[158], Y. Tsujikawa[89], I. I. Tsukerman[38], V. Tsulaia[18a], S. Tsuno[84], K. Tsuri[121], D. Tsybychev[151], Y. Tu[64b], A. Tudorache[28b], V. Tudorache[28b], S. B. Tuncay[129], S. Turchikhin[57b,57a], I. Turk Cakir[3a], R. Turra[71a], T. Turtuvshin[39,ad], P. M. Tuts[42], S. Tzamarias[158,d], E. Tzovara[102], Y. Uematsu[84], F. Ukegawa[163], P. A. Ulloa Poblete[140c,140b], E. N. Umaka[30], G. Unal[37], A. Undrus[30], G. Unel[165], J. Urban[29b], P. Urrejola[140a], G. Usai[8], R. Ushioda[160], M. Usman[110], F. Ustuner[52], Z. Uysal[82], V. Vacek[135], B. Vachon[106], T. Vafeiadis[37], A. Vaitkus[98], C. Valderanis[111], E. Valdes Santurio[47a,47b], M. Valente[37], S. Valentinetti[24b,24a], A. Valero[169], E. Valiente Moreno[169], A. Vallier[91], J. A. Valls Ferrer[169], D. R. Van Arneman[117], T. R. Van Daalen[142], A. Van Der Graaf[49], H. Z. Van Der Schyf[34g], P. Van Gemmeren[6], M. Van Rijnbach[37], S. Van Stroud[98], I. Van Vulpen[117], P. Vana[136], M. Vanadia[76a,76b], U. M. Vande Voorde[150], W. Vandelli[37], E. R. Vandewall[124], D. Vannicola[157], L. Vannoli[53], R. Vari[75a], M. Varma[178],

E. W. Varnes[7], C. Varni[18b], D. Varouchas[66], L. Varriale[169], K. E. Varvell[153], M. E. Vasile[28b], L. Vaslin[84], M. D. Vassilev[149], A. Vasyukov[39], L. M. Vaughan[124], R. Vavricka[136], T. VazquezSchroeder[13], J. Veatch[32], V. Vecchio[103], M. J. Veen[105], I. Veliscek[30], I. Velkovska[95], L. M. Veloce[161], F. Veloso[133a,133c], S. Veneziano[75a], A. Ventura[70a,70b], S. Ventura Gonzalez[138], A. Verbytskyi[112], M. Verducci[74a,74b], C. Vergis[96], M. Verissimo De Araujo[83b], W. Verkerke[117], J. C. Vermeulen[117], C. Vernieri[149], M. Vessella[165], M. C. Vetterli[148,ai], A. Vgenopoulos[102], N. Viaux Maira[140f], T. Vickey[145], O. E. Vickey Boeriu[145], G. H. A. Viehhauser[129], L. Vigani[63b], M. Vigl[112], M. Villa[24b,24a], M. Villaplana Perez[169], E. M. Villhauer[40], E. Vilucchi[53], M. Vincent[169], M. G. Vincter[35], A. Visibile[117], C. Vittori[37], I. Vivarelli[24b,24a], E. Voevodina[112], F. Vogel[111], J. C. Voigt[50], P. Vokac[135], Yu. Volkotrub[86b], E. Von Toerne[25], B. Vormwald[37], K. Vorobev[51], M. Vos[169], K. Voss[147], M. Vozak[37], L. Vozdecky[123], N. Vranjes[16], M. Vranjes Milosavljevic[16], M. Vreeswijk[117], N. K. Vu[144b,144a], R. Vuillermet[37], O. Vujinovic[102], I. Vukotic[40], I. K. Vyas[35], J. F. Wack[33], S. Wada[163], C. Wagner[149], J. M. Wagner[18a], W. Wagner[177], S. Wahdan[177], H. Wahlberg[92], C. H. Waits[123], J. Walder[137], R. Walker[111], K. Walkingshaw Pass[59], W. Walkowiak[147], A. Wall[131], E. J. Wallin[100], T. Wamorkar[18a], A. Wang[62], A. Z. Wang[139], C. Wang[102], C. Wang[11], H. Wang[18a], J. Wang[64c], P. Wang[103], P. Wang[98], R. Wang[61], R. Wang[6], S. M. Wang[154], S. Wang[14], T. Wang[62], T. Wang[62], W. T. Wang[80], W. Wang[14], X. Wang[168], X. Wang[144a], X. Wang[48], Y. Wang[114a], Y. Wang[62], Z. Wang[108], Z. Wang[144b], Z. Wang[108], C. Wanotayaroj[84], A. Warburton[106], A. L. Warnerbring[147], N. Warrack[59], S. Waterhouse[97], A. T. Watson[21], H. Watson[52], M. F. Watson[21], E. Watton[59], G. Watts[142], B. M. Waugh[98], J. M. Webb[54], C. Weber[30], H. A. Weber[19], M. S. Weber[20], S. M. Weber[63a], C. Wei[62], Y. Wei[54], A. R. Weidberg[129], E. J. Weik[120], J. Weingarten[49], C. Weiser[54], C. J. Wells[48], T. Wenaus[30], B. Wendland[49], T. Wengler[37], N. S. Wenke[112], N. Wermes[25], M. Wessels[63a], A. M. Wharton[93], A. S. White[61], A. White[8], M. J. White[1], D. Whiteson[165], L. Wickremasinghe[127], W. Wiedenmann[176], M. Wielers[137], R. Wierda[150], C. Wiglesworth[43], H. G. Wilkens[37], J. J. H. Wilkinson[33], D. M. Williams[42], H. H. Williams[131], S. Williams[33], S. Willocq[105], B. J. Wilson[103], D. J. Wilson[103], P. J. Windischhofer[40], F. I. Winkel[31], F. Winklmeier[126], B. T. Winter[54], M. Wittgen[149], M. Wobisch[99], T. Wojtkowski[60], Z. Wolffs[117], J. Wollrath[37], M. W. Wolter[87], H. Wolters[133a,133c], M. C. Wong[139], E. L. Woodward[42], S. D. Worm[48], B. K. Wosiek[87], K. W. Woźniak[87], S. Wozniewski[55], K. Wraight[59], C. Wu[161], C. Wu[21], J. Wu[159], M. Wu[114b], M. Wu[116], S. L. Wu[176], S. Wu[14], X. Wu[62], Y. Wu[62], Z. Wu[4], J. Wuerzinger[112], T. R. Wyatt[103], B. M. Wynne[52], S. Xella[43], L. Xia[114a], M. Xia[15], M. Xie[62], A. Xiong[126], J. Xiong[18a], D. Xu[14], H. Xu[62], L. Xu[62], R. Xu[131], T. Xu[108], Y. Xu[142], Z. Xu[52], Z. Xu[114a], B. Yabsley[153], S. Yacoob[34a], Y. Yamaguchi[84], E. Yamashita[159], H. Yamauchi[163], T. Yamazaki[18a], Y. Yamazaki[85], S. Yan[59], Z. Yan[105], H. J. Yang[144a,144b], H. T. Yang[62], S. Yang[62], T. Yang[64c], X. Yang[37], X. Yang[14], Y. Yang[159], Y. Yang[62], W-M. Yao[18a], C. L. Yardley[152], J. Ye[14], S. Ye[30], X. Ye[62], Y. Yeh[98], I. Yeletskikh[39], B. Yeo[18b], M. R. Yexley[98], T. P. Yildirim[129], P. Yin[42], K. Yorita[174], C. J. S. Young[37], C. Young[149], N. D. Young[126], Y. Yu[62], J. Yuan[14,114c], M. Yuan[108], R. Yuan[144b,144a], L. Yue[98], M. Zaazoua[62], B. Zabinski[87], I. Zahir[36a], A. Zaio[57b,57a], Z. K. Zak[87], T. Zakareishvili[169], S. Zambito[56], J. A. Zamora Saa[140d], J. Zang[159], R. Zanzottera[71a,71b], O. Zaplatilek[135], C. Zeitnitz[177], H. Zeng[14], J. C. Zeng[168], D. T. Zenger Jr[27], O. Zenin[38], T. Ženiš[29a], S. Zenz[96], D. Zerwas[66], M. Zhai[14,114c], D. F. Zhang[145], G. Zhang[14], J. Zhang[143a], J. Zhang[6], K. Zhang[14,114c], L. Zhang[62], L. Zhang[114a], P. Zhang[14,114c], R. Zhang[114a], S. Zhang[91], T. Zhang[159], Y. Zhang[142], Y. Zhang[98], Y. Zhang[62], Y. Zhang[114a], Z. Zhang[143a], Z. Zhang[66], H. Zhao[142], T. Zhao[143a], Y. Zhao[35], Z. Zhao[62], Z. Zhao[62], A. Zhemchugov[39], J. Zheng[114a], K. Zheng[168], X. Zheng[62], Z. Zheng[149], D. Zhong[168], B. Zhou[108], H. Zhou[7], N. Zhou[144a], Y. Zhou[15], Y. Zhou[114a], Y. Zhou[7], C. G. Zhu[143a], J. Zhu[108], X. Zhu[144b], Y. Zhu[144a], Y. Zhu[62], X. Zhuang[14], K. Zhukov[68], N. I. Zimine[39], J. Zinsser[63b], M. Ziolkowski[147], L. Živković[16], A. Zoccoli[24b,24a], K. Zoch[61], A. Zografos[37], T. G. Zorbas[145], O. Zormpa[46], L. Zwalinski[37]

[1] Department of Physics, University of Adelaide, Adelaide, Australia
[2] Department of Physics, University of Alberta, Edmonton, AB, Canada
[3] [(a)]Department of Physics, Ankara University, Ankara, Türkiye; [(b)]Division of Physics, TOBB University of Economics and Technology, Ankara, Türkiye
[4] LAPP, CNRS/IN2P3, Université Savoie Mont Blanc, Annecy, France
[5] APC, Université Paris Cité, CNRS/IN2P3, Paris, France
[6] High Energy Physics Division, Argonne National Laboratory, Argonne, IL, USA

[7] Department of Physics, University of Arizona, Tucson, AZ, USA
[8] Department of Physics, University of Texas at Arlington, Arlington, TX, USA
[9] Physics Department, National and Kapodistrian University of Athens, Athens, Greece
[10] Physics Department, National Technical University of Athens, Zografou, Greece
[11] Department of Physics, University of Texas at Austin, Austin, TX, USA
[12] Institute of Physics, Azerbaijan Academy of Sciences, Baku, Azerbaijan
[13] Institut de Física d'Altes Energies (IFAE), Barcelona Institute of Science and Technology, Barcelona, Spain
[14] Institute of High Energy Physics, Chinese Academy of Sciences, Beijing, China
[15] Physics Department, Tsinghua University, Beijing, China
[16] Institute of Physics, University of Belgrade, Belgrade, Serbia
[17] Department for Physics and Technology, University of Bergen, Bergen, Norway
[18] [(a)]Physics Division, Lawrence Berkeley National Laboratory, Berkeley, CA, USA; [(b)]University of California, Berkeley, CA, USA
[19] Institut für Physik, Humboldt Universität zu Berlin, Berlin, Germany
[20] Albert Einstein Center for Fundamental Physics and Laboratory for High Energy Physics, University of Bern, Bern, Switzerland
[21] School of Physics and Astronomy, University of Birmingham, Birmingham, UK
[22] [(a)]Department of Physics, Bogazici University, Istanbul, Türkiye; [(b)]Department of Physics Engineering, Gaziantep University, Gaziantep, Türkiye; [(c)]Department of Physics, Istanbul University, Istanbul, Türkiye
[23] [(a)]Facultad de Ciencias y Centro de Investigaciónes, Universidad Antonio Nariño, Bogotá, Colombia; [(b)]Departamento de Física, Universidad Nacional de Colombia, Bogotá, Colombia
[24] [(a)]Dipartimento di Fisica e Astronomia A. Righi, Università di Bologna, Bologna, Italy; [(b)]INFN Sezione di Bologna, Bologna, Italy
[25] Physikalisches Institut, Universität Bonn, Bonn, Germany
[26] Department of Physics, Boston University, Boston, MA, USA
[27] Department of Physics, Brandeis University, Waltham, MA, USA
[28] [(a)]Transilvania University of Brasov, Brasov, Romania; [(b)]Horia Hulubei National Institute of Physics and Nuclear Engineering, Bucharest, Romania; [(c)]Department of Physics, Alexandru Ioan Cuza University of Iasi, Iasi, Romania; [(d)]National Institute for Research and Development of Isotopic and Molecular Technologies, Physics Department, Cluj-Napoca, Romania; [(e)]National University of Science and Technology Politechnica, Bucharest, Romania; [(f)]West University in Timisoara, Timisoara, Romania; [(g)]Faculty of Physics, University of Bucharest, Bucharest, Romania
[29] [(a)]Faculty of Mathematics, Physics and Informatics, Comenius University, Bratislava, Slovak Republic; [(b)]Department of Subnuclear Physics, Institute of Experimental Physics of the Slovak Academy of Sciences, Kosice, Slovak Republic
[30] Physics Department, Brookhaven National Laboratory, Upton, NY, USA
[31] Facultad de Ciencias Exactas y Naturales, Departamento de Física, y CONICET, Instituto de Física de Buenos Aires (IFIBA), Universidad de Buenos Aires, Buenos Aires, Argentina
[32] California State University, Long Beach, CA, USA
[33] Cavendish Laboratory, University of Cambridge, Cambridge, UK
[34] [(a)]Department of Physics, University of Cape Town, Cape Town, South Africa; [(b)]iThemba Labs, Western Cape, South Africa; [(c)]Department of Mechanical Engineering Science, University of Johannesburg, Johannesburg, South Africa; [(d)]National Institute of Physics, University of the Philippines Diliman (Philippines), Quezon City, Philippines; [(e)]University of South Africa, Department of Physics, Pretoria, South Africa; [(f)]University of Zululand, KwaDlangezwa, South Africa; [(g)]School of Physics, University of the Witwatersrand, Johannesburg, South Africa
[35] Department of Physics, Carleton University, Ottawa, ON, Canada
[36] [(a)]Faculté des Sciences Ain Chock, Université Hassan II de Casablanca, Casablanca, Morocco; [(b)]Faculté des Sciences, Université Ibn-Tofail, Kénitra, Morocco; [(c)]Faculté des Sciences Semlalia, LPHEA-Marrakech, Université Cadi Ayyad, Marrakech, Morocco; [(d)]LPMR, Faculté des Sciences, Université Mohamed Premier, Oujda, Morocco; [(e)]Faculté des sciences, Université Mohammed V, Rabat, Morocco; [(f)]Institute of Applied Physics, Mohammed VI Polytechnic University, Ben Guerir, Morocco
[37] CERN, Geneva, Switzerland
[38] Affiliated with an Institute Formerly Covered by a Cooperation Agreement with CERN, Geneva, Switzerland
[39] Affiliated with an International Laboratory Covered by a Cooperation Agreement with CERN, Geneva, Switzerland

[40] Enrico Fermi Institute, University of Chicago, Chicago, IL, USA
[41] LPC, CNRS/IN2P3, Université Clermont Auvergne, Clermont-Ferrand, France
[42] Nevis Laboratory, Columbia University, Irvington, NY, USA
[43] Niels Bohr Institute, University of Copenhagen, Copenhagen, Denmark
[44] [(a)]Dipartimento di Fisica, Università della Calabria, Rende, Italy; [(b)]Laboratori Nazionali di Frascati, INFN Gruppo Collegato di Cosenza, Cosenza, Italy
[45] Physics Department, Southern Methodist University, Dallas, TX, USA
[46] National Centre for Scientific Research "Demokritos", Agia Paraskevi, Greece
[47] [(a)]Department of Physics, Stockholm University, Stockholm, Sweden; [(b)]Oskar Klein Centre, Stockholm, Sweden
[48] Deutsches Elektronen-Synchrotron DESY, Hamburg and Zeuthen, Germany
[49] Fakultät Physik , Technische Universität Dortmund, Dortmund, Germany
[50] Institut für Kern- und Teilchenphysik, Technische Universität Dresden, Dresden, Germany
[51] Department of Physics, Duke University, Durham, NC, USA
[52] SUPA-School of Physics and Astronomy, University of Edinburgh, Edinburgh, UK
[53] INFN e Laboratori Nazionali di Frascati, Frascati, Italy
[54] Physikalisches Institut, Albert-Ludwigs-Universität Freiburg, Freiburg, Germany
[55] II. Physikalisches Institut, Georg-August-Universität Göttingen, Göttingen, Germany
[56] Département de Physique Nucléaire et Corpusculaire, Université de Genève, Geneva, Switzerland
[57] [(a)]Dipartimento di Fisica, Università di Genova, Genoa, Italy; [(b)]INFN Sezione di Genova, Genoa, Italy
[58] II. Physikalisches Institut, Justus-Liebig-Universität Giessen, Giessen, Germany
[59] SUPA-School of Physics and Astronomy, University of Glasgow, Glasgow, UK
[60] LPSC, Université Grenoble Alpes, CNRS/IN2P3, Grenoble INP, Grenoble, France
[61] Laboratory for Particle Physics and Cosmology, Harvard University, Cambridge, MA, USA
[62] Department of Modern Physics and State Key Laboratory of Particle Detection and Electronics, University of Science and Technology of China, Hefei, China
[63] [(a)]Kirchhoff-Institut für Physik, Ruprecht-Karls-Universität Heidelberg, Heidelberg, Germany; [(b)]Physikalisches Institut, Ruprecht-Karls-Universität Heidelberg, Heidelberg, Germany
[64] [(a)]Department of Physics, Chinese University of Hong Kong, Shatin, N.T., Hong Kong, China; [(b)]Department of Physics, University of Hong Kong, Hong Kong, China; [(c)]Department of Physics and Institute for Advanced Study, Hong Kong University of Science and Technology, Clear Water Bay, Kowloon, Hong Kong, China
[65] Department of Physics, National Tsing Hua University, Hsinchu, Taiwan
[66] IJCLab, CNRS/IN2P3, Université Paris-Saclay, 91405 Orsay, France
[67] Centro Nacional de Microelectrónica (IMB-CNM-CSIC), Barcelona, Spain
[68] Department of Physics, Indiana University, Bloomington, IN, USA
[69] [(a)]INFN Gruppo Collegato di Udine, Sezione di Trieste, Udine, Italy; [(b)]ICTP, Trieste, Italy; [(c)]Dipartimento Politecnico di Ingegneria e Architettura, Università di Udine, Udine, Italy
[70] [(a)]INFN Sezione di Lecce, Lecce, Italy; [(b)]Dipartimento di Matematica e Fisica, Università del Salento, Lecce, Italy
[71] [(a)]INFN Sezione di Milano, Milan, Italy; [(b)]Dipartimento di Fisica, Università di Milano, Milan, Italy
[72] [(a)]INFN Sezione di Napoli, Naples, Italy; [(b)]Dipartimento di Fisica, Università di Napoli, Naples, Italy
[73] [(a)]INFN Sezione di Pavia, Pavia, Italy; [(b)]Dipartimento di Fisica, Università di Pavia, Pavia, Italy
[74] [(a)]INFN Sezione di Pisa, Pisa, Italy; [(b)]Dipartimento di Fisica E. Fermi, Università di Pisa, Pisa, Italy
[75] [(a)]INFN Sezione di Roma, Rome, Italy; [(b)]Dipartimento di Fisica, Sapienza Università di Roma, Rome, Italy
[76] [(a)]INFN Sezione di Roma Tor Vergata, Rome, Italy; [(b)]Dipartimento di Fisica, Università di Roma Tor Vergata, Rome, Italy
[77] [(a)]INFN Sezione di Roma Tre, Rome, Italy; [(b)]Dipartimento di Matematica e Fisica, Università Roma Tre, Rome, Italy
[78] [(a)]INFN-TIFPA, Povo, Italy; [(b)]Università degli Studi di Trento, Trento, Italy
[79] Universität Innsbruck, Department of Astro and Particle Physics, Innsbruck, Austria
[80] University of Iowa, Iowa City, IA, USA
[81] Department of Physics and Astronomy, Iowa State University, Ames, IA, USA
[82] Istinye University, Sariyer, Istanbul, Türkiye
[83] [(a)]Departamento de Engenharia Elétrica, Universidade Federal de Juiz de Fora (UFJF), Juiz de Fora, Brazil; [(b)]Universidade Federal do Rio De Janeiro COPPE/EE/IF, Rio de Janeiro, Brazil; [(c)]Instituto de Física,

Universidade de São Paulo, São Paulo, Brazil; [(d)]Rio de Janeiro State University, Rio de Janeiro, Brazil; [(e)]Federal University of Bahia, Bahia, Brazil
[84] KEK, High Energy Accelerator Research Organization, Tsukuba, Japan
[85] Graduate School of Science, Kobe University, Kobe, Japan
[86] [(a)]AGH University of Krakow, Faculty of Physics and Applied Computer Science, Kraków, Poland; [(b)]Marian Smoluchowski Institute of Physics, Jagiellonian University, Kraków, Poland
[87] Institute of Nuclear Physics Polish Academy of Sciences, Kraków, Poland
[88] [(a)]Khalifa University of Science and Technology, Abu Dhabi, United Arab Emirates; [(b)]University of Sharjah, Sharjah, United Arab Emirates
[89] Faculty of Science, Kyoto University, Kyoto, Japan
[90] Research Center for Advanced Particle Physics and Department of Physics, Kyushu University, Fukuoka , Japan
[91] L2IT, CNRS/IN2P3, UPS, Université de Toulouse, Toulouse, France
[92] Instituto de Física La Plata, Universidad Nacional de La Plata and CONICET, La Plata, Argentina
[93] Physics Department, Lancaster University, Lancaster, UK
[94] Oliver Lodge Laboratory, University of Liverpool, Liverpool, UK
[95] Department of Experimental Particle Physics, Jožef Stefan Institute and Department of Physics, University of Ljubljana, Ljubljana, Slovenia
[96] Department of Physics and Astronomy, Queen Mary University of London, London, UK
[97] Department of Physics, Royal Holloway University of London, Egham, UK
[98] Department of Physics and Astronomy, University College London, London, UK
[99] Louisiana Tech University, Ruston, LA, USA
[100] Fysiska institutionen, Lunds universitet, Lund, Sweden
[101] Departamento de Física Teorica C-15 and CIAFF, Universidad Autónoma de Madrid, Madrid, Spain
[102] Institut für Physik, Universität Mainz, Mainz, Germany
[103] School of Physics and Astronomy, University of Manchester, Manchester, UK
[104] CPPM, CNRS/IN2P3, Aix-Marseille Université, Marseille, France
[105] Department of Physics, University of Massachusetts, Amherst, MA, USA
[106] Department of Physics, McGill University, Montreal, QC, Canada
[107] School of Physics, University of Melbourne, Victoria, Australia
[108] Department of Physics, University of Michigan, Ann Arbor, MI, USA
[109] Department of Physics and Astronomy, Michigan State University, East Lansing, MI, USA
[110] Group of Particle Physics, University of Montreal, Montreal, QC, Canada
[111] Fakultät für Physik, Ludwig-Maximilians-Universität München, Munich, Germany
[112] Max-Planck-Institut für Physik (Werner-Heisenberg-Institut), Munich, Germany
[113] Graduate School of Science and Kobayashi-Maskawa Institute, Nagoya University, Nagoya, Japan
[114] [(a)]Department of Physics, Nanjing University, Nanjing, China; [(b)]School of Science, Shenzhen Campus of Sun Yat-sen University, Guangzhou, China; [(c)]University of Chinese Academy of Science (UCAS), Beijing, China
[115] Department of Physics and Astronomy, University of New Mexico, Albuquerque, NM, USA
[116] Institute for Mathematics, Astrophysics and Particle Physics, Radboud University/Nikhef, Nijmegen, Netherlands
[117] Nikhef National Institute for Subatomic Physics and University of Amsterdam, Amsterdam, Netherlands
[118] Department of Physics, Northern Illinois University, DeKalb, IL, USA
[119] [(a)]New York University Abu Dhabi, Abu Dhabi, United Arab Emirates; [(b)]United Arab Emirates University, Al Ain, United Arab Emirates
[120] Department of Physics, New York University, New York, NY, USA
[121] Ochanomizu University, Otsuka, Bunkyo-ku, Tokyo, Japan
[122] Ohio State University, Columbus, OH, USA
[123] Homer L. Dodge Department of Physics and Astronomy, University of Oklahoma, Norman, OK, USA
[124] Department of Physics, Oklahoma State University, Stillwater, OK, USA
[125] Palacký University, Joint Laboratory of Optics, Olomouc, Czech Republic
[126] Institute for Fundamental Science, University of Oregon, Eugene, OR, USA
[127] Graduate School of Science, University of Osaka, Osaka, Japan
[128] Department of Physics, University of Oslo, Oslo, Norway
[129] Department of Physics, Oxford University, Oxford, UK

[130] LPNHE, CNRS/IN2P3, Sorbonne Université, Université Paris Cité, Paris, France
[131] Department of Physics, University of Pennsylvania, Philadelphia, PA, USA
[132] Department of Physics and Astronomy, University of Pittsburgh, Pittsburgh, PA, USA
[133] [(a)]Laboratório de Instrumentação e Física Experimental de Partículas - LIP, Lisbon, Portugal; [(b)]Departamento de Física, Faculdade de Ciências, Universidade de Lisboa, Lisbon, Portugal; [(c)]Departamento de Física, Universidade de Coimbra, Coimbra, Portugal; [(d)]Centro de Física Nuclear da Universidade de Lisboa, Lisbon, Portugal; [(e)]Departamento de Física, Escola de Ciências, Universidade do Minho, Braga, Portugal; [(f)]Departamento de Física Teórica y del Cosmos, Universidad de Granada, Granada, Spain; [(g)]Departamento de Física, Instituto Superior Técnico, Universidade de Lisboa, Lisbon, Portugal
[134] Institute of Physics of the Czech Academy of Sciences, Prague, Czech Republic
[135] Czech Technical University in Prague, Prague, Czech Republic
[136] Faculty of Mathematics and Physics, Charles University, Prague, Czech Republic
[137] Particle Physics Department, Rutherford Appleton Laboratory, Didcot, UK
[138] IRFU, CEA, Université Paris-Saclay, Gif-sur-Yvette, France
[139] Santa Cruz Institute for Particle Physics, University of California Santa Cruz, Santa Cruz, CA, USA
[140] [(a)]Departamento de Física, Pontificia Universidad Católica de Chile, Santiago, Chile; [(b)]Millennium Institute for Subatomic Physics at High Energy Frontier (SAPHIR), Santiago, Chile; [(c)]Instituto de Investigación Multidisciplinario en Ciencia y Tecnología y Departamento de Física, Universidad de La Serena, La Serena, Chile; [(d)]Universidad Andres Bello, Department of Physics, Santiago, Chile; [(e)]Instituto de Alta Investigación, Universidad de Tarapacá, Arica, Chile; [(f)]Departamento de Física, Universidad Técnica Federico Santa María, Valparaíso, Chile
[141] Department of Physics, Institute of Science, Tokyo, Japan
[142] Department of Physics, University of Washington, Seattle, WA, USA
[143] [(a)]Institute of Frontier and Interdisciplinary Science and Key Laboratory of Particle Physics and Particle Irradiation (MOE), Shandong University, Qingdao, China; [(b)]School of Physics, Zhengzhou University, Zhengzhou, China
[144] [(a)]State Key Laboratory of Dark Matter Physics, School of Physics and Astronomy, Shanghai Jiao Tong University, Key Laboratory for Particle Astrophysics and Cosmology (MOE), SKLPPC, Shanghai, China; [(b)]State Key Laboratory of Dark Matter Physics, Tsung-Dao Lee Institute, Shanghai Jiao Tong University, Shanghai, China
[145] Department of Physics and Astronomy, University of Sheffield, Sheffield, UK
[146] Department of Physics, Shinshu University, Nagano, Japan
[147] Department Physik, Universität Siegen, Siegen, Germany
[148] Department of Physics, Simon Fraser University, Burnaby, BC, Canada
[149] SLAC National Accelerator Laboratory, Stanford, CA, USA
[150] Department of Physics, Royal Institute of Technology, Stockholm, Sweden
[151] Departments of Physics and Astronomy, Stony Brook University, Stony Brook, NY, USA
[152] Department of Physics and Astronomy, University of Sussex, Brighton, UK
[153] School of Physics, University of Sydney, Sydney, Australia
[154] Institute of Physics, Academia Sinica, Taipei, Taiwan
[155] [(a)]E. Andronikashvili Institute of Physics, Iv. Javakhishvili Tbilisi State University, Tbilisi, Georgia; [(b)]High Energy Physics Institute, Tbilisi State University, Tbilisi, Georgia; [(c)]University of Georgia, Tbilisi, Georgia
[156] Department of Physics, Technion, Israel Institute of Technology, Haifa, Israel
[157] Raymond and Beverly Sackler School of Physics and Astronomy, Tel Aviv University, Tel Aviv, Israel
[158] Department of Physics, Aristotle University of Thessaloniki, Thessaloníki, Greece
[159] International Center for Elementary Particle Physics and Department of Physics, University of Tokyo, Tokyo, Japan
[160] Graduate School of Science and Technology, Tokyo Metropolitan University, Tokyo, Japan
[161] Department of Physics, University of Toronto, Toronto, ON, Canada
[162] [(a)]TRIUMF, Vancouver, BC, Canada; [(b)]Department of Physics and Astronomy, York University, Toronto, ON, Canada
[163] Division of Physics and Tomonaga Center for the History of the Universe, Faculty of Pure and Applied Sciences, University of Tsukuba, Tsukuba, Japan
[164] Department of Physics and Astronomy, Tufts University, Medford, MA, USA
[165] Department of Physics and Astronomy, University of California Irvine, Irvine, CA, USA
[166] University of West Attica, Athens, Greece
[167] Department of Physics and Astronomy, University of Uppsala, Uppsala, Sweden
[168] Department of Physics, University of Illinois, Urbana, IL, USA

[169] Instituto de Física Corpuscular (IFIC), Centro Mixto Universidad de Valencia - CSIC, Valencia, Spain
[170] Department of Physics, University of British Columbia, Vancouver, BC, Canada
[171] Department of Physics and Astronomy, University of Victoria, Victoria, BC, Canada
[172] Fakultät für Physik und Astronomie, Julius-Maximilians-Universität Würzburg, Würzburg, Germany
[173] Department of Physics, University of Warwick, Coventry, UK
[174] Waseda University, Tokyo, Japan
[175] Department of Particle Physics and Astrophysics, Weizmann Institute of Science, Rehovot, Israel
[176] Department of Physics, University of Wisconsin, Madison, WI, USA
[177] Fakultät für Mathematik und Naturwissenschaften, Fachgruppe Physik, Bergische Universität Wuppertal, Wuppertal, Germany
[178] Department of Physics, Yale University, New Haven, CT, USA
[179] Yerevan Physics Institute, Yerevan, Armenia

[a] Also at Affiliated with an Institute Formerly Covered by a Cooperation Agreement with CERN, Geneva, Switzerland
[b] Also at An-Najah National University, Nablus, Palestine
[c] Also at Borough of Manhattan Community College, City University of New York, New York, NY, USA
[d] Also at Center for Interdisciplinary Research and Innovation (CIRI-AUTH), Thessaloníki, Greece
[e] Also at Centre of Physics of the Universities of Minho and Porto (CF-UM-UP), Porto, Portugal
[f] Also at CERN, Geneva, Switzerland
[g] Also at CMD-AC UNEC Research Center, Azerbaijan State University of Economics (UNEC), Baku, Azerbaijan
[h] Also at Département de Physique Nucléaire et Corpusculaire, Université de Genève, Geneva, Switzerland
[i] Also at Departament de Fisica de la Universitat Autonoma de Barcelona, Barcelona, Spain
[j] Also at Department of Financial and Management Engineering, University of the Aegean, Chios, Greece
[k] Also at Department of Mathematical Sciences, University of South Africa, Johannesburg, South Africa
[l] Also at Department of Modern Physics and State Key Laboratory of Particle Detection and Electronics, University of Science and Technology of China, Hefei, China
[m] Also at Department of Physics, Bolu Abant Izzet Baysal University, Bolu, Türkiye
[n] Also at Department of Physics, King's College London, London, UK
[o] Also at Department of Physics, Stanford University, Stanford, CA, USA
[p] Also at Department of Physics, Stellenbosch University, South Africa
[q] Also at Department of Physics, University of Fribourg, Fribourg, Switzerland
[r] Also at Department of Physics, University of Thessaly, Volos, Greece
[s] Also at Department of Physics, Westmont College, Santa Barbara, USA
[t] Also at Faculty of Physics, Sofia University 'St. Kliment Ohridski', Sofia, Bulgaria
[u] Also at Faculty of Physics, University of Bucharest, Bucharest, Romania
[v] Also at Hellenic Open University, Patras, Greece
[w] Also at Henan University, Henan, China
[x] Also at Imam Mohammad Ibn Saud Islamic University, Riyadh, Saudi Arabia
[y] Also at Institucio Catalana de Recerca i Estudis Avancats, ICREA, Barcelona, Spain
[z] Also at Institut für Experimentalphysik, Universität Hamburg, Hamburg, Germany
[aa] Also at Institute for Nuclear Research and Nuclear Energy (INRNE) of the Bulgarian Academy of Sciences, Sofia, Bulgaria
[ab] Also at Institute of Applied Physics, Mohammed VI Polytechnic University, Ben Guerir, Morocco
[ac] Also at Institute of Particle Physics (IPP), Toronto, Canada
[ad] Also at Institute of Physics and Technology, Mongolian Academy of Sciences, Ulaanbaatar, Mongolia
[ae] Also at Institute of Physics, Azerbaijan Academy of Sciences, Baku, Azerbaijan
[af] Also at Institute of Theoretical Physics, Ilia State University, Tbilisi, Georgia
[ag] Also at National Institute of Physics, University of the Philippines Diliman (Philippines), Quezon City, Philippines
[ah] Also at The Collaborative Innovation Center of Quantum Matter (CICQM), Beijing, China
[ai] Also at TRIUMF, Vancouver, BC, Canada
[aj] Also at Università di Napoli Parthenope, Naples, Italy
[ak] Also at Department of Physics, University of Colorado Boulder, Colorado, USA
[al] Also at University of Sienna, Siena, Italy

[am] Also at Washington College, Chestertown, MD, USA
[an] Also at Physics Department, Yeditepe University, Istanbul, Türkiye
* Deceased

[138] Department of Physics and Astronomy, University of Sheffield, Sheffield; United Kingdom
[139] Department of Physics, Shinshu University, Nagano; Japan
[140] Department Physik, Universität Siegen, Siegen; Germany
[141] Department of Physics, Simon Fraser University, Burnaby BC; Canada
[142] SLAC National Accelerator Laboratory, Stanford CA; United States of America
[143] Department of Physics, Royal Institute of Technology, Stockholm; Sweden
[144] Departments of Physics and Astronomy, Stony Brook University, Stony Brook NY; United States of America
[145] Department of Physics and Astronomy, University of Sussex, Brighton; United Kingdom
[146] School of Physics, University of Sydney, Sydney; Australia
[147] Institute of Physics, Academia Sinica, Taipei; Taiwan
[148] [(a)] E. Andronikashvili Institute of Physics, Iv. Javakhishvili Tbilisi State University, Tbilisi; [(b)] High Energy Physics Institute, Tbilisi State University, Tbilisi; [(c)] University of Georgia, Tbilisi; Georgia
[149] Department of Physics, Technion, Israel Institute of Technology, Haifa; Israel
[150] Raymond and Beverly Sackler School of Physics and Astronomy, Tel Aviv University, Tel Aviv; Israel
[151] Department of Physics, Aristotle University of Thessaloniki, Thessaloniki; Greece
[152] International Center for Elementary Particle Physics and Department of Physics, University of Tokyo, Tokyo; Japan
[153] Department of Physics, Tokyo Institute of Technology, Tokyo; Japan
[154] Department of Physics, University of Toronto, Toronto ON; Canada
[155] [(a)] TRIUMF, Vancouver BC; [(b)] Department of Physics and Astronomy, York University, Toronto ON; Canada
[156] Division of Physics and Tomonaga Center for the History of the Universe, Faculty of Pure and Applied Sciences, University of Tsukuba, Tsukuba; Japan
[157] Department of Physics and Astronomy, Tufts University, Medford MA; United States of America
[158] United Arab Emirates University, Al Ain; United Arab Emirates
[159] Department of Physics and Astronomy, University of California Irvine, Irvine CA; United States of America
[160] Department of Physics and Astronomy, University of Uppsala, Uppsala; Sweden
[161] Department of Physics, University of Illinois, Urbana IL; United States of America
[162] Instituto de Física Corpuscular (IFIC), Centro Mixto Universidad de Valencia – CSIC, Valencia; Spain
[163] Department of Physics, University of British Columbia, Vancouver BC; Canada
[164] Department of Physics and Astronomy, University of Victoria, Victoria BC; Canada
[165] Fakultät für Physik und Astronomie, Julius-Maximilians-Universität Würzburg, Würzburg; Germany
[166] Department of Physics, University of Warwick, Coventry; United Kingdom
[167] Waseda University, Tokyo; Japan
[168] Department of Particle Physics and Astrophysics, Weizmann Institute of Science, Rehovot; Israel
[169] Department of Physics, University of Wisconsin, Madison WI; United States of America
[170] Fakultät für Mathematik und Naturwissenschaften, Fachgruppe Physik, Bergische Universität Wuppertal, Wuppertal; Germany
[171] Department of Physics, Yale University, New Haven CT; United States of America

[a] Also Affiliated with an institute covered by a cooperation agreement with CERN.
[b] Also at An-Najah National University, Nablus; Palestine.
[c] Also at Borough of Manhattan Community College, City University of New York, New York NY; United States of America.
[d] Also at Bruno Kessler Foundation, Trento; Italy.
[e] Also at Center for High Energy Physics, Peking University; China.
[f] Also at Centro Studi e Ricerche Enrico Fermi; Italy.
[g] Also at CERN, Geneva; Switzerland.
[h] Also at Département de Physique Nucléaire et Corpusculaire, Université de Genève, Genève; Switzerland.
[i] Also at Departament de Fisica de la Universitat Autonoma de Barcelona, Barcelona; Spain.
[j] Also at Department of Financial and Management Engineering, University of the Aegean, Chios; Greece.
[k] Also at Department of Physics and Astronomy, Michigan State University, East Lansing MI; United States of America.
[l] Also at Department of Physics and Astronomy, University of Louisville, Louisville, KY; United States of America.
[m] Also at Department of Physics, Ben Gurion University of the Negev, Beer Sheva; Israel.
[n] Also at Department of Physics, California State University, East Bay; United States of America.
[o] Also at Department of Physics, California State University, Sacramento; United States of America.
[p] Also at Department of Physics, King's College London, London; United Kingdom.
[q] Also at Department of Physics, Stanford University, Stanford CA; United States of America.
[r] Also at Department of Physics, University of Fribourg, Fribourg; Switzerland.
[s] Also at Department of Physics, University of Thessaly; Greece.
[t] Also at Department of Physics, Westmont College, Santa Barbara; United States of America.
[u] Also at Hellenic Open University, Patras; Greece.
[v] Also at Institucio Catalana de Recerca i Estudis Avancats, ICREA, Barcelona; Spain.
[w] Also at Institut für Experimentalphysik, Universität Hamburg, Hamburg; Germany.
[x] Also at Institute for Nuclear Research and Nuclear Energy (INRNE) of the Bulgarian Academy of Sciences, Sofia; Bulgaria.
[y] Also at Institute of Particle Physics (IPP); Canada.
[z] Also at Institute of Physics, Azerbaijan Academy of Sciences, Baku; Azerbaijan.
[aa] Also at Institute of Theoretical Physics, Ilia State University, Tbilisi; Georgia.
[ab] Also at L2IT, Université de Toulouse, CNRS/IN2P3, UPS, Toulouse; France.
[ac] Also at Lawrence Livermore National Laboratory, Livermore; United States of America.
[ad] Also at National Institute of Physics, University of the Philippines Diliman (Philippines); Philippines.
[ae] Also at The City College of New York, New York NY; United States of America.
[af] Also at The Collaborative Innovation Center of Quantum Matter (CICQM), Beijing; China.
[ag] Also at TRIUMF, Vancouver BC; Canada.
[ah] Also at Università di Napoli Parthenope, Napoli; Italy.
[ai] Also at University of Chinese Academy of Sciences (UCAS), Beijing; China.
[aj] Also at University of Colorado Boulder, Department of Physics, Colorado; United States of America.
[ak] Also at Yeditepe University, Physics Department, Istanbul; Türkiye.
[*] Deceased.

Physics Reports 1116 (2025) 4–56

Contents lists available at ScienceDirect

Physics Reports

journal homepage: www.elsevier.com/locate/physrep

Characterising the Higgs boson with ATLAS data from the LHC Run-2

The ATLAS Collaboration[1]

ARTICLE INFO

Article history:
Received 15 May 2024
Received in revised form 15 October 2024
Accepted 1 November 2024
Available online 16 November 2024
Editor: Giulia Zanderighi

This work is dedicated to the memory of Prof. Peter Ware Higgs, whose groundbreaking research on broken symmetries and mass generation predicted the boson that is the focus of this Report.

Keywords:
Higgs boson
Standard model physics

ABSTRACT

The Higgs boson was discovered by the ATLAS and CMS Collaborations in 2012 using data from Run 1 of the Large Hadron Collider (2010−2012). In Run 2 (2015−2018), about 140 fb^{-1} of proton–proton collisions at a centre-of-mass energy of 13 TeV were collected by the ATLAS experiment. This review presents the most important Run 2 results obtained by the ATLAS Collaboration regarding the properties of the Higgs boson and its interactions with other particles. The performed studies significantly enhance the understanding of the Higgs boson, while hunting for deviations from the predictions of the Standard Model of particle physics.
© 2024 CERN for the benefit of the ATLAS Collaboration. Published by Elsevier B.V. This is an open access article under the CC BY license (http://creativecommons.org/licenses/by/4.0/).

Contents

1. Introduction 5
   1.1. The Higgs mechanism 5
   1.2. SM predictions for Higgs boson production and decay 5
   1.3. The LHC run 1 legacy: From the discovery of the Higgs boson to the first property measurements 7
      1.3.1. The Higgs boson discovery 7
      1.3.2. First measurements of the Higgs boson properties 7
2. Higgs boson mass and width 9
   2.1. Higgs boson mass 9
   2.2. Higgs boson width 10
3. Fiducial and differential cross-sections 12
   3.1. Fiducial and total cross-sections 12
   3.2. Differential cross-sections 13
4. Higgs boson couplings to fermions 15
   4.1. Observation of the Higgs boson couplings to third generation fermions: τ-leptons, top and bottom quarks 15
   4.2. Higgs boson couplings to the second generation fermions: $H \to c\bar{c}$ and $H \to \mu\mu$ 20
5. Search for rare loop-induced decays of the Higgs boson 21
6. Cross-sections and couplings from combined fits 22
   6.1. Global signal strength, production cross-sections and decay branching ratios 24
   6.2. Higgs boson couplings to other particles 24
   6.3. Production cross-sections in different kinematic regions and their interpretation 25
7. Study of CP properties and search for anomalous interactions 27

[1] See Appendix for more details.

https://doi.org/10.1016/j.physrep.2024.11.001
0370-1573/© 2024 CERN for the benefit of the ATLAS Collaboration. Published by Elsevier B.V. This is an open access article under the CC BY license (http://creativecommons.org/licenses/by/4.0/).

7.1. CP properties in interactions with vector bosons ... 27
7.2. CP properties in interactions with fermions ... 31
8. The Higgs boson self-coupling ... 32
8.1. Double Higgs boson production ... 32
8.2. Self-coupling constraints from single Higgs boson measurements and combination with double Higgs boson searches 35
9. Conclusion and outlook ... 36
CRediT authorship contribution statement ... 37
Declaration of competing interest ... 37
Acknowledgements ... 37
Appendix. The ATLAS collaboration ... 38
References ... 51

1. Introduction

One of the main motivations for building the Large Hadron Collider (LHC) was to investigate the nature of electroweak symmetry breaking. After the discovery of the Higgs boson [1,2] by the ATLAS and CMS Collaborations [3,4], the focus has shifted to the measurement of its properties. Ever since, an important goal has been to determine whether the Higgs boson can be a portal to so-far undiscovered phenomena.

This report summarises the expansive Higgs boson analysis programme performed by the ATLAS Collaboration with the data recorded during Run 2 of the LHC (2015−2018) and discusses the wealth of exciting results available at the time of its publication. Unless otherwise specified, all results are based on the full Run 2 data sample, corresponding to 140 fb^{-1} of proton–proton (pp) collisions recorded with the ATLAS detector [5]. For detailed discussions of technical aspects of the conducted analyses, the reader is referred to the original publications, which are cited throughout the report. Searches for exotic Higgs boson decays and additional Higgs bosons are covered elsewhere [6].

1.1. The Higgs mechanism

The Standard Model of particle physics (SM) is a relativistic quantum field theory based on gauge symmetries that describes the elementary particles and their interactions [7–10]. Seemingly forbidden by gauge invariance, massive W and Z bosons are enabled by electroweak symmetry breaking. In its simplest form, electroweak symmetry breaking is realised through the introduction of a complex doublet scalar field, which manifests itself in a neutral scalar boson, the Higgs boson [11–15]. While the Higgs field potential itself is invariant under the SU(2) transformation, its shape allows for spontaneous symmetry breaking, which keeps the gauge symmetries intact but leads to a vacuum expectation value that is non-zero and non-invariant under SU(2). Interactions between the Higgs field and the fermions, the Yukawa interactions, give rise to the masses of the fermions. The Yukawa couplings and the Higgs boson mass are free parameters in the SM.

The LHC offers a unique opportunity to study the Higgs sector and therefore the nature of electroweak symmetry breaking. With the measurement of the Higgs boson mass, the SM Higgs sector is fully determined by experimentally measured parameters. Measurements of the Higgs boson couplings to other particles and the Higgs boson self-coupling are of particular importance. The Yukawa sector describes a completely new boson–fermion interaction that is the only interaction in the SM that distinguishes between particles of different masses and therefore flavours. The Higgs boson self-coupling is mainly probed through double Higgs boson production and is an important parameter of the Higgs field potential, which is related to the structure of the vacuum and governs the properties of the electroweak phase transition in the early universe [16,17].

The SM Higgs boson is a scalar boson: spin zero and its interactions are even under charge–parity (CP) conjugation. In pp collisions, the main Higgs boson production mechanisms predicted by the SM are gluon–gluon fusion (ggF), vector-boson fusion (VBF), and associated production with vector bosons (VH, where V represents a W or Z boson), top- or bottom-quark pairs ($t\bar{t}H$, $b\bar{b}H$), or a single top quark (tH). The different production processes can be tagged through dedicated selection criteria, taking advantage of the particular signatures of the different final states. They are shown, together with the main predicted decay processes, in Fig. 1. The corresponding diagrams for double Higgs boson production through the ggF and VBF mechanisms are shown in Fig. 2. The expected width of the SM Higgs boson for a mass of 125 GeV is 4.1 MeV [18].

1.2. SM predictions for Higgs boson production and decay

Complementing the measurement programme at the LHC, there is an intense effort ongoing to calculate Higgs boson production cross-sections and branching ratios, as well as their associated uncertainties, to the best possible accuracy in various phase space regions. Furthermore, Monte Carlo (MC) simulations are developed to optimise the experimental data analysis and to compare observed and expected results. These differential predictions are more challenging and therefore only available at lower precision than the total production cross-sections.

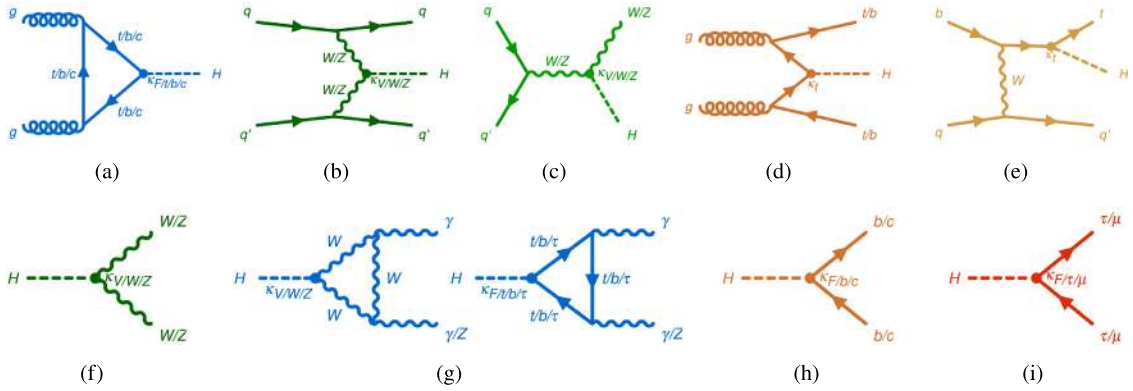

Fig. 1. Top: Higgs boson production via (a) gluon–gluon fusion, (b) vector-boson fusion, and (c) associated production with vector bosons, (d) top- or bottom-quark pairs, or (e) a single top quark. Bottom: Higgs boson decays into (f) a pair of vector bosons, (g) a pair of photons or a Z boson and a photon, (h) a pair of quarks, and (i) a pair of charged leptons [19].

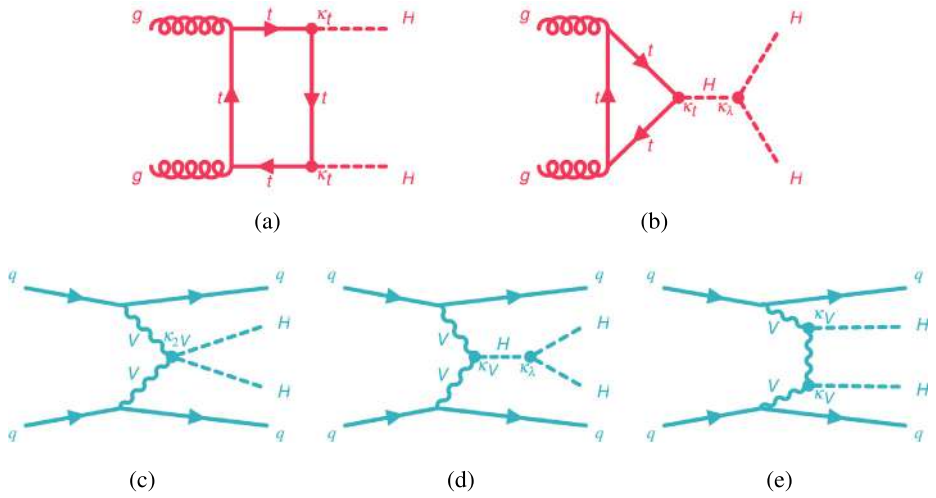

Fig. 2. Examples of leading-order Feynman diagrams for Higgs boson pair production in the (a and b) ggF HH and (c, d and e) VBF HH modes.

Table 1
SM predictions of Higgs boson production cross-sections for a Higgs boson mass of 125.09 GeV in pp collisions at a centre-of-mass energy of $\sqrt{s} = 13$ TeV. The values are based on Refs. [21–33] for ggF, Refs. [34–36] for VBF, Refs. [37–45] for WH and ZH, Refs. [46–49] for $t\bar{t}H$, Refs. [50–52] for $b\bar{b}H$, and Refs. [53,54] for tH. They are compiled in Ref. [18].

Process	Precision in QCD	Precision in EW	Cross-section [pb]	Fraction [%]
ggF	N^{3}LO	NLO	$48.5^{+2.7}_{-3.6}$	87.2
VBF	approx. NNLO	NLO	3.78±0.08	6.8
$qq \to WH$	NNLO	NLO	1.37±0.03	2.44
$qq \to ZH$	NNLO	NLO	$0.76^{+0.01}_{-0.02}$	1.35
$gg \to ZH$	NLO	LO	$0.12^{+0.03}_{-0.02}$	0.22
$t\bar{t}H$	NLO	NLO	$0.51^{+0.03}_{-0.05}$	0.92
$b\bar{b}H$	NNLO	LO	$0.49^{+0.10}_{-0.12}$	0.88
tH	NLO	LO	$0.092^{+0.006}_{-0.011}$	0.16

SM Higgs boson production cross-sections are calculated for the different production modes shown in Fig. 1(a)–(e). The total cross-sections are listed in Table 1, including the achieved accuracy in the electroweak (EW) and strong (QCD) coupling constant, i.e., tree-level or leading order (LO), next-to-leading order (NLO), next-to-next-to leading order (NNLO), etc. They are calculated assuming a Higgs boson mass of 125.09 GeV. This value is based on the combined Higgs boson mass measurement by the ATLAS and CMS Collaborations in the LHC Run 1 [20].

The SM predicts the double Higgs boson production cross-section to be more than a thousand times smaller than single Higgs boson production: $\sigma_{\text{ggF } HH} = 31.0^{+2.1}_{-7.2}$ fb [18,55–64], computed at NNLO in QCD including approximated mass top effects, and $\sigma_{\text{VBF } HH} = 1.73 \pm 0.04$ fb, at N^{3}LO in QCD, for a Higgs boson mass of 125 GeV [65–67].

Branching fractions, or decay probabilities for the different Higgs boson decays, as depicted in Fig. 1(f)–(i), also depend on the Higgs boson mass. For a mass of 125.09 GeV, the SM predicts that decays into W bosons have a branching fraction of 22%, Z bosons of 3%, photons (γ) of 0.2%, and Z boson and photon of 0.2%. Decays into fermion pairs have the following branching ratios: bottom quarks 58%, charm quarks 3%, τ leptons 6%, and muons 0.02% [68–72].

For most of the analyses discussed in this report, samples were produced with MC generators as follows: ggF events were simulated using the POWHEG NNLOPS program [33,73–77], which provides NNLO accuracy in QCD. The other production modes were simulated with the POWHEG generator [73–75,78–80] at an accuracy of NLO in QCD, except for $b\bar{b}H$ and tH, which were simulated using the MADGRAPH5_AMC@NLO generator, also at NLO accuracy in QCD [81]. In the majority of cases, the PYTHIA program is used to simulate decays and to model the effects of parton showering, hadronisation and the underlying event. To evaluate modelling uncertainties, alternative samples showered with the HERWIG program are used. The effect of multiple interactions in the same and neighbouring LHC bunch crossings (pile-up) was modelled by overlaying the original hard-scattering event with simulated inelastic pp events. The generated events were passed through a simulation of the ATLAS detector [82] using GEANT4 [83].

1.3. The LHC run 1 legacy: From the discovery of the Higgs boson to the first property measurements

1.3.1. The Higgs boson discovery

By 2012, both the LEP collider at CERN and the Tevatron collider at Fermilab had searched for the Higgs boson and excluded the existence of a SM Higgs boson with a mass below 114.4 GeV [84] or between 149 and 182 GeV [85] at 95% confidence level (CL). SM consistency fits based on precision electroweak measurements hinted at a Higgs boson with a mass of $\sim$90 $\pm$ 30 GeV [86,87].

Due to record centre-of-mass energies and a steady increase in collected pp data, Run 1 of the LHC saw a continuous widening of the excluded mass ranges for a SM Higgs boson, except for masses around 125 GeV, where, during the 2011 and 2012 data taking, the data recorded by the ATLAS and CMS detectors showed an excess over the background-only hypothesis.

On July 4th, 2012, based on approximately 10 fb^{-1} of recorded LHC data each, the ATLAS and CMS Collaborations individually announced the discovery of a neutral boson with a mass of about 125 GeV [1,2]. As shown in Fig. 3, multiple decay channels contributed to the combined significance of the excess, which exceeded the five standard deviation (σ) discovery threshold. The ones with the highest significances were the $\gamma\gamma$ and four-lepton ($ZZ^* \to 4\ell$, $\ell = e, \mu$) final states, which provide an excellent invariant mass resolution and favourable signal-to-background ratios, as well as the $WW^* \to e\nu\mu\nu$ final state. Fig. 4 shows the observed excess in the $\gamma\gamma$ and 4ℓ invariant mass distributions, and in the transverse mass distribution for the $H \to WW^* \to e\nu\mu\nu$ decay channel, where the transverse momentum of the neutrinos is estimated through the missing transverse momentum in the detector. This results in the wider distribution seen in Fig. 4(c). The transverse mass is defined as $m_{\text{T}} = \sqrt{(E_{\text{T}}^{\ell\ell} + E_{\text{T}}^{\text{miss}})^2 - |\vec{p}_{\text{T}}^{\,\ell\ell} + \vec{p}_{\text{T}}^{\,\text{miss}}|^2}$, where $\vec{p}_{\text{T}}^{\,\ell\ell}$ is the transverse momentum vector of the dilepton system, $\vec{p}_{\text{T}}^{\,\text{miss}}$ is the missing transverse momentum vector with magnitude $E_{\text{T}}^{\text{miss}}$, and $E_{\text{T}}^{\ell\ell}$ is the square root of sum in quadrature of the magnitude of $\vec{p}_{\text{T}}^{\,\ell\ell}$ and the invariant mass of the dilepton system.

1.3.2. First measurements of the Higgs boson properties

The data produced by the LHC and recorded by the ATLAS and CMS detectors in Run 1, in particular the 20 fb^{-1} of data at 8 TeV centre-of-mass energy recorded in 2012, allowed the first measurements of the properties of the newly discovered particle.

A Higgs boson mass measurement in the $H \to ZZ^* \to 4\ell$ and $H \to \gamma\gamma$ decay channels, combining ATLAS and CMS data, resulted in a value of m_H = 125.09$\pm$0.24 GeV [20]. This value is used as input to almost all measurements performed by the ATLAS Collaboration based on the LHC Run 2 data. In most measurements, the effect of the associated uncertainty is negligible.

Combining ATLAS and CMS Higgs boson measurements from Run 1 in all accessible production and decay channels, the Higgs boson signal yield relative to the SM prediction, also called signal strength μ, was measured to be 1.09 $\pm$ 0.11 [88]. Each experiment observed, with more than 5σ significance, the ggF production process and the decays into two Z bosons, two W bosons, and two photons. The combination also allowed observation of VBF production and decays into two τ-leptons. Assuming SM coupling structures, the couplings of the Higgs boson to the gauge bosons were measured with an accuracy of $\sim$10%, to top quarks and τ-leptons with $\sim$17%, and to bottom quarks with $\sim$30%.

Differential cross-section measurements were performed in the $H \to \gamma\gamma$, $H \to ZZ^* \to 4\ell$, and $H \to WW^* \to e\nu\mu\nu$ decay channels [89–92], analysing Higgs boson kinematics and properties of associated hadronic jet production.

First statements could also be made in Run 1 regarding the spin and CP properties of the newly discovered particle. The fact that decays into two bosons were observed clearly characterises the particle as a boson, with the diphoton decay excluding the spin-1 possibility [93,94]. Spin and CP studies of diboson decays [95] confronted the scalar hypothesis with several alternative spin scenarios, including non-SM spin-0 and spin-2 models with universal and non-universal couplings

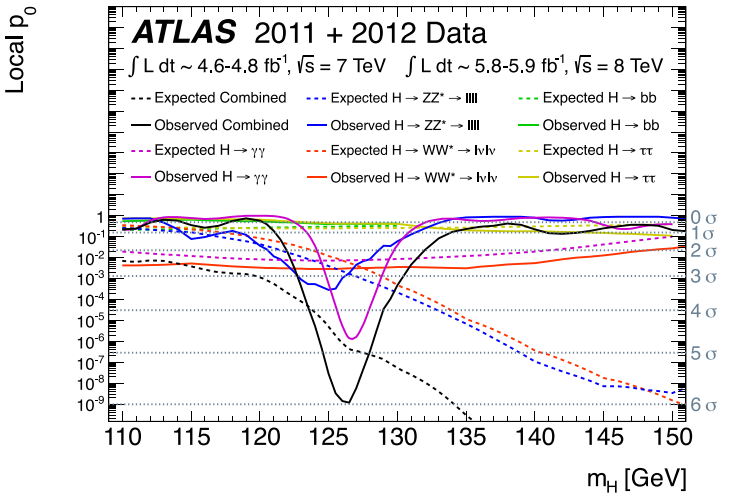

Fig. 3. Left vertical axis: The p-value, i.e., the probability for a background-only experiment to be more like the signal than the observation, for individual decay channels and their statistical combination. Right vertical axis: The translation to standard deviations. The horizontal axis shows the Higgs boson mass hypothesis [1].

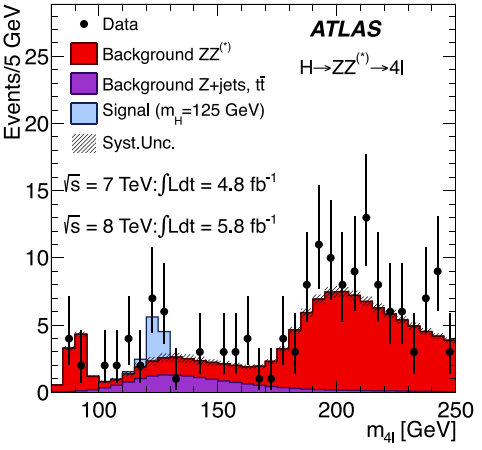

(a)

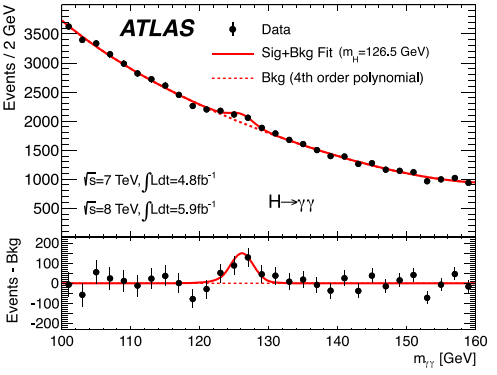

(b)

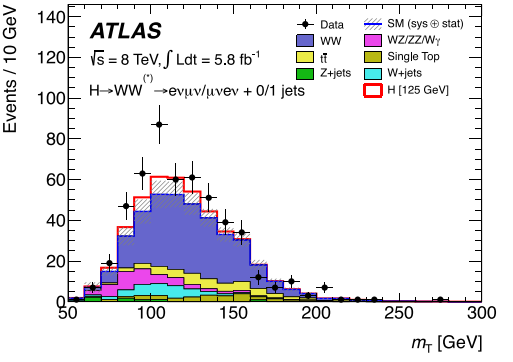

(c)

Fig. 4. Invariant mass distributions in the (a) $ZZ^* \to 4\ell$ and (b) $\gamma\gamma$ final states, and (c) the transverse mass in the $WW^* \to e\nu\mu\nu$ final state, showing the excesses in data events over the background-only hypotheses that led to the discovery of the Higgs boson [1].

to fermions and vector bosons. All tested alternative models were excluded in favour of the SM Higgs boson hypothesis at a CL of more than 99.9%. No sign of CP violation was found in VBF production with τ-lepton decays [96].

An upper limit was set on the width of the Higgs boson by the ATLAS Collaboration of 22.7 MeV [97], which corresponds to roughly six times the SM expectation. This assumed that the signal strength on the Higgs boson peak and off-shell is the same [98–101].

Within the achieved statistical and systematic uncertainties, all measurements in Run 1 agreed with the predictions for a SM Higgs boson.

In Run 2 of the LHC, the ATLAS detector recorded 140 fb^{-1} of pp collision data. For this data sample, the SM predicts a total of ∼9 million Higgs bosons produced at the ATLAS interaction point, of which 0.3% are experimentally accessible [19]. Making use of this unprecedented amount of data, the goals for Run 2 included a more precise determination of the Higgs boson mass and width (see Section 2), and of fiducial and differential cross-sections (see Section 3). Measurements of the Higgs boson couplings to fermions, in particular the direct observation of the Yukawa couplings to third generation quarks (see Section 4) were eagerly anticipated, as were the searches for rare decays (see Sections 4 and 5). The larger data sample also allowed increased precision on the measured Higgs boson production cross-sections and couplings to other particles (see Section 6) and the study of the CP properties of both the boson and fermion couplings (see Section 7). Finally, enormous progress was made regarding the search for Higgs boson pair production and the constraints on the Higgs boson self-coupling (see Section 8).

2. Higgs boson mass and width

2.1. Higgs boson mass

The SM predicts the existence of a Higgs boson but not its mass, which therefore has to be measured experimentally. Once the mass of the Higgs boson is known, together with the masses of fermions, the SM production cross-section and branching ratios can be calculated. They can then be checked experimentally to search for deviations from SM predictions due to potential new phenomena. The value of the Higgs boson mass also affects the SM predictions of the effective weak mixing angle and, logarithmically, the W boson mass (see e.g., Ref. [102]). Moreover, the shape and energy evolution of the Higgs potential are directly related to the Higgs boson mass, which therefore determines the stability of the electroweak vacuum [16,103].

Among the various decay modes, $H \to \gamma\gamma$ and $H \to ZZ^* \to 4\ell$ play a special role in the characterisation of the Higgs boson and in particular the measurement of its mass. Both final states are fully reconstructable, provide an excellent mass resolution, and are accompanied by well-understood backgrounds. Among the two, $H \to \gamma\gamma$ yields more signal events, while $H \to ZZ^* \to 4\ell$ benefits from a higher signal-to-background ratio.

The $H \to \gamma\gamma$ decay channel [104] allows the direct observation of a narrow mass peak over a smooth background that can be determined directly from the collected data. The typical mass resolution in the ATLAS detector is 1.7 GeV for a Higgs boson mass of 125 GeV. The main background process is non-resonant $\gamma\gamma$ production with a smaller contribution of about 25% from γ+jet and dijet processes where one or two of the hadronic jets are misidentified as photons. In the $H \to \gamma\gamma$ analysis, the Higgs boson properties (e.g., signal yield, mass) are measured in events with at least two isolated and well-identified photon candidates. The selection efficiency for events with a SM Higgs boson decaying into two photons is about 36%. Depending on the measurement being performed, events are classified into different categories to improve the specific sensitivity to a given observable. In the case of the Higgs boson mass measurement, the selected events are classified into 14 categories with different signal-to-background ratios, invariant mass resolutions and photon energy scale uncertainties.

The invariant diphoton mass distribution ($m_{\gamma\gamma}$) of the simulated signal in each category is found to be very well described by a double-sided Crystal Ball [105] probability density function. The normalisation factors of the signal, one for each category, are treated as free parameters in the fit to reduce the model-dependence of the measurement. In each category, the $m_{\gamma\gamma}$ distribution of the background processes is represented by either an exponential function, a power-law function, or the exponential of a second-order polynomial.

One key aspect of the mass measurement in the $H \to \gamma\gamma$ channel is the careful control of the systematic uncertainties, mainly arising from the photon energy scale. A significant effort was devoted during Run 2 to substantially reduce these uncertainties, resulting in a decrease of a factor close to four compared to the mass measurement performed with the initial 36 fb^{-1} of LHC Run 2 data [106]. This improvement in the photon energy scale calibration was achieved through a better understanding of the energy response across the longitudinal layers of the ATLAS electromagnetic calorimeter and a new correction implemented in the extrapolation of the electron energy scale measured in $Z \to ee$ events to photons [107]. The impact of the photon energy scale uncertainty on the mass measurement was reduced to 83 MeV. Systematic uncertainties related to the choice of the function used to describe the background are also taken into account, with a minor impact on the mass measurement, but more relevant for analyses targeting the measured signal yield. The measured mass of the Higgs boson in the $H \to \gamma\gamma$ final state using the full Run 2 data sample is $m_H = 125.17 \pm 0.11(\text{stat.}) \pm 0.09(\text{syst.})$ GeV. The measurement is statistically limited, hence opening the possibility for substantial improvements with the future LHC runs. The diphoton invariant mass distribution of all selected data events, weighted according to the signal-to-background ratio in the respective category, and the fitted functions are shown in Fig. 5(a).

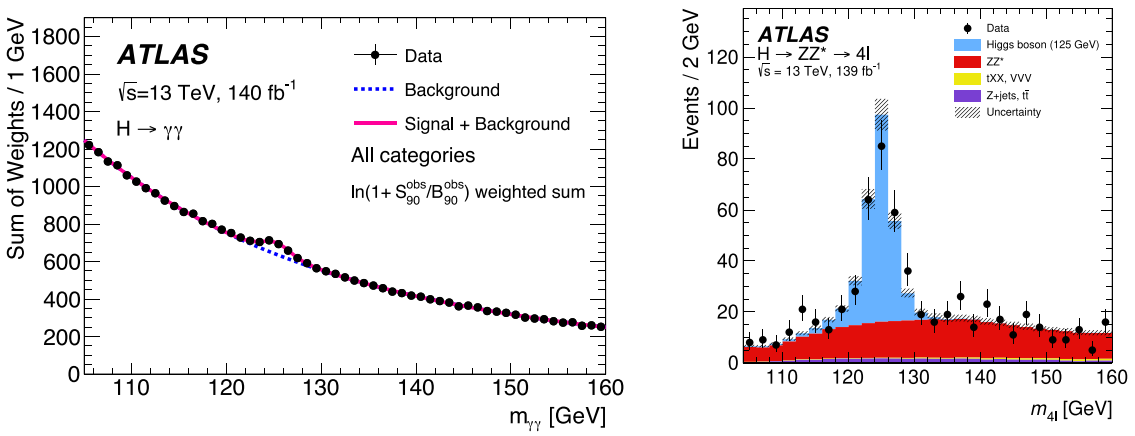

Fig. 5. (a) Weighted diphoton invariant mass distribution of all selected data events, overlaid with the result of the fit [104]. (b) Four-lepton invariant mass distribution of the selected events in data compared with the simulation [108].

***H → ZZ* → 4ℓ* decays** [108] are reconstructed by requiring two pairs of oppositely charged same-flavour isolated electrons or muons in the final state. One of the two pairs, the leading lepton pair is required to have an invariant mass compatible with that of the Z boson. The events are split into four sub-channels according to the flavour of the leading and subleading lepton pair (4μ, $2e2\mu$, $2\mu2e$, $4e$). The selection efficiency ranges between 31% and 16%, depending on the sub-channel. The dominant background process is non-resonant $ZZ \to 4\ell$ production, which is suppressed in this specific measurement by using a neural network (NN) based classifier. The measurement of the Higgs boson mass is carried out by simultaneously fitting the reconstructed invariant mass of the four-lepton system ($m_{4\ell}$) in the four sub-channels using an unbinned maximum-likelihood approach. The resolution of $m_{4\ell}$ varies from approximately 1.5 GeV to 2.1 GeV. The signal model comprises a double-sided Crystal Ball probability density function, with the mean of its Gaussian core determined as a function of m_H and the standard deviation expressed as a function of the predicted event-level resolution. In the fitting procedure, the normalisations of the signal and background components are treated as free parameters for each of the four sub-channels.

Fig. 5(b) shows the four-lepton invariant mass distribution of the selected events in data compared with the simulation. The Higgs boson mass measured in the $H \to ZZ^* \to 4\ell$ channel using the Run 2 data sample is $m_H = 124.99 \pm 0.18(\text{stat.}) \pm 0.04(\text{syst.})$ GeV, with the dominant source of systematic uncertainty arising from the uncertainties in the muon momentum scale, resolution and sagitta bias correction (28 MeV) and the electron energy scale (19 MeV).

The combination of the mass measurements performed with the $H \to \gamma\gamma$ and $H \to ZZ^* \to 4\ell$ channels using Run 1 and Run 2 [20] data results in a Higgs boson mass of $m_H = 125.11 \pm 0.09(\text{stat.}) \pm 0.06(\text{syst.})$ GeV [109], which corresponds to an experimental precision of 0.09%. With the current precision achieved in the Higgs boson mass, the impact of its uncertainty on the Higgs boson production cross-sections and branching ratios is below 1%. A summary plot of the Higgs boson mass measurements performed in Run 1 and Run 2 and their combination is shown in Fig. 6.

2.2. Higgs boson width

Once the mass of the Higgs boson is known, the SM allows the width to be computed. For a Higgs boson with a mass of 125 GeV, the expected width is only $\Gamma_H = 4.1$ MeV [18]. Any deviation from this value would indicate the presence of phenomena beyond the SM, e.g., Higgs boson decays into so-far unknown particles.

Due to the experimental mass resolution in the most precise channels ($H \to \gamma\gamma$ and $H \to ZZ^* \to 4\ell$) of the order of 1−2 GeV, a direct measurement of the SM width of the Higgs boson is not achievable from the detected lineshapes. Similarly, the corresponding lifetime is so short that the decay length is extremely small, well beyond the experimental resolution on the reconstruction of the displaced vertex from the beam spot. In addition, the width cannot be extracted from the rate measurement in the different decay channels because only cross-section times branching-ratio measurements are possible at the LHC. However, in 2012, a different method was proposed, which relies on measuring on-shell and off-shell Higgs boson production [98–101]. In the SM, despite the small total width, about 10% of the $gg \to H^* \to VV$ ($V = W, Z$) events are produced with an invariant mass larger than twice the vector bosons masses. In particular, the vector bosons from the Higgs boson decay and the top quarks running in the ggF production loop can be on-shell above the thresholds of $2m_V$ and $2m_t$, respectively. On-shell Higgs boson production is inversely proportional to the width, e.g., for ggF production with the Higgs boson decaying into two V bosons

$$\sigma^{\text{on-shell}}_{gg\to H\to VV} \propto \frac{g^2_{ggF,\text{on-shell}} g^2_{HVV,\text{on-shell}}}{\Gamma_H m_H}, \tag{1}$$

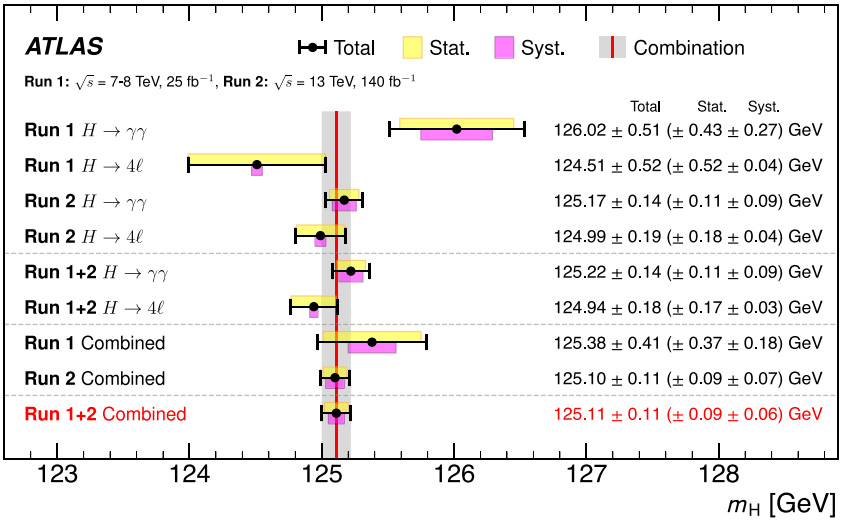

Fig. 6. ATLAS Higgs boson mass measurement combining LHC Run 1 and Run 2 results in the $H \to \gamma\gamma$ and $H \to ZZ^* \to 4\ell$ final states [109].

where $g_{ggF,\text{on-shell}}$ and $g_{HVV,\text{on-shell}}$ are the on-shell couplings associated with the Higgs boson production and decay. On the other hand, off-shell Higgs boson production has negligible dependence on the width, e.g.,

$$\sigma^{\text{off-shell}}_{gg\to H\to VV} \propto \frac{g^2_{ggF,\text{off-shell}} g^2_{HVV,\text{off-shell}}}{m^2_{VV}}. \tag{2}$$

Similar expressions apply to electroweak production, where the g_{ggF} coupling is replaced by the g_{HVV} coupling. If the effective couplings have a known relationship (e.g., the one predicted in the SM) in the on-shell and off-shell regimes, the ratio of the off-shell to the on-shell production allows the determination of Γ_H.

The off-shell Higgs boson signal cannot be treated independently of the $gg \to VV$ background due to significant negative interference between the two processes [98]. For a given off-shell signal strength $\mu_{\text{off-shell}}$, the expected number of events as a function of the invariant mass of the diboson system, m_{VV}, is positive and corresponds to the sum of the $gg \to VV$ background, the off-shell signal, which is proportional to $\mu_{\text{off-shell}}$, and the (negative) interference term, which is proportional to $\sqrt{\mu_{\text{off-shell}}}$. Additionally, when extracting the width of the Higgs boson, it must also be assumed that any new phenomena affecting the off-shell signal strength and the off-shell couplings do not modify the relative phase of the interfering signal and background processes. The full Run 2 data sample is used to study off-shell Higgs boson production and set an upper limit on the width of the Higgs boson through the $ZZ \to 4\ell$ and $ZZ \to 2\ell 2\nu$ final states [110], which were identified as the most sensitive channels in Run 1 [111].

The $ZZ \to 4\ell$ analysis selects events with two same-flavour oppositely charged dilepton pairs and a four-lepton invariant mass above the on-shell ZZ production threshold. The mass of each dilepton pair is required to be compatible with that of a Z boson. The signal regions are designed to be sensitive to both the electroweak and ggF production modes, considering only events with $m_{4\ell} > 220$ GeV, while events with $180 < m_{4\ell} < 220$ GeV are used to constrain the normalisation of the dominant $qq \to ZZ$ process. To enhance the signal sensitivity, a multi-class dense NN is used to distinguish among the off-shell Higgs boson signal, the interfering background and non-interfering background. Two separate NNs are trained for ggF and electroweak-induced signals. The NN's output is employed to define the final observable, serving as a discriminating variable in the corresponding signal region. Fig. 7(a) shows the observed distribution of the NN based discriminant in the ggF signal region compared with the SM expectations.

In the $ZZ \to 2\ell 2\nu$ final state, the presence of neutrinos prevents the kinematic reconstruction of m_{ZZ}. The discriminating variable used to enhance sensitivity to the off-shell production of the Higgs boson is therefore the transverse mass, computed from the transverse components of the momenta, defined as

$$m_{\text{T}}^{ZZ} \equiv \sqrt{\left(\sqrt{m_Z^2 + (p_{\text{T}}^{\ell\ell})^2} + \sqrt{m_Z^2 + (E_{\text{T}}^{\text{miss}})^2}\right)^2 - \left|\vec{p}_{\text{T}}^{\,\ell\ell} + \vec{p}_{\text{T}}^{\,\text{miss}}\right|^2}, \tag{3}$$

which is reconstructed from the mass of the Z boson m_Z, the transverse momentum vector of the dilepton system $\vec{p}_{\text{T}}^{\,\ell\ell}$ and the missing transverse momentum vector $\vec{p}_{\text{T}}^{\,\text{miss}}$, along with their respective magnitudes. Signal events are selected by requiring two oppositely charged electron or muon candidates with a dilepton invariant mass compatible with the Z boson mass and high $E_{\text{T}}^{\text{miss}}$, vetoing events with a third lepton. Additional selection criteria are optimised to maximise the signal significance relative to the main backgrounds, which include ZZ, WZ, WW, top-quark, and W/Z+jets processes. Fig. 7(b) shows the observed m_{T}^{ZZ} distribution compared with the SM prediction in the ggF signal region.

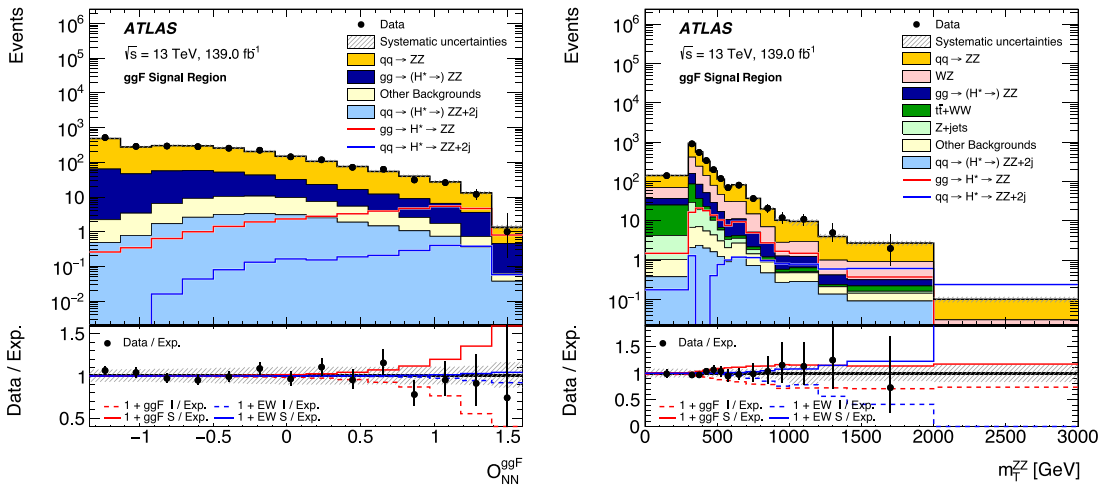

(a) (b)

Fig. 7. (a) Observed and expected distribution of the NN-based observable sensitive to the off-shell production in the 4ℓ channel in the ggF signal region [110]. (b) Observed and expected transverse mass distribution in the $2\ell 2\nu$ channel in the ggF signal region [110].

Combining the 4ℓ and $2\ell 2\nu$ channels, the ratio of the off-shell Higgs boson production rate to its SM prediction (μ_{offshell}) is measured. The data are found to be consistent with SM predictions, rejecting the hypothesis of no off-shell Higgs boson production ($\mu_{\text{offshell}} = 0$) with an observed (expected) statistical significance of 3.3 (2.2)σ, thus providing experimental evidence for this process. In addition, these results are combined with the on-shell Higgs boson measurements in the $H \to ZZ^* \to 4\ell$ channel [112], obtaining an indirect measurement of the width of the Higgs boson of $\Gamma_H = 4.5^{+3.0}_{-2.5}$ MeV, in agreement with the SM expectation, and observed (expected) lower and upper limits on the total width of $0.5\ (0.1) < \Gamma_H < 10.2\ (10.6)$ MeV at 95% CL.

3. Fiducial and differential cross-sections

Fiducial and differential cross-section measurements allow the characterisation of the Higgs boson through production- and decay-related distributions. They are usually performed inclusively over all production modes. Compared to measurements of event yields, these cross-section measurements have the advantage that they can be easily interpreted and used by physicists outside the ATLAS Collaboration, as they include corrections for detector effects.

In each final state, a fiducial phase space is chosen to reduce the extrapolation from the measured phase space and therefore the model dependence of the measurement. The fiducial phase space is defined at particle level, i.e., based on generated stable particles, approximating the selection of reconstructed events. After selecting the events, the extraction of the signal event yields and the correction to the fiducial phase space are performed simultaneously using a likelihood fit.

3.1. Fiducial and total cross-sections

Higgs boson production cross-sections are measured in the $\gamma\gamma$ and $ZZ^* \to 4\ell$ final states. The event selections are very similar to those discussed in Section 2, but the events are not separated into different categories. The Higgs boson production cross-section times branching ratio measured in the $\gamma\gamma$ fiducial volume is 67 ± 6 fb [113], while the cross-section times branching ratio measured in the $ZZ^* \to 4\ell$ fiducial volume is 3.28 ± 0.32 fb [114]. Both results are in agreement with the SM predictions (64 ± 4 fb and 3.41 ± 0.18 fb, respectively [18]), and achieve a precision of about 10%.

To allow the combination of the $ZZ^* \to 4\ell$ and $\gamma\gamma$ measurements [115], total cross-sections are extracted by extrapolating from the fiducial to the total phase space, also correcting for the branching fractions. The combination improves the statistical power by roughly doubling the analysed data sample, as the lower cross-section times branching fraction of the $ZZ^* \to 4\ell$ decay channel is balanced by a better signal-over-background ratio compared to the $\gamma\gamma$ measurement. On the other hand, the combination increases the model-dependence of the result. The extrapolation factors rely on SM predictions and uncertainties related to the measured cross-sections of the different Higgs boson production modes are taken into account. The reduction in statistical uncertainties is significantly larger than the additional uncertainties due to the extrapolation, which are at the per-cent level. The cross-sections measured at different centre-of-mass energies are presented in Fig. 8, together with the SM prediction. For pp collisions at 13 TeV centre-of-mass energy, the measured cross-section is $55.5 \pm 3.2(\text{stat.})^{+2.4}_{-2.2}(\text{syst.}) = 55.5^{+4.0}_{-3.8}$ pb, achieving a precision of about 7%. Good agreement with the SM prediction (55.6 ± 2.2 pb [18]) is observed.

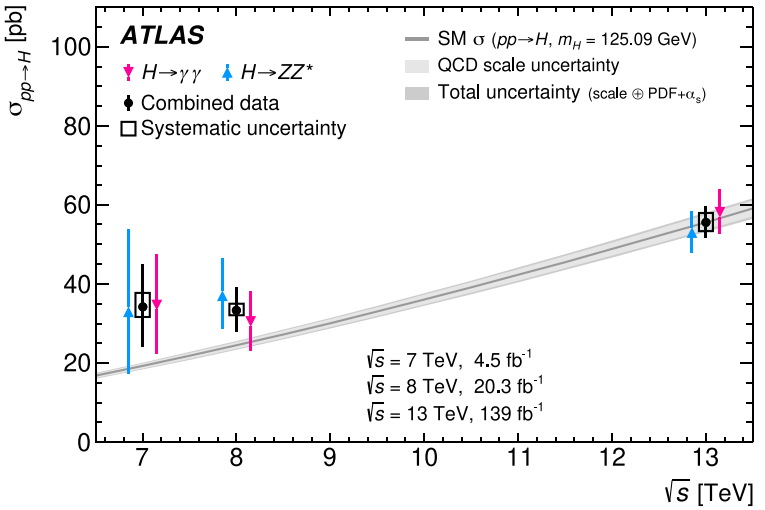

Fig. 8. Total $pp \to H + X$ cross-sections measured at centre-of-mass energies of 7, 8 and 13 TeV in the $ZZ^* \to 4\ell$ and $\gamma\gamma$ decay channels, and their combination, compared with SM predictions [115].

3.2. Differential cross-sections

Measurements of differential cross-sections allow probing of Higgs boson kinematics, such as the Higgs boson transverse momentum p_{T}^{H} and rapidity, and other aspects of Higgs boson production and decay, such as the number and properties of the associated hadronic jets. The $ZZ^* \to 4\ell$ and $\gamma\gamma$ differential cross-section measurements are performed individually and combined, to benefit from the reduced statistical uncertainties. As for the total cross-section, the necessary extrapolation introduces additional model-dependent uncertainties.

For each observable, a likelihood fit performs the extraction of the signal event yields in each bin. It uses dedicated factors for the correction of measurement inefficiencies, a migration matrix for the unfolding of resolution effects, and the measured luminosity to determine the cross-sections. No regularisation is applied. In addition to the experimental and background uncertainties, uncertainties related to the model dependence of the unfolding are included.

The p_{T}^{H} distribution of the Higgs boson is one of the most interesting observables to measure as it could be sensitive to different phenomena beyond the SM (BSM). It could differ from the SM prediction if the Higgs boson were produced together with an invisible particle or if so-far unknown particles contributed to the ggF loop. In addition, the p_{T}^{H} distribution, the overall production rate and the $H \to \gamma\gamma$ branching fraction are sensitive to the Yukawa couplings of the Higgs boson to the bottom and charm quarks. Both the contributions of these quarks to the loop-induced ggF production and $b\bar{b}$ and $c\bar{c}$ initiated Higgs boson production play an important role. The p_{T}^{H} would also be modified by the presence of new dynamics. Constraints on non-SM interactions can be set within an effective field theory model, as shown in Section 6. A combined measurement of p_{T}^{H}, extrapolated to the total phase space, is shown in Fig. 9(a). The binning was chosen to adequately capture the shape of the distribution for the subsequent interpretations. A precision of 20% is achieved in some regions. Fig. 9(b) shows the observed limits at 95% CL on the Yukawa coupling-strength modifiers of the bottom and charm quarks, defined as the ratios of the measured Yukawa couplings to their SM values [116], based on the shape and normalisation of the p_{T}^{H} distribution. The combination of these constraints with those from the $H \to b\bar{b}$ and $H \to c\bar{c}$ analyses is discussed in Section 4.

Fig. 10 shows the rapidity of the Higgs boson measured in the $H \to \gamma\gamma$ decay channel and the invariant mass of the off-shell Z boson in the $H \to ZZ^* \to 4\ell$ decay channel. The rapidity of the Higgs boson is sensitive to the parton distribution functions of the colliding protons, and is also influenced by QCD radiative corrections. The invariant mass of the off-shell Z boson would be modified by the presence of a 'dark' Z boson mixing with the SM [117,118]. It is also sensitive to anomalous couplings and can be interpreted in the pseudo-observable framework [119]. The two results are a subset of the measured distributions, which cover a broad range of observables, ranging from Higgs boson kinematics to properties of the associated hadronic jets and of the Higgs boson decay products.

Despite the missing information from the neutrinos in the final state and thanks to the relatively high branching ratio, it is also possible to measure differential cross-sections in the $WW^* \to e\nu\mu\nu$ final state [120,121]. In this channel, the measurements are not performed inclusively, but separately for ggF and VBF production. Events are selected if they contain two oppositely charged, different-flavour leptons (electrons or muons). Further requirements are applied to ensure a non-negligible missing transverse momentum in the event. To suppress $\tau\tau$ background from the Υ meson, or from an off-shell photon or Z boson (Drell–Yan) a minimum requirement on the invariant mass of the two leptons is applied. After the event selection, the dominant backgrounds to the Higgs boson signal are non-resonant WW production, top

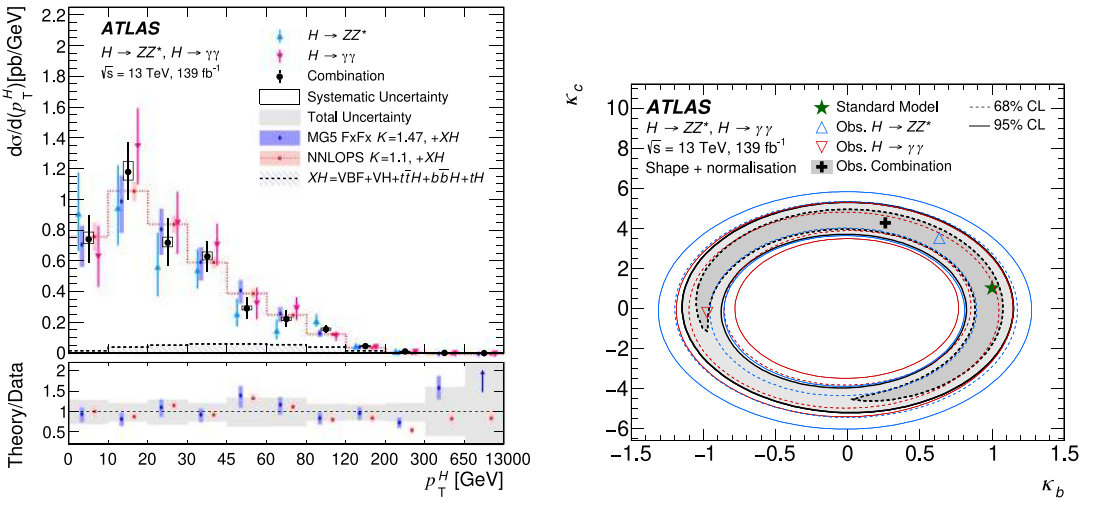

(a) (b)

Fig. 9. (a) Higgs boson transverse momentum measured in the $ZZ^* \to 4\ell$ and $\gamma\gamma$ decay channels, and their combination, compared with two SM ggF predictions, which are scaled to the total expected N^{3}LO cross-section and added to the predictions for the other production modes. (b) Observed limits at 95% CL on the Yukawa coupling-strength modifiers based on both the shape and normalisation of the Higgs boson transverse momentum distribution. The SM prediction and the observed best-fit values are also indicated [115].

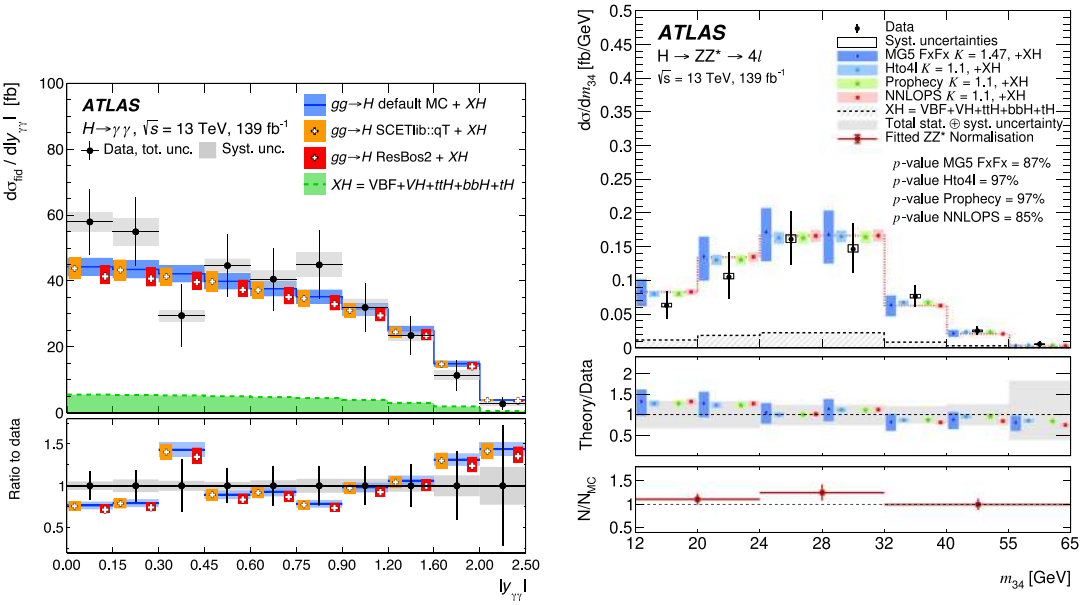

(a) (b)

Fig. 10. (a) The rapidity of the Higgs boson measured in the $H \to \gamma\gamma$ decay channel [113], and (b) the invariant mass of the off-shell Z boson in the $H \to ZZ^* \to 4\ell$ decay channel [114]. The measurements are compared with different SM ggF predictions that are added to predictions for the other production modes. For the invariant mass, the ggF predictions are scaled to the total N^{3}LO cross-sections.

pair production, the Drell–Yan process, and jets that are misidentified as leptons. Dedicated control regions are created that are enriched in these background processes. They are used in the subsequent fit to extract correction factors to the estimated yields, which are extracted from MC for most backgrounds. To estimate the background from events with jets misidentified as leptons, correction factors are determined from data and applied to the corresponding control region. In the VBF analysis, an additional control region enriched in ggF events is added to the fit to estimate this background. In the ggF analysis, the small contributions from other Higgs boson production modes are estimated by using simulated

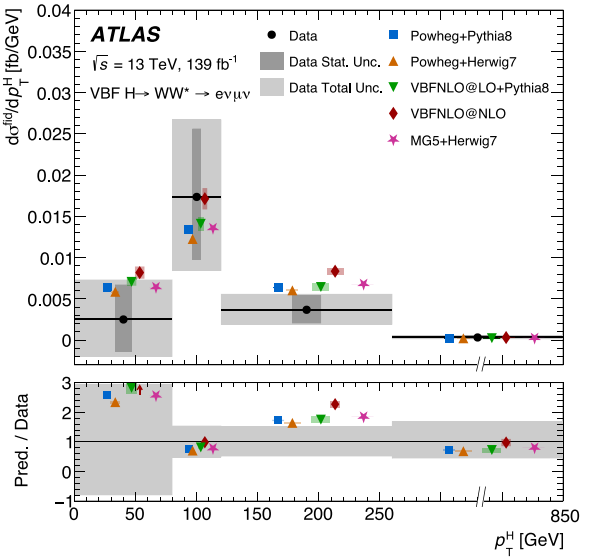

Fig. 11. Higgs boson transverse momentum measured for VBF production in the $WW^* \to e\nu\mu\nu$ decay channel compared with different SM predictions [121].

events scaled to the expected SM cross-sections. The unfolding is performed by inverting the response matrix. In the ggF analysis, a Tikhonov regularisation term [122] is included in the likelihood to avoid large statistical fluctuations. Fig. 11 shows p_{T}^{H} measured for VBF production in the $WW^* \to e\nu\mu\nu$ decay channel.

Good agreement is seen between all measured differential cross-sections and the state-of-the-art SM predictions.

4. Higgs boson couplings to fermions

4.1. Observation of the Higgs boson couplings to third generation fermions: τ-leptons, top and bottom quarks

In the SM, fermions obtain their masses by interacting with the Higgs field via the Yukawa coupling. One of the major achievements during Run 2 of the LHC was the direct confirmation of the Yukawa couplings to third generation fermions. This was accomplished by studying the fermionic decays of the Higgs boson and the associated production of the Higgs boson with pairs of top quarks.

The observation of Higgs boson decays into two τ-leptons was established during Run 1 through a combination of measurements by the ATLAS and CMS Collaborations, with a significance of 5.5σ [88]. ATLAS achieved a single-experiment observation using 36.1 fb^{-1} of Run 2 data in combination with Run 1 data [123].

All combinations of hadronic and leptonic τ-lepton decays are considered. They are treated as separate analysis channels due to differences in their background composition. In all channels, the dominant background is the $Z \to \tau\tau$ process. Therefore, the best sensitivity can be achieved for topologies in which Z boson production is suppressed, such as Lorentz-boosted ggF and VBF production. The relative contributions from other backgrounds, primarily from top-quark and vector-boson decays, as well as from misidentified leptonic or hadronic τ-lepton decays, vary considerably depending on the τ-lepton decay mode. The invariant mass of the $\tau\tau$ system is used to discriminate between Higgs boson and Z boson production and to extract the signal yield, making the mass resolution extremely important. An algorithm is employed that determines the most probable $\tau\tau$ mass for the event, assuming that the measured missing transverse momentum originates from neutrinos in a resonant $\tau\tau$ final state [124]. Several categories are defined based on the Higgs boson production mode, particularly probing VBF and boosted Higgs boson production via ggF. The normalisations of the major backgrounds are constrained using data from different control regions. The yields of the $Z \to \tau\tau$ background are estimated directly from a fit to the final discriminating variable.

In Fig. 12(a), the reconstructed invariant mass of the $\tau\tau$ system is shown for all signal regions using the 2015–2016 ATLAS data sample [123]. The $H \to \tau\tau$ signal is established with an observed (expected) significance of 4.4σ (4.1σ), which increases to 6.4σ (5.4σ) when combined with the Run 1 results.

With the data collected by the end of Run 2, it is possible to probe the $H \to \tau\tau$ cross-section in the four major production modes (ggF, VBF, VH, and $t\bar{t}H$), and as a function of the kinematic properties of the events in ggF and electroweak production processes [125]. In Fig. 12(b), the reconstructed invariant mass of the $\tau_{\mathrm{lep}}\tau_{\mathrm{had}}$ pair is shown, where one τ-lepton decays leptonically and one hadronically. The measured cross-sections times branching ratio for $|y_H| < 2.5$ in the dominant ggF and VBF production modes are $2.65 \pm 0.41(\mathrm{stat.})^{+0.91}_{-0.67}(\mathrm{syst.})$ pb and $0.197 \pm 0.028(\mathrm{stat.})^{+0.032}_{-0.026}(\mathrm{syst.})$ pb

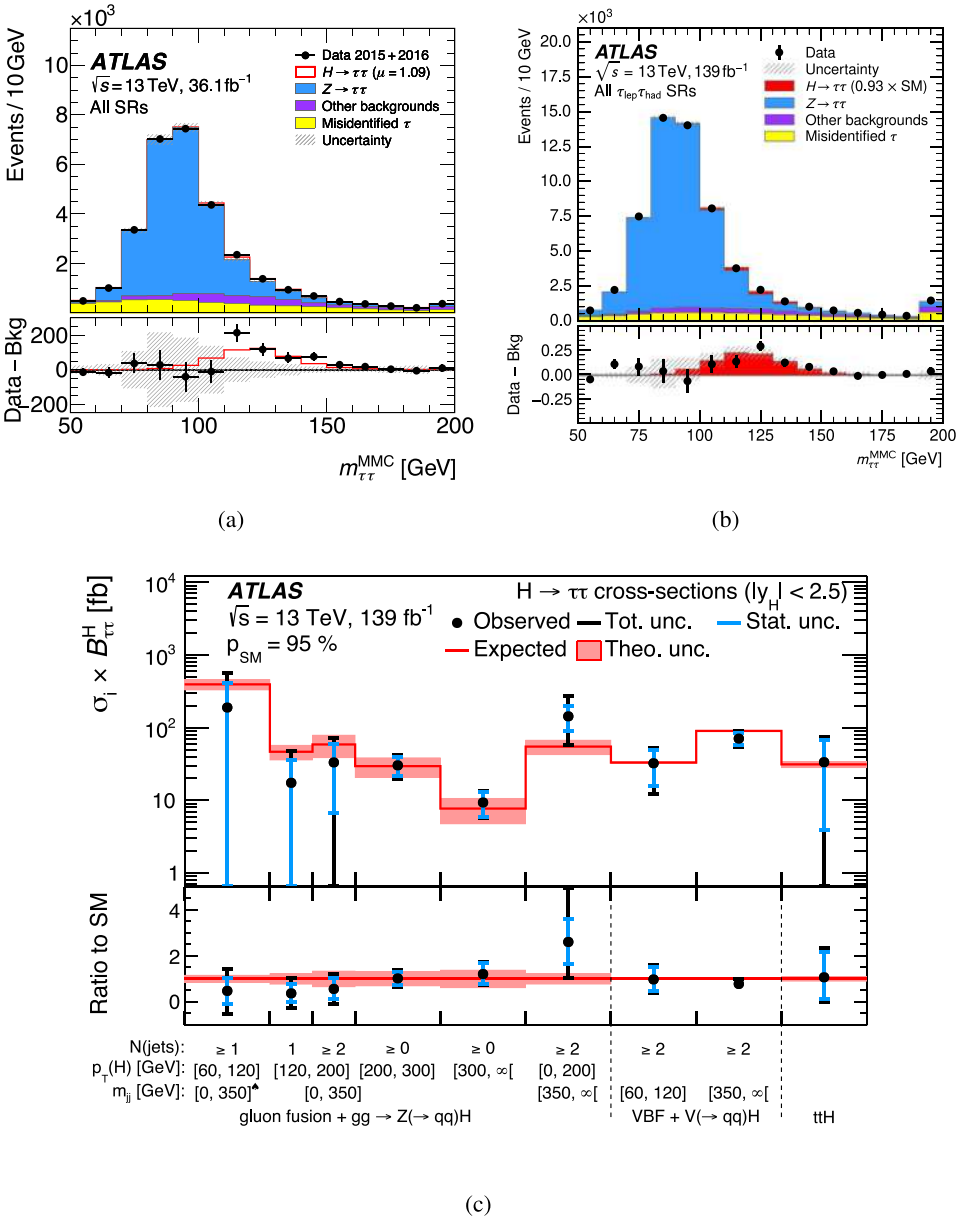

Fig. 12. (a) The invariant mass of the $\tau\tau$ system for all combinations of τ-lepton decays using 36.1 fb^{-1} of data [123]. (b) The same observable considering only signal regions with one τ-lepton decaying leptonically and one decaying hadronically for 139 fb^{-1} of data [125]. (c) The measured cross-sections times branching ratio in nine different kinematic regions compared with the SM expectations [125].

respectively, in agreement with the SM expectations. Cross-sections of the production of a Higgs boson decaying into τ-leptons are measured as a function of p_{T}^{H}, the number of jets produced in association with the Higgs boson, and the invariant mass of the two leading jets m_{jj}, as shown in Fig. 12(c). The achieved statistical and systematic uncertainties are 24% for the electroweak production of the Higgs boson with two jets and m_{jj} greater than 350 GeV and about 40% for the boosted ggF production.

The observation of $t\bar{t}H$ production [126] was an important breakthrough. Since the strength of the Yukawa interaction is proportional to the fermion mass, the predicted Yukawa coupling of the top quark is the largest one in the SM, with a value close to unity. Indirect constraints on this coupling were already obtained through ggF production and Higgs boson decays into photons, which occur via quantum loops (Fig. 1). In the SM, the dominant contribution to the former arises from diagrams featuring the top quark or the bottom quark in the loop, along with their interference. Meanwhile, in the latter case, the primary contribution is due to the W boson in the loop or the top quark [127]. However,

so-far unknown phenomena could affect these loops, therefore a direct measurement through $t\bar{t}H$ production is necessary to disentangle and probe potential BSM effects.

The presence of complex final states and large irreducible backgrounds, combined with a small predicted rate (about 1% of the total Higgs boson production), makes the measurement of $t\bar{t}H$ challenging. Different analyses using up to 79.8 fb^{-1} of Run 2 data and targeting various Higgs boson decay channels were combined, leading to the observation of this production mode in 2018 [126].

The search for $t\bar{t}H$ production via $H \to b\bar{b}$ decays [128] benefits from the large Higgs boson branching fraction to bottom quarks, but suffers from sizeable backgrounds, primarily from events with a top quark pair and additional heavy-flavour jets, which are also challenging to model. Events are selected in which one or both top quarks decay semileptonically. The events are further categorised using the jet multiplicity and the probability that a certain jet originates from a bottom quark (b-tagging). This allows nine signal-enriched regions to be defined, with a maximum purity at the level of about 5%, and ten background-enriched control regions. Multivariate discriminants based on kinematic variables are trained for each region to further enhance the signal-to-background separation. The signal yield is extracted through a global fit in which the normalisation of the $t\bar{t}$ +heavy flavour background components is allowed to float freely. An excess over the background-only hypothesis is observed (expected) with a significance of 1.4σ (1.6σ) with the 2015–2016 data sample, corresponding to 36.1 fb^{-1} of Run 2 data.

Searching for $t\bar{t}H$ production, the $H \to WW^*$, $H \to \tau\tau$, and the $H \to ZZ^*$ decays are difficult to disentangle, as they lead to similar final states featuring the presence of multiple leptons. Therefore, they are treated together in a common $t\bar{t}H, H \to$ multilepton analysis [129]. The $t\bar{t}H$, $H \to ZZ^* \to 4\ell$ contribution is studied in a dedicated analysis and minimised to be negligible in the $t\bar{t}H, H \to$ multilepton analysis with a selection based on the four-lepton invariant mass. Events are categorised into seven orthogonal categories based on the number of light leptons and hadronically decaying τ-lepton candidates. The $t\bar{t}$ background is suppressed by requiring two leptons with the same charges or at least three leptons of any charges. The defined categories have different background compositions and a wide range of total yields and signal purities. The irreducible background is predominantly composed of SM processes with prompt leptons, such as $t\bar{t}W$, $t\bar{t}Z$, and diboson production. Control regions are used to extract the normalisation for these backgrounds and estimate the backgrounds with non-prompt light leptons and mis-identified hadronically decaying τ-lepton candidates. Dedicated multivariate discriminants are employed in most of the signal regions to further enhance the signal-to-background separation. In Fig. 13(a), the observed and expected yields in the signal regions and control regions are shown. A combined profile likelihood fit across all regions extracts the signal with an observed (expected) significance of 4.1σ (2.8σ) with the 2015–2016 data sample, corresponding to 36.1 fb^{-1} of Run 2 data.

The $t\bar{t}H$, $H \to ZZ^* \to 4\ell$ final state is treated in a dedicated analysis [126], separating events in which both top quarks decay hadronically from events in which at least one top quark decays semileptonically and employing a boosted decision tree (BDT) in each region. Due to the small Higgs boson branching ratio to four leptons, the expected rates are very low. The expected background contamination is also small. The simulation predicts 0.6 signal events, and an expected significance of 1.2σ. No events are observed with 79.8 fb^{-1} of Run 2 data.

The $t\bar{t}H$ analysis using $H \to \gamma\gamma$ decays [126] benefits from a very clean signature, with a peak in the invariant mass distribution of the diphoton system over a smooth background, but it suffers from a low rate. The main background processes are non-resonant diphoton production and other Higgs boson production modes. Regarding the associated top quark decays, this analysis distinguishes between leptonic events (where at least one light lepton is present) and hadronic channels. BDTs are employed in various analysis categories to separate the signal from backgrounds. As shown in Fig. 13(b), the signal is extracted from signal-plus-background fits to the $\gamma\gamma$ invariant mass distribution, with the background constrained by the mass sidebands. The resulting observed (expected) significance is 4.1σ (3.7σ) with 79.8 fb^{-1} of Run 2 data.

Combining the various decay modes, along with the results obtained using the Run 1 data, an observed (expected) significance of 6.3σ (5.1σ) for $t\bar{t}H$ production is achieved with 36.1—79.8 fb^{-1} of Run 2 data [126]. Assuming SM branching fractions, the total $t\bar{t}H$ production cross-section at 13 TeV is measured to be $670 \pm 90(\text{stat.})^{+110}_{-100}(\text{syst.})$ fb, in agreement with the SM prediction. Fig. 13(c) shows the combined event yields in all analysis categories as a function of $\log_{10}(S/B)$, where S and B are the expected signal and background yields extracted from the fit, with a clearly visible signal-like excess over the background at high $\log_{10}(S/B)$.

Exploiting the full Run 2 data sample, it is possible to make cross-section measurements as a function of p_{T}^{H} in $t\bar{t}H$ production, both in the $H \to \gamma\gamma$ [131] and $H \to b\bar{b}$ [130] final states. Fig. 13(d) shows the results obtained in the $H \to b\bar{b}$ final state.

The observation of Higgs boson decays into bottom-quark pairs in 2018 was another significant milestone in the understanding of Higgs boson interactions [132]. This observation provides direct evidence of the Yukawa coupling of the Higgs boson with down-type quarks.

The $H \to b\bar{b}$ decay has the largest branching ratio in the SM at about 58%. However, inclusive $H \to b\bar{b}$ searches are very challenging at the LHC due to backgrounds arising from multijet production that are orders of magnitudes larger than Higgs boson production. The most sensitive analysis is based on VH production, where events are categorised according to the number of charged leptons (muons or electrons) from the vector boson decays. Events containing zero or two leptons target ZH production, while events with one lepton target WH production. All events are required to have at least two jets, of which exactly two must have a high probability to originate from bottom quarks. The primary background sources

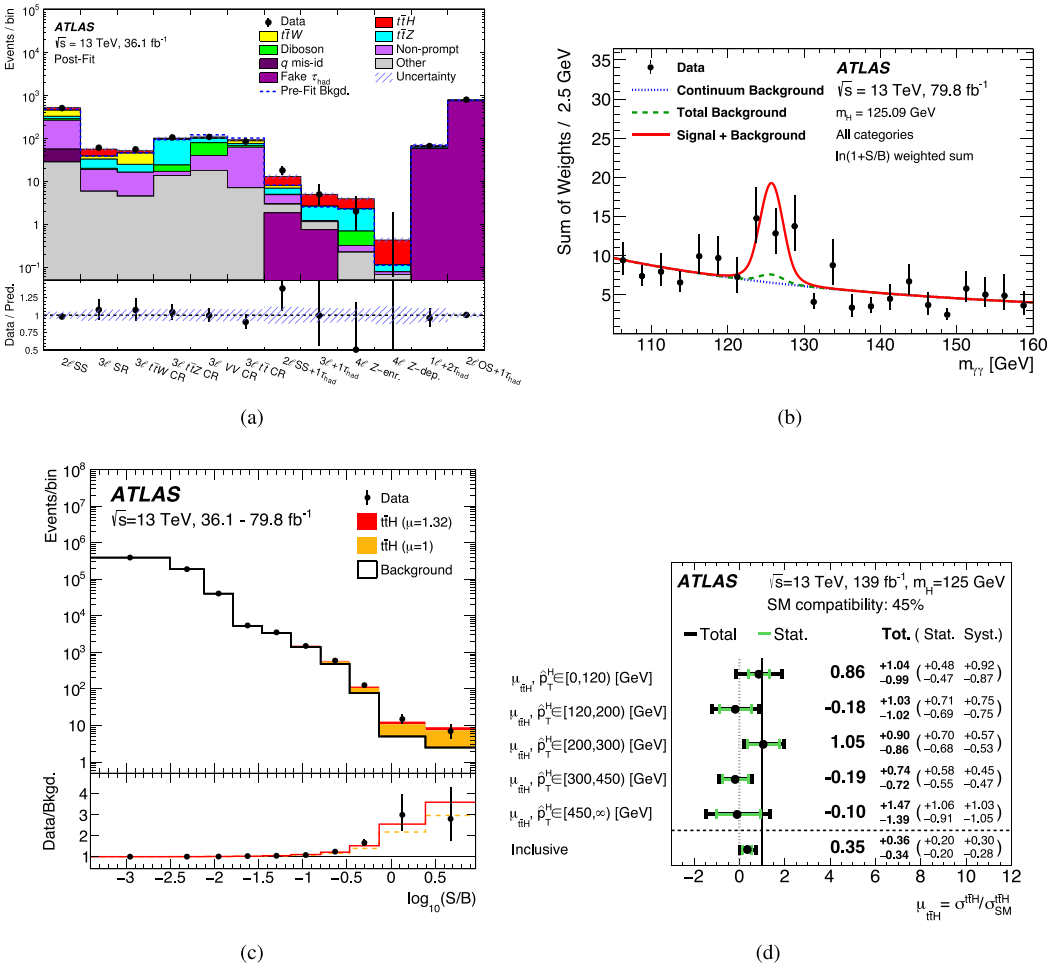

Fig. 13. (a) Comparison of the data to the prediction in the different signal and control regions of the $t\bar{t}H$, $H \to$ multilepton analysis, after the fit is performed [129]. (b) The diphoton invariant mass distribution in the $t\bar{t}H, H \to \gamma\gamma$ analysis [126]. (c) Event yields as a function of $\log_{10}(S/B)$ for data, background and a Higgs boson signal for all decay channels considered, using up to 79.8 fb^{-1} of data, leading to the observation of $t\bar{t}H$ production [126]. (d) Measured $t\bar{t}H$ production cross-sections normalised to the SM expectation as function of p_{T}^{H} in the $H \to b\bar{b}$ final state [130].

are V+jets and $t\bar{t}$ production, and their normalisation is constrained using dedicated control regions. The separation between the signal and background is achieved using the invariant mass of the $b\bar{b}$ system $m_{b\bar{b}}$ and several other kinematic observables, such as the transverse momentum of the vector boson. These observables are used as input to BDTs in the different signal regions. Based on the first 79.8 fb^{-1} of Run 2 data, the analysis yields an observed significance for VH, $H \to b\bar{b}$ production of 4.9σ (4.2σ expected). Combining this result with the searches for $H \to b\bar{b}$ in other Higgs boson production modes, a significance of 5.4σ is observed, with an expectation of 5.5σ. Furthermore, the combination of this result with the other searches for VH production provides the first observation of this process with a significance of 5.3σ (4.8σ expected).

In addition, an analysis without multivariate discriminants (cut-based analysis) is performed as a cross-check. In this case, $m_{b\bar{b}}$ is used as the discriminating variable and additional selection criteria are employed, e.g., on the separation between the two b-tagged jets, to increase the purity of the signal regions. The VZ process with the Z boson decaying into $b\bar{b}$ offers a powerful validation of the cut-based analysis, as this process closely resembles the Higgs boson signal except for the lower invariant mass of the $b\bar{b}$ system. Fig. 14(a) shows the invariant mass distribution of the $b\bar{b}$ system after subtracting all backgrounds except for the VZ process, using the first 79.8 fb^{-1} of data in Run 2. The VZ contribution is clearly visible, along with a significant excess at higher $m_{b\bar{b}}$ values due to VH production.

The full Run 2 data sample allows further improvements in the VH, $H \to b\bar{b}$ measurements [133], yielding a measured signal strength relative to the SM prediction of $\mu_{VH}^{bb} = 1.02^{+0.12}_{-0.11}(\text{stat.})^{+0.14}_{-0.13}(\text{syst.})$. Fig. 14(b) shows the observed and predicted discriminant distribution used to separate the Higgs boson signal from the backgrounds in one of the signal regions. In addition, cross-sections of associated production of a Higgs boson decaying into bottom quark pairs and a vector boson decaying into leptons are measured as a function of the vector boson transverse momentum in kinematic

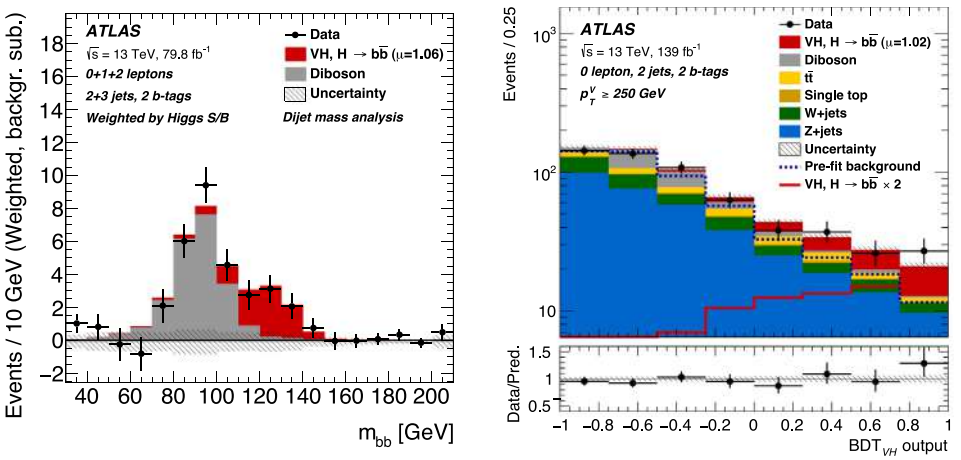

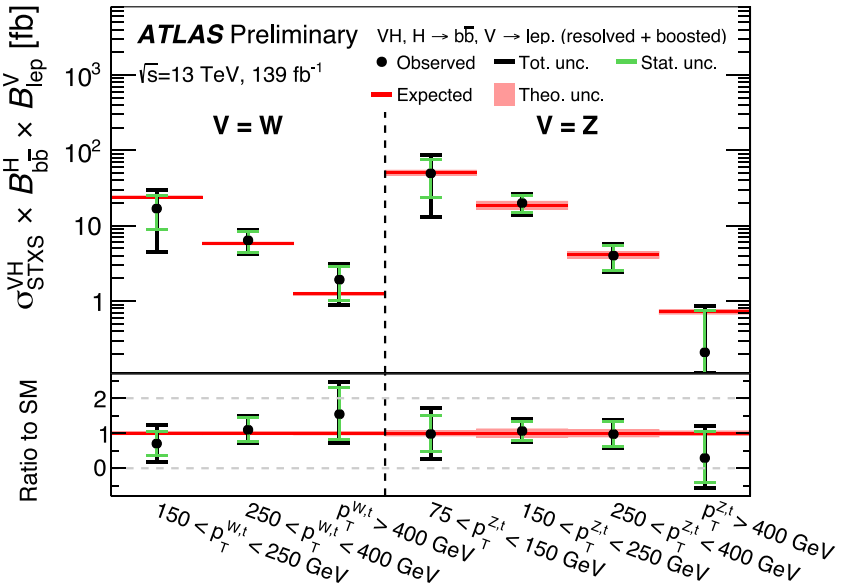

Fig. 14. (a) The S/B weighted $b\bar{b}$ invariant mass distribution for the cut-based $VH, H \to b\bar{b}$ analysis after the subtraction of all backgrounds but the WZ and ZZ diboson processes, based on Run 2 data collected up to 2017 [132]. (b) Observed and predicted distribution for one of the 14 BDTs used to separate the Higgs boson signal from the background processes in the $VH, H \to b\bar{b}$ analysis performed with the full Run 2 data sample [133]. (c) The production cross-section of the Higgs boson times the $H \to b\bar{b}$ and $V \to$ leptons branching ratios as a function of the transverse momentum of the vector boson p_{T}^{V} [134].

fiducial volumes, with uncertainties ranging from 30% in the highest p_{T}^{V} region ($p_{\mathrm{T}}^{V} > 250$ GeV) to 85% in the lowest (75 GeV $< p_{\mathrm{T}}^{Z} <$ 150 GeV).

For transverse momenta of the Higgs boson above about 300 GeV, the decay products of the Higgs boson in the $VH, H \to b\bar{b}$ process cannot always be reconstructed through two jets with a small radius parameter R ($R = 0.4$). The collimated Higgs boson decay products may however be reconstructed as a single jet with a large radius parameter ($R = 1$). This boosted region is particularly interesting due to its sensitivity to BSM physics at high energy scales. The measured signal strength for the $VH, H \to b\bar{b}$ events reconstructed as a single large-radius jet with $p_{\mathrm{T}}^{V} > 250$ GeV with the full Run 2 data is $\mu_{VH}^{bb} = 0.72^{+0.39}_{-0.36}$ [135].

A combination of the $VH, H \to b\bar{b}$ measurements targeting different transverse momentum regions by reconstructing the Higgs boson as two individual jets [133] or a single large-radius jet [135] is also performed [134]. The overlap between the two analyses is addressed by switching from the former to the latter at a p_{T}^{V} of 400 GeV. Cross-sections are measured

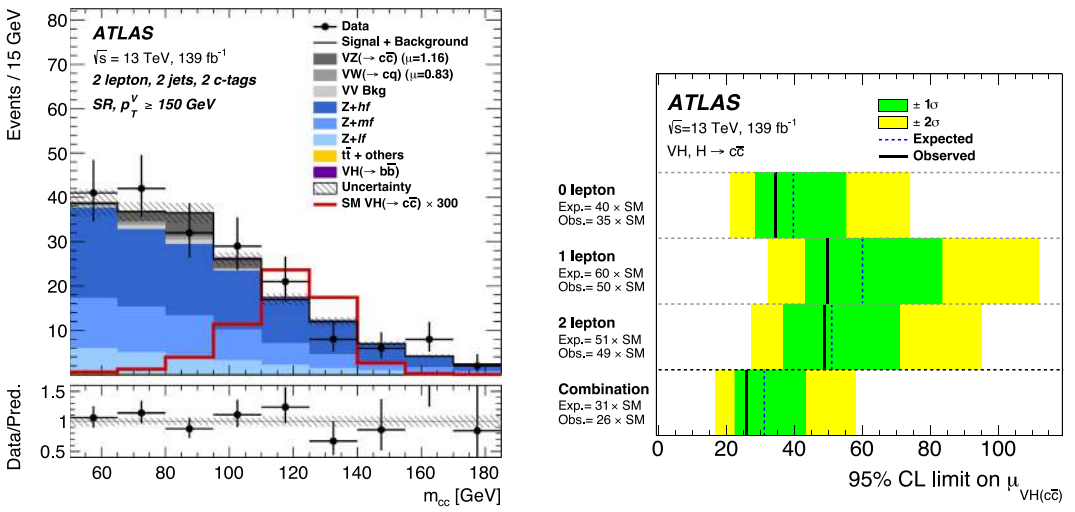

(a) (b)

Fig. 15. (a) Invariant mass distribution of the two charm-tagged jets in a selected signal region of the $H \to c\bar{c}$ analysis [116]. The $H \to c\bar{c}$ signal is also shown, scaled by 300 times the SM prediction. (b) The observed and expected 95% CL upper limits on the VH, $H \to c\bar{c}$ signal strength in the different analysis categories and for the combined fit [116].

as function of the transverse momentum of the W and Z bosons and found to be compatible with the SM expectations, as shown in Fig. 14(c).

Higgs bosons decaying into bottom-quark pairs are also studied in the VBF production mode [136], resulting in a measured yield of $0.95^{+0.38}_{-0.36}$ times the one predicted by the SM with the full Run 2 data sample, corresponding to an observed (expected) significance of 2.6σ (2.8σ).

Run 2 data are also exploited to study the inclusive production of the Higgs boson at high transverse momentum in the $H \to b\bar{b}$ decay channel [137]. The observed (expected) 95% CL upper limit on the Higgs boson production cross-section for $p_{\mathrm{T}}^{H} > 1$ TeV is 9.6 (7.4) fb, while the SM cross-section in the same kinematic region is 0.13 fb.

4.2. Higgs boson couplings to the second generation fermions: $H \to c\bar{c}$ and $H \to \mu\mu$

One of the challenges tackled during Run 2 was the investigation of the Yukawa interactions of the Higgs boson with the fermions of the second generation. As the Yukawa interaction is the only known fundamental interaction that distinguishes between fermion generations, the study of the couplings beyond the third generation is crucial.

Higgs boson decays into charm quark–antiquark pairs are usually searched for in events compatible with VH production [116]. As in the $H \to b\bar{b}$ case, this production mode provides the possibility for efficient triggering and background rejection through the leptonic decays of the associated W or Z bosons. Nevertheless, the analysis of $H \to c\bar{c}$ encounters several additional challenges. The branching ratio for Higgs boson decays into charm quark–antiquark pairs is $\mathcal{B}(H \to c\bar{c}) = 2.89\%$, approximately 20 times smaller than the branching ratio for Higgs boson decays into bottom quark–antiquark pairs. In addition, charm-hadron decays have less distinct signatures compared to those of bottom-hadron decays due to the shorter lifetime of charm hadrons. A dedicated algorithm requires jets to have a high probability to originate from charm quarks while vetoing jets likely to originate from bottom quarks, allowing the possibility to statistically combine the $H \to c\bar{c}$ and $H \to b\bar{b}$ analyses. This configuration gives an average efficiency of 27% to tag c-jets in simulated $t\bar{t}$ events, with b- and light-jet misidentification rates of 8% and 1.6%, respectively. Similarly to the $H \to b\bar{b}$ analysis, events are classified according to the number of charged leptons in the events. Additional cuts are applied in the various categories to suppress the V+jet, $t\bar{t}$ and diboson backgrounds. The VH, $H \to c\bar{c}$ signal and background yields are obtained through a simultaneous fit to the invariant mass of the charm-tagged jets ($m_{c\bar{c}}$). The analysis strategy is validated by the simultaneous measurement of diboson processes with one of the bosons decaying into at least one charm quark. Fig. 15(a) shows the observed $m_{c\bar{c}}$ distribution in data compared with the SM prediction for one of the analysis categories. The upper limit on the VH, $H \to c\bar{c}$ signal strength for each of the vector boson decay channels considered in the analysis is shown in Fig. 15(b), and their combination yields an observed (expected) upper limit on the VH, $H \to c\bar{c}$ signal strength of 26 (31) at 95% CL.

A statistical combination of the $H \to c\bar{c}$ and $H \to b\bar{b}$ analyses is performed to simultaneously constrain the coupling-strength modifiers κ_b and κ_c, which are defined as the ratios of the measured Yukawa couplings to their SM values [116]. The combination ensures a reduced model dependency of the result, as, even after the $H \to c\bar{c}$ analysis selection, the VH, $H \to b\bar{b}$ process is expected to be two to eight times larger than the VH, $H \to c\bar{c}$ contribution, depending on the signal

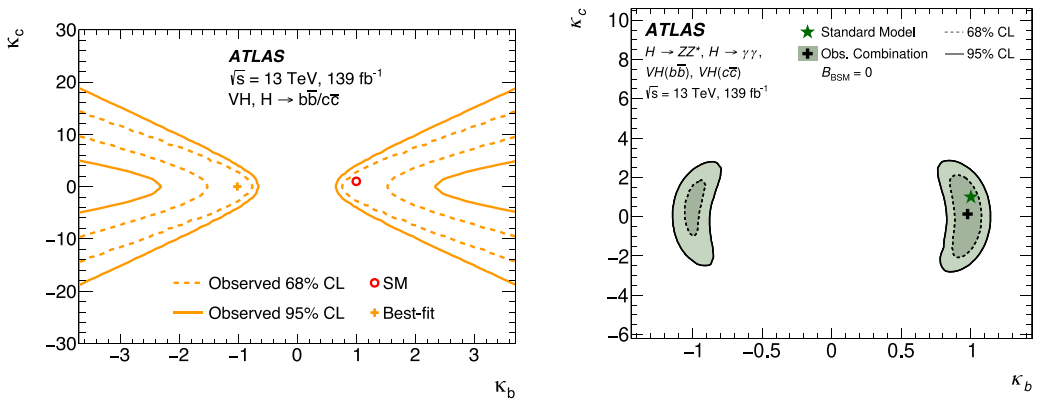

(a) (b)

Fig. 16. (a) The observed constraints on κ_b and κ_c at 68% and 95% CL from a fit to multivariate discriminants used to identify VH events with Higgs bosons decaying into $b\bar{b}$ or $c\bar{c}$, assuming no decays into BSM particles [116]. (b) Observed contours for the κ_b and κ_c parameters from a simultaneous fit to the p_{T}^{H} distributions measured in $H \to \gamma\gamma$ and $H \to ZZ^* \to 4\ell$ decays and to the multivariate discriminants in (a) [115].

region. The observed bounds in the κ_c–κ_b plane are shown in Fig. 16(a). The observed (expected) upper limit on the ratio yields $|\kappa_c/\kappa_b| < 4.5$ (5.1) at 95% CL. This bound is slightly smaller than the m_b/m_c ratio [138], indicating that the Higgs boson to charm-quark coupling is weaker than the Higgs boson to bottom-quark coupling. The direct limits on the κ_b and κ_c coupling-strength modifiers are combined with the ones from the fiducial differential cross-section measurements of p_{T}^{H} in the $H \to \gamma\gamma$ and $H \to ZZ^* \to 4\ell$ final states (Section 3). The resulting constraints are shown in Fig. 16(b) [115].

The $H \to \mu\mu$ decay channel presents a unique opportunity to investigate the interactions of the Higgs boson with second-generation fermions. Despite its low SM branching ratio (approximately 2.17×10^{-4}), the expected sensitivity in this decay channel surpasses the $H \to c\bar{c}$ decay channel, thanks to the lower background contamination and the better invariant mass resolution. Considerable effort was dedicated to further enhance the sensitivity of this decay channel during Run 2 [139], capitalising particularly on continuous improvements in analysis techniques and muon reconstruction.

Events are selected that contain two isolated muons with opposite charges and high transverse momenta, reconstructed within the acceptance of the ATLAS muon spectrometer. The dominant background is the Drell–Yan process. The selected events are then categorised using multivariate techniques that exploit kinematic and topological differences among the various Higgs boson production modes and background processes, typically resulting in a signal-to-background ratio (S/B) ranging from 0.1% to 8% in the 120 GeV $< m_{\mu\mu} <$ 130 GeV window.

Thanks to the excellent muon momentum resolution, the resonant behaviour of the Higgs boson signal in the $m_{\mu\mu}$ distribution can be utilised after categorisation to extract the signal yield and determine background normalisation and shape parameters, as shown in Fig. 17. The resolution of the $m_{\mu\mu}$ resonance is improved by including photons from QED final-state radiation through which muons can lose a significant fraction of their energy. The signal is modelled using a double-sided Crystal Ball function, with the width of the Gaussian component ranging from 2.6 to 3.2 GeV depending on the specific category.

The observed (expected) significance over the background-only hypothesis for a Higgs boson with a mass of 125.09 GeV is 2.0σ (1.7σ). The best-fit value of the signal strength parameter, defined as the ratio of the observed signal yield to the one expected in the SM, is $\mu = 1.2 \pm 0.6$.

5. Search for rare loop-induced decays of the Higgs boson

Higgs boson decays into two leptons and a photon can occur at tree level through the Yukawa coupling of a Higgs boson to leptons, or through quantum loops of virtual particles. Representative Feynman diagrams are shown in Fig. 18. The corresponding invariant mass distributions of the electron pair in $H \to ee\gamma$ decays are presented in Fig. 19. Due to the small Yukawa couplings to electrons, the tree-level diagram in Fig. 18(a) is only relevant for $H \to \mu\mu\gamma$. Rare loop processes are interesting to study, as they could be modified by so-far undiscovered particles modifying the branching ratios [140]. Furthermore, the three-particle final state might in the future allow CP studies of the corresponding couplings [141,142].

ATLAS has performed searches for Higgs boson decays into two leptons and a photon, with $m_{\ell\ell}$ below 30 GeV, mostly targeting the decay into a virtual photon and a photon [143], as well for decays with $m_{\ell\ell}$ close to the Z pole [144], dominated by decays into a Z boson and a photon. Searches for Higgs bosons decaying into a meson and a photon [145] are not discussed here, as the SM branching ratios are too small to be detectable at the LHC (see instead Ref. [6]).

Events with a photon and two electrons or two muons are selected. For the low-$m_{\ell\ell}$ analysis, the invariant mass of the two leptons $m_{\ell\ell}$ is required to be smaller than 30 GeV. For the $Z\gamma$ analysis, the dilepton invariant mass must be

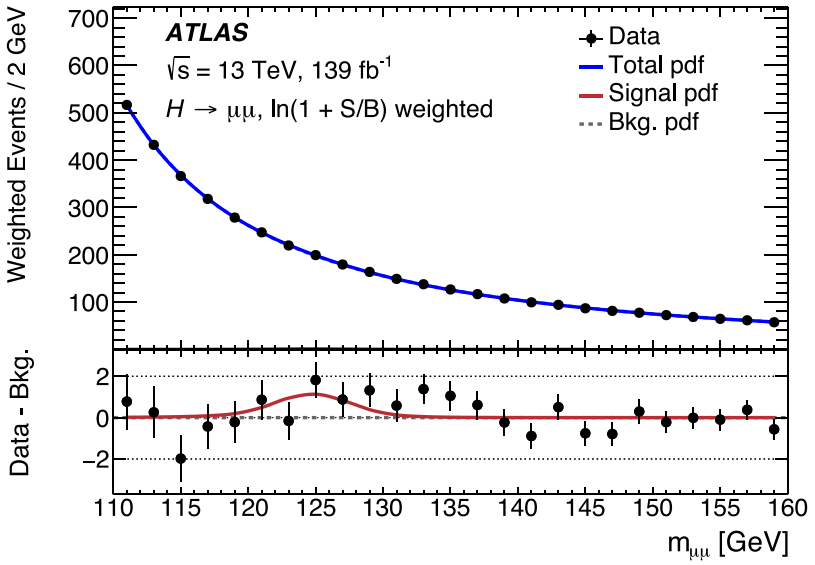

Fig. 17. Dimuon invariant mass spectrum in all analysis categories observed in data, with the events and probability density functions (pdfs) weighted by $\ln(1+S/B)$ [139] where S corresponds to the observed signal yield in the 120 GeV $< m_{\mu\mu} <$ 130 GeV window and B is the background yield in the same window, both derived by the fit to the data.

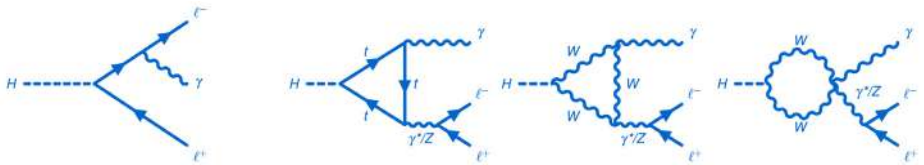

(a) (b)

Fig. 18. Representative Feynman diagrams of Higgs boson decays into two leptons and a photon.

within 10 GeV of the Z boson mass. In the $ee\gamma$ final state, for low invariant masses and high transverse momenta of the dielectron system, the two electromagnetic showers can overlap in the calorimeter. Therefore, the search for low-$m_{\ell\ell}$ final states also considers events if they contain a photon and an object that is compatible with two very close electrons. In addition to the categorisation into lepton final states, further categorisations are introduced, guided by the different signal-to-background ratios of the various Higgs boson production modes: categories targeting VBF production, $\ell\ell\gamma$ final states with high transverse momenta, and the remainder. In each of the two dilepton mass ranges, a simultaneous parameterised fit is performed over the $m_{\ell\ell\gamma}$ mass distributions in all categories, to extract the number of signal events. As in the $\gamma\gamma$ final state, uncertainties in the choice of fit function for the background are included. Overall, statistical uncertainties are dominant. Fig. 20 shows the $m_{\ell\ell\gamma}$ distributions, with each data event weighted by a category-dependent weight that depends on the signal-to-background ratio in a window around the resonance peak.

Testing the low-$m_{\ell\ell}$ regime, evidence for the $H \to \ell\ell\gamma$ process is found with a significance of 3.2σ over the background-only hypothesis, compared with an expected significance of 2.1σ for the SM prediction. The best-fit value of the signal-strength parameter is $\mu = 1.5 \pm 0.5$. The Higgs boson production cross-section times the $H \to \ell\ell\gamma$ branching ratio for $m_{\ell\ell\gamma} < 30$ GeV is determined to be $8.7^{+2.8}_{-2.7}$ fb.

In the search for the $Z\gamma$ process, the observed (expected) significance is 2.2σ (1.2σ). The best-fit value for the $H \to Z\gamma$ signal strength is found to be $\mu = 2.0^{+1.0}_{-0.9}$. As the analysis is limited by the small expected number of signal events, a combination is performed with the CMS analysis [146], effectively doubling the data sample, which pushes the significance above the evidence threshold: 3.4σ with an expectation of 1.6σ. The corresponding best-fit signal strength is $\mu = 2.2 \pm 0.7$ [147].

6. Cross-sections and couplings from combined fits

Higgs boson measurements with different decay signatures can be combined to extract as complete a portrait of the Higgs boson as possible [19]. The combination harnesses the statistical power of an unprecedented number of Higgs boson measurements to extract inclusive cross-sections and cross-sections for different production processes and

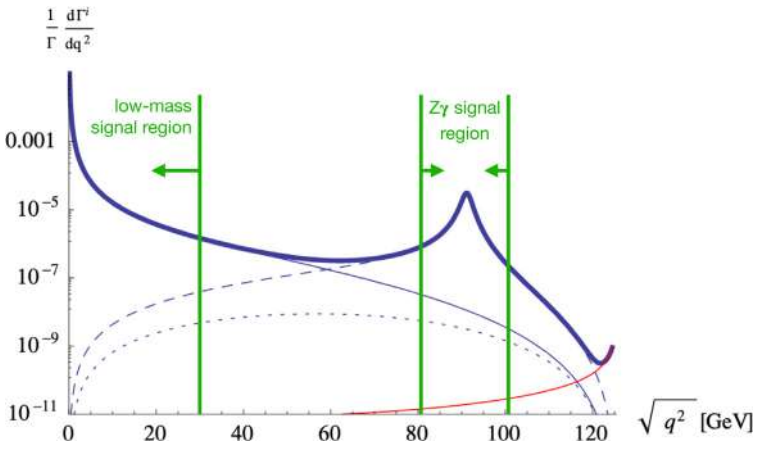

Fig. 19. Distribution of the invariant mass of the two electrons in $H \to ee\gamma$ decays [148]. The red line shows the tree level diagram, the dashed line the decay into a Z boson and a photon, and the thin blue line the decay into a virtual photon and a photon. The dotted line comes from four-point box diagrams, not discussed here. The low-$m_{\ell\ell}$ and $Z\gamma$ signal regions used in the ATLAS analyses are indicated by vertical lines.

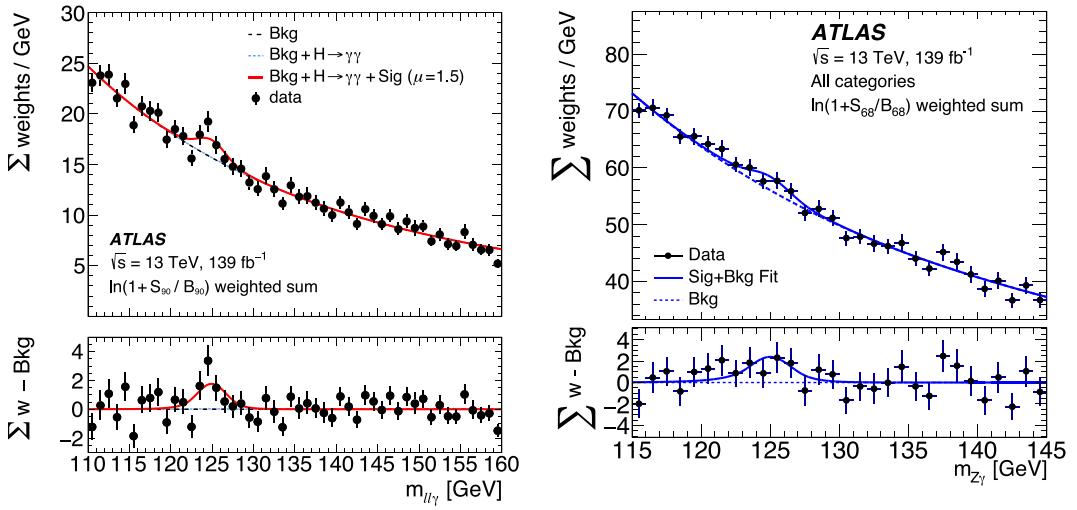

(a) (b)

Fig. 20. (a) The $m_{\ell\ell\gamma}$ distributions for the low-$m_{\ell\ell}$ analysis [143], and (b) the $Z\gamma$ analysis [144], where every data event is reweighted by a category-dependent weight, $\ln(1+S_X/B_X)$, with X = 90% (68%) for the low-$m_{\ell\ell}$ ($Z\gamma$) analysis. Here, S_X is the number of signal events in the smallest window containing X% of the expected signal, and B_X is the expected number of background events in the same window.

kinematic regions. Each production–decay process is sensitive to different combinations of Higgs boson couplings to other fundamental particles, and the combination allows all accessible couplings to be constrained simultaneously.

Analyses in the following Higgs boson decay channels are considered in the combination: $H \to \gamma\gamma$ [131], $H \to ZZ^* \to 4\ell$ [112], $H \to WW^* \to e\nu\mu\nu$ [149,150], $H \to Z\gamma \to \ell\ell\gamma$ [144], $H \to b\bar{b}$ [130,133,135–137], $H \to \tau\tau$ [125], $H \to \mu\mu$ [139], $H \to c\bar{c}$ [116]. They provide measurements in different Higgs boson production modes and phase space regions. A complementary analysis of the $t\bar{t}H$ process, sensitive to WW^*, ZZ^* and $\tau\tau$ final states is included, as well [129]. Furthermore, searches for Higgs bosons decaying into invisible particles, such as dark matter candidates, are considered, most notably those targeting the VBF and ZH production mechanisms [151,152]. These are included in a subset of the fits.

The statistical analysis of the data is based on a combined likelihood function, calculated by forming the product of the likelihood functions describing each of the input measurements [153]. A multitude of results can be extracted from the combination of the different analyses. Each result is obtained under certain assumptions, as detailed below.

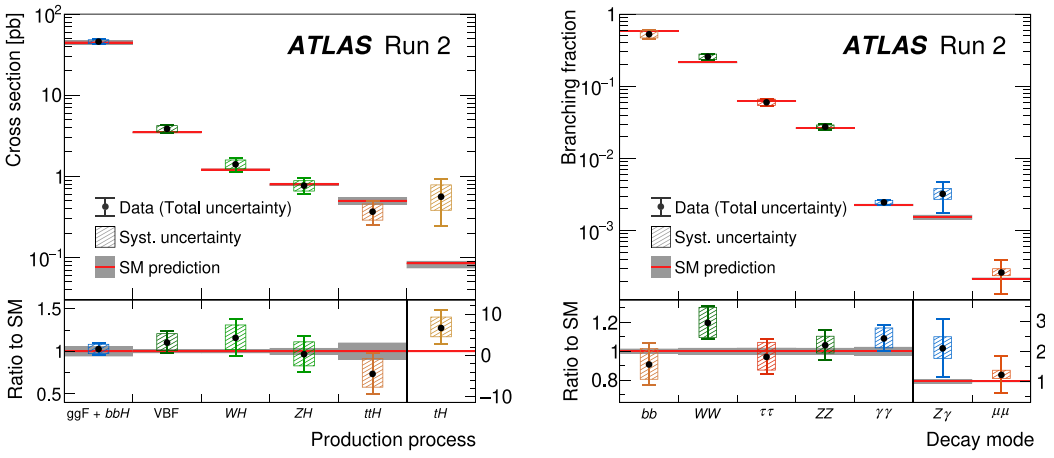

(a) (b)

Fig. 21. (a) Observed and predicted Higgs boson production cross-sections, assuming SM values for the branching ratios. (b) Observed and expected branching fractions assuming SM values for the cross-sections [19].

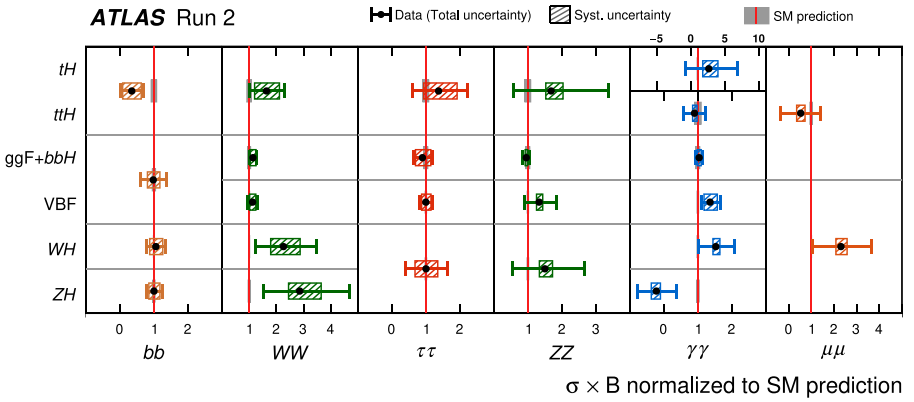

Fig. 22. Observed event rate divided by predicted SM event rate for different combinations of Higgs boson production and decay processes [19].

6.1. Global signal strength, production cross-sections and decay branching ratios

Assuming each production–decay process scales with the same global signal strength μ, the measured number of produced Higgs bosons relative to the SM prediction is
$\mu = 1.05 \pm 0.06 = 1.05 \pm 0.03(\text{stat.}) \pm 0.03(\text{exp.}) \pm 0.04(\text{sig.th.}) \pm 0.02(\text{bkg.th.})$, where the total uncertainty is split into statistical, experimental and theoretical uncertainties (signal and background).

The cross-sections of the different Higgs boson production processes are measured assuming SM values for the decay branching fractions and vice versa, as shown in Fig. 21. All major production modes are now observed, including the *WH* and *ZH* processes individually. An unprecedented upper limit at 95% CL was observed for *tH* production: 15 times the SM cross-section (7 times expected), with a strong correlation between the $t\bar{t}H$ and *tH* measurements. Fig. 22 shows the observed event rate divided by the predicted SM event rate for different combinations of Higgs boson production and decay processes. This measurement does not require any assumptions on cross-sections or branching ratios and nicely illustrates the sensitivity of the analyses in the different decay channels. Excellent overall agreement is observed with the SM predictions over multiple orders of magnitude.

6.2. Higgs boson couplings to other particles

To extract the couplings of the Higgs boson to other particles, a formalism has to be introduced. In the κ-framework [127], the cross-section times the branching fraction for an individual measurement is parameterised in terms of multiplicative coupling-strength modifiers that do not change kinematic distributions but only the strength of the coupling to a given particle compared to that expected in the SM. For example, the partial width of the decay into two bottom

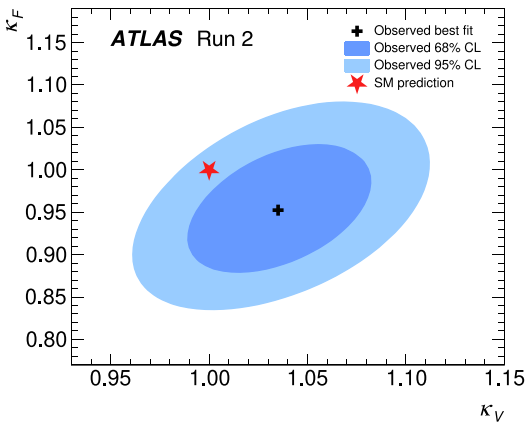

Fig. 23. Fit in the κ_F–κ_V plane, showing the best fit value and the 68% and 95% CL regions [19]. This fit is performed assuming that there are no BSM contributions to invisible or undetected Higgs boson decays.

quarks is parameterised as $\Gamma_b/\Gamma_b^{\mathrm{SM}} = \kappa_b^2$. Care is taken to adjust the total width of the Higgs boson accordingly, and in some fits BSM contributions to undetected or invisible decays are included, where undetected decays are hidden by large backgrounds. For production and decays through quantum loops (e.g., ggF and $H \to \gamma\gamma$), either effective coupling-strength modifiers are introduced (κ_g and κ_γ), or the loops are resolved into the different particle contributions according to the SM.

Assuming all coupling-strength modifiers to fermions (κ_F) scale the same way, as do all modifiers to vector bosons (κ_V), one can perform a two-dimensional fit in κ_F and κ_V, finding the best fit value and the 68% and 95% CL regions, as shown in Fig. 23. Here, the loops are assumed to be as in the SM with no BSM contributions to undetected or invisible decays allowed. The SM value lies within the 95% CL region.

Still resolving the loop-induced processes according to the SM and not allowing for additional decays, the coupling-strength modifiers for individual particles can be fit separately. The reduced coupling-strength modifiers are defined as $\sqrt{\kappa_V g_V/2v} = \sqrt{\kappa_V}(m_V/v)$ for weak bosons with a mass m_V, and $\kappa_F g_F = \kappa_F m_F/v$ for fermions with a mass m_F, where g_V and g_F are the corresponding absolute coupling strengths and $v = (\sqrt{2}G_F)^{-\frac{1}{2}} \sim 246$ GeV is the vacuum expectation value of the Higgs field, which can be derived from the measurement of the Fermi constant G_F [154]. Fig. 24 shows these reduced coupling-strength modifiers as a function of the particle masses. The SM predicts a striking diagonal line, encapsulating the essence of the SM Higgs Lagrangian, which agrees very well with the measured values over about three orders of magnitude. Two versions of the fit are performed, as the sensitivity of the analyses to the charm quark coupling is still rather low. In one, the modification to the charm quark coupling is fixed to be the same as for the top quark coupling, and in the other, the charm quark coupling is a free parameter.

Finally, a fit is performed allowing for new contributions to the loop-induced processes by using effective coupling-strength modifiers for the gluon, photon and $Z\gamma$ couplings. Fig. 25 shows the results of two fits: allowing (and not allowing) for undetected and invisible non-SM contributions to the branching ratios. When these contributions are allowed, the searches for invisibly decaying Higgs bosons produced via VBF or ZH production are included in the fit, $\kappa_V \leq 1$ is imposed to avoid degeneracies, and upper limits are set at 95% CL on the undetected and invisible branching fractions to non-SM particles. It can be seen that allowing for undetected and invisible BSM contributions does not change the fitted coupling-strength modifiers significantly. The modifiers for the coupling strength to top-quark, bottom-quark and τ-lepton are measured with uncertainties ranging from about 7% to 12%, to W and Z bosons with uncertainties of about 6%, and for the effective loop-induced coupling strength to photons and gluons with 6% and 7%, respectively. The upper limit on the invisible (undetected) BSM branching ratio is 0.13 (0.12), improving on the direct searches alone (see Ref. [6]).

6.3. Production cross-sections in different kinematic regions and their interpretation

A comprehensive study is performed measuring cross-sections separately per production mechanism in different phase space regions, referred to as simplified template cross-sections (STXS) [18,155–157]. The STXS framework has been designed to maximise the sensitivity of Higgs boson cross-section measurements to BSM effects, while minimising their theory dependence and allowing for the combination of analyses in different decay channels. The measurements and the SM predictions are shown in Fig. 26. Different kinematic regimes are targeted, for example Higgs bosons produced with high transverse momenta, which could be modified by BSM phenomena at high energies. Selections are also made based on the properties of the hadronic jets in the events, for example separating VBF- and VH-enriched $qq \to Hqq$ production. The measured cross-sections could reveal phenomena beyond the SM that are not observable

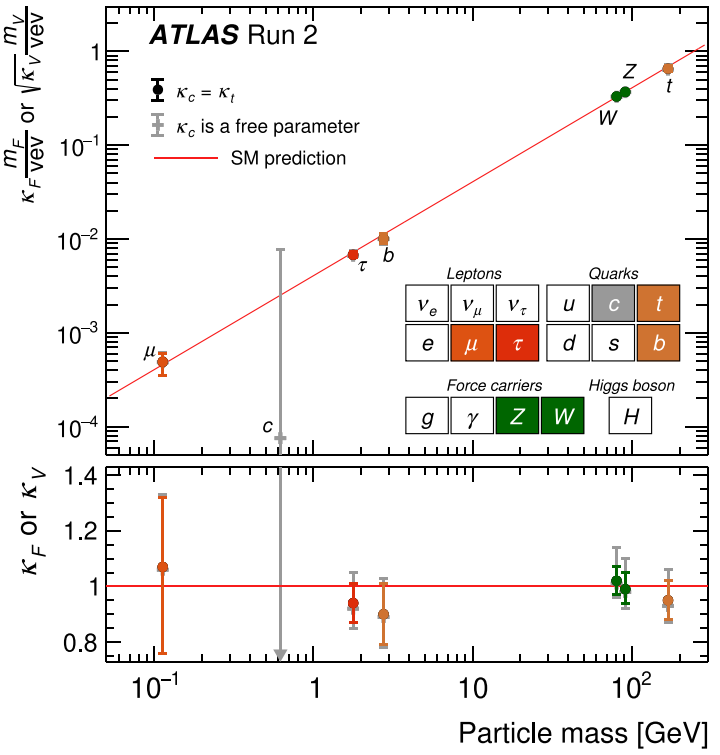

Fig. 24. Higgs boson coupling-strength modifiers and their uncertainties versus the particle masses, compared with the SM prediction [19]. For the bottom and the top quark, the masses are evaluated at a scale corresponding to that of the Higgs boson mass. Loop-induced processes are resolved according to the SM predictions, and no decays into non-SM particles are allowed.

through measurements of the coupling strengths. Furthermore they can be used as a basis for electroweak fits and BSM interpretations.

The measurement of the production cross-sections in different kinematic regions, separated by decay mode, is interpreted in the SM effective field theory (SMEFT) [158]. This allows effects of unknown phenomena at energy scales Λ that are large compared to the vacuum expectation value of the Higgs field, and that reduce to the SM at lower energies, to be searched for without having to rely on a specific model. A complete set of higher-order-in-mass operators invariant under the SM gauge group is built from the SM fields [159]. They are scaled by Wilson-coefficients, which are zero in the SM. If dimension-five operators are ignored, because they violate lepton number conservation, the leading contributions to physical observables are expected to come from dimension-six operators, which can describe CP-even or CP-odd couplings. There are several complete sets (bases), of these dimension-six operators e.g., the Warsaw [160–162], Higgs [18,163] and HISZ [164] bases.

Here, the Warsaw basis is used, and only CP-even operators are considered (see Section 7 for searches for CP-odd effects). When parameterising the cross-section times branching ratios through SMEFT, the series needs to be truncated by construction. Two different choices are considered: keeping only the linear terms of the new operators (proportional to Λ^{-2}), or including quadratic terms (proportional to Λ^{-4}) as well, along with products of different Wilson coefficients. The second choice is more complete, but also less consistent as it does not include terms from dimension-eight operators with the same suppression factor. The input measurements do not allow constraints to be put on all relevant Wilson coefficients simultaneously. The solution chosen in this analysis is a rotated basis, which allows linear combinations that combine operators with similar predicted effects on the measurements [165].

Fig. 27 shows the fitted values of the rotated coefficients for the linear and the linear+quadratic fit, including their uncertainties. All coefficients are compatible with the SM expectation of zero. The strongest constraints can be found on coefficients which affect SM processes that are suppressed by small Yukawa couplings or include quantum loops. The operators corresponding to $c_{eH,22}$, $c_{eH,33}$, c_{bH} are effectively modifiers of the Higgs Yukawa coupling to muons, τ-leptons and bottom quarks, respectively, while non-zero values of c_{Hq} would modify VH production. The eigenvectors $e^{[i]}_{\text{ggF}}$ encapsulate changes to the ggF production and $e^{[i]}_{H\gamma\gamma,Z\gamma}$ could affect the $H \to \gamma\gamma$ and $H \to Z\gamma$ decays.

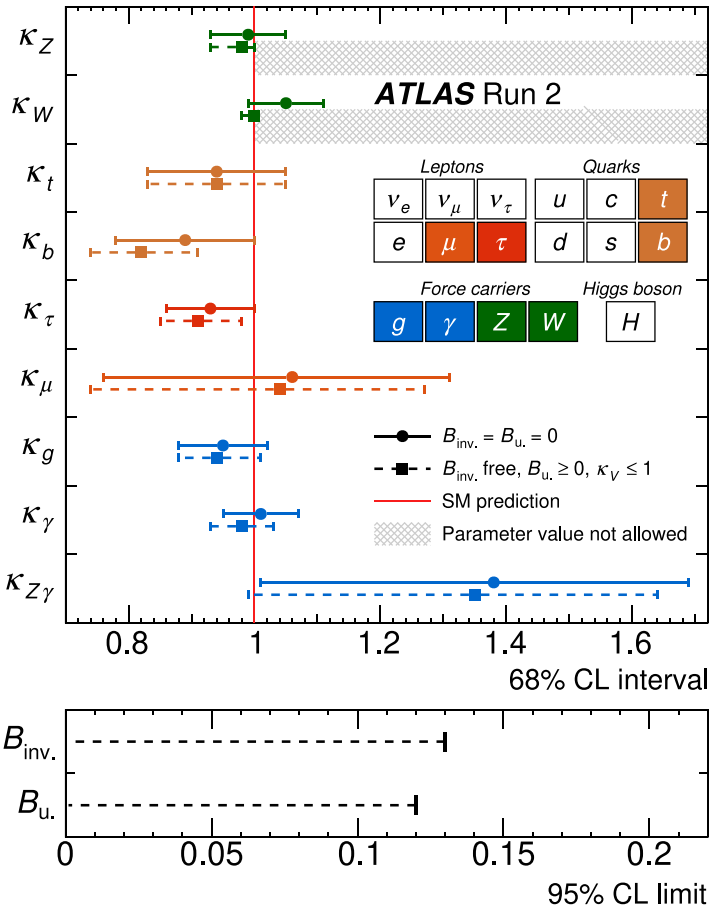

Fig. 25. Coupling-strength modifiers and their uncertainties per particle type with effective gluon, photon and $Z\gamma$ couplings, assuming the BSM contribution to undetected and invisible branching fractions to be zero (solid lines), and allowing them to contribute to the width of the Higgs boson (dashed lines). For the second case, the undetected branching ratio is assumed to be larger or equal to zero, and κ_V is assumed to be smaller or equal to one. Limits on the undetected and invisible branching fractions to non-SM particles are shown in the bottom panel [19].

7. Study of CP properties and search for anomalous interactions

In the SM, the Higgs boson is a CP-even scalar with the following quantum numbers: $J^{CP} = 0^{++}$. Any sign of CP-odd couplings in the production or decay of the Higgs boson would be an unambiguous indication of BSM phenomena. Moreover, it would provide a so-far unknown source of CP violation that could play a fundamental role in explaining the matter–antimatter asymmetry in the universe.

CP-odd Higgs boson couplings to other particles can be described by adding corresponding terms to the SM Lagrangian [159,166,167]. Couplings to bosons and fermions are investigated separately, also probing for mixtures between pure CP-odd and CP-even couplings. While a CP-odd component of the vector-boson couplings to the Higgs boson would be naturally suppressed by the scale at which BSM physics becomes relevant [159,168], this suppression does not happen for Yukawa couplings, where CP-odd Higgs−fermion couplings may be significant already at tree level [166,167].

7.1. CP properties in interactions with vector bosons

Higgs boson couplings to vector bosons are usually parameterised in the SMEFT framework (see Section 6). In the Warsaw basis, there are three relevant dimension-six operators describing CP-odd interactions at the *HVV* vertex, scaled by the following Wilson coefficients: $c_{H\tilde{B}}$, $c_{H\tilde{W}B}$, and $c_{H\tilde{W}}$. Adding these CP-odd operators to the Lagrangian, and assuming the coefficients of the CP-even dimension-six operators to be zero, the new matrix element can be written as the sum of the SM matrix element $\mathcal{M}_{SM}$ and the CP-odd BSM Matrix element $\mathcal{M}_{BSM}$. The HISZ basis also contains three coefficients to describe CP-odd interactions. By setting $\tilde{d} = \tilde{d}_B$ and the third coefficient to zero, the HISZ basis allows the strength of

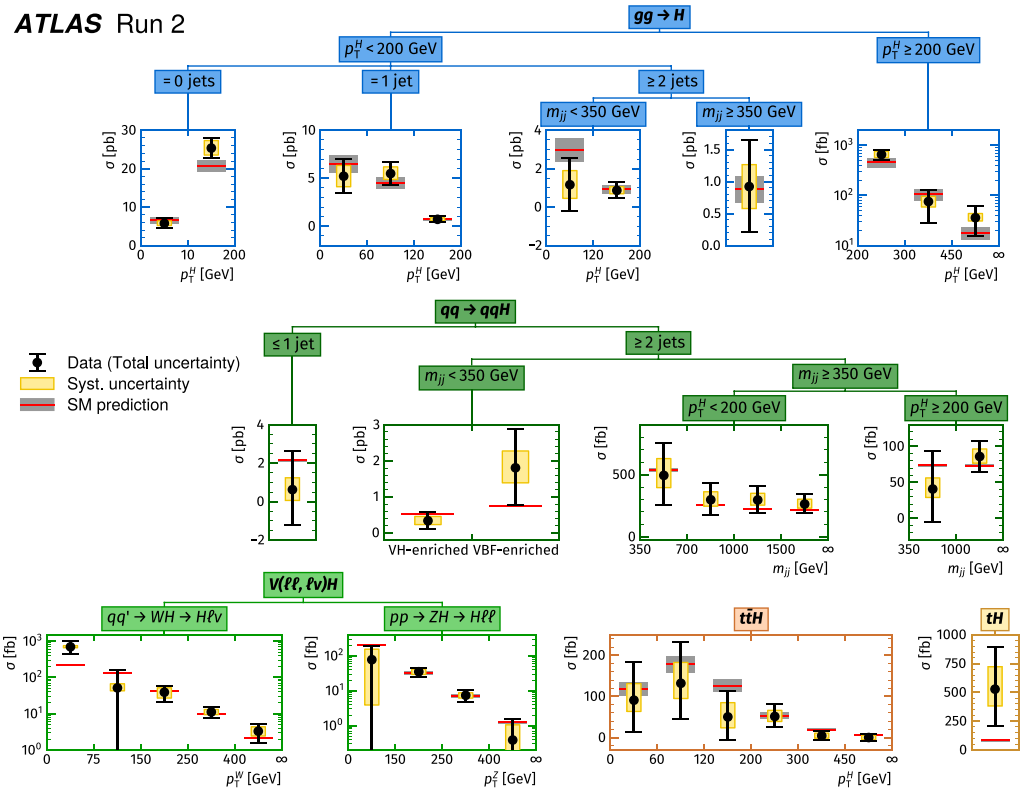

Fig. 26. Observed and predicted Higgs boson production cross-sections in different kinematic regions [19].

CP violation to be described by a single parameter $\tilde{d}$, through

$$\mathcal{M} = \mathcal{M}_{SM} + \tilde{d} \cdot \mathcal{M}_{BSM},$$

where the dependence on $\tilde{d}$ has explicitly been factored out [96,169].

Experimentally, Higgs boson couplings to vector bosons can be probed in Higgs boson production (most prominently the VBF production mode) and Higgs boson decays into Z or W bosons. BSM effects on couplings can be probed by measuring cross-sections in different kinematic regions (see Section 6) and with CP-sensitive observables (this section), which, compared to the cross-section measurements specifically target CP-odd BSM effects.

The CP-sensitive observable of choice is the matrix-element-based 'Optimal Observable' [170–172], defined as

$$\mathcal{OO} = \frac{2Re(\mathcal{M}_{SM}^{*}\mathcal{M}_{BSM})}{|\mathcal{M}_{SM}|^2}.$$

This distribution is symmetric with a mean value of zero for a CP-even Higgs boson and becomes asymmetric when contributions from CP-odd BSM couplings are present. In the measurements discussed below, only the shape of the distribution is considered, such that exclusively CP-odd BSM effects are probed.

The Optimal Observable for a given VBF event is calculated based on matrix elements extracted from MC simulations at LO in QCD. From the data, the four-momenta of the Higgs boson and the two VBF jets are used as input to $\mathcal{OO}$. The momentum fractions of the initial-state partons are extracted by making use of the energy–momentum conservation in the collision, taking into account all possible quark flavour combinations as predicted by the parton distribution function [173].

The CP properties are probed in VBF production for Higgs bosons decaying into two τ-leptons [173], two photons [174], four leptons [169], or two W bosons [121]. The $H \to ZZ^* \to 4\ell$ analysis also makes use of the decay characteristics, which are accessed through the reconstructed four-momenta of the decay leptons, to extract CP information.

In the $H \to \tau\tau$ decay channel, the variable $\mathcal{OO}$ is measured in bins of a BDT that is trained to distinguish the VBF signal from the background of non-Higgs and non-VBF processes. A simultaneous fit is performed over these signal regions and a number of control regions, enriched in the most important background processes, to extract the strength of a possible CP-odd parameter $\tilde{d}$.

In the $H \to \gamma\gamma$ decay channel, two BDTs are trained to suppress ggF and non-Higgs contributions creating a sample enriched in VBF events. To estimate the remaining background, the signal yield is extracted from a combined unbinned

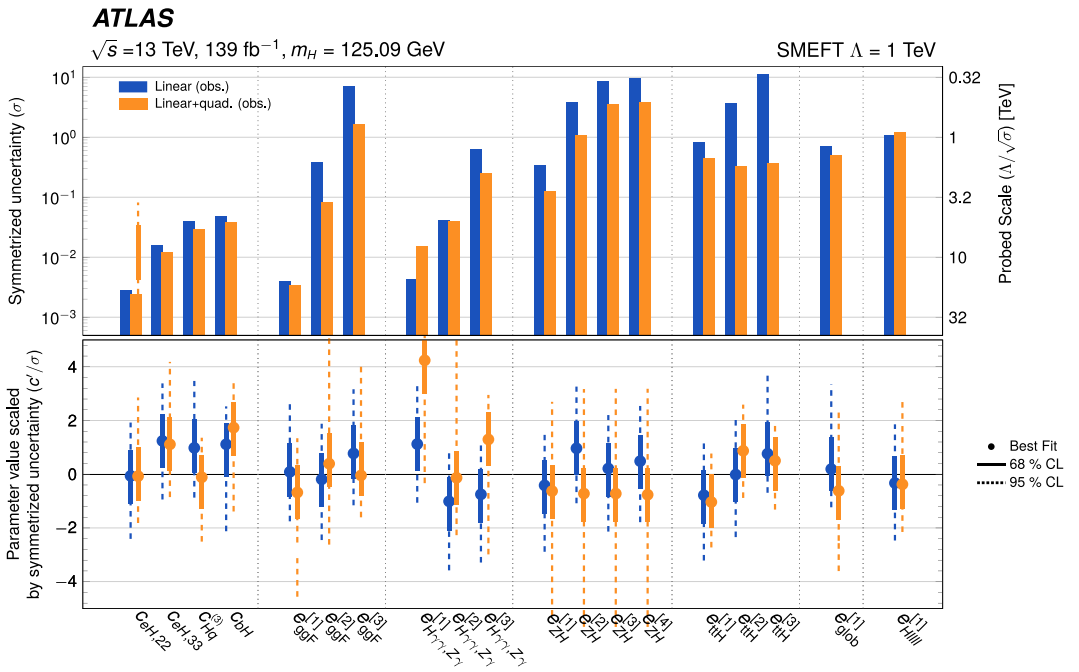

Fig. 27. Comparison of the observed parameters of the rotated basis with the SMEFT model that keeps only terms linear in the new operators (blue) and the model including quadratic terms (orange), where all other coefficients and nuisance parameters are profiled, i.e., set to the values that maximise the likelihood [158]. The top panel shows the symmetrised 68% CL uncertainty σ of each parameter measurement (left vertical axis) and the corresponding energy scale $\Lambda/\sqrt{\sigma}$, Λ = 1 TeV that is probed (right vertical axis). The bottom panel shows the measured parameter value, 68% (solid) and 95% (dashed) CL intervals, divided by the symmetrised uncertainty shown in the top panel.

maximum-likelihood fit applied to the $m_{\gamma\gamma}$ distribution of the observed data in each bin of $\mathcal{OO}$ (see Fig. 28). Using the $H \to \gamma\gamma$ channel, constraints are extracted for $\tilde{d}$ and, separately, for the Wilson coefficient of the relevant operator $c_{H\widetilde{W}}$ in the Warsaw basis.

In order to extract a constraint on $c_{H\widetilde{W}}$ in the $H \to ZZ^* \to 4\ell$ decay channel, both the VBF production and properties of the $H \to ZZ^* \to 4\ell$ decay are used. A NN is trained by creating samples depleted or enriched in VBF, and a fit is performed simultaneously over the different regions. The Wilson coefficients $c_{H\widetilde{B}}$ and $c_{H\widetilde{W}B}$, and $\tilde{d}$ are extracted from the decays. Each coefficient is fitted separately, based on a dedicated Optimal Observable.

The measurements of differential VBF cross-sections in the $H \to WW^* \to e\nu\mu\nu$ decay channel, discussed in Section 3, are used to constrain the Wilson coefficients $c_{H\widetilde{W}}$, $c_{H\widetilde{B}}$, and $c_{H\widetilde{W}B}$ [121]. The distribution of the azimuthal angle difference between the two jets produced together with the Higgs boson is used as discriminant observable.

No deviation from a pure CP-even coupling is found in any of the studies. Fig. 29 summarises some of the resulting constraints on the Wilson coefficients in both the Warsaw and HISZ bases.

The CP properties of the effective Higgs–gluon coupling are studied in the $H \to WW^* \to e\nu\mu\nu$ decay channel [175]. The Lagrangian can be extended by a CP-odd term as

$$\mathcal{L}_{Hgg} = -\frac{g_{Hgg}}{4}\kappa_{gg}(\cos\alpha\, G^a_{\mu\nu}G^{a,\mu\nu} + \sin\alpha\, G^a_{\mu\nu}\tilde{G}^{a,\mu\nu})H, \tag{4}$$

where $G^a_{\mu\nu}$ is the gluon field strength tensor, $\tilde{G}^{a,\mu\nu} = G^a_{\rho\sigma}\epsilon^{\mu\nu\rho\sigma}/2$ is the dual tensor, g_{Hgg} is the effective coupling for the SM CP-even ggF interaction, κ_{gg} is the coupling-strength modifier for the effective Higgs−gluon interaction and α is the CP-mixing angle, which is zero in the SM. The azimuthal angle difference between the two jets produced together with the Higgs boson is used as CP-sensitive observable. Events are selected with two jets and kinematics compatible with the ggF production mode. A BDT is applied to reduce the background contamination and control regions are defined for the most important backgrounds. A maximum-likelihood fit over all considered regions is performed. Using the angular distribution and the overall rate, a value of $\tan\alpha = 0.0 \pm 0.4(\text{stat.}) \pm 0.3(\text{syst.})$ is obtained for the tangent of the mixing angle for CP-even and CP-odd contributions.

The $H \to WW^* \to e\nu\mu\nu$ decay channel also allows the Higgs boson coupling to longitudinally and transversely polarised W and Z bosons to be studied separately [175]. The azimuthal angle difference between the jets and the production rates in the signal regions are used. To probe both production and decay, events are selected that are compatible with the VBF production mode. The polarisation-dependent coupling-strength modifiers are defined as the ratios of the measured polarisation-dependent coupling strengths to those predicted by the SM, and are determined to be $a_L = 0.91^{+0.10}_{-0.18}(\text{stat.})^{+0.09}_{-0.17}(\text{syst.})$ and $a_T = 1.2 \pm 0.4(\text{stat.})^{+0.2}_{-0.3}(\text{syst.})$, compatible with the SM value of 1.

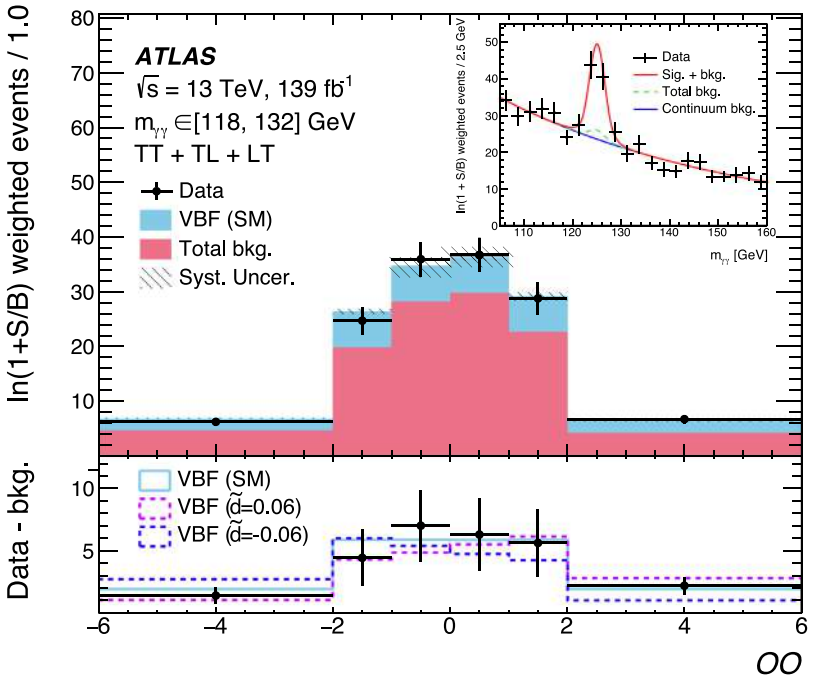

Fig. 28. Distribution of the Optimal Observable in the $H \to \gamma\gamma$ decay channel, for events enriched in the VBF production mode, with $118 < m_{\gamma\gamma} < 132$ GeV [174]. The total background includes events from non-VBF Higgs production. The bottom panel contains the background-subtracted distribution for data as well as the prediction for the SM and for two non-zero values of $\tilde{d}$. The invariant mass distribution is shown in the inset on the top right. Category-dependent weights are applied.

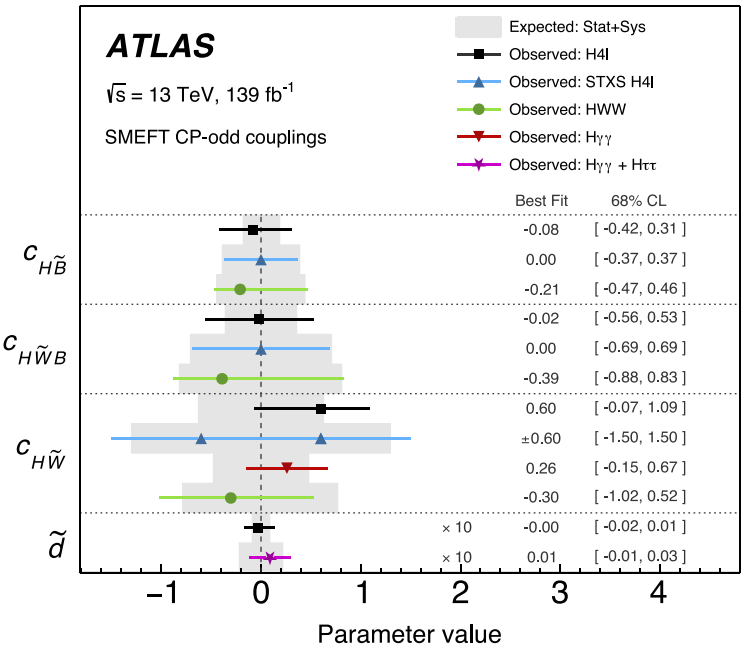

Fig. 29. Comparison of results extracted using the CP sensitive observables in the $H \to ZZ^* \to 4\ell$ channel, the $H \to WW^* \to e\nu\mu\nu$ differential cross-section measurement in the VBF production mode, the $H \to \gamma\gamma$ VBF measurement of $c_{H\tilde{W}}$ in the Warsaw basis, and the combined VBF measurement of $\tilde{d}$ in the $H \to \gamma\gamma$ and $H \to \tau\tau$ decay channels. Furthermore, the results based on the rate measurements in the $H \to ZZ^* \to 4\ell$ cross-section measurement of Ref. [112] ('STXS H4l') are added, which cannot distinguish between CP-odd and CP-even effects. The data points and 68% CL uncertainty bars show the observed values with statistical and systematic uncertainties. The $\tilde{d}$ best fit points and uncertainty bars are scaled by a factor of ten. In the $H \to ZZ^* \to 4\ell$ channel, only the linear parameterisation is considered (the effects of adding the quadratic terms are found to be negligible), while for the other analyses, the linear plus quadratic parameterisation is applied.

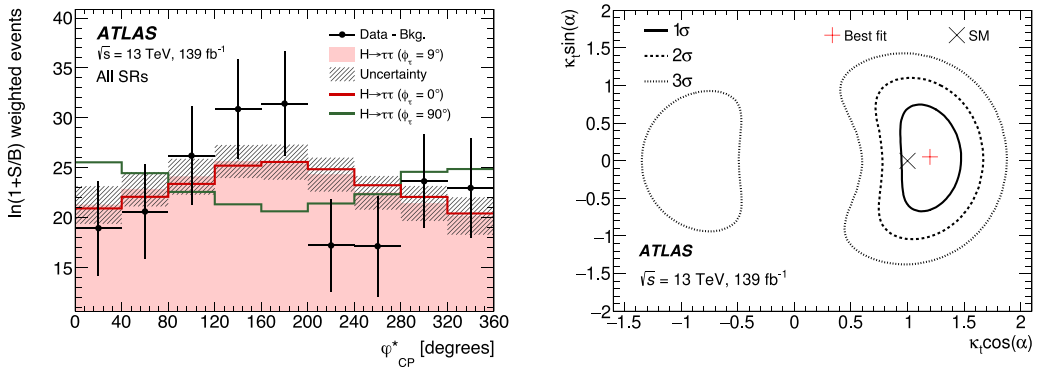

(a) (b)

Fig. 30. (a) Angle between the τ-lepton decay planes [176]. Events are weighted by $\ln(1+S/B)$, where S is the signal and B the background yield in the respective category. The best fit is shown in solid pink, while the red and green lines correspond to the predictions for the pure CP-even (scalar, SM) and pure CP-odd (pseudoscalar) hypotheses, respectively, all scaled to the best-fit $H \to \tau\tau$ yield. (b) Two-dimensional likelihood contours for $\kappa_t \cos\alpha$ and $\kappa_t \sin\alpha$, measured in the $H \to \gamma\gamma$ decay channel, with ggF and $H \to \gamma\gamma$ constrained by the Higgs boson coupling combination [177].

7.2. CP properties in interactions with fermions

The general effective Yukawa interaction between the Higgs boson and fermions, including a CP-odd term at tree level, can be parameterised as

$$\mathcal{L}_{HFF} = -\frac{m_F}{v}\kappa_F(\cos\alpha\,\bar{\psi}\psi + \sin\alpha\,\bar{\psi}i\gamma_5\psi)H. \tag{5}$$

Here, m_F is the fermion mass, v is the vacuum expectation value of the Higgs field, κ_F is the scaling factor for the Yukawa coupling, ψ are the fermion fields, and α is the CP-mixing angle. The SM corresponds to a CP-even coupling with $\alpha = 0$ and $\kappa_F = 1$ while a pure CP-odd coupling would be realised for $\alpha = 90°$. CP properties of the Higgs–τ-lepton and Higgs–top-quark couplings are probed.

The transverse spin components of the τ-leptons in the $H \to \tau\tau$ decays are affected by the CP-mixing angle α [176] and can be probed through the directions of the τ-lepton decay products. At least one of the τ-leptons is required to decay hadronically and decay planes are formed for each τ-lepton from the different visible decay products, i.e., leptons or pions, and, where necessary, the impact parameters of these objects. The angle φ^*_{CP} between these planes is calculated, which can be analytically related to α [166,167,178]. The event selection and background estimates follow the analysis discussed in Section 4. Categories are created to target VBF production and ggF production with Higgs bosons at high transverse momenta. A BDT classifier is used to further increase the purity of VBF events. In addition, $Z \to \tau\tau$ control regions are also formed. Fig. 30(a) shows the measured angle between the decay planes, which is used to extract $\phi_\tau = \alpha$.

Allowing for a free normalisation of the $H \to \tau\tau$ branching fraction, α is measured to be $9° \pm 16°$, with an expected value of $0° \pm 28°$ under the SM assumption. The pure CP-odd hypothesis is disfavoured at a level of 3.4σ.

The CP properties of the Higgs–top-quark couplings are probed in the $H \to \gamma\gamma$ [177] and $H \to b\bar{b}$ decay channels [179], using the $t\bar{t}H$ and tH production mechanisms. Both production rates and kinematic distributions depend on the CP properties, with the tH rate being particularly sensitive due to interference effects of diagrams. Furthermore, the ggF production and the $H \to \gamma\gamma$ decay rates are also affected, as there is a top-quark contribution in the loop diagrams.

For the $H \to \gamma\gamma$ channel, BDTs are used to identify the hadronic decay products for the reconstruction of the two top quarks, to reduce the background, and to separate CP-even and CP-odd contributions. The latter relies on kinematic distributions of the photons and top quarks and properties of the diphoton and $t\bar{t}$ systems, as well as various azimuthal angles. Events with at least one top quark candidate decaying semileptonically are separated from the fully hadronic events. A combined fit is performed over the $m_{\gamma\gamma}$ distributions in all signal regions and a pure CP-odd coupling of the Higgs boson to top quarks is excluded at 3.9σ, with $|\alpha| > 43°$ excluded at 95% CL. The likelihood contours as a function of $\kappa_t \cos\alpha$ and $\kappa_t \sin\alpha$ are shown in Fig. 30.

In the $H \to b\bar{b}$ case, either one or both of the top quarks are required to decay semileptonically. Signal candidate and control regions are formed based on the number of light- and heavy-flavour jets. The signal candidate regions are further split into signal and control regions with different $t\bar{t}H$ sensitivity. CP-sensitive observables are formed using the directions and azimuthal separation of the top quarks. A combined likelihood fit allows the mixing angle to be measured, resulting in $\alpha = (11\,^{+52}_{-73})°$.

In summary, no deviations from the CP-even hypothesis predicted by the SM are observed in the couplings of the Higgs boson to either bosons or fermions. The Run 2 data excludes CP-odd couplings to τ-leptons and top quarks at more than 3σ. Constraints are set on maximum mixing angles for the fermion couplings and on Wilson coefficients and matrix element mixing parameters for the boson couplings.

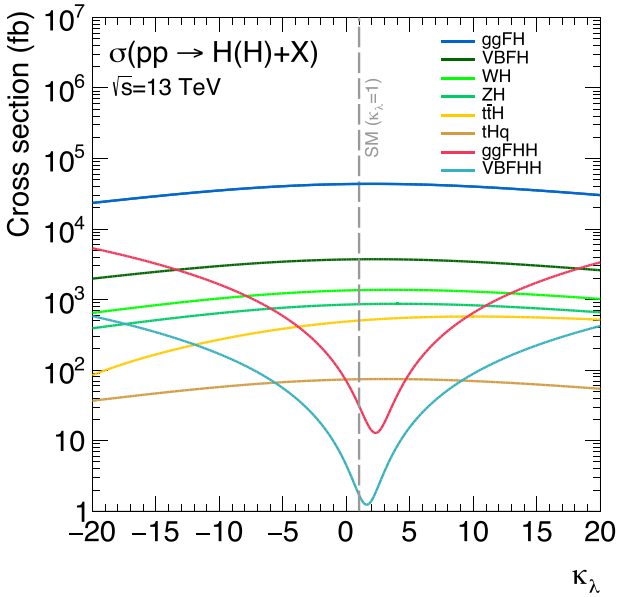

Fig. 31. Single-Higgs and double-Higgs boson production cross-sections as a function of κ_λ for $\sqrt{s} = 13$ TeV. The dashed line intercepts the values corresponding to the SM hypothesis ($\kappa_\lambda = 1$) [186].

8. The Higgs boson self-coupling

To completely understand the electroweak symmetry breaking mechanism, not only the properties of the Higgs boson, but also the Higgs field potential have to be probed experimentally. The Higgs field potential is of great interest from a cosmological perspective, as it determines the structure of the vacuum and influences the electroweak phase transition in the early universe [16,17]. A deviation of the Higgs boson self-coupling from the SM expectation might point to a first-order phase transition, a necessary condition for the electroweak baryogenesis mechanism, which in turn may help solve the matter–antimatter asymmetry puzzle. The Higgs field potential can be expressed as:

$$V(H) = \frac{1}{2} m_H^2 H^2 + \lambda_{HHH}\, v\, H^3 + \frac{1}{4}\lambda_{HHHH} H^4 + O(H^5)\,, \tag{6}$$

where m_H is the Higgs boson mass, v is the vacuum expectation value, and λ_{HHH} and λ_{HHHH} are the trilinear and quadrilinear Higgs boson self-couplings, respectively. In the SM, once m_H and the vacuum expectation value are known, the Higgs field potential and the Higgs boson self-couplings are fully determined:

$$O(H^5) = 0 \quad \text{and} \quad \lambda_{HHH}^{\text{SM}} = \lambda_{HHHH}^{\text{SM}} = \lambda\,, \quad \text{where} \quad \lambda = m_H^2/(2v^2) \sim 0.13\,. \tag{7}$$

To probe deviations from the Higgs boson self-coupling values within the SM Lagrangian structure, the self-coupling-modifier κ_λ is introduced as $\kappa_\lambda = \lambda_{HHH}/\lambda_{HHH}^{\text{SM}}$. Many BSM models predict changes in the trilinear and quadrilinear self-couplings and add additional higher-order terms to the Higgs field potential.

At the LHC, the Higgs boson trilinear self-interaction is directly accessible via the production of Higgs boson pairs (referred to as double-Higgs). The Higgs boson self-interaction also contributes to other processes via NLO EW corrections. In particular, it was shown [180–185] that single Higgs boson production cross-sections and branching ratios (referred to as single-Higgs) are modified if the Higgs boson self-coupling deviates from the SM prediction. Fig. 31 shows the expected effect of varying κ_λ on both the double- and single-Higgs boson production cross-sections. Additionally, BSM physics can give rise to resonant production of Higgs boson pairs mediated by a heavy scalar. More details of resonant double-Higgs searches can be found in Ref. [6].

8.1. Double Higgs boson production

Double Higgs boson production is sensitive to the Higgs boson trilinear self-coupling at LO. In the SM, the ggF *HH* process accounts for more than 90% of the Higgs boson pair-production at the LHC. The process with the second-highest cross-section at the LHC is VBF *HH* production. At LO, the ggF *HH* process proceeds through the destructive interference of two amplitudes: the box diagram in Fig. 2(a), which is proportional to the square of κ_t, and the triangle diagram in Fig. 2(b), which is proportional to the product of κ_t and κ_λ. The VBF *HH* process is described at LO by three Feynman diagrams: the two vector bosons radiated by the scattering quarks fuse into two Higgs bosons via a *HHVV* vertex (Fig. 2(c)),

with the corresponding amplitude proportional to $\kappa_{2V} = \lambda_{HHVV}/\lambda^{\mathrm{SM}}_{HHVV}$; the vector bosons fuse into a virtual Higgs boson that decays into two Higgs bosons via a trilinear vertex (Fig. 2(d)), with the amplitude proportional to the product of κ_V and κ_λ; the vector bosons couple with two single Higgs bosons via two *HVV* interactions (Fig. 2(e)), with an amplitude proportional to the square of κ_V. Due to negative interference, the SM predicts double Higgs boson production to be a rare process, with a total cross-section that is more than a thousand times smaller than for single Higgs boson production (see Section 1.2 for the numerical values).

The various decays of the two Higgs bosons result in many different final states. However, the most sensitive decay channels for double Higgs boson production and its properties are those that contain at least one Higgs boson decaying into a bottom-quark pair [187–192], thanks to the large branching fraction. In particular, the most sensitive ones are the three *HH* decay channels $HH \to b\bar{b}b\bar{b}$, $HH \to b\bar{b}\tau^+\tau^-$, and $HH \to b\bar{b}\gamma\gamma$.

The $HH \to b\bar{b}b\bar{b}$ decay mode has the advantage of the largest SM *HH* decay branching fraction of 33.9%. However, the double-Higgs search in this final state is also affected by a larger SM background compared to the other *HH* analyses, due to the abundance of QCD multijet processes. The search for $HH \to b\bar{b}b\bar{b}$ [187] selects events that contain at least four *b*-tagged jets, which are split between VBF *HH* and ggF *HH* categories according to the properties of the additional jets in the event. A further selection aims to reduce the contamination from $t\bar{t}$ production in the two categories through a discriminant that quantifies the probability that an event contains a hadronic top-quark decay. Finally, in each category, the signal region is defined in a two-dimensional plane of the mass of the two Higgs boson candidates m_{H1} and m_{H2}, defined respectively as the one with the highest and lowest transverse momentum, by requiring that $X_{HH} < 1.6$ with X_{HH} defined as:

$$X_{HH} = \sqrt{\left(\frac{m_{H1} - 124\ \mathrm{GeV}}{0.1\ m_{H1}}\right)^2 + \left(\frac{m_{H2} - 117\ \mathrm{GeV}}{0.1\ m_{H2}}\right)^2}, \tag{8}$$

where 124 GeV and 117 GeV are determined as the peak of the m_{H1} and m_{H2} distributions for signal events in MC simulation. The *HH* invariant mass (m_{HH}) is used as a discriminating variable in the maximum-likelihood fit to extract the final results. The background, which is composed mostly of QCD multijet and $t\bar{t}$ processes, is evaluated with a fully data-driven method based on the extrapolation of the m_{HH} distribution from control regions, defined as the signal regions except that exactly two *b*-tagged jets are required in the events. To account for differences in kinematic properties between events with four and two *b*-tagged jets, a NN trained on data is used to reweight the m_{HH} distribution. The 95% CL upper limit on the observed (expected) double-Higgs production signal strength is $\mu_{HH} < 5.4$ (8.1).

ATLAS has also performed a dedicated search for $HH \to b\bar{b}b\bar{b}$ production via VBF *HH* in the boosted regime [188], which is particularly sensitive to BSM κ_{2V} variations. It results in 95% CL observed (expected) constraints on κ_{2V} equal to $0.52 < \kappa_{2V} < 1.52$ ($0.32 < \kappa_{2V} < 1.71$). Here, and in the following, unless explicitly stated otherwise, the Higgs boson couplings to the other particles are fixed to their SM expectations. The 95% CL upper limit on μ_{HH} and the constraints on κ_λ and κ_{2V}, obtained by the combination of the two $HH \to b\bar{b}b\bar{b}$ searches, are shown in Fig. 32 and in Table 2.

The $HH \to b\bar{b}\tau^+\tau^-$ decay mode has one of the largest branching fractions (7.3%) among the possible *HH* decay channels. The $HH \to b\bar{b}\tau^+\tau^-$ search [190] includes different signal regions targeting fully hadronic and semileptonic $\tau\tau$ final states. Events in the semileptonic channel are required to have exactly one electron or muon and one hadronically decaying τ-lepton with opposite charges. Events in the fully hadronic channel are required to have exactly two reconstructed hadronically decaying τ-leptons with opposite charge. In both channels, exactly two *b*-tagged jets are required. For each final state, the events are further split in different signal regions: one targeting VBF *HH* production, and two regions, dominated by ggF *HH* and defined by requiring $m_{HH} < 350$ GeV and $m_{HH} \geq 350$ GeV, respectively. The high mass region targets SM double-Higgs production, while the low-mass region is more sensitive to BSM values of κ_λ, as the double Higgs boson production cross-section would increase in this region if the value of κ_λ is different from one. The dominant backgrounds arise from Z + heavy flavour and $t\bar{t}$ production. Other relevant background contributions are due to events with a single Higgs boson decaying into $\tau^+\tau^-$: $t\bar{t}H$, ggF $+b\bar{b}$, $Z(\to b\bar{b})H$, and also $Z(\to \tau^+\tau^-)H(\to b\bar{b})$. A multivariate discriminant is trained separately in each signal region. The fit is performed simultaneously in the signal regions plus an additional control region that is used to constrain the normalisation of the Z + heavy flavour background component. It results in the best expected sensitivity for SM double-Higgs production in a single channel. Fig. 32 shows the final 95% CL upper limit on μ_{HH} and Table 2 presents the constraints on κ_λ and κ_{2V}.

The $HH \to b\bar{b}\gamma\gamma$ decay mode has a very small branching ratio (0.26%), but due to its experimentally clean signature allows for one of the most sensitive *HH* searches. The $HH \to b\bar{b}\gamma\gamma$ search [192] selects events with two photons and two *b*-tagged jets, each consistent with a SM Higgs boson decay. The dominant background arises from the SM continuum production of photon pairs and jets and from events with a single Higgs boson decaying into a pair of photons. The selected events are split into a low- and a high-mass region according to the value of the four-body mass $m^*_{b\bar{b}\gamma\gamma} = m_{b\bar{b}\gamma\gamma} - m_{b\bar{b}} - m_{\gamma\gamma} + 250$ GeV, where 250 GeV is about twice the Higgs boson mass. Compared to $m_{b\bar{b}\gamma\gamma}$, $m^*_{b\bar{b}\gamma\gamma}$ is chosen because it improves the four-object mass resolution. In each of the two mass regions, defined by $m^*_{b\bar{b}\gamma\gamma} < 350$ GeV and $m^*_{b\bar{b}\gamma\gamma} \geq 350$ GeV, respectively, a multivariate discriminant is used to separate the signal, which includes ggF *HH* and VBF *HH* production, from the background, and to define the categories which maximise the double-Higgs significance. The final results are obtained from a simultaneous fit to the diphoton invariant mass distribution in these categories, three in the high-mass region and four in the low-mass region. The 95% CL upper limit on μ_{HH} is shown in Fig. 32 and the constraints on κ_λ and κ_{2V} are summarised in Table 2.

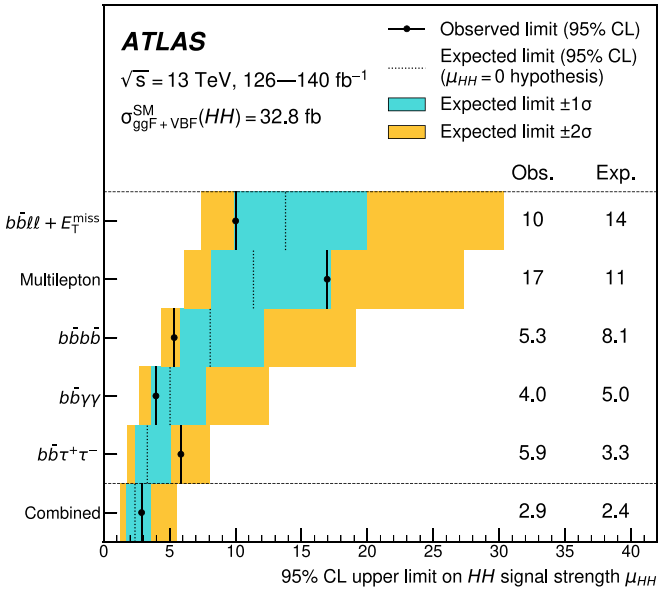

Fig. 32. Observed and expected 95% CL upper limits on μ_{HH} for double Higgs boson production in the $HH \to b\bar{b}\ell\ell + E_{\mathrm{T}}^{\mathrm{miss}}$, multilepton, $HH \to b\bar{b}\gamma\gamma$, $HH \to b\bar{b}\tau^+\tau^-$ and $HH \to b\bar{b}b\bar{b}$ decay channels and their statistical combination [193]. The expected limit is derived assuming $\mu_{HH} = 0$.

Table 2
Summary of the observed and expected constraints on κ_λ and κ_{2V} for the $HH \to b\bar{b}\gamma\gamma$, $HH \to b\bar{b}\tau^+\tau^-$, $HH \to b\bar{b}b\bar{b}$, multilepton and $HH \to b\bar{b}\ell\ell + E_{\mathrm{T}}^{\mathrm{miss}}$ analyses, and their combination [193]. In the fit, the Higgs boson couplings to the other particles are fixed to their SM expectations. The expected constraints are derived under the SM hypothesis.

Analysis	Obs. 95% CL	Exp. 95% CL	Obs. 68% CL
$HH \to b\bar{b}\gamma\gamma$	$-1.4 < \kappa_\lambda < 6.9$	$-2.9 < \kappa_\lambda < 7.8$	$\kappa_\lambda = 3.0^{+2.2}_{-2.5}$
$HH \to b\bar{b}\tau^+\tau^-$	$-3.2 < \kappa_\lambda < 9.0$	$-2.5 < \kappa_\lambda < 9.2$	$\kappa_\lambda = 0.0^{+3.3}_{-1.7}$
$HH \to b\bar{b}b\bar{b}$	$-3 < \kappa_\lambda < 11$	$-5 < \kappa_\lambda < 11$	$\kappa_\lambda = 5.8^{+3.0}_{-5.2}$
$HH \to$ multilepton	$-6 < \kappa_\lambda < 12$	$-4.5 < \kappa_\lambda < 9.6$	$\kappa_\lambda \in [-4.4, 0.6] \cup [4.3, 9.8]$
$HH \to b\bar{b}\ell\ell + E_{\mathrm{T}}^{\mathrm{miss}}$	$-6 < \kappa_\lambda < 13$	$-10 < \kappa_\lambda < 17$	$\kappa_\lambda = 3 \pm 6$
HH combination	$-1.2 < \kappa_\lambda < 7.2$	$-1.6 < \kappa_\lambda < 7.2$	$\kappa_\lambda = 3.8^{+2.1}_{-3.6}$
$HH \to b\bar{b}\gamma\gamma$	$-0.5 < \kappa_{2V} < 2.7$	$-1.1 < \kappa_{2V} < 3.3$	$\kappa_{2V} = 1.1 \pm 0.8$
$HH \to b\bar{b}\tau^+\tau^-$	$-0.5 < \kappa_{2V} < 2.7$	$-0.2 < \kappa_{2V} < 2.4$	$\kappa_{2V} = 0.4^{+1.9}_{-0.5}$
$HH \to b\bar{b}b\bar{b}$	$0.5 < \kappa_{2V} < 1.5$	$0.4 < \kappa_{2V} < 1.7$	$\kappa_{2V} = 1.01 \pm 0.23$
$HH \to$ multilepton	$-2.5 < \kappa_{2V} < 4.6$	$-1.9 < \kappa_{2V} < 4.1$	$\kappa_{2V} = -0.4^{+4.1}_{-1.2}$
$HH \to b\bar{b}\ell\ell + E_{\mathrm{T}}^{\mathrm{miss}}$	$-0.2 < \kappa_{2V} < 2.4$	$-0.5 < \kappa_{2V} < 2.7$	$\kappa_{2V} = 1.1 \pm 0.7$
HH combination	$0.6 < \kappa_{2V} < 1.5$	$0.4 < \kappa_{2V} < 1.6$	$\kappa_{2V} = 1.02^{+0.22}_{-0.23}$

The analyses in the $HH \to b\bar{b}b\bar{b}$, $HH \to b\bar{b}\tau^+\tau^-$ and $HH \to b\bar{b}\gamma\gamma$ decay channels are combined [193] to obtain more stringent constraints on the production cross-section, the Higgs boson self-coupling, and the $HHVV$ coupling. This combination includes also two other searches for double-Higgs production which target rarer or less sensitive final states: the search for HH events in $b\bar{b}ZZ^*$, VV^*VV^* ($V = W$ or Z), $VV^*\tau^+\tau^-$, $\tau^+\tau^-\tau^+\tau^-$, $\gamma\gamma VV^*$ and $\gamma\gamma\tau^+\tau^-$ decay channels with leptons in the final states (referred to as "multilepton") [194]; the search for $HH \to b\bar{b}\ell\ell + E_{\mathrm{T}}^{\mathrm{miss}}$, which probes the HH decay channels where one of the Higgs bosons decays to a b-quark pair and the other to either a boson pair (ZZ^*, WW^*) or a τ-lepton pair, which then decays to a pair of opposite-sign leptons and neutrinos [195]. The inclusion of these additional searches maximises the coverage over the combination of HH decays and improves the sensitivity to SM double-Higgs production by 4%.

The combination yields an observed 95% CL upper limit on μ_{HH} of 2.9, and an expected upper limit of 2.4 in the absence of HH production. The individual limits on the signal strength obtained from each channel and their combination are shown in Fig. 32. The best-fit value of the signal strength is $\mu_{HH} = 0.5^{+1.2}_{-1.0}$, which is compatible with the SM expectation with a p-value of 0.64. The observed (expected) significance for double-Higgs production is 0.4 (1.0) standard deviations, with respect to the hypothesis of no HH production. The 95% CL intervals for κ_λ and κ_{2V} are summarised in Table 2. The combination and the individual double-Higgs measurements are also interpreted in the context of effective field theory, as shown in Refs. [190,192,193,196].

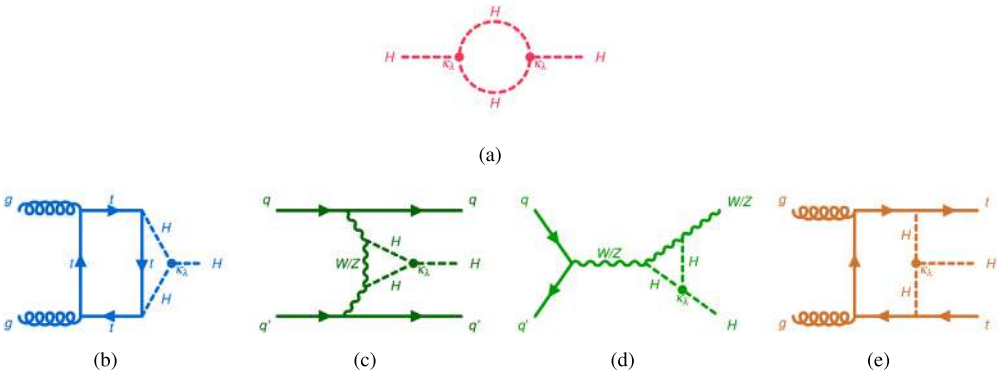

Fig. 33. Examples of one-loop λ_{HHH}-dependent diagrams for (a) the Higgs boson self-energy, and for single Higgs boson production in the (b) ggF, (c) VBF, (d) VH, and (e) $t\bar{t}H$ modes. The self-coupling vertex is indicated by the filled circle [197].

8.2. Self-coupling constraints from single Higgs boson measurements and combination with double Higgs boson searches

An alternative and complementary approach to study the Higgs boson self-coupling was proposed in Refs. [180–185]. Processes involving a single Higgs boson do not depend on λ_{HHH} at LO, but the Higgs trilinear self-coupling has to be taken into account in the calculation of the complete NLO EW corrections. In particular, λ_{HHH} contributes via Higgs boson self-energy loop corrections and additional diagrams, as illustrated for different production modes by the examples in Fig. 33.

A framework for a global fit to constrain the Higgs boson self-coupling is proposed in Refs. [180,181]. The SM predictions of the Higgs boson production and branching ratios are modified as:

$$\mu_{if}(\kappa_\lambda) = \mu_i(\kappa_\lambda) \times \mu_f(\kappa_\lambda) \equiv \frac{\sigma_i(\kappa_\lambda)}{\sigma_{\mathrm{SM},i}} \times \frac{\mathcal{B}_f(\kappa_\lambda)}{\mathcal{B}_{\mathrm{SM},f}} \,, \tag{9}$$

where μ_i and μ_f describe multiplicative corrections to the expected SM Higgs boson production cross-sections ($\sigma_{\mathrm{SM},i}$) and branching fractions ($\mathcal{B}_{\mathrm{SM},f}$) as a function of κ_λ. The functional dependence of $\mu_i(\kappa_\lambda)$ and $\mu_f(\kappa_\lambda)$ on κ_λ varies according to the production mode and the decay channel. Moreover, these functions depend on the kinematic region considered within each process, especially for the VH and $t\bar{t}H$ production modes. The cross-sections measured in different kinematic regions from the combined analysis in Section 6.3 are used to constrain κ_λ. While potential variations across kinematic regions are not considered for ggF, the differential effects of κ_λ for VBF, WH, ZH and $t\bar{t}H$ production modes are parameterised as reported in Ref. [186].

The observed (expected) 95% CL intervals for κ_λ from single Higgs boson measurements are $-4.0 < \kappa_\lambda < 10.3$ ($-5.2 < \kappa_\lambda < 11.5$) [198], which are not much looser than those obtained from the search for double Higgs boson production, despite the milder dependence of the single Higgs boson cross-sections on κ_λ. Moreover, since the two approaches are independent, they can be combined to provide the current most stringent 95% CL interval for κ_λ, equal to $-0.4 < \kappa_\lambda < 6.3$ [198]. This result and the following shown in this section, are based on the combination of a first version of the $HH \to b\bar{b}b\bar{b}$, $HH \to b\bar{b}\tau^+\tau^-$ and $HH \to b\bar{b}\gamma\gamma$ searches in the 140 fb^{-1} dataset [187,189,191], differently from the combination presented in the previous section which benefits from improved input analyses.

Double Higgs boson production does not only depend on κ_λ, but also has a significant dependence on κ_t because the two most important diagrams contributing to the ggF HH amplitude (see Fig. 2) contain the coupling of the Higgs boson to the top quark. Using only double Higgs boson analyses, it is not possible to simultaneously constrain κ_λ and κ_t without spoiling the sensitivity of the measurements of the two coupling-strength modifiers, as shown in Fig. 34. The inclusion of single Higgs boson measurements makes it possible to eliminate the degeneracy between κ_λ and κ_t and leads to a limit almost identical to that obtained by determining only κ_λ. The combination of single and double Higgs boson analyses allows a further generalisation of the fit model by simultaneously profiling κ_t, κ_b, κ_τ, and κ_V. The constraints on κ_λ in the different configurations are summarised in Table 3.

Although still not achieving the sensitivity required to probe the SM, the constraints of the trilinear Higgs boson self-coupling are starting to enter ranges predicted by BSM physics. They also have exceeded the expectations based on the Run 2 intermediate analyses [199–202]. This success can be attributed to new analysis techniques and improvements in the object identification, such as new algorithms for tagging heavy-flavour jets [203]. Future data taking will be critical to get closer to the first evidence of double Higgs boson production and increase the sensitivity to possible BSM effects on κ_λ.

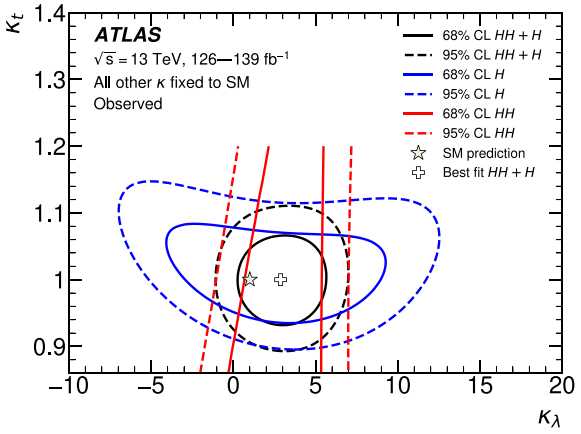

Fig. 34. Observed 68% (95%) CL contours in the κ_λ–κ_t plane from single (blue) and double (red) Higgs boson analyses and their combination (black) [198]. The Higgs boson couplings to the other particles are fixed to their SM expectations.

Table 3
Summary of observed and expected constraints on κ_λ and corresponding observed best-fit values with their uncertainties [198]. The HH combination is based on the earlier full Run 2 analyses performed by ATLAS.

	Floating parameters	Obs. 95% CL	Exp. 95% CL	Obs. value $^{+1\sigma}_{-1\sigma}$
HH combination	κ_λ	$-0.6 < \kappa_\lambda < 6.6$	$-2.1 < \kappa_\lambda < 7.8$	$\kappa_\lambda = 3.1^{+1.9}_{-2.0}$
Single-H combination	κ_λ	$-4.0 < \kappa_\lambda < 10.3$	$-5.2 < \kappa_\lambda < 11.5$	$\kappa_\lambda = 2.5^{+4.6}_{-3.9}$
$HH + H$ combination	κ_λ	$-0.4 < \kappa_\lambda < 6.3$	$-1.9 < \kappa_\lambda < 7.6$	$\kappa_\lambda = 3.0^{+1.8}_{-1.9}$
$HH + H$ combination	κ_λ, κ_t	$-0.4 < \kappa_\lambda < 6.3$	$-1.9 < \kappa_\lambda < 7.6$	$\kappa_\lambda = 3.0^{+1.8}_{-1.9}$
$HH + H$ combination	κ_λ, κ_t, κ_V, κ_b and κ_τ	$-1.4 < \kappa_\lambda < 6.1$	$-2.2 < \kappa_\lambda < 7.7$	$\kappa_\lambda = 2.3^{+2.1}_{-2.0}$

9. Conclusion and outlook

In Run 2 of the LHC (2015–2018), the ATLAS detector recorded an unprecedented amount of proton–proton collision data: 140 fb^{-1}, produced at a record centre-of-mass energy of 13 TeV. The analysis of these data significantly advances our understanding of the Higgs boson properties and its interactions with other particles.

The mass of the Higgs boson is not predicted by the SM and is a fundamental parameter in the calculation of its expected properties. It is measured to be 125.11 ± 0.11 GeV, which corresponds to a precision better than a permille, leading to negligible variations in the SM predictions for other Higgs boson properties compared to the current experimental uncertainties of the measurements. All the measurements, in particular the production cross-sections and decay branching fractions, show very good agreement with the SM predictions within the uncertainties.

Higgs boson production in association with a vector boson and its production in association with two top quarks is observed for the first time; together with the Run 1 discoveries, all major Higgs boson production modes at the LHC have now been observed. With the observation of $H \to \tau\tau$ and $H \to b\bar{b}$ decays, couplings to third generation fermions are now established, and the search for $H \to \mu\mu$, probing the Yukawa couplings to second generation fermions, yields a significance of 2σ. Evidence is found for $H \to \ell\ell\gamma$ decays, both for $H \to Z\gamma$ (in a combination of ATLAS and CMS analyses) and lepton pairs with low invariant masses.

Assuming the SM coupling structure, the Higgs boson couplings to the W and Z bosons are measured with uncertainties of about 6%, and the effective loop-induced couplings to photons and gluons with 6% and 7%, respectively. Couplings to τ-leptons are measured with uncertainties of 7%, and to the top and bottom quarks with about 12%. The measured uncertainty in the coupling to muons, which are the first second-generation fermions to be probed, is about 30%. Potential deviations from the SM predictions are also constrained within the framework of effective field theories. Searches for Higgs boson pair production achieve uncertainties in the HH cross-section of close to 100%, and reduce the possible range of the Higgs boson self-coupling (λ_{HHH}) to the interval $-0.4 < (\lambda_{HHH}/\lambda_{SM}) < 6.3$ at 95% CL.

Analyses of the data from Run 3 (2022–2025) and the High-Luminosity Runs of the LHC will build on the achieved results. Observation of the $H \to \ell\ell\gamma$ and $H \to \mu\mu$ decays are expected, as well as Higgs boson pair production, and the precision of the measured couplings and their structures will be significantly enhanced [204–206], further improving the characterisation of this key particle.

CRediT authorship contribution statement

ATLAS Collaboration: Writing – review & editing, Writing – original draft, Visualization, Validation, Supervision, Software, Resources, Project administration, Methodology, Investigation, Funding acquisition, Formal analysis, Data curation, Conceptualization.

Declaration of competing interest

The authors declare that they have no known competing financial interests or personal relationships that could have appeared to influence the work reported in this paper.

Acknowledgements

We thank CERN for the very successful operation of the LHC and its injectors, as well as the support staff at CERN and at our institutions worldwide without whom ATLAS could not be operated efficiently.

The crucial computing support from all WLCG partners is acknowledged gratefully, in particular from CERN, the ATLAS Tier-1 facilities at TRIUMF/SFU (Canada), NDGF (Denmark, Norway, Sweden), CC-IN2P3 (France), KIT/GridKA (Germany), INFN-CNAF (Italy), NL-T1 (Netherlands), PIC (Spain), RAL (UK) and BNL (USA), the Tier-2 facilities worldwide and large non-WLCG resource providers. Major contributors of computing resources are listed in Ref. [207].

We gratefully acknowledge the support of ANPCyT, Argentina; YerPhI, Armenia; ARC, Australia; BMWFW and FWF, Austria; ANAS, Azerbaijan; CNPq and FAPESP, Brazil; NSERC, NRC and CFI, Canada; CERN; ANID, Chile; CAS, MOST and NSFC, China; Minciencias, Colombia; MEYS CR, Czech Republic; DNRF and DNSRC, Denmark; IN2P3-CNRS and CEA-DRF/IRFU, France; SRNSFG, Georgia; BMBF, HGF and MPG, Germany; GSRI, Greece; RGC and Hong Kong SAR, China; ISF and Benoziyo Center, Israel; Istituto Nazionale di Fisica Nucleare, Italy; MEXT and JSPS, Japan; CNRST, Morocco; NWO, Netherlands; RCN, Norway; MNiSW, Poland; FCT, Portugal; MNE/IFA, Romania; MESTD, Serbia; MSSR, Slovakia; ARIS and MVZI, Slovenia; DSI/NRF, South Africa; MICIU/AEI, Spain; SRC and Wallenberg Foundation, Sweden; SERI, SNSF and Cantons of Bern and Geneva, Switzerland; NSTC, Taipei; TENMAK, Türkiye; STFC/UKRI, United Kingdom; DOE and NSF, United States of America.

Individual groups and members have received support from BCKDF, CANARIE, CRC and DRAC, Canada; PRIMUS 21/SCI/017, CERN-CZ and FORTE, Czech Republic; COST, ERC, ERDF, Horizon 2020, ICSC-NextGenerationEU and Marie Skłodowska-Curie Actions, European Union; Investissements d'Avenir Labex, Investissements d'Avenir Idex and ANR, France; DFG and AvH Foundation, Germany; Herakleitos, Thales and Aristeia programmes co-financed by EU-ESF and the Greek NSRF, Greece; BSF-NSF and MINERVA, Israel; Norwegian Financial Mechanism 2014–2021, Norway; NCN and NAWA, Poland; La Caixa Banking Foundation, CERCA Programme Generalitat de Catalunya and PROMETEO and GenT Programmes Generalitat Valenciana, Spain; Göran Gustafssons Stiftelse, Sweden; The Royal Society and Leverhulme Trust, United Kingdom.

In addition, individual members wish to acknowledge support from CERN: European Organisation for Nuclear Research (CERN PJAS); Chile: Agencia Nacional de Investigación *y* Desarrollo (FONDECYT 1190886, FONDECYT 1210400, FONDECYT 1230812, FONDECYT 1230987); China: Chinese Ministry of Science and Technology (MOST-2023YFA1605700), National Natural Science Foundation of China (NSFC - 12175119, NSFC 12275265, NSFC-12075060); Czech Republic: Czech Science Foundation (GACR - 24-11373S), Ministry of Education Youth and Sports (FORTE CZ.02.01.01/00/22_008/0004632), PRIMUS Research Programme (PRIMUS/21/SCI/017); EU: H2020 European Research Council (ERC - 101002463); European Union: European Research Council (ERC - 948254, ERC 101089007), Horizon 2020 Framework Programme (MUCCA - CHIST-ERA-19-XAI-00), European Union, Future Artificial Intelligence Research (FAIR-NextGenerationEU PE00000013), Italian Center for High Performance Computing, Big Data and Quantum Computing (ICSC, NextGenerationEU); France: Agence Nationale de la Recherche (ANR-20-CE31-0013, ANR-21-CE31-0013, ANR-21-CE31-0022, ANR-22-EDIR-0002), Investissements d'Avenir Labex (ANR-11-LABX-0012); Germany: Baden-Württemberg Stiftung (BW Stiftung-Postdoc Eliteprogramme), Deutsche Forschungsgemeinschaft (DFG - 469666862, DFG - CR 312/5-2); Italy: Istituto Nazionale di Fisica Nucleare (ICSC, NextGenerationEU), Ministero dell'Università e della Ricerca (PRIN - 20223N7F8K - PNRR M4.C2.1.1); Japan: Japan Society for the Promotion of Science (JSPS KAKENHI JP21H05085, JSPS KAKENHI JP22H01227, JSPS KAKENHI JP22H04944, JSPS KAKENHI JP22KK0227); Netherlands: Netherlands Organisation for Scientific Research (NWO Veni 2020 - VI.Veni.202.179); Norway: Research Council of Norway (RCN-314472); Poland: Polish National Agency for Academic Exchange (PPN/PPO/2020/1/00002/U/00001), Polish National Science Centre (NCN 2021/42/E/ST2/00350, NCN OPUS nr 2022/47/B/ST2/03059, NCN UMO-2019/34/E/ST2/00393, UMO-2020/37/B/ST2/01043, UMO-2021/40/C/ST2/00187, UMO-2022/47/O/ST2/00148); Slovenia: Slovenian Research Agency (ARIS grant J1-3010); Spain: Generalitat Valenciana (Artemisa, FEDER, IDIFEDER/2018/048), Ministry of Science and Innovation (MCIN & NextGenEU PCI2022-135018-2, MICIN & FEDER PID2021-125273NB, RYC2019-028510-I, RYC2020-030254-I, RYC2021-031273-I, RYC2022-038164-I), PROMETEO and GenT Programmes Generalitat Valenciana (CIDEGENT/2019/023, CIDEGENT/2019/027); Sweden: Swedish Research Council (Swedish Research Council 2023-04654, VR 2018-00482, VR 2022-03845, VR 2022-04683, VR 2023-03403, VR grant 2021-03651), Knut and Alice Wallenberg Foundation (KAW 2018.0157, KAW 2018.0458, KAW 2019.0447, KAW 2022.0358); Switzerland: Swiss National Science Foundation (SNSF - PCEFP2_194658); United Kingdom: Leverhulme Trust (Leverhulme Trust RPG-2020-004), Royal Society (NIF-R1-231091); United States of America: U.S. Department of Energy (ECA DE-AC02-76SF00515), Neubauer Family Foundation.

Appendix. The ATLAS collaboration

G. Aad[103], E. Aakvaag[16], B. Abbott[121], K. Abeling[55], N.J. Abicht[49], S.H. Abidi[29], M. Aboelela[44], A. Aboulhorma[35e], H. Abramowicz[153], H. Abreu[152], Y. Abulaiti[118], B.S. Acharya[69a,69b,k], A. Ackermann[63a], C. Adam Bourdarios[4], L. Adamczyk[86a], S.V. Addepalli[26], M.J. Addison[102], J. Adelman[116], A. Adiguzel[21c], T. Adye[135], A.A. Affolder[137], Y. Afik[39], M.N. Agaras[13], J. Agarwala[73a,73b], A. Aggarwal[101], C. Agheorghiesei[27c], A. Ahmad[36], F. Ahmadov[38,y], W.S. Ahmed[105], S. Ahuja[96], X. Ai[62e], G. Aielli[76a,76b], A. Aikot[164], M. Ait Tamlihat[35e], B. Aitbenchikh[35a], M. Akbiyik[101], T.P.A. Åkesson[99], A.V. Akimov[37], D. Akiyama[169], N.N. Akolkar[24], S. Aktas[21a], K. Al Khoury[41], G.L. Alberghi[23b], J. Albert[166], P. Albicocco[53], G.L. Albouy[60], S. Alderweireldt[52], Z.L. Alegria[122], M. Aleksa[36], I.N. Aleksandrov[38], C. Alexa[27b], T. Alexopoulos[10], F. Alfonsi[23b], M. Algren[56], M. Alhroob[143], B. Ali[133], H.M.J. Ali[92], S. Ali[31], S.W. Alibocus[93], M. Aliev[33c], G. Alimonti[71a], W. Alkakhi[55], C. Allaire[66], B.M.M. Allbrooke[148], J.F. Allen[52], C.A. Allendes Flores[138f], P.P. Allport[20], A. Aloisio[72a,72b], F. Alonso[91], C. Alpigiani[140], M. Alvarez Estevez[100], A. Alvarez Fernandez[101], M. Alves Cardoso[56], M.G. Alviggi[72a,72b], M. Aly[102], Y. Amaral Coutinho[83b], A. Ambler[105], C. Amelung[36], M. Amerl[102], C.G. Ames[110], D. Amidei[107], K.J. Amirie[156], S.P. Amor Dos Santos[131a], K.R. Amos[164], S. An[84], V. Ananiev[126], C. Anastopoulos[141], T. Andeen[11], J.K. Anders[36], S.Y. Andrean[47a,47b], A. Andreazza[71a,71b], S. Angelidakis[9], A. Angerami[41,aa], A.V. Anisenkov[37], A. Annovi[74a], C. Antel[56], E. Antipov[147], M. Antonelli[53], F. Anulli[75a], M. Aoki[84], T. Aoki[155], M.A. Aparo[148], L. Aperio Bella[48], C. Appelt[18], A. Apyan[26], S.J. Arbiol Val[87], C. Arcangeletti[53], A.T.H. Arce[51], E. Arena[93], J-F. Arguin[109], S. Argyropoulos[54], J.-H. Arling[48], O. Arnaez[4], H. Arnold[115], G. Artoni[75a,75b], H. Asada[112], K. Asai[119], S. Asai[155], N.A. Asbah[36], K. Assamagan[29], R. Astalos[28a], K.S.V. Astrand[99], S. Atashi[160], R.J. Atkin[33a], M. Atkinson[163], H. Atmani[35f], P.A. Atmasiddha[129], K. Augsten[133], S. Auricchio[72a,72b], A.D. Auriol[20], V.A. Austrup[102], G. Avolio[36], K. Axiotis[56], G. Azuelos[109,ae], D. Babal[28b], H. Bachacou[136], K. Bachas[154,o], A. Bachiu[34], F. Backman[47a,47b], A. Badea[39], T.M. Baer[107], P. Bagnaia[75a,75b], M. Bahmani[18], D. Bahner[54], K. Bai[124], J.T. Baines[135], L. Baines[95], O.K. Baker[173], E. Bakos[15], D. Bakshi Gupta[8], V. Balakrishnan[121], R. Balasubramanian[115], E.M. Baldin[37], P. Balek[86a], E. Ballabene[23b,23a], F. Balli[136], L.M. Baltes[63a], W.K. Balunas[32], J. Balz[101], E. Banas[87], M. Bandieramonte[130], A. Bandyopadhyay[24], S. Bansal[24], L. Barak[153], M. Barakat[48], E.L. Barberio[106], D. Barberis[57b,57a], M. Barbero[103], M.Z. Barel[115], K.N. Barends[33a], T. Barillari[111], M-S. Barisits[36], T. Barklow[145], P. Baron[123], D.A. Baron Moreno[102], A. Baroncelli[62a], G. Barone[29], A.J. Barr[127], J.D. Barr[97], F. Barreiro[100], J. Barreiro Guimarães da Costa[14a], U. Barron[153], M.G. Barros Teixeira[131a], S. Barsov[37], F. Bartels[63a], R. Bartoldus[145], A.E. Barton[92], P. Bartos[28a], A. Basan[101], M. Baselga[49], A. Bassalat[66,b], M.J. Basso[157a], R. Bate[165], R.L. Bates[59], S. Batlamous[100], B. Batool[143], M. Battaglia[137], D. Battulga[18], M. Bauce[75a,75b], M. Bauer[36], P. Bauer[24], L.T. Bazzano Hurrell[30], J.B. Beacham[51], T. Beau[128], J.Y. Beaucamp[91], P.H. Beauchemin[159], P. Bechtle[24], H.P. Beck[19,n], K. Becker[168], A.J. Beddall[82], V.A. Bednyakov[38], C.P. Bee[147], L.J. Beemster[15], T.A. Beermann[36], M. Begalli[83d], M. Begel[29], A. Behera[147], J.K. Behr[48], J.F. Beirer[36], F. Beisiegel[24], M. Belfkir[117b], G. Bella[153], L. Bellagamba[23b], A. Bellerive[34], P. Bellos[20], K. Beloborodov[37], D. Benchekroun[35a], F. Bendebba[35a], Y. Benhammou[153], K.C. Benkendorfer[61], L. Beresford[48], M. Beretta[53], E. Bergeaas Kuutmann[162], N. Berger[4], B. Bergmann[133], J. Beringer[17a], G. Bernardi[5], C. Bernius[145], F.U. Bernlochner[24], F. Bernon[36,103], A. Berrocal Guardia[13], T. Berry[96], P. Berta[134], A. Berthold[50], S. Bethke[111], A. Betti[75a,75b], A.J. Bevan[95], N.K. Bhalla[54], M. Bhamjee[33c], S. Bhatta[147], D.S. Bhattacharya[167], P. Bhattarai[145], K.D. Bhide[54], V.S. Bhopatkar[122], R.M. Bianchi[130], G. Bianco[23b,23a], O. Biebel[110], R. Bielski[124], M. Biglietti[77a], C.S. Billingsley[44], M. Bindi[55], A. Bingul[21b], C. Bini[75a,75b], A. Biondini[93], C.J. Birch-sykes[102], G.A. Bird[32], M. Birman[170], M. Biros[134], S. Biryukov[148], T. Bisanz[49], E. Bisceglie[43b,43a], J.P. Biswal[135], D. Biswas[143], I. Bloch[48], A. Blue[59], U. Blumenschein[95], J. Blumenthal[101], V.S. Bobrovnikov[37], M. Boehler[54], B. Boehm[167], D. Bogavac[36], A.G. Bogdanchikov[37], C. Bohm[47a], V. Boisvert[96], P. Bokan[36], T. Bold[86a], M. Bomben[5], M. Bona[95], M. Boonekamp[136], C.D. Booth[96], A.G. Borbély[59], I.S. Bordulev[37],

H.M. Borecka-Bielska[109], G. Borissov[92], D. Bortoletto[127], D. Boscherini[23b], M. Bosman[13], J.D. Bossio Sola[36], K. Bouaouda[35a], N. Bouchhar[164], L. Boudet[4], J. Boudreau[130], E.V. Bouhova-Thacker[92], D. Boumediene[40], R. Bouquet[57b,57a], A. Boveia[120], J. Boyd[36], D. Boye[29], I.R. Boyko[38], L. Bozianu[56], J. Bracinik[20], N. Brahimi[4], G. Brandt[172], O. Brandt[32], F. Braren[48], B. Brau[104], J.E. Brau[124], R. Brener[170], L. Brenner[115], R. Brenner[162], S. Bressler[170], D. Britton[59], D. Britzger[111], I. Brock[24], R. Brock[108], G. Brooijmans[41], E. Brost[29], L.M. Brown[166], L.E. Bruce[61], T.L. Bruckler[127], P.A. Bruckman de Renstrom[87], B. Brüers[48], A. Bruni[23b], G. Bruni[23b], M. Bruschi[23b], N. Bruscino[75a,75b], T. Buanes[16], Q. Buat[140], D. Buchin[111], A.G. Buckley[59], O. Bulekov[37], B.A. Bullard[145], S. Burdin[93], C.D. Burgard[49], A.M. Burger[36], B. Burghgrave[8], O. Burlayenko[54], J.T.P. Burr[32], C.D. Burton[11], J.C. Burzynski[144], E.L. Busch[41], V. Büscher[101], P.J. Bussey[59], J.M. Butler[25], C.M. Buttar[59], J.M. Butterworth[97], W. Buttinger[135], C.J. Buxo Vazquez[108], A.R. Buzykaev[37], S. Cabrera Urbán[164], L. Cadamuro[66], D. Caforio[58], H. Cai[130], Y. Cai[14a,14e], Y. Cai[14c], V.M.M. Cairo[36], O. Cakir[3a], N. Calace[36], P. Calafiura[17a], G. Calderini[128], P. Calfayan[68], G. Callea[59], L.P. Caloba[83b], D. Calvet[40], S. Calvet[40], M. Calvetti[74a,74b], R. Camacho Toro[128], S. Camarda[36], D. Camarero Munoz[26], P. Camarri[76a,76b], M.T. Camerlingo[72a,72b], D. Cameron[36], C. Camincher[166], M. Campanelli[97], A. Camplani[42], V. Canale[72a,72b], A.C. Canbay[3a], E. Canonero[96], J. Cantero[164], Y. Cao[163], F. Capocasa[26], M. Capua[43b,43a], A. Carbone[71a,71b], R. Cardarelli[76a], J.C.J. Cardenas[8], G. Carducci[43b,43a], T. Carli[36], G. Carlino[72a], J.I. Carlotto[13], B.T. Carlson[130,p], E.M. Carlson[166,157a], J. Carmignani[93], L. Carminati[71a,71b], A. Carnelli[136], M. Carnesale[75a,75b], S. Caron[114], E. Carquin[138f], S. Carrá[71a], G. Carratta[23b,23a], A.M. Carroll[124], T.M. Carter[52], M.P. Casado[13,h], M. Caspar[48], F.L. Castillo[4], L. Castillo Garcia[13], V. Castillo Gimenez[164], N.F. Castro[131a,131e], A. Catinaccio[36], J.R. Catmore[126], T. Cavaliere[4], V. Cavaliere[29], N. Cavalli[23b,23a], Y.C. Cekmecelioglu[48], E. Celebi[21a], S. Cella[36], F. Celli[127], M.S. Centonze[70a,70b], V. Cepaitis[56], K. Cerny[123], A.S. Cerqueira[83a], A. Cerri[148], L. Cerrito[76a,76b], F. Cerutti[17a], B. Cervato[143], A. Cervelli[23b], G. Cesarini[53], S.A. Cetin[82], D. Chakraborty[116], J. Chan[17a], W.Y. Chan[155], J.D. Chapman[32], E. Chapon[136], B. Chargeishvili[151b], D.G. Charlton[20], M. Chatterjee[19], C. Chauhan[134], Y. Che[14c], S. Chekanov[6], S.V. Chekulaev[157a], G.A. Chelkov[38,a], A. Chen[107], B. Chen[153], B. Chen[166], H. Chen[14c], H. Chen[29], J. Chen[62c], J. Chen[144], M. Chen[127], S. Chen[155], S.J. Chen[14c], X. Chen[62c,136], X. Chen[14b,ad], Y. Chen[62a], C.L. Cheng[171], H.C. Cheng[64a], S. Cheong[145], A. Cheplakov[38], E. Cheremushkina[48], E. Cherepanova[115], R. Cherkaoui El Moursli[35e], E. Cheu[7], K. Cheung[65], L. Chevalier[136], V. Chiarella[53], G. Chiarelli[74a], N. Chiedde[103], G. Chiodini[70a], A.S. Chisholm[20], A. Chitan[27b], M. Chitishvili[164], M.V. Chizhov[38,q], K. Choi[11], Y. Chou[140], E.Y.S. Chow[114], K.L. Chu[170], M.C. Chu[64a], X. Chu[14a,14e], J. Chudoba[132], J.J. Chwastowski[87], D. Cieri[111], K.M. Ciesla[86a], V. Cindro[94], A. Ciocio[17a], F. Cirotto[72a,72b], Z.H. Citron[170], M. Citterio[71a], D.A. Ciubotaru[27b], A. Clark[56], P.J. Clark[52], C. Clarry[156], J.M. Clavijo Columbie[48], S.E. Clawson[48], C. Clement[47a,47b], J. Clercx[48], Y. Coadou[103], M. Cobal[69a,69c], A. Coccaro[57b], R.F. Coelho Barrue[131a], R. Coelho Lopes De Sa[104], S. Coelli[71a], B. Cole[41], J. Collot[60], P. Conde Muiño[131a,131g], M.P. Connell[33c], S.H. Connell[33c], E.I. Conroy[127], F. Conventi[72a,af], H.G. Cooke[20], A.M. Cooper-Sarkar[127], F.A. Corchia[23b,23a], A. Cordeiro Oudot Choi[128], L.D. Corpe[40], M. Corradi[75a,75b], F. Corriveau[105,w], A. Cortes-Gonzalez[18], M.J. Costa[164], F. Costanza[4], D. Costanzo[141], B.M. Cote[120], J. Couthures[4], G. Cowan[96], K. Cranmer[171], D. Cremonini[23b,23a], S. Crépé-Renaudin[60], F. Cresciolli[128], M. Cristinziani[143], M. Cristoforetti[78a,78b], V. Croft[115], J.E. Crosby[122], G. Crosetti[43b,43a], A. Cueto[100], Z. Cui[7], W.R. Cunningham[59], F. Curcio[164], J.R. Curran[52], P. Czodrowski[36], M.M. Czurylo[36], M.J. Da Cunha Sargedas De Sousa[57b,57a], J.V. Da Fonseca Pinto[83b], C. Da Via[102], W. Dabrowski[86a], T. Dado[49], S. Dahbi[150], T. Dai[107], D. Dal Santo[19], C. Dallapiccola[104], M. Dam[42], G. D'amen[29], V. D'Amico[110], J. Damp[101], J.R. Dandoy[34], D. Dannheim[36], M. Danninger[144], V. Dao[36], G. Darbo[57b], S.J. Das[29,ag], F. Dattola[48], S. D'Auria[71a,71b], A. D'Avanzo[72a,72b], C. David[33a], T. Davidek[134], I. Dawson[95], H.A. Day-hall[133], K. De[8], R. De Asmundis[72a], N. De Biase[48], S. De Castro[23b,23a], N. De Groot[114], P. de Jong[115], H. De la Torre[116], A. De Maria[14c], A. De Salvo[75a], U. De Sanctis[76a,76b], F. De Santis[70a,70b], A. De Santo[148],

J.B. De Vivie De Regie[60], D.V. Dedovich[38], J. Degens[93], A.M. Deiana[44], F. Del Corso[23b,23a], J. Del Peso[100], F. Del Rio[63a], L. Delagrange[128], F. Deliot[136], C.M. Delitzsch[49], M. Della Pietra[72a,72b], D. Della Volpe[56], A. Dell'Acqua[36], L. Dell'Asta[71a,71b], M. Delmastro[4], P.A. Delsart[60], S. Demers[173], M. Demichev[38], S.P. Denisov[37], L. D'Eramo[40], D. Derendarz[87], F. Derue[128], P. Dervan[93], K. Desch[24], C. Deutsch[24], F.A. Di Bello[57b,57a], A. Di Ciaccio[76a,76b], L. Di Ciaccio[4], A. Di Domenico[75a,75b], C. Di Donato[72a,72b], A. Di Girolamo[36], G. Di Gregorio[36], A. Di Luca[78a,78b], B. Di Micco[77a,77b], R. Di Nardo[77a,77b], M. Diamantopoulou[34], F.A. Dias[115], T. Dias Do Vale[144], M.A. Diaz[138a,138b], F.G. Diaz Capriles[24], M. Didenko[164], E.B. Diehl[107], S. Díez Cornell[48], C. Diez Pardos[143], C. Dimitriadi[162,24], A. Dimitrievska[20], J. Dingfelder[24], I-M. Dinu[27b], S.J. Dittmeier[63b], F. Dittus[36], M. Divisek[134], F. Djama[103], T. Djobava[151b], C. Doglioni[102,99], A. Dohnalova[28a], J. Dolejsi[134], Z. Dolezal[134], K.M. Dona[39], M. Donadelli[83c], B. Dong[108], J. Donini[40], A. D'Onofrio[72a,72b], M. D'Onofrio[93], J. Dopke[135], A. Doria[72a], N. Dos Santos Fernandes[131a], P. Dougan[102], M.T. Dova[91], A.T. Doyle[59], M.A. Draguet[127], E. Dreyer[170], I. Drivas-koulouris[10], M. Drnevich[118], M. Drozdova[56], D. Du[62a], T.A. du Pree[115], F. Dubinin[37], M. Dubovsky[28a], E. Duchovni[170], G. Duckeck[110], O.A. Ducu[27b], D. Duda[52], A. Dudarev[36], E.R. Duden[26], M. D'uffizi[102], L. Duflot[66], M. Dührssen[36], I. Duminica[27g], A.E. Dumitriu[27b], M. Dunford[63a], S. Dungs[49], K. Dunne[47a,47b], A. Duperrin[103], H. Duran Yildiz[3a], M. Düren[58], A. Durglishvili[151b], B.L. Dwyer[116], G.I. Dyckes[17a], M. Dyndal[86a], B.S. Dziedzic[36], Z.O. Earnshaw[148], G.H. Eberwein[127], B. Eckerova[28a], S. Eggebrecht[55], E. Egidio Purcino De Souza[128], L.F. Ehrke[56], G. Eigen[16], K. Einsweiler[17a], T. Ekelof[162], P.A. Ekman[99], S. El Farkh[35b], Y. El Ghazali[35b], H. El Jarrari[36], A. El Moussaouy[109], V. Ellajosyula[162], M. Ellert[162], F. Ellinghaus[172], N. Ellis[36], J. Elmsheuser[29], M. Elsawy[117a], M. Elsing[36], D. Emeliyanov[135], Y. Enari[155], I. Ene[17a], S. Epari[13], P.A. Erland[87], M. Errenst[172], M. Escalier[66], C. Escobar[164], E. Etzion[153], G. Evans[131a], H. Evans[68], L.S. Evans[96], A. Ezhilov[37], S. Ezzarqtouni[35a], F. Fabbri[23b,23a], L. Fabbri[23b,23a], G. Facini[97], V. Fadeyev[137], R.M. Fakhrutdinov[37], D. Fakoudis[101], S. Falciano[75a], L.F. Falda Ulhoa Coelho[36], F. Fallavollita[111], J. Faltova[134], C. Fan[163], Y. Fan[14a], Y. Fang[14a,14e], M. Fanti[71a,71b], M. Faraj[69a,69b], Z. Farazpay[98], A. Farbin[8], A. Farilla[77a], T. Farooque[108], S.M. Farrington[52], F. Fassi[35e], D. Fassouliotis[9], M. Faucci Giannelli[76a,76b], W.J. Fawcett[32], L. Fayard[66], P. Federic[134], P. Federicova[132], O.L. Fedin[37,a], M. Feickert[171], L. Feligioni[103], D.E. Fellers[124], C. Feng[62b], M. Feng[14b], Z. Feng[115], M.J. Fenton[160], L. Ferencz[48], R.A.M. Ferguson[92], S.I. Fernandez Luengo[138f], P. Fernandez Martinez[13], M.J.V. Fernoux[103], J. Ferrando[92], A. Ferrari[162], P. Ferrari[115,114], R. Ferrari[73a], D. Ferrere[56], C. Ferretti[107], F. Fiedler[101], P. Fiedler[133], A. Filipčič[94], E.K. Filmer[1], F. Filthaut[114], M.C.N. Fiolhais[131a,131c,c], L. Fiorini[164], W.C. Fisher[108], T. Fitschen[102], P.M. Fitzhugh[136], I. Fleck[143], P. Fleischmann[107], T. Flick[172], M. Flores[33d,ab], L.R. Flores Castillo[64a], L. Flores Sanz De Acedo[36], F.M. Follega[78a,78b], N. Fomin[16], J.H. Foo[156], A. Formica[136], A.C. Forti[102], E. Fortin[36], A.W. Fortman[17a], M.G. Foti[17a], L. Fountas[9,i], D. Fournier[66], H. Fox[92], P. Francavilla[74a,74b], S. Francescato[61], S. Franchellucci[56], M. Franchini[23b,23a], S. Franchino[63a], D. Francis[36], L. Franco[114], V. Franco Lima[36], L. Franconi[48], M. Franklin[61], G. Frattari[26], Y.Y. Frid[153], J. Friend[59], N. Fritzsche[50], A. Froch[54], D. Froidevaux[36], J.A. Frost[127], Y. Fu[62a], S. Fuenzalida Garrido[138f], M. Fujimoto[103], K.Y. Fung[64a], E. Furtado De Simas Filho[83e], M. Furukawa[155], J. Fuster[164], A. Gabrielli[23b,23a], A. Gabrielli[156], P. Gadow[36], G. Gagliardi[57b,57a], L.G. Gagnon[17a], S. Gaid[161], S. Galantzan[153], E.J. Gallas[127], B.J. Gallop[135], K.K. Gan[120], S. Ganguly[155], Y. Gao[52], F.M. Garay Walls[138a,138b], B. Garcia[29], C. García[164], A. Garcia Alonso[115], A.G. Garcia Caffaro[173], J.E. García Navarro[164], M. Garcia-Sciveres[17a], G.L. Gardner[129], R.W. Gardner[39], N. Garelli[159], D. Garg[80], R.B. Garg[145], J.M. Gargan[52], C.A. Garner[156], C.M. Garvey[33a], V.K. Gassmann[159], G. Gaudio[73a], V. Gautam[13], P. Gauzzi[75a,75b], I.L. Gavrilenko[37], A. Gavrilyuk[37], C. Gay[165], G. Gaycken[48], E.N. Gazis[10], A.A. Geanta[27b], C.M. Gee[137], A. Gekow[120], C. Gemme[57b], M.H. Genest[60], A.D. Gentry[113], S. George[96], W.F. George[20], T. Geralis[46], P. Gessinger-Befurt[36], M.E. Geyik[172], M. Ghani[168], K. Ghorbanian[95], A. Ghosal[143], A. Ghosh[160], A. Ghosh[7], B. Giacobbe[23b], S. Giagu[75a,75b], T. Giani[115], P. Giannetti[74a], A. Giannini[62a], S.M. Gibson[96], M. Gignac[137], D.T. Gil[86b], A.K. Gilbert[86a],

B.J. Gilbert[41], D. Gillberg[34], G. Gilles[115], L. Ginabat[128], D.M. Gingrich[2,ae], M.P. Giordani[69a,69c], P.F. Giraud[136], G. Giugliarelli[69a,69c], D. Giugni[71a], F. Giuli[36], I. Gkialas[9,i], L.K. Gladilin[37], C. Glasman[100], G.R. Gledhill[124], G. Glemža[48], M. Glisic[124], I. Gnesi[43b,e], Y. Go[29], M. Goblirsch-Kolb[36], B. Gocke[49], D. Godin[109], B. Gokturk[21a], S. Goldfarb[106], T. Golling[56], M.G.D. Gololo[33g], D. Golubkov[37], J.P. Gombas[108], A. Gomes[131a,131b], G. Gomes Da Silva[143], A.J. Gomez Delegido[164], R. Gonçalo[131a], L. Gonella[20], A. Gongadze[151c], F. Gonnella[20], J.L. Gonski[145], R.Y. González Andana[52], S. González de la Hoz[164], R. Gonzalez Lopez[93], C. Gonzalez Renteria[17a], M.V. Gonzalez Rodrigues[48], R. Gonzalez Suarez[162], S. Gonzalez-Sevilla[56], L. Goossens[36], B. Gorini[36], E. Gorini[70a,70b], A. Gorišek[94], T.C. Gosart[129], A.T. Goshaw[51], M.I. Gostkin[38], S. Goswami[122], C.A. Gottardo[36], S.A. Gotz[110], M. Gouighri[35b], V. Goumarre[48], A.G. Goussiou[140], N. Govender[33c], I. Grabowska-Bold[86a], K. Graham[34], E. Gramstad[126], S. Grancagnolo[70a,70b], C.M. Grant[1,136], P.M. Gravila[27f], F.G. Gravili[70a,70b], H.M. Gray[17a], M. Greco[70a,70b], C. Grefe[24], I.M. Gregor[48], K.T. Greif[160], P. Grenier[145], S.G. Grewe[111], A.A. Grillo[137], K. Grimm[31], S. Grinstein[13,s], J.-F. Grivaz[66], E. Gross[170], J. Grosse-Knetter[55], J.C. Grundy[127], L. Guan[107], J.G.R. Guerrero Rojas[164], G. Guerrieri[69a,69c], F. Guescini[111], R. Gugel[101], J.A.M. Guhit[107], A. Guida[18], E. Guilloton[168], S. Guindon[36], F. Guo[14a,14e], J. Guo[62c], L. Guo[48], Y. Guo[107], R. Gupta[130], S. Gurbuz[24], S.S. Gurdasani[54], G. Gustavino[36], M. Guth[56], P. Gutierrez[121], L.F. Gutierrez Zagazeta[129], M. Gutsche[50], C. Gutschow[97], C. Gwenlan[127], C.B. Gwilliam[93], E.S. Haaland[126], A. Haas[118], M. Habedank[48], C. Haber[17a], H.K. Hadavand[8], A. Hadef[50], S. Hadzic[111], A.I. Hagan[92], J.J. Hahn[143], E.H. Haines[97], M. Haleem[167], J. Haley[122], J.J. Hall[141], G.D. Hallewell[103], L. Halser[19], K. Hamano[166], M. Hamer[24], G.N. Hamity[52], E.J. Hampshire[96], J. Han[62b], K. Han[62a], L. Han[14c], L. Han[62a], S. Han[17a], Y.F. Han[156], K. Hanagaki[84], M. Hance[137], D.A. Hangal[41], H. Hanif[144], M.D. Hank[129], J.B. Hansen[42], P.H. Hansen[42], K. Hara[158], D. Harada[56], T. Harenberg[172], S. Harkusha[37], M.L. Harris[104], Y.T. Harris[127], J. Harrison[13], N.M. Harrison[120], P.F. Harrison[168], N.M. Hartman[111], N.M. Hartmann[110], R.Z. Hasan[96,135], Y. Hasegawa[142], S. Hassan[16], R. Hauser[108], C.M. Hawkes[20], R.J. Hawkings[36], Y. Hayashi[155], S. Hayashida[112], D. Hayden[108], C. Hayes[107], R.L. Hayes[115], C.P. Hays[127], J.M. Hays[95], H.S. Hayward[93], F. He[62a], M. He[14a,14e], Y. He[139], Y. He[48], Y. He[97], N.B. Heatley[95], V. Hedberg[99], A.L. Heggelund[126], N.D. Hehir[95,*], C. Heidegger[54], K.K. Heidegger[54], W.D. Heidorn[81], J. Heilman[34], S. Heim[48], T. Heim[17a], J.G. Heinlein[129], J.J. Heinrich[124], L. Heinrich[111,ac], J. Hejbal[132], A. Held[171], S. Hellesund[16], C.M. Helling[165], S. Hellman[47a,47b], R.C.W. Henderson[92], L. Henkelmann[32], A.M. Henriques Correia[36], H. Herde[99], Y. Hernández Jiménez[147], L.M. Herrmann[24], T. Herrmann[50], G. Herten[54], R. Hertenberger[110], L. Hervas[36], M.E. Hesping[101], N.P. Hessey[157a], M. Hidaoui[35b], E. Hill[156], S.J. Hillier[20], J.R. Hinds[108], F. Hinterkeuser[24], M. Hirose[125], S. Hirose[158], D. Hirschbuehl[172], T.G. Hitchings[102], B. Hiti[94], J. Hobbs[147], R. Hobincu[27e], N. Hod[170], M.C. Hodgkinson[141], B.H. Hodkinson[127], A. Hoecker[36], D.D. Hofer[107], J. Hofer[48], T. Holm[24], M. Holzbock[111], L.B.A.H. Hommels[32], B.P. Honan[102], J.J. Hong[68], J. Hong[62c], T.M. Hong[130], B.H. Hooberman[163], W.H. Hopkins[6], M.C. Hoppesch[163], Y. Horii[112], S. Hou[150], A.S. Howard[94], J. Howarth[59], J. Hoya[6], M. Hrabovsky[123], A. Hrynevich[48], T. Hryn'ova[4], P.J. Hsu[65], S.-C. Hsu[140], T. Hsu[66], M. Hu[17a], Q. Hu[62a], S. Huang[64b], X. Huang[14a,14e], Y. Huang[141], Y. Huang[101], Y. Huang[14a], Z. Huang[102], Z. Hubacek[133], M. Huebner[24], F. Huegging[24], T.B. Huffman[127], C.A. Hugli[48], M. Huhtinen[36], S.K. Huiberts[16], R. Hulsken[105], N. Huseynov[12], J. Huston[108], J. Huth[61], R. Hyneman[145], G. Iacobucci[56], G. Iakovidis[29], L. Iconomidou-Fayard[66], J.P. Iddon[36], P. Iengo[72a,72b], R. Iguchi[155], T. Iizawa[127], Y. Ikegami[84], N. Ilic[156], H. Imam[35a], M. Ince Lezki[56], T. Ingebretsen Carlson[47a,47b], G. Introzzi[73a,73b], M. Iodice[77a], V. Ippolito[75a,75b], R.K. Irwin[93], M. Ishino[155], W. Islam[171], C. Issever[18,48], S. Istin[21a,ai], H. Ito[169], R. Iuppa[78a,78b], A. Ivina[170], J.M. Izen[45], V. Izzo[72a], P. Jacka[132], P. Jackson[1], C.S. Jagfeld[110], G. Jain[157a], P. Jain[48], K. Jakobs[54], T. Jakoubek[170], J. Jamieson[59], M. Javurkova[104], L. Jeanty[124], J. Jejelava[151a,z], P. Jenni[54,f], C.E. Jessiman[34], C. Jia[62b], J. Jia[147], X. Jia[61], X. Jia[14a,14e], Z. Jia[14c], C. Jiang[52], S. Jiggins[48], J. Jimenez Pena[13], S. Jin[14c], A. Jinaru[27b], O. Jinnouchi[139], P. Johansson[141], K.A. Johns[7], J.W. Johnson[137], D.M. Jones[148], E. Jones[48],

P. Jones[32], R.W.L. Jones[92], T.J. Jones[93], H.L. Joos[55,36], R. Joshi[120], J. Jovicevic[15], X. Ju[17a], J.J. Junggeburth[104], T. Junkermann[63a], A. Juste Rozas[13,s], M.K. Juzek[87], S. Kabana[138e], A. Kaczmarska[87], M. Kado[111], H. Kagan[120], M. Kagan[145], A. Kahn[129], C. Kahra[101], T. Kaji[155], E. Kajomovitz[152], N. Kakati[170], I. Kalaitzidou[54], C.W. Kalderon[29], N.J. Kang[137], D. Kar[33g], K. Karava[127], M.J. Kareem[157b], E. Karentzos[54], O. Karkout[115], S.N. Karpov[38], Z.M. Karpova[38], V. Kartvelishvili[92], A.N. Karyukhin[37], E. Kasimi[154], J. Katzy[48], S. Kaur[34], K. Kawade[142], M.P. Kawale[121], C. Kawamoto[88], T. Kawamoto[62a], E.F. Kay[36], F.I. Kaya[159], S. Kazakos[108], V.F. Kazanin[37], Y. Ke[147], J.M. Keaveney[33a], R. Keeler[166], G.V. Kehris[61], J.S. Keller[34], A.S. Kelly[97], J.J. Kempster[148], P.D. Kennedy[101], O. Kepka[132], B.P. Kerridge[135], S. Kersten[172], B.P. Kerševan[94], L. Keszeghova[28a], S. Ketabchi Haghighat[156], R.A. Khan[130], A. Khanov[122], A.G. Kharlamov[37], T. Kharlamova[37], E.E. Khoda[140], M. Kholodenko[37], T.J. Khoo[18], G. Khoriauli[167], J. Khubua[151b,*], Y.A.R. Khwaira[128], B. Kibirige[33g], D.W. Kim[47a,47b], Y.K. Kim[39], N. Kimura[97], M.K. Kingston[55], A. Kirchhoff[55], C. Kirfel[24], F. Kirfel[24], J. Kirk[135], A.E. Kiryunin[111], C. Kitsaki[10], O. Kivernyk[24], M. Klassen[159], C. Klein[34], L. Klein[167], M.H. Klein[44], S.B. Klein[56], U. Klein[93], P. Klimek[36], A. Klimentov[29], T. Klioutchnikova[36], P. Kluit[115], S. Kluth[111], E. Kneringer[79], T.M. Knight[156], A. Knue[49], R. Kobayashi[88], D. Kobylianskii[170], S.F. Koch[127], M. Kocian[145], P. Kodyš[134], D.M. Koeck[124], P.T. Koenig[24], T. Koffas[34], O. Kolay[50], I. Koletsou[4], T. Komarek[123], K. Köneke[54], A.X.Y. Kong[1], T. Kono[119], N. Konstantinidis[97], P. Kontaxakis[56], B. Konya[99], R. Kopeliansky[41], S. Koperny[86a], K. Korcyl[87], K. Kordas[154,d], A. Korn[97], S. Korn[55], I. Korolkov[13], N. Korotkova[37], B. Kortman[115], O. Kortner[111], S. Kortner[111], W.H. Kostecka[116], V.V. Kostyukhin[143], A. Kotsokechagia[136], A. Kotwal[51], A. Koulouris[36], A. Kourkoumeli-Charalampidi[73a,73b], C. Kourkoumelis[9], E. Kourlitis[111,ac], O. Kovanda[124], R. Kowalewski[166], W. Kozanecki[136], A.S. Kozhin[37], V.A. Kramarenko[37], G. Kramberger[94], P. Kramer[101], M.W. Krasny[128], A. Krasznahorkay[36], J.W. Kraus[172], J.A. Kremer[48], T. Kresse[50], J. Kretzschmar[93], K. Kreul[18], P. Krieger[156], S. Krishnamurthy[104], M. Krivos[134], K. Krizka[20], K. Kroeninger[49], H. Kroha[111], J. Kroll[132], J. Kroll[129], K.S. Krowpman[108], U. Kruchonak[38], H. Krüger[24], N. Krumnack[81], M.C. Kruse[51], O. Kuchinskaia[37], S. Kuday[3a], S. Kuehn[36], R. Kuesters[54], T. Kuhl[48], V. Kukhtin[38], Y. Kulchitsky[37,a], S. Kuleshov[138d,138b], M. Kumar[33g], N. Kumari[48], P. Kumari[157b], A. Kupco[132], T. Kupfer[49], A. Kupich[37], O. Kuprash[54], H. Kurashige[85], L.L. Kurchaninov[157a], O. Kurdysh[66], Y.A. Kurochkin[37], A. Kurova[37], M. Kuze[139], A.K. Kvam[104], J. Kvita[123], T. Kwan[105], N.G. Kyriacou[107], L.A.O. Laatu[103], C. Lacasta[164], F. Lacava[75a,75b], H. Lacker[18], D. Lacour[128], N.N. Lad[97], E. Ladygin[38], A. Lafarge[40], B. Laforge[128], T. Lagouri[173], F.Z. Lahbabi[35a], S. Lai[55], J.E. Lambert[166], S. Lammers[68], W. Lampl[7], C. Lampoudis[154,d], G. Lamprinoudis[101], A.N. Lancaster[116], E. Lançon[29], U. Landgraf[54], M.P.J. Landon[95], V.S. Lang[54], O.K.B. Langrekken[126], A.J. Lankford[160], F. Lanni[36], K. Lantzsch[24], A. Lanza[73a], J.F. Laporte[136], T. Lari[71a], F. Lasagni Manghi[23b], M. Lassnig[36], V. Latonova[132], A. Laudrain[101], A. Laurier[152], S.D. Lawlor[141], Z. Lawrence[102], R. Lazaridou[168], M. Lazzaroni[71a,71b], B. Le[102], E.M. Le Boulicaut[51], L.T. Le Pottier[17a], B. Leban[23b,23a], A. Lebedev[81], M. LeBlanc[102], F. Ledroit-Guillon[60], S.C. Lee[150], S. Lee[47a,47b], T.F. Lee[93], L.L. Leeuw[33c], H.P. Lefebvre[96], M. Lefebvre[166], C. Leggett[17a], G. Lehmann Miotto[36], M. Leigh[56], W.A. Leight[104], W. Leinonen[114], A. Leisos[154,r], M.A.L. Leite[83c], C.E. Leitgeb[18], R. Leitner[134], K.J.C. Leney[44], T. Lenz[24], S. Leone[74a], C. Leonidopoulos[52], A. Leopold[146], C. Leroy[109], R. Les[108], C.G. Lester[32], M. Levchenko[37], J. Levêque[4], L.J. Levinson[170], G. Levrini[23b,23a], M.P. Lewicki[87], C. Lewis[140], D.J. Lewis[4], A. Li[5], B. Li[62b], C. Li[62a], C-Q. Li[111], H. Li[62a], H. Li[62b], H. Li[14c], H. Li[14b], H. Li[62b], J. Li[62c], K. Li[140], L. Li[62c], M. Li[14a,14e], S. Li[14a,14e], S. Li[62d,62c], T. Li[5], X. Li[105], Z. Li[127], Z. Li[155], Z. Li[14a,14e], S. Liang[14a,14e], Z. Liang[14a], M. Liberatore[136], B. Liberti[76a], K. Lie[64c], J. Lieber Marin[83e], H. Lien[68], K. Lin[108], R.E. Lindley[7], J.H. Lindon[2], E. Lipeles[129], A. Lipniacka[16], A. Lister[165], J.D. Little[4], B. Liu[14a], B.X. Liu[14d], D. Liu[62d,62c], E.H.L. Liu[20], J.B. Liu[62a], J.K.K. Liu[32], K. Liu[62d], K. Liu[62d,62c], M. Liu[62a], M.Y. Liu[62a], P. Liu[14a], Q. Liu[62d,140,62c], X. Liu[62a], X. Liu[62b], Y. Liu[14d,14e], Y.L. Liu[62b], Y.W. Liu[62a], J. Llorente Merino[144], S.L. Lloyd[95], E.M. Lobodzinska[48], P. Loch[7], T. Lohse[18], K. Lohwasser[141], E. Loiacono[48], M. Lokajicek[132,*],

J.D. Lomas[20], J.D. Long[163], I. Longarini[160], R. Longo[163], I. Lopez Paz[67], A. Lopez Solis[48], N. Lorenzo Martinez[4], A.M. Lory[110], G. Löschcke Centeno[148], O. Loseva[37], X. Lou[47a,47b], X. Lou[14a,14e], A. Lounis[66], P.A. Love[92], G. Lu[14a,14e], M. Lu[66], S. Lu[129], Y.J. Lu[65], H.J. Lubatti[140], C. Luci[75a,75b], F.L. Lucio Alves[14c], F. Luehring[68], I. Luise[147], O. Lukianchuk[66], O. Lundberg[146], B. Lund-Jensen[146,*], N.A. Luongo[6], M.S. Lutz[36], A.B. Lux[25], D. Lynn[29], R. Lysak[132], E. Lytken[99], V. Lyubushkin[38], T. Lyubushkina[38], M.M. Lyukova[147], M. Firdaus M. Soberi[52], H. Ma[29], K. Ma[62a], L.L. Ma[62b], W. Ma[62a], Y. Ma[122], G. Maccarrone[53], J.C. MacDonald[101], P.C. Machado De Abreu Farias[83e], R. Madar[40], T. Madula[97], J. Maeda[85], T. Maeno[29], H. Maguire[141], V. Maiboroda[136], A. Maio[131a,131b,131d], K. Maj[86a], O. Majersky[48], S. Majewski[124], N. Makovec[66], V. Maksimovic[15], B. Malaescu[128], Pa. Malecki[87], V.P. Maleev[37], F. Malek[60,m], M. Mali[94], D. Malito[96], U. Mallik[80,*], S. Maltezos[10], S. Malyukov[38], J. Mamuzic[13], G. Mancini[53], M.N. Mancini[26], G. Manco[73a,73b], J.P. Mandalia[95], I. Mandić[94], L. Manhaes de Andrade Filho[83a], I.M. Maniatis[170], J. Manjarres Ramos[90], D.C. Mankad[170], A. Mann[110], S. Manzoni[36], L. Mao[62c], X. Mapekula[33c], A. Marantis[154,r], G. Marchiori[5], M. Marcisovsky[132], C. Marcon[71a], M. Marinescu[20], S. Marium[48], M. Marjanovic[121], A. Markhoos[54], M. Markovitch[66], E.J. Marshall[92], Z. Marshall[17a], S. Marti-Garcia[164], T.A. Martin[135], V.J. Martin[52], B. Martin dit Latour[16], L. Martinelli[75a,75b], M. Martinez[13,s], P. Martinez Agullo[164], V.I. Martinez Outschoorn[104], P. Martinez Suarez[13], S. Martin-Haugh[135], G. Martinovicova[134], V.S. Martoiu[27b], A.C. Martyniuk[97], A. Marzin[36], D. Mascione[78a,78b], L. Masetti[101], T. Mashimo[155], J. Masik[102], A.L. Maslennikov[37], P. Massarotti[72a,72b], P. Mastrandrea[74a,74b], A. Mastroberardino[43b,43a], T. Masubuchi[155], T. Mathisen[162], J. Matousek[134], N. Matsuzawa[155], J. Maurer[27b], A.J. Maury[66], B. Maček[94], D.A. Maximov[37], A.E. May[102], R. Mazini[150], I. Maznas[116], M. Mazza[108], S.M. Mazza[137], E. Mazzeo[71a,71b], C. Mc Ginn[29], J.P. Mc Gowan[166], S.P. Mc Kee[107], C.C. McCracken[165], E.F. McDonald[106], A.E. McDougall[115], J.A. Mcfayden[148], R.P. McGovern[129], G. Mchedlidze[151b], R.P. Mckenzie[33g], T.C. Mclachlan[48], D.J. Mclaughlin[97], S.J. McMahon[135], C.M. Mcpartland[93], R.A. McPherson[166,w], S. Mehlhase[110], A. Mehta[93], D. Melini[164], B.R. Mellado Garcia[33g], A.H. Melo[55], F. Meloni[48], A.M. Mendes Jacques Da Costa[102], H.Y. Meng[156], L. Meng[92], S. Menke[111], M. Mentink[36], E. Meoni[43b,43a], G. Mercado[116], S. Merianos[154], C. Merlassino[69a,69c], L. Merola[72a,72b], C. Meroni[71a,71b], J. Metcalfe[6], A.S. Mete[6], E. Meuser[101], C. Meyer[68], J-P. Meyer[136], R.P. Middleton[135], L. Mijović[52], G. Mikenberg[170], M. Mikestikova[132], M. Mikuž[94], H. Mildner[101], A. Milic[36], D.W. Miller[39], E.H. Miller[145], L.S. Miller[34], A. Milov[170], D.A. Milstead[47a,47b], T. Min[14c], A.A. Minaenko[37], I.A. Minashvili[151b], L. Mince[59], A.I. Mincer[118], B. Mindur[86a], M. Mineev[38], Y. Mino[88], L.M. Mir[13], M. Miralles Lopez[59], M. Mironova[17a], A. Mishima[155], M.C. Missio[114], A. Mitra[168], V.A. Mitsou[164], Y. Mitsumori[112], O. Miu[156], P.S. Miyagawa[95], T. Mkrtchyan[63a], M. Mlinarevic[97], T. Mlinarevic[97], M. Mlynarikova[36], S. Mobius[19], P. Mogg[110], M.H. Mohamed Farook[113], A.F. Mohammed[14a,14e], S. Mohapatra[41], G. Mokgatitswane[33g], L. Moleri[170], B. Mondal[143], S. Mondal[133], K. Mönig[48], E. Monnier[103], L. Monsonis Romero[164], J. Montejo Berlingen[13], M. Montella[120], F. Monticelli[91], S. Monzani[69a,69c], N. Morange[66], A.L. Moreira De Carvalho[48], M. Moreno Llácer[164], C. Moreno Martinez[56], P. Morettini[57b], S. Morgenstern[36], M. Morii[61], M. Morinaga[155], F. Morodei[75a,75b], L. Morvaj[36], P. Moschovakos[36], B. Moser[36], M. Mosidze[151b], T. Moskalets[54], P. Moskvitina[114], J. Moss[31,j], P. Moszkowicz[86a], A. Moussa[35d], E.J.W. Moyse[104], O. Mtintsilana[33g], S. Muanza[103], J. Mueller[130], D. Muenstermann[92], R. Müller[19], G.A. Mullier[162], A.J. Mullin[32], J.J. Mullin[129], D.P. Mungo[156], D. Munoz Perez[164], F.J. Munoz Sanchez[102], M. Murin[102], W.J. Murray[168,135], M. Muškinja[94], C. Mwewa[29], A.G. Myagkov[37,a], A.J. Myers[8], G. Myers[107], M. Myska[133], B.P. Nachman[17a], O. Nackenhorst[49], K. Nagai[127], K. Nagano[84], J.L. Nagle[29,ag], E. Nagy[103], A.M. Nairz[36], Y. Nakahama[84], K. Nakamura[84], K. Nakkalil[5], H. Nanjo[125], E.A. Narayanan[113], I. Naryshkin[37], L. Nasella[71a,71b], M. Naseri[34], S. Nasri[117b], C. Nass[24], G. Navarro[22a], J. Navarro-Gonzalez[164], R. Nayak[153], A. Nayaz[18], P.Y. Nechaeva[37], S. Nechaeva[23b,23a], F. Nechansky[48], L. Nedic[127], T.J. Neep[20], A. Negri[73a,73b], M. Negrini[23b], C. Nellist[115], C. Nelson[105], K. Nelson[107], S. Nemecek[132], M. Nessi[36,g], M.S. Neubauer[163], F. Neuhaus[101], J. Neundorf[48], P.R. Newman[20], C.W. Ng[130],

Y.W.Y. Ng[48], B. Ngair[117a], H.D.N. Nguyen[109], R.B. Nickerson[127], R. Nicolaidou[136], J. Nielsen[137], M. Niemeyer[55], J. Niermann[55], N. Nikiforou[36], V. Nikolaenko[37,a], I. Nikolic-Audit[128], K. Nikolopoulos[20], P. Nilsson[29], I. Ninca[48], G. Ninio[153], A. Nisati[75a], N. Nishu[2], R. Nisius[111], J-E. Nitschke[50], E.K. Nkadimeng[33g], T. Nobe[155], T. Nommensen[149], M.B. Norfolk[141], R.R.B. Norisam[97], B.J. Norman[34], M. Noury[35a], J. Novak[94], T. Novak[94], L. Novotny[133], R. Novotny[113], L. Nozka[123], K. Ntekas[160], N.M.J. Nunes De Moura Junior[83b], J. Ocariz[128], A. Ochi[85], I. Ochoa[131a], S. Oerdek[48,t], J.T. Offermann[39], A. Ogrodnik[134], A. Oh[102], C.C. Ohm[146], H. Oide[84], R. Oishi[155], M.L. Ojeda[48], Y. Okumura[155], L.F. Oleiro Seabra[131a], S.A. Olivares Pino[138d], G. Oliveira Correa[13], D. Oliveira Damazio[29], D. Oliveira Goncalves[83a], J.L. Oliver[160], Ö.O. Öncel[54], A.P. O'Neill[19], A. Onofre[131a,131e], P.U.E. Onyisi[11], M.J. Oreglia[39], G.E. Orellana[91], D. Orestano[77a,77b], N. Orlando[13], R.S. Orr[156], V. O'Shea[59], L.M. Osojnak[129], R. Ospanov[62a], G. Otero y Garzon[30], H. Otono[89], P.S. Ott[63a], G.J. Ottino[17a], M. Ouchrif[35d], F. Ould-Saada[126], T. Ovsiannikova[140], M. Owen[59], R.E. Owen[135], V.E. Ozcan[21a], F. Ozturk[87], N. Ozturk[8], S. Ozturk[82], H.A. Pacey[127], A. Pacheco Pages[13], C. Padilla Aranda[13], G. Padovano[75a,75b], S. Pagan Griso[17a], G. Palacino[68], A. Palazzo[70a,70b], J. Pampel[24], J. Pan[173], T. Pan[64a], D.K. Panchal[11], C.E. Pandini[115], J.G. Panduro Vazquez[135], H.D. Pandya[1], H. Pang[14b], P. Pani[48], G. Panizzo[69a,69c], L. Panwar[128], L. Paolozzi[56], S. Parajuli[163], A. Paramonov[6], C. Paraskevopoulos[53], D. Paredes Hernandez[64b], A. Pareti[73a,73b], K.R. Park[41], T.H. Park[156], M.A. Parker[32], F. Parodi[57b,57a], E.W. Parrish[116], V.A. Parrish[52], J.A. Parsons[41], U. Parzefall[54], B. Pascual Dias[109], L. Pascual Dominguez[100], E. Pasqualucci[75a], S. Passaggio[57b], F. Pastore[96], P. Patel[87], U.M. Patel[51], J.R. Pater[102], T. Pauly[36], C.I. Pazos[159], J. Pearkes[145], M. Pedersen[126], R. Pedro[131a], S.V. Peleganchuk[37], O. Penc[36], E.A. Pender[52], G.D. Penn[173], K.E. Penski[110], M. Penzin[37], B.S. Peralva[83d], A.P. Pereira Peixoto[140], L. Pereira Sanchez[145], D.V. Perepelitsa[29,ag], E. Perez Codina[157a], M. Perganti[10], H. Pernegger[36], O. Perrin[40], K. Peters[48], R.F.Y. Peters[102], B.A. Petersen[36], T.C. Petersen[42], E. Petit[103], V. Petousis[133], C. Petridou[154,d], T. Petru[134], A. Petrukhin[143], M. Pettee[17a], N.E. Pettersson[36], A. Petukhov[37], K. Petukhova[134], R. Pezoa[138f], L. Pezzotti[36], G. Pezzullo[173], T.M. Pham[171], T. Pham[106], P.W. Phillips[135], G. Piacquadio[147], E. Pianori[17a], F. Piazza[124], R. Piegaia[30], D. Pietreanu[27b], A.D. Pilkington[102], M. Pinamonti[69a,69c], J.L. Pinfold[2], B.C. Pinheiro Pereira[131a], A.E. Pinto Pinoargote[136,136], L. Pintucci[69a,69c], K.M. Piper[148], A. Pirttikoski[56], D.A. Pizzi[34], L. Pizzimento[64b], A. Pizzini[115], M.-A. Pleier[29], V. Pleskot[134], E. Plotnikova[38], G. Poddar[95], R. Poettgen[99], L. Poggioli[128], I. Pokharel[55], S. Polacek[134], G. Polesello[73a], A. Poley[144,157a], A. Polini[23b], C.S. Pollard[168], Z.B. Pollock[120], E. Pompa Pacchi[75a,75b], N.I. Pond[97], D. Ponomarenko[114], L. Pontecorvo[36], S. Popa[27a], G.A. Popeneciu[27d], A. Poreba[36], D.M. Portillo Quintero[157a], S. Pospisil[133], M.A. Postill[141], P. Postolache[27c], K. Potamianos[168], P.A. Potepa[86a], I.N. Potrap[38], C.J. Potter[32], H. Potti[1], J. Poveda[164], M.E. Pozo Astigarraga[36], A. Prades Ibanez[164], J. Pretel[54], D. Price[102], M. Primavera[70a], M.A. Principe Martin[100], R. Privara[123], T. Procter[59], M.L. Proffitt[140], N. Proklova[129], K. Prokofiev[64c], G. Proto[111], J. Proudfoot[6], M. Przybycien[86a], W.W. Przygoda[86b], A. Psallidas[46], J.E. Puddefoot[141], D. Pudzha[37], D. Pyatiizbyantseva[37], J. Qian[107], D. Qichen[102], Y. Qin[13], T. Qiu[52], A. Quadt[55], M. Queitsch-Maitland[102], G. Quetant[56], R.P. Quinn[165], G. Rabanal Bolanos[61], D. Rafanoharana[54], F. Raffaeli[76a,76b], F. Ragusa[71a,71b], J.L. Rainbolt[39], J.A. Raine[56], S. Rajagopalan[29], E. Ramakoti[37], I.A. Ramirez-Berend[34], K. Ran[48,14e], N.P. Rapheeha[33g], H. Rasheed[27b], V. Raskina[128], D.F. Rassloff[63a], A. Rastogi[17a], S. Rave[101], B. Ravina[55], I. Ravinovich[170], M. Raymond[36], A.L. Read[126], N.P. Readioff[141], D.M. Rebuzzi[73a,73b], G. Redlinger[29], A.S. Reed[111], K. Reeves[26], J.A. Reidelsturz[172], D. Reikher[153], A. Rej[49], C. Rembser[36], M. Renda[27b], M.B. Rendel[111], F. Renner[48], A.G. Rennie[160], A.L. Rescia[48], S. Resconi[71a], M. Ressegotti[57b,57a], S. Rettie[36], J.G. Reyes Rivera[108], E. Reynolds[17a], O.L. Rezanova[37], P. Reznicek[134], H. Riani[35d], N. Ribaric[92], E. Ricci[78a,78b], R. Richter[111], S. Richter[47a,47b], E. Richter-Was[86b], M. Ridel[128], S. Ridouani[35d], P. Rieck[118], P. Riedler[36], E.M. Riefel[47a,47b], J.O. Rieger[115], M. Rijssenbeek[147], M. Rimoldi[36], L. Rinaldi[23b,23a], T.T. Rinn[29], M.P. Rinnagel[110], G. Ripellino[162], I. Riu[13], J.C. Rivera Vergara[166], F. Rizatdinova[122], E. Rizvi[95], B.R. Roberts[17a], S.H. Robertson[105,w], D. Robinson[32],

C.M. Robles Gajardo[138f], M. Robles Manzano[101], A. Robson[59], A. Rocchi[76a,76b], C. Roda[74a,74b], S. Rodriguez Bosca[36], Y. Rodriguez Garcia[22a], A. Rodriguez Rodriguez[54], A.M. Rodríguez Vera[116], S. Roe[36], J.T. Roemer[160], A.R. Roepe-Gier[137], J. Roggel[172], O. Røhne[126], R.A. Rojas[104], C.P.A. Roland[128], J. Roloff[29], A. Romaniouk[37], E. Romano[73a,73b], M. Romano[23b], A.C. Romero Hernandez[163], N. Rompotis[93], L. Roos[128], S. Rosati[75a], B.J. Rosser[39], E. Rossi[127], E. Rossi[72a,72b], L.P. Rossi[61], L. Rossini[54], R. Rosten[120], M. Rotaru[27b], B. Rottler[54], C. Rougier[90], D. Rousseau[66], D. Rousso[48], A. Roy[163], S. Roy-Garand[156], A. Rozanov[103], Z.M.A. Rozario[59], Y. Rozen[152], A. Rubio Jimenez[164], A.J. Ruby[93], V.H. Ruelas Rivera[18], T.A. Ruggeri[1], A. Ruggiero[127], A. Ruiz-Martinez[164], A. Rummler[36], Z. Rurikova[54], N.A. Rusakovich[38], H.L. Russell[166], G. Russo[75a,75b], J.P. Rutherfoord[7], S. Rutherford Colmenares[32], M. Rybar[134], E.B. Rye[126], A. Ryzhov[44], J.A. Sabater Iglesias[56], P. Sabatini[164], H.F-W. Sadrozinski[137], F. Safai Tehrani[75a], B. Safarzadeh Samani[135], S. Saha[1], M. Sahinsoy[111], A. Saibel[164], M. Saimpert[136], M. Saito[155], T. Saito[155], A. Sala[71a,71b], D. Salamani[36], A. Salnikov[145], J. Salt[164], A. Salvador Salas[153], D. Salvatore[43b,43a], F. Salvatore[148], A. Salzburger[36], D. Sammel[54], E. Sampson[92], D. Sampsonidis[154,d], D. Sampsonidou[124], J. Sánchez[164], V. Sanchez Sebastian[164], H. Sandaker[126], C.O. Sander[48], J.A. Sandesara[104], M. Sandhoff[172], C. Sandoval[22b], L. Sanfilippo[63a], D.P.C. Sankey[135], T. Sano[88], A. Sansoni[53], L. Santi[75a,75b], C. Santoni[40], H. Santos[131a,131b], A. Santra[170], E. Sanzani[23b,23a], K.A. Saoucha[161], J.G. Saraiva[131a,131d], J. Sardain[7], O. Sasaki[84], K. Sato[158], C. Sauer[63b], E. Sauvan[4], P. Savard[156,ae], R. Sawada[155], C. Sawyer[135], L. Sawyer[98], C. Sbarra[23b], A. Sbrizzi[23b,23a], T. Scanlon[97], J. Schaarschmidt[140], U. Schäfer[101], A.C. Schaffer[66,44], D. Schaile[110], R.D. Schamberger[147], C. Scharf[18], M.M. Schefer[19], V.A. Schegelsky[37], D. Scheirich[134], M. Schernau[160], C. Scheulen[55], C. Schiavi[57b,57a], M. Schioppa[43b,43a], B. Schlag[145], K.E. Schleicher[54], S. Schlenker[36], J. Schmeing[172], M.A. Schmidt[172], K. Schmieden[101], C. Schmitt[101], N. Schmitt[101], S. Schmitt[48], L. Schoeffel[136], A. Schoening[63b], P.G. Scholer[34], E. Schopf[127], M. Schott[24], J. Schovancova[36], S. Schramm[56], T. Schroer[56], H-C. Schultz-Coulon[63a], M. Schumacher[54], B.A. Schumm[137], Ph. Schune[136], A.J. Schuy[140], H.R. Schwartz[137], A. Schwartzman[145], T.A. Schwarz[107], Ph. Schwemling[136], R. Schwienhorst[108], A. Sciandra[29], G. Sciolla[26], F. Scuri[74a], C.D. Sebastiani[93], K. Sedlaczek[116], S.C. Seidel[113], A. Seiden[137], B.D. Seidlitz[41], C. Seitz[48], J.M. Seixas[83b], G. Sekhniaidze[72a], L. Selem[60], N. Semprini-Cesari[23b,23a], D. Sengupta[56], V. Senthilkumar[164], L. Serin[66], M. Sessa[76a,76b], H. Severini[121], F. Sforza[57b,57a], A. Sfyrla[56], Q. Sha[14a], E. Shabalina[55], A.H. Shah[32], R. Shaheen[146], J.D. Shahinian[129], D. Shaked Renous[170], L.Y. Shan[14a], M. Shapiro[17a], A. Sharma[36], A.S. Sharma[165], P. Sharma[80], P.B. Shatalov[37], K. Shaw[148], S.M. Shaw[102], Q. Shen[62c,5], D.J. Sheppard[144], P. Sherwood[97], L. Shi[97], X. Shi[14a], C.O. Shimmin[173], J.D. Shinner[96], I.P.J. Shipsey[127,*], S. Shirabe[89], M. Shiyakova[38,u], M.J. Shochet[39], J. Shojaii[106], D.R. Shope[126], B. Shrestha[121], S. Shrestha[120,ah], M.J. Shroff[166], P. Sicho[132], A.M. Sickles[163], E. Sideras Haddad[33g], A.C. Sidley[115], A. Sidoti[23b], F. Siegert[50], Dj. Sijacki[15], F. Sili[91], J.M. Silva[52], M.V. Silva Oliveira[29], S.B. Silverstein[47a], S. Simion[66], R. Simoniello[36], E.L. Simpson[102], H. Simpson[148], L.R. Simpson[107], N.D. Simpson[99], S. Simsek[82], S. Sindhu[55], P. Sinervo[156], S. Singh[156], S. Sinha[48], S. Sinha[102], M. Sioli[23b,23a], I. Siral[36], E. Sitnikova[48], J. Sjölin[47a,47b], A. Skaf[55], E. Skorda[20], P. Skubic[121], M. Slawinska[87], V. Smakhtin[170], B.H. Smart[135], S.Yu. Smirnov[37], Y. Smirnov[37], L.N. Smirnova[37,a], O. Smirnova[99], A.C. Smith[41], D.R. Smith[160], E.A. Smith[39], H.A. Smith[127], J.L. Smith[102], R. Smith[145], M. Smizanska[92], K. Smolek[133], A.A. Snesarev[37], S.R. Snider[156], H.L. Snoek[115], S. Snyder[29], R. Sobie[166,w], A. Soffer[153], C.A. Solans Sanchez[36], E.Yu. Soldatov[37], U. Soldevila[164], A.A. Solodkov[37], S. Solomon[26], A. Soloshenko[38], K. Solovieva[54], O.V. Solovyanov[40], P. Sommer[36], A. Sonay[13], W.Y. Song[157b], A. Sopczak[133], A.L. Sopio[97], F. Sopkova[28b], J.D. Sorenson[113], I.R. Sotarriva Alvarez[139], V. Sothilingam[63a], O.J. Soto Sandoval[138c,138b], S. Sottocornola[68], R. Soualah[161], Z. Soumaimi[35e], D. South[48], N. Soybelman[170], S. Spagnolo[70a,70b], M. Spalla[111], D. Sperlich[54], G. Spigo[36], S. Spinali[92], D.P. Spiteri[59], M. Spousta[134], E.J. Staats[34], R. Stamen[63a], A. Stampekis[20], M. Standke[24], E. Stanecka[87], W. Stanek-Maslouska[48], M.V. Stange[50], B. Stanislaus[17a], M.M. Stanitzki[48], B. Stapf[48], E.A. Starchenko[37],

G.H. Stark[137], J. Stark[90], P. Staroba[132], P. Starovoitov[63a], S. Stärz[105], R. Staszewski[87], G. Stavropoulos[46], J. Steentoft[162], P. Steinberg[29], B. Stelzer[144,157a], H.J. Stelzer[130], O. Stelzer-Chilton[157a], H. Stenzel[58], T.J. Stevenson[148], G.A. Stewart[36], J.R. Stewart[122], M.C. Stockton[36], G. Stoicea[27b], M. Stolarski[131a], S. Stonjek[111], A. Straessner[50], J. Strandberg[146], S. Strandberg[47a,47b], M. Stratmann[172], M. Strauss[121], T. Strebler[103], P. Strizenec[28b], R. Ströhmer[167], D.M. Strom[124], R. Stroynowski[44], A. Strubig[47a,47b], S.A. Stucci[29], B. Stugu[16], J. Stupak[121], N.A. Styles[48], D. Su[145], S. Su[62a], W. Su[62d], X. Su[62a], D. Suchy[28a], K. Sugizaki[155], V.V. Sulin[37], M.J. Sullivan[93], D.M.S. Sultan[127], L. Sultanaliyeva[37], S. Sultansoy[3b], T. Sumida[88], S. Sun[107], S. Sun[171], O. Sunneborn Gudnadottir[162], N. Sur[103], M.R. Sutton[148], H. Suzuki[158], M. Svatos[132], M. Swiatlowski[157a], T. Swirski[167], I. Sykora[28a], M. Sykora[134], T. Sykora[134], D. Ta[101], K. Tackmann[48,t], A. Taffard[160], R. Tafirout[157a], J.S. Tafoya Vargas[66], Y. Takubo[84], M. Talby[103], A.A. Talyshev[37], K.C. Tam[64b], N.M. Tamir[153], A. Tanaka[155], J. Tanaka[155], R. Tanaka[66], M. Tanasini[147], Z. Tao[165], S. Tapia Araya[138f], S. Tapprogge[101], A. Tarek Abouelfadl Mohamed[108], S. Tarem[152], K. Tariq[14a], G. Tarna[27b], G.F. Tartarelli[71a], M.J. Tartarin[90], P. Tas[134], M. Tasevsky[132], E. Tassi[43b,43a], A.C. Tate[163], G. Tateno[155], Y. Tayalati[35e,v], G.N. Taylor[106], W. Taylor[157b], A.S. Tee[171], R. Teixeira De Lima[145], P. Teixeira-Dias[96], J.J. Teoh[156], K. Terashi[155], J. Terron[100], S. Terzo[13], M. Testa[53], R.J. Teuscher[156,w], A. Thaler[79], O. Theiner[56], N. Themistokleous[52], T. Theveneaux-Pelzer[103], O. Thielmann[172], D.W. Thomas[96], J.P. Thomas[20], E.A. Thompson[17a], P.D. Thompson[20], E. Thomson[129], R.E. Thornberry[44], C. Tian[62a], Y. Tian[55], V. Tikhomirov[37,a], Yu.A. Tikhonov[37], S. Timoshenko[37], D. Timoshyn[134], E.X.L. Ting[1], P. Tipton[173], S.H. Tlou[33g], K. Todome[139], S. Todorova-Nova[134], S. Todt[50], L. Toffolin[69a,69c], M. Togawa[84], J. Tojo[89], S. Tokár[28a], K. Tokushuku[84], O. Toldaiev[68], R. Tombs[32], M. Tomoto[84,112], L. Tompkins[145,l], K.W. Topolnicki[86b], E. Torrence[124], H. Torres[90], E. Torró Pastor[164], M. Toscani[30], C. Tosciri[39], M. Tost[11], D.R. Tovey[141], A. Traeet[16], I.S. Trandafir[27b], T. Trefzger[167], A. Tricoli[29], I.M. Trigger[157a], S. Trincaz-Duvoid[128], D.A. Trischuk[26], B. Trocmé[60], L. Truong[33c], M. Trzebinski[87], A. Trzupek[87], F. Tsai[147], M. Tsai[107], A. Tsiamis[154,d], P.V. Tsiareshka[37], S. Tsigaridas[157a], A. Tsirigotis[154,r], V. Tsiskaridze[156], E.G. Tskhadadze[151a], M. Tsopoulou[154], Y. Tsujikawa[88], I.I. Tsukerman[37], V. Tsulaia[17a], S. Tsuno[84], K. Tsuri[119], D. Tsybychev[147], Y. Tu[64b], A. Tudorache[27b], V. Tudorache[27b], A.N. Tuna[61], S. Turchikhin[57b,57a], I. Turk Cakir[3a], R. Turra[71a], T. Turtuvshin[38,x], P.M. Tuts[41], S. Tzamarias[154,d], E. Tzovara[101], F. Ukegawa[158], P.A. Ulloa Poblete[138c,138b], E.N. Umaka[29], G. Unal[36], A. Undrus[29], G. Unel[160], J. Urban[28b], P. Urrejola[138a], G. Usai[8], R. Ushioda[139], M. Usman[109], Z. Uysal[82], V. Vacek[133], B. Vachon[105], T. Vafeiadis[36], A. Vaitkus[97], C. Valderanis[110], E. Valdes Santurio[47a,47b], M. Valente[157a], S. Valentinetti[23b,23a], A. Valero[164], E. Valiente Moreno[164], A. Vallier[90], J.A. Valls Ferrer[164], D.R. Van Arneman[115], T.R. Van Daalen[140], A. Van Der Graaf[49], P. Van Gemmeren[6], M. Van Rijnbach[36], S. Van Stroud[97], I. Van Vulpen[115], P. Vana[134], M. Vanadia[76a,76b], W. Vandelli[36], E.R. Vandewall[122], D. Vannicola[153], L. Vannoli[53], R. Vari[75a], E.W. Varnes[7], C. Varni[17b], T. Varol[150], D. Varouchas[66], L. Varriale[164], K.E. Varvell[149], M.E. Vasile[27b], L. Vaslin[84], G.A. Vasquez[166], A. Vasyukov[38], R. Vavricka[101], T. Vazquez Schroeder[36], J. Veatch[31], V. Vecchio[102], M.J. Veen[104], I. Veliscek[29], L.M. Veloce[156], F. Veloso[131a,131c], S. Veneziano[75a], A. Ventura[70a,70b], S. Ventura Gonzalez[136], A. Verbytskyi[111], M. Verducci[74a,74b], C. Vergis[95], M. Verissimo De Araujo[83b], W. Verkerke[115], J.C. Vermeulen[115], C. Vernieri[145], M. Vessella[104], M.C. Vetterli[144,ae], A. Vgenopoulos[154,d], N. Viaux Maira[138f], T. Vickey[141], O.E. Vickey Boeriu[141], G.H.A. Viehhauser[127], L. Vigani[63b], M. Villa[23b,23a], M. Villaplana Perez[164], E.M. Villhauer[52], E. Vilucchi[53], M.G. Vincter[34], A. Visibile[115], C. Vittori[36], I. Vivarelli[23b,23a], E. Voevodina[111], F. Vogel[110], J.C. Voigt[50], P. Vokac[133], Yu. Volkotrub[86b], J. Von Ahnen[48], E. Von Toerne[24], B. Vormwald[36], V. Vorobel[134], K. Vorobev[37], M. Vos[164], K. Voss[143], M. Vozak[115], L. Vozdecky[121], N. Vranjes[15], M. Vranjes Milosavljevic[15], M. Vreeswijk[115], N.K. Vu[62d,62c], R. Vuillermet[36], O. Vujinovic[101], I. Vukotic[39], S. Wada[158], C. Wagner[104], J.M. Wagner[17a], W. Wagner[172], S. Wahdan[172], H. Wahlberg[91], M. Wakida[112], J. Walder[135], R. Walker[110], W. Walkowiak[143], A. Wall[129], E.J. Wallin[99], T. Wamorkar[6], A.Z. Wang[137], C. Wang[101], C. Wang[11], H. Wang[17a], J. Wang[64c], R. Wang[61],

R. Wang[6], S.M. Wang[150], S. Wang[62b], S. Wang[14a], T. Wang[62a], W.T. Wang[80], W. Wang[14a], X. Wang[14c], X. Wang[163], X. Wang[62c], Y. Wang[62d], Y. Wang[14c], Z. Wang[107], Z. Wang[62d,51,62c], Z. Wang[107], A. Warburton[105], R.J. Ward[20], N. Warrack[59], S. Waterhouse[96], A.T. Watson[20], H. Watson[59], M.F. Watson[20], E. Watton[59,135], G. Watts[140], B.M. Waugh[97], J.M. Webb[54], C. Weber[29], H.A. Weber[18], M.S. Weber[19], S.M. Weber[63a], C. Wei[62a], Y. Wei[54], A.R. Weidberg[127], E.J. Weik[118], J. Weingarten[49], C. Weiser[54], C.J. Wells[48], T. Wenaus[29], B. Wendland[49], T. Wengler[36], N.S. Wenke[111], N. Wermes[24], M. Wessels[63a], A.M. Wharton[92], A.S. White[61], A. White[8], M.J. White[1], D. Whiteson[160], L. Wickremasinghe[125], W. Wiedenmann[171], M. Wielers[135], C. Wiglesworth[42], D.J. Wilbern[121], H.G. Wilkens[36], J.J.H. Wilkinson[32], D.M. Williams[41], H.H. Williams[129], S. Williams[32], S. Willocq[104], B.J. Wilson[102], P.J. Windischhofer[39], F.I. Winkel[30], F. Winklmeier[124], B.T. Winter[54], J.K. Winter[102], M. Wittgen[145], M. Wobisch[98], T. Wojtkowski[60], Z. Wolffs[115], J. Wollrath[160], M.W. Wolter[87], H. Wolters[131a,131c], M.C. Wong[137], E.L. Woodward[41], S.D. Worm[48], B.K. Wosiek[87], K.W. Woźniak[87], S. Wozniewski[55], K. Wraight[59], C. Wu[20], M. Wu[14d], M. Wu[114], S.L. Wu[171], X. Wu[56], Y. Wu[62a], Z. Wu[4], J. Wuerzinger[111,ac], T.R. Wyatt[102], B.M. Wynne[52], S. Xella[42], L. Xia[14c], M. Xia[14b], J. Xiang[64c], M. Xie[62a], S. Xin[14a,14e], A. Xiong[124], J. Xiong[17a], D. Xu[14a], H. Xu[62a], L. Xu[62a], R. Xu[129], T. Xu[107], Y. Xu[14b], Z. Xu[52], Z. Xu[14c], B. Yabsley[149], S. Yacoob[33a], Y. Yamaguchi[139], E. Yamashita[155], H. Yamauchi[158], T. Yamazaki[17a], Y. Yamazaki[85], J. Yan[62c], S. Yan[59], Z. Yan[104], H.J. Yang[62c,62d], H.T. Yang[62a], S. Yang[62a], T. Yang[64c], X. Yang[36], X. Yang[14a], Y. Yang[44], Y. Yang[62a], Z. Yang[62a], W-M. Yao[17a], H. Ye[14c], H. Ye[55], J. Ye[14a], S. Ye[29], X. Ye[62a], Y. Yeh[97], I. Yeletskikh[38], B. Yeo[17b], M.R. Yexley[97], T.P. Yildirim[127], P. Yin[41], K. Yorita[169], S. Younas[27b], C.J.S. Young[36], C. Young[145], C. Yu[14a,14e], Y. Yu[62a], M. Yuan[107], R. Yuan[62d,62c], L. Yue[97], M. Zaazoua[62a], B. Zabinski[87], E. Zaid[52], Z.K. Zak[87], T. Zakareishvili[164], N. Zakharchuk[34], S. Zambito[56], J.A. Zamora Saa[138d,138b], J. Zang[155], D. Zanzi[54], O. Zaplatilek[133], C. Zeitnitz[172], H. Zeng[14a], J.C. Zeng[163], D.T. Zenger Jr[26], O. Zenin[37], T. Ženiš[28a], S. Zenz[95], S. Zerradi[35a], D. Zerwas[66], M. Zhai[14a,14e], D.F. Zhang[141], J. Zhang[62b], J. Zhang[6], K. Zhang[14a,14e], L. Zhang[62a], L. Zhang[14c], P. Zhang[14a,14e], R. Zhang[171], S. Zhang[107], S. Zhang[90], T. Zhang[155], X. Zhang[62c], X. Zhang[62b], Y. Zhang[62c], Y. Zhang[97], Y. Zhang[14c], Z. Zhang[17a], Z. Zhang[66], H. Zhao[140], T. Zhao[62b], Y. Zhao[137], Z. Zhao[62a], Z. Zhao[62a], A. Zhemchugov[38], J. Zheng[14c], K. Zheng[163], X. Zheng[62a], Z. Zheng[145], D. Zhong[163], B. Zhou[107], H. Zhou[7], N. Zhou[62c], Y. Zhou[14b], Y. Zhou[14c], Y. Zhou[7], C.G. Zhu[62b], J. Zhu[107], X. Zhu[62d], Y. Zhu[62c], Y. Zhu[62a], X. Zhuang[14a], K. Zhukov[37], N.I. Zimine[38], J. Zinsser[63b], M. Ziolkowski[143], L. Živković[15], A. Zoccoli[23b,23a], K. Zoch[61], T.G. Zorbas[141], O. Zormpa[46], W. Zou[41], L. Zwalinski[36].

[1]Department of Physics, University of Adelaide, Adelaide; Australia.
[2]Department of Physics, University of Alberta, Edmonton AB; Canada.
[3(a)]Department of Physics, Ankara University, Ankara; [(b)]Division of Physics, TOBB University of Economics and Technology, Ankara; Türkiye.
[4]LAPP, Université Savoie Mont Blanc, CNRS/IN2P3, Annecy; France.
[5]APC, Université Paris Cité, CNRS/IN2P3, Paris; France.
[6]High Energy Physics Division, Argonne National Laboratory, Argonne IL; United States of America.
[7]Department of Physics, University of Arizona, Tucson AZ; United States of America.
[8]Department of Physics, University of Texas at Arlington, Arlington TX; United States of America.
[9]Physics Department, National and Kapodistrian University of Athens, Athens; Greece.
[10]Physics Department, National Technical University of Athens, Zografou; Greece.
[11]Department of Physics, University of Texas at Austin, Austin TX; United States of America.
[12]Institute of Physics, Azerbaijan Academy of Sciences, Baku; Azerbaijan.
[13]Institut de Física d'Altes Energies (IFAE), Barcelona Institute of Science and Technology, Barcelona; Spain.
[14(a)]Institute of High Energy Physics, Chinese Academy of Sciences, Beijing; [(b)]Physics Department, Tsinghua University, Beijing; [(c)]Department of Physics, Nanjing University, Nanjing; [(d)]School of Science, Shenzhen Campus of Sun Yat-sen University; [(e)]University of Chinese Academy of Science (UCAS), Beijing; China.
[15]Institute of Physics, University of Belgrade, Belgrade; Serbia.
[16]Department for Physics and Technology, University of Bergen, Bergen; Norway.
[17(a)]Physics Division, Lawrence Berkeley National Laboratory, Berkeley CA; [(b)]University of California, Berkeley CA; United States of America.

[18]Institut für Physik, Humboldt Universität zu Berlin, Berlin; Germany.
[19]Albert Einstein Center for Fundamental Physics and Laboratory for High Energy Physics, University of Bern, Bern; Switzerland.
[20]School of Physics and Astronomy, University of Birmingham, Birmingham; United Kingdom.
[21(a)]Department of Physics, Bogazici University, Istanbul; [(b)]Department of Physics Engineering, Gaziantep University, Gaziantep; [(c)]Department of Physics, Istanbul University, Istanbul; Türkiye.
[22(a)]Facultad de Ciencias *y* Centro de Investigaciónes, Universidad Antonio Nariño, Bogotá; [(b)]Departamento de Física, Universidad Nacional de Colombia, Bogotá; Colombia.
[23(a)]Dipartimento di Fisica e Astronomia A. Righi, Università di Bologna, Bologna; [(b)]INFN Sezione di Bologna; Italy.
[24]Physikalisches Institut, Universität Bonn, Bonn; Germany.
[25]Department of Physics, Boston University, Boston MA; United States of America.
[26]Department of Physics, Brandeis University, Waltham MA; United States of America.
[27(a)]Transilvania University of Brasov, Brasov; [(b)]Horia Hulubei National Institute of Physics and Nuclear Engineering, Bucharest; [(c)]Department of Physics, Alexandru Ioan Cuza University of Iasi, Iasi; [(d)]National Institute for Research and Development of Isotopic and Molecular Technologies, Physics Department, Cluj-Napoca; [(e)]National University of Science and Technology Politechnica, Bucharest; [(f)]West University in Timisoara, Timisoara; [(g)]Faculty of Physics, University of Bucharest, Bucharest; Romania.
[28(a)]Faculty of Mathematics, Physics and Informatics, Comenius University, Bratislava; [(b)]Department of Subnuclear Physics, Institute of Experimental Physics of the Slovak Academy of Sciences, Kosice; Slovak Republic.
[29]Physics Department, Brookhaven National Laboratory, Upton NY; United States of America.
[30]Universidad de Buenos Aires, Facultad de Ciencias Exactas *y* Naturales, Departamento de Física, *y* CONICET, Instituto de Física de Buenos Aires (IFIBA), Buenos Aires; Argentina.
[31]California State University, CA; United States of America.
[32]Cavendish Laboratory, University of Cambridge, Cambridge; United Kingdom.
[33(a)]Department of Physics, University of Cape Town, Cape Town; [(b)]iThemba Labs, Western Cape; [(c)]Department of Mechanical Engineering Science, University of Johannesburg, Johannesburg; [(d)]National Institute of Physics, University of the Philippines Diliman (Philippines); [(e)]University of South Africa, Department of Physics, Pretoria; [(f)]University of Zululand, KwaDlangezwa; [(g)]School of Physics, University of the Witwatersrand, Johannesburg; South Africa.
[34]Department of Physics, Carleton University, Ottawa ON; Canada.
[35(a)]Faculté des Sciences Ain Chock, Université Hassan II de Casablanca; [(b)]Faculté des Sciences, Université Ibn-Tofail, Kénitra; [(c)]Faculté des Sciences Semlalia, Université Cadi Ayyad, LPHEA-Marrakech; [(d)]LPMR, Faculté des Sciences, Université Mohamed Premier, Oujda; [(e)]Faculté des sciences, Université Mohammed V, Rabat; [(f)]Institute of Applied Physics, Mohammed VI Polytechnic University, Ben Guerir; Morocco.
[36]CERN, Geneva; Switzerland.
[37]Affiliated with an institute covered by a cooperation agreement with CERN.
[38]Affiliated with an international laboratory covered by a cooperation agreement with CERN.
[39]Enrico Fermi Institute, University of Chicago, Chicago IL; United States of America.
[40]LPC, Université Clermont Auvergne, CNRS/IN2P3, Clermont-Ferrand; France.
[41]Nevis Laboratory, Columbia University, Irvington NY; United States of America.
[42]Niels Bohr Institute, University of Copenhagen, Copenhagen; Denmark.
[43(a)]Dipartimento di Fisica, Università della Calabria, Rende; [(b)]INFN Gruppo Collegato di Cosenza, Laboratori Nazionali di Frascati; Italy.
[44]Physics Department, Southern Methodist University, Dallas TX; United States of America.
[45]Physics Department, University of Texas at Dallas, Richardson TX; United States of America.
[46]National Centre for Scientific Research "Demokritos", Agia Paraskevi; Greece.
[47(a)]Department of Physics, Stockholm University; [(b)]Oskar Klein Centre, Stockholm; Sweden.
[48]Deutsches Elektronen-Synchrotron DESY, Hamburg and Zeuthen; Germany.
[49]Fakultät Physik, Technische Universität Dortmund, Dortmund; Germany.
[50]Institut für Kern- und Teilchenphysik, Technische Universität Dresden, Dresden; Germany.
[51]Department of Physics, Duke University, Durham NC; United States of America.
[52]SUPA - School of Physics and Astronomy, University of Edinburgh, Edinburgh; United Kingdom.
[53]INFN e Laboratori Nazionali di Frascati, Frascati; Italy.
[54]Physikalisches Institut, Albert-Ludwigs-Universität Freiburg, Freiburg; Germany.
[55]II. Physikalisches Institut, Georg-August-Universität Göttingen, Göttingen; Germany.
[56]Département de Physique Nucléaire et Corpusculaire, Université de Genève, Genève; Switzerland.
[57(a)]Dipartimento di Fisica, Università di Genova, Genova; [(b)]INFN Sezione di Genova; Italy.
[58]II. Physikalisches Institut, Justus-Liebig-Universität Giessen, Giessen; Germany.
[59]SUPA - School of Physics and Astronomy, University of Glasgow, Glasgow; United Kingdom.
[60]LPSC, Université Grenoble Alpes, CNRS/IN2P3, Grenoble INP, Grenoble; France.
[61]Laboratory for Particle Physics and Cosmology, Harvard University, Cambridge MA; United States of America.
[62(a)]Department of Modern Physics and State Key Laboratory of Particle Detection and Electronics, University of Science and Technology of China, Hefei; [(b)]Institute of Frontier and Interdisciplinary Science and Key Laboratory of Particle Physics

and Particle Irradiation (MOE), Shandong University, Qingdao; [c]School of Physics and Astronomy, Shanghai Jiao Tong University, Key Laboratory for Particle Astrophysics and Cosmology (MOE), SKLPPC, Shanghai; [d]Tsung-Dao Lee Institute, Shanghai; [e]School of Physics, Zhengzhou University; China.
[63a]Kirchhoff-Institut für Physik, Ruprecht-Karls-Universität Heidelberg, Heidelberg; [b]Physikalisches Institut, Ruprecht-Karls-Universität Heidelberg, Heidelberg; Germany.
[64a]Department of Physics, Chinese University of Hong Kong, Shatin, N.T., Hong Kong; [b]Department of Physics, University of Hong Kong, Hong Kong; [c]Department of Physics and Institute for Advanced Study, Hong Kong University of Science and Technology, Clear Water Bay, Kowloon, Hong Kong; China.
[65]Department of Physics, National Tsing Hua University, Hsinchu; Taiwan.
[66]IJCLab, Université Paris-Saclay, CNRS/IN2P3, 91405, Orsay; France.
[67]Centro Nacional de Microelectrónica (IMB-CNM-CSIC), Barcelona; Spain.
[68]Department of Physics, Indiana University, Bloomington IN; United States of America.
[69a]INFN Gruppo Collegato di Udine, Sezione di Trieste, Udine; [b]ICTP, Trieste; [c]Dipartimento Politecnico di Ingegneria e Architettura, Università di Udine, Udine; Italy.
[70a]INFN Sezione di Lecce; [b]Dipartimento di Matematica e Fisica, Università del Salento, Lecce; Italy.
[71a]INFN Sezione di Milano; [b]Dipartimento di Fisica, Università di Milano, Milano; Italy.
[72a]INFN Sezione di Napoli; [b]Dipartimento di Fisica, Università di Napoli, Napoli; Italy.
[73a]INFN Sezione di Pavia; [b]Dipartimento di Fisica, Università di Pavia, Pavia; Italy.
[74a]INFN Sezione di Pisa; [b]Dipartimento di Fisica E. Fermi, Università di Pisa, Pisa; Italy.
[75a]INFN Sezione di Roma; [b]Dipartimento di Fisica, Sapienza Università di Roma, Roma; Italy.
[76a]INFN Sezione di Roma Tor Vergata; [b]Dipartimento di Fisica, Università di Roma Tor Vergata, Roma; Italy.
[77a]INFN Sezione di Roma Tre; [b]Dipartimento di Matematica e Fisica, Università Roma Tre, Roma; Italy.
[78a]INFN-TIFPA; [b]Università degli Studi di Trento, Trento; Italy.
[79]Universität Innsbruck, Department of Astro and Particle Physics, Innsbruck; Austria.
[80]University of Iowa, Iowa City IA; United States of America.
[81]Department of Physics and Astronomy, Iowa State University, Ames IA; United States of America.
[82]Istinye University, Sariyer, Istanbul; Türkiye.
[83a]Departamento de Engenharia Elétrica, Universidade Federal de Juiz de Fora (UFJF), Juiz de Fora; [b]Universidade Federal do Rio De Janeiro COPPE/EE/IF, Rio de Janeiro; [c]Instituto de Física, Universidade de São Paulo, São Paulo; [d]Rio de Janeiro State University, Rio de Janeiro; [e]Federal University of Bahia, Bahia; Brazil.
[84]KEK, High Energy Accelerator Research Organisation, Tsukuba; Japan.
[85]Graduate School of Science, Kobe University, Kobe; Japan.
[86a]AGH University of Krakow, Faculty of Physics and Applied Computer Science, Krakow; [b]Marian Smoluchowski Institute of Physics, Jagiellonian University, Krakow; Poland.
[87]Institute of Nuclear Physics Polish Academy of Sciences, Krakow; Poland.
[88]Faculty of Science, Kyoto University, Kyoto; Japan.
[89]Research Center for Advanced Particle Physics and Department of Physics, Kyushu University, Fukuoka ; Japan.
[90]L2IT, Université de Toulouse, CNRS/IN2P3, UPS, Toulouse; France.
[91]Instituto de Física La Plata, Universidad Nacional de La Plata and CONICET, La Plata; Argentina.
[92]Physics Department, Lancaster University, Lancaster; United Kingdom.
[93]Oliver Lodge Laboratory, University of Liverpool, Liverpool; United Kingdom.
[94]Department of Experimental Particle Physics, Jožef Stefan Institute and Department of Physics, University of Ljubljana, Ljubljana; Slovenia.
[95]School of Physics and Astronomy, Queen Mary University of London, London; United Kingdom.
[96]Department of Physics, Royal Holloway University of London, Egham; United Kingdom.
[97]Department of Physics and Astronomy, University College London, London; United Kingdom.
[98]Louisiana Tech University, Ruston LA; United States of America.
[99]Fysiska institutionen, Lunds universitet, Lund; Sweden.
[100]Departamento de Física Teorica C-15 and CIAFF, Universidad Autónoma de Madrid, Madrid; Spain.
[101]Institut für Physik, Universität Mainz, Mainz; Germany.
[102]School of Physics and Astronomy, University of Manchester, Manchester; United Kingdom.
[103]CPPM, Aix-Marseille Université, CNRS/IN2P3, Marseille; France.
[104]Department of Physics, University of Massachusetts, Amherst MA; United States of America.
[105]Department of Physics, McGill University, Montreal QC; Canada.
[106]School of Physics, University of Melbourne, Victoria; Australia.
[107]Department of Physics, University of Michigan, Ann Arbor MI; United States of America.
[108]Department of Physics and Astronomy, Michigan State University, East Lansing MI; United States of America.
[109]Group of Particle Physics, University of Montreal, Montreal QC; Canada.
[110]Fakultät für Physik, Ludwig-Maximilians-Universität München, München; Germany.
[111]Max–Planck-Institut für Physik (Werner-Heisenberg-Institut), München; Germany.
[112]Graduate School of Science and Kobayashi-Maskawa Institute, Nagoya University, Nagoya; Japan.

[113]Department of Physics and Astronomy, University of New Mexico, Albuquerque NM; United States of America.
[114]Institute for Mathematics, Astrophysics and Particle Physics, Radboud University/Nikhef, Nijmegen; Netherlands.
[115]Nikhef National Institute for Subatomic Physics and University of Amsterdam, Amsterdam; Netherlands.
[116]Department of Physics, Northern Illinois University, DeKalb IL; United States of America.
[117(a)]New York University Abu Dhabi, Abu Dhabi; [(b)]United Arab Emirates University, Al Ain; United Arab Emirates.
[118]Department of Physics, New York University, New York NY; United States of America.
[119]Ochanomizu University, Otsuka, Bunkyo-ku, Tokyo; Japan.
[120]Ohio State University, Columbus OH; United States of America.
[121]Homer L. Dodge Department of Physics and Astronomy, University of Oklahoma, Norman OK; United States of America.
[122]Department of Physics, Oklahoma State University, Stillwater OK; United States of America.
[123]Palacký University, Joint Laboratory of Optics, Olomouc; Czech Republic.
[124]Institute for Fundamental Science, University of Oregon, Eugene, OR; United States of America.
[125]Graduate School of Science, Osaka University, Osaka; Japan.
[126]Department of Physics, University of Oslo, Oslo; Norway.
[127]Department of Physics, Oxford University, Oxford; United Kingdom.
[128]LPNHE, Sorbonne Université, Université Paris Cité, CNRS/IN2P3, Paris; France.
[129]Department of Physics, University of Pennsylvania, Philadelphia PA; United States of America.
[130]Department of Physics and Astronomy, University of Pittsburgh, Pittsburgh PA; United States of America.
[131(a)]Laboratório de Instrumentação e Física Experimental de Partículas - LIP, Lisboa; [(b)]Departamento de Física, Faculdade de Ciências, Universidade de Lisboa, Lisboa; [(c)]Departamento de Física, Universidade de Coimbra, Coimbra; [(d)]Centro de Física Nuclear da Universidade de Lisboa, Lisboa; [(e)]Departamento de Física, Universidade do Minho, Braga; [(f)]Departamento de Física Teórica *y* del Cosmos, Universidad de Granada, Granada (Spain); [(g)]Departamento de Física, Instituto Superior Técnico, Universidade de Lisboa, Lisboa; Portugal.
[132]Institute of Physics of the Czech Academy of Sciences, Prague; Czech Republic.
[133]Czech Technical University in Prague, Prague; Czech Republic.
[134]Charles University, Faculty of Mathematics and Physics, Prague; Czech Republic.
[135]Particle Physics Department, Rutherford Appleton Laboratory, Didcot; United Kingdom.
[136]IRFU, CEA, Université Paris-Saclay, Gif-sur-Yvette; France.
[137]Santa Cruz Institute for Particle Physics, University of California Santa Cruz, Santa Cruz CA; United States of America.
[138(a)]Departamento de Física, Pontificia Universidad Católica de Chile, Santiago; [(b)]Millennium Institute for Subatomic physics at high energy frontier (SAPHIR), Santiago; [(c)]Instituto de Investigación Multidisciplinario en Ciencia *y* Tecnología, *y* Departamento de Física, Universidad de La Serena; [(d)]Universidad Andres Bello, Department of Physics, Santiago; [(e)]Instituto de Alta Investigación, Universidad de Tarapacá, Arica; [(f)]Departamento de Física, Universidad Técnica Federico Santa María, Valparaíso; Chile.
[139]Department of Physics, Institute of Science, Tokyo; Japan.
[140]Department of Physics, University of Washington, Seattle WA; United States of America.
[141]Department of Physics and Astronomy, University of Sheffield, Sheffield; United Kingdom.
[142]Department of Physics, Shinshu University, Nagano; Japan.
[143]Department Physik, Universität Siegen, Siegen; Germany.
[144]Department of Physics, Simon Fraser University, Burnaby BC; Canada.
[145]SLAC National Accelerator Laboratory, Stanford CA; United States of America.
[146]Department of Physics, Royal Institute of Technology, Stockholm; Sweden.
[147]Departments of Physics and Astronomy, Stony Brook University, Stony Brook NY; United States of America.
[148]Department of Physics and Astronomy, University of Sussex, Brighton; United Kingdom.
[149]School of Physics, University of Sydney, Sydney; Australia.
[150]Institute of Physics, Academia Sinica, Taipei; Taiwan.
[151(a)]E. Andronikashvili Institute of Physics, Iv. Javakhishvili Tbilisi State University, Tbilisi; [(b)]High Energy Physics Institute, Tbilisi State University, Tbilisi; [(c)]University of Georgia, Tbilisi; Georgia.
[152]Department of Physics, Technion, Israel Institute of Technology, Haifa; Israel.
[153]Raymond and Beverly Sackler School of Physics and Astronomy, Tel Aviv University, Tel Aviv; Israel.
[154]Department of Physics, Aristotle University of Thessaloniki, Thessaloniki; Greece.
[155]International Center for Elementary Particle Physics and Department of Physics, University of Tokyo, Tokyo; Japan.
[156]Department of Physics, University of Toronto, Toronto ON; Canada.
[157(a)]TRIUMF, Vancouver BC; [(b)]Department of Physics and Astronomy, York University, Toronto ON; Canada.
[158]Division of Physics and Tomonaga Center for the History of the Universe, Faculty of Pure and Applied Sciences, University of Tsukuba, Tsukuba; Japan.
[159]Department of Physics and Astronomy, Tufts University, Medford MA; United States of America.
[160]Department of Physics and Astronomy, University of California Irvine, Irvine CA; United States of America.
[161]University of Sharjah, Sharjah; United Arab Emirates.
[162]Department of Physics and Astronomy, University of Uppsala, Uppsala; Sweden.
[163]Department of Physics, University of Illinois, Urbana IL; United States of America.

[164]Instituto de Física Corpuscular (IFIC), Centro Mixto Universidad de Valencia - CSIC, Valencia; Spain.
[165]Department of Physics, University of British Columbia, Vancouver BC; Canada.
[166]Department of Physics and Astronomy, University of Victoria, Victoria BC; Canada.
[167]Fakultät für Physik und Astronomie, Julius-Maximilians-Universität Würzburg, Würzburg; Germany.
[168]Department of Physics, University of Warwick, Coventry; United Kingdom.
[169]Waseda University, Tokyo; Japan.
[170]Department of Particle Physics and Astrophysics, Weizmann Institute of Science, Rehovot; Israel.
[171]Department of Physics, University of Wisconsin, Madison WI; United States of America.
[172]Fakultät für Mathematik und Naturwissenschaften, Fachgruppe Physik, Bergische Universität Wuppertal, Wuppertal; Germany.
[173]Department of Physics, Yale University, New Haven CT; United States of America.
[a] Also Affiliated with an institute covered by a cooperation agreement with CERN.
[b] Also at An-Najah National University, Nablus; Palestine.
[c] Also at Borough of Manhattan Community College, City University of New York, New York NY; United States of America.
[d] Also at Center for Interdisciplinary Research and Innovation (CIRI-AUTH), Thessaloniki; Greece.
[e] Also at Centro Studi e Ricerche Enrico Fermi; Italy.
[f] Also at CERN, Geneva; Switzerland.
[g] Also at Département de Physique Nucléaire et Corpusculaire, Université de Genève, Genève; Switzerland.
[h] Also at Departament de Fisica de la Universitat Autonoma de Barcelona, Barcelona; Spain.
[i] Also at Department of Financial and Management Engineering, University of the Aegean, Chios; Greece.
[j] Also at Department of Physics, California State University, Sacramento; United States of America.
[k] Also at Department of Physics, King's College London, London; United Kingdom.
[l] Also at Department of Physics, Stanford University, Stanford CA; United States of America.
[m] Also at Department of Physics, Stellenbosch University; South Africa.
[n] Also at Department of Physics, University of Fribourg, Fribourg; Switzerland.
[o] Also at Department of Physics, University of Thessaly; Greece.
[p] Also at Department of Physics, Westmont College, Santa Barbara; United States of America.
[q] Also at Faculty of Physics, Sofia University, 'St. Kliment Ohridski', Sofia; Bulgaria.
[r] Also at Hellenic Open University, Patras; Greece.
[s] Also at Institucio Catalana de Recerca i Estudis Avancats, ICREA, Barcelona; Spain.
[t] Also at Institut für Experimentalphysik, Universität Hamburg, Hamburg; Germany.
[u] Also at Institute for Nuclear Research and Nuclear Energy (INRNE) of the Bulgarian Academy of Sciences, Sofia; Bulgaria.
[v] Also at Institute of Applied Physics, Mohammed VI Polytechnic University, Ben Guerir; Morocco.
[w] Also at Institute of Particle Physics (IPP); Canada.
[x] Also at Institute of Physics and Technology, Mongolian Academy of Sciences, Ulaanbaatar; Mongolia.
[y] Also at Institute of Physics, Azerbaijan Academy of Sciences, Baku; Azerbaijan.
[z] Also at Institute of Theoretical Physics, Ilia State University, Tbilisi; Georgia.
[aa] Also at Lawrence Livermore National Laboratory, Livermore; United States of America.
[ab] Also at National Institute of Physics, University of the Philippines Diliman (Philippines); Philippines.
[ac] Also at Technical University of Munich, Munich; Germany.
[ad] Also at The Collaborative Innovation Center of Quantum Matter (CICQM), Beijing; China.
[ae] Also at TRIUMF, Vancouver BC; Canada.
[af] Also at Università di Napoli Parthenope, Napoli; Italy.
[ag] Also at University of Colorado Boulder, Department of Physics, Colorado; United States of America.
[ah] Also at Washington College, Chestertown, MD; United States of America.
[ai] Also at Yeditepe University, Physics Department, Istanbul; Türkiye.
* Deceased

References

[1] ATLAS Collaboration, Observation of a new particle in the search for the standard model Higgs boson with the ATLAS detector at the LHC, Phys. Lett. B 716 (2012) 1, arXiv:1207.7214 [hep-ex].
[2] CMS Collaboration, Observation of a new boson at a mass of 125 GeV with the CMS experiment at the LHC, Phys. Lett. B 716 (2012) 30, arXiv:1207.7235 [hep-ex].
[3] ATLAS Collaboration, The ATLAS experiment at the CERN large hadron collider, JINST 3 (2008) S08003.
[4] CMS Collaboration, The CMS experiment at the CERN LHC, JINST 3 (2008) S08004.
[5] ATLAS Collaboration, Luminosity determination in pp collisions at $\sqrt{s} = 13$ TeV using the ATLAS detector at the LHC, Eur. Phys. J. C 83 (2023) 982, arXiv:2212.09379 [hep-ex].
[6] ATLAS Collaboration, ATLAS searches for additional scalars and exotic Higgs boson decays with the LHC run 2 dataset, 2024, CERN-EP-2024-94.
[7] S. Weinberg, A model of leptons, Phys. Rev. Lett. 19 (1967) 1264–1266.
[8] S.L. Glashow, Partial symmetries of weak interactions, Nuclear Phys. 22 (1961) 579–588.
[9] A. Salam, Weak and electromagnetic interactions, Conf. Proc. C 680519 (1968) 367–377.
[10] G. 't Hooft, M. Veltman, Regularization and renormalization of gauge fields, Nuclear Phys. B 44 (1972) 189–213.
[11] P.W. Higgs, Broken symmetries, massless particles and gauge fields, Phys. Lett. 12 (1964) 132–133.

[12] P.W. Higgs, Broken symmetries and the masses of gauge bosons, in: J.C. Taylor (Ed.), Phys. Rev. Lett. 13 (1964) 508–509.
[13] F. Englert, R. Brout, Broken symmetry and the mass of gauge vector mesons, in: J.C. Taylor (Ed.), Phys. Rev. Lett. 13 (1964) 321–323.
[14] G.S. Guralnik, C.R. Hagen, T.W.B. Kibble, Global conservation laws and massless particles, in: J.C. Taylor (Ed.), Phys. Rev. Lett. 13 (1964) 585–587.
[15] T.W.B. Kibble, Symmetry breaking in nonabelian gauge theories, in: J.C. Taylor (Ed.), Phys. Rev. 155 (1967) 1554–1561.
[16] G. Degrassi, et al., Higgs mass and vacuum stability in the standard model at NNLO, JHEP 08 (2012) 098, arXiv:1205.6497 [hep-ph].
[17] M. Reichert, et al., Probing baryogenesis through the Higgs boson self-coupling, Phys. Rev. D 97 (7) (2018) 075008, arXiv:1711.00019 [hep-ph].
[18] D. de Florian, et al., Handbook of LHC Higgs cross sections: 4. Deciphering the nature of the Higgs sector, 2017, http://dx.doi.org/10.23731/CYRM-2017-002, arXiv:1610.07922 [hep-ph].
[19] ATLAS Collaboration, A detailed map of Higgs boson interactions by the ATLAS experiment ten years after the discovery, Nature 607 (7917) (2022) 52–59, arXiv:2207.00092 [hep-ex].
[20] ATLAS and CMS Collaborations, Combined measurement of the Higgs boson mass in pp collisions at $\sqrt{s} = 7$ and 8 TeV with the ATLAS and CMS experiments, Phys. Rev. Lett. 114 (2015) 191803, arXiv:1503.07589 [hep-ex].
[21] C. Anastasiou, et al., High precision determination of the gluon fusion Higgs boson cross-section at the LHC, JHEP 05 (2016) 058, arXiv:1602.00695 [hep-ph].
[22] C. Anastasiou, C. Duhr, F. Dulat, F. Herzog, B. Mistlberger, Higgs boson gluon-fusion production in QCD at three loops, Phys. Rev. Lett. 114 (2015) 212001, arXiv:1503.06056 [hep-ph].
[23] F. Dulat, A. Lazopoulos, B. Mistlberger, Ihixs 2 – inclusive Higgs cross sections, Comput. Phys. Comm. 233 (2018) 243–260, arXiv:1802.00827 [hep-ph].
[24] R.V. Harlander, K.J. Ozeren, Finite top mass effects for hadronic Higgs production at next-to-next-to-leading order, JHEP 11 (2009) 088, arXiv:0909.3420 [hep-ph].
[25] R.V. Harlander, K.J. Ozeren, Top mass effects in Higgs production at next-to-next-to-leading order QCD: Virtual corrections, Phys. Lett. B 679 (2009) 467–472, arXiv:0907.2997 [hep-ph].
[26] R.V. Harlander, H. Mantler, S. Marzani, K.J. Ozeren, Higgs production in gluon fusion at next-to-next-to-leading order QCD for finite top mass, Eur. Phys. J. C 66 (2010) 359–372, arXiv:0912.2104 [hep-ph].
[27] A. Pak, M. Rogal, M. Steinhauser, Finite top quark mass effects in NNLO Higgs boson production at LHC, JHEP 02 (2010) 025, arXiv:0911.4662 [hep-ph].
[28] S. Actis, G. Passarino, C. Sturm, S. Uccirati, NLO electroweak corrections to Higgs boson production at hadron colliders, Phys. Lett. B 670 (2008) 12–17, arXiv:0809.1301 [hep-ph].
[29] S. Actis, G. Passarino, C. Sturm, S. Uccirati, NNLO computational techniques: The cases $H \to \gamma\gamma$ and $H \to gg$, Nuclear Phys. B 811 (2009) 182–273, arXiv:0809.3667 [hep-ph].
[30] M. Bonetti, K. Melnikov, L. Tancredi, Higher order corrections to mixed QCD-EW contributions to Higgs boson production in gluon fusion, Phys. Rev. D 97 (5) (2018) 056017, arXiv:1801.10403 [hep-ph].
[31] U. Aglietti, R. Bonciani, G. Degrassi, A. Vicini, Two-loop light fermion contribution to Higgs production and decays, Phys. Lett. B 595 (2004) 432–441, arXiv:hep-ph/0404071.
[32] E. Bagnaschi, G. Degrassi, P. Slavich, A. Vicini, Higgs production via gluon fusion in the POWHEG approach in the SM and in the MSSM, JHEP 02 (2012) 088, arXiv:1111.2854 [hep-ph].
[33] K. Hamilton, P. Nason, G. Zanderighi, Finite quark-mass effects in the NNLOPS POWHEG+MiNLO Higgs generator, JHEP 05 (2015) 140, arXiv:1501.04637 [hep-ph].
[34] M. Ciccolini, A. Denner, S. Dittmaier, Strong and electroweak corrections to the production of a Higgs boson + 2 jets via weak interactions at the large hadron collider, Phys. Rev. Lett. 99 (2007) 161803, arXiv:0707.0381 [hep-ph].
[35] M. Ciccolini, A. Denner, S. Dittmaier, Electroweak and QCD corrections to Higgs production via vector-boson fusion at the CERN LHC, Phys. Rev. D 77 (2008) 013002, arXiv:0710.4749 [hep-ph].
[36] P. Bolzoni, F. Maltoni, S.-O. Moch, M. Zaro, Higgs boson production via vector-boson fusion at next-to-next-to-leading order in QCD, Phys. Rev. Lett. 105 (2010) 011801, arXiv:1003.4451 [hep-ph].
[37] O. Brein, R.V. Harlander, T.J.E. Zirke, Vh@nnlo – Higgs strahlung at hadron colliders, Comput. Phys. Comm. 184 (2013) 998–1003, arXiv:1210.5347 [hep-ph].
[38] R.V. Harlander, J. Klappert, S. Liebler, L. Simon, Vh@nnlo-v2: new physics in Higgs strahlung, JHEP 05 (2018) 089, arXiv:1802.04817 [hep-ph].
[39] O. Brein, A. Djouadi, R. Harlander, NNLO QCD corrections to the Higgs-strahlung processes at hadron colliders, Phys. Lett. B 579 (2004) 149–156, arXiv:hep-ph/0307206.
[40] O. Brein, R.V. Harlander, M. Wiesemann, T. Zirke, Top-quark mediated effects in hadronic Higgs-strahlung, Eur. Phys. J. C 72 (2012) 1868, arXiv:1111.0761 [hep-ph].
[41] L. Altenkamp, S. Dittmaier, R.V. Harlander, H. Rzehak, T.J.E. Zirke, Gluon-induced Higgs-strahlung at next-to-leading order QCD, JHEP 02 (2013) 078, arXiv:1211.5015 [hep-ph].
[42] R.V. Harlander, A. Kulesza, V. Theeuwes, T. Zirke, Soft gluon resummation for gluon-induced Higgs strahlung, JHEP 11 (2014) 082, arXiv:1410.0217 [hep-ph].
[43] A. Denner, S. Dittmaier, S. Kallweit, A. Mück, HAWK 2.0: A Monte Carlo program for Higgs production in vector-boson fusion and Higgs strahlung at hadron colliders, Comput. Phys. Comm. 195 (2015) 161–171, arXiv:1412.5390 [hep-ph].
[44] M.L. Ciccolini, S. Dittmaier, M. Krämer, Electroweak radiative corrections to associated WH and ZH production at hadron colliders, Phys. Rev. D 68 (2003) 073003, arXiv:hep-ph/0306234 [hep-ph].
[45] A. Denner, S. Dittmaier, S. Kallweit, A. Mück, Electroweak corrections to Higgs-strahlung off W/Z bosons at the tevatron and the LHC with HAWK, JHEP 03 (2012) 075, arXiv:1112.5142 [hep-ph].
[46] W. Beenakker, et al., NLO QCD corrections to $t\bar{t}H$ production in hadron collisions, Nucl. Phys. B 653 (2003) 151–203, arXiv:hep-ph/0211352.
[47] S. Dawson, C. Jackson, L. Orr, L. Reina, D. Wackeroth, Associated Higgs boson production with top quarks at the CERN large hadron collider: NLO QCD corrections, Phys. Rev. D 68 (2003) 034022, arXiv:hep-ph/0305087.
[48] Y. Zhang, W.-G. Ma, R.-Y. Zhang, C. Chen, L. Guo, QCD nlo and EW NLO corrections to $t\bar{t}H$ production with top quark decays at hadron collider, Phys. Lett. B 738 (2014) 1–5, arXiv:1407.1110 [hep-ph].
[49] S. Frixione, V. Hirschi, D. Pagani, H.-S. Shao, M. Zaro, Electroweak and QCD corrections to top-pair hadroproduction in association with heavy bosons, JHEP 06 (2015) 184, arXiv:1504.03446 [hep-ph].
[50] S. Dawson, C. Jackson, L. Reina, D. Wackeroth, Exclusive Higgs boson production with bottom quarks at hadron colliders, Phys. Rev. D 69 (2004) 074027, arXiv:hep-ph/0311067.
[51] S. Dittmaier, M. Krämer, M. Spira, Higgs radiation off bottom quarks at the Fermilab Tevatron and the CERN LHC, Phys. Rev. D 70 (2004) 074010, arXiv:hep-ph/0309204.
[52] R. Harlander, M. Krämer, M. Schumacher, Bottom-quark associated Higgs-boson production: reconciling the four- and five-flavour scheme approach, 2011, arXiv:1112.3478 [hep-ph].

[53] F. Demartin, F. Maltoni, K. Mawatari, M. Zaro, Higgs production in association with a single top quark at the LHC, Eur. Phys. J. C 75 (2015) 267, arXiv:1504.00611 [hep-ph].
[54] F. Demartin, B. Maier, F. Maltoni, K. Mawatari, M. Zaro, tWH associated production at the LHC, Eur. Phys. J. C 77 (1) (2017) 34, arXiv:1607.05862 [hep-ph].
[55] M. Grazzini, et al., Higgs boson pair production at NNLO with top quark mass effects, JHEP 05 (2018) 059, arXiv:1803.02463 [hep-ph].
[56] G. Heinrich, S.P. Jones, M. Kerner, G. Luisoni, L. Scyboz, Probing the trilinear Higgs boson coupling in di-Higgs production at NLO QCD including parton shower effects, JHEP 06 (2019) 066, arXiv:1903.08137 [hep-ph].
[57] S. Dawson, S. Dittmaier, M. Spira, Neutral Higgs-boson pair production at hadron colliders: QCD corrections, Phys. Rev. D 58 (1998) 115012, arXiv:hep-ph/9805244 [hep-ph].
[58] S. Borowka, et al., Higgs boson pair production in gluon fusion at next-to-leading order with full top-quark mass dependence, Phys. Rev. Lett. 117 (1) (2016) 012001, arXiv:1604.06447 [hep-ph].
[59] J. Baglio, et al., Gluon fusion into Higgs pairs at NLO QCD and the top mass scheme, Eur. Phys. J. C 79 (6) (2019) 459, arXiv:1811.05692 [hep-ph].
[60] R. Bonciani, G. Degrassi, P.P. Giardino, R. Gröber, Analytical method for next-to-leading-order QCD corrections to double-Higgs production, Phys. Rev. Lett. 121 (16) (2018) 162003, arXiv:1806.11564 [hep-ph].
[61] D. de Florian, J. Mazzitelli, Higgs boson pair production at next-to-next-to-leading order in QCD, Phys. Rev. Lett. 111 (2013) 201801, arXiv:1309.6594 [hep-ph].
[62] D.Y. Shao, C.S. Li, H.T. Li, J. Wang, Threshold resummation effects in Higgs boson pair production at the LHC, JHEP 07 (2013) 169, arXiv:1301.1245 [hep-ph].
[63] D. de Florian, J. Mazzitelli, Higgs pair production at next-to-next-to-leading logarithmic accuracy at the LHC, JHEP 09 (2015) 053, arXiv:1505.07122 [hep-ph].
[64] J. Baglio, et al., $gg \to HH$: Combined uncertainties, Phys. Rev. D 103.
[65] F.A. Dreyer, A. Karlberg, Vector-boson fusion Higgs pair production at N^{3}LO, Phys. Rev. D 98 (2018) 114016, arXiv:1811.07906.
[66] J. Baglio, et al., The measurement of the Higgs self-coupling at the LHC: theoretical status, JHEP 04 (4) (2013) 151, arXiv:1212.5581.
[67] L.-S. Ling, et al., NNLO QCD corrections to Higgs pair production via vector boson fusion at hadron colliders, Phys. Rev. D 89.
[68] A. Djouadi, J. Kalinowski, M. Spira, HDECAY: A program for Higgs boson decays in the standard model and its supersymmetric extension, Comput. Phys. Comm. 108 (1998) 56–74, arXiv:hep-ph/9704448.
[69] M. Spira, QCD effects in Higgs physics, Fortschr. Phys. 46 (1998) 203–284, arXiv:hep-ph/9705337.
[70] A. Bredenstein, A. Denner, S. Dittmaier, M.M. Weber, Precise predictions for the Higgs-boson decay $H \to WW/ZZ \to 4$ leptons, Phys. Rev. D 74 (2006) 013004, arXiv:hep-ph/0604011.
[71] A. Bredenstein, A. Denner, S. Dittmaier, M.M. Weber, Radiative corrections to the semileptonic and hadronic Higgs-boson decays H → W W / Z Z → 4 fermions, JHEP 02 (2007) 080, arXiv:hep-ph/0611234.
[72] L. Mihaila, B. Schmidt, M. Steinhauser, $\Gamma(H \to b\bar{b})$ To order $\alpha\alpha_s$, Phys. Lett. B 751 (2015) 442–447, arXiv:1509.02294 [hep-ph].
[73] P. Nason, A new method for combining NLO QCD with shower Monte Carlo algorithms, JHEP 11 (2004) 040, arXiv:hep-ph/0409146.
[74] S. Frixione, P. Nason, C. Oleari, Matching NLO QCD computations with parton shower simulations: the POWHEG method, JHEP 11 (2007) 070, arXiv:0709.2092 [hep-ph].
[75] S. Alioli, P. Nason, C. Oleari, E. Re, A general framework for implementing NLO calculations in shower Monte Carlo programs: the POWHEG BOX, JHEP 06 (2010) 043, arXiv:1002.2581 [hep-ph].
[76] K. Hamilton, P. Nason, E. Re, G. Zanderighi, NNLOPS simulation of Higgs boson production, JHEP 10 (2013) 222, arXiv:1309.0017 [hep-ph].
[77] S. Catani, M. Grazzini, Next-to-next-to-leading-order subtraction formalism in hadron collisions and its application to Higgs-boson production at the large hadron collider, Phys. Rev. Lett. 98 (2007) 222002, arXiv:hep-ph/0703012.
[78] P. Nason, C. Oleari, NLO Higgs boson production via vector-boson fusion matched with shower in POWHEG, JHEP 02 (2010) 037, arXiv:0911.5299 [hep-ph].
[79] G. Cullen, et al., Automated one-loop calculations with gosam, Eur. Phys. J. C 72 (2012) 1889, arXiv:1111.2034 [hep-ph].
[80] H.B. Hartanto, B. Jäger, L. Reina, D. Wackeroth, Higgs boson production in association with top quarks in the POWHEG BOX, Phys. Rev. D 91 (9) (2015) 094003, arXiv:1501.04498 [hep-ph].
[81] J. Alwall, et al., The automated computation of tree-level and next-to-leading order differential cross sections, and their matching to parton shower simulations, JHEP 07 (2014) 079, arXiv:1405.0301 [hep-ph].
[82] ATLAS Collaboration, The ATLAS simulation infrastructure, Eur. Phys. J. C 70 (2010) 823, arXiv:1005.4568 [physics.ins-det].
[83] S. Agostinelli, et al., GEANT4 - a simulation toolkit, Nucl. Instrum. Methods A 506 (2003) 250.
[84] R. Barate, et al., Search for the standard model Higgs boson at LEP, Phys. Lett. B 565 (2003) 61–75, arXiv:hep-ex/0306033.
[85] CDF and D0 Collaborations, Higgs boson studies at the tevatron, Phys. Rev. D 88 (5) (2013) 052014, arXiv:1303.6346 [hep-ex].
[86] ALEPH, CDF, D0, DELPHI, L3, OPAL, SLD, LEP Electroweak Working Group, Tevatron Electroweak Working Group, SLD Electroweak, Heavy Flavour Groups, Precision electroweak measurements and constraints on the standard model, 2010, arXiv:1012.2367 [hep-ex].
[87] M. Baak, et al., Updated status of the global electroweak fit and constraints on new physics, Eur. Phys. J. C 72 (2012) 2003, arXiv:1107.0975 [hep-ph].
[88] ATLAS and CMS Collaborations, Measurements of the Higgs boson production and decay rates and constraints on its couplings from a combined ATLAS and CMS analysis of the LHC pp collision data at $\sqrt{s} = 7$ and 8 TeV, JHEP 08 (2016) 045, arXiv:1606.02266 [hep-ex].
[89] ATLAS Collaboration, Measurements of fiducial and differential cross sections for Higgs boson production in the diphoton decay channel at $\sqrt{s} = 8$ TeV with ATLAS, JHEP 09 (2014) 112, arXiv:1407.4222 [hep-ex].
[90] ATLAS Collaboration, Fiducial and differential cross sections of Higgs boson production measured in the four-lepton decay channel in pp collisions at $\sqrt{s} = 8$ TeV with the ATLAS detector, Phys. Lett. B 738 (2014) 234, arXiv:1408.3226 [hep-ex].
[91] ATLAS Collaboration, Measurements of the total and differential Higgs boson production cross sections combining the $H \to \gamma\gamma$ and $H \to ZZ^* \to 4\ell$ decay channels at $\sqrt{s} = 8$ TeV with the ATLAS detector, Phys. Rev. Lett. 115 (2015) 091801, arXiv:1504.05833 [hep-ex].
[92] ATLAS Collaboration, Measurement of fiducial differential cross sections of gluon-fusion production of Higgs bosons decaying to $WW^* \to e\nu\mu\nu$ with the ATLAS detector at $\sqrt{s} = 8$ TeV, JHEP 08 (2016) 104, arXiv:1604.02997 [hep-ex].
[93] L.D. Landau, On the angular momentum of a system of two photons, Dokl. Akad. Nauk SSSR 60 (2) (1948) 207–209.
[94] C.-N. Yang, Selection rules for the dematerialization of a particle into two photons, Phys. Rev. 77 (1950) 242–245.
[95] ATLAS Collaboration, Study of the spin and parity of the Higgs boson in diboson decays with the ATLAS detector, Eur. Phys. J. C 75 (2015) 476, arXiv:1506.05669 [hep-ex].
[96] ATLAS Collaboration, Test of CP invariance in vector-boson fusion production of the Higgs boson using the *optimal observable* method in the ditau decay channel with the ATLAS detector, Eur. Phys. J. C 76 (2016) 658, arXiv:1602.04516 [hep-ex].
[97] ATLAS Collaboration, Constraints on the off-shell Higgs boson signal strength in the high-mass ZZ and WW final states with the ATLAS detector, Eur. Phys. J. C 75 (2015) 335, arXiv:1503.01060 [hep-ex].
[98] N. Kauer, G. Passarino, Inadequacy of zero-width approximation for a light Higgs boson signal, JHEP 08 (2012) 116, arXiv:1206.4803 [hep-ph].

[99] F. Caola, K. Melnikov, Constraining the Higgs boson width with ZZ production at the LHC, Phys. Rev. D 88 (2013) 054024, arXiv:1307.4935 [hep-ph].
[100] J.M. Campbell, R.K. Ellis, C. Williams, Bounding the Higgs width at the LHC using full analytic results for $gg \to e^- e^+ \mu^- \mu^+$, JHEP 04 (2014) 060, arXiv:1311.3589 [hep-ph].
[101] J.M. Campbell, R.K. Ellis, C. Williams, Bounding the Higgs width at the LHC: Complementary results from $H \to WW$, Phys. Rev. D 89 (5) (2014) 053011, arXiv:1312.1628 [hep-ph].
[102] Gfitter Group, J. Haller, et al., Update of the global electroweak fit and constraints on two-Higgs-doublet models, Eur. Phys. J. C 78 (8) (2018) 675, arXiv:1803.01853 [hep-ph].
[103] M. Sher, Electroweak Higgs potential and vacuum stability, Phys. Rep. 179 (1989) 273–418.
[104] ATLAS Collaboration, Measurement of the Higgs boson mass with $H \to \gamma\gamma$ decays in 140 fb^{-1} of $\sqrt{s} = 13$ TeV pp collisions with the ATLAS detector, Phys. Lett. B 847 (2023) 138315, arXiv:2308.07216 [hep-ex].
[105] M.J. Oreglia, A Study of the Reactions $\psi' \to \gamma\gamma\psi$, Appendix D (SLAC-0236, Ph.D. thesis), SLAC, 1980, URL www.slac.stanford.edu/cgi-wrap/getdoc/slac-r-236.pdf.
[106] ATLAS Collaboration, Measurement of the Higgs boson mass in the $H \to ZZ^* \to 4\ell$ and $H \to \gamma\gamma$ channels with $\sqrt{s} = 13$ TeV pp collisions using the ATLAS detector, Phys. Lett. B 784 (2018) 345, arXiv:1806.00242 [hep-ex].
[107] ATLAS Collaboration, Electron and photon energy calibration with the ATLAS detector using LHC run 2 data, JINST 19 (02) (2023) P02009, arXiv:2309.05471 [hep-ex].
[108] ATLAS Collaboration, Measurement of the Higgs boson mass in the $H \to ZZ^* \to 4\ell$ decay channel using 139 fb^{-1} of $\sqrt{s}$=13 TeV pp collisions recorded by the ATLAS detector at the LHC, Phys. Lett. B 843 (2023) 137880, arXiv:2207.00320 [hep-ex].
[109] ATLAS Collaboration, Combined measurement of the Higgs boson mass from the $H \to \gamma\gamma$ and $H \to ZZ^* \to 4\ell$ decay channels with the ATLAS detector using $\sqrt{s} = 7, 8,$ and 13 TeV pp collision data, Phys. Rev. Lett. 131 (2023) 251802, arXiv:2308.04775 [hep-ex].
[110] ATLAS Collaboration, Evidence of off-shell Higgs boson production from ZZ leptonic decay channels and constraints on its total width with the ATLAS detector, Phys. Lett. B 846 (2023) 138223, arXiv:2304.01532 [hep-ex].
[111] ATLAS Collaboration, Constraints on the off-shell Higgs boson signal strength in the high-mass ZZ and WW final states with the ATLAS detector, Eur. Phys. J. C 75 (7) (2015) 335, arXiv:1503.01060 [hep-ex].
[112] ATLAS Collaboration, Higgs boson production cross-section measurements and their EFT interpretation in the 4ℓ decay channel at $\sqrt{s} = 13$ TeV with the ATLAS detector, Eur. Phys. J. C 80 (2020) 957, arXiv:2004.03447 [hep-ex].
[113] ATLAS Collaboration, Measurements of the Higgs boson inclusive and differential fiducial cross-sections in the diphoton decay channel with pp collisions at $\sqrt{s} = 13$ TeV with the ATLAS detector, JHEP 08 (2022) 027, arXiv:2202.00487 [hep-ex].
[114] ATLAS Collaboration, Measurements of the Higgs boson inclusive and differential fiducial cross sections in the 4ℓ decay channel at $\sqrt{s} = 13$ TeV, Eur. Phys. J. C 80 (2020) 942, arXiv:2004.03969 [hep-ex].
[115] ATLAS Collaboration, Measurement of the total and differential Higgs boson production cross-sections at $\sqrt{s} = 13$ TeV with the ATLAS detector by combining the $H \to ZZ^* \to 4\ell$ and $H \to \gamma\gamma$ decay channels, JHEP 05 (2023) 028, arXiv:2207.08615 [hep-ex].
[116] ATLAS Collaboration, Direct constraint on the Higgs-charm coupling from a search for Higgs boson decays into charm quarks with the ATLAS detector, Eur. Phys. J. C 82 (2022) 717, arXiv:2201.11428 [hep-ex].
[117] D. Curtin, et al., Exotic decays of the 125 GeV Higgs boson, Phys. Rev. D 90 (7) (2014) 075004, arXiv:1312.4992 [hep-ph].
[118] D. Curtin, R. Essig, S. Gori, J. Shelton, Illuminating dark photons with high-energy colliders, JHEP 02 (2015) 157, arXiv:1412.0018 [hep-ph].
[119] M. González-Alonso, A. Greljo, G. Isidori, D. Marzocca, Pseudo-observables in Higgs decays, Eur. Phys. J. C 75 (2015) 128, arXiv:1412.6038 [hep-ph].
[120] ATLAS Collaboration, Measurements of differential cross sections of Higgs boson production through gluon fusion in the $H \to WW^* \to e\nu\mu\nu$ final state at $\sqrt{s} = 13$ TeV with the ATLAS detector, Eur. Phys. J. C 83 (9) (2023) 774, arXiv:2301.06822 [hep-ex].
[121] ATLAS Collaboration, Integrated and differential fiducial cross-section measurements for the vector boson fusion production of the Higgs boson in the $H \to WW^* \to e\nu\mu\nu$ decay channel at 13 TeV with the ATLAS detector, Phys. Rev. D 108 (2023) 072003, arXiv:2304.03053 [hep-ex].
[122] A. Tikhonov, Solution of incorrectly formulated problems and the regularization method, Sov. Math. Dokl. 5 (1963) 1035/1038, URL https://ci.nii.ac.jp/naid/10004315593/en/.
[123] ATLAS Collaboration, Cross-section measurements of the Higgs boson decaying into a pair of τ-leptons in proton–proton collisions at $\sqrt{s} = 13$ TeV with the ATLAS detector, Phys. Rev. D 99 (2019) 072001, arXiv:1811.08856 [hep-ex].
[124] A. Elagin, P. Murat, A. Pranko, A. Safonov, A new mass reconstruction technique for resonances decaying to $\tau\tau$, Nucl. Instrum. Methods A 654 (2011) 481–489, arXiv:1012.4686 [hep-ex].
[125] ATLAS Collaboration, Measurements of Higgs boson production cross-sections in the $H \to \tau^+\tau^-$ decay channel in pp collisions at $\sqrt{s} = 13$ TeV with the ATLAS detector, JHEP 08 (2022) 175, arXiv:2201.08269 [hep-ex].
[126] ATLAS Collaboration, Observation of Higgs boson production in association with a top quark pair at the LHC with the ATLAS detector, Phys. Lett. B 784 (2018) 173, arXiv:1806.00425 [hep-ex].
[127] LHC Higgs Cross Section Working Group, S. Heinemeyer, et al., Handbook of LHC Higgs Cross Sections: 3. Higgs Properties, CERN-2013-004, CERN, Geneva, 2013, arXiv:1307.1347 [hep-ph].
[128] ATLAS Collaboration, Search for the standard model Higgs boson produced in association with top quarks and decaying into a $b\bar{b}$ pair in pp collisions at $\sqrt{s} = 13$ TeV with the ATLAS detector, Phys. Rev. D 97 (2018) 072016, arXiv:1712.08895 [hep-ex].
[129] ATLAS Collaboration, Evidence for the associated production of the Higgs boson and a top quark pair with the ATLAS detector, Phys. Rev. D 97 (2018) 072003, arXiv:1712.08891 [hep-ex].
[130] ATLAS Collaboration, Measurement of Higgs boson decay into b-quarks in associated production with a top-quark pair in pp collisions at $\sqrt{s} = 13$ TeV with the ATLAS detector, JHEP 06 (2022) 097, arXiv:2111.06712 [hep-ex].
[131] ATLAS Collaboration, Measurement of the properties of Higgs boson production at $\sqrt{s} = 13$ TeV in the $H \to \gamma\gamma$ channel using 139 fb^{-1} of pp collision data with the ATLAS experiment, JHEP 07 (2023) 088, arXiv:2207.00348 [hep-ex].
[132] ATLAS Collaboration, Observation of $H \to b\bar{b}$ decays and VH production with the ATLAS detector, Phys. Lett. B 786 (2018) 59, arXiv:1808.08238 [hep-ex].
[133] ATLAS Collaboration, Measurements of WH and ZH production in the $H \to b\bar{b}$ decay channel in pp collisions at 13 TeV with the ATLAS detector, Eur. Phys. J. C 81 (2021) 178, arXiv:2007.02873 [hep-ex].
[134] ATLAS Collaboration, Combination of measurements of Higgs boson production in association with a W or Z boson in the $b\bar{b}$ decay channel with the ATLAS experiment at $\sqrt{s} = 13$ TeV, 2021, URL https://cds.cern.ch/record/2782535.
[135] ATLAS Collaboration, Measurement of the associated production of a Higgs boson decaying into b-quarks with a vector boson at high transverse momentum in pp collisions at $\sqrt{s} = 13$ TeV with the ATLAS detector, Phys. Lett. B 816 (2021) 136204, arXiv:2008.02508 [hep-ex].
[136] ATLAS Collaboration, Measurements of Higgs bosons decaying to bottom quarks from vector boson fusion production with the ATLAS experiment at $\sqrt{s} = 13$ TeV, Eur. Phys. J. C 81 (2021) 537, arXiv:2011.08280 [hep-ex].
[137] ATLAS Collaboration, Constraints on Higgs boson production with large transverse momentum using $H \to b\bar{b}$ decays in the ATLAS detector, Phys. Rev. D 105 (2022) 092003, arXiv:2111.08340 [hep-ex].

[138] Fermilab Lattice, MILC, and TUMQCD Collaborations, A. Bazavov, et al., Up-, down-, strange-, charm-, and bottom-quark masses from four-flavor lattice QCD, Phys. Rev. D 98 (5) (2018) 054517, arXiv:1802.04248 [hep-lat].
[139] ATLAS Collaboration, A search for the dimuon decay of the standard model Higgs boson with the ATLAS detector, Phys. Lett. B 812 (2021) 135980, arXiv:2007.07830 [hep-ex].
[140] A. Kachanovich, U. Nierste, I. Nišandžić, Higgs boson decay into a lepton pair and a photon revisited, Phys. Rev. D 101 (7) (2020) 073003, arXiv:2001.06516 [hep-ph].
[141] A.Y. Korchin, V.A. Kovalchuk, Angular distribution and forward–backward asymmetry of the Higgs-boson decay to photon and lepton pair, Eur. Phys. J. C 74 (11) (2014) 3141, arXiv:1408.0342 [hep-ph].
[142] Y. Chen, A. Falkowski, I. Low, R. Vega-Morales, New observables for CP violation in Higgs decays, Phys. Rev. D 90 (11) (2014) 113006, arXiv:1405.6723 [hep-ph].
[143] ATLAS Collaboration, Evidence for Higgs boson decays to a low-mass dilepton system and a photon in pp collisions at $\sqrt{s} = 13$ TeV with the ATLAS detector, Phys. Lett. B 819 (2021) 136412, arXiv:2103.10322 [hep-ex].
[144] ATLAS Collaboration, A search for the $Z\gamma$ decay mode of the Higgs boson in pp collisions at $\sqrt{s} = 13$ TeV with the ATLAS detector, Phys. Lett. B 809 (2020) 135754, arXiv:2005.05382 [hep-ex].
[145] ATLAS Collaboration, Searches for exclusive Higgs and Z boson decays into a vector quarkonium state and a photon using 139 fb^{-1} of ATLAS $\sqrt{s} = 13$ TeV proton–proton collision data, Eur. Phys. J. C 83 (9) (2023) 781, arXiv:2208.03122 [hep-ex].
[146] CMS Collaboration, Search for Higgs boson decays to a Z boson and a photon in proton–proton collisions at $\sqrt{s} = 13$ TeV, JHEP 05 (2023) 233, arXiv:2204.12945 [hep-ex].
[147] ATLAS and CMS Collaborations, Evidence for the Higgs boson decay to a Z boson and a photon at the LHC, Phys. Rev. Lett. 132 (2024) 021803, arXiv:2309.03501 [hep-ex].
[148] Y. Sun, H.-R. Chang, D.-N. Gao, Higgs decays to $\gamma l^+ l^-$ in the standard model, JHEP 05 (2013) 061, arXiv:1303.2230 [hep-ph].
[149] ATLAS Collaboration, Measurements of Higgs boson production by gluon–gluon fusion and vector-boson fusion using $H \to WW^* \to e\nu\mu\nu$ decays in pp collisions at $\sqrt{s} = 13$ TeV with the ATLAS detector, Phys. Rev. D 108 (2023) 032005, arXiv:2207.00338 [hep-ex].
[150] ATLAS Collaboration, Measurement of the production cross section for a Higgs boson in association with a vector boson in the $H \to WW^* \to \ell\nu\ell\nu$ channel in pp collisions at $\sqrt{s} = 13$ TeV with the ATLAS detector, Phys. Lett. B 798 (2019) 134949, arXiv:1903.10052 [hep-ex].
[151] ATLAS Collaboration, Search for invisible Higgs-boson decays in events with vector-boson fusion signatures using 139 fb^{-1} of proton–proton data recorded by the ATLAS experiment, JHEP 08 (2022) 104, arXiv:2202.07953 [hep-ex].
[152] ATLAS Collaboration, Search for associated production of a Z boson with an invisibly decaying Higgs boson or dark matter candidates at $\sqrt{s} = 13$ TeV with the ATLAS detector, Phys. Lett. B 829 (2022) 137066, arXiv:2111.08372 [hep-ex].
[153] The ATLAS Collaboration, The CMS Collaboration, The LHC Higgs Combination Group, Procedure for the LHC Higgs boson search combination in summer 2011, 2011, URL https://cds.cern.ch/record/1375842.
[154] Particle Data Group, R.L. Workman, et al., Review of particle physics, PTEP 2022 (2022) 083C01.
[155] J.R. Andersen, et al., Les houches 2015: Physics at TeV colliders, standard model working group report, 9th les houches workshop on physics at TeV colliders, 2016, arXiv:1605.04692 [hep-ph].
[156] N. Berger, et al., Simplified template cross sections - stage 1.1, 2019, arXiv:1906.02754 [hep-ph].
[157] S. Amoroso, et al., Les Houches 2019: Physics at TeV Colliders, Standard Model Working Group Report, 11th Les Houches Workshop on Physics at TeV Colliders, 2020, arXiv:2003.01700 [hep-ph].
[158] ATLAS Collaboration, Interpretations of the ATLAS measurements of Higgs boson production and decay rates and differential cross-sections in pp collisions at $\sqrt{s} = 13$ TeV, 2024, arXiv:2402.05742 [hep-ex].
[159] I. Brivio, M. Trott, The Standard Model as an Effective Field Theory, Phys. Rep. 793 (2019) 1–98, arXiv:1706.08945 [hep-ph].
[160] B. Grzadkowski, M. Iskrzyński, M. Misiak, J. Rosiek, Dimension-six terms in the standard model Lagrangian, JHEP 10 (2010) 085, arXiv:1008.4884 [hep-ph].
[161] I. Brivio, Y. Jiang, M. Trott, The SMEFTsim package, theory and tools, JHEP 12 (2017) 070, arXiv:1709.06492 [hep-ph].
[162] I. Brivio, SMEFTsim 3.0 — a practical guide, JHEP 04 (2021) 073, arXiv:2012.11343 [hep-ph].
[163] LHC Higgs Cross Section Working Group, Off-shell Higgs Interpretations Task Force : Models and Effective Field Theories Subgroup Report, LHCHWG-2022-001, CERN, Geneva, 2022, URL https://cds.cern.ch/record/2801789.
[164] K. Hagiwara, S. Ishihara, R. Szalapski, D. Zeppenfeld, Low energy effects of new interactions in the electroweak boson sector, Phys. Rev. D 48 (1993) 2182–2203.
[165] ATLAS Collaboration, Interpretations of the ATLAS measurements of Higgs boson production and decay rates and differential cross-sections in pp collisions at $\sqrt{s} = 13$ TeV, 2023, URL https://cds.cern.ch/record/2870216.
[166] S. Berge, W. Bernreuther, S. Kirchner, Determination of the Higgs CP-mixing angle in the tau decay channels at the LHC including the Drell–Yan background, Eur. Phys. J. C 74 (11) (2014) 3164, arXiv:1408.0798 [hep-ph].
[167] S. Berge, W. Bernreuther, S. Kirchner, Determination of the Higgs CP-mixing angle in the tau decay channels, Nucl. Part. Phys. Proc. 273–275 (2016) 841–845, arXiv:1410.6362 [hep-ph].
[168] C. Zhang, S. Willenbrock, Effective-field-theory approach to top-quark production and decay, Phys. Rev. D 83 (2011) 034006, arXiv:1008.3869 [hep-ph].
[169] ATLAS Collaboration, Test of CP-invariance of the Higgs boson in vector-boson fusion production and its decay into four leptons, JHEP 05 (2024) 105.
[170] D. Atwood, A. Soni, Analysis for magnetic moment and electric dipole moment form factors of the top quark via $e^+e^- \to t\bar{t}$, Phys. Rev. D 45 (1992) 2405–2413.
[171] M. Davier, L. Duflot, F. Le Diberder, A. Rougé, The optimal method for the measurement of tau polarization, Phys. Lett. B 306 (1993) 411–417.
[172] M. Diehl, O. Nachtmann, Optimal observables for the measurement of three gauge boson couplings in $e^+e^- \to W^+W^-$, Z. Phys. C 62 (1994) 397–412.
[173] ATLAS Collaboration, Test of CP invariance in vector-boson fusion production of the Higgs boson in the $H \to \tau\tau$ channel in proton–proton collisions at $\sqrt{s} = 13$ TeV with the ATLAS detector, Phys. Lett. B 805 (2020) 135426, arXiv:2002.05315 [hep-ex].
[174] ATLAS Collaboration, Test of *CP* invariance in Higgs boson vector-boson-fusion production using the $H \to \gamma\gamma$ channel with the ATLAS detector, Phys. Rev. Lett. 131 (2023) 061802, arXiv:2208.02338 [hep-ex].
[175] ATLAS Collaboration, Constraints on Higgs boson properties using $WW^*(\to e\nu\mu\nu)jj$ production in 36.1 fb^{-1} of $\sqrt{s} = 13$ TeV pp collisions with the ATLAS detector, Eur. Phys. J. C 82 (2022) 622, arXiv:2109.13808 [hep-ex].
[176] ATLAS Collaboration, Measurement of the CP properties of Higgs boson interactions with τ-leptons with the ATLAS detector, Eur. Phys. J. C 83 (7) (2023) 563, arXiv:2212.05833 [hep-ex].
[177] ATLAS Collaboration, *CP* Properties of Higgs boson interactions with top quarks in the $t\bar{t}H$ and tH processes using $H \to \gamma\gamma$ with the ATLAS detector, Phys. Rev. Lett. 125 (2020) 061802, arXiv:2004.04545 [hep-ex].
[178] M. Krämer, J. Kühn, M.L. Stong, P.M. Zerwas, Prospects of measuring the parity of Higgs particles, Z. Phys. C 64 (1994) 21–30, arXiv:hep-ph/9404280.

[179] ATLAS Collaboration, Probing the *CP* nature of the top-Higgs Yukawa coupling in $t\bar{t}H$ and tH events with $H \to b\bar{b}$ decays using the ATLAS detector at the LHC, Phys. Lett. B 849 (2023) 138469, arXiv:2303.05974 [hep-ex].
[180] G. Degrassi, P.P. Giardino, F. Maltoni, D. Pagani, Probing the Higgs self coupling via single Higgs production at the LHC, JHEP 12 (2016) 080, arXiv:1607.04251 [hep-ph].
[181] F. Maltoni, D. Pagani, A. Shivaji, X. Zhao, Trilinear Higgs coupling determination via single-Higgs differential measurements at the LHC, Eur. Phys. J. C 77 (12) (2017) 887, arXiv:1709.08649 [hep-ph].
[182] S. Di Vita, C. Grojean, G. Panico, M. Riembau, T. Vantalon, A global view on the Higgs self-coupling, JHEP 09 (2017) 069, arXiv:1704.01953 [hep-ph].
[183] M. Gorbahn, U. Haisch, Indirect probes of the trilinear Higgs coupling: $gg \to h$ and $h \to \gamma\gamma$, JHEP 10 (2016) 094, arXiv:1607.03773 [hep-ph].
[184] W. Bizoń, M. Gorbahn, U. Haisch, G. Zanderighi, Constraints on the trilinear Higgs coupling from vector boson fusion and associated Higgs production at the LHC, JHEP 07 (2017) 083, arXiv:1610.05771 [hep-ph].
[185] M. McCullough, An indirect model-dependent probe of the Higgs self-coupling, Phys. Rev. D 90 (1) (2014) 015001, arXiv:1312.3322 [hep-ph].
[186] LHC Higgs Cross Section Working Group, Modelling of the Single-Higgs Simplified Template Cross-Sections (STXS 1.2) for the Determination of the Higgs Boson Trilinear Self-Coupling, Tech. Rep. LHCHWG-2022-002, CERN, 2022, URL https://cds.cern.ch/record/2803606.
[187] ATLAS Collaboration, Search for nonresonant pair production of Higgs bosons in the $b\bar{b}b\bar{b}$ final state in pp collisions at $\sqrt{s}$=13 TeV with the ATLAS detector, Phys. Rev. D 108 (5) (2023) 052003, arXiv:2301.03212 [hep-ex].
[188] ATLAS Collaboration, Search for pair production of boosted Higgs bosons via vector-boson fusion in the $b\bar{b}b\bar{b}$ final state using *pp* collisions at $\sqrt{s} = 13$ TeV with the ATLAS detector, Phys. Lett. B 858 (2024) 139007.
[189] ATLAS Collaboration, Search for resonant and non-resonant Higgs boson pair production in the $b\bar{b}\tau^+\tau^-$ decay channel using 13 TeV *pp* collision data from the ATLAS detector, JHEP 07 (2023) 040, arXiv:2209.10910 [hep-ex].
[190] ATLAS Collaboration, Search for the non-resonant production of Higgs boson pairs via gluon fusion and vector-boson fusion in the $b\bar{b}\tau^+\tau^-$ final state in proton–proton collisions at $\sqrt{s} = 13$ TeV with the ATLAS detector, Phys. Rev. D 110 (3) (2024) 032012, arXiv:2404.12660 [hep-ex].
[191] ATLAS Collaboration, Search for Higgs boson pair production in the two bottom quarks plus two photons final state in *pp* collisions at $\sqrt{s} = 13$ TeV with the ATLAS detector, Phys. Rev. D 106 (5) (2022) 052001, arXiv:2112.11876 [hep-ex].
[192] ATLAS Collaboration, Studies of new Higgs boson interactions through nonresonant *HH* production in the $b\bar{b}\gamma\gamma$ final state in *pp* collisions at $\sqrt{s} = 13$ TeV with the ATLAS detector, JHEP 01 (2024) 066, arXiv:2310.12301 [hep-ex].
[193] ATLAS Collaboration, Combination of searches for Higgs boson pair production in *pp* collisions at $\sqrt{s} = 13$ TeV with the ATLAS detector, Phys. Rev. Lett. 133 (10) (2024) 101801, arXiv:2406.09971 [hep-ex].
[194] ATLAS Collaboration, Search for non-resonant Higgs boson pair production in final states with leptons, taus, and photons in *pp* collisions at $\sqrt{s}$=13 TeV with the ATLAS detector, JHEP 08 (2024) 164, arXiv:2405.20040 [hep-ex].
[195] ATLAS Collaboration, Search for non-resonant Higgs boson pair production in the $2b + 2\ell + E_{\mathrm{T}}^{\mathrm{miss}}$ final state in *pp* collisions at $\sqrt{s} = 13$TeV with the ATLAS detector, JHEP 02 (2024) 037, arXiv:2310.11286 [hep-ex].
[196] ATLAS Collaboration, HEFT interpretations of Higgs boson pair searches in $b\bar{b}\gamma\gamma$ and $b\bar{b}\tau^+\tau^-$ final states and of their combination in ATLAS, 2022, URL https://cds.cern.ch/record/2806411.
[197] ATLAS Collaboration, Constraints on the Higgs boson self-coupling from single- and double-Higgs production with the ATLAS detector using pp collisions at $\sqrt{s}$=13 TeV, Phys. Lett. B 843 (2023) 137745, arXiv:2211.01216 [hep-ex].
[198] ATLAS Collaboration, Constraints on the Higgs boson self-coupling from single- and double-Higgs production with the ATLAS detector using *pp* collisions at $\sqrt{s} = 13$ TeV, Phys. Lett. B 843 (2023) 137745, arXiv:2211.01216 [hep-ex].
[199] ATLAS Collaboration, Search for Higgs boson pair production in the $\gamma\gamma b\bar{b}$ final state with 13 TeV *pp* collision data collected by the ATLAS experiment, JHEP 11 (2018) 040, arXiv:1807.04873 [hep-ex].
[200] ATLAS Collaboration, Search for resonant and nonresonant Higgs boson pair production in the $b\bar{b}\tau^+\tau^-$ decay channel in *pp* collisions at $\sqrt{s} = 13$ TeV with the ATLAS detector, Phys. Rev. Lett. 121 (2018) 191801, arXiv:1808.00336 [hep-ex].
[201] ATLAS Collaboration, Search for pair production of Higgs bosons in the $b\bar{b}b\bar{b}$ final state using proton–proton collisions at $\sqrt{s} = 13$ TeV with the ATLAS detector, JHEP 01 (2019) 030, arXiv:1804.06174 [hep-ex].
[202] ATLAS Collaboration, Search for Higgs boson pair production in the $b\bar{b}WW^*$ decay mode at $\sqrt{s} = 13$ TeV with the ATLAS detector, JHEP 04 (2019) 092, arXiv:1811.04671 [hep-ex].
[203] ATLAS Collaboration, ATLAS flavour-tagging algorithms for the LHC run 2 pp collision dataset, Eur. Phys. J. C 83 (7) (2023) 681, arXiv:2211.16345 [physics.data-an].
[204] ATLAS and CMS Collaborations, Addendum to the report on the physics at the HL-LHC, and perspectives for the HE-LHC: Collection of notes from ATLAS and CMS, CERN Yellow Rep. Monogr. 7 (2019) Addendum, arXiv:1902.10229 [hep-ex].
[205] ATLAS and CMS Collaborations, Snowmass white paper contribution: Physics with the phase-2 ATLAS and CMS detectors, 2022, URL https://cds.cern.ch/record/2805993.
[206] ATLAS Collaboration, HL-LHC prospects for the measurement of Higgs boson pair production in the $b\bar{b}b\bar{b}$ final state and combination with the $b\bar{b}\gamma\gamma$ and $b\bar{b}\tau^+\tau^-$ final states at the ATLAS experiment, 2022, URL https://cds.cern.ch/record/2841244.
[207] ATLAS Collaboration, ATLAS computing acknowledgements, 2023, URL https://cds.cern.ch/record/2869272.

Article

A detailed map of Higgs boson interactions by the ATLAS experiment ten years after the discovery

https://doi.org/10.1038/s41586-022-04893-w

Received: 21 March 2022

Accepted: 23 May 2022

Published online: 4 July 2022

Open access

Check for updates

The ATLAS Collaboration*✉

The standard model of particle physics[1–4] describes the known fundamental particles and forces that make up our Universe, with the exception of gravity. One of the central features of the standard model is a field that permeates all of space and interacts with fundamental particles[5–9]. The quantum excitation of this field, known as the Higgs field, manifests itself as the Higgs boson, the only fundamental particle with no spin. In 2012, a particle with properties consistent with the Higgs boson of the standard model was observed by the ATLAS and CMS experiments at the Large Hadron Collider at CERN[10,11]. Since then, more than 30 times as many Higgs bosons have been recorded by the ATLAS experiment, enabling much more precise measurements and new tests of the theory. Here, on the basis of this larger dataset, we combine an unprecedented number of production and decay processes of the Higgs boson to scrutinize its interactions with elementary particles. Interactions with gluons, photons, and W and Z bosons—the carriers of the strong, electromagnetic and weak forces—are studied in detail. Interactions with three third-generation matter particles (bottom (b) and top (t) quarks, and tau leptons (τ)) are well measured and indications of interactions with a second-generation particle (muons, μ) are emerging. These tests reveal that the Higgs boson discovered ten years ago is remarkably consistent with the predictions of the theory and provide stringent constraints on many models of new phenomena beyond the standard model.

The standard model of particle physics has been tested by many experiments since its formulation[1–4] and, after accounting for the neutrino masses, no discrepancies between experimental observations and its predictions have been established so far. A central feature of the standard model is the existence of a spinless quantum field that permeates the Universe and gives mass to massive elementary particles. Testing the existence and properties of this field and its associated particle, the Higgs boson, has been one of the main goals of particle physics for several decades. In the standard model, the strength of the interaction, or 'coupling', between the Higgs boson and a given particle is fully defined by the particle's mass and type. There is no direct coupling to the massless standard model force mediators, the photons and gluons, whereas there are three types of couplings to massive particles in the theory. The first is the 'gauge' coupling of the Higgs boson to the mediators of the weak force, the W and Z vector bosons. Demonstrating the existence of gauge couplings is an essential test of the spontaneous electroweak symmetry-breaking mechanism[5–9]. The second type of coupling involves another fundamental interaction, the Yukawa interaction, between the Higgs boson and matter particles, or fermions. The third type of coupling is the 'self-coupling' of the Higgs boson to itself. A central prediction of the theory is that the couplings scale with the particle masses and they are all precisely predicted once all the particle masses are known. The experimental determination of the couplings of the Higgs boson to each individual particle therefore provides important and independent tests of the standard model. It also provides stringent constraints on theories beyond the standard model, which generally predict different patterns of coupling values.

In 2012, the ATLAS[12] and CMS[13] experiments at the Large Hadron Collider (LHC)[14] at CERN announced the discovery of a new particle with properties consistent with those predicted for the Higgs boson of the standard model[10,11]. More precise measurements that used all of the proton–proton collision data taken during the first data-taking period from 2011 to 2012 at the LHC (Run 1) showed evidence that, in contrast to all other known fundamental particles, the properties of the discovered particle were consistent with the hypothesis that it has no spin[15,16]. Alternate spin-1 and spin-2 hypotheses were also tested and were excluded at a high level of confidence. Investigations of the charge conjugation and parity (CP) properties of the new particle were also performed, demonstrating consistency with the CP-even quantum state predicted by the standard model, while still allowing for small admixtures of non-standard model CP-even or CP-odd states[15,16]. Limits on the particle's lifetime were obtained through indirect measurements of its natural width[15–19]. In addition, more precise measurements of the new particle's interactions with other elementary particles were achieved[20]. The results of all these investigations demonstrated that its properties were compatible with those of the standard model Higgs

*A list of authors and their affiliations appears in the online version of the paper. ✉e-mail: atlas.publications@cern.ch

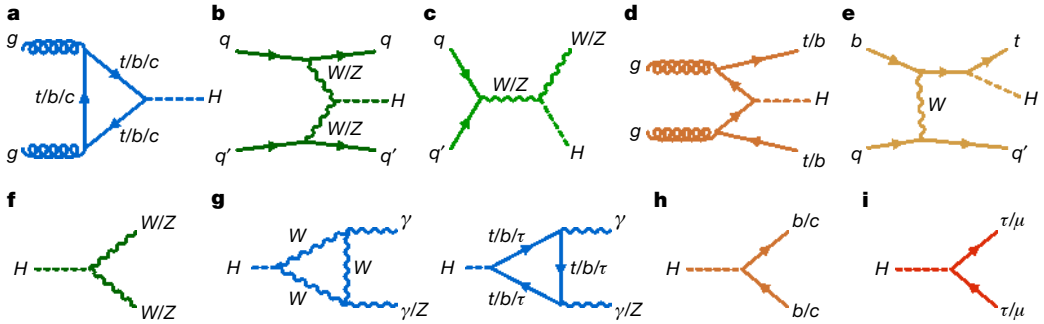

Fig. 1 | Examples of Feynman diagrams for Higgs boson production and decay. a–e, The Higgs boson is produced via gluon–gluon fusion (**a**), vector boson fusion (VBF; **b**) and associated production with vector bosons (**c**), top or *b* quark pairs (**d**), or a single top quark (**e**). **f–i**, The Higgs boson decays into a pair of vector bosons (**f**), a pair of photons or a *Z* boson and a photon (**g**), a pair of quarks (**h**), and a pair of charged leptons (**i**). Loop-induced Higgs boson interactions with gluons or photons are shown in blue, and processes involving couplings to *W* or *Z* bosons in green, to quarks in orange, and to leptons in red. Two different shades of green (orange) are used to separate the VBF and *VH* ($t\bar{t}H$ and *tH*) production processes.

boson. However, the statistical uncertainties associated with these early measurements allowed considerable room for possible interpretations of the data in terms of new phenomena beyond the standard model and left many predictions of the standard model untested.

The characterization of the Higgs boson continued during the Run 2 data-taking period between 2015 and 2018. About 9 million Higgs bosons are predicted to have been produced in the ATLAS detector during this period, of which only about 0.3% are experimentally accessible. This is 30 times more events than at the time of its discovery, owing to the higher rate of collisions and the increase of the collision energy from 8 teraelectronvolts (TeV) to 13 TeV, which raises the production rate. In this Article, the full Run 2 dataset, corresponding to an integrated luminosity of 139 inverse femtobarns (fb^{-1}), is used for the measurements of Higgs boson production and decay rates, which are used to study the couplings between the Higgs boson and the particles involved. This improves on the previous measurements obtained with partial Run 2 datasets[21,22]. The corresponding predictions depend on the value of the Higgs boson mass, which has now been measured by the ATLAS and CMS experiments[23–25] with an uncertainty of approximately 0.1%. The predictions employed in this article use the combined central value of 125.09 GeV[23].

The dominant production process at the LHC, which accounts for about 87% of Higgs boson production, is the heavy-quark loop-mediated gluon–gluon fusion process (ggF). The second most copious process is vector boson fusion (VBF), in which two weak bosons, either *Z* or *W* bosons, fuse to produce a Higgs boson (7%). Next in rate is production of a Higgs boson in association with a weak ($V = W, Z$) boson (4%). Production of a Higgs boson in association with a pair of top quarks ($t\bar{t}H$) or bottom quarks ($b\bar{b}H$) each account for about 1% of the total rate. The contribution of other $q\bar{q}H$ processes is much smaller and experimentally not accessible. Only about 0.05% of Higgs bosons are produced in association with a single top quark (*tH*). Representative Feynman diagrams of these processes are shown in Fig. 1a–e. After it is produced, the Higgs boson is predicted to decay almost instantly, with a lifetime of 1.6×10^{-22} seconds. More than 90% of these decays are via eight decay modes (Fig. 1f–i): decays into gauge boson pairs, that is, *W* bosons with a probability, or branching fraction, of 22%, *Z* bosons 3%, photons (γ) 0.2%, *Z* boson and photon 0.2%, as well as decays into fermion pairs, that is, *b* quarks 58%, *c* quarks 3%, τ leptons 6%, and muons (μ) 0.02%. There may also be decays of the Higgs boson into invisible particles, above the standard model prediction of 0.1%, which are also searched for. Such decays are possible in theories beyond the standard model, postulating, for example, the existence of dark matter particles that do not interact with the detector.

In this Article, the mutually exclusive measurements of Higgs boson production and decays probing all processes listed above are combined, taking into account the correlations among their uncertainties. In a single measurement, different couplings generally contribute in the production and decay. The combination of all measurements is therefore necessary to constrain these couplings individually. This enables key tests of the Higgs sector of the standard model to be performed, including the determination of the coupling strengths of the Higgs boson to various fundamental particles and a comprehensive study of the kinematic properties of Higgs boson production. The latter could reveal new phenomena beyond the standard model that are not observable through measurements of the coupling strengths.

The ATLAS detector at the LHC

The ATLAS experiment[12] at the LHC is a multipurpose particle detector with a forward–backward symmetric, cylindrical geometry and a near 4π coverage in solid angle. The detector records digitized signals produced by the products of LHC's proton bunch collisions, hereafter termed collision 'events'. It is designed to identify a wide variety of particles and measure their momenta and energies. These particles include electrons, muons, τ leptons and photons, as well as gluons and quarks, which produce collimated jets of particles in the detector. Because the jets from *b* quarks and *c* quarks contain hadrons with relatively long lifetimes, they can be identified by observing a decay vertex, which typically occurs at a measurable distance from the collision point. The presence of particles that do not interact with the detector, such as neutrinos, can be inferred by summing the vector momenta of the visible particles in the plane transverse to the beam and imposing conservation of transverse momenta.

The detector components closest to the collision point measure charged-particle trajectories and momenta. This inner spectrometer is surrounded by calorimeters that are used in the identification of particles and in the measurement of their energies. The calorimeters are in turn surrounded by an outer spectrometer dedicated to measuring the trajectories and momenta of muons, the only charged particle to travel through the calorimeters. A two-level trigger system was optimized for Run 2 data-taking[26] to select events of interest at a rate of about 1 kHz from the proton bunch collisions occurring at a rate of 40 MHz. An extensive software suite[27] is used in the simulation, reconstruction and analysis of real and simulated data, in detector operations, and in the trigger and data-acquisition systems of the experiment.

Input measurements and combination procedure

Physics analyses typically focus on particular production and decay processes and measure the number of Higgs boson candidates observed after accounting for non-Higgs background processes. To determine

the strengths of the interactions of the Higgs boson, simultaneous fits with different physically motivated assumptions are performed on a combined set of complementary measurements. The relative weights of the input measurements in the combination depend on the analysis selection efficiencies, on the signal rates associated with the Higgs processes studied by the analysis, on the signal-to-background ratios, and on the associated systematic uncertainties.

For each decay mode entering the combination, the production process is assessed via event classification based on the properties of particles produced in association with the Higgs boson, mostly via dedicated machine-learning approaches. Unless stated otherwise, studies of each decay mode consider all individual or combined contributions from six production processes: ggF, VBF, WH, ZH, $t\bar{t}H$ and tH. Higgs boson interactions are further explored via additional event classification of each production process based on the kinematic properties of the produced Higgs boson and the associated particles.

The input to the combined measurement includes the latest results from the decay modes that initially led to the Higgs boson discovery: $H \to ZZ \to \ell^+\ell^-\ell^+\ell^-$ decays[28] with two Z bosons that subsequently decay into a pair of oppositely charged electrons or muons; $H \to W^\pm W^\mp \to \ell^\pm \nu_\ell \ell^\mp \nu_\ell$ decays targeting separately the ggF and VBF[29], and WH and ZH[30] production processes; and $H \to \gamma\gamma$ decays[31] with two high-energy photons. The latter is the only measurement used to discriminate between the $t\bar{t}H$ and tH processes. These diboson decay modes are for the first time complemented by a search for the rare $H \to Z\gamma \to \ell^+\ell^-\gamma$ decay[32]. The decays of Higgs bosons to fermions are also extensively explored. The measurement of the dominant $H \to b\bar{b}$ decay mode is particularly challenging owing to a very large multi-jet background, which can be suppressed by requiring the presence of additional particles characteristic of the WH or ZH[33,34], VBF[35] and $t\bar{t}H$[36] production processes. As a new input, the fully hadronic $H \to b\bar{b}$ signal events with large Higgs boson transverse momentum are also considered[37], providing for the first time sensitivity to the ggF production process in this decay mode. The sensitivity of the latest measurement in the $H \to \tau^+\tau^-$ decay mode[38] is now extended to the VH and combined $t\bar{t}H$ and tH production processes. In addition to the $t\bar{t}H$ measurements obtained in the $\gamma\gamma$, $\tau^+\tau^-$ and ZZ decay modes, a complementary analysis that is sensitive to $\tau^+\tau^-$, $W^\pm W^\mp$ and ZZ decays is performed using events with multiple leptons in the final state[39]. The considerably more challenging measurements of Higgs boson couplings to second-generation fermions are explored via searches for the $H \to \mu^+\mu^-$ decay[40] and, included in the combination for the first time, $H \to c\bar{c}$ decay[41]. Owing to the large multi-jet background, the latter decay mode is currently accessed only via WH and ZH production. Finally, the inputs to the combination are complemented by the latest direct searches in the VBF and ZH production processes for Higgs boson decays into invisible particles that escape the detector[42,43]. A summary of these input measurements used in the combination is available in Extended Data Table 1.

All input measurements are performed with the full set of Run 2 data, except for the measurements of previous works[30,39], which use a partial Run 2 dataset collected during 2015 and 2016. The direct searches for invisible Higgs boson decays and the $H \to c\bar{c}$ measurements are employed only for measurements of the relevant Higgs boson coupling strengths, and the $H \to b\bar{b}$ measurements at high Higgs boson transverse momenta[37] are considered only when probing the kinematic properties of Higgs boson production. All other inputs are used for the measurements of production cross-sections, branching fractions and coupling strengths. The measurement of kinematic properties of Higgs boson production excludes input measurements from previous works[30,32,39–41], owing to their limited sensitivity.

Analyses performed with the Run 2 data introduce a number of improvements, often resulting in up to 50% better signal sensitivities compared to those expected from just the increase in the analysed amount of data. These improvements include better particle reconstruction (optimized to cope with an increased number of proton interactions per bunch crossing), dedicated reconstruction of highly Lorentz-boosted $H \to b\bar{b}$ decays, a greater number of simulated events, higher granularity of the kinematic regions that are probed in each production process, and improved signal and background theory predictions.

The standard model is tested by comparing the observed signal rates to theory predictions that require state-of-the-art calculations of Higgs boson production cross-sections and branching fractions[44–50]. All signal reconstruction efficiencies and most background rates are predicted from the simulation. The simulation is complemented by the use of dedicated signal-depleted control data for measurements of selected background processes and to constrain signal-selection efficiencies. A common set of event generators were used in all analyses to describe the gluon and quark interactions in the proton–proton collisions. The generated particles were passed through a detailed simulation of the ATLAS detector response prior to their reconstruction and identification.

The statistical analysis of the data is described in more detail in Methods. It relies on a likelihood formalism, where the product of the likelihood functions describing each of the input measurements is calculated in order to obtain a combined likelihood[51]. The effects of experimental and theoretical systematic uncertainties on the predicted signal and background yields are implemented by including nuisance parameters in the likelihood function. The values of those additional parameters are either fully determined by the included data, or constrained by Gaussian terms that multiply the likelihood. The effects of uncertainties that affect multiple measurements are propagated coherently through the fit by using common nuisance parameters.

The statistical test of a given signal hypothesis, used for the measurement of the parameters of interest, is performed with a test statistic that is based on the profile likelihood ratio[52]. The confidence intervals of the measured parameters and the p value used to test the compatibility of the results and the standard model predictions are constructed from the test statistic distribution, which is obtained using asymptotic formulae[52].

The total uncertainty in the measurement of a given parameter of interest can be decomposed into different components. The statistical uncertainty is obtained from a fit with all externally constrained nuisance parameters set to their best-fit values. The systematic uncertainty, the squared value of which is evaluated as the difference between the squares of the total uncertainty and the statistical uncertainty, can be decomposed into categories by setting all relevant subsets of nuisance parameters to their best-fit values.

Combined measurement with ATLAS Run 2 data

The Higgs boson production rates are probed by the likelihood fit to observed signal yields described earlier. Because the production cross-section σ_i and the branching fraction B_f for a specific production process i and decay mode f cannot be measured separately without further assumptions, the observed signal yield for a given process is expressed in terms of a single signal strength modifier $\mu_{if} = (\sigma_i/\sigma_i^{\mathrm{SM}})(B_f/B_f^{\mathrm{SM}})$, where the superscript 'SM' denotes the corresponding standard model prediction. Assuming that all production and decay processes scale with the same global signal strength $\mu = \mu_{if}$, the inclusive Higgs boson production rate relative to the standard model prediction is measured to be

$$\mu = 1.05 \pm 0.06$$
$$= 1.05 \pm 0.03(\mathrm{stat.}) \pm 0.03(\mathrm{exp.}) \pm 0.04(\mathrm{sig.\ th.}) \pm 0.02(\mathrm{bkg.\ th.}).$$

The total measurement uncertainty is decomposed into components for statistical uncertainties, experimental systematic uncertainties, and theory uncertainties in both signal and background modelling. Both the experimental and the theoretical uncertainties are almost

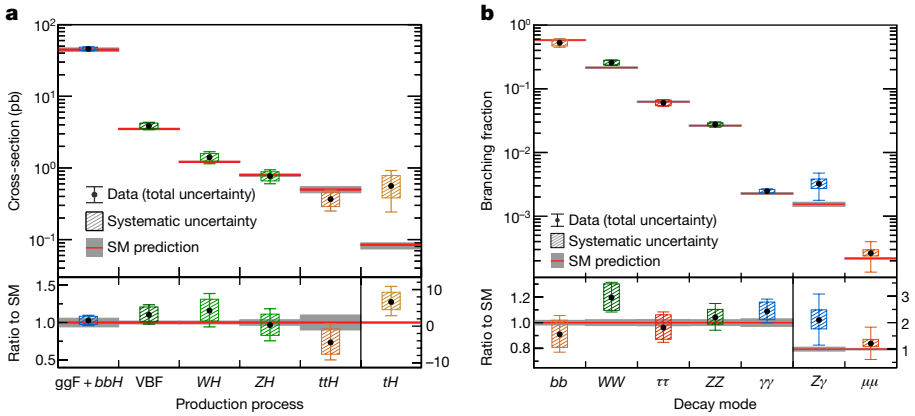

Fig. 2 | Observed and predicted Higgs boson production cross-sections and branching fractions. a, Cross-sections for different Higgs boson production processes are measured assuming standard model (SM) values for the decay branching fractions. **b**, Branching fractions for different Higgs boson decay modes are measured assuming SM values for the production cross-sections. The lower panels show the ratios of the measured values to their SM predictions. The vertical bar on each point denotes the 68% confidence interval. The p value for compatibility of the measurement and the SM prediction is 65% for **a** and 56% for **b**. Data are from ATLAS Run 2.

a factor of two lower than in the Run 1 result[20]. The presented measurement supersedes the previous ATLAS combination with a partial Run 2 dataset[22], decreasing the latest total measurement uncertainty by about 30%.

Higgs boson production is also studied per individual process. As opposed to the top quark decay products from $t\bar{t}H$ production, the identification efficiency of b jets from the $b\bar{b}H$ production is low, making the $b\bar{b}H$ process experimentally indistinguishable from ggF production. The $b\bar{b}H$ and ggF processes are therefore grouped together, with $b\bar{b}H$ contributing a relatively small amount: of the order of 1% to the total ggF + $b\bar{b}H$ production. In cases where several processes are combined, the combination assumes the relative fractions of the components to be those from the standard model within corresponding theory uncertainties. Results are obtained from the fit to the data, where the cross-section of each production process is a free parameter of the fit. Higgs boson decay branching fractions are set to their standard model values, within the uncertainties specified previously[44]. The results are shown in Fig. 2a.

All measurement results are compatible with the standard model predictions. For the ggF and VBF production processes, which were previously observed in Run 1 data, the cross-sections are measured with a precision of 7% and 12%, respectively. The following production processes are now also observed: WH with an observed (expected) signal significance of 5.8 (5.1) standard deviations (σ), ZH with 5.0σ (5.5σ) and the combined $t\bar{t}H$ and tH production processes with 6.4σ (6.6σ), where the expected signal significances are obtained under the standard model hypothesis. The separate $t\bar{t}H$ and tH measurements lead to an observed (expected) upper limit on tH production of 15 (7) times the standard model prediction at the 95% confidence level (CL), with a relatively large negative correlation coefficient of 56% between the two measurements. This is due to cross-contamination between the $t\bar{t}H$ and tH processes in the set of reconstructed events that provide the highest sensitivity to these production processes.

Branching fractions of individual Higgs boson decay modes are measured by setting the cross-sections for Higgs boson production processes to their respective standard model values. The results are shown in Fig. 2b. The branching fractions of the $\gamma\gamma$, ZZ, $W^{\pm}W^{\mp}$ and $\tau^{+}\tau^{-}$ decays, which were already observed in the Run 1 data, are measured with a precision ranging from 10% to 12%. The $b\bar{b}$ decay mode is observed with a signal significance of 7.0σ (expected 7.7σ), and the observed (expected) signal significances for the $H \to \mu^{+}\mu^{-}$ and $H \to Z\gamma$ decays are 2.0σ (1.7σ) and 2.3σ (1.1σ), respectively.

The assumptions about the relative contributions of different decay or production processes in the above measurements are relaxed by directly measuring the product of production cross-section and branching fraction for different combinations of production and decay processes. The corresponding results are shown in Fig. 3. The measurements are in agreement with the standard model prediction.

To determine the value of a particular Higgs boson coupling strength, a simultaneous fit of many individual production times branching

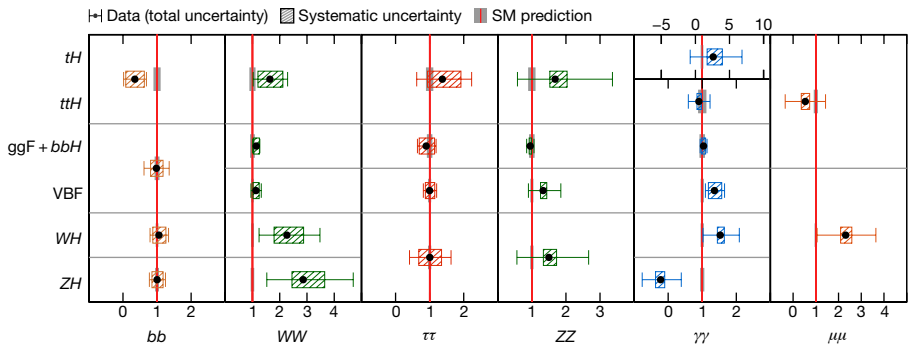

Fig. 3 | Ratio of observed rate to predicted standard model event rate for different combinations of Higgs boson production and decay processes. The horizontal bar on each point denotes the 68% confidence interval. The narrow grey bands indicate the theory uncertainties in the standard model (SM) cross-section multiplied by the branching fraction predictions. The p value for compatibility of the measurement and the SM prediction is 72%. $\sigma_i B_f$ is normalized to the SM prediction. Data are from ATLAS Run 2.

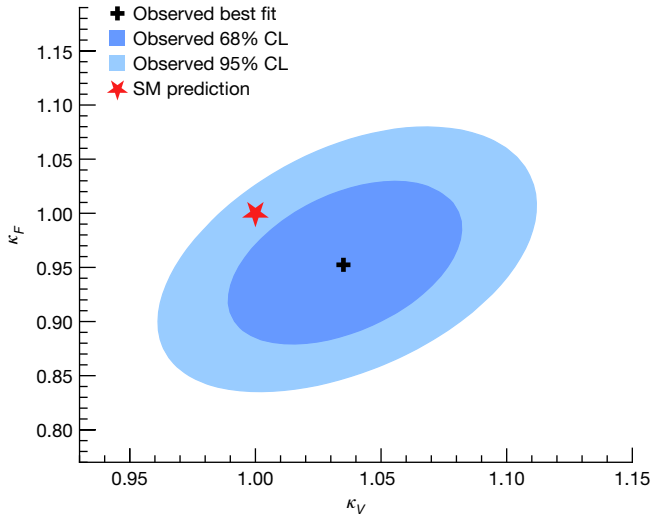

Fig. 4 | Negative log-likelihood contours corresponding to 68% and 95% CL in the (κ_V, κ_F) plane. The data are obtained from a combined fit assuming no contributions from invisible or undetected non-standard model Higgs boson decays. The p value for compatibility of the combined measurement and the standard model (SM) prediction is 14%. Data are from ATLAS Run 2.

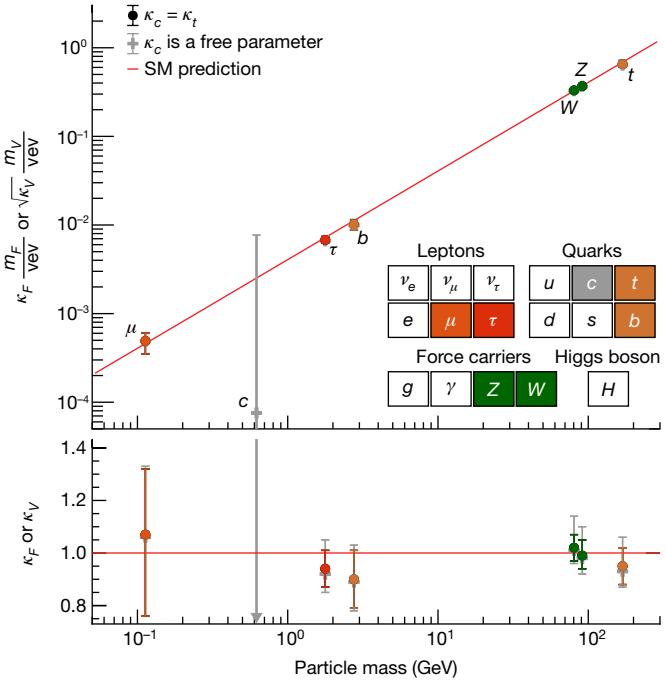

Fig. 5 | Reduced Higgs boson coupling strength modifiers and their uncertainties. They are defined as $\kappa_F m_F$/vev for fermions ($F = t, b, \tau, \mu$) and $\sqrt{\kappa_V} m_V$/vev for vector bosons as a function of their masses m_F and m_V. Two fit scenarios with $\kappa_c = \kappa_t$ (coloured circle markers), or κ_c left free-floating in the fit (grey cross markers) are shown. Loop-induced processes are assumed to have the standard model (SM) structure, and Higgs boson decays to non-SM particles are not allowed. The vertical bar on each point denotes the 68% confidence interval. The p values for compatibility of the combined measurement and the SM prediction are 56% and 65% for the respective scenarios. The lower panel shows the values of the coupling strength modifiers. The grey arrow points in the direction of the best-fit value and the corresponding grey uncertainty bar extends beyond the lower panel range. Data are from ATLAS Run 2.

fraction measurements is required. The coupling fit presented here is performed within the κ framework[53] with a set of parameters $\boldsymbol{\kappa}$ that affect the Higgs boson coupling strengths without altering any kinematic distributions of a given process.

Within this framework, the cross-section times the branching fraction for an individual measurement is parameterized in terms of the multiplicative coupling strength modifiers κ. A coupling strength modifier κ_p for a production or decay process via the coupling to a given particle p is defined as $\kappa_p^2 = \sigma_p/\sigma_p^{\text{SM}}$ or $\kappa_p^2 = \Gamma_p/\Gamma_p^{\text{SM}}$, respectively, where Γ_p is the partial decay width into a pair of particles p. The parameterization takes into account that the total decay width depends on all decay modes included in the present measurements, as well as currently undetected or invisible, direct or indirect decays predicted by the standard model (such as those to gluons, light quarks or neutrinos) and the hypothetical decays into non-standard model particles. The decays to non-standard model particles are divided into decays to invisible particles and other decays that would be undetected owing to large backgrounds. The corresponding branching fractions for the two are denoted by $B_{\text{inv.}}$ and $B_{\text{u.}}$, respectively.

In the following, three classes of models with progressively fewer assumptions about coupling strength modifiers are considered. Standard model values are assumed for the coupling strength modifiers of first-generation fermions, and the modifiers of the second-generation quarks are set to those of the third generation, except where κ_c is left free-floating in the fit. Owing to their small sizes, these couplings are not expected to noticeably affect any of the results. The ggF production and the $H \to \gamma\gamma$ and $H \to Z\gamma$ decays are loop-induced processes. They are either expressed in terms of the more fundamental coupling strength scale factors corresponding to the particles that contribute to the loop-induced processes in the standard model, or treated using effective coupling strength modifiers κ_g, κ_γ and $\kappa_{Z\gamma}$, respectively. The latter scenario accounts for possible loop contributions from particles beyond the standard model. The small contribution from the loop-induced $gg \to ZH$ process is always parameterized in terms of the couplings to the corresponding standard model particles.

The first model tests one scale factor for the vector bosons, $\kappa_V = \kappa_W = \kappa_Z$, and a second, κ_F, which applies to all fermions. In general, the standard model prediction of $\kappa_V = \kappa_F = 1$ does not hold in extensions of the standard model. For example, the values of κ_V and κ_F would be less than 1 in models in which the Higgs boson is a composite particle. The effective couplings corresponding to the ggF, $H \to \gamma\gamma$ and $H \to Z\gamma$ loop-induced processes are parameterized in terms of the fundamental standard model couplings. It is assumed that there are no invisible or undetected Higgs boson decays beyond the standard model, that is, $B_{\text{inv.}} = B_{\text{u.}} = 0$. As only the relative sign between κ_V and κ_F is physical and a negative relative sign has been excluded with a high level of confidence[20], $\kappa_V \geq 0$ and $\kappa_F \geq 0$ are assumed. Figure 4 shows the results of a combined fit in the (κ_V, κ_F) plane. The best-fit values and their uncertainties from the combined fit are $\kappa_V = 1.035 \pm 0.031$ and $\kappa_F = 0.95 \pm 0.05$, compatible with the standard model predictions. A relatively large positive correlation of 39% is observed between the two fit parameters, because some of the most sensitive input measurements involve the ggF production process (that is, via couplings to fermions) with subsequent Higgs boson decays into vector bosons.

In the second class of models, the coupling strength modifiers for W, Z, t, b, c, τ and μ are treated independently. All modifiers are assumed to be positive. It is assumed that only standard model particles contribute to the loop-induced processes, and modifications of the fermion and vector boson couplings are propagated through the loop calculations. Invisible or undetected non-standard model Higgs boson decays are not considered. These models enable testing of the predicted scaling of the couplings of the Higgs boson to the standard model particles as a function of their mass using the reduced coupling strength modifiers $\sqrt{\kappa_V g_V/2\text{vev}} = \sqrt{\kappa_V}(m_V/\text{vev})$ for weak bosons with a mass m_V and $\kappa_F g_F = \kappa_F m_F/\text{vev}$ for fermions with a mass m_F, where g_V and g_F are the corresponding absolute coupling strengths and 'vev' is the vacuum

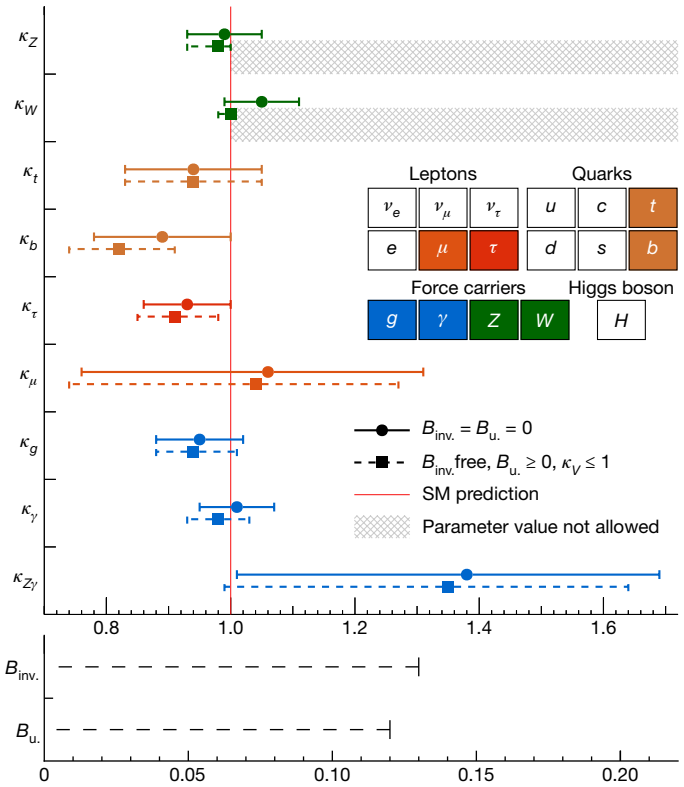

Fig. 6 | Reduced coupling strength modifiers and their uncertainties per particle type with effective photon, *Zγ* and gluon couplings. The horizontal bars on each point denote the 68% confidence interval. The scenario in which $B_{inv.} = B_{u.} = 0$ is assumed is shown as solid lines with circle markers. The *p* value for compatibility with the standard model (SM) prediction is 61% in this case. The scenario in which $B_{inv.}$ and $B_{u.}$ are allowed to contribute to the total Higgs boson decay width while assuming that $\kappa_V \leq 1$ and $B_{u.} \geq 0$ is shown as dashed lines with square markers. The lower panel shows the 95% CL upper limits on $B_{inv.}$ and $B_{u.}$. Data are from ATLAS Run 2.

expectation value of the Higgs field. Figure 5 shows the results for two scenarios: one with the coupling to *c* quarks constrained by $\kappa_c = \kappa_t$ in order to cope with the low sensitivity to this coupling; and the other with κ_c left as a free parameter in the fit. All measured coupling strength modifiers are found to be compatible with their standard model prediction. When the coupling strength modifier κ_c is left unconstrained in the fit, an upper limit of $\kappa_c < 5.7$ (7.6) times the standard model prediction is observed (expected) at 95% CL and the uncertainty in each of the other parameters increases because of the resulting weaker constraint on the total decay width. This improves the current observed (expected) limit of $\kappa_c < 8.5$ (12.4) at 95% CL from the individual measurement of $H \to c\bar{c}$ decays[41] despite the relaxed assumptions on other coupling strength modifiers, through constraints coming from the parameterization of the total Higgs boson decay width that impacts all measurements.

The third class of models in the κ framework closely follows the previous one, but allows for the presence of non-standard model particles in the loop-induced processes. These processes are parameterized by the effective coupling strength modifiers κ_g, κ_γ and $\kappa_{Z\gamma}$ instead of propagating modifications of the standard model particle couplings through the loop calculations. It is also assumed that any potential effect beyond the standard model does not substantially affect the kinematic properties of the Higgs boson decay products. The fit results for the scenario in which invisible or undetected non-standard model Higgs boson decays are assumed not to contribute to the total Higgs decay width, that is, $B_{inv.} = B_{u.} = 0$, are shown in Fig. 6 together with the results for the scenario allowing such decays. To avoid degenerate solutions, the latter constrains $B_{u.} \geq 0$ and imposes the additional constraint $\kappa_V \leq 1$ that naturally arises in various scenarios of physics beyond the standard model[54,55]. All measured coupling strength modifiers are compatible with their standard model predictions.

When allowing invisible or undetected non-standard model Higgs boson decays to contribute to the total Higgs boson decay width, the previously measured coupling strength modifiers do not change significantly, and upper limits of $B_{u.} < 0.12$ (expected 0.21) and $B_{inv.} < 0.13$ (expected 0.08) are set at 95% CL on the corresponding branching fraction. The latter improves on the current best limit of $B_{inv.} < 0.145$ (expected 0.103) from direct ATLAS searches[42].

In all tested scenarios, the statistical and the systematic uncertainty contribute almost equally to the total uncertainty in most of the κ parameter measurements. The exceptions are the κ_μ, $\kappa_{Z\gamma}$, κ_c and $B_{u.}$ measurements, for which the statistical uncertainty still dominates.

Kinematic properties of Higgs boson production probing the internal structure of its couplings are studied in the framework of simplified template cross-sections[44,56–58]. The framework partitions the phase space of standard model Higgs boson production processes into a set of regions defined by the specific kinematic properties of the Higgs boson and, where relevant, of the associated jets, *W* bosons, or *Z* bosons, as described in Methods. The regions are defined so as to provide experimental sensitivity to deviations from the standard model predictions, to avoid large theory uncertainties in these predictions, and to minimize the model-dependence of their extrapolations to the experimentally accessible signal regions. Signal cross-sections measured in each of the introduced kinematic regions are compared with those predicted when assuming that the branching fractions and kinematic properties of the Higgs boson decay are described by the standard model.

The results of the simultaneous measurement in 36 kinematic regions are presented in Fig. 7. Compared to previous results with a smaller dataset[22], a much larger number of regions are probed, particularly at high Higgs boson transverse momenta, where in many cases the sensitivity to new phenomena beyond the standard model is expected to be enhanced. All measurements are consistent with the standard model predictions.

Conclusion

In summary, the production and decay rates of the Higgs boson were measured using the dataset collected by the ATLAS experiment during Run 2 of the LHC from 2015 to 2018. The measurement results were found to be in excellent agreement with the predictions of the standard model. In different scenarios, the couplings to the three heaviest fermions, the top quark, the *b* quark and the *τ* lepton, were measured with uncertainties ranging from about 7% to 12% and the couplings to the weak bosons (*Z* and *W*) were measured with uncertainties of about 5%. In addition, indications are emerging of the presence of very rare Higgs boson decays into second-generation fermions and into a *Z* boson and a photon. Finally, a comprehensive study of Higgs boson production kinematics was performed and the results were also found to be compatible with standard model predictions. In the ten years since its discovery, the Higgs boson has undergone many experimental tests that have demonstrated that, so far, its nature is remarkably consistent with the predictions of the standard model. However, some of its key properties—such as the coupling of the Higgs boson to itself—remain to be measured. In addition, some of its rare decay modes have not yet been observed and there is ample room for new phenomena beyond the standard model to be discovered. Substantial progress on these fronts is expected in the future, given that detector upgrades are planned for the coming years, that systematic uncertainties are expected to be reduced considerably[59], and that the size of the LHC's dataset is projected to increase by a factor of 20.

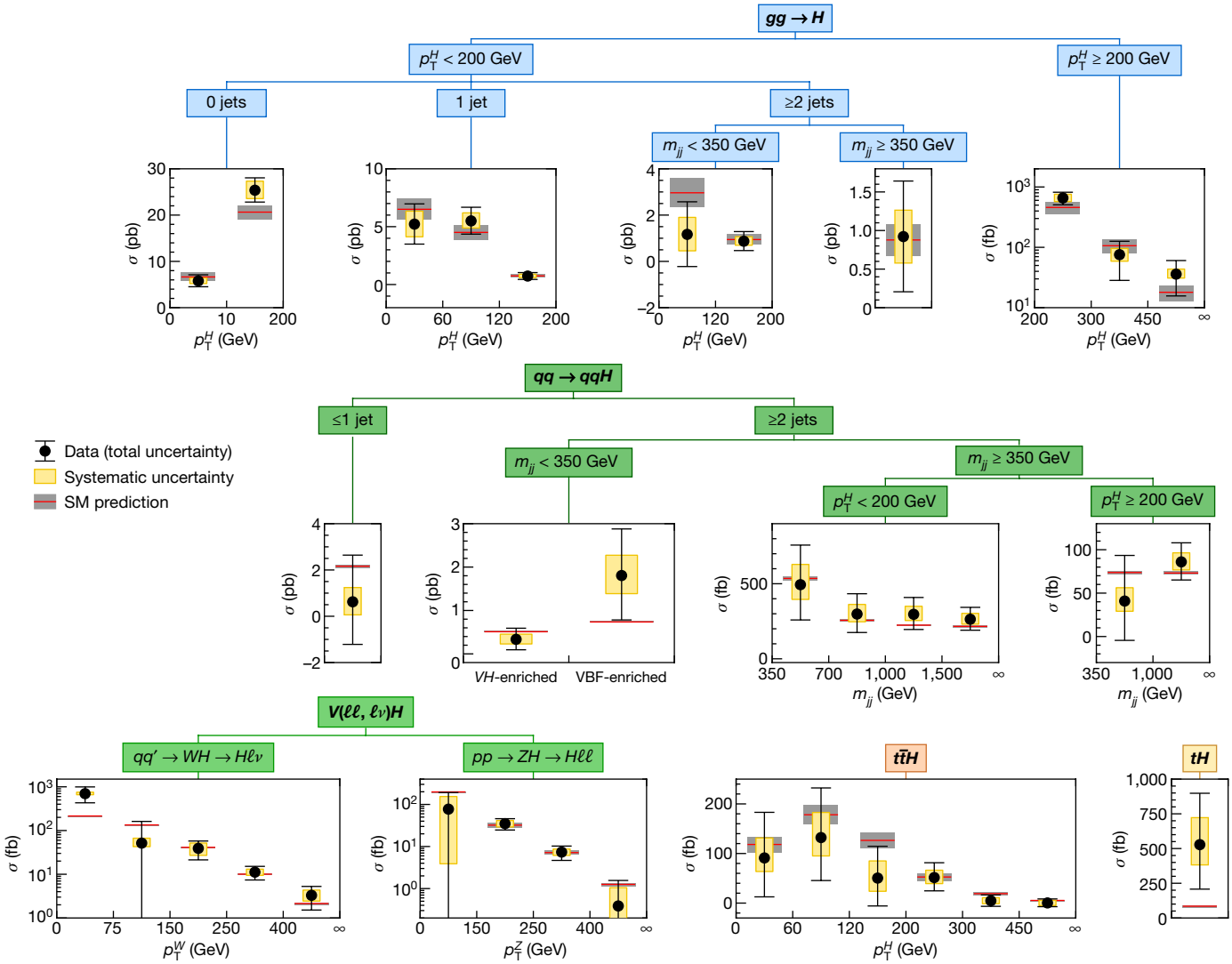

Fig. 7 | Observed and predicted Higgs boson production cross-sections in different kinematic regions. The vertical bar on each point denotes the 68% confidence interval. The *p* value for compatibility of the combined measurement and the standard model (SM) prediction is 94%. Kinematic regions are defined separately for each production process, based on the jet multiplicity, the transverse momentum of the Higgs (p_T^H) and vector bosons (p_T^W and p_T^Z) and the two-jet invariant mass (m_{jj}). The '*VH*-enriched' and 'VBF-enriched' regions with the respective requirements of $m_{jj} \in [60, 120)$ GeV and $m_{jj} \notin [60, 120)$ GeV are enhanced in signal events from *VH* and VBF productions, respectively. Data are from ATLAS Run 2.

Online content

Any methods, additional references, Nature Research reporting summaries, source data, extended data, supplementary information, acknowledgements, peer review information; details of author contributions and competing interests; and statements of data and code availability are available at https://doi.org/10.1038/s41586-022-04893-w.

1. Weinberg, S. A model of leptons. *Phys. Rev. Lett.* **19**, 1264–1266 (1967).
2. Glashow, S. L. Partial symmetries of weak interactions. *Nucl. Phys.* **22**, 579–588 (1961).
3. Salam, A. Weak and electromagnetic interactions. *Proc. 8th Nobel Symposium, Conf. Proc. C* **680519**, 367–377 (1968).
4. 't Hooft, G. & Veltman, M. J. G. Regularization and renormalization of gauge fields. *Nucl. Phys. B* **44**, 189–213 (1972).
5. Higgs, P. W. Broken symmetries, massless particles and gauge fields. *Phys. Lett.* **12**, 132–133 (1964).
6. Higgs, P. W. Broken symmetries and the masses of gauge bosons. *Phys. Rev. Lett.* **13**, 508–509 (1964).
7. Englert, F. & Brout, R. Broken symmetry and the mass of gauge vector mesons. *Phys. Rev. Lett.* **13**, 321–323 (1964).
8. Guralnik, G., Hagen, C. & Kibble, T. Global conservation laws and massless particles. *Phys. Rev. Lett.* **13**, 585–587 (1964).
9. Kibble, T. Symmetry breaking in non-Abelian gauge theories. *Phys. Rev.* **155**, 1554–1561 (1967).
10. ATLAS Collaboration. Observation of a new particle in the search for the Standard Model Higgs boson with the ATLAS detector at the LHC. *Phys. Lett. B* **716**, 1–29 (2012).
11. CMS Collaboration. Observation of a new boson at a mass of 125 GeV with the CMS experiment at the LHC. *Phys. Lett. B* **716**, 30–60 (2012).
12. ATLAS Collaboration. The ATLAS experiment at the CERN Large Hadron Collider. *J. Instrum.* **3**, S08003 (2008).
13. CMS Collaboration. The CMS experiment at the CERN LHC. *J. Instrum.* **3**, S08004 (2008).
14. Evans, L. & Bryant, P. LHC Machine. *J. Instrum.* **3**, S08001 (2008).
15. ATLAS Collaboration. Study of the spin and parity of the Higgs boson in diboson decays with the ATLAS detector. *Eur. Phys. J. C* **75**, 476 (2015).
16. CMS Collaboration. Constraints on the spin-parity and anomalous HVV couplings of the Higgs boson in proton collisions at 7 and 8 TeV. *Phys. Rev. D* **92**, 012004 (2015).
17. ATLAS Collaboration. Constraints on the off-shell Higgs boson signal strength in the high-mass ZZ and WW final states with the ATLAS detector. *Eur. Phys. J. C* **75**, 335 (2015).
18. CMS Collaboration. Search for Higgs boson off-shell production in proton–proton collisions at 7 and 8 TeV and derivation of constraints on its total decay width. *J. High Energy Phys.* **2016-09**, 51 (2016).
19. CMS Collaboration. Limits on the Higgs boson lifetime and width from its decay to four charged leptons. *Phys. Rev. D* **92**, 072010 (2015).
20. ATLAS Collaboration & CMS Collaboration. Measurements of the Higgs boson production and decay rates and constraints on its couplings from a combined ATLAS and CMS analysis of the LHC pp collision data at √s = 7 and 8 TeV. *J. High Energy Phys.* **2016-08**, 45 (2016).
21. CMS Collaboration. Combined measurements of Higgs boson couplings in proton–proton collisions at √s = 13 TeV. *Eur. Phys. J. C* **79**, 421 (2019).

22. ATLAS Collaboration. Combined measurements of Higgs boson production and decay using up to 80 fb^{-1} of proton–proton collision data at √s = 13 TeV collected with the ATLAS experiment. *Phys. Rev. D* **101**, 012002 (2020).
23. ATLAS Collaboration & CMS Collaboration. Combined measurement of the Higgs boson mass in pp collisions at √s = 7 and 8 TeV with the ATLAS and CMS experiments. *Phys. Rev. Lett.* **114**, 191803 (2015).
24. ATLAS Collaboration. Measurement of the Higgs boson mass in the H → ZZ* → 4ℓ and H → γγ channels with √s = 13 TeV pp collisions using the ATLAS detector. *Phys. Lett. B* **784**, 345–366 (2018).
25. CMS Collaboration. A measurement of the Higgs boson mass in the diphoton decay channel. *Phys. Lett. B* **805**, 135425 (2020).
26. ATLAS Collaboration. Operation of the ATLAS trigger system in Run 2. *J. Instrum.* **15**, P10004 (2020).
27. ATLAS Collaboration. *The ATLAS Collaboration Software and Firmware* Report No. ATL-SOFT-PUB-2021-001 (CERN, 2021); https://cds.cern.ch/record/2767187
28. ATLAS Collaboration. Higgs boson production cross-section measurements and their EFT interpretation in the 4ℓ decay channel at √s = 13 TeV with the ATLAS detector. *Eur. Phys. J. C* **80**, 957 (2020); erratum 81, 398 (2021).
29. ATLAS Collaboration. *Measurements of Gluon Fusion and Vector-Boson-Fusion Production of the Higgs Boson in H→ WW*→ evμv Decays using pp Collisions at √s= 13 TeV with the ATLAS Detector* Report No. CERN-EP-2022-078 (CERN, 2022).
30. ATLAS Collaboration. Measurement of the production cross section for a Higgs boson in association with a vector boson in the H → WW* → ℓνℓν channel in pp collisions at √s = 13 TeV with the ATLAS detector. *Phys. Lett. B* **798**, 134949 (2019).
31. ATLAS Collaboration. *Measurement of the Properties of Higgs Boson Production at √s= 13 TeV in the H→ γγ Channel using 139 fb^{-1} of pp Collision Data with the ATLAS Experiment* Report No. CERN-EP-2022-094 (CERN, 2022).
32. ATLAS Collaboration. A search for the Zγ decay mode of the Higgs boson in pp collisions at √s = 13 TeV with the ATLAS detector. *Phys. Lett. B* **809**, 135754 (2020).
33. ATLAS Collaboration. Measurements of *WH* and *ZH* production in the $H \to b\bar{b}$ decay channel in *pp* collisions at 13 TeV with the ATLAS detector. *Eur. Phys. J. C* **81**, 178 (2021).
34. ATLAS Collaboration. Measurement of the associated production of a Higgs boson decaying into b quarks with a vector boson at high transverse momentum in pp collisions at √s = 13 TeV with the ATLAS detector. *Phys. Lett. B* **816**, 136204 (2021).
35. ATLAS Collaboration. Measurements of Higgs bosons decaying to bottom quarks from vector boson fusion production with the ATLAS experiment at √s = 13 TeV. *Eur. Phys. J. C* **81**, 537 (2020).
36. ATLAS Collaboration. Measurement of Higgs boson decay into *b*-quarks in associated production with a top-quark pair in *pp* collisions at √s = 13 TeV with the ATLAS detector. Preprint at https://arxiv.org/abs/2111.06712 (2021).
37. ATLAS Collaboration. Constraints on Higgs boson production with large transverse momentum using $H \to b\bar{b}$ decays in the ATLAS detector. *Phys. Rev. D* **105**, 092003 (2022).
38. ATLAS Collaboration. Measurements of Higgs boson production cross-sections in the $H \to \tau^+\tau^-$ decay channel in *pp* collisions at √s = 13 TeV with the ATLAS detector. Preprint at https://arxiv.org/abs/2201.08269 (2022).
39. ATLAS Collaboration. Evidence for the associated production of the Higgs boson and a top quark pair with the ATLAS detector. *Phys. Rev. D* **97**, 072003 (2018).
40. ATLAS Collaboration. A search for the dimuon decay of the Standard Model Higgs boson with the ATLAS detector. *Phys. Lett. B* **812**, 135980 (2021).
41. ATLAS Collaboration. Direct constraint on the Higgs–charm coupling from a search for Higgs boson decays into charm quarks with the ATLAS detector. Preprint at https://arxiv.org/abs/2201.11428 (2022).
42. ATLAS Collaboration. Search for invisible Higgs boson decays in events with vector-boson fusion signatures using 139 fb^{-1} of proton–proton data recorded by the ATLAS experiment. Preprint at https://arxiv.org/abs/2202.07953 (2022).
43. ATLAS Collaboration. Search for associated production of a *Z* boson with an invisibly decaying Higgs boson or dark matter candidates at √s = 13 TeV with the ATLAS detector. *Phys. Lett. B* **829**, 137066 (2022).
44. LHC Higgs Cross Section Working Group, de Florian, D. et al. *Handbook of LHC Higgs Cross Sections: 4. Deciphering the Nature of the Higgs Sector* Report No. CERN-2017-002 (CERN, 2017); https://doi.org/10.23731/CYRM-2017-002
45. Kudashkin, K., Lindert, J. M., Melnikov, K. & Wever, C. Higgs bosons with large transverse momentum at the LHC. *Phys. Lett. B* **782**, 210–214 (2018).
46. Djouadi, A., Kalinowski, J., Mühlleitner, M. & Spira, M. HDECAY: twenty++ years after. *Comput. Phys. Commun.* **238**, 214–231 (2019).
47. Bonetti, M., Melnikov, K. & Tancredi, L. Higher order corrections to mixed QCD-EW contributions to Higgs boson production in gluon fusion. *Phys. Rev. D* **97**, 056017 (2018).
48. Dulat, F., Lazopoulos, A. & Mistlberger, B. iHixs 2 – inclusive Higgs cross sections. *Comput. Phys. Commun.* **233**, 243–260 (2018).
49. Harlander, R. V., Klappert, J., Liebler, S. & Simon, L. vh@nnlo-v2: new physics in Higgs Strahlung. *J. High Energy Phys.* **2018-05**, 89 (2018).
50. Cacciari, M., Dreyer, F. A., Karlberg, A., Salam, G. P. & Zanderighi, G. Fully differential vector-boson-fusion Higgs production at next-to-next-to-leading order. *Phys. Rev. Lett.* **115**, 082002 (2015).
51. ATLAS and CMS Collaborations & The LHC Higgs Combination Group. *Procedure for the LHC Higgs Boson Search Combination in Summer 2011* Report No. ATL-PHYS-PUB-2011-011 (CERN, 2011); https://cds.cern.ch/record/1375842
52. Cowan, G., Cranmer, K., Gross, E. & Vitells, O. Asymptotic formulae for likelihood-based tests of new physics. *Eur. Phys. J. C* **71**, 1554 (2011); erratum **73**, 2501 (2013).
53. LHC Higgs Cross Section Working Group, Heinemeyer, S. et al. *Handbook of LHC Higgs Cross Sections: 3. Higgs Properties* Report No. CERN-2013-004 (CERN, 2013); https://doi.org/10.5170/CERN-2013-004
54. Duhrssen, M. et al. Extracting Higgs boson couplings from CERN LHC data. *Phys. Rev. D* **70**, 113009 (2004).
55. Dobrescu, B. A. & Lykken, J. D. Coupling spans of the Higgs-like boson. *J. High Energy Phys.* **2103-02**, 73 (2013).
56. Andersen, J. R. et al. Les Houches 2015: Physics at TeV Colliders Standard Model Working Group Report. In *9th Les Houches Workshop on Physics at TeV Colliders* https://inspirehep.net/literature/1459079 (2016).
57. Berger, N. et al. *Simplified Template Cross Sections – Stage 1.1* Report No. LHCHXSWG-2019-003 (CERN, 2019); preprint at https://arxiv.org/abs/1906.02754
58. Amoroso, S. et al. Les Houches 2019: Physics at TeV Colliders: Standard Model Working Group Report. In *11th Les Houches Workshop on Physics at TeV Colliders: PhysTeV Les Houches* https://inspirehep.net/literature/1783782 (2020).
59. Dainese, A. et al. *Report on the Physics at the HL-LHC, and Perspectives for the HE-LHC* Report No. CERN-2019-007 (CERN, 2019); https://cds.cern.ch/record/2703572

Publisher's note Springer Nature remains neutral with regard to jurisdictional claims in published maps and institutional affiliations.

Open Access This article is licensed under a Creative Commons Attribution 4.0 International License, which permits use, sharing, adaptation, distribution and reproduction in any medium or format, as long as you give appropriate credit to the original author(s) and the source, provide a link to the Creative Commons license, and indicate if changes were made. The images or other third party material in this article are included in the article's Creative Commons license, unless indicated otherwise in a credit line to the material. If material is not included in the article's Creative Commons license and your intended use is not permitted by statutory regulation or exceeds the permitted use, you will need to obtain permission directly from the copyright holder. To view a copy of this license, visit http://creativecommons.org/licenses/by/4.0/.

© CERN 2022, corrected publication 2022, 2023

Article

The ATLAS Collaboration

G. Aad[1], B. Abbott[2], D. C. Abbott[3], K. Abeling[4], S. H. Abidi[5], A. Aboulhorma[6], H. Abramowicz[8], H. Abreu[9], Y. Abulaiti[10], A. C. Abusleme Hoffman[11], B. S. Acharya[12,13,253], B. Achkar[4], L. Adam[14], C. Adam Bourdarios[15], L. Adamczyk[16], L. Adamek[17], S. V. Addepalli[18], J. Adelman[19], A. Adiguzel[20], S. Adorni[21], T. Adye[22], A. A. Affolder[23], Y. Afik[24], M. N. Agaras[25], J. Agarwala[26,27], A. Aggarwal[14], C. Agheorghiesei[28], J. A. Aguilar-Saavedra[29], A. Ahmad[24], F. Ahmadov[30,261], W. S. Ahmed[31], S. Ahuja[32], X. Ai[33], G. Aielli[34,35], I. Aizenberg[36], M. Akbiyik[14], T. P. A. Åkesson[37], A. V. Akimov[38], K. Al Khoury[39], G. L. Alberghi[40], J. Albert[41], P. Albicocco[42], M. J. Alconada Verzini[43], S. Alderweireldt[44], M. Aleksa[24], I. N. Aleksandrov[30], C. Alexa[45], T. Alexopoulos[46], A. Alfonsi[47], F. Alfonsi[40], M. Alhroob[2], B. Ali[48], S. Ali[49], M. Aliev[38], G. Alimonti[50], C. Allaire[24], B. M. M. Allbrooke[51], P. P. Allport[52], A. Aloisio[53,54], F. Alonso[43], C. Alpigiani[55], E. Alunno Camelia[34,35], M. Alvarez Estevez[56], M. G. Alviggi[53,54], Y. Amaral Coutinho[57], A. Ambler[31], C. Amelung[24], C. G. Ames[58], D. Amidei[59], S. P. Amor Dos Santos[60], S. Amoroso[33], K. R. Amos[61], C. S. Amrouche[21], V. Ananiev[62], C. Anastopoulos[63], N. Andari[64], T. Andeen[65], J. K. Anders[66], S. Y. Andrean[67,68], A. Andreazza[50,69], S. Angelidakis[70], A. Angerami[39,263], A. V. Anisenkov[38], A. Annovi[71], C. Antel[21], M. T. Anthony[63], E. Antipov[72], M. Antonelli[42], D. J. A. Antrim[73], F. Anulli[75], M. Aoki[76], J. A. Aparisi Pozo[61], M. A. Aparo[51], L. Aperio Bella[33], C. Appelt[77], N. Aranzabal[24], V. Araujo Ferraz[78], C. Arcangeletti[42], A. T. H. Arce[79], E. Arena[80], J-F. Arguin[81], S. Argyropoulos[82], J.-H. Arling[33], A. J. Armbruster[24], O. Arnaez[17], H. Arnold[47], Z. P. Arrubarrena Tame[58], G. Artoni[75,83], H. Asada[84], K. Asai[85], S. Asai[86], N. A. Asbah[87], E. M. Asimakopoulou[88], J. Assahsah[89], K. Assamagan[5], R. Astalos[90], R. J. Atkin[91], M. Atkinson[93], N. B. Atlay[77], H. Atmani[94], P. A. Atmasiddha[59], K. Augsten[48], S. Auricchio[53,54], A. D. Auriol[52], V. A. Austrup[95], G. Avner[9], G. Avolio[24], K. Axiotis[21], M. K. Ayoub[96], G. Azuelos[81,266], D. Babal[90], H. Bachacou[64], K. Bachas[97,255], A. Bachiu[98], F. Backman[67,68], A. Badea[87], P. Bagnaia[75,83], M. Bahmani[77], A. J. Bailey[61], V. R. Bailey[93], J. T. Baines[22], C. Bakalis[46], O. K. Baker[99], P. J. Bakker[47], E. Bakos[100], D. Bakshi Gupta[101], S. Balaji[102], R. Balasubramanian[47], E. M. Baldin[38], P. Balek[103], E. Ballabene[50,69], F. Balli[64], L. M. Baltes[104], W. K. Balunas[105], J. Balz[14], E. Banas[106], M. Bandieramonte[107], A. Bandyopadhyay[108], S. Bansal[108], L. Barak[8], E. L. Barberio[109], D. Barberis[110,111], M. Barbero[1], G. Barbour[112], K. N. Barends[91], T. Barillari[113], M.-S. Barisits[24], J. Barkeloo[114], T. Barklow[115], R. M. Barnett[73], P. Baron[116], D. A. Baron Moreno[117], A. Baroncelli[118], G. Barone[5], A. J. Barr[119], L. Barranco Navarro[67,68], F. Barreiro[56], J. Barreiro Guimarães da Costa[96,120,121,122], U. Barron[8], M. G. Barros Teixeira[60], S. Barsov[38], F. Bartels[104], R. Bartoldus[115], A. E. Barton[123], P. Bartos[90], A. Basalaev[33], A. Basan[14], M. Baselga[124], I. Bashta[125,126], A. Bassalat[7,127], M. J. Basso[17], C. R. Basson[117], R. L. Bates[128], S. Batlamous[6], J. R. Batley[105], B. Batool[129], M. Battaglia[23], M. Bauce[75,83], P. Bauer[108], A. Bayirli[130], J. B. Beacham[79], T. Beau[131], P. H. Beauchemin[132], F. Becherer[82], P. Bechtle[108], H. P. Beck[66,254], K. Becker[133], C. Becot[33], A. J. Beddall[134], V. A. Bednyakov[30], C. P. Bee[135], L. J. Beemster[100], T. A. Beermann[24], M. Begalli[57,136], M. Begel[5], A. Behera[135], J. K. Behr[33], C. Beirao Da Cruz E Silva[24], J. F. Beirer[4,24], F. Beisiegel[108], M. Belfkir[138], G. Bella[8], L. Bellagamba[40], A. Bellerive[98], P. Bellos[52], K. Beloborodov[38], K. Belotskiy[38], N. L. Belyaev[38], D. Benchekroun[139], F. Bendebba[139], Y. Benhammou[8], D. P. Benjamin[5], M. Benoit[5], J. R. Bensinger[18], S. Bentvelsen[47], L. Beresford[24], M. Beretta[42], D. Berge[77], E. Bergeaas Kuutmann[88], N. Berger[15], B. Bergmann[48], J. Beringer[73], S. Berlendis[140], G. Bernardi[141], C. Bernius[115], F. U. Bernlochner[108], T. Berry[32], P. Berta[103], A. Berthold[142], I. A. Bertram[123], O. Bessidskaia Bylund[95], S. Bethke[113], A. Betti[75,83], A. J. Bevan[143], M. Bhamjee[144], S. Bhatta[135], D. S. Bhattacharya[145], P. Bhattarai[18], V. S. Bhopatkar[146], R. Bi[107], R. Bi[5,269], R. M. Bianchi[107], O. Biebel[58], R. Bielski[114], M. Biglietti[125], T. R. V. Billoud[48], M. Bindi[4], A. Bingul[147], C. Bini[75,83], S. Biondi[40,148], A. Biondini[80], C. J. Birch-sykes[117], G. A. Bird[22,52], M. Birman[36], T. Bisanz[24], D. Biswas[149,249], A. Bitadze[117], K. Bjørke[62], I. Bloch[33], C. Blocker[18], A. Blue[128], U. Blumenschein[143], J. Blumenthal[14], G. J. Bobbink[47], V. S. Bobrovnikov[38], M. Boehler[82], D. Bogavac[24], A. G. Bogdanchikov[38], C. Bohm[67], V. Boisvert[32], P. Bokan[33], T. Bold[16], M. Bomben[141], M. Bona[143], M. Boonekamp[64], C. D. Booth[32], A. G. Borbély[128], H. M. Borecka-Bielska[81], L. S. Borgna[112], G. Borissov[123], D. Bortoletto[119], D. Boscherini[40], M. Bosman[25], J. D. Bossio Sola[24], K. Bouaouda[139], J. Boudreau[107], E. V. Bouhova-Thacker[123], D. Boumediene[150], R. Bouquet[141], A. Boveia[151], J. Boyd[24], D. Boye[5], I. R. Boyko[30], J. Bracinik[52], N. Brahimi[152,153], G. Brandt[95], O. Brandt[105], F. Braren[33], B. Brau[3], J. E. Brau[114], W. D. Breaden Madden[128], K. Brendlinger[33], R. Brener[36], L. Brenner[24], R. Brenner[88], S. Bressler[36], B. Brickwedde[14], D. Britton[128], D. Britzger[113], I. Brock[108], G. Brooijmans[39], W. K. Brooks[154], E. Brost[5], P. A. Bruckman de Renstrom[106], B. Brüers[33], D. Bruncko[155,271], A. Bruni[40], G. Bruni[40], M. Bruschi[40], N. Bruscino[75,83], L. Bryngemark[115], T. Buanes[156], Q. Buat[55], P. Buchholz[129], A. G. Buckley[128], I. A. Budagov[30,272], M. K. Bugge[62], O. Bulekov[38], B. A. Bullard[87], S. Burdin[80], C. D. Burgard[33], A. M. Burger[150], B. Burghgrave[101], J. T. P. Burr[105], C. D. Burton[65], J. C. Burzynski[157], E. L. Busch[39], V. Büscher[14], P. J. Bussey[128], J. M. Butler[158], C. M. Buttar[128], J. M. Butterworth[112], W. Buttinger[22], C. J. Buxo Vazquez[159], A. R. Buzykaev[38], G. Cabras[40], S. Cabrera Urbán[61], D. Caforio[160], H. Cai[107], Y. Cai[120,122], V. M. M. Cairo[24], O. Cakir[161], N. Calace[24], P. Calafiura[73], G. Calderini[131], P. Calfayan[162], G. Callea[128], L. P. Caloba[57], D. Calvet[150], S. Calvet[150], T. P. Calvet[1], M. Calvetti[71,163], R. Camacho Toro[131], S. Camarda[24], D. Camarero Munoz[56], P. Camarri[34,35], M. T. Camerlingo[125,126], D. Cameron[62], C. Camincher[41], M. Campanelli[112], A. Camplani[164], V. Canale[53,54], A. Canesse[31], M. Cano Bret[165], J. Cantero[61], Y. Cao[93], F. Capocasa[18], M. Capua[166,167], A. Carbone[50,69], R. Cardarelli[34], J. C. J. Cardenas[101], F. Cardillo[61], T. Carli[24], G. Carlino[53], B. T. Carlson[107,256], E. M. Carlson[41,168], L. Carminati[50,69], M. Carnesale[75,83], S. Caron[169], E. Carquin[154], S. Carrá[50,69], G. Carratta[148,40], F. Carrio Argos[170], J. W. S. Carter[17], T. M. Carter[44], M. P. Casado[25,246], A. F. Casha[17], E. G. Castiglia[99], F. L. Castillo[104], L. Castillo Garcia[25], V. Castillo Gimenez[61], N. F. Castro[60,171], A. Catinaccio[24], J. R. Catmore[62], V. Cavaliere[5], N. Cavalli[40,148], V. Cavasinni[71,163], E. Celebi[130], F. Celli[119], M. S. Centonze[172,173], K. Cerny[116], A. S. Cerqueira[78], A. Cerri[51], L. Cerrito[34,35], F. Cerutti[73], A. Cervelli[40], S. A. Cetin[134], Z. Chadi[139], D. Chakraborty[19], M. Chala[29], J. Chan[149], W. S. Chan[47], W. Y. Chan[86], J. D. Chapman[105], B. Chargeishvili[174], D. G. Charlton[52], T. P. Charman[143], M. Chatterjee[66], S. Chekanov[146], S. V. Chekulaev[168], G. A. Chelkov[30,239], A. Chen[59], B. Chen[8], B. Chen[41], C. Chen[118], H. Chen[96], H. Chen[5], J. Chen[152], J. Chen[18], S. Chen[86], S. J. Chen[96], X. Chen[152], X. Chen[121,265], Y. Chen[118], C. L. Cheng[149], H. C. Cheng[176], A. Cheplakov[30], E. Cheremushkina[33], E. Cherepanova[47], R. Cherkaoui El Moursli[6], E. Cheu[140], K. Cheung[177], L. Chevalier[64], V. Chiarella[42], G. Chiarelli[71], G. Chiodini[172], A. S. Chisholm[52], A. Chitan[45], Y. H. Chiu[41], M. V. Chizhov[30], K. Choi[65], A. R. Chomont[75,83], Y. Chou[3], E. Y. S. Chow[47], T. Chowdhury[170], L. D. Christopher[170], K. L. Chu[176], M. C. Chu[176], X. Chu[120,122], J. Chudoba[178], J. J. Chwastowski[106], D. Cieri[113], K. M. Ciesla[16], V. Cindro[179], A. Ciocio[73], F. Cirotto[53,54], Z. H. Citron[36,250], M. Citterio[50], D. A. Ciubotaru[45], B. M. Ciungu[17], A. Clark[21], P. J. Clark[44], J. M. Clavijo Columbie[33], S. E. Clawson[117], C. Clement[67,68], J. Clercx[33], L. Clissa[40,148], Y. Coadou[1], M. Cobal[12,180], A. Coccaro[111], R. F. Coelho Barrue[60], R. Coelho Lopes De Sa[3], S. Coelli[50], H. Cohen[8], A. E. C. Coimbra[50,69], B. Cole[39], J. Collot[181], P. Conde Muiño[60,182], M. P. Connell[144], S. H. Connell[144], I. A. Connelly[128], E. I. Conroy[119], F. Conventi[53,267], H. G. Cooke[52], A. M. Cooper-Sarkar[119], F. Cormier[183], L. D. Corpe[24], M. Corradi[75,83], E. E. Corrigan[37], F. Corriveau[31,260], A. Cortes-Gonzalez[77], M. J. Costa[61], F. Costanza[15], D. Costanzo[63], B. M. Cote[151], G. Cowan[32], J. W. Cowley[105], K. Cranmer[10], S. Crépé-Renaudin[181], F. Crescioli[131], M. Cristinziani[129], M. Cristoforetti[184,185,241], V. Croft[132], G. Crosetti[166,167], A. Cueto[24], T. Cuhadar Donszelmann[186], H. Cui[120,122], Z. Cui[140], A. R. Cukierman[115], W. R. Cunningham[128], F. Curcio[166,167], P. Czodrowski[24], M. M. Czurylo[187], M. J. Da Cunha Sargedas De Sousa[118], J. V. Da Fonseca Pinto[57], C. Da Via[117], W. Dabrowski[16], T. Dado[124], S. Dahbi[170], T. Dai[59], C. Dallapiccola[3], M. Dam[164], G. D'amen[5], V. D'Amico[125,126], J. Damp[14], J. R. Dandoy[188], M. F. Daneri[189], M. Danninger[157], V. Dao[24], G. Darbo[111], S. Darmora[146], S. J. Das[5,269], A. Dattagupta[114], S. D'Auria[50,69], C. David[190], T. Davidek[103], D. R. Davis[79], B. Davis-Purcell[98], I. Dawson[143], K. De[101], R. De Asmundis[53], M. De Beurs[47], S. De Castro[40,148], N. De Groot[169], P. de Jong[47], H. De la Torre[159], A. De Maria[96], A. De Salvo[75], U. De Sanctis[34,35], A. De Santo[51], J. B. De Vivie De Regie[181], D. V. Dedovich[30], J. Degens[47], A. M. Deiana[191], F. Del Corso[40,148], J. Del Peso[56], F. Del Rio[104], F. Deliot[64], C. M. Delitzsch[124], M. Della Pietra[53,54], D. Della Volpe[21], A. Dell'Acqua[24], L. Dell'Asta[50,69], M. Delmastro[15], P. A. Delsart[181], S. Demers[99], M. Demichev[30], S. P. Denisov[38], L. D'Eramo[19], D. Derendarz[106], F. Derue[131], P. Dervan[80], K. Desch[108], K. Dette[17], C. Deutsch[108], P. O. Deviveiros[24], F. A. Di Bello[75,83], A. Di Ciaccio[34,35], L. Di Ciaccio[15], A. Di Domenico[75,83], C. Di Donato[53,54], A. Di Girolamo[24], G. Di Gregorio[71,163], A. Di Luca[184,185], B. Di Micco[125,126], R. Di Nardo[125,126], C. Diaconu[1], F. A. Dias[47], T. Dias Do Vale[157], M. A. Diaz[11,192], F. G. Diaz Capriles[108], M. Didenko[61], E. B. Diehl[59], L. Diehl[82], S. Díez Cornell[33], C. Diez Pardos[129], C. Dimitriadi[88,108], A. Dimitrievska[73], W. Ding[121], J. Dingfelder[108], I.-M. Dinu[45], S. J. Dittmeier[187], F. Dittus[24], F. Djama[1], T. Djobava[174], J. I. Djuvsland[156], D. Dodsworth[18], C. Doglioni[37,117], J. Dolejsi[103], Z. Dolezal[103], M. Donadelli[193], B. Dong[152], J. Donini[150], A. D'Onofrio[96], M. D'Onofrio[80], J. Dopke[22], A. Doria[53], M. T. Dova[43], A. T. Doyle[128], M. A. Draguet[119], E. Drechsler[157], E. Dreyer[36], I. Drivas-koulouris[46], A. S. Drobac[132], D. Du[118], T. A. du Pree[47], F. Dubinin[38], M. Dubovsky[90], E. Duchovni[36], G. Duckeck[58], O. A. Ducu[24], D. Duda[113], A. Dudarev[24], M. D'uffizi[117], L. Duflot[127], M. Dührssen[24], C. Dülsen[95], A. E. Dumitriu[45], M. Dunford[104], S. Dungs[124], K. Dunne[67,68], A. Duperrin[1], H. Duran Yildiz[161], M. Düren[160], A. Durglishvili[174], B. L. Dwyer[19], G. I. Dyckes[73], M. Dyndal[16], S. Dysch[117], B. S. Dziedzic[106], Z. O. Earnshaw[51], B. Eckerova[90], M. G. Eggleston[79], E. Egidio Purcino De Souza[57], L. F. Ehrke[21], G. Eigen[156], K. Einsweiler[73], T. Ekelof[88], P. A. Ekman[37], Y. El Ghazali[194], H. El Jarrari[6,49], A. El Moussaouy[139], V. Ellajosyula[88], M. Ellert[88], F. Ellinghaus[95], A. A. Elliot[143], N. Ellis[24], J. Elmsheuser[5], M. Elsing[24], D. Emeliyanov[22], A. Emerman[39], Y. Enari[86], I. Ene[73], S. Epari[25], J. Erdmann[124], A. Ereditato[66], P. A. Erland[106], M. Errenst[95], M. Escalier[127], C. Escobar[61], E. Etzion[8], G. Evans[60], H. Evans[162], M. O. Evans[51], A. Ezhilov[38], S. Ezzarqtouni[139], F. Fabbri[128], L. Fabbri[40,148], G. Facini[112], V. Fadeyev[23], R. M. Fakhrutdinov[38], S. Falciano[75], P. J. Falke[108], S. Falke[24], J. Faltova[103], Y. Fan[120], Y. Fang[120,122], G. Fanourakis[196], M. Fanti[50,69], M. Faraj[12,13], A. Farbin[101], A. Farilla[125], T. Farooque[159], S. M. Farrington[44], F. Fassi[6], D. Fassouliotis[70], M. Faucci Giannelli[34,35], W. J. Fawcett[105], L. Fayard[127], O. L. Fedin[38,239], G. Fedotov[38], M. Feickert[93], L. Feligioni[1], A. Fell[63], D. E. Fellers[114], C. Feng[94], M. Feng[121], M. J. Fenton[186], A. B. Fenyuk[38], L. Ferencz[33], S. W. Ferguson[197], J. Pretel[82], J. Ferrando[33], A. Ferrari[88], P. Ferrari[47], R. Ferrari[26], D. Ferrere[21], C. Ferretti[59], F. Fiedler[14], A. Filipčič[179], E. K. Filmer[198], F. Filthaut[169], M. C. N. Fiolhais[60,199,240], L. Fiorini[61], F. Fischer[129], W. C. Fisher[159], T. Fitschen[52,127], I. Fleck[129], P. Fleischmann[59], T. Flick[95], L. Flores[188], M. Flores[200], L. R. Flores Castillo[176], F. M. Follega[184,185], N. Fomin[156], J. H. Foo[17], B. C. Forland[162], A. Formica[64], A. C. Forti[117], E. Fortin[1], A. W. Fortman[87], M. G. Foti[73], L. Fountas[70,247], D. Fournier[127], H. Fox[123], P. Francavilla[71,163], S. Francescato[87], M. Franchini[40,148], S. Franchino[104], D. Francis[24], L. Franco[169], L. Franconi[66], M. Franklin[87], G. Frattari[18], A. C. Freegard[143], P. M. Freeman[52], W. S. Freund[57], N. Fritzsche[142], A. Froch[82], D. Froidevaux[24], J. A. Frost[119], Y. Fu[118], M. Fujimoto[85], E. Fullana Torregrosa[61,273], J. Fuster[61], A. Gabrielli[40,148], A. Gabrielli[24], P. Gadow[33], G. Gagliardi[110,111], L. G. Gagnon[73], G. E. Gallardo[119], E. J. Gallas[119], B. J. Gallop[22], R. Gamboa Goni[143], K. K. Gan[151], S. Ganguly[86], J. Gao[118], Y. Gao[44], F. M. Garay Walls[11,192], B. Garcia[5,269], C. García[61], J. E. García Navarro[61], J. A. García Pascual[120], M. Garcia-Sciveres[73], R. W. Gardner[203], D. Garg[165], R. B. Garg[115,175], S. Gargiulo[82], C. A. Garner[17], V. Garonne[5], S. J. Gasiorowski[55], P. Gaspar[57], G. Gaudio[26], V. Gautam[25], P. Gauzzi[75,83], I. L. Gavrilenko[38], A. Gavrilyuk[38], C. Gay[183], G. Gaycken[33], E. N. Gazis[46], A. A. Geanta[45], C. M. Gee[23], J. Geisen[37], M. Geisen[14], C. Gemme[111], M. H. Genest[181], S. Gentile[75,83], S. George[32], W. F. George[52], T. Geralis[196], L. O. Gerlach[4], P. Gessinger-Befurt[24], M. Ghasemi Bostanabad[41], M. Ghneimat[129], A. Ghosal[129], A. Ghosh[186], A. Ghosh[140], B. Giacobbe[40], S. Giagu[75,83], N. Giangiacomi[17], P. Giannetti[71], A. Giannini[118], S. M. Gibson[32], M. Gignac[23], D. T. Gil[204], A. K. Gilbert[16], B. J. Gilbert[39], D. Gillberg[98], G. Gilles[47], N. E. K. Gillwald[33], L. Ginabat[131], D. M. Gingrich[205,266], M. P. Giordani[12,180], P. F. Giraud[64], G. Giugliarelli[12,180], D. Giugni[50], F. Giuli[24], I. Gkialas[70,247], L. K. Gladilin[38], C. Glasman[56], G. R. Gledhill[114], M. Glisic[114], I. Gnesi[167,243], Y. Go[5,269], M. Goblirsch-Kolb[18], D. Godin[81], S. Goldfarb[109], T. Golling[21], M. G. D. Gololo[170], D. Golubkov[38], J. P. Gombas[159], A. Gomes[60,206], G. Gomes Da Silva[129], A. J. Gomez Delegido[61], R. Goncalves Gama[4], R. Gonçalo[60,199], G. Gonella[114], L. Gonella[52], A. Gongadze[30], F. Gonnella[52], J. L. Gonski[39], S. González de la Hoz[61], S. Gonzalez Fernandez[25], R. Gonzalez Lopez[80], C. Gonzalez Renteria[73], R. Gonzalez Suarez[88], S. Gonzalez-Sevilla[21], G. R. Gonzalvo Rodriguez[61], R. Y. González Andana[44], L. Goossens[24], N. A. Gorasia[52], P. A. Gorbounov[38], B. Gorini[24], E. Gorini[172,173], A. Gorišek[179], A. T. Goshaw[79], M. I. Gostkin[30], C. A. Gottardo[24], M. Gouighri[194], V. Goumarre[33], A. G. Goussiou[55], N. Govender[144], C. Goy[15], I. Grabowska-Bold[16], K. Graham[98], E. Gramstad[62], S. Grancagnolo[77], M. Grandi[51], V. Gratchev[38,274], P. M. Gravila[207], F. G. Gravili[172,173], H. M. Gray[73], M. Greco[172,173], C. Grefe[108], I. M. Gregor[33], P. Grenier[115], C. Grieco[25], A. A. Grillo[23], K. Grimm[209,251], S. Grinstein[25,258], J.-F. Grivaz[127], E. Gross[36], J. Grosse-Knetter[4], C. Grud[59], A. Grummer[210], J. C. Grundy[119], L. Guan[59], W. Guan[149], C. Gubbels[183], J. G. R. Guerrero Rojas[61], G. Guerrieri[12,13], F. Guescini[113], R. Gugel[14], J. A. M. Guhit[59], A. Guida[33], T. Guillemin[15], E. Guilloton[22,133], S. Guindon[24], F. Guo[120,122], J. Guo[152], L. Guo[127], Y. Guo[59], R. Gupta[33], S. Gurbuz[108], S. S. Gurdasani[82], G. Gustavino[24], M. Guth[21], P. Gutierrez[2], L. F. Gutierrez Zagazeta[188], C. Gutschow[112], C. Guyot[64], C. Gwenlan[119], C. B. Gwilliam[80], E. S. Haaland[62], A. Haas[10], M. Habedank[33], C. Haber[73], H. K. Hadavand[101], A. Hadef[14], S. Hadzic[113], M. Haleem[145], J. Haley[72], J. J. Hall[63], G. D. Hallewell[1], L. Halser[66], K. Hamano[41], H. Hamdaoui[6], M. Hamer[108], G. N. Hamity[44],

J. Han[94], K. Han[118], L. Han[96], L. Han[118], S. Han[73], Y. F. Han[17], K. Hanagaki[76], M. Hance[23], D. A. Hangal[39,263], M. D. Hank[203], R. Hankache[117], J. B. Hansen[164], J. D. Hansen[164], P. H. Hansen[164], K. Hara[211], D. Harada[21], T. Harenberg[95], S. Harkusha[38], Y. T. Harris[119], N. M. Harrison[151], P. F. Harrison[133], N. M. Hartman[115], N. M. Hartmann[58], Y. Hasegawa[212], A. Hasib[44], S. Haug[66], R. Hauser[159], M. Havranek[48], C. M. Hawkes[52], R. J. Hawkings[24], S. Hayashida[84], D. Hayden[159], C. Hayes[59], R. L. Hayes[183], C. P. Hays[119], J. M. Hays[143], H. S. Hayward[80], F. He[118], Y. He[213], Y. He[131], M. P. Heath[44], V. Hedberg[37], A. L. Heggelund[62], N. D. Hehir[143], C. Heidegger[82], K. K. Heidegger[82], W. D. Heidorn[214], J. Heilman[98], S. Heim[33], T. Heim[73], J. G. Heinlein[188], J. J. Heinrich[114], L. Heinrich[113,137], J. Hejbal[178], L. Helary[33], A. Held[149], S. Hellesund[62], C. M. Helling[183], S. Hellman[67,68], C. Helsens[24], R. C. W. Henderson[123], L. Henkelmann[105], A. M. Henriques Correia[24], H. Herde[115], Y. Hernández Jiménez[135], H. Herr[14], M. G. Herrmann[58], T. Herrmann[142], G. Herten[82], R. Hertenberger[58], L. Hervas[24], N. P. Hessey[168], H. Hibi[215], E. Higón-Rodriguez[61], S. J. Hillier[52], I. Hinchliffe[73], F. Hinterkeuser[108], M. Hirose[216], S. Hirose[211], D. Hirschbuehl[95], T. G. Hitchings[117], B. Hiti[179], J. Hobbs[135], R. Hobincu[217], N. Hod[36], M. C. Hodgkinson[63], B. H. Hodkinson[105], A. Hoecker[24], J. Hofer[33], D. Hohn[82], T. Holm[108], M. Holzbock[113], L. B. A. H. Hommels[105], B. P. Honan[117], J. Hong[152], T. M. Hong[107], Y. Hong[4], J. C. Honig[82], A. Hönle[113], B. H. Hooberman[93], W. H. Hopkins[146], Y. Horii[84], S. Hou[49], A. S. Howard[179], J. Howarth[128], J. Hoya[43], M. Hrabovsky[116], A. Hrynevich[38], T. Hryn'ova[15], P. J. Hsu[177], S.-C. Hsu[55], Q. Hu[39,263], Y. F. Hu[120,122,268], D. P. Huang[112], S. Huang[218], X. Huang[96], Y. Huang[118], Y. Huang[120], Z. Huang[117], Z. Hubacek[48], M. Huebner[108], F. Huegging[108], T. B. Huffman[119], M. Huhtinen[24], S. K. Huiberts[156], R. Hulsken[31], N. Huseynov[219,239], J. Huston[159], J. Huth[87], R. Hyneman[115], S. Hyrych[90], G. Iacobucci[21], G. Iakovidis[5], I. Ibragimov[129], L. Iconomidou-Fayard[127], P. Iengo[53,54], R. Iguchi[86], T. Iizawa[21], Y. Ikegami[76], A. Ilg[66], N. Ilic[17], H. Imam[139], T. Ingebretsen Carlson[67,68], G. Introzzi[26,27], M. Iodice[125], V. Ippolito[75,83], M. Ishino[86], W. Islam[149], C. Issever[33,77], S. Istin[130,270], H. Ito[220], J. M. Iturbe Ponce[176], R. Iuppa[184,185], A. Ivina[36], J. M. Izen[197], V. Izzo[53], P. Jacka[48,178], P. Jackson[198], R. M. Jacobs[33], B. P. Jaeger[157], C. S. Jagfeld[58], G. Jäkel[95], K. Jakobs[82], T. Jakoubek[36], J. Jamieson[128], K. W. Janas[16], G. Jarlskog[37], A. E. Jaspan[80], T. Javůrek[24], M. Javurkova[3], F. Jeanneau[64], L. Jeanty[114], J. Jejelava[221,262], P. Jenni[82,244], C. E. Jessiman[98], S. Jézéquel[15], J. Jia[135], X. Jia[87], X. Jia[120,122], Z. Jia[96], Y. Jiang[118], S. Jiggins[44], J. Jimenez Pena[113], S. Jin[96], A. Jinaru[45], O. Jinnouchi[213], H. Jivan[170], P. Johansson[63], K. A. Johns[140], C. A. Johnson[162], D. M. Jones[105], E. Jones[133], P. Jones[105], R. W. L. Jones[123], T. J. Jones[80], J. Jovicevic[100], X. Ju[73], J. J. Junggeburth[24], A. Juste Rozas[25,258], S. Kabana[222], A. Kaczmarska[106], M. Kado[75,83], H. Kagan[151], M. Kagan[115], A. Kahn[39], A. Kahn[188], C. Kahra[14], T. Kaji[220], E. Kajomovitz[9], N. Kakati[36], C. W. Kalderon[5], A. Kamenshchikov[17], N. J. Kang[23], Y. Kano[84], D. Kar[170], K. Karava[119], M. J. Kareem[190], E. Karentzos[82], I. Karkanias[97], S. N. Karpov[30], Z. M. Karpova[30], V. Kartvelishvili[123], A. N. Karyukhin[38], E. Kasimi[97], C. Kato[153], J. Katzy[33], S. Kaur[98], K. Kawade[212], K. Kawagoe[223], T. Kawaguchi[84], T. Kawamoto[64], G. Kawamura[4], E. F. Kay[41], F. I. Kaya[132], S. Kazakos[25], V. F. Kazanin[38], Y. Ke[135], J. M. Keaveney[91], R. Keeler[41], G. V. Kehris[87], J. S. Keller[98], A. S. Kelly[112], D. Kelsey[51], J. J. Kempster[52], J. Kendrick[52], K. E. Kennedy[39], O. Kepka[178], B. P. Kerridge[133], S. Kersten[95], B. P. Kerševan[179], L. Keszeghova[90], S. Ketabchi Haghighat[17], M. Khandoga[131], A. Khanov[72], A. G. Kharlamov[38], T. Kharlamova[38], E. E. Khoda[55], T. J. Khoo[77], G. Khoriauli[145], J. Khubua[174], Y. A. R. Khwaira[127], M. Kiehn[24], A. Kilgallon[114], D. W. Kim[67,68], E. Kim[213], Y. K. Kim[203], N. Kimura[112], A. Kirchhoff[4], D. Kirchmeier[142], C. Kirfel[108], J. Kirk[22], A. E. Kiryunin[113], T. Kishimoto[86], D. P. Kisliuk[17], C. Kitsaki[46], O. Kivernyk[108], M. Klassen[104], C. Klein[98], L. Klein[145], M. H. Klein[59], M. Klein[80], U. Klein[80], P. Klimek[24], A. Klimentov[5], F. Klimpel[113], T. Klingl[108], T. Klioutchnikova[24], F. F. Klitzner[58], P. Kluit[47], S. Kluth[113], E. Kneringer[224], T. M. Knight[17], A. Knue[82], D. Kobayashi[223], R. Kobayashi[225], M. Kocian[115], T. Kodama[86], P. Kodyš[103], D. M. Koeck[51], P. T. Koenig[108], T. Koffas[98], N. M. Köhler[24], M. Kolb[64], I. Koletsou[15], T. Komarek[116], K. Köneke[82], A. X. Y. Kong[198], T. Kono[85], N. Konstantinidis[112], B. Konya[37], R. Kopeliansky[162], S. Koperny[16], K. Korcyl[106], K. Kordas[97], G. Koren[8], A. Korn[112], S. Korn[4], I. Korolkov[25], N. Korotkova[38], B. Kortman[47], O. Kortner[113], S. Kortner[113], W. H. Kostecka[19], V. V. Kostyukhin[129], A. Kotsokechagia[127], A. Kotwal[79], A. Koulouris[24], A. Kourkoumeli-Charalampidi[26,27], C. Kourkoumelis[70], E. Kourlitis[146], O. Kovanda[51], R. Kowalewski[41], W. Kozanecki[64], A. S. Kozhin[38], V. A. Kramarenko[38], G. Kramberger[179], P. Kramer[14], M. W. Krasny[131], A. Krasznahorkay[24], J. A. Kremer[14], T. Kresse[142], J. Kretzschmar[80], K. Kreul[77], P. Krieger[17], F. Krieter[58], S. Krishnamurthy[3], A. Krishnan[187], M. Krivos[103], K. Krizka[73], K. Kroeninger[124], H. Kroha[113], J. Kroll[178], J. Kroll[188], K. S. Krowpman[159], U. Kruchonak[30], H. Krüger[108], N. Krumnack[214], M. C. Kruse[79], J. A. Krzysiak[106], A. Kubota[213], O. Kuchinskaia[38], S. Kuday[161], D. Kuechler[33], J. T. Kuechler[33], S. Kuehn[24], T. Kuhl[33], V. Kukhtin[30], Y. Kulchitsky[38,239], S. Kuleshov[192,226], M. Kumar[170], N. Kumari[1], M. Kuna[181], A. Kupco[178], T. Kupfer[124], A. Kupich[38], O. Kuprash[82], H. Kurashige[215], L. L. Kurchaninov[168], Y. A. Kurochkin[38], A. Kurova[38], E. S. Kuwertz[24], M. Kuze[213], A. K. Kvam[3], J. Kvita[116], T. Kwan[31], K. W. Kwok[176], C. Lacasta[61], F. Lacava[75,83], H. Lacker[77], D. Lacour[131], N. N. Lad[112], E. Ladygin[30], B. Laforge[131], T. Lagouri[222], S. Lai[4], I. K. Lakomiec[16], N. Lalloue[181], J. E. Lambert[2], S. Lammers[162], W. Lampl[140], C. Lampoudis[97], A. N. Lancaster[19], E. Lançon[5], U. Landgraf[82], M. P. J. Landon[143], V. S. Lang[82], R. J. Langenberg[3], A. J. Lankford[186], F. Lanni[5], K. Lantzsch[108], A. Lanza[26], A. Lapertosa[110,111], J. F. Laporte[64], T. Lari[50], F. Lasagni Manghi[40], M. Lassnig[24], V. Latonova[178], T. S. Lau[176], A. Laudrain[14], A. Laurier[98], S. D. Lawlor[32], Z. Lawrence[117], M. Lazzaroni[50,69], B. Le[117], B. Leban[179], A. Lebedev[214], M. LeBlanc[24], T. LeCompte[146], F. Ledroit-Guillon[181], A. C. A. Lee[112], G. R. Lee[156], L. Lee[87], S. C. Lee[49], S. Lee[67,68], L. L. Leeuw[144], H. P. Lefebvre[32], M. Lefebvre[41], C. Leggett[73], K. Lehmann[157], G. Lehmann Miotto[24], W. A. Leight[3], A. Leisos[97,257], M. A. L. Leite[193], C. E. Leitgeb[33], R. Leitner[103], K. J. C. Leney[191], T. Lenz[108], S. Leone[71], C. Leonidopoulos[44], A. Leopold[227], C. Leroy[81], R. Les[159], C. G. Lester[105], M. Levchenko[38], J. Levêque[15], D. Levin[59], L. J. Levinson[36], M. P. Lewicki[106], D. J. Lewis[52], B. Li[121], B. Li[94], C. Li[118], C.-Q. Li[152,153], H. Li[118], H. Li[94], H. Li[96], H. Li[94], J. Li[152], K. Li[55], L. Li[152], M. Li[120,122], Q. Y. Li[118], S. Li[152,153,242], T. Li[94], X. Li[31], Z. Li[94], Z. Li[119], Z. Li[31], Z. Li[80], Z. Liang[120], M. Liberatore[33], B. Liberti[34], K. Lie[228], J. Lieber Marin[57], K. Lin[159], R. A. Linck[162], R. E. Lindley[140], J. H. Lindon[205], A. Linss[33], E. Lipeles[188], A. Lipniacka[156], T. M. Liss[93,264], A. Lister[183], J. D. Little[15], B. Liu[120], B. X. Liu[157], D. Liu[152,153], J. B. Liu[118], J. K. K. Liu[105], K. Liu[152,153], M. Liu[118], M. Y. Liu[118], P. Liu[120], Q. Liu[55,152,153], X. Liu[118], Y. Liu[33], Y. Liu[96,122], Y. L. Liu[59], Y. W. Liu[118], M. Livan[26,27], J. Llorente Merino[157], S. L. Lloyd[143], E. M. Lobodzinska[33], P. Loch[140], S. Loffredo[34,35], T. Lohse[77], K. Lohwasser[63], M. Lokajicek[178], J. D. Long[93], I. Longarini[75,83], L. Longo[172,173], R. Longo[93], I. Lopez Paz[24], A. Lopez Solis[33], J. Lorenz[58], N. Lorenzo Martinez[15], A. M. Lory[58], A. Lösle[82], X. Lou[67,68], X. Lou[120,122], A. Lounis[127], J. Love[146], P. A. Love[123], J. J. Lozano Bahilo[61], G. Lu[120,122], M. Lu[165], S. Lu[188], Y. J. Lu[177], H. J. Lubatti[55], C. Luci[75,83], F. L. Lucio Alves[96], A. Lucotte[181], F. Luehring[162], I. Luise[135], O. Lukianchuk[127], O. Lundberg[227], B. Lund-Jensen[227], N. A. Luongo[114], M. S. Lutz[8], D. Lynn[5], H. Lyons[80], R. Lysak[178], E. Lytken[37], F. Lyu[120], V. Lyubushkin[30], T. Lyubushkina[30], H. Ma[5], L. L. Ma[94], Y. Ma[112], D. M. Mac Donell[41], G. Maccarrone[42], J. C. MacDonald[63], R. Madar[150], W. F. Mader[142], J. Maeda[215], T. Maeno[5], M. Maerker[142], V. Magerl[82], J. Magro[12,180], H. Maguire[63], D. J. Mahon[39], C. Maidantchik[57], A. Maio[60,206,229], K. Maj[16], O. Majersky[90], S. Majewski[114], N. Makovec[127], V. Maksimovic[100], B. Malaescu[131], Pa. Malecki[106], V. P. Maleev[38], F. Malek[181], D. Malito[166,167], U. Mallik[165], C. Malone[105], S. Maltezos[46], S. Malyukov[30], J. Mamuzic[25], G. Mancini[42], G. Manco[26,27], J. P. Mandalia[143], I. Mandić[179], L. Manhaes de Andrade Filho[78], I. M. Maniatis[97], M. Manisha[64], J. Manjarres Ramos[142], D. C. Mankad[36], K. H. Mankinen[37], A. Mann[58], A. Manousos[224], B. Mansoulie[64], S. Manzoni[24], A. Marantis[97,257], G. Marchiori[141], M. Marcisovsky[178], L. Marcoccia[34,35], C. Marcon[37], M. Marinescu[52], M. Marjanovic[2], Z. Marshall[73], S. Marti-Garcia[61], T. A. Martin[133], V. J. Martin[44], B. Martin dit Latour[156], L. Martinelli[75,83], M. Martinez[25,258], P. Martinez Agullo[61], V. I. Martinez Outschoorn[3], P. Martinez Suarez[25], S. Martin-Haugh[22], V. S. Martoiu[45], A. C. Martyniuk[112], A. Marzin[24], S. R. Maschek[113], L. Masetti[14], T. Mashimo[86], J. Masik[117], A. L. Maslennikov[38], L. Massa[40], P. Massarotti[53,54], P. Mastrandrea[71,163], A. Mastroberardino[166,167], T. Masubuchi[86], T. Mathisen[88], A. Matic[58], N. Matsuzawa[86], J. Maurer[45], B. Maček[179], D. A. Maximov[38], R. Mazini[49], I. Maznas[97], M. Mazza[159], S. M. Mazza[23], C. Mc Ginn[5,269], J. P. Mc Gowan[31], S. P. Mc Kee[59], T. G. McCarthy[113], W. P. McCormack[73], E. F. McDonald[109], A. E. McDougall[47], J. A. Mcfayden[51], G. Mchedlidze[174], R. P. Mckenzie[170], T. C. Mclachlan[33], D. J. Mclaughlin[112], K. D. McLean[41], S. J. McMahon[22], P. C. McNamara[109], R. A. McPherson[41,260], J. E. Mdhluli[170], S. Meehan[24], T. Megy[150], S. Mehlhase[58], A. Mehta[80], B. Meirose[197], D. Melini[9], B. R. Mellado Garcia[170], A. H. Melo[4], F. Meloni[33], E. D. Mendes Gouveia[60], A. M. Mendes Jacques Da Costa[52], H. Y. Meng[17], L. Meng[123], S. Menke[113], M. Mentink[24], E. Meoni[166,167], C. Merlassino[119], L. Merola[53,54], C. Meroni[50,69], G. Merz[59], O. Meshkov[38], J. K. R. Meshreki[129], J. Metcalfe[146], A. S. Mete[146], C. Meyer[162], J.-P. Meyer[64], M. Michetti[77], R. P. Middleton[22], L. Mijović[44], G. Mikenberg[36], M. Mikestikova[178], M. Mikuž[179], H. Mildner[63], A. Milic[17], C. D. Milke[191], D. W. Miller[203], L. S. Miller[98], A. Milov[36], D. A. Milstead[67,68], T. Min[96], A. A. Minaenko[38], I. A. Minashvili[174], L. Mince[128], A. I. Mincer[10], B. Mindur[16], M. Mineev[30], Y. Minegishi[86], Y. Mino[225], L. M. Mir[25], M. Miralles Lopez[61], M. Mironova[119], T. Mitani[220], A. Mitra[133], V. A. Mitsou[61], O. Miu[17], P. S. Miyagawa[143], Y. Miyazaki[223], A. Mizukami[76], J. U. Mjörnmark[37], T. Mkrtchyan[104], M. Mlynarikova[19], T. Moa[67,68], S. Mobius[4], K. Mochizuki[81], P. Moder[33], P. Mogg[58], A. F. Mohammed[120,122], S. Mohapatra[39], G. Mokgatitswane[170], B. Mondal[129], S. Mondal[48], K. Mönig[33], E. Monnier[1], L. Monsonis Romero[61], J. Montejo Berlingen[24], M. Montella[151], F. Monticelli[43], N. Morange[127], A. L. Moreira De Carvalho[60], M. Moreno Llácer[61], C. Moreno Martinez[25], P. Morettini[111], S. Morgenstern[133], M. Morii[87], M. Morinaga[86], V. Morisbak[62], A. K. Morley[24], F. Morodei[75,83], L. Morvaj[24], P. Moschovakos[24], B. Moser[24], M. Mosidze[174], T. Moskalets[82], P. Moskvitina[169], J. Moss[209,252], E. J. W. Moyse[3], S. Muanza[1], J. Mueller[107], D. Muenstermann[123], R. Müller[66], G. A. Mullier[37], J. J. Mullin[188], D. P. Mungo[50,69], J. L. Munoz Martinez[25], D. Munoz Perez[61], F. J. Munoz Sanchez[117], M. Murin[117], W. J. Murray[22,133], A. Murrone[50,69], J. M. Muse[2], M. Muškinja[73], C. Mwewa[5], A. G. Myagkov[38,239], A. J. Myers[101], A. A. Myers[107], G. Myers[162], M. Myska[48], B. P. Nachman[73], O. Nackenhorst[24], A. Nag[142], K. Nagai[119], K. Nagano[76], J. L. Nagle[5,269], E. Nagy[1], A. M. Nairz[24], Y. Nakahama[76], K. Nakamura[76], H. Nanjo[216], R. Narayan[191], E. A. Narayanan[210], I. Naryshkin[38], M. Naseri[98], C. Nass[108], G. Navarro[230], J. Navarro-Gonzalez[61], R. Nayak[8], P. Y. Nechaeva[38], F. Nechansky[33], T. J. Neep[52], A. Negri[26,27], M. Negrini[40], C. Nellist[169], C. Nelson[31], K. Nelson[59], S. Nemecek[178], M. Nessi[24,245], M. S. Neubauer[93], F. Neuhaus[14], J. Neundorf[33], R. Newhouse[183], P. R. Newman[52], C. W. Ng[107], Y. S. Ng[77], Y. W. Y. Ng[186], B. Ngair[6], H. D. N. Nguyen[81], R. B. Nickerson[119], R. Nicolaidou[64], J. Nielsen[23], M. Niemeyer[4], N. Nikiforou[24], V. Nikolaenko[38,239], I. Nikolic-Audit[131], K. Nikolopoulos[52], P. Nilsson[5], H. R. Nindhito[21], A. Nisati[75], N. Nishu[205], R. Nisius[113], J.-E. Nitschke[142], E. K. Nkadimeng[170], S. J. Noacco Rosende[43], T. Nobe[86], D. L. Noel[105], Y. Noguchi[225], T. Nommensen[102], M. A. Nomura[5], M. B. Norfolk[63], R. R. B. Norisam[112], B. J. Norman[98], J. Novak[179], T. Novak[33], O. Novgorodova[142], L. Novotny[48], R. Novotny[210], L. Nozka[116], K. Ntekas[186], E. Nurse[112], F. G. Oakham[98,266], J. Ocariz[131], A. Ochi[215], I. Ochoa[60], S. Oerdek[88], A. Ogrodnik[16], A. Oh[117], C. C. Ohm[227], H. Oide[213], R. Oishi[86], M. L. Ojeda[33], Y. Okazaki[225], M. W. O'Keefe[80], Y. Okumura[86], A. Olariu[45], L. F. Oleiro Seabra[60], S. A. Olivares Pino[222], D. Oliveira Damazio[5], D. Oliveira Goncalves[78], J. L. Oliver[186], M. J. R. Olsson[186], A. Olszewski[106], J. Olszowska[106,275], Ö. O. Öncel[82], D. C. O'Neil[157], A. P. O'Neill[66], A. Onofre[60,171], P. U. E. Onyisi[65], M. J. Oreglia[203], G. E. Orellana[43], D. Orestano[125,126], N. Orlando[25], R. S. Orr[17], V. O'Shea[128], R. Ospanov[118], G. Otero y Garzon[189], H. Otono[223], P. S. Ott[104], G. J. Ottino[73], M. Ouchrif[89], J. Ouellette[5,269], F. Ould-Saada[62], M. Owen[128], R. E. Owen[22], K. Y. Oyulmaz[130], V. E. Ozcan[130], N. Ozturk[101], S. Ozturk[134], J. Pacalt[116], H. A. Pacey[105], K. Pachal[79], A. Pacheco Pages[25], C. Padilla Aranda[25], G. Padovano[75,83], S. Pagan Griso[73], G. Palacino[162], A. Palazzo[172,173], S. Palazzo[44], S. Palestini[24], M. Palka[204], J. Pan[99], T. Pan[176], D. K. Panchal[65], C. E. Pandini[47], J. G. Panduro Vazquez[32], H. Pang[121], P. Pani[33], G. Panizzo[12,180], L. Paolozzi[21], C. Papadatos[81], S. Parajuli[191], A. Paramonov[146], C. Paraskevopoulos[46], D. Paredes Hernandez[218], T. H. Park[17], M. A. Parker[105], F. Parodi[110,111], E. W. Parrish[19], V. A. Parrish[44], J. A. Parsons[39], U. Parzefall[82], B. Pascual Dias[81], L. Pascual Dominguez[8], V. R. Pascuzzi[73], F. Pasquali[47], E. Pasqualucci[75], S. Passaggio[111], F. Pastore[32], P. Pasuwan[67,68], J. R. Pater[117], J. Patton[80], T. Pauly[24], J. Pearkes[115], M. Pedersen[62], R. Pedro[60], S. V. Peleganchuk[38], O. Penc[24], C. Peng[218], H. Peng[118], K. E. Penski[58], M. Penzin[38], B. S. Peralva[78,136], A. P. Pereira Peixoto[181], L. Pereira Sanchez[67,68], D. V. Perepelitsa[5,269], E. Perez Codina[168], M. Perganti[46], L. Perini[50,69,276], H. Pernegger[24], S. Perrella[24], A. Perrevoort[169], O. Perrin[150], K. Peters[33], R. F. Y. Peters[117], B. A. Petersen[24], T. C. Petersen[164], E. Petit[1], V. Petousis[48], C. Petridou[97], A. Petrukhin[129], M. Pettee[73], N. E. Pettersson[24], A. Petukhov[38], K. Petukhova[103], A. Peyaud[64], R. Pezoa[154], L. Pezzotti[24], G. Pezzullo[99], T. Pham[109], P. W. Phillips[22], M. W. Phipps[93], G. Piacquadio[135], E. Pianori[73], F. Piazza[50,69], R. Piegaia[189], D. Pietreanu[45], A. D. Pilkington[117], M. Pinamonti[12,180], J. L. Pinfold[205], B. C. Pinheiro Pereira[60], C. Pitman Donaldson[112], D. A. Pizzi[98], L. Pizzimento[34,35], A. Pizzini[47], M.-A. Pleier[5], V. Plesanovs[82], V. Pleskot[103], E. Plotnikova[30], G. Poddar[15], R. Poettgen[37], R. Poggi[21], L. Poggioli[131], I. Pogrebnyak[159], D. Pohl[108], I. Pokharel[4], S. Polacek[103], G. Polesello[26], A. Poley[157,168], R. Polifka[48], A. Polini[40], C. S. Pollard[119], Z. B. Pollock[151], V. Polychronakos[5], D. Ponomarenko[38], L. Pontecorvo[24], S. Popa[231], G. A. Popeneciu[232], D. M. Portillo Quintero[168], S. Pospisil[48], P. Postolache[28], K. Potamianos[119], I. N. Potrap[30], C. J. Potter[105], H. Potti[198], T. Poulsen[33], J. Poveda[61], G. Pownall[33], M. E. Pozo Astigarraga[24], A. Prades Ibanez[61], M. M. Prapa[196], D. Price[117], M. Primavera[172], M. A. Principe Martin[56], M. L. Proffitt[55],

N. Proklova[38], K. Prokofiev[228], G. Proto[34,35], S. Protopopescu[5], J. Proudfoot[146], M. Przybycien[16], J. E. Puddefoot[63], D. Pudzha[38], P. Puzo[127], D. Pyatiizbyantseva[38], J. Qian[59], Y. Qin[117], T. Qiu[143], A. Quadt[4], M. Queitsch-Maitland[117], G. Rabanal Bolanos[87], D. Rafanoharana[82], F. Ragusa[50,69], J. L. Rainbolt[203], J. A. Raine[21], S. Rajagopalan[5], E. Ramakoti[38], K. Ran[120,122], V. Raskina[131], D. F. Rassloff[104], S. Rave[14], B. Ravina[128], I. Ravinovich[36], M. Raymond[24], A. L. Read[62], N. P. Readioff[63], D. M. Rebuzzi[26,27], G. Redlinger[5], K. Reeves[197], J. A. Reidelsturz[95], D. Reikher[8], A. Reiss[14], A. Rej[129], C. Rembser[24], A. Renardi[33], M. Renda[45], M. B. Rendel[113], A. G. Rennie[128], S. Resconi[50], M. Ressegotti[110,111], E. D. Resseguie[73], S. Rettie[112], B. Reynolds[151], E. Reynolds[73], M. Rezaei Estabragh[95], O. L. Rezanova[38], P. Reznicek[103], E. Ricci[184,185], R. Richter[113], S. Richter[67,68], E. Richter-Was[204], M. Ridel[131], P. Rieck[10], P. Riedler[24], M. Rijssenbeek[135], A. Rimoldi[26,27], M. Rimoldi[33], L. Rinaldi[40,148], T. T. Rinn[5], M. P. Rinnagel[58], G. Ripellino[227], I. Riu[25], P. Rivadeneira[33], J. C. Rivera Vergara[41], F. Rizatdinova[72], E. Rizvi[143], C. Rizzi[21], B. A. Roberts[133], B. R. Roberts[73], S. H. Robertson[31,260], M. Robin[33], D. Robinson[105], C. M. Robles Gajardo[154], M. Robles Manzano[14], A. Robson[128], A. Rocchi[34,35], C. Roda[71,163], S. Rodriguez Bosca[104], Y. Rodriguez Garcia[230], A. Rodriguez Rodriguez[82], A. M. Rodríguez Vera[190], S. Roe[24], J. T. Roemer[186], A. R. Roepe-Gier[2], J. Roggel[95], O. Røhne[62], R. A. Rojas[41], B. Roland[82], C. P. A. Roland[162], J. Roloff[5], A. Romaniouk[38], E. Romano[26,27], M. Romano[40], A. C. Romero Hernandez[93], N. Rompotis[80], L. Roos[131], S. Rosati[75], B. J. Rosser[203], E. Rossi[15], E. Rossi[53,54], L. P. Rossi[111], L. Rossini[33], R. Rosten[151], M. Rotaru[45], B. Rottler[82], D. Rousseau[127], D. Rousso[105], G. Rovelli[26,27], A. Roy[93], A. Rozanov[1], Y. Rozen[9], X. Ruan[170], A. Rubio Jimenez[61], A. J. Ruby[80], T. A. Ruggeri[198], F. Rühr[82], A. Ruiz-Martinez[61], A. Rummler[24], Z. Rurikova[82], N. A. Rusakovich[30], H. L. Russell[41], J. P. Rutherfoord[140], E. M. Rüttinger[63], K. Rybacki[123], M. Rybar[103], E. B. Rye[62], A. Ryzhov[38], J. A. Sabater Iglesias[21], P. Sabatini[61], L. Sabetta[75,83], H. F.-W. Sadrozinski[23], F. Safai Tehrani[75], B. Safarzadeh Samani[51], M. Safdari[115], S. Saha[31], M. Sahinsoy[113], M. Saimpert[64], M. Saito[86], T. Saito[86], D. Salamani[24], G. Salamanna[125,126], A. Salnikov[115], J. Salt[61], A. Salvador Salas[25], D. Salvatore[166,167], F. Salvatore[51], A. Salzburger[24], D. Sammel[82], D. Sampsonidis[97], D. Sampsonidou[152,153], J. Sánchez[61], A. Sanchez Pineda[15], V. Sanchez Sebastian[61], H. Sandaker[62], C. O. Sander[33], J. A. Sandesara[3], M. Sandhoff[95], C. Sandoval[233], D. P. C. Sankey[22], A. Sansoni[42], L. Santi[75,83], C. Santoni[150], H. Santos[60,206], S. N. Santpur[73], A. Santra[36], K. A. Saoucha[63], J. G. Saraiva[60,229], J. Sardain[140], O. Sasaki[76], K. Sato[211], C. Sauer[187], F. Sauerburger[82], E. Sauvan[15], P. Savard[17,266], R. Sawada[86], C. Sawyer[22], L. Sawyer[234], I. Sayago Galvan[61], C. Sbarra[40], A. Sbrizzi[40,148], T. Scanlon[112], J. Schaarschmidt[55], P. Schacht[113], D. Schaefer[203], U. Schäfer[14], A. C. Schaffer[127], D. Schaile[58], R. D. Schamberger[135], E. Schanet[58], C. Scharf[77], V. A. Schegelsky[38], D. Scheirich[103], F. Schenck[77], M. Schernau[186], C. Scheulen[4], C. Schiavi[110,111], Z. M. Schillaci[18], E. J. Schioppa[172,173], M. Schioppa[166,167], B. Schlag[14], K. E. Schleicher[82], S. Schlenker[24], K. Schmieden[14], C. Schmitt[14], S. Schmitt[33], L. Schoeffel[64], A. Schoening[187], P. G. Scholer[82], E. Schopf[119], M. Schott[14], J. Schovancova[24], S. Schramm[21], F. Schroeder[95], H.-C. Schultz-Coulon[104], M. Schumacher[82], B. A. Schumm[23], Ph. Schune[64], A. Schwartzman[115], T. A. Schwarz[59], Ph. Schwemling[64], R. Schwienhorst[159], A. Sciandra[23], G. Sciolla[18], F. Scuri[71], F. Scutti[109], C. D. Sebastiani[80], K. Sedlaczek[124], P. Seema[77], S. C. Seidel[210], A. Seiden[23], B. D. Seidlitz[39], T. Seiss[203], C. Seitz[33], J. M. Seixas[57], G. Sekhniaidze[53], S. J. Sekula[191], L. Selem[15], N. Semprini-Cesari[40,148], S. Sen[79], D. Sengupta[21], V. Senthilkumar[61], L. Serin[127], L. Serkin[12,13], M. Sessa[125,126], H. Severini[2], S. Sevova[115], F. Sforza[110,111], A. Sfyrla[21], E. Shabalina[4], R. Shaheen[227], J. D. Shahinian[188], N. W. Shaikh[67,68], D. Shaked Renous[36], L. Y. Shan[120], M. Shapiro[73], A. Sharma[24], A. S. Sharma[183], P. Sharma[165], S. Sharma[33], P. B. Shatalov[38], K. Shaw[51], S. M. Shaw[117], Q. Shen[152], P. Sherwood[112], L. Shi[112], C. O. Shimmin[99], Y. Shimogama[220], J. D. Shinner[32], I. P. J. Shipsey[119], S. Shirabe[181], M. Shiyakova[30,74], J. Shlomi[36], M. J. Shochet[203], J. Shojaii[109], D. R. Shope[227], S. Shrestha[151], E. M. Shrif[170], M. J. Shroff[41], P. Sicho[178], A. M. Sickles[93], E. Sideras Haddad[170], O. Sidiropoulou[24], A. Sidoti[40], F. Siegert[142], Dj. Sijacki[100], R. Sikora[16], F. Sili[43], J. M. Silva[52], M. V. Silva Oliveira[24], S. B. Silverstein[67], S. Simion[127], R. Simoniello[24], E. L. Simpson[128], N. D. Simpson[37], S. Simsek[134], S. Sindhu[4], P. Sinervo[17], V. Sinetckii[38], S. Singh[157], S. Singh[17], S. Sinha[33], S. Sinha[170], M. Sioli[40,148], I. Siral[114], S. Yu. Sivoklokov[38,277], J. Sjölin[67,68], A. Skaf[4], E. Skorda[37], P. Skubic[2], M. Slawinska[106], V. Smakhtin[36], B. H. Smart[22], J. Smiesko[103], S. Yu. Smirnov[38], Y. Smirnov[38], L. N. Smirnova[38,239], O. Smirnova[37], A. C. Smith[39], E. A. Smith[203], H. A. Smith[119], J. L. Smith[80], R. Smith[115], M. Smizanska[123], K. Smolek[48], A. Smykiewicz[106], A. A. Snesarev[38], H. L. Snoek[47], S. Snyder[5], R. Sobie[41,260], A. Soffer[8], C. A. Solans Sanchez[24], E. Yu. Soldatov[38], U. Soldevila[61], A. A. Solodkov[38], S. Solomon[82], A. Soloshenko[30], K. Solovieva[82], O. V. Solovyanov[38], V. Solovyev[38], P. Sommer[24], A. Sonay[25], W. Y. Song[190], A. Sopczak[48], A. L. Sopio[112], F. Sopkova[155], V. Sothilingam[104], S. Sottocornola[26,27], R. Soualah[235], Z. Soumaimi[6], D. South[33], S. Spagnolo[172,173], M. Spalla[113], F. Spanò[32], D. Sperlich[82], G. Spigo[24], M. Spina[51], S. Spinali[123], D. P. Spiteri[128], M. Spousta[103], E. J. Staats[98], A. Stabile[50,69], R. Stamen[104], M. Stamenkovic[47], A. Stampekis[52], M. Standke[108], E. Stanecka[106], B. Stanislaus[73], M. M. Stanitzki[33], M. Stankaityte[119], B. Stapf[33], E. A. Starchenko[38], G. H. Stark[23], J. Stark[1,92], D. M. Starko[190], P. Staroba[178], P. Starovoitov[104], S. Stärz[31], R. Staszewski[106], G. Stavropoulos[196], J. Steentoft[88], P. Steinberg[5], A. L. Steinhebel[114], B. Stelzer[157,168], H. J. Stelzer[107], O. Stelzer-Chilton[168], H. Stenzel[160], T. J. Stevenson[51], G. A. Stewart[24], M. C. Stockton[24], G. Stoicea[45], M. Stolarski[60], S. Stonjek[113], A. Straessner[142], J. Strandberg[227], S. Strandberg[67,68], M. Strauss[2], T. Strebler[1], P. Strizenec[155], R. Ströhmer[145], D. M. Strom[114], L. R. Strom[33], R. Stroynowski[191], A. Strubig[67,68], S. A. Stucci[5], B. Stugu[156], J. Stupak[2], N. A. Styles[33], D. Su[115], S. Su[118], W. Su[55,152,153], X. Su[118,127], K. Sugizaki[86], V. V. Sulin[38], M. J. Sullivan[80], D. M. S. Sultan[184,185], L. Sultanaliyeva[38], S. Sultansoy[161,236], T. Sumida[225], S. Sun[59], S. Sun[149], O. Sunneborn Gudnadottir[88], M. R. Sutton[51], M. Svatos[178], M. Swiatlowski[168], T. Swirski[145], I. Sykora[90], M. Sykora[103], T. Sykora[103], D. Ta[14], K. Tackmann[33,259], A. Taffard[186], R. Tafirout[168], J. S. Tafoya Vargas[127], R. H. M. Taibah[131], R. Takashima[237], K. Takeda[215], E. P. Takeva[44], Y. Takubo[76], M. Talby[1], A. A. Talyshev[38], K. C. Tam[218], N. M. Tamir[8], A. Tanaka[86], J. Tanaka[86], R. Tanaka[127], M. Tanasini[110,111], J. Tang[152], Z. Tao[183], S. Tapia Araya[214], S. Tapprogge[14], A. Tarek Abouelfadl Mohamed[159], S. Tarem[9], K. Tariq[94], G. Tarna[45], G. F. Tartarelli[50], P. Tas[103], M. Tasevsky[178], E. Tassi[166,167], A. C. Tate[93], G. Tateno[86], Y. Tayalati[6], G. N. Taylor[109], W. Taylor[190], H. Teagle[80], A. S. Tee[149], R. Teixeira De Lima[115], P. Teixeira-Dias[32], J. J. Teoh[17], K. Terashi[86], J. Terron[56], S. Terzo[25], M. Testa[42], R. J. Teuscher[17,260], A. Thaler[224], N. Themistokleous[44], T. Theveneaux-Pelzer[77], O. Thielmann[95], D. W. Thomas[32], J. P. Thomas[52], E. A. Thompson[33], P. D. Thompson[52], E. Thomson[188], E. J. Thorpe[143], Y. Tian[4], V. Tikhomirov[38,239], Yu. A. Tikhonov[38], S. Timoshenko[38], E. X. L. Ting[198], P. Tipton[99], S. Tisserant[1], S. H. Tlou[170], A. Tnourji[150], K. Todome[40,148], S. Todorova-Nova[103], S. Todt[142], M. Togawa[76], J. Tojo[223], S. Tokár[90], K. Tokushuku[76], R. Tombs[105], M. Tomoto[76,84], L. Tompkins[115,175], P. Tornambe[3], E. Torrence[114], H. Torres[142], E. Torró Pastor[61], M. Toscani[189], C. Tosciri[203], D. R. Tovey[63], A. Traeet[156], I. S. Trandafir[45], T. Trefzger[145], A. Tricoli[5], I. M. Trigger[168], S. Trincaz-Duvoid[131], D. A. Trischuk[183], B. Trocmé[181], A. Trofymov[127], C. Troncon[50], L. Truong[144], M. Trzebinski[106], A. Trzupek[106], F. Tsai[135], M. Tsai[59], A. Tsiamis[97], P. V. Tsiareshka[38], S. Tsigaridas[168], A. Tsirigotis[97,257], V. Tsiskaridze[135], E. G. Tskhadadze[221], M. Tsopoulou[97], Y. Tsujikawa[225], I. I. Tsukerman[38], V. Tsulaia[73], S. Tsuno[76], O. Tsur[9], D. Tsybychev[135], Y. Tu[218], A. Tudorache[45], V. Tudorache[45], A. N. Tuna[24], S. Turchikhin[30], I. Turk Cakir[161], R. Turra[50], T. Turtuvshin[30], P. M. Tuts[39], S. Tzamarias[97], P. Tzanis[46], E. Tzovara[14], K. Uchida[86], F. Ukegawa[211], P. A. Ulloa Poblete[238], G. Unal[24], M. Unal[65], A. Undrus[5], G. Unel[186], K. Uno[86], J. Urban[155], P. Urquijo[109], G. Usai[101], R. Ushioda[213], M. Usman[81], Z. Uysal[147], V. Vacek[48], B. Vachon[31], K. O. H. Vadla[62], T. Vafeiadis[24], C. Valderanis[58], E. Valdes Santurio[67,68], M. Valente[168], S. Valentinetti[40,148], A. Valero[61], A. Vallier[1,92], J. A. Valls Ferrer[61], T. R. Van Daalen[55], P. Van Gemmeren[146], S. Van Stroud[112], I. Van Vulpen[47], M. Vanadia[34,35], W. Vandelli[24], M. Vandenbroucke[64], E. R. Vandewall[72], D. Vannicola[8], L. Vannoli[110,111], R. Vari[75], E. W. Varnes[140], C. Varni[73], T. Varol[49], D. Varouchas[127], L. Varriale[61], K. E. Varvell[102], M. E. Vasile[45], L. Vaslin[150], G. A. Vasquez[41], F. Vazeille[150], T. Vazquez Schroeder[24], J. Veatch[209], V. Vecchio[117], M. J. Veen[47], I. Veliscek[119], L. M. Veloce[17], F. Veloso[60,199], S. Veneziano[75], A. Ventura[172,173], A. Verbytskyi[113], M. Verducci[71,163], C. Vergis[108], M. Verissimo De Araujo[57], W. Verkerke[47], J. C. Vermeulen[47], C. Vernieri[115], P. J. Verschuuren[32], M. Vessella[3], M. L. Vesterbacka[10], M. C. Vetterli[157,266], A. Vgenopoulos[97], N. Viaux Maira[154], T. Vickey[63], O. E. Vickey Boeriu[63], G. H. A. Viehhauser[119], L. Vigani[187], M. Villa[40,148], M. Villaplana Perez[61], E. M. Villhauer[44], E. Vilucchi[42], M. G. Vincter[98], G. S. Virdee[52], A. Vishwakarma[44], C. Vittori[40,148], I. Vivarelli[51], V. Vladimirov[133], E. Voevodina[113], F. Vogel[58], P. Vokac[48], J. Von Ahnen[33], E. Von Toerne[108], B. Vormwald[24], V. Vorobel[103], K. Vorobev[38], M. Vos[61], J. H. Vossebeld[80], M. Vozak[47], L. Vozdecky[143], N. Vranjes[100], M. Vranjes Milosavljevic[100], M. Vreeswijk[47], R. Vuillermet[24], O. Vujinovic[14], I. Vukotic[203], S. Wada[211], C. Wagner[3], W. Wagner[95], S. Wahdan[95], H. Wahlberg[43], R. Wakasa[211], M. Wakida[84], V. M. Walbrecht[113], J. Walder[22], R. Walker[58], W. Walkowiak[129], A. M. Wang[87], A. Z. Wang[149], C. Wang[118], C. Wang[152], H. Wang[73], J. Wang[176], P. Wang[191], R.-J. Wang[14], R. Wang[87], R. Wang[146], S. M. Wang[49], S. Wang[94], T. Wang[118], W. T. Wang[165], W. X. Wang[118], X. Wang[96], X. Wang[93], X. Wang[152], Y. Wang[153], Y. Wang[96], Z. Wang[59], Z. Wang[79,152,153], Z. Wang[59], A. Warburton[31], R. J. Ward[52], N. Warrack[128], A. T. Watson[52], M. F. Watson[52], G. Watts[55], B. M. Waugh[112], A. F. Webb[65], C. Weber[5], M. S. Weber[66], S. A. Weber[98], S. M. Weber[104], C. Wei[118], Y. Wei[119], A. R. Weidberg[119], J. Weingarten[124], M. Weirich[14], C. Weiser[82], C. J. Wells[33], T. Wenaus[5], B. Wendland[124], T. Wengler[24], N. S. Wenke[113], N. Wermes[108], M. Wessels[104], K. Whalen[114], A. M. Wharton[123], A. S. White[87], A. White[101], M. J. White[198], D. Whiteson[186], L. Wickremasinghe[216], W. Wiedenmann[149], C. Wiel[142], M. Wielers[22], N. Wieseotte[14], C. Wiglesworth[164], L. A. M. Wiik-Fuchs[82], D. J. Wilbern[2], H. G. Wilkens[24], D. M. Williams[39], H. H. Williams[188], S. Williams[105], S. Willocq[3], P. J. Windischhofer[119], F. Winklmeier[114], B. T. Winter[82], M. Wittgen[115], M. Wobisch[234], A. Wolf[14], R. Wölker[119], J. Wollrath[186], M. W. Wolter[106], H. Wolters[60,199], V. W. S. Wong[183], A. F. Wongel[33], S. D. Worm[33], B. K. Wosiek[106], K. W. Woźniak[106], K. Wraight[128], J. Wu[120,122], M. Wu[176], S. L. Wu[149], X. Wu[21], Y. Wu[118], Z. Wu[64,118], J. Wuerzinger[119], T. R. Wyatt[117], B. M. Wynne[44], S. Xella[164], L. Xia[96], M. Xia[121], J. Xiang[228], X. Xiao[59], M. Xie[118], X. Xie[118], J. Xiong[73], I. Xiotidis[51], D. Xu[120], H. Xu[118], H. Xu[118], L. Xu[118], R. Xu[188], T. Xu[59], W. Xu[59], Y. Xu[121], Z. Xu[94], Z. Xu[115], B. Yabsley[102], S. Yacoob[91], N. Yamaguchi[223], Y. Yamaguchi[213], H. Yamauchi[211], T. Yamazaki[73], Y. Yamazaki[215], J. Yan[152], S. Yan[119], Z. Yan[158], H. J. Yang[152,153], H. T. Yang[73], S. Yang[118], T. Yang[228], X. Yang[118], X. Yang[120], Y. Yang[191], Z. Yang[59,118], W.-M. Yao[73], Y. C. Yap[33], H. Ye[96], J. Ye[191], S. Ye[5], X. Ye[118], Y. Yeh[112], I. Yeletskikh[30], M. R. Yexley[123], P. Yin[39], K. Yorita[220], C. J. S. Young[82], C. Young[115], M. Yuan[59], R. Yuan[94,248], L. Yue[112], X. Yue[104], M. Zaazoua[6], B. Zabinski[106], E. Zaid[44], T. Zakareishvili[174], N. Zakharchuk[98], S. Zambito[21], J. Zang[86], D. Zanzi[82], O. Zaplatilek[48], S. V. Zeißner[124], C. Zeitnitz[95], J. C. Zeng[93], D. T. Zenger Jr[18], O. Zenin[38], T. Ženiš[90], S. Zenz[143], S. Zerradi[139], D. Zerwas[127], B. Zhang[96], D. F. Zhang[63], G. Zhang[121], J. Zhang[146], K. Zhang[120,122], L. Zhang[96], R. Zhang[149], S. Zhang[59], T. Zhang[86], X. Zhang[152], X. Zhang[94], Z. Zhang[73], Z. Zhang[127], H. Zhao[55], P. Zhao[79], T. Zhao[94], Y. Zhao[23], Z. Zhao[118], A. Zhemchugov[30], Z. Zheng[115], D. Zhong[93], B. Zhou[59], C. Zhou[149], H. Zhou[140], N. Zhou[152], Y. Zhou[140], C. G. Zhu[94], C. Zhu[120,122], H. L. Zhu[118], H. Zhu[120], J. Zhu[59], Y. Zhu[152], Y. Zhu[118], X. Zhuang[120], K. Zhukov[38], V. Zhulanov[38], N. I. Zimine[30], J. Zinsser[187], M. Ziolkowski[129], L. Živković[100], A. Zoccoli[40,148], K. Zoch[21], T. G. Zorbas[63], O. Zormpa[196], W. Zou[39] & L. Zwalinski[24]

[1]CPPM, Aix-Marseille Université, CNRS/IN2P3, Marseille, France. [2]Homer L. Dodge Department of Physics and Astronomy, University of Oklahoma, Norman, OK, United States of America. [3]Department of Physics, University of Massachusetts, Amherst, MA, United States of America. [4]II. Physikalisches Institut, Georg-August-Universität Göttingen, Göttingen, Germany. [5]Physics Department, Brookhaven National Laboratory, Upton, NY, United States of America. [6]Faculté des sciences, Université Mohammed V, Rabat, Morocco. [7]Physics Department, An-Najah National University, Nablus, Palestine. [8]Raymond and Beverly Sackler School of Physics and Astronomy, Tel Aviv University, Tel Aviv, Israel. [9]Department of Physics, Technion, Israel Institute of Technology, Haifa, Israel. [10]Department of Physics, New York University, New York, NY, United States of America. [11]Departamento de Física, Pontificia Universidad Católica de Chile, Santiago, Chile. [12]INFN Gruppo Collegato di Udine, Sezione di Trieste, Udine, Italy. [13]ICTP, Trieste, Italy. [14]Institut für Physik, Universität Mainz, Mainz, Germany. [15]LAPP, Univ. Savoie Mont Blanc, CNRS/IN2P3, Annecy, France. [16]AGH University of Krakow, Faculty of Physics and Applied Computer Science, Krakow, Poland. [17]Department of Physics, University of Toronto, Toronto, ON, Canada. [18]Department of Physics, Brandeis University, Waltham, MA, United States of America. [19]Department of Physics, Northern Illinois University, DeKalb, IL, United States of America. [20]Department of Physics, Istanbul University, Istanbul, Turkey. [21]Département de Physique Nucléaire et Corpusculaire, Université de Genève, Genève, Switzerland. [22]Particle Physics Department, Rutherford Appleton Laboratory, Didcot, United Kingdom. [23]Santa Cruz Institute for Particle Physics, University of California Santa Cruz, Santa Cruz, CA, United States of America. [24]CERN, Geneva, Switzerland. [25]Institut de Física d'Altes Energies (IFAE), Barcelona Institute of Science and Technology, Barcelona, Spain. [26]INFN Sezione di Pavia, Pavia, Italy. [27]Dipartimento di Fisica, Università di Pavia, Pavia, Italy. [28]Department of Physics, Alexandru Ioan Cuza University of Iasi, Iasi, Romania. [29]Departamento de Física Teórica y del Cosmos, Universidad de Granada, Granada, Spain. [30]Affiliated with an international laboratory covered by a cooperation agreement with CERN, Geneva, Switzerland. [31]Department of Physics, McGill University, Montreal, QC, Canada.

[32]Department of Physics, Royal Holloway University of London, Egham, United Kingdom. [33]Deutsches Elektronen-Synchrotron DESY, Hamburg and Zeuthen, Germany. [34]INFN Sezione di Roma Tor Vergata, Rome, Italy. [35]Dipartimento di Fisica, Università di Roma Tor Vergata, Roma, Italy. [36]Department of Particle Physics and Astrophysics, Weizmann Institute of Science, Rehovot, Israel. [37]Fysiska institutionen, Lunds universitet, Lund, Sweden. [38]Affiliated with an institute covered by a cooperation agreement with CERN, Geneva, Switzerland. [39]Nevis Laboratory, Columbia University, Irvington, NY, United States of America. [40]INFN Sezione di Bologna, Bologna, Italy. [41]Department of Physics and Astronomy, University of Victoria, Victoria, BC, Canada. [42]INFN e Laboratori Nazionali di Frascati, Frascati, Italy. [43]Instituto de Física La Plata, Universidad Nacional de La Plata and CONICET, La Plata, Argentina. [44]SUPA - School of Physics and Astronomy, University of Edinburgh, Edinburgh, United Kingdom. [45]Horia Hulubei National Institute of Physics and Nuclear Engineering, Bucharest, Romania. [46]Physics Department, National Technical University of Athens, Zografou, Greece. [47]Nikhef National Institute for Subatomic Physics and University of Amsterdam, Amsterdam, Netherlands. [48]Czech Technical University in Prague, Prague, Czech Republic. [49]Institute of Physics, Academia Sinica, Taipei, Taiwan. [50]INFN Sezione di Milano, Milan, Italy. [51]Department of Physics and Astronomy, University of Sussex, Brighton, United Kingdom. [52]School of Physics and Astronomy, University of Birmingham, Birmingham, United Kingdom. [53]INFN Sezione di Napoli, Napoli, Italy. [54]Dipartimento di Fisica, Università di Napoli, Napoli, Italy. [55]Department of Physics, University of Washington, Seattle, WA, United States of America. [56]Departamento de Física Teorica C-15 and CIAFF, Universidad Autónoma de Madrid, Madrid, Spain. [57]Universidade Federal do Rio De Janeiro COPPE/EE/IF, Rio de Janeiro, Brazil. [58]Fakultät für Physik, Ludwig-Maximilians-Universität München, München, Germany. [59]Department of Physics, University of Michigan, Ann Arbor, MI, United States of America. [60]Laboratório de Instrumentação e Física Experimental de Partículas - LIP, Lisboa, Portugal. [61]Instituto de Física Corpuscular (IFIC), Centro Mixto Universidad de Valencia - CSIC, Valencia, Spain. [62]Department of Physics, University of Oslo, Oslo, Norway. [63]Department of Physics and Astronomy, University of Sheffield, Sheffield, United Kingdom. [64]IRFU, CEA, Université Paris-Saclay, Gif-sur-Yvette, France. [65]Department of Physics, University of Texas at Austin, Austin, TX, United States of America. [66]Albert Einstein Center for Fundamental Physics and Laboratory for High Energy Physics, University of Bern, Bern, Switzerland. [67]Department of Physics, Stockholm University, Stockholm, Sweden. [68]Oskar Klein Centre, Stockholm, Sweden. [69]Dipartimento di Fisica, Università di Milano, Milano, Italy. [70]Physics Department, National and Kapodistrian University of Athens, Athens, Greece. [71]INFN Sezione di Pisa, Pisa, Italy. [72]Department of Physics, Oklahoma State University, Stillwater, OK, United States of America. [73]Physics Division, Lawrence Berkeley National Laboratory, Berkeley, CA, United States of America. [74]Institute for Nuclear Research and Nuclear Energy (INRNE) of the Bulgarian Academy of Sciences, Sofia, Bulgaria. [75]INFN Sezione di Roma, Roma, Italy. [76]KEK, High Energy Accelerator Research Organization, Tsukuba, Japan. [77]Institut für Physik, Humboldt Universität zu Berlin, Berlin, Germany. [78]Departamento de Engenharia Elétrica, Universidade Federal de Juiz de Fora (UFJF), Juiz de Fora, Brazil. [79]Department of Physics, Duke University, Durham, NC, United States of America. [80]Oliver Lodge Laboratory, University of Liverpool, Liverpool, United Kingdom. [81]Group of Particle Physics, University of Montreal, Montreal, QC, Canada. [82]Physikalisches Institut, Albert-Ludwigs-Universität Freiburg, Freiburg, Germany. [83]Dipartimento di Fisica, Sapienza Università di Roma, Roma, Italy. [84]Graduate School of Science and Kobayashi-Maskawa Institute, Nagoya University, Nagoya, Japan. [85]Ochanomizu University, Otsuka, Bunkyo-ku, Tokyo, Japan. [86]International Center for Elementary Particle Physics and Department of Physics, University of Tokyo, Tokyo, Japan. [87]Laboratory for Particle Physics and Cosmology, Harvard University, Cambridge, MA, United States of America. [88]Department of Physics and Astronomy, University of Uppsala, Uppsala, Sweden. [89]LPMR, Faculté des Sciences, Université Mohamed Premier, Oujda, Morocco. [90]Faculty of Mathematics, Physics and Informatics, Comenius University, Bratislava, Slovak Republic. [91]Department of Physics, University of Cape Town, Cape Town, South Africa. [92]L2IT, Université de Toulouse, CNRS/IN2P3, UPS, Toulouse, France. [93]Department of Physics, University of Illinois, Urbana, IL, United States of America. [94]Institute of Frontier and Interdisciplinary Science and Key Laboratory of Particle Physics and Particle Irradiation (MOE), Shandong University, Qingdao, China. [95]Fakultät für Mathematik und Naturwissenschaften, Fachgruppe Physik, Bergische Universität Wuppertal, Wuppertal, Germany. [96]Department of Physics, Nanjing University, Nanjing, China. [97]Department of Physics, Aristotle University of Thessaloniki, Thessaloniki, Greece. [98]Department of Physics, Carleton University, Ottawa, ON, Canada. [99]Department of Physics, Yale University, New Haven, CT, United States of America. [100]Institute of Physics, University of Belgrade, Belgrade, Serbia. [101]Department of Physics, University of Texas at Arlington, Arlington, TX, United States of America. [102]School of Physics, University of Sydney, Sydney, Australia. [103]Charles University, Faculty of Mathematics and Physics, Prague, Czech Republic. [104]Kirchhoff-Institut für Physik, Ruprecht-Karls-Universität Heidelberg, Heidelberg, Germany. [105]Cavendish Laboratory, University of Cambridge, Cambridge, United Kingdom. [106]Institute of Nuclear Physics Polish Academy of Sciences, Krakow, Poland. [107]Department of Physics and Astronomy, University of Pittsburgh, Pittsburgh, PA, United States of America. [108]Physikalisches Institut, Universität Bonn, Bonn, Germany. [109]School of Physics, University of Melbourne, Victoria, Australia. [110]Dipartimento di Fisica, Università di Genova, Genova, Italy. [111]INFN Sezione di Genova, Genova, Italy. [112]Department of Physics and Astronomy, University College London, London, United Kingdom. [113]Max-Planck-Institut für Physik (Werner-Heisenberg-Institut), München, Germany. [114]Institute for Fundamental Science, University of Oregon, Eugene, OR, United States of America. [115]SLAC National Accelerator Laboratory, Stanford, CA, United States of America. [116]Palacký University, Joint Laboratory of Optics, Olomouc, Czech Republic. [117]School of Physics and Astronomy, University of Manchester, Manchester, United Kingdom. [118]Department of Modern Physics and State Key Laboratory of Particle Detection and Electronics, University of Science and Technology of China, Hefei, China. [119]Department of Physics, Oxford University, Oxford, United Kingdom. [120]Institute of High Energy Physics, Chinese Academy of Sciences, Beijing, China. [121]Physics Department, Tsinghua University, Beijing, China. [122]University of Chinese Academy of Science (UCAS), Beijing, China. [123]Physics Department, Lancaster University, Lancaster, United Kingdom. [124]Fakultät Physik, Technische Universität Dortmund, Dortmund, Germany. [125]INFN Sezione di Roma Tre, Roma, Italy. [126]Dipartimento di Matematica e Fisica, Università Roma Tre, Roma, Italy. [127]IJCLab, Université Paris-Saclay, CNRS/IN2P3, 91405, Orsay, France. [128]SUPA - School of Physics and Astronomy, University of Glasgow, Glasgow, United Kingdom. [129]Department Physik, Universität Siegen, Siegen, Germany. [130]Department of Physics, Bogazici University, Istanbul, Turkey. [131]LPNHE, Sorbonne Université, Université Paris Cité, CNRS/IN2P3, Paris, France. [132]Department of Physics and Astronomy, Tufts University, Medford, MA, United States of America. [133]Department of Physics, University of Warwick, Coventry, United Kingdom. [134]Istinye University, Sariyer, Istanbul, Turkey. [135]Departments of Physics and Astronomy, Stony Brook University, Stony Brook, NY, United States of America. [136]Rio de Janeiro State University, Rio de Janeiro, Brazil. [137]Technical University of Munich, Munich, Germany. [138]United Arab Emirates University, Al Ain, United Arab Emirates. [139]Faculté des Sciences Ain Chock, Réseau Universitaire de Physique des Hautes Energies - Université Hassan II, Casablanca, Morocco. [140]Department of Physics, University of Arizona, Tucson, AZ, United States of America. [141]APC, Université Paris Cité, CNRS/IN2P3, Paris, France. [142]Institut für Kern- und Teilchenphysik, Technische Universität Dresden, Dresden, Germany. [143]School of Physics and Astronomy, Queen Mary University of London, London, United Kingdom. [144]Department of Mechanical Engineering Science, University of Johannesburg, Johannesburg, South Africa. [145]Fakultät für Physik und Astronomie, Julius-Maximilians-Universität Würzburg, Würzburg, Germany. [146]High Energy Physics Division, Argonne National Laboratory, Argonne, IL, United States of America. [147]Department of Physics Engineering, Gaziantep University, Gaziantep, Türkiye. [148]Dipartimento di Fisica e Astronomia A. Righi, Università di Bologna, Bologna, Italy. [149]Department of Physics, University of Wisconsin, Madison, WI, United States of America. [150]LPC, Université Clermont Auvergne, CNRS/IN2P3, Clermont-Ferrand, France. [151]Ohio State University, Columbus, OH, United States of America. [152]School of Physics and Astronomy, Shanghai Jiao Tong University, Key Laboratory for Particle Astrophysics and Cosmology (MOE), SKLPPC, Shanghai, China. [153]Tsung-Dao Lee Institute, Shanghai, China. [154]Departamento de Física, Universidad Técnica Federico Santa María, Valparaíso, Chile. [155]Department of Subnuclear Physics, Institute of Experimental Physics of the Slovak Academy of Sciences, Kosice, Slovak Republic. [156]Department for Physics and Technology, University of Bergen, Bergen, Norway. [157]Department of Physics, Simon Fraser University, Burnaby, BC, Canada. [158]Department of Physics, Boston University, Boston, MA, United States of America. [159]Department of Physics and Astronomy, Michigan State University, East Lansing, MI, United States of America. [160]II. Physikalisches Institut, Justus-Liebig-Universität Giessen, Giessen, Germany. [161]Department of Physics, Ankara University, Ankara, Turkey. [162]Department of Physics, Indiana University, Bloomington, IN, United States of America. [163]Dipartimento di Fisica E. Fermi, Università di Pisa, Pisa, Italy. [164]Niels Bohr Institute, University of Copenhagen, Copenhagen, Denmark. [165]University of Iowa, Iowa City, IA, United States of America. [166]Dipartimento di Fisica, Università della Calabria, Rende, Italy. [167]INFN Gruppo Collegato di Cosenza, Laboratori Nazionali di Frascati, Frascati, Italy. [168]TRIUMF, Vancouver, BC, Canada. [169]Institute for Mathematics, Astrophysics and Particle Physics, Radboud University/Nikhef, Nijmegen, Netherlands. [170]School of Physics, University of the Witwatersrand, Johannesburg, South Africa. [171]Departamento de Física, Universidade do Minho, Braga, Portugal. [172]INFN Sezione di Lecce, Lecce, Italy. [173]Dipartimento di Matematica e Fisica, Università del Salento, Lecce, Italy. [174]High Energy Physics Institute, Tbilisi State University, Tbilisi, Georgia. [175]Department of Physics, Stanford University, Stanford CA, United States of America. [176]Department of Physics, Chinese University of Hong Kong, Shatin, N.T., Hong Kong, China. [177]Department of Physics, National Tsing Hua University, Hsinchu, Taiwan. [178]Institute of Physics of the Czech Academy of Sciences, Prague, Czech Republic. [179]Department of Experimental Particle Physics, Jožef Stefan Institute and Department of Physics, University of Ljubljana, Ljubljana, Slovenia. [180]Dipartimento Politecnico di Ingegneria e Architettura, Università di Udine, Udine, Italy. [181]LPSC, Université Grenoble Alpes, CNRS/IN2P3, Grenoble INP, Grenoble, France. [182]Instituto Superior Técnico, Universidade de Lisboa, Lisboa, Portugal. [183]Department of Physics, University of British Columbia, Vancouver, BC, Canada. [184]INFN-TIFPA, Povo, Italy. [185]Università degli Studi di Trento, Trento, Italy. [186]Department of Physics and Astronomy, University of California Irvine, Irvine, CA, United States of America. [187]Physikalisches Institut, Ruprecht-Karls-Universität Heidelberg, Heidelberg, Germany. [188]Department of Physics, University of Pennsylvania, Philadelphia, PA, United States of America. [189]Universidad de Buenos Aires, Facultad de Ciencias Exactas y Naturales, Departamento de Física, y CONICET, Instituto de Física de Buenos Aires (IFIBA), Buenos Aires, Argentina. [190]Department of Physics and Astronomy, York University, Toronto, ON, Canada. [191]Physics Department, Southern Methodist University, Dallas, TX, United States of America. [192]Millennium Institute for Subatomic physics at high energy frontier (SAPHIR), Santiago, Chile. [193]Instituto de Física, Universidade de São Paulo, São Paulo, Brazil. [194]Faculté des Sciences, Université Ibn-Tofail, Kénitra, Morocco. [196]National Centre for Scientific Research "Demokritos", Agia Paraskevi, Greece. [197]Physics Department, University of Texas at Dallas, Richardson, TX, United States of America. [198]Department of Physics, University of Adelaide, Adelaide, Australia. [199]Departamento de Física, Universidade de Coimbra, Coimbra, Portugal. [200]National Institute of Physics, University of the Philippines, Diliman (Philippines), Diliman, Philippines. [203]Enrico Fermi Institute, University of Chicago, Chicago, IL, United States of America. [204]Marian Smoluchowski Institute of Physics, Jagiellonian University, Krakow, Poland. [205]Department of Physics, University of Alberta, Edmonton, AB, Canada. [206]Departamento de Física, Faculdade de Ciências, Universidade de Lisboa, Lisboa, Portugal. [207]West University in Timisoara, Timisoara, Romania. [209]California State University, Long Beach, CA, United States of America. [210]Department of Physics and Astronomy, University of New Mexico, Albuquerque, NM, United States of America. [211]Division of Physics and Tomonaga Center for the History of the Universe, Faculty of Pure and Applied Sciences, University of Tsukuba, Tsukuba, Japan. [212]Department of Physics, Shinshu University, Nagano, Japan. [213]Department of Physics, Tokyo Institute of Technology, Tokyo, Japan. [214]Department of Physics and Astronomy, Iowa State University, Ames IA, United States of America. [215]Graduate School of Science, Kobe University, Kobe, Japan. [216]Graduate School of Science, Osaka University, Osaka, Japan. [217]University Politehnica Bucharest, Bucharest, Romania. [218]Department of Physics, University of Hong Kong, Hong Kong, China. [219]Institute of Physics, Azerbaijan Academy of Sciences, Baku, Azerbaijan. [220]Waseda University, Tokyo, Japan. [221]E. Andronikashvili Institute of Physics, Iv. Javakhishvili Tbilisi State University, Tbilisi, Georgia. [222]Instituto de Alta Investigación, Universidad de Tarapacá, Arica, Chile. [223]Research Center for Advanced Particle Physics and Department of Physics, Kyushu University, Fukuoka, Japan. [224]Universität Innsbruck, Department of Astro and Particle Physics, Innsbruck, Austria. [225]Faculty of Science, Kyoto University, Kyoto, Japan. [226]Universidad Andres Bello, Department of Physics, Santiago, Chile. [227]Department of Physics, Royal Institute of Technology, Stockholm, Sweden. [228]Department of Physics and Institute for Advanced Study, Hong Kong University of Science

and Technology, Clear Water Bay, Kowloon, Hong Kong, China. [229]Centro de Física Nuclear da Universidade de Lisboa, Lisboa, Portugal. [230]Facultad de Ciencias y Centro de Investigaciónes, Universidad Antonio Nariño, Bogotá, Colombia. [231]Transilvania University of Brasov, Brasov, Romania. [232]National Institute for Research and Development of Isotopic and Molecular Technologies, Physics Department, Cluj-Napoca, Romania. [233]Departamento de Física, Universidad Nacional de Colombia, Bogotá, Colombia. [234]Louisiana Tech University, Ruston, LA, United States of America. [235]University of Sharjah, Sharjah, United Arab Emirates. [236]Division of Physics, TOBB University of Economics and Technology, Ankara, Turkey. [237]Kyoto University of Education, Kyoto, Japan. [238]Instituto de Investigación Multidisciplinario en Ciencia y Tecnología, y Departamento de Física, Universidad de La Serena, La Serena, Chile. [239]Affiliated with an institute covered by a cooperation agreement with CERN, Geneva, Switzerland. [240]Borough of Manhattan Community College, City University of New York, New York, NY, United States of America. [241]Bruno Kessler Foundation, Trento, Italy. [242]Center for High Energy Physics, Peking University, Beijing, China. [243]Centro Studi e Ricerche Enrico Fermi, Roma, Italy. [244]CERN, Geneva, Switzerland. [245]Département de Physique Nucléaire et Corpusculaire, Université de Genève, Genève, Switzerland. [246]Departament de Fisica de la Universitat Autonoma de Barcelona, Barcelona, Spain. [247]Department of Financial and Management Engineering, University of the Aegean, Chios, Greece. [248]Department of Physics and Astronomy, Michigan State University, East Lansing MI, United States of America. [249]Department of Physics and Astronomy, University of Louisville, Louisville, KY, United States of America. [250]Department of Physics, Ben Gurion University of the Negev, Beer Sheva, Israel. [251]Department of Physics, California State University, East Bay, United States of America. [252]Department of Physics, California State University, Sacramento, United States of America. [253]Department of Physics, King's College London, London, United Kingdom. [254]Department of Physics, University of Fribourg, Fribourg, Switzerland. [255]Department of Physics, University of Thessaly, Thessaly, Greece. [256]Department of Physics, Westmont College, Santa Barbara, United States of America. [257]Hellenic Open University, Patras, Greece. [258]Institucio Catalana de Recerca i Estudis Avancats, ICREA, Barcelona, Spain. [259]Institut für Experimentalphysik, Universität Hamburg, Hamburg, Germany. [260]Institute of Particle Physics (IPP), Ottawa, Canada. [261]Institute of Physics, Azerbaijan Academy of Sciences, Baku, Azerbaijan. [262]Institute of Theoretical Physics, Ilia State University, Tbilisi, Georgia. [263]Lawrence Livermore National Laboratory, Livermore, United States of America. [264]The City College of New York, New York, NY, United States of America. [265]The Collaborative Innovation Center of Quantum Matter (CICQM), Beijing, China. [266]TRIUMF, Vancouver, BC, Canada. [267]Università di Napoli Parthenope, Napoli, Italy. [268]University of Chinese Academy of Sciences (UCAS), Beijing, China. [269]University of Colorado Boulder, Department of Physics, Colorado, United States of America. [270]Yeditepe University, Physics Department, Istanbul, Turkey. [271]Deceased: D. Bruncko. [272]Deceased: I. A. Budagov. [273]Deceased: E. Fullana Torregrosa. [274]Deceased: V. Gratchev. [275]Deceased: J. Olszowska. [276]Deceased: L. Perini. [277]Deceased: S. Yu. Sivoklokov.

Methods

Experimental set-up

The ATLAS detector[12] consists of an inner tracking detector surrounded by a thin superconducting solenoid, electromagnetic and hadron calorimeters, and a muon spectrometer incorporating three large superconducting air-core toroidal magnets.

ATLAS uses a right-handed coordinate system with its origin at the nominal interaction point in the centre of the detector and the z axis along the beam pipe. The x axis points from the interaction point to the centre of the LHC ring, and the y axis points upwards. Cylindrical coordinates (r, ϕ) are used in the transverse plane, ϕ being the azimuthal angle around the z axis. The pseudorapidity is defined in terms of the polar angle θ as $\eta = -\ln(\tan(\theta/2))$.

The inner-detector (ID) system is immersed in a 2-T axial magnetic field and provides charged-particle tracking in the range $|\eta| < 2.5$. The high-granularity silicon pixel detector covers the vertex region and typically provides four measurements per track, the first hit normally being in the insertable B-layer (IBL) installed before Run 2[60,61]. It is followed by the silicon microstrip tracker (SCT), which usually provides eight measurements per track. These silicon detectors are complemented by the transition radiation tracker (TRT), which enables radially extended track reconstruction up to $|\eta| < 2.0$. The TRT also provides electron identification information based on the fraction of hits (typically 30 in total) above a higher energy-deposit threshold corresponding to transition radiation.

The calorimeter system covers the pseudorapidity range $|\eta| < 4.9$. Within the region $|\eta| < 3.2$, electromagnetic calorimetry is provided by barrel and endcap high-granularity lead/liquid-argon (LAr) calorimeters, with an additional thin LAr presampler covering $|\eta| < 1.8$ to correct for energy loss in material upstream of the calorimeters. Hadron calorimetry is provided by the steel/scintillator-tile calorimeter, segmented into three barrel structures within $|\eta| < 1.7$, and two copper/LAr hadron endcap calorimeters. The solid angle coverage is completed with forward copper/LAr and tungsten/LAr calorimeter modules optimized for electromagnetic and hadronic energy measurements, respectively.

The muon spectrometer (MS) comprises separate trigger and high-precision tracking chambers measuring the deflection of muons in a magnetic field generated by the superconducting air-core toroidal magnets. The field integral of the toroids ranges between 2.0 and 6.0 Tm across most of the detector. Three layers of precision chambers, each consisting of layers of monitored drift tubes, covers the region $|\eta| < 2.7$, complemented by cathode-strip chambers in the forward region, where the background is highest. The muon trigger system covers the range $|\eta| < 2.4$ with resistive-plate chambers in the barrel, and thin-gap chambers in the endcap regions.

The performance of the vertex and track reconstruction in the inner detector, the calorimeter resolution in electromagnetic and hadronic calorimeters and the muon momentum resolution provided by the muon spectrometer are given previously[12].

Interesting events are selected by the first-level trigger system implemented in custom hardware, followed by selections made by algorithms implemented in software in the high-level trigger[62]. The first-level trigger accepts events from the 40-MHz bunch crossings at a rate below 100 kHz, which the high-level trigger further reduces in order to record events to disk at about 1 kHz.

Statistical framework

The results of the combination presented in this paper are obtained from a likelihood function defined as the product of the likelihoods of each input measurement. The observed yield in each category of reconstructed events follows a Poisson distribution the parameter of which is the sum of the expected signal and background contributions. The number of signal events in any category k is split into the different production and decay modes:

$$n_k^{\text{signal}} = \mathcal{L}_k \sum_i \sum_f (\sigma_i B_f)(A\epsilon)_{if}^k,$$

where the sum indexed by i runs either over the production processes (ggF, VBF, WH, ZH, $t\bar{t}H$, tH) or over the set of the measured production kinematic regions, and the sum indexed by f runs over the decay final states (ZZ, WW, $\gamma\gamma$, $Z\gamma$, $b\bar{b}$, $c\bar{c}$, $\tau^+\tau^-$, $\mu^+\mu^-$). The quantity $\mathcal{L}_k$ is the integrated luminosity of the dataset used in category k, and $(A\epsilon)_{if}^k$ is the acceptance times selection efficiency factor for production process i and decay mode f in category k. Acceptances and efficiencies are obtained from the simulation (corrected by calibration measurements in control data for the efficiencies). Their values are subject to variations due to experimental and theoretical systematic uncertainties. The cross-sections σ_i and branching fractions B_f are the parameters of interest of the model. Depending on the model being tested, they are either free parameters, set to their standard model prediction or parameterized as functions of other parameters. All cross-sections are defined in the Higgs boson rapidity range $|y_H| < 2.5$, which is related to the polar angle of the Higgs boson's momentum in the detector and corresponds approximately to the region of experimental sensitivity.

The impact of experimental and theoretical systematic uncertainties on the predicted signal and background yields is taken into account by nuisance parameters included in the likelihood function. The predicted signal yields from each production process, the branching fractions and the signal acceptance in each analysis category are affected by theory uncertainties. The combined likelihood function is therefore expressed as:

$$L(\boldsymbol{\alpha}, \boldsymbol{\theta}, \text{data}) = \prod_{k \in \text{cat}} \prod_{b \in \text{bins}} P(n_{k,b} | n_{k,b}^{\text{signal}}(\boldsymbol{\alpha}, \boldsymbol{\theta}) + n_{k,b}^{\text{bkg}}(\boldsymbol{\theta})) \prod_{\theta \in \boldsymbol{\theta}} G(\theta),$$

where $n_{k,b}$, $n_{k,b}^{\text{signal}}$ and $n_{k,b}^{\text{bkg}}$ stand for the number of observed events, the number of expected signal events and the number of expected background events in bin b of analysis category k, respectively. The parameters of interest are noted $\boldsymbol{\alpha}$, the nuisance parameters are $\boldsymbol{\theta}$, P represents the Poisson distribution, and G stands for Gaussian constraint terms assigned to the nuisance parameters. Some nuisance parameters are meant to be determined by data alone and do not have any associated constraint term. This is, for instance, the case for background normalization factors that are fitted in control categories. The effects of nuisance parameters affecting the normalizations of signal and backgrounds in a given category are generally implemented using the multiplicative expression:

$$n(\theta) = n^0(1+\sigma)^\theta,$$

where n^0 is the nominal expected yield of either signal or background and σ the value of the uncertainty. This ensures that $n(\theta) > 0$ even for negative values of θ. For the majority of nuisance parameters, including all those affecting the shapes of the distributions, a linear expression is used instead on each bin of the distributions:

$$n(\theta) = n^0(1+\sigma\theta).$$

The systematic uncertainties are broken down into independent underlying sources, so that when a source affects multiple or all analyses the associated nuisance parameter can be fully correlated across the terms in the likelihood corresponding to these analyses by using common nuisance parameters. This is the case of systematic uncertainties in the luminosity measurement[63], in the reconstruction and selection efficiencies[64–70] and in the calibrations of the energy measurements[71–74]. Their effects are propagated coherently by using common nuisance parameters whenever applicable. Only a few components of the systematic uncertainties are correlated between the analyses performed

using the full Run 2 data and those using only the 2015 and 2016 data, owing to differences in their assessment, in the reconstruction algorithms and in software releases. Systematic uncertainties associated with the modelling of background processes, as well as uncertainties due to the limited number of simulated events used to estimate the expected signal and background yields, are treated as being uncorrelated between analyses.

Uncertainties in the parton distribution functions are implemented coherently in all input measurements and all analysis categories[75]. Uncertainties in modelling the parton showering into jets of particles affect the signal acceptances and efficiencies, and are common to all input measurements within a given production process. Similarly, uncertainties due to missing higher-order quantum chromodynamics (QCD) corrections are common to a given production process. Their implementation in the kinematic regions of the simplified template cross-sections framework results in a total of 66 uncertainty sources, where overall acceptance effects are separated from migrations between the various bins (for example, between jet multiplicity regions or between dijet invariant mass regions)[76]. Both the acceptance and signal yield uncertainties affect the signal strength modifier and coupling strength modifier results, which rely on comparisons of measured and expected yields. Only acceptance uncertainties affect the cross-section and branching fraction results. The uncertainties in the Higgs boson branching fractions due to dependencies on standard model parameter values (such as b and c quark masses) and missing higher-order effects are implemented using the correlation model described previously[44].

In total, over 2,600 sources of systematic uncertainty are included in the combined likelihood. For most of the presented measurements, the systematic uncertainty is expected to be of similar size or somewhat smaller than the corresponding statistical uncertainty. The systematic uncertainties are dominant for the parameters that are measured the most precisely, that is, the global signal strength and the production cross-sections for the ggF and VBF processes. The expected systematic uncertainty of the global signal strength measurement (about 5%) is larger than the statistical uncertainty (3%), with similar contributions from the theory uncertainties in signal (4%) and background modelling (1.7%), and from the experimental systematic uncertainty (3%). The latter is predominantly composed of the uncertainty in the luminosity measurement (1.7%), followed by the uncertainties in electron, jet and b-jet reconstruction, data-driven background modelling, as well as from the limited number of simulated events (about 1% each). All other sources of experimental uncertainty combined contribute an additional 1%. The systematic uncertainty in the production cross-section of the ggF process is dominated by experimental uncertainties (3.5%) followed by signal theory uncertainties (3%), compared to a statistical uncertainty of 4%. For the VBF process, where the statistical uncertainty is 8%, the experimental uncertainties are estimated to be 5%, and the signal theory uncertainties add up to 7%. Systematic uncertainties are also dominant over the statistical uncertainties in the measurements of the branching fractions into W pairs and τ lepton pairs.

Measurements of the parameters of interest use a statistical test based on the profile likelihood ratio[52]:

$$\Lambda(\boldsymbol{\alpha}) = \frac{L(\boldsymbol{\alpha}, \hat{\hat{\boldsymbol{\theta}}}(\boldsymbol{\alpha}))}{L(\hat{\boldsymbol{\alpha}}, \hat{\boldsymbol{\theta}})},$$

where $\boldsymbol{\alpha}$ are the parameters of interest and $\boldsymbol{\theta}$ are the nuisance parameters. The $\hat{\hat{\boldsymbol{\theta}}}(\boldsymbol{\alpha})$ notation indicates that the nuisance parameters values are those that maximize the likelihood for given values of the parameters of interest. In the denominator, both the parameters of interest and the nuisance parameters are set to the values $(\hat{\boldsymbol{\alpha}}, \hat{\boldsymbol{\theta}})$ that unconditionally maximize the likelihood. The estimates of the parameters $\boldsymbol{\alpha}$ are these values $\hat{\boldsymbol{\alpha}}$ that maximize the likelihood ratio.

Owing to the usually large number of events selected in the measurements, all results presented in this paper are obtained in the asymptotic regime where the likelihood approximately follows a Gaussian distribution. It was checked in previous iterations of the individual input measurements, for instance ref. [77], that this assumption also holds in cases with low event counts by comparing the results of the asymptotic formulae with those of pseudo-experiments. This confirmed the results from a previous work[52] that the Gaussian approximation becomes valid for as few as ≥5 background events. In the asymptotic regime twice the negative logarithm of the profile likelihood $\lambda(\boldsymbol{\alpha}) = -2\ln(\Lambda(\boldsymbol{\alpha}))$ follows a χ^2 distribution with a number of degrees of freedom equal to the number of parameters of interest. Confidence intervals for a given confidence level (CL), usually 68%, are then defined as the regions fulfilling $\lambda(\boldsymbol{\alpha}) < F_n^{-1}(\mathrm{CL})$ where F_n^{-1} is the quantile function of the χ^2 distribution with n degrees of freedom, so $F_1^{-1} = 1\,(4)$ for a $1\sigma\,(2\sigma)$ CL with one degree of freedom. The values of the parameters $\boldsymbol{\alpha}$ corresponding to these confidence intervals are obtained by scanning the profile likelihood. Similarly, the p value $p_{\mathrm{SM}} = 1 - F_n(\lambda(\boldsymbol{\alpha}_{\mathrm{SM}}))$ is used to test the compatibility of the measurement and the standard model prediction. The correlations between the parameters are estimated by inverting the matrix of the second derivatives of the likelihood.

The expected significances and limits are determined using the 'Asimov' datasets[52], which are obtained by setting the observed yields to their expected values when the nuisance parameters are set to the values that maximize the likelihood $\hat{\theta}$.

Parameterization within the κ framework

Within the κ framework, the cross-section for an individual measurement is parameterized as

$$\sigma(i \to H \to f) = \sigma_i B_f = \frac{\sigma_i(\boldsymbol{\kappa})\Gamma_f(\boldsymbol{\kappa})}{\Gamma_H(\boldsymbol{\kappa}, B_{\mathrm{inv.}}, B_{\mathrm{u.}})},$$

where Γ_f is the partial width for a Higgs boson decay to the final state f and Γ_H is the total decay width of the Higgs boson. The total width is given by the sum of the partial widths of all the decay modes included. Contributions to the total Higgs boson decay width owing to phenomena beyond the standard model may manifest themselves as a value of coupling strength modifier κ_p differing from one, or a value of $B_{\mathrm{inv.}}$ or $B_{\mathrm{u.}}$ differing from zero. The Higgs boson total width is then expressed as $\Gamma_H(\boldsymbol{\kappa}, B_{\mathrm{inv.}}, B_{\mathrm{u.}}) = \kappa_H^2(\boldsymbol{\kappa}, B_{\mathrm{inv.}}, B_{\mathrm{u.}})\Gamma_H^{\mathrm{SM}}$ with

$$\kappa_H^2(\boldsymbol{\kappa}, B_{\mathrm{inv.}}, B_{\mathrm{u.}}) = \frac{\sum_p B_p^{\mathrm{SM}}\kappa_p^2}{(1 - B_{\mathrm{inv.}} - B_{\mathrm{u.}})}.$$

Higgs boson production cross-sections and partial and total decay widths are parameterized in terms of the coupling strength modifiers as shown in table 9 of ref. [22]. An improved parameterization including additional sub-leading contributions is used in this paper to match the increased precision of the measurements.

Kinematic regions probing Higgs boson production

The definitions of kinematic regions for the precision study of Higgs boson production in the framework of simplified template cross-sections[44,56–58] are based on the predicted properties of particles generated in a given production process. The partitioning follows the so-called Stage-1.2 scheme, which features a slightly finer granularity than the Stage-1.1 scheme[57] and introduces the Higgs boson transverse momentum categories for the $t\bar{t}H$ production process. Higgs bosons are required to be produced with rapidity $|y_H| < 2.5$. Associated jets of particles are constructed from all stable particles with a lifetime greater than 10 ps, excluding the decay products of the Higgs boson and leptons from W and Z boson decays, using the anti-k_t algorithm[78] with a jet radius parameter $R = 0.4$, and must have a transverse momentum $p_{\mathrm{T,jet}} > 30$ GeV. Standard model predictions are assumed for the kinematic properties of Higgs boson decays. Phenomena beyond the

standard model can substantially modify these properties, and thus the acceptance of the signal, especially for the WW or ZZ decay modes, and this should be considered when using these measurements for the relevant interpretations.

Higgs boson production is first classified according to the nature of the initial state and the associated particles, the latter including the decay products of W and Z bosons if they are present. These classes are: $t\bar{t}H$ and tH processes; $qq' \to Hqq'$ processes, with contributions from both VBF and quark-initiated VH (where $V = W, Z$) production with a hadronic decay of the vector boson; $pp \to VH$ production with a leptonic decay of the vector boson ($V(\ell\ell, \ell\nu)H$), including $gg \to ZH \to \ell\ell H$ production; and finally the ggF process combined with $gg \to ZH \to q\bar{q}H$ production to form a single $gg \to H$ process. The contribution of the $b\bar{b}H$ production process is taken into account as a 1%[44] increase of the $gg \to H$ yield in each kinematic region, because the acceptances for both processes are similar for all input analyses[44].

The input measurements in individual decay modes provide only limited sensitivity to the cross-section in some of the regions of the Stage-1.2 scheme, mainly because of the small number of events in some of these regions. In other cases, they only provide sensitivity to a combination of these regions, leading to strongly correlated measurements. To mitigate these effects, some of the Stage-1.2 kinematic regions were merged for the combined measurement.

Compared to individual input measurements, systematic theory uncertainties associated with the signal predictions have been updated for the combination to closely follow the granularity of the Stage-1.2 scheme. The QCD scale uncertainties in ggF production were updated for all input channels that are sensitive to this production process. Out of 18 uncertainty sources in total, two account for overall fixed-order and resummation effects, two cover the migrations between different jet multiplicity bins, seven are associated with the modelling of the Higgs boson transverse momentum (p_{T}^{H}) in different phase-space regions, four account for the uncertainty in the distribution of the dijet invariant mass (m_{jj}) variable, one covers the modelling of the Higgs boson plus two leading jets transverse momentum (p_{T}^{Hjj}) distribution in the ≥2-jet region, one pertains to modelling of the distribution of the Higgs boson plus one jet transverse momentum (p_{T}^{Hj}) divided by p_{T}^{H} in the high-p_{T}^{H} region, and finally, the last takes into account the uncertainty from the choice of top quark mass scheme. Theory uncertainties for the $qq' \to Hqq'$ and $t\bar{t}H$ processes are defined previously[28], and those of the $V(\ell\ell, \ell\nu)H$ kinematic region follow the scheme described in an earlier work[76]. For the kinematic regions defined by the merging of several Stage-1.2 regions, the signal acceptance factors are determined assuming that the relative fractions in each Stage-1.2 region are given by their standard model values, and the uncertainties predicted by the standard model in these fractions are taken into account.

Data availability

The experimental data that support the findings of this study are available in HEPData with the identifier https://doi.org/10.17182/hepdata.130266.

Code availability

The ATLAS data reduction software is available at the following link: https://zenodo.org/record/4772550. Statistical modelling and analysis is based on the ROOT software and its embedded RooFit and RooStats modules, available at https://zenodo.org/record/3895852. Code to configure these statistical tools and to process their output is available upon request.

60. ATLAS Collaboration. *ATLAS Insertable B-Layer: Technical Design Report* Report No. CERN-LHCC-2010-013 (CERN, 2010); https://cds.cern.ch/record/1291633
61. Abbott, B. et al. Production and integration of the ATLAS Insertable B-Layer. *J. Instrum.* **13**, T05008 (2018).
62. ATLAS Collaboration. Performance of the ATLAS trigger system in 2015. *Eur. Phys. J. C* **77**, 317 (2017).
63. ATLAS Collaboration. *Luminosity Determination in pp Collisions at √s = 13 TeV using the ATLAS Detector at the LHC* Report No. ATLAS-CONF-2019-021 (CERN, 2019); https://cds.cern.ch/record/2677054
64. ATLAS Collaboration. Electron reconstruction and identification in the ATLAS experiment using the 2015 and 2016 LHC proton–proton collision data at √s = 13 TeV. *Eur. Phys. J. C* **79**, 639 (2019).
65. ATLAS Collaboration. Performance of electron and photon triggers in ATLAS during LHC Run 2. *Eur. Phys. J. C* **80**, 47 (2020).
66. ATLAS Collaboration. Muon reconstruction and identification efficiency in ATLAS using the full Run 2 pp collision data set at √s = 13 TeV. *Eur. Phys. J. C* **81**, 578 (2021).
67. ATLAS Collaboration. *Measurement of the Tau Lepton Reconstruction and Identification Performance in the ATLAS Experiment using pp Collisions at √s = 13 TeV* Report No. ATLAS-CONF-2017-029 (CERN, 2017); https://cds.cern.ch/record/2261772
68. ATLAS Collaboration. ATLAS b-jet identification performance and efficiency measurement with $t\bar{t}$ events in pp collisions at √s = 13 TeV. *Eur. Phys. J. C* **79**, 970 (2019).
69. ATLAS Collaboration. Measurement of the c-jet mistagging efficiency in $t\bar{t}$ events using *pp* collision data at √s = 13 TeV collected with the ATLAS detector. *Eur. Phys. J. C* **82**, 95 (2022).
70. ATLAS Collaboration. Configuration and performance of the ATLAS b-jet triggers in Run 2. *Eur. Phys. J. C* **81**, 1087 (2021).
71. ATLAS Collaboration. Electron and photon performance measurements with the ATLAS detector using the 2015–2017 LHC proton–proton collision data. *J. Instrum.* **14**, P12006 (2019).
72. ATLAS Collaboration. Jet energy scale and resolution measured in proton–proton collisions at √s = 13 TeV with the ATLAS detector. *Eur. Phys. J. C* **81**, 689 (2020).
73. ATLAS Collaboration. Optimisation of large-radius jet reconstruction for the ATLAS detector in 13 TeV proton–proton collisions. *Eur. Phys. J. C* **81**, 334 (2020).
74. ATLAS Collaboration. Performance of missing transverse momentum reconstruction with the ATLAS detector using proton–proton collisions at √s = 13 TeV. *Eur. Phys. J. C* **78**, 903 (2018).
75. Butterworth, J. et al. PDF4LHC recommendations for LHC Run II. *J. Phys. G* **43**, 023001 (2016).
76. ATLAS Collaboration. *Evaluation of Theoretical Uncertainties for Simplified Template Cross Section Measurements of V-Associated Production of the Higgs Boson* Report No. ATL-PHYS-PUB-2018-035 (CERN, 2018); https://cds.cern.ch/record/2649241
77. ATLAS Collaboration. Search for the Standard Model Higgs boson in the two photon decay channel with the ATLAS detector at the LHC. *Phys. Lett. B* **705**, 452–470 (2011).
78. Cacciari, M., Salam, G. P. & Soyez, G. The anti-k_t jet clustering algorithm. *J. High Energy Phys.* **2008-04**, 063 (2008).
79. ATLAS Collaboration. *ATLAS Computing Acknowledgements* (CERN 2021); https://cds.cern.ch/record/2776662.

Acknowledgements We thank CERN for the very successful operation of the LHC, as well as the support staff from our institutions without whom ATLAS could not be operated efficiently. We acknowledge the support of ANPCyT, Argentina; YerPhI, Armenia; ARC, Australia; BMWFW and FWF, Austria; ANAS, Azerbaijan; CNPq and FAPESP, Brazil; NSERC, NRC and CFI, Canada; CERN; ANID, Chile; CAS, MOST and NSFC, China; Minciencias, Colombia; MEYS CR, Czech Republic; DNRF and DNSRC, Denmark; IN2P3-CNRS and CEA-DRF/IRFU, France; SRNSFG, Georgia; BMBF, HGF and MPG, Germany; GSRI, Greece; RGC and Hong Kong SAR, China; ISF and Benoziyo Center, Israel; INFN, Italy; MEXT and JSPS, Japan; CNRST, Morocco; NWO, Netherlands; RCN, Norway; MEiN, Poland; FCT, Portugal; MNE/IFA, Romania; MESTD, Serbia; MSSR, Slovakia; ARRS and MIZS, Slovenia; DSI/NRF, South Africa; MICINN, Spain; SRC and Wallenberg Foundation, Sweden; SERI, SNSF and Cantons of Bern and Geneva, Switzerland; MOST, Taiwan; TENMAK, Türkiye; STFC, United Kingdom; DOE and NSF, United States of America. In addition, individual groups and members have received support from BCKDF, CANARIE, Compute Canada and CRC, Canada; PRIMUS 21/SCI/017 and UNCE SCI/013, Czech Republic; COST, ERC, ERDF, Horizon 2020 and Marie Sklodowska-Curie Actions, European Union; Investissements d'Avenir Labex, Investissements d'Avenir Idex and ANR, France; DFG and AvH Foundation, Germany; Herakleitos, Thales and Aristeia programmes co-financed by EUESF and the Greek NSRF, Greece; BSF-NSF and MINERVA, Israel; Norwegian Financial Mechanism 2014-2021, Norway; NCN and NAWA, Poland; La CaixaBanking Foundation, CERCA Programme Generalitat de Catalunya and PROMETEO and GenT Programmes Generalitat Valenciana, Spain; Göran Gustafssons Stiftelse, Sweden; The Royal Society and Leverhulme Trust, United Kingdom. The crucial computing support from all WLCG partners is acknowledged gratefully, in particular from CERN, the ATLAS Tier-1 facilities at TRIUMF (Canada), NDGF (Denmark, Norway, Sweden), CC-IN2P3 (France), KIT/GridKA (Germany), INFN-CNAF (Italy), NL-T1 (Netherlands), PIC (Spain), ASGC (Taiwan), RAL (UK) and BNL (USA), the Tier-2 facilities worldwide and large non-WLCG resource providers. Major contributors of computing resources are listed at ref. 79. The copyright of this Article is held by CERN, for the benefit of the ATLAS Collaboration.

Author contributions All authors have contributed to the publication, being variously involved in the design and the construction of the detectors, in writing software, calibrating subsystems, operating the detectors and acquiring data, and finally analysing the processed data. The ATLAS Collaboration members discussed and approved the scientific results. The manuscript was prepared by a subgroup of authors appointed by the collaboration and subject to an internal collaboration-wide review process. All authors reviewed and approved the final version of the manuscript.

Competing interests The authors declare no competing interests.

Additional information

Correspondence and requests for materials should be addressed to The Atlas Collaboration.

Peer review information *Nature* thanks Matt Kenzie, Zhen Liu and David Sperka for their contribution to the peer review of this work.

Reprints and permissions information is available at http://www.nature.com/reprints.

Extended Data Table 1 | Summary of the input measurements used for the combined fit results

Decay mode	Targeted production processes	$\mathcal{L}$ [fb^{-1}]	Ref.	Fits deployed in
$H \to \gamma\gamma$	ggF, VBF, $WH, ZH, t\bar{t}H, tH$	139	31	All
$H \to ZZ$	ggF, VBF, $WH + ZH, t\bar{t}H + tH$	139	28	All
	$t\bar{t}H + tH$ (multilepton)	36.1	39	All but fit of kinematics
$H \to WW$	ggF, VBF	139	29	All
	WH, ZH	36.1	30	All but fit of kinematics
	$t\bar{t}H + tH$ (multilepton)	36.1	39	All but fit of kinematics
$H \to Z\gamma$	inclusive	139	32	All but fit of kinematics
$H \to b\bar{b}$	WH, ZH	139	33,34	All
	VBF	126	35	All
	$t\bar{t}H + tH$	139	36	All
	inclusive	139	37	Only for fit of kinematics
$H \to \tau\tau$	ggF, VBF, $WH + ZH, t\bar{t}H + tH$	139	38	All
	$t\bar{t}H + tH$ (multilepton)	36.1	39	All but fit of kinematics
$H \to \mu\mu$	ggF + $t\bar{t}H + tH$, VBF + $WH + ZH$	139	40	All but fit of kinematics
$H \to c\bar{c}$	$WH + ZH$	139	41	Only for free-floating κ_c
$H \to$ invisible	VBF	139	42	κ models with $B_{\text{u.}}$ & $B_{\text{inv.}}$
	ZH	139	43	κ models with $B_{\text{u.}}$ & $B_{\text{inv.}}$

Listed are the measured decay modes, targeted production processes and integrated luminosity ($\mathcal{L}$) used for each input analysis of the combination. The references for the input measurements and information about which combined measurements they enter are also provided. The $q\bar{q}/gg \to t\bar{t}H + tHX$ measurement in the multilepton final state[39] is complementary to other $q\bar{q}/gg \to t\bar{t}H + tHX$ measurements in the WW, ZZ and $\tau\tau$ decay modes, with no overlapping events selected by these measurements.

Published for SISSA by Springer

Received: *September 2, 2022*
Accepted: *March 19, 2023*
Published: *June 5, 2023*

Measurement of the top-quark mass using a leptonic invariant mass in pp collisions at $\sqrt{s} = 13$ TeV with the ATLAS detector

The ATLAS collaboration

E-mail: atlas.publications@cern.ch

Abstract: A measurement of the top-quark mass (m_t) in the $t\bar{t} \to$ lepton + jets channel is presented, with an experimental technique which exploits semileptonic decays of b-hadrons produced in the top-quark decay chain. The distribution of the invariant mass $m_{\ell\mu}$ of the lepton, ℓ (with $\ell = e, \mu$), from the W-boson decay and the muon, μ, originating from the b-hadron decay is reconstructed, and a binned-template profile likelihood fit is performed to extract m_t. The measurement is based on data corresponding to an integrated luminosity of 36.1 fb^{-1} of $\sqrt{s} = 13$ TeV pp collisions provided by the Large Hadron Collider and recorded by the ATLAS detector. The measured value of the top-quark mass is $m_t = 174.41 \pm 0.39$ (stat.) ± 0.66 (syst.) ± 0.25 (recoil) GeV, where the third uncertainty arises from changing the Pythia8 parton shower gluon-recoil scheme, used in top-quark decays, to a recently developed setup.

Keywords: Hadron-Hadron Scattering , Top Physics

ArXiv ePrint: 2209.00583

Open Access, Copyright CERN,
for the benefit of the ATLAS Collaboration.
Article funded by SCOAP^3.

https://doi.org/10.1007/JHEP06(2023)019

JHEP06(2023)019

Contents

1 Introduction **1**

2 ATLAS experiment **2**

3 Data and simulation **3**
- 3.1 Data sample and object definition 3
- 3.2 Object and event selections 3
- 3.3 Signal and background simulations 5
- 3.4 Modelling of heavy-quark fragmentation, hadron production and decays 7

4 Analysis **12**
- 4.1 Event yields and sample composition 12
- 4.2 Extraction of the top-quark mass 16

5 Measurement uncertainties **18**
- 5.1 Statistical and datasets 18
- 5.2 Modelling of the signal process 22
- 5.3 Modelling of background processes 25
- 5.4 Detector response 26

6 Conclusions **29**

The ATLAS collaboration **37**

JHEP06(2023)019

1 Introduction

The large mass of the top-quark plays a role in much of the dynamics of elementary particles via loop diagrams. In the Standard Model (SM), the large top-quark mass significantly affects the radiative corrections to both the Higgs boson and W-boson masses, providing a relationship that can be used for precision tests of the consistency of the SM [1]. Furthermore, a precise measurement of the top-quark mass is required to predict the evolution of the Higgs quartic coupling at high scales [2, 3]. If performed with a precision of the order of a few hundred MeV, the direct determination of the top-quark mass from its decay products, and the indirect measurements from top-quark production cross-sections or kinematic distributions, are important not only for the constraints mentioned above, but also for the challenge of the interpretation of such measurements in the context of a strongly interacting particle theory [4, 5].

A direct measurement of the top-quark mass (m_t) is presented that uses a partial, leptonic-only, invariant mass reconstruction of the top-quark decay products. The analysis

is performed from a sample of reconstructed $t\bar{t}$ events in the ℓ+jets channel, where one of the two W-bosons from the top- and antitop-quarks decays leptonically. In the top-quark decay $t \to Wb$, the invariant mass $m_{\ell\mu}$ of the lepton ℓ (with $\ell = e, \mu$) from the W-boson decay and the muon μ from a semileptonic decay of a b-hadron is constructed as the observable sensitive to the parent m_t value. The advantages of a strategy based on the invariant mass of visible leptonic decay products for the measurement of the top-quark mass rest mainly on the smaller sensitivity to the jet energy calibration and energy resolution, compared to the standard direct reconstruction methods, and on less sensitivity to top-quark production modelling (owing to the boost-invariant construction) than in methods based on the W-decay lepton alone [6]. Moreover, methods with different types of systematic uncertainties are important when combining measurements, and for testing the consistency of the theoretical interpretation of the top-quark mass.

In this analysis the $m_{\ell\mu}$ distribution from models with different top-quark mass hypotheses is compared with data, and the optimal value of m_t is determined from a binned-template profile likelihood fit. A similar technique was first employed by the CDF Collaboration at the Tevatron collider [7], and a closely related analysis with J/ψ decays has been presented by the CMS Collaboration [8]; however, both these analyses yielded uncertainties in m_t of several GeV. Until now, the most precise measurement of the top-quark mass in the $t\bar{t} \to$ ℓ+jets channel by the ATLAS Collaboration was $m_t = 172.08 \pm 0.39$ (stat.) ± 0.82 (syst.) GeV, whereas combining multiple ATLAS measurements gave $m_t = 172.69 \pm 0.48$ GeV [9]. The CMS Collaboration reports its most precise combination as $m_t = 172.44 \pm 0.49$ GeV [10], and the Tevatron experiments report a combined value of $m_t = 174.30 \pm 0.65$ GeV [11]. Finally, the mass of the top-quark is indirectly determined from global electroweak fits as $m_t = 176.4 \pm 2.1$ GeV [12].

2 ATLAS experiment

The ATLAS experiment [13] at the LHC is a multipurpose particle detector with a forward-backward symmetric cylindrical geometry and a near 4π coverage in solid angle.[1] It consists of an inner tracking detector surrounded by a thin superconducting solenoid providing a 2 T axial magnetic field, electromagnetic and hadronic calorimeters, and a muon spectrometer. The inner tracking detector covers the pseudorapidity range $|\eta| < 2.5$ and consists of silicon pixel, silicon microstrip, and transition radiation tracking detectors. The innermost layer, known as the insertable B-layer [14, 15], was added in 2014 and provides high-resolution hits at small radius to improve the tracking performance. Lead/liquid-argon (LAr) sampling calorimeters provide electromagnetic (EM) energy measurements with high granularity. A steel/scintillator-tile hadronic calorimeter covers the central pseudorapidity range ($|\eta| < 1.7$). The endcap and forward regions are instrumented with LAr calorimeters for both the EM

[1] ATLAS uses a right-handed coordinate system with its origin at the nominal interaction point (IP) in the centre of the detector and the z-axis along the beam pipe. The x-axis points from the IP to the centre of the LHC ring, and the y-axis points upwards. Cylindrical coordinates (r,ϕ) are used in the transverse plane, ϕ being the azimuthal angle around the z-axis. The pseudorapidity is defined in terms of the polar angle θ as $\eta = -\ln\tan(\theta/2)$. Angular distance is measured in units of $\Delta R \equiv \sqrt{(\Delta\eta)^2 + (\Delta\phi)^2}$.

JHEP06(2023)019

and hadronic energy measurements up to $|\eta| = 4.9$. The muon spectrometer surrounds the calorimeters and is based on three large air-core toroid superconducting magnets with eight coils each and a bending power of 2.0 to 7.5 Tm. It includes a system of precision tracking chambers covering the region $|\eta| < 2.7$ and fast detectors for triggering in the range $|\eta| < 2.4$. A two-level trigger system was used to select events [16]. The first-level trigger is implemented in hardware and uses a subset of the detector information to reduce the accepted rate to at most 100 kHz. This is followed by the software-based high-level trigger, which reduces the event rate to around 1 kHz. An extensive software suite [17] is used in the reconstruction and analysis of real and simulated data, in detector operations, and in the trigger and data acquisition systems of the experiment.

3 Data and simulation

3.1 Data sample and object definition

The analysis is performed with the 2015 and 2016 proton-proton collision data sample produced by the LHC at a centre-of-mass energy of $\sqrt{s} = 13$ TeV and collected by the ATLAS experiment, corresponding to an integrated luminosity of 36.1 fb^{-1} [18]. The data sample was recorded during stable beam conditions, and all relevant ATLAS detector subsystems were required to be operational. The average number of pp collisions in the same bunch crossing (referred to as pile-up) in the data sample is 24.1.

Electron candidates are reconstructed from energy deposits (clusters) in the electromagnetic calorimeter matched to reconstructed tracks in the inner detector. Candidates in the transition region $1.37 < |\eta_{\text{cluster}}| < 1.52$ between the calorimeter barrel and endcaps are excluded. Muon candidates are reconstructed from track segments in the layers of the muon spectrometer, and matched to tracks found in the inner detector. The final muon candidates are re-fitted using the complete track information from both detector systems. Jet candidates are reconstructed from three-dimensional topological EM-scale energy clusters [19] in the calorimeter using the anti-k_t jet algorithm [20, 21] with a radius parameter $R = 0.4$. The reconstructed jets are calibrated to the level of stable-particle jets by the application of a jet energy scale (JES) correction derived from simulation and *in situ* corrections based on 13 TeV data [22]. There is no dedicated energy scale correction for jets with semileptonic heavy-flavour hadron decays. The missing transverse momentum, $E_{\text{T}}^{\text{miss}}$, is defined as the magnitude of the negative vector sum of the transverse momentum, p_{T}, of all reconstructed and calibrated physics objects in the event, with an extra term added to account for soft energy in the event that is not associated with any of the reconstructed objects [23]. This soft term is calculated from inner-detector tracks matched to the primary vertex in order to make it more resilient to pile-up contamination.

3.2 Object and event selections

The event selection is designed to collect a sample of $t\bar{t}$ candidate events in the final state $\ell\nu bjj'\bar{b}$, where $\ell = e$ or μ and the jj' are the jets produced in the decay of the W-boson into quarks, and at least one of the b-initiated jets is associated with a muon from the

JHEP06(2023)019

semileptonic decay of a b-hadron. The goal is to select events where the lepton ℓ from the W-boson and the b-initiated jet with the muon from semileptonic decay come from the same top-quark.

Events are required to pass either a single-electron or single-muon trigger. Multiple trigger types were used: the lowest-threshold triggers include isolation requirements to reduce the trigger rate and had p_{T} thresholds of 20 GeV for muons and 24 GeV for electrons in 2015 data, and 26 GeV for both lepton types in 2016 data [16, 24, 25]. These triggers were complemented by others with higher p_{T} thresholds and no isolation requirements to increase event acceptance. Events must have at least one reconstructed vertex, i.e. at least two tracks with $p_{\mathrm{T}} > 0.4$ GeV consistent with the beam-collision region in the x–y plane. If multiple vertices are reconstructed, then the primary vertex is taken to be the one with the largest sum, over the tracks assigned to it, of the transverse momentum squared of each track.

Events are further selected based on the presence of an electron or muon candidate from the decay of a W-boson, called 'primary' leptons. Primary-lepton electron candidates must satisfy a 'tight' likelihood-based identification criterion [26], be matched to the corresponding trigger, and have $p_{\mathrm{T}} > 27$ GeV, $|\eta| < 2.47$ with the exclusion of $1.37 < |\eta| < 1.52$, longitudinal impact parameter $|z_0 \sin\theta| < 0.5$ mm and transverse impact parameter significance $|d_0/\sigma(d_0)| < 5$, where $\sigma(d_0)$ is the uncertainty in the transverse impact parameter. Background from photon conversions, hadrons, and electrons produced away from the primary vertex ('non-prompt' electrons) is reduced by requiring the primary electron candidates to pass an isolation requirement based on the surrounding tracks and topological clusters in the calorimeter [26]. Primary-lepton muon candidates must satisfy a 'medium' quality identification criterion [27], be matched to the corresponding trigger, and have $p_{\mathrm{T}} > 27$ GeV, $|\eta| < 2.5$, longitudinal impact parameter $|z_0 \sin\theta| < 0.5$ mm and transverse impact parameter significance $|d_0/\sigma(d_0)| < 3$. Background from hadrons and from muons produced away from the primary vertex ('non-prompt' muons) is reduced by requiring primary muon candidates to pass an isolation requirement based on the surrounding tracks and topological clusters in the calorimeter, and be separated by $\Delta R > 0.4$ from the nearest selected jet. If the nearest selected jet is $\Delta R \leq 0.4$ from the muon and has less than three associated tracks (including the muon track), the muon is kept and the jet is removed from the jet list, to ensure high efficiency for muons undergoing significant energy loss in the calorimeter. Events with more than one candidate primary lepton with $p_{\mathrm{T}} > 25$ GeV are vetoed, in order to reject events from the $t\bar{t}$ dileptonic decay channel.

Jet candidates are required to have $p_{\mathrm{T}} > 25$ GeV and $|\eta| < 2.5$, and a multivariate jet-vertex-tagger (JVT) is applied to suppress jets from pile-up [28]. During jet reconstruction, no distinction is made between identified electrons and jet energy deposits. Therefore, if any of the jets lie within $\Delta R = 0.2$ of a selected electron, the single closest jet is discarded in order to avoid double-counting electrons as jets. After this, electrons that are within $\Delta R = 0.4$ of a remaining jet are removed. Jets are identified as originating from a b-quark (b-tagged) using two techniques, one based on the reconstruction of a displaced jet (DJ tagging) and the other based on the semileptonic decay of a b-hadron into a so-called 'soft muon' (SMT tagging). For DJ tagging, multivariate techniques are used to combine

JHEP06(2023)019

information about the impact parameters of displaced tracks and the topological properties of secondary and tertiary decay vertices reconstructed within the jet [29]. The algorithm is trained on simulated $t\bar{t}$ events to discriminate b-jets from a background consisting of light-flavour jets and c-jets. A selection corresponding to an efficiency of 77% for b-jets in $t\bar{t}$ events is employed, with a rejection rate of a factor of 7 (100) for c-jets (light jets). The SMT tagging is performed by requiring the presence of a muon candidate satisfying the 'tight' quality identification criterion [27], $p_{\mathrm{T}} > 8$ GeV and $|\eta| < 2.5$, with loose requirements on the impact parameters ($|d_0| < 3$ mm, $|z_0 \sin\theta| < 3$ mm) and with a distance $\Delta R < 0.4$ from a selected jet candidate. The definition of the muon object for the SMT tagging was optimised by maximising the efficiency for muons originating from the semileptonic decays of b- and c-hadrons (selecting approximately 50% of b-jets containing a muon, which are in turn 20% of all b-jets produced in $t\bar{t}$ events), minimising the misidentification rate (about 10^{-3} per light-flavour jet, mostly due to the decays of pions and kaons), and minimising the uncertainty in the measured top-quark mass. If more than one muon satisfying the criteria above is found within a given jet, the muon with the highest p_{T} is chosen.

Events must have at least one SMT-tagged jet and at least one DJ-tagged jet (which could be the same jet), among a total of at least four jet candidates with $p_{\mathrm{T}} > 30$ GeV (with the exception of the SMT-tagged jet which may have a p_{T} as low as 25 GeV). If more than one SMT-tagged jet is found in the event, only the one with the highest-p_{T} muon is considered. The SMT muon and the primary lepton must be separated by $\Delta R_{\ell,\mu} < 2$. The presence of at least one neutrino in the final state is inferred from the requirements that $E_{\mathrm{T}}^{\mathrm{miss}} > 30$ GeV and $E_{\mathrm{T}}^{\mathrm{miss}} + m_{\mathrm{T}}(W) > 60$ GeV.[2] The requirement that the SMT muon and the primary lepton must be separated by $\Delta R_{\ell,\mu} < 2$ enhances the fraction of events where both leptons come from the same top-quark, in contrast to events where the two leptons originate from different top-quarks. The selected events are categorised as same-sign (SS) events or opposite-sign (OS) events according to the charge signs of the primary lepton and the soft muon. When both leptons come from the same top-quark, opposite-sign events are enriched in direct $b \to \mu X$ decays, while same-sign events have a large contribution from sequential $b \to cX' \to \mu X''$ decays; both samples carry information about the mass of the parent top-quark though. Finally, the invariant mass of the primary lepton and the soft muon ($m_{\ell\mu}$) is required to be between 15 and 80 GeV, as this is the region most sensitive to the top-quark mass. This requirement also suppresses the Z-boson, J/ψ and Υ resonances.

3.3 Signal and background simulations

A number of Monte Carlo (MC) simulation samples are used to model the expected signal of top-quark pairs and the background. The MC samples were processed either through the full ATLAS detector simulation [30] based on GEANT4 [31] or through a faster simulation making use of parameterised showers in the calorimeters [32]. Additional simulated pp collisions generated by PYTHIA 8.186 [33] with the MSTW2008 [34, 35] set of leading-order (LO) parton distribution functions (PDFs) and a set of tuned parameters called the

[2] The transverse mass is given by $m_{\mathrm{T}}(W) = \sqrt{2p_{\mathrm{T}}^{\ell} E_{\mathrm{T}}^{\mathrm{miss}}(1 - \cos\Delta\phi)}$, where p_{T}^{ℓ} is the transverse momentum of the muon (electron) and $\Delta\phi$ is the azimuthal angle separation between the lepton and the direction of the missing transverse momentum.

JHEP06(2023)019

A2 tune [36] were used to model the effects of both in-time and out-of-time pile-up. They were superimposed on the MC events, matching the luminosity profile of the recorded data. All simulated samples were processed through the same reconstruction algorithms and analysis chain as the data.

Simulated MC events were corrected so that the object identification efficiencies and energy and momentum scales and resolutions matched those determined from data control samples [22, 27, 28, 37]. The modelling of SMT muons and their misidentification due to light-hadron decays and detector background ('SMT fake') was studied using control samples as well. The efficiency of muon identification in jets was calibrated using muons from J/ψ and Z decays, and checked as a function of nearby track and calorimeter activity, and of the muon's transverse impact parameter d_0. The calibration of the misidentification rate was performed, using the sample of W+jets events described in the following of the section, with the same approach used in ref. [38]. A data-driven technique, described in detail in ref. [39], is used to measure in data the normalisation and flavour composition of such events and to derive corrections that are applied to simulated samples for the calibration. A light-jets dominated sample of $W+$ 1 jet events is then defined by selecting events where the jet is SMT-tagged but is not DJ-tagged, and using the SS category. A data-to-simulation scale factor (SF) of 1.10 ± 0.14 is measured. A slight miscalibration of the p_{T} of jets that contain a soft muon was observed, and the p_{T} of these jets was corrected in the simulation with a factor of 0.967 ± 0.024. It has been measured by studying the distribution of the ratio of the p_{T} values of the SMT-tagged jet and the average non-SMT-tagged jet in $t\bar{t}$ data and simulation.

The $t\bar{t}$ sample was generated using the *hvq* program [40] in the Powheg-Box v2 generator [41, 42] with the NNPDF3.0nlo set of PDFs [43] and the top-quark mass set to 172.5 GeV. Additional samples with different top-quark mass hypotheses were produced in the range of m_t between 165 and 180 GeV, with steps of 0.5 GeV between 170 and 175 GeV. The samples have been produced using the appropriate top-quark decay width values predicted at next-to-next-to-leading order (NNLO) as a function of m_t [44]. The *hvq* program uses on-shell matrix elements for production of $t\bar{t}$ pairs at next-to-leading order (NLO) in quantum chromodynamics (QCD). Off-shell effects and top-quark decays, including spin correlations, were approximated using Madspin [45]. Parton showers and hadronisation were modelled by Pythia 8.2 [33] using a dedicated 'A14-r_b' setting of the ATLAS A14 [46] tune, as detailed in section 3.4. The A14 tune is based on LEP and Tevatron collider data and also uses a combination of ATLAS $\sqrt{s}$=7 TeV measurements of the underlying event, jet production, Z-boson production and top-quark production in order to constrain the parameters for the showers, multiple parton interactions and colour reconnection effects. Radiation in top-quark decays was handled entirely by the parton-shower generator, which implements matrix-element corrections with an accuracy equivalent to a calculation at the NLO level. The h_{damp} parameter, which controls the p_{T} of the first additional emission beyond the Born configuration, was set to 1.5 times the top-quark mass of each sample. The main effect of the h_{damp} setting is to regulate the high-p_{T} emission against which the $t\bar{t}$ system recoils. The EvtGen v1.2.0 [47] program was used to simulate bottom and charm hadron mixing and decays. The production

JHEP06(2023)019

fractions and the branching ratios (BR) of the decay of b-hadrons and c-hadrons into muons were rescaled to the latest values from the Particle Data Group (PDG) [1], as detailed in section 3.4. The simulated $t\bar{t}$ event sample was normalised to the Top++2.0 [48] theoretical cross-section of 832^{+46}_{-51} pb, calculated at NNLO in QCD and including resummation of next-to-next-to-leading logarithmic (NNLL) soft gluon terms [49–53].

The main backgrounds to candidate signal events come from the production of a single top-quark, and from a W- or Z-boson in association with jets. A small background contribution arises from diboson (WW, WZ, ZZ) production. Events not containing prompt leptons also contribute to the selected sample via the misidentification of a jet or a photon as an electron, or the presence of non-prompt electrons or muons passing the prompt isolated lepton selection. This contribution is referred to as 'multijet' background, and was estimated using data by following the matrix method described in ref. [54].

The production of V+jets was simulated with the Sherpa 2.2.1 [55] generator using next-to-leading-order (NLO) matrix elements (ME) for up to two partons, and leading-order (LO) matrix elements for up to four partons calculated with the Comix [56] and OpenLoops [57–59] libraries. They were matched with the Sherpa parton shower [60] using the MEPS@NLO prescription [61–64] with the set of tuned parameters developed by the Sherpa authors. The NNPDF3.0nnlo set of PDFs [43] was used and the samples were normalised to a next-to-next-to-leading-order (NNLO) prediction [65]. The normalisation of the W+jet background and the fractions of W-bosons produced in association with heavy-flavour quarks are extracted from data, taking advantage of the intrinsic W-boson charge asymmetry in this process [66]. The Z+jets contribution is estimated from MC simulation and checked in a data control sample.

Diboson processes were simulated with the Sherpa 2.1.1 event generator. They were calculated using Comix and OpenLoops, and merged with the Sherpa parton shower according to the MEPS@NLO prescription. The CT10nlo PDF set [67] was used in conjunction with dedicated parton shower tuning developed by the Sherpa authors.

Samples of $t-$, Wt- and s-channel single top-quark background events were generated with Powheg-Box v1, using the 4-flavour scheme for the NLO matrix element calculations together with the fixed four-flavour PDF set CT10f4. Overlaps between the $t\bar{t}$ and Wt final states were removed with the 'diagram removal' prescription [68]. For all top processes, top-quark spin correlations were preserved (for t-channel, top quarks were decayed using Madspin). All single top-quark samples were interfaced to Pythia 6.428 [69] with the CTEQ6L1 PDF set [70] and the corresponding Perugia 2012 [71] set of tuned parameters. The EvtGen v1.2.0 program was used to model properties of the bottom and charm hadron decays. The single top-quark t- and s-channel samples were normalised to the approximate NNLO theoretical cross-sections [72–74].

3.4 Modelling of heavy-quark fragmentation, hadron production and decays

The modelling of the momentum transfer between the b-quark and the b-hadron is an important aspect of this analysis. The Monte Carlo event generators, such as the Pythia, Herwig [75, 76] and Sherpa programs, describe this transfer according to phenomenological models, namely the string and cluster models containing parameters which are tuned to data.

JHEP06(2023)019

The Pythia8 program uses parametric functions to describe the b-quark fragmentation function, while Herwig7 and Sherpa use a non-parametric model which handles the complete parton-shower evolution. The free parameters in those models are typically fit to measurements from e^+e^- colliders, and this analysis assumes that the b-quark fragmentation function is the same in e^+e^- and pp collisions, as supported by dedicated studies.

The Lund-Bowler parameterisation [77, 78] in Pythia8 was used. It is given by

$$f(z) = \frac{1}{z^{1+br_b m_b^2}}(1-z)^a \exp(-bm_{\mathrm{T}}^2/z),$$

where a, b and r_b are the function parameters, m_b is the b-quark mass, $m_{\mathrm{T}} = \sqrt{m_B^2 + p_{\mathrm{T}}^2}$ the b-hadron transverse mass (m_B being the b-hadron mass), and z is the fraction of the longitudinal energy carried by the b-hadron with respect to the b-quark, in the light-cone reference frame. The fragmentation function is defined at the hadronisation scale and it is evolved by the parton shower to the process scale through DGLAP evolution equations. In Pythia8, the values of a and b were fit to data sensitive to light-quark fragmentation [79], such as charged-particle multiplicities, event shapes and scaled momentum distributions. They are assumed to be universal for light- and heavy-quarks, while the r_b parameter is specific to b-quark fragmentation.

The description of the b-quark fragmentation in the ATLAS A14 tune is improved by fitting for the `StringZ:rFactB` Pythia8 parameter (corresponding to r_b) following the approach given in refs. [80–83]. The A14 tune sets the parton shower α_s to 0.127, whereas the value of 0.1365 is used in Monash [79]. However, both Monash and A14 set $r_b = 0.855$. Since the b-quark fragmentation is controlled both by α_s and r_b, the procedure described in the following is used to determine a value of r_b more appropriate for a value of $\alpha_s = 0.127$. The fit uses the A14 tune with e^+e^- collision data from the ALEPH, DELPHI and OPAL experiments at the LEP collider, and from the SLD experiment at the SLC collider [84–87]. The distribution of $x_B = 2p_B \cdot p_Z/m_Z^2$ from semileptonically decaying b-hadrons in $e^+e^- \to Z \to b\bar{b}$ events is used, where p_B and p_Z are the four-momenta of the b-hadron and the Z-boson, respectively. In the Z rest frame, m_Z is twice the beam energy and therefore $x_B = 2E_B/m_Z$, where E_B is the energy of the b-hadron. The fit is performed using Rivet v3.1.0 [88] to implement the measurements. The effect of the matrix-element corrections for $e^+e^- \to Z \to b\bar{b}g$ is taken into account. Eighty simulated samples of 1M $e^+e^- \to Z \to b\bar{b}$ events were produced using Pythia8 with different values of the r_b parameter in the interval [0.8–1.4] and compared to the experimental data in HEPDATA format. The extraction of the best r_b value is performed through a standard binned χ^2 test on the experimental x_B distribution where statistical and systematic uncertainties are taken into account for each of the four experiments. In addition, for the results of ALEPH, DELPHI and OPAL, bin-by-bin correlations are taken into account in the fit procedure. The SLD experiment did not provide the full covariance matrix for the total uncertainties and therefore the χ^2 fit for this experiment is performed ignoring bin-by-bin correlations. For each experiment, the χ^2 minimisation is performed and the best r_b value and its uncertainty are found. The results are summarised in table 1. The values of χ^2/ndf for DELPHI and SLD experiments show a poor modelling of the data by the simulated templates. Therefore,

JHEP06(2023)019

Experiment	r_b	χ^2/ndf
ALEPH	1.070 ± 0.035	21/18
DELPHI	1.094 ± 0.030	73/8
OPAL	1.023 ± 0.019	18/19
SLD	1.092 ± 0.018	58/21

Table 1. Results of a fit of the r_b parameter of the Lund-Bowler b-quark fragmentation function in Pythia8 to different experimental data where bin-by-bin correlations for ALEPH, DELPHI and OPAL experiments were considered.

before including these results into a global χ^2 combination, the uncertainties found in the r_b parameter for these two cases were rescaled by a factor of $S = \sqrt{\chi^2/\text{ndf}}$ following the procedure outlined in ref. [1]. After these uncertainties are rescaled, the four χ^2 curves are summed up to produce a single χ^2 curve taking into account the information of all four experiments. In this approach, the four experiments are considered uncorrelated since the dominant uncertainties on the measurements come from uncorrelated sources. This curve is then fitted with a parabola to find the minimum of the χ^2 and to extract the best value of the r_b parameter and its uncertainty, yielding $r_b = 1.05 \pm 0.02$. The values of the r_b parameter and its uncertainty for the four experiments, and their combination are shown in figure 1. A similar procedure is performed, as a cross-check, exploiting the average value $<x_B>$ of the four x_B distributions. The experimental $<x_B>$ values are compared with the predicted value of the various simulated samples, and the best r_b values and their uncertainties are extracted. A weighted average of the single results is calculated and the result is found to be compatible with the previous method.

The setting with $r_b = 1.05 \pm 0.02$ is referred to as A14-r_b and is applied in this analysis to all signal MC samples using Pythia8 for the simulation of the parton shower. The x_B distributions measured by the ALEPH, DELPHI, OPAL and SLD experiments are shown in figure 2 together with the MC predictions obtained with the A14, the A14-r_b and the Powheg+Herwig7 settings respectively. Recent b-fragmentation measurements based on LHC data [89, 90] show reasonable agreement with simulations using the A14-r_b tune.

The production fractions of weakly decaying b- and c-hadrons observed in Powheg+Pythia8 MC simulation with EvtGen are rescaled to those from the Heavy Flavour Averaging Group (HFLAV) [91] as reported by the PDG [1] and in ref. [92]. The production fraction values and corresponding scale factors for Powheg+Pythia8 simulations are shown in table 2. These scale factors refer only to the first weakly decaying hadron produced in the hadronisation process of b- and c-quarks. The scale factors are applied to each of these hadrons present in a MC simulated event, with the overall event weight given by the product of these scale factors. This procedure assumes that the production fractions of heavy-flavour quarks can be regarded as universal in the kinematic phase space relevant for this analysis, within the uncertainties accounted for here, as supported by recent results [93–99] which find deviations from universality only in the very low-p_{T} regime.

The branching ratios of the b- and c-hadron decays that contain a muon are also adjusted to match those measured by previous experiments [1]. Central values and relative

JHEP06(2023)019

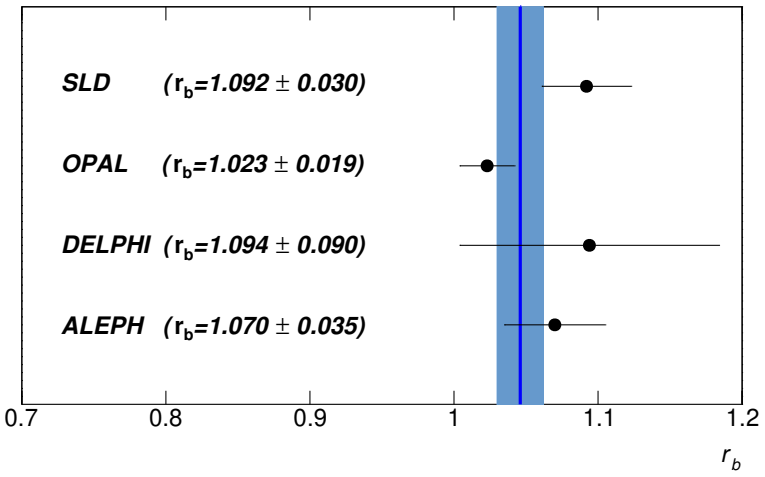

Figure 1. Fit of the r_b PYTHIA parameter to the four experiments considered: SLD, OPAL, DELPHI and ALEPH. For each experiment, the r_b fitted value is shown together with its uncertainty. These results have been obtained including bin-by-bin correlations in the experimental data (except for SLD experiment) and after rescaling the uncertainties on r_b for DELPHI and SLD experiments as explained in the text. The solid blue line represents the value of r_b obtained from the combined fit to the four experiments. The blue band represents the uncertainty from the combined fit to the four experiments.

Hadron	PDG	POWHEG+PYTHIA8	Scale Factor
B^0	0.404 ± 0.006	0.429	0.941 ± 0.014
B^+	0.404 ± 0.006	0.429	0.942 ± 0.014
B_s^0	0.103 ± 0.005	0.095	1.088 ± 0.052
b-baryon	0.088 ± 0.012	0.047	1.87 ± 0.26
D^+	0.226 ± 0.008	0.290	0.780 ± 0.027
D^0	0.564 ± 0.015	0.553	1.020 ± 0.027
D_s^0	0.080 ± 0.005	0.093	0.857 ± 0.054
c-baryon	0.109 ± 0.009	0.038	2.90 ± 0.24

Table 2. The production fraction values for b-hadrons and c-hadrons in the PDG and POWHEG+PYTHIA8. The relative scale factors applied to POWHEG+PYTHIA8 are also shown. The values in the PDG column are derived from refs. [1] and [92]. The same scale factors are applied to the charge-conjugate hadrons.

JHEP06(2023)019

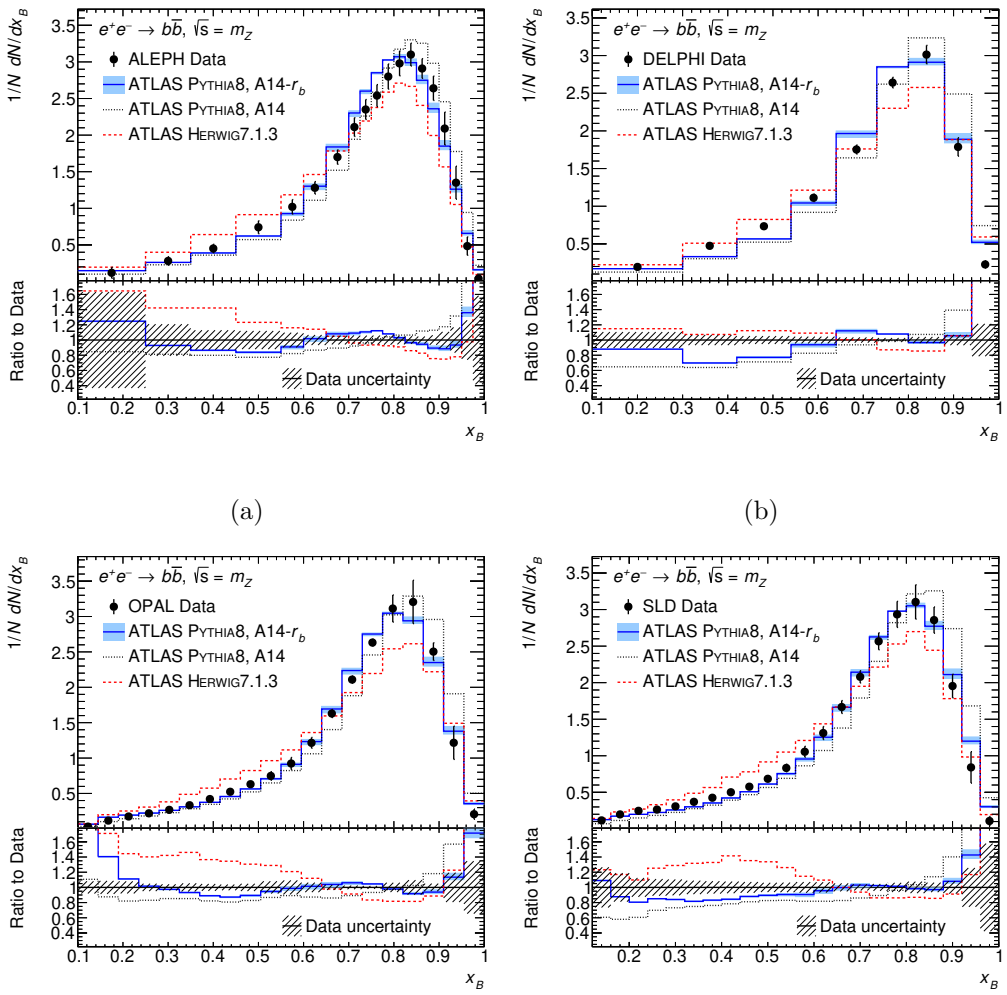

Figure 2. Distributions of x_B from semileptonically decaying b-hadrons in $e^+e^- \to Z \to b\bar{b}$ events as measured by the ALEPH, DELPHI and OPAL experiments at the LEP collider, and by the SLD experiment at the SLC collider. Each of the measured spectra is compared with a set of MC predictions. The Pythia8 A14-r_b prediction includes a systematic uncertainty band obtained considering the r_b parameter variations described in the text and included as systematic uncertainty in the analysis.

scale factors, along with the corresponding uncertainties, are shown in table 3; these are measured after applying the corrections for the production fractions described above. The $b \to \bar{c} \to \mu$ branching ratio was determined by averaging the direct measurement from DELPHI [100] and the predicted values computed by the LEP Electroweak Heavy Flavour Working Group [101]. The latter prediction is based on flavour-specific $B \to D$ and $B \to \Lambda_c^+$ rates measured at CLEO [102–104] in combination with the $B \to DD(X)$ rates measured in ALEPH [105] to extract the probabilities of producing the different c-hadrons from the initial b-hadron decays. The c-hadron semileptonic branching fractions were also used in the

JHEP06(2023)019

Hadronic Decay Mode	PDG	POWHEG PYTHIA8+EVTGEN	Scale Factor
$b \to \mu$	$0.1095\ ^{+0.0029}_{-0.0025}$	0.106	$1.032\ ^{+0.0027}_{-0.0023}$
$b \to \tau$	0.0042 ± 0.0004	0.0064	0.661 ± 0.062
$b \to c \to \mu$	0.0802 ± 0.0019	0.085	0.946 ± 0.022
$b \to \bar{c} \to \mu$	0.016 ± 0.003	0.018	0.89 ± 0.17
$c \to \mu$	0.082 ± 0.005	0.084	0.976 ± 0.059

Table 3. Hadron to muon branching ratios from the PDG and in POWHEG+PYTHIA8+EVTGEN. The relative scale factors applied to POWHEG+PYTHIA8 are also shown. The values in the PDG column are derived from refs. [1] and [92]. The $c \to \mu$ scale factor is applied only to the semileptonic decays of c-hadrons into muons when the c-hadrons do not come from a cascade b-hadron decay. The same scale factors are applied to the charge conjugate hadrons.

prediction. The $c \to \mu$ scale factor is applied only to the semileptonic decays of c-hadrons into muons when the c-hadrons do not come from a cascade b-hadron decay.

4 Analysis

4.1 Event yields and sample composition

The number of observed candidate events and the predicted signal and background are shown in table 4, for both the OS and SS regions. Over 90% of the events in the sample contain a top-quark pair, including cases where the soft muon is erroneously chosen from a $t\bar{t}$ dilepton decay, whereby a muon from the prompt W decay is found near a jet or radiates a near-collinear photon mimicking a soft muon tag, and cases where the soft muon candidate does not originate from a b decay such as in $W \to cs$ or SMT fakes. The contributions from single top-quark, W- or Z-boson in association with jets, and multijet background are not negligible. The Z+jets background gives a small contribution near the peak of the $m_{\ell\mu}$ distribution, but becomes important for $m_{\ell\mu}$ close to the Z-boson mass peak.

Of the selected $t\bar{t}$ events in the OS class, 83% are cases where the primary lepton and the soft muon belong to the decay of the same top-quark, and 10% are events where the two originate from different top-quarks. The topological requirement $\Delta R_{\ell,\mu} < 2$ is responsible for much of the purity because it is very effective in preferentially selecting the same top-quark decays. For the remaining 7% of cases, the soft muon does not originate from either of the b-quarks produced in the two top-quark decays. In the SS class, the above fractions are 57%, 41% and 2%, respectively. The rate of soft muons that are not from b-quarks is higher in OS events owing to the decay of c-quarks that come from $W \to cs$ in the top-quark decay chain.

In order to better understand the nature of the sample composition in the OS and SS regions, the expected $t\bar{t}$ events shown in the first row of table 4 are further resolved into components. Table 5 shows the components involving direct and sequential decays, and decays not belonging to the b-quark from the $t \to Wb$ transition. The direct $t \to B \to \mu$

JHEP06(2023)019

Process	Yield (OS)	Yield (SS)
$t\bar{t}$ (SMT from b- or c-hadron)	55 700 ± 3400	34 800 ± 2300
$t\bar{t}$ (SMT from $W \to \mu\nu$)	2190 ± 310	4.9 ± 3.6
$t\bar{t}$ (SMT fake)	1490 ± 210	1240 ± 170
Single top t-channel	770 ± 70	490 ± 40
Single top s-channel	63 ± 6	49 ± 4
Single top Wt channel	1840 ± 140	1260 ± 100
W+jets	1600 ± 400	1080 ± 240
Z+light jets	210 ± 80	15 ± 6
Z+HF jets	550 ± 180	310 ± 100
Diboson	17.2 ± 2.9	6.3 ± 1.4
Multijet	530 ± 140	480 ± 130
Total Expected	65 000 ± 4000	39 700 ± 2500
Data	66 891	42 087

Table 4. Event yields with $m_{\ell\mu}$ between 15 and 80 GeV, separately for OS and SS regions. Uncertainties shown include statistical and systematic contributions but not the recoil uncertainty.

decays are by far the dominant component in the OS sample, while the sequential $t \to B \to D \to \mu$ decays are also suppressed by the kinematic requirement on the soft muon. Decay channels involving τ leptons give a small contribution.

	OS [%]	SS [%]
Processes involving a μ from a t or $\bar{t}$		
$t \to B \to \mu$	73.6	51.2
$t \to B \to D \to \mu$	16.7	44.2
$t \to B \to \tau \to \mu$	2.0	1.3
$t \to B \to D \to \tau \to \mu$	0.8	0.8
Processes involving a μ not from a t or $\bar{t}$		
$B \to \mu$	0.6	0.9
$D \to \mu$	5.8	1.4
Other ($\tau \to \mu$)	0.5	0.1

Table 5. Fraction of MC-simulated $t\bar{t}$ events with a soft muon originated by a b- or c-hadron split into components of direct and sequential decays, and decays not belonging to the b-quark from the $t \to Wb$ transition, separately for the opposite-sign and same-sign event selections. The letters B and D indicate b- and c-hadrons of either charge. Only MC events with two real muons are included.

The data are compared with the sum of the predicted signal and backgrounds in figures 3 and 4, for an illustrative selection of kinematic distributions of the candidate events for the OS and SS selections: $p_{\mathrm{T}}(\mu^{\mathrm{SMT}})$, $\eta(\mu^{\mathrm{SMT}})$, $p_{\mathrm{T}}(\ell^{\text{ primary}})$ and $m_{\mathrm{T}}(W)$. The uncertainties are discussed in detail in section 5. The compatibility of the data and MC predictions is studied

JHEP06(2023)019

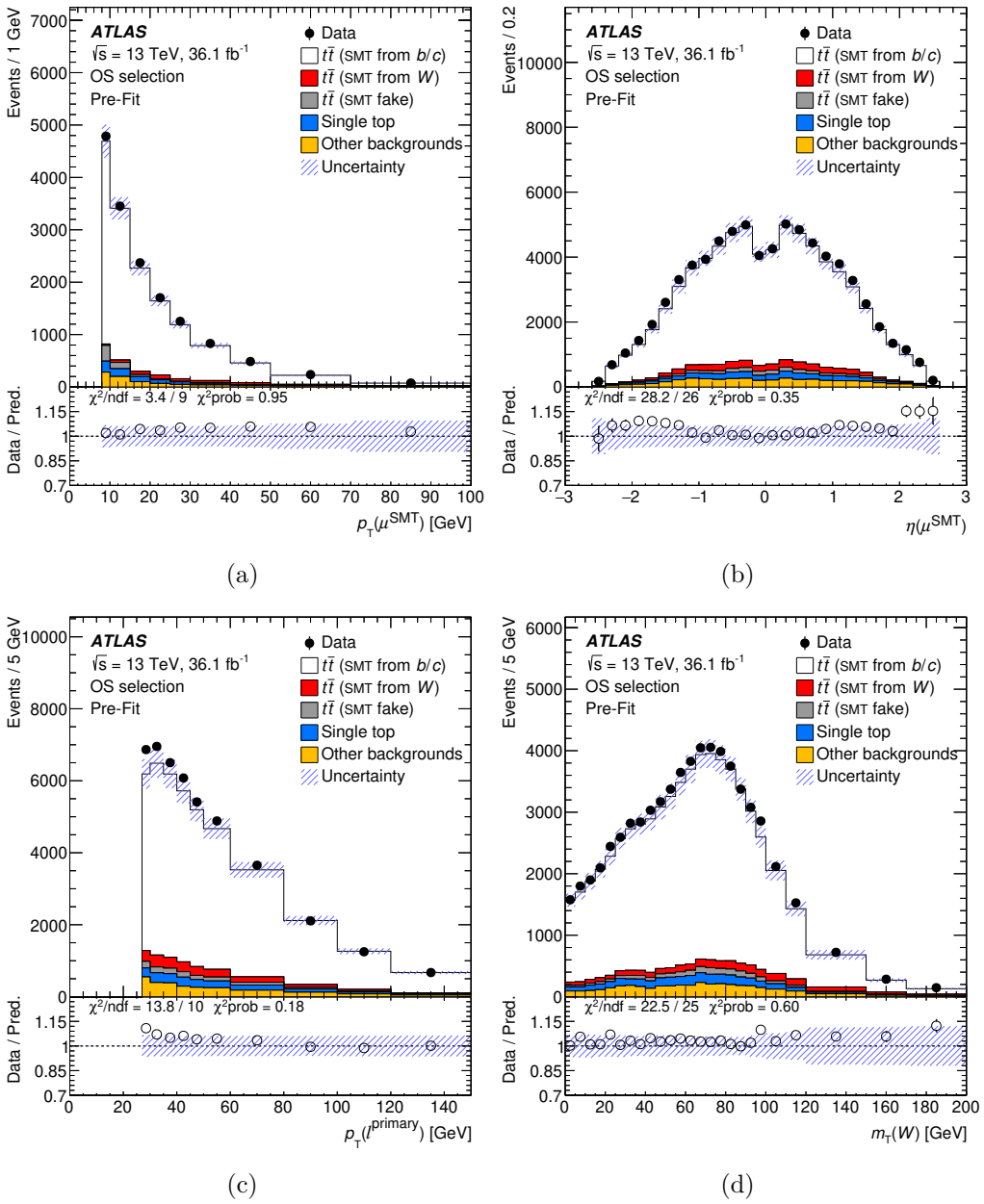

Figure 3. Comparison of data and prediction before the fit described in section 4.2 in the OS sample, i.e. for events with primary lepton and the soft muon with opposite charges, for the (a) soft muon p_{T}, (b) soft muon η, (c) primary lepton p_{T} and (d) W-boson transverse mass. The prediction reports the expected event contribution from the signal and backgrounds. The uncertainty band includes statistical and systematic uncertainties, but does not include the recoil uncertainty.

using a χ^2 test involving the bin-by-bin full correlation matrix, and for all distributions the level of agreement is better than 2 standard deviations. The slight excess of SMT muons in regions of high-η is associated with a potential small mismodelling of the efficiency for low-p_{T} muons in simulation. The corresponding impact on the measurement is negligible.

JHEP06(2023)019

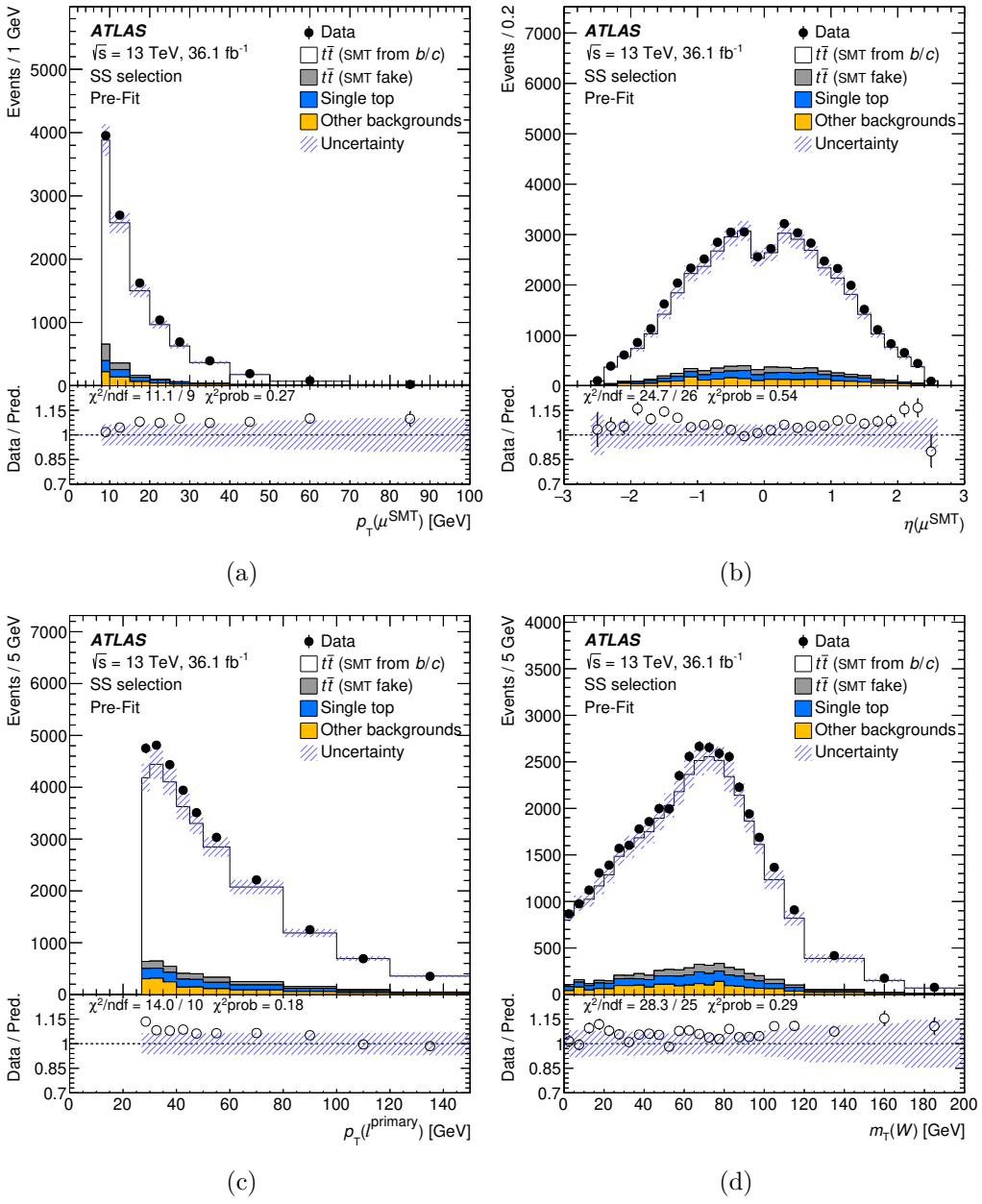

Figure 4. Comparison of data and prediction before the fit described in section 4.2 in the SS sample, i.e. for events with primary lepton and the soft muon with same charges, for the (a) soft muon p_{T}, (b) soft muon η, (c) primary lepton p_{T} and (d) W-boson transverse mass. The prediction reports the expected event contribution from the signal and backgrounds. The uncertainty band includes statistical and systematic uncertainties, but does not include the recoil uncertainty.

JHEP06(2023)019

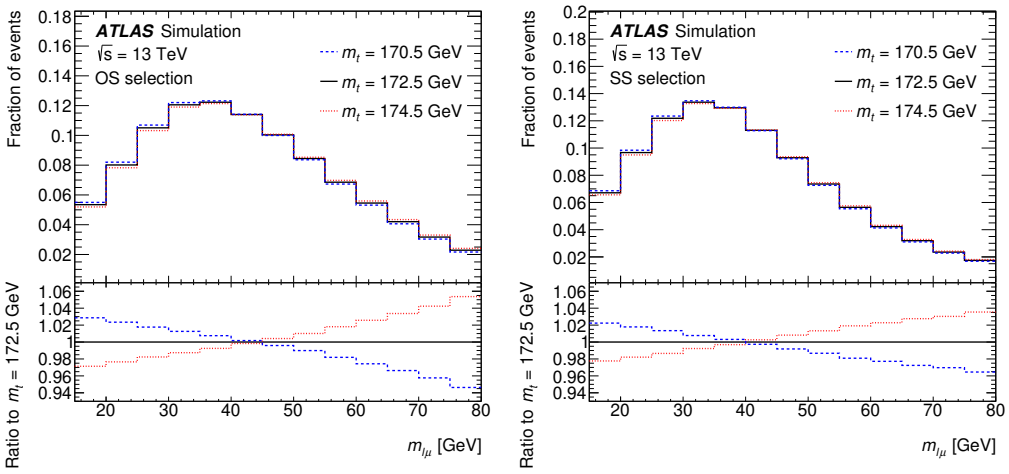

(a) (b)

Figure 5. Sensitivity of the $m_{\ell\mu}$ distribution to different input top-quark masses from simulated events, separately for the OS and SS samples.

4.2 Extraction of the top-quark mass

The distribution of the invariant mass of the primary lepton and the soft muon, $m_{\ell\mu}$ is used to determine the mass of the parent top-quark. A binned-template profile likelihood fit is performed, with a Poisson likelihood model and systematic uncertainties included as Gaussian-constrained nuisance parameters [106]. Only the range of $m_{\ell\mu}$ between 15 and 80 GeV is considered in the fit, since the tail of the $m_{\ell\mu}$ distribution is more sensitive to $t\bar{t}$ modelling uncertainties and higher-order corrections, and to the Z+jets background. The fit is performed simultaneously for the OS and SS charge-combination samples, and figure 5 shows the sensitivity of each of these distributions to variations of the top-quark mass, as well as the binning used by the templates. The SS sample has less sensitivity than the OS sample due to the larger incidence of sequential $b \to c \to \mu$ decays, where the SMT muon carries a smaller fraction of the parent b-quark momentum, and due to the larger fraction of events in which the leptons originate from different top-quarks.

The fit uses template histograms simulated as for the nominal $t\bar{t}$ sample but with different values for the input top-quark mass. The templates from the different mass samples are interpolated with piece-wise linear functions built bin by bin. To improve the stability of the method, the templates are smoothed assuming a linear dependence on m_t for the fraction of the total number of events in each bin. A maximum-likelihood fit is performed with three free parameters: m_t, which controls the shape of the $m_{\ell\mu}$ distribution for $t\bar{t}$ events, and the normalisation factors for $t\bar{t}$ events in the OS and SS samples. The normalisation factors ensure that the total of the $t\bar{t}$ signal and background events is always equal to the total number of selected data events, and no m_t information is extracted from the number of events.

The uncertainty due to the limited number of simulated events, and due to statistical fluctuations in the background estimates based on control samples, is evaluated by defining

JHEP06(2023)019

a new source of systematic uncertainty for each bin of the prediction, which modifies the bin content by its statistical uncertainty. Since a very large number of systematic uncertainties are considered *a priori*, a pruning procedure is applied to reduce the number of statistically insignificant systematic uncertainties affecting the prediction of each of the signal and background processes. A systematic variation of the $m_{\ell\mu}$ templates is excluded if the total predicted change is smaller than 0.05% of the nominal bin content for all bins. The impact on the total estimated uncertainty is smaller than 0.03 GeV.

The top-quark mass determination from the fit is found to be linear and unbiased with respect to the input top-quark mass hypothesis by means of pseudo-experiments, and its uncertainty from the likelihood ratio is also checked to ensure it reports the correct statistical coverage. The fit method and the event selection were optimised to minimise the total uncertainty in m_t in a 'blinded' approach, i.e. using pseudo-data and data without knowledge of the best-fit top-quark mass. The fit yields:

$$m_t = 174.41 \pm 0.39 \text{ (stat.)} \pm 0.66 \text{ (syst.)} \pm 0.25 \text{ (recoil) GeV},$$

where the statistical, systematic and recoil uncertainties are described in detail in section 5. Figure 6 shows the post-fit $m_{\ell\mu}$ distributions in the OS and SS samples; a goodness-of-fit test is performed using the saturated model technique [1, 107] and returns a probability of 56%. Figures 7 and 8 display the corresponding post-fit plots for the kinematic variables of figures 3 and 4. The data distributions are well described by the prediction, with the primary lepton p_{T} exhibiting a slight trend which is traced to the boost of the $t\bar{t}$ system, but which has no appreciable impact on the determined top-quark mass. This was confirmed by detailed checks, performed by testing the impact of NNLO corrections on the top quark kinematics, and by performing a test fit including the lepton pT as a second fit variable. In all cases the impact on the measurement was shown to be well within the quoted modelling uncertainties associated with ISR effects and ME generator choice. The post-fit uncertainties shown in figures 7 and 8 are significantly reduced with respect to the pre-fit ones shown in figures 3 and 4 due to the $t\bar{t}$ normalisation being treated as a free parameter in the fit procedure; the normalisation uncertainty considered at pre-fit level is thus removed after the fit procedure. The likelihood scan with the best-fit top-quark mass value is shown in figure 9.

Checks were performed by fitting the OS and SS regions separately, giving $m_t(\mathrm{OS}) = 174.63 \pm 0.47 \text{ (stat.)} \pm 0.75 \text{ (syst.) GeV}$ and $m_t(\mathrm{SS}) = 173.88 \pm 0.74 \text{ (stat.)} \pm 1.01 \text{ (syst.) GeV}$. Checks were performed by separately fitting the electron and muon channels, different W-decay lepton charges and different configurations of b-tagging and event selection, and were found to all give consistent results. Checks also included the extraction of the top-quark mass with alternative statistical methods, namely using analytic functions for $m_{\ell\mu}$ with a parametric dependence on the top-quark mass, only using the mean value of the $m_{\ell\mu}$ distribution, and using a binned-template likelihood fit without including systematic uncertainties as nuisance parameters. In particular, the inclusion of systematic uncertainties as nuisance parameters in the fit reduces the total uncertainty by 2.6%, in line with reasonable constraints from the fit.

JHEP06(2023)019

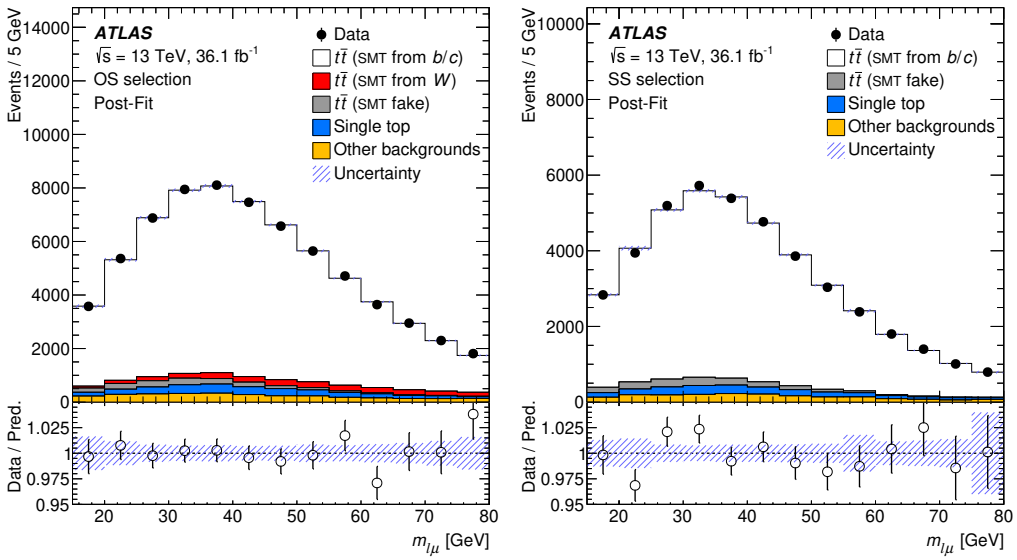

(a) (b)

Figure 6. Post-fit $m_{\ell\mu}$ distributions in the (a) OS sample and in the (b) SS sample. The prediction reports the event contribution for the signal and backgrounds. The uncertainty band includes statistical and systematic uncertainties, but does not include the recoil uncertainty. The SS (same sign) or OS (opposite sign) refers to the charge signs of the primary lepton and the soft muon.

5 Measurement uncertainties

The individual sources of uncertainty and the evaluation of their effect on m_t are described in the following. Many sources of systematic uncertainty are considered, corresponding to a total of 151 individual variations. Table 6 summarises the impact on m_t of the main sources of systematic uncertainty, and each systematic uncertainty is accompanied by an estimate of its statistical precision performed using the bootstrap method [108].

5.1 Statistical and datasets

The uncertainty related to the size of the data sample (data statistical uncertainty) is obtained by performing the fit while keeping constant all of the nuisance parameters associated with the systematic uncertainties. The data statistical uncertainty obtained by using both the OS and SS selections is ±0.39 GeV, while the OS sample alone yields ±0.47 GeV, highlighting the contribution to the sensitivity from the SS sample. The uncertainty due to the limited size of the simulated signal and background samples includes both the impact of the signal samples size on m_t-dependent templates used for the top mass interpolation, and the uncertainty of the backgrounds due to the limited size of the corresponding MC samples. This includes the multijet background, which is estimated with a data control sample. The uncertainty in the combined 2015–2016 integrated luminosity is 2.1% [18], obtained using the LUCID-2 detector [109] for the primary luminosity measurements. The distribution of the average number of interactions per bunch crossing (pile-up activity) in each MC sample

JHEP06(2023)019

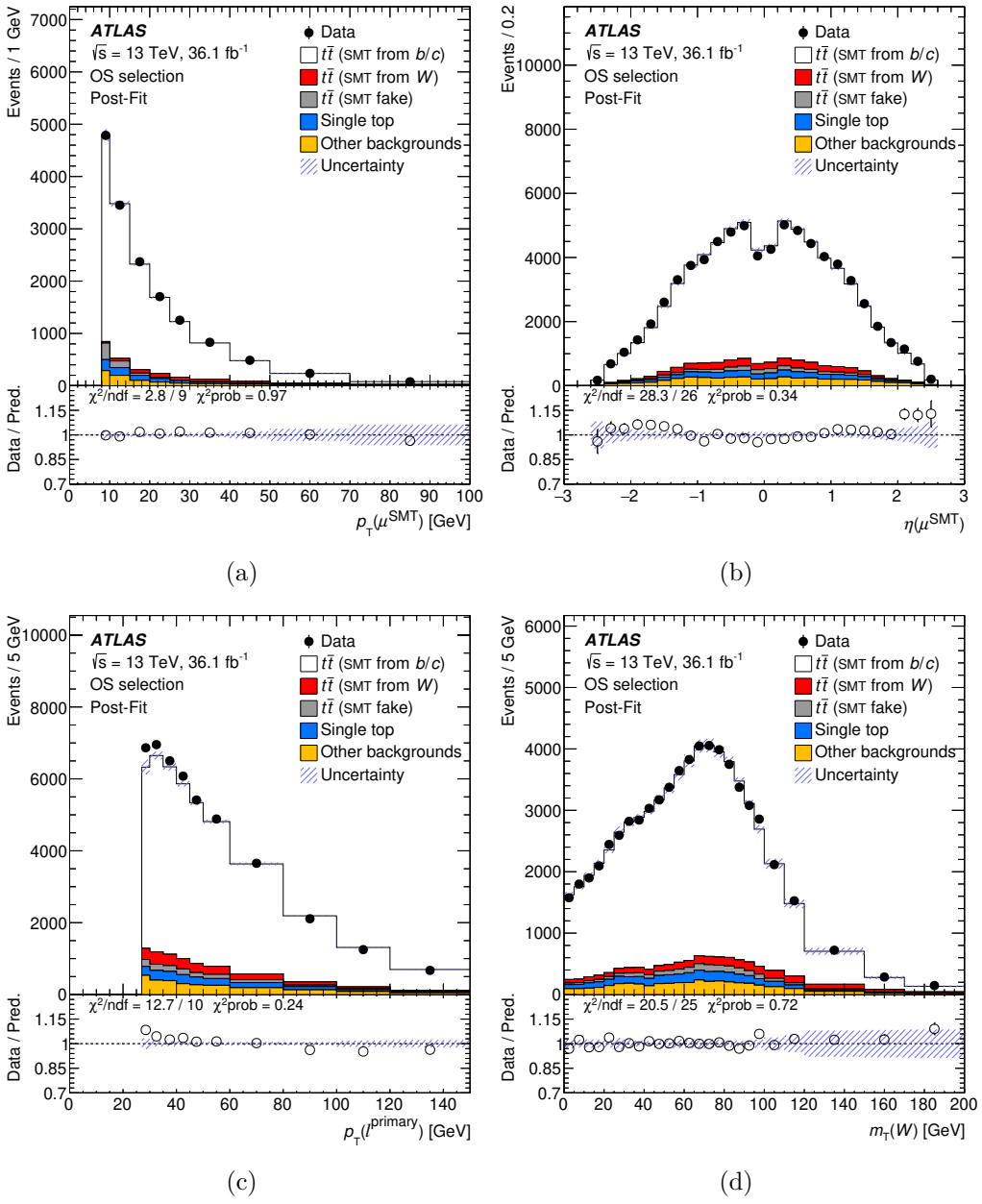

Figure 7. Post-fit comparison of data and prediction in the OS sample, i.e. for events with primary lepton and the soft muon with opposite charges, for the (a) soft muon p_{T}, (b) soft muon η, (c) primary lepton p_{T} and (d) W-boson transverse mass. The prediction reports the event contribution for the signal and backgrounds. The uncertainty band includes statistical and systematic uncertainties, but does not include the recoil uncertainty.

JHEP06(2023)019

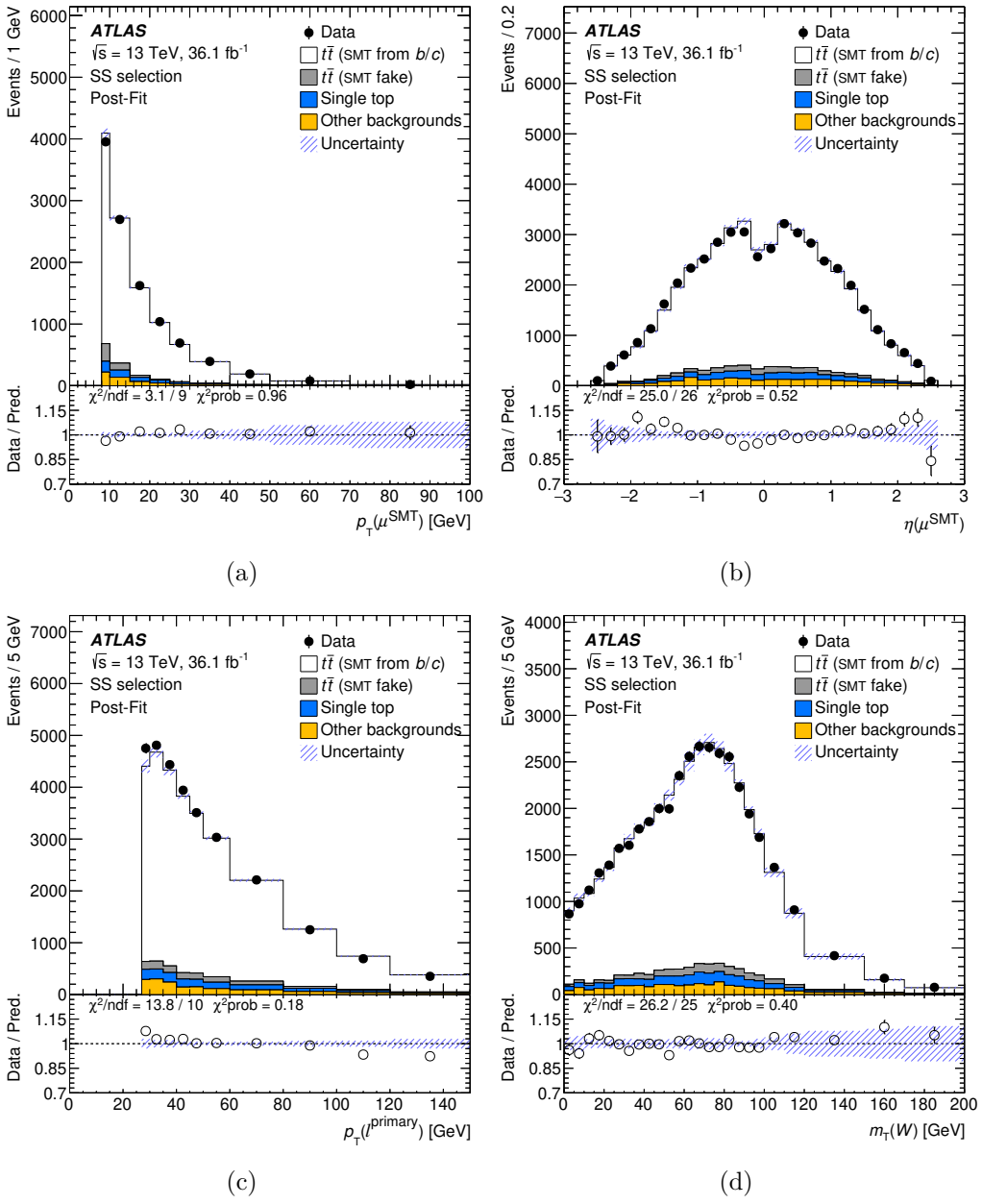

Figure 8. Post-fit comparison of data and prediction in the SS sample, i.e. for events with primary lepton and the soft muon with same charges, for the (a) soft muon p_{T}, (b) soft muon η, (c) primary lepton p_{T} and (d) W-boson transverse mass. The prediction reports the event contribution for the signal and backgrounds. The uncertainty band includes statistical and systematic uncertainties, but does not include the recoil uncertainty.

JHEP06(2023)019

Source	Unc. on m_t [GeV]	Stat. precision [GeV]
Statistical and datasets		
Data statistics	0.39	
Signal and background model statistics	0.17	
Luminosity	< 0.01	± 0.01
Pile-up	0.07	± 0.03
Modelling of signal processes		
Monte Carlo event generator	0.04	± 0.06
b, c-hadron production fractions	0.11	± 0.01
b, c-hadron decay BRs	0.40	± 0.01
b-quark fragmentation r_b	0.19	± 0.06
Parton shower α_S^{FSR}	0.07	± 0.04
Parton shower and hadronisation model	0.06	± 0.07
Initial-state QCD radiation	0.23	± 0.08
Colour reconnection	< 0.01	± 0.02
Choice of PDFs	0.07	± 0.01
Modelling of background processes		
Soft muon fake	0.16	± 0.03
Multijet	0.07	± 0.02
Single top	0.01	± 0.01
W/Z+jets	0.17	± 0.01
Detector response		
Leptons	0.12	± 0.01
Jet energy scale	0.13	± 0.02
Soft muon jet $\mathrm{p_T}$ calibration	< 0.01	± 0.01
Jet energy resolution	0.08	± 0.07
b-tagging	0.10	± 0.01
Missing transverse momentum	0.15	± 0.01
Total stat. and syst. uncertainties (excluding recoil)	0.77	± 0.03
Recoil uncertainty	0.25	
Total uncertainty	0.81	

Table 6. Impact of main sources of uncertainty on m_t. Each row of the table corresponds to a group of individual systematic variations. For each uncertainty source the fit is repeated with the corresponding group of nuisance parameters fixed to their best-fit values. The contribution from each source is then evaluated by subtracting in quadrature the uncertainty obtained in this fit from that of the full fit. The total systematic uncertainty is different from the sum in quadrature of the different groups due to correlations among nuisance parameters in the fit. The last column shows the statistical uncertainty on each of the top-quark mass uncertainties as estimated with the bootstrap method [108].

JHEP06(2023)019

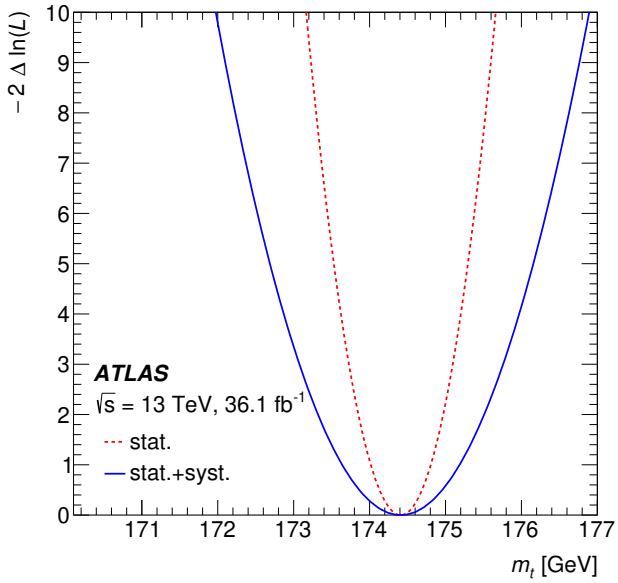

Figure 9. Likelihood scan, showing the best-fit value and the statistical and total uncertainty profiles (excluding the recoil uncertainty).

is reweighted to match the conditions in data, and a corresponding uncertainty is evaluated according to the uncertainty in the average number of interactions per bunch crossing.

5.2 Modelling of the signal process

Uncertainties in the $t\bar{t}$ signal modelling include all sources that affect the kinematics of the lepton from the W-boson decay and the kinematics of the b-hadron giving rise to the soft muon, and also the fraction of events from different soft-muon flavour components (from b-hadrons, c-hadrons, light jets and W-bosons). The $t\bar{t}$ inclusive cross-section uncertainty does not affect the measurement, since the fit is based only on the shape of the distribution from $t\bar{t}$ events after background subtraction.

Uncertainties that depend on the choice of NLO matching scheme in the $t\bar{t}$ MC generator are estimated by comparing a sample generated with Powheg+Pythia8 with a sample generated with MadGraph5_aMC@NLO+Pythia8 [110] (referred to hereafter as aMC@NLO+Pythia8). The aMC@NLO matching requires specific settings of the Pythia8 shower to retain the NLO accuracy. The matrix-element corrections are switched off for both initial-state radiation and the global-recoil settings that are used for final-state radiation emissions. These settings are different from the nominal Powheg+Pythia8. In order to have a coherent comparison, an alternative Powheg+Pythia8 sample was generated with the same Pythia8 configuration as that used to shower aMC@NLO events. Additionally, since aMC@NLO+Pythia8 is known to describe poorly the distribution of the boost of the $t\bar{t}$ system ($p_{\mathrm{T}}^{t\bar{t}}$) [111], the $p_{\mathrm{T}}^{t\bar{t}}$ in aMC@NLO+Pythia8 is reweighted to that of the Powheg+Pythia8 sample. The full difference between the top-quark masses

JHEP06(2023)019

obtained with the two samples is considered as the positive and negative uncertainty due to the MC generator NLO matching.

Uncertainties in the b-hadron production fractions and the BRs of the inclusive decays of b- and c-hadrons into muons are derived from the uncertainties in the rescaling procedure, described in section 3.4 and shown in tables 2 and 3. These uncertainties are propagated through the analysis. In addition, a check was performed to verify that the impact on $m_{\ell\mu}$ due to the different admixture of D-mesons involved in $b \to c\mu + X$ transitions was within the uncertainty assigned to $b \to \mu$ inclusive BRs. For this purpose, the exclusive decays $B^0 \to D^-\mu\nu$, $B^0 \to D^*(2010)^-\mu\nu$, $B^+ \to \overline{D^0}\mu\nu$, $B^+ \to \overline{D^*}(2007)^0\mu\nu$ and their charge conjugates were considered. For each of these decays, a kinematic selection similar to that of the main selection was applied to the events and the BR of each decay was varied within the uncertainty quoted by the PDG. The impact on $m_{\ell\mu}$ was found to be significantly smaller than the effect of varying only the BR of the inclusive $b \to \mu$ decays. The impact on $m_{\ell\mu}$ from the uncertainties in the $B^0_{(s)}$ mixing parameters is much smaller than the impact from imperfect knowledge of the b-hadron production fractions and from the heavy-quark hadrons BRs. Similarly, the impact of the modelling of the soft-muon kinematics in the exclusive semileptonic decays of b- and c-hadrons in EvtGen v1.2.0 was tested by varying the various BRs within their uncertainties. The total impact was found to be negligible with respect to the impact of the inclusive b-hadron production fractions and heavy-quark hadrons BRs uncertainties.

Uncertainties in the modelling of the parton shower and hadronisation processes include the estimation of several components. An alternative simulation of the $t\bar{t}$ sample is considered whereby the Powheg-Box generator is matched to the Herwig 7.1.3 generator for the modelling of the parton shower and hadronisation. The Herwig 7.1.3 generator release includes several improvements in the shower description for heavy-quark fragmentation, together with a new tune to e^+e^- data. The angle-ordered shower algorithm is preferred to the dipole shower for this sample, as it better describes both the shower evolution in the 7 TeV ATLAS measurement of jet shapes in $t\bar{t}$ events [112], and the x_B distribution of LEP data, although it does not describe the x_B spectrum of LEP data as well as Pythia8. The sample based on Herwig 7.1.3, when compared with the nominal $t\bar{t}$ simulation used in the fit, allows the effects of changes in the shower algorithm, and therefore in initial- and final-state emissions, to be assessed using alternative but coherent models of b-quark fragmentation and hadronisation, the underlying event and colour reconnection. The full difference between the top-quark masses obtained with the two samples of Powheg events showered with Pythia8 A14-r_b and Herwig 7.1.3 is considered as the positive and negative uncertainty from variations of the parton shower and hadronisation modelling.

To evaluate the uncertainty on the modelling of the b-quark fragmentation, additional samples were produced with the value of r_b in the fragmentation function varied by its uncertainty of ± 0.02. Additionally, the uncertainty on the choice of the renormalisation and factorisation scales in the final-state radiation (FSR) description of Pythia8 is evaluated using alternative simulated $t\bar{t}$ samples generated with the scale parameters explicitly[3] varied

[3]With explicit scale variations, dedicated alternative MC samples are generated with the $\mu_{R,F}$ scales

JHEP06(2023)019

up and down by factors of $\sqrt{2}$ [113]. For these alternative settings, the appropriate r_b values are determined following the same fit procedure described in section 3.4, in order to still correctly model the x_B distribution for LEP/SLD data. It must be noted that the x_B distribution will however be different for the $t\bar{t}$ samples with varied scales with respect to the nominal one, due to process-dependent effects. This uncertainty is labelled α_S^{FSR} in table 6.

As a check of the separate r_b and $\alpha_{\mathrm{S}}^{\mathrm{FSR}}$ uncertainties reported in table 6, a sample of Powheg events showered with Pythia using the Monash tune [79] (which has different values of α_{S} and r_b than the A14-r_b tune), is used to obtain an equivalent systematic uncertainty. The change in the measured top-quark mass obtained with this sample is 0.30 ± 0.06 GeV, consistent with the uncertainties associated with $\alpha_{\mathrm{S}}^{\mathrm{FSR}}$, r_b and the hadronisation model, listed in table 6.

In the modelling of the parton shower of the b-quark from $t \to Wb$ with Pythia 8.2, there is the possibility to change the default gluon recoil scheme from recoiling against the b-quark (the nominal setting, referred to here as RTB), to recoiling against the W-boson (recoilToColoured=off, referred to as RTW) [114]. Before Pythia version 8.160, the RTW was the only possibility, but it could give unphysical radiation patterns and it is now kept as an option to understand the effect this setting has in view of previous measurements. This setting changes the modelling of second and subsequent gluon emission from quarks produced by coloured resonance decays, such as the b-quark in a $t \to Wb$ process, but it has no impact for example on $Z \to b\bar{b}$ decays. A third recoil scheme has been recently made available via the UserHook functionality of Pythia 8.2 with the top-quark itself serving as recoiler for second and subsequent gluon emission of the b-quark (referred to as RTT).[4] The RTW and RTT setups give wider-angle gluon radiation, resulting in energy deposits that do not get clustered into the b-jet, and lower gluon-energy emission, altering the modelling of the b-quark fragmentation and hardening the b-hadron momenta. They also mildly change the W-boson p_T and the angle between the W-boson and the b-hadron resulting from the top-quark decay. The recently-developed RTT option has been considered as an additional uncertainty in the measurement, even though the implementation could only be performed based on particle-level simulation and without a dedicated tune that would normally accompany a change of setup of this nature. The change of the recoil model modifies the distribution of the momentum fraction of the b-hadron

$$x_B = \frac{1}{1 - m_W^2/m_t^2 + m_b^2/m_t^2} \frac{2p_B \cdot p_t}{m_t^2},$$

where m_w is the W-boson mass and p_t is the top four-momentum. However, the Mellin moments of this distribution derived with the RTB setup agree well with those predicted by the NLO+NLL resummation convoluted with the Kartvelishvili model tuned on ALEPH, OPAL and SLD data [80]. Therefore, the x_B distribution derived with the RTT shower is

modified in the parton shower settings, as opposed to the automated parton shower variations discussed in ref. [113], where weights are applied to the MC sample to obtain the systematic shifts. Explicitly changing $\mu_{R,F}$ by a factor $\sqrt{2}$ corresponds approximately to an automated variation of a factor 2, thanks to the implementation of the NLO compensation terms in the latter case.

[4]The code used for the RTT UserHook was provided by the Pythia authors directly.

JHEP06(2023)019

reweighted to that of the RTB simulation. The reweighting of x_B is a crude adjustment, since its distribution is controlled by the parameters of the fragmentation function and α_S^{FSR}, which are set in the A14-r_b Pythia tune, and bound by the universality of the b-quark fragmentation model. Closure tests demonstrated that the x_B reweighting provides the correct $m_{\ell\mu}$ distribution, and the correct extracted top mass, even though it does not fully address the modelling of other variables of the event. Overall, the analysis performed with the RTT shower setup as above yields a measured top-quark mass value which is larger than the one obtained with the nominal parton shower configuration by approximately 0.25 GeV. The less physically-motivated RTW setup has been also checked, and would have an effect at the same level as RTT. A one-sided shift of the measured top mass is seen with the RTT and RTW setups, but a symmetrised uncertainty of ± 0.25 GeV is assigned and indicated by "recoil". This uncertainty is considered outside of the profile likelihood fit, and quoted as a separate uncertainty on the result.

The uncertainty in the modelling of initial-state radiation (ISR) is estimated by using four variations: the first two are obtained by independently changing the Powheg ISR renormalisation and factorisation scales up and down by a factor 2.0, the third by comparing with an alternative sample obtained doubling the h_{damp} parameter with respect to the nominal settings, the fourth one corresponds to the `Var3c` up and down variations of the Pythia8 A14 tune [115].

The modelling of the underlying event and of colour reconnection (CR) can affect the amount of radiation emitted from the b-quark, as well as modify the kinematic distribution of the b-hadron. An underlying-event uncertainty is estimated using the corresponding eigentunes of the A14 Pythia8 tune. Variations of colour reconnection parameters are also provided by the A14 eigentunes, determined from measurements of the underlying event in jet production. Samples are generated where the colour reconnection strength in the Pythia8 default model is set to its maximum value (all hadrons are reconnected) and are compared with a setting with the colour reconnection switched off. To account for the possibility of colour reconnection also affecting the top-quark decay products, a comparison with the 'Early Resonance Decay' (ERD) model is performed [116]. In this model, the top-quarks and W-bosons are allowed to decay before CR takes place, so the top-quark decay products directly participate in CR. The impact on the measured top-quark mass is found to be negligible.

The systematic uncertainty due to the choice of PDFs is evaluated using the PDF4LHC15 error set [117] applied to the nominal $t\bar{t}$ MC settings, and is obtained by means of event reweighting for 30 PDF replicas. The m_t value is extracted for each of the 30 cases, and the total systematic uncertainty due to this effect is computed as the sum in quadrature of the single variations.

5.3 Modelling of background processes

Several sources of uncertainty are considered for the normalisation and shape of the background contributions. The relative uncertainty in the normalisation of the soft-muon component of $t\bar{t}$ events which arises from light-hadron decays and detector background ('Soft muon fake') is derived from the uncertainty in the calibration of the misidentification rate.

JHEP06(2023)019

An additional uncertainty is derived from the difference in shape and normalisation of the $m_{\ell\mu}$ distribution of SMT mistags between $t\bar{t}$ samples generated with Powheg+Pythia8 and Sherpa. For the $t\bar{t}$ dilepton component, uncertainties in the modelling of the ISR, in the NLO matching and in the parton shower and hadronisation model are estimated in the same way as for the nominal $t\bar{t}$ sample.

An uncertainty of $+5\%/-4\%$ is applied to the total cross-section for single top-quark production [72–74]. An additional uncertainty in the amount of initial- and final-state radiation is evaluated in a manner similar to that used for $t\bar{t}$. The uncertainty in the interference between Wt and $t\bar{t}$ production at NLO is assessed by comparing the default 'diagram removal' scheme with an alternative 'diagram subtraction' scheme [68]. The uncertainty in the event generator for the t-channel is evaluated by comparing it with a sample simulated with aMC@NLO+Pythia8. The uncertainty in the parton shower and hadronisation models for the t- and Wt-channels is derived from a comparison with samples showered with Herwig++. The impact of m_t variations on the single top-quark background has been found to yield negligible effects.

An uncertainty of 30% is applied to the Z+jets background normalisation, for both its light-flavour-jet and heavy-flavour-jet (Z+$c\bar{c}$ and Z+$b\bar{b}$) components. It was validated in a control region around the Z-boson mass peak, where the normalisations of the Z+light-jet and Z+heavy-flavour-jet are simultaneously extracted with a combined fit and are found to be in agreement with the theoretical expectation for Z+jets. The uncertainty in the normalisation and in the flavour composition of W+jets is assessed using data control regions. The total normalisation and flavour fraction uncertainty is about 22% for $Wb(b)$ and Wcc, approximately 45% for Wc, and about 23% for W+light-jets.

For the multijet background, a 30% systematic uncertainty is assigned to the predicted yields, based on comparisons with data yields in control regions similar to the signal region but enriched in events from the multijet background; the e+jet and μ+jet events are treated as uncorrelated. For the small diboson background, a 50% normalisation uncertainty is assigned and includes uncertainties in the inclusive cross-section and additional jet production [118].

5.4 Detector response

Uncertainties associated with leptons arise from the trigger, reconstruction, identification, and isolation requirements, as well as the lepton momentum scale and resolution. The reconstruction, identification and isolation efficiency for electrons and muons, as well as the efficiency of the trigger, differ slightly between data and simulation and are compensated for by dedicated SFs. Efficiency SFs are derived using data and simulated samples of $Z \to \ell^+\ell^-$ ($\ell = e, \mu$), and are applied to the simulation to correct for differences. The effect of uncertainties in these SFs is propagated through the analysis. The total uncertainty in efficiency SFs, for the high-p_{T} leptons, is $< 0.5\%$ for muons across the entire p_{T} spectrum [27] and for electrons with $p_{\mathrm{T}} > 30$ GeV, while it exceeds 1% for lower-p_{T} electrons [37]. The corresponding uncertainties are at the level of few per-mill for the momentum scale both for electrons and muons, and of 5–10% (4–7%) for the electron (muon) momentum resolution, strongly depending on the detector region and on the transverse momentum of the lepton.

JHEP06(2023)019

Additional sources of uncertainty originate from the uncertainty in the corrections applied to adjust the lepton momentum scale and resolution in the simulation to match those in data. They are measured using reconstructed $Z \to \ell^+\ell^-$ and $J/\psi \to \ell^+\ell^-$ dilepton invariant mass distributions [26, 27]. To evaluate the effect of momentum scale and resolution uncertainties, the analysis is repeated with the lepton momentum varied by $\pm 1\sigma$ and with the lepton momentum smeared, respectively. A systematic uncertainty due to the electron charge misidentification is taken from ref. [26]. Scale factors correcting for the differences in electron charge misidentification rates between data and simulation are computed using $Z \to e^+e^-$ events.

Uncertainties associated with jets arise from the efficiency of jet reconstruction and identification based on the JVT variable, as well as the JES and the jet energy resolution (JER). Although the observable $m_{\ell\mu}$ does not involve jets, the various jet uncertainties impact the analysis through the event selection. The JES and its uncertainty were derived by combining information from test-beam data, LHC collision data and simulation [22]. The JES uncertainty is about 5.5% for jets with $p_{\mathrm{T}} = 25$ GeV and decreases quickly with increasing jet p_{T}. It is below 1.5% for central jets with p_{T} in the range of approximately 100 GeV to 1.5 TeV. The highest-p_{T} jet in this analysis has an average p_{T} of around 130 GeV, with a typical range between 50 GeV and 450 GeV. The uncertainty from the soft muon jet p_{T} calibration affects the measured top-quark mass marginally, through the event selection. The magnitude of the JER uncertainty variation is parameterised in jet p_{T} and η [119], and the uncertainty is propagated by smearing the jet p_{T} in the simulation. The uncertainty in the efficiency to pass the JVT requirement is evaluated by varying the scale factors within their uncertainties [28].

The efficiencies of DJ tagging in simulated samples are corrected to match efficiencies in data. Correction scale factors are derived for jets originating from b-, c- and light-quarks separately in dedicated calibration analyses [29, 120, 121]. For jets originating from b- and c-quarks, SFs are derived as a function of p_{T}, whereas the light-jet efficiency is scaled by p_{T}- and η-dependent factors. Uncertainties in the correction scale factors are estimated by varying each source of uncertainty up and down by one standard deviation and are taken as uncorrelated between b-jets, c-jets, and light-jets. The same SFs are verified to also be applicable to jets containing soft muons by repeating the calibration procedure on a dedicated sample of events. An additional set of MC-to-MC correction factors are introduced to account for the different parton shower and hadronisation model used in the calibration samples compared to those used in this analysis. Furthermore, the efficiency of tagging the hadronic decays of τ-leptons in simulation is treated in the same way as the efficiency of tagging c-jets, and a specific uncertainty is considered for this simplified approach. An additional check is performed by changing the event selection such that there is always a DJ tagged jet other than the SMT tagged jet in the event, and the measured top-quark mass is consistent with the value measured using the nominal event selection.

The $E_{\mathrm{T}}^{\mathrm{miss}}$ reconstruction is affected by uncertainties associated with lepton and jet energy scales and resolutions, which are appropriately propagated to the $E_{\mathrm{T}}^{\mathrm{miss}}$ calculation. Additional small uncertainties associated with the modelling of the underlying event, in

JHEP06(2023)019

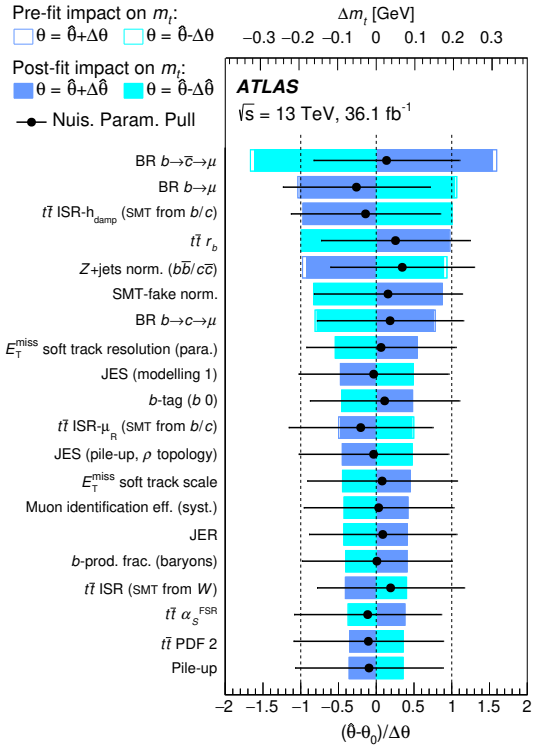

Figure 10. Ranking, from top to bottom, of the main systematic uncertainties (excluding recoil) showing the pulls and the impact of the systematic uncertainties on m_t, from the combined OS and SS binned-template profile likelihood fit to data. The θ's represent each systematic variation. The upper scale shows the uncertainty contribution to the measured top-quark mass. The PDF 2 is the set number 2 of the PDF4LHC15 error set [117].

particular its impact on the p_{T} scale and resolution of unclustered energy, are also taken into account [23].

The total systematic uncertainty is computed from the variance (σ^2) difference between the total uncertainty returned by the fit and the data statistics uncertainty. The plot in figure 10 shows the ranking of the main systematic uncertainties, including the pulls and the impact of constraining the systematic uncertainties. Uncertainties in figure 10 are from the individual nuisance parameters. They may be included within a grouped category in table 6. The leading uncertainties are due to the modelling of the b-quark fragmentation b-hadron and decay. In particular, the BRs for direct and sequential decays are important because the SMT muon p_{T} is softer when it is produced from c-hadrons in a cascade b-hadron decay, than when it comes directly from a semileptonic b-hadron decay. The BRs also impact the charge-signs combination of the primary lepton and the soft muon. Nearly all of the main systematic uncertainties are largely uncorrelated with those dominant in previous top-quark direct reconstruction measurements [9], and the uncertainty from jet energy calibration is sub-dominant with a value of ±0.13 GeV.

JHEP06(2023)019

6 Conclusions

A direct measurement of the top-quark mass has been performed using a technique that exploits a partial, leptonic-only, invariant mass reconstruction of the top-quark decay products. The analysis uses data corresponding to an integrated luminosity of 36.1 fb^{-1} of $\sqrt{s} = 13$ TeV pp collisions provided by the Large Hadron Collider and recorded by the ATLAS detector, and is based on the invariant mass, $m_{\ell\mu}$, of the lepton ℓ (with $\ell = e, \mu$) from the W-boson decay and the muon μ from a semileptonic decay of a b-hadron. A binned-template profile likelihood fit to the $m_{\ell\mu}$ distribution is performed to determine the most probable top-quark mass value. The result, $m_t = 174.41 \pm 0.39$ (stat.) ± 0.66 (syst.) ± 0.25 (recoil) GeV, corresponds to the most precise single measurement to date of the top-quark mass from the direct reconstruction of its decay products by the ATLAS Collaboration, and more precise than those performed previously with similar techniques [7, 8]. The third uncertainty arises from using a recently developed setup of the Pythia8 parton shower gluon-recoil scheme in top quark decays.

Taking into account the correlation between uncertainties, the result is consistent at the level of approximately two standard deviations with the current ATLAS combination of top-quark mass measurements from the reconstruction of the top-quark decay [9]. A similar level of consistency is found with the equivalent combination at CMS [10], while agreement with the latest Tevatron combination [11] is good. Agreement within one standard deviation is also found with the indirect prediction of the top-quark mass from global electroweak fits [12]. The main sources of systematic uncertainty are due to the modelling of top-quark pair production and b-quark fragmentation and decay, with uncertainties from backgrounds also being significant. On the other hand, the uncertainty due to the calibration of the jet energies is sub-dominant, which is advantageous in future combinations of this result with those from the standard reconstruction of the top-quark decay products.

Acknowledgments

We thank CERN for the very successful operation of the LHC, as well as the support staff from our institutions without whom ATLAS could not be operated efficiently.

We acknowledge the support of ANPCyT, Argentina; YerPhI, Armenia; ARC, Australia; BMWFW and FWF, Austria; ANAS, Azerbaijan; CNPq and FAPESP, Brazil; NSERC, NRC and CFI, Canada; CERN; ANID, Chile; CAS, MOST and NSFC, China; Minciencias, Colombia; MEYS CR, Czech Republic; DNRF and DNSRC, Denmark; IN2P3-CNRS and CEA-DRF/IRFU, France; SRNSFG, Georgia; BMBF, HGF and MPG, Germany; GSRI, Greece; RGC and Hong Kong SAR, China; ISF and Benoziyo Center, Israel; INFN, Italy; MEXT and JSPS, Japan; CNRST, Morocco; NWO, Netherlands; RCN, Norway; MEiN, Poland; FCT, Portugal; MNE/IFA, Romania; MESTD, Serbia; MSSR, Slovakia; ARRS and MIZŠ, Slovenia; DSI/NRF, South Africa; MICINN, Spain; SRC and Wallenberg Foundation, Sweden; SERI, SNSF and Cantons of Bern and Geneva, Switzerland; MOST, Taiwan; TENMAK, Türkiye; STFC, United Kingdom; DOE and NSF, United States of America. In addition, individual groups and members have received support from BCKDF,

JHEP06(2023)019

CANARIE, Compute Canada and CRC, Canada; PRIMUS 21/SCI/017 and UNCE SCI/013, Czech Republic; COST, ERC, ERDF, Horizon 2020 and Marie Skłodowska-Curie Actions, European Union; Investissements d'Avenir Labex, Investissements d'Avenir Idex and ANR, France; DFG and AvH Foundation, Germany; Herakleitos, Thales and Aristeia programmes co-financed by EU-ESF and the Greek NSRF, Greece; BSF-NSF and MINERVA, Israel; Norwegian Financial Mechanism 2014–2021, Norway; NCN and NAWA, Poland; La Caixa Banking Foundation, CERCA Programme Generalitat de Catalunya and PROMETEO and GenT Programmes Generalitat Valenciana, Spain; Göran Gustafssons Stiftelse, Sweden; The Royal Society and Leverhulme Trust, United Kingdom.

The crucial computing support from all WLCG partners is acknowledged gratefully, in particular from CERN, the ATLAS Tier-1 facilities at TRIUMF (Canada), NDGF (Denmark, Norway, Sweden), CC-IN2P3 (France), KIT/GridKA (Germany), INFN-CNAF (Italy), NL-T1 (Netherlands), PIC (Spain), ASGC (Taiwan), RAL (UK) and BNL (USA), the Tier-2 facilities worldwide and large non-WLCG resource providers. Major contributors of computing resources are listed in ref. [122].

Open Access. This article is distributed under the terms of the Creative Commons Attribution License (CC-BY 4.0), which permits any use, distribution and reproduction in any medium, provided the original author(s) and source are credited. SCOAP^3 supports the goals of the International Year of Basic Sciences for Sustainable Development.

References

[1] Particle Data Group collaboration, *Review of Particle Physics*, *Phys. Rev. D* **98** (2018) 030001 [INSPIRE].

[2] G. Degrassi et al., *Higgs mass and vacuum stability in the Standard Model at NNLO*, *JHEP* **08** (2012) 098 [arXiv:1205.6497] [INSPIRE].

[3] S. Alekhin, A. Djouadi and S. Moch, *The top quark and Higgs boson masses and the stability of the electroweak vacuum*, *Phys. Lett. B* **716** (2012) 214 [arXiv:1207.0980] [INSPIRE].

[4] P. Nason, *The Top Mass in Hadronic Collisions*, arXiv:1712.02796 [INSPIRE].

[5] G. Corcella, *The top-quark mass: challenges in definition and determination*, *Front. in Phys.* **7** (2019) 54 [arXiv:1903.06574] [INSPIRE].

[6] ATLAS collaboration, *Measurement of lepton differential distributions and the top quark mass in $t\bar{t}$ production in pp collisions at $\sqrt{s} = 8$ TeV with the ATLAS detector*, *Eur. Phys. J. C* **77** (2017) 804 [arXiv:1709.09407] [INSPIRE].

[7] CDF collaboration, *Measurement of the Top Quark Mass Using the Invariant Mass of Lepton Pairs in Soft Muon b-tagged Events*, *Phys. Rev. D* **80** (2009) 051104 [arXiv:0906.5371] [INSPIRE].

[8] CMS collaboration, *Measurement of the mass of the top quark in decays with a J/ψ meson in pp collisions at 8 TeV*, *JHEP* **12** (2016) 123 [arXiv:1608.03560] [INSPIRE].

[9] ATLAS collaboration, *Measurement of the top quark mass in the $t\bar{t} \to$ lepton+jets channel from $\sqrt{s} = 8$ TeV ATLAS data and combination with previous results*, *Eur. Phys. J. C* **79** (2019) 290 [arXiv:1810.01772] [INSPIRE].

JHEP06(2023)019

[10] CMS collaboration, *Measurement of the top quark mass using proton-proton data at* $\sqrt{(s)} = 7$ *and* 8 *TeV*, *Phys. Rev. D* **93** (2016) 072004 [arXiv:1509.04044] [INSPIRE].

[11] CDF and D0 collaborations, *Combination of CDF and D0 results on the mass of the top quark using up to* $9.7 fb^{-1}$ *at the Tevatron*, arXiv:1608.01881 [INSPIRE].

[12] J. Haller et al., *Update of the global electroweak fit and constraints on two-Higgs-doublet models*, *Eur. Phys. J. C* **78** (2018) 675 [arXiv:1803.01853] [INSPIRE].

[13] ATLAS collaboration, *The ATLAS Experiment at the CERN Large Hadron Collider*, 2008 *JINST* **3** S08003 [INSPIRE].

[14] ATLAS collaboration, *ATLAS Insertable B-Layer Technical Design Report*, CERN-LHCC-2010-013 (2010).

[15] ATLAS IBL collaboration, *Production and Integration of the ATLAS Insertable B-Layer*, 2018 *JINST* **13** T05008 [arXiv:1803.00844] [INSPIRE].

[16] ATLAS collaboration, *Performance of the ATLAS Trigger System in 2015*, *Eur. Phys. J. C* **77** (2017) 317 [arXiv:1611.09661] [INSPIRE].

[17] ATLAS collaboration, *The ATLAS Collaboration Software and Firmware*, ATL-SOFT-PUB-2021-001, CERN, Geneva (2021).

[18] ATLAS collaboration, *Luminosity determination in pp collisions at* $\sqrt{s} = 13$ *TeV using the ATLAS detector at the LHC*, ATLAS-CONF-2019-021, CERN, Geneva (2019).

[19] ATLAS collaboration, *Topological cell clustering in the ATLAS calorimeters and its performance in LHC Run 1*, *Eur. Phys. J. C* **77** (2017) 490 [arXiv:1603.02934] [INSPIRE].

[20] M. Cacciari, G.P. Salam and G. Soyez, *The anti-*k_t *jet clustering algorithm*, *JHEP* **04** (2008) 063 [arXiv:0802.1189] [INSPIRE].

[21] M. Cacciari, G.P. Salam and G. Soyez, *FastJet User Manual*, *Eur. Phys. J. C* **72** (2012) 1896 [arXiv:1111.6097] [INSPIRE].

[22] ATLAS collaboration, *Jet energy scale measurements and their systematic uncertainties in proton-proton collisions at* $\sqrt{s} = 13$ *TeV with the ATLAS detector*, *Phys. Rev. D* **96** (2017) 072002 [arXiv:1703.09665] [INSPIRE].

[23] ATLAS collaboration, *Performance of missing transverse momentum reconstruction with the ATLAS detector using proton-proton collisions at* $\sqrt{s} = 13$ *TeV*, *Eur. Phys. J. C* **78** (2018) 903 [arXiv:1802.08168] [INSPIRE].

[24] ATLAS collaboration, *Performance of electron and photon triggers in ATLAS during LHC Run 2*, *Eur. Phys. J. C* **80** (2020) 47 [arXiv:1909.00761] [INSPIRE].

[25] ATLAS collaboration, *Performance of the ATLAS muon triggers in Run 2*, 2020 *JINST* **15** P09015 [arXiv:2004.13447] [INSPIRE].

[26] ATLAS collaboration, *Electron reconstruction and identification in the ATLAS experiment using the 2015 and 2016 LHC proton-proton collision data at* $\sqrt{s} = 13$ *TeV*, *Eur. Phys. J. C* **79** (2019) 639 [arXiv:1902.04655] [INSPIRE].

[27] ATLAS collaboration, *Muon reconstruction performance of the ATLAS detector in proton-proton collision data at* $\sqrt{s} = 13$ *TeV*, *Eur. Phys. J. C* **76** (2016) 292 [arXiv:1603.05598] [INSPIRE].

[28] ATLAS collaboration, *Performance of pile-up mitigation techniques for jets in pp collisions at* $\sqrt{s} = 8$ *TeV using the ATLAS detector*, *Eur. Phys. J. C* **76** (2016) 581 [arXiv:1510.03823] [INSPIRE].

JHEP06(2023)019

[29] ATLAS collaboration, *Measurements of b-jet tagging efficiency with the ATLAS detector using $t\bar{t}$ events at $\sqrt{s} = 13$ TeV*, *JHEP* **08** (2018) 089 [arXiv:1805.01845] [INSPIRE].

[30] ATLAS collaboration, *The ATLAS Simulation Infrastructure*, *Eur. Phys. J. C* **70** (2010) 823 [arXiv:1005.4568] [INSPIRE].

[31] GEANT4 collaboration, *GEANT4 — a simulation toolkit*, *Nucl. Instrum. Meth. A* **506** (2003) 250 [INSPIRE].

[32] C. ATLAS et al., *The simulation principle and performance of the ATLAS fast calorimeter simulation FastCaloSim*, ATL-PHYS-PUB-2010-013, CERN, Geneva (2010).

[33] T. Sjöstrand, S. Mrenna and P.Z. Skands, *A Brief Introduction to PYTHIA 8.1*, *Comput. Phys. Commun.* **178** (2008) 852 [arXiv:0710.3820] [INSPIRE].

[34] A.D. Martin, W.J. Stirling, R.S. Thorne and G. Watt, *Parton distributions for the LHC*, *Eur. Phys. J. C* **63** (2009) 189 [arXiv:0901.0002] [INSPIRE].

[35] A.D. Martin, W.J. Stirling, R.S. Thorne and G. Watt, *Uncertainties on α_S in global PDF analyses and implications for predicted hadronic cross sections*, *Eur. Phys. J. C* **64** (2009) 653 [arXiv:0905.3531] [INSPIRE].

[36] ATLAS collaboration, *Summary of ATLAS Pythia 8 tunes*, ATL-PHYS-PUB-2012-003, CERN, Geneva (2012).

[37] ATLAS collaboration, *Electron and photon energy calibration with the ATLAS detector using 2015-2016 LHC proton-proton collision data*, 2019 *JINST* **14** P03017 [arXiv:1812.03848] [INSPIRE].

[38] ATLAS collaboration, *Measurements of charge and CP asymmetries in b-hadron decays using top-quark events collected by the ATLAS detector in pp collisions at $\sqrt{s} = 8$ TeV*, *JHEP* **02** (2017) 071 [arXiv:1610.07869] [INSPIRE].

[39] ATLAS collaboration, *Measurements of normalized differential cross sections for $t\bar{t}$ production in pp collisions at $\sqrt{s} = 7$ TeV using the ATLAS detector*, *Phys. Rev. D* **90** (2014) 072004 [arXiv:1407.0371] [INSPIRE].

[40] S. Frixione, P. Nason and G. Ridolfi, *A positive-weight next-to-leading-order Monte Carlo for heavy flavour hadroproduction*, *JHEP* **09** (2007) 126 [arXiv:0707.3088] [INSPIRE].

[41] P. Nason, *A new method for combining NLO QCD with shower Monte Carlo algorithms*, *JHEP* **11** (2004) 040 [hep-ph/0409146] [INSPIRE].

[42] S. Alioli, P. Nason, C. Oleari and E. Re, *A general framework for implementing NLO calculations in shower Monte Carlo programs: the POWHEG BOX*, *JHEP* **06** (2010) 043 [arXiv:1002.2581] [INSPIRE].

[43] NNPDF collaboration, *Parton distributions for the LHC Run II*, *JHEP* **04** (2015) 040 [arXiv:1410.8849] [INSPIRE].

[44] J. Gao, C.S. Li and H.X. Zhu, *Top Quark Decay at Next-to-Next-to Leading Order in QCD*, *Phys. Rev. Lett.* **110** (2013) 042001 [arXiv:1210.2808] [INSPIRE].

[45] S. Frixione, E. Laenen, P. Motylinski and B.R. Webber, *Angular correlations of lepton pairs from vector boson and top quark decays in Monte Carlo simulations*, *JHEP* **04** (2007) 081 [hep-ph/0702198] [INSPIRE].

[46] ATLAS collaboration, *ATLAS Pythia 8 tunes to 7 TeV data*, ATL-PHYS-PUB-2014-021, CERN, Geneva (2014).

[47] D.J. Lange, *The EvtGen particle decay simulation package*, *Nucl. Instrum. Meth. A* **462** (2001) 152 [INSPIRE].

JHEP06(2023)019

[48] M. Czakon and A. Mitov, *Top++: A Program for the Calculation of the Top-Pair Cross-Section at Hadron Colliders*, *Comput. Phys. Commun.* **185** (2014) 2930 [arXiv:1112.5675] [INSPIRE].

[49] M. Cacciari et al., *Top-pair production at hadron colliders with next-to-next-to-leading logarithmic soft-gluon resummation*, *Phys. Lett. B* **710** (2012) 612 [arXiv:1111.5869] [INSPIRE].

[50] P. Bärnreuther, M. Czakon and A. Mitov, *Percent Level Precision Physics at the Tevatron: First Genuine NNLO QCD Corrections to $q\bar{q} \to t\bar{t} + X$*, *Phys. Rev. Lett.* **109** (2012) 132001 [arXiv:1204.5201] [INSPIRE].

[51] M. Czakon and A. Mitov, *NNLO corrections to top-pair production at hadron colliders: the all-fermionic scattering channels*, *JHEP* **12** (2012) 054 [arXiv:1207.0236] [INSPIRE].

[52] M. Czakon and A. Mitov, *NNLO corrections to top pair production at hadron colliders: the quark-gluon reaction*, *JHEP* **01** (2013) 080 [arXiv:1210.6832] [INSPIRE].

[53] M. Czakon, P. Fiedler and A. Mitov, *Total Top-Quark Pair-Production Cross Section at Hadron Colliders Through $O(\alpha_S^4)$*, *Phys. Rev. Lett.* **110** (2013) 252004 [arXiv:1303.6254] [INSPIRE].

[54] ATLAS collaboration, *Estimation of non-prompt and fake lepton backgrounds in final states with top quarks produced in proton-proton collisions at $\sqrt{s} = 8$ TeV with the ATLAS Detector*, ATLAS-CONF-2014-058, CERN, Geneva (2014).

[55] SHERPA collaboration, *Event Generation with Sherpa 2.2*, *SciPost Phys.* **7** (2019) 034 [arXiv:1905.09127] [INSPIRE].

[56] T. Gleisberg and S. Hoeche, *Comix, a new matrix element generator*, *JHEP* **12** (2008) 039 [arXiv:0808.3674] [INSPIRE].

[57] OPENLOOPS 2 collaboration, *OpenLoops 2*, *Eur. Phys. J. C* **79** (2019) 866 [arXiv:1907.13071] [INSPIRE].

[58] F. Cascioli, P. Maierhöfer and S. Pozzorini, *Scattering Amplitudes with Open Loops*, *Phys. Rev. Lett.* **108** (2012) 111601 [arXiv:1111.5206] [INSPIRE].

[59] A. Denner, S. Dittmaier and L. Hofer, *Collier: a fortran-based Complex One-Loop LIbrary in Extended Regularizations*, *Comput. Phys. Commun.* **212** (2017) 220 [arXiv:1604.06792] [INSPIRE].

[60] S. Schumann and F. Krauss, *A parton shower algorithm based on Catani-Seymour dipole factorisation*, *JHEP* **03** (2008) 038 [arXiv:0709.1027] [INSPIRE].

[61] S. Hoeche, F. Krauss, M. Schönherr and F. Siegert, *A critical appraisal of NLO+PS matching methods*, *JHEP* **09** (2012) 049 [arXiv:1111.1220] [INSPIRE].

[62] S. Hoeche, F. Krauss, M. Schönherr and F. Siegert, *QCD matrix elements + parton showers: The NLO case*, *JHEP* **04** (2013) 027 [arXiv:1207.5030] [INSPIRE].

[63] S. Catani, F. Krauss, R. Kuhn and B.R. Webber, *QCD matrix elements + parton showers*, *JHEP* **11** (2001) 063 [hep-ph/0109231] [INSPIRE].

[64] S. Hoeche, F. Krauss, S. Schumann and F. Siegert, *QCD matrix elements and truncated showers*, *JHEP* **05** (2009) 053 [arXiv:0903.1219] [INSPIRE].

[65] C. Anastasiou, L.J. Dixon, K. Melnikov and F. Petriello, *High precision QCD at hadron colliders: Electroweak gauge boson rapidity distributions at NNLO*, *Phys. Rev. D* **69** (2004) 094008 [hep-ph/0312266] [INSPIRE].

JHEP06(2023)019

[66] ATLAS collaboration, *Measurements of differential cross sections of top quark pair production in association with jets in pp collisions at $\sqrt{s} = 13$ TeV using the ATLAS detector*, *JHEP* **10** (2018) 159 [arXiv:1802.06572] [INSPIRE].

[67] H.-L. Lai et al., *New parton distributions for collider physics*, *Phys. Rev. D* **82** (2010) 074024 [arXiv:1007.2241] [INSPIRE].

[68] S. Frixione et al., *Single-top hadroproduction in association with a W boson*, *JHEP* **07** (2008) 029 [arXiv:0805.3067] [INSPIRE].

[69] T. Sjöstrand, S. Mrenna and P.Z. Skands, *PYTHIA 6.4 Physics and Manual*, *JHEP* **05** (2006) 026 [hep-ph/0603175] [INSPIRE].

[70] J. Pumplin et al., *New generation of parton distributions with uncertainties from global QCD analysis*, *JHEP* **07** (2002) 012 [hep-ph/0201195] [INSPIRE].

[71] P.Z. Skands, *Tuning Monte Carlo Generators: The Perugia Tunes*, *Phys. Rev. D* **82** (2010) 074018 [arXiv:1005.3457] [INSPIRE].

[72] N. Kidonakis, *Two-loop soft anomalous dimensions for single top quark associated production with a W^- or H^-*, *Phys. Rev. D* **82** (2010) 054018 [arXiv:1005.4451] [INSPIRE].

[73] N. Kidonakis, *NNLL resummation for s-channel single top quark production*, *Phys. Rev. D* **81** (2010) 054028 [arXiv:1001.5034] [INSPIRE].

[74] N. Kidonakis, *Next-to-next-to-leading-order collinear and soft gluon corrections for t-channel single top quark production*, *Phys. Rev. D* **83** (2011) 091503 [arXiv:1103.2792] [INSPIRE].

[75] M. Bähr et al., *Herwig++ Physics and Manual*, *Eur. Phys. J. C* **58** (2008) 639 [arXiv:0803.0883] [INSPIRE].

[76] J. Bellm et al., *Herwig 7.0/Herwig++ 3.0 release note*, *Eur. Phys. J. C* **76** (2016) 196 [arXiv:1512.01178] [INSPIRE].

[77] B. Andersson, G. Gustafson, G. Ingelman and T. Sjöstrand, *Parton Fragmentation and String Dynamics*, *Phys. Rept.* **97** (1983) 31 [INSPIRE].

[78] M.G. Bowler, *e^+e^- Production of heavy quarks in the string model*, *Z. Phys. C* **11** (1981) 169 [INSPIRE].

[79] P. Skands, S. Carrazza and J. Rojo, *Tuning PYTHIA 8.1: the Monash 2013 Tune*, *Eur. Phys. J. C* **74** (2014) 3024 [arXiv:1404.5630] [INSPIRE].

[80] G. Corcella and V. Drollinger, *Bottom-quark fragmentation: Comparing results from tuned event generators and resummed calculations*, *Nucl. Phys. B* **730** (2005) 82 [hep-ph/0508013] [INSPIRE].

[81] G. Corcella and F. Mescia, *A Phenomenological Study of Bottom Quark Fragmentation in Top Quark Decay*, *Eur. Phys. J. C* **65** (2010) 171 [arXiv:0907.5158] [INSPIRE].

[82] G. Corcella and F. Mescia, *Erratum to: A Phenomenological Study of Bottom Quark Fragmentation in Top Quark Decay*, *Eur. Phys. J. C* **68** (2010) 687.

[83] G. Corcella, R. Franceschini and D. Kim, *Fragmentation Uncertainties in Hadronic Observables for Top-quark Mass Measurements*, *Nucl. Phys. B* **929** (2018) 485 [arXiv:1712.05801] [INSPIRE].

[84] ALEPH collaboration, *Study of the fragmentation of b quarks into B mesons at the Z peak*, *Phys. Lett. B* **512** (2001) 30 [hep-ex/0106051] [INSPIRE].

[85] DELPHI collaboration, *A study of the b-quark fragmentation function with the DELPHI detector at LEP I and an averaged distribution obtained at the Z Pole*, *Eur. Phys. J. C* **71** (2011) 1557 [arXiv:1102.4748] [INSPIRE].

JHEP06(2023)019

[86] OPAL collaboration, *Inclusive analysis of the b quark fragmentation function in Z decays at LEP*, *Eur. Phys. J. C* **29** (2003) 463 [hep-ex/0210031] [INSPIRE].

[87] SLD collaboration, *Precise measurement of the b quark fragmentation function in Z0 boson decays*, *Phys. Rev. Lett.* **84** (2000) 4300 [hep-ex/9912058] [INSPIRE].

[88] C. Bierlich et al., *Robust Independent Validation of Experiment and Theory: Rivet version 3*, *SciPost Phys.* **8** (2020) 026 [arXiv:1912.05451] [INSPIRE].

[89] ATLAS collaboration, *Measurement of b-quark fragmentation properties in jets using the decay $B^{\pm} \to J/\psi K^{\pm}$ in pp collisions at $\sqrt{s} = 13$ TeV with the ATLAS detector*, *JHEP* **12** (2021) 131 [arXiv:2108.11650] [INSPIRE].

[90] ATLAS collaboration, *Measurements of jet observables sensitive to b-quark fragmentation in $t\bar{t}$ events at the LHC with the ATLAS detector*, *Phys. Rev. D* **106** (2022) 032008 [arXiv:2202.13901] [INSPIRE].

[91] HFLAV collaboration, *Averages of b-hadron, c-hadron, and τ-lepton properties as of summer 2014*, arXiv:1412.7515 [INSPIRE].

[92] E. Lohrmann, *A Summary of Charm Hadron Production Fractions*, arXiv:1112.3757 [INSPIRE].

[93] LHCb collaboration, *Evidence for modification of b quark hadronization in high-multiplicity pp collisions at $\sqrt{s} = 13$ TeV*, arXiv:2204.13042 [INSPIRE].

[94] LHCb collaboration, *Measurement of the fragmentation fraction ratio f_s/f_d and its dependence on B meson kinematics*, *JHEP* **04** (2013) 001 [arXiv:1301.5286] [INSPIRE].

[95] LHCb collaboration, *Measurement of f_s/f_u Variation with Proton-Proton Collision Energy and B-Meson Kinematics*, *Phys. Rev. Lett.* **124** (2020) 122002 [arXiv:1910.09934] [INSPIRE].

[96] LHCb collaboration, *Precise measurement of the f_s/f_d ratio of fragmentation fractions and of B^0_s decay branching fractions*, *Phys. Rev. D* **104** (2021) 032005 [arXiv:2103.06810] [INSPIRE].

[97] LHCb collaboration, *Measurement of b-hadron production fractions in* 7 TeV *pp collisions*, *Phys. Rev. D* **85** (2012) 032008 [arXiv:1111.2357] [INSPIRE].

[98] LHCb collaboration, *Measurement of b hadron fractions in 13 TeV pp collisions*, *Phys. Rev. D* **100** (2019) 031102 [arXiv:1902.06794] [INSPIRE].

[99] ALICE collaboration, *Charm-quark fragmentation fractions and production cross section at midrapidity in pp collisions at the LHC*, *Phys. Rev. D* **105** (2022) L011103 [arXiv:2105.06335] [INSPIRE].

[100] DELPHI collaboration, *Measurement of the semileptonic b branching fractions and average b mixing parameter in Z decays*, *Eur. Phys. J. C* **20** (2001) 455 [hep-ex/0105080] [INSPIRE].

[101] LEP Electroweak Working Group and the SLD Heavy Flavour and Electroweak Groups, *Final input parameters for the LEP/SLD heavy flavour analyses*, DELPHI-2001-134 PHYS 908 (2001) [INSPIRE].

[102] CLEO collaboration, *Flavor-specific inclusive B decays to charm*, *Phys. Rev. Lett.* **80** (1998) 1150 [hep-ex/9710028] [INSPIRE].

[103] CLEO collaboration, *Measurements of $B \to D^+_s X$ decays*, *Phys. Rev. D* **53** (1996) 4734 [INSPIRE].

[104] CLEO collaboration, *Study of flavor tagged baryon production in B decay*, *Phys. Rev. D* **55** (1997) 13 [INSPIRE].

JHEP06(2023)019

[105] ALEPH collaboration, *Observation of doubly charmed B decays at LEP*, *Eur. Phys. J. C* **4** (1998) 387 [INSPIRE].

[106] K. Cranmer et al., *HistFactory: A tool for creating statistical models for use with RooFit and RooStats*, CERN-OPEN-2012-016, (2012).

[107] S. Baker and R.D. Cousins, *Clarification of the Use of Chi Square and Likelihood Functions in Fits to Histograms*, *Nucl. Instrum. Meth.* **221** (1984) 437 [INSPIRE].

[108] ATLAS collaboration, *Evaluating statistical uncertainties and correlations using the bootstrap method*, ATL-PHYS-PUB-2021-011, CERN, Geneva (2021).

[109] G. Avoni et al., *The new LUCID-2 detector for luminosity measurement and monitoring in ATLAS*, 2018 *JINST* **13** P07017 [INSPIRE].

[110] J. Alwall et al., *The automated computation of tree-level and next-to-leading order differential cross sections, and their matching to parton shower simulations*, *JHEP* **07** (2014) 079 [arXiv:1405.0301] [INSPIRE].

[111] ATLAS collaboration, *Measurements of top-quark pair differential and double-differential cross-sections in the ℓ+jets channel with pp collisions at $\sqrt{s} = 13$ TeV using the ATLAS detector*, *Eur. Phys. J. C* **79** (2019) 1028 [*Erratum ibid.* **80** (2020) 1092] [arXiv:1908.07305] [INSPIRE].

[112] ATLAS collaboration, *Measurement of jet shapes in top-quark pair events at $\sqrt{s} = 7$ TeV using the ATLAS detector*, *Eur. Phys. J. C* **73** (2013) 2676 [arXiv:1307.5749] [INSPIRE].

[113] S. Mrenna and P. Skands, *Automated Parton-Shower Variations in Pythia 8*, *Phys. Rev. D* **94** (2016) 074005 [arXiv:1605.08352] [INSPIRE].

[114] H. Brooks and P. Skands, *Coherent showers in decays of colored resonances*, *Phys. Rev. D* **100** (2019) 076006 [arXiv:1907.08980] [INSPIRE].

[115] ATLAS collaboration, *Simulation of top-quark production for the ATLAS experiment at $\sqrt{s} = 13$ TeV*, ATL-PHYS-PUB-2016-004, CERN, Geneva (2016).

[116] S. Argyropoulos and T. Sjöstrand, *Effects of color reconnection on $t\bar{t}$ final states at the LHC*, *JHEP* **11** (2014) 043 [arXiv:1407.6653] [INSPIRE].

[117] J. Butterworth et al., *PDF4LHC recommendations for LHC Run II*, *J. Phys. G* **43** (2016) 023001 [arXiv:1510.03865] [INSPIRE].

[118] ATLAS collaboration, *Multi-Boson Simulation for 13 TeV ATLAS Analyses*, ATL-PHYS-PUB-2016-002, CERN, Geneva (2016).

[119] ATLAS collaboration, *Jet Calibration and Systematic Uncertainties for Jets Reconstructed in the ATLAS Detector at $\sqrt{s} = 13$ TeV*, ATL-PHYS-PUB-2015-015, CERN, Geneva (2015).

[120] ATLAS collaboration, *Measurement of b-tagging Efficiency of c-jets in $t\bar{t}$ Events Using a Likelihood Approach with the ATLAS Detector*, ATLAS-CONF-2018-001, CERN, Geneva (2018).

[121] ATLAS collaboration, *Calibration of light-flavour b-jet mistagging rates using ATLAS proton-proton collision data at $\sqrt{s} = 13$ TeV*, ATLAS-CONF-2018-006, CERN, Geneva (2018).

[122] ATLAS collaboration, *ATLAS Computing Acknowledgements*, ATL-SOFT-PUB-2021-003, CERN, Geneva (2021).

JHEP06(2023)019

The ATLAS collaboration

G. Aad[103], B. Abbott[122], D.C. Abbott[104], A. Abed Abud[36], K. Abeling[55], D.K. Abhayasinghe[95], S.H. Abidi[159], O.S. AbouZeid[42], N.L. Abraham[149], H. Abramowicz[154], H. Abreu[153], Y. Abulaiti[6], B.S. Acharya[69a,69b,o], B. Achkar[55], S. Adachi[156], L. Adam[101], C. Adam Bourdarios[5], L. Adamczyk[85a], L. Adamek[159], J. Adelman[117], M. Adersberger[110], A. Adiguzel[12c,ag], S. Adorni[56], T. Adye[136], A.A. Affolder[138], Y. Afik[153], C. Agapopoulou[67], M.N. Agaras[40], A. Aggarwal[115], C. Agheorghiesei[27c], J.A. Aguilar-Saavedra[132f,132a,af], F. Ahmadov[38,ad], W.S. Ahmed[105], X. Ai[18a], G. Aielli[76a,76b], S. Akatsuka[87], T.P.A. Åkesson[98], E. Akilli[56], A.V. Akimov[37], K. Al Khoury[67], G.L. Alberghi[23b], J. Albert[168], M.J. Alconada Verzini[154], S. Alderweireldt[36], M. Aleksa[36], I.N. Aleksandrov[38], C. Alexa[27b], T. Alexopoulos[10], A. Alfonsi[116], F. Alfonsi[23b,23a], M. Alhroob[122], B. Ali[134], M. Aliev[37], G. Alimonti[71a], C. Allaire[67], B.M.M. Allbrooke[149], B.W. Allen[125], P.P. Allport[21], A. Aloisio[72a,72b], F. Alonso[90], C. Alpigiani[141], A.A. Alshehri[59], E. Alunno Camelia[76a,76b], M. Alvarez Estevez[100], M.G. Alviggi[72a,72b], Y. Amaral Coutinho[82b], A. Ambler[105], L. Ambroz[128], C. Amelung[26], D. Amidei[107], S.P. Amor Dos Santos[132a], S. Amoroso[48], C.S. Amrouche[56], F. An[81], C. Anastopoulos[142], N. Andari[137], T. Andeen[11], C.F. Anders[63b], J.K. Anders[20], A. Andreazza[71a,71b], V. Andrei[63a], C.R. Anelli[168], S. Angelidakis[40], A. Angerami[41], A.V. Anisenkov[37], A. Annovi[74a], C. Antel[56], M.T. Anthony[142], E. Antipov[123], M. Antonelli[53], D.J.A. Antrim[163], F. Anulli[75a], M. Aoki[83], J.A. Aparisi Pozo[166], L. Aperio Bella[15a], J.P. Araque[132a], V. Araujo Ferraz[82b], R. Araujo Pereira[82b], C. Arcangeletti[53], A.T.H. Arce[51], F.A. Arduh[90], J-F. Arguin[109], S. Argyropoulos[54], J.-H. Arling[48], A.J. Armbruster[36], A. Armstrong[163], O. Arnaez[159], H. Arnold[116], Z.P. Arrubarrena Tame[110], G. Artoni[128], S. Artz[101], S. Asai[156], T. Asawatavonvanich[158], N.A. Asbah[61], E.M. Asimakopoulou[164], L. Asquith[149], J. Assahsah[35d], K. Assamagan[29], R. Astalos[28a], R.J. Atkin[33a], M. Atkinson[165], N.B. Atlay[19], H. Atmani[67], K. Augsten[134], G. Avolio[36], M.K. Ayoub[15a], G. Azuelos[109,ao], H. Bachacou[137], K. Bachas[70a,70b], M. Backes[128], F. Backman[47a,47b], P. Bagnaia[75a,75b], H. Bahrasemani[145], A.J. Bailey[166], V.R. Bailey[165], J.T. Baines[136], C. Bakalis[10], O.K. Baker[175], P.J. Bakker[116], D. Bakshi Gupta[8], S. Balaji[150], E.M. Baldin[37], P. Balek[172], F. Balli[137], W.K. Balunas[128], J. Balz[101], E. Banas[86], A. Bandyopadhyay[24], Sw. Banerjee[173,j], A.A.E. Bannoura[174], L. Barak[154], W.M. Barbe[40], E.L. Barberio[106], D. Barberis[57b,57a], M. Barbero[103], G. Barbour[96], T. Barillari[111], M-S. Barisits[36], J. Barkeloo[125], T. Barklow[146], R. Barnea[153], B.M. Barnett[136], R.M. Barnett[18a], Z. Barnovska-Blenessy[62a], A. Baroncelli[62a], G. Barone[29], A.J. Barr[128], L. Barranco Navarro[47a,47b], F. Barreiro[100], J. Barreiro Guimarães da Costa[15a], S. Barsov[37], R. Bartoldus[146], G. Bartolini[103], A.E. Barton[91], P. Bartos[28a], A. Basalaev[48], A. Basan[101], A. Bassalat[67,aj], M.J. Basso[159], R.L. Bates[59], S. Batlamous[35e], J.R. Batley[32], B. Batool[144], M. Battaglia[138], M. Bauce[75a,75b], F. Bauer[137,*], K.T. Bauer[163], H.S. Bawa[31], J.B. Beacham[51], T. Beau[129], P.H. Beauchemin[162], F. Becherer[54], P. Bechtle[24], H.C. Beck[55], H.P. Beck[20,r], K. Becker[170], C. Becot[48], A. Beddall[12d], A.J. Beddall[12a],

JHEP06(2023)019

V.A. Bednyakov[38], M. Bedognetti[116], C.P. Bee[148], T.A. Beermann[174], M. Begalli[82b], M. Begel[29], A. Behera[148], J.K. Behr[48], F. Beisiegel[24], A.S. Bell[96], G. Bella[154], L. Bellagamba[23b], A. Bellerive[34], P. Bellos[9], K. Beloborodov[37], K. Belotskiy[37], N.L. Belyaev[37], D. Benchekroun[35a], N. Benekos[10], Y. Benhammou[154], D.P. Benjamin[6], M. Benoit[56], J.R. Bensinger[26], S. Bentvelsen[116], L. Beresford[128], M. Beretta[53], D. Berge[19], E. Bergeaas Kuutmann[164], N. Berger[5], B. Bergmann[134], L.J. Bergsten[26], J. Beringer[18a], S. Berlendis[7], G. Bernardi[129], C. Bernius[146], F.U. Bernlochner[24], T. Berry[95], P. Berta[101], C. Bertella[15a], I.A. Bertram[91], O. Bessidskaia Bylund[174], N. Besson[137], A. Bethani[102], S. Bethke[111], A. Betti[44], A.J. Bevan[94], J. Beyer[111], D.S. Bhattacharya[169], P. Bhattarai[26], R. Bi[131], R.M. Bianchi[131], O. Biebel[110], D. Biedermann[19], R. Bielski[36], K. Bierwagen[101], N.V. Biesuz[74a,74b], M. Biglietti[77a], T.R.V. Billoud[109], M. Bindi[55], A. Bingul[12d], C. Bini[75a,75b], S. Biondi[23b,23a], M. Birman[172], T. Bisanz[55], D. Biswas[173,j], A. Bitadze[102], C. Bittrich[50], K. Bjørke[127], T. Blazek[28a], I. Bloch[48], C. Blocker[26], A. Blue[59], U. Blumenschein[94], G.J. Bobbink[116], V.S. Bobrovnikov[37], S.S. Bocchetta[98], A. Bocci[51], D. Bogavac[14], A.G. Bogdanchikov[37], C. Bohm[47a], V. Boisvert[95], P. Bokan[55], T. Bold[85a], A.E. Bolz[63b], M. Bomben[129], M. Bona[94], J.S. Bonilla[125], M. Boonekamp[137], C.D. Booth[95], H.M. Borecka-Bielska[92], L.S. Borgna[96], A. Borisov[37], G. Borissov[91], J. Bortfeldt[36], D. Bortoletto[128], D. Boscherini[23b], M. Bosman[14], J.D. Bossio Sola[105], K. Bouaouda[35a], J. Boudreau[131], E.V. Bouhova-Thacker[91], D. Boumediene[40], S.K. Boutle[59], A. Boveia[120], J. Boyd[36], D. Boye[33b,ak], I.R. Boyko[38], A.J. Bozson[95], J. Bracinik[21], N. Brahimi[103], G. Brandt[174], O. Brandt[32], F. Braren[48], B. Brau[104], J.E. Brau[125], W.D. Breaden Madden[59], K. Brendlinger[48], L. Brenner[48], R. Brenner[164], S. Bressler[172], B. Brickwedde[101], D.L. Briglin[21], D. Britton[59], D. Britzger[111], I. Brock[24], R. Brock[108], G. Brooijmans[41], W.K. Brooks[139c], E. Brost[29], J.H Broughton[21], P.A. Bruckman de Renstrom[86], D. Bruncko[28b,*], A. Bruni[23b], G. Bruni[23b], L.S. Bruni[116], S. Bruno[76a,76b], M. Bruschi[23b], N. Bruscino[75a,75b], P. Bryant[39], L. Bryngemark[98], T. Buanes[17], Q. Buat[36], P. Buchholz[144], A.G. Buckley[59], I.A. Budagov[38,*], M.K. Bugge[127], F. Bührer[54], O. Bulekov[37], T.J. Burch[117], S. Burdin[92], C.D. Burgard[116], A.M. Burger[123], B. Burghgrave[8], J.T.P. Burr[48], C.D. Burton[11], J.C. Burzynski[104], V. Büscher[101], E. Buschmann[55], P.J. Bussey[59], J.M. Butler[25], C.M. Buttar[59], J.M. Butterworth[96], P. Butti[36], W. Buttinger[36], C.J. Buxo Vazquez[108], A. Buzatu[151], A.R. Buzykaev[37], G. Cabras[23b,23a], S. Cabrera Urbán[166], D. Caforio[58], H. Cai[165], V.M.M. Cairo[146], O. Cakir[4a], N. Calace[36], P. Calafiura[18a], A. Calandri[103], G. Calderini[129], P. Calfayan[68], G. Callea[59], L.P. Caloba[82b], A. Caltabiano[76a,76b], S. Calvente Lopez[100], D. Calvet[40], S. Calvet[40], T.P. Calvet[148], M. Calvetti[74a,74b], R. Camacho Toro[129], S. Camarda[36], D. Camarero Munoz[100], P. Camarri[76a,76b], D. Cameron[127], C. Camincher[36], S. Campana[36], M. Campanelli[96], A. Camplani[42], A. Campoverde[144], V. Canale[72a,72b], A. Canesse[105], M. Cano Bret[62c], J. Cantero[123], T. Cao[154], Y. Cao[165], M.D.M. Capeans Garrido[36], M. Capua[43b,43a], R. Cardarelli[76a], F. Cardillo[142], I. Carli[135], T. Carli[36], G. Carlino[72a], B.T. Carlson[131], L. Carminati[71a,71b], R.M.D. Carney[146], S. Caron[115], E. Carquin[139c], S. Carrá[48], J.W.S. Carter[159], M.P. Casado[14,f], A.F. Casha[159], D.W. Casper[163], R. Castelijn[116],

JHEP06(2023)019

F.L. Castillo[166], L. Castillo Garcia[14], V. Castillo Gimenez[166], N.F. Castro[132a,132e], A. Catinaccio[36], J.R. Catmore[127], A. Cattai[36], V. Cavaliere[29], E. Cavallaro[14], M. Cavalli-Sforza[14], V. Cavasinni[74a,74b], E. Celebi[12b], L. Cerda Alberich[166], K. Cerny[124], A.S. Cerqueira[82a], A. Cerri[149], L. Cerrito[76a,76b], F. Cerutti[18a], A. Cervelli[23b], S.A. Cetin[12b], Z. Chadi[35a], D. Chakraborty[117], J. Chan[173], W.S. Chan[116], W.Y. Chan[92], J.D. Chapman[32], B. Chargeishvili[152b], D.G. Charlton[21], T.P. Charman[94], C.C. Chau[34], S. Che[120], S. Chekanov[6], S.V. Chekulaev[160a], G.A. Chelkov[38,a], B. Chen[81], C. Chen[62a], C.H. Chen[81], H. Chen[29], J. Chen[62a], J. Chen[41], J. Chen[26], S. Chen[130], S.J. Chen[15c], X. Chen[15b,an], Y-H. Chen[48], H.C. Cheng[65a], H.J. Cheng[15a], A. Cheplakov[38], E. Cheremushkina[37], R. Cherkaoui El Moursli[35e], E. Cheu[7], K. Cheung[66], T.J.A. Chevalérias[137], L. Chevalier[137], V. Chiarella[53], G. Chiarelli[74a], G. Chiodini[70a], A.S. Chisholm[21], A. Chitan[27b], I. Chiu[156], Y.H. Chiu[168], M.V. Chizhov[38], K. Choi[11], A.R. Chomont[75a,75b], S. Chouridou[155], E.Y.S. Chow[116], M.C. Chu[65a], X. Chu[15a,15d], J. Chudoba[133], J.J. Chwastowski[86], L. Chytka[124], D. Cieri[111], K.M. Ciesla[86], D. Cinca[49], V. Cindro[93], I.A. Cioară[27b], A. Ciocio[18a], F. Cirotto[72a,72b], Z.H. Citron[172,k], M. Citterio[71a], D.A. Ciubotaru[27b], B.M. Ciungu[159], A. Clark[56], M.R. Clark[41], P.J. Clark[52], C. Clement[47a,47b], Y. Coadou[103], M. Cobal[69a,69c], A. Coccaro[57b], J. Cochran[81], R. Coelho Lopes De Sa[104], H. Cohen[154], A.E.C. Coimbra[36], B. Cole[41], A.P. Colijn[116], J. Collot[60], P. Conde Muiño[132a,132h], S.H. Connell[33b], I.A. Connelly[59], S. Constantinescu[27b], F. Conventi[72a,ap], A.M. Cooper-Sarkar[128], G. Corcella[53], F. Cormier[167], K.J.R. Cormier[159], L.D. Corpe[96], M. Corradi[75a,75b], E.E. Corrigan[98], F. Corriveau[105,ac], M.J. Costa[166], F. Costanza[5], D. Costanzo[142], G. Cowan[95], J.W. Cowley[32], J. Crane[102], K. Cranmer[118], S.J. Crawley[59], R.A. Creager[130], S. Crépé-Renaudin[60], F. Crescioli[129], M. Cristinziani[24], V. Croft[162], G. Crosetti[43b,43a], A. Cueto[5], T. Cuhadar Donszelmann[142], A.R. Cukierman[146], W.R. Cunningham[59], S. Czekierda[86], P. Czodrowski[36], M.J. Da Cunha Sargedas De Sousa[62b], J.V. Da Fonseca Pinto[82b], C. Da Via[102], W. Dabrowski[85a], F. Dachs[36], T. Dado[28a], S. Dahbi[33d], T. Dai[107], C. Dallapiccola[104], M. Dam[42], G. D'amen[29], V. D'Amico[77a,77b], J. Damp[101], J.R. Dandoy[130], M.F. Daneri[30], N.S. Dann[102], M. Danninger[145], V. Dao[36], G. Darbo[57b], O. Dartsi[5], A. Dattagupta[125], T. Daubney[48], S. D'Auria[71a,71b], C. David[160b], T. Davidek[135], D.R. Davis[51], I. Dawson[142], K. De[8], R. De Asmundis[72a], M. De Beurs[116], S. De Castro[23b,23a], S. De Cecco[75a,75b], N. De Groot[115], P. de Jong[116], H. De la Torre[108], A. De Maria[15c], D. De Pedis[75a], A. De Salvo[75a], U. De Sanctis[76a,76b], M. De Santis[76a,76b], A. De Santo[149], K. De Vasconcelos Corga[103], J.B. De Vivie De Regie[67], C. Debenedetti[138], D.V. Dedovich[38], A.M. Deiana[44], J. Del Peso[100], Y. Delabat Diaz[48], D. Delgove[67], F. Deliot[137,q], C.M. Delitzsch[7], M. Della Pietra[72a,72b], D. Della Volpe[56], A. Dell'Acqua[36], L. Dell'Asta[76a,76b], M. Delmastro[5], C. Delporte[67], P.A. Delsart[60], D.A. DeMarco[159], S. Demers[175], M. Demichev[38], G. Demontigny[109], S.P. Denisov[37], L. D'Eramo[129], D. Derendarz[86], J.E. Derkaoui[35d], F. Derue[129], P. Dervan[92], K. Desch[24], C. Deterre[48], K. Dette[159], C. Deutsch[24], M.R. Devesa[30], P.O. Deviveiros[36], F.A. Di Bello[56], A. Di Ciaccio[76a,76b], L. Di Ciaccio[5], W.K. Di Clemente[130], C. Di Donato[72a,72b], A. Di Girolamo[36], G. Di Gregorio[74a,74b], B. Di Micco[77a,77b],

JHEP06(2023)019

R. Di Nardo[77a,77b], K.F. Di Petrillo[61], R. Di Sipio[159], C. Diaconu[103], F.A. Dias[42], T. Dias Do Vale[132a], M.A. Diaz[139a], J. Dickinson[18a], E.B. Diehl[107], J. Dietrich[19], S. Díez Cornell[48], A. Dimitrievska[18a], W. Ding[15b], J. Dingfelder[24], F. Dittus[36], F. Djama[103], T. Djobava[152b], J.I. Djuvsland[17], M.A.B. Do Vale[140], M. Dobre[27b], D. Dodsworth[26], C. Doglioni[98], J. Dolejsi[135], Z. Dolezal[135], M. Donadelli[82c], B. Dong[62c], J. Donini[40], A. D'Onofrio[15c], M. D'Onofrio[92], J. Dopke[136], A. Doria[72a], M.T. Dova[90], A.T. Doyle[59], E. Drechsler[145], E. Dreyer[145], T. Dreyer[55], A.S. Drobac[162], D. Du[62b], Y. Duan[62b], F. Dubinin[37], M. Dubovsky[28a], A. Dubreuil[56], E. Duchovni[172], G. Duckeck[110], A. Ducourthial[129], O.A. Ducu[109], D. Duda[111], A. Dudarev[36], A.C. Dudder[101], E.M. Duffield[18a], L. Duflot[67], M. Dührssen[36], C. Dülsen[174], M. Dumancic[172], A.E. Dumitriu[27b], A.K. Duncan[59], M. Dunford[63a], A. Duperrin[103], H. Duran Yildiz[4a], M. Düren[58], A. Durglishvili[152b], D. Duschinger[50], B. Dutta[48], B.L. Dwyer[117], G.I. Dyckes[130], M. Dyndal[36], S. Dysch[102], B.S. Dziedzic[86], K.M. Ecker[111], M.G. Eggleston[51], T. Eifert[8], G. Eigen[17], K. Einsweiler[18a], T. Ekelof[164], H. El Jarrari[35e], R. El Kosseifi[103], V. Ellajosyula[164], M. Ellert[164], F. Ellinghaus[174], A.A. Elliot[94], N. Ellis[36], J. Elmsheuser[29], M. Elsing[36], D. Emeliyanov[136], A. Emerman[41], Y. Enari[156], M.B. Epland[51], J. Erdmann[49], A. Ereditato[20], P.A. Erland[86], M. Errenst[36], M. Escalier[67], C. Escobar[166], O. Estrada Pastor[166], E. Etzion[154], H. Evans[68], A. Ezhilov[37], F. Fabbri[59], L. Fabbri[23b,23a], V. Fabiani[115], G. Facini[170], R.M. Faisca Rodrigues Pereira[132a], R.M. Fakhrutdinov[37], S. Falciano[75a], P.J. Falke[5], S. Falke[5], J. Faltova[135], Y. Fang[15a], Y. Fang[15a,15d], G. Fanourakis[46], M. Fanti[71a,71b], M. Faraj[69a,69c,s], A. Farbin[8], A. Farilla[77a], E.M. Farina[73a,73b], T. Farooque[108], S.M. Farrington[52], P. Farthouat[36], F. Fassi[35e], P. Fassnacht[36], D. Fassouliotis[9], M. Faucci Giannelli[52], W.J. Fawcett[32], L. Fayard[67], O.L. Fedin[37,a], W. Fedorko[167], M. Feickert[165], L. Feligioni[103], A. Fell[142], C. Feng[62b], M. Feng[51], M.J. Fenton[163], A.B. Fenyuk[37], S.W. Ferguson[45], J. Ferrando[48], A. Ferrante[165], A. Ferrari[164], P. Ferrari[116], R. Ferrari[73a], D.E. Ferreira de Lima[63b], A. Ferrer[166], D. Ferrere[56], C. Ferretti[107], F. Fiedler[101], A. Filipčič[93], F. Filthaut[115], K.D. Finelli[25], M.C.N. Fiolhais[132a,132c,b], L. Fiorini[166], F. Fischer[110], W.C. Fisher[108], I. Fleck[144], P. Fleischmann[107], T. Flick[174], B.M. Flierl[110], L. Flores[130], L.R. Flores Castillo[65a], F.M. Follega[78a,78b], N. Fomin[17], J.H. Foo[159], G.T. Forcolin[78a,78b], A. Formica[137], F.A. Förster[14], A.C. Forti[102], A.G. Foster[21], M.G. Foti[128], D. Fournier[67], H. Fox[91], P. Francavilla[74a,74b], S. Francescato[75a,75b], M. Franchini[23b,23a], S. Franchino[63a], D. Francis[36], L. Franconi[20], M. Franklin[61], A.N. Fray[94], P.M. Freeman[21], B. Freund[109], W.S. Freund[82b], E.M. Freundlich[49], D.C. Frizzell[122], D. Froidevaux[36], J.A. Frost[128], C. Fukunaga[157], E. Fullana Torregrosa[166,*], T. Fusayasu[112], J. Fuster[166], A. Gabrielli[23b,23a], A. Gabrielli[18a], S. Gadatsch[56], P. Gadow[111], G. Gagliardi[57b,57a], L.G. Gagnon[109], B. Galhardo[132a], G.E. Gallardo[128], E.J. Gallas[128], B.J. Gallop[136], G. Galster[42], R. Gamboa Goni[94], K.K. Gan[120], S. Ganguly[172], J. Gao[62a], Y. Gao[52], Y.S. Gao[31,m], C. García[166], J.E. García Navarro[166], J.A. García Pascual[15a], C. Garcia-Argos[54], M. Garcia-Sciveres[18a], R.W. Gardner[39], S. Gargiulo[54], C.A. Garner[159], V. Garonne[127], S.J. Gasiorowski[141], P. Gaspar[82b], A. Gaudiello[57b,57a], G. Gaudio[73a], I.L. Gavrilenko[37], A. Gavrilyuk[37], C. Gay[167], G. Gaycken[48], E.N. Gazis[10],

JHEP06(2023)019

A.A. Geanta[27b], C.M. Gee[138], C.N.P. Gee[136], J. Geisen[98], M. Geisen[101], C. Gemme[57b], M.H. Genest[60], C. Geng[107], S. Gentile[75a,75b], S. George[95], T. Geralis[46], L.O. Gerlach[55], P. Gessinger-Befurt[101], G. Gessner[49], S. Ghasemi[144], M. Ghasemi Bostanabad[168], M. Ghneimat[144], A. Ghosh[67], A. Ghosh[80], B. Giacobbe[23b], S. Giagu[75a,75b], N. Giangiacomi[23b,23a], P. Giannetti[74a], A. Giannini[72a,72b], G. Giannini[14], S.M. Gibson[95], M. Gignac[138], D. Gillberg[34], G. Gilles[174], D.M. Gingrich[3,ao], M.P. Giordani[69a,69c], P.F. Giraud[137], G. Giugliarelli[69a,69c], D. Giugni[71a], F. Giuli[76a,76b], S. Gkaitatzis[155], I. Gkialas[9,h], E.L. Gkougkousis[14], P. Gkountoumis[10], L.K. Gladilin[37], C. Glasman[100], J. Glatzer[14], P.C.F. Glaysher[48], A. Glazov[48], G.R. Gledhill[125], M. Goblirsch-Kolb[26], D. Godin[109], S. Goldfarb[106], T. Golling[56], D. Golubkov[37], A. Gomes[132a,132b], R. Goncalves Gama[55], R. Gonçalo[132a], G. Gonella[125], L. Gonella[21], A. Gongadze[38], F. Gonnella[21], J.L. Gonski[41], S. González de la Hoz[166], S. Gonzalez Fernandez[14], S. Gonzalez-Sevilla[56], G.R. Gonzalvo Rodriguez[166], L. Goossens[36], N.A. Gorasia[21], P.A. Gorbounov[37], B. Gorini[36], E. Gorini[70a,70b], A. Gorišek[93], A.T. Goshaw[51], M.I. Gostkin[38], C.A. Gottardo[115], M. Gouighri[35b], A.G. Goussiou[141], N. Govender[33b], C. Goy[5], E. Gozani[153], I. Grabowska-Bold[85a], E.C. Graham[92], J. Gramling[163], E. Gramstad[127], S. Grancagnolo[19], M. Grandi[149], V. Gratchev[37,*], P.M. Gravila[27f], F.G. Gravili[70a,70b], C. Gray[59], H.M. Gray[18a], C. Grefe[24], K. Gregersen[98], I.M. Gregor[48], P. Grenier[146], K. Grevtsov[48], C. Grieco[14], N.A. Grieser[122], A.A. Grillo[138], K. Grimm[31,l], S. Grinstein[14,x], J.-F. Grivaz[67], S. Groh[101], E. Gross[172], J. Grosse-Knetter[55], Z.J. Grout[96], C. Grud[107], A. Grummer[114], L. Guan[107], W. Guan[173], C. Gubbels[167], J. Guenther[36], A. Guerguichon[67], J.G.R. Guerrero Rojas[166], F. Guescini[111], R. Gugel[54], T. Guillemin[5], S. Guindon[36], U. Gul[59], J. Guo[62c], W. Guo[107], Y. Guo[62a], Z. Guo[103], R. Gupta[48], S. Gurbuz[12c], G. Gustavino[122], M. Guth[54], P. Gutierrez[122], C. Gutschow[96], C. Guyot[137], C. Gwenlan[128], C.B. Gwilliam[92], A. Haas[118], C. Haber[18a], H.K. Hadavand[8], A. Hadef[62a], M. Haleem[169], J. Haley[123], G. Halladjian[108], G.D. Hallewell[103], K. Hamacher[174], P. Hamal[124], K. Hamano[168], H. Hamdaoui[35e], M. Hamer[24], G.N. Hamity[52], K. Han[62a,v], L. Han[62a], S. Han[15a], Y.F. Han[159], K. Hanagaki[83], M. Hance[138], D.M. Handl[110], B. Haney[130], R. Hankache[129], E. Hansen[98], J.B. Hansen[42], J.D. Hansen[42], M.C. Hansen[24], P.H. Hansen[42], E.C. Hanson[102], K. Hara[161], T. Harenberg[174], S. Harkusha[37], P.F. Harrison[170], N.M. Hartmann[110], Y. Hasegawa[143], A. Hasib[52], S. Hassani[137], S. Haug[20], R. Hauser[108], L.B. Havener[41], M. Havranek[134], C.M. Hawkes[21], R.J. Hawkings[36], D. Hayden[108], C. Hayes[107], R.L. Hayes[167], C.P. Hays[128], J.M. Hays[94], H.S. Hayward[92], S.J. Haywood[136], F. He[62a], M.P. Heath[52], V. Hedberg[98], S. Heer[24], K.K. Heidegger[54], W.D. Heidorn[81], J. Heilman[34], S. Heim[48], T. Heim[18a], B. Heinemann[48,al], J.J. Heinrich[125], L. Heinrich[36], J. Hejbal[133], L. Helary[63b], A. Held[118], S. Hellesund[127], C.M. Helling[138], S. Hellman[47a,47b], C. Helsens[36], R.C.W. Henderson[91], Y. Heng[173], L. Henkelmann[63a], S. Henkelmann[167], A.M. Henriques Correia[36], H. Herde[26], V. Herget[169], Y. Hernández Jiménez[33d], H. Herr[101], M.G. Herrmann[110], T. Herrmann[50], G. Herten[54], R. Hertenberger[110], L. Hervas[36], T.C. Herwig[130], G.G. Hesketh[96], N.P. Hessey[160a], A. Higashida[156], S. Higashino[83], E. Higón-Rodriguez[166], K. Hildebrand[39], J.C. Hill[32], K.K. Hill[29], K.H. Hiller[48],

JHEP06(2023)019

S.J. Hillier[21], M. Hils[50], I. Hinchliffe[18a], F. Hinterkeuser[24], M. Hirose[126], S. Hirose[54], D. Hirschbuehl[174], B. Hiti[93], O. Hladik[133], D.R. Hlaluku[33d], X. Hoad[52], J. Hobbs[148], N. Hod[172], M.C. Hodgkinson[142], A. Hoecker[36], D. Hohn[54], D. Hohov[67], T. Holm[24], T.R. Holmes[39], M. Holzbock[110], L.B.A.H. Hommels[32], S. Honda[161], T.M. Hong[131], J.C. Honig[54], A. Hönle[111], B.H. Hooberman[165], W.H. Hopkins[6], Y. Horii[113], P. Horn[50], L.A. Horyn[39], S. Hou[151], A. Hoummada[35a], J. Howarth[102], J. Hoya[90], M. Hrabovsky[124], J. Hrdinka[79], I. Hristova[19], J. Hrivnac[67], A. Hrynevich[37], T. Hryn'ova[5], P.J. Hsu[66], S.-C. Hsu[141], Q. Hu[29], S. Hu[62c], Y.F. Hu[15a,15d], D.P. Huang[96], Y. Huang[62a], Y. Huang[15a], Z. Hubacek[134], F. Hubaut[103], M. Huebner[24], F. Huegging[24], T.B. Huffman[128], M. Huhtinen[36], R.F.H. Hunter[34], P. Huo[148], N. Huseynov[38,ad], J. Huston[108], J. Huth[61], R. Hyneman[107], S. Hyrych[28a], G. Iacobucci[56], G. Iakovidis[29], I. Ibragimov[144], L. Iconomidou-Fayard[67], P. Iengo[36], R. Ignazzi[42], O. Igonkina[116,z,*], R. Iguchi[156], T. Iizawa[56], Y. Ikegami[83], M. Ikeno[83], A. Ilg[20], N. Ilic[115,159,ac], F. Iltzsche[50], G. Introzzi[73a,73b], M. Iodice[77a], K. Iordanidou[160a], V. Ippolito[75a,75b], M.F. Isacson[164], M. Ishino[156], W. Islam[123], C. Issever[19,48], S. Istin[153], F. Ito[161], J.M. Iturbe Ponce[65a], R. Iuppa[78a,78b], A. Ivina[172], H. Iwasaki[83], J.M. Izen[45], V. Izzo[72a], P. Jacka[133], P. Jackson[1], R.M. Jacobs[24], B.P. Jaeger[145], V. Jain[2], G. Jäkel[174], K.B. Jakobi[101], K. Jakobs[54], T. Jakoubek[133], J. Jamieson[59], K.W. Janas[85a], R. Jansky[56], M. Janus[55], P.A. Janus[85a], G. Jarlskog[98], N. Javadov[38,ad], T. Javůrek[36], M. Javurkova[104], F. Jeanneau[137], L. Jeanty[125], J. Jejelava[152a,ae], A. Jelinskas[170], P. Jenni[54,c], N. Jeong[48], S. Jézéquel[5], H. Ji[173], J. Jia[148], H. Jiang[81], Y. Jiang[62a], Z. Jiang[146,p], S. Jiggins[54], F.A. Jimenez Morales[40], J. Jimenez Pena[111], S. Jin[15c], A. Jinaru[27b], O. Jinnouchi[158], H. Jivan[33d], P. Johansson[142], K.A. Johns[7], C.A. Johnson[68], R.W.L. Jones[91], S.D. Jones[149], S. Jones[7], T.J. Jones[92], J. Jongmanns[63a], P.M. Jorge[132a], J. Jovicevic[36], X. Ju[18a], J.J. Junggeburth[111], A. Juste Rozas[14,x], A. Kaczmarska[86], M. Kado[75a,75b], H. Kagan[120], M. Kagan[146], A. Kahn[41], C. Kahra[101], T. Kaji[171], E. Kajomovitz[153], C.W. Kalderon[29], A. Kaluza[101], A. Kamenshchikov[37], M. Kaneda[156], N.J. Kang[138], S. Kang[81], L. Kanjir[93], Y. Kano[113], V.A. Kantserov[37], J. Kanzaki[83], L.S. Kaplan[173], D. Kar[33d], K. Karava[128], M.J. Kareem[160b], S.N. Karpov[38], Z.M. Karpova[38], V. Kartvelishvili[91], A.N. Karyukhin[37], L. Kashif[173], A. Kastanas[47a,47b], C. Kato[62d,62c], J. Katzy[48], K. Kawade[143], K. Kawagoe[89], T. Kawaguchi[113], T. Kawamoto[137], G. Kawamura[55], E.F. Kay[168], V.F. Kazanin[37], R. Keeler[168], R. Kehoe[44], J.S. Keller[34], E. Kellermann[98], D. Kelsey[149], J.J. Kempster[21], J. Kendrick[21], K.E. Kennedy[41], O. Kepka[133], S. Kersten[174], B.P. Kerševan[93], S. Ketabchi Haghighat[159], M. Khader[165], F. Khalil-Zada[13], M. Khandoga[137], A. Khanov[123], A.G. Kharlamov[37], T. Kharlamova[37], E.E. Khoda[167], A. Khodinov[37], T.J. Khoo[56], J. Khubua[152b], S. Kido[84], M. Kiehn[56], C.R. Kilby[95], E. Kim[158], Y.K. Kim[39], N. Kimura[96], O.M. Kind[19], B.T. King[92,*], D. Kirchmeier[50], J. Kirk[136], A.E. Kiryunin[111], T. Kishimoto[156], D.P. Kisliuk[159], V. Kitali[48], O. Kivernyk[5], T. Klapdor-Kleingrothaus[54], M. Klassen[63a], C. Klein[32], M.H. Klein[107], M. Klein[92], U. Klein[92], K. Kleinknecht[101], P. Klimek[117], A. Klimentov[29], T. Klingl[24], T. Klioutchnikova[36], F.F. Klitzner[110], P. Kluit[116], S. Kluth[111], E. Kneringer[79], E.B.F.G. Knoops[103], A. Knue[54], D. Kobayashi[89], T. Kobayashi[156], M. Kobel[50],

JHEP06(2023)019

M. Kocian[146], T. Kodama[156], P. Kodyš[135], P.T. Koenig[24], T. Koffas[34], N.M. Köhler[36], M. Kolb[137], I. Koletsou[5], T. Komarek[124], T. Kondo[83], K. Köneke[54], A.X.Y. Kong[1], A.C. König[115], T. Kono[119], R. Konoplich[118,ai], V. Konstantinides[96], N. Konstantinidis[96], B. Konya[98], R. Kopeliansky[68], S. Koperny[85a], K. Korcyl[86], K. Kordas[155], G. Koren[154], A. Korn[96], I. Korolkov[14], E.V. Korolkova[142], N. Korotkova[37], O. Kortner[111], S. Kortner[111], T. Kosek[135], V.V. Kostyukhin[142,37], A. Kotsokechagia[67], A. Kotwal[51], A. Koulouris[10], A. Kourkoumeli-Charalampidi[73a,73b], C. Kourkoumelis[9], E. Kourlitis[142], V. Kouskoura[29], A.B. Kowalewska[86], R. Kowalewski[168], W. Kozanecki[102], A.S. Kozhin[37], V.A. Kramarenko[37], G. Kramberger[93], D. Krasnopevtsev[62a], M.W. Krasny[129], A. Krasznahorkay[36], D. Krauss[111], J.A. Kremer[85a], J. Kretzschmar[92], P. Krieger[159], F. Krieter[110], A. Krishnan[63b], K. Krizka[18a], K. Kroeninger[49], H. Kroha[111], J. Kroll[133], J. Kroll[130], K.S. Krowpman[108], U. Kruchonak[38], H. Krüger[24], N. Krumnack[81], M.C. Kruse[51], J.A. Krzysiak[86], T. Kubota[106], O. Kuchinskaia[37], S. Kuday[4b], D. Kuechler[48], J.T. Kuechler[48], S. Kuehn[36], A. Kugel[63a], T. Kuhl[48], V. Kukhtin[38], R. Kukla[103], Y. Kulchitsky[37,a], S. Kuleshov[139c], Y.P. Kulinich[165], M. Kuna[60], T. Kunigo[87], A. Kupco[133], T. Kupfer[49], O. Kuprash[54], H. Kurashige[84], L.L. Kurchaninov[160a], Y.A. Kurochkin[37], A. Kurova[37], M.G. Kurth[15a,15d], E.S. Kuwertz[36], M. Kuze[158], A.K. Kvam[141], J. Kvita[124], T. Kwan[105], L. La Rotonda[43b,43a], F. La Ruffa[43b,43a], C. Lacasta[166], F. Lacava[75a,75b], D.P.J. Lack[102], H. Lacker[19], D. Lacour[129], E. Ladygin[38], R. Lafaye[5], B. Laforge[129], T. Lagouri[139b], S. Lai[55], I.K. Lakomiec[85a], S. Lammers[68], W. Lampl[7], C. Lampoudis[155], E. Lançon[29], U. Landgraf[54], M.P.J. Landon[94], M.C. Lanfermann[56], V.S. Lang[48], J.C. Lange[55], R.J. Langenberg[104], A.J. Lankford[163], F. Lanni[29], K. Lantzsch[24], A. Lanza[73a], A. Lapertosa[57b,57a], S. Laplace[129], J.F. Laporte[137], T. Lari[71a], F. Lasagni Manghi[23b], M. Lassnig[36], T.S. Lau[65a], A. Laudrain[67], A. Laurier[34], M. Lavorgna[72a,72b], S.D. Lawlor[95], M. Lazzaroni[71a,71b], B. Le[106], E. Le Guirriec[103], A. Lebedev[81], M. LeBlanc[7], T. LeCompte[6], F. Ledroit-Guillon[60], A.C.A. Lee[96], C.A. Lee[29], G.R. Lee[17], L. Lee[61], S.C. Lee[151], S. Lee[81], B. Lefebvre[160a], H.P. Lefebvre[95], M. Lefebvre[168], C. Leggett[18a], K. Lehmann[145], N. Lehmann[174], G. Lehmann Miotto[36], W.A. Leight[48], A. Leisos[155,u], M.A.L. Leite[82c], C.E. Leitgeb[110], R. Leitner[135], D. Lellouch[172,*], K.J.C. Leney[44], T. Lenz[24], R. Leone[7], S. Leone[74a], C. Leonidopoulos[52], A. Leopold[129], C. Leroy[109], R. Les[159], C.G. Lester[32], M. Levchenko[37], J. Levêque[5], D. Levin[107], L.J. Levinson[172], D.J. Lewis[21], B. Li[15b], B. Li[107], C-Q. Li[62a], F. Li[62c], H. Li[62a], H. Li[62b], J. Li[62c], K. Li[141], L. Li[62c], M. Li[15a,15d], Q. Li[15a,15d], Q.Y. Li[62a], S. Li[62d,62c], X. Li[48], Y. Li[48], Z. Li[62b], Z. Li[105], Z. Liang[15a], B. Liberti[76a], A. Liblong[159], K. Lie[65c], S. Lim[29], C.Y. Lin[32], K. Lin[108], T.H. Lin[101], R.A. Linck[68], J.H. Lindon[21], A.L. Lionti[56], E. Lipeles[130], A. Lipniacka[17], T.M. Liss[165,am], A. Lister[167], J.D. Little[8], B. Liu[81], B.X. Liu[6], H.B. Liu[29], H. Liu[107], J.B. Liu[62a], J.K.K. Liu[39], K. Liu[62d,62c], M. Liu[62a], P. Liu[15a], Y. Liu[48], Y. Liu[15a,15d], Y.L. Liu[107], Y.W. Liu[62a], M. Livan[73a,73b], A. Lleres[60], J. Llorente Merino[145], S.L. Lloyd[94], C.Y. Lo[65b], E.M. Lobodzinska[48], P. Loch[7], S. Loffredo[76a,76b], T. Lohse[19], K. Lohwasser[142], M. Lokajicek[133], J.D. Long[165], R.E. Long[91], L. Longo[36], K.A. Looper[120], J.A. Lopez[139c], I. Lopez Paz[102],

JHEP06(2023)019

A. Lopez Solis[142], J. Lorenz[110], N. Lorenzo Martinez[5], A.M. Lory[110], P.J. Lösel[110], A. Lösle[54], X. Lou[48], X. Lou[15a,15d], A. Lounis[67], J. Love[6], P.A. Love[91], J.J. Lozano Bahilo[166], M. Lu[62a], Y.J. Lu[66], H.J. Lubatti[141], C. Luci[75a,75b], A. Lucotte[60], C. Luedtke[54], F. Luehring[68], I. Luise[129], L. Luminari[75a], B. Lund-Jensen[147], M.S. Lutz[104], D. Lynn[29], H. Lyons[92], R. Lysak[133], E. Lytken[98], F. Lyu[15a], V. Lyubushkin[38], T. Lyubushkina[38], H. Ma[29], L.L. Ma[62b], Y. Ma[62b], G. Maccarrone[53], A. Macchiolo[111], C.M. Macdonald[142], J. Machado Miguens[130], D. Madaffari[166], R. Madar[40], W.F. Mader[50], M. Madugoda Ralalage Don[123], N. Madysa[50], J. Maeda[84], T. Maeno[29], M. Maerker[50], V. Magerl[54], N. Magini[81], D.J. Mahon[41], C. Maidantchik[82b], T. Maier[110], A. Maio[132a,132b,132d], K. Maj[85a], O. Majersky[28a], S. Majewski[125], Y. Makida[83], N. Makovec[67], B. Malaescu[129], Pa. Malecki[86], V.P. Maleev[37], F. Malek[60], U. Mallik[80], D. Malon[6], C. Malone[32], S. Maltezos[10], S. Malyukov[38], J. Mamuzic[166], G. Mancini[53], I. Mandić[93], L. Manhaes de Andrade Filho[82a], I.M. Maniatis[155], J. Manjarres Ramos[50], K.H. Mankinen[98], A. Mann[110], A. Manousos[79], B. Mansoulie[137], I. Manthos[155], S. Manzoni[116], A. Marantis[155,u], G. Marceca[30], L. Marchese[128], G. Marchiori[129], M. Marcisovsky[133], L. Marcoccia[76a,76b], C. Marcon[98], C.A. Marin Tobon[36], M. Marjanovic[122], Z. Marshall[18a], M.U.F. Martensson[164], S. Marti-Garcia[166], C.B. Martin[120], T.A. Martin[170], V.J. Martin[52], B. Martin dit Latour[17], L. Martinelli[77a,77b], M. Martinez[14,x], V.I. Martinez Outschoorn[104], S. Martin-Haugh[136], V.S. Martoiu[27b], A.C. Martyniuk[96], A. Marzin[36], S.R. Maschek[111], L. Masetti[101], T. Mashimo[156], R. Mashinistov[37], J. Masik[102], A.L. Maslennikov[37], L. Massa[23b], P. Massarotti[72a,72b], P. Mastrandrea[74a,74b], A. Mastroberardino[43b,43a], T. Masubuchi[156], D. Matakias[29], A. Matic[110], N. Matsuzawa[156], P. Mättig[24], J. Maurer[27b], B. Maček[93], D.A. Maximov[37], R. Mazini[151], I. Maznas[155], S.M. Mazza[138], S.P. Mc Kee[107], T.G. McCarthy[111], W.P. McCormack[18a], E.F. McDonald[106], J.A. Mcfayden[36], G. Mchedlidze[152b], M.A. McKay[44], K.D. McLean[168], S.J. McMahon[136], P.C. McNamara[106], C.J. McNicol[170], R.A. McPherson[168,ac], J.E. Mdhluli[33d], Z.A. Meadows[104], S. Meehan[36], T. Megy[54], S. Mehlhase[110], A. Mehta[92], T. Meideck[60], B. Meirose[45], D. Melini[153], B.R. Mellado Garcia[33d], J.D. Mellenthin[55], M. Melo[28a], F. Meloni[48], A. Melzer[24], S.B. Menary[102], E.D. Mendes Gouveia[132a,132e], L. Meng[36], X.T. Meng[107], S. Menke[111], E. Meoni[43b,43a], S. Mergelmeyer[19], S.A.M. Merkt[131], C. Merlassino[128], P. Mermod[56,*], L. Merola[72a,72b], C. Meroni[71a], G. Merz[107], O. Meshkov[37], J.K.R. Meshreki[144], A. Messina[75a,75b], J. Metcalfe[6], A.S. Mete[6], C. Meyer[68], J-P. Meyer[137], H. Meyer Zu Theenhausen[63a], F. Miano[149], M. Michetti[19], R.P. Middleton[136], L. Mijović[52], G. Mikenberg[172], M. Mikestikova[133], M. Mikuž[93], H. Mildner[142], M. Milesi[106], A. Milic[159], D.A. Millar[94], D.W. Miller[39], A. Milov[172], D.A. Milstead[47a,47b], R.A. Mina[146], A.A. Minaenko[37], M. Miñano Moya[166], I.A. Minashvili[152b], A.I. Mincer[118], B. Mindur[85a], M. Mineev[38], Y. Minegishi[156], L.M. Mir[14], A. Mirto[70a,70b], K.P. Mistry[130], T. Mitani[171], J. Mitrevski[110], V.A. Mitsou[166], M. Mittal[62c], O. Miu[159], A. Miucci[20], P.S. Miyagawa[142], A. Mizukami[83], J.U. Mjörnmark[98], T. Mkrtchyan[63a], M. Mlynarikova[135], T. Moa[47a,47b], K. Mochizuki[109], P. Mogg[54], S. Mohapatra[41], R. Moles-Valls[24], M.C. Mondragon[108], K. Mönig[48], J. Monk[42], E. Monnier[103], A. Montalbano[145], J. Montejo Berlingen[36],

JHEP06(2023)019

M. Montella[96], F. Monticelli[90], N. Morange[67], D. Moreno[22], M. Moreno Llácer[166], C. Moreno Martinez[14], P. Morettini[57b], M. Morgenstern[153], S. Morgenstern[50], D. Mori[145], M. Morii[61], M. Morinaga[171], V. Morisbak[127], A.K. Morley[36], G. Mornacchi[36], A.P. Morris[96], L. Morvaj[148], P. Moschovakos[36], B. Moser[116], M. Mosidze[152b], T. Moskalets[137], H.J. Moss[142], J. Moss[31,n], E.J.W. Moyse[104], S. Muanza[103], J. Mueller[131], R.S.P. Mueller[110], D. Muenstermann[91], G.A. Mullier[98], D.P. Mungo[71a,71b], J.L. Munoz Martinez[14], F.J. Munoz Sanchez[102], P. Murin[28b], W.J. Murray[170,136], A. Murrone[71a,71b], M. Muškinja[18a], C. Mwewa[33a], A.G. Myagkov[37,a], A.A. Myers[131], J. Myers[125], M. Myska[134], B.P. Nachman[18a], O. Nackenhorst[49], A. Nag[50], K. Nagai[128], K. Nagano[83], Y. Nagasaka[64], J.L. Nagle[29], E. Nagy[103], A.M. Nairz[36], Y. Nakahama[113], K. Nakamura[83], T. Nakamura[156], I. Nakano[121], H. Nanjo[126], F. Napolitano[63a], R.F. Naranjo Garcia[48], R. Narayan[44], I. Naryshkin[37], T. Naumann[48], G. Navarro[22], P.Y. Nechaeva[37], F. Nechansky[48], T.J. Neep[21], A. Negri[73a,73b], M. Negrini[23b], C. Nellist[115], M.E. Nelson[47a,47b], S. Nemecek[133], M. Nessi[36,e], M.S. Neubauer[165], F. Neuhaus[101], M. Neumann[174], R. Newhouse[167], P.R. Newman[21], C.W. Ng[131], Y.S. Ng[19], Y.W.Y. Ng[163], B. Ngair[35e], H.D.N. Nguyen[103], T. Nguyen Manh[109], E. Nibigira[40], R.B. Nickerson[128], R. Nicolaidou[137], D.S. Nielsen[42], J. Nielsen[138], N. Nikiforou[11], V. Nikolaenko[37,a], I. Nikolic-Audit[129], K. Nikolopoulos[21], P. Nilsson[29], H.R. Nindhito[56], Y. Ninomiya[83], A. Nisati[75a], N. Nishu[62c], R. Nisius[111], I. Nitsche[49], T. Nitta[171], T. Nobe[156], Y. Noguchi[87], I. Nomidis[129], M.A. Nomura[29], M. Nordberg[36], T. Novak[93], O. Novgorodova[50], R. Novotny[134], L. Nozka[124], K. Ntekas[163], E. Nurse[96], F.G. Oakham[34,ao], H. Oberlack[111], J. Ocariz[129], A. Ochi[84], I. Ochoa[41], J.P. Ochoa-Ricoux[139a], K. O'Connor[26], S. Oda[89], S. Odaka[83], S. Oerdek[55], A. Ogrodnik[85a], A. Oh[102], S.H. Oh[51], C.C. Ohm[147], H. Oide[158], M.L. Ojeda[159], H. Okawa[161], Y. Okazaki[87], M.W. O'Keefe[92], Y. Okumura[156], T. Okuyama[83], A. Olariu[27b], L.F. Oleiro Seabra[132a], S.A. Olivares Pino[139a], D. Oliveira Damazio[29], J.L. Oliver[1], M.J.R. Olsson[163], A. Olszewski[86], J. Olszowska[86,*], D.C. O'Neil[145], A.P. O'Neill[128], A. Onofre[132a,132e], P.U.E. Onyisi[11], H. Oppen[127], M.J. Oreglia[39], G.E. Orellana[90], D. Orestano[77a,77b], N. Orlando[14], R.S. Orr[159], V. O'Shea[59], R. Ospanov[62a], G. Otero y Garzon[30], H. Otono[89], P.S. Ott[63a], M. Ouchrif[35d], J. Ouellette[29], F. Ould-Saada[127], A. Ouraou[137,*], Q. Ouyang[15a], M. Owen[59], R.E. Owen[21], V.E. Ozcan[12c], N. Ozturk[8], J. Pacalt[124], H.A. Pacey[32], K. Pachal[51], A. Pacheco Pages[14], C. Padilla Aranda[14], S. Pagan Griso[18a], M. Paganini[175], G. Palacino[68], S. Palazzo[52], S. Palestini[36], M. Palka[85b], D. Pallin[40], P. Palni[85a], I. Panagoulias[10], C.E. Pandini[36], J.G. Panduro Vazquez[95], P. Pani[48], G. Panizzo[69a,69c], L. Paolozzi[56], C. Papadatos[109], K. Papageorgiou[9,h], S. Parajuli[44], A. Paramonov[6], D. Paredes Hernandez[65b], S.R. Paredes Saenz[128], B. Parida[37], T.H. Park[159], A.J. Parker[31], M.A. Parker[32], F. Parodi[57b,57a], E.W. Parrish[117], J.A. Parsons[41], U. Parzefall[54], L. Pascual Dominguez[129], V.R. Pascuzzi[159], J.M.P. Pasner[138], F. Pasquali[116], E. Pasqualucci[75a], S. Passaggio[57b], F. Pastore[95], P. Pasuwan[47a,47b], S. Pataraia[101], J.R. Pater[102], A. Pathak[173,j], J. Patton[92], T. Pauly[36], J. Pearkes[146], B. Pearson[111], M. Pedersen[127], L. Pedraza Diaz[115], R. Pedro[132a], T. Peiffer[55],

JHEP06(2023)019

S.V. Peleganchuk[37], O. Penc[133], H. Peng[62a], B.S. Peralva[82a], M.M. Perego[67], A.P. Pereira Peixoto[132a], D.V. Perepelitsa[29], F. Peri[19], L. Perini[71a,71b,*], H. Pernegger[36], S. Perrella[132a], A. Perrevoort[116], K. Peters[48], R.F.Y. Peters[102], B.A. Petersen[36], T.C. Petersen[42], E. Petit[103], A. Petridis[1], C. Petridou[155], M. Petrov[128], F. Petrucci[77a,77b], M. Pettee[175], N.E. Pettersson[104], K. Petukhova[135], A. Peyaud[137], R. Pezoa[139c], L. Pezzotti[73a,73b], T. Pham[106], F.H. Phillips[108], P.W. Phillips[136], M.W. Phipps[165], G. Piacquadio[148], E. Pianori[18a], A. Picazio[104], R.H. Pickles[102], R. Piegaia[30], D. Pietreanu[27b], J.E. Pilcher[39], A.D. Pilkington[102], M. Pinamonti[69a,69c], J.L. Pinfold[3], M. Pitt[154], L. Pizzimento[76a,76b], M.-A. Pleier[29], V. Pleskot[135], E. Plotnikova[38], P. Podberezko[37], R. Poettgen[98], R. Poggi[56], L. Poggioli[129], I. Pogrebnyak[108], D. Pohl[24], I. Pokharel[55], G. Polesello[73a], A. Poley[18a], A. Policicchio[75a,75b], R. Polifka[135], A. Polini[23b], C.S. Pollard[48], V. Polychronakos[29], D. Ponomarenko[37], L. Pontecorvo[36], S. Popa[27a], G.A. Popeneciu[27d], L. Portales[5], D.M. Portillo Quintero[60], S. Pospisil[134], K. Potamianos[48], I.N. Potrap[38], C.J. Potter[32], H. Potti[11], T. Poulsen[98], J. Poveda[36], T.D. Powell[142], G. Pownall[48], M.E. Pozo Astigarraga[36], P. Pralavorio[103], S. Prell[81], D. Price[102], M. Primavera[70a], S. Prince[105], M.L. Proffitt[141], N. Proklova[37], K. Prokofiev[65c], S. Protopopescu[29], J. Proudfoot[6], M. Przybycien[85a], D. Pudzha[37], A. Puri[165], P. Puzo[67], J. Qian[107], Y. Qin[102], A. Quadt[55], M. Queitsch-Maitland[36], A. Qureshi[1], M. Racko[28a], F. Ragusa[71a,71b], G. Rahal[99], J.A. Raine[56], S. Rajagopalan[29], A. Ramirez Morales[94], K. Ran[15a,15d], T. Rashid[67], S. Raspopov[5], D.M. Rauch[48], F. Rauscher[110], S. Rave[101], B. Ravina[142], I. Ravinovich[172], J.H. Rawling[102], M. Raymond[36], A.L. Read[127], N.P. Readioff[60], M. Reale[70a,70b], D.M. Rebuzzi[73a,73b], A. Redelbach[169], G. Redlinger[29], K. Reeves[45], L. Rehnisch[19], J. Reichert[130], D. Reikher[154], A. Reiss[101], A. Rej[144], C. Rembser[36], A. Renardi[48], M. Renda[27b], M. Rescigno[75a], S. Resconi[71a], E.D. Resseguie[18a], S. Rettie[96], B. Reynolds[120], E. Reynolds[21], O.L. Rezanova[37], P. Reznicek[135], E. Ricci[78a,78b], R. Richter[111], S. Richter[48], E. Richter-Was[85b], O. Ricken[24], M. Ridel[129], P. Rieck[111], O. Rifki[48], M. Rijssenbeek[148], A. Rimoldi[73a,73b], M. Rimoldi[48], L. Rinaldi[23b,23a], G. Ripellino[147], I. Riu[14], J.C. Rivera Vergara[168], F. Rizatdinova[123], E. Rizvi[94], C. Rizzi[36], R.T. Roberts[102], S.H. Robertson[105,ac], M. Robin[48], D. Robinson[32], C.M. Robles Gajardo[139c], M. Robles Manzano[101], A. Robson[59], A. Rocchi[76a,76b], E. Rocco[101], C. Roda[74a,74b], S. Rodriguez Bosca[166], A. Rodriguez Perez[14], D. Rodriguez Rodriguez[166], A.M. Rodríguez Vera[160b], S. Roe[36], O. Røhne[127], R. Röhrig[111], R.A. Rojas[139c], B. Roland[54], C.P.A. Roland[68], J. Roloff[29], A. Romaniouk[37], M. Romano[23b], N. Rompotis[92], M. Ronzani[118], L. Roos[129], S. Rosati[75a], G. Rosin[104], B.J. Rosser[130], E. Rossi[48], E. Rossi[77a,77b], E. Rossi[72a,72b], L.P. Rossi[57b], L. Rossini[71a,71b], R. Rosten[14], M. Rotaru[27b], J. Rothberg[141,*], B. Rottler[54], D. Rousseau[67], G. Rovelli[73a,73b], A. Roy[11], D. Roy[33d], A. Rozanov[103], Y. Rozen[153], X. Ruan[33d], F. Rühr[54], A. Ruiz-Martinez[166], A. Rummler[36], Z. Rurikova[54], N.A. Rusakovich[38], H.L. Russell[105], L. Rustige[40,49], J.P. Rutherfoord[7], E.M. Rüttinger[142], M. Rybar[41], G. Rybkin[67], E.B. Rye[127], A. Ryzhov[37], J.A. Sabater Iglesias[48], P. Sabatini[55], G. Sabato[116], S. Sacerdoti[67], H.F-W. Sadrozinski[138], F. Safai Tehrani[75a], B. Safarzadeh Samani[149], M. Safdari[146], P. Saha[117], S. Saha[105],

JHEP06(2023)019

M. Sahinsoy[63a], A. Sahu[174], M. Saimpert[48], M. Saito[156], T. Saito[156], H. Sakamoto[156], A. Sakharov[118,ai], D. Salamani[56], G. Salamanna[77a,77b], J.E. Salazar Loyola[139c], A. Salnikov[146], J. Salt[166], D. Salvatore[43b,43a], F. Salvatore[149], A. Salvucci[65a,65b,65c], A. Salzburger[36], J. Samarati[36], D. Sammel[54], D. Sampsonidis[155], D. Sampsonidou[155], J. Sánchez[166], A. Sanchez Pineda[69a,36,69c], H. Sandaker[127], C.O. Sander[48], I.G. Sanderswood[91], M. Sandhoff[174], C. Sandoval[22], D.P.C. Sankey[136], M. Sannino[57b,57a], Y. Sano[113], A. Sansoni[53], C. Santoni[40], H. Santos[132a,132b], S.N. Santpur[18a], A. Santra[166], J.G. Saraiva[132a,132d], J. Sardain[129], O. Sasaki[83], K. Sato[161], F. Sauerburger[54], E. Sauvan[5], P. Savard[159,ao], R. Sawada[156], C. Sawyer[136], L. Sawyer[97,ah], C. Sbarra[23b], A. Sbrizzi[23a], T. Scanlon[96], J. Schaarschmidt[141], P. Schacht[111], B.M. Schachtner[110], D. Schaefer[39], L. Schaefer[130], J. Schaeffer[101], S. Schaepe[36], U. Schäfer[101], A.C. Schaffer[67], D. Schaile[110], R.D. Schamberger[148], N. Scharmberg[102], V.A. Schegelsky[37], D. Scheirich[135], F. Schenck[19], M. Schernau[163], C. Schiavi[57b,57a], L.K. Schildgen[24], Z.M. Schillaci[26], E.J. Schioppa[36], M. Schioppa[43b,43a], K.E. Schleicher[54], S. Schlenker[36], K.R. Schmidt-Sommerfeld[111], K. Schmieden[36], C. Schmitt[101], S. Schmitt[48], S. Schmitz[101], J.C. Schmoeckel[48], L. Schoeffel[137], A. Schoening[63b], P.G. Scholer[54], E. Schopf[128], M. Schott[101], J.F.P. Schouwenberg[115], J. Schovancova[36], S. Schramm[56], F. Schroeder[174], A. Schulte[101], H-C. Schultz-Coulon[63a], M. Schumacher[54], B.A. Schumm[138], Ph. Schune[137], A. Schwartzman[146], T.A. Schwarz[107], Ph. Schwemling[137], R. Schwienhorst[108], A. Sciandra[138], G. Sciolla[26], M. Scodeggio[48], M. Scornajenghi[43b,43a], F. Scuri[74a], F. Scutti[106], L.M. Scyboz[111], C.D. Sebastiani[75a,75b], P. Seema[19], S.C. Seidel[114], A. Seiden[138], B.D. Seidlitz[29], T. Seiss[39], J.M. Seixas[82b], G. Sekhniaidze[72a], S.J. Sekula[44], N. Semprini-Cesari[23b,23a], S. Sen[51], C. Serfon[79], L. Serin[67], L. Serkin[69a,69b], M. Sessa[62a], H. Severini[122], S. Sevova[146], T. Šfiligoj[93], F. Sforza[57b,57a], A. Sfyrla[56], E. Shabalina[55], J.D. Shahinian[138], N.W. Shaikh[47a,47b], D. Shaked Renous[172], L.Y. Shan[15a], J.T. Shank[25], M. Shapiro[18a], A. Sharma[128], A.S. Sharma[1], P.B. Shatalov[37], K. Shaw[149], S.M. Shaw[102], M. Shehade[172], Y. Shen[122], A.D. Sherman[25], P. Sherwood[96], L. Shi[151], S. Shimizu[83], C.O. Shimmin[175], Y. Shimogama[171], M. Shimojima[112], I.P.J. Shipsey[128], S. Shirabe[158], M. Shiyakova[38,aa], J. Shlomi[172], A. Shmeleva[37], M.J. Shochet[39], J. Shojaii[106], D.R. Shope[122], S. Shrestha[120], E.M. Shrif[33d], E. Shulga[172], P. Sicho[133], A.M. Sickles[165], P.E. Sidebo[147], E. Sideras Haddad[33d], O. Sidiropoulou[36], A. Sidoti[23b], F. Siegert[50], Dj. Sijacki[16], M.Jr. Silva[173], M.V. Silva Oliveira[82a], S.B. Silverstein[47a], S. Simion[67], R. Simoniello[101], S. Simsek[12b], P. Sinervo[159], V. Sinetckii[37], N.B. Sinev[125], S. Singh[145], M. Sioli[23b,23a], I. Siral[125], S.Yu. Sivoklokov[37,*], J. Sjölin[47a,47b], E. Skorda[98], P. Skubic[122], M. Slawinska[86], K. Sliwa[162], R. Slovak[135], V. Smakhtin[172], B.H. Smart[136], J. Smiesko[28b], N. Smirnov[37], S.Yu. Smirnov[37], Y. Smirnov[37], L.N. Smirnova[37,a], O. Smirnova[98], J.W. Smith[55], M. Smizanska[91], K. Smolek[134], A. Smykiewicz[86], A.A. Snesarev[37], H.L. Snoek[116], I.M. Snyder[125], S. Snyder[29], R. Sobie[168,ac], A. Soffer[154], A. Søgaard[52], F. Sohns[55], C.A. Solans Sanchez[36], E.Yu. Soldatov[37], U. Soldevila[166], A.A. Solodkov[37], A. Soloshenko[38], O.V. Solovyanov[37], V. Solovyev[37], P. Sommer[142], H. Son[162], W. Song[136], W.Y. Song[160b], A. Sopczak[134], A.L. Sopio[96], F. Sopkova[28b], C.L. Sotiropoulou[74a,74b], S. Sottocornola[73a,73b],

JHEP06(2023)019

R. Soualah[69a,69c,g], D. South[48], S. Spagnolo[70a,70b], M. Spalla[111], M. Spangenberg[170], F. Spanò[95], D. Sperlich[54], T.M. Spieker[63a], G. Spigo[36], M. Spina[149], D.P. Spiteri[59], M. Spousta[135], A. Stabile[71a,71b], R. Stamen[63a], M. Stamenkovic[116], E. Stanecka[86], B. Stanislaus[128], M.M. Stanitzki[48], M. Stankaityte[128], B. Stapf[116], E.A. Starchenko[37], G.H. Stark[138], J. Stark[60], P. Staroba[133], P. Starovoitov[63a], S. Stärz[105], R. Staszewski[86], G. Stavropoulos[46], M. Stegler[48], P. Steinberg[29], A.L. Steinhebel[125], B. Stelzer[145], H.J. Stelzer[131], O. Stelzer-Chilton[160a], H. Stenzel[58], T.J. Stevenson[149], G.A. Stewart[36], M.C. Stockton[36], G. Stoicea[27b], M. Stolarski[132a], S. Stonjek[111], A. Straessner[50], J. Strandberg[147], S. Strandberg[47a,47b], M. Strauss[122], P. Strizenec[28b], R. Ströhmer[169], D.M. Strom[125], R. Stroynowski[44], A. Strubig[52], S.A. Stucci[29], B. Stugu[17], J. Stupak[122], N.A. Styles[48], D. Su[146], W. Su[62c], S. Suchek[63a], V.V. Sulin[37], M.J. Sullivan[92], D.M.S. Sultan[56], S. Sultansoy[4c], T. Sumida[87], S. Sun[107], X. Sun[102], K. Suruliz[149], C.J.E. Suster[150], M.R. Sutton[149], S. Suzuki[83], M. Svatos[133], M. Swiatlowski[39], S.P. Swift[2], T. Swirski[169], A. Sydorenko[101], I. Sykora[28a], M. Sykora[135], T. Sykora[135], D. Ta[101], K. Tackmann[48,y], J. Taenzer[154], A. Taffard[163], R. Tafirout[160a], H. Takai[29], R. Takashima[88], K. Takeda[84], T. Takeshita[143], E.P. Takeva[52], Y. Takubo[83], M. Talby[103], A.A. Talyshev[37], N.M. Tamir[154], J. Tanaka[156], M. Tanaka[158], R. Tanaka[67], S. Tapia Araya[165], S. Tapprogge[101], A. Tarek Abouelfadl Mohamed[129], S. Tarem[153], K. Tariq[62b], G. Tarna[27b,d], G.F. Tartarelli[71a], P. Tas[135], M. Tasevsky[133], T. Tashiro[87], E. Tassi[43b,43a], A. Tavares Delgado[132a], Y. Tayalati[35e], A.J. Taylor[52], G.N. Taylor[106], W. Taylor[160b], A.S. Tee[91], R. Teixeira De Lima[146], P. Teixeira-Dias[95], H. Ten Kate[36], J.J. Teoh[116], S. Terada[83], K. Terashi[156], J. Terron[100], S. Terzo[14], M. Testa[53], R.J. Teuscher[159,ac], S.J. Thais[175], T. Theveneaux-Pelzer[48], F. Thiele[42], D.W. Thomas[95], J.O. Thomas[44], J.P. Thomas[21], P.D. Thompson[21], L.A. Thomsen[175], E. Thomson[130], E.J. Thorpe[94], R.E. Ticse Torres[55], V. Tikhomirov[37,a], Yu.A. Tikhonov[37], S. Timoshenko[37], P. Tipton[175], S. Tisserant[103], K. Todome[23b,23a], S. Todorova-Nova[135], S. Todt[50], J. Tojo[89], S. Tokár[28a], K. Tokushuku[83], E. Tolley[120], K.G. Tomiwa[33d], M. Tomoto[113], L. Tompkins[146,p], B. Tong[61], P. Tornambe[104], E. Torrence[125], H. Torres[50], E. Torró Pastor[141], C. Tosciri[128], J. Toth[103,ab], D.R. Tovey[142], A. Traeet[17], C.J. Treado[118], T. Trefzger[169], F. Tresoldi[149], A. Tricoli[29], I.M. Trigger[160a], S. Trincaz-Duvoid[129], D.A. Trischuk[167], B. Trocmé[60], A. Trofymov[137], C. Troncon[71a], F. Trovato[149], L. Truong[33b], M. Trzebinski[86], A. Trzupek[86], F. Tsai[48], J.C-L. Tseng[128], P.V. Tsiareshka[37,a], A. Tsirigotis[155,u], V. Tsiskaridze[148], E.G. Tskhadadze[152a], M. Tsopoulou[155], I.I. Tsukerman[37], V. Tsulaia[18a], S. Tsuno[83], D. Tsybychev[148], Y. Tu[65b], A. Tudorache[27b], V. Tudorache[27b], T.T. Tulbure[27a], A.N. Tuna[61], S. Turchikhin[38], D. Turgeman[172], I. Turk Cakir[4b,t], R.J. Turner[21], R. Turra[71a], P.M. Tuts[41], S. Tzamarias[155], E. Tzovara[101], G. Ucchielli[49], K. Uchida[156], F. Ukegawa[161], G. Unal[36], A. Undrus[29], G. Unel[163], F.C. Ungaro[106], Y. Unno[83], K. Uno[156], J. Urban[28b], P. Urquijo[106], G. Usai[8], Z. Uysal[12d], V. Vacek[134], B. Vachon[105], K.O.H. Vadla[127], A. Vaidya[96], C. Valderanis[110], E. Valdes Santurio[47a,47b], M. Valente[56], S. Valentinetti[23b,23a], A. Valero[166], L. Valéry[48], R.A. Vallance[21], A. Vallier[36], J.A. Valls Ferrer[166], T.R. Van Daalen[14], P. Van Gemmeren[6], I. Van Vulpen[116], M. Vanadia[76a,76b], W. Vandelli[36], M. Vandenbroucke[137],

JHEP06(2023)019

E.R. Vandewall[123], A. Vaniachine[37], D. Vannicola[75a,75b], R. Vari[75a], E.W. Varnes[7], C. Varni[57b,57a], T. Varol[151], D. Varouchas[67], K.E. Varvell[150], M.E. Vasile[27b], G.A. Vasquez[168], F. Vazeille[40], D. Vazquez Furelos[14], T. Vazquez Schroeder[36], J. Veatch[55], V. Vecchio[77a,77b], M.J. Veen[116], L.M. Veloce[159], F. Veloso[132a,132c], S. Veneziano[75a], A. Ventura[70a,70b], N. Venturi[36], A. Verbytskyi[111], V. Vercesi[73a], M. Verducci[74a,74b], C.M. Vergel Infante[81], C. Vergis[24], W. Verkerke[116], A.T. Vermeulen[116], J.C. Vermeulen[116], M.C. Vetterli[145,ao], N. Viaux Maira[139c], M. Vicente Barreto Pinto[56], T. Vickey[142], O.E. Vickey Boeriu[142], G.H.A. Viehhauser[128], L. Vigani[63b], M. Villa[23b,23a], M. Villaplana Perez[3], E. Vilucchi[53], M.G. Vincter[34], G.S. Virdee[21], A. Vishwakarma[48], C. Vittori[23b,23a], I. Vivarelli[149], M. Vogel[174], P. Vokac[134], S.E. von Buddenbrock[33d], E. Von Toerne[24], V. Vorobel[135], K. Vorobev[37], M. Vos[166], J.H. Vossebeld[92], M. Vozak[102], N. Vranjes[16], M. Vranjes Milosavljevic[16], V. Vrba[134,*], M. Vreeswijk[116], R. Vuillermet[36], I. Vukotic[39], P. Wagner[24], W. Wagner[174], J. Wagner-Kuhr[110], S. Wahdan[174], H. Wahlberg[90], V.M. Walbrecht[111], J. Walder[91], R. Walker[110], S.D. Walker[95], W. Walkowiak[144], V. Wallangen[47a,47b], A.M. Wang[61], A.Z. Wang[173], C. Wang[62c], F. Wang[173], H. Wang[18a], H. Wang[3], J. Wang[65a], J. Wang[63b], P. Wang[44], Q. Wang[122], R.-J. Wang[101], R. Wang[62a], R. Wang[6], S.M. Wang[151], W.T. Wang[62a], W.X. Wang[62a], Y. Wang[62a], Z. Wang[62c], C. Wanotayaroj[48], A. Warburton[105], C.P. Ward[32], D.R. Wardrope[96], N. Warrack[59], A. Washbrook[52], A.T. Watson[21], M.F. Watson[21], G. Watts[141], B.M. Waugh[96], A.F. Webb[11], S. Webb[101], C. Weber[175], M.S. Weber[20], S.A. Weber[34], S.M. Weber[63a], A.R. Weidberg[128], J. Weingarten[49], M. Weirich[101], C. Weiser[54], P.S. Wells[36], T. Wenaus[29], T. Wengler[36], S. Wenig[36], N. Wermes[24], M.D. Werner[81], M. Wessels[63a], T.D. Weston[20], K. Whalen[125], N.L. Whallon[141], A.M. Wharton[91], A.S. White[107], A. White[8], M.J. White[1], D. Whiteson[163], B.W. Whitmore[91], W. Wiedenmann[173], C. Wiel[50], M. Wielers[136], N. Wieseotte[101], C. Wiglesworth[42], L.A.M. Wiik-Fuchs[54], H.G. Wilkens[36], L.J. Wilkins[95], H.H. Williams[130], S. Williams[32], C. Willis[108], S. Willocq[104], I. Wingerter-Seez[5], E. Winkels[149], F. Winklmeier[125], O.J. Winston[149], B.T. Winter[54], M. Wittgen[146], M. Wobisch[97], A. Wolf[101], T.M.H. Wolf[116], R. Wolff[103], R. Wölker[128], J. Wollrath[54], M.W. Wolter[86], H. Wolters[132a,132c], V.W.S. Wong[167], N.L. Woods[138], S.D. Worm[21], B.K. Wosiek[86], K.W. Woźniak[86], K. Wraight[59], S.L. Wu[173], X. Wu[56], Y. Wu[62a], T.R. Wyatt[102], B.M. Wynne[52], S. Xella[42], Z. Xi[107], X. Xiao[107], I. Xiotidis[149], D. Xu[15a], H. Xu[62a], H. Xu[62a], L. Xu[29], T. Xu[137], W. Xu[107], Z. Xu[62b], Z. Xu[146], B. Yabsley[150], S. Yacoob[33a], K. Yajima[126], D.P. Yallup[96], N. Yamaguchi[89], Y. Yamaguchi[158], A. Yamamoto[83], M. Yamatani[156], T. Yamazaki[156], Y. Yamazaki[84], Z. Yan[25], H.J. Yang[62c,62d], H.T. Yang[18a], S. Yang[62a], T. Yang[65c], X. Yang[62b,60], Y. Yang[156], W-M. Yao[18a], Y.C. Yap[48], Y. Yasu[83], E. Yatsenko[62c,62d], H. Ye[15c], J. Ye[44], S. Ye[29], I. Yeletskikh[38], M.R. Yexley[91], E. Yigitbasi[25], K. Yorita[171], K. Yoshihara[130], C.J.S. Young[36], C. Young[146], J. Yu[81], R. Yuan[62b,i], X. Yue[63a], M. Zaazoua[35e], B. Zabinski[86], G. Zacharis[10], E. Zaffaroni[56], T. Zakareishvili[152b], N. Zakharchuk[34], S. Zambito[61], D. Zanzi[36], D.R. Zaripovas[59], S.V. Zeißner[49], C. Zeitnitz[174], G. Zemaityte[128], J.C. Zeng[165], O. Zenin[37], T. Ženiš[28a], D. Zerwas[67], M. Zgubič[128], B. Zhang[15c], D.F. Zhang[15b], G. Zhang[15b], H. Zhang[15c], J. Zhang[6],

JHEP06(2023)019

L. Zhang[15c], L. Zhang[62a], M. Zhang[165], R. Zhang[173], S. Zhang[107], X. Zhang[62b], Y. Zhang[15a,15d], Z. Zhang[65a], Z. Zhang[67], P. Zhao[51], Z. Zhao[62a], A. Zhemchugov[38], Z. Zheng[107], D. Zhong[165], B. Zhou[107], C. Zhou[173], M.S. Zhou[15a,15d], M. Zhou[148], N. Zhou[62c], Y. Zhou[7], C.G. Zhu[62b], C. Zhu[15a,15d], H.L. Zhu[62a], H. Zhu[15a], J. Zhu[107], Y. Zhu[62a], X. Zhuang[15a], K. Zhukov[37], V. Zhulanov[37], D. Zieminska[68], N.I. Zimine[38], S. Zimmermann[54,*], Z. Zinonos[111], M. Ziolkowski[144], L. Živković[16], G. Zobernig[173], A. Zoccoli[23b,23a], K. Zoch[55], T.G. Zorbas[142], R. Zou[39], L. Zwalinski[36]

[1] *Department of Physics, University of Adelaide, Adelaide; Australia*
[2] *Physics Department, SUNY Albany, Albany NY; United States of America*
[3] *Department of Physics, University of Alberta, Edmonton AB; Canada*
[4] [(a)] *Department of Physics, Ankara University, Ankara;* [(b)] *Istanbul Aydin University, Application and Research Center for Advanced Studies, Istanbul;* [(c)] *Division of Physics, TOBB University of Economics and Technology, Ankara; Türkiye*
[5] *LAPP, Univ. Savoie Mont Blanc, CNRS/IN2P3, Annecy; France*
[6] *High Energy Physics Division, Argonne National Laboratory, Argonne IL; United States of America*
[7] *Department of Physics, University of Arizona, Tucson AZ; United States of America*
[8] *Department of Physics, University of Texas at Arlington, Arlington TX; United States of America*
[9] *Physics Department, National and Kapodistrian University of Athens, Athens; Greece*
[10] *Physics Department, National Technical University of Athens, Zografou; Greece*
[11] *Department of Physics, University of Texas at Austin, Austin TX; United States of America*
[12] [(a)] *Bahcesehir University, Faculty of Engineering and Natural Sciences, Istanbul;* [(b)] *Istanbul Bilgi University, Faculty of Engineering and Natural Sciences, Istanbul;* [(c)] *Department of Physics, Bogazici University, Istanbul;* [(d)] *Department of Physics Engineering, Gaziantep University, Gaziantep; Türkiye*
[13] *Institute of Physics, Azerbaijan Academy of Sciences, Baku; Azerbaijan*
[14] *Institut de Física d'Altes Energies (IFAE), Barcelona Institute of Science and Technology, Barcelona; Spain*
[15] [(a)] *Institute of High Energy Physics, Chinese Academy of Sciences, Beijing;* [(b)] *Physics Department, Tsinghua University, Beijing;* [(c)] *Department of Physics, Nanjing University, Nanjing;* [(d)] *University of Chinese Academy of Science (UCAS), Beijing; China*
[16] *Institute of Physics, University of Belgrade, Belgrade; Serbia*
[17] *Department for Physics and Technology, University of Bergen, Bergen; Norway*
[18] [(a)] *Physics Division, Lawrence Berkeley National Laboratory, Berkeley CA;* [(b)] *University of California, Berkeley CA; United States of America*
[19] *Institut für Physik, Humboldt Universität zu Berlin, Berlin; Germany*
[20] *Albert Einstein Center for Fundamental Physics and Laboratory for High Energy Physics, University of Bern, Bern; Switzerland*
[21] *School of Physics and Astronomy, University of Birmingham, Birmingham; United Kingdom*
[22] *Facultad de Ciencias y Centro de Investigaciónes, Universidad Antonio Nariño, Bogotá; Colombia*
[23] [(a)] *Dipartimento di Fisica e Astronomia A. Righi, Università di Bologna, Bologna;* [(b)] *INFN Sezione di Bologna; Italy*
[24] *Physikalisches Institut, Universität Bonn, Bonn; Germany*
[25] *Department of Physics, Boston University, Boston MA; United States of America*
[26] *Department of Physics, Brandeis University, Waltham MA; United States of America*
[27] [(a)] *Transilvania University of Brasov, Brasov;* [(b)] *Horia Hulubei National Institute of Physics and Nuclear Engineering, Bucharest;* [(c)] *Department of Physics, Alexandru Ioan Cuza University of Iasi, Iasi;* [(d)] *National Institute for Research and Development of Isotopic and Molecular Technologies, Physics Department, Cluj-Napoca;* [(e)] *University Politehnica Bucharest, Bucharest;* [(f)] *West University in Timisoara, Timisoara; Romania*
[28] [(a)] *Faculty of Mathematics, Physics and Informatics, Comenius University, Bratislava;* [(b)] *Department of Subnuclear Physics, Institute of Experimental Physics of the Slovak Academy of Sciences, Kosice; Slovak Republic*

JHEP06(2023)019

[29] Physics Department, Brookhaven National Laboratory, Upton NY; United States of America
[30] Universidad de Buenos Aires, Facultad de Ciencias Exactas y Naturales, Departamento de Física, y CONICET, Instituto de Física de Buenos Aires (IFIBA), Buenos Aires; Argentina
[31] California State University, CA; United States of America
[32] Cavendish Laboratory, University of Cambridge, Cambridge; United Kingdom
[33] [(a)] Department of Physics, University of Cape Town, Cape Town;[(b)] Department of Mechanical Engineering Science, University of Johannesburg, Johannesburg;[(c)] University of South Africa, Department of Physics, Pretoria;[(d)] School of Physics, University of the Witwatersrand, Johannesburg; South Africa
[34] Department of Physics, Carleton University, Ottawa ON; Canada
[35] [(a)] Faculté des Sciences Ain Chock, Réseau Universitaire de Physique des Hautes Energies — Université Hassan II, Casablanca;[(b)] Faculté des Sciences, Université Ibn-Tofail, Kénitra;[(c)] Faculté des Sciences Semlalia, Université Cadi Ayyad, LPHEA-Marrakech;[(d)] LPMR, Faculté des Sciences, Université Mohamed Premier, Oujda;[(e)] Faculté des sciences, Université Mohammed V, Rabat; Morocco
[36] CERN, Geneva; Switzerland
[37] Affiliated with an institute covered by a cooperation agreement with CERN
[38] Affiliated with an international laboratory covered by a cooperation agreement with CERN
[39] Enrico Fermi Institute, University of Chicago, Chicago IL; United States of America
[40] LPC, Université Clermont Auvergne, CNRS/IN2P3, Clermont-Ferrand; France
[41] Nevis Laboratory, Columbia University, Irvington NY; United States of America
[42] Niels Bohr Institute, University of Copenhagen, Copenhagen; Denmark
[43] [(a)] Dipartimento di Fisica, Università della Calabria, Rende;[(b)] INFN Gruppo Collegato di Cosenza, Laboratori Nazionali di Frascati; Italy
[44] Physics Department, Southern Methodist University, Dallas TX; United States of America
[45] Physics Department, University of Texas at Dallas, Richardson TX; United States of America
[46] National Centre for Scientific Research "Demokritos", Agia Paraskevi; Greece
[47] [(a)] Department of Physics, Stockholm University;[(b)] Oskar Klein Centre, Stockholm; Sweden
[48] Deutsches Elektronen-Synchrotron DESY, Hamburg and Zeuthen; Germany
[49] Fakultät Physik, Technische Universität Dortmund, Dortmund; Germany
[50] Institut für Kern- und Teilchenphysik, Technische Universität Dresden, Dresden; Germany
[51] Department of Physics, Duke University, Durham NC; United States of America
[52] SUPA — School of Physics and Astronomy, University of Edinburgh, Edinburgh; United Kingdom
[53] INFN e Laboratori Nazionali di Frascati, Frascati; Italy
[54] Physikalisches Institut, Albert-Ludwigs-Universität Freiburg, Freiburg; Germany
[55] II. Physikalisches Institut, Georg-August-Universität Göttingen, Göttingen; Germany
[56] Département de Physique Nucléaire et Corpusculaire, Université de Genève, Genève; Switzerland
[57] [(a)] Dipartimento di Fisica, Università di Genova, Genova;[(b)] INFN Sezione di Genova; Italy
[58] II. Physikalisches Institut, Justus-Liebig-Universität Giessen, Giessen; Germany
[59] SUPA — School of Physics and Astronomy, University of Glasgow, Glasgow; United Kingdom
[60] LPSC, Université Grenoble Alpes, CNRS/IN2P3, Grenoble INP, Grenoble; France
[61] Laboratory for Particle Physics and Cosmology, Harvard University, Cambridge MA; United States of America
[62] [(a)] Department of Modern Physics and State Key Laboratory of Particle Detection and Electronics, University of Science and Technology of China, Hefei;[(b)] Institute of Frontier and Interdisciplinary Science and Key Laboratory of Particle Physics and Particle Irradiation (MOE), Shandong University, Qingdao;[(c)] School of Physics and Astronomy, Shanghai Jiao Tong University, Key Laboratory for Particle Astrophysics and Cosmology (MOE), SKLPPC, Shanghai;[(d)] Tsung-Dao Lee Institute, Shanghai; China
[63] [(a)] Kirchhoff-Institut für Physik, Ruprecht-Karls-Universität Heidelberg, Heidelberg;[(b)] Physikalisches Institut, Ruprecht-Karls-Universität Heidelberg, Heidelberg; Germany
[64] Faculty of Applied Information Science, Hiroshima Institute of Technology, Hiroshima; Japan

JHEP06(2023)019

[65] [(a)] Department of Physics, Chinese University of Hong Kong, Shatin, N.T., Hong Kong;[(b)] Department of Physics, University of Hong Kong, Hong Kong;[(c)] Department of Physics and Institute for Advanced Study, Hong Kong University of Science and Technology, Clear Water Bay, Kowloon, Hong Kong; China
[66] Department of Physics, National Tsing Hua University, Hsinchu; Taiwan
[67] IJCLab, Université Paris-Saclay, CNRS/IN2P3, 91405, Orsay; France
[68] Department of Physics, Indiana University, Bloomington IN; United States of America
[69] [(a)] INFN Gruppo Collegato di Udine, Sezione di Trieste, Udine;[(b)] ICTP, Trieste;[(c)] Dipartimento Politecnico di Ingegneria e Architettura, Università di Udine, Udine; Italy
[70] [(a)] INFN Sezione di Lecce;[(b)] Dipartimento di Matematica e Fisica, Università del Salento, Lecce; Italy
[71] [(a)] INFN Sezione di Milano;[(b)] Dipartimento di Fisica, Università di Milano, Milano; Italy
[72] [(a)] INFN Sezione di Napoli;[(b)] Dipartimento di Fisica, Università di Napoli, Napoli; Italy
[73] [(a)] INFN Sezione di Pavia;[(b)] Dipartimento di Fisica, Università di Pavia, Pavia; Italy
[74] [(a)] INFN Sezione di Pisa;[(b)] Dipartimento di Fisica E. Fermi, Università di Pisa, Pisa; Italy
[75] [(a)] INFN Sezione di Roma;[(b)] Dipartimento di Fisica, Sapienza Università di Roma, Roma; Italy
[76] [(a)] INFN Sezione di Roma Tor Vergata;[(b)] Dipartimento di Fisica, Università di Roma Tor Vergata, Roma; Italy
[77] [(a)] INFN Sezione di Roma Tre;[(b)] Dipartimento di Matematica e Fisica, Università Roma Tre, Roma; Italy
[78] [(a)] INFN-TIFPA;[(b)] Università degli Studi di Trento, Trento; Italy
[79] Universität Innsbruck, Department of Astro and Particle Physics, Innsbruck; Austria
[80] University of Iowa, Iowa City IA; United States of America
[81] Department of Physics and Astronomy, Iowa State University, Ames IA; United States of America
[82] [(a)] Departamento de Engenharia Elétrica, Universidade Federal de Juiz de Fora (UFJF), Juiz de Fora;[(b)] Universidade Federal do Rio De Janeiro COPPE/EE/IF, Rio de Janeiro;[(c)] Instituto de Física, Universidade de São Paulo, São Paulo; Brazil
[83] KEK, High Energy Accelerator Research Organization, Tsukuba; Japan
[84] Graduate School of Science, Kobe University, Kobe; Japan
[85] [(a)] AGH University of Science and Technology, Faculty of Physics and Applied Computer Science, Krakow;[(b)] Marian Smoluchowski Institute of Physics, Jagiellonian University, Krakow; Poland
[86] Institute of Nuclear Physics Polish Academy of Sciences, Krakow; Poland
[87] Faculty of Science, Kyoto University, Kyoto; Japan
[88] Kyoto University of Education, Kyoto; Japan
[89] Research Center for Advanced Particle Physics and Department of Physics, Kyushu University, Fukuoka; Japan
[90] Instituto de Física La Plata, Universidad Nacional de La Plata and CONICET, La Plata; Argentina
[91] Physics Department, Lancaster University, Lancaster; United Kingdom
[92] Oliver Lodge Laboratory, University of Liverpool, Liverpool; United Kingdom
[93] Department of Experimental Particle Physics, Jožef Stefan Institute and Department of Physics, University of Ljubljana, Ljubljana; Slovenia
[94] School of Physics and Astronomy, Queen Mary University of London, London; United Kingdom
[95] Department of Physics, Royal Holloway University of London, Egham; United Kingdom
[96] Department of Physics and Astronomy, University College London, London; United Kingdom
[97] Louisiana Tech University, Ruston LA; United States of America
[98] Fysiska institutionen, Lunds universitet, Lund; Sweden
[99] Centre de Calcul de l'Institut National de Physique Nucléaire et de Physique des Particules (IN2P3), Villeurbanne; France
[100] Departamento de Física Teorica C-15 and CIAFF, Universidad Autónoma de Madrid, Madrid; Spain
[101] Institut für Physik, Universität Mainz, Mainz; Germany
[102] School of Physics and Astronomy, University of Manchester, Manchester; United Kingdom
[103] CPPM, Aix-Marseille Université, CNRS/IN2P3, Marseille; France
[104] Department of Physics, University of Massachusetts, Amherst MA; United States of America
[105] Department of Physics, McGill University, Montreal QC; Canada

JHEP06(2023)019

[106] School of Physics, University of Melbourne, Victoria; Australia
[107] Department of Physics, University of Michigan, Ann Arbor MI; United States of America
[108] Department of Physics and Astronomy, Michigan State University, East Lansing MI; United States of America
[109] Group of Particle Physics, University of Montreal, Montreal QC; Canada
[110] Fakultät für Physik, Ludwig-Maximilians-Universität München, München; Germany
[111] Max-Planck-Institut für Physik (Werner-Heisenberg-Institut), München; Germany
[112] Nagasaki Institute of Applied Science, Nagasaki; Japan
[113] Graduate School of Science and Kobayashi-Maskawa Institute, Nagoya University, Nagoya; Japan
[114] Department of Physics and Astronomy, University of New Mexico, Albuquerque NM; United States of America
[115] Institute for Mathematics, Astrophysics and Particle Physics, Radboud University/Nikhef, Nijmegen; Netherlands
[116] Nikhef National Institute for Subatomic Physics and University of Amsterdam, Amsterdam; Netherlands
[117] Department of Physics, Northern Illinois University, DeKalb IL; United States of America
[118] Department of Physics, New York University, New York NY; United States of America
[119] Ochanomizu University, Otsuka, Bunkyo-ku, Tokyo; Japan
[120] Ohio State University, Columbus OH; United States of America
[121] Faculty of Science, Okayama University, Okayama; Japan
[122] Homer L. Dodge Department of Physics and Astronomy, University of Oklahoma, Norman OK; United States of America
[123] Department of Physics, Oklahoma State University, Stillwater OK; United States of America
[124] Palacký University, Joint Laboratory of Optics, Olomouc; Czech Republic
[125] Institute for Fundamental Science, University of Oregon, Eugene, OR; United States of America
[126] Graduate School of Science, Osaka University, Osaka; Japan
[127] Department of Physics, University of Oslo, Oslo; Norway
[128] Department of Physics, Oxford University, Oxford; United Kingdom
[129] LPNHE, Sorbonne Université, Université Paris Cité, CNRS/IN2P3, Paris; France
[130] Department of Physics, University of Pennsylvania, Philadelphia PA; United States of America
[131] Department of Physics and Astronomy, University of Pittsburgh, Pittsburgh PA; United States of America
[132] [(a)] Laboratório de Instrumentação e Física Experimental de Partículas — LIP, Lisboa;[(b)] Departamento de Física, Faculdade de Ciências, Universidade de Lisboa, Lisboa;[(c)] Departamento de Física, Universidade de Coimbra, Coimbra;[(d)] Centro de Física Nuclear da Universidade de Lisboa, Lisboa;[(e)] Departamento de Física, Universidade do Minho, Braga;[(f)] Departamento de Física Teórica y del Cosmos, Universidad de Granada, Granada (Spain);[(g)] Dep Física and CEFITEC of Faculdade de Ciências e Tecnologia, Universidade Nova de Lisboa, Caparica;[(h)] Departamento de Física, Instituto Superior Técnico, Universidade de Lisboa, Lisboa; Portugal
[133] Institute of Physics of the Czech Academy of Sciences, Prague; Czech Republic
[134] Czech Technical University in Prague, Prague; Czech Republic
[135] Charles University, Faculty of Mathematics and Physics, Prague; Czech Republic
[136] Particle Physics Department, Rutherford Appleton Laboratory, Didcot; United Kingdom
[137] IRFU, CEA, Université Paris-Saclay, Gif-sur-Yvette; France
[138] Santa Cruz Institute for Particle Physics, University of California Santa Cruz, Santa Cruz CA; United States of America
[139] [(a)] Departamento de Física, Pontificia Universidad Católica de Chile, Santiago;[(b)] Universidad Andres Bello, Department of Physics, Santiago;[(c)] Departamento de Física, Universidad Técnica Federico Santa María, Valparaíso; Chile
[140] Universidade Federal de São João del Rei (UFSJ), São João del Rei; Brazil
[141] Department of Physics, University of Washington, Seattle WA; United States of America
[142] Department of Physics and Astronomy, University of Sheffield, Sheffield; United Kingdom
[143] Department of Physics, Shinshu University, Nagano; Japan

JHEP06(2023)019

[144] Department Physik, Universität Siegen, Siegen; Germany
[145] Department of Physics, Simon Fraser University, Burnaby BC; Canada
[146] SLAC National Accelerator Laboratory, Stanford CA; United States of America
[147] Department of Physics, Royal Institute of Technology, Stockholm; Sweden
[148] Departments of Physics and Astronomy, Stony Brook University, Stony Brook NY; United States of America
[149] Department of Physics and Astronomy, University of Sussex, Brighton; United Kingdom
[150] School of Physics, University of Sydney, Sydney; Australia
[151] Institute of Physics, Academia Sinica, Taipei; Taiwan
[152] [(a)] E. Andronikashvili Institute of Physics, Iv. Javakhishvili Tbilisi State University, Tbilisi;[(b)] High Energy Physics Institute, Tbilisi State University, Tbilisi; Georgia
[153] Department of Physics, Technion, Israel Institute of Technology, Haifa; Israel
[154] Raymond and Beverly Sackler School of Physics and Astronomy, Tel Aviv University, Tel Aviv; Israel
[155] Department of Physics, Aristotle University of Thessaloniki, Thessaloniki; Greece
[156] International Center for Elementary Particle Physics and Department of Physics, University of Tokyo, Tokyo; Japan
[157] Graduate School of Science and Technology, Tokyo Metropolitan University, Tokyo; Japan
[158] Department of Physics, Tokyo Institute of Technology, Tokyo; Japan
[159] Department of Physics, University of Toronto, Toronto ON; Canada
[160] [(a)] TRIUMF, Vancouver BC;[(b)] Department of Physics and Astronomy, York University, Toronto ON; Canada
[161] Division of Physics and Tomonaga Center for the History of the Universe, Faculty of Pure and Applied Sciences, University of Tsukuba, Tsukuba; Japan
[162] Department of Physics and Astronomy, Tufts University, Medford MA; United States of America
[163] Department of Physics and Astronomy, University of California Irvine, Irvine CA; United States of America
[164] Department of Physics and Astronomy, University of Uppsala, Uppsala; Sweden
[165] Department of Physics, University of Illinois, Urbana IL; United States of America
[166] Instituto de Física Corpuscular (IFIC), Centro Mixto Universidad de Valencia — CSIC, Valencia; Spain
[167] Department of Physics, University of British Columbia, Vancouver BC; Canada
[168] Department of Physics and Astronomy, University of Victoria, Victoria BC; Canada
[169] Fakultät für Physik und Astronomie, Julius-Maximilians-Universität Würzburg, Würzburg; Germany
[170] Department of Physics, University of Warwick, Coventry; United Kingdom
[171] Waseda University, Tokyo; Japan
[172] Department of Particle Physics and Astrophysics, Weizmann Institute of Science, Rehovot; Israel
[173] Department of Physics, University of Wisconsin, Madison WI; United States of America
[174] Fakultät für Mathematik und Naturwissenschaften, Fachgruppe Physik, Bergische Universität Wuppertal, Wuppertal; Germany
[175] Department of Physics, Yale University, New Haven CT; United States of America

[a] Also Affiliated with an institute covered by a cooperation agreement with CERN
[b] Also at Borough of Manhattan Community College, City University of New York, New York NY; United States of America
[c] Also at CERN, Geneva; Switzerland
[d] Also at CPPM, Aix-Marseille Université, CNRS/IN2P3, Marseille; France
[e] Also at Département de Physique Nucléaire et Corpusculaire, Université de Genève, Genève; Switzerland
[f] Also at Departament de Fisica de la Universitat Autonoma de Barcelona, Barcelona; Spain
[g] Also at Department of Applied Physics and Astronomy, University of Sharjah, Sharjah; United Arab Emirates
[h] Also at Department of Financial and Management Engineering, University of the Aegean, Chios; Greece
[i] Also at Department of Physics and Astronomy, Michigan State University, East Lansing MI; United States of America

JHEP06(2023)019

[j] Also at Department of Physics and Astronomy, University of Louisville, Louisville, KY; United States of America
[k] Also at Department of Physics, Ben Gurion University of the Negev, Beer Sheva; Israel
[l] Also at Department of Physics, California State University, East Bay; United States of America
[m] Also at Department of Physics, California State University, Fresno; United States of America
[n] Also at Department of Physics, California State University, Sacramento; United States of America
[o] Also at Department of Physics, King's College London, London; United Kingdom
[p] Also at Department of Physics, Stanford University, Stanford CA; United States of America
[q] Also at Department of Physics, University of Adelaide, Adelaide; Australia
[r] Also at Department of Physics, University of Fribourg, Fribourg; Switzerland
[s] Also at Dipartimento di Matematica, Informatica e Fisica, Università di Udine, Udine; Italy
[t] Also at Giresun University, Faculty of Engineering, Giresun; Türkiye
[u] Also at Hellenic Open University, Patras; Greece
[v] Also at IJCLab, Université Paris-Saclay, CNRS/IN2P3, 91405, Orsay; France
[w] Associated at INFN e Laboratori Nazionali di Frascati, Frascati; Italy
[x] Also at Institucio Catalana de Recerca i Estudis Avancats, ICREA, Barcelona; Spain
[y] Also at Institut für Experimentalphysik, Universität Hamburg, Hamburg; Germany
[z] Also at Institute for Mathematics, Astrophysics and Particle Physics, Radboud University/Nikhef, Nijmegen; Netherlands
[aa] Also at Institute for Nuclear Research and Nuclear Energy (INRNE) of the Bulgarian Academy of Sciences, Sofia; Bulgaria
[ab] Also at Institute for Particle and Nuclear Physics, Wigner Research Centre for Physics, Budapest; Hungary
[ac] Also at Institute of Particle Physics (IPP); Canada
[ad] Also at Institute of Physics, Azerbaijan Academy of Sciences, Baku; Azerbaijan
[ae] Also at Institute of Theoretical Physics, Ilia State University, Tbilisi; Georgia
[af] Also at Instituto de Fisica Teorica, IFT-UAM/CSIC, Madrid; Spain
[ag] Also at Istanbul University, Dept. of Physics, Istanbul; Türkiye
[ah] Also at Louisiana Tech University, Ruston LA; United States of America
[ai] Also at Manhattan College, New York NY; United States of America
[aj] Also at Physics Department, An-Najah National University, Nablus; Palestine
[ak] Also at Physics Dept, University of South Africa, Pretoria; South Africa
[al] Also at Physikalisches Institut, Albert-Ludwigs-Universität Freiburg, Freiburg; Germany
[am] Also at The City College of New York, New York NY; United States of America
[an] Also at The Collaborative Innovation Center of Quantum Matter (CICQM), Beijing; China
[ao] Also at TRIUMF, Vancouver BC; Canada
[ap] Also at Università di Napoli Parthenope, Napoli; Italy
[*] Deceased

JHEP06(2023)019

Published for SISSA by Springer

Received: November 15, 2021
Revised: February 26, 2022
Accepted: May 16, 2022
Published: June 17, 2022

Measurement of Higgs boson decay into b-quarks in associated production with a top-quark pair in pp collisions at $\sqrt{s} = 13$ TeV with the ATLAS detector

The ATLAS collaboration

E-mail: atlas.publications@cern.ch

Abstract: The associated production of a Higgs boson and a top-quark pair is measured in events characterised by the presence of one or two electrons or muons. The Higgs boson decay into a b-quark pair is used. The analysed data, corresponding to an integrated luminosity of 139 fb^{-1}, were collected in proton-proton collisions at the Large Hadron Collider between 2015 and 2018 at a centre-of-mass energy of $\sqrt{s} = 13$ TeV. The measured signal strength, defined as the ratio of the measured signal yield to that predicted by the Standard Model, is $0.35^{+0.36}_{-0.34}$. This result is compatible with the Standard Model prediction and corresponds to an observed (expected) significance of 1.0 (2.7) standard deviations. The signal strength is also measured differentially in bins of the Higgs boson transverse momentum in the simplified template cross-section framework, including a bin for specially selected boosted Higgs bosons with transverse momentum above 300 GeV.

Keywords: Hadron-Hadron Scattering

ArXiv ePrint: 2111.06712

Open Access, Copyright CERN,
for the benefit of the ATLAS Collaboration.
Article funded by SCOAP^3.

https://doi.org/10.1007/JHEP06(2022)097

JHEP06(2022)097

Contents

1 Introduction **1**

2 ATLAS detector **3**

3 Signal and background modelling **4**
- 3.1 Signal modelling 5
- 3.2 $t\bar{t}$ + jets background 5
- 3.3 Other backgrounds 7

4 Object and event selection **8**

5 Analysis strategy **10**
- 5.1 Analysis regions 11
- 5.2 Multivariate analysis 12

6 Systematic uncertainties **14**
- 6.1 Experimental uncertainties 15
- 6.2 Theoretical modelling uncertainties 16

7 Results **19**

8 Conclusion **33**

A Input variables to the classification BDTs **34**

The ATLAS collaboration **46**

1 Introduction

The Higgs boson [1–3] was discovered by the ATLAS and CMS collaborations [4, 5] in 2012, with a mass of around 125 GeV [6]. Since then, the analysis of proton-proton (pp) collision data at centre-of-mass energies of 7 TeV, 8 TeV and 13 TeV delivered by the Large Hadron Collider (LHC) [7] has led to more detailed measurements of its properties and couplings, testing the predictions of the Standard Model (SM). Of particular interest is the Yukawa coupling to the top quark, the heaviest elementary particle in the SM, which could be very sensitive to effects of physics beyond the SM (BSM) [8].

Both the ATLAS and CMS collaborations have observed the interaction of the Higgs boson with third-generation fermions of the SM. The coupling to τ-leptons was measured in the observation of $H \to \tau\tau$ decays [9–11], while the observation of the decay of the Higgs boson into b-quark pairs provided direct evidence for the Yukawa coupling to down-type quarks [12, 13]. The interaction of the Higgs boson with the top quark was indirectly constrained (assuming no BSM phenomena in the loops) from measurements of gluon-gluon fusion Higgs production and decay to $\gamma\gamma$ [9], before being directly measured in the observation of Higgs boson production in association with a pair of top quarks ($t\bar{t}H$) [14, 15].

JHEP06(2022)097

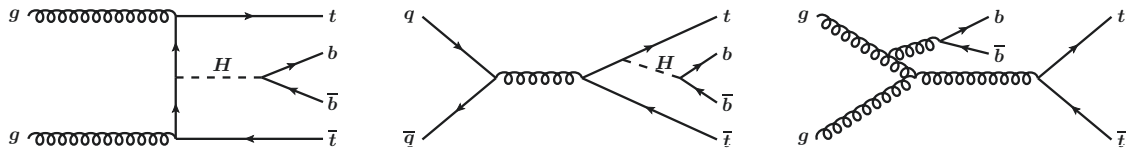

(a) $t\bar{t}H(b\bar{b})$ t-channel (b) $t\bar{t}H(b\bar{b})$ s-channel (c) $t\bar{t}+b\bar{b}$

Figure 1. Representative tree-level Feynman diagrams for the production of a Higgs boson in association with a top-quark pair ($t\bar{t}H$) in (a) the t-channel and (b) the s-channel and the subsequent decay of the Higgs boson into $b\bar{b}$, and for (c) the main $t\bar{t}+b\bar{b}$ background.

The $t\bar{t}H$ production mode, in which the top quark couples to the Higgs boson at tree level, is the most favourable to extract direct information on the top-quark Yukawa coupling without assumptions about the potential presence of BSM physics [16–19].

Although this production mode contributes only around 1% of the total Higgs boson production cross-section at the LHC [20], the top quarks in the final state offer a distinctive signature and allow access to many Higgs boson decay modes. The decay into two b-quarks ($H \to b\bar{b}$) is the most probable, with a SM branching fraction of about 58% [20]. Furthermore, in the $H \to b\bar{b}$ decay mode the reconstruction of the Higgs boson kinematics is possible, which allows the extraction of additional information about the structure of the top-Higgs interaction [21–24]. This analysis therefore aims to select events with a Higgs boson produced in association with a pair of top quarks and decaying into a pair of b-quarks $\left(t\bar{t}H(b\bar{b})\right)$, in which one or both top quarks decay semileptonically, producing an electron or a muon, collectively referred to as leptons (ℓ).[1] With many final-state particles, the main challenges are the low efficiency to reconstruct and identify all of them, the large combinatorial ambiguities when trying to match the observed objects to the decay products of the Higgs boson and top quarks, and the large background of $t\bar{t}+$jets processes (in particular when these jets originate from b- or c-quarks), which have a much larger production cross-section than the signal. Representative Feynman diagrams for the $t\bar{t}H(b\bar{b})$ signal and dominant $t\bar{t}+b\bar{b}$ background are shown in figure 1.

The ATLAS Collaboration searched for $t\bar{t}H(b\bar{b})$ production at $\sqrt{s} = 8\,\text{TeV}$ in final states with at least one [25] or no lepton [26], and at $\sqrt{s} = 13\,\text{TeV}$ with at least one lepton in the final state with data collected in 2015 and 2016, corresponding to an integrated luminosity of $36.1\,\text{fb}^{-1}$ [27]. A combined signal strength (defined as the ratio of the measured signal yield to that predicted by the Standard Model) of $0.84^{+0.64}_{-0.61}$ was measured, with an observed (expected) significance of 1.4 (1.6) standard deviations. This result was combined with analyses of Higgs boson decays into massive vector bosons, τ-leptons, or photons to reach observation of the $t\bar{t}H$ production mode [14]. The CMS Collaboration searched for the same processes using $35.9\,\text{fb}^{-1}$ of data collected at $\sqrt{s} = 13\,\text{TeV}$ in 2016, in events with at least one lepton [28] or no lepton [29], and measured a signal strength of 0.72 ± 0.45 and 0.9 ± 1.5, respectively. These results also contributed to the observation of the $t\bar{t}H$ production mode [15].

In this paper, a measurement of the $t\bar{t}H$ production cross-section in the $H \to b\bar{b}$ channel is performed using the LHC Run 2 pp collision data collected by the ATLAS detector,

[1] Electrons and muons from the decay of a τ-lepton itself originating from a W boson are included.

JHEP06(2022)097

corresponding to an integrated luminosity of 139 fb^{-1} at $\sqrt{s} = 13$ TeV. Events with either one lepton or two leptons are analysed separately in exclusive single-lepton or dilepton categories depending on the number of leptons, the number of jets and the number of jets identified as originating from b-hadrons (b-jets). In the single-lepton channel (but not in the dilepton channel because the expected number of events is small), a specific category, referred to as 'boosted' in the following, is designed to select events in which the Higgs boson is produced with high transverse momentum (p_{T}). The non-boosted categories, where the Higgs boson decay products are less collimated, are referred to as 'resolved'. Machine-learning algorithms are used to classify events into signal-rich categories, which are analysed together with the signal-depleted ones in a combined profile likelihood fit. The output distributions of these multivariate algorithms are used as the main discriminant to extract the signal. This signal extraction fit simultaneously determines the event yields for the signal and for the most important background components, while constraining the overall background model within the assigned systematic uncertainties. In addition, making use of the possibility to reconstruct the Higgs boson kinematics in the $H \to b\bar{b}$ channel, the cross-section is measured as a function of the Higgs boson 'truth' transverse momentum $\hat{p}_{\text{T}}^{H}$, as obtained from Monte Carlo simulation, in the simplified template cross-sections (STXS) formalism [20], which aims to reduce the theory dependencies that are folded into the measurements.

Several aspects of the analysis have been improved relative to the previous version [27]. The full Run 2 dataset is analysed, with improved reconstruction algorithms and detector calibrations, which in turn enhance the performance of the b-tagging algorithm. This allows the use of tighter selection criteria to reject events in poorly modelled regions of phase space, and to define analysis regions differential in Higgs boson p_{T}. An enhanced model is adopted for the $t\bar{t}+$jets background, with updated event generator versions, a higher-order precision prediction for the $t\bar{t}+b\bar{b}$ process, an increased number of simulated events, and an improved assessment of uncertainties. Finally, a new deep neural network improves the performance of the boosted channel.

This paper is organised as follows. The ATLAS detector is described in section 2. The signal and background modelling is presented in section 3. Section 4 summarises the selection criteria for reconstructed objects and events, while section 5 describes the analysis strategy. Systematic uncertainties are discussed in section 6. Results are presented in section 7, and the conclusions in section 8.

2 ATLAS detector

The ATLAS experiment [30–33] at the LHC is a multipurpose particle detector with a forward-backward symmetric cylindrical geometry and a near 4π coverage in solid angle.[2]

[2]ATLAS uses a right-handed coordinate system with its origin at the nominal interaction point (IP) in the centre of the detector and the z-axis along the beam pipe. The x-axis points from the IP to the centre of the LHC ring, and the y-axis points upwards. Cylindrical coordinates (r, ϕ) are used in the transverse plane, ϕ being the azimuthal angle around the z-axis. The rapidity is defined as $y = (1/2)\ln[(E + p_z)/(E - p_z)]$ where E is the energy and p_z is the longitudinal component of the momentum along the beam pipe. The pseudorapidity is defined in terms of the polar angle θ as $\eta = -\ln\tan(\theta/2)$. Angular distance is measured in units of $\Delta R \equiv \sqrt{(\Delta\eta)^2 + (\Delta\phi)^2}$.

JHEP06(2022)097

It consists of an inner tracking detector surrounded by a thin superconducting solenoid providing a 2 T axial magnetic field, electromagnetic and hadron calorimeters, and a muon spectrometer. The inner tracking detector (ID) covers the pseudorapidity range $|\eta| < 2.5$. It consists of silicon pixel, silicon microstrip, and transition radiation tracking detectors. Lead/liquid-argon (LAr) sampling calorimeters provide electromagnetic (EM) energy measurements with high granularity. A steel/scintillator-tile hadron calorimeter covers the central pseudorapidity range $|\eta| < 1.7$. The endcap and forward regions are instrumented with LAr calorimeters for both the EM and hadronic energy measurements up to $|\eta| = 4.9$. The muon spectrometer surrounds the calorimeters and is based on three large air-core toroidal superconducting magnets with eight coils each. The field integral of the toroids ranges between 2 and 6 T m across most of the detector. The muon spectrometer includes a system of precision chambers for tracking and fast detectors for triggering. A two-level trigger system is used to select events. The first-level trigger is implemented in hardware and uses a subset of the detector information to accept events at a rate below 100 kHz. This is followed by a software-based trigger that reduces the accepted event rate to 1 kHz on average depending on the data-taking conditions [34]. An extensive software suite [35] is used in the reconstruction and analysis of real and simulated data, in detector operations, and in the trigger and data acquisition systems of the experiment.

3 Signal and background modelling

Simulated event samples are used to model the $t\bar{t}H$ signal and the background processes. The numbers of selected events and the distribution shapes of variables used to discriminate between signal and background enter into the signal extraction fit, which also constrains the modelling of the background processes. The Monte Carlo (MC) samples were produced using either the full ATLAS detector simulation [36] based on GEANT4 [37] or a faster simulation where the full GEANT4 simulation of the calorimeter response is replaced by a detailed parameterisation of the shower shapes [36]. For the observables used in the analysis, the two simulations were found to give similar modelling. To simulate the effects of multiple interactions in the same and neighbouring bunch crossings (pile-up), additional interactions were generated using PYTHIA 8.186 [38] with a set of tuned parameters called the A3 tune [39] and overlaid onto the simulated hard-scatter event. Simulated events are reweighted to match the pile-up conditions observed in the full Run 2 dataset, with a mean number of pp interactions per bunch crossing of 34. All simulated events are processed through the same reconstruction algorithms and analysis chain as the data.

In all samples where the parton shower (PS), hadronisation, and multi-parton interactions (MPI) were generated with either PYTHIA 8 or HERWIG 7 [40, 41], the decays of b- and c-hadrons were simulated using the EVTGEN 1.6.0 program [42]. The b-quark mass was set to $m_b = 4.80$ GeV (4.50 GeV) for samples using PYTHIA 8 (HERWIG 7). For PYTHIA 8, the A14 tune [43] and the NNPDF2.3LO parton distribution function (PDF) set [44] were used. For HERWIG 7, the H7UE tune [41] was used with the MMHT2014LO PDF set [45]. The Higgs boson mass was set to $m_H = 125.0$ GeV, and the top-quark mass to $m_t = 172.5$ GeV. The precision of the matrix element (ME) generators is next-to-leading order (NLO) in

JHEP06(2022)097

quantum chromodynamics (QCD) for most samples. Some samples are normalised to higher precision in QCD (next-to-next-to-leading order, NNLO, or next-to-next-to-leading logarithm, NNLL) or with electroweak (EW) corrections. A summary of all generated samples is presented in table 1, which includes both the samples used for nominal predictions and other samples used to assess systematic uncertainties. Further details are provided in the following subsections.

3.1 Signal modelling

In $t\bar{t}H$ events the production and decays were modelled in the five-flavour scheme using the Powheg Box [61–65] generator at NLO in QCD with the NNPDF3.0nlo [66] PDF set. The h_{damp} parameter[3] was set to $0.75 \times (m_t + m_{\bar{t}} + m_H) = 352.5\,\text{GeV}$, and the functional form of the renormalisation and factorisation scales were both set to $\sqrt[3]{m_{\text{T}}(t) \cdot m_{\text{T}}(\bar{t}) \cdot m_{\text{T}}(H)}$ (where $m_{\text{T}} = \sqrt{m^2 + p_{\text{T}}^2}$ is the transverse mass of a particle). The events were showered by Pythia 8 and all Higgs boson decay modes are considered. The samples are normalised to the fixed-order cross-section calculation, $\sigma_{t\bar{t}H} = 507^{+35}_{-50}\,\text{fb}$, which includes NLO QCD and EW corrections [20] for a Higgs boson mass of 125 GeV.

3.2 $t\bar{t}$ + jets background

Simulated $t\bar{t}$ + jets events are categorised according to the flavour of additional jets in the event, using the procedure described in ref. [25]. For this purpose, jets are reconstructed from stable particles (mean lifetime $\tau > 3 \times 10^{-11}$ s) using the anti-k_t algorithm [67, 68], and the number of b- or c-hadrons within $\Delta R = 0.4$ of the jet axis is considered (with $p_{\text{T}} > 5\,\text{GeV}$ for the leading b- or c-hadron around the jet), excluding particles produced by the top-quark decay. Events are labelled as $t\bar{t} + \geq 1b$ if at least one b-flavour jet is identified, or else as $t\bar{t} + \geq 1c$ if at least one c-flavour jet is identified, and otherwise as $t\bar{t}$ + light. Where necessary, the $t\bar{t} + \geq 1b$ events are further separated into $t\bar{t} + 1b$ (where exactly one jet is matched to at least one b-hadron) and $t\bar{t} + \geq 2b$ (all remaining events).

To accurately model the dominant $t\bar{t} + \geq 1b$ background, a sample with $t\bar{t} + b\bar{b}$ MEs was produced at NLO QCD accuracy in the four-flavour scheme with the Powheg Box Res [69] generator and OpenLoops [70, 71], using a pre-release of the implementation of this process in Powheg Box Res provided by the authors [72], with the NNPDF3.0nlo nf4 [66] PDF set, and using Pythia 8 for the PS and hadronisation. The factorisation scale was set to $0.5 \times \Sigma_{i=t,\bar{t},b,\bar{b},j} m_{\text{T}}(i)$ (where j stands for extra partons), the renormalisation scale was set to $\sqrt[4]{m_{\text{T}}(t) \cdot m_{\text{T}}(\bar{t}) \cdot m_{\text{T}}(b) \cdot m_{\text{T}}(\bar{b})}$, and the h_{damp} parameter was set to $0.5 \times \Sigma_{i=t,\bar{t},b,\bar{b}} m_{\text{T}}(i)$. The mass of the two b-quarks produced in the ME in association with the two top quarks was set to the same value as the mass of the b-quarks from the top-quark decays, $m_b = 4.95\,\text{GeV}$.

Inclusive $t\bar{t}$ + jets events were also generated with $t\bar{t}$ MEs in the five-flavour scheme using the Powheg Box v2 generator at NLO in QCD, using Pythia 8 for the PS and hadronisation. Here, the h_{damp} parameter was set to 1.5 m_t [60], and the functional form of

[3] The h_{damp} parameter controls the p_{T} of the first additional emission beyond the leading-order Feynman diagram in the PS and therefore regulates the high-p_{T} emission against which the $t\bar{t}H$ system recoils.

JHEP06(2022)097

Process	ME generator	ME PDF	PS	Normalisation
Higgs boson				
$t\bar{t}H$	Powheg Box v2	NNPDF3.0nlo	Pythia 8.230	NLO+NLO (EW) [20]
	Powheg Box v2	NNPDF3.0nlo	Herwig 7.04	NLO+NLO (EW) [20]
	MadGraph5_aMC@NLO 2.6.0	NNPDF3.0nlo	Pythia 8.230	NLO+NLO (EW) [20]
$tHjb$	MadGraph5_aMC@NLO 2.6.2	NNPDF3.0nlo nf4	Pythia 8.230	–
tWH	MadGraph5_aMC@NLO 2.6.2 [DR]	NNPDF3.0nlo	Pythia 8.235	–
$t\bar{t}$ + jets and single-top				
$t\bar{t}$	Powheg Box v2	NNPDF3.0nlo	Pythia 8.230	NNLO+NNLL [46–52]
	Powheg Box v2	NNPDF3.0nlo	Herwig 7.04	NNLO+NNLL [46–52]
	MadGraph5_aMC@NLO 2.6.0	NNPDF3.0nlo	Pythia 8.230	NNLO+NNLL [46–52]
$t\bar{t}+b\bar{b}$	Powheg Box Res	NNPDF3.0nlo nf4	Pythia 8.230	–
	Sherpa 2.2.1	NNPDF3.0nnlo nf4	Sherpa	–
tW	Powheg Box v2 [DR]	NNPDF3.0nlo	Pythia 8.230	NLO+NNLL [53, 54]
	Powheg Box v2 [DS]	NNPDF3.0nlo	Pythia 8.230	NLO+NNLL [53, 54]
	Powheg Box v2 [DR]	NNPDF3.0nlo	Herwig 7.04	NLO+NNLL [53, 54]
	MadGraph5_aMC@NLO 2.6.2 [DR]	CT10nlo	Pythia 8.230	NLO+NNLL [53, 54]
t-channel	Powheg Box v2	NNPDF3.0nlo nf4	Pythia 8.230	NLO [55, 56]
	Powheg Box v2	NNPDF3.0nlo nf4	Herwig 7.04	NLO [55, 56]
	MadGraph5_aMC@NLO 2.6.2	NNPDF3.0nlo nf4	Pythia 8.230	NLO [55, 56]
s-channel	Powheg Box v2	NNPDF3.0nlo	Pythia 8.230	NLO [55, 56]
	Powheg Box v2	NNPDF3.0nlo	Herwig 7.04	NLO [55, 56]
	MadGraph5_aMC@NLO 2.6.2	NNPDF3.0nlo	Pythia 8.230	NLO [55, 56]
Other				
W+jets	Sherpa 2.2.1 (NLO [2j], LO [4j])	NNPDF3.0nnlo	Sherpa	NNLO [57]
Z+jets	Sherpa 2.2.1 (NLO [2j], LO [4j])	NNPDF3.0nnlo	Sherpa	NNLO [57]
VV (had.)	Sherpa 2.2.1	NNPDF3.0nnlo	Sherpa	–
VV (lep.)	Sherpa 2.2.2	NNPDF3.0nnlo	Sherpa	–
VV (lep.) + jj	Sherpa 2.2.2 (LO [EW])	NNPDF3.0nnlo	Sherpa	–
$t\bar{t}W$	MadGraph5_aMC@NLO 2.3.3	NNPDF3.0nlo	Pythia 8.210	NLO+NLO (EW) [20]
	Sherpa 2.0.0 (LO [2j])	NNPDF3.0nnlo	Sherpa	NLO+NLO (EW) [20]
$t\bar{t}\ell\ell$	MadGraph5_aMC@NLO 2.3.3	NNPDF3.0nlo	Pythia 8.210	NLO+NLO (EW) [20]
	Sherpa 2.0.0 (LO [1j])	NNPDF3.0nnlo	Sherpa	NLO+NLO (EW) [20]
$t\bar{t}Z$ $(qq, \nu\nu)$	MadGraph5_aMC@NLO 2.3.3	NNPDF3.0nlo	Pythia 8.210	NLO+NLO (EW) [20]
	Sherpa 2.0.0 (LO [2j])	NNPDF3.0nnlo	Sherpa	NLO+NLO (EW) [20]
$t\bar{t}t\bar{t}$	MadGraph5_aMC@NLO 2.3.3	NNPDF3.1nlo	Pythia 8.230	NLO+NLO (EW) [58]
tZq	MadGraph5_aMC@NLO 2.3.3 (LO)	CTEQ6L1	Pythia 8.212	–
tWZ	MadGraph5_aMC@NLO 2.3.3 [DR]	NNPDF3.0nlo	Pythia 8.230	–

Table 1. Table summarising the generator set-ups for samples used in this analysis. The first row for each sample details the nominal settings used for this process in the analysis. Any additional rows describe samples which are used to evaluate the modelling and performance of the analysis. For overlap between $t\bar{t}$ and tW-like diagrams, samples using the diagram removal scheme [59] are listed as [DR] and samples using the diagram subtraction scheme [59, 60] are listed as [DS]. The precision of the ME generator is NLO in QCD if no additional information is provided in parentheses. The higher-order cross-section used to normalise these samples is listed in the last column and refers to the order of QCD processes if no additional information is provided. If no information is present in this column, no higher-order K-factor is applied to this process. For the VV Sherpa samples, 'lep.' ('had.') means that both bosons decay leptonically (one decays leptonically and one hadronically).

JHEP06(2022)097

the renormalisation and factorisation scales was set to $m_{\mathrm{T}}(t)$.[4] The $t\bar{t}+\geq 1c$ and $t\bar{t}+$ light events using this prediction are combined with the previously described $t\bar{t}+\geq 1b$ sample to form the nominal $t\bar{t}$ model, while the $t\bar{t}+\geq 1b$ events from this five-flavour scheme are used only to assign modelling uncertainties.

3.3 Other backgrounds

The QCD $V+$jets processes (i.e. $W+$jets and $Z+$jets) were simulated with the Sherpa 2.2.1 generator [73]. In this set-up, NLO-accurate MEs for up to two partons, and leading-order (LO) accurate MEs for up to four partons were calculated with the Comix [74] and OpenLoops libraries. They were matched with the Sherpa parton shower [75] by using the MEPS@NLO prescription [76–79] with the set of tuned parameters developed by the Sherpa authors and based on the NNPDF3.0nnlo set of PDFs [66]. A data-driven correction to the normalisation was derived for $Z+$jets predictions containing at least two heavy-flavour jets (where heavy-flavour means jets originating from b-hadrons and c-hadrons). Events are selected, with objects passing the selection discussed in section 4, in dedicated control regions in data defined by requiring at least two jets and two opposite-electric-charge same-flavour leptons (e^+e^- or $\mu^+\mu^-$) with an invariant mass inside the Z-boson mass window 83–99 GeV. A 25% yield increase is found to improve the modelling of $Z+$jets events with at least two heavy-flavour jets, consistent with ref. [80].

Diboson events were simulated with the Sherpa 2.2.1 and 2.2.2 generators. In this set-up multiple MEs were matched and merged with the Sherpa PS based on Catani-Seymour dipole factorisation [74, 75] using the MEPS@NLO prescription. For semileptonically and fully leptonically decaying diboson event samples, as well as loop-induced diboson event samples, the virtual QCD correction for MEs at NLO accuracy was provided by the OpenLoops library. For EW $VVjj$ production, the calculation was performed in the G_μ scheme, ensuring an optimal description of pure EW interactions at the EW scale [81–83]. All samples were generated using the NNPDF3.0nnlo PDF set, along with the dedicated set of tuned PS parameters developed by the Sherpa authors.

The associated production of a single top quark and a Higgs boson is treated as background. Samples for two subprocesses, $tHjb$ and tWH production, were generated using the MadGraph5_aMC@NLO 2.6.2 generator at NLO in QCD. The functional form of the renormalisation and factorisation scale was set to $0.5 \times \sum_i m_{\mathrm{T}}(i)$, where the sum runs over all the particles generated from the ME calculation. For $tHjb$ (tWH), events were generated in the four-flavour (five-flavour) scheme using the NNPDF3.0nlo nf4 (NNPDF3.0nlo) PDF set, and the diagram removal scheme was employed to handle the interference with $t\bar{t}H$ in the tWH sample [59, 84].

Single-top t-channel, s-channel, and tW production were modelled using the Powheg Box v2 [85–87] generator at NLO in QCD. For t-channel production, events were generated in the four-flavour scheme with the NNPDF3.0nlo nf4 PDF set, and the functional form of the renormalisation and factorisation scales was set to $m_{\mathrm{T}}(b)$ following the recommendation of ref. [85]. For s-channel and tW production, events were generated

[4] This scale is calculated in the $t\bar{t}$ rest-frame and hence the p_{T} values of the top quark and top antiquark are equivalent.

JHEP06(2022)097

in the five-flavour scheme with the NNPDF3.0NLO PDF set, and the functional form of the renormalisation and factorisation scales was set to the top-quark mass. For tW production, the diagram removal scheme [59] was employed to handle the interference with $t\bar{t}$ production [60]. An additional sample which applies the diagram subtraction scheme [59, 60] was used to assess an uncertainty in the modelling of this interference.

The production and decay of a top-quark pair in association with a vector boson (i.e. $t\bar{t}W$ or $t\bar{t}Z$), referred to collectively as $t\bar{t}V$, was modelled using the MadGraph5_aMC@NLO 2.3.3 generator at NLO in QCD. The functional form of the renormalisation and factorisation scale was set to $0.5 \times \sum_i m_{\mathrm{T}}(i)$, where the sum runs over all the particles generated from the ME calculation.

For events with four top quarks ($t\bar{t}t\bar{t}$) the production and decays were modelled using the MadGraph5_aMC@NLO 2.3.3 generator at NLO in QCD with the NNPDF3.1NLO [66] PDF set. The functional form of the renormalisation and factorisation scales was set to $0.25 \times \sum_i m_{\mathrm{T}}(i)$, where the sum runs over all the particles generated from the ME calculation, following the recommendation of ref. [58].

The tZq events were generated using the MadGraph5_aMC@NLO 2.3.3 generator in the four-flavour scheme at LO in QCD, with the CTEQ6L1 [88] PDF set. Following the recommendations of ref. [85], the renormalisation and factorisation scales were set to $4 \times m_{\mathrm{T}}(b)$, where the b-quark is the one coming from the gluon splitting.

The tWZ sample was produced using the MadGraph5_aMC@NLO 2.3.3 generator at NLO in QCD with the NNPDF3.0NLO PDF set. The renormalisation and factorisation scales were set to the top-quark mass. The diagram removal scheme was employed to handle the interference between tWZ and $t\bar{t}Z$.

In the single-lepton channel, a negligible contribution is found from events with a jet or a photon misidentified as a lepton, or from events with a non-prompt lepton. In the dilepton channel, the contribution from events with non-prompt leptons is estimated from simulated events (from $t\bar{t}$, $t\bar{t}Z$, $t\bar{t}W$, diboson, $Z+$jets, $W+$jets, tW, s-channel and t-channel single top production) where at least one of the reconstructed leptons does not match a true lepton in the event record. These events are collectively referred to as fakes.

4 Object and event selection

Events are selected from pp collisions at $\sqrt{s} = 13\,\mathrm{TeV}$ recorded by the ATLAS detector between 2015 and 2018, corresponding to an integrated luminosity of $139\,\mathrm{fb}^{-1}$. Only events for which the LHC beams were in stable-collision mode and all relevant subsystems were operational are considered [89]. Events are required to have at least one primary vertex with two or more tracks with $p_{\mathrm{T}} > 0.5\,\mathrm{GeV}$. If more than one vertex is found, the hard-scattering primary vertex is selected as the one with the highest sum of squared transverse momenta of associated tracks [90].

Events were recorded using single-lepton triggers with either a low p_{T} threshold and a lepton isolation requirement, or a higher threshold but a looser identification criterion and without any isolation requirement. The lowest p_{T} threshold in the single-muon trigger was 20 (26) GeV [91] for data taken in 2015 (2016–2018), while in the single-electron trigger it was 24 (26) GeV [92]).

JHEP06(2022)097

Electrons are reconstructed from tracks in the ID associated with topological clusters of energy depositions in the calorimeter [93] and are required to have $p_{\mathrm{T}} > 10\,\mathrm{GeV}$ and $|\eta| < 2.47$. Candidates in the calorimeter barrel-endcap transition region ($1.37 < |\eta| < 1.52$) are excluded. Electrons must satisfy the *Medium* likelihood identification criterion. Muon candidates are identified by matching ID tracks to full tracks or track segments reconstructed in the muon spectrometer, using the *Loose* identification criterion [94]. Muons are required to have $p_{\mathrm{T}} > 10\,\mathrm{GeV}$ and $|\eta| < 2.5$. Lepton tracks must match the primary vertex of the event, i.e. they have to satisfy $|z_0 \sin(\theta)| < 0.5$ mm and $|d_0/\sigma(d_0)| < 5\,(3)$ for electrons (muons), where z_0 is the longitudinal impact parameter relative to the primary vertex and d_0 (with uncertainty $\sigma(d_0)$) is the transverse impact parameter relative to the beam line.

Jets are reconstructed from noise-suppressed topological clusters of calorimeter energy depositions [95] calibrated at the electromagnetic scale [96], using the anti-k_t algorithm with a radius parameter of 0.4. These are referred to as small-R jets. The average energy contribution from pile-up is subtracted according to the jet area and jets are calibrated as described in ref. [96] with a series of simulation-based corrections and in situ techniques. Jets are required to satisfy $p_{\mathrm{T}} > 25\,\mathrm{GeV}$ and $|\eta| < 2.5$. The effect of pile-up is reduced by an algorithm requiring that the calorimeter-based jets are consistent with originating from the primary vertex using tracking information [97].

Jets containing b-hadrons are identified (b-tagged) with the MV2c10 multivariate algorithm [98], which combines information about the transverse impact parameters of displaced tracks and the topological properties of secondary and tertiary decay vertices reconstructed within the jet. Four working points, defined by different thresholds for the MV2c10 discriminant, are used in this analysis, corresponding to efficiencies ranging from 85% to 60% for b-jets with $p_{\mathrm{T}} > 20\,\mathrm{GeV}$ as determined in simulated $t\bar{t}$ events. The corresponding rejection rates are in the range 2–22 for c-jets (containing c-hadrons and no b-hadrons) and 27–1150 for light-jets. Jets are then assigned a pseudo-continuous b-tagging value [98] according to the tightest working point they satisfy. Correction factors are applied to the simulated events to compensate for differences between data and simulation in the b-tagging efficiency for b-, c-, and light-jets [98–100].

Hadronically decaying τ-leptons (τ_{had}) are distinguished from jets using their track multiplicity and a multivariate discriminant based on calorimetric shower shapes and tracking information [101]. They are required to have $p_{\mathrm{T}} > 25\,\mathrm{GeV}$ and $|\eta| < 2.5$, and to pass the *Medium* τ-identification working point.

An overlap removal procedure is applied to prevent double-counting of objects. The closest jet within $\Delta R_y = \sqrt{(\Delta y)^2 + (\Delta\phi)^2} = 0.2$ of a selected electron is removed. If the nearest jet surviving that selection is within $\Delta R_y = 0.4$ of the electron, the electron is discarded. Muons are usually removed if they are separated from the nearest jet by $\Delta R_y < 0.4$, since this reduces the background from heavy-flavour decays inside jets. However, if this jet has fewer than three associated tracks, the muon is kept and the jet is removed instead; this avoids an inefficiency for high-energy muons undergoing significant energy loss in the calorimeter. A τ_{had} candidate is rejected if it is separated by $\Delta R_y < 0.2$ from any selected electron or muon. No overlap removal is performed between jets and τ_{had} candidates.

JHEP06(2022)097

The missing transverse momentum (with magnitude $E_{\mathrm{T}}^{\mathrm{miss}}$) is reconstructed as the negative vector sum of the p_{T} of all the selected electrons, muons, τ_{had} and jets described above, with an extra 'soft term' built from additional tracks associated with the primary vertex, to make it resilient to pile-up contamination [102]. The missing transverse momentum is not used for event selection but is included in the inputs to the multivariate discriminants that are built in the most sensitive analysis categories (see section 5.2).

For the boosted category, the small-R jets are reclustered [103] using the anti-k_t algorithm with a radius parameter of 1.0, resulting in a collection of large-R jets (referred to as RC jets). These RC jets are required to have a reconstructed invariant mass higher than 50 GeV, $p_{\mathrm{T}} > 200$ GeV and at least two small-R constituent jets. RC jets are used as input to a deep neural network (DNN), described in section 5.2, to identify high-p_{T} (boosted) top-quark and Higgs boson candidates decaying into collimated hadronic final states. The event is flagged as containing a boosted Higgs boson candidate if one of the RC jets has a high probability of originating from a Higgs boson, as estimated by the DNN.

Events are required to have exactly one lepton in the single-lepton channels and exactly two leptons with opposite electric charge in the dilepton channel. At least one of the leptons must have $p_{\mathrm{T}} > 27$ GeV and match a corresponding object at trigger level. In the ee and $\mu\mu$ channels, the dilepton invariant mass must be above 15 GeV and outside the Z-boson mass window 83–99 GeV. To maintain orthogonality with other $t\bar{t}H$ channels [104], events are vetoed if they contain one or more (two or more) τ_{had} candidates in the dilepton (single-lepton) channel. Leptons are further required to satisfy additional identification and isolation criteria to increase background rejection: electrons (muons) must pass the *Tight* (*Medium*) identification criterion and the *Gradient* (*FixedCutTightTrackOnly*) isolation criteria [93, 105].

5 Analysis strategy

In order to target the $t\bar{t}H(b\bar{b})$ final state, events are categorised into mutually exclusive regions defined by the number of leptons, the number of jets, the number of b-tagged jets at different b-tagging efficiencies (60%, 70%, 77%, or 85%) and the number of boosted Higgs boson candidates (see section 5.1).

The analysis regions with higher signal-to-background ratio are referred to as 'signal regions' (SR). Higgs boson candidates are reconstructed using a DNN in the boosted category, and boosted decision trees (BDT) referred to as 'reconstruction BDTs' in the resolved categories, aiming at associating the reconstructed jets to the final state partons. Kinematic variables of these Higgs boson candidates, such as their transverse momentum p_{T}^{H}, are computed and used together with several other variables as input to other BDTs. These, referred to as 'classification BDTs', are then employed to separate signal from background, in each of the SRs (see section 5.2). The remaining analysis regions, depleted in signal, are referred to as 'control regions' (CR). They provide stringent constraints on the normalisation of the backgrounds and on systematic uncertainties when used in a combined fit with the signal regions.

JHEP06(2022)097

5.1 Analysis regions

Table 2 defines the 16 regions into which the events are classified: 11 SRs (dilepton $\mathrm{SR}^{\geq 4j}_{\geq 4b}$, single-lepton $\mathrm{SR}^{\geq 6j}_{\geq 4b}$ and $\mathrm{SR}_{\mathrm{boosted}}$, split according to the reconstructed p_{T}^{H} into four, five and two regions, respectively), and five CRs.

In the single-lepton channel, events are assigned to the boosted category if they contain at least four jets b-tagged at the 85% working point, one boosted Higgs boson candidate, and at least two jets not belonging to the boosted Higgs boson candidate which are b-tagged at the 77% working point. The boosted Higgs boson candidate must satisfy $p_{\mathrm{T}} > 300\,\mathrm{GeV}$, have an invariant mass in the range 100–140 GeV, a DNN score $P(H) > 0.6$ (see section 5.2), and exactly two jet constituents b-tagged at the 85% working point. If more than one candidate is identified, the one with a mass closest to the Higgs boson mass is chosen. The selected RC jet is used to determine the kinematic properties of the boosted Higgs boson candidate (reconstructed p_{T}^{H}, $m_{b\bar{b}}$, etc.). All other selected events belong to the resolved categories.

The analysis regions are further split according to the reconstructed p_{T}^{H} to allow the extraction of multiple signal parameters, sensitive to new physics effects. The p_{T}^{H} ranges are the same as used to define STXS bins with 'truth' $\hat{p}_{\mathrm{T}}^{H}$ (where the 'truth' $\hat{p}_{\mathrm{T}}^{H}$ is taken from the MC event record before the Higgs boson decays), and were chosen to minimise the correlation among signal strengths in different STXS bins. The split goes as follows:

- The single-lepton resolved signal region, $\mathrm{SR}^{\geq 6j}_{\geq 4b}$, is split in five reconstructed p_{T}^{H} regions: 0–120 GeV, 120–200 GeV, 200–300 GeV, 300–450 GeV and ≥ 450 GeV.
- The dilepton signal region, $\mathrm{SR}^{\geq 4j}_{\geq 4b}$, is split in a similar manner, with the two highest p_{T}^{H} bins merged because only a small number of events are expected.
- The boosted signal region, $\mathrm{SR}_{\mathrm{boosted}}$, is split into two reconstructed p_{T}^{H} regions: 300–450 GeV and ≥ 450 GeV.
- Control regions are inclusive in reconstructed p_{T}^{H} to maintain the constraints on the background composition.

After these selections are applied, $t\bar{t}$ + heavy-flavour jets dominate the background composition and the $t\bar{t}H$ selection efficiency is 1.2%. Although all Higgs boson decay modes are considered, $H \to b\bar{b}$ events account for at least 94% of $t\bar{t}H$ events selected in the signal regions. In the SRs the shape and normalisation of a multivariate discriminant distribution is used in the statistical analysis, except in the highest reconstructed p_{T}^{H} bin of the single-lepton resolved analysis, where only the event yield is used.

In the dilepton CRs, only the event yield is used to correct the amount of $t\bar{t} + \geq 1c$ predicted from the inclusive $t\bar{t}+$ jets sample. In the single-lepton channel the distribution shape and normalisation of the average ΔR for all possible combinations of b-tagged jet pairs, $\Delta R_{bb}^{\mathrm{avg}}$, is used in the CRs to help better constrain the background contributions and correct their shape. Control regions have different ratios of $t\bar{t} + \geq 1b$ to $t\bar{t} + \geq 1c$ events: regions labelled 'hi', referring to a higher b-tagging probability, are enriched in $t\bar{t} + \geq 1b$, while in regions labelled 'lo', the proportion of $t\bar{t} + \geq 1c$ events is increased. The different

JHEP06(2022)097

Region	Dilepton				Single-lepton			
	$\mathrm{SR}^{\geq 4j}_{\geq 4b}$	$\mathrm{CR}^{\geq 4j}_{3b\ \mathrm{hi}}$	$\mathrm{CR}^{\geq 4j}_{3b\ \mathrm{lo}}$	$\mathrm{CR}^{3j}_{3b\ \mathrm{hi}}$	$\mathrm{SR}^{\geq 6j}_{\geq 4b}$	$\mathrm{CR}^{5j}_{\geq 4b\ \mathrm{hi}}$	$\mathrm{CR}^{5j}_{\geq 4b\ \mathrm{lo}}$	$\mathrm{SR}_{\mathrm{boosted}}$
#leptons	$= 2$				$= 1$			
#jets	≥ 4			$= 3$	≥ 6	$= 5$		≥ 4
#b-tag @85%	–				≥ 4			
#b-tag @77%	–				–			$\geq 2^{\dagger}$
#b-tag @70%	≥ 4	$= 3$			≥ 4			—
#b-tag @60%	—	$= 3$	< 3	$= 3$	—	≥ 4	< 4	—
#boosted cand.	–				0			≥ 1
Fit input	BDT	Yield			BDT/Yield	$\Delta R^{\mathrm{avg}}_{bb}$		BDT

Table 2. Definition of the analysis regions, split according to the number of leptons, jets, and b-tagged jets using different working points, and the number of boosted Higgs candidates. For $\mathrm{SR}_{\mathrm{boosted}}$, b-tagged jets flagged with † are extra b-jets not part of the boosted Higgs boson candidate. All SRs are further split in reconstructed p_{T}^{H} as described in the text. The last row specifies the type of input to the fit used in each region: normalisation only (Yield) or shape and normalisation of the classification BDT or $\Delta R^{\mathrm{avg}}_{bb}$ distribution. In the highest bin ($p_{\mathrm{T}}^{H} \geq 450\,\mathrm{GeV}$) of the single-lepton resolved analysis, only the event yield is used.

proportions of $t\bar{t}+\geq 1b$ and $t\bar{t}+\geq 1c$ in the control regions allow the signal extraction fit to better constrain the relative fractions of these processes in the signal regions.

5.2 Multivariate analysis

Multivariate classifiers are used in two parts of this analysis: identifying Higgs boson candidate objects and classifying $t\bar{t}H$ signal events. In all SRs of the resolved categories, the multivariate classifiers are constructed analogously to the reconstruction and classification BDTs used in the previous analysis [27] and trained with TMVA [106]. The training for the reconstruction BDTs is identical to this previous analysis, matching reconstructed jets to the partons emitted from top-quark and Higgs boson decays. For this purpose, W-boson, top-quark and Higgs boson candidates are built from combinations of jets and leptons. The b-tagging information is used to discard combinations containing jet-parton assignments inconsistent with the correct parton candidate flavour. The combination of jets with the highest reconstruction BDT score is selected, allowing the computation of kinematic properties of the Higgs boson candidate (reconstructed p_{T}^{H}, $m_{b\bar{b}}$, etc.) by summing the four-momenta of the two jets associated with the Higgs boson candidate in this combination.

In the boosted channel the Higgs boson candidate is found using a DNN with a three-node softmax output layer trained with Keras [107] and a TensorFlow backend [108] on a sample of RC jets from signal events. The DNN quantifies the probability that an RC jet is originated from a Higgs boson (labelled $P(H)$ and shown in figure 2), top quark or any other process (mostly multijet production). The most important DNN input variables for identifying a Higgs boson candidate jet are built from the small-R jet constituent masses

JHEP06(2022)097

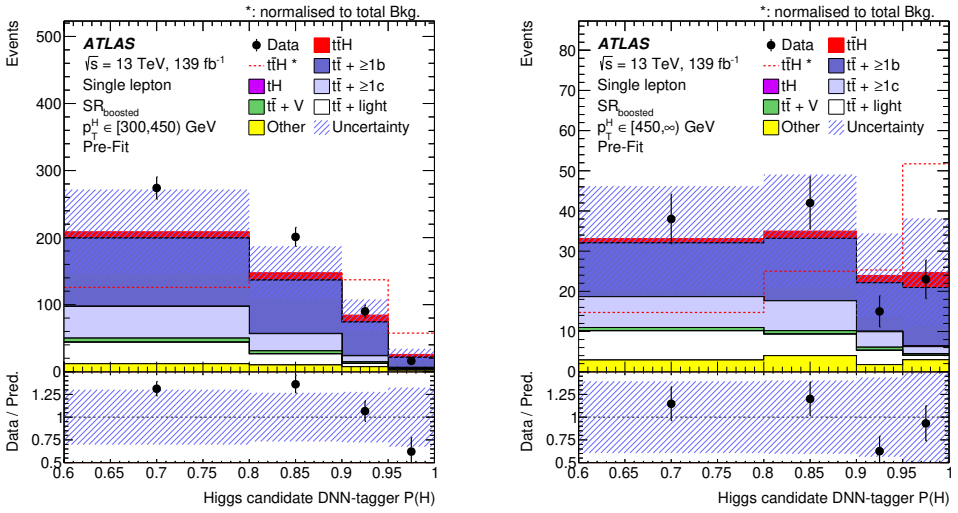

(a) (b)

Figure 2. Comparison between data and prediction for the DNN $P(H)$ output for the Higgs boson candidate prior to any fit to the data in the single-lepton boosted channel for (a) $300 \leq p_{\mathrm{T}}^{H} < 450\,\mathrm{GeV}$ and (b) $p_{\mathrm{T}}^{H} \geq 450\,\mathrm{GeV}$. The dashed line shows the $t\bar{t}H$ signal distribution normalised to the total background prediction. The uncertainty band includes all uncertainties and their correlations.

and pseudo-continuous b-tagging values, while substructure variables [109] also contribute. The Higgs boson jets are correctly identified 76% of the time, while top-quark jets are identified in 67% of the cases, in signal events.

The performance of the reconstruction in the three channels is reported in figure 3, which shows the migration matrix for Higgs boson candidates between reconstructed p_{T}^{H} bins and 'truth' $\hat{p}_{\mathrm{T}}^{H}$ bins, for all reconstructed Higgs boson candidates. When applying the reconstruction BDT or the DNN (which are trained with $t\bar{t}H$ events to match b-jets to a Higgs boson candidate) to the $t\bar{t} + \geq 1b$ sample, the two selected jets do not originate from the top-quark decay products about half (two-thirds) of the time in the lower (higher) p_{T}^{H} bin. The number of events with both jets originating from top-quark decays is negligible.

The classification BDTs have been retrained since the previous analysis to profit from the improved background modelling and from the increased number of simulated events, using the signal and components of the nominal background model presented in this paper. The dilepton BDT is trained only against $t\bar{t} + b\bar{b}$ events (as it constitutes most of the background), the single-lepton resolved BDT is trained against $t\bar{t} +$ jets events (because $t\bar{t} + \geq 1c$ and $t\bar{t} +$ light events also contribute) and the single-lepton boosted BDT is trained against all background processes.

These BDTs are built by combining kinematic variables, such as invariant masses and angular separations of pairs of reconstructed jets and leptons, outputs of the reconstruction discriminants, as well as the pseudo-continuous b-tagging discriminant of selected jets. The complete lists of input variables can be found in appendix A. The reconstruction discriminants provide their own output value as well as variables derived from the selected combination of jets with the highest reconstruction BDT score in the resolved channels.

JHEP06(2022)097

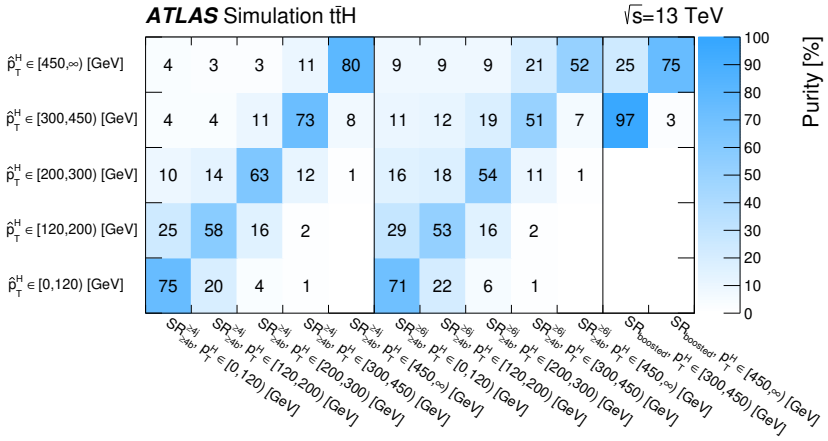

Figure 3. Performance of the Higgs boson reconstruction algorithms. For each row of 'truth' $\hat{p}_{\mathrm{T}}^{H}$, the matrix shows (in percentages) the fraction of all Higgs boson candidates with reconstructed p_{T}^{H} in the various bins of the dilepton (left), single-lepton resolved (middle) and boosted (right) channels.

In the single-lepton resolved channel, a likelihood discriminant method that combines the signal and background probabilities of all possible jet combinations in each event is also used as input to the classification BDT [27]. In the boosted channel, information from the DNN is used as input to the classification BDT, including the Higgs probability, $P(H)$. Distributions of the output of these BDT classifiers serve as SR inputs to the signal extraction fit.

The most important variables entering the dilepton BDT include the reconstruction BDT score for the Higgs boson candidate identified using Higgs boson information, the average $\Delta\eta$ between b-tagged jets, the minimum invariant mass of a b-tagged jet pair, the ΔR between the Higgs candidate and the $t\bar{t}$ candidate system, and the number of b-tagged jet pairs with an invariant mass within 30 GeV of 125 GeV. The most important variables entering the single-lepton resolved BDT include the likelihood discriminant, the average ΔR for all possible combinations of two b-tagged jets ($\Delta R_{bb}^{\mathrm{avg}}$), the invariant mass of the two b-tagged jets with the smallest ΔR, the reconstruction BDT score for the Higgs boson candidate identified using Higgs boson information, and the ΔR between the two highest-p_{T} b-tagged jets. The most important variables entering the single-lepton boosted BDT include the DNN $P(H)$ output for the Higgs boson candidate, the sum of b-tagging discriminants of small-R jets from Higgs, hadronic top and leptonic top candidates, the hadronic top candidate's invariant mass, the small-R jet multiplicity and, in the sum of b-tagging discriminants, the fraction due to all jets not associated with the Higgs or hadronic top candidates.

6 Systematic uncertainties

Many sources of systematic uncertainty affect this analysis, impacting the categorisation of events as well as the shape and normalisation of the final discriminants used in the signal extraction fit. All sources of experimental uncertainty considered, with the exception of the

JHEP06(2022)097

uncertainty in the luminosity, affect both the normalisations and shapes of distributions in all the simulated event samples. Uncertainties related to the theoretical modelling of the signal and background processes affect both the normalisations and shapes of the distributions, with the exception of cross-section and normalisation uncertainties which only affect the overall yield of the considered sample. Nonetheless, the normalisation uncertainties modify the relative fractions of the different samples leading to a shape uncertainty in the distribution of the final discriminant for the total prediction in the different analysis regions.

A single independent nuisance parameter is assigned to each source of systematic uncertainty. Some of the systematic uncertainties, in particular most of the experimental uncertainties, are decomposed into several independent sources, as specified in the following. Each individual source then has a correlated effect across all the channels, analysis regions, and signal and background samples. Modelling uncertainties are typically broken down into components which target specific physics effects in the event generation, such as scale variations or changing the hadronisation model, and are uncorrelated between different samples.

6.1 Experimental uncertainties

The uncertainty in the combined 2015–2018 integrated luminosity is 1.7% [110], obtained using the LUCID-2 detector [111] for the primary luminosity measurement. An uncertainty associated with the modelling of pile-up in the simulation is included to cover the difference between the predicted and measured inelastic cross-section values [112].

The jet energy scale uncertainty is derived by combining information from test-beam data, LHC collision data and simulation, and the jet energy resolution uncertainty is obtained by combining dijet p_{T}-balance measurements and simulation [96]. Additional considerations related to jet flavour, pile-up corrections, η dependence and high-p_{T} jets are included. These uncertainties are further propagated into the single-lepton boosted analysis by applying the reclustering described in section 4 with systematically varied inputs. A total of 40 independent contributions are considered. While the uncertainties are not large, varying between 1% and 5% per jet (depending on the jet p_{T}), the effects are amplified by the large number of jets considered in the final state. The efficiency to identify and remove jets from pile-up is measured with $Z \to \mu^+\mu^-$ events in data using techniques similar to those used in ref. [97]. All small-R jet constituent uncertainties are propagated to RC jets.

The efficiency to correctly tag b-jets is measured using dileptonic $t\bar{t}$ events [98]. The mis-tag rate for c-jets is measured using single-lepton $t\bar{t}$ events, exploiting the c-jets from the hadronic W-boson decays using techniques similar to those in ref. [99]. The mis-tag rate for light-jets is measured using a negative-tag method similar to that in ref. [100] applied to Z+jets events. The uncertainty in tagging b-jets is 2%–10% depending on the working point and jet p_{T}. The uncertainty in mis-tagging c-jets (light-jets) is 10%–25% (15%–50%) depending on the working point and jet p_{T}. For the calibration of the four working points used in this analysis, a large number of uncertainty components are considered, yielding 45, 20, and 20 uncorrelated sources of uncertainty for b-, c- and light-jets, respectively.

Uncertainties associated with leptons arise from the trigger, reconstruction, identification, and isolation, as well as the lepton momentum scale and resolution. Efficiencies are measured and scale and resolution calibrations are performed using leptons in $Z \to \ell^+\ell^-$

JHEP06(2022)097

and $J/\psi \to \ell^+\ell^-$ events [93, 105]. Systematic uncertainties in these measurements account for 22 independent sources but have only a small impact on the final result.

All uncertainties related to the energy scales or resolution of the reconstructed objects are propagated to the calculation of the missing transverse momentum. Three additional uncertainties associated with the scale and resolution of the soft term are also included. As the missing transverse momentum is only used for event reconstruction and not for event selection, these uncertainties have a minimal impact.

6.2 Theoretical modelling uncertainties

Uncertainties in the predicted SM $t\bar{t}H$ signal cross-section are evaluated with a particular focus on the impact on STXS bins. An uncertainty of $\pm 3.6\%$ from varying the PDF and α_s in the fixed-order calculation is applied [20, 113–117]. The effect of PDF variations on the shape of the distributions considered in this analysis is found to be negligible. Uncertainties in the Higgs boson branching fractions are also considered, and amount to 2.2% for the $b\bar{b}$ decay mode [20]. An uncertainty related to the amount of initial-state radiation (ISR) is estimated by simultaneously varying the renormalisation and factorisation scales in the ME and α_s^{ISR} in the PS [118], while an uncertainty related to final-state radiation (FSR) is estimated by varying α_s^{FSR} in the PS. The nominal Powheg Box + Pythia 8 sample is also compared with the Powheg Box + Herwig 7 sample to assess an uncertainty related to the choice of PS and hadronisation model, and with the MadGraph5_aMC@NLO + Pythia 8 sample to assess an uncertainty arising from changing the NLO matching procedure (sample details are given in table 1). Uncertainties due to missing higher-order terms in the perturbative QCD calculations affecting the total cross-section and event migration between STXS bins are estimated by varying the renormalisation and factorisation scales independently by a factor of two, as well as evaluating the ISR and FSR uncertainties. The largest effect was found to originate from the ISR uncertainty, corresponding to a 9.2% variation of the total cross-section, leading to an uncertainty of 10%–17% in bin migrations estimated using the Stewart-Tackmann procedure [119]. All signal uncertainties are correlated across STXS bins, with the exception of bin migration uncertainties.

The systematic uncertainties affecting the $t\bar{t}$ + jets background modelling are summarised in table 3. An uncertainty of 6% is assumed for the inclusive $t\bar{t}$ production cross-section predicted at NNLO+NNLL, including effects from varying the factorisation and renormalisation scales, the PDFs, α_s, and the top-quark mass [46–52]. This uncertainty is applied to $t\bar{t}$ + light samples only, since this component is dominant in $t\bar{t}$ production in the full phase-space. An uncertainty of 100% in the normalisation of $t\bar{t} + \geq 1c$ events is applied, motivated by the fitted value of this normalisation in the previous analysis [27]. The normalisation of $t\bar{t} + \geq 1b$ is allowed to float freely in the signal extraction fit. The $t\bar{t} + \geq 1b$, $t\bar{t} + \geq 1c$ and $t\bar{t}$ + light processes are affected by different types of uncertainties: $t\bar{t}$ + light profits from relatively precise measurements in data; $t\bar{t} + \geq 1b$ and $t\bar{t} + \geq 1c$ can have similar or different diagrams depending on the precision of the ME and the flavour scheme used for the PDF, and the different masses of the c- and b-quarks contribute to additional differences between these two processes. For these reasons, all uncertainties in the $t\bar{t}$ + jets background

JHEP06(2022)097

Uncertainty source	Description		Components
$t\bar{t}$ cross-section	±6%		$t\bar{t}+$ light
$t\bar{t}+\geq 1b$ normalisation	Free-floating		$t\bar{t}+\geq 1b$
$t\bar{t}+\geq 1c$ normalisation	±100%		$t\bar{t}+\geq 1c$
NLO matching	MadGraph5_aMC@NLO + Pythia 8 vs Powheg Box + Pythia 8		All
PS & hadronisation	Powheg Box + Herwig 7 vs Powheg Box + Pythia 8		All
ISR	Varying α_s^{ISR} (PS), μ_r & μ_f (ME)	in Powheg Box Res + Pythia 8	$t\bar{t}+\geq 1b$
		in Powheg Box + Pythia 8	$t\bar{t}+\geq 1c$, $t\bar{t}+$ light
FSR	Varying α_s^{FSR} (PS)	in Powheg Box Res + Pythia 8	$t\bar{t}+\geq 1b$
		in Powheg Box + Pythia 8	$t\bar{t}+\geq 1c$, $t\bar{t}+$ light
$t\bar{t}+\geq 1b$ fractions	Powheg Box + Herwig 7 vs Powheg Box + Pythia 8		$t\bar{t}+1b$, $t\bar{t}+\geq 2b$
p_{T}^{bb} shape	Shape mismodelling measured from data		$t\bar{t}+\geq 1b$

Table 3. Summary of the sources of systematic uncertainty for $t\bar{t}+$jets modelling. The systematic uncertainties listed in the second section of the table are evaluated in such a way as to have no impact on the normalisation of the three $t\bar{t}+\geq 1b$, $t\bar{t}+\geq 1c$, and $t\bar{t}+$ light components in the phase-space selected in this analysis. The last column of the table indicates the $t\bar{t}+$jets components to which a systematic uncertainty is assigned. All systematic uncertainty sources are treated as uncorrelated across the three components.

modelling are assigned independent nuisance parameters for the $t\bar{t}+\geq 1b$, $t\bar{t}+\geq 1c$ and $t\bar{t}+$ light processes. The effect of PDF uncertainties was found to be negligible.

Systematic uncertainties in the acceptance and the distribution shapes are extracted from comparisons between the nominal prediction and different samples or settings. The fraction of $t\bar{t}+\geq 1b$ events in the selected phase-space in all alternative samples is reweighted to match the fraction in the nominal sample. This is to allow the normalisation of $t\bar{t}+\geq 1b$ to be driven solely by the free-floating parameter in the signal extraction fit to data. The systematic uncertainties related to varying the amount of ISR, the amount of FSR, the PS and hadronisation model, and the NLO matching procedure are estimated using the same procedure as for $t\bar{t}H$, comparing the nominal prediction with alternative samples. In the specific case of $t\bar{t}+\geq 1b$, relative uncertainties are used to estimate the effect of changing the PS and hadronisation model or the NLO matching procedure by comparing predictions from the NLO $t\bar{t}$ generators (see table 3). These comparisons are made using predictions in which the additional b-quarks were generated at leading-log precision from gluon splitting. A check was performed, comparing the nominal $t\bar{t}+\geq 1b$ prediction with a smaller $t\bar{t}+b\bar{b}$ sample produced with Sherpa 2.2.1. The size of the difference estimated from $t\bar{t}$ samples was observed to be generally the same as or larger than the difference between the two $t\bar{t}+b\bar{b}$ NLO predictions. The impact of these uncertainties on the final results is reported in section 7.

Special consideration is given to the correlation of modelling uncertainties across different p_{T}^{H} bins, in order to provide the fit with enough flexibility to cover background mismodelling without biasing the signal extraction. The $t\bar{t}+\geq 1b$ NLO matching uncertainty is shown to depend on p_{T}^{H} and is therefore decorrelated across p_{T} bins in the SRs. The NLO matching uncertainty and the PS and hadronisation uncertainties for $t\bar{t}+\geq 1b$ are further

JHEP06(2022)097

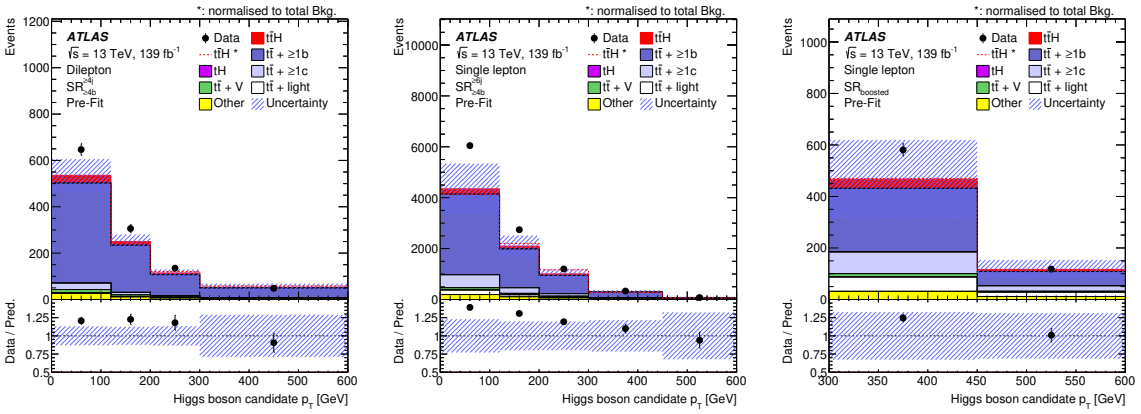

(a) (b) (c)

Figure 4. Pre-fit distributions of the reconstructed Higgs boson candidate p_{T}^{H} for the (a) dilepton $\mathrm{SR}^{\geq 4j}_{\geq 4b}$, (b) single-lepton resolved $\mathrm{SR}^{\geq 6j}_{\geq 4b}$ and (c) single-lepton boosted $\mathrm{SR}_{\mathrm{boosted}}$ signal regions. The dashed line shows the $t\bar{t}H$ signal distribution normalised to the total background prediction. The uncertainty band includes all uncertainties and their correlations, except for the uncertainty in the $k(t\bar{t}+\geq 1b)$ normalisation factor which is not defined pre-fit. The last bin includes the overflow.

decorrelated between the single-lepton and dilepton channels in order to avoid the transfer of constraints from the single-lepton resolved channel to the dilepton channel, which is less sensitive to the high-p_{T}^{H} regime and produces less additional radiation. The pre-fit distributions of the reconstructed p_{T}^{H} are shown in figure 4. An additional uncertainty is derived for the $t\bar{t}+\geq 1b$ sample to cover the mismodelling observed in this distribution. After removing the overall normalisation difference by scaling the $t\bar{t}+\geq 1b$ background in the dilepton $\mathrm{SR}^{\geq 4j}_{\geq 4b}$ (single-lepton $\mathrm{SR}^{\geq 6j}_{\geq 4b}$), a weight is computed in each reconstructed p_{T}^{H} bin of the dilepton $\mathrm{SR}^{\geq 4j}_{\geq 4b}$ (single-lepton $\mathrm{SR}^{\geq 6j}_{\geq 4b}$), which corrects the predicted $t\bar{t}+\geq 1b$ contribution so that the data and background model yields agree in each p_{T}^{H} bin. The derived weights are not applied to the nominal sample: instead they define the $+1\sigma$ variation of an additional uncertainty in the $t\bar{t}+\geq 1b$ sample in each reconstructed p_{T}^{H} bin. The weights derived in the single-lepton resolved channel are also applied in the boosted channel. This uncertainty enters the signal extraction fit as a single nuisance parameter (p_{T}^{bb} shape), correlated across all channels, such that a pull of $+1\sigma$ corresponds to applying this weight, effectively correcting the reconstructed p_{T}^{H} spectrum.

To account for variations in the $t\bar{t}+\geq 1b$ subcomponent fractions found in different predictions, an additional nuisance parameter is introduced to cover the largest discrepancy between two models for the fraction of $t\bar{t}+1b$ and $t\bar{t}+\geq 2b$. The 1σ variation of this nuisance parameter corresponds to reducing the amount of $t\bar{t}+\geq 2b$ by 13% and increasing the amount of $t\bar{t}+1b$ by 22%. This uncertainty is correlated across all regions, and impacts each region differently due to the varying compositions of $t\bar{t}+\geq 1b$.

An uncertainty of 5% is considered for the cross-sections of the three single-top production modes [55, 56, 120, 121]. Uncertainties associated with the PS and hadronisation model, and with the NLO matching scheme, are evaluated by comparing, for each process,

JHEP06(2022)097

the nominal Powheg Box + Pythia 8 sample with a sample produced using Powheg Box + Herwig 7 and MadGraph5_aMC@NLO + Pythia 8, respectively. The uncertainty associated with the interference between tW and $t\bar{t}$ production at NLO [59] is assessed by comparing the nominal Powheg Box + Pythia 8 sample produced using the diagram removal scheme with the alternative sample produced with the same generator but using the diagram subtraction scheme.

An uncertainty of 40% is assumed for the $W+$jets cross-section, with an additional 30% normalisation uncertainty used for $W+$ heavy-flavour jets, taken as uncorrelated between events with two and more than two heavy-flavour jets. These uncertainties are based on variations of the factorisation and renormalisation scales and of the Sherpa matching parameters. An uncertainty of 35% is applied to the $Z+$jets normalisation, uncorrelated across jet bins, to account for both the variations of the scales and Sherpa matching parameters and the uncertainty in the extraction from data of the correction factor for the heavy-flavour component.

The uncertainty in the $t\bar{t}V$ NLO cross-section prediction is 15% [122], split into PDF and scale uncertainties as for $t\bar{t}H$. An additional $t\bar{t}V$ modelling uncertainty, related to the choice of PS and hadronisation model and NLO matching scheme is assessed by comparing the nominal MadGraph5_aMC@NLO + Pythia 8 samples with alternative ones generated with Sherpa.

The uncertainty in the diboson background is assumed to be 50%, which includes uncertainties in the inclusive cross-section and additional jet production [123]. A 50% normalisation uncertainty is considered for the four-top background, covering effects from varying the factorisation and renormalisation scales, the PDFs and α_s [124].

The small backgrounds from tZq and tWZ are each assigned cross-section uncertainties; for tZq two uncertainties are used, 7.9% accounting for factorisation and renormalisation scale variations and 0.9% accounting for PDFs, and for tWZ a single uncertainty of 50% is used [124]. Uncertainties in the associated production of a single top quark and a Higgs boson include factorisation and renormalisation scale variations as well as PDF uncertainties: they amount to $+6.5/-14.9\%$ ($+6.5/-6.7\%$) and $\pm 3.7\%$ ($\pm 6.3\%$) for $tHjb$ (tWH), respectively [20]. Finally, a 25% normalisation uncertainty is considered for the fake lepton background in the dilepton channel.

7 Results

The distributions of the classification BDT in the signal regions, and the event yield or the $\Delta R_{bb}^{\text{avg}}$ distributions in the dilepton or single-lepton control regions, respectively, are combined in a profile likelihood fit to extract the signal, while simultaneously determining the yields and constraining the normalisation and shape of differential distributions of the most important background components. The binning of these distributions is optimised to maximise the analysis sensitivity while keeping the total MC statistical uncertainty in each bin to a level adjusted to avoid biases due to fluctuations in the predicted number of events.

The statistical analysis is based on a binned likelihood function $\mathcal{L}(\mu, \theta)$ constructed as a product of Poisson probability terms over all bins considered in the analysis. The

JHEP06(2022)097

likelihood function depends on the signal-strength parameter μ, defined as $\mu = \sigma/\sigma_{\text{SM}}$ (where σ is the measured cross-section and σ_{SM} is the Standard Model prediction), and a set of nuisance parameters θ which characterise the effects of systematic uncertainties in the signal and background expectations. They are implemented in the likelihood function as Gaussian or Poisson priors, with the exception of the unconstrained normalisation factor $k(t\bar{t} + \geq 1b)$ for the $t\bar{t} + \geq 1b$ background, of which no prior knowledge from theory or subsidiary measurements is assumed. The statistical uncertainty in the prediction, which incorporates the statistical uncertainty arising from the limited number of simulated events, is included in the likelihood in the form of additional nuisance parameters, one for each of the considered bins. In the statistical analysis, the number of events expected in a given bin depends on μ and θ. The nuisance parameters θ adjust the expectations for signal and background according to the corresponding systematic uncertainties, and their fitted values correspond to the amount that best fits the data. The test statistic t_μ is defined as the profile likelihood ratio: $t_\mu = -2\ln(\mathcal{L}(\mu, \hat{\hat{\theta}}_\mu)/\mathcal{L}(\hat{\mu}, \hat{\theta}))$, where $\hat{\mu}$ and $\hat{\theta}$ are the values of the parameters that maximise the likelihood function, and $\hat{\hat{\theta}}_\mu$ are the values of the nuisance parameters that maximise the likelihood function for a given value of μ [125]. This test statistic, as implemented in the RooStat framework [126, 127], is used to assess the compatibility of the observed data with the background-only hypothesis (i.e. for $\mu = 0$) and to make statistical inferences about μ. The uncertainty in the best-fit value of the signal strength is extracted by finding the values of μ that correspond to varying t_μ by one unit.

Tables 4 and 5 show the observed and predicted signal and background event yields in all SRs and CRs before and after the inclusive fit to data. Post-fit values are summarised in figure 5, where the precision increases post-fit due to profiling and the uncertainties can be observed to increase as a function of p_{T}^H, ranging from 2% to 12%. The SR BDT distributions are presented in figures 6 and 7, while the $\Delta R_{bb}^{\text{avg}}$ distributions in the single-lepton resolved CRs are shown in figure 8. All distributions are compatible with the data. The normalisation factor for the $t\bar{t}+\geq 1b$ background is found to be $k(t\bar{t}+\geq 1b) = 1.28 \pm 0.08$. The best-fit μ value is

$$\mu = 0.35 \pm 0.20\,(\text{stat.})\,^{+0.30}_{-0.28}\,(\text{syst.}) = 0.35^{+0.36}_{-0.34},$$

corresponding to an observed (expected) significance of 1.0 (2.7) standard deviations with respect to the background-only hypothesis. This observed inclusive μ and its uncertainty, common to all channels, cannot affect the shape of the signal distributions but only their normalisation, leading to post-fit signal yield uncertainties very close to 100%.

The statistical uncertainty is obtained by repeating the fit to data after fixing all nuisance parameters to their post-fit values, with the exception of the free normalisation factors in the fit: $k(t\bar{t} + \geq 1b)$ and μ. The total systematic uncertainty is obtained by subtracting the statistical variance from the total variance, i.e. $\sigma_{\text{syst}} = \sqrt{\sigma_{\text{tot}}^2 - \sigma_{\text{stat}}^2}$. The expected significance is computed from a fit to a pseudo-dataset, built using the pulls from the nominal fit when fixing $\mu = 1$. Figure 9 shows the event yield in data compared with the post-fit prediction for all events entering the analysis selection, grouped and ordered by the signal-to-background ratio of the corresponding final-discriminant bins.

JHEP06(2022)097

	$SR^{\geq 4j}_{\geq 4b}$, $p_T^H \in$ [0,120) GeV		$SR^{\geq 4j}_{\geq 4b}$, $p_T^H \in$ [120,200) GeV		$SR^{\geq 4j}_{\geq 4b}$, $p_T^H \in$ [200,300) GeV		$SR^{\geq 4j}_{\geq 4b}$, $p_T^H \in$ [300,∞) GeV	
	Pre-fit	Post-fit	Pre-fit	Post-fit	Pre-fit	Post-fit	Pre-fit	Post-fit
$t\bar{t}H$	33.6 ± 4.1	12 ± 12	15.6 ± 1.8	5.5 ± 5.3	7.71 ± 0.89	2.7 ± 2.6	3.72 ± 0.44	1.3 ± 1.3
tH	0.249 ± 0.065	0.249 ± 0.064	0.148 ± 0.063	0.146 ± 0.061	0.043 ± 0.032	0.043 ± 0.031	0.031 ± 0.027	0.031 ± 0.025
$t\bar{t} + \geq 1b$	432 ± 59	546 ± 24	203 ± 27	263 ± 12	92 ± 14	116.9 ± 8.8	42 ± 15	37.9 ± 6.0
$t\bar{t} + \geq 1c$	27 ± 29	48.5 ± 9.1	11 ± 12	16.3 ± 5.0	4.0 ± 4.2	6.5 ± 1.4	1.9 ± 2.1	3.69 ± 0.96
$t\bar{t} + Z$	12.5 ± 2.0	12.6 ± 2.0	7.4 ± 1.6	7.6 ± 1.6	4.18 ± 0.72	4.15 ± 0.70	2.05 ± 0.45	2.06 ± 0.44
$t\bar{t} + W$	0.75 ± 0.31	0.75 ± 0.31	0.38 ± 0.12	0.40 ± 0.11	0.27 ± 0.12	0.27 ± 0.11	0.124 ± 0.068	0.127 ± 0.068
$t\bar{t}$ + light	3.6 ± 4.9	4.8 ± 6.2	0.97 ± 0.96	0.92 ± 0.74	0.46 ± 0.65	0.41 ± 0.47	0.22 ± 0.31	0.22 ± 0.25
$t\bar{t}t\bar{t}$	3.1 ± 1.5	3.0 ± 1.5	2.4 ± 1.2	2.3 ± 1.2	1.38 ± 0.70	1.36 ± 0.69	0.81 ± 0.41	0.79 ± 0.40
Fakes	3.7 ± 1.1	3.7 ± 1.1	1.33 ± 0.51	1.33 ± 0.51	0.40 ± 0.23	0.40 ± 0.23	0.57 ± 0.30	0.57 ± 0.30
Other sources	19.1 ± 6.9	19.3 ± 7.0	7.1 ± 4.4	7.7 ± 4.3	4.3 ± 4.0	4.5 ± 4.1	2.0 ± 1.5	2.0 ± 1.5
Total	536 ± 71	651 ± 21	249 ± 32	305 ± 11	114 ± 16	137.2 ± 8.1	53 ± 15	48.7 ± 5.7
Data	647		306		135		48	

	$CR^{3j}_{3b\ \mathrm{hi}}$		$CR^{\geq 4j}_{3b\ \mathrm{hi}}$		$CR^{\geq 4j}_{3b\ \mathrm{lo}}$	
	Pre-fit	Post-fit	Pre-fit	Post-fit	Pre-fit	Post-fit
$t\bar{t}H$	25.2 ± 3.1	8.8 ± 8.6	117 ± 13	42 ± 41	76.4 ± 8.4	27 ± 27
tH	1.26 ± 0.15	1.23 ± 0.15	2.06 ± 0.39	2.02 ± 0.38	1.19 ± 0.53	1.12 ± 0.50
$t\bar{t} + \geq 1b$	1900 ± 510	2010 ± 130	2810 ± 300	4070 ± 210	1730 ± 210	2550 ± 160
$t\bar{t} + \geq 1c$	350 ± 360	550 ± 130	700 ± 710	1190 ± 240	1500 ± 1500	2550 ± 470
$t\bar{t} + Z$	11.1 ± 1.8	10.8 ± 1.7	57.1 ± 7.4	57.5 ± 7.3	51.7 ± 7.0	52.3 ± 6.7
$t\bar{t} + W$	1.88 ± 0.59	1.84 ± 0.55	10.8 ± 1.6	10.9 ± 1.6	21.5 ± 3.7	21.8 ± 3.4
$t\bar{t}$ + light	128 ± 74	119 ± 61	200 ± 120	210 ± 120	850 ± 350	900 ± 340
$t\bar{t}t\bar{t}$	0.047 ± 0.026	0.044 ± 0.024	12.3 ± 6.1	12.0 ± 6.1	8.9 ± 4.5	8.8 ± 4.4
Fakes	6.3 ± 1.8	6.4 ± 1.8	47 ± 12	47 ± 12	56 ± 14	56 ± 14
Other sources	125 ± 35	125 ± 34	211 ± 62	211 ± 62	251 ± 73	257 ± 73
Total	2540 ± 630	2835 ± 54	4160 ± 810	5855 ± 79	4500 ± 1600	6431 ± 83
Data	2827		5865		6429	

Table 4. Pre-fit and post-fit event yields in the dilepton channel (top) signal regions and (bottom) control regions. Post-fit yields are after the inclusive fit in all channels. All uncertainties are included, taking into account correlations in the post-fit case. The $k(t\bar{t} + \geq 1b)$ uncertainty is not defined pre-fit and therefore only included in the post-fit uncertainties. For the $t\bar{t}H$ signal, the pre-fit yield values correspond to the theoretical prediction and corresponding uncertainties, while the post-fit yield and uncertainties correspond to those in the inclusive signal-strength measurement. 'Other sources' refers to s-channel, t-channel, tW, tWZ, tZq, $Z+$jets and diboson events.

The global goodness of fit, including all input variables to the classification BDTs and to a fit using the saturated model [128], is 92%, validating the good post-fit modelling achieved. Some of the most important variables used in the classification BDTs are shown in figure 10 for the dilepton channel, figure 11 for the single-lepton resolved channel and figure 12 for the single-lepton boosted channel. The probability of obtaining a level of agreement worse than observed between the fitted predictions and data was evaluated by calculating the χ^2 for a given number of degrees of freedom and integrating the cumulative probability distribution to $+\infty$. For all channels combined, the mean probability is 80% for classification BDT outputs and 60% for classification BDT training variables in all SRs. Post-fit distributions of the reconstructed Higgs boson candidate mass in the three SRs are shown in figure 13.

JHEP06(2022)097

	$SR^{\geq 6j}_{\geq 4b}$, $p_T^H \in$ [0,120) GeV		$SR^{\geq 6j}_{\geq 4b}$, $p_T^H \in$ [120,200) GeV		$SR^{\geq 6j}_{\geq 4b}$, $p_T^H \in$ [200,300) GeV		$SR^{\geq 6j}_{\geq 4b}$, $p_T^H \in$ [300,450) GeV		$SR^{\geq 6j}_{\geq 4b}$, $p_T^H \in$ [450,∞) GeV	
	Pre-fit	Post-fit	Pre-fit	Post-fit	Pre-fit	Post-fit	Pre-fit	Post-fit	Pre-fit	Post-fit
$t\bar{t}H$	213±29	76±73	113±15	40±39	59.9±7.8	21±21	13.9±2.0	4.8±4.7	3.09±0.49	1.0±1.0
tH	3.01±0.47	3.03±0.44	1.81±0.44	1.83±0.40	1.24±0.26	1.28±0.25	0.26±0.17	0.25±0.14	0.000±0.041	0.000±0.041
$t\bar{t}+\geq 1b$	3160±490	4530±160	1530±210	2050±80	720±130	865±47	215±61	240±22	55±27	44.7±8.5
$t\bar{t}+\geq 1c$	510±540	930±190	220±230	401±83	96±100	176±36	26±27	45±10	6.9±7.5	12.8±3.2
$t\bar{t}+W$	7.0±1.2	7.1±1.1	4.31±0.90	4.37±0.84	2.47±0.52	2.49±0.46	1.05±0.32	1.06±0.30	0.47±0.15	0.47±0.14
$t\bar{t}+Z$	77±11	77±10	44.6±6.6	45.6±6.3	30.1±4.9	30.8±4.8	11.5±2.4	11.6±2.3	2.05±0.64	2.11±0.64
$t\bar{t}$ + light	180±120	220±130	85±58	97±58	37±23	43±25	10.5±7.7	11.6±7.8	2.2±2.1	2.7±2.3
Single top tW	71±40	76±42	40±26	42±27	17.9±7.6	18.3±7.7	8.5±7.9	9.5±9.0	6.0±5.3	6.0±5.4
$t\bar{t}t\bar{t}$	15.9±8.0	15.7±7.9	12.6±6.3	12.5±6.3	7.7±3.9	7.6±3.8	2.7±1.4	2.7±1.3	0.98±0.50	0.95±0.49
Other top sources	46±24	45±24	23±16	24±16	13±10	12.7±9.6	4.3±2.8	4.4±2.6	1.08±0.54	1.06±0.54
V & VV + jets	60±24	60±23	29±11	29±11	19.7±8.3	19.7±7.9	7.8±3.4	7.8±3.2	1.90±0.88	1.84±0.82
Total	4350±810	6045±82	2100±360	2745±48	1000±180	1198±33	301±72	339±16	80±29	73.7±7.2
Data	6047		2742		1199		331		75	

	SR_{boosted}, $p_T^H \in$ [300,450) GeV		SR_{boosted}, $p_T^H \in$ [450,∞) GeV		$CR^{5j}_{\geq 4b\ \text{lo}}$		$CR^{5j}_{\geq 4b\ \text{hi}}$	
	Pre-fit	Post-fit	Pre-fit	Post-fit	Pre-fit	Post-fit	Pre-fit	Post-fit
$t\bar{t}H$	35.1±4.1	12±12	8.5±1.1	3.0±2.9	61.7±8.1	21±21	62.1±8.6	22±21
tH	1.31±0.31	1.31±0.29	0.42±0.10	0.42±0.10	3.15±0.41	3.15±0.40	3.16±0.42	3.18±0.42
$t\bar{t}+\geq 1b$	246±49	295±23	55±24	52.5±9.3	1370±160	1581±89	1000±150	1118±51
$t\bar{t}+\geq 1c$	84±90	156±35	21±23	38±10	390±410	650±140	56±59	93±23
$t\bar{t}+W$	1.86±0.39	1.88±0.35	0.55±0.18	0.56±0.17	2.53±0.53	2.58±0.45	0.54±0.13	0.53±0.12
$t\bar{t}+Z$	10.7±2.1	10.9±2.1	2.21±0.60	2.32±0.59	26.4±3.7	26.0±3.5	23.5±3.4	23.0±3.2
$t\bar{t}$ + light	56±26	61±25	17±10	16.2±7.3	260±120	270±95	22±16	20±14
Single top tW	13.1±8.0	13.7±8.3	6.1±5.8	5.3±4.6	58±32	59±32	27±20	28±20
$t\bar{t}t\bar{t}$	1.76±0.89	1.74±0.88	0.42±0.22	0.41±0.21	0.33±0.17	0.31±0.16	0.24±0.13	0.23±0.12
Other top sources	4.3±3.2	4.4±3.1	0.80±0.78	0.82±0.77	41±16	41±16	27±11	26±10
V & VV + jets	12.4±5.7	12.4±5.4	4.3±2.3	4.2±2.0	42±16	41±15	24.2±8.8	24.2±8.5
Total	470±120	571±22	117±38	123.8±9.7	2260±490	2694±53	1250±170	1359±36
Data	581		118		2696		1362	

Table 5. Pre-fit and post-fit event yields in the single-lepton (top) resolved signal regions and (bottom) boosted signal regions and control regions. Post-fit yields are after the inclusive fit in all channels. All uncertainties are included, taking into account correlations in the post-fit case. The $k(t\bar{t}+\geq 1b)$ uncertainty is not defined pre-fit and therefore only included in the post-fit uncertainties. For the $t\bar{t}H$ signal, the pre-fit yield values correspond to the theoretical prediction and corresponding uncertainties, while the post-fit yield and uncertainties correspond to those in the inclusive signal-strength measurement. 'Other top sources' refers to s-channel, t-channel, tWZ and tZq events.

The probability of the obtained signal strength being compatible with the SM prediction is 8.5%, estimated by redoing the fit while fixing $\mu = 1$. The measured signal strength is compatible with that obtained previously [27] from part of the dataset, and the impact of systematic uncertainties has been reduced by about a factor of two. The main improvements come from improved theoretical knowledge in $t\bar{t}+\geq 1b$ modelling, from the much larger size of simulated event samples for systematic uncertainty estimation as well as from the refined b-tagging scale factors and jet energy scale and resolution measurements.

JHEP06(2022)097

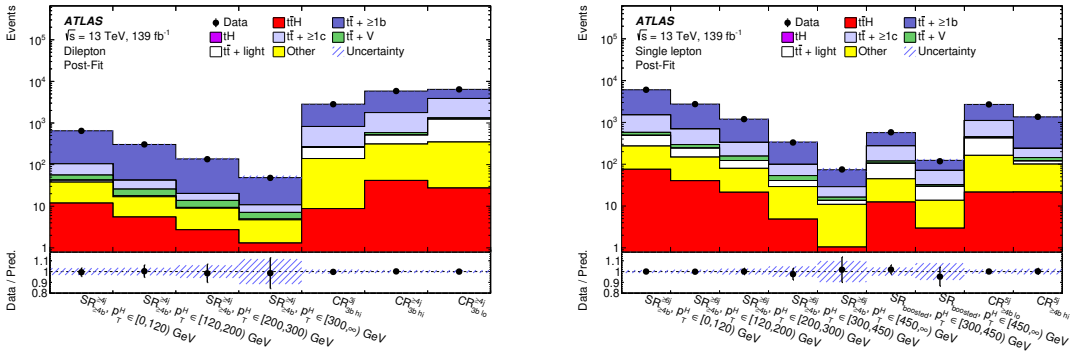

(a) (b)

Figure 5. Comparison of predicted and observed event yields in each of the control and signal regions in the (a) dilepton and (b) single-lepton channels after the fit to the data. The uncertainty band includes all uncertainties and their correlations.

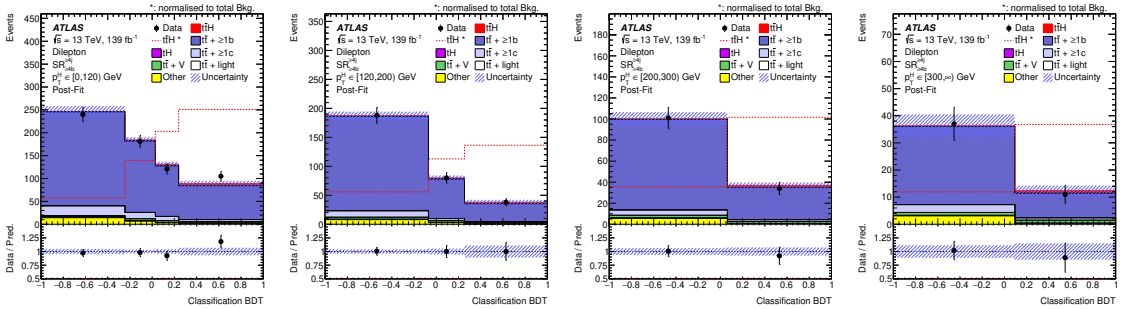

(a) (b) (c) (d)

Figure 6. Comparison between data and prediction for the BDT discriminant in the dilepton SRs after the inclusive fit to the data, for (a) $0 \leq p_{\mathrm{T}}^{H} < 120\,\mathrm{GeV}$, (b) $120 \leq p_{\mathrm{T}}^{H} < 200\,\mathrm{GeV}$, (c) $200 \leq p_{\mathrm{T}}^{H} < 300\,\mathrm{GeV}$ and (d) $p_{\mathrm{T}}^{H} \geq 300\,\mathrm{GeV}$. The $t\bar{t}H$ signal yield (solid red) is normalised to the fitted μ value from the inclusive fit. The dashed line shows the $t\bar{t}H$ signal distribution normalised to the total background prediction. The uncertainty band includes all uncertainties and their correlations.

The fit is repeated with three independent signal strengths, one each for the dilepton, single-lepton resolved and single-lepton boosted channels. Figure 14 shows the μ value obtained for each channel and the single signal strength from the previous fit. In this fit the normalisation factor for the $t\bar{t}+\geq 1b$ background is found to be $k(t\bar{t}+\geq 1b) = 1.27 \pm 0.08$, compatible with the value in the single μ fit. The probability of obtaining a discrepancy between these three μ values equal to or larger than the one observed is 90%.

The measurement is largely dominated by systematic uncertainties. Their contributions to the fit to μ are reported in table 6. The dominant impact comes from the modelling of the $t\bar{t}+\geq 1b$ background, followed by the signal modelling, tW modelling and b-tagging efficiency uncertainties. The largest observed pull on systematic uncertainties, as shown in figure 15, is seen in the $t\bar{t}+\geq 1b$ ISR uncertainty, and is about 1.2σ, mostly driven by the

JHEP06(2022)097

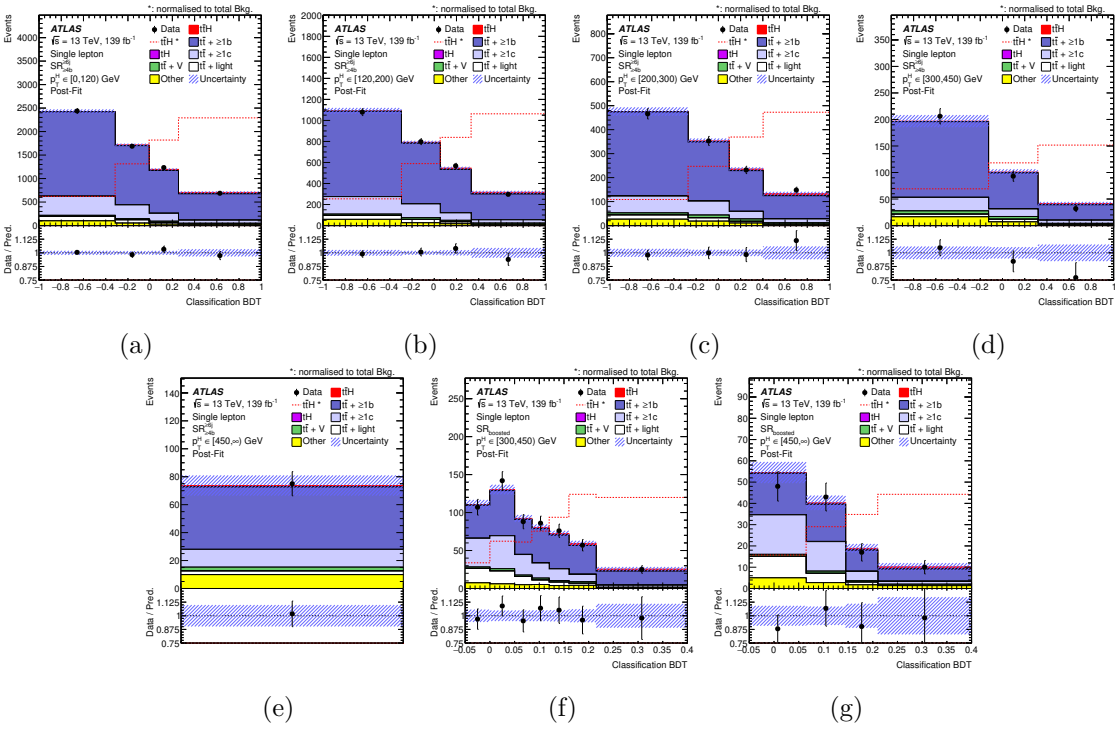

Figure 7. Comparison between data and prediction for the BDT discriminant in the single-lepton SRs after the inclusive fit to the data. The resolved channel is shown for (a) $0 \leq p_{\mathrm{T}}^{H} < 120\,\mathrm{GeV}$, (b) $120 \leq p_{\mathrm{T}}^{H} < 200\,\mathrm{GeV}$, (c) $200 \leq p_{\mathrm{T}}^{H} < 300\,\mathrm{GeV}$, (d) $300 \leq p_{\mathrm{T}}^{H} < 450\,\mathrm{GeV}$ and (e) $p_{\mathrm{T}}^{H} \geq 450\,\mathrm{GeV}$ (yield only). The boosted channel is shown for (f) $300 \leq p_{\mathrm{T}}^{H} < 450\,\mathrm{GeV}$ and (g) $p_{\mathrm{T}}^{H} \geq 450\,\mathrm{GeV}$. The $t\bar{t}H$ signal yield (solid red) is normalised to the fitted μ value from the inclusive fit. The dashed line shows the $t\bar{t}H$ signal distribution normalised to the total background prediction. The uncertainty band includes all uncertainties and their correlations.

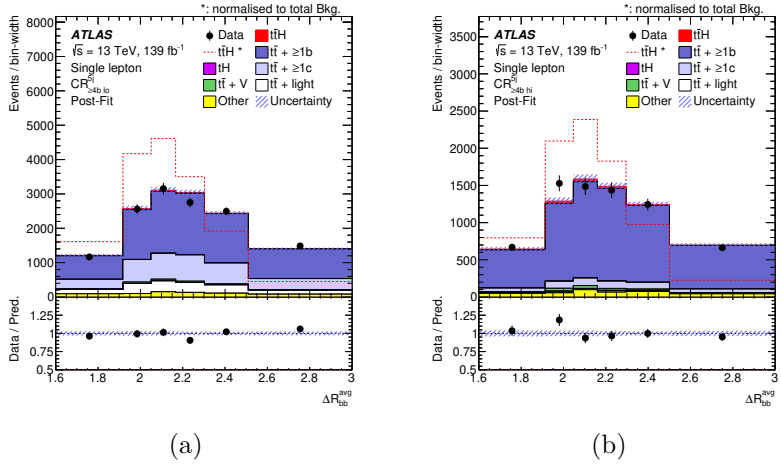

Figure 8. Comparison between data and prediction for $\Delta R_{bb}^{\mathrm{avg}}$ after the inclusive fit to the data in the single-lepton (a) $\mathrm{CR}^{5j}_{\geq 4b\ \mathrm{lo}}$ and (b) $\mathrm{CR}^{5j}_{\geq 4b\ \mathrm{hi}}$ control regions. The $t\bar{t}H$ signal yield (solid red) is normalised to the fitted μ value from the inclusive fit. The dashed line shows the $t\bar{t}H$ signal distribution normalised to the total background prediction. The uncertainty band includes all uncertainties and their correlations. The first (last) bin includes the underflow (overflow).

JHEP06(2022)097

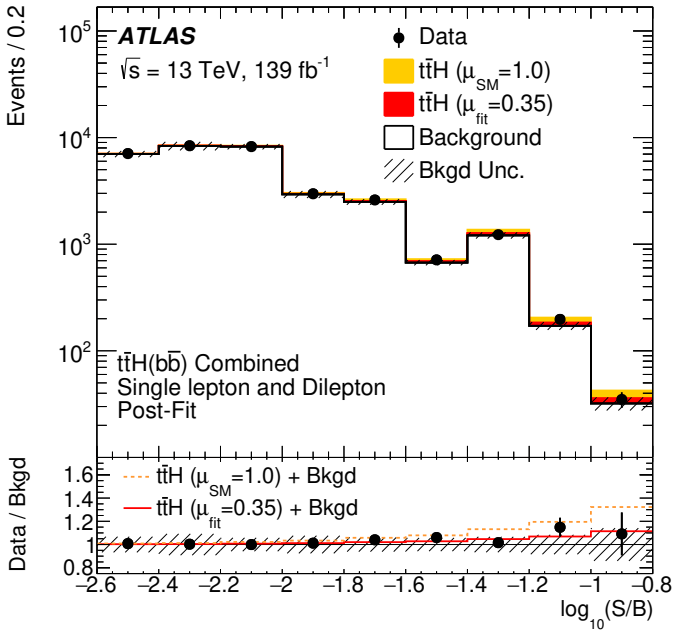

Figure 9. Post-fit yields of signal (S) and total background (B) as a function of $\log(S/B)$, compared with data. Final-discriminant bins in all dilepton and single-lepton analysis regions are combined into bins of $\log(S/B)$, with the signal normalised to the SM prediction used for the computation of $\log(S/B)$. The signal is then shown normalised to the best-fit value and the SM prediction. The lower frame reports the ratio of data to background, and this is compared with the expected $t\bar{t}H$-signal-plus-background yield divided by the background-only yield for the best-fit signal strength (solid red line) and the SM prediction (dashed orange line).

renormalisation scale. This pull indicates that the data favours a softer renormalisation scale in the ME calculation, as also suggested in ref. [129] where a lower scale in $t\bar{t}b\bar{b}$ calculations gives better agreement with $t\bar{t}b\bar{b}j$ calculations. This effect was shown to not affect the BDT shapes in each individual region, while correcting a mismodelling in the distribution of the number of jets in the event (by adjusting the amount of additional radiation), which affects the categorisation of events. The distributions of the number of jets in the three SRs are shown in figure 16 pre-fit and post-fit. Decorrelating this uncertainty between the dilepton and single-lepton channels leads to very similar fitted μ values and nuisance parameter pulls.

Another large pull is on the reconstructed p_{T}^{bb} shape uncertainty in the $t\bar{t}+\geq 1b$ background, as expected from the pre-fit mismodelling (see figure 4) and how this uncertainty is defined: a $+1\sigma$ variation corresponds to correcting the reconstructed p_{T}^{H} shape such that it agrees between data and the background model (see section 6.2). The sensitivity of the result to this uncertainty was tested by replacing the data-driven mismodelling with decorrelated free-floating $t\bar{t}+\geq 1b$ normalisation factors across the STXS bins and analysis regions, and no bias was observed on the fitted signal strength. The reconstructed p_{T}^{H} distributions display good post-fit agreement, as shown in figure 17 (to be compared with the pre-fit discrepancies shown in figure 4).

JHEP06(2022)097

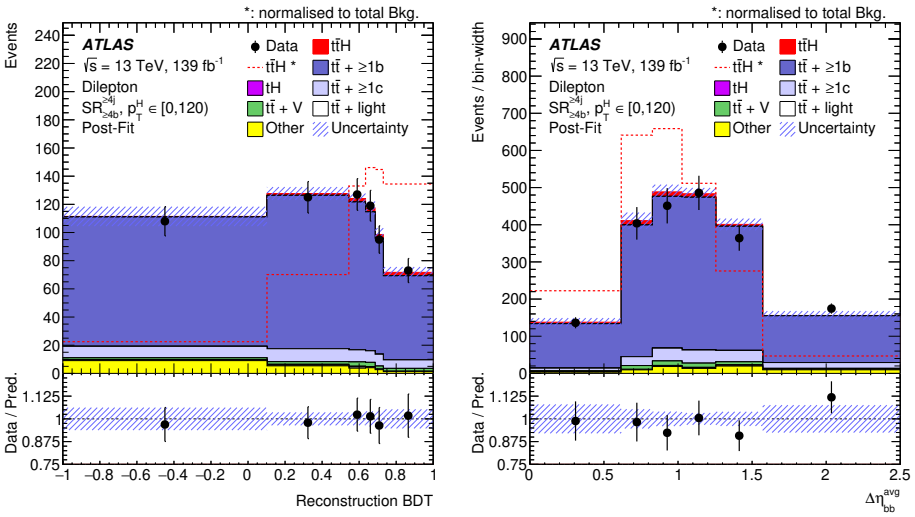

(a) (b)

Figure 10. Comparison between data and prediction for (a) the reconstruction BDT score for the Higgs boson candidate identified using Higgs boson information, and (b) the average $\Delta\eta$ between b-tagged jets, after the inclusive fit to the data in the dilepton resolved channel for $0 \leq p_{\mathrm{T}}^{H} < 120\,\mathrm{GeV}$. The $t\bar{t}H$ signal yield (solid red) is normalised to the fitted μ value from the inclusive fit. The dashed line shows the $t\bar{t}H$ signal distribution normalised to the total background prediction. The uncertainty band includes all uncertainties and their correlations.

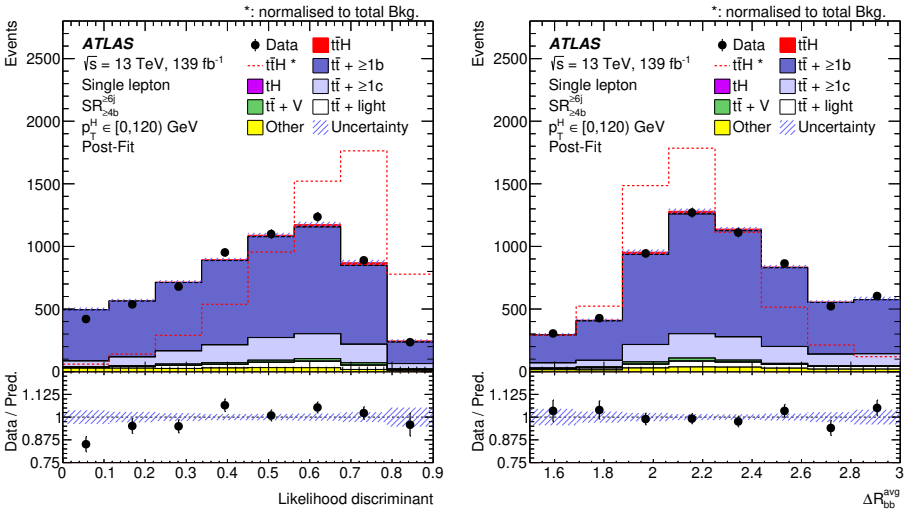

(a) (b)

Figure 11. Comparison between data and prediction for (a) the likelihood discriminant, and (b) the average ΔR for all possible combinations of b-tagged jet pairs, after the inclusive fit to the data in the single-lepton resolved channel for $0 \leq p_{\mathrm{T}}^{H} < 120\,\mathrm{GeV}$. The $t\bar{t}H$ signal yield (solid red) is normalised to the fitted μ value from the inclusive fit. The dashed line shows the $t\bar{t}H$ signal distribution normalised to the total background prediction. The uncertainty band includes all uncertainties and their correlations.

JHEP06(2022)097

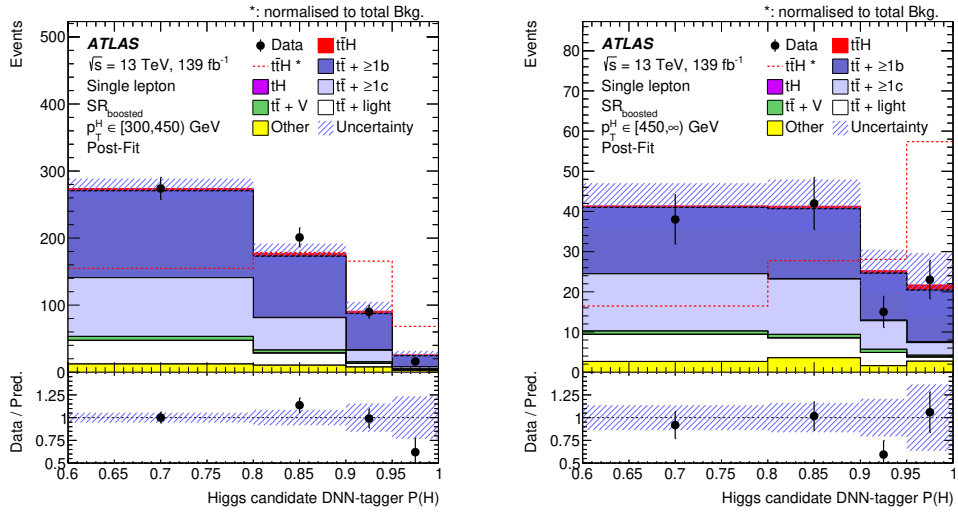

(a) (b)

Figure 12. Comparison between data and prediction for the DNN $P(H)$ output for the Higgs boson candidate after the inclusive fit to the data in the single-lepton boosted channel for (a) $300 \leq p_{\mathrm{T}}^{H} < 450\,\mathrm{GeV}$ and (b) $p_{\mathrm{T}}^{H} \geq 450\,\mathrm{GeV}$. The $t\bar{t}H$ signal yield (solid red) is normalised to the fitted μ value from the inclusive fit. The dashed line shows the $t\bar{t}H$ signal distribution normalised to the total background prediction. The uncertainty band includes all uncertainties and their correlations.

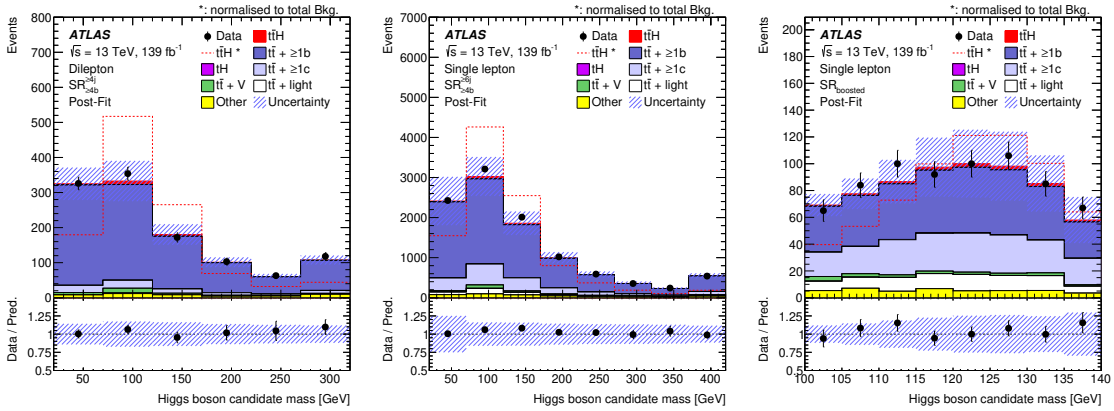

(a) (b) (c)

Figure 13. Post-fit distributions of the reconstructed Higgs boson candidate mass for the (a) dilepton $\mathrm{SR}^{\geq 4j}_{\geq 4b}$, (b) single-lepton resolved $\mathrm{SR}^{\geq 6j}_{\geq 4b}$ and (c) single-lepton boosted $\mathrm{SR}_{\mathrm{boosted}}$ signal regions. The $t\bar{t}H$ signal yield (solid red) is normalised to the fitted μ value from the inclusive fit. The dashed line shows the $t\bar{t}H$ signal distribution normalised to the total background prediction. The uncertainty band includes all uncertainties and their correlations. The first (last) bin includes the underflow (overflow).

JHEP06(2022)097

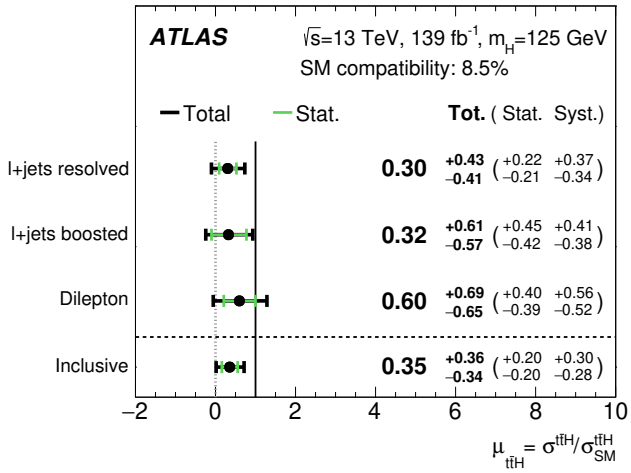

Figure 14. Fitted values of the $t\bar{t}H$ signal-strength parameter in the individual channels and in the inclusive signal strength measurement.

Additionally, a large pull is observed in the $t\bar{t}+\geq 1b$ NLO matching uncertainty in the dilepton channel in the $0 \leq p_{\mathrm{T}}^{H} < 120\,\mathrm{GeV}$ bin, as shown in figure 15 where it is ranked sixth for the impact on this measurement. Due to the large number of nuisance parameters entering into the likelihood fit, there is a non-negligible probability that any one of the $t\bar{t}+\geq 1b$ NLO matching uncertainties could be pulled to a value at least as extreme as that observed from a purely statistical standpoint. The probability is calculated to be 17%. Despite the large differences between models (see section 6.2), the varying $t\bar{t}+\geq 1b$ composition in the CRs and SRs allows the $t\bar{t}+\geq 1b$ subcomponent fraction systematic uncertainty to be constrained. In general the fit mostly constrains the $t\bar{t}+\geq 1b$ modelling uncertainties and the normalisation of the $t\bar{t}+\geq 1c$ background, which is pulled to 0.6σ and agrees very well with the previous publication [27]. To further validate the robustness of the fit, a pseudo-data sample was built from simulated events by replacing the nominal $t\bar{t}+\geq 1b$ background with the alternative $t\bar{t}+b\bar{b}$ MC sample generated with Sherpa 2.2.1. The fit to this pseudo-data sample did not reveal any significant bias in the signal extraction, the signal strength being compatible with unity within uncertainties.

The fit is also performed with multiple signal strengths corresponding to the five 'truth' $\hat{p}_{\mathrm{T}}^{H}$ bins. Figure 18 shows the values obtained. The normalisation factor is found to be $k(t\bar{t}+\geq 1b) = 1.28 \pm 0.08$, in perfect agreement with the single μ fit value. The global goodness of fit is 88%, summarising the good post-fit modelling obtained. The probability that the obtained signal strengths are compatible with the SM predictions is 45%, estimated by redoing the fit while fixing the μ value to 1 in the five bins. Overall, pulls and constraints similar to those in the inclusive measurement are observed. The measurement is dominated by systematic uncertainties in the lowest bin of 'truth' $\hat{p}_{\mathrm{T}}^{H}$ (mostly from the $t\bar{t}+\geq 1b$ background modelling), and by statistical uncertainties in the upper three bins.

Cross-section upper limits are also derived in the STXS framework. In this case, the likelihood function is slightly different from the one used to extract signal strengths: the effects of signal scale and PDF uncertainties on the predicted cross-section are not included

JHEP06(2022)097

Uncertainty source	$\Delta\mu$	
Process modelling		
$t\bar{t}H$ modelling	+0.13	−0.05
$t\bar{t}+\geq 1b$ modelling		
$t\bar{t}+\geq 1b$ NLO matching	+0.21	−0.20
$t\bar{t}+\geq 1b$ fractions	+0.12	−0.12
$t\bar{t}+\geq 1b$ FSR	+0.10	−0.11
$t\bar{t}+\geq 1b$ PS & hadronisation	+0.09	−0.08
$t\bar{t}+\geq 1b$ p_{T}^{bb} shape	+0.04	−0.04
$t\bar{t}+\geq 1b$ ISR	+0.04	−0.04
$t\bar{t}+\geq 1c$ modelling	+0.03	−0.04
$t\bar{t}+$ light modelling	+0.03	−0.03
tW modelling	+0.08	−0.07
Background-model statistical uncertainty	+0.04	−0.05
b-tagging efficiency and mis-tag rates		
b-tagging efficiency	+0.03	−0.02
c-mis-tag rates	+0.03	−0.03
l-mis-tag rates	+0.02	−0.02
Jet energy scale and resolution		
b-jet energy scale	+0.00	−0.01
Jet energy scale (flavour)	+0.01	−0.01
Jet energy scale (pile-up)	+0.00	−0.01
Jet energy scale (remaining)	+0.01	−0.01
Jet energy resolution	+0.02	−0.02
Luminosity	+0.01	−0.00
Other sources	+0.03	−0.03
Total systematic uncertainty	+0.30	−0.28
$t\bar{t}+\geq 1b$ normalisation	+0.04	−0.07
Total statistical uncertainty	+0.20	−0.20
Total uncertainty	+0.36	−0.34

Table 6. Breakdown of the contributions to the uncertainties in μ. The contributions from the different sources of uncertainty are evaluated after the fit. The $\Delta\mu$ values are obtained by repeating the fit after having fixed a certain set of nuisance parameters corresponding to a group of systematic uncertainties, and then evaluating $(\Delta\mu)^2$ by subtracting the resulting squared uncertainty of μ from its squared uncertainty found in the full fit. The same procedure is followed when quoting the effect of the $t\bar{t}+\geq 1b$ normalisation. The total uncertainty is different from the sum in quadrature of the different components due to correlations between nuisance parameters existing in the fit.

JHEP06(2022)097

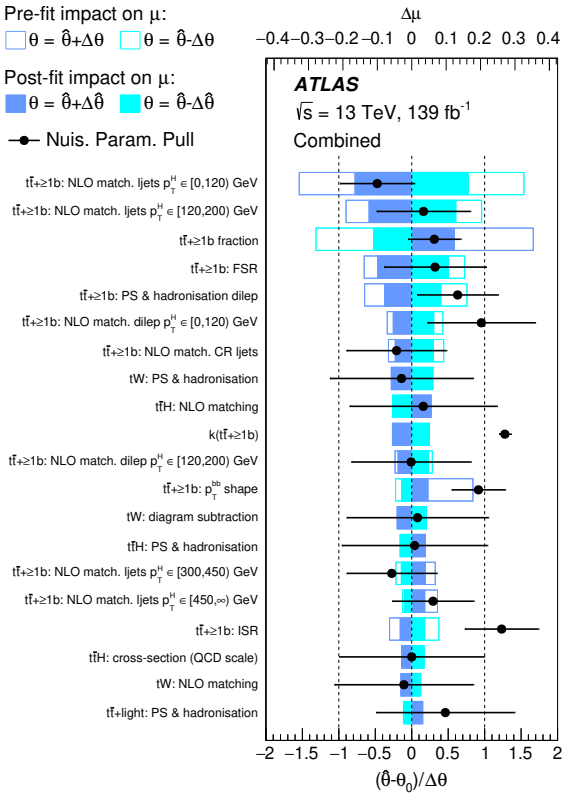

Figure 15. Ranking of the 20 nuisance parameters with the largest post-fit impact on μ in the fit. Nuisance parameters corresponding to statistical uncertainties in the simulated event samples are not included. The empty blue rectangles correspond to the pre-fit impact on μ and the filled blue ones to the post-fit impact on μ, both referring to the upper scale. The impact of each nuisance parameter, $\Delta\mu$, is computed by comparing the nominal best-fit value of μ with the result of the fit when fixing the considered nuisance parameter to its best-fit value, $\hat{\theta}$, shifted by its pre-fit (post-fit) uncertainties $\pm\Delta\theta$ ($\pm\Delta\hat{\theta}$). The black points show the pulls of the nuisance parameters relative to their nominal values, θ_0. These pulls and their relative post-fit errors, $\Delta\hat{\theta}/\Delta\theta$, refer to the lower scale. The 'ljets' ('dilep') label refers to the single-lepton (dilepton) channel.

because, while affecting the signal-strength measurements, they do not affect the cross-section measurements. Scale effects are still present in the statistical model though, via the ISR uncertainty, but with no impact on the overall cross-section. The inclusive cross-section of 507 fb is used to calculate these limits, scaled by the fraction of events in each $\hat{p}_{\mathrm{T}}^{H}$ bin to establish the fiducial cross-section for each STXS bin. The measured 95% confidence level (CL) cross-section upper limits in each STXS bin are shown in figure 19, where the hatched uncertainty bands correspond to the theoretical uncertainty in the fiducial cross-section prediction in each bin.

JHEP06(2022)097

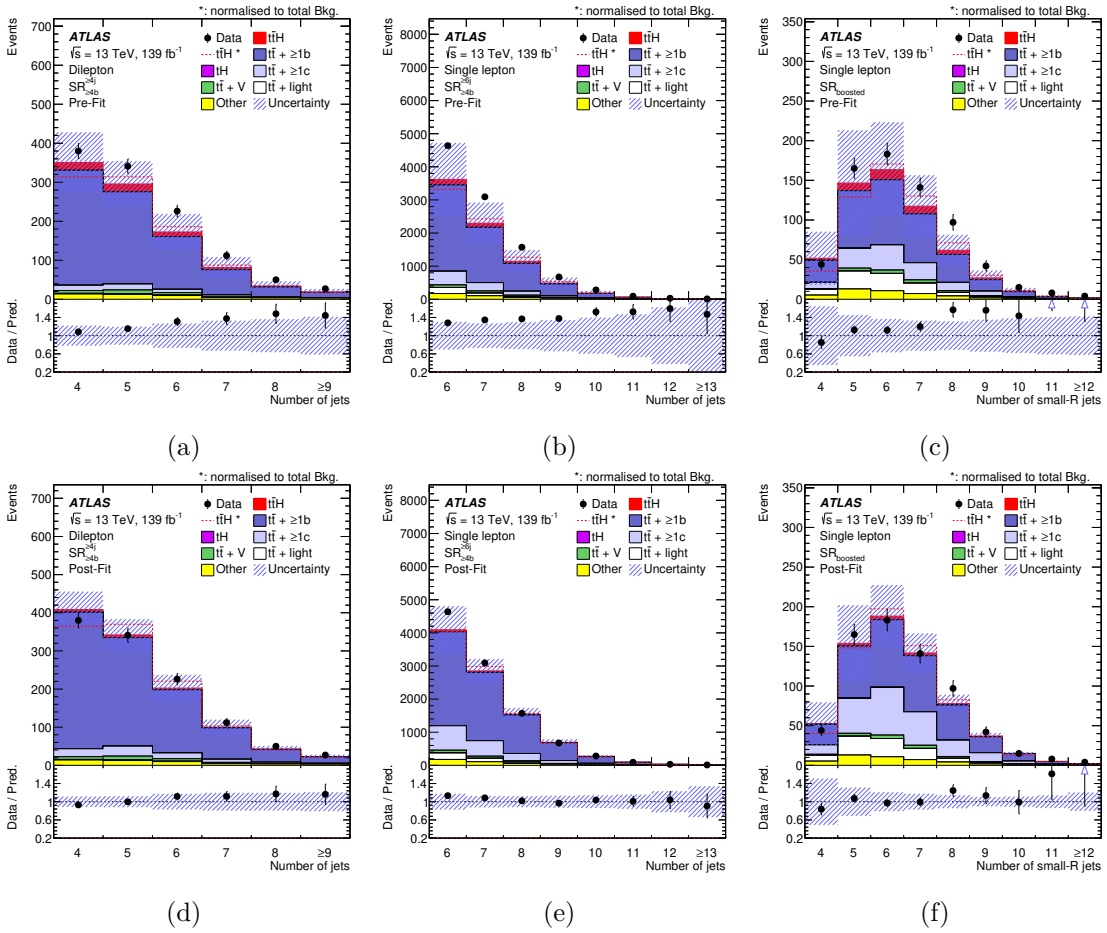

Figure 16. Pre-fit (top) and post-fit (bottom) distributions of the number of jets in the (a, d) dilepton $\mathrm{SR}^{\geq 4j}_{\geq 4b}$, (b, e) single-lepton resolved $\mathrm{SR}^{\geq 6j}_{\geq 4b}$ and (c, f) single-lepton boosted $\mathrm{SR}_{\mathrm{boosted}}$ signal regions. The $t\bar{t}H$ signal yield (solid red) is normalised to the Standard Model expectation (the fitted μ value from the inclusive fit) in the pre-fit (post-fit) distributions. The dashed line shows the $t\bar{t}H$ signal distribution normalised to the total background prediction. The uncertainty band includes all uncertainties and their correlations, except in the pre-fit distributions where the uncertainty in the $k(t\bar{t}+\geq 1b)$ normalisation factor is not defined.

JHEP06(2022)097

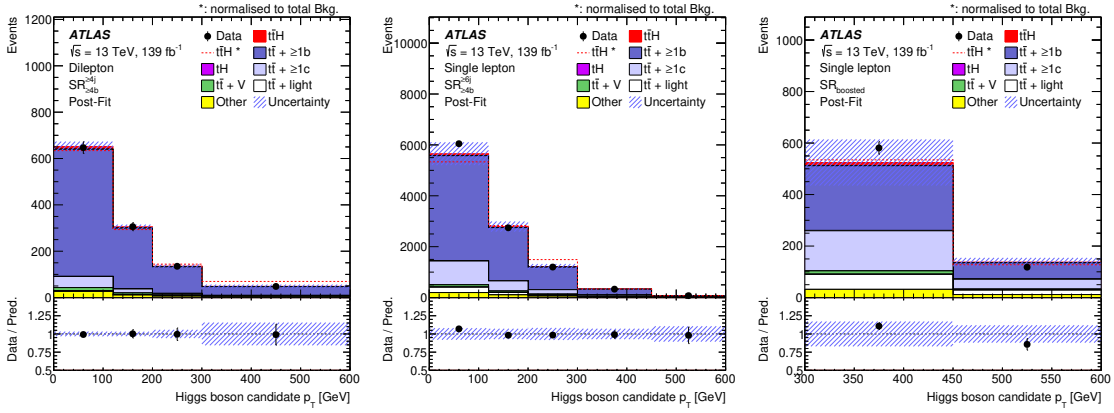

(a) (b) (c)

Figure 17. Post-fit distributions of the reconstructed Higgs boson candidate p_{T}^{H} for the (a) dilepton $\mathrm{SR}^{\geq 4j}_{\geq 4b}$, (b) single-lepton resolved $\mathrm{SR}^{\geq 6j}_{\geq 4b}$ and (c) single-lepton boosted $\mathrm{SR}_{\mathrm{boosted}}$ signal regions. The $t\bar{t}H$ signal yield (solid red) is normalised to the fitted μ value from the inclusive fit. The dashed line shows the $t\bar{t}H$ signal distribution normalised to the total background prediction. The uncertainty band includes all uncertainties and their correlations. The last bin includes the overflow.

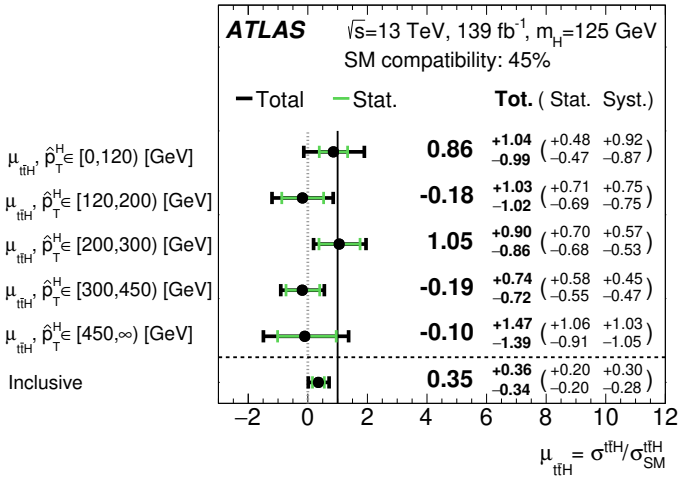

Figure 18. Signal-strength measurements in the individual STXS $\hat{p}_{\mathrm{T}}^{H}$ bins, as well as the inclusive signal strength.

JHEP06(2022)097

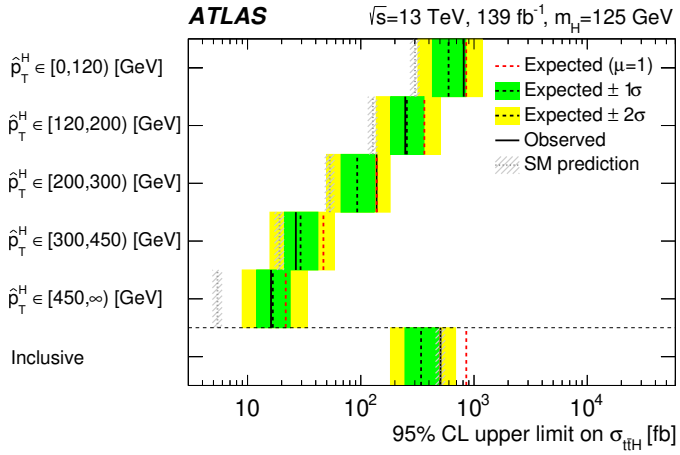

Figure 19. 95% CL simplified template cross-section upper limits in the individual STXS $\hat{p}_{\mathrm{T}}^{H}$ bins, as well as the inclusive limit. The observed limits are shown (solid black lines), together with the expected limits both in the background-only hypothesis (dotted black lines) and in the SM hypothesis (dotted red lines). In the case of the expected limits in the background-only hypothesis, one- and two-standard-deviation uncertainty bands are also shown. The hatched uncertainty bands correspond to the theory uncertainty in the fiducial cross-section prediction in each bin.

8 Conclusion

Measurements of a Standard Model Higgs boson produced in association with a pair of top quarks and decaying into a pair of b-quarks are performed. The results are based on the Run 2 dataset of pp collision data collected at $\sqrt{s} = 13\,\mathrm{TeV}$ by the ATLAS detector at the LHC, corresponding to an integrated luminosity of $139\,\mathrm{fb}^{-1}$. The event selection targets top-quark pair decays to a final state containing one or two leptons. Machine-learning techniques are used to discriminate between signal and background events, the latter being dominated by $t\bar{t}$ + jets production. The measured signal strength is $0.35^{+0.36}_{-0.34}$, corresponding to an observed (expected) significance of 1.0 (2.7) standard deviations. The probability of the obtained signal strength being compatible with the SM prediction is 8.5%. The measurement uncertainty is dominated by systematic uncertainties, despite significant improvement relative to the previous measurement [27], especially regarding theoretical knowledge of the $t\bar{t} + \geq 1b$ background process, which still drives the sensitivity. To further test the Standard Model, the first differential measurement of the $t\bar{t}H$ signal strength was performed in five bins of Higgs boson transverse momentum in the STXS framework, including a bin for specially selected boosted Higgs bosons with transverse momentum above 300 GeV. Upper limits on the STXS cross-sections are also derived. Observed results are compatible with Standard Model expectations within uncertainties.

Acknowledgments

We thank CERN for the very successful operation of the LHC, as well as the support staff from our institutions without whom ATLAS could not be operated efficiently.

JHEP06(2022)097

We acknowledge the support of ANPCyT, Argentina; YerPhI, Armenia; ARC, Australia; BMWFW and FWF, Austria; ANAS, Azerbaijan; SSTC, Belarus; CNPq and FAPESP, Brazil; NSERC, NRC and CFI, Canada; CERN; ANID, Chile; CAS, MOST and NSFC, China; Minciencias, Colombia; MEYS CR, Czech Republic; DNRF and DNSRC, Denmark; IN2P3-CNRS and CEA-DRF/IRFU, France; SRNSFG, Georgia; BMBF, HGF and MPG, Germany; GSRI, Greece; RGC and Hong Kong SAR, China; ISF and Benoziyo Center, Israel; INFN, Italy; MEXT and JSPS, Japan; CNRST, Morocco; NWO, Netherlands; RCN, Norway; MEiN, Poland; FCT, Portugal; MNE/IFA, Romania; JINR; MES of Russia and NRC KI, Russian Federation; MESTD, Serbia; MSSR, Slovakia; ARRS and MIZŠ, Slovenia; DSI/NRF, South Africa; MICINN, Spain; SRC and Wallenberg Foundation, Sweden; SERI, SNSF and Cantons of Bern and Geneva, Switzerland; MOST, Taiwan; TAEK, Turkey; STFC, United Kingdom; DOE and NSF, United States of America. In addition, individual groups and members have received support from BCKDF, CANARIE, Compute Canada and CRC, Canada; COST, ERC, ERDF, Horizon 2020 and Marie Skłodowska-Curie Actions, European Union; Investissements d'Avenir Labex, Investissements d'Avenir Idex and ANR, France; DFG and AvH Foundation, Germany; Herakleitos, Thales and Aristeia programmes co-financed by EU-ESF and the Greek NSRF, Greece; BSF-NSF and GIF, Israel; Norwegian Financial Mechanism 2014–2021, Norway; NCN and NAWA, Poland; La Caixa Banking Foundation, CERCA Programme Generalitat de Catalunya and PROMETEO and GenT Programmes Generalitat Valenciana, Spain; Göran Gustafssons Stiftelse, Sweden; The Royal Society and Leverhulme Trust, United Kingdom.

The crucial computing support from all WLCG partners is acknowledged gratefully, in particular from CERN, the ATLAS Tier-1 facilities at TRIUMF (Canada), NDGF (Denmark, Norway, Sweden), CC-IN2P3 (France), KIT/GridKA (Germany), INFN-CNAF (Italy), NL-T1 (Netherlands), PIC (Spain), ASGC (Taiwan), RAL (U.K.) and BNL (U.S.A.), the Tier-2 facilities worldwide and large non-WLCG resource providers. Major contributors of computing resources are listed in ref. [130].

A Input variables to the classification BDTs

In this appendix, the full list of variables used as inputs to the classification BDT, described in section 5.2, in each of the signal regions is reported. Variables are listed separately in table 7 for the dilepton channel, in table 8 for the resolved single-lepton channel and in table 9 for the single-lepton boosted channel. Variables from the reconstruction BDT exploit the chosen jet-parton assignment (see section 5.2). The b-tagging discriminant assigned to each jet and the large-R jets used to build the Higgs-boson and top-quark candidates in the boosted category are defined in section 4. Some kinematic and topological variables are built considering only b-tagged jets in the event. In the resolved and boosted single-lepton channels, b-tagged jets are defined as the four jets with the largest value of the b-tagging discriminant. If two jets have the same b-tagging discriminant value, they are ordered by decreasing jet p_{T} value. In the dilepton channel, jets are required to pass the 70% working point to be b-tagged.

JHEP06(2022)097

Variable	Definition	
General kinematic variables		
m_{bb}^{min}	Minimum invariant mass of a b-tagged jet pair	
$m_{bb}^{\text{min } \Delta R}$	Invariant mass of the b-tagged jet pair with minimum ΔR	
$m_{jj}^{\text{max } p_{\text{T}}}$	Invariant mass of the jet pair with maximum p_{T}	
$m_{bb}^{\text{max } p_{\text{T}}}$	Invariant mass of the b-tagged jet pair with maximum p_{T}	
$\Delta\eta_{bb}^{\text{avg}}$	Average $\Delta\eta$ for all b-tagged jet pairs	
$N_{bb}^{\text{Higgs 30}}$	Number of b-tagged jet pairs with invariant mass within 30 GeV of the Higgs boson mass	
Variables from reconstruction BDT		
BDT outputs	Output of the reco. BDT w/ Higgs info. for the combination selected by the reco. BDTs w/ or w/o Higgs info.	‡
m_{bb}^{Higgs}	Higgs candidate mass	
$\Delta R_{H,t\bar{t}}$	ΔR between Higgs candidate and $t\bar{t}$ candidate system	†
$\Delta R_{H,\ell}^{\text{min}}$	Minimum ΔR between Higgs candidate and lepton	
$\Delta R_{H,b}^{\text{min}}$	Minimum ΔR between Higgs candidate and b-jet from top	

Table 7. Variables used in the classification BDTs in the dilepton channel. For variables depending on b-tagged jets, only jets b-tagged using the 70% working point are considered. For variables from the reconstruction BDT, those with a † are from the BDT using Higgs boson information, those with no sign are from the BDT without Higgs boson information while for those with a ‡ both versions are used.

JHEP06(2022)097

Variable	Definition	
General kinematic variables		
$\Delta R_{bb}^{\text{avg}}$	Average ΔR for all b-tagged jet pairs	
$\Delta R_{bb}^{\text{max } p_{\text{T}}}$	ΔR between the two b-tagged jets with the largest vector sum p_{T}	
$\Delta\eta_{jj}^{\text{max}}$	Maximum $\Delta\eta$ between any two jets	
$m_{bb}^{\text{min } \Delta R}$	Mass of the combination of two b-tagged jets with the smallest ΔR	
$N_{bb}^{\text{Higgs 30}}$	Number of b-tagged jet pairs with invariant mass within 30 GeV of the Higgs boson mass	
Aplanarity	$1.5\lambda_2$, where λ_2 is the second eigenvalue of the momentum tensor [*Phys. Rev. D* **48** (1993) R3953] built with all jets	
H_1	Second Fox-Wolfram moment computed using all jets and the lepton	
Variables from reconstruction BDT		
BDT output	Output of the reconstruction BDT	†
m_{bb}^{Higgs}	Higgs candidate mass	
$m_{H,b_{\text{lep top}}}$	Mass of Higgs candidate and b-jet from leptonic top candidate	
$\Delta R_{bb}^{\text{Higgs}}$	ΔR between b-jets from the Higgs candidate	
$\Delta R_{H,t\bar{t}}$	ΔR between Higgs candidate and $t\bar{t}$ candidate system	†
$\Delta R_{H,\text{lep top}}$	ΔR between Higgs candidate and leptonic top candidate	
Variables from likelihood calculations		
LHD	Likelihood discriminant	
Variables from b-tagging		
$w_{b\text{-tag}}^{\text{Higgs}}$	Sum of b-tagging discriminants of jets from best Higgs candidate from the reconstruction BDT	
B_{jet}^{3}	3$^{\text{rd}}$ largest jet b-tagging discriminant	
B_{jet}^{4}	4$^{\text{th}}$ largest jet b-tagging discriminant	
B_{jet}^{5}	5$^{\text{th}}$ largest jet b-tagging discriminant	

Table 8. Input variables to the classification BDTs in the single-lepton resolved channel. For variables depending on b-tagged jets, jets are sorted by their pseudo-continuous b-tag score, and by their p_{T} when they have the same pseudo-continuous b-tag score. For variables from the reconstruction BDT, those with a † are from the BDT using Higgs boson information, those with no † are from the BDT without Higgs boson information.

JHEP06(2022)097

Variable	Definition
m_{bb}^{Higgs}	Higgs candidate mass
p_{T}^{H}	Higgs candidate transverse momentum
$\eta_{\text{lep}}^{\text{Higgs}}$	η of the Higgs candidate relative to the lepton
$P(H)$	DNN Higgs probability for the Higgs candidate
$m_{\text{had top}}$	Hadronic top candidate mass
$p_{\text{T}}^{\text{had top}}$	Hadronic top candidate transverse momentum
$\eta_{\text{had top}}^{\text{lep}}$	η of the hadronic top candidate relative to the lepton
$B_{\text{had top}}^{i}$	i^{th} largest jet b-tagging discriminant associated to the hadronic top candidate
$m_{\text{lep top}}$	Leptonic top candidate mass
$p_{\text{T}}^{\text{lep top}}$	Leptonic top candidate transverse momentum
$B_{\text{lep top}}$	b-tagging discriminant of the jet associated to the leptonic top candidate
n_{jets}	Small-R jets multiplicity
$\Delta R_{H,\text{had top}}$	ΔR between the Higgs and the hadronic top candidates
$\Delta R_{H,\text{lep top}}$	ΔR between the Higgs and the leptonic top candidates
$\Delta R_{\text{had top,lep top}}$	ΔR between the hadronic top and the leptonic top candidates
$p_{\text{T}}^{t\bar{t}H}$	$t\bar{t}H$ system transverse momentum
$p_{\text{T}}^{t\bar{t}}$	$t\bar{t}$ system transverse momentum
$w_{b\text{-tag}}^{\text{sum}}$	Sum of b-tagging discriminants of jets from Higgs, hadronic and leptonic top candidates
$w_{b\text{-tag}}^{\text{add jet}}$	Fraction of the sum of b-tagging discriminants of all jets not associated to Higgs or hadronic top candidates

Table 9. Input variables to the classification BDT in the single-lepton boosted channel. For variables depending on b-tagged jets, jets are sorted by their pseudo-continuous b-tag score, and by their p_{T} when they have the same pseudo-continuous b-tag score. The i index runs from zero to two.

JHEP06(2022)097

Open Access. This article is distributed under the terms of the Creative Commons Attribution License (CC-BY 4.0), which permits any use, distribution and reproduction in any medium, provided the original author(s) and source are credited.

References

[1] F. Englert and R. Brout, *Broken Symmetry and the Mass of Gauge Vector Mesons*, *Phys. Rev. Lett.* **13** (1964) 321 [INSPIRE].

[2] P.W. Higgs, *Broken Symmetries and the Masses of Gauge Bosons*, *Phys. Rev. Lett.* **13** (1964) 508 [INSPIRE].

[3] G.S. Guralnik, C.R. Hagen and T.W.B. Kibble, *Global Conservation Laws and Massless Particles*, *Phys. Rev. Lett.* **13** (1964) 585 [INSPIRE].

[4] ATLAS collaboration, *Observation of a new particle in the search for the Standard Model Higgs boson with the ATLAS detector at the LHC*, *Phys. Lett. B* **716** (2012) 1 [arXiv:1207.7214] [INSPIRE].

[5] CMS collaboration, *Observation of a new boson at a mass of* 125 *GeV with the CMS experiment at the LHC*, *Phys. Lett. B* **716** (2012) 30 [arXiv:1207.7235] [INSPIRE].

[6] ATLAS and CMS collaborations, *Combined Measurement of the Higgs Boson Mass in pp Collisions at* $\sqrt{s} = 7$ *and* 8 *TeV with the ATLAS and CMS Experiments*, *Phys. Rev. Lett.* **114** (2015) 191803 [arXiv:1503.07589] [INSPIRE].

[7] L. Evans and P. Bryant, eds., *LHC Machine*, 2008 *JINST* **3** S08001 [INSPIRE].

[8] C. Englert et al., *Precision measurements of Higgs couplings: implications for new physics scales*, *J. Phys. G* **41** (2014) 113001 [arXiv:1403.7191] [INSPIRE].

[9] ATLAS and CMS collaborations, *Measurements of the Higgs boson production and decay rates and constraints on its couplings from a combined ATLAS and CMS analysis of the LHC pp collision data at* $\sqrt{s} = 7$ *and* 8 *TeV*, *JHEP* **08** (2016) 045 [arXiv:1606.02266] [INSPIRE].

[10] ATLAS collaboration, *Cross-section measurements of the Higgs boson decaying into a pair of* τ*-leptons in proton-proton collisions at* $\sqrt{s} = 13$ *TeV with the ATLAS detector*, *Phys. Rev. D* **99** (2019) 072001 [arXiv:1811.08856] [INSPIRE].

[11] CMS collaboration, *Observation of the Higgs boson decay to a pair of* τ *leptons with the CMS detector*, *Phys. Lett. B* **779** (2018) 283 [arXiv:1708.00373] [INSPIRE].

[12] ATLAS collaboration, *Observation of* $H \to b\bar{b}$ *decays and* VH *production with the ATLAS detector*, *Phys. Lett. B* **786** (2018) 59 [arXiv:1808.08238] [INSPIRE].

[13] CMS collaboration, *Observation of Higgs Boson Decay to Bottom Quarks*, *Phys. Rev. Lett.* **121** (2018) 121801 [arXiv:1808.08242] [INSPIRE].

[14] ATLAS collaboration, *Observation of Higgs boson production in association with a top quark pair at the LHC with the ATLAS detector*, *Phys. Lett. B* **784** (2018) 173 [arXiv:1806.00425] [INSPIRE].

[15] CMS collaboration, *Observation of* $t\bar{t}H$ *Production*, *Phys. Rev. Lett.* **120** (2018) 231801 [arXiv:1804.02610] [INSPIRE].

[16] J.N. Ng and P. Zakarauskas, *QCD-parton calculation of conjoined production of Higgs bosons and heavy flavors in* $p\bar{p}$ *collision*, *Phys. Rev. D* **29** (1984) 876 [INSPIRE].

JHEP06(2022)097

[17] Z. Kunszt, *Associated production of heavy Higgs boson with top quarks*, *Nucl. Phys. B* **247** (1984) 339 [INSPIRE].

[18] S. Dawson, L.H. Orr, L. Reina and D. Wackeroth, *Next-to-leading order QCD corrections to $pp \to t\bar{t}h$ at the CERN Large Hadron Collider*, *Phys. Rev. D* **67** (2003) 071503 [hep-ph/0211438] [INSPIRE].

[19] W. Beenakker, S. Dittmaier, M. Krämer, B. Plumper, M. Spira and P.M. Zerwas, *Higgs Radiation Off Top Quarks at the Tevatron and the LHC*, *Phys. Rev. Lett.* **87** (2001) 201805 [hep-ph/0107081] [INSPIRE].

[20] LHC Higgs Cross Section Working Group collaboration, *Handbook of LHC Higgs Cross Sections: 4. Deciphering the Nature of the Higgs Sector*, arXiv:1610.07922 [INSPIRE].

[21] J. Ellis, D.S. Hwang, K. Sakurai and M. Takeuchi, *Disentangling Higgs-top couplings in associated production*, *JHEP* **04** (2014) 004 [arXiv:1312.5736] [INSPIRE].

[22] F. Boudjema, D. Guadagnoli, R.M. Godbole and K.A. Mohan, *Laboratory-frame observables for probing the top-Higgs boson interaction*, *Phys. Rev. D* **92** (2015) 015019 [arXiv:1501.03157] [INSPIRE].

[23] M.R. Buckley and D. Goncalves, *Boosting the Direct CP Measurement of the Higgs-Top Coupling*, *Phys. Rev. Lett.* **116** (2016) 091801 [arXiv:1507.07926] [INSPIRE].

[24] S. Amor Dos Santos et al., *Probing the CP nature of the Higgs coupling in $t\bar{t}h$ events at the LHC*, *Phys. Rev. D* **96** (2017) 013004 [arXiv:1704.03565] [INSPIRE].

[25] ATLAS collaboration, *Search for the Standard Model Higgs boson produced in association with top quarks and decaying into $b\bar{b}$ in pp collisions at $\sqrt{s} = 8$ TeV with the ATLAS detector*, *Eur. Phys. J. C* **75** (2015) 349 [arXiv:1503.05066] [INSPIRE].

[26] ATLAS collaboration, *Search for the Standard Model Higgs boson decaying into $b\bar{b}$ produced in association with top quarks decaying hadronically in pp collisions at $\sqrt{s} = 8$ TeV with the ATLAS detector*, *JHEP* **05** (2016) 160 [arXiv:1604.03812] [INSPIRE].

[27] ATLAS collaboration, *Search for the standard model Higgs boson produced in association with top quarks and decaying into a $b\bar{b}$ pair in pp collisions at $\sqrt{s} = 13$ TeV with the ATLAS detector*, *Phys. Rev. D* **97** (2018) 072016 [arXiv:1712.08895] [INSPIRE].

[28] CMS collaboration, *Search for $t\bar{t}H$ production in the $H \to b\bar{b}$ decay channel with leptonic $t\bar{t}$ decays in proton-proton collisions at $\sqrt{s} = 13$ TeV*, *JHEP* **03** (2019) 026 [arXiv:1804.03682] [INSPIRE].

[29] CMS collaboration, *Search for $t\bar{t}H$ production in the all-jet final state in proton-proton collisions at $\sqrt{s} = 13$ TeV*, *JHEP* **06** (2018) 101 [arXiv:1803.06986] [INSPIRE].

[30] ATLAS collaboration, *The ATLAS Experiment at the CERN Large Hadron Collider*, 2008 *JINST* **3** S08003 [INSPIRE].

[31] ATLAS collaboration, *ATLAS Insertable B-Layer Technical Design Report*, CERN-LHCC-2010-013, ATLAS-TDR-19 (2010).

[32] ATLAS collaboration, *ATLAS Insertable B-Layer Technical Design Report Addendum*, CERN-LHCC-2012-009, ATLAS-TDR-19-ADD-1 (2012).

[33] ATLAS IBL collaboration, *Production and integration of the ATLAS Insertable B-Layer*, 2018 *JINST* **13** T05008 [arXiv:1803.00844] [INSPIRE].

JHEP06(2022)097

[34] ATLAS collaboration, *Performance of the ATLAS trigger system in 2015*, *Eur. Phys. J. C* **77** (2017) 317 [arXiv:1611.09661] [INSPIRE].

[35] ATLAS collaboration, *The ATLAS Collaboration Software and Firmware*, ATL-SOFT-PUB-2021-001 (2021).

[36] ATLAS collaboration, *The ATLAS Simulation Infrastructure*, *Eur. Phys. J. C* **70** (2010) 823 [arXiv:1005.4568] [INSPIRE].

[37] GEANT4 collaboration, *GEANT4 — a simulation toolkit*, *Nucl. Instrum. Meth. A* **506** (2003) 250 [INSPIRE].

[38] T. Sjöstrand et al., *An introduction to PYTHIA 8.2*, *Comput. Phys. Commun.* **191** (2015) 159 [arXiv:1410.3012] [INSPIRE].

[39] ATLAS collaboration, *The Pythia 8 A3 tune description of ATLAS minimum bias and inelastic measurements incorporating the Donnachie-Landshoff diffractive model*, ATL-PHYS-PUB-2016-017 (2016).

[40] M. Bahr et al., *Herwig++ physics and manual*, *Eur. Phys. J. C* **58** (2008) 639 [arXiv:0803.0883] [INSPIRE].

[41] J. Bellm et al., *Herwig 7.0/Herwig++ 3.0 release note*, *Eur. Phys. J. C* **76** (2016) 196 [arXiv:1512.01178] [INSPIRE].

[42] D.J. Lange, *The EvtGen particle decay simulation package*, *Nucl. Instrum. Meth. A* **462** (2001) 152 [INSPIRE].

[43] ATLAS collaboration, *ATLAS Pythia 8 tunes to 7 TeV data*, ATL-PHYS-PUB-2014-021 (2014).

[44] R.D. Ball et al., *Parton distributions with LHC data*, *Nucl. Phys. B* **867** (2013) 244 [arXiv:1207.1303] [INSPIRE].

[45] L.A. Harland-Lang, A.D. Martin, P. Motylinski and R.S. Thorne, *Parton distributions in the LHC era: MMHT 2014 PDFs*, *Eur. Phys. J. C* **75** (2015) 204 [arXiv:1412.3989] [INSPIRE].

[46] M. Beneke, P. Falgari, S. Klein and C. Schwinn, *Hadronic top-quark pair production with NNLL threshold resummation*, *Nucl. Phys. B* **855** (2012) 695 [arXiv:1109.1536] [INSPIRE].

[47] M. Cacciari, M. Czakon, M. Mangano, A. Mitov and P. Nason, *Top-pair production at hadron colliders with next-to-next-to-leading logarithmic soft-gluon resummation*, *Phys. Lett. B* **710** (2012) 612 [arXiv:1111.5869] [INSPIRE].

[48] P. Bärnreuther, M. Czakon and A. Mitov, *Percent-Level-Precision Physics at the Tevatron: Next-to-Next-to-Leading Order QCD Corrections to $q\bar{q} \to t\bar{t} + X$*, *Phys. Rev. Lett.* **109** (2012) 132001 [arXiv:1204.5201] [INSPIRE].

[49] M. Czakon and A. Mitov, *NNLO corrections to top-pair production at hadron colliders: the all-fermionic scattering channels*, *JHEP* **12** (2012) 054 [arXiv:1207.0236] [INSPIRE].

[50] M. Czakon and A. Mitov, *NNLO corrections to top pair production at hadron colliders: the quark-gluon reaction*, *JHEP* **01** (2013) 080 [arXiv:1210.6832] [INSPIRE].

[51] M. Czakon, P. Fiedler and A. Mitov, *Total Top-Quark Pair-Production Cross Section at Hadron Colliders Through $O(\alpha_S^4)$*, *Phys. Rev. Lett.* **110** (2013) 252004 [arXiv:1303.6254] [INSPIRE].

[52] M. Czakon and A. Mitov, *Top++: A program for the calculation of the top-pair cross-section at hadron colliders*, *Comput. Phys. Commun.* **185** (2014) 2930 [arXiv:1112.5675] [INSPIRE].

JHEP06(2022)097

[53] N. Kidonakis, *Two-loop soft anomalous dimensions for single top quark associated production with a W^- or H^-*, *Phys. Rev. D* **82** (2010) 054018 [arXiv:1005.4451] [INSPIRE].

[54] N. Kidonakis, *Top Quark Production*, in *Helmholtz International Summer School on Physics of Heavy Quarks and Hadrons (HQ 2013)*, pp. 139–168 (2014) [DOI] [arXiv:1311.0283] [INSPIRE].

[55] M. Aliev, H. Lacker, U. Langenfeld, S. Moch, P. Uwer and M. Wiedermann, *HATHOR — HAdronic Top and Heavy quarks crOss section calculatoR*, *Comput. Phys. Commun.* **182** (2011) 1034 [arXiv:1007.1327] [INSPIRE].

[56] P. Kant et al., *HatHor for single top-quark production: Updated predictions and uncertainty estimates for single top-quark production in hadronic collisions*, *Comput. Phys. Commun.* **191** (2015) 74 [arXiv:1406.4403] [INSPIRE].

[57] C. Anastasiou, L.J. Dixon, K. Melnikov and F. Petriello, *High precision QCD at hadron colliders: Electroweak gauge boson rapidity distributions at next-to-next-to leading order*, *Phys. Rev. D* **69** (2004) 094008 [hep-ph/0312266] [INSPIRE].

[58] R. Frederix, D. Pagani and M. Zaro, *Large NLO corrections in $t\bar{t}W^{\pm}$ and $t\bar{t}t\bar{t}$ hadroproduction from supposedly subleading EW contributions*, *JHEP* **02** (2018) 031 [arXiv:1711.02116] [INSPIRE].

[59] S. Frixione, E. Laenen, P. Motylinski, C. White and B.R. Webber, *Single-top hadroproduction in association with a W boson*, *JHEP* **07** (2008) 029 [arXiv:0805.3067] [INSPIRE].

[60] ATLAS collaboration, *Studies on top-quark Monte Carlo modelling for Top2016*, ATL-PHYS-PUB-2016-020 (2016).

[61] P. Nason, *A new method for combining NLO QCD with shower Monte Carlo algorithms*, *JHEP* **11** (2004) 040 [hep-ph/0409146] [INSPIRE].

[62] S. Frixione, P. Nason and C. Oleari, *Matching NLO QCD computations with parton shower simulations: the POWHEG method*, *JHEP* **11** (2007) 070 [arXiv:0709.2092] [INSPIRE].

[63] S. Alioli, P. Nason, C. Oleari and E. Re, *A general framework for implementing NLO calculations in shower Monte Carlo programs: the POWHEG BOX*, *JHEP* **06** (2010) 043 [arXiv:1002.2581] [INSPIRE].

[64] H.B. Hartanto, B. Jager, L. Reina and D. Wackeroth, *Higgs boson production in association with top quarks in the POWHEG BOX*, *Phys. Rev. D* **91** (2015) 094003 [arXiv:1501.04498] [INSPIRE].

[65] S. Frixione, G. Ridolfi and P. Nason, *A positive-weight next-to-leading-order Monte Carlo for heavy flavour hadroproduction*, *JHEP* **09** (2007) 126 [arXiv:0707.3088] [INSPIRE].

[66] NNPDF collaboration, *Parton distributions for the LHC run II*, *JHEP* **04** (2015) 040 [arXiv:1410.8849] [INSPIRE].

[67] M. Cacciari, G.P. Salam and G. Soyez, *The anti-k_t jet clustering algorithm*, *JHEP* **04** (2008) 063 [arXiv:0802.1189] [INSPIRE].

[68] M. Cacciari, G.P. Salam and G. Soyez, *FastJet user manual*, *Eur. Phys. J. C* **72** (2012) 1896 [arXiv:1111.6097] [INSPIRE].

[69] T. Ježo, J.M. Lindert, N. Moretti and S. Pozzorini, *New NLOPS predictions for $t\bar{t}$ + b-jet production at the LHC*, *Eur. Phys. J. C* **78** (2018) 502 [arXiv:1802.00426] [INSPIRE].

JHEP06(2022)097

[70] F. Cascioli, P. Maierhöfer and S. Pozzorini, *Scattering Amplitudes with Open Loops*, *Phys. Rev. Lett.* **108** (2012) 111601 [arXiv:1111.5206] [INSPIRE].

[71] A. Denner, S. Dittmaier and L. Hofer, *COLLIER: A fortran-based complex one-loop library in extended regularizations*, *Comput. Phys. Commun.* **212** (2017) 220 [arXiv:1604.06792] [INSPIRE].

[72] T. Ježo, *Powheg-box-res ttbb source code*, https://gitlab.cern.ch/tjezo/powheg-box-res_ttbb/ (2019).

[73] SHERPA collaboration, *Event generation with Sherpa 2.2*, *SciPost Phys.* **7** (2019) 034 [arXiv:1905.09127] [INSPIRE].

[74] T. Gleisberg and S. Hoeche, *Comix, a new matrix element generator*, *JHEP* **12** (2008) 039 [arXiv:0808.3674] [INSPIRE].

[75] S. Schumann and F. Krauss, *A parton shower algorithm based on Catani-Seymour dipole factorisation*, *JHEP* **03** (2008) 038 [arXiv:0709.1027] [INSPIRE].

[76] S. Höche, F. Krauss, M. Schonherr and F. Siegert, *A critical appraisal of NLO+PS matching methods*, *JHEP* **09** (2012) 049 [arXiv:1111.1220] [INSPIRE].

[77] S. Höche, F. Krauss, M. Schonherr and F. Siegert, *QCD matrix elements + parton showers. The NLO case*, *JHEP* **04** (2013) 027 [arXiv:1207.5030] [INSPIRE].

[78] S. Catani, F. Krauss, B.R. Webber and R. Kuhn, *QCD Matrix Elements + Parton Showers*, *JHEP* **11** (2001) 063 [hep-ph/0109231] [INSPIRE].

[79] S. Höche, F. Krauss, S. Schumann and F. Siegert, *QCD matrix elements and truncated showers*, *JHEP* **05** (2009) 053 [arXiv:0903.1219] [INSPIRE].

[80] ATLAS collaboration, *Measurements of the production cross-section for a Z boson in association with b-jets in proton-proton collisions at* $\sqrt{s} = 13$ *TeV with the ATLAS detector*, *JHEP* **07** (2020) 044 [arXiv:2003.11960] [INSPIRE].

[81] A. Denner, S. Dittmaier, M. Roth and L.H. Wieders, *Electroweak corrections to charged-current* $e^+e^- \to 4$ *fermion processes: Technical details and further results*, *Nucl. Phys. B* **724** (2005) 247 [*Erratum ibid.* **854** (2012) 504] [hep-ph/0505042] [INSPIRE].

[82] S. Dittmaier and M. Huber, *Radiative corrections to the neutral-current Drell-Yan process in the Standard Model and its minimal supersymmetric extension*, *JHEP* **01** (2010) 060 [arXiv:0911.2329] [INSPIRE].

[83] J.R. Andersen et al., *Les Houches 2013: Physics at TeV Colliders: Standard Model Working Group Report*, arXiv:1405.1067 [INSPIRE].

[84] F. Demartin, B. Maier, F. Maltoni, K. Mawatari and M. Zaro, *tWH associated production at the LHC*, *Eur. Phys. J. C* **77** (2017) 34 [arXiv:1607.05862] [INSPIRE].

[85] R. Frederix, E. Re and P. Torrielli, *Single-top t-channel hadroproduction in the four-flavour scheme with POWHEG and aMC@NLO*, *JHEP* **09** (2012) 130 [arXiv:1207.5391] [INSPIRE].

[86] S. Alioli, P. Nason, C. Oleari and E. Re, *NLO single-top production matched with shower in POWHEG: s- and t-channel contributions*, *JHEP* **09** (2009) 111 [*Erratum ibid.* **02** (2010) 011] [arXiv:0907.4076] [INSPIRE].

[87] E. Re, *Single-top Wt-channel production matched with parton showers using the POWHEG method*, *Eur. Phys. J. C* **71** (2011) 1547 [arXiv:1009.2450] [INSPIRE].

JHEP06(2022)097

[88] J. Pumplin, D.R. Stump, J. Huston, H.L. Lai, P.M. Nadolsky and W.K. Tung, *New Generation of Parton Distributions with Uncertainties from Global QCD Analysis*, *JHEP* **07** (2002) 012 [hep-ph/0201195] [INSPIRE].

[89] ATLAS collaboration, *ATLAS data quality operations and performance for 2015–2018 data-taking*, 2020 *JINST* **15** P04003 [arXiv:1911.04632] [INSPIRE].

[90] ATLAS collaboration, *Reconstruction of primary vertices at the ATLAS experiment in Run 1 proton-proton collisions at the LHC*, *Eur. Phys. J. C* **77** (2017) 332 [arXiv:1611.10235] [INSPIRE].

[91] ATLAS collaboration, *Performance of the ATLAS muon triggers in Run 2*, 2020 *JINST* **15** P09015 [arXiv:2004.13447] [INSPIRE].

[92] ATLAS collaboration, *Performance of electron and photon triggers in ATLAS during LHC Run 2*, *Eur. Phys. J. C* **80** (2020) 47 [arXiv:1909.00761] [INSPIRE].

[93] ATLAS collaboration, *Electron and photon performance measurements with the ATLAS detector using the 2015–2017 LHC proton-proton collision data*, 2019 *JINST* **14** P12006 [arXiv:1908.00005] [INSPIRE].

[94] ATLAS collaboration, *Muon reconstruction and identification efficiency in ATLAS using the full Run 2 pp collision data set at* $\sqrt{s} = 13$ *TeV*, *Eur. Phys. J. C* **81** (2021) 578 [arXiv:2012.00578] [INSPIRE].

[95] ATLAS collaboration, *Topological cell clustering in the ATLAS calorimeters and its performance in LHC Run 1*, *Eur. Phys. J. C* **77** (2017) 490 [arXiv:1603.02934] [INSPIRE].

[96] ATLAS collaboration, *Jet energy scale and resolution measured in proton-proton collisions at* $\sqrt{s} = 13$ *TeV with the ATLAS detector*, *Eur. Phys. J. C* **81** (2021) 689 [arXiv:2007.02645] [INSPIRE].

[97] ATLAS collaboration, *Performance of pile-up mitigation techniques for jets in pp collisions at* $\sqrt{s} = 8$ *TeV using the ATLAS detector*, *Eur. Phys. J. C* **76** (2016) 581 [arXiv:1510.03823] [INSPIRE].

[98] ATLAS collaboration, *ATLAS b-jet identification performance and efficiency measurement with* $t\bar{t}$ *events in pp collisions at* $\sqrt{s} = 13$ *TeV*, *Eur. Phys. J. C* **79** (2019) 970 [arXiv:1907.05120] [INSPIRE].

[99] ATLAS collaboration, *Measurement of b-tagging efficiency of c-jets in* $t\bar{t}$ *events using a likelihood approach with the ATLAS detector*, ATLAS-CONF-2018-001 (2018).

[100] ATLAS collaboration, *Calibration of light-flavour b-jet mistagging rates using ATLAS proton-proton collision data at* $\sqrt{s} = 13$ *TeV*, ATLAS-CONF-2018-006 (2018).

[101] ATLAS collaboration, *Measurement of the tau lepton reconstruction and identification performance in the ATLAS experiment using pp collisions at* $\sqrt{s} = 13$ *TeV*, ATLAS-CONF-2017-029 (2017).

[102] ATLAS collaboration, *Performance of missing transverse momentum reconstruction with the ATLAS detector using proton-proton collisions at* $\sqrt{s} = 13$ *TeV*, *Eur. Phys. J. C* **78** (2018) 903 [arXiv:1802.08168] [INSPIRE].

[103] B. Nachman, P. Nef, A. Schwartzman, M. Swiatlowski and C. Wanotayaroj, *Jets from jets: re-clustering as a tool for large radius jet reconstruction and grooming at the LHC*, *JHEP* **02** (2015) 075 [arXiv:1407.2922] [INSPIRE].

JHEP06(2022)097

[104] ATLAS collaboration, *Evidence for the associated production of the Higgs boson and a top quark pair with the ATLAS detector*, *Phys. Rev. D* **97** (2018) 072003 [arXiv:1712.08891] [INSPIRE].

[105] ATLAS collaboration, *Muon reconstruction performance of the ATLAS detector in proton-proton collision data at* $\sqrt{s} = 13$ *TeV*, *Eur. Phys. J. C* **76** (2016) 292 [arXiv:1603.05598] [INSPIRE].

[106] A. Hoecker et al., *TMVA — Toolkit for Multivariate Data Analysis*, physics/0703039 [INSPIRE].

[107] F. Chollet et al., *Keras*, https://keras.io (2015).

[108] M. Abadi et al., *TensorFlow: Large-scale machine learning on heterogeneous systems*, https://www.tensorflow.org/ (2015).

[109] ATLAS collaboration, *Performance of jet substructure techniques for large-R jets in proton-proton collisions at* $\sqrt{s} = 7$ *TeV using the ATLAS detector*, *JHEP* **09** (2013) 076 [arXiv:1306.4945] [INSPIRE].

[110] ATLAS collaboration, *Luminosity determination in pp collisions at* $\sqrt{s} = 13$ *TeV using the ATLAS detector at the LHC*, ATLAS-CONF-2019-021 (2019).

[111] G. Avoni et al., *The new LUCID-2 detector for luminosity measurement and monitoring in ATLAS*, 2018 *JINST* **13** P07017 [INSPIRE].

[112] ATLAS collaboration, *Measurement of the Inelastic Proton-Proton Cross Section at* $\sqrt{s} = 13$ *TeV with the ATLAS Detector at the LHC*, *Phys. Rev. Lett.* **117** (2016) 182002 [arXiv:1606.02625] [INSPIRE].

[113] R. Raitio and W.W. Wada, *Higgs-boson production at large transverse momentum in quantum chromodynamics*, *Phys. Rev. D* **19** (1979) 941 [INSPIRE].

[114] W. Beenakker, S. Dittmaier, M. Krämer, B. Plumper, M. Spira and P.M. Zerwas, *NLO QCD corrections to* $t\bar{t}H$ *production in hadron collisions*, *Nucl. Phys. B* **653** (2003) 151 [hep-ph/0211352] [INSPIRE].

[115] S. Dawson, C. Jackson, L.H. Orr, L. Reina and D. Wackeroth, *Associated Higgs boson production with top quarks at the CERN Large Hadron Collider: NLO QCD corrections*, *Phys. Rev. D* **68** (2003) 034022 [hep-ph/0305087] [INSPIRE].

[116] Y. Zhang, W.-G. Ma, R.-Y. Zhang, C. Chen and L. Guo, *QCD NLO and EW NLO corrections to* $t\bar{t}H$ *production with top quark decays at hadron collider*, *Phys. Lett. B* **738** (2014) 1 [arXiv:1407.1110] [INSPIRE].

[117] S. Frixione, V. Hirschi, D. Pagani, H.S. Shao and M. Zaro, *Electroweak and QCD corrections to top-pair hadroproduction in association with heavy bosons*, *JHEP* **06** (2015) 184 [arXiv:1504.03446] [INSPIRE].

[118] ATLAS collaboration, *Study of top-quark pair modelling and uncertainties using ATLAS measurements at* $\sqrt{s} = 13$ *TeV*, ATL-PHYS-PUB-2020-023 (2020).

[119] I.W. Stewart and F.J. Tackmann, *Theory uncertainties for Higgs mass and other searches using jet bins*, *Phys. Rev. D* **85** (2012) 034011 [arXiv:1107.2117] [INSPIRE].

[120] A.D. Martin, W.J. Stirling, R.S. Thorne and G. Watt, *Parton distributions for the LHC*, *Eur. Phys. J. C* **63** (2009) 189 [arXiv:0901.0002] [INSPIRE].

JHEP06(2022)097

[121] A.D. Martin, W.J. Stirling, R.S. Thorne and G. Watt, *Uncertainties on α_S in global PDF analyses and implications for predicted hadronic cross sections*, *Eur. Phys. J. C* **64** (2009) 653 [arXiv:0905.3531] [INSPIRE].

[122] J.M. Campbell and R.K. Ellis, *$t\bar{t}W^{\pm}$ production and decay at NLO*, *JHEP* **07** (2012) 052 [arXiv:1204.5678] [INSPIRE].

[123] *Multi-boson simulation for 13 TeV ATLAS analyses*, ATL-PHYS-PUB-2016-002 (2016).

[124] J. Alwall et al., *The automated computation of tree-level and next-to-leading order differential cross sections, and their matching to parton shower simulations*, *JHEP* **07** (2014) 079 [arXiv:1405.0301] [INSPIRE].

[125] G. Cowan, K. Cranmer, E. Gross and O. Vitells, *Asymptotic formulae for likelihood-based tests of new physics*, *Eur. Phys. J. C* **71** (2011) 1554 [*Erratum ibid.* **73** (2013) 2501] [arXiv:1007.1727] [INSPIRE].

[126] W. Verkerke and D.P. Kirkby, *The RooFit toolkit for data modeling*, *eConf* **C 0303241** (2003) MOLT007 [physics/0306116] [INSPIRE].

[127] L. Moneta et al., *The RooStats project*, *PoS* **ACAT2010** (2010) 057 [arXiv:1009.1003] [INSPIRE].

[128] R.D. Cousins, *Generalization of chisquare goodness-of-fit test for binned data using saturated models, with application to histograms*, http://www.physics.ucla.edu/~cousins/stats/cousins_saturated.pdf (2013).

[129] F. Buccioni, S. Kallweit, S. Pozzorini and M.F. Zoller, *NLO QCD predictions for $t\bar{t}b\bar{b}$ production in association with a light jet at the LHC*, *JHEP* **12** (2019) 015 [arXiv:1907.13624] [INSPIRE].

[130] ATLAS collaboration, *ATLAS Computing Acknowledgements*, ATL-SOFT-PUB-2021-003 (2021).

JHEP06(2022)097

The ATLAS collaboration

G. Aad[98], B. Abbott[124], D.C. Abbott[99], A. Abed Abud[34], K. Abeling[51], D.K. Abhayasinghe[91], S.H. Abidi[27], A. Aboulhorma[33e], H. Abramowicz[157], H. Abreu[156], Y. Abulaiti[5], A.C. Abusleme Hoffman[142a], B.S. Acharya[64a,64b,o], B. Achkar[51], L. Adam[96], C. Adam Bourdarios[4], L. Adamczyk[81a], L. Adamek[162], S.V. Addepalli[24], J. Adelman[116], A. Adiguzel[11c,ac], S. Adorni[52], T. Adye[139], A.A. Affolder[141], Y. Afik[34], C. Agapopoulou[62], M.N. Agaras[12], J. Agarwala[68a,68b], A. Aggarwal[114], C. Agheorghiesei[25c], J.A. Aguilar-Saavedra[135f,135a,ab], A. Ahmad[34], F. Ahmadov[77,z], W.S. Ahmed[100], X. Ai[44], G. Aielli[71a,71b], I. Aizenberg[175], S. Akatsuka[83], M. Akbiyik[96], T.P.A. Åkesson[94], A.V. Akimov[107], K. Al Khoury[37], G.L. Alberghi[21b], J. Albert[171], P. Albicocco[49], M.J. Alconada Verzini[86], S. Alderweireldt[48], M. Aleksa[34], I.N. Aleksandrov[77], C. Alexa[25b], T. Alexopoulos[9], A. Alfonsi[115], F. Alfonsi[21b], M. Alhroob[124], B. Ali[137], S. Ali[154], M. Aliev[161], G. Alimonti[66a], C. Allaire[34], B.M.M. Allbrooke[152], P.P. Allport[19], A. Aloisio[67a,67b], F. Alonso[86], C. Alpigiani[144], E. Alunno Camelia[71a,71b], M. Alvarez Estevez[95], M.G. Alviggi[67a,67b], Y. Amaral Coutinho[78b], A. Ambler[100], L. Ambroz[130], C. Amelung[34], D. Amidei[102], S.P. Amor Dos Santos[135a], S. Amoroso[44], K.R. Amos[169], C.S. Amrouche[52], V. Ananiev[129], C. Anastopoulos[145], N. Andari[140], T. Andeen[10], J.K. Anders[18], S.Y. Andrean[43a,43b], A. Andreazza[66a,66b], S. Angelidakis[8], A. Angerami[37], A.V. Anisenkov[117b,117a], A. Annovi[69a], C. Antel[52], M.T. Anthony[145], E. Antipov[125], M. Antonelli[49], D.J.A. Antrim[16], F. Anulli[70a], M. Aoki[79], J.A. Aparisi Pozo[169], M.A. Aparo[152], L. Aperio Bella[44], N. Aranzabal[34], V. Araujo Ferraz[78a], C. Arcangeletti[49], A.T.H. Arce[47], E. Arena[88], J-F. Arguin[106], S. Argyropoulos[50], J.-H. Arling[44], A.J. Armbruster[34], A. Armstrong[166], O. Arnaez[162], H. Arnold[34], Z.P. Arrubarrena Tame[110], G. Artoni[130], H. Asada[112], K. Asai[122], S. Asai[159], N.A. Asbah[57], E.M. Asimakopoulou[167], L. Asquith[152], J. Assahsah[33d], K. Assamagan[27], R. Astalos[26a], R.J. Atkin[31a], M. Atkinson[168], N.B. Atlay[17], H. Atmani[58b], P.A. Atmasiddha[102], K. Augsten[137], S. Auricchio[67a,67b], V.A. Austrup[177], G. Avner[156], G. Avolio[34], M.K. Ayoub[13c], G. Azuelos[106,aj], D. Babal[26a], H. Bachacou[140], K. Bachas[158], A. Bachiu[32], F. Backman[43a,43b], A. Badea[57], P. Bagnaia[70a,70b], H. Bahrasemani[148], A.J. Bailey[169], V.R. Bailey[168], J.T. Baines[139], C. Bakalis[9], O.K. Baker[178], P.J. Bakker[115], E. Bakos[14], D. Bakshi Gupta[7], S. Balaji[153], R. Balasubramanian[115], E.M. Baldin[117b,117a], P. Balek[138], E. Ballabene[66a,66b], F. Balli[140], L.M. Baltes[59a], W.K. Balunas[130], J. Balz[96], E. Banas[82], M. Bandieramonte[134], A. Bandyopadhyay[22], S. Bansal[22], L. Barak[157], E.L. Barberio[101], D. Barberis[53b,53a], M. Barbero[98], G. Barbour[92], K.N. Barends[31a], T. Barillari[111], M-S. Barisits[34], J. Barkeloo[127], T. Barklow[149], B.M. Barnett[139], R.M. Barnett[16], A. Baroncelli[58a], G. Barone[27], A.J. Barr[130], L. Barranco Navarro[43a,43b], F. Barreiro[95], J. Barreiro Guimarães da Costa[13a], U. Barron[157], S. Barsov[133], F. Bartels[59a], R. Bartoldus[149], G. Bartolini[98], A.E. Barton[87], P. Bartos[26a], A. Basalaev[44], A. Basan[96], M. Baselga[44], I. Bashta[72a,72b], A. Bassalat[62,ag], M.J. Basso[162], C.R. Basson[97], R.L. Bates[55], S. Batlamous[33e], J.R. Batley[30], B. Batool[147], M. Battaglia[141], M. Bauce[70a,70b], F. Bauer[140,*], P. Bauer[22], H.S. Bawa[29], A. Bayirli[11c], J.B. Beacham[47], T. Beau[131], P.H. Beauchemin[165], F. Becherer[50], P. Bechtle[22], H.P. Beck[18,q], K. Becker[173], C. Becot[44], A.J. Beddall[11a], V.A. Bednyakov[77], C.P. Bee[151], T.A. Beermann[34], M. Begalli[78b], M. Begel[27], A. Behera[151], J.K. Behr[44], C. Beirao Da Cruz E Silva[34], J.F. Beirer[51,34], F. Beisiegel[22], M. Belfkir[4], G. Bella[157], L. Bellagamba[21b], A. Bellerive[32], P. Bellos[19], K. Beloborodov[117b,117a], K. Belotskiy[108], N.L. Belyaev[108], D. Benchekroun[33a], Y. Benhammou[157], D.P. Benjamin[27], M. Benoit[27], J.R. Bensinger[24], S. Bentvelsen[115], L. Beresford[34], M. Beretta[49], D. Berge[17], E. Bergeaas Kuutmann[167], N. Berger[4], B. Bergmann[137], L.J. Bergsten[24], J. Beringer[16], S. Berlendis[6], G. Bernardi[131], C. Bernius[149], F.U. Bernlochner[22], T. Berry[91], P. Berta[138], A. Berthold[46], I.A. Bertram[87], O. Bessidskaia Bylund[177], S. Bethke[111], A. Betti[40], A.J. Bevan[90],

JHEP06(2022)097

S. Bhatta[151], D.S. Bhattacharya[172], P. Bhattarai[24], V.S. Bhopatkar[5], R. Bi[134], R. Bi[27], R.M. Bianchi[134], O. Biebel[110], R. Bielski[127], N.V. Biesuz[69a,69b], M. Biglietti[72a], T.R.V. Billoud[137], M. Bindi[51], A. Bingul[11d], C. Bini[70a,70b], S. Biondi[21b,21a], A. Biondini[88], C.J. Birch-sykes[97], G.A. Bird[19,139], M. Birman[175], T. Bisanz[34], J.P. Biswal[2], D. Biswas[176,j], A. Bitadze[97], C. Bittrich[46], K. Bjørke[129], I. Bloch[44], C. Blocker[24], A. Blue[55], U. Blumenschein[90], J. Blumenthal[96], G.J. Bobbink[115], V.S. Bobrovnikov[117b,117a], M. Boehler[50], D. Bogavac[12], A.G. Bogdanchikov[117b,117a], C. Bohm[43a], V. Boisvert[91], P. Bokan[44], T. Bold[81a], M. Bomben[131], M. Bona[90], M. Boonekamp[140], C.D. Booth[91], A.G. Borbély[55], H.M. Borecka-Bielska[106], L.S. Borgna[92], G. Borissov[87], D. Bortoletto[130], D. Boscherini[21b], M. Bosman[12], J.D. Bossio Sola[34], K. Bouaouda[33a], J. Boudreau[134], E.V. Bouhova-Thacker[87], D. Boumediene[36], R. Bouquet[131], S.K. Boutle[55], A. Boveia[123], J. Boyd[34], D. Boye[27], I.R. Boyko[77], A.J. Bozson[91], J. Bracinik[19], N. Brahimi[58d,58c], G. Brandt[177], O. Brandt[30], F. Braren[44], B. Brau[99], J.E. Brau[127], W.D. Breaden Madden[55], K. Brendlinger[44], R. Brener[175], L. Brenner[34], R. Brenner[167], S. Bressler[175], B. Brickwedde[96], D.L. Briglin[19], D. Britton[55], D. Britzger[111], I. Brock[22], R. Brock[103], G. Brooijmans[37], W.K. Brooks[142e], E. Brost[27], P.A. Bruckman de Renstrom[82], B. Brüers[44], D. Bruncko[26b], A. Bruni[21b], G. Bruni[21b], M. Bruschi[21b], N. Bruscino[70a,70b], L. Bryngemark[149], T. Buanes[15], Q. Buat[151], P. Buchholz[147], A.G. Buckley[55], I.A. Budagov[77], M.K. Bugge[129], O. Bulekov[108], B.A. Bullard[57], S. Burdin[88], C.D. Burgard[44], A.M. Burger[125], B. Burghgrave[7], J.T.P. Burr[30], C.D. Burton[10], J.C. Burzynski[148], E.L. Busch[37], V. Büscher[96], P.J. Bussey[55], J.M. Butler[23], C.M. Buttar[55], J.M. Butterworth[92], W. Buttinger[139], C.J. Buxo Vazquez[103], A.R. Buzykaev[117b,117a], G. Cabras[21b], S. Cabrera Urbán[169], D. Caforio[54], H. Cai[134], V.M.M. Cairo[149], O. Cakir[3a], N. Calace[34], P. Calafiura[16], G. Calderini[131], P. Calfayan[63], G. Callea[55], L.P. Caloba[78b], D. Calvet[36], S. Calvet[36], T.P. Calvet[98], M. Calvetti[69a,69b], R. Camacho Toro[131], S. Camarda[34], D. Camarero Munoz[95], P. Camarri[71a,71b], M.T. Camerlingo[72a,72b], D. Cameron[129], C. Camincher[171], M. Campanelli[92], A. Camplani[38], V. Canale[67a,67b], A. Canesse[100], M. Cano Bret[75], J. Cantero[125], Y. Cao[168], F. Capocasa[24], M. Capua[39b,39a], A. Carbone[66a,66b], R. Cardarelli[71a], J.C.J. Cardenas[7], F. Cardillo[169], G. Carducci[39b,39a], T. Carli[34], G. Carlino[67a], B.T. Carlson[134], E.M. Carlson[171,163a], L. Carminati[66a,66b], M. Carnesale[70a,70b], R.M.D. Carney[149], S. Caron[114], E. Carquin[142e], S. Carrá[44], G. Carratta[21b,21a], J.W.S. Carter[162], T.M. Carter[48], D. Casadei[31c], M.P. Casado[12,g], A.F. Casha[162], E.G. Castiglia[178], F.L. Castillo[59a], L. Castillo Garcia[12], V. Castillo Gimenez[169], N.F. Castro[135a,135e], A. Catinaccio[34], J.R. Catmore[129], A. Cattai[34], V. Cavaliere[27], N. Cavalli[21b,21a], V. Cavasinni[69a,69b], E. Celebi[11b], F. Celli[130], M.S. Centonze[65a,65b], K. Cerny[126], A.S. Cerqueira[78a], A. Cerri[152], L. Cerrito[71a,71b], F. Cerutti[16], A. Cervelli[21b], S.A. Cetin[11b], Z. Chadi[33a], D. Chakraborty[116], M. Chala[135f], J. Chan[176], W.S. Chan[115], W.Y. Chan[88], J.D. Chapman[30], B. Chargeishvili[155b], D.G. Charlton[19], T.P. Charman[90], M. Chatterjee[18], S. Chekanov[5], S.V. Chekulaev[163a], G.A. Chelkov[77,ae], A. Chen[102], B. Chen[157], B. Chen[171], C. Chen[58a], C.H. Chen[76], H. Chen[13c], H. Chen[27], J. Chen[58c], J. Chen[24], S. Chen[132], S.J. Chen[13c], X. Chen[58c], X. Chen[13b], Y. Chen[58a], Y-H. Chen[44], C.L. Cheng[176], H.C. Cheng[60a], A. Cheplakov[77], E. Cheremushkina[44], E. Cherepanova[77], R. Cherkaoui El Moursli[33e], E. Cheu[6], K. Cheung[61], L. Chevalier[140], V. Chiarella[49], G. Chiarelli[69a], G. Chiodini[65a], A.S. Chisholm[19], A. Chitan[25b], Y.H. Chiu[171], M.V. Chizhov[77,s], K. Choi[10], A.R. Chomont[70a,70b], Y. Chou[99], Y.S. Chow[115], T. Chowdhury[31f], L.D. Christopher[31f], M.C. Chu[60a], X. Chu[13a,13d], J. Chudoba[136], J.J. Chwastowski[82], D. Cieri[111], K.M. Ciesla[82], V. Cindro[89], I.A. Cioară[25b], A. Ciocio[16], F. Cirotto[67a,67b], Z.H. Citron[175,k], M. Citterio[66a], D.A. Ciubotaru[25b], B.M. Ciungu[162], A. Clark[52], P.J. Clark[48], J.M. Clavijo Columbie[44], S.E. Clawson[97], C. Clement[43a,43b], L. Clissa[21b,21a], Y. Coadou[98], M. Cobal[64a,64c], A. Coccaro[53b], J. Cochran[76], R.F. Coelho Barrue[135a], R. Coelho Lopes De Sa[99], S. Coelli[66a], H. Cohen[157], A.E.C. Coimbra[34], B. Cole[37], J. Collot[56],

JHEP06(2022)097

P. Conde Muiño[135a,135g], S.H. Connell[31c], I.A. Connelly[55], E.I. Conroy[130], F. Conventi[67a,ak], H.G. Cooke[19], A.M. Cooper-Sarkar[130], F. Cormier[170], L.D. Corpe[34], M. Corradi[70a,70b], E.E. Corrigan[94], F. Corriveau[100,y], M.J. Costa[169], F. Costanza[4], D. Costanzo[145], B.M. Cote[123], G. Cowan[91], J.W. Cowley[30], K. Cranmer[121], S. Crépé-Renaudin[56], F. Crescioli[131], M. Cristinziani[147], M. Cristoforetti[73a,73b,b], V. Croft[165], G. Crosetti[39b,39a], A. Cueto[34], T. Cuhadar Donszelmann[166], H. Cui[13a,13d], A.R. Cukierman[149], W.R. Cunningham[55], F. Curcio[39b,39a], P. Czodrowski[34], M.M. Czurylo[59b], M.J. Da Cunha Sargedas De Sousa[58a], J.V. Da Fonseca Pinto[78b], C. Da Via[97], W. Dabrowski[81a], T. Dado[45], S. Dahbi[31f], T. Dai[102], C. Dallapiccola[99], M. Dam[38], G. D'amen[27], V. D'Amico[72a,72b], J. Damp[96], J.R. Dandoy[132], M.F. Daneri[28], M. Danninger[148], V. Dao[34], G. Darbo[53b], S. Darmora[5], A. Dattagupta[127], S. D'Auria[66a,66b], C. David[163b], T. Davidek[138], D.R. Davis[47], B. Davis-Purcell[32], I. Dawson[90], K. De[7], R. De Asmundis[67a], M. De Beurs[115], S. De Castro[21b,21a], N. De Groot[114], P. de Jong[115], H. De la Torre[103], A. De Maria[13c], D. De Pedis[70a], A. De Salvo[70a], U. De Sanctis[71a,71b], M. De Santis[71a,71b], A. De Santo[152], J.B. De Vivie De Regie[56], D.V. Dedovich[77], J. Degens[115], A.M. Deiana[40], J. Del Peso[95], Y. Delabat Diaz[44], F. Deliot[140], C.M. Delitzsch[6], M. Della Pietra[67a,67b], D. Della Volpe[52], A. Dell'Acqua[34], L. Dell'Asta[66a,66b], M. Delmastro[4], P.A. Delsart[56], S. Demers[178], M. Demichev[77], S.P. Denisov[118], L. D'Eramo[116], D. Derendarz[82], J.E. Derkaoui[33d], F. Derue[131], P. Dervan[88], K. Desch[22], K. Dette[162], C. Deutsch[22], P.O. Deviveiros[34], F.A. Di Bello[70a,70b], A. Di Ciaccio[71a,71b], L. Di Ciaccio[4], A. Di Domenico[70a,70b], C. Di Donato[67a,67b], A. Di Girolamo[34], G. Di Gregorio[69a,69b], A. Di Luca[73a,73b,b], B. Di Micco[72a,72b], R. Di Nardo[72a,72b], C. Diaconu[98], F.A. Dias[115], T. Dias Do Vale[135a], M.A. Diaz[142a], F.G. Diaz Capriles[22], J. Dickinson[16], M. Didenko[169], E.B. Diehl[102], J. Dietrich[17], S. Díez Cornell[44], C. Diez Pardos[147], A. Dimitrievska[16], W. Ding[13b], J. Dingfelder[22], I-M. Dinu[25b], S.J. Dittmeier[59b], F. Dittus[34], F. Djama[98], T. Djobava[155b], J.I. Djuvsland[15], M.A.B. Do Vale[143], D. Dodsworth[24], C. Doglioni[94], J. Dolejsi[138], Z. Dolezal[138], M. Donadelli[78c], B. Dong[58c], J. Donini[36], A. D'onofrio[13c], M. D'Onofrio[88], J. Dopke[139], A. Doria[67a], M.T. Dova[86], A.T. Doyle[55], E. Drechsler[148], E. Dreyer[148], T. Dreyer[51], A.S. Drobac[165], D. Du[58a], T.A. du Pree[115], F. Dubinin[107], M. Dubovsky[26a], A. Dubreuil[52], E. Duchovni[175], G. Duckeck[110], O.A. Ducu[34,25b], D. Duda[111], A. Dudarev[34], M. D'uffizi[97], L. Duflot[62], M. Dührssen[34], C. Dülsen[177], A.E. Dumitriu[25b], M. Dunford[59a], S. Dungs[45], K. Dunne[43a,43b], A. Duperrin[98], H. Duran Yildiz[3a], M. Düren[54], A. Durglishvili[155b], B. Dutta[44], B.L. Dwyer[116], G.I. Dyckes[16], M. Dyndal[81a], S. Dysch[97], B.S. Dziedzic[82], B. Eckerova[26a], M.G. Eggleston[47], E. Egidio Purcino De Souza[78b], L.F. Ehrke[52], T. Eifert[7], G. Eigen[15], K. Einsweiler[16], T. Ekelof[167], Y. El Ghazali[33b], H. El Jarrari[33e], A. El Moussaouy[33a], V. Ellajosyula[167], M. Ellert[167], F. Ellinghaus[177], A.A. Elliot[90], N. Ellis[34], J. Elmsheuser[27], M. Elsing[34], D. Emeliyanov[139], A. Emerman[37], Y. Enari[159], J. Erdmann[45], A. Ereditato[18], P.A. Erland[82], M. Errenst[177], M. Escalier[62], C. Escobar[169], O. Estrada Pastor[169], E. Etzion[157], G. Evans[135a], H. Evans[63], M.O. Evans[152], A. Ezhilov[133], F. Fabbri[55], L. Fabbri[21b,21a], G. Facini[173], V. Fadeyev[141], R.M. Fakhrutdinov[118], S. Falciano[70a], P.J. Falke[22], S. Falke[34], J. Faltova[138], Y. Fan[13a], Y. Fang[13a], G. Fanourakis[42], M. Fanti[66a,66b], M. Faraj[58c], A. Farbin[7], A. Farilla[72a], E.M. Farina[68a,68b], T. Farooque[103], S.M. Farrington[48], P. Farthouat[34], F. Fassi[33e], D. Fassouliotis[8], M. Faucci Giannelli[71a,71b], W.J. Fawcett[30], L. Fayard[62], O.L. Fedin[133,p], G. Fedotov[133], M. Feickert[168], L. Feligioni[98], A. Fell[145], C. Feng[58b], M. Feng[13b], M.J. Fenton[166], A.B. Fenyuk[118], L. Ferencz[44], S.W. Ferguson[41], J. Ferrando[44], A. Ferrari[167], P. Ferrari[115], R. Ferrari[68a], D. Ferrere[52], C. Ferretti[102], F. Fiedler[96], A. Filipčič[89], F. Filthaut[114], M.C.N. Fiolhais[135a,135c,a], L. Fiorini[169], F. Fischer[147], W.C. Fisher[103], T. Fitschen[19], I. Fleck[147], P. Fleischmann[102], T. Flick[177], B.M. Flierl[110], L. Flores[132], M. Flores[31d], L.R. Flores Castillo[60a], F.M. Follega[73a,73b], N. Fomin[15], J.H. Foo[162], B.C. Forland[63], A. Formica[140], F.A. Förster[12], A.C. Forti[97], E. Fortin[98], M.G. Foti[130],

JHEP06(2022)097

L. Fountas[8], D. Fournier[62], H. Fox[87], P. Francavilla[69a,69b], S. Francescato[57], M. Franchini[21b,21a], S. Franchino[59a], D. Francis[34], L. Franco[4], L. Franconi[18], M. Franklin[57], G. Frattari[70a,70b], A.C. Freegard[90], P.M. Freeman[19], W.S. Freund[78b], E.M. Freundlich[45], D. Froidevaux[34], J.A. Frost[130], Y. Fu[58a], M. Fujimoto[122], E. Fullana Torregrosa[169], J. Fuster[169], A. Gabrielli[21b,21a], A. Gabrielli[34], P. Gadow[44], G. Gagliardi[53b,53a], L.G. Gagnon[16], G.E. Gallardo[130], E.J. Gallas[130], B.J. Gallop[139], R. Gamboa Goni[90], K.K. Gan[123], S. Ganguly[159], J. Gao[58a], Y. Gao[48], Y.S. Gao[29,m], F.M. Garay Walls[142a], C. García[169], J.E. García Navarro[169], J.A. García Pascual[13a], M. Garcia-Sciveres[16], R.W. Gardner[35], D. Garg[75], R.B. Garg[149], S. Gargiulo[50], C.A. Garner[162], V. Garonne[129], S.J. Gasiorowski[144], P. Gaspar[78b], G. Gaudio[68a], P. Gauzzi[70a,70b], I.L. Gavrilenko[107], A. Gavrilyuk[119], C. Gay[170], G. Gaycken[44], E.N. Gazis[9], A.A. Geanta[25b], C.M. Gee[141], C.N.P. Gee[139], J. Geisen[94], M. Geisen[96], C. Gemme[53b], M.H. Genest[56], S. Gentile[70a,70b], S. George[91], W.F. George[19], T. Geralis[42], L.O. Gerlach[51], P. Gessinger-Befurt[34], M. Ghasemi Bostanabad[171], A. Ghosh[166], A. Ghosh[75], B. Giacobbe[21b], S. Giagu[70a,70b], N. Giangiacomi[162], P. Giannetti[69a], A. Giannini[67a,67b], S.M. Gibson[91], M. Gignac[141], D.T. Gil[81b], B.J. Gilbert[37], D. Gillberg[32], G. Gilles[115], N.E.K. Gillwald[44], D.M. Gingrich[2,aj], M.P. Giordani[64a,64c], P.F. Giraud[140], G. Giugliarelli[64a,64c], D. Giugni[66a], F. Giuli[71a,71b], I. Gkialas[8,h], P. Gkountoumis[9], L.K. Gladilin[109], C. Glasman[95], P.C.F. Glaysher[44], G.R. Gledhill[127], M. Glisic[127], I. Gnesi[39b,d], M. Goblirsch-Kolb[24], D. Godin[106], S. Goldfarb[101], T. Golling[52], D. Golubkov[118], J.P. Gombas[103], A. Gomes[135a,135b], R. Goncalves Gama[51], R. Gonçalo[135a,135c], G. Gonella[127], L. Gonella[19], A. Gongadze[77], F. Gonnella[19], J.L. Gonski[37], S. González de la Hoz[169], S. Gonzalez Fernandez[12], R. Gonzalez Lopez[88], C. Gonzalez Renteria[16], R. Gonzalez Suarez[167], S. Gonzalez-Sevilla[52], G.R. Gonzalvo Rodriguez[169], R.Y. González Andana[142a], L. Goossens[34], N.A. Gorasia[19], P.A. Gorbounov[119], H.A. Gordon[27], B. Gorini[34], E. Gorini[65a,65b], A. Gorišek[89], A.T. Goshaw[47], M.I. Gostkin[77], C.A. Gottardo[114], M. Gouighri[33b], V. Goumarre[44], A.G. Goussiou[144], N. Govender[31c], C. Goy[4], I. Grabowska-Bold[81a], K. Graham[32], E. Gramstad[129], S. Grancagnolo[17], M. Grandi[152], V. Gratchev[133], P.M. Gravila[25f], F.G. Gravili[65a,65b], H.M. Gray[16], C. Grefe[22], I.M. Gregor[44], P. Grenier[149], K. Grevtsov[44], C. Grieco[12], N.A. Grieser[124], A.A. Grillo[141], K. Grimm[29,l], S. Grinstein[12,v], J.-F. Grivaz[62], S. Groh[96], E. Gross[175], J. Grosse-Knetter[51], C. Grud[102], A. Grummer[113], J.C. Grundy[130], L. Guan[102], W. Guan[176], C. Gubbels[170], J. Guenther[34], J.G.R. Guerrero Rojas[169], F. Guescini[111], D. Guest[17], R. Gugel[96], A. Guida[44], T. Guillemin[4], S. Guindon[34], F. Guo[13a], J. Guo[58c], L. Guo[62], Y. Guo[102], Z. Guo[98], R. Gupta[44], S. Gurbuz[22], G. Gustavino[124], M. Guth[52], P. Gutierrez[124], L.F. Gutierrez Zagazeta[132], C. Gutschow[92], C. Guyot[140], C. Gwenlan[130], C.B. Gwilliam[88], E.S. Haaland[129], A. Haas[121], M. Habedank[44], C. Haber[16], H.K. Hadavand[7], A. Hadef[96], S. Hadzic[111], M. Haleem[172], J. Haley[125], J.J. Hall[145], G. Halladjian[103], G.D. Hallewell[98], L. Halser[18], K. Hamano[171], H. Hamdaoui[33e], M. Hamer[22], G.N. Hamity[48], K. Han[58a], L. Han[13c], L. Han[58a], S. Han[16], Y.F. Han[162], K. Hanagaki[79,t], M. Hance[141], M.D. Hank[35], R. Hankache[97], E. Hansen[94], J.B. Hansen[38], J.D. Hansen[38], M.C. Hansen[22], P.H. Hansen[38], K. Hara[164], T. Harenberg[177], S. Harkusha[104], Y.T. Harris[130], P.F. Harrison[173], N.M. Hartman[149], N.M. Hartmann[110], Y. Hasegawa[146], A. Hasib[48], S. Hassani[140], S. Haug[18], R. Hauser[103], M. Havranek[137], C.M. Hawkes[19], R.J. Hawkings[34], S. Hayashida[112], D. Hayden[103], C. Hayes[102], R.L. Hayes[170], C.P. Hays[130], J.M. Hays[90], H.S. Hayward[88], S.J. Haywood[139], F. He[58a], Y. He[160], Y. He[131], M.P. Heath[48], V. Hedberg[94], A.L. Heggelund[129], N.D. Hehir[90], C. Heidegger[50], K.K. Heidegger[50], W.D. Heidorn[76], J. Heilman[32], S. Heim[44], T. Heim[16], B. Heinemann[44,ah], J.G. Heinlein[132], J.J. Heinrich[127], L. Heinrich[34], J. Hejbal[136], L. Helary[44], A. Held[121], C.M. Helling[141], S. Hellman[43a,43b], C. Helsens[34], R.C.W. Henderson[87], L. Henkelmann[30], A.M. Henriques Correia[34], H. Herde[149], Y. Hernández Jiménez[151], H. Herr[96], M.G. Herrmann[110], T. Herrmann[46], G. Herten[50],

JHEP06(2022)097

R. Hertenberger[110], L. Hervas[34], N.P. Hessey[163a], H. Hibi[80], S. Higashino[79], E. Higón-Rodriguez[169], K.H. Hiller[44], S.J. Hillier[19], M. Hils[46], I. Hinchliffe[16], F. Hinterkeuser[22], M. Hirose[128], S. Hirose[164], D. Hirschbuehl[177], B. Hiti[89], O. Hladik[136], J. Hobbs[151], R. Hobincu[25e], N. Hod[175], M.C. Hodgkinson[145], B.H. Hodkinson[30], A. Hoecker[34], J. Hofer[44], D. Hohn[50], T. Holm[22], T.R. Holmes[35], M. Holzbock[111], L.B.A.H. Hommels[30], B.P. Honan[97], J. Hong[58c], T.M. Hong[134], Y. Hong[51], J.C. Honig[50], A. Hönle[111], B.H. Hooberman[168], W.H. Hopkins[5], Y. Horii[112], L.A. Horyn[35], S. Hou[154], J. Howarth[55], J. Hoya[86], M. Hrabovsky[126], A. Hrynevich[105], T. Hryn'ova[4], P.J. Hsu[61], S.-C. Hsu[144], Q. Hu[37], S. Hu[58c], Y.F. Hu[13a,13d,al], D.P. Huang[92], X. Huang[13c], Y. Huang[58a], Y. Huang[13a], Z. Hubacek[137], F. Hubaut[98], M. Huebner[22], F. Huegging[22], T.B. Huffman[130], M. Huhtinen[34], S.K. Huiberts[15], R. Hulsken[56], N. Huseynov[77,z], J. Huston[103], J. Huth[57], R. Hyneman[149], S. Hyrych[26a], G. Iacobucci[52], G. Iakovidis[27], I. Ibragimov[147], L. Iconomidou-Fayard[62], P. Iengo[34], R. Iguchi[159], T. Iizawa[52], Y. Ikegami[79], A. Ilg[18], N. Ilic[162], H. Imam[33a], T. Ingebretsen Carlson[43a,43b], G. Introzzi[68a,68b], M. Iodice[72a], V. Ippolito[70a,70b], M. Ishino[159], W. Islam[176], C. Issever[17,44], S. Istin[11c,am], J.M. Iturbe Ponce[60a], R. Iuppa[73a,73b], A. Ivina[175], J.M. Izen[41], V. Izzo[67a], P. Jacka[136], P. Jackson[1], R.M. Jacobs[44], B.P. Jaeger[148], C.S. Jagfeld[110], G. Jäkel[177], K. Jakobs[50], T. Jakoubek[175], J. Jamieson[55], K.W. Janas[81a], G. Jarlskog[94], A.E. Jaspan[88], T. Javůrek[34], M. Javurkova[99], F. Jeanneau[140], L. Jeanty[127], J. Jejelava[155a,aa], P. Jenni[50,e], S. Jézéquel[4], J. Jia[151], Z. Jia[13c], Y. Jiang[58a], S. Jiggins[48], J. Jimenez Pena[111], S. Jin[13c], A. Jinaru[25b], O. Jinnouchi[160], H. Jivan[31f], P. Johansson[145], K.A. Johns[6], C.A. Johnson[63], D.M. Jones[30], E. Jones[173], R.W.L. Jones[87], T.J. Jones[88], J. Jovicevic[14], X. Ju[16], J.J. Junggeburth[34], A. Juste Rozas[12,v], S. Kabana[142d], A. Kaczmarska[82], M. Kado[70a,70b], H. Kagan[123], M. Kagan[149], A. Kahn[37], A. Kahn[132], C. Kahra[96], T. Kaji[174], E. Kajomovitz[156], C.W. Kalderon[27], A. Kamenshchikov[118], M. Kaneda[159], N.J. Kang[141], S. Kang[76], Y. Kano[112], D. Kar[31f], K. Karava[130], M.J. Kareem[163b], I. Karkanias[158], S.N. Karpov[77], Z.M. Karpova[77], V. Kartvelishvili[87], A.N. Karyukhin[118], E. Kasimi[158], C. Kato[58d], J. Katzy[44], K. Kawade[146], K. Kawagoe[85], T. Kawaguchi[112], T. Kawamoto[140], G. Kawamura[51], E.F. Kay[171], F.I. Kaya[165], S. Kazakos[12], V.F. Kazanin[117b,117a], Y. Ke[151], J.M. Keaveney[31a], R. Keeler[171], J.S. Keller[32], A.S. Kelly[92], D. Kelsey[152], J.J. Kempster[19], J. Kendrick[19], K.E. Kennedy[37], O. Kepka[136], S. Kersten[177], B.P. Kerševan[89], S. Ketabchi Haghighat[162], M. Khandoga[131], A. Khanov[125], A.G. Kharlamov[117b,117a], T. Kharlamova[117b,117a], E.E. Khoda[144], T.J. Khoo[17], G. Khoriauli[172], E. Khramov[77], J. Khubua[155b], S. Kido[80], M. Kiehn[34], A. Kilgallon[127], E. Kim[160], Y.K. Kim[35], N. Kimura[92], A. Kirchhoff[51], D. Kirchmeier[46], C. Kirfel[22], J. Kirk[139], A.E. Kiryunin[111], T. Kishimoto[159], D.P. Kisliuk[162], C. Kitsaki[9], O. Kivernyk[22], T. Klapdor-Kleingrothaus[50], M. Klassen[59a], C. Klein[32], L. Klein[172], M.H. Klein[102], M. Klein[88], U. Klein[88], P. Klimek[34], A. Klimentov[27], F. Klimpel[111], T. Klingl[22], T. Klioutchnikova[34], F.F. Klitzner[110], P. Kluit[115], S. Kluth[111], E. Kneringer[74], T.M. Knight[162], A. Knue[50], D. Kobayashi[85], R. Kobayashi[83], M. Kobel[46], M. Kocian[149], T. Kodama[159], P. Kodys[138], D.M. Koeck[152], P.T. Koenig[22], T. Koffas[32], N.M. Köhler[34], M. Kolb[140], I. Koletsou[4], T. Komarek[126], K. Köneke[50], A.X.Y. Kong[1], T. Kono[122], V. Konstantinides[92], N. Konstantinidis[92], B. Konya[94], R. Kopeliansky[63], S. Koperny[81a], K. Korcyl[82], K. Kordas[158], G. Koren[157], A. Korn[92], S. Korn[51], I. Korolkov[12], E.V. Korolkova[145], N. Korotkova[109], B. Kortman[115], O. Kortner[111], S. Kortner[111], W.H. Kostecka[116], V.V. Kostyukhin[147,161], A. Kotsokechagia[62], A. Kotwal[47], A. Koulouris[34], A. Kourkoumeli-Charalampidi[68a,68b], C. Kourkoumelis[8], E. Kourlitis[5], O. Kovanda[152], R. Kowalewski[171], W. Kozanecki[140], A.S. Kozhin[118], V.A. Kramarenko[109], G. Kramberger[89], P. Kramer[96], D. Krasnopevtsev[58a], M.W. Krasny[131], A. Krasznahorkay[34], J.A. Kremer[96], J. Kretzschmar[88], K. Kreul[17], P. Krieger[162], F. Krieter[110], S. Krishnamurthy[99], A. Krishnan[59b], M. Krivos[138], K. Krizka[16], K. Kroeninger[45], H. Kroha[111], J. Kroll[136], J. Kroll[132], K.S. Krowpman[103], U. Kruchonak[77], H. Krüger[22], N. Krumnack[76], M.C. Kruse[47], J.A. Krzysiak[82],

JHEP06(2022)097

A. Kubota[160], O. Kuchinskaia[161], S. Kuday[3a], D. Kuechler[44], J.T. Kuechler[44], S. Kuehn[34], T. Kuhl[44], V. Kukhtin[77], Y. Kulchitsky[104,ad], S. Kuleshov[142c], M. Kumar[31f], N. Kumari[98], M. Kuna[56], A. Kupco[136], T. Kupfer[45], O. Kuprash[50], H. Kurashige[80], L.L. Kurchaninov[163a], Y.A. Kurochkin[104], A. Kurova[108], M.G. Kurth[13a,13d], E.S. Kuwertz[34], M. Kuze[160], A.K. Kvam[144], J. Kvita[126], T. Kwan[100], K.W. Kwok[60a], C. Lacasta[169], F. Lacava[70a,70b], H. Lacker[17], D. Lacour[131], N.N. Lad[92], E. Ladygin[77], R. Lafaye[4], B. Laforge[131], T. Lagouri[142d], S. Lai[51], I.K. Lakomiec[81a], N. Lalloue[56], J.E. Lambert[124], S. Lammers[63], W. Lampl[6], C. Lampoudis[158], E. Lançon[27], U. Landgraf[50], M.P.J. Landon[90], V.S. Lang[50], J.C. Lange[51], R.J. Langenberg[99], A.J. Lankford[166], F. Lanni[27], K. Lantzsch[22], A. Lanza[68a], A. Lapertosa[53b,53a], J.F. Laporte[140], T. Lari[66a], F. Lasagni Manghi[21b], M. Lassnig[34], V. Latonova[136], T.S. Lau[60a], A. Laudrain[96], A. Laurier[32], M. Lavorgna[67a,67b], S.D. Lawlor[91], Z. Lawrence[97], M. Lazzaroni[66a,66b], B. Le[97], B. Leban[89], A. Lebedev[76], M. LeBlanc[34], T. LeCompte[5], F. Ledroit-Guillon[56], A.C.A. Lee[92], G.R. Lee[15], L. Lee[57], S.C. Lee[154], S. Lee[76], L.L. Leeuw[31c], B. Lefebvre[163a], H.P. Lefebvre[91], M. Lefebvre[171], C. Leggett[16], K. Lehmann[148], N. Lehmann[18], G. Lehmann Miotto[34], W.A. Leight[44], A. Leisos[158,u], M.A.L. Leite[78c], C.E. Leitgeb[44], R. Leitner[138], K.J.C. Leney[40], T. Lenz[22], S. Leone[69a], C. Leonidopoulos[48], A. Leopold[150], C. Leroy[106], R. Les[103], C.G. Lester[30], M. Levchenko[133], J. Levêque[4], D. Levin[102], L.J. Levinson[175], D.J. Lewis[19], B. Li[13b], B. Li[58b], C. Li[58a], C-Q. Li[58c,58d], H. Li[58a], H. Li[58b], H. Li[58b], J. Li[58c], K. Li[144], L. Li[58c], M. Li[13a,13d], Q.Y. Li[58a], S. Li[58d,58c,c], T. Li[58b], X. Li[44], Y. Li[44], Z. Li[58b], Z. Li[130], Z. Li[100], Z. Li[88], Z. Liang[13a], M. Liberatore[44], B. Liberti[71a], K. Lie[60c], J. Lieber Marin[78b], K. Lin[103], R.A. Linck[63], R.E. Lindley[6], J.H. Lindon[2], A. Linss[44], E. Lipeles[132], A. Lipniacka[15], T.M. Liss[168,ai], A. Lister[170], J.D. Little[7], B. Liu[13a], B.X. Liu[148], J.B. Liu[58a], J.K.K. Liu[35], K. Liu[58d,58c], M. Liu[58a], M.Y. Liu[58a], P. Liu[13a], Q. Liu[58d,144,58c], X. Liu[58a], Y. Liu[44], Y. Liu[13c,13d], Y.L. Liu[102], Y.W. Liu[58a], M. Livan[68a,68b], J. Llorente Merino[148], S.L. Lloyd[90], E.M. Lobodzinska[44], P. Loch[6], S. Loffredo[71a,71b], T. Lohse[17], K. Lohwasser[145], M. Lokajicek[136], J.D. Long[168], I. Longarini[70a,70b], L. Longo[34], R. Longo[168], I. Lopez Paz[12], A. Lopez Solis[44], J. Lorenz[110], N. Lorenzo Martinez[4], A.M. Lory[110], A. Lösle[50], X. Lou[43a,43b], X. Lou[13a], A. Lounis[62], J. Love[5], P.A. Love[87], J.J. Lozano Bahilo[169], G. Lu[13a], M. Lu[58a], S. Lu[132], Y.J. Lu[61], H.J. Lubatti[144], C. Luci[70a,70b], F.L. Lucio Alves[13c], A. Lucotte[56], F. Luehring[63], I. Luise[151], L. Luminari[70a], O. Lundberg[150], B. Lund-Jensen[150], N.A. Luongo[127], M.S. Lutz[157], D. Lynn[27], H. Lyons[88], R. Lysak[136], E. Lytken[94], F. Lyu[13a], V. Lyubushkin[77], T. Lyubushkina[77], H. Ma[27], L.L. Ma[58b], Y. Ma[92], D.M. Mac Donell[171], G. Maccarrone[49], C.M. Macdonald[145], J.C. MacDonald[145], R. Madar[36], W.F. Mader[46], M. Madugoda Ralalage Don[125], N. Madysa[46], J. Maeda[80], T. Maeno[27], M. Maerker[46], V. Magerl[50], J. Magro[64a,64c], D.J. Mahon[37], C. Maidantchik[78b], A. Maio[135a,135b,135d], K. Maj[81a], O. Majersky[26a], S. Majewski[127], N. Makovec[62], V. Maksimovic[14], B. Malaescu[131], Pa. Malecki[82], V.P. Maleev[133], F. Malek[56], D. Malito[39b,39a], U. Mallik[75], C. Malone[30], S. Maltezos[9], S. Malyukov[77], J. Mamuzic[169], G. Mancini[49], J.P. Mandalia[90], I. Mandić[89], L. Manhaes de Andrade Filho[78a], I.M. Maniatis[158], M. Manisha[140], J. Manjarres Ramos[46], K.H. Mankinen[94], A. Mann[110], A. Manousos[74], B. Mansoulie[140], I. Manthos[158], S. Manzoni[115], A. Marantis[158,u], G. Marchiori[131], M. Marcisovsky[136], L. Marcoccia[71a,71b], C. Marcon[94], M. Marjanovic[124], Z. Marshall[16], S. Marti-Garcia[169], T.A. Martin[173], V.J. Martin[48], B. Martin dit Latour[15], L. Martinelli[70a,70b], M. Martinez[12,v], P. Martinez Agullo[169], V.I. Martinez Outschoorn[99], S. Martin-Haugh[139], V.S. Martoiu[25b], A.C. Martyniuk[92], A. Marzin[34], S.R. Maschek[111], L. Masetti[96], T. Mashimo[159], J. Masik[97], A.L. Maslennikov[117b,117a], L. Massa[21b], P. Massarotti[67a,67b], P. Mastrandrea[69a,69b], A. Mastroberardino[39b,39a], T. Masubuchi[159], D. Matakias[27], T. Mathisen[167], A. Matic[110], N. Matsuzawa[159], J. Maurer[25b], B. Maček[89], D.A. Maximov[117b,117a], R. Mazini[154], I. Maznas[158], S.M. Mazza[141], C. Mc Ginn[27], J.P. Mc Gowan[100], S.P. Mc Kee[102], T.G. McCarthy[111],

JHEP06(2022)097

W.P. McCormack[16], E.F. McDonald[101], A.E. McDougall[115], J.A. Mcfayden[152], G. Mchedlidze[155b], M.A. McKay[40], K.D. McLean[171], S.J. McMahon[139], P.C. McNamara[101], R.A. McPherson[171,y], J.E. Mdhluli[31f], Z.A. Meadows[99], S. Meehan[34], T. Megy[36], S. Mehlhase[110], A. Mehta[88], B. Meirose[41], D. Melini[156], B.R. Mellado Garcia[31f], A.H. Melo[51], F. Meloni[44], A. Melzer[22], E.D. Mendes Gouveia[135a], A.M. Mendes Jacques Da Costa[19], H.Y. Meng[162], L. Meng[34], S. Menke[111], M. Mentink[34], E. Meoni[39b,39a], C. Merlassino[130], P. Mermod[52,*], L. Merola[67a,67b], C. Meroni[66a], G. Merz[102], O. Meshkov[107,109], J.K.R. Meshreki[147], J. Metcalfe[5], A.S. Mete[5], C. Meyer[63], J-P. Meyer[140], M. Michetti[17], R.P. Middleton[139], L. Mijović[48], G. Mikenberg[175], M. Mikestikova[136], M. Mikuž[89], H. Mildner[145], A. Milic[162], C.D. Milke[40], D.W. Miller[35], L.S. Miller[32], A. Milov[175], D.A. Milstead[43a,43b], T. Min[13c], A.A. Minaenko[118], I.A. Minashvili[155b], L. Mince[55], A.I. Mincer[121], B. Mindur[81a], M. Mineev[77], Y. Minegishi[159], Y. Mino[83], L.M. Mir[12], M. Miralles Lopez[169], M. Mironova[130], T. Mitani[174], V.A. Mitsou[169], M. Mittal[58c], O. Miu[162], P.S. Miyagawa[90], Y. Miyazaki[85], A. Mizukami[79], J.U. Mjörnmark[94], T. Mkrtchyan[59a], M. Mlynarikova[116], T. Moa[43a,43b], S. Mobius[51], K. Mochizuki[106], P. Moder[44], P. Mogg[110], A.F. Mohammed[13a], S. Mohapatra[37], G. Mokgatitswane[31f], B. Mondal[147], S. Mondal[137], K. Mönig[44], E. Monnier[98], L. Monsonis Romero[169], A. Montalbano[148], J. Montejo Berlingen[34], M. Montella[123], F. Monticelli[86], N. Morange[62], A.L. Moreira De Carvalho[135a], M. Moreno Llácer[169], C. Moreno Martinez[12], P. Morettini[53b], S. Morgenstern[173], D. Mori[148], M. Morii[57], M. Morinaga[159], V. Morisbak[129], A.K. Morley[34], A.P. Morris[92], L. Morvaj[34], P. Moschovakos[34], B. Moser[115], M. Mosidze[155b], T. Moskalets[50], P. Moskvitina[114], J. Moss[29,n], E.J.W. Moyse[99], S. Muanza[98], J. Mueller[134], R. Mueller[18], D. Muenstermann[87], G.A. Mullier[94], J.J. Mullin[132], D.P. Mungo[66a,66b], J.L. Munoz Martinez[12], F.J. Munoz Sanchez[97], M. Murin[97], P. Murin[26b], W.J. Murray[173,139], A. Murrone[66a,66b], J.M. Muse[124], M. Muškinja[16], C. Mwewa[27], A.G. Myagkov[118,ae], A.J. Myers[7], A.A. Myers[134], G. Myers[63], M. Myska[137], B.P. Nachman[16], O. Nackenhorst[45], A.Nag Nag[46], K. Nagai[130], K. Nagano[79], J.L. Nagle[27], E. Nagy[98], A.M. Nairz[34], Y. Nakahama[112], K. Nakamura[79], H. Nanjo[128], F. Napolitano[59a], R. Narayan[40], E.A. Narayanan[113], I. Naryshkin[133], M. Naseri[32], C. Nass[22], T. Naumann[44], G. Navarro[20a], J. Navarro-Gonzalez[169], R. Nayak[157], P.Y. Nechaeva[107], F. Nechansky[44], T.J. Neep[19], A. Negri[68a,68b], M. Negrini[21b], C. Nellist[114], C. Nelson[100], K. Nelson[102], S. Nemecek[136], M. Nessi[34,f], M.S. Neubauer[168], F. Neuhaus[96], J. Neundorf[44], R. Newhouse[170], P.R. Newman[19], C.W. Ng[134], Y.S. Ng[17], Y.W.Y. Ng[166], B. Ngair[33e], H.D.N. Nguyen[106], R.B. Nickerson[130], R. Nicolaidou[140], D.S. Nielsen[38], J. Nielsen[141], M. Niemeyer[51], N. Nikiforou[10], V. Nikolaenko[118,ae], I. Nikolic-Audit[131], K. Nikolopoulos[19], P. Nilsson[27], H.R. Nindhito[52], A. Nisati[70a], N. Nishu[2], R. Nisius[111], T. Nitta[174], T. Nobe[159], D.L. Noel[30], Y. Noguchi[83], I. Nomidis[131], M.A. Nomura[27], M.B. Norfolk[145], R.R.B. Norisam[92], J. Novak[89], T. Novak[44], O. Novgorodova[46], L. Novotny[137], R. Novotny[113], L. Nozka[126], K. Ntekas[166], E. Nurse[92], F.G. Oakham[32,aj], J. Ocariz[131], A. Ochi[80], I. Ochoa[135a], J.P. Ochoa-Ricoux[142a], S. Oda[85], S. Odaka[79], S. Oerdek[167], A. Ogrodnik[81a], A. Oh[97], C.C. Ohm[150], H. Oide[160], R. Oishi[159], M.L. Ojeda[44], Y. Okazaki[83], M.W. O'Keefe[88], Y. Okumura[159], A. Olariu[25b], L.F. Oleiro Seabra[135a], S.A. Olivares Pino[142d], D. Oliveira Damazio[27], D. Oliveira Goncalves[78a], J.L. Oliver[166], M.J.R. Olsson[166], A. Olszewski[82], J. Olszowska[82], Ö.O. Öncel[22], D.C. O'Neil[148], A.P. O'neill[130], A. Onofre[135a,135e], P.U.E. Onyisi[10], R.G. Oreamuno Madriz[116], M.J. Oreglia[35], G.E. Orellana[86], D. Orestano[72a,72b], N. Orlando[12], R.S. Orr[162], V. O'Shea[55], R. Ospanov[58a], G. Otero y Garzon[28], H. Otono[85], P.S. Ott[59a], G.J. Ottino[16], M. Ouchrif[33d], J. Ouellette[27], F. Ould-Saada[129], A. Ouraou[140,*], Q. Ouyang[13a], M. Owen[55], R.E. Owen[139], K.Y. Oyulmaz[11c], V.E. Ozcan[11c], N. Ozturk[7], S. Ozturk[11c], J. Pacalt[126], H.A. Pacey[30], K. Pachal[47], A. Pacheco Pages[12], C. Padilla Aranda[12], S. Pagan Griso[16], G. Palacino[63], S. Palazzo[48], S. Palestini[34], M. Palka[81b], P. Palni[81a], D.K. Panchal[10], C.E. Pandini[52], J.G. Panduro Vazquez[91], P. Pani[44], G. Panizzo[64a,64c],

JHEP06(2022)097

L. Paolozzi[52], C. Papadatos[106], S. Parajuli[40], A. Paramonov[5], C. Paraskevopoulos[9], D. Paredes Hernandez[60b], S.R. Paredes Saenz[130], B. Parida[175], T.H. Park[162], A.J. Parker[29], M.A. Parker[30], F. Parodi[53b,53a], E.W. Parrish[116], J.A. Parsons[37], U. Parzefall[50], L. Pascual Dominguez[157], V.R. Pascuzzi[16], F. Pasquali[115], E. Pasqualucci[70a], S. Passaggio[53b], F. Pastore[91], P. Pasuwan[43a,43b], J.R. Pater[97], A. Pathak[176], J. Patton[88], T. Pauly[34], J. Pearkes[149], M. Pedersen[129], L. Pedraza Diaz[114], R. Pedro[135a], T. Peiffer[51], S.V. Peleganchuk[117b,117a], O. Penc[136], C. Peng[60b], H. Peng[58a], M. Penzin[161], B.S. Peralva[78a], A.P. Pereira Peixoto[135a], L. Pereira Sanchez[43a,43b], D.V. Perepelitsa[27], E. Perez Codina[163a], M. Perganti[9], L. Perini[66a,66b], H. Pernegger[34], S. Perrella[34], A. Perrevoort[115], K. Peters[44], R.F.Y. Peters[97], B.A. Petersen[34], T.C. Petersen[38], E. Petit[98], V. Petousis[137], C. Petridou[158], P. Petroff[62], F. Petrucci[72a,72b], A. Petrukhin[147], M. Pettee[178], N.E. Pettersson[34], K. Petukhova[138], A. Peyaud[140], R. Pezoa[142e], L. Pezzotti[34], G. Pezzullo[178], T. Pham[101], P.W. Phillips[139], M.W. Phipps[168], G. Piacquadio[151], E. Pianori[16], F. Piazza[66a,66b], A. Picazio[99], R. Piegaia[28], D. Pietreanu[25b], J.E. Pilcher[35], A.D. Pilkington[97], M. Pinamonti[64a,64c], J.L. Pinfold[2], C. Pitman Donaldson[92], D.A. Pizzi[32], L. Pizzimento[71a,71b], A. Pizzini[115], M.-A. Pleier[27], V. Plesanovs[50], V. Pleskot[138], E. Plotnikova[77], P. Podberezko[117b,117a], R. Poettgen[94], R. Poggi[52], L. Poggioli[131], I. Pogrebnyak[103], D. Pohl[22], I. Pokharel[51], G. Polesello[68a], A. Poley[148,163a], A. Policicchio[70a,70b], R. Polifka[138], A. Polini[21b], C.S. Pollard[130], Z.B. Pollock[123], V. Polychronakos[27], D. Ponomarenko[108], L. Pontecorvo[34], S. Popa[25a], G.A. Popeneciu[25d], L. Portales[4], D.M. Portillo Quintero[163a], S. Pospisil[137], P. Postolache[25c], K. Potamianos[130], I.N. Potrap[77], C.J. Potter[30], H. Potti[1], T. Poulsen[44], J. Poveda[169], T.D. Powell[145], G. Pownall[44], M.E. Pozo Astigarraga[34], A. Prades Ibanez[169], P. Pralavorio[98], M.M. Prapa[42], S. Prell[76], D. Price[97], M. Primavera[65a], M.A. Principe Martin[95], M.L. Proffitt[144], N. Proklova[108], K. Prokofiev[60c], F. Prokoshin[77], S. Protopopescu[27], J. Proudfoot[5], M. Przybycien[81a], D. Pudzha[133], P. Puzo[62], D. Pyatiizbyantseva[108], J. Qian[102], Y. Qin[97], T. Qiu[90], A. Quadt[51], M. Queitsch-Maitland[34], G. Rabanal Bolanos[57], F. Ragusa[66a,66b], J.A. Raine[52], S. Rajagopalan[27], K. Ran[13a,13d], D.F. Rassloff[59a], D.M. Rauch[44], S. Rave[96], B. Ravina[55], I. Ravinovich[175], M. Raymond[34], A.L. Read[129], N.P. Readioff[145], D.M. Rebuzzi[68a,68b], G. Redlinger[27], K. Reeves[41], D. Reikher[157], A. Reiss[96], A. Rej[147], C. Rembser[34], A. Renardi[44], M. Renda[25b], M.B. Rendel[111], A.G. Rennie[55], S. Resconi[66a], M. Ressegotti[53b,53a], E.D. Resseguie[16], S. Rettie[92], B. Reynolds[123], E. Reynolds[19], M. Rezaei Estabragh[177], O.L. Rezanova[117b,117a], P. Reznicek[138], E. Ricci[73a,73b], R. Richter[111], S. Richter[44], E. Richter-Was[81b], M. Ridel[131], P. Rieck[111], P. Riedler[34], O. Rifki[44], M. Rijssenbeek[151], A. Rimoldi[68a,68b], M. Rimoldi[44], L. Rinaldi[21b,21a], T.T. Rinn[168], M.P. Rinnagel[110], G. Ripellino[150], I. Riu[12], P. Rivadeneira[44], J.C. Rivera Vergara[171], F. Rizatdinova[125], E. Rizvi[90], C. Rizzi[52], B.A. Roberts[173], B.R. Roberts[16], S.H. Robertson[100,y], M. Robin[44], D. Robinson[30], C.M. Robles Gajardo[142e], M. Robles Manzano[96], A. Robson[55], A. Rocchi[71a,71b], C. Roda[69a,69b], S. Rodriguez Bosca[59a], A. Rodriguez Rodriguez[50], A.M. Rodríguez Vera[163b], S. Roe[34], A.R. Roepe[124], J. Roggel[177], O. Røhne[129], R.A. Rojas[171], B. Roland[50], C.P.A. Roland[63], J. Roloff[27], A. Romaniouk[108], M. Romano[21b], A.C. Romero Hernandez[168], N. Rompotis[88], M. Ronzani[121], L. Roos[131], S. Rosati[70a], B.J. Rosser[132], E. Rossi[162], E. Rossi[4], E. Rossi[67a,67b], L.P. Rossi[53b], L. Rossini[44], R. Rosten[123], M. Rotaru[25b], B. Rottler[50], D. Rousseau[62], D. Rousso[30], G. Rovelli[68a,68b], A. Roy[10], A. Rozanov[98], Y. Rozen[156], X. Ruan[31f], A.J. Ruby[88], T.A. Ruggeri[1], F. Rühr[50], A. Ruiz-Martinez[169], A. Rummler[34], Z. Rurikova[50], N.A. Rusakovich[77], H.L. Russell[34], L. Rustige[36], J.P. Rutherfoord[6], E.M. Rüttinger[145], M. Rybar[138], E.B. Rye[129], A. Ryzhov[118], J.A. Sabater Iglesias[44], P. Sabatini[169], L. Sabetta[70a,70b], H.F-W. Sadrozinski[141], R. Sadykov[77], F. Safai Tehrani[70a], B. Safarzadeh Samani[152], M. Safdari[149], S. Saha[100], M. Sahinsoy[111], A. Sahu[177], M. Saimpert[140], M. Saito[159], T. Saito[159], D. Salamani[34], G. Salamanna[72a,72b],

JHEP06(2022)097

A. Salnikov[149], J. Salt[169], A. Salvador Salas[12], D. Salvatore[39b,39a], F. Salvatore[152], A. Salzburger[34], D. Sammel[50], D. Sampsonidis[158], D. Sampsonidou[58d,58c], J. Sánchez[169], A. Sanchez Pineda[4], V. Sanchez Sebastian[169], H. Sandaker[129], C.O. Sander[44], I.G. Sanderswood[87], J.A. Sandesara[99], M. Sandhoff[177], C. Sandoval[20b], D.P.C. Sankey[139], M. Sannino[53b,53a], A. Sansoni[49], C. Santoni[36], H. Santos[135a,135b], S.N. Santpur[16], A. Santra[175], K.A. Saoucha[145], A. Sapronov[77], J.G. Saraiva[135a,135d], J. Sardain[98], O. Sasaki[79], K. Sato[164], C. Sauer[59b], F. Sauerburger[50], E. Sauvan[4], P. Savard[162,aj], R. Sawada[159], C. Sawyer[139], L. Sawyer[93], I. Sayago Galvan[169], C. Sbarra[21b], A. Sbrizzi[21b,21a], T. Scanlon[92], J. Schaarschmidt[144], P. Schacht[111], D. Schaefer[35], U. Schäfer[96], A.C. Schaffer[62], D. Schaile[110], R.D. Schamberger[151], E. Schanet[110], C. Scharf[17], N. Scharmberg[97], V.A. Schegelsky[133], D. Scheirich[138], F. Schenck[17], M. Schernau[166], C. Schiavi[53b,53a], L.K. Schildgen[22], Z.M. Schillaci[24], E.J. Schioppa[65a,65b], M. Schioppa[39b,39a], B. Schlag[96], K.E. Schleicher[50], S. Schlenker[34], K. Schmieden[96], C. Schmitt[96], S. Schmitt[44], L. Schoeffel[140], A. Schoening[59b], P.G. Scholer[50], E. Schopf[130], M. Schott[96], J. Schovancova[34], S. Schramm[52], F. Schroeder[177], H-C. Schultz-Coulon[59a], M. Schumacher[50], B.A. Schumm[141], Ph. Schune[140], A. Schwartzman[149], T.A. Schwarz[102], Ph. Schwemling[140], R. Schwienhorst[103], A. Sciandra[141], G. Sciolla[24], F. Scuri[69a], F. Scutti[101], C.D. Sebastiani[88], K. Sedlaczek[45], P. Seema[17], S.C. Seidel[113], A. Seiden[141], B.D. Seidlitz[27], T. Seiss[35], C. Seitz[44], J.M. Seixas[78b], G. Sekhniaidze[67a], S.J. Sekula[40], L. Selem[4], N. Semprini-Cesari[21b,21a], S. Sen[47], C. Serfon[27], L. Serin[62], L. Serkin[64a,64b], M. Sessa[72a,72b], H. Severini[124], S. Sevova[149], F. Sforza[53b,53a], A. Sfyrla[52], E. Shabalina[51], R. Shaheen[150], J.D. Shahinian[132], N.W. Shaikh[43a,43b], D. Shaked Renous[175], L.Y. Shan[13a], M. Shapiro[16], A. Sharma[34], A.S. Sharma[1], S. Sharma[44], P.B. Shatalov[119], K. Shaw[152], S.M. Shaw[97], P. Sherwood[92], L. Shi[92], C.O. Shimmin[178], Y. Shimogama[174], J.D. Shinner[91], I.P.J. Shipsey[130], S. Shirabe[52], M. Shiyakova[77], J. Shlomi[175], M.J. Shochet[35], J. Shojaii[101], D.R. Shope[150], S. Shrestha[123], E.M. Shrif[31f], M.J. Shroff[171], E. Shulga[175], P. Sicho[136], A.M. Sickles[168], E. Sideras Haddad[31f], O. Sidiropoulou[34], A. Sidoti[21b], F. Siegert[46], Dj. Sijacki[14], J.M. Silva[19], M.V. Silva Oliveira[34], S.B. Silverstein[43a], S. Simion[62], R. Simoniello[34], N.D. Simpson[94], S. Simsek[11b], P. Sinervo[162], V. Sinetckii[109], S. Singh[148], S. Singh[162], S. Sinha[44], S. Sinha[31f], M. Sioli[21b,21a], I. Siral[127], S.Yu. Sivoklokov[109], J. Sjölin[43a,43b], A. Skaf[51], E. Skorda[94], P. Skubic[124], M. Slawinska[82], K. Sliwa[165], V. Smakhtin[175], B.H. Smart[139], J. Smiesko[138], S.Yu. Smirnov[108], Y. Smirnov[108], L.N. Smirnova[109,r], O. Smirnova[94], E.A. Smith[35], H.A. Smith[130], M. Smizanska[87], K. Smolek[137], A. Smykiewicz[82], A.A. Snesarev[107], H.L. Snoek[115], S. Snyder[27], R. Sobie[171,y], A. Soffer[157], F. Sohns[51], C.A. Solans Sanchez[34], E.Yu. Soldatov[108], U. Soldevila[169], A.A. Solodkov[118], S. Solomon[50], A. Soloshenko[77], O.V. Solovyanov[118], V. Solovyev[133], P. Sommer[145], H. Son[165], A. Sonay[12], W.Y. Song[163b], A. Sopczak[137], A.L. Sopio[92], F. Sopkova[26b], S. Sottocornola[68a,68b], R. Soualah[120c], A.M. Soukharev[117b,117a], Z. Soumaimi[33e], D. South[44], S. Spagnolo[65a,65b], M. Spalla[111], M. Spangenberg[173], F. Spanò[91], D. Sperlich[50], T.M. Spieker[59a], G. Spigo[34], M. Spina[152], D.P. Spiteri[55], M. Spousta[138], A. Stabile[66a,66b], R. Stamen[59a], M. Stamenkovic[115], A. Stampekis[19], M. Standke[22], E. Stanecka[82], B. Stanislaus[34], M.M. Stanitzki[44], M. Stankaityte[130], B. Stapf[44], E.A. Starchenko[118], G.H. Stark[141], J. Stark[98], D.M. Starko[163b], P. Staroba[136], P. Starovoitov[59a], S. Stärz[100], R. Staszewski[82], G. Stavropoulos[42], P. Steinberg[27], A.L. Steinhebel[127], B. Stelzer[148,163a], H.J. Stelzer[134], O. Stelzer-Chilton[163a], H. Stenzel[54], T.J. Stevenson[152], G.A. Stewart[34], M.C. Stockton[34], G. Stoicea[25b], M. Stolarski[135a], S. Stonjek[111], A. Straessner[46], J. Strandberg[150], S. Strandberg[43a,43b], M. Strauss[124], T. Strebler[98], P. Strizenec[26b], R. Ströhmer[172], D.M. Strom[127], L.R. Strom[44], R. Stroynowski[40], A. Strubig[43a,43b], S.A. Stucci[27], B. Stugu[15], J. Stupak[124], N.A. Styles[44], D. Su[149], S. Su[58a], W. Su[58d,144,58c], X. Su[58a], K. Sugizaki[159], V.V. Sulin[107], M.J. Sullivan[88], D.M.S. Sultan[52], L. Sultanaliyeva[107], S. Sultansoy[3c], T. Sumida[83], S. Sun[102], S. Sun[176], X. Sun[97], O. Sunneborn Gudnadottir[167], C.J.E. Suster[153], M.R. Sutton[152], M. Svatos[136], M. Swiatlowski[163a], T. Swirski[172], I. Sykora[26a],

JHEP06(2022)097

M. Sykora[138], T. Sykora[138], D. Ta[96], K. Tackmann[44,w], A. Taffard[166], R. Tafirout[163a], R.H.M. Taibah[131], R. Takashima[84], K. Takeda[80], T. Takeshita[146], E.P. Takeva[48], Y. Takubo[79], M. Talby[98], A.A. Talyshev[117b,117a], K.C. Tam[60b], N.M. Tamir[157], A. Tanaka[159], J. Tanaka[159], R. Tanaka[62], J. Tang[58c], Z. Tao[170], S. Tapia Araya[76], S. Tapprogge[96], A. Tarek Abouelfadl Mohamed[103], S. Tarem[156], K. Tariq[58b], G. Tarna[25b], G.F. Tartarelli[66a], P. Tas[138], M. Tasevsky[136], E. Tassi[39b,39a], G. Tateno[159], Y. Tayalati[33e], G.N. Taylor[101], W. Taylor[163b], H. Teagle[88], A.S. Tee[176], R. Teixeira De Lima[149], P. Teixeira-Dias[91], H. Ten Kate[34], J.J. Teoh[115], K. Terashi[159], J. Terron[95], S. Terzo[12], M. Testa[49], R.J. Teuscher[162,y], N. Themistokleous[48], T. Theveneaux-Pelzer[17], O. Thielmann[177], D.W. Thomas[91], J.P. Thomas[19], E.A. Thompson[44], P.D. Thompson[19], E. Thomson[132], E.J. Thorpe[90], Y. Tian[51], V. Tikhomirov[107,af], Yu.A. Tikhonov[117b,117a], S. Timoshenko[108], E.X.L. Ting[1], P. Tipton[178], S. Tisserant[98], S.H. Tlou[31f], A. Tnourji[36], K. Todome[21b,21a], S. Todorova-Nova[138], S. Todt[46], M. Togawa[79], J. Tojo[85], S. Tokár[26a], K. Tokushuku[79], E. Tolley[123], R. Tombs[30], M. Tomoto[79,112], L. Tompkins[149], P. Tornambe[99], E. Torrence[127], H. Torres[46], E. Torró Pastor[169], M. Toscani[28], C. Tosciri[35], J. Toth[98,x], D.R. Tovey[145], A. Traeet[15], C.J. Treado[121], T. Trefzger[172], A. Tricoli[27], I.M. Trigger[163a], S. Trincaz-Duvoid[131], D.A. Trischuk[170], W. Trischuk[162], B. Trocmé[56], A. Trofymov[62], C. Troncon[66a], F. Trovato[152], L. Truong[31c], M. Trzebinski[82], A. Trzupek[82], F. Tsai[151], M. Tsai[102], A. Tsiamis[158], P.V. Tsiareshka[104], A. Tsirigotis[158,u], V. Tsiskaridze[151], E.G. Tskhadadze[155a], M. Tsopoulou[158], Y. Tsujikawa[83], I.I. Tsukerman[119], V. Tsulaia[16], S. Tsuno[79], O. Tsur[156], D. Tsybychev[151], Y. Tu[60b], A. Tudorache[25b], V. Tudorache[25b], A.N. Tuna[34], S. Turchikhin[77], I. Turk Cakir[3a], R.J. Turner[19], R. Turra[66a], P.M. Tuts[37], S. Tzamarias[158], P. Tzanis[9], E. Tzovara[96], K. Uchida[159], F. Ukegawa[164], P.A. Ulloa Poblete[142b], G. Unal[34], M. Unal[10], A. Undrus[27], G. Unel[166], F.C. Ungaro[101], K. Uno[159], J. Urban[26b], P. Urquijo[101], G. Usai[7], R. Ushioda[160], M. Usman[106], Z. Uysal[11d], V. Vacek[137], B. Vachon[100], K.O.H. Vadla[129], T. Vafeiadis[34], C. Valderanis[110], E. Valdes Santurio[43a,43b], M. Valente[163a], S. Valentinetti[21b,21a], A. Valero[169], R.A. Vallance[19], A. Vallier[98], J.A. Valls Ferrer[169], T.R. Van Daalen[144], P. Van Gemmeren[5], S. Van Stroud[92], I. Van Vulpen[115], M. Vanadia[71a,71b], W. Vandelli[34], M. Vandenbroucke[140], E.R. Vandewall[125], D. Vannicola[157], L. Vannoli[53b,53a], R. Vari[70a], E.W. Varnes[6], C. Varni[16], T. Varol[154], D. Varouchas[62], K.E. Varvell[153], M.E. Vasile[25b], L. Vaslin[36], G.A. Vasquez[171], F. Vazeille[36], D. Vazquez Furelos[12], T. Vazquez Schroeder[34], J. Veatch[51], V. Vecchio[97], M.J. Veen[115], I. Veliscek[130], L.M. Veloce[162], F. Veloso[135a,135c], S. Veneziano[70a], A. Ventura[65a,65b], A. Verbytskyi[111], M. Verducci[69a,69b], C. Vergis[22], M. Verissimo De Araujo[78b], W. Verkerke[115], A.T. Vermeulen[115], J.C. Vermeulen[115], C. Vernieri[149], P.J. Verschuuren[91], M. Vessella[99], M.L. Vesterbacka[121], M.C. Vetterli[148,aj], A. Vgenopoulos[158], N. Viaux Maira[142e], T. Vickey[145], O.E. Vickey Boeriu[145], G.H.A. Viehhauser[130], L. Vigani[59b], M. Villa[21b,21a], M. Villaplana Perez[169], E.M. Villhauer[48], E. Vilucchi[49], M.G. Vincter[32], G.S. Virdee[19], A. Vishwakarma[48], C. Vittori[21b,21a], I. Vivarelli[152], V. Vladimirov[173], E. Voevodina[111], M. Vogel[177], P. Vokac[137], J. Von Ahnen[44], E. Von Toerne[22], B. Vormwald[34], V. Vorobel[138], K. Vorobev[108], M. Vos[169], J.H. Vossebeld[88], M. Vozak[97], L. Vozdecky[90], N. Vranjes[14], M. Vranjes Milosavljevic[14], V. Vrba[137,*], M. Vreeswijk[115], N.K. Vu[98], R. Vuillermet[34], O.V. Vujinovic[96], I. Vukotic[35], S. Wada[164], C. Wagner[99], W. Wagner[177], S. Wahdan[177], H. Wahlberg[86], R. Wakasa[164], M. Wakida[112], V.M. Walbrecht[111], J. Walder[139], R. Walker[110], S.D. Walker[91], W. Walkowiak[147], A.M. Wang[57], A.Z. Wang[176], C. Wang[58a], C. Wang[58c], H. Wang[16], J. Wang[60a], P. Wang[40], R.-J. Wang[96], R. Wang[57], R. Wang[116], S.M. Wang[154], S. Wang[58b], T. Wang[58a], W.T. Wang[75], W.X. Wang[58a], X. Wang[13c], X. Wang[168], X. Wang[58c], Y. Wang[58a], Z. Wang[102], Z. Wang[102], C. Wanotayaroj[34], A. Warburton[100], C.P. Ward[30], R.J. Ward[19], N. Warrack[55], A.T. Watson[19], M.F. Watson[19], G. Watts[144], B.M. Waugh[92], A.F. Webb[10], C. Weber[27], M.S. Weber[18], S.A. Weber[32], S.M. Weber[59a], C. Wei[58a],

JHEP06(2022)097

Y. Wei[130], A.R. Weidberg[130], J. Weingarten[45], M. Weirich[96], C. Weiser[50], T. Wenaus[27], B. Wendland[45], T. Wengler[34], S. Wenig[34], N. Wermes[22], M. Wessels[59a], K. Whalen[127], A.M. Wharton[87], A.S. White[57], A. White[7], M.J. White[1], D. Whiteson[166], L. Wickremasinghe[128], W. Wiedenmann[176], C. Wiel[46], M. Wielers[139], N. Wieseotte[96], C. Wiglesworth[38], L.A.M. Wiik-Fuchs[50], D.J. Wilbern[124], H.G. Wilkens[34], L.J. Wilkins[91], D.M. Williams[37], H.H. Williams[132], S. Williams[30], S. Willocq[99], P.J. Windischhofer[130], I. Wingerter-Seez[4], E. Winkels[152], F. Winklmeier[127], B.T. Winter[50], M. Wittgen[149], M. Wobisch[93], A. Wolf[96], R. Wölker[130], J. Wollrath[166], M.W. Wolter[82], H. Wolters[135a,135c], V.W.S. Wong[170], A.F. Wongel[44], S.D. Worm[44], B.K. Wosiek[82], K.W. Woźniak[82], K. Wraight[55], J. Wu[13a,13d], S.L. Wu[176], X. Wu[52], Y. Wu[58a], Z. Wu[140,58a], J. Wuerzinger[130], T.R. Wyatt[97], B.M. Wynne[48], S. Xella[38], L. Xia[13c], M. Xia[13b], J. Xiang[60c], X. Xiao[102], M. Xie[58a], X. Xie[58a], I. Xiotidis[152], D. Xu[13a], H. Xu[58a], H. Xu[58a], L. Xu[58a], R. Xu[132], T. Xu[58a], W. Xu[102], Y. Xu[13b], Z. Xu[58b], Z. Xu[149], B. Yabsley[153], S. Yacoob[31a], N. Yamaguchi[85], Y. Yamaguchi[160], M. Yamatani[159], H. Yamauchi[164], T. Yamazaki[16], Y. Yamazaki[80], J. Yan[58c], S. Yan[130], Z. Yan[23], H.J. Yang[58c,58d], H.T. Yang[16], S. Yang[58a], T. Yang[60c], X. Yang[58a], X. Yang[13a], Y. Yang[159], Z. Yang[102,58a], W-M. Yao[16], Y.C. Yap[44], H. Ye[13c], J. Ye[40], S. Ye[27], I. Yeletskikh[77], M.R. Yexley[87], P. Yin[37], K. Yorita[174], K. Yoshihara[76], C.J.S. Young[50], C. Young[149], M. Yuan[102], R. Yuan[58b,i], X. Yue[59a], M. Zaazoua[33e], B. Zabinski[82], G. Zacharis[9], E. Zaid[48], A.M. Zaitsev[118,ae], T. Zakareishvili[155b], N. Zakharchuk[32], S. Zambito[34], D. Zanzi[50], O. Zaplatilek[137], S.V. Zeißner[45], C. Zeitnitz[177], J.C. Zeng[168], D.T. Zenger Jr[24], O. Zenin[118], T. Ženiš[26a], S. Zenz[90], S. Zerradi[33a], D. Zerwas[62], B. Zhang[13c], D.F. Zhang[145], G. Zhang[13b], J. Zhang[5], K. Zhang[13a], L. Zhang[13c], M. Zhang[168], R. Zhang[176], S. Zhang[102], X. Zhang[58c], X. Zhang[58b], Z. Zhang[62], P. Zhao[47], T. Zhao[58b], Y. Zhao[141], Z. Zhao[58a], A. Zhemchugov[77], Z. Zheng[149], D. Zhong[168], B. Zhou[102], C. Zhou[176], H. Zhou[6], N. Zhou[58c], Y. Zhou[6], C.G. Zhu[58b], C. Zhu[13a,13d], H.L. Zhu[58a], H. Zhu[13a], J. Zhu[102], Y. Zhu[58a], X. Zhuang[13a], K. Zhukov[107], V. Zhulanov[117b,117a], D. Zieminska[63], N.I. Zimine[77], S. Zimmermann[50,*], J. Zinsser[59b], M. Ziolkowski[147], L. Živković[14], A. Zoccoli[21b,21a], K. Zoch[52], T.G. Zorbas[145], O. Zormpa[42], W. Zou[37], L. Zwalinski[34].

[1] *Department of Physics, University of Adelaide, Adelaide; Australia*

[2] *Department of Physics, University of Alberta, Edmonton AB; Canada*

[3] [(a)] *Department of Physics, Ankara University, Ankara;* [(b)] *Istanbul Aydin University, Application and Research Center for Advanced Studies, Istanbul;* [(c)] *Division of Physics, TOBB University of Economics and Technology, Ankara; Turkey*

[4] *LAPP, Univ. Savoie Mont Blanc, CNRS/IN2P3, Annecy; France*

[5] *High Energy Physics Division, Argonne National Laboratory, Argonne IL; United States of America*

[6] *Department of Physics, University of Arizona, Tucson AZ; United States of America*

[7] *Department of Physics, University of Texas at Arlington, Arlington TX; United States of America*

[8] *Physics Department, National and Kapodistrian University of Athens, Athens; Greece*

[9] *Physics Department, National Technical University of Athens, Zografou; Greece*

[10] *Department of Physics, University of Texas at Austin, Austin TX; United States of America*

[11] [(a)] *Bahcesehir University, Faculty of Engineering and Natural Sciences, Istanbul;* [(b)] *Istanbul Bilgi University, Faculty of Engineering and Natural Sciences, Istanbul;* [(c)] *Department of Physics, Bogazici University, Istanbul;* [(d)] *Department of Physics Engineering, Gaziantep University, Gaziantep; Turkey*

[12] *Institut de Física d'Altes Energies (IFAE), Barcelona Institute of Science and Technology, Barcelona; Spain*

[13] [(a)] *Institute of High Energy Physics, Chinese Academy of Sciences, Beijing;* [(b)] *Physics Department, Tsinghua University, Beijing;* [(c)] *Department of Physics, Nanjing University, Nanjing;* [(d)] *University of Chinese Academy of Science (UCAS), Beijing; China*

[14] *Institute of Physics, University of Belgrade, Belgrade; Serbia*

[15] *Department for Physics and Technology, University of Bergen, Bergen; Norway*

JHEP06(2022)097

[16] *Physics Division, Lawrence Berkeley National Laboratory and University of California, Berkeley CA; United States of America*
[17] *Institut für Physik, Humboldt Universität zu Berlin, Berlin; Germany*
[18] *Albert Einstein Center for Fundamental Physics and Laboratory for High Energy Physics, University of Bern, Bern; Switzerland*
[19] *School of Physics and Astronomy, University of Birmingham, Birmingham; United Kingdom*
[20] [(a)] *Facultad de Ciencias y Centro de Investigaciónes, Universidad Antonio Nariño, Bogotá;* [(b)] *Departamento de Física, Universidad Nacional de Colombia, Bogotá; Colombia*
[21] [(a)] *Dipartimento di Fisica e Astronomia A. Righi, Università di Bologna, Bologna;* [(b)] *INFN Sezione di Bologna; Italy*
[22] *Physikalisches Institut, Universität Bonn, Bonn; Germany*
[23] *Department of Physics, Boston University, Boston MA; United States of America*
[24] *Department of Physics, Brandeis University, Waltham MA; United States of America*
[25] [(a)] *Transilvania University of Brasov, Brasov;* [(b)] *Horia Hulubei National Institute of Physics and Nuclear Engineering, Bucharest;* [(c)] *Department of Physics, Alexandru Ioan Cuza University of Iasi, Iasi;* [(d)] *National Institute for Research and Development of Isotopic and Molecular Technologies, Physics Department, Cluj-Napoca;* [(e)] *University Politehnica Bucharest, Bucharest;* [(f)] *West University in Timisoara, Timisoara; Romania*
[26] [(a)] *Faculty of Mathematics, Physics and Informatics, Comenius University, Bratislava;* [(b)] *Department of Subnuclear Physics, Institute of Experimental Physics of the Slovak Academy of Sciences, Kosice; Slovak Republic*
[27] *Physics Department, Brookhaven National Laboratory, Upton NY; United States of America*
[28] *Departamento de Física (FCEN) and IFIBA, Universidad de Buenos Aires and CONICET, Buenos Aires; Argentina*
[29] *California State University, CA; United States of America*
[30] *Cavendish Laboratory, University of Cambridge, Cambridge; United Kingdom*
[31] [(a)] *Department of Physics, University of Cape Town, Cape Town;* [(b)] *iThemba Labs, Western Cape;* [(c)] *Department of Mechanical Engineering Science, University of Johannesburg, Johannesburg;* [(d)] *National Institute of Physics, University of the Philippines Diliman (Philippines);* [(e)] *University of South Africa, Department of Physics, Pretoria;* [(f)] *School of Physics, University of the Witwatersrand, Johannesburg; South Africa*
[32] *Department of Physics, Carleton University, Ottawa ON; Canada*
[33] [(a)] *Faculté des Sciences Ain Chock, Réseau Universitaire de Physique des Hautes Energies — Université Hassan II, Casablanca;* [(b)] *Faculté des Sciences, Université Ibn-Tofail, Kénitra;* [(c)] *Faculté des Sciences Semlalia, Université Cadi Ayyad, LPHEA-Marrakech;* [(d)] *LPMR, Faculté des Sciences, Université Mohamed Premier, Oujda;* [(e)] *Faculté des sciences, Université Mohammed V, Rabat;* [(f)] *Mohammed VI Polytechnic University, Ben Guerir; Morocco*
[34] *CERN, Geneva; Switzerland*
[35] *Enrico Fermi Institute, University of Chicago, Chicago IL; United States of America*
[36] *LPC, Université Clermont Auvergne, CNRS/IN2P3, Clermont-Ferrand; France*
[37] *Nevis Laboratory, Columbia University, Irvington NY; United States of America*
[38] *Niels Bohr Institute, University of Copenhagen, Copenhagen; Denmark*
[39] [(a)] *Dipartimento di Fisica, Università della Calabria, Rende;* [(b)] *INFN Gruppo Collegato di Cosenza, Laboratori Nazionali di Frascati; Italy*
[40] *Physics Department, Southern Methodist University, Dallas TX; United States of America*
[41] *Physics Department, University of Texas at Dallas, Richardson TX; United States of America*
[42] *National Centre for Scientific Research "Demokritos", Agia Paraskevi; Greece*
[43] [(a)] *Department of Physics, Stockholm University;* [(b)] *Oskar Klein Centre, Stockholm; Sweden*
[44] *Deutsches Elektronen-Synchrotron DESY, Hamburg and Zeuthen; Germany*
[45] *Fakultät Physik, Technische Universität Dortmund, Dortmund; Germany*
[46] *Institut für Kern- und Teilchenphysik, Technische Universität Dresden, Dresden; Germany*
[47] *Department of Physics, Duke University, Durham NC; United States of America*
[48] *SUPA — School of Physics and Astronomy, University of Edinburgh, Edinburgh; United Kingdom*

JHEP06(2022)097

[49] INFN e Laboratori Nazionali di Frascati, Frascati; Italy
[50] Physikalisches Institut, Albert-Ludwigs-Universität Freiburg, Freiburg; Germany
[51] II. Physikalisches Institut, Georg-August-Universität Göttingen, Göttingen; Germany
[52] Département de Physique Nucléaire et Corpusculaire, Université de Genève, Genève; Switzerland
[53] [(a)] Dipartimento di Fisica, Università di Genova, Genova;[(b)] INFN Sezione di Genova; Italy
[54] II. Physikalisches Institut, Justus-Liebig-Universität Giessen, Giessen; Germany
[55] SUPA — School of Physics and Astronomy, University of Glasgow, Glasgow; United Kingdom
[56] LPSC, Université Grenoble Alpes, CNRS/IN2P3, Grenoble INP, Grenoble; France
[57] Laboratory for Particle Physics and Cosmology, Harvard University, Cambridge MA; United States of America
[58] [(a)] Department of Modern Physics and State Key Laboratory of Particle Detection and Electronics, University of Science and Technology of China, Hefei;[(b)] Institute of Frontier and Interdisciplinary Science and Key Laboratory of Particle Physics and Particle Irradiation (MOE), Shandong University, Qingdao;[(c)] School of Physics and Astronomy, Shanghai Jiao Tong University, Key Laboratory for Particle Astrophysics and Cosmology (MOE), SKLPPC, Shanghai;[(d)] Tsung-Dao Lee Institute, Shanghai; China
[59] [(a)] Kirchhoff-Institut für Physik, Ruprecht-Karls-Universität Heidelberg, Heidelberg;[(b)] Physikalisches Institut, Ruprecht-Karls-Universität Heidelberg, Heidelberg; Germany
[60] [(a)] Department of Physics, Chinese University of Hong Kong, Shatin, N.T., Hong Kong;[(b)] Department of Physics, University of Hong Kong, Hong Kong;[(c)] Department of Physics and Institute for Advanced Study, Hong Kong University of Science and Technology, Clear Water Bay, Kowloon, Hong Kong; China
[61] Department of Physics, National Tsing Hua University, Hsinchu; Taiwan
[62] IJCLab, Université Paris-Saclay, CNRS/IN2P3, 91405, Orsay; France
[63] Department of Physics, Indiana University, Bloomington IN; United States of America
[64] [(a)] INFN Gruppo Collegato di Udine, Sezione di Trieste, Udine;[(b)] ICTP, Trieste;[(c)] Dipartimento Politecnico di Ingegneria e Architettura, Università di Udine, Udine; Italy
[65] [(a)] INFN Sezione di Lecce;[(b)] Dipartimento di Matematica e Fisica, Università del Salento, Lecce; Italy
[66] [(a)] INFN Sezione di Milano;[(b)] Dipartimento di Fisica, Università di Milano, Milano; Italy
[67] [(a)] INFN Sezione di Napoli;[(b)] Dipartimento di Fisica, Università di Napoli, Napoli; Italy
[68] [(a)] INFN Sezione di Pavia;[(b)] Dipartimento di Fisica, Università di Pavia, Pavia; Italy
[69] [(a)] INFN Sezione di Pisa;[(b)] Dipartimento di Fisica E. Fermi, Università di Pisa, Pisa; Italy
[70] [(a)] INFN Sezione di Roma;[(b)] Dipartimento di Fisica, Sapienza Università di Roma, Roma; Italy
[71] [(a)] INFN Sezione di Roma Tor Vergata;[(b)] Dipartimento di Fisica, Università di Roma Tor Vergata, Roma; Italy
[72] [(a)] INFN Sezione di Roma Tre;[(b)] Dipartimento di Matematica e Fisica, Università Roma Tre, Roma; Italy
[73] [(a)] INFN-TIFPA;[(b)] Università degli Studi di Trento, Trento; Italy
[74] Institut für Astro- und Teilchenphysik, Leopold-Franzens-Universität, Innsbruck; Austria
[75] University of Iowa, Iowa City IA; United States of America
[76] Department of Physics and Astronomy, Iowa State University, Ames IA; United States of America
[77] Joint Institute for Nuclear Research, Dubna; Russia
[78] [(a)] Departamento de Engenharia Elétrica, Universidade Federal de Juiz de Fora (UFJF), Juiz de Fora;[(b)] Universidade Federal do Rio De Janeiro COPPE/EE/IF, Rio de Janeiro;[(c)] Instituto de Física, Universidade de São Paulo, São Paulo; Brazil
[79] KEK, High Energy Accelerator Research Organization, Tsukuba; Japan
[80] Graduate School of Science, Kobe University, Kobe; Japan
[81] [(a)] AGH University of Science and Technology, Faculty of Physics and Applied Computer Science, Krakow;[(b)] Marian Smoluchowski Institute of Physics, Jagiellonian University, Krakow; Poland
[82] Institute of Nuclear Physics Polish Academy of Sciences, Krakow; Poland
[83] Faculty of Science, Kyoto University, Kyoto; Japan
[84] Kyoto University of Education, Kyoto; Japan

JHEP06(2022)097

[85] Research Center for Advanced Particle Physics and Department of Physics, Kyushu University, Fukuoka; Japan
[86] Instituto de Física La Plata, Universidad Nacional de La Plata and CONICET, La Plata; Argentina
[87] Physics Department, Lancaster University, Lancaster; United Kingdom
[88] Oliver Lodge Laboratory, University of Liverpool, Liverpool; United Kingdom
[89] Department of Experimental Particle Physics, Jožef Stefan Institute and Department of Physics, University of Ljubljana, Ljubljana; Slovenia
[90] School of Physics and Astronomy, Queen Mary University of London, London; United Kingdom
[91] Department of Physics, Royal Holloway University of London, Egham; United Kingdom
[92] Department of Physics and Astronomy, University College London, London; United Kingdom
[93] Louisiana Tech University, Ruston LA; United States of America
[94] Fysiska institutionen, Lunds universitet, Lund; Sweden
[95] Departamento de Física Teorica C-15 and CIAFF, Universidad Autónoma de Madrid, Madrid; Spain
[96] Institut für Physik, Universität Mainz, Mainz; Germany
[97] School of Physics and Astronomy, University of Manchester, Manchester; United Kingdom
[98] CPPM, Aix-Marseille Université, CNRS/IN2P3, Marseille; France
[99] Department of Physics, University of Massachusetts, Amherst MA; United States of America
[100] Department of Physics, McGill University, Montreal QC; Canada
[101] School of Physics, University of Melbourne, Victoria; Australia
[102] Department of Physics, University of Michigan, Ann Arbor MI; United States of America
[103] Department of Physics and Astronomy, Michigan State University, East Lansing MI; United States of America
[104] B.I. Stepanov Institute of Physics, National Academy of Sciences of Belarus, Minsk; Belarus
[105] Research Institute for Nuclear Problems of Byelorussian State University, Minsk; Belarus
[106] Group of Particle Physics, University of Montreal, Montreal QC; Canada
[107] P.N. Lebedev Physical Institute of the Russian Academy of Sciences, Moscow; Russia
[108] National Research Nuclear University MEPhI, Moscow; Russia
[109] D.V. Skobeltsyn Institute of Nuclear Physics, M.V. Lomonosov Moscow State University, Moscow; Russia
[110] Fakultät für Physik, Ludwig-Maximilians-Universität München, München; Germany
[111] Max-Planck-Institut für Physik (Werner-Heisenberg-Institut), München; Germany
[112] Graduate School of Science and Kobayashi-Maskawa Institute, Nagoya University, Nagoya; Japan
[113] Department of Physics and Astronomy, University of New Mexico, Albuquerque NM; United States of America
[114] Institute for Mathematics, Astrophysics and Particle Physics, Radboud University/Nikhef, Nijmegen; Netherlands
[115] Nikhef National Institute for Subatomic Physics and University of Amsterdam, Amsterdam; Netherlands
[116] Department of Physics, Northern Illinois University, DeKalb IL; United States of America
[117] [(a)] Budker Institute of Nuclear Physics and NSU, SB RAS, Novosibirsk;[(b)] Novosibirsk State University Novosibirsk; Russia
[118] Institute for High Energy Physics of the National Research Centre Kurchatov Institute, Protvino; Russia
[119] Institute for Theoretical and Experimental Physics named by A.I. Alikhanov of National Research Centre "Kurchatov Institute", Moscow; Russia
[120] [(a)] New York University Abu Dhabi, Abu Dhabi;[(b)] United Arab Emirates University, Al Ain;[(c)] University of Sharjah, Sharjah; United Arab Emirates
[121] Department of Physics, New York University, New York NY; United States of America
[122] Ochanomizu University, Otsuka, Bunkyo-ku, Tokyo; Japan
[123] Ohio State University, Columbus OH; United States of America
[124] Homer L. Dodge Department of Physics and Astronomy, University of Oklahoma, Norman OK; United States of America
[125] Department of Physics, Oklahoma State University, Stillwater OK; United States of America

JHEP06(2022)097

[126] Palacký University, Joint Laboratory of Optics, Olomouc; Czech Republic
[127] Institute for Fundamental Science, University of Oregon, Eugene, OR; United States of America
[128] Graduate School of Science, Osaka University, Osaka; Japan
[129] Department of Physics, University of Oslo, Oslo; Norway
[130] Department of Physics, Oxford University, Oxford; United Kingdom
[131] LPNHE, Sorbonne Université, Université Paris Cité, CNRS/IN2P3, Paris; France
[132] Department of Physics, University of Pennsylvania, Philadelphia PA; United States of America
[133] Konstantinov Nuclear Physics Institute of National Research Centre "Kurchatov Institute", PNPI, St. Petersburg; Russia
[134] Department of Physics and Astronomy, University of Pittsburgh, Pittsburgh PA; United States of America
[135] [(a)] Laboratório de Instrumentação e Física Experimental de Partículas — LIP, Lisboa;[(b)] Departamento de Física, Faculdade de Ciências, Universidade de Lisboa, Lisboa;[(c)] Departamento de Física, Universidade de Coimbra, Coimbra;[(d)] Centro de Física Nuclear da Universidade de Lisboa, Lisboa;[(e)] Departamento de Física, Universidade do Minho, Braga;[(f)] Departamento de Física Teórica y del Cosmos, Universidad de Granada, Granada (Spain);[(g)] Instituto Superior Técnico, Universidade de Lisboa, Lisboa; Portugal
[136] Institute of Physics of the Czech Academy of Sciences, Prague; Czech Republic
[137] Czech Technical University in Prague, Prague; Czech Republic
[138] Charles University, Faculty of Mathematics and Physics, Prague; Czech Republic
[139] Particle Physics Department, Rutherford Appleton Laboratory, Didcot; United Kingdom
[140] IRFU, CEA, Université Paris-Saclay, Gif-sur-Yvette; France
[141] Santa Cruz Institute for Particle Physics, University of California Santa Cruz, Santa Cruz CA; United States of America
[142] [(a)] Departamento de Física, Pontificia Universidad Católica de Chile, Santiago;[(b)] Instituto de Investigación Multidisciplinario en Ciencia y Tecnología, y Departamento de Física, Universidad de La Serena;[(c)] Universidad Andres Bello, Department of Physics, Santiago;[(d)] Instituto de Alta Investigación, Universidad de Tarapacá, Arica;[(e)] Departamento de Física, Universidad Técnica Federico Santa María, Valparaíso; Chile
[143] Universidade Federal de São João del Rei (UFSJ), São João del Rei; Brazil
[144] Department of Physics, University of Washington, Seattle WA; United States of America
[145] Department of Physics and Astronomy, University of Sheffield, Sheffield; United Kingdom
[146] Department of Physics, Shinshu University, Nagano; Japan
[147] Department Physik, Universität Siegen, Siegen; Germany
[148] Department of Physics, Simon Fraser University, Burnaby BC; Canada
[149] SLAC National Accelerator Laboratory, Stanford CA; United States of America
[150] Department of Physics, Royal Institute of Technology, Stockholm; Sweden
[151] Departments of Physics and Astronomy, Stony Brook University, Stony Brook NY; United States of America
[152] Department of Physics and Astronomy, University of Sussex, Brighton; United Kingdom
[153] School of Physics, University of Sydney, Sydney; Australia
[154] Institute of Physics, Academia Sinica, Taipei; Taiwan
[155] [(a)] E. Andronikashvili Institute of Physics, Iv. Javakhishvili Tbilisi State University, Tbilisi;[(b)] High Energy Physics Institute, Tbilisi State University, Tbilisi; Georgia
[156] Department of Physics, Technion, Israel Institute of Technology, Haifa; Israel
[157] Raymond and Beverly Sackler School of Physics and Astronomy, Tel Aviv University, Tel Aviv; Israel
[158] Department of Physics, Aristotle University of Thessaloniki, Thessaloniki; Greece
[159] International Center for Elementary Particle Physics and Department of Physics, University of Tokyo, Tokyo; Japan
[160] Department of Physics, Tokyo Institute of Technology, Tokyo; Japan
[161] Tomsk State University, Tomsk; Russia
[162] Department of Physics, University of Toronto, Toronto ON; Canada

JHEP06(2022)097

[163] [(a)] TRIUMF, Vancouver BC; [(b)] Department of Physics and Astronomy, York University, Toronto ON; Canada
[164] Division of Physics and Tomonaga Center for the History of the Universe, Faculty of Pure and Applied Sciences, University of Tsukuba, Tsukuba; Japan
[165] Department of Physics and Astronomy, Tufts University, Medford MA; United States of America
[166] Department of Physics and Astronomy, University of California Irvine, Irvine CA; United States of America
[167] Department of Physics and Astronomy, University of Uppsala, Uppsala; Sweden
[168] Department of Physics, University of Illinois, Urbana IL; United States of America
[169] Instituto de Física Corpuscular (IFIC), Centro Mixto Universidad de Valencia — CSIC, Valencia; Spain
[170] Department of Physics, University of British Columbia, Vancouver BC; Canada
[171] Department of Physics and Astronomy, University of Victoria, Victoria BC; Canada
[172] Fakultät für Physik und Astronomie, Julius-Maximilians-Universität Würzburg, Würzburg; Germany
[173] Department of Physics, University of Warwick, Coventry; United Kingdom
[174] Waseda University, Tokyo; Japan
[175] Department of Particle Physics and Astrophysics, Weizmann Institute of Science, Rehovot; Israel
[176] Department of Physics, University of Wisconsin, Madison WI; United States of America
[177] Fakultät für Mathematik und Naturwissenschaften, Fachgruppe Physik, Bergische Universität Wuppertal, Wuppertal; Germany
[178] Department of Physics, Yale University, New Haven CT; United States of America

[a] Also at Borough of Manhattan Community College, City University of New York, New York NY; United States of America
[b] Also at Bruno Kessler Foundation, Trento; Italy
[c] Also at Center for High Energy Physics, Peking University; China
[d] Also at Centro Studi e Ricerche Enrico Fermi; Italy
[e] Also at CERN, Geneva; Switzerland
[f] Also at Département de Physique Nucléaire et Corpusculaire, Université de Genève, Genève; Switzerland
[g] Also at Departament de Fisica de la Universitat Autonoma de Barcelona, Barcelona; Spain
[h] Also at Department of Financial and Management Engineering, University of the Aegean, Chios; Greece
[i] Also at Department of Physics and Astronomy, Michigan State University, East Lansing MI; United States of America
[j] Also at Department of Physics and Astronomy, University of Louisville, Louisville, KY; United States of America
[k] Also at Department of Physics, Ben Gurion University of the Negev, Beer Sheva; Israel
[l] Also at Department of Physics, California State University, East Bay; United States of America
[m] Also at Department of Physics, California State University, Fresno; United States of America
[n] Also at Department of Physics, California State University, Sacramento; United States of America
[o] Also at Department of Physics, King's College London, London; United Kingdom
[p] Also at Department of Physics, St. Petersburg State Polytechnical University, St. Petersburg; Russia
[q] Also at Department of Physics, University of Fribourg, Fribourg; Switzerland
[r] Also at Faculty of Physics, M.V. Lomonosov Moscow State University, Moscow; Russia
[s] Also at Faculty of Physics, Sofia University, 'St. Kliment Ohridski', Sofia; Bulgaria
[t] Also at Graduate School of Science, Osaka University, Osaka; Japan
[u] Also at Hellenic Open University, Patras; Greece
[v] Also at Institucio Catalana de Recerca i Estudis Avancats, ICREA, Barcelona; Spain
[w] Also at Institut für Experimentalphysik, Universität Hamburg, Hamburg; Germany
[x] Also at Institute for Particle and Nuclear Physics, Wigner Research Centre for Physics, Budapest; Hungary
[y] Also at Institute of Particle Physics (IPP); Canada

JHEP06(2022)097

[z] Also at Institute of Physics, Azerbaijan Academy of Sciences, Baku; Azerbaijan
[aa] Also at Institute of Theoretical Physics, Ilia State University, Tbilisi; Georgia
[ab] Also at Instituto de Fisica Teorica, IFT-UAM/CSIC, Madrid; Spain
[ac] Also at Istanbul University, Dept. of Physics, Istanbul; Turkey
[ad] Also at Joint Institute for Nuclear Research, Dubna; Russia
[ae] Also at Moscow Institute of Physics and Technology State University, Dolgoprudny; Russia
[af] Also at National Research Nuclear University MEPhI, Moscow; Russia
[ag] Also at Physics Department, An-Najah National University, Nablus; Palestine
[ah] Also at Physikalisches Institut, Albert-Ludwigs-Universität Freiburg, Freiburg; Germany
[ai] Also at The City College of New York, New York NY; United States of America
[aj] Also at TRIUMF, Vancouver BC; Canada
[ak] Also at Università di Napoli Parthenope, Napoli; Italy
[al] Also at University of Chinese Academy of Sciences (UCAS), Beijing; China
[am] Also at Yeditepe University, Physics Department, Istanbul; Turkey
[*] Deceased

JHEP06(2022)097

LHCP2023 - (other lhcp conferences)

for readers

22-26 May 2023
Belgrade, Serbia
published July 18, 2024

Entries on ADS

The eleventh annual Large Hadron Collider Physics (LHCP2023) conference will be held in Belgrade, Serbia from 22nd to 27th May 2023. The LHCP conference series started in 2013 as a successful fusion of two international conferences, "Physics at the Large Hadron Collider Conference" and the "Hadron Collider Physics Symposium". The conference programme will contain a detailed review of the latest experimental and theoretical results on the collider physics, including the results of the Large Hadron Collider Run II and Run III (LHC at CERN, Geneva), and discussions on further research directions within the high energy particle physics community, both in theory and experiment. The main goal of the conference is to provide intense and lively discussions between experimenters and theorists in research areas as the Standard Model Physics and Beyond, the Higgs Boson Physics, Supersymmetry, Heavy Quark Physics and Heavy Ion Physics, as well as to share recent progress in the high luminosity upgrades of LHC and future collider developments.

Editorial Board

1. Jelena Jovicevic, Jelena.Jovicevic@cern.ch, Institute of Physics Belgrade.
2. Nikola Konjik, konjik@ipb.ac.rs, Faculty of Physics, University of Belgrade
3. Igor Salom, isalom@ipb.ac.rs, Institute of Physics Belgrade
4. Lidija Zivkovic, Lidija.Zivkovic@cern.ch, Institute of Physics Belgrade
5. Predrag Milenovic, Predrag.Milenovic@cern.ch, Faculty of Physics, University of Belgrade

Sessions
session Upgrades and Future Projects
session Top Physics
session QCD Physics
session Performance and Tools
session Outreach, Diversity and Education

International Meeting

Excited QCD

Sicily, Italy, 23–29 October, 2022

Sponsored by:

Istituto Nazionale di Fisica Nucleare
The Center for Exploration of Energy and Matter of Indiana University

ALESSANDRO PILLONI
PEDRO BICUDO
ROMAN HÖLLWIESER
JELENA JOVIĆEVIĆ
ROBERT KAMIŃSKI
MARINA MARINKOVIĆ
Editors of the Proceedings

ORGANIZING COMMITTEE

Alessandro Pilloni
Jelena Jovićević
Robert Kamiński
Marina Marinković
Nuno Cardoso
Pedro Bicudo
Roman Höllwieser

Simplified template cross sections – Stage 1.1 and 1.2

Nicolas Berger[1], Claudia Bertella[2,3], Matteo Bonanomi[4], Nihal Brahimi[1], Thomas P. Calvet[5], Milene Calvetti[6], Valerio Dao[2], Marco Delmastro[1], Michael Duehrssen-Debling[2], Paolo Francavilla[6], Yacine Haddad[7], Sarah Heim[8,4], Jelena Jovicevic[9], Oleh Kivernyk[1], Maria Moreno Llacer[10], Jonathon M. Langford[11], Changqiao Li[12], Giovanni Marchiori[13], Josh A. McFayden[14], Johannes K. L. Michel[15], Predrag Milenovic[2,16], Carlo E. Pandini[2], Edward Scott[11], Frank J. Tackmann[8], Kerstin Tackmann[8,4], Lorenzo Viliani[17], Meng Xiao[18], and Hongtao Yang[12]

Part of the Regular Reports Collection
published in the LHC Higgs Working Group Reports Series

Abstract

Simplified Template Cross Sections (STXS) have been adopted by the LHC experiments as a common framework for Higgs measurements. Their purpose is to reduce the theoretical uncertainties that are directly folded into the measurements as much as possible, while at the same time allowing for the combination of the measurements between different decay channels as well as between experiments. We report the complete, revised definition of the STXS kinematic bins (stage 1.1 and stage 1.2), which have been used for the measurements by the ATLAS and CMS experiments using the full LHC Run 2 datasets. The main focus is on the four dominant Higgs production processes, namely gluon-fusion, vector-boson fusion, production in association with a vector boson and in association with a $t\bar{t}$ pair. We also comment briefly on the treatment of other production modes.

Copyright N. Berger *et al.*
This work is licensed under the Creative Commons Attribution 4.0 International License.
Published by the SciPost Foundation.

Received 2025-07-11
Accepted 2025-12-04
Published 2026-01-07
doi:10.21468/SciPostPhysCommRep.15

1 LAPP, Annecy, France
2 CERN, Geneva, Switzerland
3 Institute of High Energy Physics, Chinese Academy of Sciences, Beijing, China
4 University of Hamburg, Hamburg, Germany
5 Stony Brook University, Stony Brook, NY, USA
6 Università and INFN Sezione di Pisa, Pisa, Italy
7 Northeastern University, Boston, MA, USA
8 Deutsches Elektronen-Synchrotron (DESY), Hamburg, Germany
9 Institute of Physics Belgrade, Belgrade, Serbia
10 University of Valencia and CSIC, Spain
11 Imperial College, London, United Kingdom
12 University of Science and Technology of China, Hefei, China
13 LPNHE, Sorbonne Université, Paris Diderot Sorbonne Paris Cité, CNRS/IN2P3, Paris, France

14 University of Sussex, Brighton, United Kingdom
15 University of Amsterdam, Amsterdam, Netherlands
16 University of Belgrade, Belgrade, Serbia
17 Università and INFN Sezione di Firenze, Firenze, Italy
18 Johns Hopkins University, Baltimore, MD, USA

Contents

1 Introduction **2**

2 Overview **3**
2.1 Sub-bin boundaries for theory uncertainties 4

3 Definition of final-state objects **5**
3.1 Higgs boson 5
3.2 Leptons and leptonically decaying vector bosons 5
3.3 Jets 6

4 Bin definitions **6**
4.1 Gluon-fusion Higgs production ($gg \to H$) 6
4.2 Electroweak qqH production (VBF + hadronic VH) 8
4.3 Associated Higgs production (leptonic VH) 10
4.4 $t\bar{t}H$ production 11
4.5 Other production modes 11
4.5.1 $b\bar{b} \to H$ production 11
4.5.2 tH production 11

5 Conclusions **12**

References **12**

1 Introduction

Simplified Template Cross Sections (STXS) have been adopted by the LHC experiments as an evolution of the signal strength measurements performed during Run 1 of the LHC. They were first discussed in detail in Section III.3 of [1] and Section III.2 of [2]. Their purpose is twofold. They provide more fine-grained measurements for individual Higgs production modes in various kinematic regions, and reduce the theoretical uncertainties that are directly folded into the measurements. At the same time, they allow for the use of multivariate analysis techniques and provide a common framework for the combination of measurements in different decay channels and eventually between experiments. Currently, STXS measurements are available in all five major Higgs decay channels, namely $H \to \gamma\gamma$ [3,4], $H \to ZZ^* \to 4\ell$ [5,6], $H \to WW^* \to 2\ell 2\nu$ [7,8], $H \to \tau\tau$ [9,10], and $H \to b\bar{b}$ [11–13] (only shortly after its discovery [14,15]), as well as from the combination of several decay channels [16–20]. Both

individual and combined STXS measurements can then be used as inputs for subsequent interpretations in and beyond the Standard Model (SM). This can be the determination of overall signal strengths or coupling scale factors, SMEFT coefficients, or tests of specific BSM models, see for example [21–25].

After the first successful STXS measurements and the experience gained from them, several refinements to the definitions of the kinematic STXS bins given in [1, 2] (henceforth referred to as stage 1.0) were necessary. This paper provides the complete and revised definitions of the STXS bins, referred to as stage 1.1 and its subsequent further refinement stage 1.2. They are the result of many fruitful discussions and dedicated studies by members of the ATLAS and CMS experiments and the theory community. The STXS stages 1.1 and 1.2 presented here have been agreed upon in the context of the LHC Higgs Cross Section Working Group, and they have been used as the baseline for the measurements based on the full Run 2 datasets by ATLAS and CMS.

As discussed in more detail in Section 4.2, the vector-boson fusion (VBF) process in particular required a substantial reorganization compared to the previous stage 1.0 to be able to better exploit the potential improvements in the full Run 2 measurements for this process. For this reason, the changes are also not backward compatible with the previous stage 1.0, in the sense that they do not just correspond to a splitting of the previously defined bins. This also lead to corresponding changes in the VBF-like bins of the gluon-fusion ($gg \to H$) process. All other refinements for the $gg \to H$ and VH processes are backward-compatible with stage 1.0.

The remainder of this paper is organized as follows. In Section 2, we briefly review the main features and goals of the STXS framework. In Section 3, we summarize the truth definitions of the relevant final-state objects, namely leptons, jets, and the Higgs boson itself. In Section 4, we give the complete bin definitions for $gg \to H$ (Section 4.1), electroweak qqH production (Section 4.2), leptonic VH production (Section 4.3), and $t\bar{t}H$ production (Section 4.4). In Section 4.5, we briefly comment on the current treatment of $b\bar{b} \to H$ and tH production. We conclude in Section 5.

2 Overview

The STXS are physical cross sections (in contrast to e.g. signal strengths). They are defined in mutually exclusive regions of phase space ("bins"). Their primary features and design goals are briefly reviewed in the following.

First, the kinematic cuts defining the bins are abstracted and simplified compared to the exact fiducial volumes of the individual analyses in different Higgs decay channels. In particular, the STXS are defined inclusively in the Higgs boson decay (up to an overall cut on the rapidity of the Higgs boson). The measurements are unfolded to the STXS bins, which are common for all analyses. This is the key feature that allows for a subsequent global combination of all measurements in different decay channels as well as from ATLAS and CMS. When combining measurements in different decay channels, one can either assume the SM branching ratios or consider the ratios of the branching ratios as additional free parameters.

While being simplified to allow for the combination of different measurements, the bin definitions nevertheless try to be as close as possible to the typical experimental kinematic selections or more generally the kinematic regions that dominate the experimental sensitivity. The goal is to allow for the use of advanced analysis techniques such as event categorization or multivariate techniques in order to achieve maximal sensitivity, while still keeping the unfolding uncertainties small. In particular, an important goal is to avoid any unnecessary extrapolations and as much as possible reduce the dependence on theory predictions and uncertainties that are folded into the measurements.

The second key feature of STXS is that they are defined for specific production modes, with the SM production processes serving as kinematic templates. This separation into production modes is an essential aspect to reduce the model dependence, i.e., to eliminate the dependence of the measurements on the relative fractions of the production modes in the SM.

From the above discussion it should be clear that STXS measurements should not replace measurements of fully fiducial and differential cross sections in individual decay channels. Rather, they complement each other and are optimized for somewhat different purposes. In particular, the STXS allow testing the SM in the kinematics of the different Higgs production modes with an improved sensitivity from combining all decay channels.

For the concrete definitions of the STXS bins, several considerations have to be taken into account. The key goals are to

- minimize the dependence on theory uncertainties that are folded into the measurements,
- maximize the experimental sensitivity,
- isolate possible BSM effects,
- and limit the number of bins to match the experimental sensitivity.

The last point in particular deserves to be stressed, as it is an important practical consideration. It is often in direct competition with the other requirements, and so they must be balanced against each other. In practice, for an analysis to contribute to the global combination, it needs to implement the complete split at the truth level, even if it only measures a small subset of bins. Therefore, keeping the number of bins at a manageable level is essential to facilitate the practical implementation and keep the required overhead manageable for all analyses. In addition, it reduces the technical complications that arise when one has to statistically combine many weakly constrained or unconstrained measurements.

The number of separately measured bins can evolve with time, such that the measurements can become more fine-grained as the size of the available dataset increases. For this purpose, different stages are defined, corresponding to increasingly fine-grained measurements. The stage 0 bin definitions essentially correspond to the production mode measurements of Run 1. The stages 1.1 and 1.2 reported here update the original stage 1.0, and target the full Run 2 measurements. Compared to stage 1.1, in stage 1.2 the $gg \to H$ binning has been extended and a binning for the $t\bar{t}H$ process has been added. It should be stressed that the goal is not that the complete set of bins should be measurable by any single analysis, but rather that the full granularity should become accessible in the combination of all decay channels with the full Run 2 dataset. In individual analyses several bins can be merged and only their sum be measured according to the sensitivity of each analysis and decay channel.

2.1 Sub-bin boundaries for theory uncertainties

One important goal is to reduce the theory dependence of the measurements. First, this requires avoiding that the measurements have to extrapolate from a certain measured region in phase space to a much larger region of phase space, in particular when such an extrapolation entails nontrivial theory uncertainties. More generally, it requires avoiding cases with a large variation in the experimental acceptance or sensitivity within a given bin, as this introduces a direct dependence on the theory predictions for the kinematic distribution of the signal within that bin. Ideally, if such a residual theory dependence becomes a relevant source of uncertainty, the bin in question can be split further into two or more smaller bins, which moves this theory dependence on the signal distribution from the measurement into the interpretation step.

However, within many experimental analyses, the theory uncertainties on the predictions of the STXS bins, which by default should only enter in the interpretation step, do explicitly reenter the measurements whenever two bins have to be merged, e.g., due to limited statistics

or separation power. For this reason, in practice, a common treatment of theory uncertainties for all bins is important already for the measurements, even if just to know where the uncertainties are and whether two bins can be safely merged if needed or whether they should be kept split if at all possible. The detailed treatment of theory uncertainties is beyond the scope of this work and will be discussed in a separate document in preparation.

However, it is important to realize that the same basic issue also arises for the residual theory uncertainties on the signal distribution within a bin. To test and account for this dependence, essentially the same theoretical guidance is needed. For this purpose, stages 1.1 and 1.2 introduce additional sub-bin boundaries. They are meant for tracking a potential dominant source of residual theory uncertainties within a given bin. They can be viewed as potential future boundaries where a bin could be split if it becomes necessary. Defining the sub-bin boundaries already at this stage has several advantages. First, it allows for a smoother evolution of the binning, since the experimental and theoretical implementation for the new bin will already be in place in case it gets split. Secondly, it puts the treatment of the residual theory uncertainties within a not-yet split bin on a common footing with the treatment of the explicit theory uncertainties that enter in the merging of two bins. Overall, this makes the framework more robust since after all the distinction between these two cases is ultimately a matter of convention.

3 Definition of final-state objects

Usually, the measured event categories in all decay channels are unfolded by a fit to the STXS bins. For this purpose, and for the comparison between the measured bins and theoretical predictions from either analytic calculations or Monte Carlo (MC) simulations, the truth final state particles need to be defined unambiguously. The definition of the final-state objects, namely leptons, jets, and in particular the Higgs boson itself, are explicitly kept simpler and more idealized than in the fiducial cross section measurements. Treating the Higgs boson as on-shell final-state particle is what allows for the combination of the different decay channels.

3.1 Higgs boson

The STXS are defined for the production of an on-shell Higgs boson, and the unfolding should be done accordingly. A global cut on the Higgs rapidity at $|Y_H| < 2.5$ is included in all bins. As the current measurements have no sensitivity beyond this rapidity range, this part of phase space would only be extrapolated by the MC simulation. On the other hand, it is in principle possible to use electrons at very forward rapidities (up to $|\eta| \sim 5$) in $H \to ZZ^* \to 4\ell$ and extend the accessible rapidity range. For this purpose, an additional otherwise inclusive bin for $|Y_H| > 2.5$ can be included for each production process. This forward bin is not explicitly included in the following.

3.2 Leptons and leptonically decaying vector bosons

Leptonically decaying vector bosons, e.g. from VH production, are defined from the sum of all their leptonic decay products including neutrinos. Electrons and muons from such vector-boson decays are defined as dressed, i.e., all FSR photons should be added back to the electron or muon. There should be no restriction on the transverse momentum or the rapidity of the leptons. That is, for a leptonically decaying vector boson the full decay phase space is included. Similarly, if leptonic decays to τ leptons are considered, the τ is defined from the sum of all its decay products for any τ decay mode.

3.3 Jets

Truth jets are defined as anti-k_T jets with a jet radius of $R = 0.4$, and are built from all stable particles, including neutrinos, photons, and leptons from hadron decays or produced in the shower. Stable particles here have the usual definition, having a lifetime greater than 10 ps, i.e., those particles that are passed to GEANT4 in the experimental simulation chain.

All decay products from the Higgs boson decay are removed from the inputs to the jet algorithm, as they are accounted for by the truth Higgs boson. Similarly, all decay products from leptonic decays of signal V bosons are removed, as they are treated separately. In contrast, the decay products from hadronically decaying signal V bosons are included in the inputs to the truth jet building.

By default, truth jets are defined without restriction on their rapidity. A possible cut on the jet rapidity can be included in the bin definition. Unless otherwise specified, a common $p_T = 30\,\text{GeV}$ threshold for jets is used for all truth jets. In principle, a lower threshold would have the advantage to split the events more evenly between the different jet bins. Experimentally, a higher threshold at 30 GeV is favored to suppress jets from pile-up interactions, and is therefore used for the jet definition to limit the amount of extrapolation in the measurements.

4 Bin definitions

In this section, we give the explicit definitions of the stage 1.1 and 1.2 bins, where stage 1.2 provides an extension of stage 1.1. The sub-bin boundaries as discussed in Section 2.1 are included in the definitions and are indicated by dashed lines in the diagrams.

4.1 Gluon-fusion Higgs production ($gg \to H$)

The gluon-fusion template process is defined in the usual way based on the Born $gg \to H$ process plus higher-order QCD and electroweak corrections. Typically, calculations only include the virtual electroweak corrections to the Born $gg \to H$ process. We stress that here it also includes real electroweak radiation, so in particular the $gg \to Z(\to q\bar{q})H$ process.

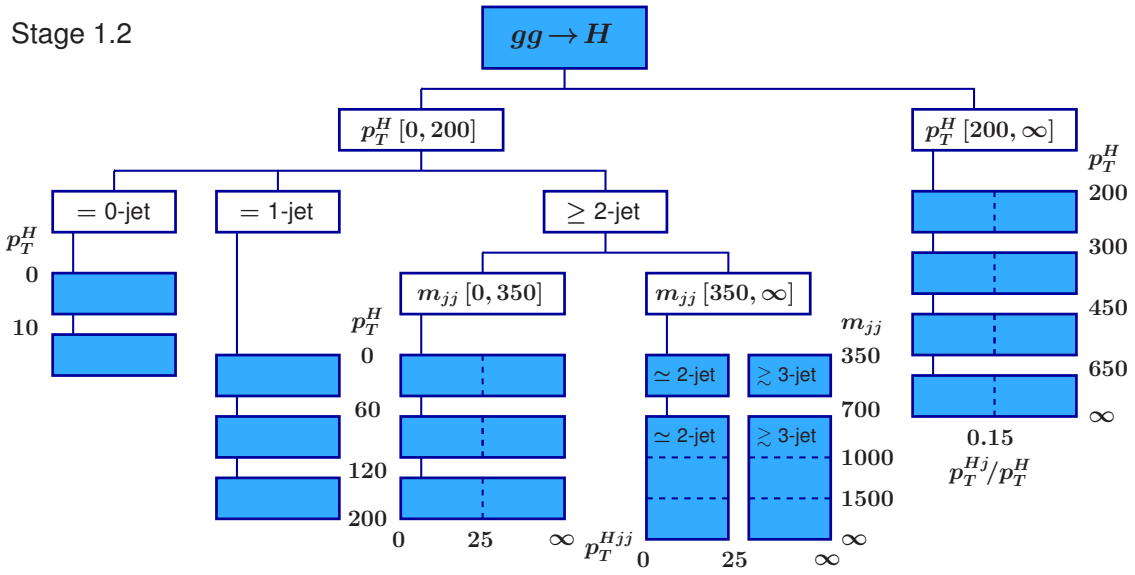

Figure 1: Stage 1.2 bins for gluon-fusion Higgs production $gg \to H$. In stage 1.1 all bins at $p_T^H > 200\,\text{GeV}$ were merged into a single bin.

The changes with respect to the previous stage 1.0 are primarily in the treatment of the BSM sensitive high-p_T region, which is now split out directly as the first cut, and in a modified $N_j \geq 2$ selection matching the changes for the VBF production (see Section 4.2). Although the selection order has changed with respect to stage 1.0, the bins that describe the bulk of the $gg \to H$ production are unchanged.

The stage 1.2 bins are depicted in Figure 1 and are described briefly in the following:

- The cross section is first split into $\boxed{p_T^H < 200\,\text{GeV}}$ and $\boxed{p_T^H > 200\,\text{GeV}}$ bins. The high-p_T^H region is split out first now to better enable its dedicated treatment.
  - The $\boxed{p_T^H > 200\,\text{GeV}}$ bin is primarily sensitive to BSM effects. In stage 1.0, it was part of the 1-jet and $\geq$ 2-jet bins, but in most experimental analyses it is actually merged across jet bins. This was a single bin with $p_T^H > 200\,\text{GeV}$ in stage 1.1, while in stage 1.2 it is further split into four bins, using $p_T^H = 300, 400, 650\,\text{GeV}$ as bin boundaries, to increase the sensitivity to the tails of the p_T^H distribution, which can be probed by dedicated boosted analyses.
    An additional sub-bin at $p_T^{Hj}/p_T^H = 0.15$ is also introduced to more evenly divide the cross section, and to avoid increasingly large theory uncertainties that would otherwise arise from the large scale separation between a fixed jet p_T threshold and the hard scale set by p_T^H.
  - The $\boxed{p_T^H < 200\,\text{GeV}}$ bin contains most of the cross section and is the starting point for the remaining binning.
- The $\boxed{p_T^H < 200\,\text{GeV}}$ bin is split into $\boxed{0\text{-jet}}$, $\boxed{1\text{-jet}}$, and $\boxed{\geq 2\text{-jet}}$ bins, similarly to the stage 1.0 splitting.
  - Compared to stage 1.0, the $\boxed{0\text{-jet}}$ bin is split into two p_T^H bins with a boundary at $p_T^H = 10\,\text{GeV}$ to probe the very low p_T region of Higgs production, which contains a sizeable fraction of the cross section.
  - The $\boxed{1\text{-jet}}$ bin is split into 3 p_T^H bins with boundaries at $p_T^H = 60$ and $120\,\text{GeV}$, which are unchanged with respect to stage 1.0.
  - The $\boxed{\geq 2\text{-jet}}$ bin is slightly reorganized with a more dedicated split into low-m_{jj} and high-m_{jj} regions.
- The $\boxed{\geq 2\text{-jet}}$ bin is split into low-m_{jj} and high-m_{jj} bins with $\boxed{m_{jj} < 350\,\text{GeV}}$ and $\boxed{m_{jj} > 350\,\text{GeV}}$, following the analogous cuts in the VBF bins. In stage 1.0, the analogous separation was implicit and it has now been made explicit. (As for the VBF bins described in Section 4.2, the m_{jj} cut has been lowered from 400 GeV to 350 GeV and the $|\Delta\eta_{jj}|$ cut has been dropped.)

  In addition, a bin boundary is defined at $p_T^{Hjj} = 25\,\text{GeV}$, which provides a separation into 2-jet like and $\geq$ 3-jet like phase-space regions to facilitate the uncertainty treatment for $gg \to H$ as background to VBF.
  - The $\boxed{m_{jj} < 350\,\text{GeV}}$ bin contains the bulk of the $\geq$ 2-jet region. It is further split into 3 p_T^H bins with boundaries at $p_T^H = 60$ and $120\,\text{GeV}$, aligned with the 1-jet bin.

This allows for an almost inclusive measurement of the $gg \to H$ p_T^H spectrum in combination with the other jet bins. The p_T^{Hjj} boundary here is kept as a sub-bin boundary.

– The $\boxed{m_{jj} > 350\,\text{GeV}}$ bin contains only a small fraction of the total $gg \to H$ cross section, which however constitutes the main background to VBF production. Hence it uses the same splitting as the corresponding high-m_{jj} VBF bin in Section 4.2 with boundaries defined at $m_{jj} = 700, 1000$, and $1500\,\text{GeV}$. Currently, the $m_{jj} = 700\,\text{GeV}$ boundary defines an explicit bin separation, while the higher m_{jj} boundaries are kept as sub-bins. The p_T^{Hjj} boundary is an explicit bin separation.

4.2 Electroweak qqH production (VBF + hadronic VH)

The VBF template process is defined more precisely as electroweak qqH production. It includes the usual VBF topology and also the $pp \to V(\to q\bar{q})H$ topology with hadronic $V \to q\bar{q}$ decays. The two topologies lead to the same final state through the same interactions and therefore represent the t-channel and s-channel contributions to the same physical process. Hence, they can only be distinguished by enriching one or the other type of contribution via kinematic cuts, which is achieved by the STXS bins as described below.

The changes compared to the previous stage 1.0 is the treatment of the BSM sensitive high-p_T region (which is now split out after the m_{jj} separation), a more fine-grained m_{jj} binning along with dropping the additional $|\Delta\eta_{jj}|$ cut, and the separation of the previous "Rest"-bin, which contained a combination of different jet topologies and kinematic regions. These are now separated to allow for an easier treatment, in particular for the estimation of theory uncertainties.

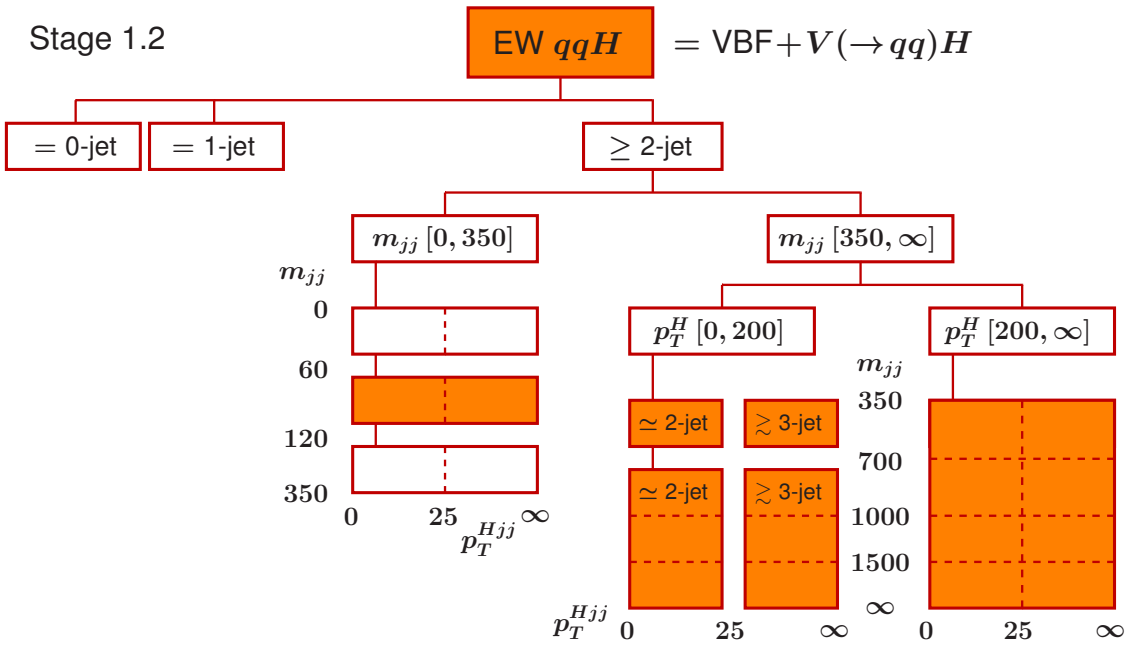

Figure 2: Stage 1.2 bins for electroweak qqH production, VBF+$V(\to qq)H$. The stage 1.1 bins are identical.

The stage 1.2 bins, identical to the stage 1.1 ones, are depicted in Figure 2 and are described briefly in the following:

- The cross section is first split into $\boxed{\text{0-jet}}$, $\boxed{\text{1-jet}}$, and $\boxed{\geq \text{2-jet}}$ bins.
  - The $\boxed{\text{0-jet}}$ and $\boxed{\text{1-jet}}$ bins are very hard to access experimentally, and are likely to remain merged. It might be possible to get some sensitivity to the $\boxed{\text{1-jet}}$ bin using dedicated analyses. Previously they where included in the "Rest" bin.
  - The $\boxed{\geq \text{2-jet}}$ bin is the starting point for the remaining binning.
- The $\boxed{\geq \text{2-jet}}$ bin is split into low-m_{jj} and high-m_{jj} bins with $\boxed{m_{jj} < 350\,\text{GeV}}$ and $\boxed{m_{jj} > 350\,\text{GeV}}$, respectively.
  - The $\boxed{m_{jj} < 350\,\text{GeV}}$ bin was previously part of the "Rest"-bin as well as the previous "VH"-bin. In this kinematic region, contributions from the actual VBF process of interest are still very hard to distinguish from the overwhelming gluon-fusion background. This bin is split into 3 m_{jj} regions with cuts at $m_{jj} = 60$ and 120 GeV. The middle $\boxed{60\,\text{GeV} < m_{jj} < 120\,\text{GeV}}$ bin targets the hadronic VH-like production. (It is equivalent to the previous "VH"-bin.) In addition, sub-bin boundaries at $p_T^{Hjj} = 25\,\text{GeV}$ are defined for all m_{jj} bins, primarily for consistency with the higher m_{jj} bins.
  - The $\boxed{m_{jj} > 350\,\text{GeV}}$ bin targets the nominal VBF production process. Compared to the previous "VBF"-bin, the m_{jj} threshold is slightly lowered (from previously 400 GeV) to capture more of the VBF signal. Furthermore, the $|\Delta\eta_{jj}|$ cut is dropped in favor of a more fine-grained m_{jj} binning. This allows one to better account for the fact that different analyses can have substantially different sensitivities to different m_{jj} regions. It also allows for an easier treatment of theory uncertainties, which can now be based on considering the one-dimensional m_{jj} spectrum.
- The $\boxed{m_{jj} > 350\,\text{GeV}}$ bin is split into low-p_T^H and high-p_T^H bins with $\boxed{p_T^H < 200\,\text{GeV}}$ and $\boxed{p_T^H > 200\,\text{GeV}}$, respectively. The p_T separation is moved inside the nominal VBF-like region to allow for a better isolation of the high-p_T region of the actual VBF process. In addition, the p_T variable is changed from the p_T of the leading jet, which was used in stage 1.0, to the p_T^H of the Higgs boson. The sensitivity to possible BSM effects at high p_T is roughly similar for both variables. On the other hand, using p_T^H has the important advantage that it better aligns with the use of p_T^H in the $gg \to H$ bins, which have a large cross section and are hard to distinguish experimentally from the VBF process in this kinematic region. This allows for a much cleaner merging of corresponding bins across the VBF and $gg \to H$ processes if necessary.

  The bin has m_{jj} boundaries defined at $m_{jj} = 700, 1000$, and 1500 GeV. In addition, it has a bin boundary defined at $p_T^{Hjj} = 25\,\text{GeV}$, which provides a separation into 2-jet like and $\geq$ 3-jet like phase-space regions (as in stage 1.0), which is essential for the discrimination against the large gluon-fusion contributions.

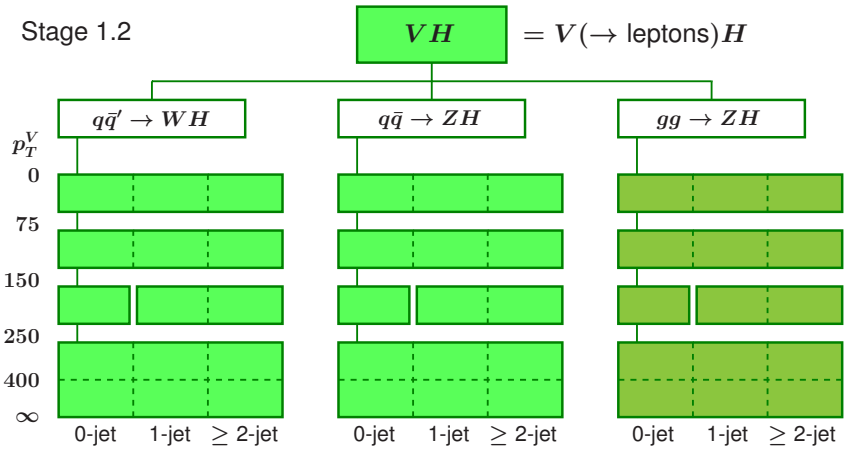

Figure 3: Stage 1.2 bins for VH production, $V(\to \text{leptons})H$. The stage 1.1 bins are identical.

- The $\boxed{p_T^H < 200\,\text{GeV}}$ bin contains most of the (accessible) VBF signal. The $m_{jj} = 700\,\text{GeV}$ boundary is an explicit bin separation, while the higher m_{jj} boundaries are kept as sub-bins at the current stage. The p_T^{Hjj} boundary is an explicit bin separation. Hence, a total of four bins are defined at this stage. However, explicitly splitting out the higher m_{jj} bins at the defined m_{jj} boundaries is encouraged if there is sufficient sensitivity from dedicated analyses to allow for their separate measurement.
- The $\boxed{p_T^H > 200\,\text{GeV}}$ bin only contains a small fraction of the VBF signal and is therefore kept as a single bin at this stage, with all m_{jj} boundaries and the p_T^{Hjj} boundary kept as sub-bin boundaries.

4.3 Associated Higgs production (leptonic VH)

The VH template process is defined as Higgs production in association with a leptonically decaying vector boson, $pp \to V(\to \text{leptons})H$. It is separated into the three underlying processes $q\bar{q}' \to W(\to \ell\bar{\nu})H$, $q\bar{q} \to Z(\to \ell\bar{\ell})H$, and $gg \to Z(\to \ell\bar{\ell})H$. The hadronic VH processes $q\bar{q} \to V(\to q\bar{q})H$ are part of the electroweak qqH template process (see Section 4.2). Similarly, the gluon-induced $gg \to Z(\to q\bar{q})H$ process is included as part of the $gg \to H$ template process (see Section 4.1), for which it represents an electroweak real-emission correction. The extensions in stage 1.1 are additional p_T^V and jet-bin boundaries, and are fully backward compatible with the previous stage 1.0.

The stage 1.2 bins, identical to the stage 1.1 ones, are depicted in Figure 3 and are summarized in the following:

- The total cross section is first split into the subprocesses $\boxed{q\bar{q}' \to WH}$, $\boxed{q\bar{q} \to ZH}$ and $\boxed{gg \to ZH}$.
  - The $\boxed{q\bar{q}' \to WH}$ and $\boxed{q\bar{q} \to ZH}$ subprocesses are split into p_T^V bins with boundaries at $p_T^V = 75, 150, 250$, and $400\,\text{GeV}$, where the $p_T^V = 400\,\text{GeV}$ bin boundary is kept as sub-bin at this stage. Compared to stage 1.0, the boundaries at $p_T^V = 75$ and $400\,\text{GeV}$ were added. This more fine grained p_T^V binning better reflects the experimental sensitivity in the low p_T^V range and also allows one to provide the theory uncertainties with sufficient detail.

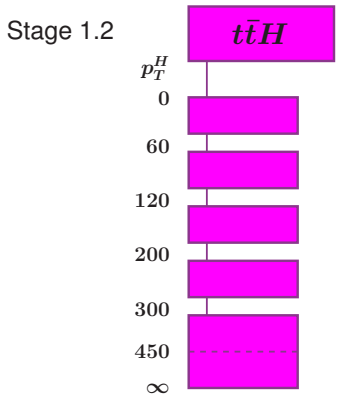

Figure 4: Stage 1.2 bins for $t\bar{t}H$ production. In stage 1.1 this production mode is not binned.

  - Exactly the same binning as for $\boxed{q\bar{q} \to ZH}$ is now used for $\boxed{gg \to ZH}$. This allows for a more consistent merging of individual bins across the two subprocesses, which at present are hard to separate experimentally. In addition, it facilitates a better treatment of the sizeable theory uncertainties for $gg \to ZH$.

- As in stage 1.0, the $\boxed{150\,\text{GeV} < p_T^V < 250\,\text{GeV}}$ bin is split explicitly into $\boxed{0\text{-jet}}$ and $\boxed{\geq 1\text{-jet}}$ bins. Stage 1.1 and 1.2 now also add 0-jet, 1-jet, $\geq$ 2-jet sub-bins in all p_T^V bins to allow for a more fine-grained estimate of theory uncertainties.

4.4 $t\bar{t}H$ production

The $t\bar{t}H$ template process is defined as Higgs production in association with a $t\bar{t}$ pair. While in stage 1.1 this process is not split into bins, stage 1.2 incorporates five bins in p_T^H with boundaries at $p_T^H = 60, 120, 200$, and 300 GeV. An additional sub-bin boundary at $p_T^H > 450$ GeV is also introduced to enhance sensitivity to the boosted topology. The stage 1.2 bins for the $t\bar{t}H$ production mode are depicted in Figure 4. The observable p_T^H is chosen for the binning, as it has good sensitivity to potential BSM effects, while being simpler than other, more complex observables. In particular, it has the key advantage that it does not require one to define a top quark or top jet as a truth-level object.

4.5 Other production modes

4.5.1 $b\bar{b} \to H$ production

So far it is not possible in experimental analyses to separate the $b\bar{b} \to H$ process from the by far larger $gg \to H$ process, and this is likely to remain the case in the near future. For this reason, the two processes are currently merged and $b\bar{b} \to H$ should hence be used with a binning that follows that of $gg \to H$ as needed by each analysis.

4.5.2 tH production

Due to the low experimental sensitivity using the LHC Run 2 dataset to measure Higgs boson production in association with a single top quark, comprising tHq and tWH production modes, these processes are treated commmonly as tH production and are not split into bins in stages 1.1. and 1.2. The split of these processes is planned for a future stage.

5 Conclusions

We have presented the complete definitions of Simplified Template Cross Sections in stage 1.2 and its predecessor stage 1.1. These have been used for the measurements based on the full Run 2 datasets by the ATLAS and CMS experiments. Compared to the previous stage 1.0, several refinements and extensions have been introduced, in particular for the VBF process. For stage 1.2, measurements in the $t\bar{t}H$ production mode are divided into bins.

A new feature in stage 1.1 and stage 1.2 is the introduction of sub-bin boundaries. Their purpose is to allow for an improved treatment of residual theory uncertainties in the signal distributions and their propagation to the measured parameters. For this reason, the full granularity including sub-bins is higher than the experimental sensitivity with the full Run 2 datasets. The sub-bin boundaries should be considered as possible boundaries for splitting bins, allowing for a smoother evolution of the binning in the future. The final bin splitting or merging should be optimized by the experiments based on the available statistics at a given time.

Acknowledgments

Funding information This work was supported in part by the French Agence Nationale de la Recherche under the project "PhotonPortal" (ANR-16-CE31-0016); the US National Science Foundation award 1806579; Imperial College London and the Science and Technology Facilities Council, UK; and the Deutsche Forschungsgemeinschaft (DFG) under Germany's Excellence Strategy – EXC 2121 "Quantum Universe" – 390833306.

References

[1] J. R. Andersen et al., *Les Houches 2015: Physics at TeV colliders Standard Model working group report*, in *The 2015 Les Houches workshop on physics at TeV colliders*, Les Houches, France (2015) [preprint doi:10.48550/arXiv.1605.04692].

[2] D. de Florian et al. (eds.), *Handbook of LHC Higgs cross sections: 4. Deciphering the nature of the Higgs sector*, CERN, Geneva, Switzerland, ISBN 9789290834427 (2017), doi:10.23731/CYRM-2017-002 [preprint doi:10.48550/arXiv.1610.07922].

[3] ATLAS collaboration: G. Aad et al., *Measurement of the properties of Higgs boson production at $\sqrt{s} = 13$ TeV in the $H \to \gamma\gamma$ channel using 139fb^{-1} of pp collision data with the ATLAS experiment*, J. High Energy Phys. **07**, 088 (2023), doi:10.1007/JHEP07(2023)088 [preprint doi:10.48550/arXiv.2207.00348].

[4] CMS collaboration: A. M. Sirunyan et al., *Measurements of Higgs boson production cross sections and couplings in the diphoton decay channel at $\sqrt{s} = 13$ TeV*, J. High Energy Phys. **07**, 027 (2021), doi:10.1007/JHEP07(2021)027 [preprint doi:10.48550/arXiv.2103.06956].

[5] ATLAS collaboration: G. Aad et al., *Higgs boson production cross-section measurements and their EFT interpretation in the 4ℓ decay channel at $\sqrt{s} = 13$ TeV with the ATLAS detector*, Eur. Phys. J. C **80**, 957 (2020), doi:10.1140/epjc/s10052-020-8227-9 [preprint doi:10.48550/arXiv.2004.03447].

[6] CMS collaboration: A. M. Sirunyan et al., *Measurements of production cross sections of the Higgs boson in the four-lepton final state in proton-proton collisions at $\sqrt{s} = 13$ TeV*, Eur. Phys. J. C **81**, 488 (2021), doi:10.1140/epjc/s10052-021-09200-x [preprint doi:10.48550/arXiv.2103.04956].

[7] ATLAS collaboration: G. Aad et al., *Measurements of Higgs boson production by gluon-gluon fusion and vector-boson fusion using $H \to WW^* \to e\nu\mu\nu$ decays in pp collisions at $\sqrt{s} = 13$ TeV with the ATLAS detector*, Phys. Rev. D **108**, 032005 (2023), doi:10.1103/PhysRevD.108.032005 [preprint doi:10.48550/arXiv.2207.00338].

[8] CMS collaboration: A. Tumasyan et al., *Measurements of the Higgs boson production cross section and couplings in the W boson pair decay channel in proton-proton collisions at $\sqrt{s} = 13$ TeV*, Eur. Phys. J. C **83**, 667 (2023), doi:10.1140/epjc/s10052-023-11632-6 [preprint doi:10.48550/arXiv.2206.09466].

[9] ATLAS collaboration: G. Aad et al., *Differential cross-section measurements of Higgs boson production in the $H \to \tau^+\tau^-$ decay channel in pp collisions at $\sqrt{s} = 13$ TeV with the ATLAS detector*, J. High Energy Phys. **03**, 010 (2025), doi:10.1007/JHEP03(2025)010 [preprint doi:10.48550/arXiv.2407.16320].

[10] CMS collaboration: A. Tumasyan et al., *Measurements of Higgs boson production in the decay channel with a pair of τ leptons in proton-proton collisions at $\sqrt{s} = 13$ TeV*, Eur. Phys. J. C **83**, 562 (2023), doi:10.1140/epjc/s10052-023-11452-8 [preprint doi:10.48550/arXiv.2204.12957].

[11] ATLAS collaboration: G. Aad et al., *Measurements of WH and ZH production with Higgs boson decays into bottom quarks and direct constraints on the charm Yukawa coupling in 13 TeV pp collisions with the ATLAS detector*, J. High Energy Phys. **04**, 075 (2025), doi:10.1007/JHEP04(2025)075 [preprint doi:10.48550/arXiv.2410.19611].

[12] ATLAS collaboration: G. Aad et al., *Measurements of WH and ZH production in the $H \to b\bar{b}$ decay channel in pp collisions at 13 TeV with the ATLAS detector*, Eur. Phys. J. C **81**, 178 (2021), doi:10.1140/epjc/s10052-020-08677-2 [preprint doi:10.48550/arXiv.2007.02873].

[13] CMS collaboration, *Measurement of simplified template cross sections of the Higgs boson produced in association with $\sqrt{s} = 13$ TeV*, Phys. Rev. D **109**, 092011 (2024), doi:10.1103/PhysRevD.109.092011 [preprint doi:10.48550/arXiv.2312.07562].

[14] ATLAS collaboration: M. Aaboud et al., *Observation of $H \to b\bar{b}$ decays and VH production with the ATLAS detector*, Phys. Lett. B **786**, 59 (2018), doi:10.1016/j.physletb.2018.09.013 [preprint doi:10.48550/arXiv.1808.08238].

[15] CMS collaboration: A. M. Sirunyan et al., *Observation of Higgs boson decay to bottom quarks*, Phys. Rev. Lett. **121**, 121801 (2018), doi:10.1103/PhysRevLett.121.121801 [preprint doi:10.48550/arXiv.1808.08242].

[16] ATLAS collaboration: G. Aad et al., *A detailed map of Higgs boson interactions by the ATLAS experiment ten years after the discovery*, Nature **607**, 52 (2022), doi:10.1038/s41586-022-04893-w [preprint doi:10.48550/arXiv.2207.00092].

[17] CMS collaboration: A. Tumasyan et al., *A portrait of the Higgs boson by the CMS experiment ten years after the discovery*, Nature **607**, 60 (2022), doi:10.1038/s41586-022-04892-x [preprint doi:10.48550/arXiv.2207.00043].

[18] ATLAS collaboration, *Combined measurements of Higgs boson production and decay using up to 80fb^{-1} of proton–proton collision data at $\sqrt{s} = 13$ TeV collected with the ATLAS experiment*, Tech. Rep. ATLAS-CONF-2018-031, CERN, Geneva, Switzerland (2018), https://cds.cern.ch/record/2629412.

[19] ATLAS collaboration, *Combined measurements of Higgs boson production and decay using up to 80fb^{-1} of proton–proton collision data at $\sqrt{s} = 13$ TeV collected with the ATLAS experiment*, Tech. Rep. ATLAS-CONF-2019-005, CERN, Geneva, Switzerland (2019), https://cds.cern.ch/record/2668375.

[20] CMS collaboration: A. M. Sirunyan et al., *Combined measurements of Higgs boson couplings in proton-proton collisions at $\sqrt{s} = 13$ TeV*, Eur. Phys. J. C **79**, 421 (2019), doi:10.1140/epjc/s10052-019-6909-y [preprint doi:10.48550/arXiv.1809.10733].

[21] C. Hays, V. S. Gonzalez and G. Zemaityte, *Constraining EFT parameters using simplified template cross sections*, Tech. Rep. LHCHXSWG-INT-2017-001, CERN, Geneva, Switzerland (2017), https://cds.cern.ch/record/2290628.

[22] J. Ellis, C. W. Murphy, V. Sanz and T. You, *Updated global SMEFT fit to Higgs, diboson and electroweak data*, J. High Energy Phys. **06**, 146 (2018), doi:10.1007/JHEP06(2018)146 [preprint doi:10.48550/arXiv.1803.03252].

[23] ATLAS collaboration: G. Aad et al., *Interpretations of the ATLAS measurements of Higgs boson production and decay rates and differential cross-sections in pp collisions at $\sqrt{s} = 13$ TeV*, J. High Energy Phys. **11**, 097 (2024), doi:10.1007/JHEP11(2024)097 [preprint doi:10.48550/arXiv.2402.05742].

[24] ATLAS collaboration, *Constraint of the Higgs boson self-coupling from Higgs boson differential production and decay measurements*, Tech. Rep. ATL-PHYS-PUB-2019-009, CERN, Geneva, Switzerland (2019), https://cds.cern.ch/record/2667570.

[25] CMS collaboration, *Combined Higgs boson production and decay measurements with up to 137fb^{-1} of proton–proton collision data at $\sqrt{s} = 13$ tev*, Tech. Rep. CMS-PAS-HIG-19-005, CERN, Geneva, Switzerland (2020), https://cds.cern.ch/record/2706103.

ATLAS PUB Note

ATL-PHYS-PUB-2023-031

1st November 2023

Evaluation of QCD uncertainties for Higgs boson production through gluon fusion and in association with two top quarks for simplified template cross-section measurements

The ATLAS Collaboration

This note summarizes the QCD uncertainties for Higgs boson production through gluon fusion and in association with two top quarks. The uncertainties are evaluated using a variation of the Stewart-Tackmann procedure in phase space regions defined by the stage 1.2 simplified template cross-section framework. They are used in the relevant ATLAS Run-2 Higgs boson measurements to assign uncertainties on the cross-section and acceptance predictions.

© 2023 CERN for the benefit of the ATLAS Collaboration.
Reproduction of this article or parts of it is allowed as specified in the CC-BY-4.0 license.

1 Introduction

The simplified template cross-section (STXS) framework has been designed to maximize the sensitivity of Higgs boson cross-section measurements to beyond-the-Standard-Model effects, while minimizing their theory dependence and allowing for the combination of analyses in different decay channels [1, 2]. In the STXS framework, cross-section measurements are performed in mutually exclusive phase space regions (also referred to as bins) specific to the different Higgs boson production modes.

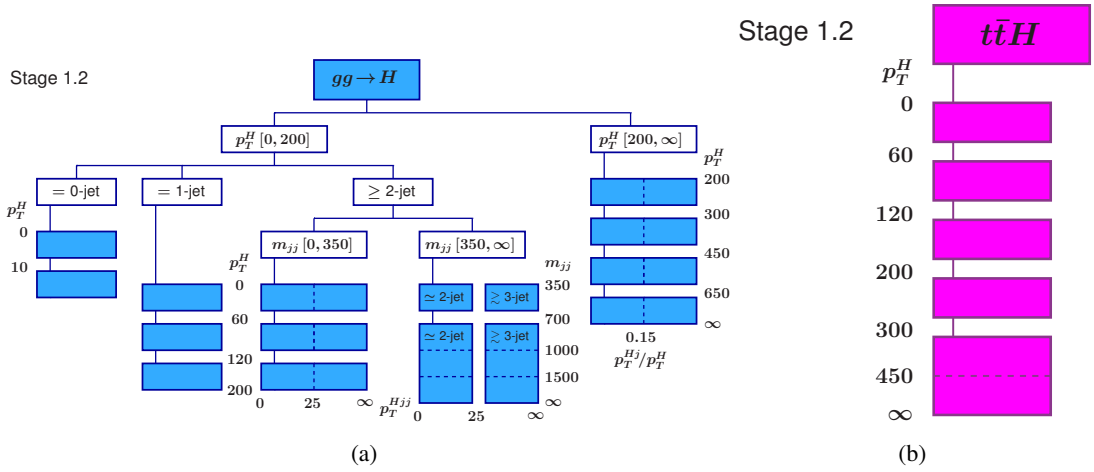

(a) (b)

Figure 1: The mutually exclusive phase space regions of the STXS framework, stage 1.2, for the (a) ggF and (b) $t\bar{t}H$ production modes.

This note provides a summary of the QCD uncertainties on the cross-section predictions in STXS stage 1.2 bins for Higgs boson production through gluon fusion (ggF) and in association with a $t\bar{t}$ pair ($t\bar{t}H$) as shown in Figure 1. The STXS 1.2 splitting is based on the number of jets, the transverse momentum of the Higgs boson p_{T}^{H}, the invariant mass of the two jets m_{jj}, the transverse momentum of the system formed by the Higgs boson and the two highest-p_{T} jets p_{T}^{Hjj}, as well as the combined transverse momentum of the Higgs boson and the leading jet divided by the transverse momentum of the Higgs boson $p_{\mathrm{T}}^{Hj}/p_{\mathrm{T}}^{H}$. For the STXS bin definitions, particle-level jets are built from stable particles (particles with lifetime $c\tau$ >10 mm) including neutrinos, photons, and leptons from hadron decays or those produced in the parton shower. All Higgs boson decay products, as well as the leptons and neutrinos from the decays of the associated vectors bosons are excluded from the jet building, while the decay products from hadronically decaying associated vector bosons are included. The anti-k_t jet reconstruction algorithm [3, 4] with a radius parameter R = 0.4 is used. The jets are required to have $p_{\mathrm{T}} > 30$ GeV, with no restrictions on rapidity.

The described QCD uncertainties have been used in a number of ATLAS publications, in particular cross-section and couplings measurements, combining analyses in all accessible decay channels [5]. They are used for the Standard Model cross-section and acceptance predictions. The uncertainties on the cross sections of the other Higgs boson production modes (vector boson fusion and associated production with a vector boson) will be discussed elsewhere.

The reason a special procedure is needed to estimate the uncertainties in STXS bins due to unknown higher-order perturbative corrections instead of the usual variations of the renormalization (μ_{r}) and factorization (μ_{f}) scales is multifold. In some regions of phase space, the standard variations can lead to unrealistically small uncertainty estimates for fixed order calculations through cancellation effects, which

is described in the proposal of the Stewart-Tackmann (ST) procedure [6]. The standard procedure can also mismodel correlations of uncertainties between bins, since the higher-order effects approximated by the scale variations may include a number of different contributions.

The desired result is an uncertainty scheme that produces sensible results, both for the uncertainty values and their correlations.

A variation of the ST procedure is applied (the so-called long-range ST method), which includes a single uncertainty on the inclusive cross section, while the other components describe migration uncertainties in the fraction of events passing the selections defining the STXS regions. The goal is to have a full description of the cross-section uncertainty in each STXS region using a Hessian scheme, where the full uncertainty is split into components that are uncorrelated with respect to each other, while each is fully correlated across the STXS bins. Each uncertainty component can then be assigned an individual nuisance parameter in a profile likelihood fit.

The note is structured as follows: Section 2 describes the simulated samples used for the extraction of the uncertainties, Section 3 introduces the principles of the long-range ST procedure and Section 4 shows the extracted uncertainties for ggF and $t\bar{t}H$ production cross sections.

2 Simulated event samples and theoretical calculations

Several simulated samples and theoretical calculations with varying approximations and different accuracy are used to evaluate and cross check the systematic uncertainties associated to the cross-section predictions in various STXS bins. A description of these samples and calculations are provided below and summarized in Table 1.

2.1 ggF

Higgs boson production via ggF is simulated at NNLO accuracy in QCD using Powheg Box v2 [7–11] (Powheg NNLOPS). The simulation achieves NNLO accuracy for arbitrary inclusive $gg \to H$ observables by reweighting the Higgs boson rapidity spectrum in MiNLO HJ [12–14] to that of the HNNLO prediction [15]. Top- and bottom-quark mass effects are included up to next-to-leading order (NLO). The renormalization and factorization scales are set to half of the Higgs boson mass and the PDF4LHC15nnlo PDF set [16] is used. The matrix elements are matched to the parton shower of Pythia 8.2 [17] which uses the AZNLO tune [18]. The decays of bottom and charm hadrons are performed by EvtGen 1.6.0 [19].

The QCD scale uncertainties are obtained using 9-point scale variations of the NLO renormalization and factorization scales μ_r and μ_f by factors of 0.5 and 2, and applying the NNLO reweighting to those variations, including up and down variations of $\mu_r = \mu_f$ by 0.5 and 2 around the central value for the NNLO part, yielding a total of 27 scale variations. Using these settings but without the reweighting, additional simulations are created with MiNLO HJ [12–14] and MiNLO HJJ [20] using the Powheg Box v2 generator. In addition to the Powheg samples, MG5_aMC@NLO simulations [21, 22] are used for uncertainty evaluations and cross-checks. The MG5_aMC@NLO samples are generated using PDF set NNPDF30_nlo_as_0118 [23] with infinite top-quark mass and zero bottom-quark mass.

Some sources of uncertainties are estimated with analytic calculations. The Boughezal-Liu-Petriello-Tackmann-Walsh (BLPTW) method [2, 24] utilizes resummed and fixed-order calculations and provides

cross sections in bins of jet multiplicity, as well as associated uncertainties. Other calculations including finite-top-quark mass effects at NLO ("SM_NLO") [25] are used for the evaluation of the p_{T}^{H} migration in the high-p_{T}^{H} region. Calculations at leading order (LO) with various top-quark mass settings [26–30] are used to estimate the uncertainty due to the choice of the top-quark mass scheme. These are listed as "Pole mass" in Table 1.

Table 1: Samples, calculations, and variations used to derive QCD uncertainties in bins of STXS stage 2 for the ggF and $t\bar{t}H$ processes.

Generated Samples

Process	Name	Description	Generator	Pythia 8 shower tune	PDF	Variations	Other Notes
ggF	Powheg NNLOPS	H+0j@NNLO	Powheg	AZNLO	PDF4LHC15_nlo_30_pdfas	(μ_r, μ_f) variations (9-point NLO, 3-point NNLO)	NNLOPS reweighting Rescaled for quark mass effects Low-p_T^H and p_T^{Hj}/p_T^H migration
ggF	MiNLO HJ	H+1j@NLO	Powheg	AZNLO	PDF4LHC15_nlo_30_pdfas	9-point (μ_r, μ_f) variations	Rescaled quark mass effects Cross-check for high-p_T^H spectrum
ggF	MiNLO HJJ	H+2j@NLO	Powheg	AZNLO	PDF4LHC15_nlo_30_pdfas	9-point (μ_r, μ_f) variations	Rescaled quark mass effects Cross-check for m_{jj} and p_T^{Hjj} migration
ggF	H+0,1,2j MG5_aMC@NLO (FxFx)	H+0,1,2j@NLO	MG5_aMC@NLO	AZNLO	NNPDF30_nlo_as_0118	9-point (μ_r, μ_f) variations	FxFx merging merging scale = 30 GeV HC_NLO_X0-heft model m_{top} = inf, m_b = 0 m_{jj} and p_T^{Hjj} migration Cross-check for p_T^{Hj}/p_T^H migration
ggF	H+1j MG5_aMC@NLO	H+1j@NLO	MG5_aMC@NLO	AZNLO	NNPDF30_nlo_as_0118	9-point (μ_r, μ_f) variations	HC_NLO_X0-heft model m_{top} = inf, m_b = 0 Cross-check for high-p_T^H spectrum
$t\bar{t}H$	Powheg	NLO	Powheg	A14	NNPDF3.0nlo	9-point (μ_r, μ_f) around $E_T = \sqrt[3]{m_T(t) \cdot m_T(\bar{t}) \cdot m_T(H)}$ 4-point (ISR, FSR) variations	p_T^H migration

Calculations

Process	Name	Description	PDF	Variations	Other Notes
ggF	NLO_SM	H+1j@NLO with finite top mass	PDF4LHC15_nnlo_mc	9-point variations of (μ_r, μ_f) around $E_T = \sqrt{m_H^2 + p_{T,H}^2}$	m_{top} = 173.05 GeV $\geq$ 1 jet with p_T > 30 GeV High-p_T^H migration
ggF	Pole mass (and other top mass variations)	H+1j@LO with finite top mass	-	$\overline{MS}$ mass variations m_{top} (m_{top}), m_{top} (E_T/2), m_{top} (E_T), m_{top} (2E_T), with $E_T = \sqrt{m_H^2 + p_{T,H}^2}$	Top mass scheme uncertainty

2.2 $t\bar{t}H$

The production of $t\bar{t}H$ events is modelled using the POWHEG BOX v2 generator [9–11, 31, 32] , which provides matrix elements at next-to-leading order (NLO) in the strong coupling constant α_s in the five-flavour scheme with the NNPDF3.0NLO PDF set [33]. The functional form of the renormalisation and factorisation scales is set to $\sqrt[3]{m_T(t) \cdot m_T(\bar{t}) \cdot m_T(H)}$. The events are interfaced to PYTHIA 8.2 [17] using the A14 tune [34] and the NNPDF2.3LO PDF set [33]. The decays of bottom and charm hadrons are performed by EVTGEN 1.6.0 [19].

Uncertainties due to missing higher-order corrections are evaluated through simultaneous variations of the renormalisation and factorisation scales by factors of 2 and 0.5 (using seven-point variations). For $t\bar{t}H$, unlike ggF, no resummed calculations are available binned in the number of jets, so to capture parton shower/resummation effects, more QCD uncertainty sources are included in the calculation: Scale variations affecting initial and final state radiation (ISR and FSR) and parton shower variations. The uncertainty in the ISR is estimated from simultaneous variation of the renormalization and factorization scales and the Var3c up/down variations of the A14 tune. The uncertainties in FSR are estimated by varying the renormalization scale by a factor of 2 and 0.5.

3 QCD uncertainty parameterization

To avoid underestimates of the QCD uncertainties in exclusive phase space regions through artificial cancellations in the calculations, the Stewart Tackmann method suggests using QCD scale variations to determine uncertainties for inclusive cross sections, and use these to extract uncertainties for exclusive cross sections. As an example the uncertainty in the region with exactly one jet ($N_{\text{jet}} = 1$) can be estimated from the quadratic sum of the uncertainties in the regions $N_{\text{jet}} \geq 2$ and $N_{\text{jet}} \geq 1$.

The presented uncertainties are split into two types:

- **Yield uncertainties** which affect the overall normalization and, if they depend on any of the probed observables, also the shape.
- **Migration uncertainties** which affect the shape but not the normalization, and hence will have impacts that sum to 0 across all regions of phase

Each uncertainty component is uncorrelated from each other and can therefore be assigned to an independent nuisance parameter in the likelihood model of Higgs boson production cross-section measurements.

In many cases, theoretical calculations are available for the yield uncertainties. Otherwise, they are estimated with scale variations.

For the migration uncertainties, the long-range ST method us applied, similarly to what is proposed in Ref. [35]. Different from the original Stewart–Tackmann method, which assigns the selection effects only to the two adjacent jet bins separated by the selection cut, the migration uncertainties in the STXS framework are considered to propagate from the bin below a boundary to all bins above the boundary. For instance, a requirement on the dijet invariant mass $m_{jj} = 700$ GeV induces uncertainties caused by migration of events from the bin $m_{jj} = [350,700]$ GeV to all bins above 700 GeV. This is captured in the uncertainty scheme by placing the relative uncertainty evaluated for $m_{jj} \geq 700$ GeV on all individual bins falling into that region, and a relative uncertainty calculated from the same absolute uncertainty but opposite sign on the $m_{jj} = [350,700]$ GeV bin. In addition, a scale factor ρ is applied to account for the double-counting

effects from multiple sources of migration uncertainties that are considered for a specific bin. For the ggF uncertainties, $\rho = 0.5$ allows the derived numbers to roughly match the largest scale uncertainties in each bin (the largest uncertainties are taken to avoid underestimation). For the $t\bar{t}H$ uncertainties, $\rho = 0.7$ was found to be appropriate.

In the next two sections, the strategies and results for the uncertainty estimates of the ggF and $t\bar{t}H$ production cross sections are discussed. For the ggF process, most migration uncertainties are estimated with the long-range ST method based on the (symmetrized) scale variation with the largest impact. As stated before, for $t\bar{t}H$, unlike ggF, no resummed calculations are available in bins of jets, so to capture parton shower/resummation effects, scale variations affecting initial and final state radiation and parton-shower uncertainties are included as additional sources of QCD-related uncertainties. In the derivation of the $t\bar{t}H$ uncertainties, events outside the nominal STXS Higgs boson rapidity selection $|y| > 2.5$ are included. They contribute 1.3% of the total yield.

The uncertainties presented in this note are applied to the state-of-the-art predictions (Powheg NNLOPS for ggF and Powheg NLO for $t\bar{t}H$ as described in Table 1). The cross section values for each STXS bin, estimated by multiplying the production cross sections from Ref. [2] with the acceptances calculated from the samples listed above, are summarized in Appendix B. For reference, the cross sections for the STXS bins of the other production modes are listed in Appendix C.

4 Results

4.1 ggF production mode

4.1.1 ggF low-p_{T}^{H} ($p_{\mathrm{T}}^{H} < 200$ GeV) region

Yield uncertainties and jet migration: The renormalization, resummation, and migration uncertainties due to the split into bins of different jet multiplicities were calculated using the BLPTW method (see Section 2) and published in Table 20 in the Yellow Report 4 [2]. Since the publication of this report, N3LO calculations as well as EW corrections [2, 36–47] have become available, increasing the overall ggF cross section by 2.5%. The numbers from Table 20 in the Yellow Report 4 were converted into absolute uncertainties and scaled by a factor of 1.025 due to this cross section increase. The absolute uncertainties were then applied to the jet multiplicity distribution from NNLOPS, normalized to the best available total cross section. The shape of the NNLOPS distribution is compatible with the shape used in the Yellow Report within uncertainties. However, small differences in the central values lead to small changes in the resulting relative uncertainties. The uncertainties obtained from the procedure described above are shown in Table 2, where the symbol λ_i denotes the relative uncertainty induced by the source i. The yield uncertainty is calculated separately for each bin and is split into a part due to scale variations λ_μ and a resummation uncertainty λ_{res}.

Table 2: Yield (λ_μ, λ_{res}) and jet bin migration ($\lambda_{0/1}$, $\lambda_{1/2}$) uncertainties for the 0/1/2-jet bins for p_{T}^{j} = 30 GeV.

ggF	BLPTW		
Jet bin	0	1	≥ 2
λ_μ [%]	3.8	5.2	7.9
λ_{res} [%]	0.1	4.5	7.9
$\lambda_{0/1}$ [%]	-4.2	7.9	3.9
$\lambda_{1/2}$ [%]	-	-6.8	16.1
Total [%]	5.6	12.5	19.9

p_{T}^{H} bins in 0-jet region: Due to the complex theoretical uncertainties affecting the low p_{T}^{H} region in the 0-jet topology, the values are obtained from a different approach than the long-range ST method. Besides the renormalization scale μ_{r} and the factorization scale μ_{f}, the HNNLO scale for NNLOPS reweighing is also considered. Figure 2 shows the p_{T}^{H} spectrum for the scale variations that have significant effects.

The number of events that pass a typical Higgs boson analysis selection usually depends on p_{T}^{H}. To avoid discontinuities in the systematic variations of this acceptance, the uncertainties are parameterized in two p_{T}^{H} ranges by a linear interpolation as a function of p_{T}^{H}, based on the largest variation in each range. To extract the migration effects only, the p_{T}^{H} spectra of the variations are normalized to unit area. The parameterization is illustrated in Figure 3 and the resulting uncertainty values are shown in Table 3. Care was taken that the integral up to p_{T}^{H} < 10 GeV matches the best available uncertainty prediction from resummed calculations.

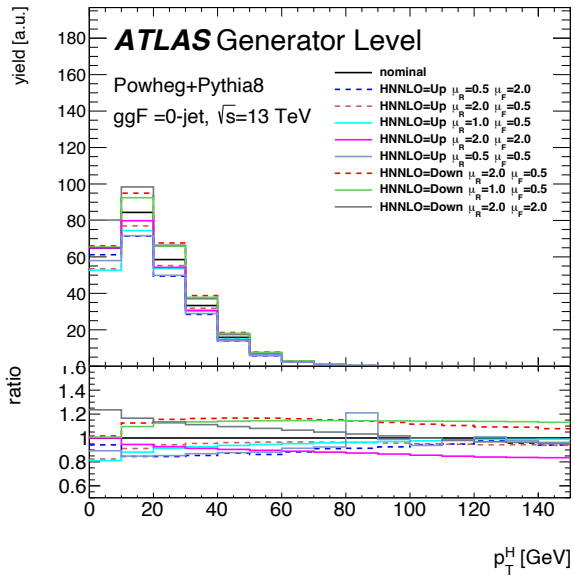

Figure 2: The largest scale variations of the Powheg NNLOPS sample as a function of p_{T}^{H} in the 0-jet region, used to evaluate p_{T}^{H} migration uncertainties in the p_{T}^{H} < 200 GeV region. The bottom panel shows the scale variations with respect to the nominal prediction.

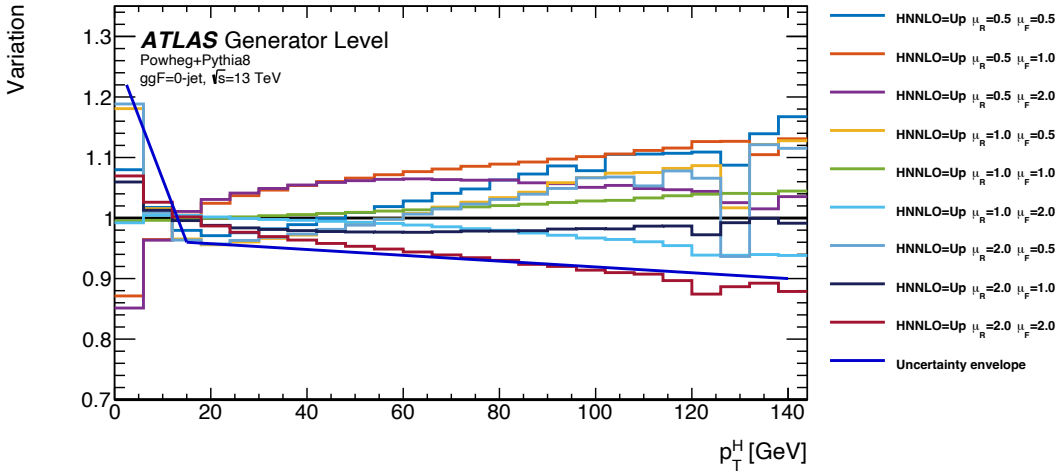

Figure 3: Parameterization of the p_{T}^{H} uncertainty in the 0-jet region. The various coloured histograms show the impact on the (normalized) cross section from QCD scale variations in this region. The solid blue line presents the functional parameterization used to evaluate the uncertainty as described in Table 3.

Table 3: p_{T}^{H} migration uncertainties for ggF events with no jets ($p_{\mathrm{T}}^{j} > 30$ GeV)

.

ggF	Powheg NNLOPS	
p_{T}^{H} [GeV] bin in 0-jet region	< 10	≥ 10
$\lambda_{p_{\mathrm{T}}^{H}=10}$ [%]	11.2	-3.6

p_{T}^{H} bins in 1-jet and ≥2-jet regions: In the 1-jet and ≥2-jet regions, the uncertainty evaluation follows the long-range ST method. The scale variations considered include the renormalization scale μ_{r}, factorization scale μ_{f}, and the HNNLO scale. Figure 4 shows the p_{T}^{H} spectrum for the scale variations that have significant effects. The p_{T}^{H} uncertainties are estimated in the jet-inclusive region to avoid double-counting of the jet migration effects, and are covered by a single nuisance parameter in both the 1-jet and ≥2-jet regions.

For the ≥2-jet region, the p_{T}^{H} bins are further split by m_{jj}. Hence, the m_{jj} dependence on the p_{T}^{H} uncertainties is investigated. To check the effect, the ratios of the largest variations over the nominal p_{T}^{H} spectrum in each m_{jj} region are compared. As shown in Figure 5, the differences between the ratios in each m_{jj} region are within the statistical uncertainty (the ratios are smoother than the statistical bands because scale variations are implemented as internal reweighting, and because the numerator and denominator of the ratio use the same events but with a different weight and are therefore correlated, while the statistical uncertainties are propagated as if uncorrelated). Therefore, the p_{T}^{H} uncertainties are treated as m_{jj} independent and it is safe to apply the long-range ST method in the m_{jj}-inclusive region for evaluation.

As in the 0-jet case, a smoothing procedure is applied on the resulting uncertainties to avoid discontinuities in the acceptance of event selections depending on p_{T}^{H}. The smoothing is performed by a linear interpolation

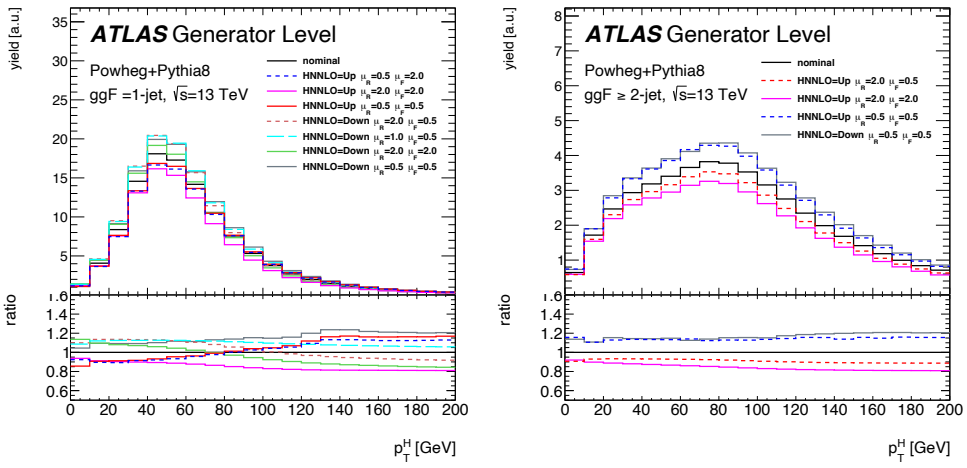

Figure 4: The largest scale variations of the Powheg NNLOPS sample as a function of p_{T}^{H} in the 1-jet (left) and ≥2-jet (right) region, used to evaluate p_{T}^{H} migration uncertainties in the $p_{T}^{H} < 200$ GeV region. The bottom panel shows the scale variations with respect to the nominal prediction.

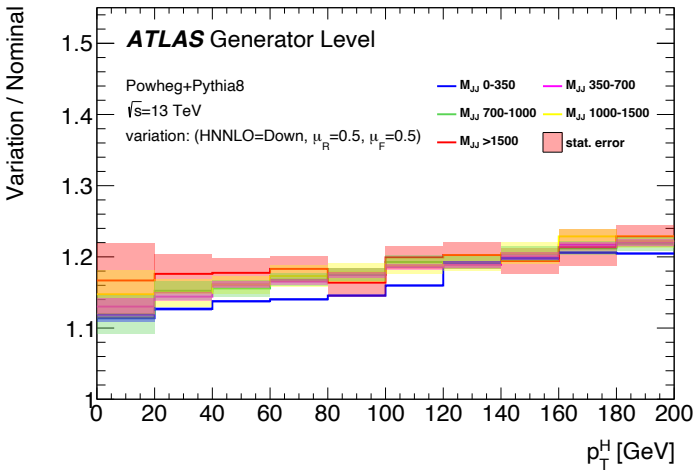

Figure 5: The ratio of the most extreme scale variation to the nominal distribution, as a function of p_{T}^{H} in each m_{jj} bins. The solid coloured lines represent the ratios, while the coloured bands are the statistical errors.

as a function of p_{T}^{H}, inspired by the normalized distributions of the scale variations across the p_{T}^{H} spectrum. The form was also determined to ensure that the total migration effects cancel in the inclusive region. The original values of the p_{T}^{H} uncertainties in 1-jet and ≥2-jet regions by the long-range ST method are shown in Table 4 and the smoothed ones are shown in Figure 6.

Table 4: p_{T}^{H} uncertainties obtained from the long-range ST method with $\rho = 0.5$, evaluated in the ≥1-jet region. The overall normalization uncertainty λ_y is to be replaced by the values found in Table 2 but is shown here for completeness.

ggF	Powheg NNLOPS		
p_{T}^{H} [GeV] bin in ≥1-jet region	< 60	[60,120)	[120,200)
λ_y [%]	13.1	13.1	13.1
$\lambda_{p_T^H=60}$ [%]	-8.1	+7.6	+7.6
$\lambda_{p_T^H=120}$ [%]		-2.9	+10.3
Total [%]	15.4	15.5	18.3

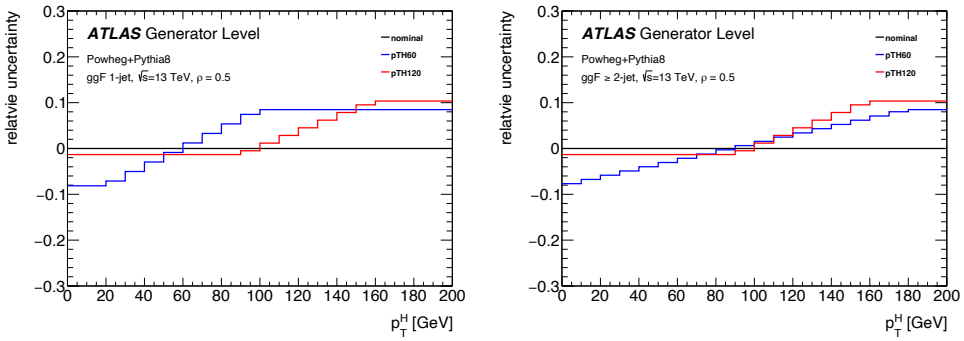

Figure 6: p_{T}^{H} uncertainties in the 1-jet (left) and the ≥2-jet (right) $p_{\mathrm{T}}^{H} < 200$ GeV regions obtained from the long-range ST method with $\rho = 0.5$. The uncertainties are shown after smoothing via linear interpolation is performed to remove unphysical discontinuities.

***m_{jj}* bins:** The m_{jj} migration is evaluated by the long-range ST method in the 2-jet inclusive region. The variations considered are the renormalization scale μ_{r} and the factorization scale μ_{f}. The $H + 0, 1, 2j$ MG5_aMC@NLO (FxFx) sample is chosen to estimate the uncertainties, with the scale variations across the m_{jj} spectrum shown in Figure 7. The evaluated uncertainties are shown in Table 5. The values were validated with the NNLOPS, $H + 2j$ MG5_aMC@NLO and MiNLO HJJ samples as described in Table 1.

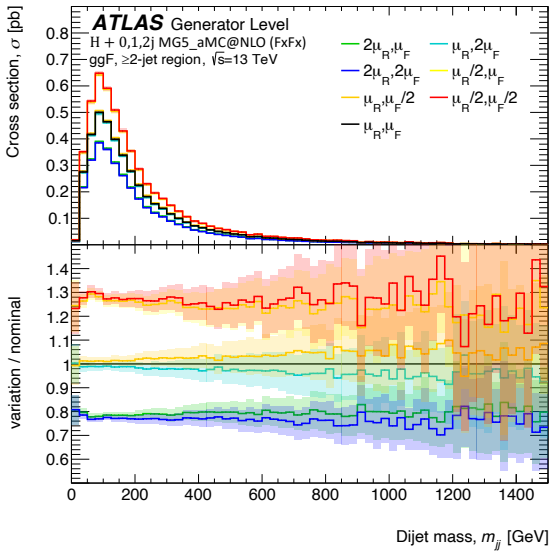

Figure 7: Cross sections for different scale variations in the $H + 2j$ dijet mass spectrum predicted by the $H + 0, 1, 2j$ MG5_aMC@NLO (FxFx) generator, used to evaluate m_{jj} migration uncertainties. The bottom panel shows the scale variations with respect to the nominal prediction.

Table 5: m_{jj} migration uncertainties obtained from the long-range ST method with $\rho = 0.5$. The overall normalization uncertainty λ_y is to be replaced by the values found in Table 2 but is shown here for completeness.

ggF	$H + 0, 1, 2j$ MG5_aMC@NLO (FxFx)				
m_{jj} [GeV] bin	< 350	[350,700)	[700,1000)	[1000,1500)	≥ 1500
λ_y [%]	23.0	23.0	23.0	23.0	23.0
$\lambda_{m_{jj}=350}$ [%]	-2.9	+11.8	+11.8	+11.8	+11.8
$\lambda_{m_{jj}=700}$ [%]		-5.7	+12.4	+12.4	+12.4
$\lambda_{m_{jj}=1000}$ [%]			-11.1	+12.6	+12.6
$\lambda_{m_{jj}=1500}$ [%]				-6.8	+13.0
Total [%]	23.2	26.5	30.7	32.0	33.9

p_{T}^{Hjj} bins: The observable p_{T}^{Hjj} is used as an indirect probe to separate 2-jet and ≥3-jet events. Table 6 shows the contributions of exclusive 2-jet and inclusive 3-jet events to the p_{T}^{Hjj} <25 GeV and p_{T}^{Hjj} ≥25 GeV categories.

Table 6: p_{T}^{Hjj} composition across the 25 GeV boundary for $N_{\mathrm{jet}} = 2$ and $N_{\mathrm{jet}} \geq 3$.

ggF	$H + 0, 1, 2j$ MG5_aMC@NLO (FxFx)	
p_{T}^{Hjj} [GeV] bin	$\sigma_{<25}/\sigma_{tot}$ [%]	$\sigma_{\geq 25}/\sigma_{tot}$ [%]
$N_{\mathrm{jet}} = 2$	91	9
$N_{\mathrm{jet}} \geq 3$	55	45

Since there is only one p_{T}^{Hjj} boundary, no ρ scale factor is applied in the uncertainty evaluation. The uncertainties are estimated from the $H+0, 1, 2j$ MG5_aMC@NLO (FxFx) sample, with the renormalization and factorization scale variations considered. Figure 8 shows the scale variations across the p_{T}^{Hjj} spectrum in the 2-jet inclusive, 2-jet exclusive and 3-jet inclusive regions. The uncertainty values are cross-checked with the NNLOPS, $H + 2j$ MG5_aMC@NLO and MiNLO HJJ samples. The resulting uncertainties are shown in Table 7, with one modification: The value of λ_{25} in the $\sigma_{\geq 25}$ bin derived from the $H + 0, 1, 2j$ MG5_aMC@NLO (FxFx) is 23.8%, but is conservatively increased to 30% to account for differences in the shape of the $H + 0, 1, 2j$ MG5_aMC@NLO FxFx sample, from which numbers are derived, and the NNLOPS sample, to which they are applied. This prevents this migration NP from having an overall normalization impact.

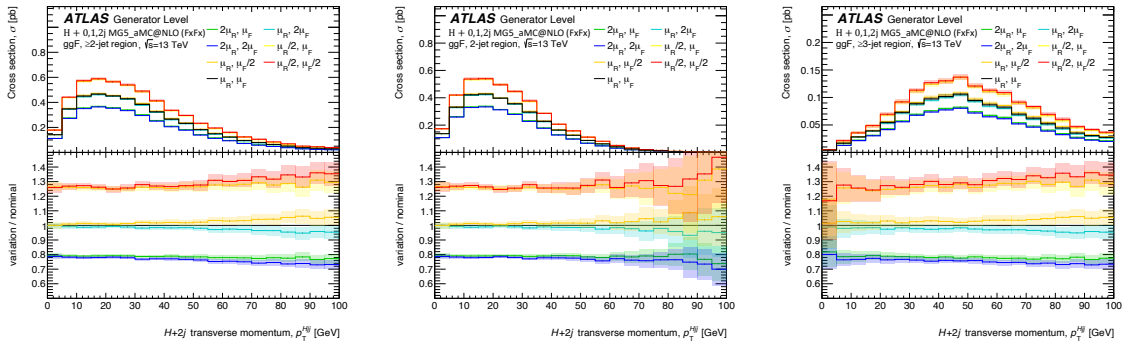

(a) ≥ 2-jet selection (b) 2-jet selection (c) ≥ 3-jet selection

Figure 8: Cross sections for different scale variations in the $H + 2j$ transverse momentum spectrum predicted by $H + 0, 1, 2j$ MG5_aMC@NLO FxFx generator for the (a) ≥ 2-jet selection, (b) 2-jet selection and (c) ≥ 3-jet selection. The bottom panel shows the scale variations with respect to the nominal prediction.

Table 7: p_{T}^{Hjj} migration uncertainties obtained from the long-range ST method with $\rho = 0.5$. The overall normalization uncertainty λ_y is to be replaced by the values found in Table 2 but is shown here for completeness.

ggF	$H + 0, 1, 2j$ MG5_aMC@NLO (FxFx)	
p_{T}^{Hjj} [GeV] bin	< 25	≥ 25
λ_y [%]	23.0	23.0
λ_{25} [%]	-33.7	+30.0
Total [%]	40.8	37.8

4.1.2 ggF high-p_{T}^{H} ($p_{\mathrm{T}}^{H} > 200$ GeV) region

Due to effects of the resolved top-quark loop in the high-p_{T}^{H} region, the extraction of the theoretical uncertainties, including the yield uncertainty, is separated from the low-p_{T}^{H} region. Thanks to recent improvements of theoretical calculations at high-p_{T}^{H} (see Section 2), the uncertainties in this region can now be more carefully evaluated.

Three types of uncertainties are considered in the high-p_{T}^{H} region. The first and second type are the yield uncertainty and migration uncertainties caused by the splitting of the $\boldsymbol{p_{\mathrm{T}}^{H}}$ and $\boldsymbol{p_{\mathrm{T}}^{Hj}/p_{\mathrm{T}}^{H}}$ bins (QCD perturbative uncertainties). To cover the resolved top-quark-loop contribution, effects due to the **choice of the top mass scheme** are included, as well.

$\boldsymbol{p_{\mathrm{T}}^{H}}$ bins: The uncertainties are derived using the calculation of the $H + 1j$ cross-section at NLO accuracy with finite top mass (NLO_SM). The renormalization and factorization scales are considered in the derivation. The central value of the cross section and the scale variations are cross-checked with the NNLOPS and the MiNLO HJ amples [1]. In addition, the envelopes of the scale variations are validated among the samples. The comparisons are shown in Figure 9(a) and 9(b) respectively. The yield uncertainty in the high-p_{T}^{H} region and the p_{T}^{H} migration are both evaluated using the long-range ST method, as shown in Table 8.

Table 8: p_{T}^{H} uncertainties obtained from the long-range ST method with $\rho = 0.5$ in the $p_{\mathrm{T}}^{H} > 200$ GeV region.

ggF	NLO_SM				
p_{T}^{H} [GeV] bin	≥ 200	[200,300)	[300,450)	[450,650)	≥ 650
$\lambda_{\mathrm{high}-p_{\mathrm{T}}^{H}}$ [%]	22.1	22.1	22.1	22.1	22.1
$\lambda_{p_{\mathrm{T}}^{H}=300}$ [%]		-2.8	10.4	10.4	10.4
$\lambda_{p_{\mathrm{T}}^{H}=450}$ [%]			-1.7	10.3	10.3
$\lambda_{p_{\mathrm{T}}^{H}=650}$ [%]				-1.4	10.4
Total [%]	22.1	22.2	24.4	26.5	28.4

[1] Comparisons with samples generated in the infinite top mass scheme are presented in Appendix A

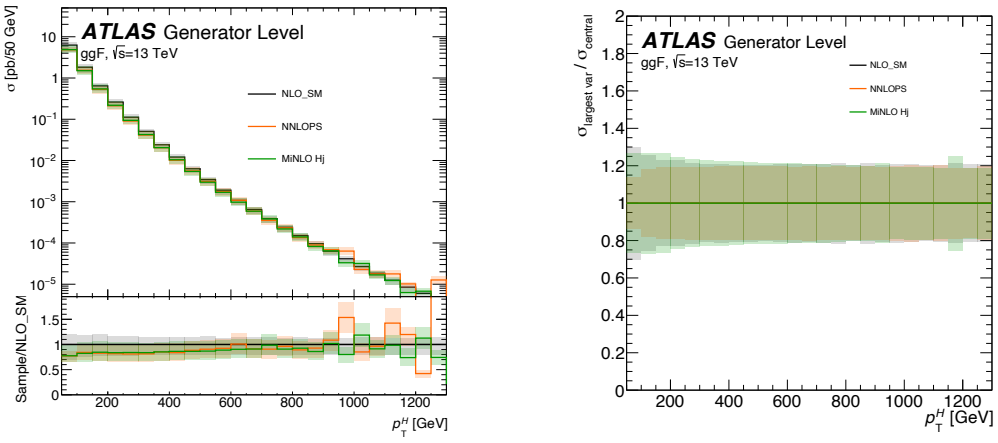

(a) (b)

Figure 9: (a) Cross sections and scale variations as a function of p_{T}^{H} for the NLO_SM sample, compared to the NNLOPS and MiNLO HJ samples. The bottom panel shows the ratio to the NLO_SM prediction. (b) Envelopes of scale variations divided by central value as a function of p_{T}^{H} for the NLO_SM sample, compared to the NNLOPS and MiNLO HJ samples. The uncertainty envelope is created by symmetrizing the largest scale variation.

$p_{\mathrm{T}}^{Hj}/p_{\mathrm{T}}^{H}$ bins: $p_{\mathrm{T}}^{Hj}/p_{\mathrm{T}}^{H}$ is an observable used to probe the 1-jet exclusive and 2-jet inclusive events. Since the NLO_SM calculation is a function of p_{T}^{H} only, the $p_{\mathrm{T}}^{Hj}/p_{\mathrm{T}}^{H}$ migration is estimated using the NNLOPS sample and cross-checked with the $H+0,1,2j$ MG5_aMC@NLO (FxFx) sample.

Before deriving the uncertainty, the p_{T}^{H} dependence of the NNLOPS scale variations as a function of $p_{\mathrm{T}}^{Hj}/p_{\mathrm{T}}^{H}$ was investigated. As shown in Figure 10, the envelope of the scale uncertainty over the $p_{\mathrm{T}}^{Hj}/p_{\mathrm{T}}^{H}$ spectrum is consistent among all p_{T}^{H} regions. Therefore, it is appropriate to evaluate the $p_{\mathrm{T}}^{Hj}/p_{\mathrm{T}}^{H}$ migration using the long-range ST method in the p_{T}^{H} inclusive region. The resulting uncertainties are shown in Table 9. Note that no ρ scale factor is applied in this case since there is only one boundary.

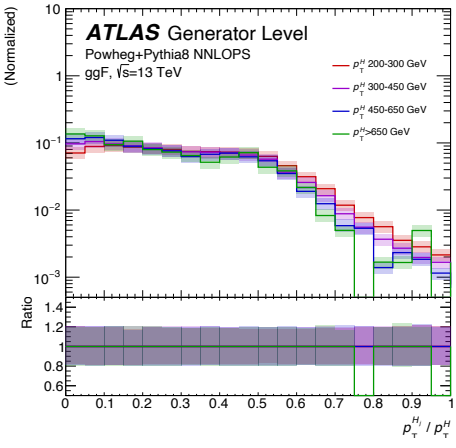

Figure 10: Cross sections and envelopes of scale variations as a function of $p_{\mathrm{T}}^{Hj}/p_{\mathrm{T}}^{H}$ on NNLOPS, split by p_{T}^{H} bin. The bottom panel shows the scale variations envelope with respect to the nominal prediction for each p_{T}^{H} bin.

Table 9: Scale uncertainties obtained with the long-range ST method in bins of $p_{\mathrm{T}}^{Hj}/p_{\mathrm{T}}^{H}$. The overall normalization uncertainty λ_y is to be replaced by the number from scale variations on the NLO_SM sample, shown as $\lambda_{\mathrm{high}-p_{\mathrm{T}}^{H}}$ in Table 8, but is shown for completeness.

ggF	NNLOPS	
$p_{\mathrm{T}}^{Hj}/p_{\mathrm{T}}^{H}$ bin	< 0.15	≥ 0.15
λ_y [%]	20.7	20.7
$\lambda_{p_{\mathrm{T}}^{Hj}/p_{\mathrm{T}}^{H}=0.15}$ [%]	-51.0	18.1
Total [%]	55.0	27.4

Top mass scheme uncertainty: For the NLO_SM calculation, the top mass is set to the pole mass, which is 173.05 GeV. To estimate the uncertainty due to the choice of the top mass scheme, another theoretical calculation at LO accuracy with various top mass settings is used. The top mass choices of the calculation include the pole mass and the $\overline{MS}$ scheme with a dynamical scale E_{T}: $m_{\mathrm{top}}(E_{\mathrm{T}})$, $m_{\mathrm{top}}(2E_{\mathrm{T}})$, $m_{\mathrm{top}}(E_{\mathrm{T}}/2)$.

The effect due to the top mass scheme across the p_{T}^{H} bins is handled by a single nuisance parameter. The uncertainty is taken from the difference of the cross sections calculated with the pole mass and the $\bar{M}S$ scheme. Since the cross sections are only at LO accuracy, the uncertainty is estimated to be half of the difference to account for the expected improvement with a NLO calculation. The resulting uncertainties are shown in Table 10.

Table 10: Uncertainty due to the top mass scheme, in bins of p_{T}^{H}.

ggF	LO finite top mass samples				
p_{T}^{H} [GeV] bin	≥ 200	[200,300)	[300,450)	[450,650)	≥ 650
$\lambda_{m_{\mathrm{top}}}$ [%]	3.7	2.8	6.4	10.3	14.1

4.2 $t\bar{t}H$ production mode

Yield uncertainties: The yield uncertainties are due to missing higher-order terms in the perturbative QCD calculations and are estimated to be 9.2% [48] by μ_{f} and μ_{r} scale variations.

p_{T}^{H} migration: The p_{T}^{H} migration is evaluated with the long-range ST method. Renormalization, factorization scales variations, ISR (μ_R, μ_F and shower variation Var3cDo), and FSR variations are taken into account in the evaluation. Figure 11 shows the effect of the simultaneous variation of the renormalization and factorization scales (top left), ISR (top right) and FSR (down) on the p_{T}^{H} spectrum. The values of the relative uncertainties on the cross sections binned in inclusive p_{T}^{H} regions are shown in

Figure 12. It can be seen that the maximal relative uncertainty originates from the ISR variation with μ_r = 2, μ_f = 2.

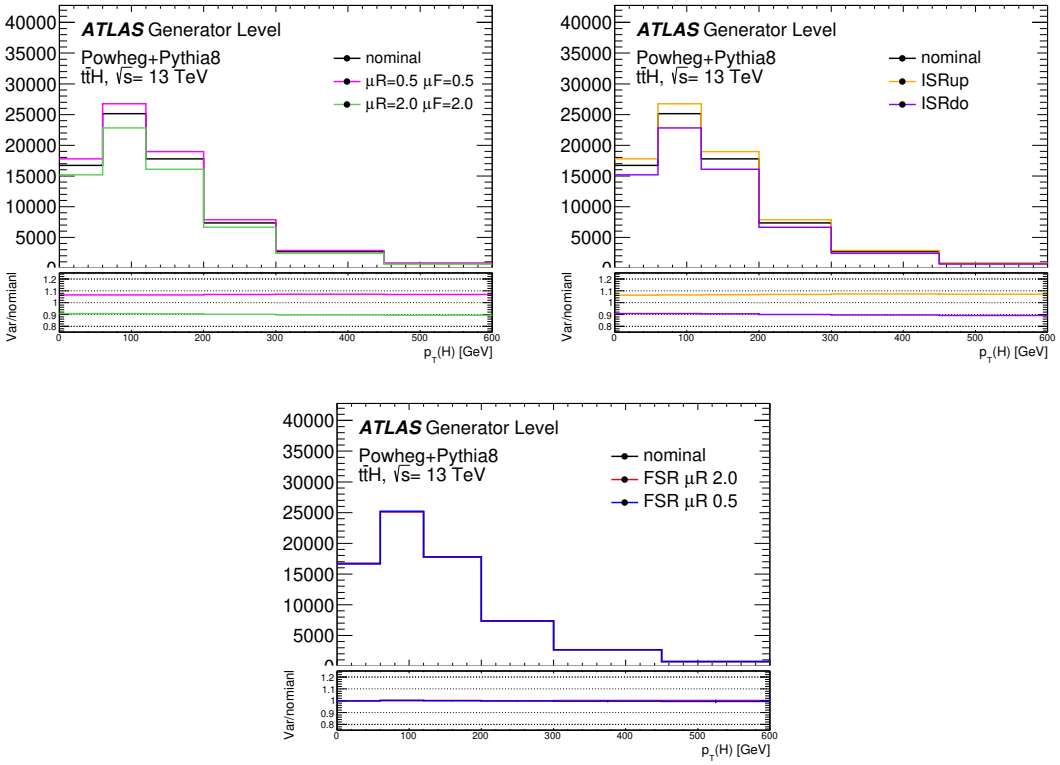

Figure 11: Effect of renormalization, factorization, ISR, and FSR variations on the yield in each p_T^H bin.

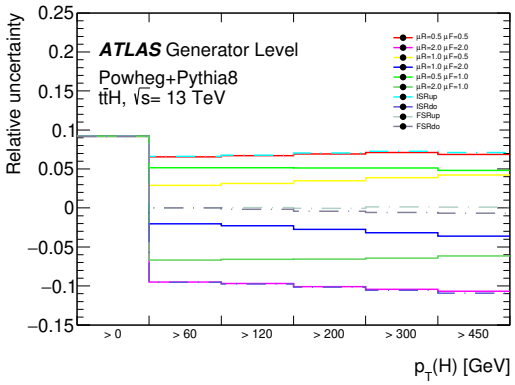

Figure 12: Relative uncertainty on the cross sections due to the scale variations, as well as the ISR and FSR uncertainty in the inclusive p_T^H bins. (Note that the relative variations in the inclusive bin $p_T^H > 0$ GeV correspond to the overall cross-section uncertainty of 9.2%.)

Since the maximal relative uncertainty is originating from the ISRdo(wn) variation (shown in Figure 13 along with the overall uncertainty of 9.2%), it is used to estimate the migration uncertainty with the long-range ST method. The migration across the p_T^H = 120, 200, 300, 450 GeV boundaries are evaluated with the standard long-range ST method, using $\rho = 0.7$. However, for the calculation of $\lambda_{p_T^H=60}$, the

long-range ST method is applied in the opposite direction given that the bulk of the $t\bar{t}H$ events is in the bin p_{T}^{H} =[60, 120] GeV and the standard procedure would overestimate the uncertainty in the p_{T}^{H} =[0, 60] GeV bin.

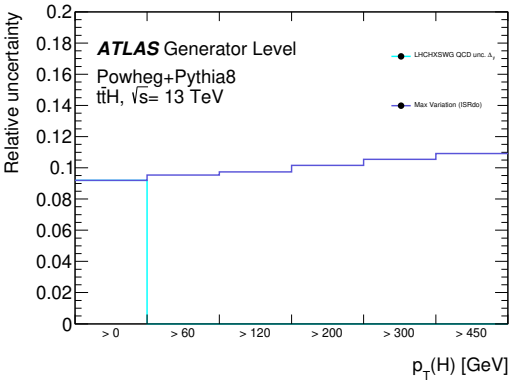

Figure 13: Same as Fig. 12, but showing the absolute value of the maximal variation (overall cross-section uncertainty in first bin and the ISR down variation in the others) in each bin only.

The corresponding migration uncertainties, as well as the total uncertainty in each p_{T}^{H} bin are shown in Figure 14 and presented in Table 11.

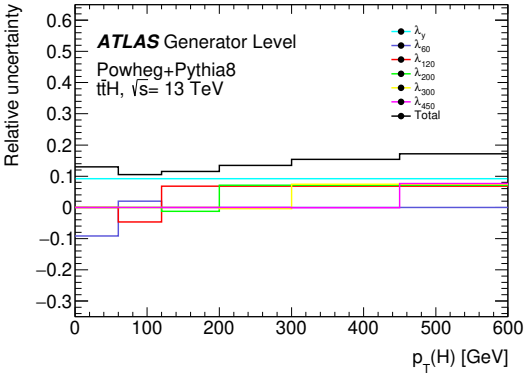

Figure 14: Yield, p_{T}^{H} migration, and total uncertainties obtained by the long-range ST method with $\rho = 0.7$.

The effect of using an alternative NLO generator (MG5_aMC@NLO) or an alternative parton shower algorithm (Herwig) on the shape of the p_{T}^{H} spectrum was also checked and found to be negligible. It is therefore not used for the evaluation of the migration uncertainties.

Table 11: Yield, p_{T}^{H} migration, and total uncertainties obtained with the long-range ST method with $\rho = 0.7$.

$t\bar{t}H$	Powheg					
p_{T}^{H} [GeV] bin	< 60	[60,120)	[120,200)	[200,300)	[300,450)	≥ 450
λ_y [%]	9.2	9.2	9.2	9.2	9.2	9.2
$\lambda_{p_{\mathrm{T}}^{H}=60}$ [%]	-9.2	2.0				
$\lambda_{p_{\mathrm{T}}^{H}=120}$ [%]		-4.6	6.8	6.8	6.8	6.8
$\lambda_{p_{\mathrm{T}}^{H}=200}$ [%]			-1.3	7.1	7.1	7.1
$\lambda_{p_{\mathrm{T}}^{H}=300}$ [%]				-0.4	7.4	7.4
$\lambda_{p_{\mathrm{T}}^{H}=450}$ [%]					-0.1	7.6
Total [%]	13.0	10.5	11.5	13.5	15.4	17.2

5 Conclusion

The uncertainties on the cross-section predictions for ggF and $t\bar{t}H$ were evaluated in bins of the simplified template cross-section framework, stage 1.2. To estimate the uncertainties in exclusive phase space regions, the long-range Stewart-Tackmann method was applied. These uncertainties are used in ATLAS Run-2 Higgs boson measurements, to assign uncertainties on the cross-section predictions and acceptance effects.

References

[1] J. R. Andersen et al.,
Les Houches 2015: Physics at TeV Colliders Standard Model Working Group Report, (2016),
arXiv: 1605.04692 [hep-ph],
URL: http://lss.fnal.gov/archive/2016/conf/fermilab-conf-16-175-ppd-t.pdf
(cit. on p. 2).

[2] D. de Florian et al.,
Handbook of LHC Higgs Cross Sections: 4. Deciphering the Nature of the Higgs Sector, (2016),
arXiv: 1610.07922 [hep-ph] (cit. on pp. 2, 3, 7, 24, 25).

[3] M. Cacciari, G. P. Salam and G. Soyez, *The anti-k_t jet clustering algorithm*, JHEP **04** (2008) 063,
arXiv: 0802.1189 [hep-ph] (cit. on p. 2).

[4] M. Cacciari, G. P. Salam and G. Soyez, *FastJet user manual*, Eur. Phys. J. C **72** (2012) 1896,
arXiv: 1111.6097 [hep-ph] (cit. on p. 2).

[5] ATLAS Collaboration,
A detailed map of Higgs boson interactions by the ATLAS experiment ten years after the discovery,
Nature **607** (2022) 52, arXiv: 2207.00092 [hep-ex] (cit. on p. 2).

[6] I. W. Stewart and F. J. Tackmann,
Theory uncertainties for Higgs mass and other searches using jet bins,
Physical Review D **85** (2012), ISSN: 1550-2368,
URL: http://dx.doi.org/10.1103/PhysRevD.85.034011 (cit. on p. 3).

[7] K. Hamilton, P. Nason, E. Re and G. Zanderighi, *NNLOPS simulation of Higgs boson production*,
JHEP **10** (2013) 222, arXiv: 1309.0017 [hep-ph] (cit. on p. 3).

[8] K. Hamilton, P. Nason and G. Zanderighi,
Finite quark-mass effects in the NNLOPS POWHEG+MiNLO Higgs generator, JHEP **05** (2015) 140,
arXiv: 1501.04637 [hep-ph] (cit. on p. 3).

[9] S. Alioli, P. Nason, C. Oleari and E. Re, *A general framework for implementing NLO calculations in shower Monte Carlo programs: the POWHEG BOX*, JHEP **06** (2010) 043,
arXiv: 1002.2581 [hep-ph] (cit. on pp. 3, 6).

[10] P. Nason, *A new method for combining NLO QCD with shower Monte Carlo algorithms*,
JHEP **11** (2004) 040, arXiv: hep-ph/0409146 (cit. on pp. 3, 6).

[11] S. Frixione, P. Nason and C. Oleari,
Matching NLO QCD computations with parton shower simulations: the POWHEG method,
JHEP **11** (2007) 070, arXiv: 0709.2092 [hep-ph] (cit. on pp. 3, 6).

[12] K. Hamilton, P. Nason and G. Zanderighi, *MINLO: multi-scale improved NLO*,
JHEP **10** (2012) 155, arXiv: 1206.3572 [hep-ph] (cit. on p. 3).

[13] J. M. Campbell et al., *NLO Higgs boson production plus one and two jets using the POWHEG BOX, MadGraph4 and MCFM*, JHEP **07** (2012) 092, arXiv: 1202.5475 [hep-ph] (cit. on p. 3).

[14] K. Hamilton, P. Nason, C. Oleari and G. Zanderighi, *Merging H/W/Z + 0 and 1 jet at NLO with no merging scale: a path to parton shower + NNLO matching*, JHEP **05** (2013) 082,
arXiv: 1212.4504 [hep-ph] (cit. on p. 3).

[15] S. Catani and M. Grazzini, *Next-to-Next-to-Leading-Order Subtraction Formalism in Hadron Collisions and its Application to Higgs-boson Production at the Large Hadron Collider*,
Phys. Rev. Lett. **98** (2007) 222002, arXiv: hep-ph/0703012 [hep-ph] (cit. on p. 3).

[16] J. Butterworth et al., *PDF4LHC recommendations for LHC Run II*, J. Phys. G **43** (2016) 023001,
arXiv: 1510.03865 [hep-ph] (cit. on p. 3).

[17] T. Sjöstrand et al., *An introduction to PYTHIA 8.2*, Comput. Phys. Commun. **191** (2015) 159,
arXiv: 1410.3012 [hep-ph] (cit. on pp. 3, 6).

[18] ATLAS Collaboration, *Measurement of the Z/γ^* boson transverse momentum distribution in pp collisions at $\sqrt{s} = 7$ TeV with the ATLAS detector*, JHEP **09** (2014) 145,
arXiv: 1406.3660 [hep-ex] (cit. on p. 3).

[19] D. J. Lange, *The EvtGen particle decay simulation package*, Nucl. Instrum. Meth. A **462** (2001) 152
(cit. on pp. 3, 6).

[20] R. Frederix and K. Hamilton, *Extending the MINLO method*, JHEP **05** (2016) 042,
arXiv: 1512.02663 [hep-ph] (cit. on p. 3).

[21] J. Alwall et al., *The automated computation of tree-level and next-to-leading order differential cross sections, and their matching to parton shower simulations*,
Journal of High Energy Physics **2014** (2014),
URL: https://doi.org/10.1007%2Fjhep07%282014%29079 (cit. on p. 3).

[22] R. Frederix and S. Frixione, *Merging meets matching in MC@NLO*, Journal of High Energy Physics **2012** (2012), URL: https://doi.org/10.1007%2Fjhep12%282012%29061 (cit. on p. 3).

[23] R. D. Ball et al., *Parton distributions for the LHC run II*, Journal of High Energy Physics **2015** (2015), URL: https://doi.org/10.1007/JHEP04(2015)040 (cit. on p. 3).

[24] R. Boughezal, X. Liu, F. Petriello, F. J. Tackmann and J. R. Walsh, *Combining Resummed Higgs Predictions Across Jet Bins*, Phys. Rev. D **89** (2014) 074044, arXiv: 1312.4535 [hep-ph] (cit. on p. 3).

[25] S. P. Jones, M. Kerner and G. Luisoni, *Next-to-Leading-Order QCD Corrections to Higgs Boson Plus Jet Production with Full Top-Quark Mass Dependence*, Phys. Rev. Lett. **120** (2018) 162001, arXiv: 1802.00349 [hep-ph] (cit. on p. 4).

[26] S. Amoroso et al., *Les Houches 2019: Physics at TeV Colliders: Standard Model Working Group Report*, 2020, arXiv: 2003.01700 [hep-ph] (cit. on p. 4).

[27] J. Baglio et al., *Gluon fusion into Higgs pairs at NLO QCD and the top mass scheme*, The European Physical Journal C **79** (2019), ISSN: 1434-6052, URL: http://dx.doi.org/10.1140/epjc/s10052-019-6973-3 (cit. on p. 4).

[28] J. Baglio et al., *Higgs-Pair Production via Gluon Fusion at Hadron Colliders: NLO QCD Corrections*, JHEP **04** (2020) 181, arXiv: 2003.03227 [hep-ph] (cit. on p. 4).

[29] J. Baglio et al., *gg→HH : Combined uncertainties*, Physical Review D **103** (2021), ISSN: 2470-0029, URL: http://dx.doi.org/10.1103/PhysRevD.103.056002 (cit. on p. 4).

[30] J. Baglio et al., *Gluon fusion into Higgs pairs at NLO QCD and the top mass scheme*, Eur. Phys. J. C **79** (2019) 459, arXiv: 1811.05692 [hep-ph] (cit. on p. 4).

[31] S. Frixione, G. Ridolfi and P. Nason, *A positive-weight next-to-leading-order Monte Carlo for heavy flavour hadroproduction*, JHEP **09** (2007) 126, arXiv: 0707.3088 [hep-ph] (cit. on p. 6).

[32] H. B. Hartanto, B. Jäger, L. Reina and D. Wackeroth, *Higgs boson production in association with top quarks in the POWHEG BOX*, Phys. Rev. D **91** (2015) 094003, arXiv: 1501.04498 [hep-ph] (cit. on p. 6).

[33] R. D. Ball et al., *Parton distributions for the LHC run II*, JHEP **04** (2015) 040, arXiv: 1410.8849 [hep-ph] (cit. on p. 6).

[34] ATLAS Collaboration, *ATLAS Pythia 8 tunes to 7 TeV data*, ATL-PHYS-PUB-2014-021, 2014, URL: https://cds.cern.ch/record/1966419 (cit. on p. 6).

[35] S. Gangal and F. J. Tackmann, *Next-to-leading-order uncertainties in Higgs+2 jets from gluon fusion*, Phys. Rev. D **87** (2013) 093008, arXiv: 1302.5437 [hep-ph] (cit. on p. 6).

[36] C. Anastasiou, C. Duhr, F. Dulat, F. Herzog and B. Mistlberger, *Higgs Boson Gluon-Fusion Production in QCD at Three Loops*, Phys. Rev. Lett. **114** (2015) 212001, arXiv: 1503.06056 [hep-ph] (cit. on p. 7).

[37] C. Anastasiou et al.,
High precision determination of the gluon fusion Higgs boson cross-section at the LHC,
JHEP **05** (2016) 058, arXiv: 1602.00695 [hep-ph] (cit. on p. 7).

[38] F. Dulat, A. Lazopoulos and B. Mistlberger, *iHixs 2 – Inclusive Higgs cross sections*,
Comput. Phys. Commun. **233** (2018) 243, arXiv: 1802.00827 [hep-ph] (cit. on p. 7).

[39] R. V. Harlander and K. J. Ozeren,
Finite top mass effects for hadronic Higgs production at next-to-next-to-leading order,
JHEP **11** (2009) 088, arXiv: 0909.3420 [hep-ph] (cit. on p. 7).

[40] R. V. Harlander and K. J. Ozeren,
Top mass effects in Higgs production at next-to-next-to-leading order QCD: Virtual corrections,
Phys. Lett. B **679** (2009) 467, arXiv: 0907.2997 [hep-ph] (cit. on p. 7).

[41] R. V. Harlander, H. Mantler, S. Marzani and K. J. Ozeren,
Higgs production in gluon fusion at next-to-next-to-leading order QCD for finite top mass,
Eur. Phys. J. C **66** (2010) 359, arXiv: 0912.2104 [hep-ph] (cit. on p. 7).

[42] A. Pak, M. Rogal and M. Steinhauser,
Finite top quark mass effects in NNLO Higgs boson production at LHC, JHEP **02** (2010) 025,
arXiv: 0911.4662 [hep-ph] (cit. on p. 7).

[43] S. Actis, G. Passarino, C. Sturm and S. Uccirati,
NLO electroweak corrections to Higgs boson production at hadron colliders,
Phys. Lett. B **670** (2008) 12, arXiv: 0809.1301 [hep-ph] (cit. on p. 7).

[44] S. Actis, G. Passarino, C. Sturm and S. Uccirati,
NNLO computational techniques: The cases $H \to \gamma\gamma$ and $H \to gg$, Nucl. Phys. B **811** (2009) 182,
arXiv: 0809.3667 [hep-ph] (cit. on p. 7).

[45] C. Anastasiou, R. Boughezal and F. Petriello,
Mixed QCD-electroweak corrections to Higgs boson production in gluon fusion,
JHEP **04** (2009) 003, arXiv: 0811.3458 [hep-ph] (cit. on p. 7).

[46] U. Aglietti, R. Bonciani, G. Degrassi and A. Vicini,
Two-loop light fermion contribution to Higgs production and decays, Phys. Lett. B **595** (2004) 432,
arXiv: hep-ph/0404071 (cit. on p. 7).

[47] M. Bonetti, K. Melnikov and L. Tancredi, *Higher order corrections to mixed QCD-EW contributions to Higgs boson production in gluon fusion*, Phys. Rev. D **97** (2018) 056017,
arXiv: 1801.10403 [hep-ph], Erratum: Phys. Rev. D **97** (2018) 099906 (cit. on p. 7).

[48] ATLAS Collaboration, *Measurement of Higgs boson decay into b-quarks in associated production with a top-quark pair in pp collisions at $\sqrt{s} = 13$ TeV with the ATLAS detector*,
JHEP **06** (2021) 097, arXiv: 2111.06712 [hep-ex] (cit. on p. 16).

Appendices

A Generator comparison in the high-p_{T}^{H} region for ggF

The p_{T}^{H} migration in the high-p_{T}^{H} region of the ggF production is evaluated with the NLO_SM calculation, which is derived using a finite top mass. In Section 4.1.2, central values and the variations of this calculation are cross-checked with the ATLAS recommended samples NNLOPS and MiNLO HJ, in which corrections are applied to account for top mass effects. In this section, we further present the comparisons with the alternative generator MG5_aMC@NLO, for which no corrections are applied for top mass effects. The comparison is shown in Figure 15(a). It can be seen that the central values have a strong dependence on the handling of the top mass. The figure also shows the success of the NNLOPS and MiNLO HJ samples in approximating the finite top mass spectrum.

Figure 15(b) compares the sizes of uncertainties predicted by each sample, which are compatible with each other.

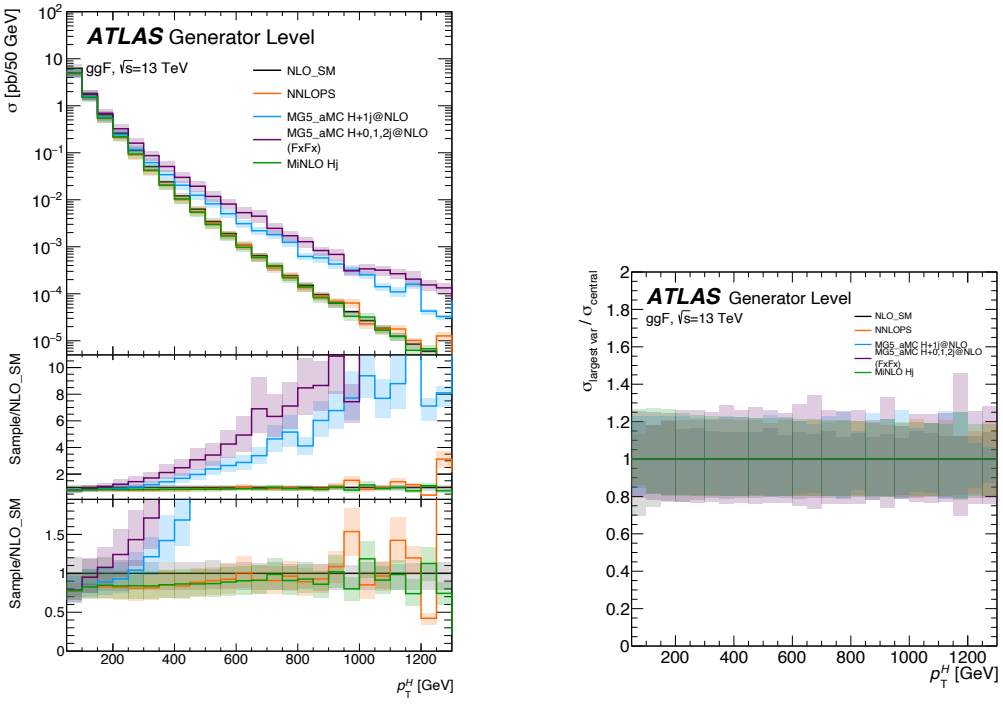

(a) (b)

Figure 15: (a) Cross sections and scale variations as a function of p_{T}^{H} estimated with the NLO_SM calculation, compared to samples generated with (NNLOPS and MiNLO HJ) or without (MG5_aMC@NLO) corrections for top mass effects. (b) Envelope of the scale variations for each sample.

B STXS stage 1.2 cross-sections for ggF and $t\bar{t}H$

This appendix summarizes the cross sections for each ggF and $t\bar{t}H$ bin in STXS stage 1.2. They are calculated by multiplying the Higgs boson production cross sections from Ref. [2] with the acceptances calculated from Powheg NNLOPS for ggF and Powheg NLO for $t\bar{t}H$. Table 12 shows the nominal ATLAS samples for all production modes along with the cross sections from Ref. [2]. More details on the ggF and $t\bar{t}H$ samples can be found in Table 1.

The STXS cross sections for ggF production are shown in Table 13 and for $t\bar{t}H$ production in Table 14.

Table 12: Configuration of MC simulation of SM Higgs boson production and the predicted cross sections at $\sqrt{s}$ = 13 TeV from Ref. [2] .

Process	Generator (ME+PS)	PDF (ME)	PDF, Tune (PS, UE)	Cross section [pb] ($\sqrt{s}$ = 13 TeV)
ggF	Powheg NNLOPS + Pythia 8	PDF4LHC15	CTEQ6, AZNLO	48.5
VBF	Powheg Box + Pythia 8	PDF4LHC15	CTEQ6, AZNLO	3.78
WH	Powheg Box + Pythia 8	PDF4LHC15	CTEQ6, AZNLO	1.37
$q\bar{q} \to ZH$	Powheg Box + Pythia 8	PDF4LHC15	CTEQ6, AZNLO	0.76
$t\bar{t}H$	Powheg Box + Pythia 8	PDF4LHC15	NNPDF2.3, A14	0.51
$gg \to ZH$	Powheg Box + Pythia 8	PDF4LHC15	CTEQ6, AZNLO	0.12
$b\bar{b}H$	Powheg Box + Pythia 8	PDF4LHC15	NNPDF2.3, A14	0.49
$tHbj$	aMC@NLO + Pythia 8	NNPDF3.0	NNPDF2.3, A14	0.074
tWH	aMC@NLO + Pythia 8	NNPDF3.0	NNPDF2.3, A14	0.015

Table 13: Cross section of each STXS bin for $gg \to H$ production.

$gg \to H$ STXS bin	cross-section [fb]	$gg \to H$ STXS bin	Cross section [fb]
0J_ptH_0_10	6.64×10^3	ge2J_mJJ_gt1500_ptH_0_200_ptHJJ_gt25	24.4
0J_ptH_gt10	2.06×10^4	ptH_200_300_ptHJoverptH_0_15	104
1J_ptH_0_60	6.5×10^3	ptH_300_450_ptHJoverptH_0_15	29.3
1J_ptH_60_120	4.5×10^3	ptH_450_650_ptHJoverptH_0_15	4.99
1J_ptH_120_200	747	ptH_gt650_ptHJoverptH_0_15	0.719
ge2J_mJJ_0_350_ptH_0_60_ptHJJ_0_25	647	ptH_200_300_ptHJoverptH_gt15	344
ge2J_mJJ_0_350_ptH_60_120_ptHJJ_0_25	961	ptH_300_450_ptHJoverptH_gt15	75.1
ge2J_mJJ_0_350_ptH_120_200_ptHJJ_0_25	356	ptH_450_650_ptHJoverptH_gt15	10.6
ge2J_mJJ_0_350_ptH_0_60_ptHJJ_gt25	522	ptH_gt650_ptHJoverptH_gt15	1.46
ge2J_mJJ_0_350_ptH_60_120_ptHJJ_gt25	833	ptH_200_300_ptHJoVerptH_0_15	0.471
ge2J_mJJ_0_350_ptH_120_200_ptHJJ_gt25	587	ptH_300_450_ptHJoVerptH_0_15	0.105
ge2J_mJJ_350_700_ptH_0_200_ptHJJ_0_25	2.5×10^2	ptH_450_650_ptHJoVerptH_0_15	0.0186
ge2J_mJJ_350_700_ptH_0_200_ptHJJ_gt25	361	ptH_gt650_ptHJoVerptH_0_15	0.00173
ge2J_mJJ_700_1000_ptH_0_200_ptHJJ_0_25	56.9	ptH_200_300_ptHJoVerptH_gt15	9.68
ge2J_mJJ_700_1000_ptH_0_200_ptHJJ_gt25	87.3	ptH_300_450_ptHJoVerptH_gt15	1.82
ge2J_mJJ_1000_1500_ptH_0_200_ptHJJ_0_25	31.7	ptH_450_650_ptHJoVerptH_gt15	0.171
ge2J_mJJ_1000_1500_ptH_0_200_ptHJJ_gt25	48.8	ptH_gt650_ptHJoVerptH_gt15	0.0122
ge2J_mJJ_gt1500_ptH_0_200_ptHJJ_0_25	16.4		

Table 14: Cross section of each STXS bin for $t\bar{t}H$ production.

$t\bar{t}H$ STXS bin	Cross section [fb]
ptH_0_60	118
ptH_60_120	178
ptH_120_200	126
ptH_200_300	52.6
ptH_300_450	19.0
ptH_gt450	5.38

C STXS stage 1.2 cross-sections for the other production modes

This appendix summarizes the cross section for each bin in STXS stage 1.2 for the Higgs boson production modes not discussed in this note, calculated by multiplying the Higgs boson production cross sections from Ref. [2] with the acceptances calculated from the samples listed in Table 12.

Table 15: Cross section of each STXS bin for $qq \to Hqq$ production.

$qq \to Hqq$ STXS bin	Cross section [fb]	$qq \to Hqq$ STXS bin	Cross section [fb]
0J	371	ge2J_MJJ_gt1500_ptH_gt200_ptHJJ_gt25	10.9
1J	1.79×10^3	ge2J_mJJ_0_60_ptHJJ_0_25	20.9
ge2J_MJJ_0_60_ptHJJ_0_25	19.3	ge2J_mJJ_0_60_ptHJJ_gt25	29.2
ge2J_MJJ_0_60_ptHJJ_gt25	30.9	ge2J_mJJ_1000_1500_ptH_0_200_ptHJJ_0_25	0.243
ge2J_MJJ_1000_1500_ptH_0_200_ptHJJ_0_25	1.8×10^2	ge2J_mJJ_1000_1500_ptH_0_200_ptHJJ_gt25	1.9
ge2J_MJJ_1000_1500_ptH_0_200_ptHJJ_gt25	41.5	ge2J_mJJ_1000_1500_ptH_gt200_ptHJJ_0_25	0.122
ge2J_MJJ_1000_1500_ptH_gt200_ptHJJ_0_25	21.0	ge2J_mJJ_1000_1500_ptH_gt200_ptHJJ_gt25	0.75
ge2J_MJJ_1000_1500_ptH_gt200_ptHJJ_gt25	10.7	ge2J_mJJ_120_350_ptHJJ_0_25	50.2
ge2J_MJJ_120_350_ptHJJ_0_25	288	ge2J_mJJ_120_350_ptHJJ_gt25	158
ge2J_MJJ_120_350_ptHJJ_gt25	139	ge2J_mJJ_350_700_ptH_0_200_ptHJJ_0_25	6.07
ge2J_MJJ_350_700_ptH_0_200_ptHJJ_0_25	383	ge2J_mJJ_350_700_ptH_0_200_ptHJJ_gt25	29.9
ge2J_MJJ_350_700_ptH_0_200_ptHJJ_gt25	116	ge2J_mJJ_350_700_ptH_gt200_ptHJJ_0_25	1.29
ge2J_MJJ_350_700_ptH_gt200_ptHJJ_0_25	19.9	ge2J_mJJ_350_700_ptH_gt200_ptHJJ_gt25	7.76
ge2J_MJJ_350_700_ptH_gt200_ptHJJ_gt25	15.3	ge2J_mJJ_60_120_ptHJJ_0_25	2.5×10^2
ge2J_MJJ_60_120_ptHJJ_0_25	36.4	ge2J_mJJ_60_120_ptHJJ_gt25	177
ge2J_MJJ_60_120_ptHJJ_gt25	46.9	ge2J_mJJ_700_1000_ptH_0_200_ptHJJ_0_25	0.743
ge2J_MJJ_700_1000_ptH_0_200_ptHJJ_0_25	199	ge2J_mJJ_700_1000_ptH_0_200_ptHJJ_gt25	4.39
ge2J_MJJ_700_1000_ptH_0_200_ptHJJ_gt25	52.2	ge2J_mJJ_700_1000_ptH_gt200_ptHJJ_0_25	0.25
ge2J_MJJ_700_1000_ptH_gt200_ptHJJ_0_25	17.3	ge2J_mJJ_700_1000_ptH_gt200_ptHJJ_gt25	1.67
ge2J_MJJ_700_1000_ptH_gt200_ptHJJ_gt25	10.3	ge2J_mJJ_gt1500_ptH_0_200_ptHJJ_0_25	0.0699
ge2J_MJJ_gt1500_ptH_0_200_ptHJJ_0_25	184	ge2J_mJJ_gt1500_ptH_0_200_ptHJJ_gt25	0.622
ge2J_MJJ_gt1500_ptH_0_200_ptHJJ_gt25	30.8	ge2J_mJJ_gt1500_ptH_gt200_ptHJJ_0_25	0.0356
ge2J_MJJ_gt1500_ptH_gt200_ptHJJ_0_25	29.4	ge2J_mJJ_gt1500_ptH_gt200_ptHJJ_gt25	0.245

Table 16: Cross section of each STXS bin for $qq \to Hl\nu$ production.

$qq \to Hl\nu$ STXS bin	Cross section [fb]
ptV_0_75_0J	1.5×10^2
ptV_0_75_1J	45.6
ptV_0_75_ge2J	19.8
ptV_75_150_0J	84.2
ptV_75_150_1J	33.3
ptV_75_150_ge2J	16.9
ptV_150_250_0J	22.7
ptV_150_250_1J	11.4
ptV_150_250_ge2J	7.11
ptV_250_400_0J	4.97
ptV_250_400_1J	2.9
ptV_250_400_ge2J	2.17
ptV_gt400_0J	0.963
ptV_gt400_1J	0.634
ptV_gt400_ge2J	0.541

Table 17: Cross-section of each STXS bin for $qq \to Hll$ production.

$qq \to Hll$ STXS bin	Cross section [fb]
ptV_0_75_0J	72.9
ptV_0_75_1J	22.6
ptV_0_75_ge2J	9.71
ptV_75_150_0J	43.2
ptV_75_150_1J	17.6
ptV_75_150_ge2J	8.97
ptV_150_250_0J	12.0
ptV_150_250_1J	6.15
ptV_150_250_ge2J	3.9
ptV_250_400_0J	2.59
ptV_250_400_1J	1.54
ptV_250_400_ge2J	1.17
ptV_gt400_0J	0.487
ptV_gt400_1J	0.322
ptV_gt400_ge2J	0.279

Table 18: Cross section of each STXS bin for $gg \to Hll$ production.

$gg \to Hll$ STXS bin	Cross section [fb]
ptV_0_75_0J	2.9
ptV_0_75_1J	2.27
ptV_0_75_ge2J	1.37
ptV_75_150_0J	7.72
ptV_75_150_1J	5.81
ptV_75_150_ge2J	3.39
ptV_150_250_0J	3.47
ptV_150_250_1J	3.81
ptV_150_250_ge2J	2.89
ptV_250_400_0J	0.317
ptV_250_400_1J	0.646
ptV_250_400_ge2J	0.882
ptV_gt400_0J	0.0139
ptV_gt400_1J	0.0453
ptV_gt400_ge2J	0.109

Table 19: Cross section of each STXS bin for tHW, $tHqb$, and bbH productions.

STXS bin	Cross section [fb]
tHW	15.0
$tHqb$	69.7
bbH	444